

**HANDBOOK OF POLYMER
SYNTHESIS, CHARACTERIZATION,
AND PROCESSING**



HANDBOOK OF POLYMER SYNTHESIS, CHARACTERIZATION, AND PROCESSING

Edited by

ENRIQUE SALDÍVAR-GUERRA

Centro de Investigación en Química Aplicada
Saltillo Coahuila, México

EDUARDO VIVALDO-LIMA

Facultad de Química, Universidad Nacional Autónoma de México
Ciudad Universitaria, México, D.F., México

 **WILEY**

A JOHN WILEY & SONS, INC., PUBLICATION





Copyright © 2013 by John Wiley & Sons, Inc. All rights reserved

Published by John Wiley & Sons, Inc., Hoboken, New Jersey
Published simultaneously in Canada

No part of this publication may be reproduced, stored in a retrieval system, or transmitted in any form or by any means, electronic, mechanical, photocopying, recording, scanning, or otherwise, except as permitted under Section 107 or 108 of the 1976 United States Copyright Act, without either the prior written permission of the Publisher, or authorization through payment of the appropriate per-copy fee to the Copyright Clearance Center, Inc., 222 Rosewood Drive, Danvers, MA 01923, (978) 750-8400, fax (978) 750-4470, or on the web at www.copyright.com. Requests to the Publisher for permission should be addressed to the Permissions Department, John Wiley & Sons, Inc., 111 River Street, Hoboken, NJ 07030, (201) 748-6011, fax (201) 748-6008, or online at <http://www.wiley.com/go/permission>.



Limit of Liability/Disclaimer of Warranty: While the publisher and author have used their best efforts in preparing this book, they make no representations or warranties with respect to the accuracy or completeness of the contents of this book and specifically disclaim any implied warranties of merchantability or fitness for a particular purpose. No warranty may be created or extended by sales representatives or written sales materials. The advice and strategies contained herein may not be suitable for your situation. You should consult with a professional where appropriate. Neither the publisher nor author shall be liable for any loss of profit or any other commercial damages, including but not limited to special, incidental, consequential, or other damages.

For general information on our other products and services or for technical support, please contact our Customer Care Department within the United States at (800) 762-2974, outside the United States at (317) 572-3993 or fax (317) 572-4002.

Wiley also publishes its books in a variety of electronic formats. Some content that appears in print may not be available in electronic formats. For more information about Wiley products, visit our web site at www.wiley.com.

Library of Congress Cataloging-in-Publication Data:

Handbook of polymer synthesis, characterization, and processing / edited by Enrique Saldívar-Guerra, Centro de Investigación en Química Aplicada, Saltillo Coahuila, Mexico, Eduardo Vivaldo-Lima, Facultad de Química, Departamento de Ingeniería Química, Universidad Nacional Autónoma de Mexico, Mexico, D.F., Mexico.

pages cm

Includes bibliographical references and index.

ISBN 978-0-470-63032-7 (cloth)

1. Polymerization. I. Saldívar-Guerra, Enrique, editor of compilation. II. Vivaldo-Lima, Eduardo, editor of compilation.

TP156.P6H36 2013

547'.28—dc23

2012025752

Printed in the United States of America

ISBN: 9780470630327

10 9 8 7 6 5 4 3 2 1





*To Amparo, Adriana and Andrés, with love
To Adriana, Eduardo Abraham and Luis Ángel, with appreciation and love*



CONTENTS

PREFACE	xv
ACKNOWLEDGMENTS	xvii
CONTRIBUTORS	xix
PART I BASIC CONCEPTS	1
1 Introduction to Polymers and Polymer Types	3
<i>Enrique Saldívar-Guerra and Eduardo Vivaldo-Lima</i>	
1.1 Introduction to Polymers	3
1.2 Classification of Polymers	8
1.3 Nomenclature	12
References	13
2 Polymer States and Properties	15
<i>J. Betzabe González-Campos, Gabriel Luna-Bárcenas, Diana G. Zárate-Triviño, Arturo Mendoza-Galván, Evgen Prokhorov, Francisco Villaseñor-Ortega, and Isaac C. Sanchez</i>	
2.1 Introduction	15
2.2 Glass Transition Temperature (α -Relaxation) Controversy in Chitin, Chitosan, and PVA	16
2.3 Glass Transition Related to the α -Relaxation	16
2.4 Moisture Content Effects on Polymer's Molecular Relaxations	17
2.5 Dielectric Fundamentals	18
2.6 Chitin, Chitosan, and PVA Films Preparation for Dielectric Measurements	21
2.7 Dielectric Relaxations in Chitin: Evidence for a Glass Transition	22
2.8 Dielectric Relaxations in Neutralized and Nonneutralized Chitosan: The Stronger Water Content Effect on the α -Relaxation and the Glass Transition Phenomenon	30
2.9 PVA Dielectric Relaxations	35
References	38

vii

PART II POLYMER SYNTHESIS AND MODIFICATION	41
3 Step-Growth Polymerization	43
<i>Luis E. Elizalde, Gladys de los Santos-Villarreal, José L. Santiago-García, and Manuel Aguilar-Vega</i>	
3.1 Introduction	43
3.2 Polymerization Kinetics	46
3.3 Polyamides	48
3.4 Polyimides	50
3.5 Polyesters	50
3.6 Inorganic Condensation Polymers	53
3.7 Dendrimers	54
3.8 Thermoset Polycondensation Polymers	55
3.9 Controlled Molecular Weight Condensation Polymers	57
References	62
4 Free Radical Polymerization	65
<i>Ramiro Guerrero-Santos, Enrique Saldívar-Guerra, and José Bonilla-Cruz</i>	
4.1 Introduction	65
4.2 Basic Mechanism	66
4.3 Other Free Radical Reactions	68
4.4 Kinetics and Polymerization Rate	71
4.5 Molecular Weight and Molecular Weight Distribution	74
4.6 Experimental Determination of Rate Constants	76
4.7 Thermodynamics of Polymerization	77
4.8 Controlled Radical Polymerization	78
References	81
5 Coordination Polymerization	85
<i>João B. P. Soares and Odilia Pérez</i>	
5.1 Introduction	85
5.2 Polymer Types	87
5.3 Catalyst Types	87
5.4 Coordination Polymerization Mechanism	93
5.5 Polymerization Kinetics and Mathematical Modeling	93
References	101
6 Copolymerization	105
<i>Marc A. Dubé, Enrique Saldívar-Guerra, and Iván Zapata-González</i>	
6.1 Introduction	105
6.2 Types of Copolymers	106
6.3 Copolymer Composition and Microstructure	107
6.4 Reaction Conditions: Considerations	118
References	121
7 Anionic Polymerization	127
<i>Roderic Quirk</i>	
7.1 Introduction	127
7.2 Living Anionic Polymerization	127
7.3 General Considerations	129
7.4 Kinetics and Mechanism of Polymerization	134

7.5 Stereochemistry	144
7.6 Copolymerization of Styrenes and Dienes	148
7.7 Synthetic Applications of Living Anionic Polymerization	150
References	157
8 Cationic Polymerizations	163
<i>Filip E. Du Prez, Eric J. Goethals, and Richard Hoogenboom</i>	
8.1 Introduction	163
8.2 Carbocationic Polymerization	163
8.3 Cationic Ring-Opening Polymerization	172
8.4 Summary and Prospects	181
Acknowledgment	181
References	181
9 Crosslinking	187
<i>Julio César Hernández-Ortiz and Eduardo Vivaldo-Lima</i>	
9.1 Introduction	187
9.2 Background on Polymer Networks	187
9.3 Main Chemical Routes for Synthesis of Polymer Networks	191
9.4 Characterization of Polymer Networks and Gels	193
9.5 Theory and Mathematical Modeling of Crosslinking	195
Appendix A Calculation of Average Chain Length	200
Appendix B Calculation of Sol and Gel Fractions	201
Acknowledgments	202
References	202
10 Polymer Modification: Functionalization and Grafting	205
<i>José Bonilla-Cruz, Mariamne Dehonor, Enrique Saldívar-Guerra, and Alfonso González-Montiel</i>	
10.1 General Concepts	205
10.2 Graft Copolymers	207
References	219
11 Polymer Additives	225
<i>Rudolf Pfaendner</i>	
11.1 Introduction	225
11.2 Antioxidants	227
11.3 PVC Heat Stabilizers	231
11.4 Light Stabilizers	233
11.5 Flame Retardants	235
11.6 Plasticizers	238
11.7 Scavenging Agents	239
11.8 Additives to Enhance Processing	240
11.9 Additives to Modify Plastic Surface Properties	240
11.10 Additives to Modify Polymer Chain Structures	241
11.11 Additives to Influence Morphology and Crystallinity of Polymers	242
11.12 Antimicrobials	243
11.13 Additives to Enhance Thermal Conductivity	243
11.14 Active Protection Additives (Smart Additives)	243
11.15 Odor Masking	244

11.16 Animal Repellents	244
11.17 Markers	244
11.18 Blowing Agents	244
11.19 Summary and Trends in Polymer Additives	245
References	245
Further Reading	246
PART III POLYMERIZATION PROCESSES AND ENGINEERING	249
12 Polymer Reaction Engineering	251
<i>Alexander Penlidis, Eduardo Vivaldo-Lima, Julio César Hernández-Ortiz, and Enrique Saldívar-Guerra</i>	
12.1 Introduction	251
12.2 Mathematical Modeling of Polymerization Processes	252
12.3 Useful Tips on Polymer Reaction Engineering (PRE) and Modeling	257
12.4 Examples of Several Free Radical (Co)Polymerization Schemes and the Resulting Kinetic and Molecular Weight Development Equations	264
Acknowledgments	270
References	270
13 Bulk and Solution Processes	273
<i>Marco A. Villalobos and Jon Deblng</i>	
13.1 Definition	273
13.2 History	273
13.3 Processes for Bulk and Solution Polymerization	274
13.4 Energy Considerations	287
13.5 Mass Considerations	289
References	292
14 Dispersed-Phase Polymerization Processes	295
<i>Jorge Herrera-Ordóñez, Enrique Saldívar-Guerra, and Eduardo Vivaldo-Lima</i>	
14.1 Introduction	295
14.2 Emulsion Polymerization	295
14.3 Microemulsion Polymerization	303
14.4 Miniemulsion Polymerization	304
14.5 Applications of Polymer Latexes	304
14.6 Dispersion and Precipitation Polymerizations	305
14.7 Suspension Polymerization	305
14.8 Controlled Radical Polymerization (CRP) in Aqueous Dispersions	308
References	310
15 New Polymerization Processes	317
<i>Eduardo Vivaldo-Lima, Carlos Guerrero-Sánchez, Christian H. Hornung, Iraís A. Quintero-Ortega, and Gabriel Luna-Bárcenas</i>	
15.1 Introduction	317
15.2 Polymerizations in Benign or Green Solvents	317
15.3 Alternative Energy Sources for Polymerization Processes	327
15.4 Polymerization in Microreactors	329

Acknowledgments	331
References	331
PART IV POLYMER CHARACTERIZATION	335
16 Polymer Spectroscopy and Compositional Analysis	337
<i>Gladys de los Santos-Villarreal and Luis E. Elizalde</i>	
16.1 Introduction	337
16.2 Elemental Analysis	337
16.3 Infrared Spectroscopy	339
16.4 Nuclear Magnetic Resonance of Polymers in Solution	343
16.5 Mass Spectrometry	351
References	353
17 Polymer Molecular Weight Measurement	355
<i>María Guadalupe Neira-Velázquez, María Teresa Rodríguez-Hernández, Ernesto Hernández-Hernández, and Antelmo R. Y. Ruiz-Martínez</i>	
17.1 Introduction	355
17.2 Historical Background	355
17.3 Principles of GPC	356
17.4 Measurement of Intrinsic Viscosity	362
References	365
18 Light Scattering and its Applications in Polymer Characterization	367
<i>Roberto Alexander-Katz</i>	
18.1 Introduction	367
18.2 Principles of Static and Dynamic Light Scattering	367
18.3 Static Light Scattering by Dilute Polymer Solutions	370
18.4 Dynamic Light Scattering	377
References	387
19 Small-Angle X-Ray Scattering of Polymer Systems	391
<i>Carlos A. Avila-Orta and Francisco J. Medellín-Rodríguez</i>	
19.1 Introduction	391
19.2 Polymer Morphology	391
19.3 Small-Angle X-Ray Scattering	393
19.4 Analysis in Reciprocal Space	395
19.5 Analysis in Real Space	399
Appendix A Procedure to Obtain Morphological Data from 1D SAXS Profiles	404
References	406
20 Microscopy	409
<i>Mariamne Dehonor, Carlos López-Barrón, and Christopher W. Macosko</i>	
20.1 Introduction	409
20.2 Transmission Electron Microscopy	409
20.3 Three-Dimensional Microscopy	416
References	421

21 Structure and Mechanical Properties of Polymers	425
<i>Manuel Aguilar-Vega</i>	
21.1 Structure of Polymer Chains	425
21.2 Mechanical Properties of Polymers	426
21.3 Mechanical Properties of Polymer Composites	431
References	434
 PART V POLYMER PROCESSING	
22 Polymer Rheology	435
<i>Estanislao Ortíz-Rodríguez</i>	
22.1 Introduction to Polymer Rheology Fundamentals	437
22.2 Linear Viscoelasticity	440
22.3 Viscometric Techniques for Polymer Melts	441
22.4 Overview of Constitutive Equations	443
22.5 Brief Overview on Other Relevant Polymer Rheology Aspects	445
References	448
23 Principles of Polymer Processing	451
<i>Luis F. Ramos-de Valle</i>	
23.1 General	451
23.2 Compounding	451
23.3 Extrusion	452
23.4 Bottle Blowing	455
23.5 Injection Molding	455
23.6 Thermoforming	460
References	461
Further Reading	461
24 Blown Films and Ribbons Extrusion	463
<i>Jorge R. Robledo-Ortíz, Daniel E. Ramírez-Arreola, Denis Rodrigue, and Rubén González-Núñez</i>	
24.1 Introduction	463
24.2 Extrusion Processes for Blown Films and Ribbons	463
24.3 Equations	465
24.4 Ribbon and Film Dimensions	467
24.5 Cooling Process and Stretching Force	467
24.6 Morphology and Mechanical Properties	469
References	472
25 Polymer Solutions and Processing	473
<i>Dámaso Navarro Rodríguez</i>	
25.1 Introduction	473
25.2 Polymer Solution Thermodynamics and Conformation of Polymer Chains: Basic Concepts	474
25.3 Semidilute Polymer Solutions	481
25.4 Processing of Polymer Solutions	482
References	488

26 Wood and Natural Fiber-Based Composites (NFCs)	493
<i>Jorge R. Robledo-Ortíz, Francisco J. Fuentes-Talavera, Rubén González-Núñez, and José A. Silva-Guzmán</i>	
26.1 Introduction	493
26.2 Background	493
26.3 Raw Materials	494
26.4 Manufacturing Process	497
26.5 Properties of Composite Materials	497
26.6 Durability	498
26.7 Factors that Affect Decay of Wood–Plastic Composites	500
26.8 Uses of Wood–Plastic Composites	501
References	501
27 Polymer Blends	505
<i>Saúl Sánchez-Valdes, Luis F. Ramos-de Valle, and Octavio Manero</i>	
27.1 Introduction	505
27.2 Miscibility in Polymer Blends	505
27.3 Compatibility in Polymer Blends	508
27.4 Techniques for Studying Blend Microstructure	509
27.5 Preparation of Polymer Blends	510
27.6 Factors Influencing the Morphology of a Polymer Blend	511
27.7 Properties of Polymer Blends	513
27.8 Applications of Polymer Blends	516
References	517
28 Thermosetting Polymers	519
<i>Jean-Pierre Pascault and Roberto J.J. Williams</i>	
28.1 Introduction	519
28.2 Chemistries of Network Formation	520
28.3 Structural Transformations During Network Formation	521
28.4 Processing	524
28.5 Conclusions	532
References	532
PART VI POLYMERS FOR ADVANCED TECHNOLOGIES	535
29 Conducting Polymers	537
<i>María Judith Percino and Víctor Manuel Chapela</i>	
29.1 Introduction	537
29.2 Historical Background	538
29.3 The Structures of Conducting Polymers	539
29.4 Charge Storage	539
29.5 Doping	541
29.6 Polyanilines	543
29.7 Charge Transport	544
29.8 Syntheses	545
29.9 Conducting Polymers	545
29.10 Characterization Techniques	551
29.11 Present and Future Potential	552
References	555

xiv CONTENTS

30 Dendritic Polymers	559
<i>Jason Dockendorff and Mario Gauthier</i>	
30.1 Introduction	559
30.2 Dendrimers	561
30.3 Hyperbranched Polymers	567
30.4 Dendrigraft Polymers	574
30.5 Concluding Remarks	581
References	582
31 Polymer Nanocomposites	585
<i>Octavio Manero and Antonio Sanchez-Solis</i>	
31.1 Introduction	585
31.2 Polyester/Clay Nanocomposites	586
31.3 Polyolefin/Clay Nanocomposites	590
31.4 Polystyrene/Clay Nanocomposites	593
31.5 Polymer/Carbon Black Nanocomposites	596
31.6 Nanoparticles of Barium Sulfate	597
31.7 Polymer/Graphene Nanocomposites	598
31.8 Conclusions	601
Acknowledgments	601
References	601
INDEX	605



PREFACE

The industry of polymers is very complex, in part because it encompasses many aspects that are of multidisciplinary nature. The chain of production of polymers requires expert knowledge in different areas: (i) polymer synthesis, both from the chemistry and the engineering aspects; (ii) polymer characterization, including chemical, physicochemical, rheological properties and others; and (iii) polymer processing and transformation into final products.

The aim of this handbook is to serve as the first source and comprehensive reference to all aspects of interest in the polymer industry. Given the complexity of this industry and the specialized knowledge required in each area of polymer production and application, most of the books dealing with polymer science and technology cover only some aspects of the polymer production chain; however, we believe that a professional working in the polymer industry or, in general, in polymer science and technology would greatly benefit from a book summarizing all the aspects involved in the production chain of the polymer industry. The book has been written with the underlying idea of meeting this need. An effort has been made in every chapter to include the fundamentals of the chapter's subject, the relevant literature, and the new trends in the field.

The book is addressed mainly to professionals in virtually all positions in the polymer industry: manufacturing, quality control, R&D, sales, technical assistance, and so on. Another group of potential readers is the undergraduate and graduate students in fields related to polymer science and technology. Finally, academic researchers of universities and institutes, working in different areas of polymerization and polymers, will find the book useful for expanding their knowledge beyond their area of expertise. The book can be used to establish the first approach to a specific topic by anyone in the target audience, to broaden the knowledge

of industrial practitioners wanting to know more about the polymer production chain, and to look for references in order to deepen the understanding of specialized aspects of a topic. It can also be used as a textbook in the first course in polymer science or engineering, at the undergraduate or graduate level, especially if a broad coverage of the field is desired.

After an introduction to the basic concepts of polymers and polymerization (Chapter 1) and thermodynamic polymer states (Chapter 2)¹, the second part of the handbook is devoted to the main synthesis techniques of polymers (Chapters 3–5 and 7–8), including chapters covering concepts that may be applicable to all the synthesis techniques (crosslinking and grafting in Chapters 9 and 10, respectively). The important subject of copolymers (Chapter 6) is also included in this section, as synthesis and structure are closely related areas. The subject of additives is included in the synthesis section because, from the point of view of properties and applications, they have become an important part of the polymeric material being synthesized. The third part of the handbook is dedicated to the engineering principles and the different types of polymerization processes used in industry (Chapters 12–14); the new trends, from an engineering perspective, are also discussed (Chapter 15). Part IV, which includes Chapters 16–21, provides the scope of the main techniques used for polymer characterization and testing, at both the fundamental and the applied levels. Chapters 22–28 cover polymer processing principles, techniques, and equipment. Chapter 28 (Thermosetting Polymers) is included here because of the emphasis on industrial processes, although it implies simultaneous reaction and shaping. Finally, Chapters 29–31 deal with advanced

¹Some important thermodynamic concepts related to polymers are dealt with in Chapter 25.

and more specialized subjects in the polymer field, which are of increasing importance (nanomaterials, dendrimers, and conjugated polymers).

The handbook represents the joint effort of a large number of scientists and researchers working in the many

diverse fields of polymer science and technology. Many years of study and experience have been put together in an organized manner in this work; hopefully, the handbook will serve its purpose with a large audience.



ACKNOWLEDGMENTS

We are deeply grateful to the authors of all the chapters for their contribution and for sharing their expert knowledge. We also thank the Wiley-Blackwell editors and team for their support and guidance throughout the writing and editing of the handbook.

We also thank the several sponsors who have allowed us to carry out fundamental and applied research to an extent where we feel that we have added a few salt grains to the polymer science and engineering fields. E.V.-L. is indebted

to UNAM (PAIP and PAPIIT Project 119510), CONACyT (Project 101682), and ICyTDF (Project PICSA11-56). E.S.-G. acknowledges CIQA and CONACyT for continuous support.

Last but not least, we thank our families for their support and understanding during the editing of the handbook, and to some of our students and office staff at CIQA and FQ-UNAM for taking some extra work load that allowed us to invest time in this project.

CONTRIBUTORS

Manuel Aguilar-Vega, Materials Unit, Membranes Laboratory, Centro de Investigación Científica de Yucatán, Mérida, Yucatán, México

Roberto Alexander-Katz, Departamento de Física, Universidad Autónoma Metropolitana-Iztapalapa, Col. Vicentina, Mexico

Carlos A. Avila-Orta, Centro de Investigación en Química Aplicada, Saltillo, Coahuila, México

José Bonilla-Cruz, Centro de Investigación en Materiales Avanzados, Apodaca, Nuevo León, México

Víctor Manuel Chapela, Laboratorio de Polímeros, Instituto de Ciencias, Benemérita Universidad Autónoma de Puebla, Puebla, Pue., México

Jon Debling, BASF Corp., Wyandotte, MI, USA

Mariamne Dehonor, Macro-M S.A. de C.V. Lerma, Edo. de México, México

Jason Dockendorff, Department of Chemistry, Institute for Polymer Research, University of Waterloo, Waterloo, Ontario, Canada

Filip E. Du Prez, Department of Organic Chemistry, Polymer Chemistry Research group, Ghent University, Ghent, Belgium

Marc A. Dubé, Department of Chemical and Biological Engineering, Centre for Catalysis Research and Innovation, University of Ottawa, Ottawa, Ontario, Canada

Luis E. Elizalde, Centro de Investigación en Química Aplicada, Saltillo, Coahuila, México

Francisco J. Fuentes-Talavera, Departamento de Madera, Celulosa y Papel, Universidad de Guadalajara, Las Agujas, Zapopan, Jalisco, México

Mario Gauthier, Department of Chemistry, Institute for Polymer Research, University of Waterloo, Waterloo, Ontario, Canada

Eric J. Goethals, Department of Organic Chemistry, Polymer Chemistry Research group, Ghent University, Ghent, Belgium

J. Betzabe González-Campos, Universidad Michoacana de San Nicolás de Hidalgo, Instituto de Investigaciones Químico-Biológicas, Morelia, Michoacán, México

Alfonso González-Montiel, Macro M S.A. de C.V. Lerma, Edo. De México, México

Rubén González-Núñez, Departamento de Ingeniería Química, Universidad de Guadalajara, Guadalajara, Jalisco, México

Carlos Guerrero-Sánchez, CSIRO, Materials Science and Engineering Division, Victoria, Australia

Ramiro Guerrero-Santos, Centro de Investigación en Química Aplicada, Saltillo, Coahuila, México

Ernesto Hernández-Hernández, Centro de Investigación en Química Aplicada, Saltillo, Coahuila, México

Julio César Hernández-Ortiz, Departamento de Ingeniería Química, Facultad de Química, Universidad Nacional Autónoma de México, México D.F., México

Jorge Herrera-Ordóñez, Centro de Investigación en Química Aplicada, Saltillo, Coahuila, México

- Richard Hoogenboom**, Department of Organic Chemistry, Supramolecular Chemistry group, Ghent University, Ghent, Belgium
- Christian H. Hornung**, CSIRO, Materials Science and Engineering Division, Victoria, Australia
- Carlos López-Barrón**, Center for Neutron Science, Department of Chemical and Biomolecular Engineering, University of Delaware, Newark, DE, USA
- Gabriel Luna-Bárcenas**, Centro de Investigación y de Estudios Avanzados (CINVESTAV) del IPN, Unidad Querétaro, Querétaro, México
- Christopher W. Macosko**, Dept. of Chemical Engineering and Materials Science, University of Minnesota, Minneapolis, MN, USA
- Octavio Manero**, Instituto de Investigaciones en Materiales, Universidad Nacional Autónoma de México, México D.F., México
- Francisco J. Medellín-Rodríguez**, Facultad de Ciencias Químicas, Universidad Autónoma de San Luis Potosí, San Luis Potosí, San Luis Potosí, México
- Arturo Mendoza-Galván**, Centro de Investigación y de Estudios Avanzados (CINVESTAV) del IPN, Unidad Querétaro, Querétaro, México
- Dámaso Navarro Rodríguez**, Centro de Investigación en Química Aplicada, Saltillo, Coahuila, México
- María Guadalupe Neira-Velázquez**, Centro de Investigación en Química Aplicada, Saltillo, Coahuila, México
- Estanislao Ortíz-Rodríguez**, A. Schulman de México, San Luis Potosí, México
- Jean-Pierre Pascault**, Université de Lyon, UMR-CNRS 5223, INSA-Lyon, Ingénierie des Matériaux Polymères/Laboratoire des Matériaux Macromoléculaires, Villeurbanne, France
- Alexander Penlidis**, Department of Chemical Engineering, Institute for Polymer Research (IPR), University of Waterloo, Waterloo, Ontario, Canada
- María Judith Percino**, Laboratorio de Polímeros, Instituto de Ciencias, Benemérita Universidad Autónoma de Puebla, Puebla, Pue., México
- Odilia Pérez**, Centro de Investigación en Química Aplicada, Saltillo, Coahuila, México
- Rudolf Pfaendner**, Fraunhofer Institute for Structural Durability and System Reliability LBF, Division Plastics, Darmstadt, Germany
- Evgen Prokhorov**, Centro de Investigación y de Estudios Avanzados (CINVESTAV) del IPN, Unidad Querétaro, Querétaro, México
- Iraís A. Quintero-Ortega**, División de Ciencias e Ingenierías, Universidad de Guanajuato, León, México
- Roderic Quirk**, Dept. of Polymer Science, The University of Akron, Akron, OH, USA
- Daniel E. Ramírez-Arreola**, Departamento de Ingenierías, Universidad de Guadalajara, Autlán de Navarro, Jalisco, México
- Jorge R. Robledo-Ortíz**, Departamento de Madera, Celulosa y Papel, Universidad de Guadalajara, Las Agujas, Zapopan, Jalisco, México
- Denis Rodrigue**, Department of Chemical Engineering and CERMA, Université Laval, Quebec City, Quebec, Canada
- María Teresa Rodríguez-Hernández**, Centro de Investigación en Química Aplicada, Saltillo, Coahuila, México
- Antelmo R. Y. Ruiz-Martínez**, Centro de Investigación en Química Aplicada, Saltillo, Coahuila, México
- Enrique Saldívar-Guerra**, Centro de Investigación en Química Aplicada, Saltillo, Coahuila, México
- Isaac C. Sanchez**, Chemical Engineering Department, The University of Texas at Austin
- Antonio Sanchez-Solis**, Instituto de Investigaciones en Materiales, Universidad Nacional Autónoma de México, México D.F., México
- José L. Santiago-García**, Materials Unit, Membranes Laboratory, Centro de Investigación Científica de Yucatán, Mérida, Yucatán, México
- Gladys de los Santos-Villarreal**, Centro de Investigación en Química Aplicada, Saltillo, Coahuila, México
- José A. Silva-Guzmán**, Departamento de Madera, Celulosa y Papel, Universidad de Guadalajara, Las Agujas, Zapopan, Jalisco, México
- João B. P. Soares**, Department of Chemical Engineering, University of Waterloo, Waterloo, Ontario, Canada
- Saúl Sánchez-Valdes**, Centro de Investigación en Química Aplicada, Saltillo, México
- Luis F. Ramos-de Valle**, Centro de Investigación en Química Aplicada, Saltillo, México
- Marco A. Villalobos**, Cabot Corp., Billerica, MA, USA
- Francisco Villaseñor-Ortega**, Department of Biochemical Engineering, Instituto Tecnológico de Celaya, Celaya, Guanajuato, México
- Eduardo Vivaldo-Lima**, Departamento de Ingeniería Química, Facultad de Química, Universidad Nacional Autónoma de México, México, D.F., México

Roberto J. J. Williams, Institute of Materials Science and Technology (INTEMA), University of Mar del Plata and National Research Council (CONICET), Mar del Plata, Argentina

Iván Zapata-González, Facultad de Ciencias Químicas, Universidad Autónoma de Coahuila, Saltillo, Coahuila, México

Diana G. Zárate-Triviño, Centro de Investigación y de Estudios Avanzados (CINVESTAV) del IPN, Unidad Querétaro, Querétaro, Querétaro, México



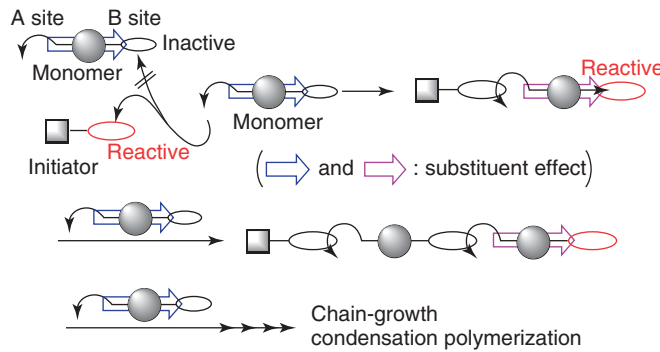


Figure 3.24 Scheme of chain-growth condensation polymerization. Source: Reprinted with permission from Yokoyama A, Yokozawa T. *Macromolecules* 2007;40:4093 [73]. Copyright 2007 American Chemical Society.

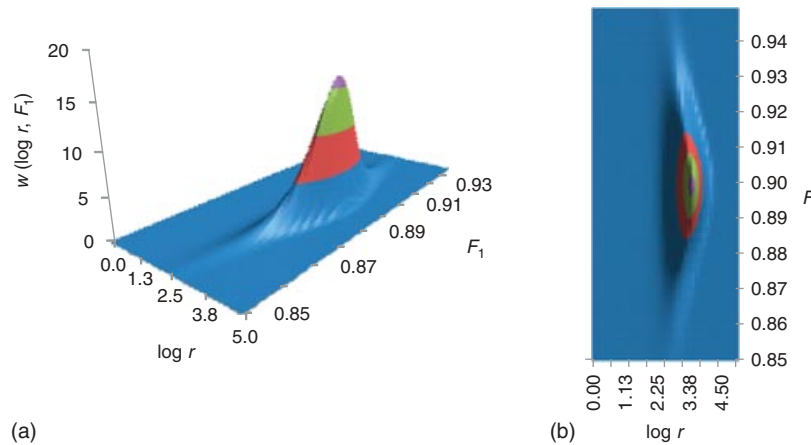


Figure 5.10 The Stockmayer distribution for a copolymer made with a single-site catalyst. (a) Three-dimensional plot, (b) Bird's eye view.

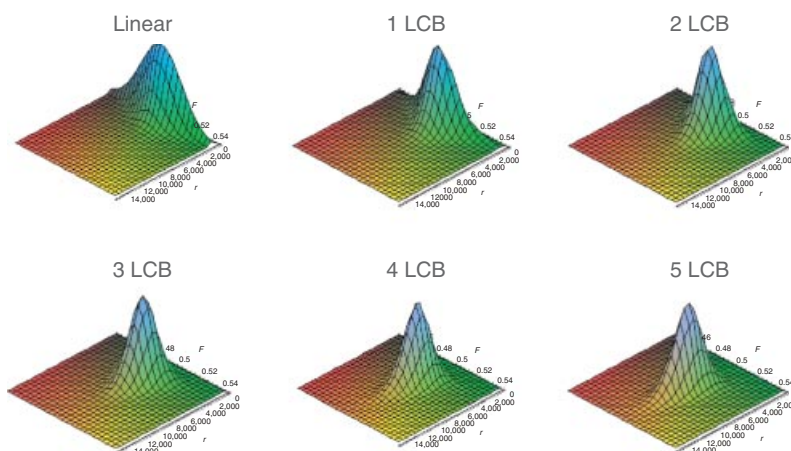


Figure 5.11 Trivariate distribution for a model polymer.

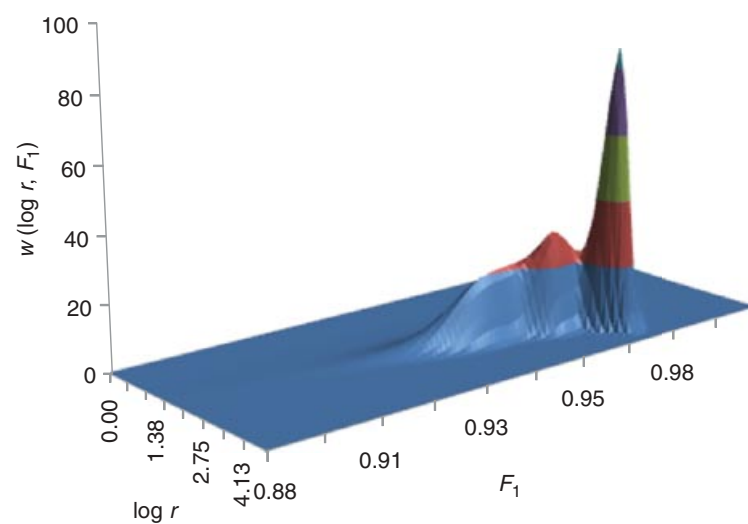


Figure 5.12 Simulated chain length and chemical composition distributions of a polymer made from a three-site catalyst.

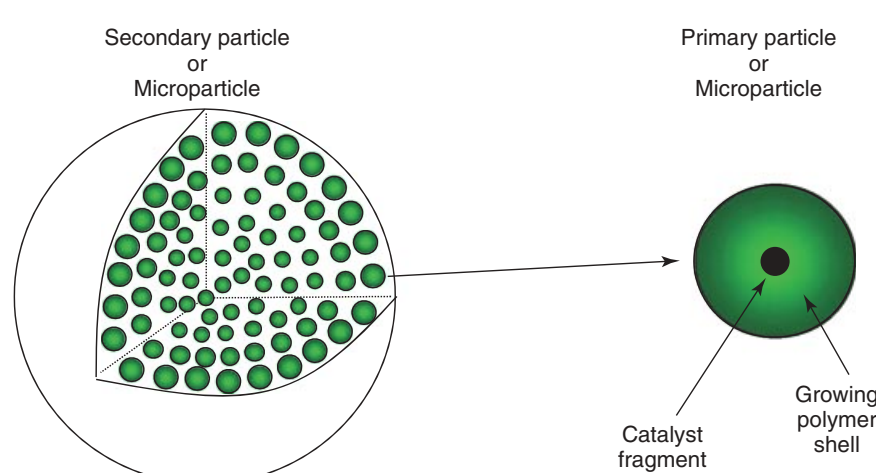


Figure 5.13 The multigrain model (MGM).

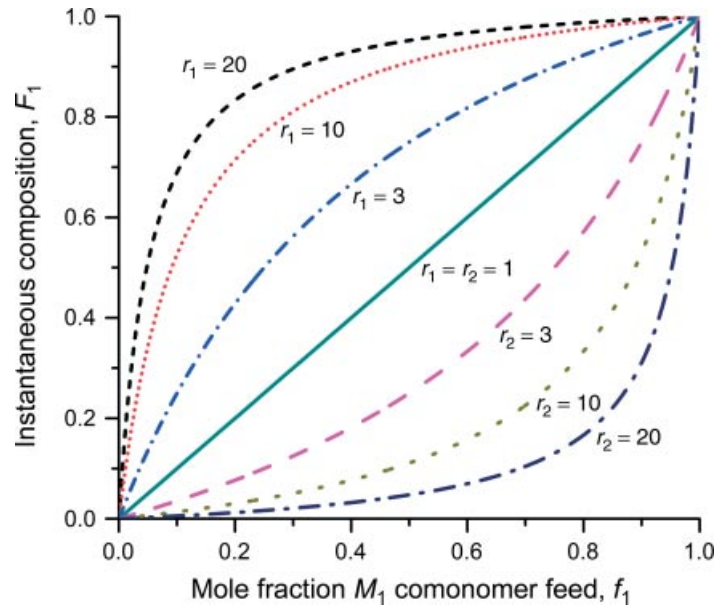


Figure 6.6 Dependence of instantaneous copolymer composition F_1 on initial comonomer feed composition f_1 in an ideal copolymer. The reactivity ratios satisfy $r_1 r_2 = 1$.

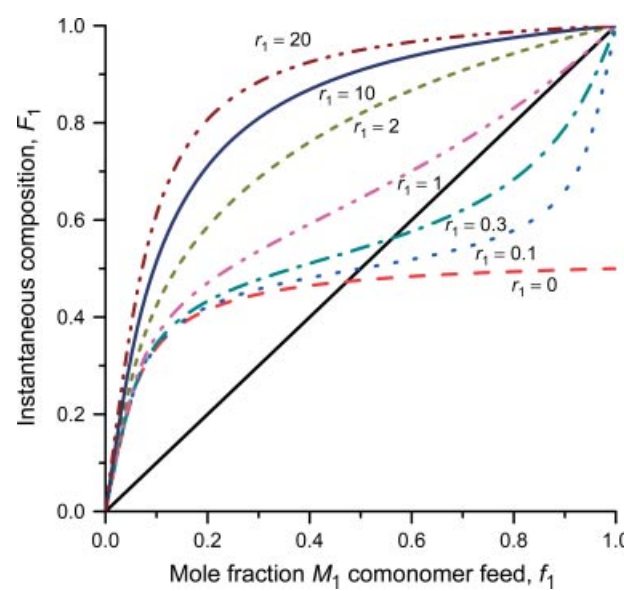


Figure 6.8 Dependence of instantaneous copolymer composition F_1 on initial comonomer feed composition f_1 for different values of r_1 ; $r_2 = 0.1$.

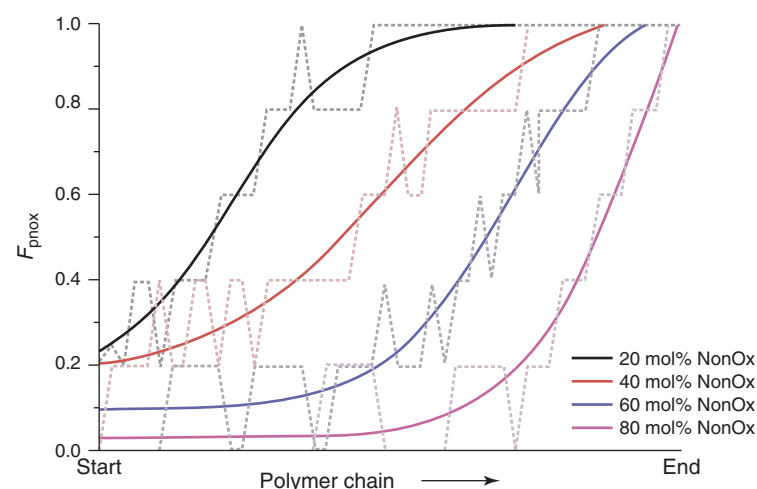


Figure 8.4 Monomer distribution along the polymer chain for statistical copolymers of 2-nonyl-2-oxazoline (NonOx) and 2-phenyl-2-oxazoline (PhOx). *Source:* Reprinted with permission Lambermont-Thijs HML, Jochems MJ, Hoogenboom R, Schubert US. *J Polym Sci A Polym Chem* 2009;47:6433 [176]. Copyright 2009 John Wiley and Sons, Inc.

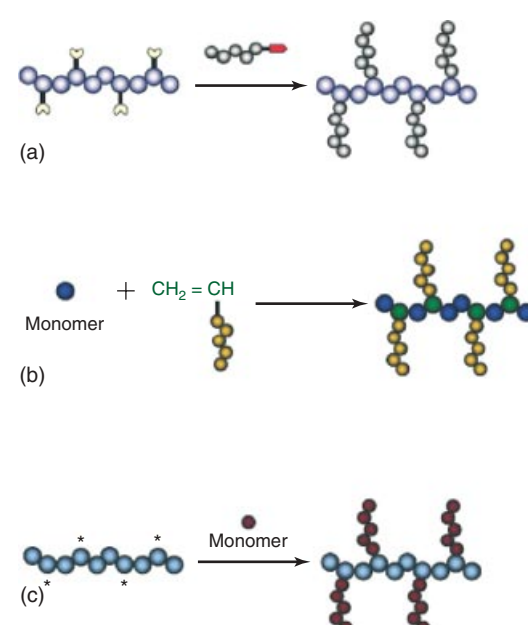


Figure 10.1 Schematic representation of (a) grafting-onto, (b) grafting-through, and (c) grafting-from methods.

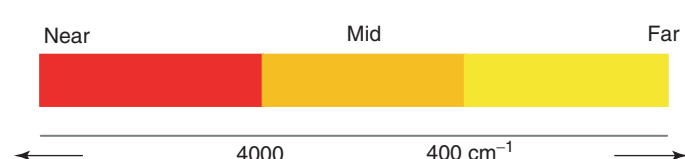


Figure 16.3 Regions for the study of IR: near, middle, and far.

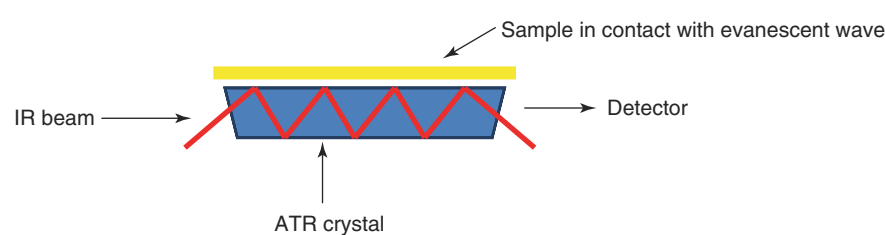


Figure 16.4 Mechanism of IR analysis by attenuated total reflectance.

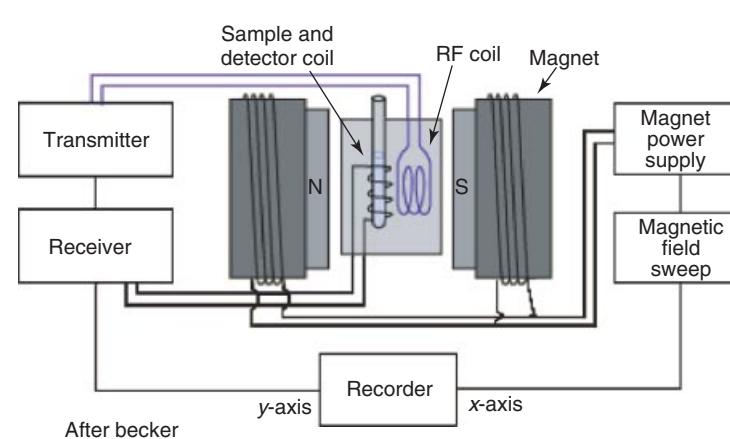


Figure 16.11 Diagram of an FT-NMR spectrometer.

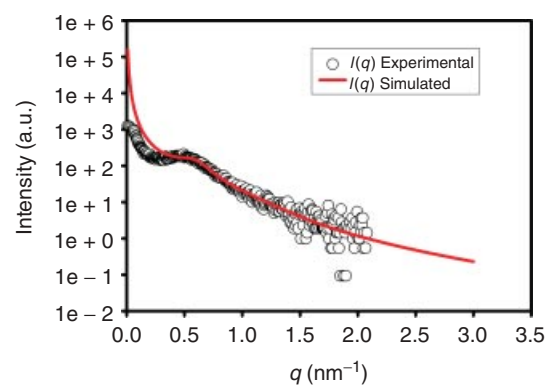


Figure 19.A.1 Intensity plot.

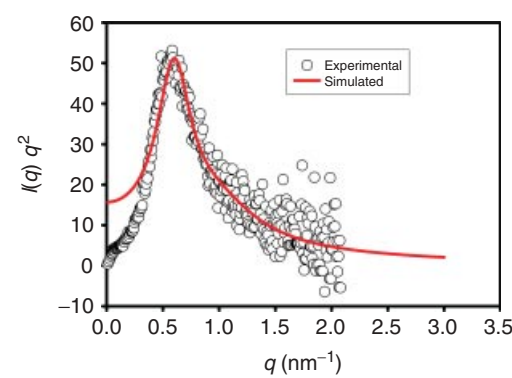


Figure 19.A.2 The Lorentz plot.

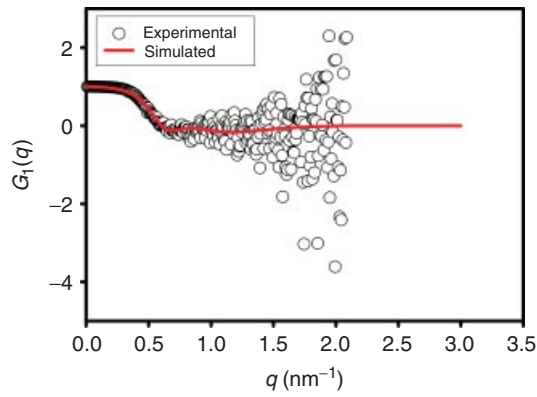


Figure 19.A.3 Interference function.

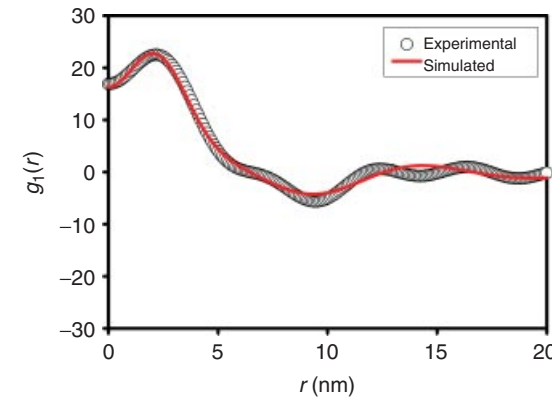


Figure 19.A.4 Interface distribution function.

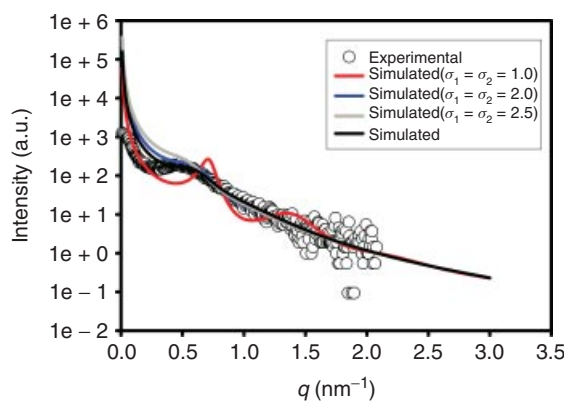


Figure 19.A.5 Statistical effect on the intensity plot.

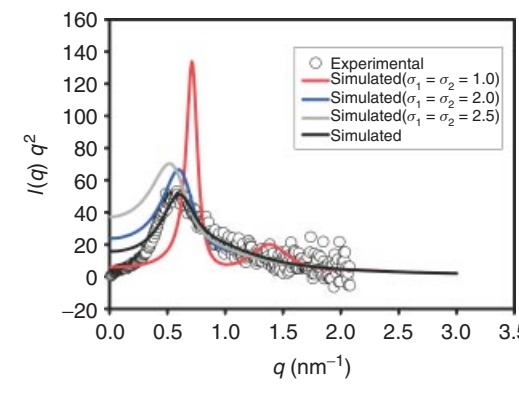


Figure 19.A.6 Statistical effect on the Lorentz plot.

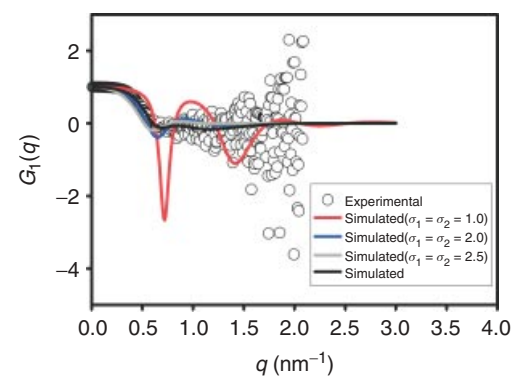


Figure 19.A.7 Statistical effect on the interference function.

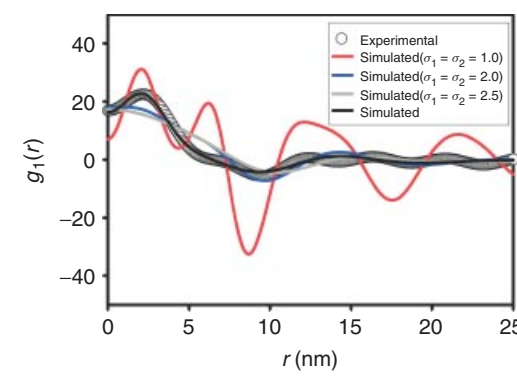


Figure 19.A.8 Statistical effect on the interface distribution function.

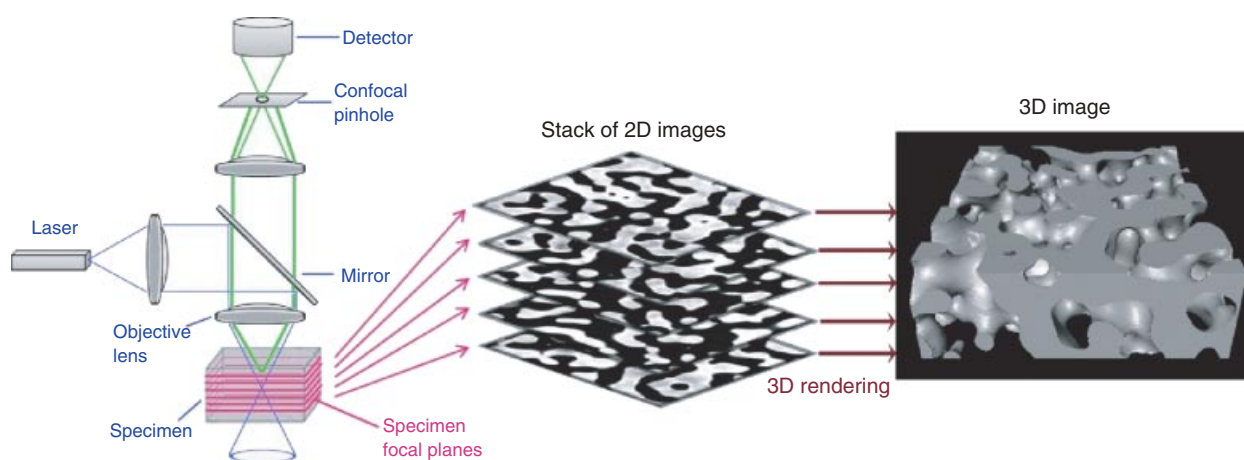


Figure 20.1 Schematic of LSCM. A stack of 2D images is recorded at different focal planes in the specimen and subsequently reconstructed in three dimensions using the marching cubes algorithm [136].

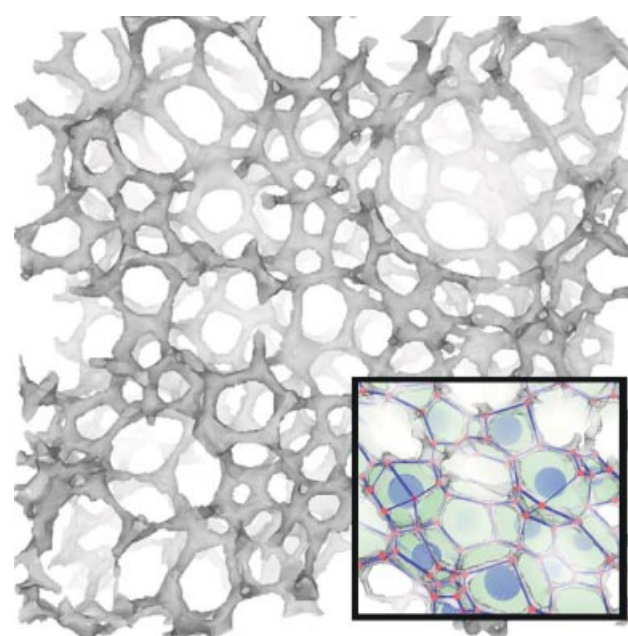


Figure 20.2 3D-rendered image of a polyurethane foam obtained via X-ray μ -CT. The black voxels within this image represent the locations of foam struts, while the white areas represent void space. The inset shows a close-up of the foam structure showing the correlation between the detected strut, vertex, and cell locations and the original foam volume. The large blue spheres in the image indicate the centers of detected foam cells. *Source:* Reprinted with permission from Journal of Colloid and Interface Science, Vol. 280, M.D. Montminy, A.R. Tannenbaum, C.W. Macosko, The 3D structure of real polymer foams, Journal of Colloid and Interface Science 2004, 280, pages 202–211 [152]. Copyright 2004 Elsevier.

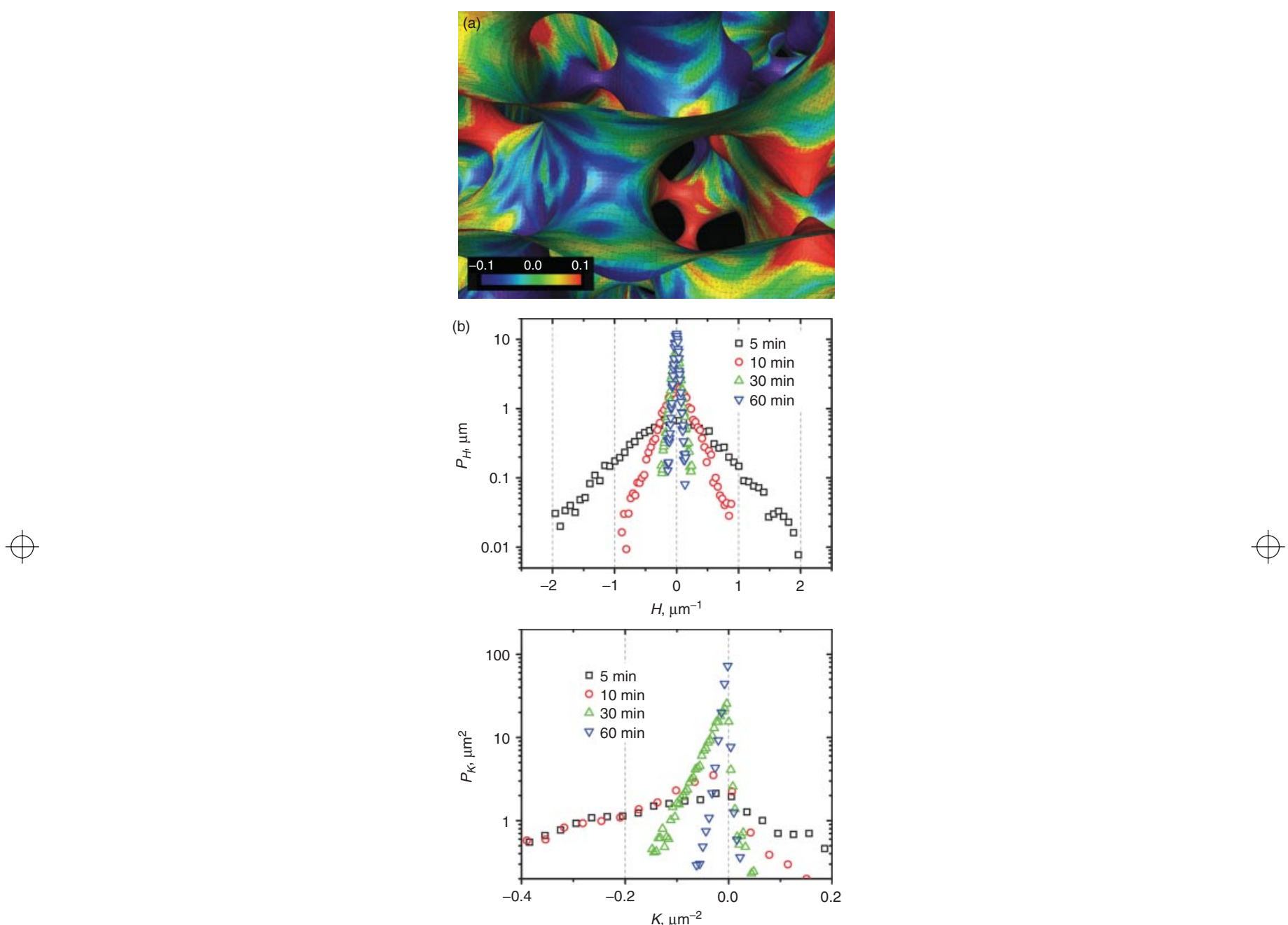


Figure 20.4 (a) 3D-rendered interface of 50/50 PS/SAN cocontinuous blend. The color in each triangle represents the value of the mean curvature given by the color bar scale. *Source:* Reproduced with permission from López-Barrón C, Macosko CW. A new model for the coarsening of cocontinuous morphologies. *Soft Matter* 2010;6:2637–2647 [149]. Copyright 2010 The Royal Society of Chemistry. (b) Probability densities of the mean and the Gaussian curvatures of the 50/50 PS/SAN interface at different annealing times. *Source:* Reprinted with permission from Lopez-Barron C, Macosko CW. Characterizing interface shape evolution in immiscible polymer blends via 3D image analysis. *Langmuir* 2009;25:9392–9404 [148]. Copyright 2009 American Chemical Society.

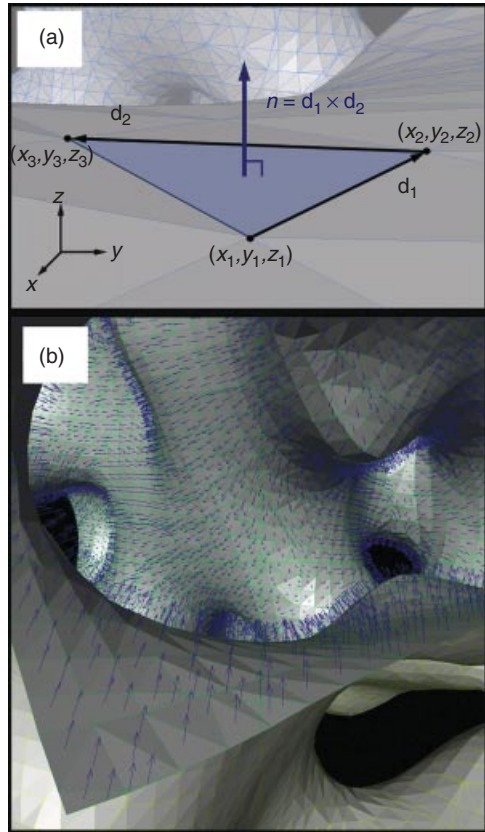


Figure 20.6 (a) Schematic of the computation of the vector normal to a triangle. (b) Detail of the normal vector field generated with the LCPM on a cocontinuous interface. *Source:* Reprinted with permission from López-Barrón CR, Macosko CW. Direct measurement of interface anisotropy of bicontinuous structures via 3D image analysis. *Langmuir* 2010;26 (17):14284–14293 [150]. Copyright 2010 American Chemical Society.

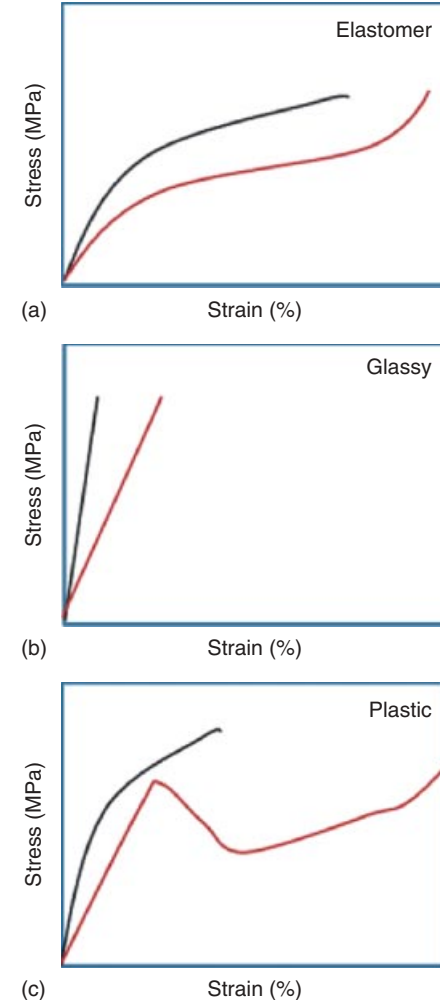


Figure 21.4 Typical stress-strain curves for different types of polymers: (a) elastomer, (b) glassy, and (c) plastic.

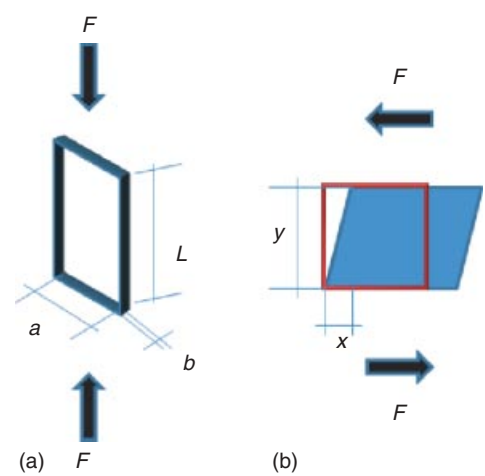


Figure 21.3 Common force fields for applied forces in a material (a) tension and (b) shear.

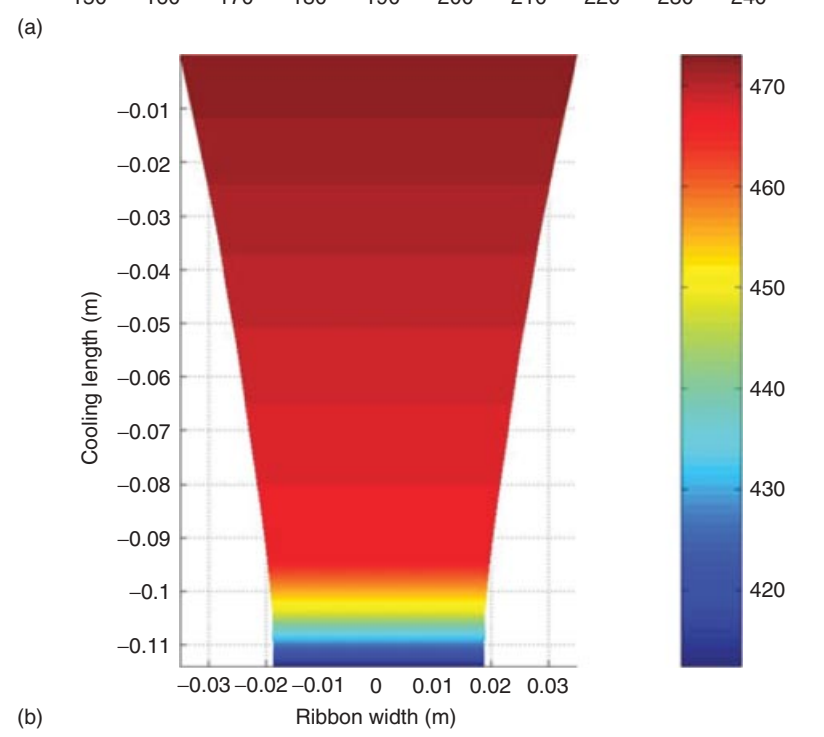
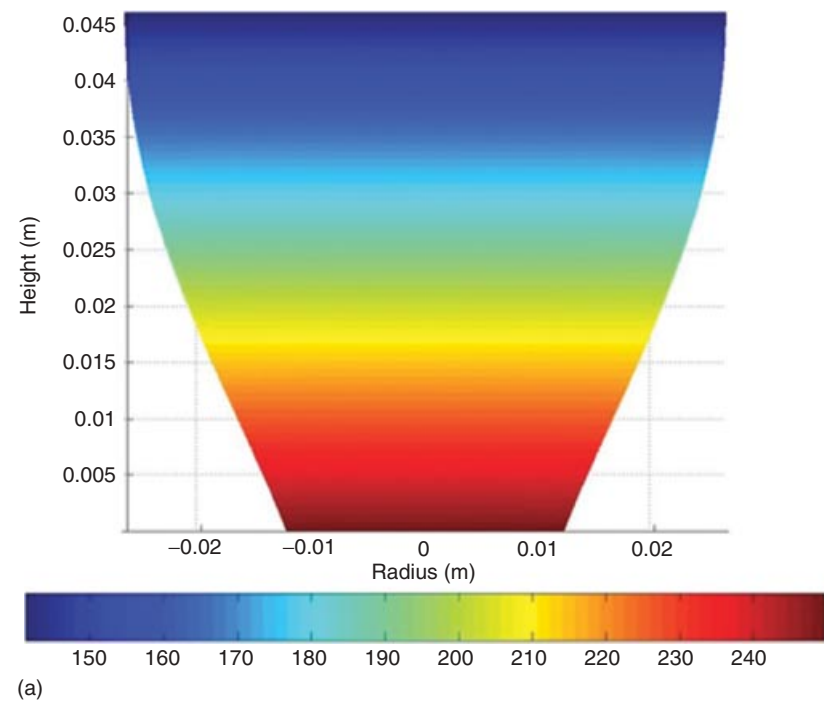


Figure 24.3 Simulated (a) bubble radius, (b) ribbon width, and temperature profiles.

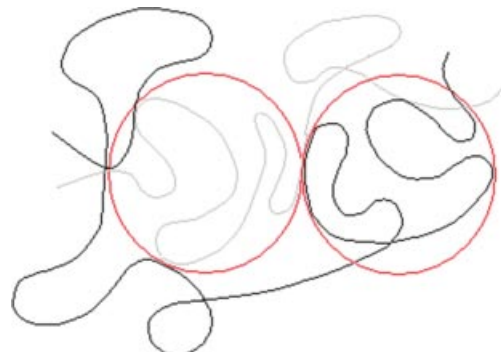


Figure 25.6 Representation of blobs in a polymer chain.

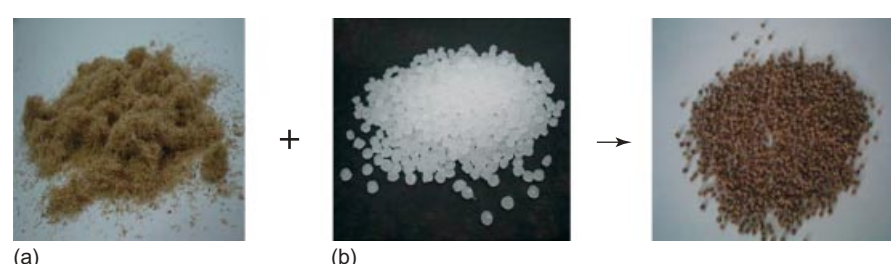


Figure 26.1 Typical composite components: (a) fiber, (b) polymer and additives.

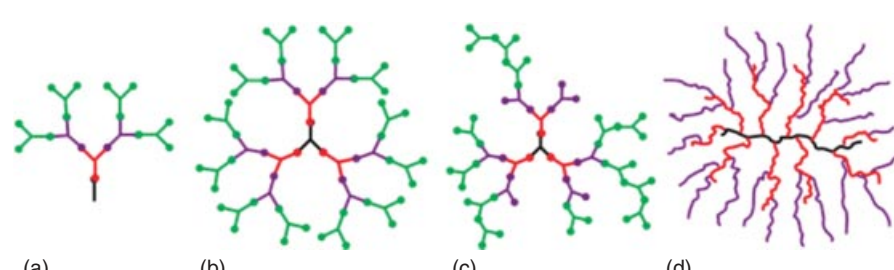


Figure 30.1 Structure of four types of dendritic polymers: (a) dendron, (b) dendrimer, (c) hyperbranched polymer, and (d) dendrigraft polymer.

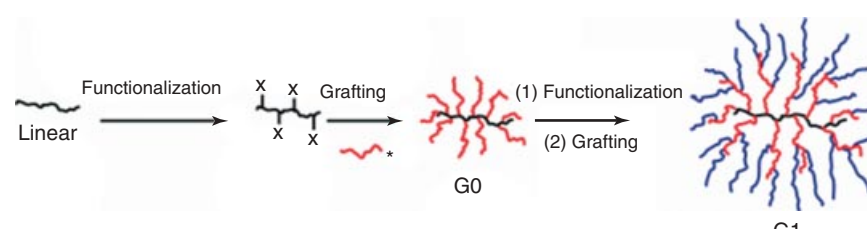


Figure 30.9 Schematic representation of the generation-based synthesis of dendrigraft polymers by a divergent *grafting-onto* method.

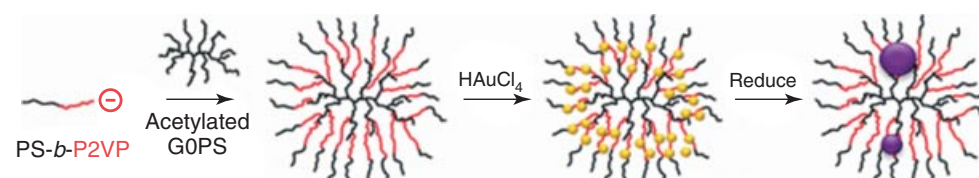
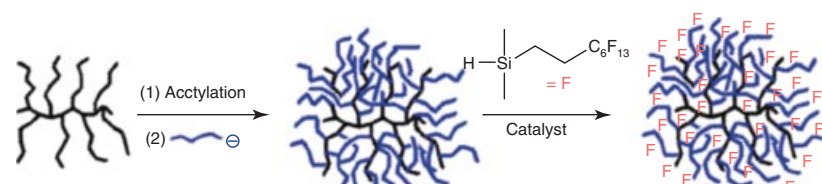


Figure 30.11 Synthesis of an arborescent copolymer, G0PS-*g*-(P2VP-*b*-PS), its application to templating HAuCl₄ deposition, and reduction to gold nanoparticles.



Scheme 30.19 Synthesis of G0PS-*g*-PIP copolymer followed by hydrosilation with a fluorohydrosilane for use as a processing aid. *Source:* Reproduced with permission from Gauthier M, Lin W-Y, Teertstra SJ, Tzoganakis C. Polymer 2010;51:3123 [121]. Copyright 2010 Elsevier.

PART I

BASIC CONCEPTS





1

INTRODUCTION TO POLYMERS AND POLYMER TYPES

ENRIQUE SALDÍVAR-GUERRA AND EDUARDO VIVALDO-LIMA

1.1 INTRODUCTION TO POLYMERS

1.1.1 Basic Concepts

Polymers are very large molecules, or macromolecules, formed by the union of many smaller molecules. These smaller units are termed *monomers* before they are converted into polymers. In fact, the word “polymer” has a Greek origin meaning “many members.” Natural polymers have been around since the early times in Planet Earth. Life itself is linked to polymers since deoxyribonucleic acid (DNA), ribonucleic acid (RNA), and proteins, which are essential to all known forms of life, are macromolecules. Cellulose, lignin, starch, and natural rubber are just a few other examples of natural polymers. Some of these polymers were used by early human civilizations to produce simple artifacts; for example, the play balls from natural rubber for the ball game of several of the Mesoamerican civilizations (which contained ritual content and not only entertaining purposes). In the 1800s, natural polymers began to be chemically modified to produce many materials, such as vulcanized rubber, gun cotton, and celluloid. Although natural polymers are very important, this book is mainly concerned with synthetic polymers, especially organic synthetic polymers. The chemical reaction by which polymers are synthesized from monomers is termed *polymerization*; however, this is a generic term, since there are a number of chemical mechanisms involved in different polymerization reactions.

Synthetic polymers are relatively modern materials, since they entered into the technological and practical scene only in the first decades of the twentieth century. This makes them very different from some other materials that have been known to humanity for centuries or millennia.

Also, given the fact that synthetic polymers are created by chemical reactions, the possibilities of building different polymers are virtually endless, only restricted by chemical and thermodynamic laws and by the creativity of the synthetic polymer chemist. These endless possibilities have given rise to an enormous variety of synthetic polymers that find application in almost every conceivable field of human activity that deals with matter or physical objects. In addition, the enormous molecular structural versatility that is derived from the rich synthetic possibilities, translates into materials with extremely diverse properties, and therefore applications.

We can find polymers as components of many of the objects that surround us, as well as in a broad diversity of applications in daily life: clothing, shoes, personal care products, furniture, electrical and electronic appliances, packaging, utensils, automobile parts, coatings, paints, adhesives, tires, and so on. The list is endless, and these few examples should provide an idea of the importance of synthetic polymers to modern society, in terms of both their usefulness and the economic value that they represent.

1.1.2 History

Some synthetic polymers were inadvertently prepared since the mid-nineteenth century by chemists working in organic synthesis without necessarily knowing the chemical structure of these materials, although some of them may have had some intuition of the right character of these molecules as very large ones [1]. Only in 1920, Staudinger [2] proposed the concept of polymers as macromolecules, and this idea slowly gained acceptance among the scientific community during the next decade. Some of the supporting

4 INTRODUCTION TO POLYMERS AND POLYMER TYPES

evidence for the macromolecular concept came from measurements of high molecular weight molecules in rubber using physicochemical methods. Later, around 1929, Carothers [3] started an experimental program aimed at the synthesis of polymers of defined structures using well-known reactions of organic chemistry; this work, together with the confirmation of high molecular weight molecules by other experimental measurements (e.g., the viscosity of polymer solutions), helped to confirm the correctness of the macromolecular hypothesis of Staudinger. An interesting book on the history of polymer science is that by Morawetz [4].

1.1.3 Mechanical and Rheological Properties

1.1.3.1 Mechanical Properties Long chains with high molecular weights impart unique properties to polymers as materials. This can be illustrated by analyzing the change in the properties of the homologous series of the simplest hydrocarbon chains, the alkanes, which can be seen as constituted of ethylene repeating units (with methyl groups at the chain ends),¹ as the number of repeating units increase. At relatively low molecular weights (C_6-C_{10}), compounds in these series are relatively volatile liquids (gasolines). As the number of ethylene units increases, the compounds in this series start to behave as waxes with low melting points. However, if the number of ethylene units exceeds some 200–300, such that the molecular weight of the chains is in the order of 5000–8000, the material starts to behave as a solid exhibiting the higher mechanical properties associated with a polymer (polyethylene in this case). In general, above some minimum molecular weight, polymers exhibit increased mechanical properties and they are considered “high polymers”, alluding to their high molecular weight.

The mechanical behavior of a polymer is characterized by stress–strain curves in which the stress (force per unit area) needed to stretch the material to a certain elongation is plotted. In order to experimentally generate these curves, a tension stress is applied on a polymer sample of known dimensions, which is elongated until it breaks. The elongation is expressed as a fractional or percentage increase of the original length of the sample, which is denominated strain, ε , and is defined as

$$\varepsilon = \frac{\Delta L}{L} \quad (1.1)$$

where L is the original length of the sample and ΔL is the increase in length under the applied tension. The nature of the stress–strain curve for a given polymer defines its

¹Strictly speaking, this is valid only for alkanes with a pair number of carbon atoms starting from butane, since ethylene has 2 C; however, this precision is irrelevant for this discussion (especially at high number of carbons).

possible use as elastomer, fiber, or thermoplastic. Figure 1.1 shows the form of the stress–strain curves for these types of polymers, and Table 1.1 shows typical values of some of the mechanical properties that can be defined as a function of the stress–strain behavior.

The elastic or Young’s modulus is the initial slope of the stress–strain curve and gives a measure of the resistance to deformation of the material. The ultimate tensile strength is the stress required to rupture the sample, and the ultimate elongation is the extent of elongation at which the rupture of the sample occurs.

Mechanical properties are discussed here only in an introductory manner in order to understand the main applications of polymers. An extended discussion of the mechanical properties of polymers and their measurement can be found in Chapter 21.

1.1.3.2 Rheological Properties Thermoplastics are processed and shaped in the molten state. This can be loosely defined as a state in which a polymer flows under the action of heat and pressure. Molten polymers are non-Newtonian fluids, as opposed to the simpler Newtonian fluids. In the latter, the stress σ (force per unit area) is proportional to the shear rate $\dot{\gamma}$ (velocity per unit length) with a proportionality factor μ (viscosity) which is constant at a given temperature. Newtonian fluids follow the law

$$\sigma = \mu \dot{\gamma} \quad (1.2)$$

On the other hand, in a non-Newtonian fluid, the viscosity depends on the shear rate. Besides showing very high non-Newtonian viscosities, polymers exhibit a complex viscoelastic flow behavior, that is, their flow exhibits “memory”, as it includes an elastic component in addition to the purely viscous flow. Rheological properties are those that define the flow behavior, such as the viscosity and the melt elasticity, and they determine how easy or difficult is to process these materials, as well as the performance of the polymer in some applications. The rheology of the polymers and its effect on the processing of these materials are studied in Chapters 22 and 23.

1.1.4 Polymer States

There are several scales at which polymers can be observed. The repeating unit in a polymeric chain lies in the scale of a few angstroms, while a single polymer molecule or chain has characteristic lengths of a few to some tens of nanometers (considering the contour length of a chain). At the next scale, or mesoscale, clusters of chains can be observed. This scale is rather important since it defines the polymer morphology based on the order or disorder exhibited by the chains. Ordered regions are termed *crystalline* and disordered ones *amorphous*. In the crystalline regions, the polymer chains are packed in regular arrays termed

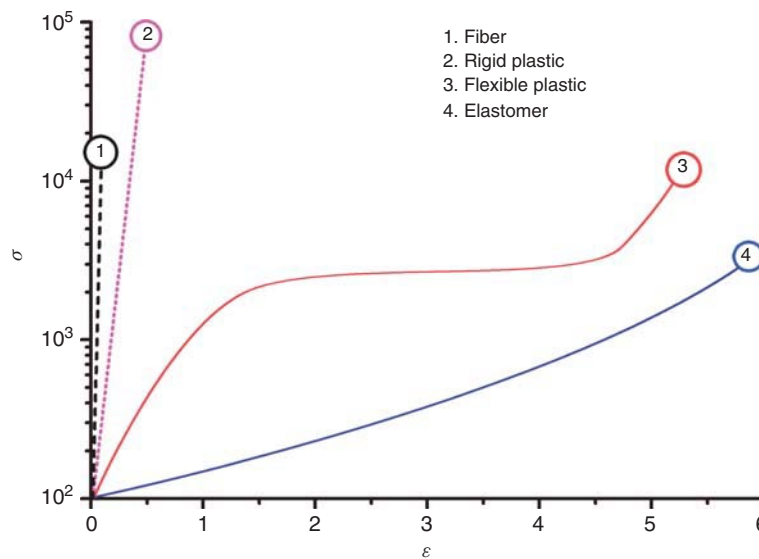


Figure 1.1 Schematic stress–strain curves for different types of polymers.

TABLE 1.1 Typical Values of Mechanical Properties for Different Polymer Types

Type of Polymer (use)	Modulus (N/m ²)	Typical Elongations (Strain %)	Examples
Elastomers	<2 × 10 ⁶	400–1000	Polybutadiene, polyisoprene, butyl rubber
Fibers	>2 × 10 ⁹	100–150	Nylon (polyamide), polypropylene
Flexible thermoplastics	0.15–3.5 × 10 ⁹	20–800	Polyethylene
Rigid thermoplastics	0.7–3.5 × 10 ⁹	0.5–10	Polystyrene, PMMA, phenol-formaldehyde resins

Abbreviation: PMMA, Poly(methyl methacrylate).

crystallites. Crystalline morphology is favored by structural regularity in the polymer chain and by strong intermolecular forces, as well as by some chain flexibility. Usually, in a crystalline polymer, both ordered and disordered regions are found; thus, the so-called crystalline polymers are actually semicrystalline. Examples of highly crystalline polymers are polyethylene and polyamides. On the other hand, completely amorphous polymers that owe their disordered morphology to bulky substituents and rigid chains are common, atactic polystyrene and poly methyl methacrylate being good examples of this category.

There are two important thermal properties that define the state of a polymer; these are the glass-transition temperature or T_g and the melting temperature, T_m . Below the glass-transition temperature, the amorphous regions of a polymer are in a glassy state showing practically no chain motions (at least in a practical time scale). Above the T_g , the polymer behaves as a viscous liquid reflecting motions of the polymer chains or chain segments. Also, at the T_g , many of the physicochemical properties of the polymer change in a relatively abrupt way (Fig. 1.2). The T_g can be defined in more precise thermodynamic terms, but this is further discussed in Chapter 2.

On the other hand, the T_m is a property exhibited by the crystalline regions of a polymer and is the temperature

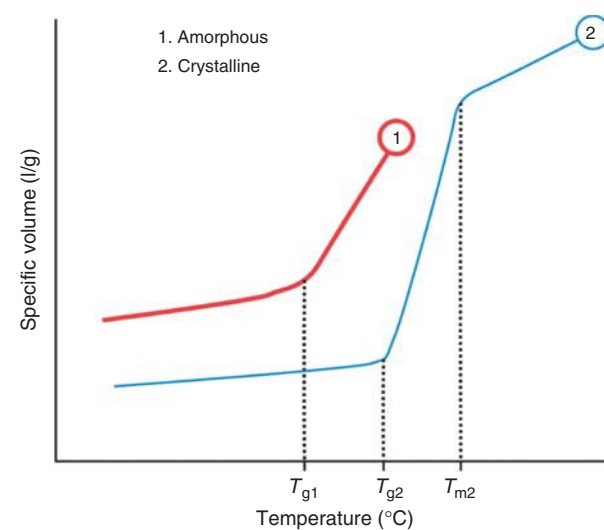


Figure 1.2 Schematic representation of the main thermal transitions in polymers in a plot of specific volume–temperature.

above which the crystalline regions melt and become disordered or amorphous. Since, for a given polymer $T_m > T_g$, above the melting point, the polymer will flow as a viscous liquid. Amorphous polymers exhibit only a T_g , while semicrystalline polymers exhibit both, a T_g and a T_m .

1.1.5 Molecular Weight

Compounds made of small molecules exhibit a unique well-defined molecular weight; on the other hand, polymers exhibit a distribution of molecular weights since not all the polymer chains of a given sample will have the same molecular weight or chain length. Therefore, in order to characterize a given polymer sample, it is necessary to either describe the full molecular weight distribution (MWD) or some average quantities related to the distribution. Also, the MWD can be plotted in different ways using either length or weight for the abscissa and, for example, number average or weight average for the ordinate; the classical paper of Ray [5] shows different representations of the MWD. Two of the most common averages are the number average and weight average molecular weights, \bar{M}_n and \bar{M}_w , respectively, which are defined as

$$\bar{M}_n = \sum_x f_x^n M_x \quad (1.3)$$

$$\bar{M}_w = \sum_x f_x^w M_x \quad (1.4)$$

where f_x^n is the number fraction of chains having x monomer units and M_x is the molecular weight of a chain having x monomer units. Also,

$$M_x = x M_0 \quad (1.5)$$

with M_0 being the molecular weight of the monomer unit. f_x^w is the weight fraction of chains having x monomer units. In these definitions, and assuming long chains, the contribution of any initiator fragment at the end of a chain has been neglected. In mathematical terms, the number and weight fractions are defined as follows:

$$f_x^n = \frac{N_x}{\sum_x N_x} \quad (1.6)$$

$$f_x^w = \frac{x N_x}{\sum_x x N_x} \quad (1.7)$$

where N_x is the number of chains having x monomer units. Also note that

$$f_x^w = \frac{x N_x}{\sum_x x N_x} = \frac{x f_x^n}{\sum_x x f_x^n} \quad (1.8)$$

Other related quantities that are frequently used are the number average chain length (NACL) and the weight average chain length (WACL); also represented as \bar{r}_n and \bar{r}_w , respectively, in some texts. The NACL is also simply

termed the *degree of polymerization* or DP_n . They are simply related to \bar{M}_n and \bar{M}_w by the following equations:

$$\text{NACL} = \frac{\bar{M}_n}{M_0} \quad (1.9)$$

$$\text{WACL} = \frac{\bar{M}_w}{M_0} \quad (1.10)$$

Instead of giving average based on the weight of the repeating unit, these two quantities are based on the number of repeating units.

1.1.5.1 Moments of the Molecular Weight Distribution

Since the molecular weight is a distributed quantity, the concepts and properties of statistical distributions can be applied to the MWD. A statistical definition that is particularly useful is that of moment of a distribution. In statistics, the S th moment of the discrete distribution² f of a discrete random variable y_i is defined as

$$\mu_S = \sum_{i=1}^{\infty} y_i^S f(y_i), \quad S = 0, 1, 2, \dots \quad (1.11)$$

A graphical representation of the discrete distribution $f(y_i)$ is shown in Figure 1.3a. Figure 1.3b shows the analogous MWD represented as the (number) distribution f_x^n of the discrete variable M_x (notice the equivalence of the concept of distribution with those of fraction or frequency).

Equivalently, the S th moment of the MWD can be defined as

$$\mu_S = \sum_{x=1}^{\infty} M_x^S f_x^n, \quad S = 0, 1, 2, \dots \quad (1.12)$$

Now, the average molecular weights of the MWD can be more simply defined in terms of the moments (Eq. 1.12).

The number average molecular weight is simply

$$\overline{M}_n = \frac{\mu_1}{\mu_0} \quad (1.13)$$

since

$$\frac{\mu_1}{\mu_0} = \frac{\sum_{x=1}^{\infty} M_x f_x^n}{\sum_{x=1}^{\infty} f_x^n} = \frac{\overline{M}_n}{1} \quad (1.14)$$

²Notice that here we use the concept of distribution in a non-rigorous statistical sense. In rigorous statistical terms “distribution” usually alludes to the cumulative distribution function. Here, as in common language, by “distribution” we mean what in rigorous statistical terms is denoted as “density function” or “probability function”.

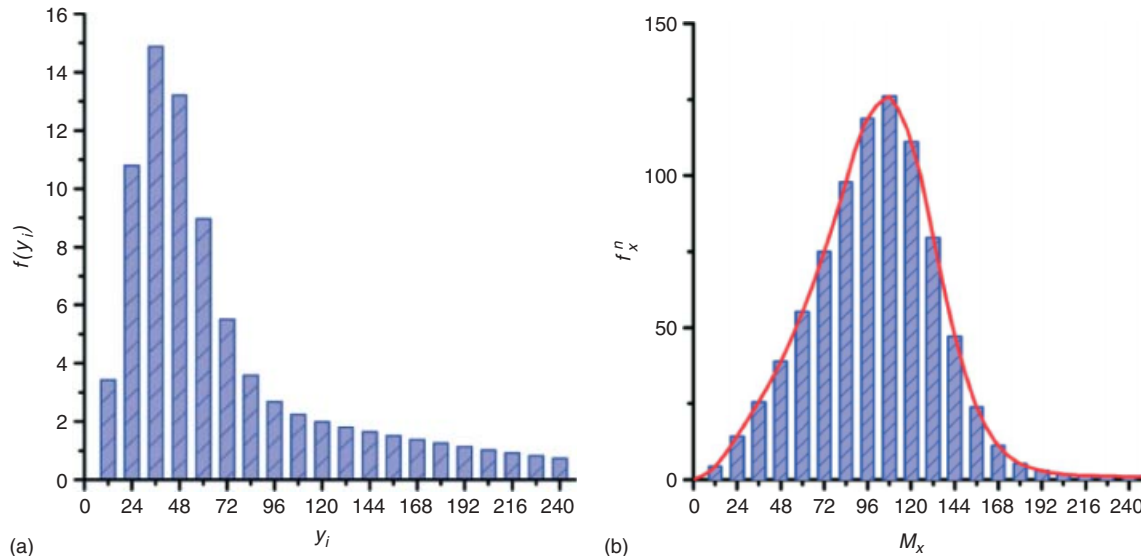


Figure 1.3 (a) A statistical discrete distribution (density) function f of the discrete random variable y_i . (b) Example of a discrete molecular weight distribution of a polymer represented as the number distribution f_x^n (or number fraction) of the discrete variable M_x .

Notice also that an equivalent physical definition of \overline{M}_n is

$$\overline{M}_n = \frac{\text{Polymer mass}}{\text{Polymer moles}} = \sum_x f_x^n M_x = \frac{\sum_x N_x M_x}{\sum_x N_x} \quad (1.15)$$

where the two right-most equalities come from application of Equations (1.3) and (1.6), respectively.

It is also possible to demonstrate (by application of equations (1.12), (1.5), (1.8), and (1.4) in that order) that

$$\overline{M}_w = \frac{\mu_2}{\mu_1} \quad (1.16)$$

Averages based on higher order moments are also used, for example,

$$\overline{M}_z = \frac{\mu_3}{\mu_2}; \quad \overline{M}_{z+1} = \frac{\mu_4}{\mu_3} \quad (1.17)$$

It should be emphasized that the discrete variable used here is M_x . In some textbooks and research papers, the moments of the MWD are defined in terms of the chain length distribution (CLD) (with chain length, x , being the discrete variable), which means that, in that case, the corresponding averages of the MWD defined in equations analogous to Equations (1.13), (1.16), and (1.17) need to be multiplied by M_0 .

A special average that can be estimated by measurements of the polymer solution intrinsic viscosity is the viscosimetric average molecular weight, which in terms of moments

is defined as

$$\overline{M}_v = \left(\frac{\mu_{\alpha+1}}{\mu_1} \right)^{1/\alpha} \quad (1.18)$$

where α is the exponent in the Mark-Houwink-Sakurada expression:

$$[\eta] = K \overline{M}_v^\alpha \quad (1.19)$$

in which $[\eta]$ is the intrinsic viscosity of a polymer solution and K and α are constants at a given temperature and for a given pair polymer–solvent [6].

Finally, the polydispersity index or molecular weight dispersity³ \mathcal{D} is defined as

$$\mathcal{D} = \frac{\overline{M}_w}{\overline{M}_n} \quad (1.20)$$

and it is a measure of the broadness of the MWD. It can be demonstrated that \mathcal{D} is related to the variance of the MWD by the following expression:

$$\sigma_{M_x}^2 = M_n^2 (\mathcal{D} - 1) \quad (1.21)$$

1.1.6 Main Types and Uses

In Section 1.2, we review in more detail the different criteria for the classification of polymers; however, at this point, it is convenient to describe some of the main types of polymers according to their use. On the basis of this, they

³The term “dispersity” instead of “polydispersity index” is now recommended by the IUPAC [7].

8 INTRODUCTION TO POLYMERS AND POLYMER TYPES

can be identified as plastics, thermosets, elastomers, fibers, paints, and coatings. These uses naturally derive from some of the thermodynamic and mechanical properties of the polymers, which were briefly described in Sections 1.1.3 and 1.1.4.

Plastics or *thermoplastics* are materials that can be shaped under heating. Once they are heated above certain temperature these materials flow as very viscous liquids and can adopt the shape of a mold; once they are cooled down again, they keep the new molded shape. In general terms, this process of heating and molding can be repeated a number of times; however, after some reprocessing of this sort, the polymeric chains can break or undergo reactions leading to reduced physical properties, a fact that sets practical limits to the recyclability of thermoplastics. Some of the most important thermoplastics by volume are polyethylene (low density polyethylene (LDPE) and high density polyethylene (HDPE)), polypropylene (PP), poly(vinyl chloride) (PVC) and polystyrene (PS or PSt), to name a few. Thermoplastics are synthesized in large amounts in polymerization plants and are then transformed by other users in processing equipment to form objects useful in packaging or as utensils, for example.

Thermosets, on the other hand, are polymers formed by the mixing and chemical reaction of fluid precursors into a mold; once the precursors react, a crosslinked network that cannot flow anymore under heating is created; therefore, reaction and molding into the final shape usually take place at the same time (by the RIM or reaction injection molding process). Examples of common thermosets are some polyesters, phenol-formaldehyde resins, epoxy resins, and polyurethanes, among others. Chapter 28 of this handbook elaborates on this topic.

Elastomers or *rubbers* are flexible materials that are mainly used in tires, hoses, and seals; as adhesives; or as impact modifiers of thermoplastics. They exhibit high resistance to impact, even at low temperatures at which materials increase their rigidity. For some of the applications (e.g., tires or hoses), these materials have to be slightly crosslinked once they are formed into the desired shape in order to impart them dimensional stability, since otherwise they tend to slowly flow. Elastomers are polymers that are used above their glass-transition temperature (T_g). Some examples of common elastomers are polybutadiene, which is used as an impact modifier of rigid plastics; SBR (copolymer of styrene and butadiene), mainly used in tires; EPDM (copolymer of ethylene, propylene, and a diene monomer, usually norbornene); NBR (copolymer of acrylonitrile and butadiene); and so on.

Fibers are polymers with very high moduli and very high resistance to deformation; therefore, they elongate very little. Some examples of polymers used as fibers are nylon (polyamide), polyesters, and polyacrylonitrile (acrylic fiber).

Paints and coatings are based on polymers that can form a film. The polymer is considered the binder or vehicle that carries the pigments and additives that are used to impart color or protect the surface of the substrates on which the paint or coating is applied. Some examples of polymers used as paint base are copolymers of styrene–butyl acrylate or of acrylic monomer–vinyl acetate. In the product, the polymer is either finely dispersed in water forming a latex or dissolved in a solvent (in oil-based paints). Latexes for paints are usually produced by emulsion polymerization (Chapter 14).

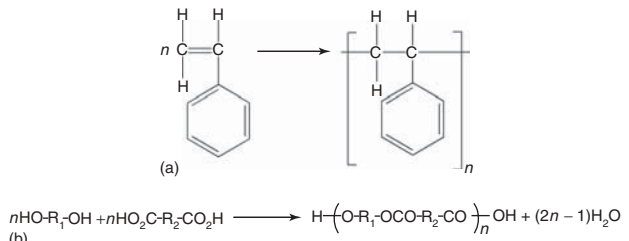
1.2 CLASSIFICATION OF POLYMERS

Given the versatility of polymers, they can be classified according to different criteria. In this section, we review some of these classifications.

1.2.1 Classification Based on Structure

This is one of the oldest and most important classification criteria originally proposed by Carothers [3] in 1929 and the one that splits polymers into two major types: addition and condensation polymers. The basis for the distinction is better understood by illustration with two examples belonging each one to one category: polystyrene as an addition polymer and a polyester as a condensation polymer. They are produced by the reactions shown in Scheme 1.1.

In both the cases, the structure shown in parenthesis or brackets in the main product of the reaction is called *repeating unit*. In an addition polymer, the repeating unit has the same composition as that of the monomer; the only difference is the change of chemical bonds with respect to those of the monomer. On the other hand, in a condensation polymer, according to the original idea of Carothers, some atoms of the monomer are lost as a condensation compound when the monomers react to form the repeating unit of the polymer. Some years after the original Carothers classification, it became clear that some polymers, for example, polyurethane, which is synthesized by the reaction between a diol and a diisocyanate, would not generate any condensation molecule, so they could not be classified as a condensation polymer; still their chemistry and structure had much more in common with those of condensation polymers than with those of addition polymers; therefore, the criterion for classification of a polymer as one of condensation type was changed to include this type of cases. The modern accepted criterion determines that a condensation polymer is that which satisfies any of the following conditions: (i) some atoms of the monomer are lost as a small molecule during their synthesis or (ii) they contain functional groups as part of the main polymer



Scheme 1.1 Examples of the synthesis reactions of (a) an addition polymer, polystyrene and (b) a condensation polymer, generic polyester with R_1 and R_2 being aliphatic or aromatic groups.

chain, such as ester, urethane, amide, or ether. If a polymer does not satisfy any of these criteria then it is an addition polymer.⁴ This issue is further discussed in Odian [8].

1.2.2 Classification Based on Mechanism

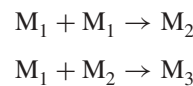
A second major classification of polymers was proposed by Flory [1] in 1953. This is based on the kinetic mechanism of the polymerization reaction. Flory classifies polymerizations into two categories:

1. Step-growth polymerization;
2. Chain polymerization.

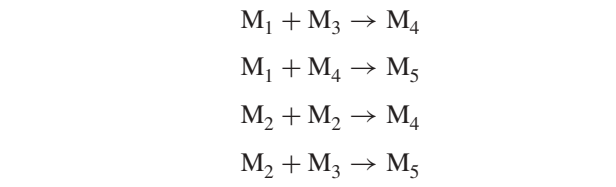
1.2.2.1 Step-growth Polymerization The simplest scheme of this polymerization involves the reaction of a difunctional monomer AB, which contains both functional groups A and B in the molecule. For example, A can be an amine and B a carboxylic acid group. Another scheme involves the reaction between two difunctional monomers of the type AA and BB. In any case, each polymer linkage will have involved the reaction of the functional groups A and B coming from two molecules (monomers or chains). Some examples of polymers synthesized by this mechanism are polyurethane, polyamide, and polyester.

This mechanism shows the following features:

1. The chain growth occurs by steps; at each step, a reaction between the functional groups belonging to two monomers or chains occurs. If M_1 denotes monomer, M_2 dimer, M_3 trimer, and so on, the mechanism can be schematically represented as follows:



⁴IUPAC only defines the term polycondensation, but no condensation polymers; however this last classification is of widespread use.

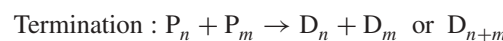
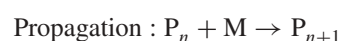
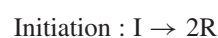


2. The size of the chains increases gradually and relatively slowly.
3. Any two species in the system can react as long as they possess unreacted dissimilar functional groups.
4. Monomer disappears at low conversions.
5. Conversion is measured in terms of the functional groups reacted.

1.2.2.2 Chain Polymerization

This is characterized by:

1. It requires a generator of active centers (usually an initiator for free radicals, anions, or cations).
2. Chain growth occurs by propagation of the active center (chain reaction of the active center with monomer).
3. The monomer only reacts with active centers (not with more monomer).
4. Monomer is present throughout all the reaction.
5. There is high molecular weight polymer present at any time during the polymerization, so the contents of the reaction at any time are unreacted monomer, unreacted initiator, and high molecular weight polymer. There are no significant amounts of intermediate size species (dimer, trimers, etc.).
6. Since there is a clear distinction between monomer and polymer, the conversion is measured in terms of the monomer already incorporated in a polymer chain.
7. The reaction mechanism for free radical polymerization as an example can be represented as follows:



In the initiation steps, the initiator I decomposes generating two active centers (primary radicals) R, which react with a monomer M to produce an active polymer of length 1, P_1 , having an active center. The active polymer grows by propagation of the active center adding a monomer unit in each propagation reaction. Finally, two active centers react, forming dead polymer of length n , D_n .

TABLE 1.2 Differences Between the Step-Growth and the Chain Polymerization Mechanisms

Feature	Step-Growth Mechanism	Chain (Living)	Chain (with Termination)
Number and class of reactions	Only one between dissimilar groups (A and B)	Two reactions: initiation and propagation	Three reactions: initiation, propagation, and termination
Reactive species	Two species of any size having dissimilar groups	Active species of any size with monomer	Active species of any size with monomer or among them (termination)
Monomer consumption	Monomer disappears early in the reaction	Monomer is present up to high conversion	Monomer is present up to high conversion
Conversion	On the basis of reacted functional groups	On the basis of polymerized monomer	On the basis of polymerized monomer
Average molecular weight versus conversion			

Source: Adapted from Ref 9. Copyright 1995, Wiley-VCH Verlag GmbH & Co. KGaA. Reproduced with permission.

The differences between the step-growth and the chain polymerization mechanisms are summarized in Table 1.2. Notice that chain polymerizations may include bimolecular termination reactions (as in the free radical mechanism) or may not (as in living anionic or cationic polymerizations).

Although sometimes the classifications of condensation and step-growth polymers are considered to be interchangeable, as well as those of addition and chain-growth polymers, one must be aware that the classification of a polymer only by structure or only by mechanism may lead to ambiguities. Odian [8] recommends to classify a polymer attending both, structure and mechanism, in order to avoid this problem. Tables 1.3 and 1.4 contain examples of common addition and condensation polymers, respectively.

1.2.3 Classification by Chain Topology

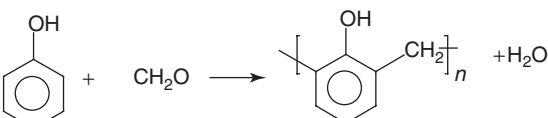
Two polymers having the same chemical composition but different chain topology can exhibit profound differences in crystallinity, physical properties, rheological behavior, and so on. For example, the differences in density, crystallinity, as well as mechanical and rheological properties of LDPE and HDPE derive from the presence or not of long and short branches along the polymer chain. Linear chains are those with no branches; these are shown schematically in Figure 1.4a. Branched chains have at least one branch along the main chain. These branches are classified as short (usually less than 10 repeating units) or long, and they are schematically illustrated in Figure 1.4b. Branches can also be classified, according to Flory, as trifunctional or tetrafunctional, depending on the number of paths departing from the branching point. If the branches are formed by repeating units (monomer) different from those forming

TABLE 1.3 Examples of Common Addition Polymers

Addition Polymers	Repeating Unit
Polyacrylonitrile	$\text{---CH}_2\text{---CH}(\text{CN})\text{---}$
Polybutadiene	$\text{---CH}_2\text{---CH}(\text{CH}_2\text{---CH}=\text{CH}_2)\text{---}$
Polyethylene	$\text{---CH}_2\text{---CH}_2\text{---}$
Poly(methyl methacrylate)	$\text{---CH}_2\text{---C(CH}_3\text{)}_2\text{---CO}_2\text{CH}_3\text{---}$
Polypropylene	$\text{---CH}_2\text{---CH(CH}_3\text{)}\text{---}$
Polystyrene	$\text{---CH}_2\text{---CH}(\text{---C}_6\text{H}_4\text{---CH}_2\text{---})\text{---}$
Poly(vinyl chloride)	$\text{---CH}_2\text{---CH(Cl)}\text{---}$

the main chain, the branched polymer is a graft copolymer (Figure 1.4c, see also Chapter 6). Crosslinked polymers are those forming a three-dimensional network and are shown in Figure 1.4d; they are insoluble and have very restricted chain-segment mobility; therefore, they do not flow (a discussion on the processes leading to crosslinked polymers can be found in Chapter 9).

TABLE 1.4 Examples of Common Condensation Polymers

Polymer	Synthesis Reaction → Repeating Unit
Polyamide	$\text{H}_2\text{N}-\text{R}_1-\text{NH}_2 + \text{HO}_2\text{C}-\text{R}_2-\text{CO}_2\text{H} \longrightarrow [\text{NH}-\text{R}_1-\text{NHCO}-\text{R}_2-\text{CO}]_n\text{OH} + \text{H}_2\text{O}$
Polyester	$\text{HO}-\text{R}_1-\text{OH} + \text{HO}_2\text{C}-\text{R}_2-\text{CO}_2\text{H} \longrightarrow [\text{O}-\text{R}_1-\text{OCO}-\text{R}_2-\text{CO}]_n\text{OH} + \text{H}_2\text{O}$
Phenol-formaldehyde	
Urea-formaldehyde	$\text{H}_2\text{N}-\text{CO}-\text{NH}_2 + \text{CH}_2\text{O} \longrightarrow [\text{HN}-\text{CO}-\text{NH}-\text{CH}_2]_n + \text{H}_2\text{O}$
Polyurethane	$\text{HO}-\text{R}_1-\text{OH} + \text{OCN}-\text{R}_2-\text{NCO} \longrightarrow [\text{O}-\text{R}_1-\text{OCO}-\text{NH}-\text{R}_2-\text{NH}-\text{CO}]_n$

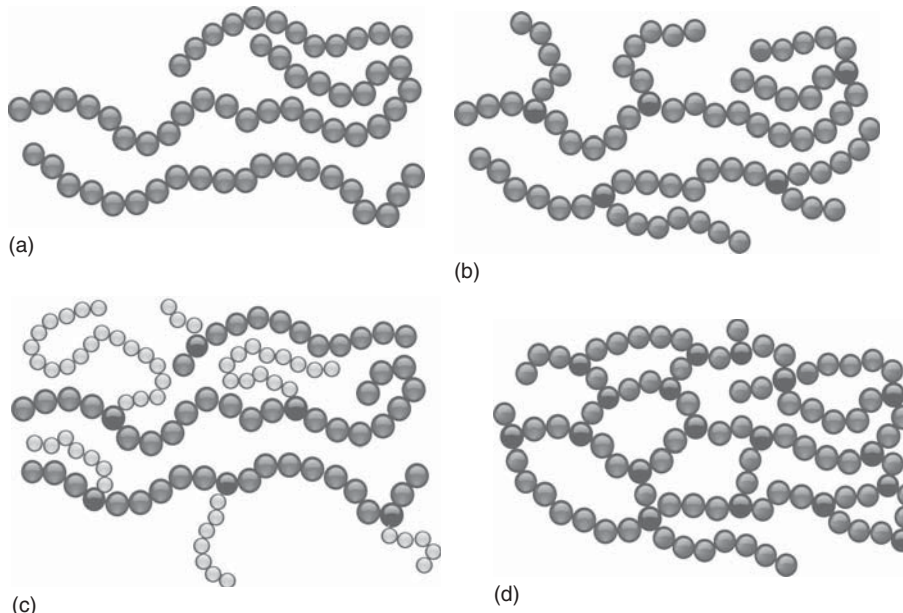


Figure 1.4 Different polymer chain topologies: (a) linear polymer; (b) branched polymer; (c) graft copolymer; and (d) crosslinked polymer. Dotson NE, Galván R, Laurence RL, Tirrell M. Polymerization Process Modeling. VCH Publishers; 1995. p 35 [8]. Copyright 1995 Wiley-VCH Verlag GmbH & Co. KGaA.

1.2.4 Other Classification Criteria

1.2.4.1 Homopolymer and Copolymer If only one type of monomer or repeating unit constitutes the macromolecule (without considering the chain ends) then the polymeric substance is termed a *homopolymer*. If, on the other hand, more than one type of repeating unit is present in the macromolecule, the polymeric substance is a *copolymer*. The macromolecule produced in the specific case of a reacting mixture containing three different monomers or monomer units is termed *terpolymer*. Depending on the randomness or order in which two or more types of repeating units are present in the macromolecule, there are

different types of copolymers: random, block, alternate, and so on. These are described in Chapter 6.

1.2.4.2 Origin Another possible classification of polymeric substances can be based on the origin of the material or the repeating units. In this sense, one can have *natural* and *synthetic* polymers, if they occur in nature or if they are synthesized in a chemical laboratory, respectively. Of course, natural polymers are of great importance, but they fall out of the scope of this handbook, which is mainly concerned with synthetic polymers.

Also, among the synthetic polymers, one can distinguish between organic and inorganic polymers, depending on

the presence or absence of carbon atoms in the polymer chain backbone. Synthetic organic polymers are by far the most studied and utilized polymeric substances of the two categories, mainly because of the availability of organic monomers coming from the petrochemical industry, and this handbook is mainly concerned with this type of polymers.

On the other hand, inorganic polymers have long been known, and recently, increasing research is being done in this field. Typical inorganic polymers contain oxygen, silicon, nitrogen, or phosphorus in their backbones [10]. Inorganic polymers can overcome some of the disadvantages of organic polymers, such as degradability at relatively low temperatures, or in the presence of oxygen or radiation, and they are expected to become more important in the future. The reader can find more details on this subject elsewhere [10].

1.2.4.3 Biodegradability *Biodegradable polymers* are those that degrade by the action of biological agents (e.g., microorganisms, bacteria or fungi) in ambient or mild conditions, and in relatively short times. In order to be more specific, it is necessary to set a time frame for degradability, to define the environmental conditions under which degradation is supposed to occur, and also to what extent the polymer must degrade in order to be considered biodegradable [11]. Most of the commodity polymers are not biodegradable: polyethylenes, poly(ethylene terephthalate) (PET), PVC, polystyrene, and so on. The development and commercialization of biodegradable polymers in significant amounts is relatively recent (since around the year 2001), but an accelerated growth of this industry is expected because of worldwide growing environmental concerns. Some examples of biodegradable polymers are poly(lactic acid) (PLA), poly(hydroxyalkanoates) (PHA) [12], and polycaprolactones.

1.2.4.4 Production Volume Finally, polymers can be classified by production volume. Large production volume polymers are *commodities*, and they are usually produced by continuous processes with very low profit margins per weight unit. Mostly, mature technologies are used to produce them, and the investment in R&D that is used to improve the production processes or products tends to be relatively low. Main examples of commodities are polyethylene (LDPE and HDPE), polypropylene, PVC, PET, polystyrene, and derivatives. These five families of polymers constitute those produced in largest volume. Estimated worldwide production of polymers in 2003 was around 200 million Tons, with an annual estimated global growth rate of 3.4% [13]. About 80% of the total polymer production is composed of the five families of commodities mentioned above.

On the other hand, *specialty polymers* are produced in smaller quantities, in batch or semibatch processes, and have high profit margins per weight unit. They require high investment in R&D in order to offer significant advantages over existing products for specific applications.

1.3 NOMENCLATURE

Unfortunately, at present, the naming of polymers is not uniform. The International Union for Pure and Applied Chemistry (IUPAC) has established some systematic rules for the naming of polymers, but they are not used by everyone. For some polymers, there are common or trade names that are used almost exclusively, instead of the more systematic IUPAC names. The lack of rigor and uniformity in naming polymers may occasionally give rise to confusions; in this book, different types of names are used as long as there is no ambiguity in the identification of the polymer.

Three naming systems are briefly discussed here: (i) conventional nomenclature based on source or structure, (ii) IUPAC structure-based nomenclature, and (iii) trade and common names and abbreviations. A deeper discussion can be found in the text by Odian [8].

1.3.1 Conventional Nomenclature.

The most common nonofficial (non-IUPAC) convention used to name polymers is based on the source from which the polymer is formed. This is particularly useful for polymers formed of a single monomer (homopolymers) synthesized by addition, ring-opening, or condensation polymerizations (Section 1.2). This rule consists in using the prefix “poly” followed by the name of the monomer (repeating unit), frequently enclosed in parentheses, although, in many cases, the name of the monomer is simply written after the prefix without separation. Examples of this convention are poly(methyl methacrylate), polystyrene, polypropylene, PVC, poly(ethylene oxide), and PLA. The parentheses are used in cases in which otherwise ambiguity would arise.

For condensation polymers formed by two bifunctional monomers (of the type AA and BB, where A and B are different functional groups, see Section 1.2) the rule varies to reflect the structure of the repeating unit. In this case, instead of the monomer(s) name, the name of the structural group formed by the reaction of the two functional groups (A and B) is used as the base for the nomenclature and is enclosed in parentheses following the prefix “poly.” Consider, for example, the polymer formed by the reaction of ethylene glycol HO—CH₂—CH₂—OH (a monomer containing two OH or “A” groups) and terephthalic acid HO₂C—C₆H₄—CO₂H (monomer containing two COOH or “B” groups). The reaction between the carboxyl and

TABLE 1.5 Widespread Abbreviations for Some Common Polymers

Abbreviation	Polymer	Abbreviation	Polymer
ABS	Acrylonitrile-butadiene-styrene terpolymer	PET	Poly(ethylene terephthalate)
BR	Butyl rubber or poly(isobutylene)	PLA	Poly(lactic acid)
EPDM	Ethylene-propylene-diene monomer rubber	PMMA	Poly(methyl methacrylate)
EPR	Ethylene-propylene rubber	PS (or GPPS)	Polystyrene or general purpose polystyrene
EPS	Expandable polystyrene	PP	Polypropylene
HDPE	High density polyethylene	PTFE	Poly(tetrafluoroethylene)
HIPS	High impact polystyrene	PU	Polyurethane
LDPE	Low density polyethylene	PVA	Poly(vinyl alcohol)
LLDPE	Linear low density polyethylene	PVC	Poly(vinyl chloride)
MBS	Methyl methacrylate-butadiene-styrene	PVDC	Poly(vinylidene chloride)
NBR	Acrylonitrile-butadiene rubber	PVDF	Poly(vinylidene fluoride)
PA	Polyamide	SAN	Styrene acrylonitrile copolymer
PAN	Polyacrylonitrile	SBR	Styrene-butadiene rubber
PBT	Poly(butylene terephthalate)	SBS	Styrene-butadiene-styrene block copolymer
PC	Polycarbonate	SIS	Styrene-isoprene-styrene block copolymer
PEO	Poly(ethylene oxide)	SMA	Styrene-maleic anhydride copolymer

the hydroxyl groups can be considered to yield the ester group or repeating structural unit “ethylene terephthalate.” Therefore, the resulting polymer is denoted poly(ethylene terephthalate).

1.3.2 IUPAC Structure-based Nomenclature

The IUPAC nomenclature is not discussed here in detail, only the main idea behind it. Complete details can be found in the text by Odian [8] or in the original source [14].

The IUPAC rules for naming polymers are applicable to *single-strand* polymers, which are those comprising constitutional units connected in such a way that adjacent constitutional units are linked one to another by two atoms, one on each constitutional unit. The large majority of common polymers are single-strand ones. The IUPAC nomenclature is based on the selection of a preferred constitutional repeating unit or CRU, where the CRU is the smallest possible repeating unit of the polymer. This is named by the prefix poly followed by the name of the CRU in parentheses or brackets. This rule coincides with the simpler non-IUPAC rule given before, except for polymers in which the repeating unit (monomer) is formed by two identical halves (such as ethylene). The IUPAC naming system is more powerful and general than other conventional systems since the CRU is named following the rules for small organic compounds.

1.3.3 Trade Names, Common Names, and Abbreviations

Trade names have become well established for certain polymers. A good example is nylon, which is the trade name of the generic family of polyamides. When the polyamide is

based on the condensation of a diamine and a dicarboxylic acid, the word nylon is followed by two numbers, for example, nylon 6,6, which correspond to the number of carbon atoms in the diamine and the dicarboxylic acid parts of the repeating unit, respectively. On the other hand, if the polyamide is based on a single monomer, a single number reflecting the number of carbon atoms in the repeating unit follows the word nylon, as in nylon 6.

Other examples of well-established trade names are Kevlar (poly(paraphenylene terephthalamide)), Plexiglass (sheets of poly(methyl methacrylate)), Teflon (poly(tetrafluoroethylene)), and Dacron (PET fiber).

Abbreviations and common names are also widely used, especially in industry and also to some extent in technical journals and academic environments. Table 1.5 contains a nonexhaustive list of some of the more common abbreviations in use; many of them refer to copolymers (for more information on copolymer naming rules, see Chapter 6). The reader must be aware of some details regarding the brief polymer description in Table 1.5 (columns 2 and 4); some of these materials are not pure polymers, but rather a complex mixture of two or three different polymers forming a two-phase material, such as in the case of high impact polystyrene (HIPS), acrylonitrile-butadiene-styrene (ABS), and methyl methacrylate-butadiene-styrene (MBS); see Chapter 10 for more details on the structure of these materials.

REFERENCES

- Flory PJ. *Principles of Polymer Chemistry*. Ithaca (NY): Cornell University Press; 1953.
- Staudinger H. Ber Deut Chem Ges 1920;53(6):1073.
- Carothers WH. J Am Chem Soc 1929;51:2548.

14 INTRODUCTION TO POLYMERS AND POLYMER TYPES

4. Morawetz H. *Polymers: The Origin and Growth of a Science*. Mineola (NY): Dover Publications Inc.; 2002.
5. Ray WH. J Macromol Sci Rev Macromol Chem Phys 1972;C8(1):1.
6. Brandrup J, Immergut EH, Grulke EA, editors. *Polymer Handbook*. 4thSection VII ed. New York: John Wiley & Sons Inc.; 1999.
7. Stepto RFT. Pure Appl Chem 2009;81(2):351.
8. Odian G. *Principles of Polymerization*. 4th ed. Hoboken (NJ): Wiley Interscience; 2004.
9. Dotson NE, Galván R, Laurence RL, Tirrell M. *Polymerization Process Modeling*. New York (NY): Wiley VCH; 1996. p 35.
10. Mark JE, Allcock HR, West R. *Inorganic Polymers*. 2nd ed. New York (NY): Oxford University Press; 2005.
11. Narayan R, Pettigrew C. ASTM Standardization News; 1999 December: 36–42.
12. Kolybaba M, Tabil LG, Panigrahi S, Crerar WJ, Powell J, Wang B. Paper RRV03-0007 presented at the 2003 CSAE/ASAE Annual Intersectoral Meeting. Fargo (ND): The Society for Engineering in Agricultural, Food and Biological Systems; 2003. Accessed 2012, October.
13. [a] Lothar R. China Particuology 2006;4(2):47. [b] VLEEM2 EC/DG Research Contract ENG1-CT 2002-00645, Final Report, Annex 2, Detailed results on bulk materials. Available at <http://www.enerdata.net/VLEEM/PDF/30-05-05/anx2.pdf>.
14. [a] Metanomski WV. (*IUPAC Compendium of Macromolecular Nomenclature (The Purple Book)*). 1st ed. Oxford: Blackwell Scientific; 1991. [b] Kahovec J, Fox RB, Hatada K. Pure Appl Chem 2002;74(10):1921.

2

POLYMER STATES AND PROPERTIES

J. BETZABE GONZÁLEZ-CAMPOS, GABRIEL LUNA-BÁRCENAS, DIANA G. ZÁRATE-TRIVIÑO, ARTURO MENDOZA-GALVÁN, EVGEN PROKHOROV, FRANCISCO VILLASEÑOR-ORTEGA, AND ISAAC C. SANCHEZ

2.1 INTRODUCTION

Polymers can be either amorphous or semicrystalline in structure. The structure of amorphous materials cannot be described in terms of repeating unit cells such as that of crystalline materials; because of nonperiodicity, the unit cell of an amorphous material would comprise all atoms. The physics and chemistry of the amorphous state remain poorly understood in many aspects. Although numerous experiments and theoretical studies have been performed, many of the amorphous-state features remain unexplained and others are controversial. One such controversial problem is the nature of glass-liquid transition.

Glass transition is a key phenomenon that is useful to understand how external conditions affect physical changes on materials. Theories that predict and describe the glass transition as well as different experimental methods to detect and characterize this phenomenon are of great interest for food, medical, pharmaceutical, and polymer industries [1–4]. It is important to emphasize that the materials of relevance in these industries are interchangeably sharing similar issues on functionality and their association with the glass transition phenomenon.

The glassy state of materials corresponds to a nonequilibrium solid state, in which the molecules forming the material are randomly arranged occupying a volume larger than that of the crystalline state and having a similar composition. Since glassy solids are considered to be in a state of nonequilibrium, the stability of the material is therefore dependent on several factors, which include temperature, water content, molecular weight, and the thermal history undergone by the material before reaching the specific glassy state. The glass transition plays an important role in the

stability of various foods and drugs, as well as in polymer manufacturing. Several theories have been developed to understand the glass transition phenomenon from kinetics and thermodynamics standpoints by presenting existing models that are able to estimate the glass transition temperature [1–3]. The development of new materials and understanding the physicochemical behavior of existing ones require a scientific foundation that translates into safe and high quality products with improved quality and functional efficacy of polymers used in different industries.

The glass transition can be measured using different techniques and sometimes they give different results. In the case of chitin (Ch), chitosan (CS), poly(vinyl alcohol) (PVA), and their composites [5–7], improper water elimination analysis had led to a misinterpretation of thermal relaxations, and in some cases, the glass transition phenomenon had not been observed because of this. However, once moisture was properly eliminated, the α -relaxation related to the glass transition phenomenon was revealed [5–7]. In all cases, this behavior was observed through the analysis of their molecular dynamics using dielectric spectroscopy (DS). This is a poorly known tool and not commonly used in the glass transition temperature analysis.

DS has been demonstrated to be a useful tool for the analysis of the glass transition phenomenon in both natural and synthetic polymers, especially under the influence of water, and its application on composites molecular dynamics analysis was also demonstrated [5–7]. This chapter addresses the glass transition phenomenon from an experimental standpoint by exploring a dielectric method used for the characterization of the glass transition phenomenon in natural and synthetic polymers.

2.2 GLASS TRANSITION TEMPERATURE (α -RELAXATION) CONTROVERSY IN CHITIN, CHITOSAN, AND PVA

Solids and liquids are phase separated at the melting point. Polymers have an intermediate boundary called the *glass transition temperature* at which there are remarkable changes in the properties of the polymers. The glass transition temperature (T_g) of a noncrystalline material is the critical temperature at which the material changes its behavior from being “glassy” to being “rubbery.” Glassy in this context means hard and brittle (and therefore relatively easy to break), while rubbery means elastic and flexible.

Although fundamentally important, the nature of the glass transition is not well understood. The glass transition is accompanied by significant changes in physical properties such as conductivity and viscosity. Additionally, physicochemical properties of a material such as dissolution, bioavailability, processing, and handling qualities can be related to the material’s T_g [8]. Rearrangements that occur in an amorphous material at the glass transition temperature lead to characteristic discontinuities of derivative thermodynamic parameters such as the coefficient of thermal expansion (CTE) or the specific heat. The glass transition temperature can also be considered a measure of compatibility or miscibility in polymer blends.

In polymers, the glass transition phenomenon has been related to the dielectric α -relaxation processes through the Vogel-Fulcher-Tammann (VFT) equation [9], and it can be characterized by means of their molecular dynamics analysis.

In semicrystalline polymers, such as chitin and CS, the value of the glass transition temperature characteristic of the amorphous material was controversial even as to whether polysaccharides exhibit a glass transition temperature (T_g). For many natural polymers, T_g is above the thermal degradation temperature [10]. For chitin, some authors have not observed a glass transition [11], while others report an apparent α -relaxation at 236 °C for α -chitin [12] and 170 °C for β -chitin [13] using DMTA measurements. Lee et al. [14] report an apparent α -relaxation at 182 °C for β -chitin by dielectric measurements.

Regarding CS, some authors using several techniques, including differential scanning calorimetry (DSC) and dynamic mechanical thermal analysis (DMTA), have reported T_g values from 20 to 203 °C [4, 14–18], while others do not observe the glass transition by DSC and DMTA measurements [19]. Some authors have reported molecular dynamics analysis in CS by dielectric measurements with no evidence associated with a glass transition. [19–21] These studies reported local main chain motions at the high frequency side, the β -relaxation process, and at higher temperature the so-called σ -relaxation produced by proton migration [20, 21]. It is well known that this biopolymer is

highly hydrophilic and that small amounts of water affect its molecular relaxations. This effect has been reported on wet CS, since it exhibits an additional relaxation referred to as the β_{wet} -relaxation [19–21].

Regarding PVA, it has been shown by DSC, dynamic mechanical analysis (DMA), and DS that the T_g of PVA can be modified by the inclusion of ions, ceramics, monomers, nanoparticles, nanotubes, and other polymers [22–26]. In addition, a plasticizing effect of small amounts of water on T_g could lead to slight differences in the T_g values reported elsewhere [27]. However, most of these analyses were carried out without taking into account the effect of moisture content. In the 30–100 °C temperature range, the temperature dependence of the conductivity and the relaxation time for PVA have been commonly described as Arrhenius-type behavior [28–34]. This behavior can be ascribed to a secondary relaxation process and related to the rotation of hydroxyl groups. Nevertheless, other authors observed a VTF behavior, associated with a primary α -relaxation process [25, 35, 36]. Thermal relaxations of PVA at this temperature range have been subject to contradictory interpretations; therefore, a deep analysis in a wider temperature range is needed to gain a better insight into the molecular dynamics of PVA and its blends, composites, and PVA-based materials.

On the other hand, the physical and chemical properties of polymers can be significantly changed by the presence of small amounts of water [37]; chitin, CS, and PVA have a strong affinity for water and, therefore, can be readily hydrated forming macromolecules with rather disordered structures [38]. A true understanding of hydration properties is essential for several applications in materials science, food industry, and biotechnology [37]. DS is an important technique used to investigate the hydration properties related to the molecular dynamics of materials. The α -relaxation related to the glass transition can be clearly analyzed by this technique. The main advantage of dielectric techniques over others that attempt to measure molecular dynamics is the extremely broad frequency range covered [37]. In this chapter, the glass transition phenomenon is analyzed and described by means of the molecular dynamics analysis.

2.3 GLASS TRANSITION RELATED TO THE α -RELAXATION

The concept of T_g applies only to noncrystalline solids, which are mostly either glasses or rubbers. Noncrystalline materials are also known as *amorphous materials*. Amorphous materials are materials that do not have their atoms or molecules arranged on a lattice that repeats periodically in space. For amorphous solids, whether glasses, organic polymers, or even metals, T_g is the critical temperature that

separates their glassy and rubbery behaviors. If a material is at a temperature below its T_g , large-scale molecular motion is not possible because the material is essentially frozen. If it is at a temperature above its T_g , molecular motion on the scale of its repeat unit (such as a single mer in a polymer) takes place, allowing it to be "soft" or "rubbery." A small change in temperature T_g could result in pronounced changes in the mechanical, thermal, and dielectric properties of amorphous materials.

DSC defines the glass transition as a change in the heat capacity as the polymer matrix goes from the glassy state to the rubbery state. This is a second-order endothermic transition (requires heat to go through the transition), and so in DSC the transition appears as a step transition and not a peak such as might be seen with a melt transition. DSC is the classic and "official" way to determine T_g even though in some cases there are polymeric materials that do not exhibit a sharp T_g by DSC; this has been the case of chitin and CS as well as cellulose [12, 39].

Thermal mechanical analysis (TMA) defines the glass transition in terms of a change in the CTE as the polymer goes from glass to rubber states with the associated change in free molecular volume. Each of these techniques measures a different result of the change from glass to rubber. DSC measures the heat effect, whereas TMA measures the physical effect, that is, the CTE. Both techniques assume that the effect happens over a narrow range of a few degrees in temperature. If the glass transition is very broad, it may not be seen with either approach.

From the practical point of view, fundamental information on the processability of polymers is usually obtained through thermal analysis, which provides knowledge of the main polymer transitions (melting and glass-to-rubber transition to the crystalline and amorphous phases, respectively). In addition to the well-established calorimetric techniques, experimental methods capable of revealing the motional phenomena occurring in the solid state have attracted increasing attention.

In amorphous polymers, α -relaxation, as determined by DS and DMA, corresponds to the glass transition and reflects motions of fairly long chain segments in the amorphous domains of the polymer (long range motions). Relaxations at lower temperatures (labeled β , γ , δ , etc.) are generally due to local movements of the main chain, or rotations and vibrations of terminal groups or other side chains (short range motions). DS and DMA are well-established techniques for the measurement of thermal transitions including the glass transition; they are especially available in detecting T_g of a sample that cannot be observed by normal calorimetric measurements. For example, T_g of polymers having crosslinked network structure [14]. In general, the same relaxation/retardation processes are responsible for the mechanical and dielectric dispersion observed in polar materials [40]. In materials

with low polarity, the dielectric relaxations are very weak and cannot be easily detected. However, these two techniques have not been explored at the maximum in relation to the glass transition temperature assignation in natural and synthetic polymers, even though it is demonstrated that they are very effective for the glass transition temperature analysis in hydrophilic polymers [5–7].

The α -relaxation is related to the glass transition of the systems and for that reason this relaxation is also called *dynamic glass transition*. In general, the α -relaxation and the related glass transition phenomenon are not well understood, and the actual microscopic description of the relaxation remains unsolved besides it is a current problem in polymer science [41]. However, it is well accepted that the dynamics of the glass transition is associated with the segmental motion of chains being cooperative in nature [9], which means that a specific segment moves together with its environment. For most amorphous polymers, the α -relaxation has some peculiarities, describe later.

In the α -process, the viscosity and consequently the relaxation time increase drastically as the temperature decreases. Thus, molecular dynamics is characterized by a wide distribution of relaxation times. A strong temperature dependence presenting departure from linearity or non-Arrhenius thermal activation is present, owing to the abrupt increase in relaxation time with the temperature decrease, thus developing a curvature near T_g . This dependence can be well described by the Vogel-Fulcher-Tammann-Hesse (VFTH) equation [40, 41], given by Equation 2.1:

$$\tau = \tau_0 \exp\left(\frac{DT_0}{T - T_0}\right) \quad (2.1)$$

where τ_0 is the pre-exponential factor $\sim 10^{10}$ – 10^{13} Hz, D is a material's constant, and T_0 is the so-called ideal glass transition or Vogel temperature, which is generally 30–70 K below the glass transition temperature (T_g) [9, 41].

2.4 MOISTURE CONTENT EFFECTS ON POLYMER'S MOLECULAR RELAXATIONS

It is well known that moisture content has a significant influence on chitin, CS, and PVA physical properties [5–7]. A true understanding of hydration properties is essential for several practical applications in materials science, food industry, biotechnology, etc. [42]. CS moisture content is affected by the number of ionic groups in the material as well as their nature. The important binding sites for water molecules in CS are the hydroxyl and amine groups present in the polymer. Several studies have been performed to gain an understanding of the adsorption of water; thermal methods such as thermogravimetry (TGA),

DSC, and dynamical mechanical thermal analysis (DMTA) have emerged as powerful thermoanalytical techniques to monitor physical and chemical changes in both natural and synthetic polymers.

Chitin and CS are a hydrophilic, hence, water-insoluble polysaccharides. The glass transition phenomenon could be also affected by moisture content, since it can work as a plasticizer. Plasticization occurs only in the amorphous region, such that the degree of hydration is quoted as moisture content in the amorphous region. In general, the following three states of water adsorbed on chitin and CS are distinguished:

1. *Nonfreezing Water*. Water that is strongly bound to hydrophilic groups and shows no thermal transition by DSC;
2. *Freezable Bound Water*. Water that is weakly bound to the polymer chain (or weakly bound to the nonfreezing water) and that melts on heating at temperatures greater than 0°C due to these bonding interactions; and
3. *Free Water*. Water that has the same phase transitions as bulk water.

Polymers that contain the amide group, such as chitin and CS, usually show a low temperature mechanical and dielectric relaxation in the vicinity of -70°C (at 1 Hz) [43] which is commonly called *water relaxation* since it is sensibly affected by changes in the moisture content of the polymer. Typically the peak intensity, very low when samples are dried, increases with increasing moisture content, whereas correspondingly the peak maximum shifts to lower temperatures. This relaxation has been assigned as the β -wet relaxation attributed to the motion of water–polymer complex in the amorphous regions [20, 21].

Two basic contributions are expected to the variation of dielectric properties of a hydrated material with respect to those of a dry one: that of the polar water molecules themselves and the second one due to the modification of the various polarization and relaxation mechanisms of the matrix material itself by water [37]. In the low frequency region of measurements, there is a third contribution, often ignored in works dealing with high frequency measurements, which arises from the influence of moisture on conductivity and conductivity effects. The increase of electrical conductivity of the sample is the major effect present in wet samples; dielectric response is often masked by conductivity, and it superposes the dielectric processes in the loss spectra and demands a conductivity correction of the dielectric loss spectra [9]. This dc conductivity strongly affects the modified loss factor, ϵ'' . In this case, it can be expressed as shown in the following equation:

$$\epsilon'' = \epsilon''_{\text{exp}} - \frac{\sigma_{\text{dc}}}{\omega \epsilon_0} \quad (2.2)$$

In Equation 2.2, ϵ''_{exp} is the experimental loss factor value; σ_{dc} is direct current conductivity; d and S are thickness and area of sample, respectively; $\omega = 2\pi f$ (f is frequency); and ϵ_0 is the permittivity of vacuum. As a general rule for polymers, σ_{dc} is determined from fitting of the real component of the complex conductivity ($\sigma_{\text{dc}} = \sigma_0 n^a$, where σ_0 and n are fitting parameters) measured in the low frequency range where a plateau is expected to appear.

However, generally in composites with conductive inclusions, ionic current and interfacial polarization could often mask the real dielectric relaxation processes in the low frequency range. Therefore, to analyze the dielectric process in detail, the complex permittivity ϵ^* can be converted to the complex electric modulus M^* by using the following equation:

$$M^* = \frac{1}{\epsilon^*} = M' + iM'' = \frac{\epsilon'}{\epsilon'^2 + \epsilon''^2} + \frac{\epsilon''}{\epsilon'^2 + \epsilon''^2} \quad (2.3)$$

where M' is the real and M'' the imaginary parts of electric modulus, and ϵ' is the real and ϵ'' the imaginary parts of permittivity.

Interpreting the experimental data in this form nowadays is a commonly employed method to obtain information about the relaxation processes in ionic conductive materials and polymer-conductivity nanoparticles composites. In this representation, interfacial polarization and electrode contributions are essentially suppressed [44, 45]. The peak in the imaginary part of M'' depends on temperature, which can be related to the translational ionic motions. The corresponding relaxation time $\tau_\sigma = 1/(2\pi f_p)$, where f_p is the peak frequency, therefore is called *conductivity relaxation time*.

In this case, this chapter presents both analyses; in the case of chitin and CS, the analysis by means of the real (ϵ') and the imaginary (ϵ'') parts of permittivity and for PVA the case of the analysis by the complex electric modulus, M^* .

2.5 DIELECTRIC FUNDAMENTALS

DS measures the dielectric permittivity as a function of frequency and temperature. It can be applied to all nonconducting materials. The frequency range extends over nearly 18 orders in magnitude: from the microhertz to terahertz range close to the infrared region. This remarkable breadth is the key feature that enables one to relate the observed dielectric response to slow (low frequency) and/or fast (high frequency) molecular events. DS is sensitive to dipolar species as well as localized charges in a material; it determines their strength, kinetics, and interactions. Thus, DS is a powerful tool for the electrical characterization of nonconducting materials in relation to their structure.

2.5.1 The Origin of Dielectric Response

When a metal body is exposed to an electric field, free electrons are displaced by electric forces until the field in the body vanishes. In an ideal dielectric (dc conductivity is zero), there exists only bound charges (electrons, ions) that can be displaced from their equilibrium positions until the field force and the oppositely acting elastic force are equal. This phenomenon is called *displacement polarization* (electronic or ionic polarization). A dipole moment is induced in every atom or between ion pairs. The molecular dipoles can only be rotated by an electric field. Usually, their dipole moments are randomly oriented. In an external field, however, an orientation parallel to the field direction is preferred so that a dipole moment is induced. This process is called *orientational polarization*.

In an alternating electric field, the displacement polarization leads to electric oscillations. This is a resonant process with resonant frequencies of 10^{15} – 10^{14} Hz for the electronic and of 10^{13} – 10^{12} Hz for the ionic polarization.

Orientational polarization is not a resonant process since the molecular dipoles have inertia. The response of the orientational polarization to a charge of the electric field is, therefore, always retarded. This process is called *dielectric relaxation*. The characteristic time constant of such a relaxation process—this is the time for reaching new equilibrium after changing the excitation—is called *relaxation time* (τ). It is strongly temperature dependent, since it is closely related to the viscosity of the material. At room temperature, the relaxation times of the orientational polarization in crystals are of 10^{-11} – 10^{-9} s. In amorphous solids and polymers, however, they can reach a few seconds or even hours, days, and years, depending on the temperature.

In polymer materials that are studied by DS, there are two major polarization mechanisms: (i) polarization due to charge migration and (ii) polarization due to the orientation of permanent dipoles. Let us look at charge migration first. Migration of charges gives rise to conductivity [20]. The measured conductivity encompasses contributions from extrinsic migrating charges (e.g., ionic impurities) and intrinsic migrating charges (e.g., proton transfers along hydrogen bonds). Regarding dipole orientation, while electronic and atomic polarization result from induce dipoles, there are many materials that contain permanent dipoles. When such materials are placed in the electric field, dipole orientation or dipole polarization is produced as a result of the alignment of dipoles in the direction of the applied field. The orientation (polarization) of permanent dipoles involves cooperative motions of molecular segments in a viscous medium with time-scales measurable by DS.

Real dielectrics also contain charge carriers that can be moved by electric forces between potential walls, formed by non-ohmic or blocking contacts or internal boundaries,

for example, between crystalline and amorphous phases in a semicrystalline material. This leads to a space charge polarization (electrode polarization or Maxwell–Wagner polarization, respectively), which on the other hand is limited by diffusion. These processes are also relaxation processes and are called *charge-carrier relaxations*. Because these processes are closely related to the conductivity, they are sometimes also named *conductivity relaxations*.

The dielectric (ϵ^*) and loss (ϵ'') constants are important properties of interest because these two parameters, among others, determine the suitability of a material for a given application. Dielectric relaxations are studied to reduce energy losses in materials used in practically important areas of insulation and mechanical strength.

2.5.2 Dielectric Relaxation in Solid Polymers

Several and different relaxation processes are usually present in solid polymeric materials, and these are dielectrically active if they incur significant orientation of molecular dipoles. The multiplicity of relaxation process is seen most easily in a scan dielectric loss at constant frequency as a function of temperature. As temperature is raised, molecular mobilities of various types become successively energized and available for dipolar orientation. By convention, the dielectric relaxation processes are labeled α , β , and so on, beginning at the high temperature end. The same relaxation processes are generally responsible for dispersions in mechanical properties too, although a particular molecular rearrangement process may produce a stronger dielectric than mechanical effect or vice versa [40].

Some polymers are completely amorphous, and there is only one phase present in the solid material. In such cases, there is always a high temperature α -relaxation associated with the micro-Brownian motion of the whole chains and, in addition, at least one low temperature (β , γ , etc.) subsidiary relaxation. The relative strength of the α - and β -dielectric relaxations depends on how much orientation of the dipolar groups can occur through the limited mobility allowed by the β -process before the more difficult but more expensive mobility of the α -process comes into play: there is a partitioning of the total dipolar alignment among the molecular rearrangement processes.

A detailed examination of the relaxations requires isothermal scans of relative permittivity and dielectric loss factor as a function of frequency, f , so that the effective dipole movements and activation energies of relaxation times may be obtained. A typical pair of plots of ϵ'' and ϵ' values against $\log f$ is shown in Figure 2.1. Plots of dielectric data of this kind are sometimes called *dielectric spectra*. From a series of such plots, the relaxation times can be obtained for the individual relaxation processes as a function of temperature.

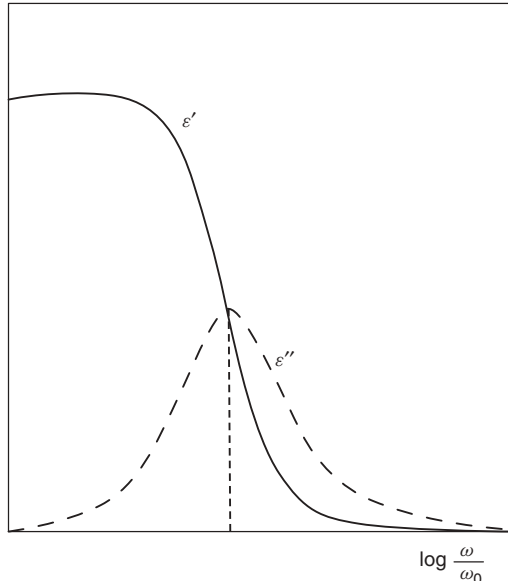


Figure 2.1 Dielectric relaxation curves commonly found in dielectric processes.

Molecular processes cover a broad frequency range being associated with the length scale of the conformational mobility in the polymeric chain. Hence, relaxation processes in polymeric materials involve hierarchy that goes from very local motions (β , δ , γ , etc.) to segmental mobility involving cooperativity (α -process), or even relaxation processes involving large or complete polymeric segments [40].

When studying a polymer on a large frequency/time scale, the response of a given material under a dynamic stimulus usually exhibits several relaxations. Moreover, the peaks are usually broad and sometimes are associated with superposed processes. The relaxation rate, shape of the loss peak, and relaxation strength depend on the motion associated with a given relaxation process [41]. In general, the same relaxation/retardation processes are responsible for the mechanical and dielectric dispersion observed in polar materials [40]. In materials with low polarity, the dielectric relaxations are very weak and cannot be easily detected. The main relaxation processes detected in polymeric systems are analyzed next.

2.5.3 α -Relaxation

The α -relaxation and its features were described in Section 2.4. As mentioned before, a strong temperature dependence presenting departure from linearity or non-Arrhenius thermal activation is present as shown in Figure 2.2, due to the abrupt increase in relaxation time with the temperature decrease, thus developing a curvature near T_g . This dependence can be well described by the VFT equation.

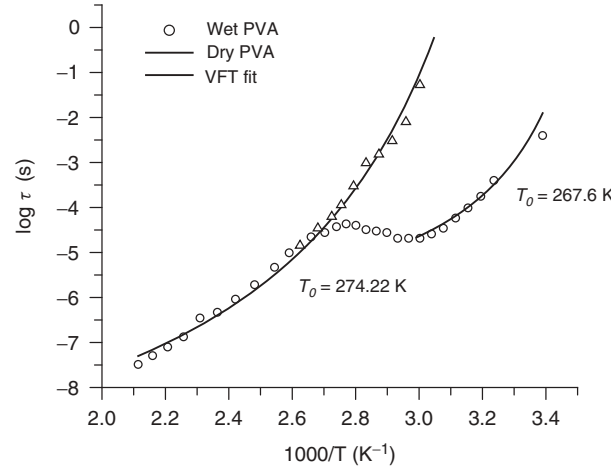


Figure 2.2 Relaxation time (τ) versus $1000/T$ for PVA disclosing the α -relaxation obtained by dielectric spectroscopy. The solid line is the VFT fitting of the dielectric data. *Source:* Reproduced with permission from González-Campos JB, García-Carvajal ZY, Prokhorov E, Luna-Bárcenas JG, Mendoza-Duarte ME, Lara-Romero J, Del Río RE, Sanchez IC. *J Appl Polym Sci* 2012;125:4082 [7]. Copyright 2012 John Wiley and Sons, Inc.

In general, the α -process is well defined in the frequency domain and shows a relatively broad and asymmetric peak. Several functions such as the Cole–Cole and Cole–Davison in the frequency domain are able to describe broad symmetric and asymmetric peaks. The most general one is the model function of Havriliak and Negami (HN function) [41].

2.5.4 β -Relaxation

Localized motions, involving either in-chain movements or side groups laterally attached to the main chain, are the origin this process. This type of local dynamic stays active even when the polymer is in the glassy state [40], that is, when the large length scale backbone motions are frozen.

This process is thermally activated and the temperature dependence of the relaxation rate is found to be Arrhenius-like, that is,

$$\tau = \tau_0 \exp^{\Delta E_a / RT} \quad (2.4)$$

where τ_0 is the pre-exponential factor and E_a is activation energy. For truly activated process, τ_{dc} should be of the magnitude of 10^{12} – 10^{13} Hz. The activation energy is associated with the slope of $\log \tau_{dc}$ versus $1/T$ and depends on both, the internal rotation barriers and the environment of a moving unit.

In the frequency domain, the dielectric β -relaxation displays a broad and in the most cases symmetric loss peak with half widths of four to six decades [41]. The variety of molecular environments (structural heterogeneity) of the

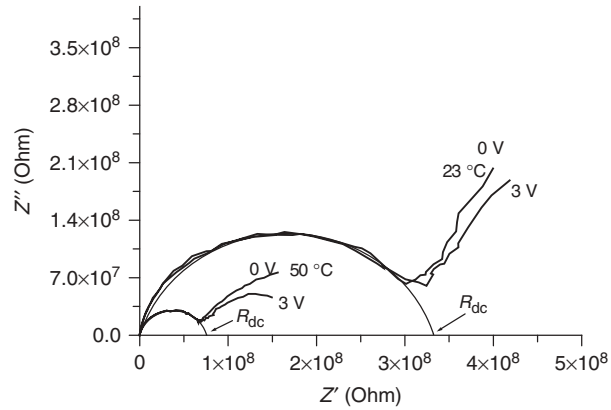


Figure 2.3 Dielectric spectra of wet chitin films at different bias applied voltage. Contact effect is observed when applied voltage is changed from 0 V to 3 V in the quasilinear response (outside the semicircle). *Source:* Reproduced with permission from González-Campos JB, Prokhorov E, Luna-Bárcenas G, Mendoza-Galván A, Sanchez IC, Nuño-Donlucas SM, García-Gaitan B, Kovalenko Y. *J Polym Sci B Polym Phys* 2009;47:932 [5]. Copyright 2009 John Wiley and Sons, Inc.

relaxation unit and, consequently, a variety of energy barriers contribute to the extremely broad peak developing [40]. Generally, dielectric strength ($\Delta\epsilon_\beta$) increases with temperature and it is much lower in the β -relaxation process, relatively to the α -process. The relative strength depends on how much orientation of the dipolar groups can occur through the limited mobility allowed by the β -process.

2.5.5 dc Conductivity Calculation

The dc conductivity (σ_{dc}) of polymer's films can be calculated by dielectric measurements using the methodology previously described by González-Campos et al. [5, 6]. R_{dc} is obtained from the intersection of the semicircle and the real-part axis on the impedance plane ($Z'' = 0$); σ_{dc} can be calculated by the following relationship: $\sigma_{dc} = d/(R_{dc} \times A)$, where d is the thickness and A the area of the film.

In chitin, CS and PVA complex dielectric spectra (Z'' versus Z' plot shown in Fig. 2.3), two different behaviors are identified: (i) a typical semicircle at "high" frequencies, which corresponds to the bulk material signal and (ii) a quasilinear response at "low" frequencies associated with interfacial polarization in the bulk of the films and/or surface and contact effects [46, 47]. This low frequency part of the electrical response is easily influenced by imperfect contact between the metal electrode and the sample; as it was previously tested elsewhere [5], there is no influence of gold contact on the polymer impedance spectra (high frequency part of the spectra corresponding to the bulk of the film) and it is discarded for further analysis.

2.6 CHITIN, CHITOSAN, AND PVA FILMS PREPARATION FOR DIELECTRIC MEASUREMENTS

2.6.1 Chitin Films Preparation

Chitin was purchased from Sigma-Aldrich (1.2% of ash content, 96% degree of acetylation, and bulk density of 1.425 g/ml). Chitin was purified according to the procedure reported in Reference 48. The viscosity average molecular weight, $\overline{M}_v = 300,000$, was determined according to Mirzadeh et al. [49] by means of the Mark–Houwink relationship. Hexafluoroisopropanol (HFIP) was purchased from Sigma-Aldrich and was used as received. Chitin was dissolved in HFIP to prepare a 0.5% w/v solution. This solution was magnetically stirred for 24 h to promote chitin dissolution. Films were prepared by the solvent cast method by pouring the solution into a plastic Petri dish and allowing the solvent to evaporate at room temperature.

2.6.2 Neutralized and Nonneutralized Chitosan Films Preparation

CS medium molecular weight ($M_w = 150,000$ g/gmol) and 82% of degree of deacetylation (DD) reported by the supplier and calculated according to Reference 49 was purchased from Sigma-Aldrich. Acetic acid from J. T. Baker was used as received without further purification. CS films were obtained by dissolving 1 wt% of CS in a 1 wt% aqueous acetic acid solution with subsequent stirring to promote dissolution. As chitin films, CS films were prepared by the solvent cast method by pouring the solution into a plastic Petri dish and allowing the solvent to evaporate at 60 °C. CS films prepared from acetic acid solution have the amino side group protonated (NH_3^+ groups); therefore, the films need to be neutralized. The films were immerse into a 0.1 M NaOH solution for 30 min and washed with distilled water until neutral pH; a subsequent drying step in furnace at 130 °C for 14 h was needed. The results of both neutralized as well as nonneutralized CS films are shown.

PVA, $M_w \approx 89,800$ – $98,000$ g/mol and hydrolysis degree >99%, was purchased from Sigma-Aldrich and used as received. PVA films were obtained by dissolving a known amount of PVA in water to obtain a 7.8 wt% solution under stirring. Films were prepared by the solvent casting method, by pouring the former solution into plastic Petri dishes and allowing the solvent to evaporate at 60 °C.

These films had thicknesses of circa 40 μm measured by a Mitutoyo micrometer. A thin layer of gold was vacuum deposited onto both film sides to serve as electrodes. Rectangular small pieces (4 mm × 3 mm) of these films were prepared for measurements and the contact areas were measured with a digital calibrator (Mitutoyo).

2.6.3 Electrode Preparation for Dielectric Measurements

In both chitin and CS films, a thin layer of gold was vacuum deposited onto both film sides to serve as electrodes, using a device (Plasma Sciences Inc.) with a gold target (Purity 99.99%) and Argon as gas carrier. Gas pressure was set to 30 mTorr and voltage to 0.2 kV. Sputtering time was 4 min onto each side. Rectangular small pieces (5 mm × 4 mm) of these films were prepared for dielectric measurements. The contact area and thickness were measured with a digital calibrator (Mitutoyo) and a micrometer (Mitutoyo), respectively. This method allows obtaining films of circa 10 μm of thickness.

2.7 DIELECTRIC RELAXATIONS IN CHITIN: EVIDENCE FOR A GLASS TRANSITION

2.7.1 Effect of Moisture on Dielectric Spectra

Figure 2.4 shows the dependence of dc resistance, capacitance, and weight loss (TGA measurements) versus temperature for wet chitin (12.3% water). It can be observed that in the temperature range 20–80 °C the resistance increases, and capacitance and weight rapidly decrease. This behavior is caused by a water modification effect on the relaxation mechanism of the matrix since water has a lower resistance and higher dielectric constant. When water is present, biopolymer's resistance decreases; if temperature increases, water evaporates and resistance increases (weight loss in the TGA measurements is registered). When water content is nearly zero (dry annealed), the real dielectric behavior of chitin is revealed. Films with near zero moisture content exhibit higher resistances at room temperature and lower resistance as temperature increases (see window inset in Fig. 2.4,

dry annealed film). In summary, to obtain the dielectric behavior of pure chitin without moisture influence, it is necessary to evaporate it by annealing; otherwise, its evaporation may mask the electrical properties of the biopolymer.

For dry chitin films, we emulated dielectric measuring conditions for TGA measurements: after overnight annealing in an oven at 120 °C, these films were handled in ambient conditions for 10–15 min for TGA measurements (time to weight samples for TGA ~ time for sample handling prior to dielectric measurements). The weight loss, and therefore moisture content, is circa 3.5% (Fig. 2.5), which indicates that chitin reabsorbs water readily during the 10–15 min handling from the oven to the vacuum cell. Hence, a second heat treatment in the vacuum cell before dielectric measurements is needed. These films were reheated at 120 °C in the impedance vacuum cell for 1 h (dry annealed films).

As illustrated in Figure 2.5, the water content in chitin films is circa 12.3% as calculated by TGA. These films were kept at normal ambient conditions before dielectric and TGA measurements and were designated as wet samples. This moisture content is in agreement with those reported for chitin and CS [17, 19, 49].

After this annealing step, no resistance change is observed, indicating that the residual water has been removed. This fact is clearly shown by the Cole–Cole plot in Figure 2.6a. Here, the change of Z'' versus Z' with thermal treatment is greatly affected by its water content. It is noteworthy that the wet chitin sample with no heat treatment shows a completely different behavior as compared to the thermally treated samples. On the other hand, Figure 2.6b shows the commonly used ϵ'' versus frequency plot after dc conductivity correction in the low frequency part of the spectra, and as can be seen, no clear change with heat treatment can be detected; this is

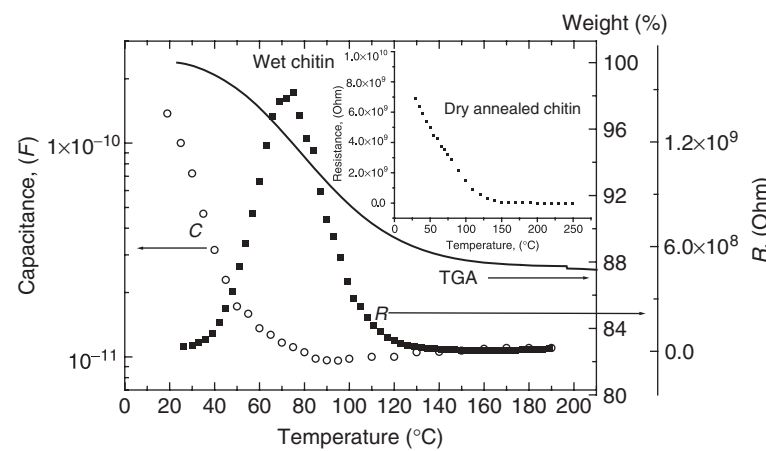


Figure 2.4 Resistance (solid squares) and capacitance (open circles) as a function of temperature for wet film. Thermogravimetric response is also shown. Note that as temperature increases resistance increases due to water evaporation and finally decreases. Window inset shows the opposite behavior for dry film after water evaporation by annealing.

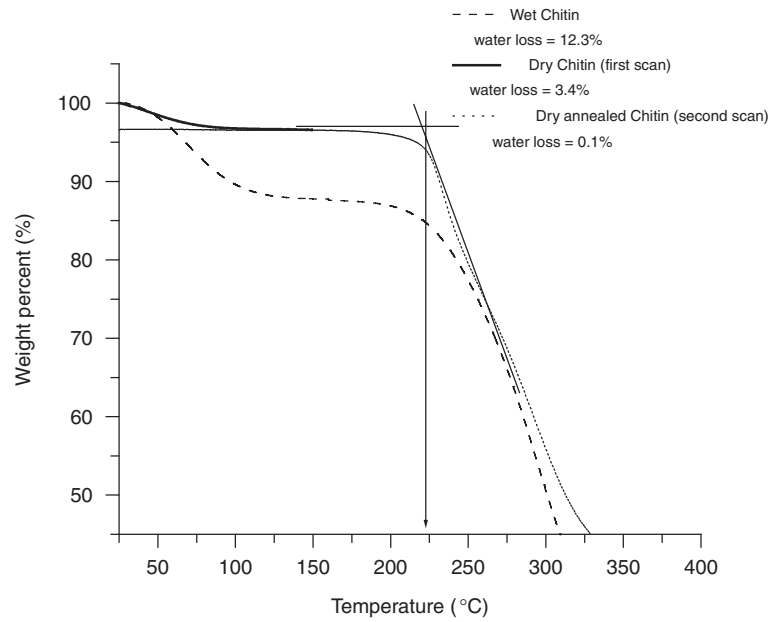


Figure 2.5 Thermogravimetric analysis of solvent-cast α -chitin films. Wet chitin (solid line), dry chitin: first scan (dashed line), and dry annealed chitin: second scan (dash-dotted line) from 20 to 250 °C. Note that above 210 °C α -chitin thermally decomposes. A construction of tangent lines is operationally used to determine the onset of degradation (circa >210 °C). Source: Reproduced with permission from González-Campos JB, Prokhorov E, Luna-Bárcenas G, Mendoza-Galván A, Sanchez IC, Nuño-Donlucas SM, García-Gaitan B, Kovalenko Y. *J Polym Sci B Polym Phys* 2009;47:932 [5]. Copyright 2009 John Wiley and Sons, Inc.

a critical issue since moisture effects are observable in one representation of the dielectric data, but not in the other.

These films are cooled under vacuum from 120 °C to room temperature (20 °C) and then a second measurement is performed in the dry annealed films. To calculate water content on these films, TGA measurements were performed in dry samples (heated at 120 °C in oven overnight). After 1 h at 120 °C (dry annealed films), no further change in weight is observed; the films were cooled to 20 °C and reheated. The second TGA scan for dry annealed chitin films shows free water content of circa 0.1% (dash-dotted line, Fig. 2.5). Using the same annealing methodology in the dielectric and TGA measurements, we can monitor the water content in the samples.

Modulated DSC thermograms (Fig. 2.7) for chitin films after water removal were scanned a second time from 20 to 250 °C. The objective was to see whether a glass transition would manifest. However, as stated in Section 2.1, controversy centers on whether a glass transition can be detected. In our case, there is no clear evidence of the glass transition; hence, it is not possible to draw any conclusion from the thermal analysis. As explained earlier, some authors assign no T_g for chitin [11], while others [12] assign approximately 236 °C for β -chitin, which is in chitin's degradation temperature range (210–280 °C). As can be seen in Figure 2.5 by TGA measurements, the onset

of degradation is about circa 220 °C from the intersection of two tangent lines (by DSC the onset of degradation is circa 210 °C). Other authors report a surprisingly high value of T_g of 350–412 °C for β -chitin, which has a degradation temperature of 450 °C [50].

2.7.2 X-Ray Diffraction Measurements

Crystal structure analysis was performed using a 2100-Rigaku diffractometer equipped with the CuK α radiation ($\lambda = 1.5406 \text{ \AA}$) in the 2θ range from 5° to 55°, at 30 and 120 °C and operating at 30 kV and 16 mA.

It is well known that chitin is a semicrystalline polymer. Consequently, it is necessary to verify whether chitin's crystalline volume fraction changes with heat treatment and its influence on relaxation behaviors. The diffraction pattern of purified α -chitin powder is shown in Figure 2.8. The five characteristic crystalline reflections for α -chitin are present [51]. They are indexed as (020), (110), (120), (101), and (130) for 9.24°, 19.13°, 20.5°, 23.31°, and 26.2°, respectively. α -Chitin has an orthorhombic unit cell with P212121 symmetry [52], indicating an antiparallel arrangement of the chitin chain with intermolecular hydrogen bonding. The peak at $2\theta = 9.24^\circ$ is associated with the most ordered regions involving the acetamide groups [53]. The strongest reflection of an α -chitin crystalline sample is obtained at $2\theta = 19.13^\circ$.

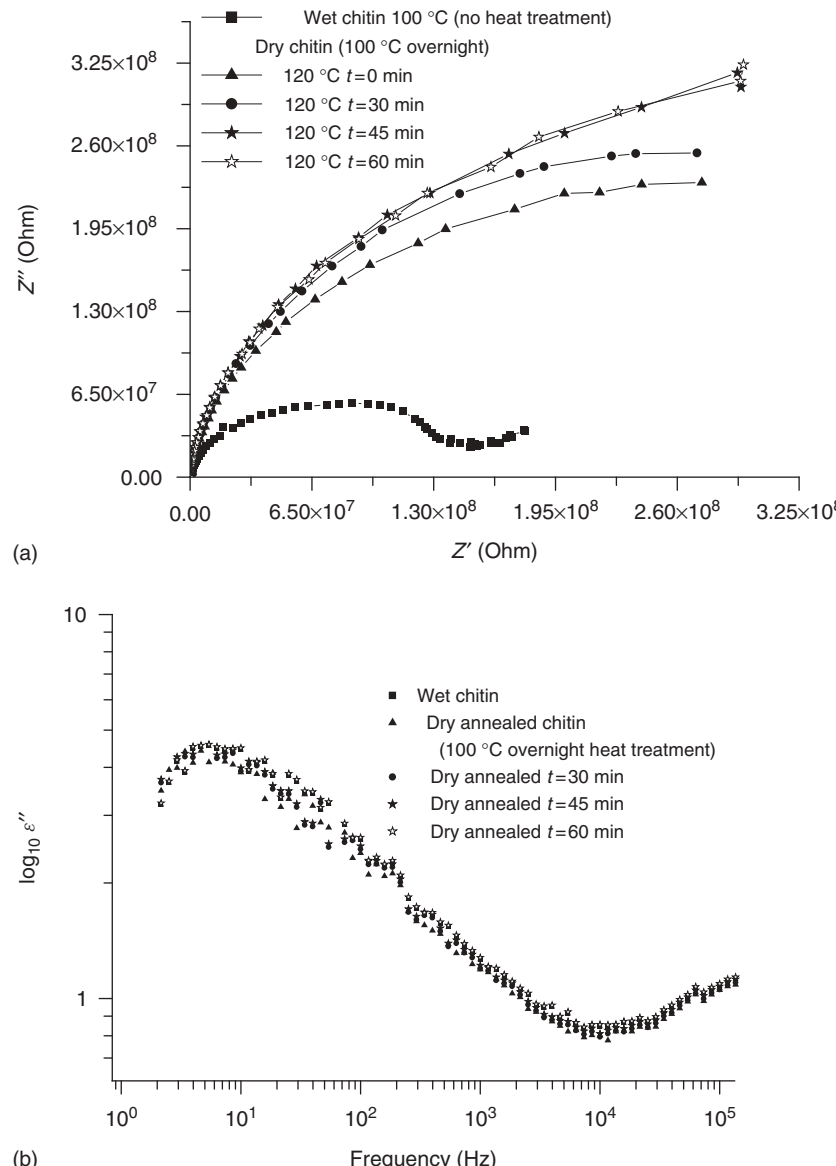


Figure 2.6 (a) Cole–Cole plot for chitin under second heat treatment in vacuum cell. Water completely drives off after 1 h evidenced by no resistance change. (b) $\log 10 \epsilon''$ versus frequency for chitin in vacuum cell; the data were corrected for dc conductivity contribution. Note that conventional plots of $\log \epsilon''$ versus frequency do not show a clearly change in function of time after water removal. *Source:* Reproduced with permission from González-Campos JB, Prokhorov E, Luna-Bárcenas G, Mendoza-Galván A, Sanchez IC, Nuño-Donlucas SM, García-Gaitan B, Kovalenko Y. *J Polym Sci B Polym Phys* 2009;47:932 [5]. Copyright 2009 John Wiley and Sons, Inc.

The estimation of crystalline volume fraction was based on the standard approach that assumes the fact that the experimental intensity curve is a linear combination of intensities of crystalline and amorphous phases. For bulk α -chitin, the crystalline volume fraction is about 30% and about 10% for film samples. A similar behavior was found for CS acetate after dissolution into acid solutions [54].

The films crystalline volume fraction does not change after annealing at 120 °C, and so the amorphous phase volume fraction is constant during the dielectric measurements at the annealing temperature employed. In subsequent analyses, we make the usual assumption that crystalline units are immobile relative to amorphous units and do not contribute to relaxations.

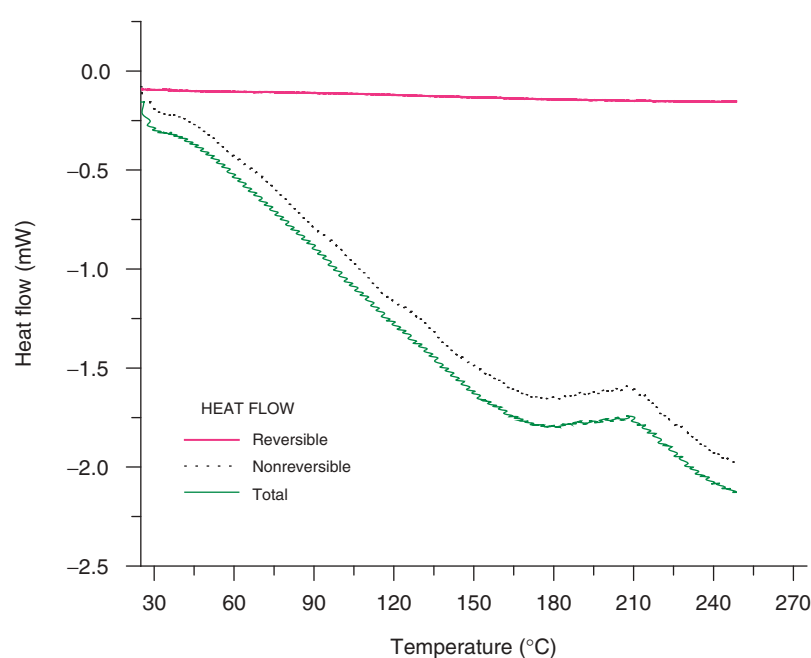


Figure 2.7 DSC analysis for chitin films.

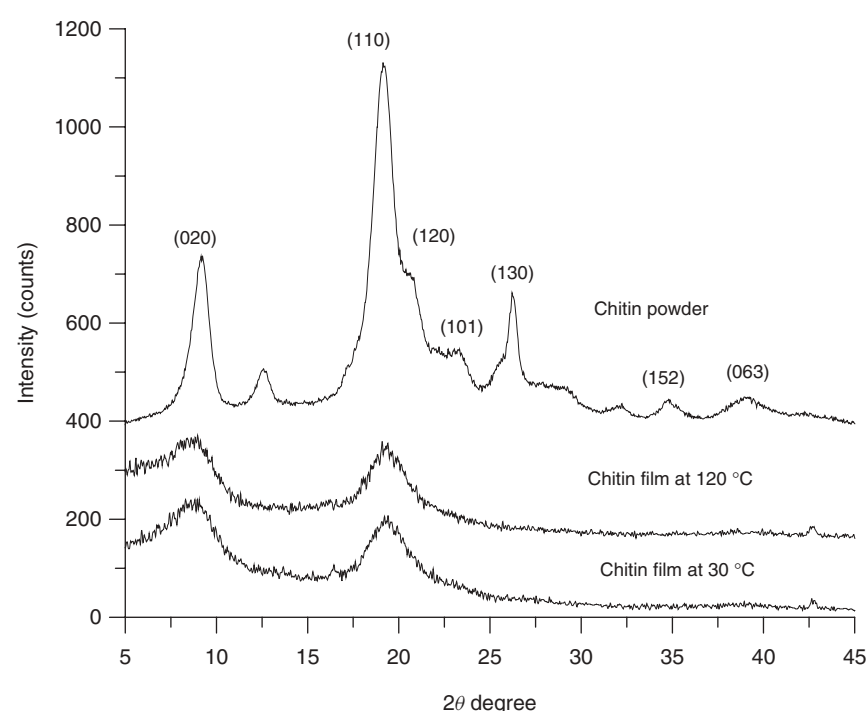


Figure 2.8 X-Ray diffraction pattern for (powder and film) α -chitin. *Source:* Reproduced with permission from González-Campos JB, Prokhorov E, Luna-Bárcenas G, Mendoza-Galván A, Sanchez IC, Nuño-Donlucas SM, García-Gaitan B, Kovalenko Y. *J Polym Sci B Polym Phys* 2009;47:932 [5]. Copyright 2009 John Wiley and Sons, Inc.

2.7.3 Dielectric Spectra: General Features

Figure 2.9 shows the complex Cole–Cole plot for wet (Fig. 2.9a) and dry annealed chitin films (Fig. 2.9b) measured at 25, 50, 70, and 130 °C, respectively. A Cole–Cole type plot of Z'' versus Z' for wet films exhibit characteristic semicircles at high frequencies and a quasilinear response at low frequencies. This behavior is due to the presence of water in the samples, that is, water reduces the resistivity of films and could be modifying the relaxation mechanism of the matrix material.

However, for dry annealed samples (Fig. 2.9b), the semicircle is not fully resolved due to an increase in film's resistivity at 25 °C. As temperature increases, resistivity decreases and the full semicircle starts to appear. For temperatures above 130 °C, the semicircle is now fully resolved. Water evaporation effect in wet and dry samples

is clearly identified when comparing the wide difference in the resistance value at 70 °C in dry annealed and wet samples as it is shown in Figure 2.9a and b. For dry annealed chitin (Fig. 2.9b), resistance drastically decreases as temperature increases, and the opposite behavior is present in wet samples (Fig. 2.9a); it means that heat treatment allows unmasking the real electrical properties of dry annealed chitin present below 70 °C. For wet samples, water evaporation on heating increases chitin resistivity response; however, this trend changes above 70 °C once water has been removed and water effect vanishes.

The same dielectric behavior in dry annealed and wet samples is developed above 110 °C. These observations are very important since they suggest an extra relaxation process [16] in the absence of water, which is analyzed in detail in the next section. On the other hand, the linear response at low frequencies in wet and dry chitin can be associated with interfacial polarization in the bulk films and/or surface and metal contact effects [47]. To analyze the dielectric relaxation of chitin films is necessary to understand the nature of the low frequency part of dielectric spectrum.

2.7.3.1 Electrode and Interfacial Polarization Effects

It is well known that contact metal–polymers for many systems can be interpreted as Schottky barriers [55–57] or heterojunction [58, 59]. To test the influence of gold contact on the chitin dielectric spectra, a nonsymmetrical contact array was prepared in the following manner: a circular chitin film was covered on one side with a piece of gold sheet with a small circular orifice in the center during gold-sputtering. The other side of the film was totally gold-sputtered. This way a top surface available for electrode contact is circa 0.008 cm^2 . The bottom surface area is circa 0.75 cm^2 . Because of contact surface area differences, the current depends on the properties of the top electrode.

Figure 2.10 shows dielectric measurements on wet chitin sample with different applied bias voltage at 23 and 50 °C. The bias increase leads to a reduction of barrier resistance that changes the low frequency contribution of dielectric spectra (which occur at large values of Z'). As can be seen, a deviation from a semicircle is seen at both temperatures, and the response depends on the bias voltage. These data are a good indication of contact polarization effects related to the (partial) blocking of charge carriers at the sample/electrode interface [60]. This low frequency part of the electrical response is easily influenced by imperfect contact between the metal electrode and the sample. In fitting dielectric data to models, this low frequency data needs to be discarded.

In addition to this electrode polarization, interfacial polarization effects are observed in the high temperature range (>170 °C) for all chitin films. This effect manifests as a “bulge” on the semicircle. Figure 2.10 illustrates this

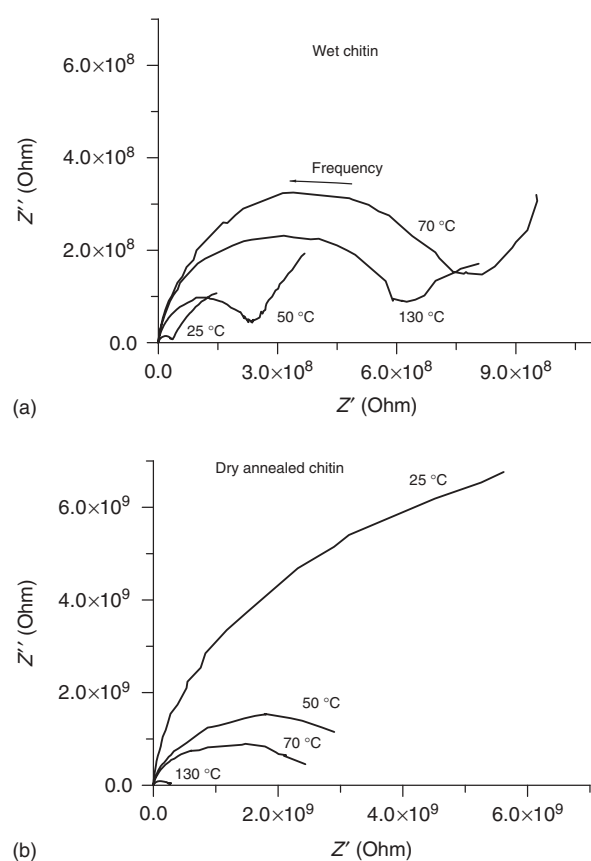


Figure 2.9 Complex dielectric spectrums of wet and dry annealed chitin films. Note the strong free water effect: for wet samples, resistance increases as temperature increases. An opposite effect is observed in dry annealed samples. *Source:* Reproduced with permission from González-Campos JB, Prokhorov E, Luna-Bárcenas G, Mendoza-Galván A, Sanchez IC, Nuño-Donlucas SM, García-Gaitan B, Kovalenko Y. *J Polym Sci B Polym Phys* 2009;47:932 [5]. Copyright 2009 John Wiley and Sons, Inc.

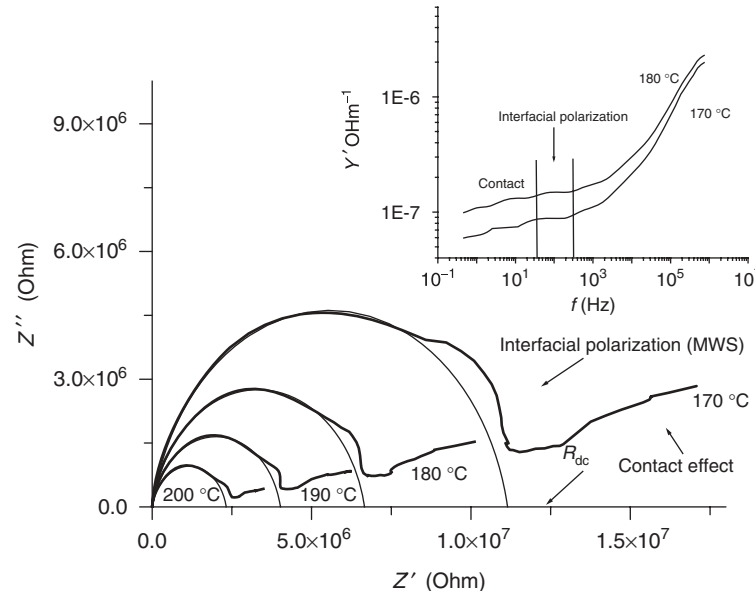


Figure 2.10 Dielectric spectra of chitin films with Maxwell–Wagner (MW) polarization at low frequency and high temperature. Interfacial polarization can be detected by the appearance of an extra semicircle. *Source:* Reproduced with permission from González-Campos JB, Prokhorov E, Luna-Bárcenas G, Mendoza-Galván A, Sanchez IC, Nuño-Donlucas SM, García-Gaitan B, Kovalenko Y. *J Polym Sci B Polym Phys* 2009;47:932 [5]. Copyright 2009 John Wiley and Sons, Inc.

effect at 170, 180, 190, and 200 °C. This is a common form of a discontinuity occurring in an inhomogeneous solid dielectric associated with internal interfaces; it is well known as the Maxwell–Wagner–Sillars (MWS) relaxation. The simplest model to describe interfacial polarization is the MWS double-layer model where each layer is characterized by its permittivity and conductivity. An equivalent circuit for interfacial polarization is constructed of two RC elements in series [9]. In polysaccharides [20] and biopolymers [21], the interfacial polarization (MWS polarization) was observed in low frequency and high temperature ranges. According to the classical model, the appearance of the interfacial polarization in dielectric spectrum can be observed as appearance of additional semicircle [41].

In the low frequency range, both contact and interfacial polarizations were observed in all samples. These polarizations have to be carefully considered; it is important to take into account only the so-called depressed semicircle that does not include contact and interfacial polarization effects.

Another critical issue is depicted in the inset of Figure 2.9. For most polysaccharides, a commonly used plot of admittance versus frequency does not reveal the appearance of the extra semicircle related to interfacial polarization. It is noteworthy that data treatment proposed in this study allows one to identify and separate these

two processes (contact and interfacial polarization effects). A model-based analysis can be misleading if appropriate contact and interfacial polarizations are not considered.

2.7.3.2 dc Conductivity Correction A correction must be applied to all samples (specially the wet ones) since they exhibit a large conductivity contribution in the low frequency range. This dc conductivity strongly modifies the dielectric loss factor ϵ'' on the low frequency side (see Fig. 2.10 at 80 °C) where dielectric effects are completely masked. In this case, the ϵ'' can be expressed with Equation 2.2.

Commonly, ac conductivity is measured in the low frequency range where a plateau is expected to appear [20]. However, in our samples, this plateau is not resolved, as a consequence polarization and contact effects cannot be discerned and the correct dc conductivity cannot be calculated by this method (see inset in Fig. 2.10). To circumvent this problem, the alternative procedure described in Section 2.5.5 can be used.

2.7.3.3 Dielectric Relaxations Analysis Figure 2.11 shows the permittivity loss coefficient (ϵ'') data for dry annealed chitin before (80 °C, solid triangles) and after dc conductivity correction (open triangles). From dielectric measurements the frequencies at which contact/polarization effects become relevant (about 2 Hz for the contact effects

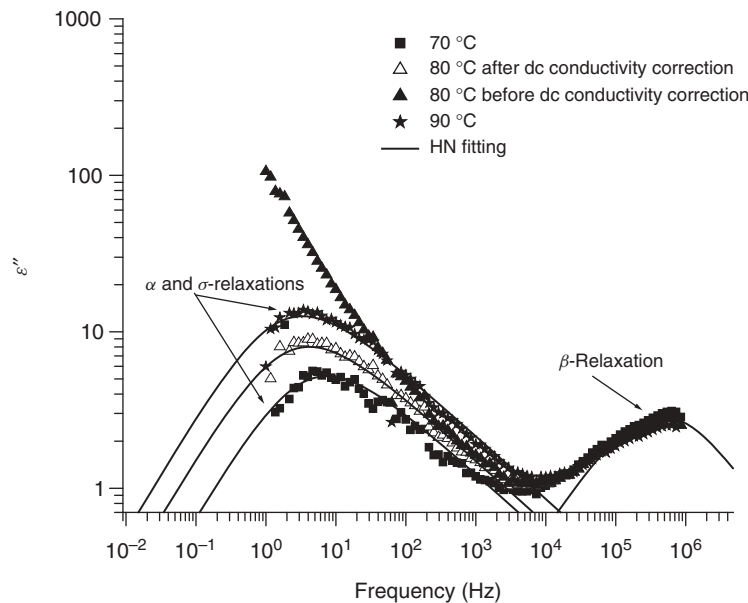


Figure 2.11 Loss coefficient curve (ϵ'') versus log frequency. *Source:* Reproduced with permission from González-Campos JB, Prokhorov E, Luna-Bárcenas G, Mendoza-Galván A, Sanchez IC, Nuño-Donlucas SM, García-Gaitan B, Kovalenko Y. *J Polym Sci B Polym Phys* 2009;47:932 [5]. Copyright 2009 John Wiley and Sons, Inc.

and about 100–300 Hz for polarization effects at the temperatures higher than 170 °C) have been estimated and are not considered for further analysis; above 80 °C a low frequency relaxation with Arrhenius temperature dependence (as will be shown later) is revealed, and below 80 °C a different relaxation with a non-Arrhenius temperature dependence that we designate as the primary or α -relaxation is disclosed. A similar behavior is seen at lower temperatures (not illustrated). Also notice in Figure 2.11 that the well-known β -relaxation found in β -chitin and CS [20, 21] is present on the high frequency side of the spectrum.

The activation plot of relaxation time for the non-Arrhenius dependence present in the low frequency range below 80 °C (Fig. 2.11) was obtained using the empirical HN [20]. For secondary relaxations with Arrhenius behavior, we used the Cole–Cole simple model [9] to obtain the activation plot for relaxation time. Some authors [21, 61] have used the model of HN to describe relaxations in polysaccharides. However, this requires more adjustable parameters. On the other hand, several authors have shown that these secondary relaxations are well described by the simpler Cole–Cole model (HN model with $\beta = 1$); this model has been successfully applied for the fitting of lateral group motions representing the β -relaxation [18, 62–64] and for describing the motion of ions ascribed to the α -relaxation [65].

For β -chitin as well as for various cellulose-based materials, starches, and nonpolymeric glass forming liquids, it was found that the activation energies from the dc

conductivity plot and the dielectric α - and β -relaxation times (or α -peak frequency) are well correlated [66–68]. In glass-forming liquids, at high temperatures, both dc conductivity and relaxation time show an Arrhenius behavior with the same activation energy. Below a cross over temperature (T_c), a VFTH behavior was observed [68].

The two different temperature dependencies described above for glass-forming liquids are present in α -chitin, and the similarity between dc conductivity and relaxation time for the two low frequency relaxations is clearly observed in Figure 2.12a and b. Both dependencies (dc conductivity (σ_{dc}) and relaxation time (τ) versus $1/T$ plots) show the same features: an Arrhenius type relaxation will yield a straight line above 80 °C, whereas a non-Arrhenius relaxation will manifest as a curved line that suggests a VFTH type or glass transition below 80 °C in dry annealed samples. For wet and dry samples, the decrease of conductivity as the temperature is increased from 20 to 80 °C is likely due to the motion of water–polymer complex since water could be modifying the relaxation mechanism of the matrix material.

At higher temperatures, a thermally activated behavior similar to that of dry annealed chitin is recovered. For all chitin samples, the dc conductivity decreases and relaxation time increases (see Fig. 2.12a and compare with Fig. 2.12b) as temperature increases until circa 210 °C. This temperature signals polymer degradation; in agreement with thermogravimetric analysis in Figure 2.5, the onset of degradation is about 210 °C. Nonreversible degradation

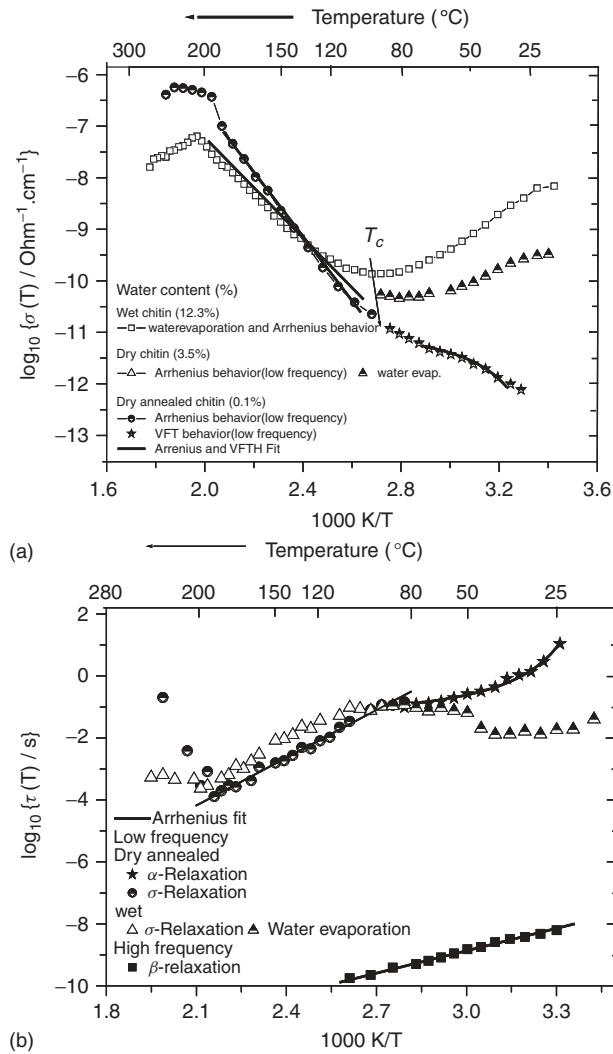


Figure 2.12 (a) Low frequency dc conductivity dependence with reciprocal temperature $1/T$ for wet and dry annealed α -chitin. (b) Relaxation time dependence versus $1/T$ at low frequency. *Source:* Reproduced with permission from González-Campos JB, Prokhorov E, Luna-Bárcenas G, Mendoza-Galván A, Sanchez IC, Nuño-Donlucas SM, García-Gaitan B, Kovalenko Y. *J Polym Sci B Polym Phys* 2009;47:932 [5]. Copyright 2009 John Wiley and Sons, Inc.

at high temperatures ($T > 210^\circ\text{C}$) is common to many polymers and polymer blends [69, 70].

Low Frequency Relaxations

THE LOW TEMPERATURE RELAXATION Although three different sample types are illustrated in Figure 2.12a and b (wet, dry, and dry annealed), let us focus on the dry annealed sample containing minimal moisture ($\sim 0.1\%$). Above 80°C , the temperature dependence is linear (Arrhenius), whereas below 80°C it is non-Arrhenius. This shows

that in this low frequency range (0.1 Hz to 1 MHz) a transition between two dynamical regions occurs at a crossover temperature (T_c) of $\sim 80^\circ\text{C}$. This crossover temperature, discussed by Ferrari et al. [71], separates a cooperative motional process that obeys the VFT equation from an activated process, described by Arrhenius equation. It can also be considered as the temperature where cooperative motion of the α -relaxation sets in [68]. Schönhals et al. [72] as well as Cutroni et al. [68] showed similar behavior for glycerol and propylene glycol.

For most polymers, the relationship between the glass transition temperature T_g and T_0 is $T_g = T_0 + C$ where C is a constant that in many dielectric studies is about 50 K [9, 73, 74]. On the basis of the usual uncertainty in C and the above $T_0 = 285\text{ K}$, we estimate that T_g for dry annealed chitin is $62 \pm 10^\circ\text{C}$. This low value for the T_g of a stiff polymer such as α -chitin is slightly surprising, but it is consistent with the low T_g 's found in polypeptides (-70 to -50°C) [75–77]. The common denominator between polysaccharides and polypeptides is extensive hydrogen bonding; significant thermal disruption of H-bonding and the onset of main chain molecular motions are probably closely related.

HIGH TEMPERATURE RELAXATION Even though the α -relaxation in amorphous polymers exhibits the typical VFT behavior in the whole temperature range above T_g , this is not the case for β -chitin and other hydrogen bonding polymers such as polypeptides [75]. In polysaccharides, there is another mechanism that intervenes and can mask the α -relaxation or glass transition. This activated process agrees very well with the σ -relaxation, which according to Reference 20 is thought to be associated with proton mobility. From the slope of the conductivity plot and relaxation time calculated with the Cole–Cole empirical model (HN equation with $\beta = 1$), it can be seen that above 80°C the commonly VFT behavior developed by the α -relaxation changes to Arrhenius behavior to the onset of degradation. The activation energy for this σ -relaxation is calculated to be $113 \pm 3\text{ kJ/mol}$ for dry annealed chitin and $89 \pm 1\text{ kJ/mol}$ in wet samples. These values agree with those reported for other polysaccharides (95–110 kJ/mol) [66] in the high temperature range ($>80^\circ\text{C}$) (Table 2.1) and the closely related CS [21].

High Frequency Relaxation As illustrated in Figure 2.11, in dry annealed chitin samples, a high frequency secondary relaxation is observed, the so-called β -relaxation. This relaxation is found in other polysaccharides [66] and is thought to be associated with molecular motions via the glucosidic bond [20, 61]. The fitting parameter $\alpha = 0.45 - 0.49 \pm 0.08$ and the intensity of β -relaxation have a weak dependence on temperature. $\beta = 1$ values in the HN model describe a symmetric relaxation by the simple Cole–Cole model. It can be seen

TABLE 2.1 Parameter Values for the Arrhenius-Type Dependence in σ -Relaxation from dc Conductivity and Relaxation Time. Low Frequency Relaxation in the 80–210 °C Range

Sample	Conductivity Relaxation Time		
	$E_{a\sigma}$	σ_0 (S cm ⁻¹)	$E_{a\tau}$ (kJ/mol)
Wet chitin (this study)	88.9 ± 1	79.8 ± 2.2	91.9 ± 4.4
Dry annealed chitin (this study)	113.2 ± 3	1.32 × 10 ⁵ ± 2.6	110.7 ± 3.7
Polysaccharides Einfeldt et al. [20]	—	—	95–110
Chitosan (dry annealed) Viciosa et al. [21]	—	—	Not reported
		94 ± 2	0.2 × 10 ⁻¹⁶

TABLE 2.2 Arrhenius Parameters for the Secondary Relaxation Process Found at High Frequencies

	β -Relaxation	
	E_a (kJ/mol)	τ_0 (s)
<i>Einfeldt et al.</i> [20]		
β-Chitin	44.7	3.9 × 10 ⁻¹⁶
<i>Viciosa et al.</i> [21]		
Chitosan	49.0 ± 1	0.44 ± 0.07 × 10 ⁻¹⁶
<i>This Study</i>		
α-Chitin (dry annealed)	44.6 ± 0.9	1.33 × 10 ⁻¹⁶

that the experimental data could be well fitted to the Cole–Cole model, involving less number of parameters in agreement with other authors [9, 62, 63]. The temperature dependence of the relaxation time is Arrhenius with activation energy of 45 ± 1 kJ/mol for dry annealed chitin (Table 2.2) in agreement with previous reports on β-chitin and CS [20, 21]. The same Arrhenius behavior is kept above and below the glass transition temperature.

2.7.4 Chitin Molecular Relaxations Conclusions

Impedance spectroscopy measurements have been used to investigate molecular dynamics in α-chitin. After dc conductivity correction, the exclusion of contact and interfacial polarization effects, and obtaining a condition of minimum moisture content (~0.1%), the α-relaxation process that likely represents the glass transition is unveiled.

The α-relaxation in dry annealed α-chitin can be observed by DS measurements. On this basis, the glass transition temperature was estimated at 61 ± 10 °C. Moisture content is a key factor to observe the glass transition in chitin and it could be related to the controversy about the glass transition temperature detection and designation in this biopolymer.

The secondary β-relaxation is also observed in α-chitin from 80 °C to the onset of thermal degradation (~210 °C). It exhibits a normal Arrhenius-type temperature dependence with activation energy of 113 ± 3 kJ/mol.

Finally, a high frequency secondary σ-relaxation is observed in dry annealed chitin with Arrhenius activation energy of 45 ± 1 kJ/mol comparable to that occurring in β-chitin, CS, and cellulose.

2.8 DIELECTRIC RELAXATIONS IN NEUTRALIZED AND NONNEUTRALIZED CHITOSAN: THE STRONGER WATER CONTENT EFFECT ON THE α-RELAXATION AND THE GLASS TRANSITION PHENOMENON

2.8.1 Low Frequency Relaxations: The Influence of Moisture Content on Dielectric Measurements

Once contact and interfacial polarization were discarded and dc corrections are carried out, high and low frequency relaxations are identified in CS films. Figure 2.13 shows the \log_{10} conductivity versus $1/T$ dependence in the low (10^0 – 10^3 Hz) and high (10^3 – 10^6 Hz) frequency ranges. Both neutralized and nonneutralized films with different moisture contents show similar behavior; the nonneutralized CS films show higher conductivity values, which could indicate higher mobility and/or number of conducting species (NH_3^+ groups) [21]. Once again, these low frequency relaxations can be analyzed in two different temperature ranges: the nonlinear “low temperature relaxation” with the characteristic trend of the glass transition phenomenon present from 20 to 70 °C, and the Arrhenius-type “high temperature relaxation” from 70 °C to the onset of degradation ~210 °C.

2.8.1.1 Low Temperature Relaxation The low temperature relaxation is highly influenced by moisture content; in wet samples, the conductivity decreases as water evaporates, disguising the actual dielectric properties of CS above 100 °C, while for moisture contents lower than 3 wt% and higher than 0.5 wt% (dry films), a non-Arrhenius behavior appears. However, in dry annealed CS (moisture contents <0.05 wt%), this low temperature relaxation vanishes after the second heat treatment.

As in chitin, the \log_{10} conductivity versus $1/T$ also shows the nonlinear behavior developed in dry samples. This nonlinear dependence is the typical trend of the

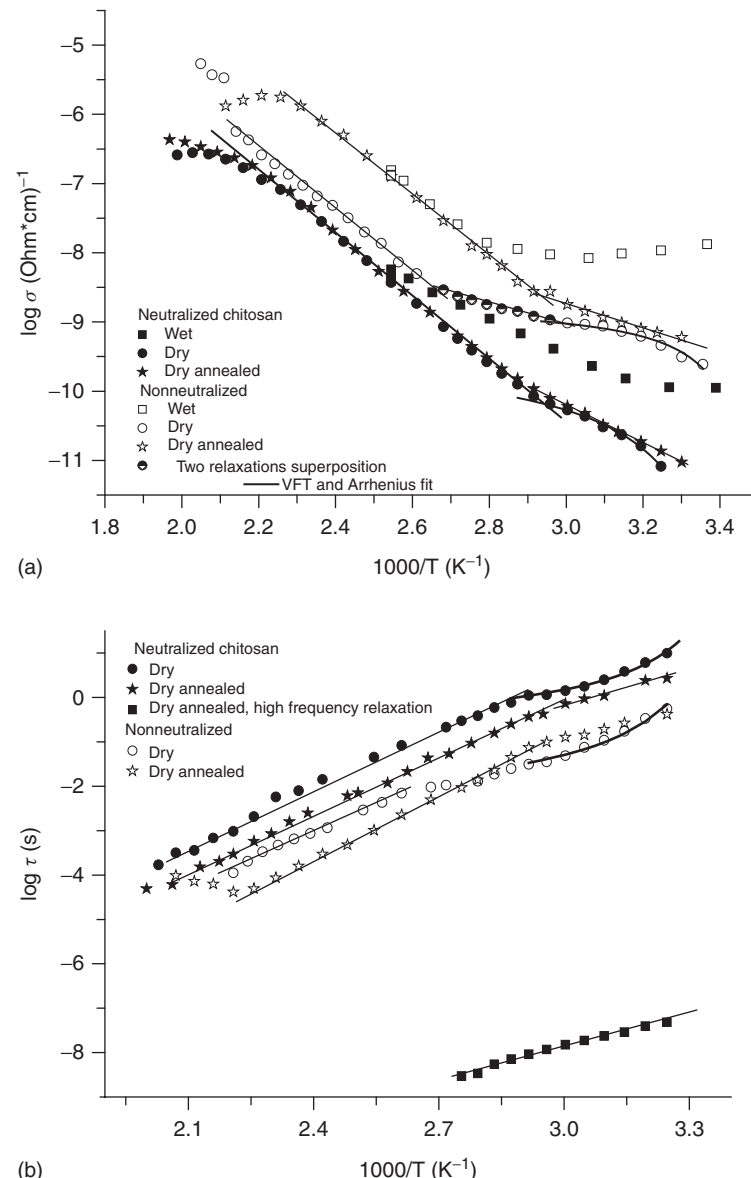


Figure 2.13 (a) $\log_{10} \sigma$ versus $1/T$ for wet, dry, and dry annealed chitosan (neutralized and nonneutralized). (b) \log_{10} relaxation time versus $1/T$. Source: Reproduced with permission from González-Campos JB, Prokhorov E, Luna-Bárcenas G, Fonseca-García A, Sanchez IC. J Polym Sci B Polym Phys 2009;47:2259 [6]. Copyright 2009 John Wiley and Sons, Inc.

α -relaxation behavior related to the dynamic glass transition [9, 37]. The temperature dependence of conductivity and relaxation time calculated are well described by the VFT equation [9]. There is an excellent agreement between the Vogel temperature calculated by conductivity and relaxation time independently ($T_0 = 284$ K in both cases). Note that nonneutralized films exhibit higher conductivity than the neutralized ones, which is consistent with the excess number of protons in the nonneutralized films (NH_3^+ groups are present). In addition, the T_0 value is independent of the presence of NH_3^+ groups. With this T_0 value, a T_g value

can be estimated for neutralized and nonneutralized CS of 61 °C.

A strong effect of moisture content on the VFT behavior describing the α -relaxation process is evidenced in Figure 2.14, since for dry samples the glass transition temperature shifts to higher values as moisture content decreases. It is possible to identify this effect when different annealing temperatures (Fig. 2.13) are used during measurements on the same sample. This shifting of the glass transition temperature to higher values for lower moisture contents suggests a plasticizing effect of water

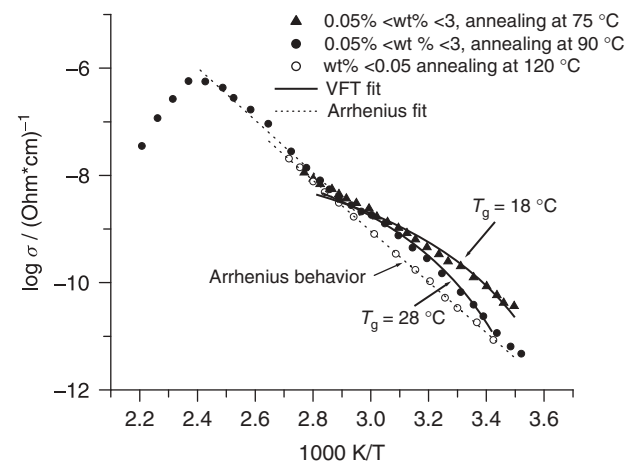


Figure 2.14 \log_{10} conductivity versus $1/T$ for nonneutralized chitosan. Source: Reproduced with permission from González-Campos JB, Prokhorov E, Luna-Bárcenas G, Fonseca-García A, Sanchez IC. J Polym Sci B Polym Phys 2009;47:2259 [6]. Copyright 2009 John Wiley and Sons, Inc.

on CS glass transition. In our case, the accurate moisture content in the 0.05–3 wt% range according to the annealing treatment at different temperatures is difficult to determine since all the measurements are performed in a vacuum cell. However, it is noteworthy that moisture contents between 0.05 and 3 wt% are needed to distinguish the α -relaxation process by dielectric measurements before it vanishes at 0.05 wt% moisture content with the 120 °C annealing treatment (Figs 2.13a and b, and 2.14).

As mentioned before, there exists a great controversy about the glass transition temperature (T_g) of CS; some authors show no evidence of a glass transition by DSC, DMTA, and dielectric measurements [19–21], while others report a wide variety of values. Sakurai et al. [18] assigned a T_g of 203 °C in nonneutralized films by DSC and DMTA techniques; however, our TGA, DSC (Figs 2.5 and 2.6), and dielectric measurements show that this value is very close to chemical degradation. Additionally, to eliminate the effect of moisture, Sakurai et al. [18] performed two cycles of heating and cooling runs by heating up to 180 °C; however, as previously explained, degradation of CS starts at 170 °C. Liu et al. assigned a T_g of 91.8 °C [17]. It is not clear if their DSC measurements come from the first or second scan; this result seems to correspond to water elimination rather than a glass transition.

Lazaridou et al. [78] estimated a $T_g \sim 95$ °C, by DMTA measurements, for dry CS through the relationship between T_g and moisture in samples with an empirical equation. Using the same technique, Toffey et al. [79] determined a $T_g = 82$ °C for CS acetate. Quijada-Garrido et al. [80] by DSC measurements found no glass transition evidence; however, by DMTA they assigned ~ 85 – 90 °C (depending

on frequency). Mucha et al. [16] reported an α -relaxation assigned by DMTA measurements in the 156–170 °C range and by DSC in the range of 170–180 °C. They also found other molecular relaxation at 43 °C, which lies in the temperature range proposed in the present work. However, Mucha et al. [16] relate this molecular event to reorganization of packing of CS molecules due to an increase of residual water mobility, volume expansion, and following a change of hydrogen bond strength. Dong et al. [4] by four different techniques (including DMTA) assigned 140–150 °C as the glass transition temperature of CS. Kaymin et al. [81], using linear dilatometry and thermomechanical analysis, stated 55 °C as the glass transition temperature, which is very close to the result presented in this work.

CS has functional groups such as hydroxyls, amines, and amides, which can act as hydrogen bond acceptors or donors. For this reason, CS can be bonded or linked with hydrogen bond donors or acceptor compounds like water [80]. In the case of glass transition temperature, plasticization occurs only in the amorphous region, such that the degree of hydration is quoted as moisture content in the amorphous region [82]. As reported in the literature review, in these biopolymers, water can be present in three states: (i) nonfreezing water, (ii) freezable bond water, and (iii) free water [38, 80, 66]. According to Reference 83, the water sorption mechanism is composed of two main steps: water sorption on polymer sites and water clustering surrounding the first absorbed water molecules.

The α -relaxation process is strongly affected by the moisture content in the films as shown in Fig. 2.13a and b. While at percentages higher than 3 wt%, this process cannot be distinguished because of the free water effect, at lower percents (<3 wt% freezable bond water) a glass transition temperature can be assigned by the motion of a water–polymer complex in amorphous regions; a glass transition temperature can be assigned depending upon moisture content limited to be between 0.05 and 3 wt%. According to Reference 80, the glass transition must be interpreted as torsional oscillations between two glucosamine rings across glucosidic oxygens and a cooperative hydrogen bonds reordering. Water sorption in hydrophilic polymers is usually a nonideal process leading to plasticization [83]. Water leads to an increase in the amounts of hydrogen bonds producing an increase in cooperative motion. Water hydrogen bonds between CS chains and increases free volume. When this happens, chains can slide past each other more easily, and so the time scale of the cooperative motion matches that of the experiment and the glass transition can be detected.

If sample moisture is minimized (<0.05 wt%), chains are able to interact with each other giving rise to a denser packing. Thereby, the mobility of polymer chains decreases and the glass transition phenomenon is not easily detected.

Because of the absence of water, the glass transition temperature could shift to temperatures above 70 °C (more rigid backbone). Ogura et al. [84] report by DMA analyses that chitin and CS's dynamic mechanical properties of wet films were greatly affected by the presence of water. For chitin, they observed a loss peak at 50 °C and it was attributed it to the glass transition of chitin plasticized with water. Regarding dry CS films, a glass transition was assigned at circa 140 °C [82]. However, these results are not theoretically connected to a glass transition, and so it is difficult to assign the observations to a specific molecular relaxation.

When water is minimized (0.05 wt% of water, Fig. 2.13a) and plasticization is absent, the glass transition temperature could shift to higher temperatures. At this point (above 70 °C), another molecular relaxation takes place and the α -relaxation is weaker and cannot be observed because of the high temperature relaxation effect; this is clearly observed in dry annealed CS below 70 °C (Fig. 2.13a and b) by a change of the VFT behavior to a linear one with a different slope than that for the high temperature process. This “new” slope is a behavior halfway between the nonlinear VFT behavior and the Arrhenius high temperature one, since under certain conditions of minimum moisture, the high temperature relaxation process is observed in the whole temperature range before the onset of thermal degradation as shown in Figure 2.14.

The controversy and particularly the discrepancy in the glass transition temperature of CS can be related to an inefficient elimination of water, a heat treatment near the degradation temperature of CS, the film preparation technique, neutralization process, or even deacetylation degree (%DD) (even though Dong et al. [4] showed no %DD influence on T_g value, Maria Mucha et al. [16] found the opposite). But without doubt, the moisture content determines whether the glass transition temperature in CS can be observed. As it can be seen, the presence of water drastically affects the CS backbone mobility, especially in the α -relaxation region that corresponds to the cooperative motion. Moisture content is probably the main cause of the wide glass transition temperatures range reported in literature.

2.8.1.2 High Temperature Relaxation The “high temperature” relaxation arises at 80 °C until the onset of degradation ~210 °C (Figs. 2.13a and b). It can be well described by the Arrhenius model and is present in both neutralized and nonneutralized CS. The slope of these curve represent the activation energy of each process. The temperature dependence of dc conductivity and relaxation time are Arrhenius type. For this relaxation, nonneutralized CS films seem to be more sensitive to water, since in the dry state

presents a particular behavior in the 70–100 °C temperature range, which is recognized as a superposition of two relaxation processes, giving raise a different slope value.

The shape of this relaxation seems to be symmetric; the HN fitting parameters [9] $\alpha = 0.72 \pm 0.08$ and $\beta = 1.0 \pm 0.09$ are temperature independent in both CS forms, in agreement with previous studies [20]. A value of $\beta = 1$ describes a symmetric relaxations that can be described by the simpler Cole–Cole model. It can be seen that the experimental data could be fitted with the Cole–Cole model involving less parameters in agreement with other authors [62, 65].

Activation energy calculations are in agreement with previous reports for neutralized and nonneutralized CS [21, 5] and for polysaccharides [20]. The activation energy values for both films are quite close. Einfeldt et al. [20] observed this relaxation process in the high temperature range (>80 °C); however, on minimum moisture conditions (Figs 2.13 and 2.14), this relaxation process discloses in the whole temperature range until the onset of thermal degradation. This process, the so-called σ -relaxation, has been widely studied and is associated with the hopping motion of ions in the disordered structure of the biomaterial [20].

For the case of nonneutralized films, moisture has a strong effect on the σ -relaxation. This is shown in the dry nonneutralized samples in the 70–100 °C temperature range with moisture content in the range of 0.05–3.5 wt% (Figs 2.13a and 2.14). Note that a lower slope (lower activation energy) ascribed to the superposition of α - and σ -relaxations (as explained above) describes this “new” Arrhenius-type σ -relaxation for nonneutralized films. Activation energy is circa $E_{a\sigma}$ (conductivity) ≈ 28.8 and $E_{a\tau}$ (time relaxation) ≈ 38.34 kJ/mol, which is much smaller than that of neutralized films with similar moisture content (~80–85 kJ/mol; Table 2.2). The activation energy value of the relaxation time for the σ -relaxation process in the dry samples shows that water exerts a greater effect on the nonneutralized CS form; this is because of its superior ability to form hydrogen bonds providing a lower activation barrier for motion of ions. In this CS form, the σ -relaxation process is shifted to slightly higher frequencies compared to neutralized CS as shown in Figure 2.15. This implies lower relaxation times (Fig. 2.13b) and lower pre-exponential factor values (Table 2.1). As mentioned before, the nonneutralized films possesses higher conductivity conferred by NH_3^+ groups, and so ion mobility in nonneutralized CS is facilitated than in neutralized samples. Solid lines represent the HN fitting; it is in excellent agreement with the experimental results.

Pizzoli et al. [85] by DMA and dielectric measurements observed a “high temperature relaxation” near 140 °C; the calculated activation energy was ~100 kJ/mol, and this value is in agreement with the activation energy of the

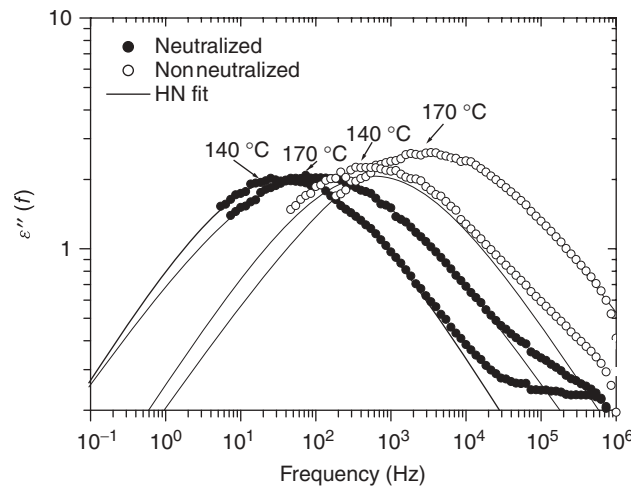


Figure 2.15 Loss factor (ε'') versus frequency. σ -Relaxation process shifts to higher frequencies with temperature for non-neutralized chitosan. *Source:* Reproduced with permission from González-Campos JB, Prokhorov E, Luna-Bárcenas G, Fonseca-García A, Sanchez IC. *J Polym Sci B Polym Phys* 2009;47:2259 [6]. Copyright 2009 John Wiley and Sons, Inc.

σ -relaxation mentioned before. They did not interpret it as a glass transition and suggested that this relaxation arises from a molecular motion having a less cooperative character than the glass-to-rubber transition. Some authors have attributed this relaxation to the glass transition [4, 16]; nonetheless, it seems to be ion motion that yields this peak in dynamic mechanical spectra and not the glass transition, because the activation energy for segmental mobility should be greater.

A change from positive slope in the conductivity (Fig. 2.13a) to negative in the relaxation time (Fig. 2.13b) plots is present at 210 °C and above; it denotes the onset of degradation, at this temperature the dependence of resistance and capacitance versus temperature also experiment a change in the slope (not shown). TGA and DSC (not shown) measurements confirm this degradation.

The large decreases of the electrical conductivity, which have been observed for all those materials, correspond to an irreversible chemical degradation of the polymer film. During heating, CS films change color from white to brown at temperatures above 200 °C. This effect has also been reported for fibrous CS [86], which changed color from white to pale yellow at 140 °C and to yellowish brown at 160 °C. DSC and TGA analyses have shown that CS's thermal degradation starts about 170 °C [87, 88].

2.8.2 High Frequency Relaxation

In the high frequency region (104–108 Hz) for dry and dry annealed neutralized and nonneutralized CS, a secondary relaxation process is identified as β -relaxation. In wet

(11% moisture content) samples, this relaxation is not well resolved and model-fitting is complicated. This is the reason we cannot identify the β_{wet} relaxation process documented by other authors attributed to motion due to biopolymer-swollen water [85, 88]. For wet polysaccharides, Enfieldt et al. [20] reported a superposition of two relaxation processes: β - and β_{wet} relaxations that merge into one common β -relaxation process as water is driven off.

The temperature dependence of the relaxation time for this high frequency relaxation is found to be Arrhenius type; this behavior is shown in Figure 2.13b. Note an excellent linear fitting of the relaxation time as a function of $1/T$. Table 2.3 lists the parameter values obtained for this process in both CS samples.

These activation energy values are in excellent agreement with previous reports enlisted in Table 4.6. This β -relaxation is the most commonly reported relaxation process in CS [20, 21]; it has been related to side group motions by means of the glucosidic linkage [20, 79]. β -Relaxation is the main relaxation process found in all pure polysaccharides in the low temperature range (−135 to +20 °C) and corresponds to local chain dynamics [20]. For CS, we have found this secondary relaxation in the high temperature range in agreement with other authors (higher than 20 °C) [20, 61]; however, it is expected to appear in the high temperature range at the very high frequency end as Einfeldt et al. [20] stated. They found this high frequency relaxation at temperatures as high as 120 °C.

2.8.3 Chitosan Molecular Relaxations: Conclusions

The molecular dynamics of neutralized and nonneutralized CS was studied by DS and DMA. The low frequency α -relaxation associated with the glass transition can be clearly observed by DS. This relaxation process seems

TABLE 2.3 Arrhenius Parameters for the Secondary Relaxation Process Found at High Frequencies

	β -Relaxation	
	E_{at} (kJ/mol)	τ_0 (s)
<i>Dry Chitosan (This Study)</i>		
Neutralized	46.0 ± 1.3	(8.2 ± 1.6) × 10 ^{−16}
Nonneutralized	46.0 ± 1.3	(1.9 ± 0.5) × 10 ^{−15}
<i>Dry Annealed Chitosan (This Study)</i>		
Neutralized	48.5 ± 1.8	(6.3 ± 1.9) × 10 ^{−17}
Nonneutralized	46.7 ± 0.4	(6.4 ± 1.1) × 10 ^{−15}
<i>Viciosa et al. [61]</i>		
Neutralized	46 ± 2	(5.1 ± 2.4) × 10 ^{−16}
Nonneutralized	47 ± 1	(3.4 ± 1.6) × 10 ^{−16}
<i>Einfeldt et al. [20]</i>		
β -Chitin (dry annealed)	44.7	3.9 × 10 ^{−16}
Chitosan	47.8	0.8 × 10 ^{−16}

to be independent of the CS form evaluated (neutralized and nonneutralized) and is strongly influenced by moisture content; a glass transition can be calculated depending upon moisture content.

A plasticizing effect on CS α -relaxation is observed by DS. For moisture contents less than 0.05 wt%, the glass transition is difficult to observe due to the superposition of two relaxation process.

Impedance spectroscopy is a powerful tool to monitor the plasticizing effect of water on CS glass transition.

The well-known secondary σ -relaxation often associated with proton mobility is also observed in CS (neutralized and nonneutralized) from 80 °C to the onset of degradation. On minimum moisture content conditions, this relaxation process could be noticed in the whole temperature range before the onset of thermal degradation. It is strongly affected by moisture content for dry samples; by water effects, the activation energy shifts to lower values when compared to dry annealed samples. The nonneutralized CS showed an easier mobility in this ion motion process. This relaxation process exhibits a normal Arrhenius-type temperature dependence with activation energy of 80–90 kJ/mol.

Finally, the high frequency secondary β -relaxation is also observed with Arrhenius activation energy of 46–48 kJ/mol.

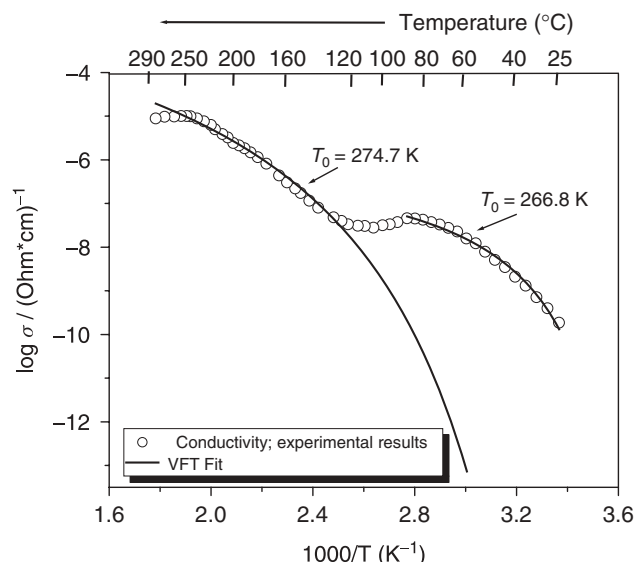


Figure 2.16 dc Conductivity (σ_{dc}) as a function of $1000/T_{PVA}$. Note: two different regions with VFT behavior are observed. Source: Reproduced with permission from González-Campos JB, García-Carvajal ZY, Prokhorov E, Luna-Bárcenas JG, Mendoza-Duarte ME, Lara-Romero J, Del Río RE, Sanchez IC. *J Appl Polym Sci* 2012;125:4082 [7]. Copyright 2012 John Wiley and Sons, Inc.

2.9 PVA DIELECTRIC RELAXATIONS

Figure 2.16 shows the change in dc conductivity as a function of temperature from 25 to 300 °C for a wet PVA II film (only one scan with no annealing treatment). It can be seen that conductivity increases as temperature increases and this dependence unveils two well-defined regions at low and high temperatures, with an intermediate discontinuity between 80 and 140 °C that is associated with water evaporation. Both relaxation regions disclose a well-defined non-Arrhenius behavior usually observed in many glass-formers and well described by the well-known VFT related to the α -relaxation. This is a clear evidence of the glass transition phenomenon; however, this behavior is not disclosed in the whole temperature range.

As illustrated in Figure 2.16, two different Vogel temperatures (T_0) can be calculated by fitting the experimental data to the VFT model described above. The low temperature region (below 80 °C) displays a lower Vogel temperature than the high temperature region (above 130 °C), suggesting a plasticizing effect of water on PVA.

Figure 2.16 shows two regions: one from 25 to 80 °C and another one from 120 to 227 °C. A conductivity decrease is observed from 80 to 120 °C due to water evaporation, as noted above. It is noteworthy that these two different temperature regions have been previously described by Hanafy [30] for pure PVA and $GdCl_3$ -doped PVA films. Hanafy [30] classified these two regions as region I from circa 30 to 60 °C and region II from circa 84 to 135 °C to propose two Arrhenius-type relaxations for pure PVA films. However, if we compare the data of Hanafy [30] with our study, one may argue the validity of the linear relationship (Arrhenius-type) of the conductivity with reciprocal temperature. When data are taken up to 300 °C (Fig. 2.16), a non-Arrhenius-type relationship is evidenced in both low (25–80 °C) and high (120–227 °C) temperature regions. This subtlety has been previously addressed by our group in polysaccharides and polysaccharides nanocomposites to resolve a non-Arrhenius-type versus an Arrhenius-type relaxation controversy [5–7].

In the above context, Bhargav et al. [89] reported a single Arrhenius behavior for the dependence of conductivity in the 30–100 °C temperature range for pure PVA, but their activation energy is almost two times higher than that of Hanafy [30]. On the other hand, Agrawal et al. [90] also suggested a VFT behavior of conductivity in pure PVA and PVA with ammonium salt films, but no further discussion is provided on the nature of the relaxations.

Figure 2.16 suggests that on heating a PVA film with moisture contents >3.5% are plasticized such that the first low temperature region (25–80 °C), described by VFT model, represents the depressed T_g of PVA circa 44 °C. As heating continues, water evaporates at 80–120 °C and the conductivity decreases. Further heating, after moisture

removal, produces an increase in conductivity up to 227 °C. At higher temperatures (227–300 °C) conductivity decreases denoting the onset of the melting point.

A VFT fitting in the high temperature region (120–227 °C) allows one to perform an extrapolation to lower temperatures. This extrapolation suggests a continuation of the primary relaxation in the high temperature that extends to lower temperatures circa 60 °C (see model extrapolation in Fig. 2.16). Under special sample conditions, the low temperature region will vanish, thus revealing a single VFT-type relaxation.

We now propose to perform dielectric measurements on samples of controlled moisture contents based on the above observations. Similarly, as those samples prepared for DSC and DMA analyses, we study samples PVA films annealed at 130 °C (water content <0.01% as calculated by TGA) and wet samples with moisture contents <3.5%. The results are shown in Figure 2.17.

Figure 2.17 shows that dry (annealed) PVA films only exhibit one VFT-type relaxation in the whole temperature range of our study and that the low temperature region vanishes (in wet samples). These results strongly suggest that the low temperature region in wet samples is related to the depressed T_g . The high temperature region (after moisture evaporation) is the VFT-type trace of dry PVA films. This is exactly shown in Figure 2.17 when comparing wet and dry (annealed) PVA films.

Calculations on VFT model show that Vogel temperatures for dry PVA is $T_0 = 267.2$ K; then, on the basis of

the 50 K rule explained above, a T_g of 317.2 K = 44.0 °C can be now proposed from dielectric measurements for dry PVA.

By means of the imaginary part (Z'') impedance spectra, it is possible to get more details about the α -relaxation dependence on temperature and water content as shown in Figure 2.18a and b. For wet samples, it is possible to observe the α -peak in the low frequency side merely above 70 °C, and it is clear that the relaxation frequency increases with rise in temperature (Fig. 2.18a). Above 195 °C, a second relaxation related to crystalline PVA regions (melting) begins to appear in the low frequency side of the spectra, remaining the α -relaxation but now in the high frequency side. The α -peaks exhibited by the dry film shift to lower frequencies for temperatures below 100 °C (Fig. 2.18b), with an increase in magnitude compared to wet ones; this displacement is a clear signal about the masking effect of water on the real dielectric properties of PVA.

The relaxation time obtained for each temperature from the maximum of the imaginary part of the dielectric modulus (M^*), the M'' peak ($K = 1/2\pi f_{\max}$) is shown in window inset of Figure 2.18a. Wet films display the trend akin to conductivity as temperature increases; two VFT behaviors in the high and low temperature range separated by water evaporation effect in the 80–140 °C temperature range. The T_0 calculated from the VFT model to the relaxation time data (Fig. 2.18) is in agreement with that obtained by the conductivity plot (Fig. 2.16). The observed T_g is commonly considered as the temperature

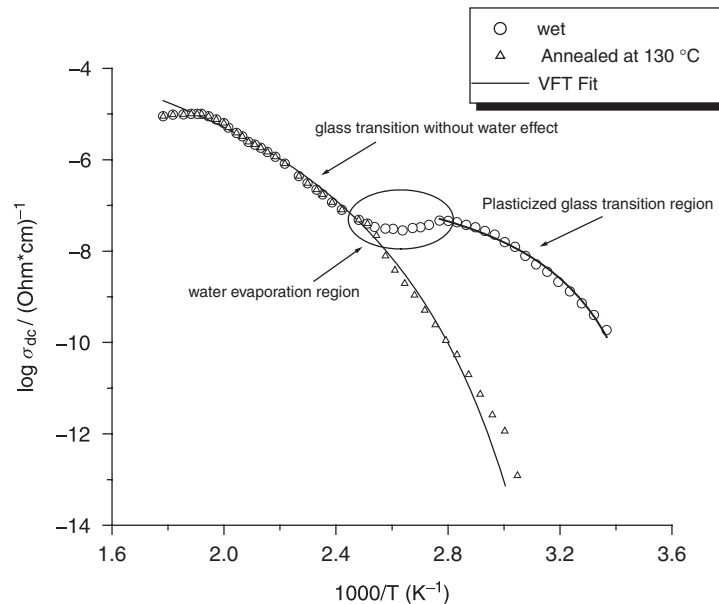


Figure 2.17 $\log \sigma_{dc}$ versus $1000/T$ for wet and dry PVA. Note: the VFT is extended in the whole temperature range after annealing at 130 °C, both low and high temperature regions merge into one. Window inset: $1000/T$ dependence of relaxation time (τ).

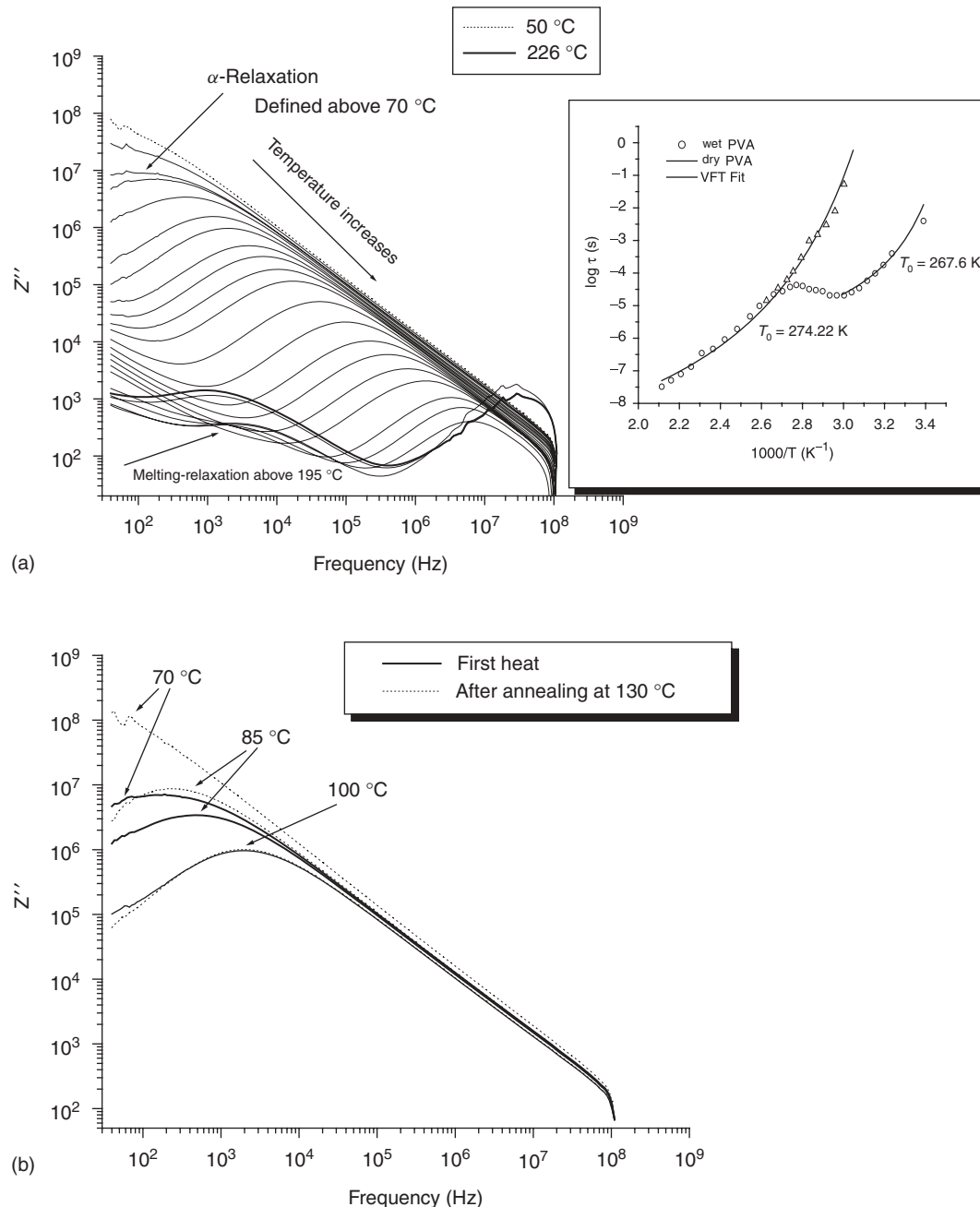


Figure 2.18 Impedance imaginary part (Z'') of the spectra versus frequency for (a) wet PVA and (b) wet and dry PVA. Note: α -Relaxation shifts to lower frequencies in dry films. Window inset: Relaxation time (τ) versus $1000/T$; the same behavior has conductivity plot is displayed. Source: Reproduced with permission from González-Campos JB, García-Carvajal ZY, Prokhorov E, Luna-Bárcenas JG, Mendoza-Duarte ME, Lara-Romero J, Del Río RE, Sanchez IC. *J Appl Polym Sci* 2012;125:4082 [7]. Copyright 2012 John Wiley and Sons, Inc.

at which the characteristic relaxation time of the material equals about 100 s [91]. With this assumption and the calculated VFT parameters for dry PVA, we can determine a $T_g(\tau = 100\text{ s}) = 43.7^\circ\text{C}$, which is in excellent agreement to those obtained with the $T_g = T_0 + 50\text{ K}$ rule.

2.9.1 PVA Dielectric Relaxations Conclusions

Two VFT relaxations processes exist in PVA, depending on moisture conditions relaxations. Wet PVA shows two different VFT behaviors separated by the moisture evaporation region (from 80 to 120°C), observed in the low (from 20 to

80 °C) and high temperature (above 120 °C) ranges. Previously, these two regions were erroneously assigned to two Arrhenius-type relaxations. While dry PVA shows a single α -relaxation non-Arrhenius, VFT-type relaxation clearly revealed after water evaporation.

REFERENCES

1. Morrel H, Grest GS. *Phys Rev B* 1979;20:1077.
2. Metatla N, Soldera A. *Macromolecules* 2007;40:9680.
3. Schut J, Bolikal D, Khan I, Pesnell A, Rege A, Rojas R, Shehiet L, Murthy NS, Kohn J. *Polymer* 2007;48:6115.
4. Dong Y, Ruan Y, Wang H, Zhao Y, Bi D. *J Appl Polym Sci* 2004;93:1553.
5. González-Campos JB, Prokhorov E, Luna-Bárcenas G, Mendoza-Galván A, Sanchez IC, Nuño-Donlucas SM, García-Gaitan B, Kovalenko Y. *J Polym Sci B Polym Phys* 2009;47:932.
6. González-Campos JB, Prokhorov E, Luna-Bárcenas G, Fonseca-García A, Sanchez IC. *J Polym Sci B Polym Phys* 2009;47:2259.
7. González-Campos JB, García-Carvajal ZY, Prokhorov E, Luna-Bárcenas JG, Mendoza-Duarte ME, Lara-Romero J, Del Río RE, Sanchez IC. *J Appl Polym Sci* 2012;125:4082.
8. Jadhav NR, Gaikwad VL, Nair KJ, Kadam HM. *Asian J Pharm* 2009;3:82.
9. Raju GG. *Dielectrics in Electrical Fields*. New York: Marcel Dekker Inc.; 2003.
10. Sorlier P, Viton C, Domard A. *Biomacromolecules* 2002;3:1336.
11. Sato H, Ohtani H, Tsuge S, Aoi K, Takasu A, Okada M. *Macromolecules* 2000;33:357.
12. Kim SS, Kim SJ, Moon YD, Lee YM. *Polymer* 1994;35:3212.
13. Kim SS, Kim SH, Lee YM. *J Polym Sci B Polym Phys* 1996;34:2367.
14. Lee YM, Kim SH, Kim SJ. *Polymer* 1996;37:5897.
15. Ratto JA, Chen CC, Blumstein RB. *J Appl Polym Sci* 1996;59:1451.
16. Mucha M, Pawlak A. *Thermochim Acta* 2005;427:69.
17. Liu Y, Zhang R, Zhang J, Zhou W, Li S. *Iran Polym J* 2006;15:935.
18. Sakurai K, Maegawa T, Takahashi T. *Polymer* 2000;41:7051.
19. Pizzoli M, Ceccorulli G, Scandola M. *Carbohydr Res* 1991;222:205.
20. Einfeldt J, Meißner D, Kwasniewski A. *Prog Polym Sci* 2001;26:1419.
21. Viciosa MT, Dionisio M, Silva RM, Mano JF. *Biomacromolecules* 2003;2004:5.
22. Huang RYM, Shieh JJ. *J Appl Polymer Sci* 1998;327. Huang RYM, Shieh JJ. *Rad Phys Chem* 2009;78:927.
23. Raju CHL, Rao JL, Reddy BCV, Brahman KV. *Bull Mater Sci* 2007;30:215.
24. Lagashetty A, Havanoor V, Basavaraja S, Venkataraman A. *Bull Mater Sci* 2005;28:477.
25. Linares A, Nogales A, Rueda DR, Ezquerra TA. *J Polym Sci B Polym Phys* 2007;45:1653.
26. Lee YM, Kim SS. *Korea Polymer J* 1996;4:178.
27. Cendoya I, López D, Alegría A, Mijangos C. *J Polym Sci B Polym Phys* 1968;2001:39.
28. Bhargav PB, Sarada BA, Sharma AK, Rao VVRN. *J Macromol Sci Pure Appl Chem* 2010;46:131.
29. Migahed MD, Bakr NA, Abdel-Hamid MI, El-Hanafy O, El-Nimr M. *J Appl Polym Sci* 1995;59:655.
30. Hanafy TA. *J Appl Polym Sci* 2008;108:2540.
31. Singh KP, Gupta PN. *Eur Polym J* 1998;7:1023.
32. Ogura K, Tonosaki T, Shiigi H. *J Electrochem Soc* 2001;148:H21.
33. Hema M, Selvasekarpandian S, Arunkumar D, Sakunthala A, Nithya A. *J Non-Cryst Solids* 2009;355:84.
34. Harun MH, Saion E, Kassim A, Hussain MY, Mustafa IS, Omer MAA. *Malaysian Polymer J* 2008;3:27.
35. Agrawal SL, Awadhia A. *Bull Mater Sci* 2004;27:523.
36. Rajendran S, Sivakumar M, Subadevi R. *Mater Lett* 2004;58:641.
37. Pissis P. Water in polymers and biopolymers by dielectric techniques. In: *Electromagnetic Aquometry*. Berlin Heidelberg: Springer; 2005.
38. Neto CGT, Giacometti JA, Job AE, Ferreira FC, Fonseca JLC, Pereira MR. *Carbohydr Polym* 2005;62:97.
39. Yu-Bey W, Shu-Huei Y, Fwu-Long M, Chung-Wei W, Shin-Shing S, Chih-Kang P, An-Chong C. *Carbohydr Polym* 2004;57:435.
40. M. Dionísio, N. M. Alves, J. F. Mano. e-polymers, 1618-7229. 2004, 044
41. Runt JP, Fitzgerald JJ. *Dielectric Spectroscopy of Polymeric Materials: fundamentals and applications*. Washington (DC): American Chemical Society; 1997.
42. Rowland SP. *Water in polymers*. Washington (DC): American Chemical Society; 1980.
43. Pezzin G. *Polym Eng Sci* 1978;18:821.
44. Köhler M, Lunkenheimer P, Loidl A. *Eur Phys J* 2008;E:27:115.
45. Tsangaris GM, Psarras GC, Kouloumbi N. *J Mater Sci* 2007;1998:33.
46. Huang H, Yuan Q, Yang X. *Colloids Surf B Biointerfaces* 2004;39:31.
47. Wintle HJ. In: Bartnikas R, Eichorn RM, editors. *Engineering Dielectrics*. Volume IIA. Philadelphia (PA): ASTM Especial Technical Publication; 1983. p 239–354.
48. Khor E. *Chitin: Fulfilling a Biomaterials Promise*. Oxford, UK: Elsevier; 2001.
49. Mirzadeh H, Yaghobi N, Amanpour S, Ahmadi H, Moghheghi MA, Hormozi F. *Iran Polym J* 2002;11:63.
50. Chandumpia A, Singhpibulpor N, Faroongsarng D, Sornpratisit P. *Carbohydr Polym* 2004;58:467.

51. Zhang Y, Xue C, Xue Y, Gao R, Zhang X. *Carbohydr Res* 1914;2005:340.
52. Sung L, Du Y, Yang J, Shi X, Li J, Wang X, Kennedy JF. *Carbohydr Polym* 2006;66:168.
53. Andrade CT, Silva KMP, Tavares MI, Simão RA, Achete C, Pérez CA. *J Appl Polym Sci* 2002;83:151.
54. Balau L, Lisa G, Popa MI, Tura V, Melnig V. *Cent Eur J Chem* 2004;2:638–647.
55. Abthagir PS, Saraswathi R. *Org. Electron* 2004;5:299.
56. Ram MK, Gowri K, Malhotra BD. *J Appl Polym Sci* 1997;63:141.
57. Bantikassegn W, Inganäs O. *J Phys D Appl Phys* 1996;29:2971.
58. Lenzmann FO, O'Regan BC, Smits JJT, Kuipers HPCE, Sommeling PM, Slooff LH, van Roosmalen JAM. *Prog Photovolt Res Appl* 2005;13:333.
59. Bekkali AEH, Thurzo I, Kampen TU, Zahn DRT. *Appl Surf Sci* 2004;234:149.
60. Kremer F, Schönhals A, editors. *Broadband Dielectric Spectroscopy*. Berlin: Springer-Verlag; 2003.
61. Viciosa MT, Dionisio M, Mano JF. *Biopolymers* 2005;81:149.
62. Yagihara S, Yamada M, Asano M, Kanai Y, Shinyashiki N, Máximo S, Ngai KL. *J Non-Cryst Solids* 1998;235–237:412.
63. Kundu SK, Choe SG, Yamamoto W, Kita R, Yagihara S. *Mater Res Soc Symp Proc* 2007;1019.
64. Schwart GA, Bergman R, Wenson J. *J Chem Phys* 2004;120(12):5736.
65. Lu Y, Fujii M, Kanai H. *Int J Food Sci Tech* 1998;33:393.
66. Einfeldt J, Meiβner D, Kwasniewski A. *J Non-Cryst Solids* 2003;320:40.
67. Stickel F, Fischer EW, Richert R. *J Chem Phys* 2003;1996:104.
68. Cutroni M, Mandanici A. *J Chem Phys* 2001;114:7118.
69. Zhou J, Tzamalis G, Zaidi NA, Comfort NP, Monkman AP. *J Appl Polym Sci* 2001;79:2503.
70. Joussemae V, Morsli M, Bonnet A. *J Appl Polym Sci* 1948;2002:84.
71. Ferrari L, Mott NF, Russo G. *Philosophical Magazine* 1989;59:263.
72. Schönhals A, Kremer F, Hofmann A, Fischer EW. *Phys Rev Lett* 1993;70:3459.
73. Garcia F, Garcia-Bernabe A, Compan V, Diaz-Calleja R, Guzman J, Riande E. *J Polym Sci B: Polym Phys* 2001;39:286.
74. Compan V, Guzman J, Diaz-Calleja R, Riande E. *J Polym Sci B Polym Phys* 1999;37:3027.
75. Lee AL, Wand AJ. *Nature* 2001;411:501.
76. Sokolov AP. *Science, New Series* 1996;273:1675.
77. Rasmussen BF, Stock AM, Ringe D, Petsko GA. *Nature* 1992;357:423.
78. Lazaridou A, Biliaderis CG. *Carbohydr Polym* 2002;48:179.
79. Toffey A, Glasser WG. *Cellulose* 2001;8:35.
80. Quijada-Garrido I, Iglesias-González V, Mazón-Arechederra JM, Barrales-Rienda JM. *Carbohydr Polym* 2007;68:173.
81. Kaymin IF, Ozolinya GA, Plisko YEA. *Polym Sci* 1980;22:171.
82. Hodge RM, Bastow TJ, Edward GH, Simon GP, Hill AJ. *Macromolecules* 1996;29:8137.
83. Despond S, Espuche E, Cartier N, Domard A. *J Polym Sci B Polym Phys* 2005;43:48.
84. Ogura K, Kanamoto T, Itch M, Miyashiro H, Tanaka K. *Polym Bull* 1980;2:301.
85. Pizzoli M, Ceccorulli G, Scandola M. *Carbohydr Res* 1991;222:205.
86. L.Y. Lim, E. Khor, C.E.J. Ling, *Biomed Mater Res (Appl Biomater)*, 1999;48:111.
87. Machado AAS, Martins VCA, Plepis MG. *J Therm Anal Calorim*, 2002;67:491.
88. Balau L, Lisa G, Popa MI, Tura V, Melnig V. *Cent Eur J Chem* 2004;2:638.
89. Bhargav PB, Sarada BA, Sharma AK, Rao VVRN. *J Macromol Sci Pure Appl Chem* 2010;46:131.
90. Agrawal SL, Awadhia A. *Bull Mater Sci* 2004;27:523.
91. Saiter JM, Grenet J, Dargent E, Saiter A, Delbreilh L. *Macromol Symp* 2007;258:152.

PART II

POLYMER SYNTHESIS AND MODIFICATION

3

STEP-GROWTH POLYMERIZATION

LUIS E. ELIZALDE, GLADYS DE LOS SANTOS-VILLARREAL, JOSÉ L. SANTIAGO-GARCÍA, AND MANUEL AGUILAR-VEGA

3.1 INTRODUCTION

3.1.1 General Principles

A rational classification of polymers has been discussed for several decades. The debate began when Carothers proposed a classification according to the polymer reactivity and considered mainly two types of polymers: polymers prepared through condensation reactions (condensation polymers) and those prepared by addition reactions (addition polymers). Chapter 1 of this handbook also discusses this topic, and although there are some overlaps in the topics covered here and in Chapter 1, the two chapters can be considered complementary.

Carothers defined addition polymers as those in which the molecular formula of the monomer is identical to that of the structural unit, so that the monomer can be obtained back from the polymer by thermolysis and, vice versa, the polymer can be synthesized from the monomer by self-addition. Condensation polymers, according to Carothers, are those where the molecular formula of the monomer differs from that of the structural unit; in this case, the monomer can be obtained from the polymer by hydrolysis or an equivalent reaction, and the polymer can be synthesized from the monomer by poly-intermolecular condensation. In this type of polymerization, the elimination of simpler molecules (H_2O , HCl , $NaCl$, etc.) is common [1].

In 1994, the IUPAC Commission on Macromolecular Nomenclature redefined the polymerization types according to the following rules [2].

1. *Chain Polymerization.* In this case, the polymer is formed through a chain reaction in which the

growth proceeds exclusively by reaction(s) between monomer(s) and reactive site(s) on the polymer chain, with regeneration of the reactive site(s) at the end of each growth step. In this kind of reactions, the polymerization is conducted by chain reaction without the formation of any small molecules.

2. *Polycondensation.* In this polymerization process, the polymers are formed through a condensation reaction between molecules of all degrees of polymerization. A condensation reaction is understood as the chemical reaction in which two functional groups (reactive groups with different chemical properties) interact to form a different functional group with the loss of a small molecule. The word “condensation” suggests a process in which two or more entities are brought “together” (from the Latin “con”) to form a “dense” entity, such as in the condensation of a gas into the liquid state; this does not imply, however, that condensation reaction products have greater density than the reactants. When the two functional groups reacting are in the same molecule, the condensation is termed *intramolecular*; on the other hand, when the functional groups are in different molecules, it is termed *intermolecular condensation*.
3. *Polyaddition.* It is a polymerization reaction in which the growth of the polymer chains proceeds by addition reactions between molecules of all degrees of polymerization.

In addition to these definitions, there is another classification for the polymers that is based on the mechanism involved during the formation of the polymer chain.

Step-growth and chain-growth polymerizations are defined by virtue of this classification, [3].

In step-growth polymerization, only one kind of reaction is involved in the formation of a polymer and the reaction proceeds step by step. The main feature of this type of reactions is that two monomers, which bear different functionalities, can react with each other, or with a polymer of any size, through the same kind of reactions. In this case, the individual polymer molecules can grow over the course of the whole process; each reaction step of a polymer molecule implies that the reactive end of a monomer or polymer encounters another species with which it can form a link. The functional group at the end of a monomer is usually assumed to have the same reactivity as that on a polymer chain of any size. The polymerizations proceed by the stepwise reaction between the functional groups of reactants as in the reactions described in Chapter 1, Section 1.2.2, of this handbook. The size of the polymer molecules increases at a relatively slow pace in polymerizations that proceed from monomer to dimer, trimer, tetramer, pentamer, and so on.

As a consequence of this mechanism, it is expected that the molecular weight grows in a slow manner at early stages of the reaction, where the reactions of oligomerization are the predominant ones. However, considering that the reactivity of the functional groups is the same during the formation of oligomers and during later stages of the reaction to form high polymer, the evolution of the average molecular weight with conversion follows the behavior shown in Figure 3.1. For this reason, a reaction

with high conversion of functional groups is required to produce polymers with high molecular weight. Therefore, if polymers with high molecular weight are required, high conversions must be reached and side reactions must be avoided; in this case, the purity of the monomers plays an important role.

Many step-growth polymerizations involve an equilibrium between reactants and products, the latter comprising macromolecular species and (usually) eliminated small molecules.

The course of these polymerizations and of the distribution of the molecular weights is statistically controlled. High polymers cannot coexist with much monomer in a system in equilibrium. Step-growth polymerizations are evidently reversible and also involve interchange reactions in which terminal functional groups in a growing chain react with linking units of other molecules producing changes in the molecular weight distributions.

There are step-growth polymerization reactions in which a small molecule is not produced (e.g., the reaction between a diol and a diisocyanate); these reactions are considered irreversible and are usually very fast, leading to high degrees of polymerization.

3.1.2 Number-Average Degree of Polymerization

As mentioned before, the main characteristic of the step-growth polymerization is that it proceeds stepwise, according to the reactivity of the two functionalities involved in the formation of the new linkage. The average

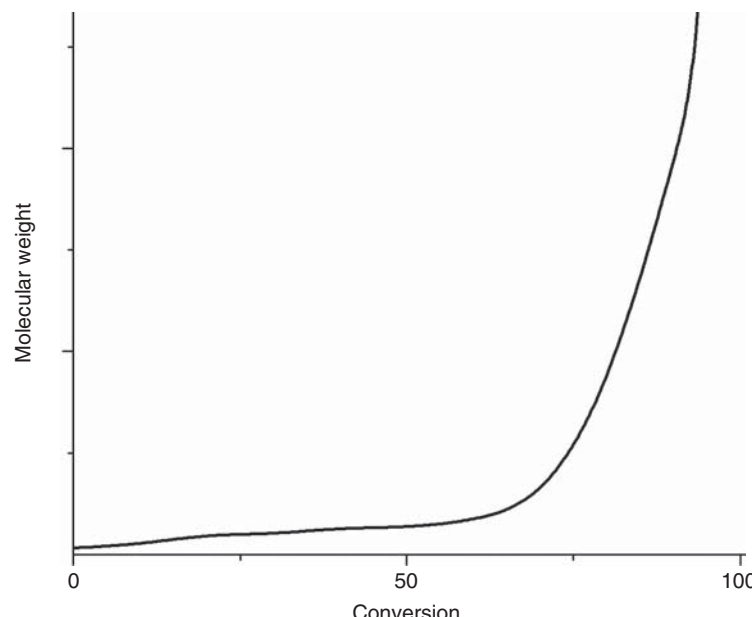


Figure 3.1 Profile of molecular weight versus conversion in a step-growth polymerization.

TABLE 3.1 Polyester Polymerization of 1,2-Ethanediol with Adipic Acid

Reagent	Reagent Concentration (% w/w)	Moles	Functionality	Equivalents
1,2-Ethanediol	99	0.99	2	1.98
Ethanol	1 (impurity in ethanediol)	0.0135	1	0.0135
1,6-Hexanedioic acid (adipic acid)	100	1	2	2
Total		2.0035		3.9935

functionality f_{av} is the average number of functional groups per monomer molecule and it is defined by Equation 3.1.

$$f_{av} \equiv \frac{\sum N_i f_i}{\sum N_i} \quad (3.1)$$

where N_i is the number of molecules of the species i and f_i is the functionality of monomeric species i . This equation is valid when the opposite functionality is present in equal concentration and in the absence of side reactions.

Consider a polymerization that forms AB links and in which $n_A < n_B$, where n_i is the number of equivalents of the functional groups of type i . In this case, the number of B equivalents that can react cannot exceed n_A , and Equation 3.1 adopts the form of Equation 3.2.

$$f_{av} = \frac{2n_A}{\sum N_i} = \frac{2n_A}{N_A + N_B} \quad (3.2)$$

The number-average degree of polymerization in the reaction mixture (X_n) is defined as the average number of structural units (or monomer units) per polymer molecule. A structural unit equals a monomer unit, that is, the residue of each monomer in the polymer. For an AB polymerization, a repeating unit is made of two structural units. This differs from what some authors term the *average degree* of polymerization (D_p , i.e., the average number of repeating units per polymer molecule). In the step-growth polymerization of a single molecule that bears two functionalities and can form a polymer, $X_n = D_p$, and when two monomers are involved, $X_n = 2D_p$, and is defined as

$$X_n = \frac{N_0}{2N_0 - N_0 p f_{av}} = \frac{2}{2 - p f_{av}} \quad (3.3)$$

where N_0 is the initial number of monomer molecules and p is the extent of reaction, which is equal to the fraction of functional groups that have reacted $0 \leq p \leq 1$. An example of the use of the number-average degree of polymerization concept is the reaction between 1,2-ethanediol with 1,6-hexanedioic acid (adipic acid). In this system, an esterification reaction takes place through the two functionalities, alcohol and acid, in the monomers and a polymer is formed. The repeating unit is $[OCH_2-CH_2-O-C(O)-(CH_2)_4-C(O)]$,

which has a molecular weight of 172 g/mol. If the monomers are in equivalent concentrations, then $f_{av} = 2$ and $X_n = 2/(2 - 2p)$. When the conversion is 90%, the number-average degree of polymerization is $X_n = 2/(2 - 2 * 0.9) = 10$ and the molecular weight is 860 g/mol. On the other hand, when the conversion is almost complete (99.5%), $X_n = 2/(2 - 2 * 0.995) = 200$ and the molecular weight is 17,200 g/mol. From this concept, the effect of conversion on molecular weight in step-growth polymerizations is clear.

Now consider the situation in which the 1,2-ethanediol monomer has a 99% (w/w) purity and contains ethanol in a concentration of 1% (w/w), as shown in Table 3.1. When 146 g of adipic acid (1 mol) is reacted with 62 g of 1,2-ethanediol (0.99 mol, considering the purity reported), at nearly complete (99.5%) conversion, the number-average degree of polymerization is $X_n = 2/(2 - 0.995 * 1.9935) = 121$ and the molecular weight obtained is 10,440 g/mol. This result clearly contrasts with the previous data found of $X_n = 200$ and molecular weight of 17,200 g/mol for the same polymerization and conversion, but with pure monomer. This example also clarifies the enormous effect of the monomers' purity on the course of a step-growth polymerization.

3.1.3 Molecular Weight Distribution

The prediction of the molecular weight distribution for a step-growth polymerization assumes that both the probability of the reaction and the reaction rate of two functional groups are independent of the sizes of the involved molecules (monomers or growing chains), as explained by Rudin [4].

For a polymerization system involving functional groups, A, reacting with another functional group (say B), the probability of finding by random selection a growing molecule with i monomer units is given by the probability that $i - 1$ A groups have reacted (p^{i-1}) multiplied by the probability that the last functional group has not reacted, which is $1 - p$ (since the probabilities that a given functional group has reacted or not must add up to 1). The resulting probability is evidently $p^{i-1}(1 - p)$. Then, the probability that a randomly selected molecule will be an i -mer equals the mole fraction x_i of i -mers in the reaction

mixture and is calculated as

$$x_i = (1-p) p^{i-1} \quad (3.4)$$

On the other hand, the total number N of molecules remaining at an extent of reaction p is

$$N = N_0 (1-p) \quad (3.5)$$

Therefore, the number N_i of i -mer molecules is given by $Nx_i = N_0(1-p)^2 p^{i-1}$, and the molecular weight of an i -mer is iM_0 .

Since the total weight of all molecules equals $N_0 M_0$ (neglecting unreacted ends), the weight fraction w_i of i -mers is

$$\begin{aligned} w_i &= \frac{N_0 i M_0 (1-p)^2 p^{i-1}}{N_0 M_0} \\ w_i &= i(1-p)^2 p^{i-1} \end{aligned} \quad (3.6)$$

Equation 3.6, together with Equation 3.4, describes a random distribution of molecular sizes; this distribution is also known as the *Flory–Schulz distribution* or the *most probable distribution* [5]. Recently, Wutz and Kricheldorf [6] proposed a model describing the frequency distribution (f_i) and formulated the weight distribution (w_i) of linear chains in step-growth polymerizations considering the cyclization reaction, which is one of the most important side reactions in step-growth polymerization.

The number-average molecular weight M_n , defined as the total weight of a polymer sample divided by the total number of molecules, is given by

$$M_n = M_0 X_n = \frac{M_0}{1-p} \quad (3.7)$$

where M_0 is the formula weight of the repeating unit.

3.1.4 Polymers Obtained by Step-Growth Polymerization

Step-growth polymerization is a very important method for the preparation of some of the most important engineering and specialty polymers. Polymers such as polyamides [7], poly(ethylene terephthalate) [8], polycarbonates [9], polyurethanes [10], polysiloxanes [11], polyimides [12], phenol polymers and resins, urea, and melamine-formaldehyde polymers can be obtained by step-growth polymerization through different types of reactions such as esterification, polyamidation, formylation, substitution, and hydrolysis. A detailed list of reaction types is shown in Table 3.2.

3.2 POLYMERIZATION KINETICS

Step-growth polymerizations are condensation reactions that usually occur in equilibrium, a fact that intrinsically leads to a high degree of reversibility. From the kinetic point of view, the most studied reactions are those of polyester and polyamide formation [13]. In these reactions, the value of the rate constant, k , can be considered independent of the polymer chain length, which is equivalent to assuming that the polymerization mechanism is the same throughout the entire reaction. In general, it is assumed that the polymerization is a first-order reaction with respect to the active functional groups; therefore,

$$-\frac{d[A]}{dt} = k[A][B] \quad (3.8)$$

This is the case of, for example, externally catalyzed reactions. If the stoichiometric balance is exact, then Equation 3.8 can be written as

$$-\frac{d[A]}{dt} = k[A]^2 \quad (3.9)$$

On integration,

$$[A] = \frac{[A_0]}{1 + [A_0]kt} \quad (3.10)$$

If the reaction is acid self-catalyzed, as in the case of polyesters, the reaction becomes a globally third-order reaction that can be written as

$$-\frac{d[A]}{dt} = k[A]^2[B] \quad (3.11)$$

Also, if $[A] = [B]$ (stoichiometric concentrations), the reaction equation can be reduced to

$$-\frac{d[A]}{dt} = k[A]^3 \quad (3.12)$$

On integration,

$$[A]^2 = \frac{[A_0]^2}{2kt [A_0]^2 + 1} \quad (3.13)$$

In general, the reactions for polyamide formation are seldom catalyzed. The reactions to produce thermosets, such as melamine-urea or phenol-formaldehyde, require a basic or an acidic catalyst. Some polyurethane formation reactions are catalyzed by basic reactants. Equation 3.11 applies when the rate constant of the externally catalyzed reaction (k') is much larger than that of the self-catalyzed

TABLE 3.2 Some Step-Growth Polymers and their Synthesis Reactions

Type	Interunit Linkage	Monomer	Monomer	Polymer	Small Molecule Formed
Polyamide	$-\text{C}(\text{O})\text{N}-$	$\text{H}_2\text{N}-\text{R}-\text{NH}_2$	$\text{HO}_2\text{C}-\text{R}'-\text{CO}_2\text{H}$	$\left[\text{H}-\text{NRHN-C(R)-C(OH)}_n \right]$	Water
				$\left[\text{H}-\text{NRHN-C(R)-C(OH)}_n \right]$	Hydrochloric acid
Polyester	$-\text{C}(\text{O})-\text{O}-$	$\text{H}_2\text{N}-\text{R}-\text{CO}_2\text{H}$	$\text{Cl}-\text{C}(\text{O})-\text{R}'-\text{C}-\text{Cl}$	$\left[\text{H}-\text{NR(OH)-C(R)-C(OH)}_n \right]$	Water
			None	$\left[\text{H}-\text{NR(OH)-C(R)-C(OH)}_n \right]$	Water
		$\text{HO}-\text{R}-\text{OH}$	$\text{HO}_2\text{C}-\text{R}'-\text{CO}_2\text{H}$	$\left[\text{H}-\text{ORO-C(R)-C(OH)}_n \right]$	Water
		$\text{HO}-\text{R}-\text{OH}$	$\text{R}'\text{O}_2\text{C}-\text{R}'-\text{CO}_2\text{R}''$	$\left[\text{H}-\text{ORO-C(R)-C(OH)}_n \right]$	Alcohol ($\text{R}''\text{OH}$)
		$\text{HO}-\text{R}-\text{CO}_2\text{H}$	None	$\left[\text{H}-\text{OR-C(OH)}_n \right]$	Water
Polyurethane	$-\text{O}(\text{C=O})\text{N}-$	$\text{HO}-\text{R}-\text{OH}$	OCN-R'-NCO	$\left[\text{R}-\text{O-C(NH-R)-N(C)}_n \right]$	None
		$-\text{Si}(\text{R})\text{O}-$	—	$\left[\text{H}-\text{O-Si(R)-O-H}_n \right]$	Hydrochloric acid or water
Polysiloxane	$\text{X}-\overset{\text{R}}{\underset{\text{R}}{\text{Si}}}-\text{X}$ $\text{X} = \text{OH, Cl}$	OH	CH_2O	$\left[\text{H}-\text{O-C(CH}_2)_n-\text{O-H}_n \right]$	Water
Resins (phenol-formaldehyde)	OH	$\text{H}_2\text{N}-\text{C}(\text{O})-\text{NH}_2$	CH_2O	$\left[\text{H}-\text{C(OH)}-\text{N-CH}_2 \right]_n$	Water
Resins (urea-formaldehyde)	$-\text{C}(\text{O})-\text{N-CH}_2-$	$\text{H}_2\text{N}-\text{C}(\text{O})-\text{NH}_2$	CH_2O	$\left[\text{H}-\text{N-C(OH)}-\text{N-CH}_2 \right]_n$	Water
Resin (melamine-formaldehyde)	$-\text{HN}-\text{C}_6\text{H}_3(\text{NH}_2)_2-\text{CH}_2-$	$\text{H}_2\text{N}-\text{C}_6\text{H}_3(\text{NH}_2)_2-\text{N}$	CH_2O	$\left[\text{H}-\text{N-C}_6\text{H}_3(\text{NH}_2)_2-\text{N} \right]_n$	Water
Polysulfide	$-S-\text{R}-$	$\text{Cl}-\text{R}-\text{Cl}$	Na_2S	$\left[\text{S-R} \right]_n$	NaCl
Polyacetal	$-\text{O}-\overset{\text{R}}{\underset{\text{R}}{\text{C}}}-\text{O}-$	$\text{HO}-\text{R}-\text{OH}$	$-\text{R}'-\overset{\text{O}}{\underset{\text{C}}{\text{C}}}-\text{H}$	$\left[\text{O-R-O-C(H)}_n \right]$	Water

reaction (k). If this is not the case, the rate of reaction expression has to be written as

$$-\frac{d[A]}{dt} = k[A]^3 + k'[A]^2 \quad (3.14)$$

On integration,

$$k't = \frac{k}{k'} \ln \frac{[A]k([A_0] + k')}{(k[A] + k')[A_0]} + \frac{1}{[A]} - \frac{1}{[A_0]} \quad (3.15)$$

This expression takes into account the values of the k' and k in the polymerization reaction.

3.3 POLYAMIDES

Polyamides are polymers containing recurring amide groups (-CONH-) as integral parts of the main polymer chain. Polyamides are among the first polycondensation polymers; they were first prepared by Carothers at Dupont in 1938 [14] and were an enormous success as a substitute of natural fibers. They are prepared from hexamethylenediamine and sebacoyl chloride. Nowadays, polyamides of different types are highly appreciated due to their thermal resistance and high mechanical strength.

Polyamides can be prepared with aliphatic or aromatic monomers, either acids or amines. Aliphatic polyamides are usually hygroscopic materials, and the introduction of the aromatic ring in the monomer structure can reduce this characteristic. Water in polyamides is an important impurity when they are processed through injection molding.

Polyamides are commonly named as *Nylon* followed by two numbers, in which the first one denotes the number of carbon atoms in the diamine monomer and the second one refers to the number of carbon atoms in the diacid monomer. If a cycle is part of the polyamide, either in the amine or the acid moiety, the first letter of the cycle name must be used. In addition, if the polyamide is derived from an amino acid, only one number has to be used that describes the number of carbon atoms between the two functionalities. These rules are shown in Table 3.3.

TABLE 3.3 Codes to be Used with the Different Polyamides in the Nylon Nomenclature

	Structure	Code
Diamine		
Hydrazine	H ₂ NNH ₂	0
Ethylenediamine	H ₂ N-CH ₂ CH ₂ .NH ₂	2
Hexamethylenediamine	H ₂ N-(CH ₂) ₆ -NH ₂	6
1,8-Octanediamine	H ₂ N-(CH ₂) ₈ -NH ₂	8
Piperazine		Pip
Diacids		
Carbonic acid		1
Oxalic	HO ₂ C-CO ₂ H	2
Glutaric acid	HO ₂ C-(CH ₂) ₃ -CO ₂ H	5
Adipic acid	HO ₂ C-(CH ₂) ₄ -CO ₂ H	6
Suberic acid	HO ₂ C-(CH ₂) ₆ -CO ₂ H	8
Isophthalic acid		I
Terephthalic acid		T

3.3.1 Polyamidation

Most polyamides are prepared by a direct amidation reaction between diacids and diamines, and numerous combinations of monomers are possible. This reaction is accompanied by the elimination of water, and the amount of water released can serve as a measure of the extent of the reaction. In addition to this, the intramolecular reaction of the amino acids can also produce a polyamide (Fig. 3.2).

The reaction path involves acid-base reaction between the monomers or the amino acid, generating the carboxylic ammonium salt, followed by loss of water, generating the amide linkage. It has been reported that this reaction can be accelerated by the use of microwave energy [15] (Fig. 3.3).

The amidation is also possible through the use of diesters instead of diacids, generating polyamides and alcohols. The use of diamides of low molecular weight in reaction with a diacid monomer also produces polyamides and acid as a by-product.

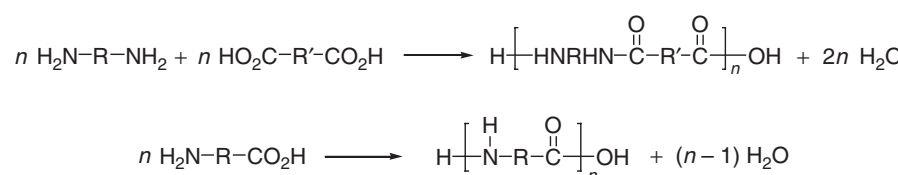
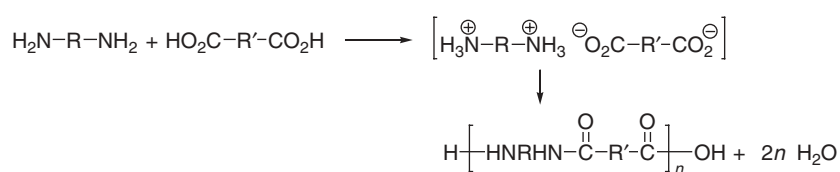
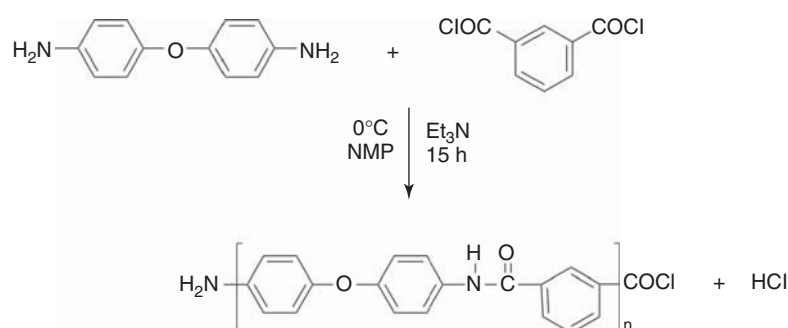


Figure 3.2 Polyamidation of amino acids or diacids and diamines.

**Figure 3.3** Reaction path of the amidation reaction.**Figure 3.4** Interfacial polyamidation of terephthalic chloride.

The reaction of diamines with diacid chlorides produces at least two types of polymerization. The first type is an interfacial polymerization in which the diamine is dissolved in water and the diacid chloride is in the organic phase. This reaction can be improved by the addition of an inorganic base to the aqueous solution or by the inclusion of a surfactant; the reaction will take place in the interface. The second type is a polymerization in solution in which both diamine and diacid chloride are dissolved in an organic solvent. With this method, a high molecular weight polyamide can be prepared.

One example is the reaction between aromatic polyether isophthalic amine and terephthalic chloride [16] at a low temperature generating a polyamide, as discussed later (Fig. 3.4).

The resulting polyamides also have high molecular weight and the monomer reactants are carefully kept in stoichiometric amounts.

The polyamides can be prepared by ring-opening reaction of the correspondent lactam; according to its mechanism, this reaction cannot be properly considered as a step-growth polymerization.

3.3.2 Aromatic Polyamides

Aromatic polyamides totally built (or at least 85%) from adjacent-to-aromatic-monomer links are called *aramids*. It was long recognized that highly favorable properties might be obtained with a polyamide that is made entirely of aromatic rings directly connected to the amide links. These

properties would result from the stiffness and stability of the rings and the complete absence of aliphatic content. Owing to the unique properties that aromatic rings impart to a macromolecule of this kind, poly(*p*-phenylene terephthalamide), better known as *Kevlar*, has become one of the most famous of the specialty polymers. However, one of the main problems in making such polymers is to maintain them in a liquid state, necessary for forming. This and other obstacles have been overcome by researchers who proposed different polymerization processes for their synthesis. Among the type of reactions that is commonly used for their preparation, the first one was developed by Yamasaki [17], and involves the use of triphenyl phosphate and pyridine in an aprotic solvent, such as *N*-methylpyrrolidinone (NMP) or dimethylformamide (DMF). A typical example of this reaction would be the preparation of polyhexafluoro isopropylidene isophthalamide or the preparation of a poly(fluorenylidene) isophthalamide as described in the scheme of Figure 3.5.

Using this method, a number of poly-isophthalamides with trifunctional monomers [18] or poly-trimethyl and *tert*-butylhydroquinone aromatic polyamides can be prepared [19]. Another interesting example of the use of Yamasaki's reaction is the preparation of organosoluble aromatic polyamides containing phosphorus [20] or the preparation of polyamides with a diamantane moiety embedded in the structure of the principal chain [21].

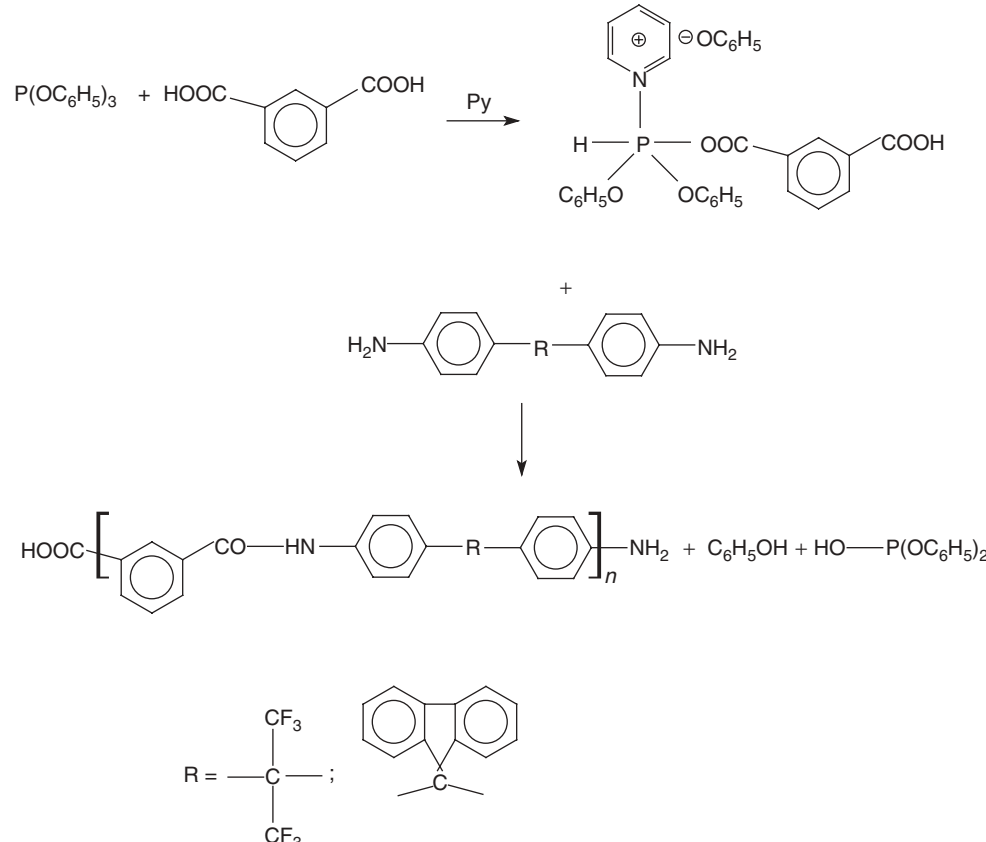


Figure 3.5 Preparation of polyaromatic amides.

3.4 POLYIMIDES

The progress of modern science and technology would not have been possible without polyimide materials; polyimides have had a significant impact on the development of various fields of science and technology. Polyimides have found applications as films, fibers, foams, membranes, plastics, composites, glues, adhesives, and coatings and are widely used for the fabrication and coating of various structures, units, and parts operating under extreme temperature conditions. One of the fields in which the use of polyamides is crucial is membrane technology, specifically in applications of gas processing technology and energy storage.

Polyimides can be prepared through several step-growth processes. One of the most common methods used for this purpose is the reaction of dianhydrides with diamines (Fig. 3.6). The first product obtained is poly(amic acid), which has the advantage of being soluble in organic solvents (normally aprotic polar solvents are used, such as dimethyl sulfoxide, DMF, dimethylacetamide, and NMP). The solution of poly(amic acid) can easily be manipulated or processed. The acid can then be cycled thermally, generating the polyamide, which is insoluble in most of the common organic solvents.

In addition, other preparation methods of polyimides use bis(methylol imide) in reaction with diamines, diisocyanates, or dinitrile compounds, according to the scheme shown in Figure 3.7.

3.5 POLYESTERS

3.5.1 Polyesters from Diacids

The polycondensation of difunctional oligomers leads to the preparation of well-defined polymer structures. Monomers in this type of reactions must be soluble in the reaction mixture and stable when the reaction is carried out in the melt, which is the case for some aromatic polymers prepared by polycondensation [22]. As previously described, polycondensation can occur with monomers bearing the same or a different functional group at both ends of the molecule. When one of the reactive functional groups is a hydroxyl moiety, several types of materials can be prepared, such as polyethers, polyesters, and polyurethanes, independently if they are used to form homopolymers, copolymers, or hyperbranched polymers.

Block copolymers can be prepared by polycondensation of difunctional oligomers (which are previously prepared

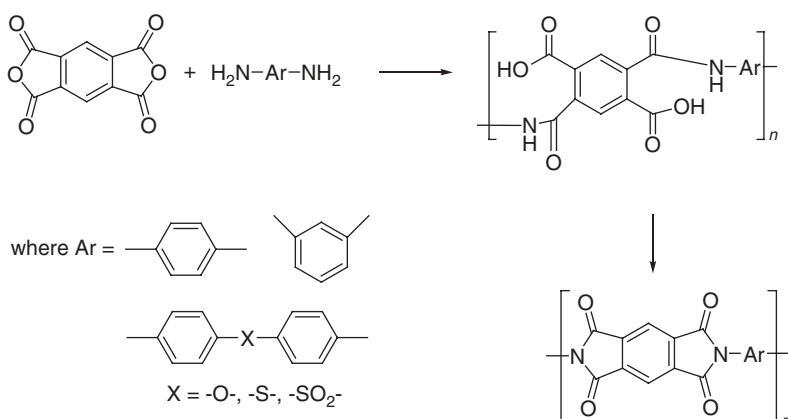


Figure 3.6 Synthesis of polyimides by the reaction of diacid anhydrides and diamines.

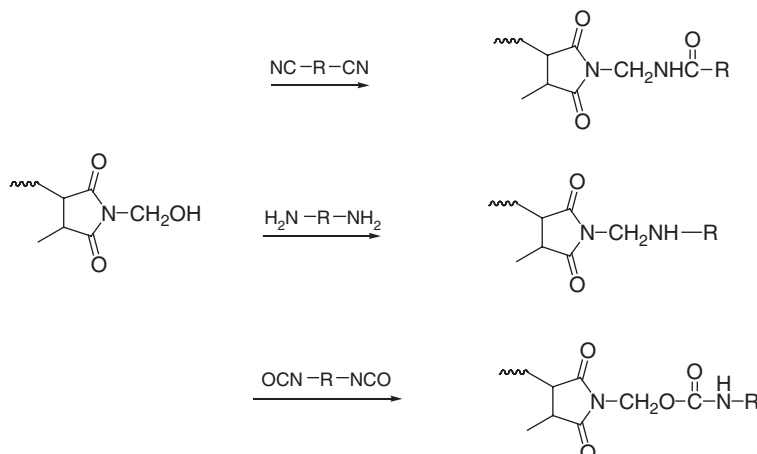


Figure 3.7 Preparation of polyimides with the use of bis(methylol imide).

by polycondensation or polyaddition reactions), reacting as precursors of each block. They can also be prepared by the coupling of different difunctional oligomers, usually no more than two, since otherwise structures that are complex and difficult to handle can be obtained.

Efforts aimed at the synthesis of highly branched polymers have followed two major pathways: one directed toward the synthesis of the desired structures by stepwise growth polymerization and another one that uses one-pot or “click” polymerization of difunctional monomers.

In addition, there has been an increasing interest in new synthetic methods for the preparation of well-defined polymers with controlled chain-end functional groups [23], such as telechelic polymers, which are characterized by the presence of reactive functional groups placed at both chain ends. These materials can then be used as precursors in the synthesis of block copolymers, as modifiers of the thermal and mechanical properties of condensation polymers, as precursors in the preparation of polymer networks, and as compatibilizers in polymer blends [24].

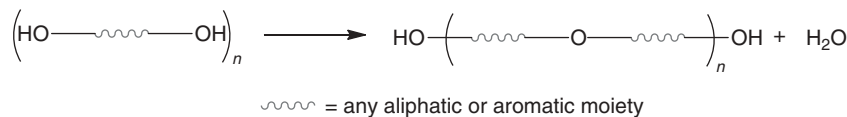
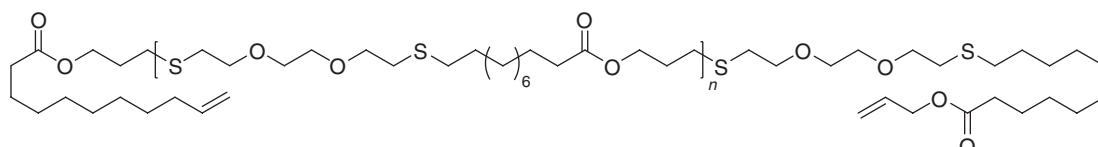
3.5.2 Polyethers

The simplest method to prepare a polyether oligomer by condensation reactions is by the use of hydroxyl functionalized monomers, as described in Figure 3.8.

Polycondensation reactions have also been used to develop an efficient and versatile “one-step” method for the preparation of some polymers by “click processes,” which has been applied for the synthesis of telechelic polymers [25].

Alkene-functionalized linear polymers, such as the polyether-thioether described in Figure 3.9, was prepared by thiol-ene click step-growth polymerization using a fast, efficient, and green approach for the synthesis of macromonomers with a variety of functionalities.

Synthesis of polyethers by polycondensation of alcohols can also be performed by the classical interfacial reaction between functionalized monomers. By this procedure, an organotin polyether was synthesized in a rapid (15 s) and high yield reaction (>80%) [26].

**Figure 3.8** General representation of a polycondensation reaction in alcohols.**Figure 3.9** Polyether-thioether based on undecanoic acid synthesized by a two-step click condensation process.

3.5.3 Polyesters

Polyesters are among the most widely used fibers in the world today. Generally, they can also be prepared by step-growth polymerization involving the condensation reaction between diols and carboxylic acids or its derivatives, which has been extensively studied. Functionalization in polyesters is usually achieved using a prefunctional monomer such as maleic acid, or any other monomer bearing a double bond, thus providing a large amount of possibilities for combinations between monomers and polymerization techniques [27].

All polymerization reactions can be categorized into two different types: chain- and step-growth polymerization, which are incompatible in terms of monomer structure, experimental conditions, reaction rates, etc. In the past years, research concerning step-growth polymerization has been oriented to the preparation of new polyester materials by the combination of condensation and free radical techniques [28], as shown in Figure 3.10.

Another example that uses the same synthetic strategy is the synthesis of aliphatic polyesters bearing pendant alkyne groups. These polyesters can be successfully prepared by

step-growth polymerization of different building blocks, such as adipic and succinic acid, in combination with an acetylene-based diol, examples of which are 2-methyl-2-propargyl-1,3-propanediol, 1,4-butanediol, and the most common ethylene glycol. Alkyne groups can survive the high reaction temperatures (200°C) in the presence of a radical inhibitor. Subsequently, the alkyne groups are reacted by a “click” cycloaddition reaction to obtain a functionalized polyester based on poly(ethylene succinate) and poly(butylene adipate) [29].

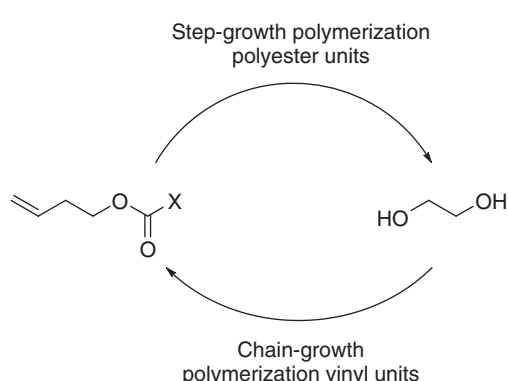
On the other hand, owing to the rising demand for specialty polymers with novel properties and characteristics designed for specific applications, hyperbranched polymers have attracted much investigation in the past decades [30]. The growing strategy uses the symmetrical nature of the molecules to construct macromolecules functionalized at each end [31].

Recently, the synthesis of seed oil-modified polyester with a hyperbranched polyether core was reported [32]. This methodology involved the preparation of a carboxyl-terminated prepolymer from the monoglyceride of the oil, which was condensed with phthalic and maleic anhydrides.

Also, 10,11-undecanoic acid in the presence of a quaternary ammonium or phosphonium bromide as initiator undergoes polymerization via ring opening of the epoxide group with the carboxylic acid moiety to yield a hydroxyl-functionalized aliphatic polyester [33].

3.5.4 Polyurethanes

Polyurethanes are widely used in several important applications including foams, elastomers, coatings, and adhesives. They result from the reaction between an alcohol and an isocyanate, and from this reaction, hyperbranched polymers can also be prepared from AB_2 monomers having both functional groups in the proper ratio. The high reactivity of isocyanates, even in self-condensation, can lead to the formation of dimer or carbamates by reaction with

**Figure 3.10** Polymerization of bifunctional monomers by step-growth and chain polymerizations.

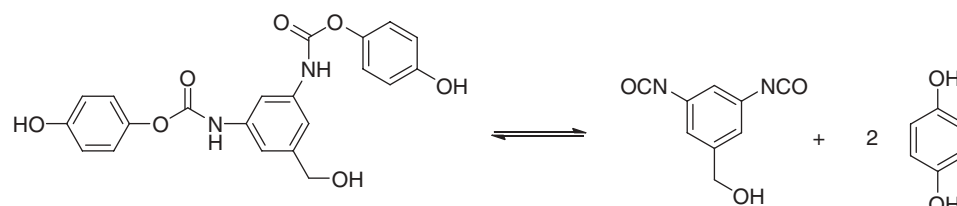


Figure 3.11 Step-growth polymerization reaction between an isocyanate and an aromatic alcohol.

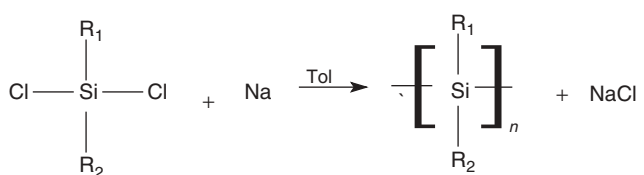


Figure 3.12 General condensation reaction for polysilane preparation. Tol, toluene.

an alcohol molecule. This requires the protection of the isocyanate moiety during storage.

Figure 3.11 shows the preparation of polyurethane by the reaction between an isocyanate molecule and an aromatic alcohol [34].

Hyperbranched polyurethanes have also been synthesized by step-growth polymerization reactions such as the reaction between 3,5-diaminobenzoic acid and 2-hydroxypropyl[3, 5-bis{(benzoxycarbonyl)imino}]benzyl ether to prepare an AB_2 -type blocked isocyanate monomer functionalized with an ester group [35]. Several years earlier, Barmar et al. had reported the preparation of a polyurethane-based thickener starting from an ethoxylated urethane prepolymer that was reacted with polyethylene glycol and dicyclohexylmethane diisocyanate [36].

3.6 INORGANIC CONDENSATION POLYMERS

3.6.1 Polysilanes

Polysilanes, which are only slightly different from polysiloxanes, are a class of interesting inorganic polymers that, depending on the molecular weight and lateral substitutions on the silane atom, could be useful as

photoinitiators or UV photoresists because of the presence of a σ -bond along the chain [37]. The condensation reaction commonly used for polysilane preparation is the denominated Wurtz reaction that proceeds by the coupling of organodichlorosilanes with sodium metal under toluene reflux, as depicted schematically in Figure 3.12.

In a complete and extensive review by Miller and Milch [38], it is indicated that sodium is favored over lithium because Li tends to undergo oligomerization. Potassium tends to promote degradation and cyclization instead of the formation of linear polymers. Gauthier and Worsfold [39] investigated the effect of phase-transfer catalyst, crown ethers, quaternary ammonium salts, and cryptands to increase the stability and repeatability of the final polysilane (see also Chapter 30 in this handbook). They found an increased reproducibility and better molecular weight distribution of the polymer produced and a certain dependence of the molecular weight upon the concentration of the crown ether. The effect was attributed to the presence of anionic species involved in the polymerization process.

In order to produce polysilanes with controlled optical properties, the substituents have to be picked up properly; thus, poly(alkyl(methoxyphenyl)silane) homo and copolymers are reported by Nakashima and Fujiki [40], who found that poly(alkyl(alkoxyphenyl)silane) with methyl, ethyl and *n*-hexyl moieties showed a typical absorption peak around 340–360 nm attributed to the delocalized σ -conjugation.

Other combinations, such as doped poly(disilanylene-oligothienylene)s, have been prepared [41] (Fig. 3.13), that are photoconducting when irradiated with visible light at 480 nm.

There are also reports on the optical properties of poly[(octamethyltetrasilylene)methylene] [42], a periodic polycarbosilane, in the presence of crown ethers. A large study on the effect of the substituents R_1 and R_2 in polysilanes and their effect on the different UV radiation absorptions was carried out by Herzog and West [43], who synthesized phenylalkyldicholorosilanes with *n*-propyl, *n*-hexyl, *n*-octyl, and *p*-MeOC₆H₄SiHexCl₂ using the Wurtz reaction. They describe changes in the absorption of UV radiation depending on the alkyl substitution, as well as the presence of halogen atoms. More recently, Reuss and Frey [44] described a strategy to obtain multihydroxy-functional polysilanes using an acetal-protecting group that

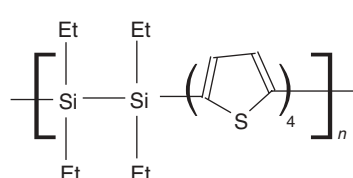


Figure 3.13 Structure of poly(disilanylene-oligothienylene).

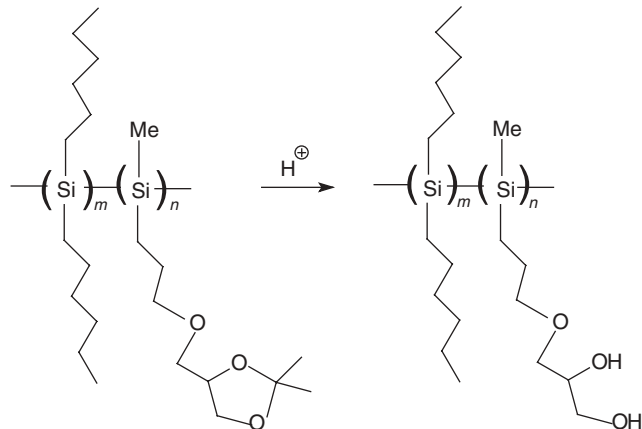


Figure 3.14 Preparation of copolysilane PHDS-*co*-GMS.

is achieved by the coupling of dichloro(3-(2,2-dimethyl-1,3-dioxolane-4-yloxy)propyl)methylsilane and poly[di-n-hexylsilane-*co*-(isopropylidene glyceryl propyl ether)methylsilane] (P(DHS-*co*-IMS)), eliminating at the end the dioxol moiety by protonation to form the hydroxyl groups, poly[di-n-hexylsilane-*co*-(glyceryl propyl ether)methylsilane] (P(DHS-*co*-GMS)) (Fig. 3.14).

3.6.2 Polyphosphazenes

Polyphosphazenes are inorganic polymers in which the backbone consists of alternating P and N atoms with two lateral groups. Polyphosphazene monomers are prepared by a condensation reaction involving phosphorus pentachloride

and ammonia. The reaction takes place in a stepwise process by elimination of the hydrogen chloride to form the cyclic chlorophosphazene monomer that undergoes ring-opening polymerization (Fig. 3.15).

Similar processes are followed for the preparation of cyclic arylphosphazenes that have a similar tendency to form cyclic phosphazenes [45].

On the other hand, Wisian-Neilson and Neilson [46–48] report a condensation method that leads to the formation of polyphosphazenes. In this route, $\text{NH}-(\text{Si}-\text{CH}_3)_3$ is reacted in the presence of *n*-butyllithium and PCl_3 to form the dichloride phosphazene using the Grignard reactant, as depicted in Figure 3.16

It is reported that this polydimethyl phosphazene can lead to exchange reactions with Li to produce anionic species that could be reacted with organic or organometallic halides to produce pending alkyl polyphosphazenes.

3.7 DENDRIMERS

The use of monomers with functionality larger than two allows the formation of tridimensional structures by step-growth polymerization. In particular, the use of monomers with the general formula A_xB_y could generate several architectures such as hyperbranched, dendrimers, and star polymers. Each architecture will have different physical and chemical properties. In particular, dendrimers are regularly branched polymers that can be produced by the divergent approach or the convergent approach [49]. In the divergent approach, the dendrimer grows

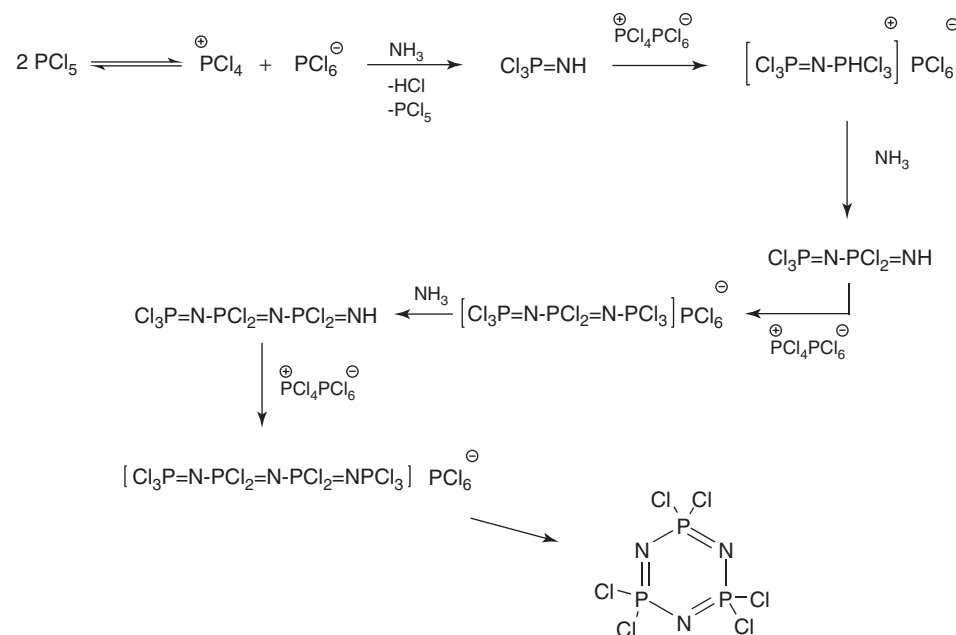


Figure 3.15 Schematic of phosphazene monomer preparation.

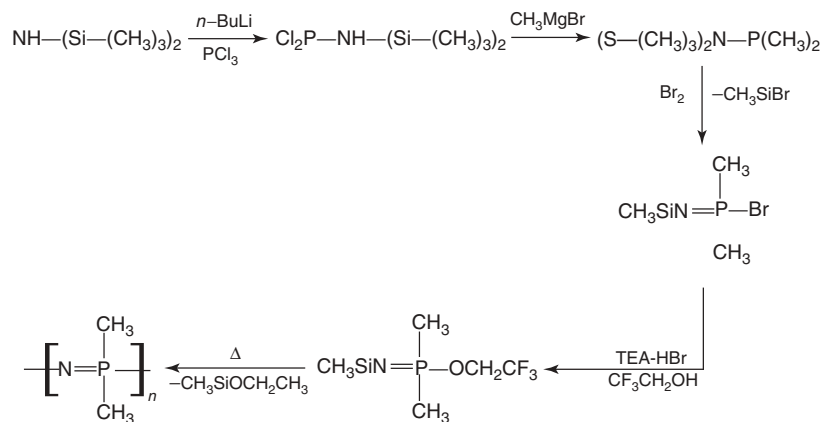


Figure 3.16 Preparation of polydimethyl phosphazene by a stepwise reaction.

from the center and spreads radially out in layers, each of them built by a stepwise reaction. In the convergent approach the dendrimer production starts at the end with the so-called surface functional groups coupled to AB_y building blocks, which allows the preparation of a larger dendron, and the process is repeated to increase the size of the dendrons. At the end, the dendrons are attached to a multifunctional core molecule to produce dendrimers [50]. Examples of AB_y monomer used, for example, in polyesters, are those where A and B are $-COOH$ and $-OH$ groups, respectively, or in some cases their derivatives such as $-COCl$, $-O-(CH_2)_2-OH$, $-O-Si(CH_3)_3$, or CH_3COO^- . A recent example of a dendrimer formation is the synthesis of 3,5-bis(hydroxymethyl)benzylbromide dendrimer unit reported by Kathiresan et al. [51]. They described the divergent approach using a CB_2 branching unit to form the dendrimer, as depicted in Figure 3.17.

This approach is used in several instances to control the arms, molecular weight, and crystallinity of the resulting polymer [52]. The convergent approach is illustrated elsewhere [53, 54]. This subject is not reviewed here in detail because a whole chapter of this handbook (Chapter 30) is dedicated to it.

3.8 THERMOSET POLYCONDENSATION POLYMERS

This section focuses on polycondensation reactions to synthesize thermoset polymers. Specific condensation chemistries are studied here; a more extensive treatment of the subject of thermoset polymers can be found in Chapter 28 of this handbook.

The most common applications of these materials are as paints and coatings. However, their uses are extremely diversified and include boat and marine construction

materials, automotive and aircraft bodies, luggage, furnishing, appliances, textiles, and packaging. Owing to their industrial applications, these materials are commonly known as *resins*. The resin industry is quite mature and is predominantly characterized by well-known and established products, applications, and processes [55, 56]. However, the synthesis of these resins requires a different approach because of their differences in chemical composition. Polyester, epoxy, alkyd, and phenolic resins are among the crosslinking polymers that are more commonly synthesized by a stepwise reaction.

3.8.1 Polyester Resins

In general, polyester resins are synthesized by the reaction between carboxylic acids and alcohols, with three or more reactive groups. Recently, unsaturated polyesters were incorporated in various ways to produce terminal, pendant, and internal double bonds [57–59]. In the case of unsaturated polyesters, maleic anhydride is most commonly used to produce internal unsaturation. The double bond present on unsaturated polyester reacts with a vinyl monomer, mainly styrene, resulting in a 3D crosslinked structure. This structure acts as a thermoset. The crosslinking is initiated through an exothermic reaction involving an organic peroxide, such as methyl ethyl ketone peroxide or benzoyl peroxide (Fig. 3.18).

3.8.2 Epoxy Resins

Epoxy resins are among the most important of the high performance thermosetting polymers and have been widely used as structural adhesives and matrix for fiber composites. Epoxy resins are characterized by the presence of epoxide groups before cure, and they may also contain aliphatic, aromatic, or heterocyclic structures in the backbone. The epoxy group can react with amines, phenols, mercaptans,

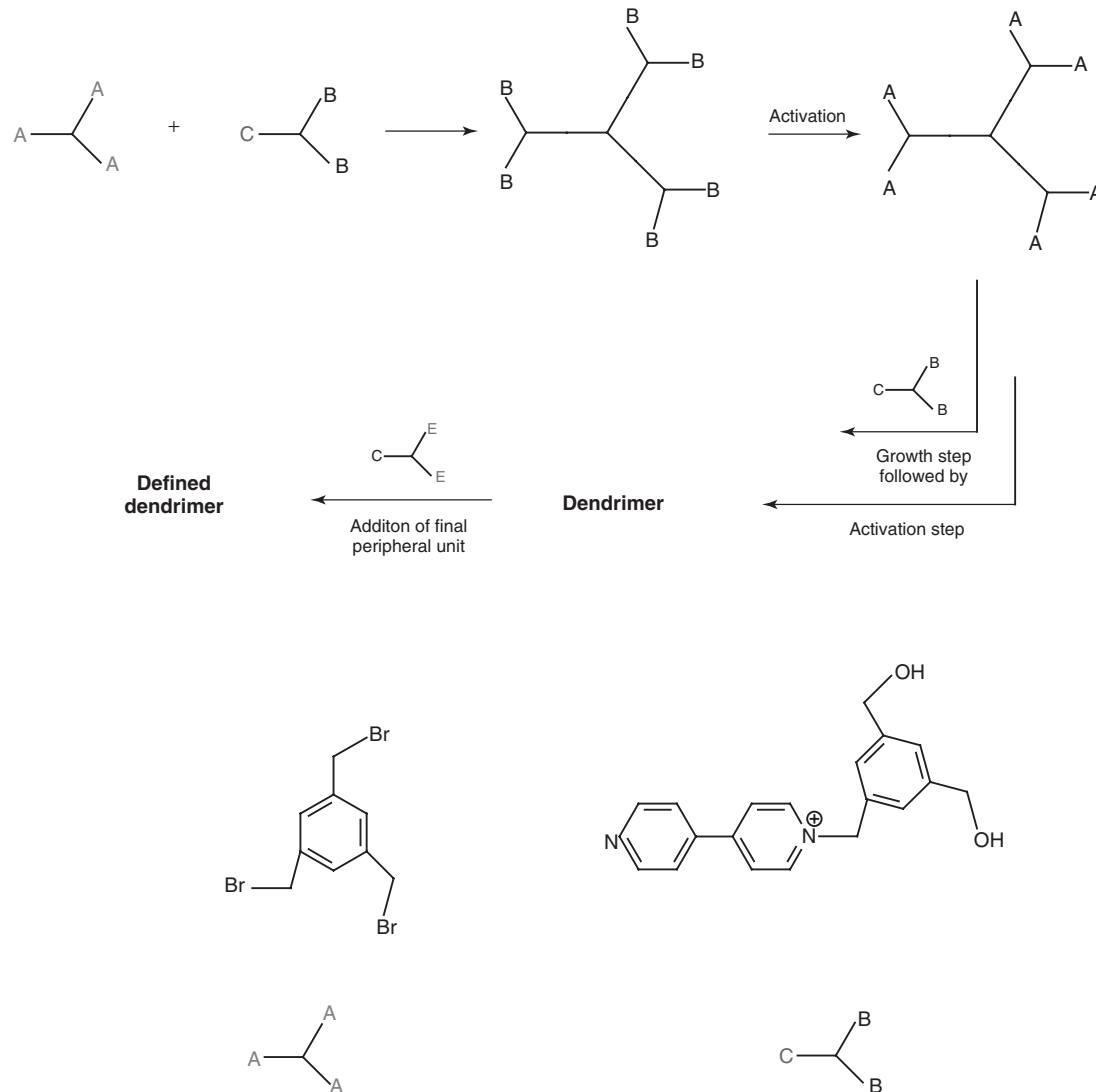


Figure 3.17 Dendrimer prepared by the divergent approach.

isocyanates, anhydrides, or acids as the first step (Fig. 3.19). Usually, aliphatic and aromatic diamines are widely used as curing agents [60].

3.8.3 Alkyd Resins

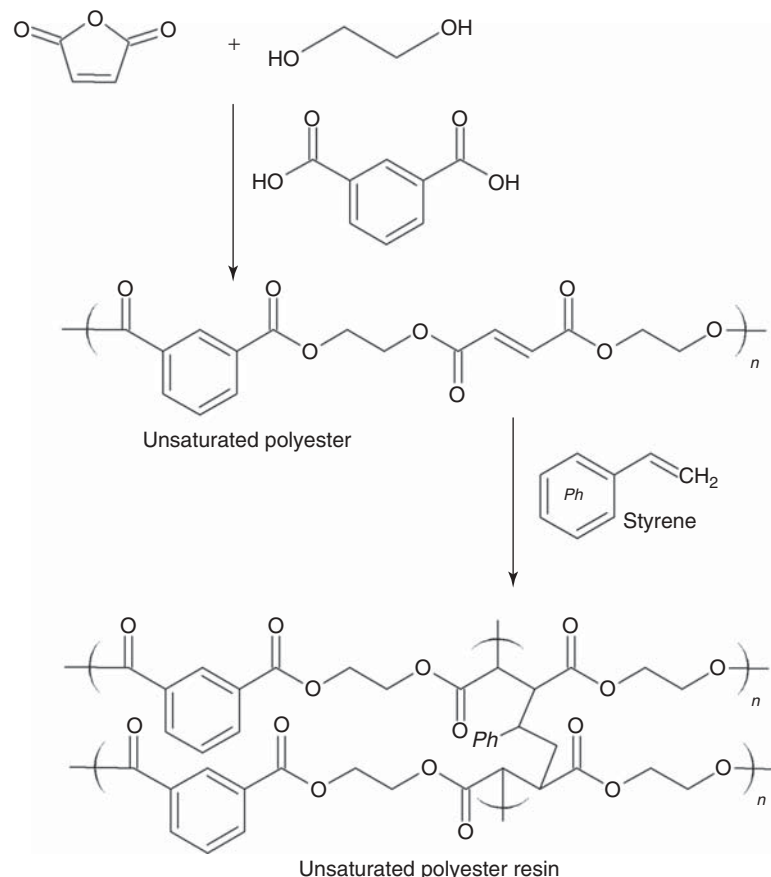
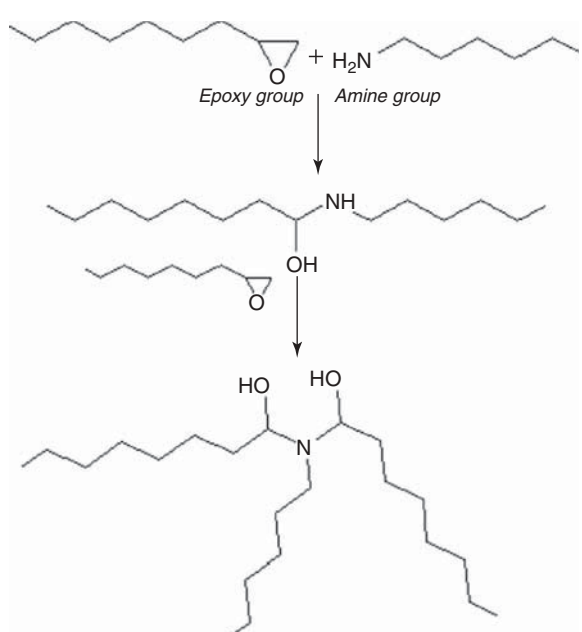
Alkyd resins are based on polymeric resins developed in the 1920s. The first alkyd resins sold commercially under the name *Glyptal* were made by the General Electric Company (Fig. 3.20). Alkyd resins are a class of polyesters synthesized by condensation between an alcohol and an acid or anhydride. Actually, the anhydride is modified with a monofunctional acid, most commonly C₁₈ fatty acid, which can be obtained from vegetable oil (rubber seed oil (RSO) or palm oil) [61–63]. The major advantage of the alkyd resins is their components (fatty acids and triglyceride

derivatives), which are obtained from low cost renewable resources.

The synthesis of alkyd resins using vegetable oils proceeds in two stages. For example, pentaerythritol, the tetraol of choice and mainly responsible for the degree of branching of the alkyd [64], and a vegetable oil are reacted to form an ester by transesterification. Then, a slight excess of phthalic anhydride is added to obtain a crosslinked alkyd resin (Fig. 3.21) [65]. Both reactions are monitored by acidity and viscosity measurements [66].

3.8.4 Phenolic Resins

Phenolic resins are a generic name given to a wide range of crosslinked polymers produced by phenol and formaldehyde. There are two types of phenolic resins, Resol and Novolac. The type of resin being made depends on the pH of the catalyst and the ratio of phenol to formaldehyde.

**Figure 3.18** Synthesis of unsaturated polyester resin.**Figure 3.19** Crosslinking polymers using epoxy-amine-cured reactions.

Novolac is made under acidic conditions, and the ratio of phenol to formaldehyde used ranges from 1.49 to 1.72, whereas Resol resins are synthesized in a basic medium using a ratio of phenol to formaldehyde in the range of 1.0 to 0.33 [54, 67, 68]. A synthetic route for both resins is shown in Figure 3.22.

3.9 CONTROLLED MOLECULAR WEIGHT CONDENSATION POLYMERS

Traditionally, a nonstoichiometric polycondensation method is used to control the number-average molecular weight of a condensation polymer [69–71]. This method assumes that no side reactions take place and that the average degree of polycondensation X_n (number of monomer units in the oligomer) at conversion p of the functional groups A and B is given by Carother's equation [72]. Generally, two dissimilar reactive difunctional monomers are used to synthesize telechelic oligomers, which have the same end-group functionality that the monomer used in excess (Fig. 3.23).

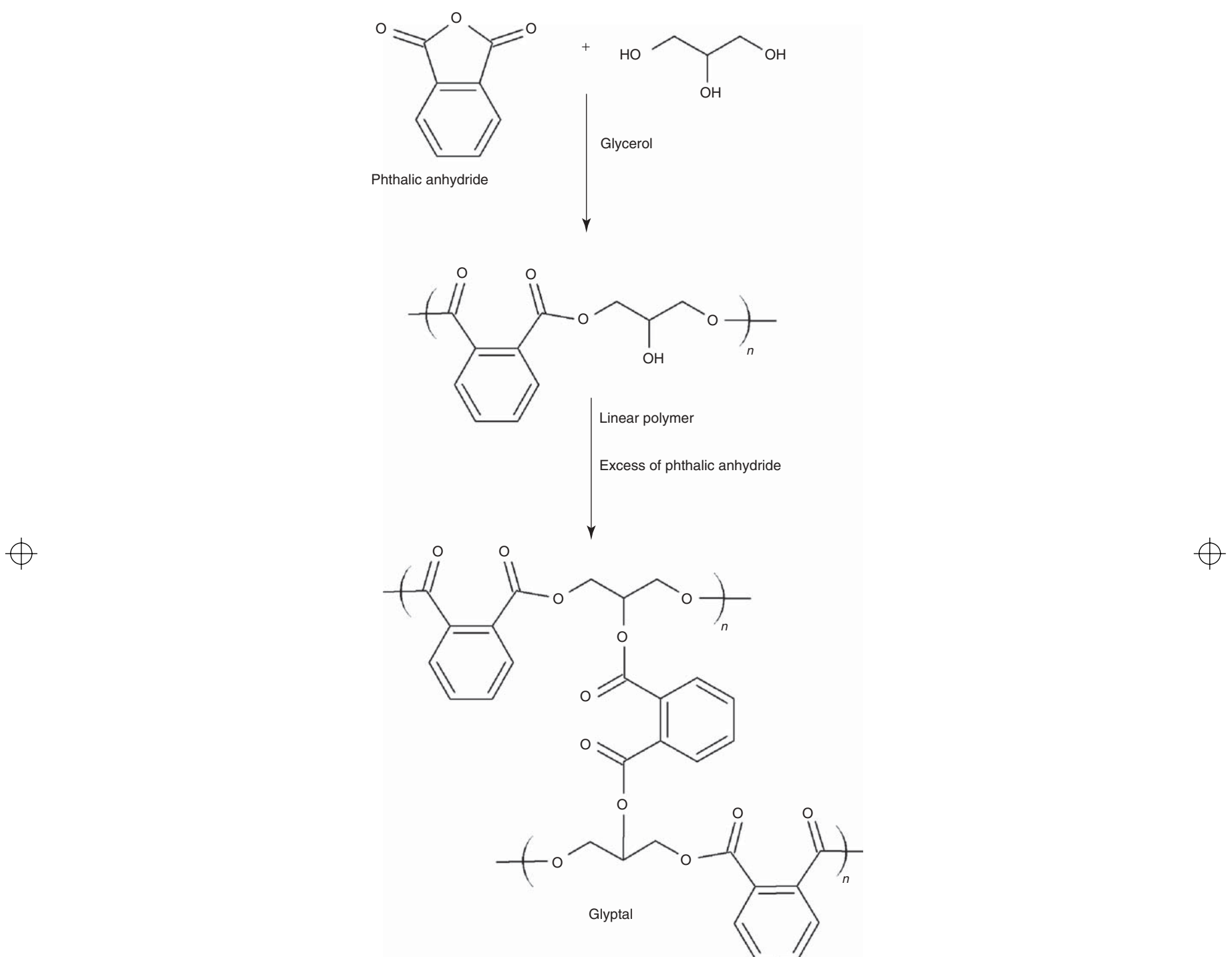


Figure 3.20 Schematic representation of the synthesis of Glyptal.

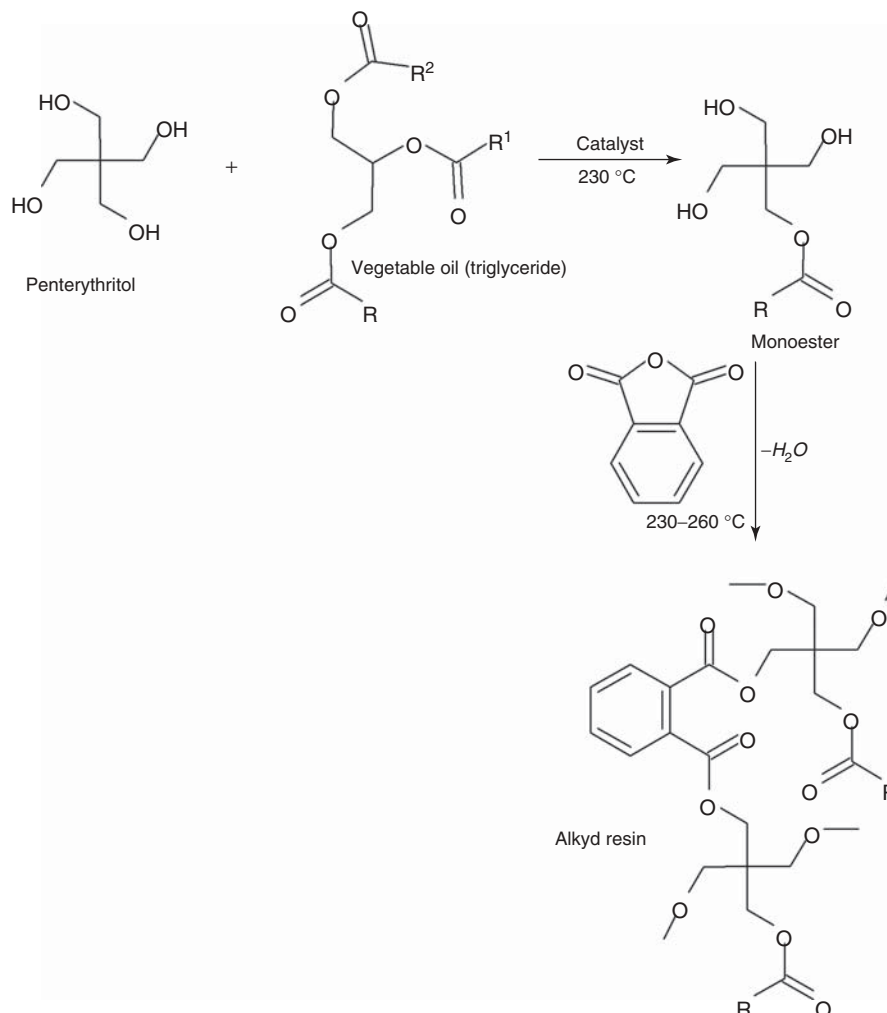


Figure 3.21 Schematic representation of alkyd resins preparation.

Recently, well-defined condensation polymers have been synthesized via substituent effect-assisted chain-growth condensation polymerization, in which the polymer-propagating ends are more reactive than the monomers because of resonance or inductive effects between the functional groups of the terminal monomer units. Figure 3.24 shows a schematic illustration of this concept in the polymerization of AB-type monomers. In this monomer, the substituent effect of the A site diminishes the reactivity of the B site, suppressing undesired step-growth polymerization between monomers. When the monomer reacts with an initiator that has a reactive site, the substituent reactivity has a change. If the substituent effect is to enhance the reactivity of the formed bond of the polymer end group, the next monomer

will react selectively with the polymer-propagating end [73].

3.9.1 Solid-Phase Synthesis

Solid-phase synthesis has been used in the preparation of well-defined polymers enabling the convergence between synthetic organic chemistry and polymer chemistry. Solid-phase synthesis has the following advantages over solution-phase methods: ease of purification, speed, and easier sequencing and control of the monomers [74]. A more complete report on techniques, supports, linkers, and reaction types on solid-phase syntheses is given by Zaragoza-Dörwald [75]. In general, this procedure can be realized using

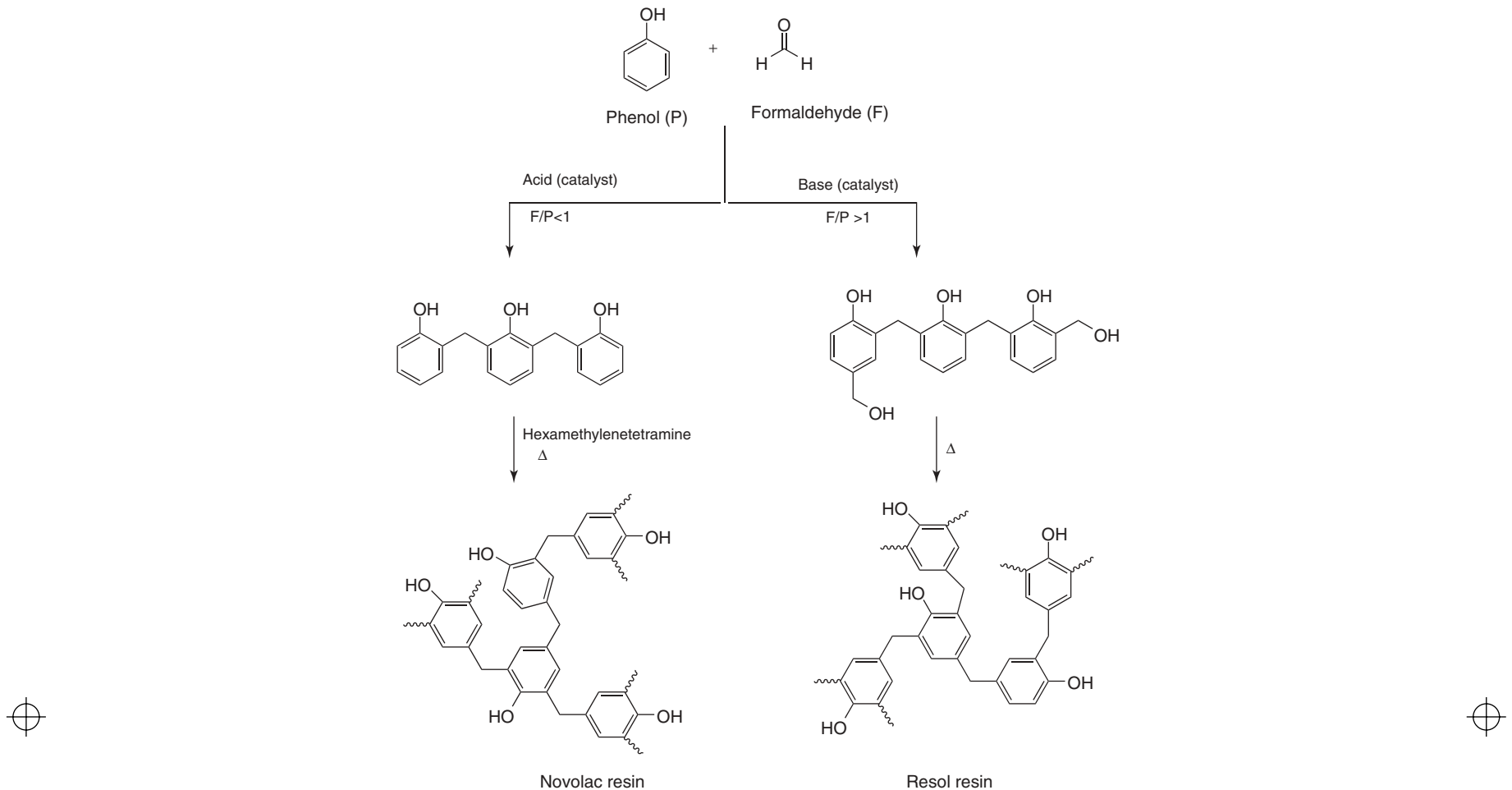


Figure 3.22 Synthetic route for phenolic resins.

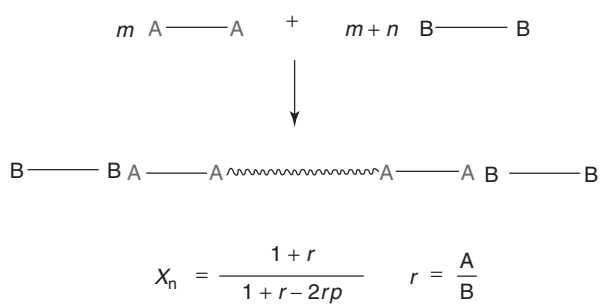
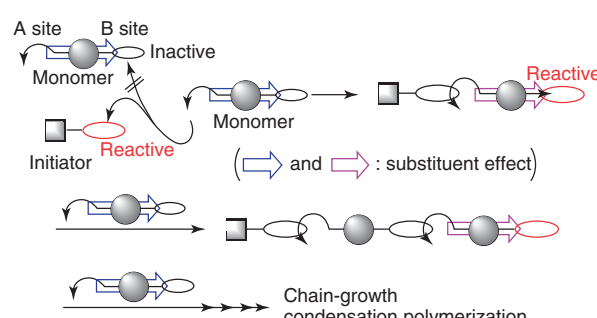


Figure 3.23 Carother's equation and synthesis of telechelic oligomers by a nonstoichiometric polycondensation method.

Figure 3.24 Scheme of chain-growth condensation polymerization. Source: Reprinted with permission from Yokoyama A, Yokozawa T. *Macromolecules* 2007;40:4093 [73]. Copyright 2007 American Chemical Society. (See insert for the color representation of the figure.)

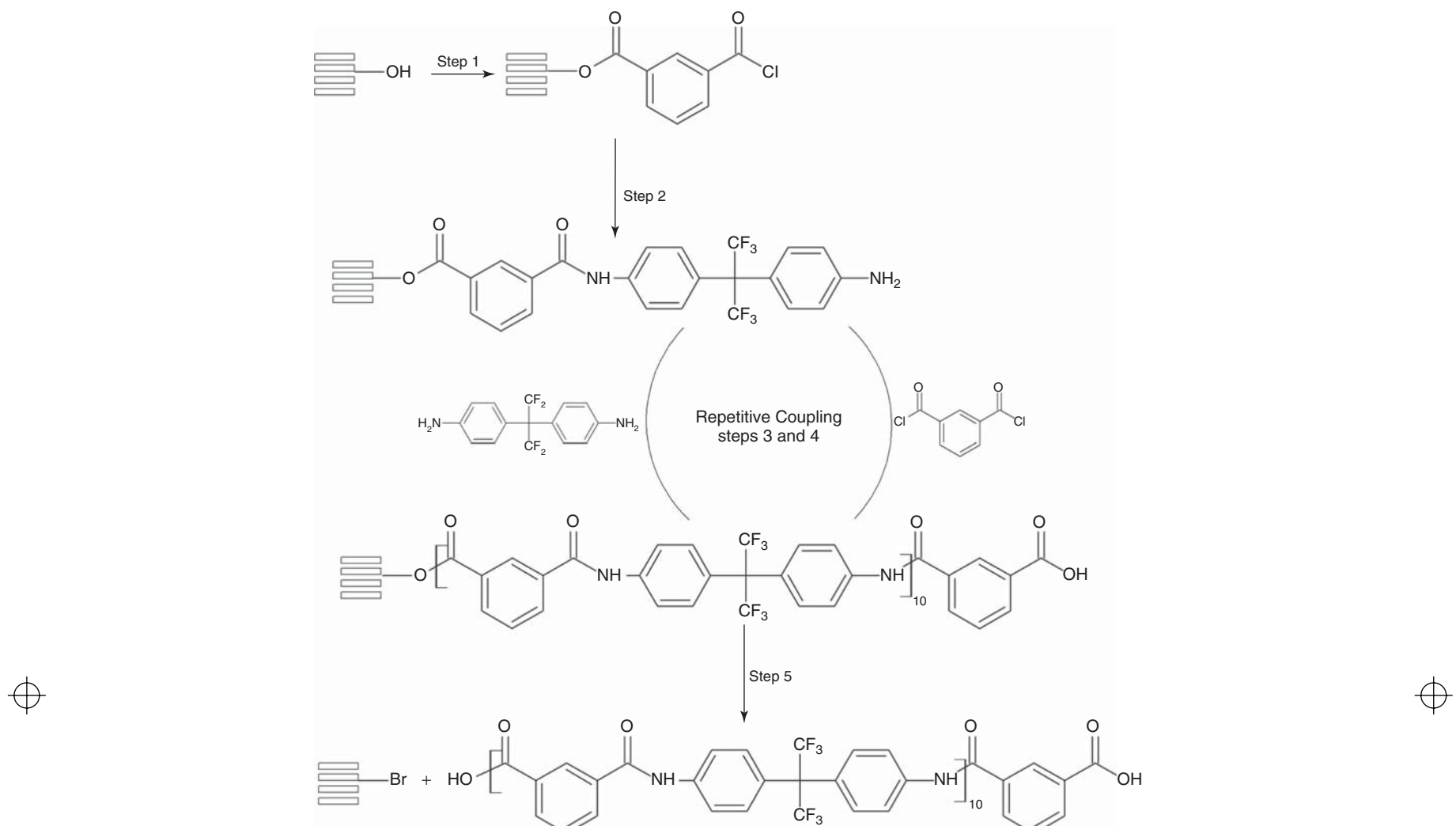


Figure 3.25 Solid-phase synthesis of aromatic oligoamides. Source: Reproduced with permission from Santiago-García JL, Aguilar-Vega M. *Eur Polym J* 2009;45:3210 [79]. Copyright 2009 Elsevier Ltd.

condensation monomers with different or equal functionalities [76–79]. Figure 3.25 shows a representative example of the synthesis of aromatic oligoamides using the solid-phase synthesis on SynPhase Lanterns as supports. This procedure shares most features of the key elements of solid-phase peptide synthesis described by Merrifield [80].

3.9.2 Use of Macromonomers in Condensation Reactions

Macromolecular monomers, called *macromonomers* or *macromers*, are a relatively new category of functionalized polymer materials having a molecular weight range of 10^3 – 10^4 and possessing one or more reactive polymerizable end groups [81] of those described in Table 3.2. The

most intensively studied macromers consist of telechelic polymers that can be used as crosslinkers, chain extenders, and precursors for block and graft copolymers, and their synthesis and modifications have been studied in detail and covered by several authors [82, 83]. One of the most often used methods to synthesize telechelic polymers is polycondensation using Carother's equation, described earlier. Figure 3.26 shows the synthesis of HFATERT-*b*-DBFISO block copolyaramides using different-size macromers [71, 84], via a condensation reaction between diacid and diamino end groups on the HFATERT and DBFISO oligomers. On the other hand, AB₂ macromonomers can be used for the synthesis of polymer with dendritic and hyperbranched structures, DendriMacs and HyperMacs, respectively [85].

62 STEP-GROWTH POLYMERIZATION

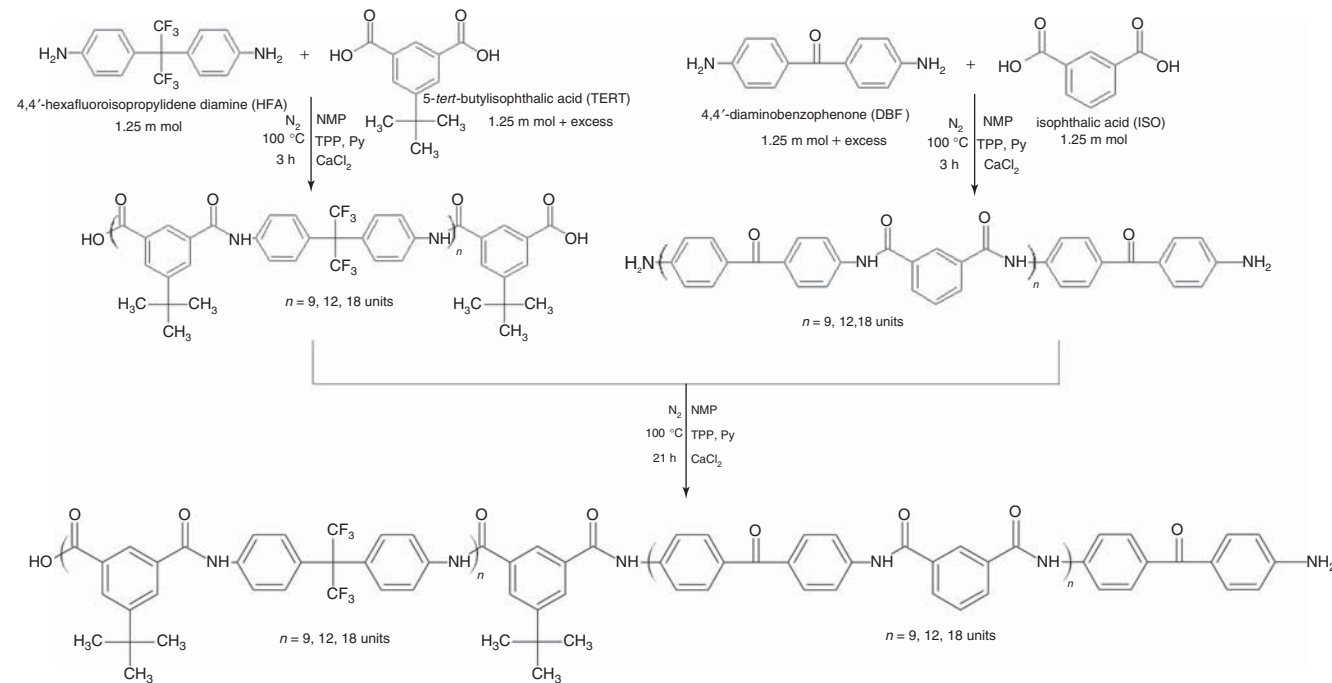


Figure 3.26 Synthesis of HFATERT-*b*-DBFISO rigid block copolyaramides by polycondensation of macromers.

REFERENCES

1. Carothers WA. J Am Chem Soc 1929;51:2548.
2. Stepto MR, Suter FT. Pure App Chem 1994;66:2483.
3. Kricheldorf HR. Macromol Symp 2003;199:1.
4. Rudin A. *The Elements of Polymer Science and Engineering*. 2nd ed. San Diego: Academic Press; 1999. p 175.
5. Flory PJ. *Principles of Polymer Chemistry*. Ithaca, NY: Cornell University Press; 1953. p 91.
6. Wutz C, Kricheldorf HR. Macromol Theory Simul 2012;1:1.
7. Marchildon K. Macromol React Eng 2011;5:22.
8. Ben D. J Appl Polym Sci 2002;83:1288.
9. Hualun C, Xiuju Z, Kai X, Huan L, Jiangxun S, Xin L, Zien F, Ying G, Mingcui C. Polym Adv Technol 2012;23:765.
10. Sharma V, Kundu PP. Prog Polym Sci 2008;33:1199.
11. Zhou Q, Yan S, Han CC, Xie P, Zhang R. Adv Mater 2008;20:2970.
12. Sazanov YN. Russ J Appl Chem 2001;74:12533.
13. Odian G. *Principles of Polymerization*. New York, NY: John Wiley & Sons; 1991. p 54.
14. Carothers WH, inventor. US patent 2130947. 1938.
15. Takashi N, Ritsuko N, Kazuhiko T. Mini Rev Org Chem 2011;8:306.
16. Morgan PW. J Polym Sci Polym Symp 1985;72:27.
17. Rivas BL, Barria B, Canessa GS, Rabagliati FM, Preston J. Macromolecules 1996;29:4449.
18. Carretero P, Sandin R, Molina S, Martinez-de la Campa A, Jose G, Lozano AE, de Abajo J. Eur Polym J 2011;47:1054.
19. Yagci H, Mathias LJ. Polymer 1998;39:3779.
20. Liu YL, Tsai SH. Polymer 2002;43:5757.
21. Chern YT, Wang WL. Polymer 1998;39:5501.
22. Fakirov S, editor. *Handbook of Condensation Thermoplastic Elastomers*. Weinheim, Germany: Wiley-VCH; 2005.
23. Percec V. Chem Rev 2009;109:4961.
24. Boutevin B, David G, Boyer C. Adv Polym Sci 2007;206:135.
25. Lluch C, Ronda JC, Galia M, Lligadas G, Cádiz V. Biomacromolecules 2010;11:1646.
26. Carraher CE, Truong NT, Roner RM. 242nd ACS National Meeting & Exposition; 2011 Aug 28–Sep 1; Denver, CO.
27. Parthiban A, Babu Rao TR. 223rd ACS National Meeting; 2007 Mar 25–29; Chicago, IL, POLY-342.
28. Mizutani M, Satoh K, Kamigaito M. J Am Chem Soc 2010;132:7498.
29. Billiet L, Fournier D, Du Prez F. J Polym Sci A Polym Chem 2008;46:6552.
30. Tomalia DA, Baker H, Dewald J, Hall M, Kallos G, Martin S, Roeck J, Ryder J, Smith P. Polymer J 1985;17:117.
31. Hawker CJ, Fréchet JM. J Am Chem Soc 1990;112:7638.
32. Uday K, Niranjan K. Polymer J 2011;43:565.
33. White JE, Earls JD, Sherman JW, Lopez LC, Dettloff ML. Polymer 2007;48:3990.
34. Spindler R, Fréchet JM. Macromolecules 1993;26:4809.
35. Vanjinathan M, Shanavas A, Raghavan A, Sultan NA. J Polym Sci A Polym Chem 2007;45:3877.
36. Barmar M, Barikani M, Kaffashi B. Iran Polym J 2001;10:331.

37. Origuchi R, Onishi Y, Hayase S. *Macromolecules* 1988;21:304.
38. Miller RD, Milch J. *Chem Rev* 1989;89:1359.
39. Gauthier S, Worsfold DJ. *Macromolecules* 1989;22:2213.
40. Nakashima H, Fujiki M. *Macromolecules* 2001;34:7558.
41. Kakimoto M, Kashihara H, Kashiwagi T, Takiguchi T, Ohshita J, Ishikawa M. *Macromolecules* 1997;30:7816.
42. Isaka H. *Macromolecules* 1997;30:344.
43. Herzog W, West R. *Macromolecules* 1999;32:2210.
44. Reuss VS, Frey H. *Macromolecules* 2010;43:8462.
45. Mark JE, Allcock HR, West R. *Inorganic Polymers*. Englewood Cliffs, NJ: Prentice Hall Inc; 1992. p 75.
46. Wisian-Neilson P, Neilson RH. *J Am Chem Soc* 1980;102:2848.
47. Neilson RH, Wisian-Neilson P. *Chem Rev* 1988;88:541.
48. Weisian-Neilson P, Ford RR, Neilson RH, Ray AK. *Macromolecules* 1986;19:2089.
49. Inoue K. *Prog Polym Sci* 2000;25:453.
50. Rogers ME, Long TE. *Synthetic Methods in Step-Growth Polymers*. Hoboken, NJ: John Wiley & Sons; 2003. p 8.
51. Kathiresan M, Walder L, Ye F, Reuter H. *Tetrahedron Lett* 2010;51:2188.
52. Zhao Y-L, Cai Q, Jiang J, Shuai X-T, Bei J-Z, Chen C-F, Xi F. *Polymer* 2002;43:5819.
53. Endo K, Ito Y, Higashihara T, Ueda M. *Eur Polym J* 1994;30:945.
54. Tractin AA. *Coatings and Technology Handbook*. 3rd ed. Boca Raton: CRC Press; 2006.
55. Cook WD, Lau M, Mehrabi M, Dean K, Zipper M. *Polym Int* 2001;50:129.
56. Zetterlund PB, Gosden RG, Weaver W, Johnson AF. *Polym Int* 2003;52:149.
57. Vargas MA, Sachsenheimer K, Guthausen G. *Polym Test* 2012;31:127.
58. Pascual JP, Williams RJ. *Epoxy Polymers: New Materials and Innovations*. Weinheim: Wiley-VCH; 2010.
59. Gan S-N, Tan BY. *J Appl Polymer Sci* 2001;80:2309.
60. Aigbodion AI, Pillai CKS. *J Appl Polymer Sci* 2001;79:2431.
61. Ikuoria EU, Okieimen FE, Obazee EO, Erhabor T. *Afr J Biotechnol* 1913;2011:10.
62. Holmberg K. Alkyd resins. In: Tractin AA, editor. *Coatings and Technology Handbook*. 3rd ed. Boca Raton: CRC Press; 2006. p 51.
63. Patel VC, Varughese J, Krishnamoorthy PA, Jain RC, Singh AK, Ramamoorthy M. *J Appl Polymer Sci* 2008;107:1724.
64. Singh S. *J Sci Ind Res* 2009;68:807.
65. Bourlier K. Phenolic resins. In: Tractin AA, editor. *Coatings and Technology Handbook*. 3rd ed. Boca Raton: CRC Press; 2006. p 53.
66. Pilato L. Resin chemistry. In: Pilatos L, editor. *Phenolic Resins: A Century of Progress*. Berlin Heidelberg: Springer Verlag; 2010. p 41.
67. Ogata S, Kakimoto M, Imai Y. *Macromolecules* 1985;18:851.
68. Rogers ME, Long TE, Turner SR. Introduction to synthetic methods in step-growth polymerization. In: Rogers ME, Long TE, editors. *Synthetic Methods in Step-Growth Polymers*. Hoboken, NJ: John Wiley and Sons, Inc; 2003. p 1.
69. Korematsu A, Furuzono T, Kishida A. *Macromol Mater Eng* 2005;290:66.
70. de Ruijter C, Jager WF, Groenewold J. *Macromolecules* 2006;39:3824.
71. Loría-Bastarrachea MI, Aguilar-Vega M. *J Membr Sci* 2011;369:40.
72. Odian G. *Principles of Polymerization*. 4th ed. New York: John Wiley & Sons, Inc; 2003.
73. Yokoyama A, Yokozawa T. *Macromolecules* 2007;40:4093.
74. Moore JS, Hill DJ, Mio MJ. Solid-phase synthesis of sequence-specific phenylacetylene oligomers. In: Burgess K, editor. *Solid-Phase Organic Synthesis*. New York: John Wiley Sons, Inc.; 2000. p 119–147.
75. Zaragoza-Dörwald F. *Organic Synthesis on Solid Phase: Supports, Linkers, Reactions*. 2nd ed. Weinheim: Wiley-VCG; 2002.
76. Nakata S, Brisson J. *Eur Polym J* 2000;36:831.
77. König HM, Abbel R, Schollmeyer D, Kilbinger AFM. *Org Lett* 1819;2006:8.
78. Hartmann L, Krause E, Antonietti M, Börner HG. *Biomacromolecules* 2006;7:1239.
79. Santiago-García JL, Aguilar-Vega M. *Eur Polym J* 2009;45:3210.
80. Merrifield RB. *J Am Chem Soc* 1963;65:2149.
81. Ito K, Kawaguchi S. *Adv Polym Sci* 1999;142:129.
82. Yagci Y, Nuyken O, Graubner V-M. Telechelic polymers. In: Kroschwitz JJ, editor. *Encyclopedia of Polymer Science and Technology*. 3rd ed. Volume 12. New York: Wiley and Sons; 2005. p 57–130.
83. Lee H-S, Roy A, Lane O, McGrath JE. *Polymer* 2008;49:5387.
84. Hutchings LR, Dodds JM, Roberts-Bleming SJ. *Macromolecules* 2005;38:5970.
85. Hutchings LR, Roberts-Bleming SJ. *Macromolecules* 2006;39:2144.

4

FREE RADICAL POLYMERIZATION

RAMIRO GUERRERO-SANTOS, ENRIQUE SALDÍVAR-GUERRA, AND JOSÉ BONILLA-CRUZ

4.1 INTRODUCTION

There have been many amazing discoveries in human history. Some of them have a direct utility and others have been combined with other innovations to fit an enormous diversity of applications. Free radical polymerization (FRP) is one of these discoveries. The first papers in this area were published in the 1940s and 1950s. However, even before that, in the 1930s, the applicability of this technique rapidly propelled this method to the commercial scale for the manufacture of diverse polymers starting from oil derivatives. Nowadays, FRP is the solid foundation of many industrial processes and a source of a number of polymeric materials. Materials such as polyethylene, polystyrene, polyvinylalcohol, polyvinylacetate, polybutadienes, and other well-known commodities have significantly improved day-to-day life. However, the considerable growth of this petrochemical segment over seven decades is now in danger because of environmental issues and high oil prices. Hence, to improve profit margins and avoid reputation losses, the industry has been moving toward bioresourced polymers during the last two decades. In addition, during the mid-1990s, FRP was revitalized with the introduction of the reversible deactivation techniques—commonly known as *controlled/living RP* [1–3]—opening the possibility to form very diverse block copolymers or more complex structures, which could not be synthesized earlier by FRP techniques. The ability to manipulate and control the termination reaction is a major milestone that represents a good possibility to produce an alteration in the landscape of vinyl polymers.

The crucial feature of an FRP is an adjustable radical source, which is commonly materialized by a thermolabile substance—or initiator—that splits apart under heating to form free radicals, that is, highly reactive species with an

unsatisfied electron valence pair. At the simplest, these species add to a monomer molecule to initiate propagation and turn out to be one of the end groups of a linear chain. Generally, the rate of addition of a monomer is higher if a resonance-stabilized radical is formed from a non-resonance-stabilized monomer and vice versa.

To be polymerized, vinyl monomers use the property that with the addition of each monomer, the resulting free radical maintains the same structure as that of the attacking radical and sustains the ability to add new molecules. In the formation of monomeric unit chains, the variation of entropy is negative, that is, the monomer-to-polymer conversion entails a reduction of disorder, while a compensation of the enthalpy term is observed. The alteration results in a negative variation of enthalpy; therefore, the reaction is exothermic.

The rates of addition to the unsaturated 1- and 1,1-disubstituted olefins are thought to be mainly determined by polar factors. Electron-withdrawing substituents will facilitate the addition of nucleophilic species, while electron-donating substituents will enhance the addition of electrophilic species. The addition of an initiating free radical to a monomer is called the *initiation step*, which is the first step of a chain reaction or propagation that ends through a termination reaction, in which two radicals interact in a mutually destructive reaction to form covalent bonds and cease propagation.

Generally, peroxides and azo compounds are commercially employed as initiators of a large number of monomers. The monomer and initiator industries are based on mature technologies and very few improvements centered on lower energy processes have been developed in recent years. The major worldwide players of organic peroxide initiators are Arkema, Akzo Nobel, Degussa-Huls

AG, and Nippon Oil & Fats Co. Bulk amounts of styrene, vinylacetate, vinylchloride, ethylene, and numerous other monomers are produced worldwide by many petrochemical companies.

This chapter deals with the description of the FRP mechanism and presents a review of the latest advances in the termination reaction control.

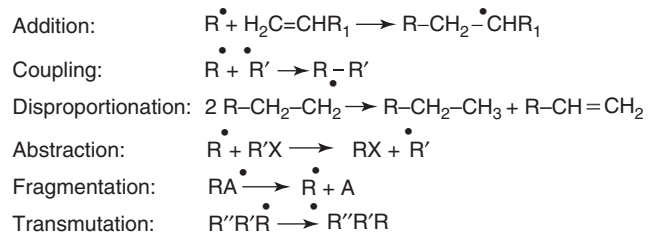
4.2 BASIC MECHANISM

The most conventional kinetic scheme of FRP includes initiation, propagation, and bimolecular termination reaction steps. Additional reactions such as chain transfer are introduced to improve the process description. Free radicals are highly reactive chemical species produced by the homolytic dissociation of covalent bonds. Such species are produced through physical (thermoexcitation, radiation) or chemical methods (oxidation-reduction, addition, etc.). Generally, their survival time is less than a second, except for those radicals highly stabilized by specific chemical groups; the hybridization state is sp^2 .

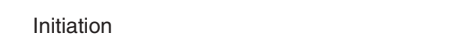
Free radicals react in six different manners as illustrated in Scheme 4.1 [4, 5].

In an FRP, all these reactions are susceptible to occur, but in a concentrated monomer environment, the dominating reactions are the addition (propagation) and termination by disproportionation or coupling. The fragmentation, abstraction, and transmutation reactions are detrimental for the chain formation; however, sometimes they can be induced to regulate the degree of polymerization.

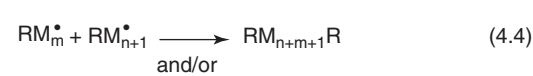
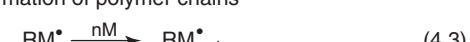
The central mechanism of chain formation involves the generation of free radicals (reaction (i)), the initiation (reaction (ii)), propagation (reaction (iii)), and termination (reactions (iv) and (v)) (Scheme 4.2). The radical generation and the first monomer *addition* to an initiating radical constitute the initiation step, whereas the successive monomer *additions* over a new free radical and the termination of chain growth by *disproportionation* and/or *coupling* actually constitute the formation of chains as represented in Scheme 4.2.



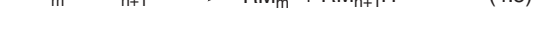
Scheme 4.1 Free radical reactions.



Formation of polymer chains



and/or



Scheme 4.2 Reactions induced by an initiating radical generated from the initiator A.

4.2.1 Initiation

Chemical initiation involves the decomposition of initiator molecules A to form very active primary radicals R^\bullet capable of initiating new polymer chains. The stability of A is measured by the half-life time ($t_{1/2}$) defined in terms of its dissociation constant k_d as follows:

$$[A] = [A]_0 \exp(-k_d t) \quad (4.1)$$

or

$$\ln \frac{[A]_0}{[A]} = k_d t \quad (4.2)$$

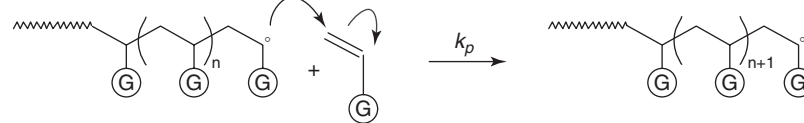
If $[A]_0/[A] = 2$, then

$$t_{1/2} = 0.693/k_d \quad (4.3)$$

Owing to the very close proximity of any two radicals generated from A, not all of them can eventually escape from their solvent "cage" to react with monomer molecules. Some radicals will either self-terminate or will react with other near-neighboring molecules before diffusing out of the cage. To account for this, an empirical initiator efficiency factor, f , which represents the fraction of all generated initiator primary radicals leading to the formation of new polymer chains, has been introduced. This parameter may have values between zero and unity. Even if the radical R^\bullet escapes from the cage, any of the possible side reactions (reactions (ii)-(v)) can be produced, although they are minimized by the ubiquitous presence of monomer.

The concentration of initiating radicals R^\bullet depends on $[A]$, k_d , and f . The initiator's efficiency itself depends on the ability of R^\bullet to add to the monomer instead of undergoing termination. Thus, the efficiency depends on the monomer concentration and the ratio k_i/k_p , where k_i is the rate constant of the initiation reaction and k_p is the rate constant of the propagation reaction.

Only some radicals R^\bullet succeed in the initiation step to form RM^\bullet , which becomes the precursor of a polymer chain. Initiating radicals are generated from a compound

**Scheme 4.3** Schematic representation of the propagation reaction.

A with kinetics governed by k_d , the rate constant of dissociation.

4.2.2 Propagation

It is an addition reaction that generates the polymer chain by a series of fast successive steps of monomer addition over the propagating radical. The microstructure of the polymer, which determines its properties, is established through this reaction.

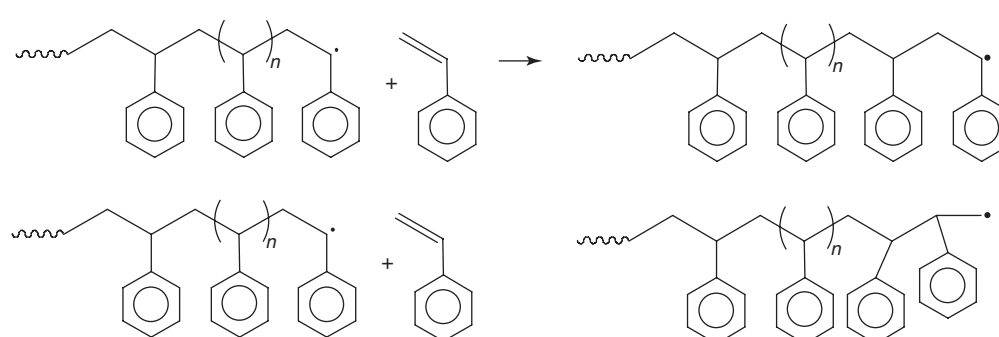
The addition of a monomer unit results in a radical structurally similar to the radical before the addition; therefore, there is no alteration in the stability of the growing radical. The group substituent (G in Scheme 4.3) has an effect on the stability of both the double bond and the resulting radical. An increase in the stabilizing effect of G produces a reduction of k_p , the rate constant of the propagation reaction, as indicated in Table 4.1. To simplify the mathematical treatment of the kinetics in the radical polymerization, it is assumed that k_p is independent of the size of the propagating radical. Nevertheless, it is known that the diffusivity of species affects the rate constant, a fact that is more evident at low molecular weights (MWs).

Given that the propagation involves the addition of unsymmetrical alkenes, regioselectivity is an important issue. As a general rule, the less-substituted carbon is more preferred to produce a bond. However, the more-substituted carbon is not totally discriminated. Thus, for a given monomer, different modes of bonding are observed and their percentages depend on the nature of substituent G. For a substituent providing a strong stabilization to the end-free radical, the regioselectivity increases, that is, the head-to-tail addition (Scheme 4.4) is predominant in comparison with the head-to-head addition.

For conjugated dienes such as butadiene, the delocalization of the radical induces the formation of species with the unpaired electron in carbon 2 or carbon 4 at the last monomer unit in the propagating chain. Such species can then add the next butadiene unit by carbon 1 or carbon 4 forming additions called 1–2 or 1–4, respectively. In the case of monosubstituted dienes, such as isoprene or chloroprene, additions 3–4 can also occur depending on

TABLE 4.1 Propagation Rate Constants of Some Monomers at 25°C

Monomer	Chemical Structure	k_p (l/(mol s))
Vinylidene chloride		9
Styrene		35
Chloroprene		228
Acrylic acid		650
Methyl methacrylate		1,010
Vinyl chloride		3,200
Acrylamide		18,000
Acrylonitrile		28,000

**Scheme 4.4** Head-to-tail and head-to-head (bottom) additions.

the regioselectivity of the monomer. As an example, in the polymerization of butadiene, 1–4 additions account for 80% of the total additions.

In FRP, the monomer addition is practically not stereoselective, as at the moment of the monomer additions, there is no preferred conformation of the radical. Therefore, there is no regular conformation of monomer units in the polymer chain. The sp^2 hybridization in the carbon atoms of a double bond and the resulting π bond favor a planar arrangement of the two carbon atoms and the four immediate ligand atoms. On the other hand, the geometry of alkyl radicals is considered to be a shallow pyramid, somewhere between sp^2 and sp^3 hybridization; the energy required to invert the pyramid is very small. In practice, one can usually think of alkyl radicals as if they were sp^2 hybridized and then their conformation is undefined at the moment of the radical addition over the planar double bond. Only the steric hindrance or electrostatic forces slightly affect the orientation of the monomer substituent and the resulting polymer is atactic, that is, it does have a random spatial orientation of substituent G. The formation of isotactic or syndiotactic polymers is not possible via radical polymerization.

4.2.3 Termination

Termination is also a fundamental reaction. Since the rate constants of this reaction are very high ($k_t = 1 \times 10^7$ to 1×10^8 l/(mol s)), the very low concentration of propagating chains is critical for the radical to survive some seconds or fractions of a second before the encounter with another radical species. A propagating chain can be deactivated through one of several possible reactions to become a polymer molecule. Termination is generally associated with reactions involving coupling and disproportionation processes, but a propagating radical can also participate in abstraction reactions resulting in growth deactivation; this type of reaction is called *chain transfer*.

The formation of polystyrene chains initiated by radicals generated by thermolysis of AIBN (2,2' azobisisobutyronitrile) can be quoted as an example. The 2-cyanoprop-2-yl radical adds to styrene, opening the π bond to form a new carbon-centered radical. This new species rapidly add to another styrene molecule and chain growth is produced by the successive additions of new styrene in a repetitive process occurring at very high rates. The active center is thus continuously relocated at the end of the growing polystyrenyl chain. This propagation stops when two radical species encounter each other and recombine to form a larger chain or disproportionate resulting in two inactive polystyrene chains. Termination rate is diffusion controlled, which means that its speed is determined by how fast the molecules move.

The speed of movement mainly depends on the molecule size and some other related factors, such as the number of obstacles around the polymer and the temperature of the system. In fact, this is the origin of the complexity of the termination reaction.

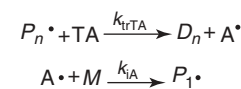
There is no precise method for the measurement of the termination rate. Major difficulties in rate constant (k_t) determination arise from the diffusion control of this reaction. Termination rate may depend on segmental and translation diffusion (and reaction diffusion) of radical species occurring in an increasingly viscous medium that change with monomer conversion. In other words, because of the decrease of the diffusion coefficient with molecular size, the termination rate coefficient is lower at higher chain lengths.

The size or MW is self-regulated by the termination reaction and the inherent side reactions. Externally, MW can be also adjusted by the reaction conditions. An increase of temperature causes faster AIBN decomposition, resulting in a lower MW because more chains are created; on the contrary, higher pressure increases the propagation and inhibits the termination resulting in higher MW. The increase of the AIBN concentration has a similar effect to that of the increase of temperature.

4.3 OTHER FREE RADICAL REACTIONS

4.3.1 Chain Transfer to Small Species

A propagating chain (live species) can also terminate via chain transfer reaction to a small molecule. This will lead to termination of the propagating chain, along with the generation of a radical on the small molecule that can initiate another propagating chain. This is schematically represented in Scheme 4.5, where P_n^\bullet is a propagating chain having n number of units, TA is a small molecule to which the activity is being transferred, D_n is dead polymer having n number of units, and A^\bullet is the radical resulting from the activation of the small molecule. In the process, the atom or species T is transferred to the growing chain and is incorporated in the dead polymer molecule. Usually, the net effect of the chain transfer is negligible on the polymerization rate, since there is no net creation or destruction of radicals (their *nature* of them changes but *not* their *number*), but it causes a decrease in MW. However, other effects may occur depending on the relative values of k_{trTA} and k_{IA} with respect to k_p . The units of the rate coefficients are liter per mole per second or cubic meter



Scheme 4.5 Simplified mechanism of chain transfer to a small species TA.

per mole per second. It is common practice to report the ratio of the transfer rate coefficient to the propagation rate coefficient, and this quantity is denoted as transfer constant $C_{\text{trTA}} = k_{\text{trTA}}/k_p$; it is defined to measure the ability of each substance to produce a chain transfer reaction.

The small species TA can be a monomer (M), a solvent (S), a chain transfer agent (CTA), an initiator (I), or an impurity (X) in the system. Chain transfer reactions occur spontaneously because of the inherent reactivity of free radicals; however, such reactions can be also induced by adding a CTA having a high proclivity to react with growing chains. A chain transfer agent is a species specifically added to the system to control the MW. In the following, the characteristics of the chain transfer reaction to specific species are considered.

4.3.2 Chain Transfer to Monomer

This reaction is generally described by the simple scheme shown above (Scheme 4.5) with TA being monomer and T (the transferred atom) being H; therefore the rate of C_M is $k_{\text{trM}} [P][M]$, where [P] is the total concentration of propagating chains. However, Moad and Solomon [5] consider that this mechanism is reasonable for monomers having aliphatic labile hydrogens (such as methyl methacrylate, vinyl acetate, and allyl monomers), but it is not likely to occur for monomers having only vinylic or aromatic protons (such as styrene or vinyl chloride), due to the difficulty of breaking the strong C–H bond in these cases. The details of the exact mechanisms for these monomers remain to be of a speculative character. Table 4.2 lists C_M values for some common monomers. In the absence of other transfer reactions, chain transfer to monomer will impose an upper limit to the maximum MW achievable in the polymerization of the corresponding monomer. This does not mean that this reaction will in general be the controlling step determining the MW; indeed bimolecular termination usually plays this role. However,

TABLE 4.2 Values of Chain Transfer to Monomer Constant C_M for Some Common Monomers

Monomer	Temperature (°C)	$C_M \times 10^4$
Acrylonitrile	60	0.26–1.02
Butyl acrylate	60	0.333–1.05
Ethylene	60	0.4–4.2
Methyl methacrylate	60	0.07–0.18
Styrene	60	0.07–1.37
	70	0.6–2.0
Vinyl acetate	60	1.75–2.8
Vinyl chloride	50	8.5
	60	12.3

All values are taken from Reference [6] except for vinyl chloride [7].

there are monomers for which C_M is so high (e.g., vinyl chloride) that transfer to monomer becomes the controlling factor. High values of transfer constants to monomer are associated with high reactivity of the propagating radical.

4.3.3 Chain Transfer to Initiator

Values for chain transfer constants to initiator are listed in Table 4.3. Note that these values are generally larger than those of transfer to monomer; however, the effect of this reaction is attenuated by the fact that the initiator is present in very small amount with respect to the monomer, as the rate of transfer to initiator is $k_{\text{trI}} [P][I]$.

4.3.4 Chain Transfer to Solvent and Chain Transfer Agents

When polymerization takes place in a solvent, it is important to be aware of possible chain transfer to solvent reactions. On the other hand, there are many instances, especially in industrial processes, in which it is convenient to include in the polymerization recipe some species (called *chain transfer agent*) that have a

TABLE 4.3 Values of Chain Transfer to Initiator Constant C_M for Some Common Polymerization Systems

Initiator	Temperature (°C)	Styrene	Methyl Methacrylate	Vinyl Acetate
AIBN (2,2' azobisisobutyronitrile)	60	0–0.16	0	—
Benzoyl peroxide	60	—	0–0.02	0.032–0.15
	70	0–0.18	—	—
	80	0.13–0.813	—	—
Lauroyl peroxide	60	—	—	0.10
	70	0–0.024	—	—
Palmytoil peroxide	60	—	0.10–0.17	0–0.16
	70	0.142	—	—
Tert-butyl peroxide	70	0.031	—	—
	80	0.0022–0.0033	—	—

All values are taken from Reference [6].

TABLE 4.4 Values of Chain Transfer to the Solvent or CTA constant C_s/C_{CTA} for Some Common Polymerization Systems

Solvent or CTA	Temperature (°C)		C_s	
		Ethylene	Methyl methacrylate	Styrene
Acetone	60	—	0.195	0.32–4.1
	80	—	0.225–0.275	—
	130	160–168	—	—
1-Butanethiol	60	—	0.66–0.67	21.0–25
	70	—	—	15.0
	80	—	—	17.0
	130	5.8	—	—
Carbon tetrachloride	60	—	0.42–20.11	69–148
	70	—	1.74	—
	80	—	2.4–24.4	133
	140	1,600–180,000	—	—
Chloroform	60	—	0.454–1.77	0.41–3.4
	80	—	1.129–1.9	0.50–0.916
	140	3,210–37,600	—	—
Ethyl benzene	60	—	0.766	0.67–2.7
	80	—	1.311–2.1	1.07–1.113
	100	—	—	1.38–2.33
Hexane	100	—	—	0.9
	130	68	—	—
	189	225	—	—
Propane	130	27–31	—	—
Toluene	60	—	0.17–0.45	0.105–2.05
	70	—	0.561	—
	80	—	0.292–0.91	0.15–0.813
	100	—	—	0.53–0.8
	130	130–180	—	—
1-Dodecanethiol	60	—	0.7	—
	70	—	0.55	0.69–19
	80	—	0.42	—
	90	—	0.33	1.3
	100	—	—	13.0
	110	—	—	26.0

All values are taken from Reference [6].

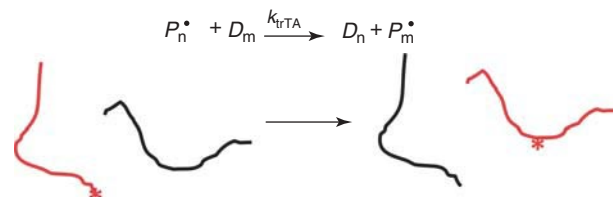
high chain transfer constant in order to lower the MW of the polymer being formed. Among many different substances used for that purpose, thiols are by far the most popular chain transfer agents. Evidently, depending on the nature of T, the chain transfer reaction occurs at different rates. The addition of a CTA is rather common in, for example, emulsion polymerization, in which the compartmentalized nature of the reaction tends to produce very high MW polymer due to the relative isolation of the propagating radicals in very small particles. The rates of reaction of chain transfer to a solvent and to a CTA are conceptually the same: $k_{trS} [P][S]$ and $k_{trCTA} [P][CTA]$, respectively. The values of chain transfer constants to solvent and to CTAs are usually reported in one table, as they lie in a continuum going from low values for solvents to rather high values for CTAs (see Table 4.4 for illustrative values).

4.3.5 Chain Transfer to Impurities

Impurities can also act as chain transfer agents. In some instances, as in the production of low density polyethylene via high pressure radical polymerization, impurities and/or the so-called inerts (methane, ethane, and propane), which come as impurities in the ethylene, are used as effective chain transfer agents to lower the MW of the polymer.

4.3.6 Chain Transfer to Polymer

The mechanism of Scheme 4.5 can also occur when the TA species is not a small molecule, but an inactive or a dead polymer instead. In this case, it is convenient to rewrite the reaction mechanism for clarity (Scheme 4.6).



Scheme 4.6 Simplified mechanism of chain transfer to a small species TA.

Evidence suggests that the mechanism proceeds by hydrogen abstraction, but this has been proved only for a few monomers [5]. However, since the hydrogen abstraction on the inactive chain D_m can occur at any monomeric unit along the chain, the free radical left in the reactivated chain will most likely give rise to a branch (unless the activation occurs at a chain end), once that monomer propagates from the just activated site. The mechanism represented in Scheme 4.6 corresponds to the intermolecular chain transfer, which involves two independent polymer chains (one active and the other dead); it is also possible that intramolecular chain transfer occurs (also called *backbiting*), in which the hydrogen abstraction occurs in the same active chain, a few carbons (about five) before the active end of the growing polymer. Intermolecular transfer will give rise to long branches, while intramolecular transfer will be the origin of short branches. Both short and long branches have a profound influence in the physical and rheological properties of the polymer formed.

The experimental determination of the chain transfer to polymer constant is difficult, as it does not necessarily result in a decrease of the MW of the polymer. Therefore, there is a large spread of values reported in the literature for this constant [6]. Since it involves hydrogen abstraction, the activation energy of chain transfer to polymer is relatively high (compared to propagation) and it is reported in the range of 9000 cal/mol in the case of ethylene [8]. Reaction conditions that favor transfer to polymer are high temperatures and high conversions (due to the high concentration of dead polymer present).

4.3.7 Backbiting

Recent studies convincingly proved the existence of mid-chain radicals (MCRs) and the secondary reactions that are responsible for the formation of MCRs during the polymerization process [9]. For instance, the polymerization of butyl acrylate (BA), and in general of the acrylate monomer family, proceeds with the presence of two radicals: a chain-end (secondary) radical and an MCR (tertiary and significantly

less reactive) that are predominantly formed by the backbiting process, an intramolecular transfer to polymer, that produces short-chain branches.

The MCRs can also be formed by intermolecular chain transfer to polymer (leading to long-chain branches), but its contribution is small.

Backbiting generates a tertiary (mid-chain) radical, R_t , by abstraction of a hydrogen atom from an acrylate unit on the backbone of the secondary (chain-end) radical R_s , most likely via the formation of a six-membered ring, as shown in Scheme 4.7 for BA. Subsequent addition of monomer to R_t creates a short-chain branch (SCB) in the polymer and leads to re-formation of a chain-end radical. The propagation rate coefficient for monomer addition to the MCR, k_{pt} , is significantly lower than that for addition to the secondary chain end [10].

4.3.8 Inhibition

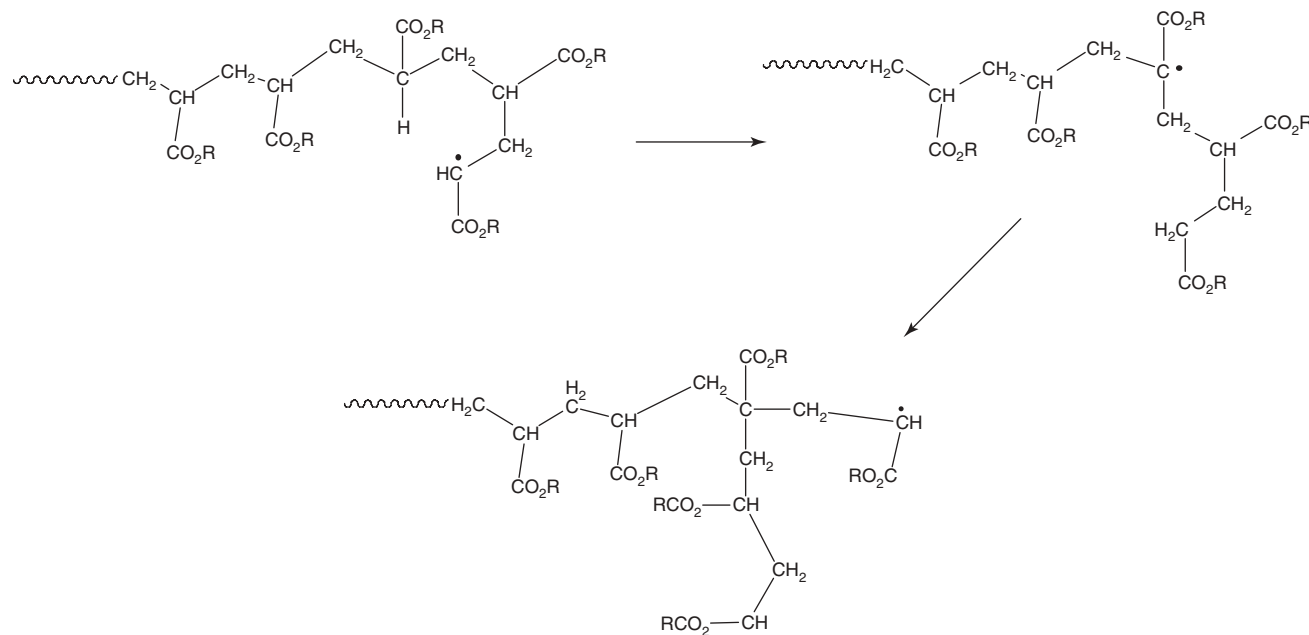
An inhibitor is used to completely stop the conversion of monomer to polymer produced by accidental initiation during storage. To induce the inhibition, some stable radicals are mixed with the monomer. Such radicals are incapable for initiation the polymerization, but they are very effective in combining with any propagating radical. Diphenylpicrylhydrazyl and tetramethylpiperidinyloxy (TEMPO) are two examples of radicals used to inhibit the radical polymerization. The chemical reactions of the inhibition produced by these compounds are shown in Scheme 4.8.

It is worth mentioning that these radicals are very effective at low temperature, but at temperatures above 100 °C, these reactions are reversible. Some other compounds, such as phenols, quinones or hydroxyquinones, or even molecular oxygen, are also employed to inhibit the polymerization; the mechanism of action of these compounds involves the transformation of the propagating radical to an oxygen-centered radical that is unable to initiate polymerization. The case of quinones is shown in Scheme 4.9.

4.4 KINETICS AND POLYMERIZATION RATE

In its simplest and essential form, the mechanism of FRP involves the steps of initiation (radical generation), propagation, and bimolecular termination. The corresponding reaction rates for the three steps are denoted by R_i , R_p , and R_t , respectively. To derive a rate expression, for the sake of generality, the simplified mechanism and expressions in columns 2 and 3 of Table 4.5 are considered first; later a more detailed mechanism (column 4 of Table 4.5), specific for chemical initiation and involving termination by disproportionation and combination, is analyzed.

In FRP, the progress of the reaction is measured in terms of conversion of monomer into polymer (this is different

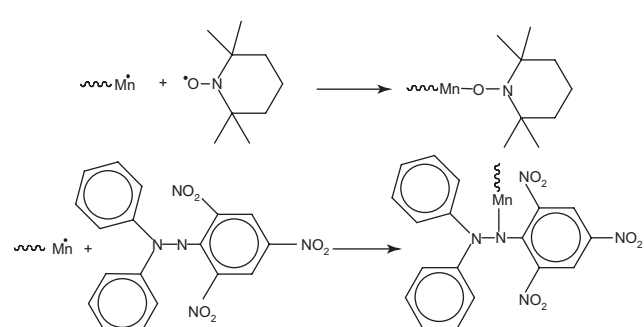


Scheme 4.7 Backbiting reaction or intramolecular transfer to polymer.

TABLE 4.5 Simple Kinetic Mechanism for Free Radical Polymerization

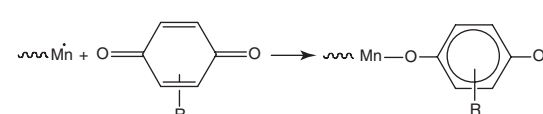
Reaction step	Simplified Mechanism	Rate Expression	Detailed Mechanism for Chemical Initiation
Initiation	None specified	R_i	$I \xrightarrow{k_d} 2R$ $R + M \xrightarrow{k_i} P_1$
Propagation	$P + M \xrightarrow{k_p} P$	$R_p = k_p[M][P]$	$P_n + M \xrightarrow{k_p} P_{n+1}$
Termination	$P + P \xrightarrow{k_t} D$	$R_t = k_t[P]^2$	$P_n + P_m \xrightarrow{k_{td}} D_n + D_m$ $P_n + P_m \xrightarrow{k_{tc}} D_{n+m}$

P , M , and D are the growing radicals, monomer, and dead polymer, respectively. I and R are the chemical initiator and primary radicals, respectively. When included, the subindex in polymeric species (P and D) represents chain length.



Scheme 4.8 Schematic representation of inhibition reactions with TEMPO and with diphenylpicrylhydrazyl.

from the polycondensation case, in which the conversion is measured in terms of reacted functional groups). It is assumed that, independently of the initiation method used, most of the monomer is consumed by the propagation reaction (this is the so-called long chain hypothesis or



Scheme 4.9 Schematic representation of inhibition reactions with quinones.

LCH); therefore, the rate of polymerization is defined as

$$R_p = -\frac{d[M]}{dt} = k_p [M] [P] \quad (4.4)$$

with units of liter per mole per second. The experimental measurement of $[P]$ is difficult¹ given the low concentrations of growing radicals in a typical polymerization; therefore, it is convenient to write this quantity in terms

¹Electron spin resonance (ESR), also called *electron paramagnetic resonance* (EPR), can be used to experimentally measure $[P]$ [72].

of other species that are easier to measure. To do this, a differential mass balance on $[P]$ is written:

$$\frac{d[P]}{dt} = R_i - k_t [P]^2 \quad (4.5)$$

The growing radicals are very reactive intermediate species that conform to what in chemical kinetics is called a *quasi-steady state* (QSS) or *stationary state hypothesis* [11, 12]. This means that the rate of formation and consumption of that species become nearly equal in a very short timescale; as a consequence, the absolute value of the derivative becomes very small and negligible compared with the derivatives of other species in the system (e.g., $d[M]/dt$) and for practical purposes can be approximated as zero. Note, however, that this does not imply constancy of the value of $[P]$, as sometimes interpreted by some authors, but this will be more clear later. By making the QSS approximation in Equation 4.5

$$R_i - k_t [P]^2 \approx 0 \quad (4.6)$$

and

$$[P] = \left(\frac{R_i}{k_t} \right)^{1/2} \quad (4.7)$$

Equation 4.7 is a general expression for the QSS concentration of growing radicals in a FRP. Other features related to the QSS are noticeable from this expression. (a) The high reactivity of the growing radicals is reflected in a rather high value of k_t (in the order of 10^7 – 10^8 l/(mol s)), which is also consistent with a rather low value of the QSS concentration of $[P]$ (typical values are 10^{-7} to 10^{-9} mol/l) as this concentration is inversely proportional to the value of k_t . (b) Since R_i and k_t may change during the course of a polymerization (as they usually do), the value of $[P]$ will not be constant; it will change following the changes in the “slow” variables of the system (initiator and monomer concentration, kinetic coefficients, etc.) instead.² Finally, in writing expressions 4.6 and 4.7, the convention that a single radical has been consumed by the termination reaction (instead of the other convention in which two radicals are consumed) has been used. It has been recently noted that the convention used here is the correct one

²The apparent paradox of a zero derivative for $[P]$ with the simultaneous possibility of a changing value for the same quantity is cleared by noting that the time derivative of $[P]$ is not really zero; it is very small instead, compared with the derivatives of other “slow” species in the system. In dynamic terms, the time for $[P]$ to reach a QSS value (e.g., from the start of a polymerization when $[P] = 0$) is extremely short (in the order of a second) compared with the characteristic time of a polymerization (minutes or hours). Seen from the point of view of the polymerization timescale, the value of $[P]$ is instantaneously and continuously adjusted (and therefore always at a QSS value) to reflect the slow changes occurring for the slow species in the reaction system.

[13], according to the rules of formulation of kinetic rate equations. Nonetheless, the reader should be aware that both conventions are still amply used in the technical literature.

When a specific type of initiation is used, the expression for R_i will be more detailed. The fourth column in Table 4.5 includes the kinetic mechanism for the commonly used initiation via a chemical initiator (such as a peroxide or an azo compound). In that case, the effective rate of generation of polymeric radicals is given by the second initiation step. The resulting expression is

$$R_i = k_i [R] [M] \quad (4.8)$$

Again, it is desirable to write the rate expression without explicitly including the concentration of primary radicals R , which is difficult to measure. A differential balance for the primary radicals, followed by the application of the QSS, results in

$$\frac{d[R]}{dt} = 2f k_d [I] - k_i [R] [M] \approx 0 \quad (4.9)$$

which, combined with Equation (4.8), results in

$$R_i = 2f k_d [I] \quad (4.10)$$

The factor f , called *initiator efficiency*, takes into account that not all the primary radicals R effectively initiate polymer chains; some can be lost due to the so-called cage effect. This implies secondary reactions of the radicals within a “cage” of solvent surrounding the initiator [5] (the effect can be more pronounced at high conversions/viscosities due to diffusion limitations). The values of f usually lie in the range 0.3–0.8.

The resulting expressions for the reaction rate are then

$$R_p = k_p [M] \left(\frac{R_i}{k_t} \right)^{1/2} \quad (4.11)$$

$$R_p = k_p [M] \left(\frac{2f k_d [I]}{k_t} \right)^{1/2} \quad (4.12)$$

for any R_i or for chemical initiation, respectively.

4.4.1 Variations of k_p and k_t with Length and Conversion: Autoacceleration

In the above derivations, the values of k_p and k_t have been implicitly considered as constants independent of the reaction medium and of the chain length of the polymeric chains involved in the reactions. For propagation, it is known that this is true only to a first approximation, since there is increasing evidence that the value of k_p should be greater for the first few propagation steps, when the chain

length of the growing chain is in the single-digit range, than for longer chains (length > 20) [5]. In addition, it is well established that the termination among radicals is a diffusion-controlled process, which may be affected by the reaction medium (polymer concentration, temperature) and the lengths of the individual chains reacting; therefore, the value of k_t is not really constant.

A phenomenon that has a particularly significant effect in the value of k_t and has been studied for many years is the so-called gel effect, which is also known as *Trommsdorff* or *Norrish-Smith effect* [14, 15]. This consists in an autoacceleration of the reaction rate as the conversion increases, and it is due to an effective decrease in the termination rate as the growing radicals encounter more difficulty in diffusing in the increasingly viscous medium. As the value of k_t decreases by several orders of magnitude in the course of the polymerization as a consequence of this phenomenon, the concentration of growing radicals [P] increases, as well as the polymerization rate (Eq. 4.7, 4.11, and 4.12). A broadening of the molecular weight distribution (MWD) simultaneously occurs. The gel effect is a complex phenomenon and it is mainly determined by translational (center of mass) and segmental diffusion (internal movement or rearrangement of the polymer coil) [16], although other motion mechanisms can also have an influence on it, for example, reptation and reaction-diffusion (chain-end motion by monomer addition at the reactive end). Experimental evidence for the gel effect usually takes the form of a rise in the slope of a plot of monomer conversion versus time. At low conversion, the slope is nearly constant. At intermediate levels of conversion, the magnitude of which depends on the monomer and other factors, the polymerization rate begins to increase to a much higher level, resulting in a steeper slope.

The quantitative modeling of this phenomenon has been addressed by many authors, but the problem is rather complex, and so far no single model is generally accepted. Most of the modeling studies have used styrene and methyl methacrylate polymerization experimental data for comparison, as in these systems the presence of the gel effect is quite clear. For several other systems, the extent of the effect has not been clearly assessed. It has been argued that the diffusion-controlled termination is present from the very start of the polymerization [17]; however, the sharp autoacceleration of the reaction rate (or gel effect onset) occurs at some moderate-to-medium conversion (20–80% depending on the system) and this point is expected to be correlated with the polymer concentration needed for chain entanglement [18]. Early attempts at modeling this phenomenon were mostly empirical or semi-empirical [19–26], in which the values of the propagation and termination constants were written as a function of some system parameters such as viscosity, conversion, temperature, or free volume. For example, see the models

of Friis and Hamielec [21] (temperature and conversion), Marten and Hamielec [20], and Ross and Laurence [22] (temperature and free volume). Other models were based on more fundamental concepts [17, 27–29], for example, reptation [29], or in the division of growing radicals into two classes: one below the critical length for chain entanglement and one above this limit [30–32].

Some reviews on previous gel effect models or on the concepts on which they are based have also been published [33–36].

For the systems in which this phenomenon is clearly present, its effects on reaction rate and process control can be significant, and so this has important practical consequences for the design of polymerization reactors and processes, especially in bulk polymerization. When solvents are used, the effect is attenuated and/or its onset is retarded to higher conversions, and so at high dilutions, the effect can be very mild or insignificant. In addition, the use of chain transfer agents will diminish the MW of the polymer formed, lowering the viscosity of the reaction medium and therefore retarding or attenuating the effect [36].

At very high conversions, the reaction medium becomes a glassy matrix, and the diffusion is very slow. At this stage, the controlling mechanism for termination is reaction-diffusion, and so the value of the termination constant becomes controlled by the propagation step. The propagation itself may become controlled by diffusion at very high conversions (which is called *glass effect*), but this effect must be separated from the lowering in the initiator efficiency, which also occurs at high conversion due to diffusion limitations. In the case of the bulk polymerization of styrene, the glass effect occurs at monomer conversions roughly above 70–90% where even diffusion of styrene is impeded. A consequence of this phenomenon is the freezing of the reaction mixture at conversions about 95% for styrene.

4.5 MOLECULAR WEIGHT AND MOLECULAR WEIGHT DISTRIBUTION

The random character of the events defining the length of each polymeric chain will lead to a distribution of MWs instead of a unique MW as in the case of small molecules. However, in the case where all chains terminate by bimolecular termination, a number average MW can be easily obtained by making the following quotient:

$$M_n = \frac{R_p}{R_i = R_t} M_0 = \frac{k_p[M][P]}{k_t[P]^2} M_0 = \frac{k_p[M]}{(2k_t f k_d[I])^{1/2}} M_0 \quad (4.13)$$

which represents the ratio of the number of events of chain growth per event of chain initiation for the case of termination by disproportionation (one dead chain per each

TABLE 4.6 Kinetic Scheme for Detailed MWD

Step	Reaction	Rate constant
Initiation	$I \xrightarrow{f k_d} 2R^\bullet$	k_d
First propagation	$R^\bullet + M \xrightarrow{k_i} P_1^\bullet$	k_i
Propagation	$P_r^\bullet + M \xrightarrow{k_p} P_{r+1}^\bullet, r \geq 1$	k_p
Transfer to monomer	$P_r^\bullet + M \xrightarrow{k_{trM}} P_1^\bullet + D_r, r \geq 1$	k_{trM}
Transfer to solvent	$P_r^\bullet + S \xrightarrow{k_{trS}} P_1^\bullet + D_r, r \geq 1$	k_{trS}
Termination by combination	$P_n^\bullet + P_m^\bullet \xrightarrow{k_{tc}} D_{n+m}, n, m \geq 1$	k_{tc}
Termination by Disproportionation	$P_n^\bullet + P_m^\bullet \xrightarrow{k_{td}} D_n + D_m, n, m \geq 1$	k_{td}

R^\bullet , P_r^\bullet are primary radicals and length- r growing radicals, respectively. I , M , S , and D_r are initiator, monomer, solvent, and length- r dead polymer, respectively.

initiated chain). When termination by combination occurs instead, the above expression must be multiplied by two.

When other termination reactions are also allowed (transfer to initiator, monomer, and solvent), the above expression must be modified, ending up in

$$M_n = \frac{R_p}{R_t + k_{trM}[P][M] + k_{trS}[P][S] + k_{trI}[P][I]} M_0 \quad (4.14)$$

or

$$\frac{1}{M_n} = \frac{1}{M_0} \left[\frac{k_t R_p}{k_p^2 [M]^2} + C_M + C_S \frac{[S]}{[M]} + C_I \frac{[I]}{[M]} \right] \quad (4.15)$$

Equation 4.15 is the Mayo equation and can be used for experimental determination of some of the transfer constants (C_M , C_S , C_I).

4.5.1 Full Molecular Weight Distribution

The full MWD can be obtained either by probabilistic arguments [4] or by a kinetic approach. Flory showed that the form of the MWD in FRP is the same as in condensation polymerization (the most probable or Flory–Schulz distribution), when termination occurs by disproportionation or transfer to a small molecule; however, in a free radical mechanism, it represents only the distribution obtained at a given instant of the polymerization or under constant reaction conditions (as those occurring, e.g., in a continuous tank reactor operating at steady state). According to Flory, letting p represent the probability of a growing chain continuing to grow instead of terminating:

$$p = \frac{R_p}{R_p + R_{td} + R_{trS}} \quad (4.16)$$

where R_i represent reaction rates with $i = p$, propagation, $i = td$, termination by disproportionation, and $i = trS$, transfer to solvent S ; hence, only the last two mechanisms

are considered for chain termination (Table 4.6). The probability that a terminated polymer chain has exactly x monomer units is given by

$$n_x = (1 - p) p^{x-1} \quad (4.17)$$

This also represents the number fraction of polymer chains having x monomer units.

If N_0 is the number of monomer moles in polymer chains, $N = N_0(1 - p)$ is the number of polymer moles, since $(1 - p)$ represents the probability of termination of a chain. Therefore, the number of moles of polymer having x monomer units is

$$N_x = N_0 (1 - p)^2 p^{x-1} \quad (4.18)$$

And the weight fraction w_x of polymer moles having x monomer units is xN_x/N_0 or

$$w_x = x (1 - p)^2 p^{x-1} \quad (4.19)$$

For termination by combination, a sharper distribution results, but a general derivation including various types of termination is more easily obtained using kinetic instead of probabilistic arguments. In the kinetic approach, differential rate expressions are written for each polymer species and the QSS approximation is used. The derivation is based on the kinetic scheme listed in Table 4.6.

The final and general result is given by the following expression [37]:

$$w_x = (\tau + \beta) \left\{ \tau + \frac{1}{2} \beta (\tau + \beta) (x - 1) \right\} x \varphi^{x+1} \quad (4.20)$$

where

$$\varphi = \frac{1}{1 + \tau + \beta} \quad (4.21)$$

$$\tau = \frac{k_{\text{td}} [\text{P}] + k_{\text{trM}} [\text{M}] + k_{\text{trS}} [\text{S}]}{k_p [\text{M}]} \quad (4.22)$$

$$\beta = \frac{k_{\text{tc}} [\text{P}]}{k_p [\text{M}]} \quad (4.23)$$

$[\text{P}]$ can be calculated by the expression at QSS (Eq. 4.7). Equation 4.20 is a convenient general form of the instantaneous weight MWD for the mechanism listed in Table 4.6. The reader must be aware that the real distribution obtained from a reaction running up to moderate or high conversions will be the addition of many instantaneous distributions that may differ from each other due to the continuously changing conditions (e.g., in a batch reactor), which will affect the concentrations of monomer, initiator, and so on and can even affect the rate coefficients (gel effect). To obtain the final MWD, an integration procedure adding the differential contributions at each reaction moment should be performed [38].

From distribution expressions such as Equation 4.17, 4.19, or 4.20, the instantaneous number and weight average MW, as well as the instantaneous polydispersity, can be obtained. The moments of the distributions are most useful as intermediate quantities for these calculations and they are defined as (see also Chapter 1)

$$\mu_s = \sum_{x=1}^{\infty} x^s n_x, \lambda_s = \sum_{x=1}^{\infty} x^s w_x; s = 0, 1, 2, \dots \quad (4.24)$$

μ_s and λ_s are the s -moments of the number chain length distribution (NCLD) and weight chain length distribution (WCLD), respectively. The number average (M_n) and weight average (M_w) MWs are then given by

$$M_n = \frac{\mu_1}{\mu_0} M_0 \quad (4.25)$$

$$M_w = \frac{\mu_2}{\mu_1} M_0 = \frac{\lambda_1}{\lambda_0} M_0 \quad (4.26)$$

and the polydispersity index (PDI)³ is simply given by the ratio $\text{PDI} = M_w/M_n$

Closed expressions can be obtained for M_n , M_w , and PDI, depending on the specific reaction mechanisms taken into account. For example, for the distribution given by Equation 4.17 (termination only by disproportionation or transfer to solvent), the evaluation of moments and

summations in Equations 4.24–4.26⁴ leads to the following expressions:

$$M_n = \frac{M_0}{(1-p)} \quad (4.27)$$

$$M_w = M_0 \frac{(1+p)}{(1-p)} \quad (4.28)$$

$$\text{PDI} = 1 + p \quad (4.29)$$

4.6 EXPERIMENTAL DETERMINATION OF RATE CONSTANTS

Up to the 1980s, the determination of k_p and k_t was carried out mainly by the rotating sector method [39]. However, since the late 1980s, given the advances in pulsed laser techniques and size exclusion chromatography, as well as the IUPAC recommendations for the search of a more reliable and reproducible method for the measurement of rate constants of polymerization, *pulsed laser polymerization* (PLP) has become the preferred method for the measurement of these two kinetic constants [40]. In this method, a reaction mixture of monomer and photoinitiator is radiated by a pulsed laser beam. Each laser flash (≈ 1 ns pulse) generates radicals that initiate the polymerization during the illuminated period, while no radicals are formed during dark periods (≈ 1 s). All the radicals formed during an illuminated period grow approximately at the same rate, since all of them are started at approximately the same time; hence, they generate a narrow MWD. After a dark period of length t_0 , the next laser pulse generates another burst of radicals, some of which annihilate most of the growing radicals still active and initiated during the previous pulse, which terminate with approximately the same chain length L_0 (generated during the time interval t_0 between light periods). As some of the radicals survive the next pulse, after several cycles (illuminated–dark), the concentration of radicals with lengths $2L_0$, $3L_0$, and so on increases with each pulse. In the end, a final, well-defined MWD is obtained, with peaks at L_0 and at its multiples. The chain length $L_{0,n}$ of a radical that has grown by n periods (pulses) is related with k_p as $L_{0,n} = nk_p [\text{M}] t_0$. From this and experimental measurements of $L_{0,n}$ (via SEC), $[\text{M}]$, and for a known t_0 , k_p can be estimated. The measurement of k_t/k_p can be done by similar techniques. A detailed description of the technique can be found elsewhere (40c).

⁴The following identities are useful for the evaluation of summations appearing in moment expressions:

$$\sum_{x=1}^{\infty} x p^{x-1} = \frac{1}{(1-p)^2}; \sum_{x=1}^{\infty} x^2 p^{x-1} = \frac{(1+p)}{(1-p)^3}; \sum_{x=1}^{\infty} x^3 p^{x-1} = \frac{(1+4p+p^2)}{(1-p)^4}$$

³Although the term *polydispersity* or *polydispersity index* is widely used, its use is now discouraged by IUPAC. The term *dispersity* is recommended instead [73].

4.7 THERMODYNAMICS OF POLYMERIZATION

The thermodynamics of polymerization has been reviewed by several authors [41–43].

The propagation reaction of alkenes implies the formation of a σ -bond from a π -bond and this makes the enthalpy of propagation (ΔH) negative (exothermic and favorable). On the other hand, the entropy of propagation (ΔS) is negative and unfavorable (the polymer chain represents a more ordered state than the unbound monomer molecules); however, the absolute value of ΔH is dominant. Therefore, the resulting ΔG ($\Delta G = \Delta H - T\Delta S$) is negative and favorable. Table 4.7 lists values of the enthalpies of polymerization for some common monomers. Most values fall in the range of 50–120 kJ/mol. There is some scattering in the data reported by different authors, and this scattering is attributed to the effect of the physical state of the monomer and the polymer. Note also that, from the point of view of polymerization process engineering, the values of ΔH on a mass basis, instead of molar, are of more significance, since differences in exothermicity among different polymerization systems tend to be more pronounced in this way (see, e.g., the high value corresponding to ethylene polymerization on mass basis).

The propagation step is potentially reversible and, owing to entropic effects, the depropagation reaction will be favored by higher temperatures. The equilibrium temperature at which the propagation and depropagation rates are equal is known as the ceiling temperature, or T_c . Most common monomers show negligible depropagation

rates at typical polymerization temperatures, but some with alkyl substituents in the α -position, such as α -methyl styrene, will show lower T_c .

Using the notation and kinetic scheme of Table 4.5 and adding to it the depropagation reaction:



The equilibrium is reached when $k_p[P][M] = k_{rev}[P]$ and the equilibrium constant is given by

$$K = \frac{k_p}{k_{rev}} = \frac{1}{[M_c]} \quad (4.31)$$

From thermodynamic relationships $\Delta G = \Delta G^\circ + RT \ln K$ and at equilibrium $\Delta G = 0$, so

$$\Delta G^\circ = \Delta H^\circ - T \Delta S^\circ = RT \ln [M_c] \quad (4.32)$$

Therefore,

$$\ln [M_c] = \frac{\Delta H^\circ}{(RT_c)} - \frac{\Delta S^\circ}{R} \quad (4.33)$$

and

$$T_c = \frac{\Delta H^\circ}{\Delta S^\circ + RT \ln [M_c]} \quad (4.34)$$

From Equation 4.34 it is concluded that T_c increases with larger $[M_c]$ (negative ΔH) and there is not a single value for T_c . Usually, the reported values of T_c are for pure monomers and therefore they represent the maximum value for that monomer. In general, at higher temperatures, the depropagation becomes increasingly important in relation to the forward propagation reaction. Equation 4.34 also implies that in a solution polymerization at a given temperature T (which must be initiated with a monomer concentration larger than the $[M_c]$ corresponding to T), the monomer is consumed and its concentration decreases until it possibly reaches the $[M_c]$ corresponding to T , where the reaction will stop.

4.7.1 Floor Temperature

Most monomers exhibit an exothermic polymerization reaction (negative and large ΔH) with a small but negative entropy change. In that case, they have a ceiling temperature as described in the previous section. However, a few exceptional monomers (e.g., cyclic sulfur) exhibit a very small ΔH (either positive or negative) with a positive entropy change. In these cases, the polymerization will have a floor temperature T_f below which the polymerization does not proceed.

TABLE 4.7 Heat of Polymerization of Some Common Monomers in Different Units

Monomer	ΔH_p (kJ/mol)	ΔH_p (kcal/mol)	ΔH_p (cal/g)	T (°C)
Butadiene	73	17.5	323	25
Isoprene	75	17.9	263	25
Ethylene	101.5	24.3	866	25
Acrylonitrile	76.5	18.3	345	74.5
Methacrylic acid	64.5	15.4	179	25
Methyl methacrylate	55.6	13.4	134	74.5
	56	13.4	134	130
Acrylic acid	67	16.0	222	74.5
Methyl acrylate	78	18.7	217	76.8
	81.8	19.6	227	80
Ethyl acrylate	78	18.7	187	74.5
	80.7	19.3	193	90
Butyl acrylate	78	18.7	146	74.5
Styrene	70	16.7	160	25
	73	17.5	168	127
Vinyl chloride	71–111.5	17–27	272–432	25
	96	23	368	74.5
Vinyl acetate	88	21.1	245	74.5

4.8 CONTROLLED RADICAL POLYMERIZATION

The year 1994 can be considered as the starting year of a revolutionary change in the field of chemistry of FRP, due to the advent of the techniques generically called *controlled/living radical polymerization* (CRP) [44, 45]. Recently, the term *reversible deactivation radical polymerization* has been recommended by the IUPAC [46] instead of other terms; however, in this section, we adhere to the older notation that is still in common use. These new techniques preserve the robustness of traditional FRP (tolerance to impurities and water) and its versatility in terms of range of monomers, reaction conditions, and types of industrial processes [47]. On the other hand, CRP techniques can produce polymers with a precisely controlled architecture and composition that had never been produced before: polymers with narrow MW distributions; block, gradient, and graft copolymers; and hybrid materials in which well-controlled organic polymers are chemically linked to inorganic materials, among others [1, 47, 48]. These materials cannot be produced via traditional FRP and some of them were produced before by using techniques that require extremely clean conditions (such as anionic polymerizations) and that lead to costly industrial processes, when feasible. In summary, CRP combines some of the best features of traditional FRP (robustness and versatility) and of true living polymerizations (such as anionic), with the capability of the latter of producing precisely controlled architectures.

The term *control* in CRP refers to the capability of producing a polymer with low polydispersity and with a prespecified MW. On the other hand, the term *livingness* refers to the potential of a chain to be extended by the addition of extra monomer (of the same or different chemical nature) after a first batch of monomer has been exhausted.

CRP is one of the most rapidly expanding areas of chemistry and polymer science due to the effectiveness already demonstrated by these techniques and their enormous potential for the synthesis of a broad variety of polymeric or polymer-related materials. The degree of control of the molecular architecture that can be achieved with these techniques is the driving force that has led many groups interested in the synthesis of materials with specific functionality, properties, or structures, to work in this field. The number of publications in this field (papers and patents) has seen an exponential increase in the last decade and it is estimated that in a single year (2005) more than a thousand publications were brought out [47].

The mechanism of all CRP techniques is based on a dynamic equilibrium between very small concentrations of propagating radicals and dormant species (Fig. 4.1), which can be reactivated by virtue of this equilibrium [48, 2]. A key factor for achieving good control (low polydispersities and good MW prediction) is a fast

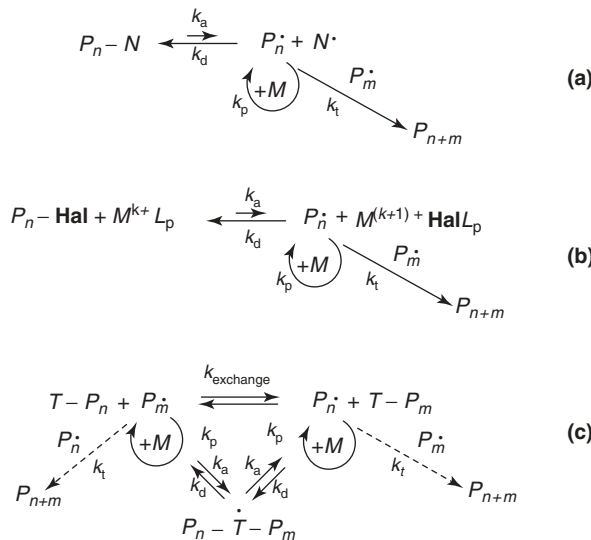


Figure 4.1 Controlled radical polymerization mechanisms via (a) NMRP, (b) ATRP, and (c) RAFT.

exchange between dormant and active species; however, it is possible for some of these processes to exhibit livingness, even in the absence of good control, when the exchange is not sufficiently fast. Since irreversible termination between radicals is always present, CRP is never completely living. In FRP, all the chains terminate; however, in CRP there is a large concentration of polymer chains (10^{-1} M, as opposed to 10^{-3} M, in FRP) and out of them only a small percentage (around 1%) are terminated chains, while the vast majority are dormant chains [47].

There are several techniques for performing CRP, but the most popular and successful ones so far are as follows: stable free radical (SFR) or nitroxide-mediated radical polymerization (NMRP) [44, 45, 49], atom transfer radical polymerization (ATRP) [50, 51], and degenerative transfer techniques, including particularly reversible addition-fragmentation transfer (RAFT) polymerization [3]. These are examined in some detail in the following sections.

In general, CRP techniques are based on either an SFR that exhibits the persistent radical effect (PRE) [52–55] (e.g., N in NMRP), an inactive species $M^{(k+1)+} HalL_p$ in ATRP (which acts as a persistent radical), or, as in the RAFT case, a highly active chain transfer agent ($T - R$) (refer to Fig. 4.1 for notation).

4.8.1 Stable Free Radical Polymerization (SFRP) or Nitroxide-Mediated Radical Polymerization (NMRP)

NMRP (also called *NMP*, *nitroxide-mediated polymerization*) or SFRP (stable free radical polymerization) was first disclosed by Solomon et al. from CSIRO (Commonwealth Scientific Industrial Research Organization) in 1984. Their patent [49] describing a unimolecular process in which an

alkoxyamine thermally breaks and produces both an initiating radical and a nitroxide radical that will control the polymerization (Scheme 4.10a) was an important landmark; however, this process required the previous synthesis of the alkoxyamine and had little diffusion. Ten years later, Georges et al. at Xerox published a couple of patents [44] disclosing the bimolecular process that, from the point of view of industrial application, was simpler to implement than the monomolecular process. In the second case, a stable (nitroxide) radical (e.g., TEMPO, 2,2,6,6 tetramethylpiperidine *N*-oxyl) and a radical initiator are added to the polymerization recipe to achieve a controlled polymerization (Scheme 4.10b).

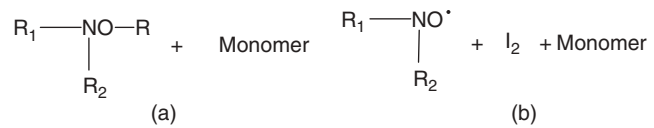
Conceptually, both processes are similar, because in the bimolecular process an alkoxyamine is formed *in situ*. The mechanism for both processes is represented by Scheme 4.11. The steps in the scheme occur in addition to the regular steps in FRP listed in Table 4.5.

The kinetic analysis of NMRP using the concept of PRE was made by Fischer [52–55]; nitroxide radicals do not terminate between themselves as propagating radicals do; hence, during a polymerization, some propagating radicals will terminate between themselves, decreasing their concentration, while the nitroxide radical concentration will remain nearly constant or will increase to satisfy the quasi-equilibrium:

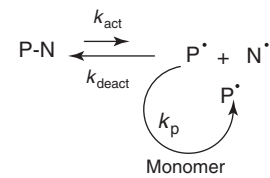
$$k_{\text{act}} [\text{P} - \text{N}] \approx k_{\text{deact}} [\text{P}] [\text{N}] \quad (4.35)$$

where the dots have been removed from the radicals for simplicity of notation. The polymerization in the presence of nitroxide will proceed near the equilibrium given by

$$K_{\text{eq}} = \frac{k_{\text{act}}}{k_{\text{deact}}} = \frac{[\text{P}] [\text{N}]}{[\text{P} - \text{N}]} \quad (4.36)$$



Scheme 4.10 (a) Monomolecular process using an alkoxyamine as an initiator and a controller; and (b) bimolecular process using a nitroxide radical as a controller and radical initiator (I_2) to generate radicals.



Scheme 4.11 Reversible activation–deactivation of the growing radical P^\cdot with the nitroxide radical N^\cdot .

which is highly biased toward the dormant polymer. Typical values for the equilibrium constant are in the range 10^{-7} – 10^{-12} M, strongly depending on the chemical structure of the nitroxide radical. A significant number of nitroxide structures have been synthesized and reported in the literature (2, 58, 59); a small sample of these is shown in Figure 4.2. Fischer [52, 53] recognized three regimes in the kinetics of a monomolecular NMP. In the first regime (which lasts only for a period in the order of a fraction of a second or seconds), living and persistent radicals appear in equal concentrations as the alkoxyamine decomposes. In the intermediate state, the quasi-equilibrium in Equation 4.35 is established.

Finally, at long reaction times, a steady state of the persistent radical is reached. Fischer [52–55] and Fukuda [2, 56] first developed kinetic equations that describe the evolution of the nitroxide radicals with reaction time t . These equations were later refined by Tang et al. to take into account the variation of the alkoxyamine initiator with time, not considered before [57], resulting in

$$\frac{I_0^2}{I_0 - N} + 2I_0 \ln \frac{I_0 - N}{I_0} - (I_0 - N) = 2k_t K_{\text{eq}}^2 t \quad (4.37)$$

where k_t is the termination constant and I_0 is the initial alkoxyamine concentration. This is an approximated expression based on the assumptions that $|dN/dt| \gg |dP/dt|$ and quasi-equilibrium (Eq. 4.35). In their analysis, Tang et al. identified three periods that differ slightly from those described by Fischer. The quasi-equilibrium (Eq. 4.35) is the third period in this last analysis, and this is preceded by a pre-equilibrium (similar to the first regime of Fischer) and a transition period (not identified by Fischer). In this study, an equation was also derived for the monomer conversion in terms of the nitroxide concentration (N) at time t :

$$\ln \left(\frac{M_0}{M} \right) = \frac{k_p}{2k_t K_{\text{eq}}} \left(I_0 \ln \left\{ \frac{I_0}{I_0 - N} \right\} - N \right) \quad (4.38)$$

k_p , M , and M_0 are the propagation constant, monomer concentration, and initial monomer concentration, respectively. The degree of polymerization DP_n is simply calculated by

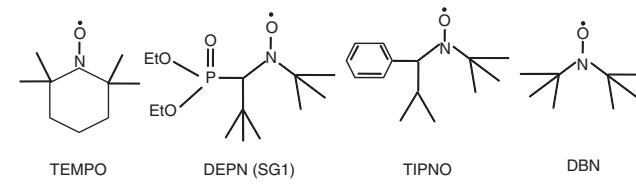


Figure 4.2 Some common nitroxide radicals and their acronyms.

Equation 4.39:

$$DP_n = \frac{[M]_0 x}{I_0} \quad (4.39)$$

where x is monomer conversion and the subindex 0 refers to initial conditions.

Numerous polymers and copolymers have been synthesized using NMP techniques. See, for example, the reviews by Hawker [58, 59]. Graft copolymers and hybrid materials synthesized by NMP are reviewed in Chapter 10.

4.8.2 Atom Transfer Radical Polymerization (ATRP)

The basic concept of ATRP was simultaneously and independently disclosed by Matyjaszewski [50] and Sawamoto [51]. In ATRP, the dormant species, $P_n\text{-Hal}$ (Fig. 4.1b), is formed by the reaction between propagating species P_n^\bullet and halogen atoms (Hal) [53], as illustrated in mechanism (b) of Figure 4.1. Ingredients included in an ATRP recipe are as follows: an initiator (usually an alkyl halide), an organometallic complex that acts as a catalyst or an activator, formed by a metal halide and a ligand, as well as the monomer. The metal is of the transition type (M^{k+}), which can expand its coordination sphere and increase its oxidation number (k). The halogen from the dormant species reversibly binds to the metal complex (M^{k+}/Lp) increasing its oxidation state by one unit ($M^{(k+1)+}\text{Hal}/Lp$) and producing propagating radicals ($P_n\cdot$) with an activation constant k_a . The oxidized state of the metallic complex, also known as *metalloradical*, plays the role of persistent radical [53], which does not propagate or finish. Meanwhile, the propagating radicals may terminate irreversibly or continue their propagation in the presence of monomer. Copper metal complexes were the first ones used extensively, but others have also been tested [53], such as Fe, Ni, Re, Rh, Ru, and Pd (among others) in the ATRP of a widespread variety of monomers. The ligands are nitrogen based, the common ones being bidentatebipyridyl ligands. Since poor solubility of the complex in the reaction media may be an issue, bipyridyl ligands possessing long alkyl chains are preferred. Other ligands exhibit better solubility when forming the complex, for example, TMEDA (tetramethylethylenediamine) and PMDETA (N,N,N',N',N'' -pentamethyldiethylenetriamine) [5].

The kinetics of ATRP has been studied and summarized by Matyjaszewski [60]. Assuming fast equilibrium, complete initiation, and neglecting termination, the total concentration of propagating radicals, $[P]$, is given by

$$[P] = \frac{k_a}{k_d} \frac{[P_n\text{-Hal}][M^k]}{[M^{k+1}\text{Hal}]} \quad (4.40)$$

and the polymerization rate R_p is [60]

$$R_p = k_p[P][M] = k_p \frac{k_a}{k_d} \frac{[P_n\text{-Hal}][M^k]}{[M^{k+1}\text{Hal}]} \quad (4.41)$$

In Equation 4.41, the concentration of dormant species $[P_n\text{-Hal}]$ can be replaced by the initial initiator concentration $[R\text{-Hal}]_0$ under the assumption of complete initiation.

The degree of polymerization DP_n can be simply calculated by Equation 4.42 [60]:

$$DP_n = \frac{[M]_0 x}{[R\text{-Hal}]_0} \quad (4.42)$$

where x is the monomer conversion. Finally, the MW dispersity, \mathbb{D} , is given by [60]

$$\mathbb{D} = \frac{\overline{M_w}}{\overline{M_n}} = 1 + \frac{k_p[R\text{-Hal}]_0}{k_d[M^{k+1}\text{Hal}]} \left| \frac{2}{x} - 1 \right| \quad (4.43)$$

Following the development of the original ATRP, the group of Matyjaszewski invented modified versions of the procedure. Reverse ATRP [61] was created to avoid some of the problems of this process when it is taken to an industrial scale or performed in aqueous dispersions, as the components of this recipe are less sensitive to air and moisture. In this version, the transition metal is added to the system in its higher oxidation state, and the catalyst or activator $M^k Lp$ is generated *in situ* by the decomposition of a conventional free radical initiator. Simultaneous reverse and normal atom transfer radical polymerization (SR/N ATRP) [62] is another modality of the process that allows for the use of more active (and sensitive) catalyst systems. The activator generated by electron transfer or AGET-ATRP process [63] is similar to SR/N ATRP, but instead of using a free radical initiator, it uses a reducing agent to generate the activator from the higher oxidation state of the metal complex. Looking for the ways to reduce the concentration of metal used in the ATRP procedure, ARGET (activator regenerated by electron transfer) ATRP [64] was proposed; in this case, proper reducing agents are used that continuously regenerate the activator from the metal in its higher oxidation state present in species formed by irreversible termination, thus allowing for a net reduction of the metal concentration in the system. Finally, ICAR (initiator for continuous activator regeneration) ATRP [65] is similar to ARGET, but it uses a traditional free radical initiator to compensate for the loss of M^k activator, which is consumed by the termination reactions at these low concentrations of catalysts. A review of the multiple applications of polymer synthesis using ATRP techniques has been presented by Matyjaszewski and Xia [66].

4.8.3 Reversible Addition-Fragmentation Chain Transfer Polymerization (RAFT)

RAFT is a variant of a degenerative transfer [67]. It requires a careful election of the RAFT agent (T-R) depending on the monomer to polymerize (see mechanism (c), Fig. 4.1). Dithioesters, dithiocarbamates, tri-thiocarbonates, and xanthates are examples of some RAFT agents that have been successfully used as transfer agents to produce novel polymeric topologies with high MW and narrow polydispersity [68]. The exchange reactions can be very fast, providing good control in these systems due to the presence of highly active transfer agents [53].

The kinetic mechanism was first proposed by the CSIRO group in its seminal 1998 paper [3] and is schematically represented by the lower path in scheme of Figure 4.1c (the higher path with the k_{exchange} kinetic constant is rather a representation of all degenerative transfer processes). The representation of the figure corresponds to the core equilibrium. Before that, a similar equilibrium is first established with the RAFT chain transfer agent T-R instead of the species $T-P_n$ (see left side of Fig. 4.1c) and with primary radicals from a radical initiator instead of the polymeric radical $T-P_m\cdot$. Moad and Barner-Kowollik have reviewed the kinetics of the process [69]. The degree of polymerization and MWD dispersity (under negligible contributions of bimolecular termination and external initiation, as well as uniform transfer activity throughout the whole reaction) are given by [69]

$$DP_n = \frac{[M]_0 x}{[T - R]_0 + df(I_0 - 1)} \quad (4.44)$$

$$\Theta = 1 + \frac{1}{DP_n} + \left| \frac{2 - x}{x} \right| \frac{1}{C_{\text{tr}}} \quad (4.45)$$

where d is the number of chains produced in a bimolecular termination reaction, f is the initiator efficiency, and C_{tr} is the chain transfer constant. To obtain the number average MW, one must multiply expression (Eq. 4.43) by $(M_0 + M_{T-R})$ (where the terms are the MWs of the monomer and the CTA, respectively). C_{tr} can be estimated experimentally using Equation 4.45 or, in some conditions [69], from the approximated expression (Eq. 4.46):

$$\frac{d[T - R]}{d[M]} \approx C_{\text{tr}} \frac{d[T - R]}{d[M]} \quad (4.46)$$

Common RAFT chain transfer agents (T-R) are of the thiocarbonylthio type, $RSC(Z) = S$, in which the chemical nature of the groups Z and R are key to effective control of the reaction. The group Z must provide stability to the intermediate radical $P_n - \dot{T} - P_m$ (Fig. 4.1c), while the salient group R must reinitiate a chain readily with the monomer. A careful selection of the CTA must be done depending on the monomer or monomers to be

polymerized. The CSIRO group has published a number of excellent reviews on the fundamentals and practical application of the RAFT technique for the synthesis of a variety of polymeric structures [68–71]. A current challenge in this field is the discovery of an universal CTA able to polymerize a vast number of monomer families.

4.8.4 Outlook of CRP Techniques

All the CRP techniques have advantages and drawbacks; some of these techniques will be more suitable for some applications than others. In general terms, SFRP or NMP is perhaps the simplest from the chemical point of view and it is rather robust, but it requires relatively high temperatures and it works better with styrenics. Milder reaction conditions are needed for ATRP and RAFT polymerizations, and these two techniques work better with a larger number of monomers than NMRP, does although in both cases a final step of metal (ATRP) or color (RAFT) removal from the polymer may be necessary. In terms of the number of reported applications/publications, ATRP is the leading technique, followed by RAFT, and then NMRP, but a further expansion, maturity, and eventual extended industrial application of all of them are expected.

REFERENCES

- Matyjaszewski K. Overview: fundamentals of controlled/living radical polymerization. In: Matyjaszewski K, editor. *Controlled Radical Polymerization*. ACS Symposium Series. Volume 685. Washington (DC): 1998. p 2.
- Goto A, Fukuda T. *Prog Polym Sci* 2004;29:329.
- Chiefari Y, Chong K, Ercole F, Krstina J, Jeffery J, Le TPT, Mayadunne RTA, Meijis GF, Moad CL, Moad G, Rizzardo E, Thang SH. *Macromolecules* 1998;31:5559.
- Flory PJ. *Principles of Polymer Chemistry*. Ithaca (NY): Cornell University Press; 1953.
- Moad G, Solomon DH. *The Chemistry of Radical Polymerization*. 2nd ed. New York: Elsevier Science Inc; 2006.
- Brandrup J, Immergut EH, Grulke EA, editors. *Polymer Handbook*. 4th ed. New York: John Wiley & Sons Inc; 1999.
- Brandrup J, Immergut EH, editors. *Polymer Handbook*. 1st ed. Interscience; 1966.
- Wells GJ, Ray WH. *Macromol Mater Eng* 2005;290: 319–346.
- Moscatelli D, Dossi M, Cavallotti C, Storti G. *J Phys Chem* 2010;115(1):52.
- Nikitin AN, Hutchinson RA, Buback M, Hesse P. *Macromolecules* 2007;40:8631.
- Bodenstein M, Link SC. *Z Phys Chem* 1907;57:168.

12. Stockmayer WH. *J Phys Chem* 1944;12:143.
13. Szymanski R. *Macromol Theor Simul* 2011;20:8–12.
14. Trommsdorff E, Kohle H, Lagally P. *Makromol Chem*. 1948;1:169.
15. Norrish RGW, Smith RR. *Nature* 1942;150:336.
16. Odian G. *Principles of Polymerization*. 4th ed. Hoboken: John Wiley and Sons; 2004.
17. [a] Tulig TJ, Tirrell M. *Macromolecules* 1981;14:1501. [b] Chiu WY, Carrat GM, Soong DS. *Macromolecules* 1983;16:348.
18. Dotson NA, Galván R, Laurence RL, Tirrell M. *Polymerization Process Modeling*. New York (NY): Wiley VCH; 1996.
19. Balke ST, Hamielec AE. *J Appl Polym Sci* 1973;17:905.
20. Marten FL, Hamielec AE. *J Appl Polym Sci* 1982;27:489.
21. Friis N, Hamielec AE. *Polymer Preprint* 1975;16:192.
22. Ross RT, Laurence RL. *AIChE Symp Series* 1976;160:74.
23. Soh SK, Sundberg DC. *J Polym Sci Polym Chem Ed* 1982;20:1299.
24. Soh SK, Sundberg DC. *J Polym Sci Polym Chem Ed* 1982;20:1315.
25. Soh SK, Sundberg DC. *J Polym Sci Polym Chem Ed* 1982;20:1331.
26. Soh SK, Sundberg DC. *J Polym Sci Polym Chem Ed* 1982;20:1345.
27. Ito K. *Polymer J* 1980;12:499.
28. Coyle DJ, Tulig TJ, Tirrell M. *Ind Eng Chem Fund* 1985;24:343.
29. Achillias DS, Kiparissides C. *Macromolecules* 1992;24:3739.
30. Cardenas JN, O'Driscoll KF. *J Polym Sci Polym Chem Ed* 1976;14:883.
31. O'Shaughnessy B, Yu J. *Macromolecules* 1994;27:5079.
32. O'Shaughnessy B, Yu J. *Macromolecules* 1994;27:5067.
33. Mita I, Horie K. *J Macromol Sci Rev Macromol Chem Phys* 1987;C27(I):91.
34. Achillias DS, Kiparissides C. *J Appl Polym Sci* 1988;35:1303.
35. Russell GT. *Macromol Theor Simul* 1994;3:439.
36. Wang X, Ruckenstein E. *J Appl Polym Sci* 1993;49:2179.
37. Hamielec AE. *Ullmann's Encyclopedia of Industrial Chemistry*. 5th ed. Volume A21. Weinheim, Germany: Wiley-VCH; 1992. p 324–330.
38. Saldívar-Guerra E, Infante-Martínez R, Vivaldo-Lima E, Flores-Tlacaúhac A. *Macromol Theor Simul* 2010;19:151.
39. Odian G. *Principles of Polymerization*. 3rd ed. New York: John Wiley and Sons; 1991.
40. [a] Olaj OF, Bitai I, Hinkelmann F. *Makromol Chem* 1987;188:1689. [b] Beuermann S, Buback M. *Prog Polym Sci* 2002;27:191.
41. Sawada H. *Thermodynamics of Polymerization*. New York: Marcel Dekker Inc.; 1976.
42. Sawada H. *J Macromol Sci Rev Macromol Chem* 1969;C3:313.
43. Busfield WK. In: Brandrup J, Immergut EH, editors. *Polymer Handbook*. 3rd ed. New York: Wiley; 1989. p II/295.
44. Georges MK, Veregin RPN, Kazmaier PM, Hamer GK, inventors; Xerox Co. US patent 5,322,912. 1994; US patent 5401804. 1995.
45. Georges MK, Veregin RPN, Kazmaier PM, Hamer GK. *Macromolecules* 1993;26:2987.
46. Jenkins AD, Jones RG, Moad G. *Pure Appl Chem* 2010;82(2):483.
47. Matyjaszewski K. Controlled living radical polymerization: state of the art in 2005. In: Matyjaszewski K, editor. *Controlled Living Radical Polymerization: From Synthesis to Materials*. ACS Symposium Series. Volume 944. Washington (DC): American Chemical Society; 2006. p 2.
48. Matyjaszewski K, Davis TP. *Handbook of Radical Polymerization*. Hoboken (NJ): John Wiley and Sons; 2002.
49. Solomon DH, Rizzardo E, Cacioli P, inventors; CSIRO. US patent 4,581,429. 1986.
50. Wang JS, Matyjaszewski K. *J Am Chem Soc* 1995;117:5614.
51. Kato M, Kamigaito M, Sawamoto M, Higashimura T. *Macromolecules* 1995;28:1721.
52. Fischer H. *Chem Rev* 2001;101:3581.
53. Fischer H. *J Polym Sci Polym Chem* 1885;1999:37.
54. Fischer H. *Macromolecules* 1997;30:5666.
55. Souaille M, Fischer H. *Macromolecules* 2000;33:7378. Souaille M, Fischer H. *Macromolecules* 2001;34:2830. Souaille M, Fischer H. *Macromolecules* 2002;35:248.
56. Fukuda T, Goto A, Ohno K. *Macromol Rapid Commun* 2000;21:151.
57. Tang W, Fukuda T, Matyjaszewski K. *Macromolecules* 2006;39:4332.
58. Hawker CJ, Bosman AW, Harth E. *Chem Rev* 2001;101: 3661.
59. Hawker CJ. Nitroxide-Mediated Living Radical Polymerizations. In: Matyjaszewski K, Davis TP, editors. *Handbook of Radical Polymerization*. Hoboken (NJ): John Wiley and Sons; 2002. p 463.
60. Matyjaszewski K. Mechanistic aspects of atom transfer radical polymerization. In: Matyjaszewski K, editor. *Controlled Radical Polymerization*. ACS Symposium Series. Volume 685. Washington (DC): American Chemical Society; 1998. p 258.
61. Xia J, Matyjaszewski K. *Macromolecules* 1997;30:7692.
62. Li M, Min K, Matyjaszewski K. *Macromolecules* 2004;37:2106.
63. Min K, Gao H, Matyjaszewski K. *J Am Chem Soc* 2005;127:3825.
64. Jakubowski W, Min K, Matyjaszewski K. *Macromolecules* 2006;39:39.
65. Dong H, Tang W, Matyjaszewski K. *Macromolecules* 2007;40:2974.
66. Matyjaszewski K, Xia J. Fundamentals of atom transfer radical polymerization. In: Matyjaszewski K, Davis TP, editors. *Handbook of Radical Polymerization*. Hoboken: John Wiley & Sons; 2002. p 523.
67. Braunecker WA, Matyjaszewski K. *Prog Polym Sci* 2007;32:93.

68. Moad G, Rizzardo E, Thang SH. Aust J Chem 2006;59: 669.
69. Moad G, Barner-Kowollik C. The mechanism and kinetics of the RAFT process: overview, rates, stabilities, side reactions, product spectrum and outstanding challenges. In: Barner-Kowollik C, editor. *Handbook of RAFT Polymerization*. Weinheim: Wiley VCH; 2008. p 51.
70. Moad G, Rizzardo E, Thang SH. Aust J Chem 2005;58:379.
71. [a] Moad G, Rizzardo E, Thang SH. Aust J Chem 2009;62:1402. [b] Moad G, Rizzardo E, Thang SH. Aust J Chem 2012;65:985.
72. [a] Yamada B, Westmoreland DG, Kobatake S, Konosu O. Prog Polym Sci 1999;24:565. [b] Kamachi M. J Polym Sci A Polym Chem 2001;40:269.
73. Stepto RFT. Pure Appl Chem 2009;81(2):351. Stepto RFT. Pure Appl Chem 2009;81(4):779.

5

COORDINATION POLYMERIZATION

JOÃO B. P. SOARES AND ODILIA PÉREZ

5.1 INTRODUCTION

This chapter describes the coordination polymerization of acyclic and cyclic vinylic monomers, conjugated dienes, and polar vinylic monomers with the most important catalytic systems known in this area. A chronological classification for the development of the main coordination catalyst types is outlined, as well as polymerization kinetics and mechanisms and applications of polymers obtained through different metallic complexes.

The reaction where vinylic monomers polymerize through coordination at the metallic center of some catalytic species is called *coordination polymerization*. Although the first catalytic system based on this kind of coordination chemistry was reported by Phillips Petroleum Co., most of the literature concerning coordination polymerization refers to the Ziegler–Natta catalysts because of their versatility in controlling chemical composition distribution (CCD) and of the wider variety of monomers they can polymerize [1].

The main early advances in the knowledge and understanding of coordination polymerization were established by studying the catalyst discovered by Ziegler in the early 1950s for ethylene polymerization, and utilized by Natta for polymerization of propylene and α -olefins. The most important contribution of Natta's works consisted in developing the Ziegler catalysts that could control polymer stereoregularity. Natta separated and characterized the three polypropylene stereoisomers—isotactic, syndiotactic, and atactic, thus opening the doors to a revolution on polyolefin applications that is still seen today.

The contributions by Ziegler and Natta caused great industrial impact and large advances in research and development of polymer science and engineering, as new kinds of

polymers—such as high density polyethylene (HDPE); isotactic polypropylene (iPP); ethylene, propylene, and higher α -olefin copolymers; cis- and trans-polydienes; ethylene-propylene elastomers (EPEs); and ethylene-propylene-diene monomer (EPDM) copolymers—became commercially available in the mid-1950s. For these remarkable advances, Karl Ziegler and Giulio Natta were awarded the Nobel Prize in Chemistry in 1963, and their original discoveries have been called the *Ziegler–Natta catalysts* since then.

Other kinds of coordination catalytic systems developed few years before the Ziegler–Natta catalysts were based on chromium and molybdenum oxides supported on SiO_2 , Al_2O_3 and other supports. The catalysts were patented by Phillips Petroleum and Standard Oil companies of Indiana for the synthesis of polyolefins. Although Phillips catalysts were the first to produce a fraction of crystalline polypropylene, these systems were more useful for the production of polyethylene. In fact, the Phillips and the Ziegler–Natta catalysts are currently the two commercial systems that dominate the production of HDPE [2].

The discovery of Ziegler–Natta catalysts led to many industrial and academic investigations on other kinds of metallic complexes for polymerization of different monomers. Several organometallic and coordination compounds have been synthesized and probed as catalytic systems. They have been classified based on generations or groups, transition-metal type, the chemical structure, the type of activator, and their applications in polymerization processes [2]. Currently, there are different groups of initiator systems based on early and late transition metals or lanthanide complexes, which have been studied in polymerization catalysis [3].

First-generation Ziegler–Natta catalysts $TiCl_4/AlEt_3$ and $TiCl_3/AlEt_2Cl$ were applied for the polymerization of ethylene and propylene, respectively. Since the mid-1970s, modifications of the original Ziegler–Natta catalysts, including crystallinity, surface area, support type, and the effect of internal and external donors, led to the development of new catalyst generations with improved activity and stereoregularity, totaling five catalyst generations for polypropylene technology [4].

Homogeneous catalytic systems based on Cp_2TiCl_2 complexes (titanocenes) activated with alkyl or alkyl chloride aluminum compounds were also investigated by Natta and Breslow in the mid-1950s; however, they showed very low activity for ethylene polymerization and were inactive for propylene polymerization [4].

In the early 1980s, Kaminsky and Sinn discovered an efficient way to activate homogeneous metallocene catalysts with methylaluminoxane (MAO). Titanocene and zirconocene complexes activated with MAO exhibited very high activity for ethylene polymerization; these early systems, however, still had low activity for propylene polymerization and formed atactic polypropylene [5]. Metallocene/MAO systems containing stereospecific ligands could be used to catalyze the polymerization of prochiral olefins (α -olefins) through the use of catalysts with well-defined active sites [6]. Later, Brintzinger [7] and Ewen [8] reported group 4 ansa-metallocenes that are useful for obtaining iPP, and they proposed for the first time the relationship between structure and symmetry of the precursor catalysts with the stereoregularity of the polymers produced.

One of the remarkable advantages of metallocene catalysts is their ability to make polyolefins with much more uniform microstructure than the Ziegler–Natta or the Phillips catalysts. Metallocene catalysts are considered to have only one type of active site (single-site catalysts) making polymer chains with the same average properties, while heterogeneous Ziegler–Natta and Phillips catalysts are multiple-site catalyst that makes polyolefins with broad, and sometimes multimodal, microstructural distributions [9].

Monocyclopentadienyl-based organometallic complexes also promote the stereoregular polymerization of higher α -olefins and styrene [9]. Ishihara first reported the use of different “half-sandwich” titanocenes activated with MAO for the production of enriched syndiotactic polystyrene [10]. Other monocyclopentadienyl-based catalysts that show stereoregular control are the constrained geometry catalysts (CGCs) [11], which contain fixed ligands, through the ansa-heteroatom bond to the metallic center. The first CGC, reported by Dow Chemical, was the *ansa*- Cp -amido M_TX_2 used in the polymerization and copolymerization of higher α -olefins and styrene [12]. CGCs are also considered single-site catalysts. Stereoregular

polymers usually show improved mechanical properties and higher melting temperatures because of their higher crystallinity.

Nonmetallocene precursors, based on early transition metals of groups 3, 4, and 5 [13], or lanthanide complexes [3] have also been reported as single-site catalytic systems useful for the polymerization of olefins or conjugated dienes [14]. Several systems containing bulky chelated diamine [15], phosphinimide [16], phenoxyimine [17], or bisphenolic ligands [18], among others, can produce very high active systems, such as 2-salicylaldimine dichloride zirconium, known as *phenoxyimine catalyst* (FI catalyst), which exhibits high activity for ethylene polymerizations when activated with MAO [17].

Other kinds of nonmetallocene complexes based on early transition metals (mainly Ti and Zr) containing dibenzyl-chelated diamido dipyrrole [19] or tetra-amido tetrapyrrole [20] ligands, as well as some amidinate, guanidinate [21], or amidopyridine [22] groups in organometallic or coordination complexes, exhibit moderate activity for olefin and diene polymerizations and some applications to living olefin polymerization [23].

Catalytic systems for diene polymerization based on lanthanide complexes mixed with aluminum compounds were reported since 1964. La, Nd, Ce, and Sm have been the most studied metals as Ziegler–Natta-type catalysts. Lanthanide-containing organic ligands such as allyl complexes were later reported for polybutadiene syntheses, and by the mid-1990s, the number of publications on lanthanide catalysts based on cyclopentadienyl ligands increased considerably [3, 24]. Lanthanidocene complexes with bridged or unbridged ligands have been studied as catalysts for non-polar and polar olefin polymerization or copolymerization reactions [25].

On the other hand, late transition-metal catalysts using Ni, Fe, Co, or Pd showed high activity for olefin polymerizations as well as for the incorporation of functionalized monomers [26]. Owing to their higher electronic density and bulky chelated ligands, late transition-metal catalysts are more stable and more capable of polymerizing monomers with different functional groups. Branched and hyperbranched polymeric structures can also be synthesized using late transition-metal catalysts due to the chain walking mechanism [27]. These systems were developed by Brookhart and Johnson [28], Gibson [29], Grubbs [30], and others and correspond to the later advances in catalytic systems for coordination polymerization.

Definitions, chemical and physical properties, and general features of the most relevant catalyst types used in coordination polymerizations are described in Section 5.3, after the classification by type of monomers most frequently used and studied in this kind of polymerization reactions.

TABLE 5.1 Main Polymers made by Coordination Polymerization

Thermoplastics	Copolymers (Thermoplastics)	Elastomers and Plastomers
High density polyethylene (HDPE)	Ethylene-propylene copolymers	<i>cis</i> -1,4-polybutadiene
Linear low density polyethylene (LLDPE)	Styrene-ethylene copolymers	<i>trans</i> -1,4-Polyisoprene
Isotactic polypropylene (iPP)		Random ethylene- α -olefin copolymers
Syndiotactic polypropylene (sPP)		Ethylene-propylene rubber (EPR)
<i>trans</i> -1,4-Polyisoprene		Ethylene-propylene-diene copolymers (EPDM)
Syndiotactic polystyrene (sPS)		
Cycloolefins		

The last part of this chapter deals with coordination polymerization kinetics and mechanism, mathematical models at different scales, as well as some analyses on the supported catalyst particle breakup and growth.

5.2 POLYMER TYPES

Polymerization by coordination is one of the most versatile methods to produce a variety of polymers. Stereoregularity is one of the outstanding characteristics of the coordination polymerization that relies on the use of catalytic systems based on organometallic or coordination complexes of special structures and symmetries to make highly stereospecific polymers.

Table 5.1 shows the main families of polymers obtained by coordination polymerization (most of them commercial polymers), which were grouped according to their thermomechanical behavior, such as polymer and copolymers, thermoplastics, elastomers, and plastomers. Most of the polymers synthesized by coordination mechanisms correspond to different grades of polyolefins and polydienes, made with Ziegler–Natta or Phillips catalyst [31].

5.3 CATALYST TYPES

5.3.1 Phillips Catalyst

The Phillips-type catalyst, first reported by Hogan in the early 1950s at the Phillips Petroleum Co., is defined as chromium oxide (CrO_3) supported on activated mixtures of silica and alumina particles with a ratio $\text{Si}/\text{Al} = 87:13$. Usually, the support particles have high surface area around

600 m^2/g . After supporting, the catalyst is activated at 500–800 °C using a dry air current, where the impregnated chromium, between 1 and 5 wt%, is stabilized as Cr(VI). Hogan determined by several methods that just 0.1% of the total supported Cr were active centers, and on the basis of the water formed per CrO_3 molecules, the chromate structure prevailed, rather than dichromate, as represented in Figure 5.1 [2].

Other researchers suspected that Cr with different valence states could lead to distinct active centers; Krauss proposed that hexavalent chromium linked to a support could be reduced to the coordinative unsaturated Cr(II) when the olefin is coordinated and starts depolymerization reaction [32].

Phillips catalysts behave in the classic coordination polymerization way: the initiation step corresponds to the generation of the active species by reduction of Cr(VI) to Cr(II); the insertion of consecutive olefins to the growing chain is the propagation step, where very high molecular weights can be obtained; and β -hydride elimination is the main chain transfer mechanism. The addition of molecular hydrogen or α -olefins promotes chain termination, producing lower molecular weight polyolefins.

Different from classical coordination polymerization, Phillips catalysts do not require activation with a cocatalyst; however, alkylaluminum complexes are usually used as scavengers in the polymerization medium [33].

5.3.2 Classical Ziegler–Natta Catalysts

Ziegler–Natta catalysts have been defined as catalytic systems containing two components—generally, the initiator

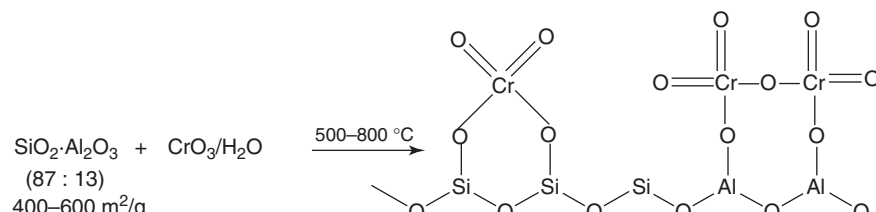


Figure 5.1 The Phillips catalyst synthesis.

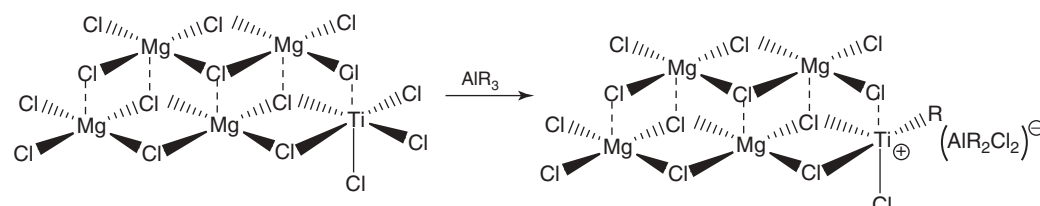


Figure 5.2 The classical Ziegler–Natta heterogenized catalyst.

or precatalyst and the component cocatalyst or activator. In the early 1950s, Ziegler determined that the mixture of metal transition halides and metallic alkyls of the main metal groups I–III (M_TCl_4 and MR_3) resulted in highly active system for the linear polymerization of ethylene. Ziegler and collaborators tried a wide variety of components using different types of transition metals, as well as metallic alkyls, determining the Ti, V, Co, and Mo, as the main transition metals potentially applied in the polymerization of different monomers. As for the cocatalysts, among the studies carried out with Al, B, Ga, Be, Mg, Li, Na, and others, the aluminum alkyls and aluminum halide-alkyls showed the best performance for the several functions carried out by the activators. Activators have three main functions in a coordination polymerization reaction: activation, stabilization, and scavenging of the polymerization medium. The activation step corresponds to the ionization of the metal by subtractions of the halide and replacement of the alkyl group in the transition metal, the conjugated base stabilizes the cationic species, and the excess of the activator works as scavenger of the polymerization medium [1].

The year following Ziegler's discovery, Natta and coworkers found that the combination of $TiCl_3$ and $AlEt_2Cl$ polymerized propylene giving a mixture of three different polymeric materials, which could be separated and characterized according to their crystallization properties. The highly crystallizable polypropylene fraction showed important physicomechanical properties such as high melting temperature, and Natta's group focused on the selective synthesis of this stereoisomer. It is important to mention again the important contribution of Natta's research group, related to the advances of stereoregularity and microstructure in the polymers obtained from propylene polymerizations or higher α -olefins, such as 1-butene, 1-hexene, and 1-octene. Natta also determined that the crystallographic structure of $TiCl_3$ was a determinant of the microstructure of the formed polypropylene. Among the allotropic crystalline structures of $TiCl_3$ (α , β , γ , and δ), the δ structure showed higher activity and better control of polypropylene stereoregularity [3, 33].

Natta also developed several techniques for the determination of the microstructure of the three stereoisomers obtained from the propylene polymerization reactions and

established the terms *isotactic*, *syndiotactic*, and *atactic polypropylenes* according to the configurational position of the substituents.

After Natta found that $TiCl_3$ was the best precatalyst for propylene stereoregular polymerization and determined the importance of the physical state of the catalytic systems, his group and many other researchers strived to improve the performance of these first-generation Ziegler–Natta systems. Figure 5.2 shows the heterogenized structure of a classical Ziegler–Natta catalyst.

Currently, most of the commercial iPP is made using fourth-generation Ziegler–Natta catalysts with different internal and external donors that increase the productivity to 25 kg polypropylene/g catalyst and isotacticity from 95% to 99%. Shell Oil Co. and Montedison started commercializing these catalytic systems in the early 1980s. Shell reported the use of benzoic acid as internal and external donors, and Montedison utilized alkyl phthalates and silyl ethers as internal and external donors, respectively [3].

Polypropylene produced with these catalytic systems did not require further atactic polypropylene removal or catalyst deashing. In addition, the morphology of the polypropylene particles was considerably improved.

Recently, Basell (currently, LyondelBasell) reported the use of catalysts classified as fifth-generation Ziegler–Natta systems, through the use of Spheripol technology [34]. Very high productivities, around 100 kg polypropylene/g catalyst have been reported in this process, using 1,3-diether and succinate compounds as internal and external donors, respectively.

These techniques and synthetic methods developed for propylene by Natta and others represented the basis for the study of other stereoregular polymers, which could be obtained using the Ziegler–Natta catalysts and the more recently discovered catalytic systems. Stereospecific polymers could be made in the polymerization of other prochiral monomers such as α -olefins. The Ziegler–Natta systems also had high catalytic activity for the synthesis of polymers using dienes and could produce geometric isomers such as *cis*- or *trans*-diene polymers.

5.3.2.1 Conjugated and Non-conjugated Diene Polymerizations

1,3-Butadienes, isoprene, and 1,3-pentadiene are the conjugated diene monomers most

studied in coordination polymerization. Cyclic dienes have also been polymerized by coordination catalysts; however, the activity is lower compared to acyclic conjugated dienes, and the versatility of their isomeric structures is limited.

The first Ziegler–Natta systems used for the production of several elastomers, and crystalline polydienes, were based on Ti, Co, V, Ni, or Cr halide or nonhalide catalyst [35]. The nature of the cocatalyst is also important for the control of the stereoregularity in the polymers synthesized from dienes. AlR_3 , AlR_2Cl , AlRCl_2 , and LiAlR_4 , where R is usually an ethyl group, have been the most used cocatalysts. The reduction and alkylating power decreases with the decrease in alkyl groups in the aluminum compounds. Although some of the catalytic systems could be similar to those used for olefin polymerizations, precatalysts containing nonhalogenated ligands showed better results for polydiene stereoregularity control, combined with the above aluminum components. Other polymerization conditions such as type of solvent, temperature, Al/M_T ratios, and crystalline structure of the M_T (Ti) are also different from that reported for olefin polymerizations. A number of articles and reviews were published by the research groups of Natta, Cooper, Marconi, and many others, and some tendencies could be related to the structure of the transition metals and the alkyl aluminum cocatalysts. It was evident that nonhalogenated cobalt based systems showed better results for the synthesis of *cis*-1,4 isomers at the expense of 1,2-units in butadiene polymerizations. For example, high *cis*-1,4-polybutadiene (99.3%) was reported by Takahasi et al. using bis(salicylaldehyde)Co(II) activated with AlEt_2Cl . The *trans*-1,4-polybutadiene was obtained with VCl_3 , VOCl_3 , or VCl_4 using AlEt_3 and AlEt_2Cl as activators, and 1,2-isotactic and syndiotactic isomers were obtained with Ti and Cr catalysts, respectively. The selectivity obtained using these catalytic systems were the highest, compared to other polymerization methods, such as anionic or cationic initiation.

The physical state of the catalytic system is another parameter that could affect the behavior of the complexes, mostly related to the stereoregularity of the materials. Highly isotactic α -olefin polymers were synthesized using heterogeneous Ziegler–Natta catalysts such as $\text{VCl}_3/\text{AlEt}_3$, where VCl_3 is insoluble in hydrocarbon solvents. On the other hand, highly syndiotactic polypropylene could be obtained using soluble Ziegler–Natta catalysts such as VCl_4 and AlEt_2Cl at -78°C [35].

After the Ziegler–Natta classical catalysts, other kind of metallic complexes were reported for the polymerization of butadienes, such as Ni-based catalysts, half-sandwich titanium complexes, or transition-metal imido compounds activated with BF_3OEt_2 , AlEt_3 , $\text{B}(\text{C}_6\text{F}_5)_4$, or MAO [3].

Recently, several lanthanide complexes, based on Nd, Ln, Sm, or Yb, have been studied for controlling stereoregularity and activity of diene polymerizations and copolymerizations. Specifically, Nd-based catalysts have shown very good stereoregularity control over the production of high *cis*-polybutadiene rubber [36].

5.3.3 Single-Site Catalysts

5.3.3.1 Metallocenes and Constrained Geometry Catalysts The introduction of organic ligands on titanium halide complexes gave rise to the obtention of new homogenous catalytic systems based on well-defined complexes, called *single-site catalysts*. Since the early 1950s, Natta and Breslow [4] (independently) studied the effect of organic ligands on Ziegler–Natta catalysts, synthesizing bis-cyclopentadienyltitanium dichloride (Cp_2TiCl_2) activated with traditional alkyl aluminum compounds, such as AlEt_3 ; however, this catalyst had very low activity for ethylene polymerization and could not polymerize propylene. Owing to its low activity, this organometallic system did not have commercial interest, but its discrete structure was useful for polymerization mechanistic studies.

Until the late 1970s and early 1980s, there was no significant progress in the catalytic activity of titanocene or zirconocene complexes, but then, Sinn and Kaminsky reported the use of MAO as an effective activator for metallocene compounds. MAO was synthesized by the controlled hydrolysis of AlMe_3 , based on the observations of Reichert and Meyer, who by adding small amounts of water to the $\text{Cp}_2\text{TiCl}_2/\text{AlEtCl}_2$ system observed significant increase in its activity. The direct activation of group 4 metallocenes with MAO gave catalysts that were more active than the heterogeneous Ziegler–Natta complexes for ethylene polymerization and also showed high activity for propylene and higher α -olefin polymerization, but without stereoregularity control [5].

A wide variety of metallocenes containing different ligands based on indenyl (Ind) or fluorenyl (Fl) derivatives, which are isoelectronic and equivalent to cyclopentadienyl (Cp) ligands, have since been synthesized. The Cp ligands in metallocenes stabilize and control the steric environment around to the metallic center, which is the active site for olefin coordination.

In 1984, Ewen [6] and Kaminsky [5, 8], based on the study of different metallocene structures activated with MAO for the polymerization of prochiral monomers, related the symmetry of the metallocene ligands to the stereoregularity of the polymers produced. Later, Brintzinger [7] reported metallocene complexes with fixed ligands, containing interannular bridges between Cp or derivative of Cp ligands (ansa-metallocenes), giving rise to a wider variety of metallocene symmetries. Figure 5.3

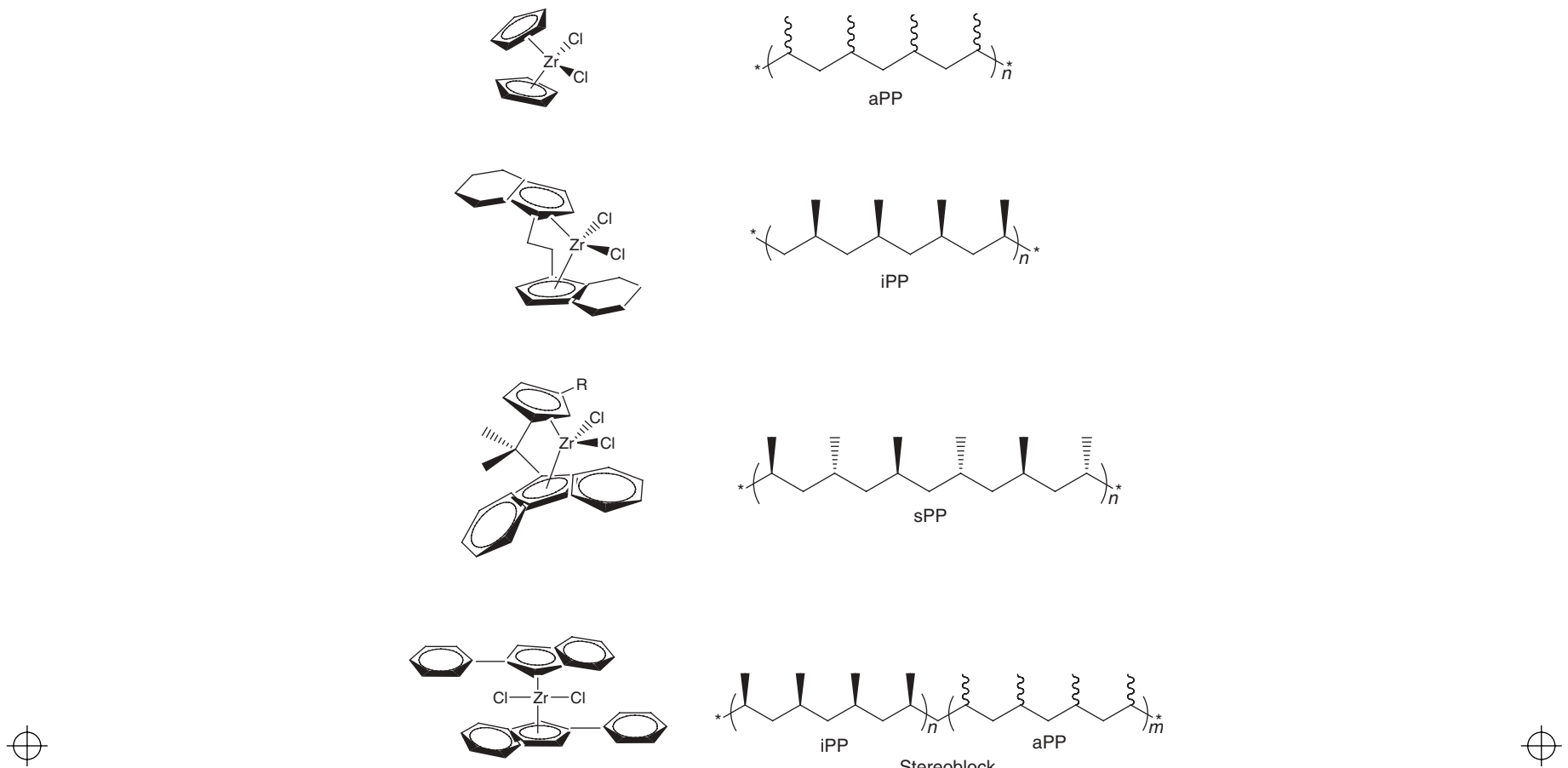


Figure 5.3 Zirconocene precursors for propylene polymerization. aPP, atactic polypropylene; sPP, syndiotactic polypropylene.

summarizes the most representative zirconocene structures, where the symmetry of the precatalysts is related to the stereoregularity of the produced polymers.

Metallocene catalysts were commercialized in 1991 by Exxon Chemical for the industrial production of ethylene-propylene (EP) elastomers in solution polymerization using zirconocene catalysts [37]. As a result of extensive research of different metallocenes applied to the stereoregular control of polymeric materials, these systems were able to produce novel polymers such as syndiotactic polystyrene and ethylene-styrene copolymers, which were not possible to produce with traditional Ziegler–Natta catalysts.

In 1985, Ishihara [10] at Indemitsu, Japan, reported that monocyclopentadienyl, indenyl, or fluorenyl titanium complexes, with different substituents on the Cp derivatives, were highly active for styrene polymerization, producing syndiotactic polystyrene with high melting temperature. Ishihara studied early transition metals from group 3 or 4; systems based on late transition metals such as Ni were inactive for styrene homo- or copolymerization. Monocyclopentadienyl complexes, also

called *half-sandwich catalysts* (Fig. 5.4), were useful for styrene-ethylene copolymerizations, alternated copolymers, or block copolymers (alternated styrene-ethylene with sPS segments) when styrene is present, since it is well known that the aromatic ring helps stabilize the cationic active species through a weak coordination to the metallic center [11, 12].

Owing to its excellent physical properties, such as high melting temperature $T_m = 265\text{--}270^\circ\text{C}$ and glass-transition temperature $T_g = 100^\circ\text{C}$, besides its high resistance to solvents and chemicals, syndiotactic polystyrene is an important engineering thermoplastic utilized for different industrial applications. After the first report by Ishihara, a wide variety of monocyclopentadienyl derivative systems have been tested for styrene polymerization. Carpenter et al. [38] summarized the most relevant systems investigated for the synthesis of syndiotactic polystyrene, which are mainly based on monocyclopentadienyl Ti complexes. Different kinds of substituted indenyl, fluorenyl, and monocyclopentadienyl ligands, or dinuclear Ti half-sandwich complexes, have been reported, as well as amidinate,

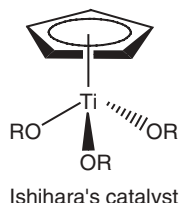


Figure 5.4 Monocyclopentadienyl complex used for styrene polymerizations.

bis-phenolate, or titanatrane derivatives with different ancillary ligands, and the order of activity was reported as benzimidinate < titanatrane < half-sandwich complexes < bis-indenyl < bis-phenolate [39]. Ancillary ligands' effect was also reported, observing the highest activities and stereoregularity for complexes containing OiPr ligands.

Other kinds of monocyclopentadienyl catalysts, containing fixed Cp ligands, correspond to *ansa*-monocyclopentadienyl group 4 complexes. Owing to their geometry, they have been called the *constrained geometry catalysts* [40]. CGCs have been active for different kinds of monomers, but the highest performance has been observed in the polymerization and copolymerization of olefins and α -olefins. The less-hindered geometry (or more open structure) at the metallic center is given by the bridged substituent from the ligand that pulls back the substituents, giving easier access to the coordination of bulkier monomers, such as styrene (Fig. 5.5).

CGCs are able to polymerize prochiral monomers, producing stereoregular polymers. Among the group 4 transition metals, titanium has shown higher activities, compared to Zr or Hf analogous systems. CGCs can make ethylene-styrene copolymers, long-chain branched (LCB) polyolefins, and polyethylene with a wide range of densities. Currently, CGCs are used in industries for producing styrene-ethylene copolymers and polyethylene resins of several densities, but it was the first catalytic system commercialized by Dow in 1991 for producing elastomers based on EP copolymers and EPDM [11].

CGCs have also been obtained with other isoelectronic Cp ligands, such as indenyl with several substituents, where

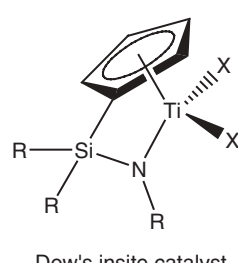


Figure 5.5 Constrained geometry catalyst (CGC).

the effect of the structures on the stereoregularity control of the polymers produced have been studied [40].

Other active single-site early transition-metal-based catalysts for nonpolar monomers correspond to different bis-cyclopentadienyl group 3 and lanthanide complexes, such as L_2MR ($M = Sc, Y, La, Nd, Sm, Lu$; $R = alkyl$ or H). Usually, these systems do not require the activator component to generate high activity catalysts for olefin polymerizations [3].

5.3.3.2 Non-metallocene Early Transition-Metal-Based Single-Site Catalysts Intense research about new highly active catalysts for ethylene polymerization and copolymerization led to the development of new postmetallocene systems [26]. Usually, non-metallocene-based catalysts are coordination or organometallic compounds that contain bidentate or multidentate ligands such as imine, diamine, tetramine, bisphenolic, or *ortho*-phenoxyimine groups, stabilized with different bulky substituents. These systems usually are tetra-coordinated complexes, but also can be hexacoordinated, with octahedral geometry, where two or more donor groups containing nitrogen, oxygen, or phosphorus atoms form highly stable bonds with the transition metal (Fig. 5.6). Combined with the appropriate activators, nonmetallocene catalysts can promote olefin polymerization with activities comparable to those of group 4 metallocene catalysts, showing, in some cases, even higher activities.

Among the different postmetallocene catalysts in Figure 5.6, the complexes bearing phenoxyimine [17] ligands (FI catalysts) exhibit the highest ethylene polymerization activity. FI catalysts were developed by Fujita and coworkers [41] at Mitsui Chemicals, Japan, in the late 1990s.

Subsequent research accomplished by Mulhaupt [42], Cavallo [43], and others afforded the production of a wide

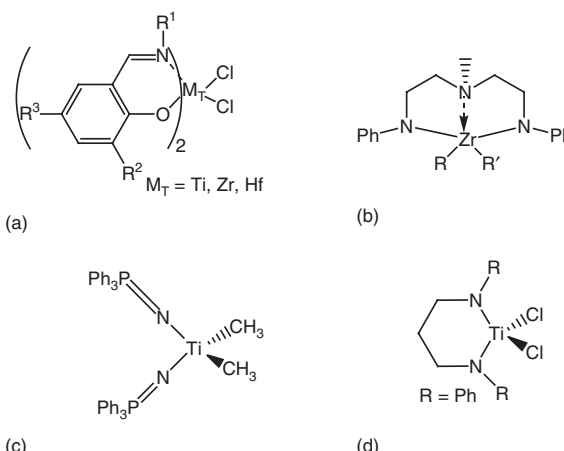


Figure 5.6 Postmetallocenes' catalytic systems: (a) phenoxyimine (FI), (b) Schrock, (c) Stephan, (d) McConville.

range of polyolefins that could not be synthesized with metallocenes efficiently. Steric and electronic effects of a variety of substituents on the phenoxyimine ligands allow these systems to produce a wide assortment of stereoregular and stereospecific polymers and copolymers, such as new differentiated polyolefins, high performance linear low density polyethylene (LLDPE), polyolefinic elastomers, cyclic olefinic copolymers, ethylene-styrene copolymers, highly isotactic and syndiotactic polypropylenes, and highly syndiotactic polystyrene, and, more recently, FI catalysts have been able to synthesize hyperbranched polyethylene [17], ethylene-polar monomer copolymers [43, 44], monodisperse poly(higher α -olefins) [18], or higher α -olefin-based block copolymers [28, 45], which are difficult to produce using the classical group 4 metallocenes or CGCs.

DFT (Density Functional Theory) calculations performed on metallocene and FI catalyst structures suggested that ethylene polymerizations involve higher energy states for metallocenes in the process of ligands exchanging, during the insertion step, than the energy states observed for FI catalysts [17]. Later, Koji and Terunor [44] postulated that the high activity of the FI complexes is based on their higher capacity for moving electronic density from the coordinating olefin, insertion and migration of the bonds and usually in all the electronic arrangement.

5.3.3.3 Late Transition-Metal Catalysts Late transition-metal catalysts typically produce branched polyethylene from polymerizing ethylene as a sole monomer, without the addition of comonomers via the mechanism of chain walking. Among the different catalytic species studied by coordination polymerization, cationic or neutral nonmetallocene complexes containing mainly Fe, Co, Ni, and Pd exhibited different ethylene polymerization behavior and single-site polymerization mechanisms (Fig. 5.7) [26]. Owing to the larger number of valence electrons, late transition-metal-based catalysts are less sensitive to protic impurities, poisons, and even polar monomers compared to catalysts based on early transition metals, such as group 4 metallocenes.

In 1981, Keim and Peuckert [45] synthesized the first branched polyethylene using iminophosphonamide-nickel

complexes. The systems produced low molecular weight polyethylene with physical properties similar to LDPE. Traditionally, this kind of catalytic species is prone to facile chain transfer reactions, useful for producing ethylene dimers and oligomeric materials.

More recently, Brookhart and Johnson [28] and Gibson et al. [29] modified the structure of late transition-metal catalysts (Fig. 5.7) by introducing tridentate and bulky substituents in the ligands, thus retarding the chain termination processes in the polymerizations.

These postmetallocene single-site catalysts [46, 47] are highly active for the synthesis of branched and hyperbranched polyethylene, polypropylene, and ethylene copolymers with different α -olefins. Branching frequency and length can be controlled by varying ligand structure, temperature, and pressure during polymerization. Formation of short-chain branches during ethylene homopolymerization occurs via the chain walking mechanism, with the competition between isomerization of the chain end and the insertion for the linear growth of the polymeric chain.

Late transition-metal complexes can also polymerize nonpolar and polar comonomers, such as alkyl acrylates, acrylonitrile, or carbon monoxide. Polyketones have been efficiently produced through CO-ethylene copolymerizations [46].

Palladium/phosphine-sulfonate neutral complexes, reported by Drent, Pugh, and coworkers, could incorporate several polar comonomers such as methyl acrylate, vinyl ethers, methyl vinyl ketones, and silyl vinyl ethers. Other common comonomers such as vinyl acetate, acrylonitrile, and vinyl chloride showed very low comonomer incorporation, between 1% and 2% [48].

5.3.3.4 Supported Single-Site Catalysts Catalysts supporting is considered a prerequisite for the application of most coordination catalytic systems. The most important polymerization methods (slurry and gas phase) require the use of supported or heterogenized catalysts. Particle morphology and bulk density are the main physical features of a supported catalytic system, determining its application in commercial processes [49].

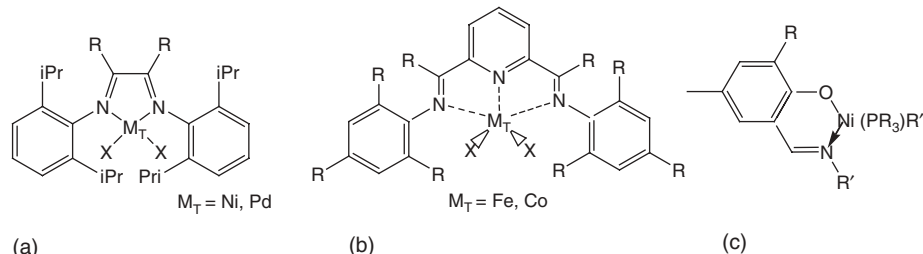


Figure 5.7 Main late transition-metal catalysts: (a) Versipol catalyst, (b) Brookhart/Gibson, (c) Grubbs/Johnson.

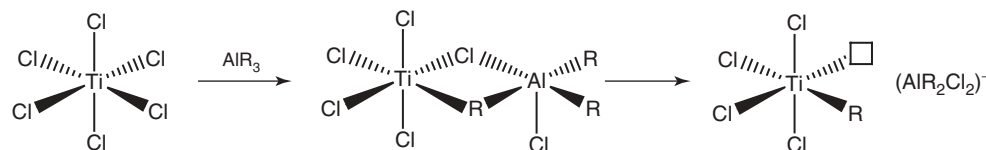


Figure 5.8 Active species formation in a classical Ziegler–Natta catalyst.

Single-site catalysts have been successfully supported on silica previously modified with MAO or trimethylaluminum, avoiding the direct contact with the Si-O or Si-OH groups of the silica support, but many other supporting techniques have been investigated. Ribeiro et al. [50] described in detail the main immobilization methods used for metallocenes, which have been extended with some modifications for other single-site catalysts. More recently, Choi and Soares have reviewed the main supporting techniques used for metallocene and postmetallocene catalysts.

5.4 COORDINATION POLYMERIZATION MECHANISM

Because of the nature of the active species, coordination polymerization has been classified as ionic polymerization, which follows the polyaddition mechanism's characteristic steps, in the growing of the polymeric chain: initiation, propagation, and termination. As for the initiation step, the ionic active species is produced by the reaction between the catalyst and cocatalyst. Usually, the catalysts are actually precursor catalysts or precatalysts, which become the real cationic active species after the activation or reaction with the cocatalyst (Fig. 5.8).

Figure 5.9 outlines the steps for the chain polyaddition mechanism involved in the coordination polymerizations for any kind of active species initiated through different cocatalysts. The counteranion species was suppressed for practical representation of the active site. Once the cationic species is created, it starts the growth of the polymeric chain through continuous addition of monomer. The propagation step is forward described in Figure 5.9 according to the most accepted reaction cycle proposed by Cossee and Arlman, which is known as the *Cossee–Arlman mechanism* [51].

As for the termination step, different reactions have been detected, according to the structure of the polymers, such as terminal vinylic groups, which are evidence of β -hydride elimination from the polymeric chains.

5.5 POLYMERIZATION KINETICS AND MATHEMATICAL MODELING

Mathematical models for olefin polymerization with coordination catalysts are usually classified into microscale,

mesoscale, and macroscale models [52]. Polymerization kinetics and microstructural models are defined at the microscale level, mesoscale phenomena includes catalyst particle breakup and growth and particle mass and heat transfer resistances during polymerization, and finally, transport phenomena at the reactor level are treated in macroscale models.

This division is very useful during model development and implementation. Differentiated emphasis should be placed on these modeling scales depending on the model objectives. For instance, detailed polymerization kinetics is important if the precise prediction of polyolefin microstructure is required. On the other hand, apparent kinetics suffices if the model's objective is to follow the evolution of particle fragmentation or to describe reactor residence time effects on polymerization. These ideas are detailed in the following sections.

5.5.1 Polymer Microstructural Models

Polyethylene microstructure is defined by its distributions of chain length (CLD) or molecular weight (MWD), chemical composition (CCD), comonomer sequence length (CSLD), and LCB. In addition, polypropylene microstructure is further characterized by its distribution of regio- and stereoregularity [53, 54].

Polymer chain microstructure depends on polymerization mechanism and reactor conditions. The polymerization

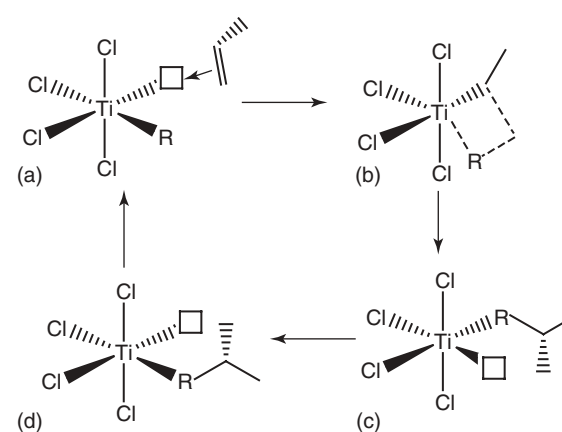


Figure 5.9 The Cossee–Arlman mechanism a) Olefin coordination, b) Olefin concerted insertion, c) Insertion step, d) Chain migration.

mechanism with coordination catalysts has been investigated extensively and is reviewed only briefly herein [39]. During polymerization, either of the two events may happen: the chain may propagate by insertion of a monomer molecule in the carbon-transition-metal bond at the end of the chain or it may terminate following several chain transfer steps. Propagation may take place with one of several comonomers or, more rarely, with a dead polymer chain having a terminal reactive double bond (macromonomer) [55]. Highly sophisticated mathematical models have been developed based on these few mechanistic steps.

Table 5.2 lists the basic kinetics steps for the homopolymerization of olefins with coordination catalysts. There are four main types of reactions: catalyst activation, monomer propagation, chain transfer, and catalyst poisoning. The reaction of the catalyst precursor, C, with the cocatalyst, Al (generally an alkylaluminum or alkylaluminoxane compound), is considered to be almost instantaneous and leads to the formation of the active catalyst site, C*. Initiation and propagation steps with monomer, M, leads to the formation of a growing polymer chain of length r , P_r. The four most common chain transfer steps are listed in Table 5.2; they produce active sites¹ that are available to grow other polymer chains and dead polymer chains of length r , D_r. Finally, the catalyst may be deactivated via first- or second-order processes or by reaction with impurities, although the

details of these mechanistic steps are still poorly understood.

This kinetic model is extended to binary copolymerization of monomer types M₁ and M₂ (e.g., ethylene and 1-hexene) in Table 5.3. Not all steps from Table 5.2 are repeated in Table 5.3 to avoid unnecessary repetition, but they can be easily deduced by analogy. For copolymerizations that follow the terminal model shown in Table 5.3, the last monomer added to the living chains influences the subsequent reactions due to steric and electronic effects. For instance, four propagation steps are needed in copolymerization, since the last monomer molecule added to the chain is assumed to influence the next propagation step with monomer M₁ or M₂. Despite its apparent complexity, copolymerization models can be rendered as simple as homopolymerization ones using the pseudoconstant model developed by Hamielec and coworkers [56–59].

The kinetic steps shown in Tables 5.2 and 5.3 are widely accepted and are commonly used to develop polyolefin microstructural models, but they do not describe all aspects of olefin polymerization with coordination catalysts: (i) hydrogen not only acts as a chain transfer agent but also accelerates the polymerization rate of propylene and reduces the polymerization rate of ethylene with most Ziegler–Natta catalysts and metallocenes [60–65]; (ii) α -olefin accelerates the rate of ethylene polymerization significantly with most coordination catalysts, the so-called comonomer effect [61, 66, 67]; and (iii) the rate of polymerization with respect to monomer concentration may vary from 1 to 2 [68]. Several alternative hypotheses have been proposed to explain these phenomena, but there is no unified mechanism that can account for all of them.

TABLE 5.2 Basic Mechanism for Olefin Homopolymerization with Coordination Catalysts

Description	Chemical Equations
Site activation	C + Al \rightarrow C*
Initiation	C* + M \rightarrow P ₁
Propagation	P _r + M \rightarrow P _{r+1}
β -Hydride elimination	P _r \rightarrow C* + D _r
Transfer to H ₂	P _r + H ₂ \rightarrow C* + D _r
Transfer to monomer	P _r + M \rightarrow C* + D _r
Transfer to cocatalyst	P _r + Al \rightarrow C* + D _r
First-order deactivation	P _r \rightarrow C _d + D _r
	C* \rightarrow C _d
Second-order deactivation	2P _r \rightarrow 2C _d + 2D _r
	2C* \rightarrow 2C _d
Poisoning	P _r + I \rightarrow C _d + D _r
	C* + I \rightarrow C _d

Abbreviations: C, catalyst precursor; C*, active site; C_d, deactivated site; Al, cocatalyst; M, monomer; P_r, living chain of length r ; D_r, dead chain of length r ; H₂, hydrogen; I, catalyst poison.

¹Active sites produced after different chain transfer steps may differ slightly. For instance, a metal hydride site is obtained after chain transfer to hydrogen, while a metal-C₂H₅ site is obtained after chain transfer to polymer. For the sake of simplicity, these sites are not differentiated in Table 5.2; for most modeling applications, these differences are also irrelevant.

TABLE 5.3 Simplified Terminal Model for Binary Copolymerization of Olefins

Description	Chemical Equations
Initiation	C* + M ₁ \rightarrow P ₁ ¹
	C* + M ₂ \rightarrow P ₁ ²
Propagation	P _r ¹ + M ₁ \rightarrow P _{r+1} ¹
	P _r ¹ + M ₂ \rightarrow P _{r+1} ²
	P _r ² + M ₁ \rightarrow P _{r+1} ¹
	P _r ² + M ₂ \rightarrow P _{r+1} ²
β -Hydride elimination	P _r ¹ \rightarrow C* + D _r
	P _r ² \rightarrow C* + D _r
Transfer to hydrogen	P _r ¹ + H ₂ \rightarrow C* + D _r
	P _r ² + H ₂ \rightarrow C* + D _r
Monomolecular deactivation	P _r ¹ \rightarrow C _d + D _r
	P _r ² \rightarrow C _d + D _r

M₁ and M₂, monomer types.
Superscripts 1 and 2 indicate the type of last monomer added to the chain.

The method of moments is one of the oldest techniques used to model the MWD of polyolefins [69]. First, it is necessary to develop population balances for living and dead chains (P_r and D_r) of all lengths using the mechanisms proposed in Table 5.2 or 5.3. For high polymers, this procedure generates a very large system of ordinary differential equations (ODEs), with one equation for each chain having from 1 to r_{\max} monomer units, where r_{\max} is the number of monomer molecules in the longest chain in the polymer population. Solving the resulting set of ODEs requires sophisticated algorithms and considerable computational effort. If the whole distribution is not required, moment equations can be derived from the ODE system, resulting in a much smaller set of ODEs. For instance, the number-average chain length (r_n) is calculated as the ratio of the first to the zeroth moment; the weight-average chain length (r_w), as the ratio of the second to the first moment; higher chain length averages are found in a similar way. The method of moments not only reduces the required computational effort significantly but also results in a considerable loss of information since only averages are computed instead of the complete CLD. Tutorial-style descriptions of this method have been published recently in the literature [53, 54].

Alternatively, the complete population balance can be solved dynamically using efficient ODE solvers [70, 71]. The versatile commercial software PREDICI can solve population balances that describe polymerizations with coordination catalysts and many other polymerization mechanisms [72]. In this approach, the complete microstructural distributions are modeled, leading to a detailed description of the polymer microstructure.

In some specific cases, analytical solutions for the population balances can also be derived. For instance, Soares and Hamielec [73, 74] obtained analytical dynamic solutions to describe how the CLD of polyolefins varied as a function of time in stopped-flow reactors commonly used for mechanistic studies on olefin polymerization kinetics and mechanism [75–78]. These analytical solutions combine the power of full population balance numerical solutions with the ease and convenience of using closed form equations; they are, unfortunately, difficult to attain for more complex cases.

Different from analytical dynamic solutions, *instantaneous distributions* are derived to describe the polymer microstructure made at a particular instant in time during the polymerization. These distributions are “snapshots” of the polymer microstructure at a given moment during the polymerization. A classic instantaneous distribution used to describe the CLD of linear polyolefins and other polymers that follow analogous chain growth kinetics was developed independently by Schulz [79] and Flory [80, 81]

$$w(r) = r \tau^2 e^{-r\tau} \quad (5.1)$$

where $w(r)$ is the weight CLD, r is the polymer chain length, and the parameter τ is the reciprocal of the number-average chain length for the polymer. Therefore, τ is also given by the ratio of overall chain transfer, R_t , to propagation, R_p ,

$$\tau = \frac{R_t}{R_p} \quad (5.2)$$

Using the mechanism proposed in Table 5.2, Equation 5.2 becomes

$$\tau = \frac{k_{tM}}{k_p} + \frac{k_{t\beta} + k_{tH}[H_2] + k_{tAl}[Al]}{k_p[M]} \quad (5.3)$$

where k_p , k_{tM} , $k_{t\beta}$, k_{tH} , and k_{tAl} are the rate constants for propagation, transfer to monomer, β -hydride elimination, transfer to hydrogen, and transfer to cocatalyst, respectively.

Equation 5.1 is applicable to polyolefins made with single-site catalysts, such as metallocenes, and predicts a polydispersity index of 2.0. It is discussed later how this equation can also be used to model the CLD of polyolefins made with multiple-site catalysts, such as heterogeneous Ziegler–Natta and Phillips catalysts. Despite its simplicity, this equation can be used to predict the complete CLD of single-site polyolefins instantaneously using an easy-to-estimate parameter, τ .

Stockmayer [82] extended the Flory distribution to also include the CCD of linear polyolefins,

$$w(r, y) = r \tau^2 e^{-r\tau} \sqrt{\frac{r}{2\pi\beta}} e^{-\frac{ry^2}{2\beta}} \quad (5.4)$$

where y is the difference between the molar fraction of monomer 1 (e.g., ethylene) in the copolymer chain, F_1 , and the average molar fraction of monomer 1 in the whole copolymer sample, \bar{F}_1 ,

$$y = F_1 - \bar{F}_1 \quad (5.5)$$

and the parameter β is defined as

$$\beta = \bar{F}_1 (1 - \bar{F}_1) \sqrt{1 - 4\bar{F}_1 (1 - \bar{F}_1) (1 - r_1 r_2)} \quad (5.6)$$

where r_1 and r_2 are the reactivity ratios. The variable r and the parameter τ have the same meaning as in the Flory most probable distribution (Eq. 5.1). The average molar fraction of comonomer 1 in the copolymer, \bar{F}_1 , is calculated with the classical Mayo–Lewis equation [83]. The Stockmayer distribution is illustrated in Figure 5.10 for a single-site catalyst.

The Stockmayer distribution is an extension of the Flory distribution for copolymers. When Equation 5.4 is integrated over all chemical compositions, it is reduced to

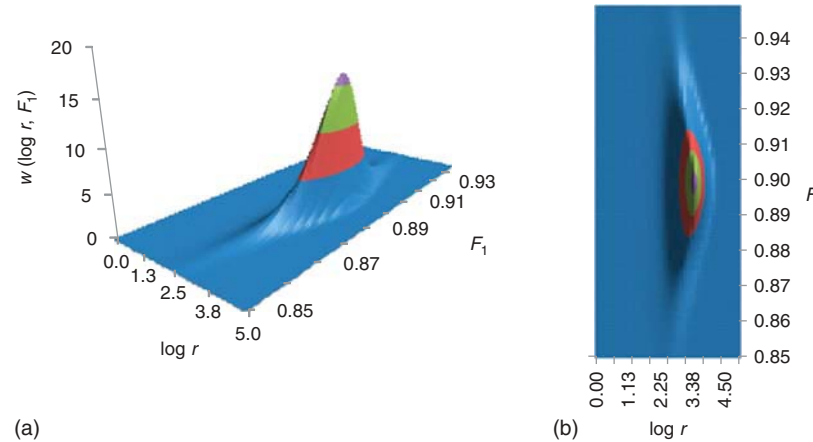


Figure 5.10 The Stockmayer distribution for a copolymer made with a single-site catalyst.
a) Three-dimensional plot, b) Bird's eye view. (See insert for the color representation of the figure.)

the Flory distribution; similarly, when it is integrated over all chain lengths, the CCD component is isolated [84–86].

CSLD is another important microstructural characteristic of polyolefins. It is usually expressed by their dyad, triad, tetrads, and higher “ad” distributions, as measured by ^{13}C NMR. CSLD is described with Markovian statistical models [87, 88]. The order of a Markovian model indicates the number of monomer units in the growing chain that affect the propagation of the next monomer molecule. For a given catalyst, zeroth-order models assume that monomer propagation depends only on the type of monomer being inserted and not on the chain end type—these models are also called *Bernoullian models*. First-order models assume that propagation depends on the type of monomer being inserted *and* on the type of monomer at the chain end bonded to the active site—this is the terminal model discussed in Table 5.3 and also assumed in the Mayo–Lewis equation. Second-order models suppose that the type of propagating monomer and the last two monomers added to the chain influence propagation (penultimate model). Higher Markovian models follow an analogous rationale. For olefin polymerization, the terminal model is generally enough to describe the CSLD of most polyolefins, with the penultimate model being used much more rarely. A similar approach may also be used to model stereo- and regiosequences for polypropylene.

Soares and Hamielec extended the Stockmayer distribution for copolymers containing LCBs, where the mechanism of LCB formation is terminal branching via macromonomer incorporation [89, 90]. The resulting trivariate distribution is given by the expression

$$w(r, y, k) = \frac{1}{(2k+1)!} r^{2k+1} \tau_B^{2k+2} e^{-r\tau_B} \sqrt{\frac{r}{2\pi\beta}} e^{-\frac{r^2}{2\beta}} \quad (5.7)$$

where k is the number of LCBs per chain and the parameter τ_B is a modification of the parameter τ given

in Equation 5.2 to account for the rate of LCB formation, R_{LCB} ,

$$\tau_B = \tau + \frac{R_{\text{LCB}}}{R_p} \quad (5.8)$$

Figure 5.11 illustrates how the CLD and CCD vary for polymer populations with different number of LCBs per chain. Several other related distributions have been developed to describe these branched homopolymers and copolymers [55].

Polymer reactor dynamics involves changes in polymerization temperature, monomer/hydrogen ratio, monomer/comonomer ratio, etc. Most olefin polymerization reactors are operated under steady-state conditions; therefore, these changes are important only during grade transitions or process instabilities. They are generally very slow compared to the chain growth and termination dynamics that determine the polymer microstructures described with the instantaneous distributions mentioned earlier. Consequently, except in special cases, these distributions can be integrated in time to describe the microstructure of polymers made during non-steady-state conditions. For instance, the cumulative CLD of a polyolefin made in the time interval Δt at transient conditions, $\bar{w}(r)$, can be calculated with the equation

$$\bar{w}(r) = \frac{\int_t^{t+\Delta t} w(r, t) R_p(t) dt}{\int_t^{t+\Delta t} R_p(t) dt} \quad (5.9)$$

Since the reactor conditions are not at steady state, the instantaneous distribution $w(r, t)$ becomes a function of time. For instance, changes in hydrogen/ethylene

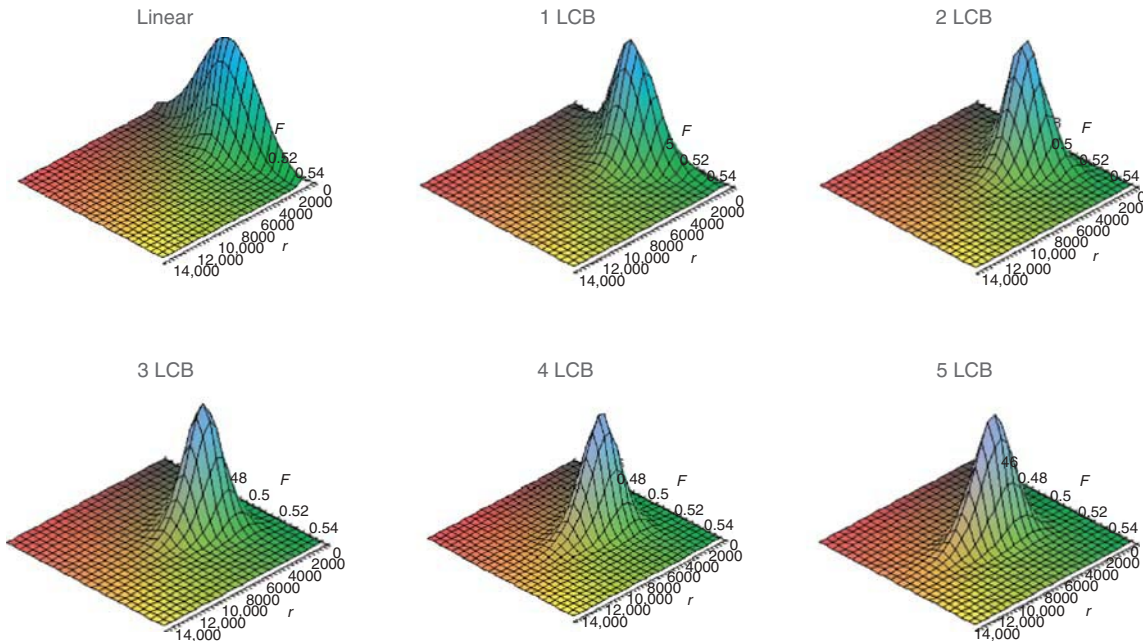


Figure 5.11 Trivariate distribution for a model polymer. (See insert for the color representation of the figure.)

ratio during a grade transition will make the molecular weight averages drift from one steady-state value to another.

Analogous equations can be used with any other instantaneous distribution. This relatively easy integration extends the use of instantaneous distributions to transient reactor operation and considerably broadens the use of this powerful technique. When compared with the method of moments, instantaneous distribution allows for the complete prediction of CLD and CCD instead of only averages; when contrasted to the full solution of the population balances, the method of instantaneous distributions provides the same information at a much shorter time using a more elegant solution, allows the modeler to analyze the problem with a simple glance at the equation, and can even be implemented on simple commercial spreadsheets for easy calculation.

The Monte Carlo techniques are the most powerful of all modeling approaches used to describe the microstructure of polyolefins, because chains are built individually and, in principle, *all* microstructural details can be retrieved at the end of the simulation. The main concept behind the Monte Carlo simulation is relatively simple, although model implementation and algorithm development may become sophisticated to enhance computational efficiency. One starts by defining model probabilities based on the polymerization mechanism and then uses a random number generator to decide which event should take place during polymerization. In the simplest of all cases, one can start by assuming that only two events take place during

polymerization: propagation and chain transfer. This leads to the definition of a propagation probability, P_p , and a termination probability, P_t ,

$$P_p = \frac{R_p}{R_p + R_t} \quad (5.10)$$

$$P_t = \frac{R_t}{R_p + R_t} = 1 - P_p \quad (5.11)$$

These two probabilities are used to build chains, one by one, during the simulation. A random number is generated between 0 and 1 and its value is compared to P_p (or P_t). If the random number is lower than P_p , the chain grows by one monomer unit; otherwise, it terminates. The CLD can be obtained through this approach after the generation of a sufficiently large number of polymer chains; generally, several hundred thousand chains are required to obtain a smooth distribution.

It is evident that this approach is impractical for this simple problem because the Flory distribution provides the same information in a much more efficient way. The Monte Carlo methods become more attractive when modeling complex microstructures for which no analytical solutions are possible, such as for terpolymers, branched or crosslinked chains, and chains with branching resulting from chain walking with late transition-metal catalysts. The Monte Carlo techniques have been used to model a variety of polyolefin microstructures effectively and are the most powerful, albeit the most computational time consuming, of all modeling techniques [91–96].

The simple approach discussed above is valid for steady-state Monte Carlo simulations, but dynamic simulations are also possible. In this case, the model probabilities must be updated frequently, generally after every iteration. A detailed discussion of these methods would be too lengthy to be included herein; the most common algorithm for dynamic Monte Carlo simulation follows the approach proposed by Gillespie, which requires the discretization of the polymerization reactor with small control volumes and the conversion of the polymerization kinetic rates into molecular collision frequencies [97, 98].

The methods discussed above for single-site catalysts (metallocenes and late transition-metal catalysts) can be extended directly to multiple-site catalysts (Ziegler–Natta and Phillips catalysts) by assuming that each site type behaves essentially as single-site catalysts [87, 88, 99, 100, 101]. Therefore, the microstructural distribution of a polymer made with a multiple-site catalyst is treated as a weighted sum of several single-type distributions [102],

$$w(r, y) = \sum_{j=1}^n m_j w(r, y)_j \quad (5.12)$$

where m_j is the mass fraction of polymer made on site type j for a catalyst having n site types. The simulated bivariate distribution of a polymer made on a three-site-type catalyst is shown in Figure 5.12.

This approach has been used by several researchers to model the microstructures of polymers made with the Ziegler–Natta and the Phillips catalysts using the method of instantaneous distributions, method of moments, or the Monte Carlo simulation. Several techniques have also been developed to help estimate model parameters for these multiple-site models, but it still remains a difficult problem

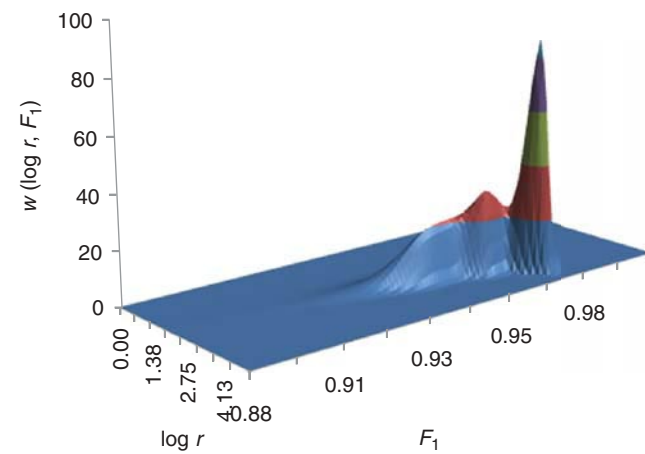


Figure 5.12 Simulated chain length and chemical composition distributions of a polymer made from a three-site catalyst. (See insert for the color representation of the figure.)

due to the relatively large number of parameters that are required [103–111]. Other modeling techniques have also been proposed to model multiple-site catalysts [112], but the approach illustrated in Equation 5.12 still remains the most common, likely because of its relative simplicity.

5.5.2 Particle Breakup, Inter- and Intraparticle Mass and Heat Transfer Resistance Models

With the exception of solution processes, all other commercial olefin polymerization processes use heterogeneous catalysts [53, 54]. When a fresh catalyst particle is introduced in the polymerization reactor (or prepolymerization reactor), monomer molecules diffuse into the catalyst pores and start forming polymer chains. In a properly designed catalyst, the polymer chains fill the pores until the force they exert on the pore walls exceeds their mechanical strength, causing the catalyst particle to break up into smaller fragments. These catalyst fragments are surrounded by entangled growing polymer chains that act as a binder, keeping the fragments together in the expanding polymer/catalyst particle. This particle breakup and exfoliation process is known as the *replication phenomenon* because the polymer particles replicate the shape and size distribution of the catalyst particles.

As usual in heterogeneous catalysis processes [113], inter- and intraparticle mass and heat transfer resistances may develop during polymerization with heterogeneous Ziegler–Natta, Phillips, and supported metallocene catalysts. If significant, the resulting temperature and concentration radial profiles may affect not only the apparent polymerization rate but also the polymer microstructure. The models described in the previous section remain valid, but only locally: slightly different microstructural distributions would be required to describe the polymer made at different radial positions because temperature, monomer/comonomer ratio, and monomer/hydrogen ratio may also be varied. In fact, the original motivation for the development of particle mass and heat transfer models for olefin polymerization was to explain the production of polyolefins with broad MWDs made with heterogeneous Ziegler–Natta catalysts [114]. If significant monomer concentration or temperature profiles occur in the polymer particle, the polymer average molecular weight becomes a function of radial position, broadening the MWD [5].²

Several models have been proposed to describe intraparticle heat and mass transfer with heterogeneous coordination catalysts [114], but the most commonly accepted is the multigrain model (MGM) [115–126]. In the MGM, the

²Currently, it is accepted that the main reason behind broad MWDs is the presence of more than one type of active site in these catalysts, with mass and heat transfer limitations being a secondary broadening effect of varying importance depending on catalyst type and polymerization conditions.

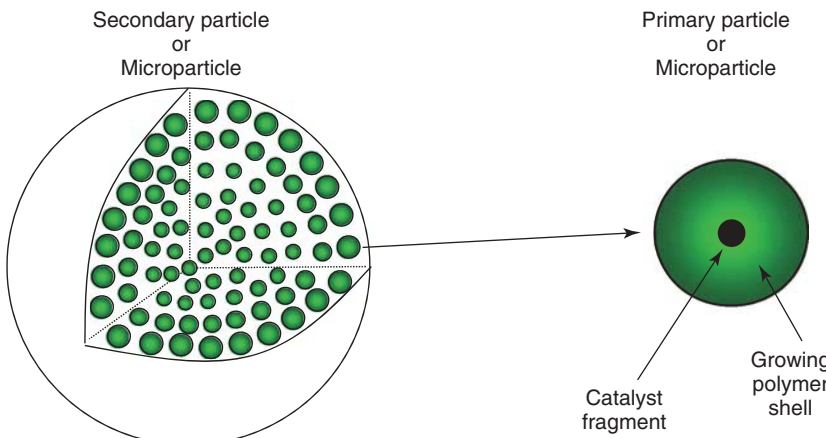


Figure 5.13 The multigrain model (MGM). (See insert for the color representation of the figure.)

growing polymer particle (macroparticle or secondary particle) is considered to be composed of several hundreds of catalyst fragments surrounded by growing polymer chains (microparticles or primary particles). Figure 5.13 shows a schematic for the MGM.

Another common single-particle model is the polymeric flow model (PFM), in which a pseudohomogenous hypothesis is made for the macroparticle [127–129]. Instead of being located at the center of microparticles, as in the MGM, active sites are considered to be dispersed in a pseudohomogenous medium with varying radial concentrations. The PFM is somewhat easier to implement than the MGM and leads to similar prediction trends. Several models that combine features of the MGM and PGM have also been developed over the years [114, 130].

The set of equations defining the PGM and MGM are the classic diffusion–reaction equations in spherical coordinates, with and without the pseudohomogenous approximation, respectively, but they must be solved under moving boundary conditions since the particle expands during polymerization; these model equations have been explained in detail in a review dedicated to single-particle models [114].

A few general conclusions have been reached from the extensive use of these single-particle models: (i) intraparticle mass transfer resistances in gas-phase processes are less important than those in slurry processes since gas-phase diffusion coefficients are 2 to 3 orders of magnitude greater than those in slurry; (ii) interparticle heat transfer resistances are more significant in gas-phase processes since gases are poor heat conductors; (iii) heat transfer resistances are greatest in larger catalyst particles because the amount of heat released is proportional to the particle volume, whereas energy removal from the particle is proportional to surface area; (iv) similarly, mass transfer resistances are also more significant in larger catalyst particles since the polymerization rate is proportional to particle

volume, while monomer flux to the particle is proportional to surface area; and (v) as the polymer particles grow, both mass and heat transfer limitations decrease, as the number of active sites either remains constant or decreases through deactivation reactions, causing both the heat generation rate and the rate of monomer consumption per unit volume to decrease, while heat and mass flux increase with the expanding surface area.

Figure 5.14 shows how the microstructural distributions developed in the previous section can be used in conjunction with the MGM [131].

The summation of these distributions over the polymer particle, weighted by the amount of polymer made at each radial position, gives the distribution for the whole particle at a given instant in time $w_p(r, y)$,

$$w_p(r, y) = \frac{\int_0^{R_s} R_p(r_s) w(r, y) dr_s}{\int_0^{R_s} R_p(r_s) dr_s} \quad (5.13)$$

where $R_p(r_s)$ is the rate of polymerization at a given radial position and R_s is the macroparticle radius. These instantaneous distributions can then be integrated in time to obtain the cumulative distribution in the reactor per polymer particle, $\bar{w}_p(r, y)$,

$$w_p(r, y) = \frac{\int_0^t \int_0^{R_s} R_p(r_s) w(r, y) dr_s dt}{\int_0^t \int_0^{R_s} R_p(r_s) dr_s dt} \quad (5.14)$$

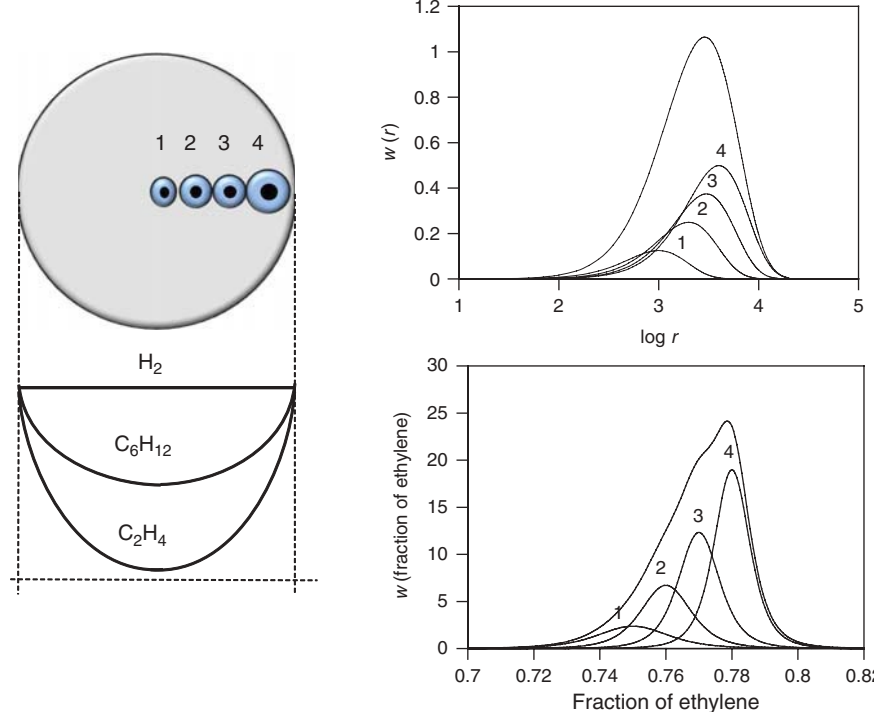


Figure 5.14 Effect of radial concentration profiles on the chain length and chemical composition distributions of an ethylene/1-hexene copolymer (four microparticle layers were used for simplicity sake: many more layers are required in an actual MGM simulation) [131].

A similar approach can be applied for a catalyst containing n site types: the instantaneous CLD and CCD in the particle equal the summation of the distributions over all site types and all radial positions,

$$w_p(r, y) = \frac{\int_0^{R_s} \sum_{j=1}^n R_{p,j}(r_s) w_j(r, y) dr_s}{\int_0^{R_s} \sum_{j=1}^n R_{p,j}(r_s) dr_s} \quad (5.15)$$

Despite being well established, the MGM and PFM can only describe a relatively minor set of phenomena that are important in particle fragmentation and growth. These models usually assume that particle fragmentation is instantaneous and cannot account for a series of important phenomena such as prepolymerization effect, particle agglomeration, fine formation, and reactor fouling, which are issues of significant industrial interest, but difficult to describe even with a semiquantitative mathematical model. Several other models, generally variations of the MGM or PFM, have been developed to try to capture different aspects of particle morphology development during olefin polymerization with heterogeneous catalysts [130, 132–148].

5.5.3 Polymerization Reactor Models

Phenomena taking place from microscale to macroscale influence olefin polymerization rates and polyolefin microstructure. Catalyst type ultimately determines the polymer microstructure for a given set of polymerization conditions such as temperature, monomer/comonomer ratio, and hydrogen concentration, but the polymerization conditions at the active sites are a consequence of the type of catalyst support and reactor used to produce the polyolefin.

A complete phenomenological mathematical model for olefin polymerization in industrial reactors should, in principle, consider phenomena taking place from microscale to macroscale, but this is seldom the case. Most models assume that the conditions in the polymerization reactor are uniform and neglect any mesoscale phenomena, which may be a good approximation for solution polymerization reactors, but may not apply to polymerizations using heterogeneous catalysts.

The reason this relatively weak hypothesis is often made is that the effort required to integrate phenomena taking place from micro- to macroscale in a single model does not necessarily lead to better quantitative predictions when it comes to industrial reactors. Uncertainties in model parameter values, especially for multiple-site catalysts, are

too high to try to decouple the “true” polymerization kinetics from particle mass and heat transfer effects; often apparent kinetic parameters will do an equally good job from an engineering perspective.

Several macroscale models with varying levels of complexity and covering macroscale phenomena such as the reactor residence time effects and micro- and macromixing behavior have been developed for olefin polymerization but is not discussed here in detail for the sake of brevity [149–157].

REFERENCES

- Boor J. *Ziegler-Natta Catalysts and Polymerizations*. New York: Academic Press, Inc.; 1979.
- [a] McDaniel Max P. *Adv Cat* 2010;53:123. [b] Sailors HR, Hogan JP. *Polymer News* 1981;7:152. [c] Eley DD, Rochester CH, Scurrell MS. *Proc Roy Soc Lond A* 1972;329:361.
- [a] Osakada K, Takeuchi D. *Adv Polym Sci* 2004;171:137. [b] Moore EP Jr. *Polypropylene Handbook*. Munich, Vienna, New York: Hanser Publishers; 1996. p 12.
- [a] Long WP, Breloow DS. *J Am Chem Soc* 1960;1953. [b] Halterman RL. *Chem Rev* 1992;92:965.
- Sinn H, Kaminsky W. *Adv Organomet Chem* 1980;18:99.
- [a] Soga K, Uozumi T, Kaji E. In: Scheirs J, Kaminsky W, editors. *Metallocene-Based Polyolefins*. Chichester: John Wiley and Sons Ltd.; 2000. p I/381. [b] Ewen JA, Jones RL, Razavi A, Ferrara JD. *J Am Chem Soc* 1988;110:6255. [c] Spaleck W, Küber F, Winter A, Rohrmann J, Bachmann B, Antberg M, Dolle V, Paulus FF. *Organometallics* 1994;13(3):954. [d] Collins S, Gauthier WJ, Holden DA, Kuntz BA, Taylor NJ, Ward DG. *Organometallics* 1991;10:2061.
- [a] Burger P, Debold J, Gutmann S, Hund HU, Brintzinger HH. *Organometallics* 1992;11:1319. [b] Röll W, Brintzinger HH, Rieger B, Zalk R. *Angew Chem Int Ed Engl* 1990;29:279.
- [a] Ewen JA. In: Scheirs J, Kaminsky W, editors. *Metallocene-Based Polyolefins*. Chichester: John Wiley and Sons Ltd.; 2000. p I/3. [b] Ewen JA, Elder MJ, Jones RL, Haspeslagh L, Atwood JL, Bott SG, Robinson K. *Makromol Chem Macromol Symp* 1991;48/49:253.
- [a] Soares JBP, McKenna TF, Cheng CP. Coordination polymerization. In: Asua JM, editor. *Polymer Reaction Engineering*. Blackwell Publishing; 2007. p 29–117. [b] Soares JBP. *Chem Eng Sci* 2001;56:4131. [c] Tomotsu N, Malanga M, Schellenberg J. *Synthesis of syndiotactic polystyrene*. In: Scheirs J, Priddy D, editors. *Modern Styrenic Polymers*. John Wiley and Sons; 2003. p 365. [d] Schellenberg J, Tomotsu N. *Prog Polym Sci* 2002;27(9):1925.
- [a] Ishihara N, Seimija T, Kuramoto M, Uoi M. *Macromolecules* 1986;19:2464. [b] Ishihara N, Kuramoto M, Uoi M. *Macromolecules* 1988;21:3356.
- [a] Chum SP, Kao CI, Knight GW. In: Scheirs J, Kaminsky W, editors. *Metallocene-Based Polyolefins*. Chichester: John Wiley and Sons Ltd.; 2000. p I/134, 261. [b] Braunschweig H, Breitling FM. *Coord Chem Rev* 2006;250(21–22):2691.
- [a] Pellecchia C, Pappalardo D, D'Arco M, Zambelli A. *Macromolecules* 1996;29:1158. [b] Lai SY, Wilson JR, Knight GW, Stevens JC, inventors; Dow Chemical Co., assignee. US patent 5, 665, 800. 1997.
- [a] Kempe R. *Chem Eur J* 2007;13:2764. [b] Yu Vasil'eva M, Fedorov SP, Nikolaev DA, Oleinik II, Ivanchev SS. *Polymer Sci B* 2010;52(7–8):443.
- [a] Kuran W. In: Kuran W, editor. *Principles of Coordination Polymerisation*. John Wiley and Sons Ltd.; 2001. p 275. [b] Burford RP. *J Macromol Sci Chem* 1982;A17(1):123.
- Scollard JD, McConville DH, Vittal JJ. *Organometallics* 1995;14:5478.
- [a] Beddie C, Wei P, Stephan DW. *Can J Chem* 2006;84:755. [b] Stephan DW, Guérin F, Spence REH, Koch L, Gao X, Brown SJ, Swabey JW, Wang Q, Xu W, Zoricak P, Harrison DG. *Organometallics* 1999;18:2046.
- [a] Kaivalchatchawal P, Suttipatkwong P, Samingprai S, Praserthdam P, Jongsomjit B. *Molecules* 2011;16:1655. [b] ChunHong W, HuaYi L, YuQi F, YouLiang HU. *Chin Sci Bull* 2008;53:3164.
- [a] Capacchione C, Proto A, Ebeling E, Mulhaupt R, Moller K, Spaniol TP, Okuda J. *J Am Chem Soc* 2003;125:4964. [b] Gibson VC, Spitzmessner SK. *Chem Rev* 2003;103:283.
- [a] Scollard JD, McConville DH, Payne NC, Vittal JJ. *Macromolecules* 1996;29:5241. [b] Liang LCH, Schrock RR, Davis WW, McConville DH. *J Am Chem Soc* 1999;121:5797. [c] Lee CHH, La Y-H, Park JW. *Organometallics* 2000;19:344.
- Mohebbi S, Rayati S. *Transit Met Chem* 2007;32:1035.
- Collins S. *Coord Chem Rev* 2011;255:118.
- [a] Britovsek GJP, Bruce M, Gibson VC, Kymberly BS, Maddox PJ, Mastrianni S, McTravish SJ, Redshaw C, Solan GA, Strömberg S, White AJP, Williams DJ. *J Am Chem Soc* 1999;121:8728. [b] Gibson VC, Redshaw C, Solan GA. *Chem Rev* 2007;107:1745.
- [a] Mitani M, Mohri J-I, Yoshida Y, Saito J, Ishii S, Tsuru K, Matsui S, Furuyama R, Nakano T, Tanaka H, Kojoh S-I, Matsugi T, Kashiwa N, Fujita T. *J Am Chem Soc* 2002;124:3327. [b] Tian J, Hustad D, Coates GW. *J Am Chem Soc* 2001;123:5134.
- Friebe PL, Nuyken O, Obrecht W. In: Nuyken O, editor. *Advances in polymer science*. Berlin, Heidelberg: Springer-Verlag; 2006. p 204.
- Hou Z, Wakatsuki Y. *Coord Chem Rev* 2002;231:1.
- Michalak A, Ziegler T. *Top Organomet Chem* 2005; 12:145.
- Guan Z, Cotts PM, McCord EF, McLain SJ. *Science* 1999;283:2059 Available at www.sciencemag.org.
- [a] Ittel SD, Johnson LK, Brookhart M. *Chem Rev* 2000;100:1169. [b] Johnson LK, Mecking S, Brookhart M. *J Am Chem Soc* 1996;118:267.

29. [a] Gibson VC, Redshaw C, Solan GA. *Chem Rev* 2007;107:1745. [b] Gibson VC. *J Chem Soc Chem Comm* 1998;849.
30. Wang C, Friedrich S, Younkin TR, Li RT, Grubbs RH, Bransleben DA, Day MW. *Organometallics* 1998;17:3149.
31. Vandenberg EJ, Repka BC. *Ziegler type polymerizations*. In: Schildknecht C, Skeits I, editors. *Polymerization Processes*. New York: Wiley (Interscience); 1975. p 337.
32. [a] Krauss HL. *Proceedings International Congress of Catalysis 5th*, 1972, 1973;1:207. [b] Thüne PC, Like R, van Gennip WJH, de Jong AM, Niemantsverdriet JW. *J Phys Chem B* 2001;105:3073.
33. [a] Pecherskaya YI, Kazanskii VB, Voevodskii VV. *Actes Congr Int Catal 2nd* 1961 paper 108. [b] Hogan JP. *J Polymer Sci A* 1970;18:2637.
34. Zheng Z-W, Shi DP, Su PL, Luo ZH, Li XJ. *Ind Eng Chem Res* 2011;50(1):322.
35. [a] Boor J. *Ziegler-Natta Catalysts and Polymerizations*. New York: Academic Press, Inc.; 1979. p 141. [b] Boor J. *Ziegler-Natta Catalysts and Polymerizations*. New York: Academic Press, Inc.; 1979. p 125.
36. Quirk RP, Kells AM. *Polym Int* 2000;49:751.
37. [a] EXXON. Jpn patent JP1-503788. 1989; [b] Montagna AA, Floyd JC. MetCon'93; 1993, May 26–28; Houston, TX. Catalyst Consultants Inc., p 171.
38. [a] Rodríguez AS, Kirillov E, Carpenter JF. *Coord Chem Rev* 2008;252:2115. [b] Knjazhanski SY, Cadenas G, García M, Pérez CM. *Organometallics* 2002;21:3094.
39. Soares JBP. *Chem Eng Sci* 2001;56:4131.
40. Cano J, Kunz K. *J Organomet Chem* 2007;692(21):4411.
41. Makio H, Terao H, Iwashita A, Fujita T. *Chem Rev* 2011;111(3):2363.
42. Klee JE, Schneider C, Holter D, Burgath A, Frey H, Mulhaupt R. *Polymers Adv Tech* 2001;12(6):346.
43. [a] Zhang Y, Ning Y, Caporaso L, Cavallo L. *J Am Chem Soc* 2010;132(8):2695. [b] Talarico G, Cavallo L. *Kinet Catal* 2006;47(2):289.
44. Kawai K, Fujita T. Topics in organometallic chemistry. In: Zhibin G, editor. *Metal Catalysts in Olefin Polymerization*. Springer; 2009. p 256.
45. Peuckert M, Keim W. *J Mol Catal* 1984;22(3):289.
46. Nakamura A, Ito S, Nozaki K. *Chem Rev* 2009;109:5215.
47. L. Johnson, A. Bennett, P. Butera, K. Dobbs, N. Drysdale, E. Hauptman, A. Ionkin, A. Ittel, E. McCord, S. McLain, C. Radzewich, A. Rinehart, RS. Schiffino, KJ. Sweetman, J. Uradnisheck, L. Wang, Y. Wang and Z. Yin, *Abstracts of Papers, 225th ACS National Meeting, New Orleans, LA, United States, March 23–27, 2003*, p. 356, POLY-Publisher: American Chemical Society.
48. Drent E, Dijk RV, Ginkel RV, Oort BV, Pugh RI. *Chem Commun* 2002:744.
49. Fink G, Steinmetz B, Zechlin J, Przybyla C, Tesche B. *Chem Rev* 2000;100:1377.
50. [a] Ribeiro MR, Deffieux A, Portela MF. *Ind Eng Chem Res* 1997;36(4):1224. [b] Y Choi, JBP Soares. *Can J Chem Eng* 2011, 10.1002/cjce.20583.
51. [a] Arlman EJ. *J Catal* 1964;3:89. [b] Arlman EJ, Cossee P. *J Catal* 1964;3:99.
52. Ray WH. Berlin Busengesellschaft fuer Physikalische Chemie 1986;90:947.
53. Soares JBP, McKenna TF, Cheng CP. Coordination polymerization. In: Asua JM, editor. *Polymer Reaction Engineering*. Oxford: Blackwell Publishing; 2007. p 29.
54. Soares JBP, Simon LC. Coordination polymerization. In: Meyer T, Keurentjes J, editors. *Handbook of Polymer Reaction Engineering*. Weinheim: Wiley-VCH; 2005. p 365.
55. Soares JBP. *Macromol Mater Eng* 2004;289:70.
56. Hamielec AE, MacGregor JF, Penlidis A. *Makromol Chem Macromol Symp* 1987;10/11:521.
57. Hamielec AE, MacGregor JF, Penlidis A. Copolymerization. In: Allan SG, editor. *Comprehensive Polymer Science*. Oxford: Pergamon Press; 1989. p 17.
58. Xie T, Hamielec AE. *Makromol Chem Theory Simul* 1993;2:421.
59. Xie T, Hamielec AE. *Makromol Chem Theory Simul* 1993;2:455.
60. Kissin YV. *J Mol Catal* 1989;56:220.
61. Kissin YV, Mink RI, Nowlin TE, Brandolini AJ. *Top Catal* 1999;7:69.
62. Resconi L, Cavallo L, Fait A, Piemontesi F. *Chem Rev* 2000;100:1253.
63. Garoff T, Johansson S, Pesonen K, Waldvogel P, Lindgren D. *Eur Polymer J* 2002:121.
64. Kissin YV, Rishina LA, Polym J. *J Polymer Sci Chem A* 2002;40:1353.
65. Kissin YV, Rishina LA, Polym J. *J Polymer Sci Chem A* 2002;40:1899.
66. Yestenes M. *J Catal* 1991;129:383.
67. Wester TS, Yestenes M. *Macromol Chem Phys* 1997;198:1623.
68. Shaffer WKA, Ray WH. *J Appl Polym Sci* 1997;65:1053.
69. Ray WH. *J Macromol Sci Rev Macromol Chem* 1972;C8:1.
70. Canu P, Ray WH. *Comput Chem Eng* 1991;15:549.
71. Wulkov M. *Macromol Theory Simul* 1996;5:393.
72. Wulkov M. *Macromol React Eng* 2008;2:494.
73. Soares JBP, Hamielec AE. *Macromol React Eng* 2007;1:53.
74. Soares JBP, Hamielec AE. *Macromol React Eng* 2008;2:115.
75. Keii T, Terano M, Kimura K, Ishii K. *Makromol Chem Rapid Commun* 1987;8:853.
76. Liu B, Matsuoka H, Terano M. *Macromol Rapid Commun* 2001;22:1.
77. Mori H, Terano M. *Trends Polymer Sci* 1977;5:314.
78. Di Martino A, Broyer JP, Spitz R, Weickert G, McKenna TF. *Macromol Rapid Commun* 2005;26:215.
79. Schulz GV. *Z Physik Chem* 1935;B30:379.

80. Flory PJ. J Am Chem Soc 1877;1936:58.
81. Flory PJ. J Am Chem Soc 1937;59:241.
82. Stockmayer WH. J Chem Phys 1945;13:199.
83. Mayo FR, Lewis FM. J Am Chem Soc 1944;66:1594.
84. Randal JC. *Polymer sequence determination*. In: *Carbon-13 NMR Method*. New York: Academic Press; 1977.
85. Bovey FA, Mirau PA. *NMR of Polymers*. San Diego: Academic Press; 1996.
86. Soares JBP. Macromol Symp 2007;257:1.
87. de Carvalho AB, Gloor PE, Hamielec AE. Polymer 1989;30:280.
88. Rincon-Rubio LM, Wilen CE, Lindfords LE. Eur Polymer J 1990;26:171.
89. Soares JBP, Hamielec AE. Macromol Theory Simul 1996;5:547.
90. Soares JBP, Hamielec AE. Macromol Theory Simul 1997;6:591.
91. Beigzadeh D, Soares JBP, Penlidis A. Polym React Eng 1999;7:195.
92. Simon LC, Soares JBP, de Souza RF. AICHE J 2000;45:1234.
93. Simon LC, Soares JBP, de Souza RF. Chem Eng Sci 2001;56:4181.
94. Simon LC, Soares JBP. Macromol Theory Simul 2002; 11:184.
95. Simon LC, Soares JBP. Ind Eng Chem Res 2005;44:2461.
96. Haag MC, Simon LC, Soares JBP. Macromol Theory Simul 2003;12:142.
97. Gillespie DT. J Phys Chem 1977;81:2340.
98. Soares JBP, Nguyen T. Macromol Symp 2007;260:189.
99. Galvan R, Tirrell M. Chem Eng Sci 1986;41:2385.
100. McAuley KB, MacGregor JF, Hamielec AE. AICHE J 1990;36:837.
101. Soares JBP, Hamielec AE. Polym React Eng 1996;3:261.
102. Soares JBP, Hamielec AE. Macromol Theory Simul 1995;4:305.
103. Vickroy VV, Schneider H, Abbott RF. J Appl Polym Sci 1993;50:551.
104. Soares JBP, Hamielec AE. Polymer 1995;36:2257.
105. Kissin YV, Rishina LA, Vizen EI. J Polymer Sci A: Polymer Chem 2002;40:1899.
106. Kissin YV, Mirabella FM, Neverden CC. J Polym Sci A: Polymer Chem 2005;43:4351.
107. da Silva Filho AA, de Galand GB, Soares JBP. Macromol Chem Phys 2000;201:1226.
108. Sarzotti DM, Soares JBP, Penlidis A. J Polymer Sci, Part B: Polymer Phys 2002;40:2595.
109. Alghyamah AA, Soares JBP. Macromol Rapid Commun 2009;30:384.
110. Soares JBP, Abbott RF, Willis JN, Liu X. Macromol Chem Phys 1996;197:3383.
111. Faldi A, Soares JBP. Polymer 2001;42:3057.
112. Soares JBP. Polym React Eng 1998;6:225.
113. Smith JM. *Chemical Engineering Kinetics*. New York: McGraw-Hill; 1981.
114. McKenna TF, Soares JBP. Chem Eng Sci 2001;56:3931.
115. Crabtree JR, Grimsby FN, Nummelin AJ, Sketchley JM. J Appl Polym Sci 1973;17:959.
116. Nagel EJ, Kirilov VA, Ray WH. Ind Eng Chem Prod Res Dev 1980;19:372.
117. Taylor TW, Choi KY, Yuan H, Ray WH. Physicochemical kinetics of liquid phase propylene polymerization. In: Quirk RP, editor. *Transition Metal Catalyzed Polymerization*. MMI Symposium Series 11. Volume 4. 1981. p 191.
118. Floyd S, Choi KY, Taylor TW, Ray WH. J Appl Polym Sci 1986;32:2935.
119. Floyd S, Choi KY, Taylor TW, Ray WH. J Appl Polym Sci 1986;31:2231.
120. Floyd S, Hutchinson RA, Ray WH. J Appl Polym Sci 1986;32:5451.
121. Hutchinson RA, Chen CM, Ray WH. J Appl Polym Sci 1992;44:1389.
122. Hutchinson RA, Ray WH. J Appl Polym Sci 1987;34:657.
123. Hutchinson RA, Ray WH. J Appl Polym Sci 1990;41:51.
124. Hutchinson RA, Ray WH. J Appl Polym Sci 1991;43:1271.
125. Hutchinson RA, Ray WH. J Appl Polym Sci 1991;43: 1387.
126. Deblng JA, Ray WH. Ind Eng Chem Res 1995;34:3466.
127. Schmeal WR, Street JR. AICHE J 1971;17:1189.
128. Schmeal WR, Street JR. J Polymer Sci Polymer Phys 1972;10:2173.
129. Singh D, Merril RP. Macromolecules 1971;4:599.
130. McKenna TFL, Di Martino A, Weickert G, Soares JBP. Macromol React Eng 2010;4:40.
131. Soares JBP, Hamielec AE. Polym React Eng 1995;3:261.
132. Ferrero MA, Chiovetta MG. Polym Eng Sci 1987;27:1436.
133. Ferrero MA, Chiovetta MG. Polym Eng Sci 1987;27:1448.
134. Ferrero MA, Chiovetta MG. Polym Eng Sci 1991;31:886.
135. Ferrero MA, Chiovetta MG. Polym Eng Sci 1991;31:904.
136. Estenoz DA, Chiovetta MG. Polym Eng Sci 1996;36: 2208.
137. Estenoz DA, Chiovetta MG. Polym Eng Sci 1996;36: 2229.
138. Estenoz DA, Chiovetta MG. J Appl Polym Sci 2001; 81:285.
139. Chiovetta MG, Estenoz DA. Macromol Mater Eng 2004;289:1012.
140. Merquior DM, Lima EL, Pinto JC. Polym React Eng 2003;11:133.
141. Merquior DM, Lima EL, Pinto JC. Macromol Mater Eng 2005;290:511.
142. Grof Z, Kosek J, Marek M, Adler PM. AICHE J 2003;49:1002.
143. Kittilsen P, Svendsen HF, McKenna TF. AICHE J 2003;49:1495.

104 COORDINATION POLYMERIZATION

144. Di Martino A, Weickert G, Sidoroff F, McKenna TFL. *Macromol React Eng* 2007;1:338.
145. Noristi L, Marchetti E, Barruzzi G, Sgarzi P. *J Polymer Sci A: Polymer Chem* 1994;32:3047.
146. Grof Z, Kosek J, Marek M. *AICHE J* 2008;54:51.
147. Grof Z, Kosek J, Marek M. *Ind Eng Chem Res* 2005;44:2389.
148. Horackova B, Grof Z, Kosek J. *Chem Eng Sci* 2007;62: 5264.
149. Soares JBP, Hamielec AE. *Polym React Eng* 1996;4:153.
150. Soares JBP, Hamielec AE. *Macromol Theory Simul* 1995;4:1085.
151. Zacca JJ, Deblng JA, Ray WH. *Chem Eng Sci* 1996;51:4859.
152. Zacca JJ, Deblng JA, Ray WH. *Chem Eng Sci* 1994;51:1941.
153. Zacca JJ, Ray WH. *Chem Eng Sci* 1993;48:3743.
154. Deblng JA, Han GC, Kuipers F, VerBurg J, Zacca JJ, Ray WH. *AICHE J* 1994;40:506.
155. Deblng JA, Zacca JJ, Ray WH. *Chem Eng Sci* 1969;1997:52.
156. Hatzantonis H, Yiannoulakis H, Yiagopoulos A, Kiparissidis C. *Chem Eng Sci* 2000;55:3237.
157. Kim JY, Choi KY. *Chem Eng Sci* 2001;56:4069.

6

COPOLYMERIZATION

MARC A. DUBÉ, ENRIQUE SALDÍVAR-GUERRA, AND IVÁN ZAPATA-GONZÁLEZ

6.1 INTRODUCTION

6.1.1 What Are Copolymers?

It often occurs that it is desirable to modify the properties of a homopolymer to achieve certain application-specific characteristics that are perhaps not possible by solely manipulating the polymer molecular weight or by chemical modification of the final product. Perhaps one is interested in achieving properties that are intermediate to two homopolymers. Properties of interest could include crystallinity, flexibility, tensile strength, melting point, glass-transition temperature, and many others.

One option would be to blend one homopolymer with another. This would result in a physical mixture prepared via mechanical means such as screw compounding and extrusion. Polymer blending is not straightforward as there is a tendency toward phase separation owing to the inherent incompatibility between most polymers. Thus, one can introduce specific interactive functionalities on the homopolymer pairs (e.g., hydrogen bondings, acid–base interactions, and ion–dipole interactions) and use processing aids and compatibilizing compounds such as ionomers to maintain a uniform blend. There are estimates that 36% of worldwide polymer consumption is accounted for by polymer blends [1].

An alternative to physical blending is the polymerization of two or more monomers referred to as *copolymerization*. When more than two monomers are used, the product is referred to as a *multicomponent copolymer*, and in the special case of three monomers, the term *terpolymer* is used. Of course, adding more than one monomer type to the reaction mixture results in added complexity in the kinetic reaction mechanisms. This complexity arises

due to the relative rates of polymerization that depend on the structure of each monomer as well as that of the radicals. This affects the polymer composition (relative amounts of each monomer unit incorporated into the copolymer chain), the monomer sequence distribution (the arrangement of the comonomers in the polymer chain backbone), and the polymer molecular weight. Despite this added complexity, a broad range of application properties that are simply not possible via homopolymerization can be achieved.

6.1.2 Commercial Copolymer Examples

Copolymerization products are widespread. Several important commercial examples are presented below: [2, 3]

Ethylene-Vinyl Acetate (EVA). The addition of vinyl acetate to ethylene imparts flexibility, impact and stress crack resistance, optical clarity, and melt adhesive properties. EVA copolymers are used extensively as hot-melt adhesives, in biomedical applications as drug delivery devices, and as a foam in a broad range of sports equipment.

Ethylene-Acrylic Acid (EAA). The addition of acrylic acid (15–20%) to ethylene results in a copolymer with an ionic nature, which offers improved adhesive properties. It is used in applications similar to that of EVA and primarily as a hot-melt adhesive.

Styrene-Butadiene Rubber (SBR). The homopolymer of styrene is relatively brittle and has a low resistance to impact and solvents. The addition of butadiene significantly increases the abrasion resistance resulting in a copolymer that is most widely used as tire

rubber. Other applications include automotive belts and gaskets, flooring, shoe heels and soles, electrical insulation, and chewing gum.

Styrene-Acrylonitrile (SAN). The addition of acrylonitrile to styrene improves the polymer's resistance to oils and grease, stress cracking, and crazing, leading to a transparent copolymer with high impact strength. SAN copolymers find application in a broad range of household items including packaging, furniture, and electronics.

Acrylonitrile-Butadiene-Styrene (ABS) Terpolymer. The acrylonitrile and styrene copolymer is grafted onto polybutadiene. The properties of SAN are combined with a greatly improved impact resistance and heat distortion resistance. ABS terpolymers find application as engineering plastics, in household appliances, luggage, telephone housings, automotive parts, and many more.

Butadiene-Acrylonitrile (Nitrile Rubber (NBR)). Acrylonitrile imparts resistance to hydrocarbon oil and gasoline. NBR finds use as an adhesive (low molecular weight), in nonlatex gloves for the health-care industry, and in automotive parts such as fuel tanks, O-rings, gaskets, belts, and hoses. NBR is also commonly blended with other polymers.

Vinylidene Chloride-Vinyl Chloride (VDC/VCM). VDC/VCM copolymers are tough, flexible, and durable. As a film, they find significant use in the food packaging industry. They are also manufactured as a fiber used in car upholstery and garden furniture fabrics.

Ethylene-Propylene-Diene-Monomer (EPDM) Rubber. The main properties of EPDM are its outstanding heat, ozone and weather resistance, as well as its electrical insulating properties. EPDM rubber finds use in vehicles (weather seals in windows and trunks, cooling system hoses), in safety equipment (seals in respirators), roofing (waterproofing of roofs), and playground surfacing.

6.1.3 Step-Growth Copolymerization

As a last point, let us consider how copolymerization relates to the polymer growth mechanism. First, most step-growth polymerizations (e.g., the production of nylon 6/6 by the reaction of hexamethylene diamine with adipic acid) use two monomers to produce the final polymer. One can say that these are inherently copolymerizations. Considering

the copolymer composition in a step-growth polymerization, we expect to achieve a final composition more or less identical to the monomer feed composition. This is due to the one-to-one ratio of functional groups required for step growth as well as the need to achieve nearly 100% conversion to yield high molecular weight polymer. The focus of this chapter is primarily on chain growth copolymerization. In certain cases (e.g., copolymer microstructure, composition measurement methods), applicability of the topic to step-growth copolymerization should be obvious.

6.2 TYPES OF COPOLYMERS

Copolymers composed of two monomers can be classified according to the relative arrangement of the two types of monomer units along the chain or, in other words, according to the monomer distribution. For linear chains, one can have four types of copolymers: statistical/random, alternating, block, and gradient.

6.2.1 Statistical Copolymers

Statistical copolymers are those in which the monomer sequence follows a specific statistical law (e.g., Markovian statistics of order zero, one, two). Random copolymers are a special case of statistical copolymers in which the nature of a monomeric unit is independent of the nature of the adjacent unit (Bernoullian or zero-order Markovian statistics). They exhibit the structure shown in Figure 6.1. If A and B are the two monomers forming the copolymer, the nomenclature is poly (A-stat-B) for statistical copolymers and poly (A-ran-B) for the random case. It should be noted that sometimes the terms random and statistical are used indistinctly. The commercial examples of these copolymers include SAN: poly (styrene-ran-acrylonitrile) [4] and poly (styrene-ran-methyl methacrylate) (MMA) [5].

6.2.2 Alternating Copolymers

Alternating copolymers contain the two monomers in equimolar composition following a regularly alternating pattern (Fig. 6.2). The nomenclature for this type of structure is poly (A-alt-B). A commercial example of this type of copolymers is poly (styrene-alt-maleic anhydride).

Random and alternating copolymers have been usually synthesized by traditional techniques (free radical, anionic, and cationic); however, in the past two decades, many copolymers have been synthesized using the relatively new



Figure 6.1 Schematic representation of a random copolymer.



Figure 6.2 Schematic representation of an alternating copolymer.

controlled/living radical polymerization (or CRP for short; see Chapter 4 for a discussion of this topic), which has expanded the ability of polymer chemists to synthesize macromolecules with defined microstructural characteristics. The most popular CRP techniques are as follows: stable radical polymerization or nitroxide-mediated polymerization (NMP), atom transfer radical polymerization (ATRP), and reversible addition fragmentation transfer (RAFT) polymerization. Random copolymerizations have recently been reported by using NMP [6], ATRP [7], and RAFT [8]. Alternating copolymers have also been obtained by NMP [9], ATRP [10], and RAFT [11].

6.2.3 Block Copolymers

Block copolymers contain long sequences of each of the monomer types [12, 13]. At least one long sequence of each of the monomers must be present, but in the so-called multiblock copolymers [14, 15], several long alternating sequences can be present. The recommended nomenclature for these copolymers is poly A-*block*-poly B, although sometimes they are named as poly (A-*block*-B) or simply poly (A-*b*-B) [16]. Figure 6.3 shows an illustration of a multiblock copolymer. Commercial examples of these copolymers include several products prepared by anionic polymerization [12]: diblock polystyrene-*block*-polybutadiene (SB) rubbers and triblock poly (styrene-*b*-butadiene-*b*-styrene). Another interesting family of triblock copolymers has the structure polyethylene oxide-*block*-poly propylene oxide-*block*-polyethylene oxide; they find many applications as surfactants, as well as in pharmacy and drug delivery [17]. Since the synthesis of block copolymers usually requires living processes (with reduced or null termination reactions), CRP techniques such as NMP [18], ATRP [19], and RAFT [20] have also been used to this end.

6.2.4 Gradient Copolymers

Gradient copolymers are those in which an initial portion of the chain is rich in one monomer and poor in the other, and the concentration of this monomer gradually

decreases along the chain length, while the concentration of the second monomer gradually increases, as shown in Figure 6.4. There is no recommended nomenclature for this type of structure. Because of the control required in the synthesis of gradient copolymers, NMP [21], ATRP [22], and RAFT [23] have been successfully used recently to build these structures.

6.2.5 Graft Copolymers

Branched chains formed of a main chain of homopolymer of one monomer type and one or several branches of homopolymer of a second monomer type are called *graft copolymers*; they are illustrated in Figure 6.5. The nomenclature for these copolymers is polyA-*graft*-polyB [24]. They are sometimes referred to as poly(A-*graft*-B). Chapter 10 reviews the topic of graft copolymers, and the reader is also referred to the review by Hadjichristidis [25] for example. CRP has also been used to synthesize this kind of polymer via NMP [26], ATRP [27], and RAFT [28].

6.2.6 Notes on Nomenclature

For linear copolymers in which the sequence distribution is not specified, the recommended notation is poly (A-*co*-B).

The general naming rules given above define the source-based nomenclature recommended by IUPAC [29]. There is another more detailed structure-based nomenclature that can be used when the exact copolymer structure is known, but this is rarely used, mainly because of the difficulty of experimentally determining the exact structure of a synthesized copolymer.

6.3 COPOLYMER COMPOSITION AND MICROSTRUCTURE

6.3.1 Terminal Model Kinetics

The following discussion is valid for chain copolymerization, regardless of the type of mechanism (radical, anionic, or cationic). The prediction of the copolymerization rate for



Figure 6.3 Schematic representation of a block copolymer.



Figure 6.4 Schematic representation of a gradient copolymer.

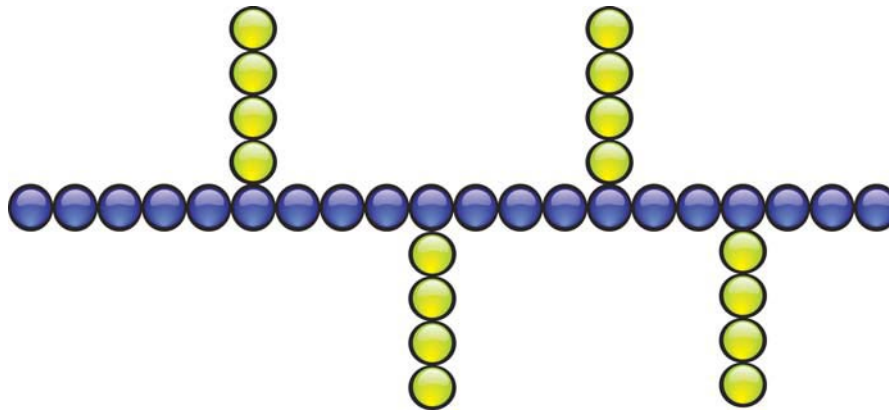
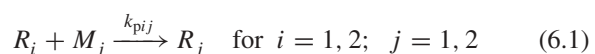


Figure 6.5 Schematic representation of a graft copolymer.

a given system is still an open question in polymer science. In general, it is very difficult to predict the rate of copolymerization of two monomers based on the knowledge of the individual homopolymerization rates of the monomers. However, for most copolymerization systems, it is possible to determine and model the copolymer composition using the so-called terminal model. This model, originally proposed by Mayo and Lewis in 1944 [30], postulates that the chemical reactivity of a propagating chain depends only on the chemical nature of the active monomer unit at the chain end. According to the terminal model, if R_i is a growing chain ending in monomer i (or type i propagating chain), and k_{pij} is the rate constant for the propagation of monomer j with a type i propagating chain, there are four possible propagation reactions in a copolymerization system:



From the mass balance for each monomer type, assuming that long chains are formed (long chain hypothesis or LCH), the monomers are mainly consumed in propagation reactions:

$$\frac{d[M_1]}{dt} = -k_{p11}[R_1][M_1] - k_{p21}[R_2][M_1] \quad (6.2)$$

$$\frac{d[M_2]}{dt} = -k_{p12}[R_1][M_2] - k_{p22}[R_2][M_2] \quad (6.3)$$

From Equations 6.2 and 6.3 and by using the chain rule, it is possible to write the following differential equation:

$$\frac{d[M_1]}{d[M_2]} = \frac{k_{p11}[R_1][M_1] + k_{p21}[R_2][M_1]}{k_{p12}[R_1][M_2] + k_{p22}[R_2][M_2]} \quad (6.4)$$

To eliminate the concentrations of the propagating radicals from Equation 6.4, the quasi-steady-state assumption

(QSSA) for propagating chains can be used. By virtue of this, the rate of conversion of a type 1 propagating chain into one of type 2 is exactly the same as the rate of conversion of a type 2 propagating chain into one of type 1. This implicitly assumes that the rates of chain type interconversion are much faster than the rates of formation or termination of a chain or, in other words, that the reaction environment (in particular, the relative concentration of the two monomers) does not change significantly during the growth of a chain. Mathematically, this results in

$$k_{p12}[R_1][M_2] = k_{p21}[R_2][M_1] \quad (6.5)$$

or

$$[R_1] = \frac{k_{p21}[R_2][M_1]}{k_{p12}[M_2]} \quad (6.6)$$

Replacement of the concentration of Equation 6.6 in Equation 6.4, followed by division of the resulting numerator and denominator by $k_{p21}[R_2][M_1]$, rearrangement, and writing of the result in terms of the parameters r_1 and r_2 defined by Equation 6.8 result in

$$\frac{d[M_1]}{d[M_2]} = \frac{[M_1]}{[M_2]} \left(\frac{r_1[M_1] + [M_2]}{[M_1] + r_2[M_2]} \right) \quad (6.7)$$

where

$$r_1 = \frac{k_{p11}}{k_{p12}} \quad r_2 = \frac{k_{p22}}{k_{p21}} \quad (6.8)$$

The parameters r_1 and r_2 are known as the *reactivity ratios of monomers 1 and 2*, respectively. They represent the tendency of a given propagating chain type toward homopropagation divided by the tendency toward cross-propagation with the other monomer. There are extensive literature reports of values of reactivity ratios for many copolymerization systems. Table 6.1 lists some illustrative values, but extended lists have been compiled and published

TABLE 6.1 Reactivity Ratios

$M_B \backslash M_A$	Acrylic acid	Acrylonitrile	Butadiene	Ethylene	Styrene	Maleic anhydride	Methacrylic acid	Methyl methacrylate	Methyl acrylate	Butyl acrylate	Vinyl acetate
Acrylic acid					0.35 0.22 [33]			1.22 0.83 [34]			2.39 0.03 [35]
Acrylonitrile			0.03 0.20 [36]	7.00 0.00 [37]	0.55 0.22 [38]	6.0 0.0 [39]	0.26 3.44 [40]	0.14 0.19 [41]	1.27 0.87 [42]	1.08 0.83 [42]	9.32 10^{-4} [43]
Butadiene		0.20 0.03 [36]			1.55 0.37 [44]			0.70 0.32 [45]	1.09 0.07 [46]	1.04 0.07 [46]	
Ethylene		0.00 7.00 [37]			0.05 14.88 [47]	0.04 0.0 [48]		0.02 19.40 [49]	0.01 13.94 [50]	0.79 1.40 [51]	
Styrene	0.22 0.35 [33]	0.22 0.55 [38]	0.37 1.55 [44]	14.88 0.05 [47]		0.04 0.02 [52]	0.14 0.67 [53]	0.43 0.49 [54]	0.72 0.17 [55]	0.354 0.119 [56]	48.0 0.05 [57]
Maleic anhydride		0.0 6.0 [39]		0.0 0.04 [48]	0.02 0.04 [52]			0.01 3.4 [58]	0.012 2.79 [59]		0.06 0.019 [59]
Methacrylic acid		3.44 0.26 [40]			0.67 0.14 [53]			0.63 0.32 [60]		1.25 0.31 [61]	0.20 0.01 [62]
Methyl methacrylate	0.83 1.22 [34]	0.19 0.14 [41]	0.32 0.70 [45]		0.49 0.43 [54]	3.4 0.01 [58]	0.32 0.63 [60]	28.6 0.04 [63]	1.79 0.29 [64]	24.02 0.026 [64]	
Methyl acrylate		0.87 1.27 [42]	0.07 1.09 [46]	19.40 0.02 [49]	0.17 0.72 [55]	2.79 0.012 [59]		0.04 28.6 [63]		6.38 0.03 [66]	
Butyl acrylate		0.83 1.08 [42]	0.07 1.04 [46]	13.94 0.01 [50]	0.119 0.354 [56]		0.31 1.25 [61]	0.29 1.79 [64]		5.94 0.026 [64]	r_{AB} (Reference)
Vinyl acetate	0.03 2.39 [35]	10^{-4} 9.32 [43]		1.40 0.79 [51]	0.05 48.0 [57]	0.019 −0.06 [59]	0.01 0.20 [62]	0.026 24.02 [64]	0.03 6.38 [66]	0.026 5.94 [64]	r_{BA}

[31, 32]. Equation 6.7 is known as the *copolymerization* or the *Mayo–Lewis equation*. The physical meaning of Equation 6.7 is better appreciated by writing it in terms of mole fractions. If f_i is the mole fraction of unreacted monomer i and F_i is the mole fraction of monomer i in the copolymer formed instantaneously, then

$$f_1 = \frac{[M_1]}{[M_1] + [M_2]}; f_2 = 1 - f_1 \quad (6.9)$$

and

$$F_1 = \frac{\frac{d[M_1]}{dt}}{\frac{d[M_1]}{dt} + \frac{d[M_2]}{dt}}; F_2 = 1 - F_1 \quad (6.10)$$

Note that Equation 6.10 defines a molar fraction in the copolymer formed at a given instant, that is, an

instantaneous molar fraction. If the composition in the feed changes during the course of the copolymerization (as in a batch reactor), it is necessary to integrate the quantity in Equation 6.10 with respect to time or conversion to calculate a cumulative F_i .

By using the definitions of Equations 6.9 and 6.10 in combination with Equation 6.7 and the chain rule, Equation 6.7 can be written as

$$F_1 = \frac{r_1 f_1^2 + f_1 f_2}{r_1 f_1^2 + 2f_1 f_2 + r_2 f_2^2} \quad (6.11)$$

Equation 6.11 is another form of the copolymerization equation and in this form it directly provides the instantaneous composition of a copolymer formed when the composition of the feed is given by f_1, f_2 .

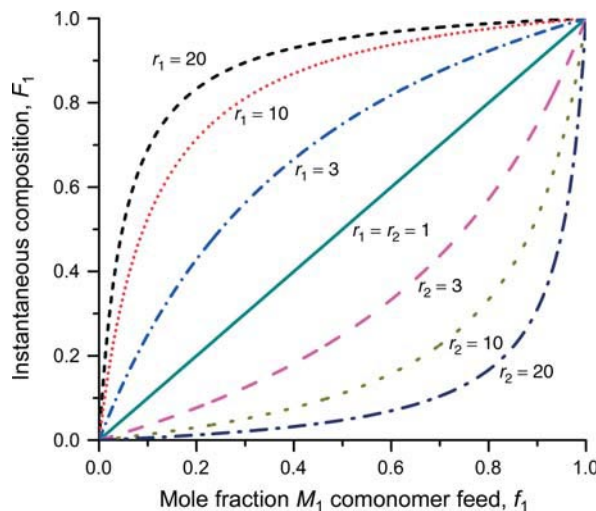


Figure 6.6 Dependence of instantaneous copolymer composition F_1 on initial comonomer feed composition f_1 in an ideal copolymer. The reactivity ratios satisfy $r_1 r_2 = 1$. (See insert for the color representation of the figure.)

In the derivation of the copolymerization equation use has been made of the QSSA; however, this is not a necessary but a sufficient condition for its derivation. It is possible to derive the equation based on statistical arguments [67], without resorting to the QSSA, but using instead the “chain continuity” condition as defined by Farina [68]. A possible physical interpretation of this condition is that the environment surrounding the chain during its formation (in particular, the monomer composition) should not change significantly, while the chain grows sufficiently to reach a statistical average composition. From a system dynamics point of view, this condition is a consequence of the dynamic decoupling (widely different time constants) of the phenomena defining the chain composition and the phenomena defining the rate of change of “slow” variables (global kinetics, unreacted monomer composition) [69].

6.3.1.1 Copolymer Composition Behavior Depending on the relative values of the reactivity ratios, copolymerization systems show different composition behavior. It is instructive to analyze some model behaviors.

Ideal Copolymerization This is defined by the condition $r_1 r_2 = 1$ and corresponds to systems in which both types of propagating chains show the same relative preference for propagation with one or the other of the monomers, since in this case

$$\frac{k_{p11}}{k_{p12}} = \frac{k_{p21}}{k_{p22}} \quad (6.12)$$

By using the mathematical condition that defines the ideal copolymerization, the two forms of the copolymer equation, Equations 6.7 and 6.11, adopt simplified forms given by Equations 6.13 and 6.14, respectively:

$$\frac{d[M_1]}{d[M_2]} = r_1 \frac{[M_1]}{[M_2]} \quad (6.13)$$

$$F_1 = \frac{r_1 f_1}{r_1 f_1 + f_2} \quad (6.14)$$

The term *ideal* for this copolymerization was adopted by Wall [70] due to the similitude that plots of Equation 6.14 for this kind of systems have with plots of vapor–liquid equilibrium for ideal binary solutions, but it has no other implication. Figure 6.6 shows a plot of Equation 6.14 for different values of the reactivity ratio r_1 . Note that when one of the two ratios is much larger than the other, the copolymer composition of the monomer with the larger ratio will be much higher than the composition of that monomer in the feed. In a batch reaction, this would lead to a fast depletion of that monomer and therefore to a significant drift of composition with the progress of the reaction conversion. This is illustrated in Figure 6.7 and, in particular, in Figure 6.7b for a system in which $r_1 = 28.6$ and the initial monomer feed is $f_1 = 0.2$. Procedures to deal with this problem are discussed in Section 6.4.5.

Alternating Copolymerization This is defined by the condition $r_1 = r_2 = 0$, which indicates that in these systems, cross-propagation is favored over homopropagation. This is clear, since in this case

$$\frac{k_{p11}}{k_{p12}} = \frac{k_{p22}}{k_{p21}} = 0 \quad (6.15)$$

The copolymerization equation in these systems adopts the simple forms

$$\frac{d[M_1]}{d[M_2]} = 1 \quad (6.16)$$

$$F_1 = 0.5 \quad (6.17)$$

This indicates that for any feed composition, the copolymer formed will have an equimolar regularly alternating composition. The chemistry behind these systems has been extensively discussed in the literature, and the charge-transfer complex concept was for a long time the prevailing theory to explain this behavior [73–75]. More recently, Hall and Padias [76, 77] have proposed an alternate explanation based on polar effects when an electron-donor and an electron-acceptor monomer interact. This last theory has the additional virtue of explaining the fact that many

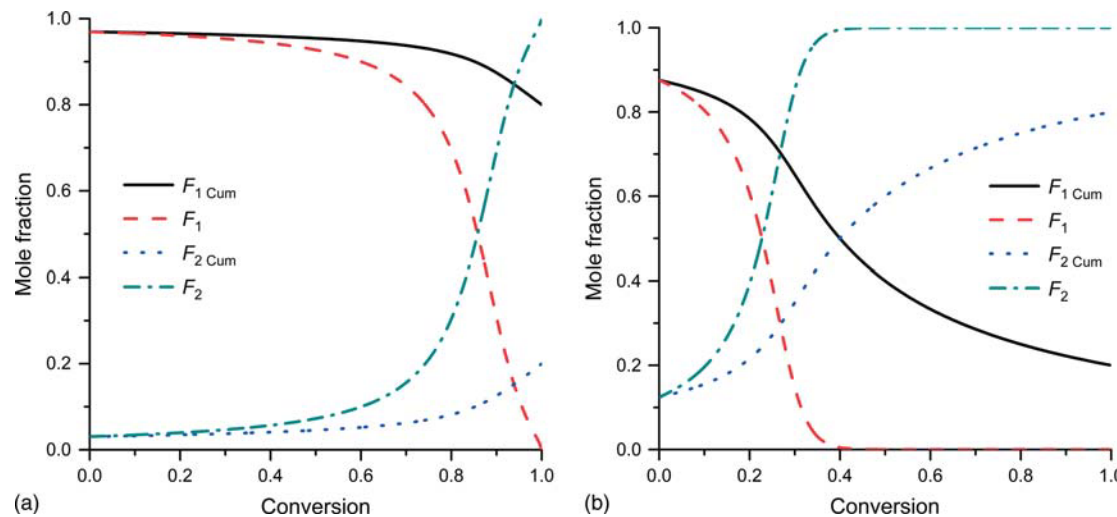


Figure 6.7 Variations in both cumulative ($F_{1 \text{ Cum}}$) and instantaneous (F_1) copolymer compositions with conversion for: (a) acrylamide (M_1)–styrene (M_2) system, $f_{1,0} = 0.8$, $f_{2,0} = 0.2$, $r_1 = 8.97$, $r_2 = 0.65$ [71]; (b) MMA (M_1)–vinyl acetate (M_2) system, $f_{1,0} = 0.2$, $f_{2,0} = 0.8$, $r_1 = 28.6$, $r_2 = 0.04$ [72].

systems that behave as alternating copolymerizations also show spontaneous initiation [78].

Some copolymerization systems are not strictly alternating, but still they show a tendency toward alternation. This occurs when both r_1 and $r_2 < 1$. The alternating trend increases as the reactivity ratios approach zero. An interesting feature of these systems is that they present the so-called azeotropic composition, at which $F_1 = f_1$. At this composition, the copolymer formed has the same composition as the monomers in the feed and, therefore, systems copolymerizing at this condition do not show compositional drift. It can be shown that a necessary condition that the reactivity ratios have to satisfy in order for a copolymerization system to show an azeotropic point is that either both r_1 and $r_2 < 1$ or both r_1 and $r_2 > 1$.

To obtain an equation for calculating the azeotropic composition, one can start by using the equivalent azeotropic condition $\frac{d[M_1]}{d[M_2]} = \frac{[M_1]}{[M_2]}$ in Equation 6.7, then writing the result in terms of mole fractions, as in the derivation of Equation 6.11, and finally solving for f_1 . The result is

$$f_1 = \frac{(1 - r_2)}{(2 - r_1 - r_2)} \quad (6.18)$$

Figure 6.8 shows several plots of Equation 6.11 for different values of r_1 at a fixed value of $r_2 = 0.1$. As the value of r_1 increases from 0.1 to 20, the behavior of the system changes from that of a nearly alternating copolymerization system to an ideal one (and even beyond when, e.g., $r_1 = 20$). Note that all the curves corresponding to values of $r_2 < 1$ cross the line of $F_1 = f_1$ at their azeotropic compositions. Figure 6.9 shows the change of

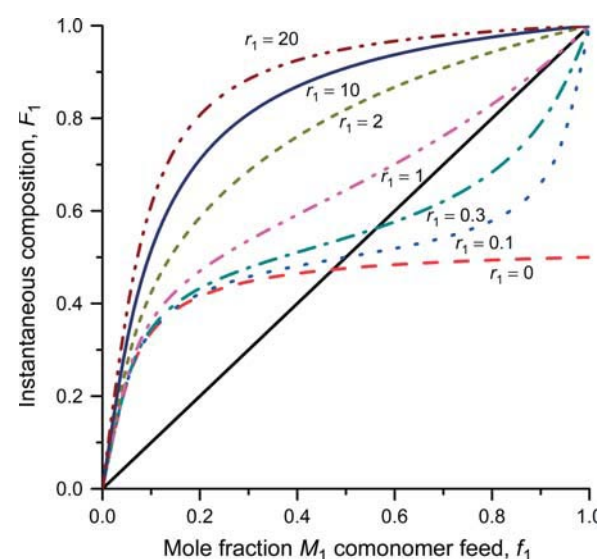


Figure 6.8 Dependence of instantaneous copolymer composition F_1 on initial comonomer feed composition f_1 for different values of r_1 ; $r_2 = 0.1$. (See insert for the color representation of the figure.)

composition with conversion for two different systems in which the composition drift is relatively small. One of them belongs to a system approaching ideal behavior, but in which both reactivity ratios are near 1. This is typical of copolymerizations involving two monomers of the same chemical family (MMA and benzyl methacrylate (BzMA) in this example). The other case is a system exhibiting an azeotropic point that is initially fed with a monomer composition near that point (styrene, St, and MMA).

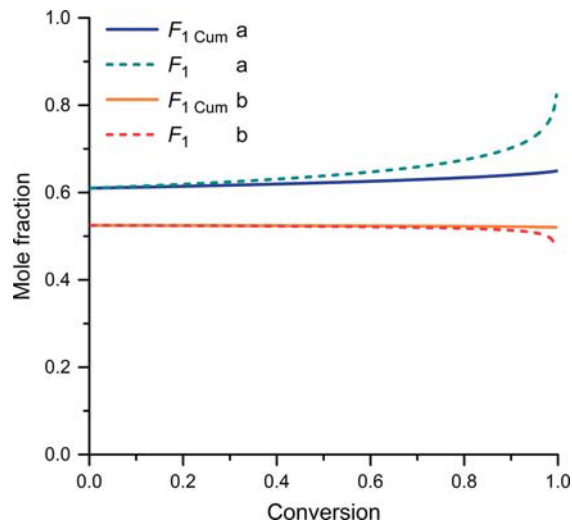


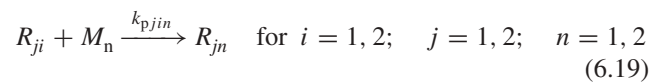
Figure 6.9 Variations in both cumulative ($F_1 \text{ Cum}$) and instantaneous (F_1) copolymer compositions with conversion for two systems. The initial conditions are as follows: (a) MMA (M_1)–BzMA (M_2) system with $f_{1,0} = 0.65, f_{2,0} = 0.35, r_1 = 0.808, r_2 = 1.112$ [79]; (b) St (M_1), MMA (M_2) system with $f_{1,0} = 0.52, f_{2,0} = 0.48, r_1 = 0.52, r_2 = 0.45$ [80].

6.3.2 Other Copolymerization Models

Although the terminal model is very useful for the correlation of composition data in copolymerization, its predictions deviate from the real behavior for systems that do not satisfy all the assumptions on which it is based. For those systems meeting all the assumptions, the terminal model can predict both the composition and the copolymerization rate. On the other hand, copolymerization systems that are not adequately described by the terminal model can be classified in two categories. In one category, the terminal model explains well the behavior of composition, but it is incapable of adequately predicting the rate of copolymerization; an example of this is the copolymerization of styrene with MMA [81]. Why is this so? The apparent reason for this is the dynamic decoupling of the phenomena determining the chain composition (linked to the rate of exchange of growing chain types) and the polymerization rate (linked to the total population of growing chains). Note that the copolymerization equation, which explains the composition behavior, is independent of the absolute propagation rate coefficients and depends only of the reactivity ratios. The same has been proved for three monomers (Eq. 6.43) [82] and for four monomers [83], and it has been also shown that the composition is independent of absolute propagation rate coefficients for any number of monomers [84, 85]. In the second category, there are some systems in which not even the composition behavior can be explained by the terminal model. In this last case, it is possible that the reactivity of the growing chain depends not only on the last unit but also

on the penultimate (or even other) units. In other systems, the reversibility of the propagating reaction can be of importance and this has been neglected in the derivation of the copolymerization equation. In the following, some models that take into account these phenomena are presented.

6.3.2.1 Penultimate Model Some copolymerization systems in which the values for reactivity ratios measured at different compositions are inconsistent can be adequately represented by the penultimate model [86]. In this case, the reactivity of the propagating chain depends on the chemical nature of the last two monomeric units: the one at the active end and the previous one (penultimate) [87, 88]. This is common in systems in which the monomers contain bulky substituents such as the fumaronitrile–styrene copolymerization [89]. In other systems, the penultimate effect has been reported to be limited [90]. The penultimate model can be formulated as follows. Consider the reaction of a growing chain having a penultimate unit j and terminal unit i with a monomer n, M_n :



There are eight possible reactions of this type obtained by combining the possible values of i, j , and n . Applying the QSSA to the four types of growing chains (four combinations of i, j values), it is possible to write the relationship between F_1 and f_1 in a form similar to the copolymerization equation, but using pseudoreactivity ratios, r_i^* , as follows [91]:

$$F_1 = \frac{r_1^* f_1^2 + f_1 f_2}{r_1^* f_1^2 + 2f_1 f_2 + r_2^* f_2^2} \quad (6.20)$$

The pseudoreactivity ratios are defined as

$$r_1^* = r_{21} \frac{r_{11} f_1 + f_2}{r_{21} f_1 + f_2} \quad (6.21)$$

$$r_2^* = r_{12} \frac{f_1 + r_{22} f_2}{f_1 + r_{12} f_2} \quad (6.22)$$

Additionally, four reactivity ratios must be defined:

$$r_{11} = \frac{k_{p111}}{k_{p112}} \quad (6.23)$$

$$r_{12} = \frac{k_{p122}}{k_{p121}} \quad (6.24)$$

$$r_{21} = \frac{k_{p211}}{k_{p212}} \quad (6.25)$$

$$r_{22} = \frac{k_{p222}}{k_{p221}} \quad (6.26)$$

6.3.2.2 Depropagation Models In some copolymerizations, one or both monomers can present a tendency toward depropagation because they are near their ceiling temperature. This trend is increased with higher reaction temperatures and lower monomer concentrations, and these systems will show composition behavior that deviates from terminal model predictions. Several systems fall in this category: styrene- α -methyl styrene [92], MMA- α -methyl styrene [93], *N*-phenylmaleimide-styrene [94] among others. One of the most relevant models for these systems was developed by Lowry [95]. In his development, Lowry considers two cases in which monomer 1 does not show any tendency to depropagation, but monomer 2 depropagates depending on the nature of the 1 or 2 units preceding the chain end. In the first case analyzed by Lowry, monomer 2 (M_2) depropagates if the penultimate unit is also M_2 . In the second case, monomer 2 depropagates if it is preceded by a sequence of at least two monomer 2 units. These cases are shown schematically in Figure 6.10.

For the first case of Lowry, the copolymer composition can be represented as follows:

$$F_1 = \frac{(r_1 [M_1] + [M_2])(1 - \alpha)}{r_1 [M_1](1 - \alpha) + [M_2](2 - \alpha)} \quad (6.27)$$

where

$$\alpha = 0.5 \left\{ \left[1 + K [M_2] + \left(\frac{K [M_1]}{r_2} \right) \right] - \left[\left(1 + K [M_2] + \left(\frac{K [M_1]}{r_2} \right) \right) - 4K [M_2] \right]^{1/2} \right\} \quad (6.28)$$

and K is the equilibrium constant for the first case reaction in Figure 6.10.

For the second case, the expression for the copolymer composition is

$$F_1 = \frac{\left\{ \frac{[r_1 M_1]}{[M_2]} + 1 \right\} \left\{ \alpha \gamma + \frac{\alpha}{1 - \alpha} \right\}}{\left\{ \frac{[r_1 M_1]}{[M_2]} + 1 \right\} \left\{ \alpha \gamma + \frac{\alpha}{1 - \alpha} \right\} + \alpha \gamma - 1 + \frac{1}{(1 - \alpha)^2}} \quad (6.29)$$

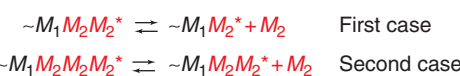


Figure 6.10 Schematic representation of depropagation first and second cases defined by Lowry.

where

$$\gamma = \frac{[K [M_2] + (K [M_1]/r_2) - \alpha]}{K [M_2]} \quad (6.30)$$

where α is also given by Equation 6.28 but the equilibrium constant K , there and in Equation 6.30, is that of the second case reaction in Figure 6.10.

There is the third case in the Lowry theory corresponding to systems in which both monomers can depropagate as long as they are preceded by a sequence of two M_2 units; however, the mathematical expressions are rather intricate and they are not reproduced here. In general, more recent work analyzes the general case of depropagation including the important topic of cross-depropagation. Kruger studied a copolymerization system starting from the terminal model [96] and Szymanski developed an equilibrium theory for depropagating systems having any number of comonomers [97]; this treatment includes the terminal and penultimate models. Recently, several systems (co- and terpolymerizations) have been analyzed experimentally and by mathematical modeling by Penlidis et al. [93, 98, 99].

This work also includes the mathematical analysis for up to six monomers [100]. The trend in these more general treatments is oriented toward the use of numerical methods for the solution of the mathematical problems associated, since closed, analytical expressions are difficult to handle and are of little practical use.

6.3.2.3 Models Involving the Participation of Complexes As mentioned in Section 3.1, several copolymerizations that lead to alternating copolymers have been analyzed by the use of the concept of chain transfer complexes. Some of these systems are styrene-maleic anhydride [101–103], allyl acetate-maleic anhydride [104], and norbornene-maleic anhydride [105].

In these models, the complex formed by the monomer pair competes with the individual monomer molecules for the propagation reaction with the radicals. There are two variations of this approach: in the complex participation model, the pair of monomers form a complex and are added to the chain radical [106–109]. On the other hand, in the complex dissociation model, the complex participates in the propagation process, but dissociates upon reaction and only one of the monomers is added to the chain [101, 103]. Although there is ample experimental evidence for the existence of such complexes in these copolymerizations (such as the bright colors associated with them) [76], it is questionable whether the complexes actually participate in the propagation step [76]. Additionally, for several years, Hall and Padias have accumulated experimental and theoretical evidence that refutes the validity of the models based on complex participation [76, 77]. Both the complex participation and the penultimate models were combined in the so-called comppen model [110].

6.3.2.4 Model Discrimination This is an extensive and difficult topic, and therefore, no detailed treatment of the subject is provided here; it involves elements not only of polymer science but also of statistics. Instead, some general considerations are provided. Generally, caution must be exerted when a model is applied to a particular copolymerization. The kinetics of copolymerization are complex for several reasons: (i) it involves at least four propagation constants; (ii) it is not clear yet if a chemical or a diffusion-controlled termination occurs; (iii) for systems with diffusion-controlled termination, the value of the termination constant may depend on the chain length; etc. In many copolymerizations, several of the kinetic constants are unknown, let alone the parameter values for multicomponent (three or more monomer) systems. In addition, it has been reported that the propagation step can often influence the determination of the termination constant or, in copolymerization systems exhibiting self-initiation, propagation, and initiation phenomena can be difficult to separate [78].

For all these reasons, careful assessment of the model adequacy, aided by statistical techniques, must be used to discriminate among competing models aimed at explaining copolymerization data. Statistical experimental design should also be used whenever possible.

The need of using experimental data on sequence distribution to discriminate among models has been mentioned [101, 111]. Burke et al. [112, 113] compared several statistical techniques for model discrimination and applied them to discriminate among the terminal and the penultimate model. They conclude that the Buzzi–Ferraris technique [114–116], which is based on sequential experimental designs that maximize the information needed at each stage (either for parameter refinement or for emphasizing model differences), is capable of model discrimination in relatively few experiments and can detect even small penultimate effects. Most authors agree that the error associated with measurements also contributes to the difficulty of discerning among competing models [32]; therefore, statistical techniques are strongly recommended for this type of analysis.

6.3.3 Reactivity Ratio Estimation

Having established the importance of reactivity ratios, it falls to the researcher to have to estimate their values. Given the number of statistical tools and computational devices available over the past several decades, one would expect this to be straightforward. However, there has been resistance to using proper parameter estimation techniques and the reader is advised to exercise caution when using reactivity ratios found in the literature [117]. A good practice is to consider reevaluating these from

their raw data if at all possible. In any case, the objective in this section is to outline a methodology to estimate reactivity ratios of the highest precision possible.

A first important question concerns whether the goal is to discriminate between competing models (i.e., terminal vs penultimate model kinetics) or to seek the best parameter estimates. We first assume that terminal model kinetics are being considered and later discuss implications regarding the assumption of penultimate model kinetics. As seen in the previous section, for terminal model kinetics, reactivity ratios are typically estimated using the instantaneous copolymer composition equation or the Mayo–Lewis equation, expressed in two common forms, Equations 6.7 and 6.11.

When considering the estimation of parameters, a protocol such as suggested by Polic et al. [118] is a wise choice. The general protocol consists of the following: (i) parameter sensitivity analysis, (ii) statistical design of experiments, and estimation of (iii) parameters, and (iv) confidence regions. Parameter sensitivity analysis answers the question about which measured response gives the best parameter estimates. Most reactivity ratio estimates have been derived from polymer composition data measured directly, for example, using spectroscopic techniques such as NMR or IR or indirectly by measuring residual monomer using gas chromatography (GC). Recent work offers a review on the use of triad sequence distribution data with case studies demonstrating improved precision of the reactivity ratio estimates [119].

The statistical design of experiments includes the consideration of reaction conditions (e.g., temperature and feed composition) as well as extent of reaction or conversion, number of experimental points and replicates, and the relative location of the design points (e.g., several equidistant points versus selected points on the feed composition scale). As discussed later, reactivity ratios are generally insensitive to moderate temperature changes (i.e., $\pm 20^\circ\text{C}$). Evidently, one would prefer to design experiments within the application range. The use of Equation 6.7, a differential equation, implies only small changes in copolymer composition can be used, and thus, the use of low conversion experiments ($<5\%$) for data collection is necessary. Depending on the copolymer system, this constraint can either be relaxed to say 10% conversion or may even necessitate ultralow conversions near 1% [120]. If higher conversion data are unavoidable, integration of Equation 6.7 or 6.11 is necessary [121]. A methodology dictating the feed composition, number of experimental points, and number of replicate experiments for unconstrained cases is given by Tidwell and Mortimer [122]. Their recommendation is to perform several replicates, say four, at two unique monomer feed compositions f_1' and f_1'' [117, 120]:

$$f'_1 = \frac{2}{2 + r_1^*} \quad (6.31)$$

$$f''_1 = \frac{r_2^*}{2 + r_2^*} \quad (6.32)$$

where r_1^* and r_2^* are initial estimates of the reactivity ratios that can be estimated using the well-known, yet highly approximate, Q-e scheme [123]. Alternatively, screening experiments (e.g., a set of equidistant points along the feed composition axis) can be used. The use of several equidistant points is more practical for model discrimination [112, 124]. In the event of comonomer feed composition constraints, the methodology described by Burke et al. can be used [125].

The next step in the protocol answers the question about what is the best method to estimate the reactivity ratios. Historically, because of its simplicity, linearization techniques such as the Fineman–Ross, Kelen–Tudos, and extended Kelen–Tudos methods have been used. Easily performed on a simple calculator, these techniques suffer from inaccuracies due to the linearization of the inherently nonlinear Mayo–Lewis model. Such techniques violate basic assumptions of linear regression and have been repeatedly shown to be invalid [117, 119, 126]. Nonlinear least squares (NLLS) techniques and other more advanced nonlinear techniques such as the error-in-variables-model (EVM) method have been readily available for several decades [119, 120, 126, 127].

Finally, we are concerned with the precision of the reactivity ratios or, in other words, the joint confidence regions of the parameter estimates. We have stated at the beginning of this section that our objective is to estimate reactivity ratios of maximum precision. This is equivalent to minimizing the joint confidence region of the parameters. The joint confidence regions can be generated using methods such as shown by Polc et al. [117].

Regarding the question of alternative copolymerization kinetic models, as mentioned earlier, in the event of discriminating between competing models (e.g., terminal model kinetics vs penultimate model kinetics), a set of equidistant monomer feed compositions along the entire composition range can serve as an appropriate design of experiments. Once one has determined that an alternative model is operative, the same four questions noted for the terminal model above should be revisited. There are several examples of the estimation of penultimate unit kinetic parameters in the literature [125, 112].

6.3.4 Sequence Length Distribution

Apart from considering the effect of the macroscopic copolymer composition on polymer properties, the exact arrangement or sequence of individual monomers bound

in the copolymer chains can also have a significant effect. While copolymers are often referred to as *random*, for most cases (i.e., other than the truly random case of $r_1 = r_2 = 1$) there is a definite trend toward a regular microstructure. For example, if $r_2 > 1$, sequences of M_2 will tend to be formed. The copolymer microstructure is defined by the distribution of the various lengths of M_1 and M_2 sequences, that is, the *sequence length distribution*.

The probability (P_{11}) of forming a M_1M_1 sequence (or dyad) in the copolymer chain is given by the ratio of the rate of adding M_1 to M_1^* to the sum of the rates of adding M_1 and M_2 to M_1^* :

$$P_{11} = \frac{k_{p11} [M_1^*] [M_1]}{k_{p11} [M_1^*] [M_1] + k_{p12} [M_1^*] [M_2]} \\ = \frac{r_1 [M_1]}{r_1 [M_1] + [M_2]} \quad (6.33)$$

Similarly, the probabilities P_{12} , P_{21} , and P_{22} for forming the dyads, M_1M_2 , M_2M_1 , and M_2M_2 , respectively, are given by

$$P_{12} = \frac{[M_2]}{r_1 [M_1] + [M_2]} \quad (6.34)$$

$$P_{21} = \frac{[M_1]}{r_2 [M_2] + [M_1]} \quad (6.35)$$

$$P_{22} = \frac{r_2 [M_2]}{r_2 [M_2] + [M_1]} \quad (6.36)$$

The number-average sequence length of monomer M_1 , in a way that is completely analogous to the definition of number-average molecular weight, is

$$\bar{n}_1 = \sum_{x=1}^{\infty} x (N_1)_x = (N_1)_1 + 2(N_1)_2 + 3(N_1)_3 + \dots \quad (6.37)$$

where $(N_1)_x$ is the mole fraction of a sequence of monomer 1 units of length x . $(N_1)_x$ is the probability of forming such a sequence and is defined as

$$(N_1)_x = (P_{11})^{(x-1)} P_{12} \quad (6.38)$$

Similarly, for sequences of monomer 2, we have

$$(N_2)_x = (P_{22})^{(x-1)} P_{21} \quad (6.39)$$

Equations 6.38 and 6.39 enable one to calculate the distribution of different sequence lengths for each monomer.

The fractions of triad sequences, A_{ijk} , are related by the probability functions, P_{ij} , as shown below [128]:

$$A_{iii} = (P_{ii})^2 = \left(\frac{r_{ij} f_i}{f_i + r_{ij} f_i} \right)^2 \quad (6.40)$$

$$A_{jij} = (P_{ij})^2 = \left(\frac{f_j}{f_j + r_{ij} f_i} \right)^2 \neq P_{ji} P_{ij} \quad (6.41)$$

$$A_{iji} = A_{jii} = P_{ii} P_{ij} = \frac{r_{ji} f_i f_j}{(f_i + r_{ij} f_i)^2} \quad (6.42)$$

As mentioned earlier, these sequence distributions can be used to derive the copolymer composition equation. Furthermore, employing experimental triad distribution data, one can also calculate the reactivity ratios [119]. The measurement of triad and dyad sequences is largely accomplished via ^1H and ^{13}C NMR spectroscopy.

6.3.5 Composition Measurement Methods

As alluded to earlier, copolymer composition measurement can be achieved by direct and indirect measurements. In some cases, one can infer the copolymer composition by measuring the amounts of monomers consumed in the process. Alternatively, one can directly measure the composition by sensing the characteristic moieties of the individual monomers bound in the copolymer chains. Several techniques are available for each of the direct or indirect measurement of the copolymer composition.

As an example of an indirect measure, we can consider chromatography, which is a technique for separating a mixture into its individual components for identification and quantification. For copolymer composition, GC is often used due to the volatility of most monomers. The unreacted monomers are thus vaporized at a temperature below 400°C , detected in the chromatograph, and the polymer composition is thus inferred from the disappearance of the monomers.

Nuclear magnetic resonance (NMR) spectroscopy is a popular direct measurement technique that provides quantitative information about the chemical structure of copolymers. ^1H and ^{13}C isotopes are the two commonly employed nuclei, but other isotopes (^{15}N , ^{19}F , ^{19}F , ^{29}Si , and ^{31}P) can be used depending on the comonomers. Other spectroscopic techniques (e.g., infrared, ultraviolet, and Raman spectroscopy) are also used [129–132].

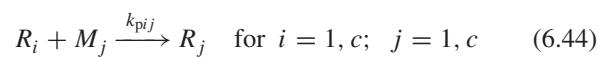
It is worth noting the emergence of several online or in-line composition measurement techniques such as ATR-FTIR and Raman spectroscopy as well as the application of GC and NMR in an online manner [133].

6.3.6 Extensions to Multicomponent Copolymerization

The terminal model for copolymerization can be naturally extended to multicomponent systems involving three or more monomers. Multicomponent copolymerizations find practical application in many commercial processes that involve three to five monomers to impart different properties to the final polymer (e.g., chemical resistance or a certain degree of crosslinking) [134]. There is a classical mathematical development for the terpolymerization or three-monomer case, the Alfrey–Goldfinger equation (Eq. 6.43) [82], and for special cases of this equation when restrictions are imposed on the reactivity ratios of some of the monomer pairs [135–137]; also in addition, the tetrapolymer case has been mathematically analyzed in the literature [83a]. However, as one introduces more monomers, the mathematical manipulation becomes more and more complex and cumbersome. The N -monomer case has been treated using determinants by Walling and Briggs [84] and has been recently reformulated in matrix form [85], more amenable for computational work; this is discussed below.

$$\begin{aligned} F_1 : F_2 : F_3 &= [M_1] \left(\frac{[M_1]}{r_{31}r_{21}} + \frac{[M_2]}{r_{21}r_{32}} + \frac{[M_3]}{r_{31}r_{23}} \right) \\ &\times \left([M_1] + \frac{[M_2]}{r_{12}} + \frac{[M_3]}{r_{13}} \right) : \\ &[M_2] \left(\frac{[M_1]}{r_{12}r_{31}} + \frac{[M_2]}{r_{12}r_{13}} + \frac{[M_3]}{r_{32}r_{13}} \right) \\ &\times \left(\frac{[M_1]}{r_{21}} + [M_2] + \frac{[M_3]}{r_{23}} \right) : \\ &[M_3] \left(\frac{[M_1]}{r_{31}r_{21}} + \frac{[M_2]}{r_{23}r_{12}} + \frac{[M_3]}{r_{13}r_{23}} \right) \\ &\times \left(\frac{[M_1]}{r_{31}} + \frac{[M_2]}{r_{32}} + [M_3] \right) \quad (6.43) \end{aligned}$$

The general mathematical multicomponent approach, based on matrix notation, can be advantageous from the practical point of view for the modeling of this kind of systems [138, 139]. Consider the application of the terminal model to a general multicomponent copolymerization of c comonomers. A general propagation step can be written as follows:



Material balances on the propagating chains of type i result in

$$\frac{d[R_i]}{dt} = \sum_{j=1}^c k_{pji} [R_j] [M_i] - \sum_{j=1}^c k_{pij} [R_i] [M_j] \quad i = 1, c \quad (6.45)$$

which by virtue of the application of the QSSA yields:

$$\sum_{j=1}^c k_{pji} [R_j] [M_i] - \sum_{j=1}^c k_{pij} [R_i] [M_j] \quad i = 1, c \quad (6.46)$$

Defining the fraction, p_i , of a type i propagating chain as

$$p_i = \frac{[R_i]}{\sum_{j=1}^c [R_j]} \quad i = 1, c \quad (6.47)$$

and dividing Equation 6.46 by the product $\sum_{j=1}^c [R_j] \sum_{j=1}^c [M_j]$, Equation 6.46 can be written in terms of the dimensionless variables p_i and f_i , yielding

$$\sum_{j=1}^c k_{pji} p_j f_i = \sum_{j=1}^c k_{pij} p_i f_j \quad (6.48)$$

Considerable simplification of the mathematical treatment is achieved by noting that Equation 6.48 is linear on the p_i , $i = 1, c$ (probabilities of propagating chain types). Out of the c equations in Equation 6.48, only $c-1$ are linearly independent, and so, to solve for the p_i , $i = 1, c$, in terms of the f_i , $i = 1, c$, an additional consistency equation, which can be seen as a dimensionless expression of the mass balance of the propagating chain types directly arising from the definition 6.47, is necessary:

$$\sum_{j=1}^c p_j = 1 \quad (6.49)$$

Taking $c-1$ equations of Equation 6.48, together with Equation 6.49, a linear system of equations can be written in matrix form as follows:

$$\mathbf{X}\mathbf{p} = \mathbf{b} \quad (6.50)$$

where \mathbf{p} is the $c \times 1$ vector of the p_i (distribution of propagating chain types); \mathbf{b} is a $c \times 1$ vector with all terms equal to zero, except for the last one (c -th term), which is unity; and \mathbf{X} is a $c \times c$ matrix having as elements:

$$\begin{aligned} X_{ij} &= k_{pji} p_i, \quad i = 1, \dots, c-1; \\ &\quad j = 1, \dots, c \quad i \neq j \\ X_{ii} &= -\sum_{\substack{j=1 \\ j \neq i}}^c k_{pij} f_j, \quad i = 1, \dots, c-1; \\ X_{cj} &= 1, \quad j = 1, \dots, c \end{aligned} \quad (6.51)$$

Equation 6.50 is easily solved for \mathbf{p} by matrix inversion as

$$\mathbf{p} = \mathbf{X}^{-1} \mathbf{b} \quad (6.52)$$

Once the distribution of propagating chain types is known, the instantaneous composition of the copolymer is given by

$$F_i = \frac{\frac{d[M_i]}{dt}}{\sum_{k=1}^c \frac{d[M_k]}{dt}} \quad (6.53)$$

which from the mass balances of the monomers can be written as

$$F_i = \frac{\sum_{j=1}^c k_{pji} [R_j] [M_i]}{\sum_{k=1}^c \sum_{j=1}^c k_{pjk} [R_j] [M_k]} \quad (6.54)$$

or dividing the numerator and the denominator by the product of the total radical and the total monomer concentrations, the result is

$$F_i = \frac{\sum_{j=1}^c k_{pji} p_j f_i}{\sum_{k=1}^c \sum_{j=1}^c k_{pjk} p_j f_k} \quad (6.55)$$

The application of Equation 6.52, followed by Equation 6.55, provides the instantaneous multicomponent copolymer composition under the terminal model and it is especially useful in the framework of mathematical modeling involving kinetic calculations (conversion – time) since, in this case, explicit p_i values are required (see the pseudokinetic [140] or pseudo-homopolymer approach [138] for kinetic calculations in Chapter 12). A drawback of this approach with respect, for example, to the copolymerization (two monomers) or the Alfrey–Goldfinger (three monomers) equations, is that in this case explicit values for all the homopropagation and cross-propagation kinetic constants are required, instead of reactivity ratios only. Often, however, only the composition behavior of a system in terms of reactivity ratios is required, since the values of the homopropagation kinetic constants is unknown or unreliable. Recently, a matrix approach, similar to that used in Equations 6.50–6.52, has been proposed that provides the composition behavior for N -monomers based only on reactivity ratios [85]; this represents a more efficient formulation than the original work of Walling and Briggs [84], which is of little practical use.

In another extension for copolymerizations involving several monomers, Tobita has studied the full multivariate distribution of chain length and compositions for multi-component free radical polymerization by using generating functions [141, 142].

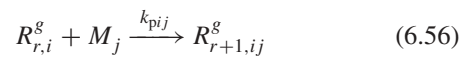
6.4 REACTION CONDITIONS: CONSIDERATIONS

These effects are dependent on the type of mechanism: radical, anionic, and cationic. The treatment here is restricted to radical copolymerizations; see Chapters 7 and 8 for a discussion of the anionic and cationic polymerization cases.

6.4.1 Copolymerization Rate

Unlike the copolymer composition, the rate of copolymerization depends on initiation and termination, as well as on propagation. In a way similar to the modeling of homopolymerizations, one must take into account that the termination and, at higher conversions, initiation and propagation are diffusion controlled to properly model the gel effect. In addition, one must consider the various alternative models for propagation and termination (e.g., terminal vs penultimate; inclusion of depropagation). For multicomponent polymerizations, the use of the pseudokinetic rate constant method for modeling the rate is highly effective [143–145].

Using terminal model kinetics as an example, the propagation equations for copolymerization are as follows:



where $R_{r,i}^g$ is a radical of chain length r ending in monomer i , and k_{pij} is the rate parameter for the addition of monomer j to a radical ending in monomer i . In other words, the forward rate of reaction of a growing polymer chain is assumed to depend only on the type of monomer on the chain that bears a free radical. According to the pseudokinetic rate constant method, it is useful to define overall rate parameters. The overall propagation pseudokinetic rate parameter for an N -component polymerization can be defined as [143]

$$k_{po} = \sum_{i=1}^N \sum_{j=1}^N k_{pij} \varphi_i f_j \quad (6.57)$$

For a copolymerization reaction, the φ_i values are as follows:

$$\varphi_1 = \frac{k_{p21} f_1}{k_{p21} f_1 + k_{p12} f_2} \quad (6.58)$$

$$\varphi_2 = 1 - \varphi_1 = \frac{k_{p12} f_2}{k_{p21} f_1 + k_{p12} f_2} \quad (6.59)$$

The overall termination pseudokinetic rate parameter may be defined as

$$k_{to} = \sum_{i=1}^N \sum_{j=1}^N k_{toij} \varphi_i \varphi_j \quad (6.60)$$

The cross-termination rate constant can be defined, for example, as a function of the instantaneous copolymer composition, F_i , or other alternative models can be invoked [144]:

$$k_{toij} = k_{toi} F_i + k_{toj} F_j \quad (6.61)$$

Diffusion-control models can be invoked for the individual rate parameters using, for example, the free volume theory [144, 145].

Similarly, all other rate parameters may be defined using the pseudokinetic approach. For example, the overall chain transfer to CTA (Chain Transfer Agent) pseudokinetic rate parameter is calculated as

$$k_{fcta} = \sum_{j=1}^N k_{fcta,j} \varphi_j \quad (6.62)$$

where $k_{fcta,j}$ is the rate parameter for the transfer of a growing radical to chain transfer agent j . An overall pseudokinetic rate parameter for transfer to monomer is calculated as

$$k_{fm} = \sum_{i=1}^N \sum_{j=1}^N k_{fmi,j} \varphi_i f_j \quad (6.63)$$

where $k_{fmi,j}$ is the rate parameter for the transfer of a radical to monomer i from a radical ending in monomer j .

When depropagation effects are ignored, polymerization rates for individual monomer species are defined as

$$R_{pj} = \left(\frac{R_I}{2\bar{k}_t} \right)^{1/2} [M] f_j \sum_{i=1}^N k_{pij} \varphi_i \quad (6.64)$$

where R_I is the rate of initiation. The overall rate of polymerization, R_{po} , can be obtained as the sum of the rates of polymerization of the individual species, or as

$$R_{po} = \left(\frac{R_I}{2\bar{k}_t} \right)^{1/2} [M] k_{po} \quad (6.65)$$

6.4.2 Effect of Temperature

Many industrial scale polymerization reactions are carried out at relatively low temperatures (20–80 °C). Not surprisingly, most of the published research has focused on studying copolymerization reactions in this lower temperature

range. However, there is significant interest in copolymerization at elevated temperatures (80–160 °C). This interest relates to frequent excursions into higher temperature ranges that often occur during industrial scale polymerizations due to poor heat transfer [146, 147], and since higher temperature stages at the end of the polymerization are often used to consume any residual monomers or initiators [148]. The higher temperature operation can provide benefits such as higher reaction rates and lower viscosity (and thus better mixing and heat transfer). There are some drawbacks including the presence of unwanted side reactions and perhaps, significant depropagation.

Copolymerization reactivity ratios are often considered to be more or less temperature invariant, but this is strictly true only over moderate temperature ranges. Considering the reactivity ratios in terms of their homopropagation and cross-propagation rate constants, one can express their temperature dependence using an Arrhenius-type equation:

$$r_1 = \frac{k_{p11}}{k_{p12}} = \frac{A_{11}}{A_{12}} \exp\left(-\frac{E_{11} - E_{12}}{RT}\right) \quad (6.66)$$

$$r_2 = \frac{k_{p22}}{k_{p21}} = \frac{A_{22}}{A_{21}} \exp\left(-\frac{E_{22} - E_{21}}{RT}\right) \quad (6.67)$$

k_{pij} is the rate constant for the addition of monomer j to a growing polymer chain on which the active radical center is located on a monomer i unit. A_{ij} and E_{ij} are the frequency factors and activation energies for the propagation reactions, respectively. Normally, the activation energies for the homopropagation and corresponding cross-propagations are similar (the difference has been reported to be less than 10 kJ/mol for several monomer pairs [32]); thus, the reactivity ratios depend only weakly on temperature. However, if the reaction temperature differs greatly from the conditions used to estimate the reactivity ratios, say, by 20 °C or more, significant changes to the reactivity ratios can result. Thus, any attempts to rely on these parameters in a model may seriously compromise the predictions unless their temperature dependence is accounted for.

As mentioned above, when operating at elevated temperatures, depropagation or depolymerization may become significant. This will occur when the reaction temperature is in the vicinity of the ceiling temperature of the system [149]. Fortunately, for most systems, the ceiling temperatures are far beyond the range of conventional polymerization temperatures and, thus, have little or no effect on the reaction kinetics. However, in light of the interest in higher temperature reactions for the reasons noted above, the depropagation reaction may be of significance and may affect the reaction kinetics. For example, poly(MMA) has a ceiling temperature near 220 °C and its reaction kinetics

may begin to exhibit depropagation effects at elevated temperatures. This has been demonstrated even in the copolymerization of butyl acrylate and MMA [150].

Should depropagation become significant, the Mayo–Lewis equation would fail to adequately describe the copolymerization kinetics and one could detect the importance of depropagation by verifying the adequacy of the Arrhenius equations (Eqs. 6.66 and 6.67) to represent the reactivity ratio data. In other words, a plot of the reactivity ratios versus temperature should result in a straight line fit and failure to do so would constitute evidence of significant depropagation effects. The models proposed by Wittmer [151], and later modified by Kruger et al. [96], have been shown useful in modeling copolymerizations with a depropagating monomer. Examples with the copolymerization of α -methylstyrene, a monomer with a low ceiling temperature, and MMA have been published (93a, 150, 152).

6.4.3 Reaction Medium

Several reviews have been published on the effect of solvent in copolymerization [153–156]. Given the radical-mediated mechanism involved, in early studies on radical copolymerization the solvent was expected to have little effect on the reactivity ratios in these systems [157]; however, there are many instances in which this is not true. This early concept may have been supported by the difficulty of distinguishing variations in reactivity ratios due to experimental uncertainties of the associated measurements. Actually, this matter is still a factor to take into account when analyzing differences in reactivity ratios.

Despite the experimental difficulties, it has been established that for systems in which one of the comonomers is ionizable or forms hydrogen bonds, for example, methacrylic acid–MMA, the solvent has a decisive effect that can even change the nature of the copolymerization (alternating or ideal) [24]. Reactivity ratios of nonprotic monomers, such as styrene, MMA, or vinyl acetate, show only a slight solvent effect, but the cause is still unknown [24].

Harwood [158] has proposed that the solvent may influence the way the polymer chains are solvated with monomers, suggesting that the relative concentration of monomers surrounding the active chain end may be different than their global relative concentrations (bootstrap effect). This can be expressed in terms of a partition coefficient:

$$K = \frac{[M_1]_v/[M_2]_v}{[M_1]/[M_2]} \quad (6.68)$$

where $[M_i]_v$ are the monomer concentrations in the vicinity of the reactive chain end and $[M_i]$ are the global monomer concentrations. This may explain the observed effects of

solvents on the reactivity ratios. Mounting experimental evidence consistent with this theory is being accumulated [159–161].

On the other hand, when dealing with heterogeneous systems (e.g., suspension or emulsion polymerizations), it is important not to confuse thermodynamic effects of monomer partitioning among phases with variations in reactivity ratios. For the calculation of these, the concentrations of the monomers at the reaction site should be considered (at the particles) instead of global concentrations in the system.

6.4.4 Effect of Pressure

The analysis for the effect of pressure is similar to that for the temperature effect. When the pressure is taken into account, Equation 6.69 becomes

$$r_1 = \frac{k_{p11}}{k_{p12}} = \frac{A_{11}}{A_{12}} \exp \left[-\frac{(E_{11} - E_{12}) + (\Delta V_{11} - \Delta V_{12}) P}{RT} \right] \quad (6.69)$$

where ΔV_{ij} are the activation volumes for the propagation of a radical type i with monomer j . Activation volumes are usually low, but their effect is magnified at high pressures. On the other hand, the pressure effect will be somehow attenuated for the reactivity ratio since it will be proportional to the difference $(\Delta V_{11} - \Delta V_{12})$ only.

The influence of pressure and temperature on activity, monomer content, molar masses, and glass-transition temperatures of copolymers has been assessed [162].

6.4.5 Achieving Uniform Copolymer Composition

More often than not, reactivity differs from monomer to monomer. This is evident when the reactivity ratios differ from a value of one. Thus, if one is operating at concentrations other than the azeotropic composition, batch copolymerization will result in a changing copolymer composition throughout the reaction. For example, a copolymerization with $r_1 > 1$ and $r_2 < 1$ would result in the instantaneous copolymer composition decreasing in monomer 1 as monomer conversion increases. The degree of compositional drift that leads to a heterogeneous copolymer composition depends on the ratio of reactivity ratios (r_1/r_2), where heterogeneity increases with r_1/r_2 , the initial monomer composition (f_{10}) and monomer conversion (x). Compositional heterogeneity usually leads to inferior properties, especially optical, rheological, and strength properties. As a result, industrial semibatch processes have

been developed to reduce composition drift [163]. One should keep in mind, however, that in certain instances heterogeneous compositions may be desired [164–166]. In the latter case, one may still wish to control the composition to achieve the desired heterogeneity.

Two basic monomer feed policies employed in a semibatch copolymerization can be used to minimize composition drift [163]. Many highly effective commercial processes are based on one or a combination of these policies. Additional promising derivations of these policies have also been presented [167–173]. Henceforth, we refer to the two basic feed policies as Policy I and Policy II, as described in following sections.

6.4.5.1 Policy I Using the copolymer composition equation (Eq. 6.11), we first calculate the desired monomer feed composition (F_1) to achieve the desired copolymer composition (F_1). All of the less reactive monomer and sufficient of the more reactive monomer to achieve the desired F_1 are added to the reactor initially. Thereafter, the more reactive monomer is fed to the reactor at a time-varying feed rate to maintain the molar ratio of monomer 1 to monomer 2 (N_1/N_2 where N_i is the number of moles of monomer i) in the reactor constant. Thus, F_1 remains constant and, consequently, F_1 also remains unchanged.

6.4.5.2 Policy II As for Policy I, we use the desired F_1 in Equation 6.11 to calculate the desired F_1 . A “heel” or an initial reactor charge of monomers 1 and 2 at a concentration level equivalent to the desired F_1 is added to the reactor initially. Thereafter, monomers 1 and 2 are fed to the reactor with time-varying feed rates to maintain the monomer concentrations ($[M_1]$ and $[M_2]$) and F_1 constant with time. With feed Policy II, a batch finishing step is required if the residual monomer is beyond acceptable levels. During this final step, some composition drift is likely to occur but will typically be small and probably tolerable from a quality point of view given that it will occur during the final stages of polymerization.

To produce a copolymer with a homogeneous composition in a semibatch process, the following equations should be solved:

$$\frac{dN_1}{dt} = -N_1 (k_{p11}\phi_1 + k_{p21}\phi_2) [P^g] + F_{1,in} \quad (6.70)$$

$$\frac{dN_2}{dt} = -N_2 (k_{p12}\phi_1 + k_{p22}\phi_2) [P^g] + F_{2,in} \quad (6.71)$$

$$\begin{aligned} \frac{dV}{dt} = & \frac{F_{1,in}MW_1}{\rho_{m1}} + \frac{F_{2,in}MW_2}{\rho_{m2}} - \left[R_{p1}MW_1 \left(\frac{1}{\rho_{m1}} - \frac{1}{\rho_p} \right) \right. \\ & \left. + R_{p2}MW_2 \left(\frac{1}{\rho_{m2}} - \frac{1}{\rho_p} \right) \right] V \end{aligned} \quad (6.72)$$

with initial conditions

$$t = 0, N_1 = N_{10}, N_2 = N_{20}, V = V_0 \quad (6.73)$$

For a binary copolymerization,

$$\phi_1 = \frac{[P_1^g]}{[P^g]} = \frac{k_{p21}f_1}{k_{21}f_1 + k_{p12}f_2} \quad (6.74)$$

In Equations 6.70–6.74, k_{pij} is the propagation rate coefficient for the addition of monomer j to a growing polymer radical ending in monomer i , ϕ_i is the mole fraction of radicals ending in monomer i , $[P^g]$ is the total concentration of radicals in the reactor, $F_{i,in}$ is the time-varying feed rate of monomer i to the semibatch reactor, V is the reactor volume, MW_i is the molecular weight of monomer i , R_{pi} is the rate of polymerization of monomer i , and ρ_{mi} and ρ_p are the densities of monomer i and the polymer, respectively.

According to the definition of Policy I,

$$F_{2,in} = 0 \quad \text{and} \quad \frac{d(N_1/N_2)}{dt} = 0 \quad (6.75)$$

and for Policy II,

$$\frac{d[M_1]}{dt} = \frac{d[M_2]}{dt} = 0 \quad (6.76)$$

Since both F_1 and F_2 are constant, ϕ_1 is also constant. Given that the total polymer radical concentration ($[P^g]$) varies during the reaction, one can readily solve for the time-varying monomer feed rates, $F_{1,in}$ and $F_{2,in}$, using Equations 6.70–6.76.

The practical implementation of the above policies is not necessarily as straightforward as solving the above equations. As can be deduced from Equations 6.70–6.76, $F_{i,in}$ is a function of the propagation rate coefficients, the monomer concentrations, and most importantly, the total radical concentration. Hence, to precalculate the optimal monomer feed rates, the radical concentration must be specified in advance and kept constant via an initiator feed policy and/or a heat production policy. This is especially important considering that a constant radical concentration is not a typical polymer production reality. This raises the notion that one could increase the reactor temperature or the initiator concentration over time to manipulate the radical concentration rather than manipulate the monomer feed flowrates, that is, keep $F_{i,in}$ constant for simpler pump operation. Furthermore, these semibatch policies provide the “open-loop” or “off-line” optimal feed rates required to produce a constant composition product. The “online” or “closed-loop” implementation of these policies necessitates a consideration of online sensors for monomer

and polymer composition and polymer reactor control methodologies. The use of process control methodologies would permit adjustment for uncontrolled variations in monomer feed rates, the presence of impurities, and other disturbances to the total radical concentration. Finally, but most importantly, we must give consideration to the potential impact of these semibatch feed policies on important polymer properties other than composition.

For the case of Policy I, given the constant monomer ratio, the reaction would proceed in a way similar to a batch reaction. That is, the reaction would commence at a relatively high monomer concentration and proceed with a decrease in overall monomer concentration akin to a batch process. The molecular weight profile and any long-chain branching would therefore be similar to a batch case and would only be of concern toward the end of the reaction.

When operating under semibatch Policy II, common practice is to maintain the reactor contents at low or “starved” monomer concentrations. This provides for relatively straightforward temperature control and overall reactor operation. However, when such low monomer concentrations are used over the duration of the polymerization, the potential for significant long-chain branching and crosslinking exists. The molecular weight profile would, therefore, be radically different from a batch process.

Another practical consideration relates to the use of the semibatch feed policies in emulsion copolymerization. One would need to account for the partitioning of monomers in the different phases as well as the presence of monomer droplets (desired or not) during the particle nucleation and growth stages.

REFERENCES

- Utracki LA. *Polymer Blends Handbook*. Volume 1. Dordrecht, The Netherlands: Kluwer Academic Publishers; 2002.
- Harper Ir2.pptcasotpl,rtcnCA. *Modern Plastics Handbook*. USA: McGraw-Hill; 2000.
- Louie DK. *Elastomers*. In: *Handbook of Sulphuric Acid Manufacturing*. Richmond Hill, Canada: DKL Engineering, Inc; 2005. p 16.
- The Down Chemical Co, assignee. US patent 4,268,652. 1981.
- Imperial Chemical Industries Ltd., assignee. FR patent 2085462. 1972.
- [a] Lessard B, Maric M. *Macromolecules* 2008;41:7881.
[b] Lessard B, Schmidt SC, Maric M. *Macromolecules* 2008;41:3446. [c] Abraham S, Choi JH, Lee JK, Ha CS, Kim I. *Macromol Res* 2007;15:324.

7. [a] Drockenmuller E. *J Polym Sci A Polym Chem* 2009;47:3803. [b] Flores M, Elizalde L, Santos G. *J Macromol Sci Pure Appl Chem* 2009;46:223. [c] Deepak VD, Asha SK. *J Polym Sci A Polym Chem* 2008;46:1278. [d] Harris HV, Holder SJ. *Polymer* 2006;47:5701.
8. [a] Li K, Cao Y. *Soft Materials* 2010;8:226. [b] Liu W, Greytak AB, Lee J, Wong C, Park J, Marshall L, Jiang W, Curtin P, Ting AY, Nocera DG, Fukumura D, Jain R, Bawendi M. *J Am Chem Soc* 2010;132:472. [c] Nguyen MN, Bressy C, Margallan A. *Polymer* 2009;50:3086.
9. Lessard B, Maric M. *Macromolecules* 2010;43:879.
10. [a] Yin J, Ge Z, Liu H, Liu S. *J Polym Sci A Polym Chem* 2009;47:2608. [b] Wenyan H, Huili P, Bibiao J, Qiang R, Guangqun Z, Lizhi K, Dongliang Z, Jianhai C. *J Appl Polym Sci* 2011;119:977. [c] Ishizu K, Yamada H, Hiroe. *Macromolecules* 2007;40:3056.
11. [a] Maki Y, Mori H, Endo T. *Macromol Chem Phys* 2010;211:1137. [b] Maki Y, Mori H, Endo T. *Macromolecules* 2008;41:8397.
12. Hadjichristidis N, Pispas S, Floudas G. *Block Copolymers: Synthetic Strategies, Physical Properties, and Applications*. Hoboken, New Jersey: Wiley; 2003.
13. Tsitsilianis C. Synthesis of block and graft copolymers, Chapter 8. In: *Controlled and Living Polymerizations: From Mechanisms to Applications*. Weinheim, Germany: Wiley-VCH Verlag GmbH & Co. KGaA; 2010. p 445–492.
14. Bae B, Miyatake K, Watanabe M. *Macromolecules* 2010;43:2684.
15. Yamada T, Suginome M. *Macromolecules* 2010;43:3999.
16. Hamley IW. *Developments in Block Copolymer Science and Technology*. New York: John Wiley and Sons; 2004.
17. Schmolka IR, inventor; BASF Wyandotte Co., assignee. US patent 3,925,241. 1975.
18. Diaz T, Fischer A, Jonquieres A, Bremilla A, Lochon P. *Macromolecules* 2003;36:2235.
19. [a] Acik G, Kahveci MU, Yagci Y. *Macromolecules* 2010;43:9198. [b] Liu X, Ni P, He J, Zhang M. *Macromolecules* 2010;43:4771. [c] Markova D, Kumar A, Klapper M, Müller K. *Polymer* 2009;50:3411.
20. Mori H, Kudo E, Saito Y, Onuma A, Morishima M. *Macromolecules* 2010;43:7021.
21. [a] Wang L, Broadbelt LJ. *Macromolecules* 2009;42:7961. [b] Phan TN, Maiez S, Pascault JP, Bonnet A, Gerard P, Guerret O, Bertin D. *Macromolecules* 2007;40:4516. [c] Karaky K, Pere E, Pouchan C, Garay H, Khoukh A, Francois J, Desbrieres J, Billon L. *New J Chem* 2006;30:698. [d] Woo D, Kim J, Suh M, Lee S, Torkelson J. *Polymer Preprint* 2005;46:405.
22. [a] Penfold H, Holder S, McKenzie B. *Polymer* 1904;2010:51. [b] Min K, Oh J, Matyjaszewski K. *J Polym Sci A Polym Chem* 2007;45:1413. [c] Wang R, Luo Y, Li BG. *AIChE J* 2007;53:174. [d] Min KE, Li M, Matyjaszewski K. *J Polym Sci A Polym Chem* 2005;43:3616.
23. [a] Li Z, Serelis A, Reed W, Alb A. *Polymer Preprint* 2010;51:84. [b] Chen Y, Zhang Y. *Polymer Preprint* 2009;50:620. [c] Ribaut T, Lacroix P, Fournel B, Sarrade S. *J Polym Sci A Polym Chem* 2009;47:5448.
24. Moad G, Solomon DH. *The Chemistry of Radical Polymerization*. 2nd ed. New York: Elsevier Science Inc; 2006.
25. Hadjichristidis N, Pitsikalis M, Iatrou H, Driva P, Chatzichristidi M, Sakellariou G, Lohse D. *Graft Copolymers*. New York: John Wiley & Sons, Inc.; 2002.
26. [a] Saldívar-Guerra E, Matyjaszewski K. *Macromolecular Symposia: New Trends in Polymer Science*. Volume 1. Wiley; 2009. p 110–119. [b] Mohajery S, Rahmani S, Entezami AA. *Polym Adv Technol* 2008;19:1528. [c] Chenal M, Mura S, Marchal C, Gigmes D, Charleux B, Fattal E, Couvreur P, Nicolas J. *Macromolecules* 2010;43:9291.
27. [a] Yamamoto S, Pietrasik J, Matyjaszewski K. *Macromolecules* 2008;41:7013. [b] Tsarevsky NV, Matyjaszewski K. *Chem Rev* 2007;107:2270. [c] Xue J, Chen L, Wang HL, Zhang ZB, Zhu XL, Kang ET, Neoh KG. *Langmuir* 2008;24:14151.
28. [a] Li Y, Zhang Y, Zhai S, Deng Y, Xiong H, Lu G, Huang X. *J Polym Sci A Polym Chem* 2011;49:23. [b] Zhang Y, Shen Z, Yang D, Feng C, Hu J, Lu G, Huang X. *Macromolecules* 2010;43:117.
29. Ring W, Mita I, Jenkins AD, Bikales NM. *Pure Appl Chem* 1985;57:1427.
30. Mayo FR, Lewis FM. *J Am Chem Soc* 1944;66:1594.
31. Greenley R. Z. Free Radical Copolymerization Reactivity Ratios chapter II, In: Brandrup J, Immergut E. H, Grulke E. A, editors. *Polymer Handbook*. New York: J. Wiley & Sons Inc; 1999.
32. [a] Odian G. *Principles of Polymerization*. 2nd ed., New York: Wiley Interscience; 1982. [b] Odian G. *Principles of Polymerization*. 4th ed., New York: Wiley Interscience; 1990.
33. Wang S, Poehlein GW. *J Appl Polym Sci* 1993;49:991.
34. Brar AS, Arunan E, Kapur GS. *Polym J (Tokyo)* 1989;21:689.
35. Zaldivar C, del Sol O, Iglesias GD. *Polymer* 1998;39:245.
36. Embree WH, Mitchell JM, Williams HL. *Can J Chem* 1951;29:253.
37. Gromov VF, Khomikovskii PM, Abkin AD. *Vysokomol Soedin* 1961;3:1015.
38. Tazuke S, Okamura S. *J Polym Sci A-I* 1968;6:2907.
39. Mayo FR, Lewis FM, Walling C. *J Am Chem Soc* 1948;70:1529.
40. Alfrey T, Overberger CG, Pinner SH. *J Am Chem Soc* 1953;75:4221.
41. Matsuda M, Iino M, Tokura N. *Makromol Chem* 1963;65:232.
42. Tamikado T, Iwakura Y. *J Polymer Sci* 1959;36:529.
43. Fordyce RG, Chapinand EC, Ham GE. *J Am Chem Soc* 1948;70:2489.
44. Meehan EJ. *J Polymer Sci* 1946;1:318.
45. Margaritova MF, Raiskaya VA. *Tr.Mosk Khim-Tekhnol Inst* 1953;4:37.
46. Walling C, Davison JA. *J Am Chem Soc* 1951;73:5736.

47. Terteryan RPptcaa(wd,aps)jir47A, Livshits SD. Sb. Nauchn. Tr.-Vses. Nauchno-Issled. Inst. Pererab. Nefti 1982;41:118.
48. Terteryan RA, Khrapov VS. Vysokomol Soedin A 1983;25:1850.
49. Raetsch M, Lange H. Plaste Kautsch 1979;26:6.
50. Burkhardt RD, Zutty NL. J Polym Sci A 1963;1:1137.
51. Van der Meer R, German AL. J Polym Sci Polym Chem Ed 1979;17:571.
52. Tsuchida E, Ohtani Y, Nakadai H, Shinohara I. Kogyo Kagaku Zasshi 1967;70:573.
53. Chapin EC, Ham GE, Mills CL. J Polymer Sci 1949;4:597.
54. San Roman J, Madruga EL, del Puerto MA. Angew Makromol Chem 1979;78:129.
55. Marvel CS, Schwen R. J Am Chem Soc 1957;79:6003.
56. McManus NT, Pendilis A, Dubé MA. Polymer 2002;43:1607.
57. Nakata T, Otsu T, Imoto M. J Polym Sci A 1965;3:3383.
58. Tsuchida E, Shimomura T, Fujimura K, Ohtani Y, Shinohara I. Kogyo Kagaku Zasshi 1966;70:1230.
59. DeWilde MC, Smets G. J Polymer Sci 1950;5:253.
60. Georgiev GS, Dakova IG, Simpson SJ. J Polym Sci A Polym Chem 1995;32:497.
61. Paxton TR. J Polym Sci B 1963;1:73.
62. Alfrey T. Jr., Bohrer J. & Mark, H. *Copolymerisation*. Interscience, New York, 1952;p. 34, 35, 38, 39, 40.
63. Zubov VR, Valuev LI, Kabanov VA, Kargin VA. J Polym Sci A-I 1971;9:833.
64. Dubé MA, Penlidis A. Polymer 1995;36:587.
65. Hakim M, Verhoeven V, McManus NT, Dubé MA, Penlidis A. J Appl Polym Sci 2000;77:602.
66. Mayo FR, Walling C, Lewis FM, Hulse WF. J Am Chem Soc 1948;70:1523.
67. Goldfinger G, Kane T. J Polymer Sci 1948;3:462.
68. Farina M. Makromol Chem 1990;191:2795.
69. Saldívar-Guerra E, Vivaldo-Lima E, Infante-Martínez R, Flores-Tlacuahuac A. Macromol Theory Simul 2010;19:151.
70. Wall FT. J Am Chem Soc 1944;66:2050.
71. Minsk LM, Kotlarchik C, Meyer GN. J Polym Sci Polym Chem Ed 1973;11:3037.
72. Atherton JN, North AM. Trans Faraday Soc 1962;58:2049.
73. Shirota Y, Kroschwitz JI, Bikales N, Overberger CG, and Menges G. *Charge-transfer complexes*. In: Kroschwitz JI, Bikales N, Overberger CG, Menges G, editors. *Encyclopedia of Polymer Science and Engineering*. Volume 3. New York, NY: Wiley; 1985. p 327.
74. Tirrell DA, Kroschwitz JI, Bikales N, Overberger CG, and Menges G. Copolymerization. In: Kroschwitz JI, Bikales N, Overberger CG, Menges G, editors. *Encyclopedia of Polymer Science and Engineering*. Volume 4. New York, NY: Wiley; 1985. p 192.
75. Cowie JMG. *Alternating Copolymers*. New York: Plenum; 1985.
76. Hall HK, Padias AB. J Polym Sci A Polym Chem 2001;39:2069.
77. Hall HK, Padias AB. J Polym Sci A Polym Chem 2004;42:2845.
78. Mota-Morales JD, Quintero-Ortega I, Saldívar-Guerra E, Luna-Bárcenas G, Albores-Velasco M, Percino J, Chapela V, Ocampo MA. Macromol React Eng 2010;4:222.
79. Garcia A, Ocampo MA, Luna-Bárcenas G, Saldívar-Guerra E. Macromol Symp 2009;283–284:336–341.
80. Asai H, Imoto T. J Polym Sci B 1964;2:553.
81. Fukuda T, Ma YD, Inagaki H. Macromolecules 1985;18:17.
82. Alfrey T, Goldfinger G. J Chem Phys 1946;14:115.
83. [a] Chen WC, Chuang Y, Chiu WY. J Appl Polymer Sci 2001;79:853. [b] Schmidt G, Drache M, Koppers F. Chem Ing Tech 2007;79:1155.
84. Walling C, Briggs ER. J Am Chem Soc 1945;67:1774.
85. Saldívar-Guerra E, Zapata-González I. Macromol Theory Simul 2012;21(1):24.
86. [a] Merz E, Alfrey T, Goldfinger G. J Polymer Sci 1946;1:75. [b] Deb PC. Polymer 2007;48:4932.
87. Rounsefell TD, Pittman CU Jr., J Macromol Sci Chem 1979;A13:153.
88. Devasia R, Reghunadhan CP, Ninan KN. Eur Polym J 2002;38:2003.
89. Fordyce RG, Ham GE. J Am Chem Soc 1951;73:1186.
90. Kaim A. Macromol Theory Simul 1997;6:907.
91. Dotson NA, Galván R, Laurence RL, Tirrell M. *Polymerization Process Modeling*. New York: VCH Publishers Inc.; 1996.
92. O'Driscoll KF, Gasparro FP. J Macromol Sci Chem 1967;A1:643.
93. [a] Palmer DE, McManus NT, Penlidis A. J Polym Sci A Polym Chem 2000;38:1981. [b] Palmer DE, McManus NT, Penlidis A. J Polym Sci A Polym Chem 2001;39:1753.
94. Florjańczyk Z, Krawiec W. Die Makromol Chem 1989;190:2141.
95. Lowry GG. J Polymer Sci 1960;42:463.
96. Kruger H, Bauer J, Rubner J. Makromol Chem 1987;188:2163.
97. Szymanski R. Makromol Chem 1987;188:2605.
98. Cheong SI, Penlidis A. J Appl Polym Sci 2004;93:261.
99. [a] Leamen MJ, McManus NT, Penlidis A. J Polym Sci A Polym Chem 2005;43:3868. [b] Leamen MJ, McManus NT, Penlidis A. Chem Eng Sci 2006;61:7774.
100. Dorschner D. Multicomponent free radical polymerization model refinements and extensions with depropagation [M.S. thesis]. Waterloo, Ontario, Canada: University of Waterloo; 2010.
101. Hill DJT, O'Donnell JH, O'Sullivan PW. Macromolecules 1983;16:1295.
102. Dodgson K, Ebdon JR. Makromol Chem 1979;180:1251.
103. Tsuchida E, Tomono T. Makromol Chem 1971;141:265.
104. Bartlett PD, Nozaki K. J Am Chem Soc 1946;68:1495.
105. Ito H, Miller D, Sveum N, Sherwood M. J Polym Sci A Polym Chem 2000;38:3521.

106. [a] Seiner JA, Litt M. *Macromolecules* 1971;4:308. [b] Litt M. *Macromolecules* 1971;4:312. [c] Litt M, Seiner JA. *Macromolecules* 1971;4:314. [d] Litt M, Seiner JA. *Macromolecules* 1971;4:316.
107. Cais RE, Farmer RG, Hill DJT, O'Donnell JH. *Macromolecules* 1979;12:835.
108. Deb PC. *J Polym Sci Polym Lett Ed* 1985;23:233.
109. Deb PC, Meyerhoff G. *Eur Polym J* 1984;20:713.
110. Brown P, Fujimori K. *J Polym Sci A Polym Chem* 1994;32:2971.
111. Hill DJT, O'Donnell JH, O'Sullivan PW. *Macromolecules* 1982;15:960.
112. Burke AL, Duever TA, Penlidis A. *Macromolecules* 1994;27:386.
113. Burke AL, Duever TA, Penlidis A. *J Polym Sci A Polym Chem* 1996;34:2665.
114. Buzzi-Ferraris G, Forzatti P. *Chem Eng Sci* 1983;38:225.
115. Buzzi-Ferraris G, Forzatti P, Emig G, Hofmann H. *Chem Eng Sci* 1984;39:81.
116. Buzzi-Ferraris G, Forzatti P, Canu P. *Chem Eng Sci* 1990;45(2):477.
117. Polic AL, Duever TA, Penlidis A. *J Polym Sci A Polym Chem* 1998;36:813.
118. Polic AL, Lona LMF, Duever TA, Penlidis A. *Macromol Theory Simul* 2004;13:115.
119. Hauch E, Zhou X, Duever TA, Penlidis A. *Macromol Symp* 2008;271:48–63.
120. Dubé MA, Sanaye RA, Penlidis A, O'Driscoll KF, Reilly PM. *J Polym Sci A Polym Chem* 1991;29:703.
121. Scorah MJ, Hua H, Dubé MA. *J Appl Polym Sci* 2001;82:1238.
122. Tidwell PW, Mortimer GA. *J Polym Sci A* 1965;3:369–387.
123. Greenley RZ. Q and e values for free radical copolymerizations of vinyl monomers and telogens. In: Brandrup J, Immergut EH, Grulke EA, editors. *Polymer Handbook*. 4th ed. New York: Wiley; 1999. p 309.
124. Burke AL, Duever TA, Penlidis A. *Ind Eng Chem Res* 1997;36(4):1016.
125. Burke AL, Duever TA, Penlidis A. *J Polym Sci A Polym Chem* 1993;31:3065.
126. Rossignoli PJ, Duever TA. *Polym React Eng* 1995;3:361.
127. Chee KK, Ng SC. *Macromolecules* 1986;19:2779.
128. Koenig J. *Chemical Microstructure of Polymer Chains*. New York: John Wiley & Sons Ltd; 1980.
129. Schmidt C, Töpfer O, Langhoff A, Oppermann W, Schmidt G. *Chem Mater* 2007;19:4277.
130. Canak TC, Kizilcan N, Serhatli IE. *J Appl Polym Sci* 2011;119:183.
131. Raihane M, Castevetro V, Bianchi S, Altas S, Ameduri B. *J Polym Sci A Polym Chem* 2010;48:4900.
132. Junil S, Pal A, Gude R, Devi S. *Eur Polym Sci* 2010;46:958.
133. Fonseca G, Dubé MA, Penlidis A. *Macromol React Eng* 2009;3:327.
134. Sahloul NA. *Diss Abstr Int* 2005;65:5275.
135. Ham GE. *J Macromol Sci Chem* 1983;A19:693.
136. Braun D, Hu F. *Prog Polym Sci* 2006;31:239.
137. [a] Schmidt G, Schmidt H, Litauski B, Bieger W. *Macromol Chem* 1990;191:2963. [b] Schmidt G, Schmidt H, Litauski B, Berger W. *Macromol Chem* 1990;191:3033. [c] Schmidt G, Schmidt H, Litauski B. *Wiss Z Tech Univ Dresden* 1998;37:145.
138. Storti G, Carrà S, Morbidelli M, Vita G. *J Polym Sci A Polym Chem* 1989;37:2443.
139. Saldívar E, Dafniotis P, Ray WH. *J Macromol Sci Rev Macromol Chem Phys* 1998;C38:207.
140. Tobita H, Hamielec AE. *Polymer* 1991;32:2641.
141. Tobita H. *Macromol Theory Simul* 2003;12:470.
142. Tobita H. *Macromol Theory Simul* 2003;12:463.
143. Hamielec AE, MacGregor JF, Penlidis A. Copolymerization. In: Sir Allen G, editor. *Comprehensive Polymer Science*. Volume 3. Oxford, UK: Pergamon Press; 1989. p 17.
144. Dubé MA, Soares JBP, Penlidis A, Hamielec AE. *Ind Eng Chem Res* 1997;36:966.
145. Gao J, Penlidis A. *J Macromol Sci Rev Macromol Chem Phys* 1998;C38:651.
146. Armitage PD, Hill S, Johnson AF, Mykytiuk J, Turner JMC. *Polymer* 1988;29:2221.
147. Zhu S, Hamielec AE. *Polymer* 1991;32:3021.
148. Maxwell IA, Verdurmen EMFJ, German AL. *Makromol Chem* 1992;193:2677.
149. Badeen C, Dubé MA. *Polym React Eng* 2003;1:53.
150. Dubé MA, Hakim M, Verhoeven V, McManus NT, Penlidis A. *Macromol Chem Phys* 2002;203:2446.
151. Wittmer P. *Adv Chem* 1971;99:140.
152. Martinet F, Guillot J. *J Appl Polym Sci* 1999;72:1611.
153. Barton J, Borsig E. *Complexes in Free Radical Polymerization*. Amsterdam: Elsevier; 1988.
154. Plochocka KJ. *J Macromol Sci Rev Macromol Chem Phys* 1981;C20:67.
155. Coote ML, Davis TP, Klumperman B, Monteiro MJ. *J Macromol Sci Rev Macromol Chem Phys* 1998;C38:567.
156. Madruga EL. *Prog Polym Sci* 2002;27:1879.
157. Mayo FR, Walling C. *Chem Rev* 1950;46:191.
158. Harwood HJ. *Makromol Chem Macromol Symp* 1987;10/11:331.
159. Coote ML, Johnston LPM, Davis TP. *Macromolecules* 1997;30:8191.
160. Chambard G, Klumperman B, German AL. *Polymer* 1999;40:4459.
161. Fernández-Monreal C, Martínez G, Sánchez-Chaves M, Madruga EL. *J Polym Sci A Polym Chem* 2001;39:2043.
162. Boggioni L, Zampa C, Ravasio A, Ferro DR, Tritto I. *Macromolecules* 2008;41:5107.
163. Hamielec AE, MacGregor JF, Penlidis A. *Makromol Chem Macromol Symp* 1987;10/11:521.
164. Bassett DR, Hamielec AE, editors. *Emulsion Polymers and*

- Emulsion Polymerization. ACS Symposium Series.* Volume 165. Washington, DC: American Chemical Society; 1981.
165. de la Cal JC, Echevarria A, Meira GR, Asua JM. *J Appl Polym Sci* 1995;57:1063.
 166. Echevarria A, de la Cal JC, Asua JM. *J Appl Polym Sci* 1995;57:1217.
 167. Arzamendi G, Asua JM. *Ind Eng Chem Res* 1991;30:1342.
 168. Arzamendi G, de la Cal JC, Asua JM. *Angew Makromol Chem* 1992;194:47.
 169. Leiza JR, Arzamendi G, Asua JM. *Polym Int* 1993;30:455.
 170. Canegallo S, Canu P, Morbidelli M, Storti G. *J Appl Polym Sci* 1994;54:1919.
 171. Canu P, Canegallo S, Morbidelli M, Storti G. *J Appl Polym Sci* 1994;54:1899.
 172. Schoonbrood HAS, van Eijnatten RCPM, German AL. *J Polym Sci A Polym Chem* 1996;34:949.
 173. Arzamendi G, Asua JM. *J Appl Polym Sci* 1989;38:2019.

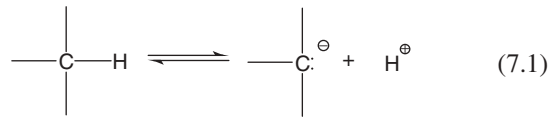
7

ANIONIC POLYMERIZATION

RODERIC QUIRK

7.1 INTRODUCTION

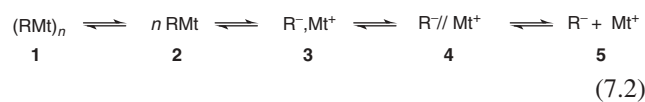
This chapter describes the general aspects of anionic polymerization of vinyl, carbonyl, and heterocyclic monomers, with emphasis on alkyl lithium-initiated polymerization of vinyl monomers. Anionic polymerization is defined as a chain reaction polymerization in which the active centers for propagation are anions, which can be in the form of free ions, paired ions, or aggregated species [1]. The term “anion” will be considered as an atom or group of atoms with a negative charge and an unshared pair of electrons. Anions can be considered to be the conjugate bases of the corresponding Bronsted acids, as shown in Equation 7.1.



The stability and reactivity of anionic species can be deduced from pK_a values for the equilibria depicted in Equation 7.1 [2, 3]. The more acidic conjugate acids (lower pK_a values) are associated with a correspondingly more stable anionic species.

In general, these anions are associated with a counterion, typically an alkali metal cation. The exact nature of the anion can be quite varied depending on the structure of the anion, counterion, solvent, and temperature [3–5]. The range of possible propagating species in anionic polymerization is depicted in terms of a Winstein spectrum of structures as shown in Equation 7.2 for a carbanionic chain end (R^-) [3, 6]. In addition to the aggregated (associated) (1) and unaggregated (unassociated) (2) species, it is necessary to consider the intervention of free ions (5), contact

ion pairs (3), and solvent-separated ion pairs (4); Mt^+ represents a metallic counterion such as an alkali metal cation. In hydrocarbon media, species (1–3) would be expected to predominate. Polar solvents tend to shift the Winstein spectrum to the right, that is, toward more reactive, less associated, more ionic species. With respect to the nature of the bonding in organoalkali metal compounds, it is generally agreed that the carbon–alkali metal bond is ionic for sodium, potassium, rubidium, and cesium. In contrast, experimental evidence and theoretical studies indicate that the carbon–lithium bond includes some covalent character, that is, it is a semipolar bond [3, 7]; however, there is disagreement about the relative amounts of covalent versus ionic bonding [8].



One unique aspect of anionic polymerization is that the reactive propagating species are not transient intermediates. Carbanions and organometallic species can be prepared and investigated independently of the polymerization process. These species can also be characterized and monitored during the polymerization.

7.2 LIVING ANIONIC POLYMERIZATION

One of the most important advances in the science and technology of anionic polymerization was the report in 1956 by Michael Szwarc and coworkers delineating the characteristics of living anionic polymerizations, that is, that they proceed in the absence of the kinetic steps of chain transfer

and chain termination [9, 10]. The most recent IUPAC definition of a living polymerization is a chain polymerization in which chain termination and irreversible intermolecular chain transfer are absent [1]; it should be noted that chain termination is defined as a chemical reaction in which a chain carrier is converted *irreversibly* into a nonpropagating species without the formation of a new chain carrier. The importance of living polymerizations is that they provide methodologies for the synthesis of polymers with control of the major variables that affect polymer properties including molecular weight, molecular weight distribution, copolymer composition and microstructure, stereochemistry, chain-end functionality, and molecular architecture [3, 11]. This inherent control aspect of living anionic polymerization stimulated tremendous industrial research activity which led to the development of numerous technologies for the preparation of important commodity and specialty materials [3]. Today, anionic polymerization is used for the commercial production of more than three million tons of polymers annually, including polybutadiene, polyisoprene, styrene-butadiene rubber (SBR), and styrene-diene-styrene triblock copolymers plus their hydrogenated analogs [12].

A general mechanism for living anionic polymerization of a vinyl monomer is illustrated in Scheme 7.1, encompassing only initiation and propagation steps; chains are terminated only by the deliberate addition of a Bronsted acid or an electrophile. Important aspects of this mechanism, and that of any living polymerization, are that one initiator generates one polymer chain and that the product after all of the monomer has been consumed is a polymer

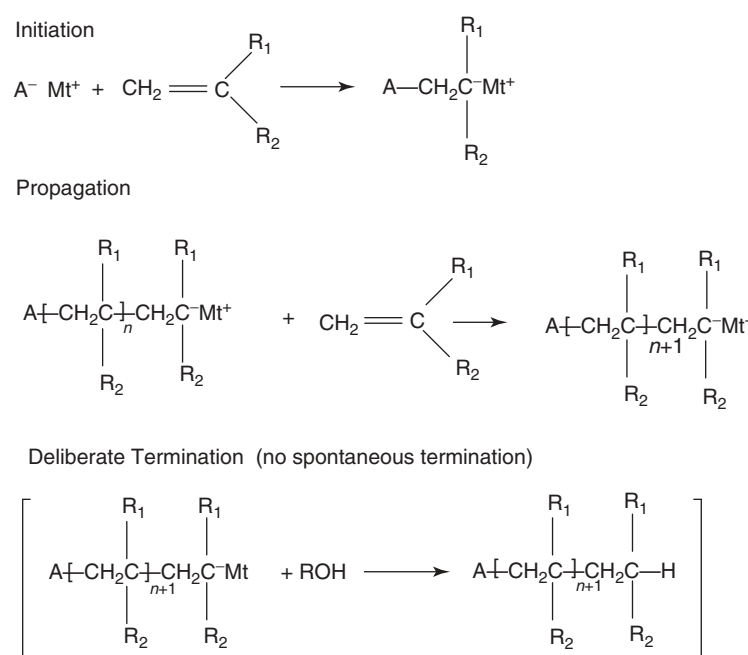
with an active anionic chain end. With this mechanism, the defining characteristics of living polymerizations with respect to the synthesis of a wide variety of polymers with low degrees of compositional heterogeneity can be understood.

7.2.1 Molecular Weight Control

Molecular weight is one of the most important variables affecting polymer properties. The number average molecular weight (M_n) in living anionic polymerization is a simple function of the stoichiometry and the degree of monomer conversion, since one polymer is formed for each initiator molecule. The expected M_n can be calculated as shown in Equation 7.3 as a function of monomer conversion. From a practical point of view, polymers can be prepared with predictable molecular weights ranging from $\approx 10^3$ to $> 10^6$ g/mol using living anionic polymerizations.

$$M_n = \frac{\text{Grams of monomer consumed}}{\text{Moles of initiator}} \quad (7.3)$$

The ability to predict and control molecular weight depends critically on the absence of significant amounts of terminating species that react with the initiator, decrease the effective number of initiator molecules, and thus increase the observed molecular weight relative to the calculated molecular weight. In many cases, the impurities react quickly with initiators, especially alkylolithium initiators, so that molecular weight control can still be achieved by determining the impurity level and compensating for this



Scheme 7.1 General mechanism for a living anionic polymerization.

by the addition of more initiator than the stoichiometric amount, Equation 7.3.

7.2.2 Molecular Weight Distribution

In principle, it is possible to prepare a polymer with a narrow molecular weight distribution (Poisson distribution) using living polymerization when the rate of initiation is competitive with or faster than the rate of propagation and monomer addition is irreversible [14, 15]. This condition ensures that all of the chains grow for essentially the same period of time. The relationship between the polydispersity and the degree of polymerization for a living polymerization is shown in Equation 7.4; the second approximation is valid for high molecular weights [13]. The Poisson distribution represents the ideal limit for termination-free polymerizations. Thus, it is predicted that the molecular weight distribution will decrease with increasing molecular weight for a living polymerization system. Broader molecular weight distributions are obtained using less active initiators, with mixtures of initiators, or with continuous addition of initiator as involved in a continuous-flow stirred-tank reactor. Thus, living polymerizations can form polymers with broader molecular weight distributions. It has been proposed that a narrow molecular weight distribution (monodisperse) polymer should exhibit $M_w/M_n \leq 1.1$ [16]. Molecular weight distribution affects melt viscosity and processing characteristics of polymers [17].

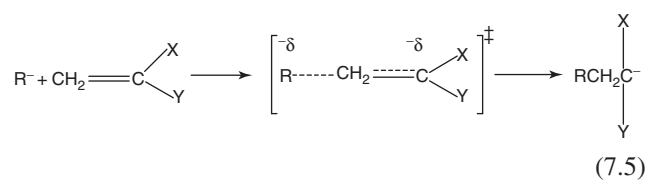
$$\frac{X_w}{X_n} = 1 + \left[\frac{X_n}{(X_n + 1)^2} \right] \approx 1 + \left[\frac{1}{X_n} \right] \quad (7.4)$$

7.3 GENERAL CONSIDERATIONS

7.3.1 Monomers

Two broad types of monomers can be polymerized anionically: vinyl, diene, and carbonyl-type monomers with difunctionality provided by one or more double bonds; and cyclic (e.g., heterocyclic) monomers with difunctionality provided by a ring that can open by reaction with nucleophiles. For vinyl monomers, it is generally considered that there must be substituents on the double bond that can stabilize the negative charge that develops in the transition state for monomer addition as shown in Equation 7.5. These substituents must also be stable to the anionic chain ends; thus, relatively acidic, proton-donating groups (e.g., amino, hydroxyl, carboxyl, acetylene functional groups) or strongly electrophilic functional groups (e.g., cyano, carbonyl, nitro, sulfonyl) that can react with bases and nucleophiles must not be present or must be protected by conversion to a suitable derivative. In general, substituents that stabilize negative charge by anionic charge

delocalization render vinyl monomers polymerizable by an anionic mechanism. Such substituents include aromatic rings, double bonds, as well as carbonyl, ester, cyano, sulfoxide, sulfone, and nitro groups. The general types of monomers that can be polymerized anionically without the incursion of termination and chain transfer reactions include styrenes, styrenes with stable or protected functional groups [14, 18–20], vinylaromatics, dienes (e.g., 1,3-butadiene and isoprene), alkyl methacrylates, vinylpyridines, aldehydes, epoxides, episulfides (thiiranes), cyclic siloxanes, lactones, and lactams. Monomers with polar substituents such as carbonyl, cyano, and nitro groups often undergo side reactions with initiators and propagating anions; therefore, controlled anionic polymerization to provide high molecular weight polymers is generally not possible. Many types of polar monomers can be polymerized anionically, but do not produce living, stable, carbanionic chain ends. These types of polar monomers include acrylonitriles, propylene oxide, vinyl ketones, acrolein, vinyl sulfones, vinyl sulfoxides, vinyl silanes, halogenated monomers, ketenes, nitroalkenes, and isocyanates.



The simplest vinyl monomer, ethylene, although it has no stabilizing moiety, can be polymerized by an anionic mechanism using butyllithium complexed with *N,N,N',N'*-tetramethylethylenediamine (TMEDA) as a complexing ligand [20, 21]. The conversion of a double bond to two single bonds provides the energetic driving force for this reaction. Because of the insolubility of the crystalline high density polyethylene formed by anionic polymerization, the polymer precipitates from solution during the polymerization.

Although cyclopropane itself is not anionically polymerizable, cyclopropanes with two electron-withdrawing groups on one of the ring carbons, for example, $-\text{CO}_2\text{R}$ or $-\text{CN}$ substitution, undergo anionic polymerization [22, 23]. Another anionically reactive monomer is trimethylvinylsilane [$\text{CH}_2=\text{CHSi}(\text{CH}_3)_3$] in which the silicon atom with available d orbitals can stabilize the resulting carbanion [24]. 4-Vinyltriphenylamine undergoes living alkylolithium-initiated polymerization to form a polymer of interest as a hole transport layer in light-emitting diodes [25]. The living polymerization of 4-vinylbenzocyclobutene using *sec*-butyllithium in benzene has been reported [26]. For some styrene monomers with potentially reactive functional groups, anionic polymerization can be effected in polar media (tetrahydrofuran (THF) [27] or THF/*N,N*-dimethylacetamide [28])

at low temperatures (-78°C), for example, 4-(4-(2-isopropenylphenoxy)butyl)styrene [27] and 4-cyanostyrene [28]. There has been renewed interest in the anionic polymerization of 1,3-cyclohexadiene, even though chain transfer and chain termination reactions can occur [29–33]. 1,3,5-Trienes such as *trans*-1,3,5-hexatriene can be polymerized by alkyllithium-initiated anionic polymerization, but it was not possible to eliminate branching reactions [34]. Monoaddition to poly(styryl)lithium was effected by addition of 1.2 equivalents of *trans*-1,3,5-hexatriene at -10°C in toluene to form the corresponding diene-functionalized macromonomer [35].

7.3.2 Solvents

The range of useful solvents for anionic polymerization is limited by the high reactivity (basicity and nucleophilicity) of the initiators and propagating carbanionic chain ends. For styrene and diene monomers, the solvents of choice are alkanes, cycloalkanes, aromatic hydrocarbons, and ethers [3, 36–38]; the use of alkenes has also been described, although some chain transfer can occur, especially at elevated temperatures and in the presence of Lewis bases [39]. Aromatic hydrocarbon solvents such as benzene and toluene provide enhanced rates of initiation and propagation relative to the alkanes [40]; however, chain transfer reactions can occur with alkylated aromatic solvents, for example, toluene and ethylbenzene [41, 42]. A useful alternative is *t*-butylbenzene which has no reactive benzylic hydrogens and has a much lower freezing point (-58°C), making it useful for low temperature processes [43].

Polar solvents such as ethers and amines react with organometallic initiators, as well as propagating polystyryl and polydienyl carbanions, to decrease the concentration of active centers [3, 44, 45]. The rate of reaction with ethers decreases in the order Li > Na > K. For example, dilute solutions of poly(styryl)lithium in THF at room temperature decompose at the rate of a few percent each minute. Alkyllithium initiators also react relatively rapidly with ethers; the order of reactivity of organolithium compounds with ethers is tertiary RLi > secondary RLi > primary RLi > phenyllithium > methylolithium > benzyllithium [44]. An approximate order of reactivity of ethers toward alkyllithium compounds is dimethoxyethane, THF > tetrahydropyran > diethyl ether > diisopropyl ether. Tertiary amines can also react with alkyllithium compounds. The importance of these reactions can be minimized by working at lower temperatures (e.g., $<0^{\circ}\text{C}$); it is also advisable to use only the minimum amounts of ethers and other Lewis bases required as additives.

For less reactive anionic chain ends such as those involved in propagation of heterocyclic monomers, a wider range of solvents can be utilized. For example, dipolar

aprotic solvents such as dimethylsulfoxide (DMSO), *N,N*-dimethylformamide (DMF), and hexamethylphosphoramide (HMPA) can be used for polymerizations of epoxides.

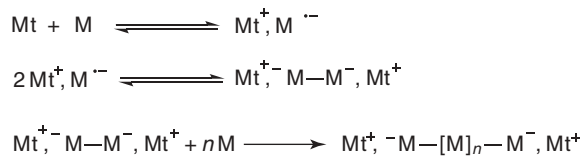
7.3.3 Initiators

The choice of a suitable initiator is essential for the preparation of polymers with well-defined structures and low degrees of compositional heterogeneity. A useful guide to choose an appropriate initiator for anionic polymerization of a given monomer is that the initiator should have a reactivity (stability) similar to that of the propagating anionic species, that is, the $\text{p}K_{\text{a}}$ of the conjugate acid of the propagating anion should correspond closely to the $\text{p}K_{\text{a}}$ of the conjugate acid of the initiating species [3, 46]. If the initiator is too reactive, then side reactions are promoted. If the initiator is relatively unreactive, the initiation reaction may be slow or inefficient. For example, the $\text{p}K_{\text{a}}$ values for the propagating carbanions in styrene and diene monomers are 43–44 [2]. Thus alkyl organometallic compounds with $\text{p}K_{\text{a}}$ values >56 are generally used as initiators for polymerizations of these monomers [3]. Initiators can be classified in terms of their mechanisms of initiation: (i) initiation by electron transfer (alkali and alkaline-earth metals and radical anions) and (ii) nucleophilic addition. The following sections discuss each of these initiator types.

7.3.3.1 Initiation by Electron Transfer

Alkali Metals The direct use alkali metals and alkaline-earth metals as initiators for anionic polymerization of diene monomers as first reported in 1910 is primarily of historical interest because these are uncontrolled, heterogeneous processes [4]. One of the most significant developments in anionic vinyl polymerization was the discovery reported in 1956 by Stavely and coworkers at Firestone Tire and Rubber Company that polymerization of neat isoprene with lithium dispersion produced high *cis*-1,4-polyisoprene, similar in structure and properties to *Hevea* natural rubber [47]. This discovery led to development of commercial anionic solution polymerization processes using alkyllithium initiators.

The mechanism of the anionic polymerization of styrenes and 1,3-dienes initiated by alkali metals has been described in detail by Szwarc [48]. Initiation is a heterogeneous process occurring on the surface of the metal (Mt) by reversible transfer of an electron to adsorbed monomer (M) as shown in Scheme 7.2. The initially formed radical anions (M^-) rapidly dimerize to form dianions. Monomer addition to these dianions forms adsorbed oligomers that desorb and continue chain growth in solution. This heterogeneous initiation reaction continues to generate new active chain ends during the course of the subsequent propagation reactions. Consequently, there is little control of molecular weight, and relatively broad molecular weight distributions

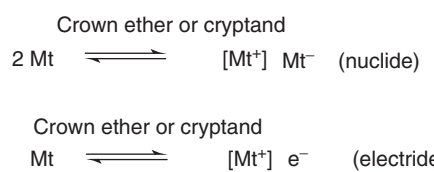


Scheme 7.2

have been reported for the soluble polymer obtained from these bulk polymerizations ($M_w/M_n = 3-10$) [47]; formation of a high degree of branching and gel content (45%) has also been reported for these processes [47, 49].

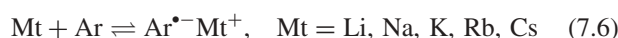
Alkali metals can dissolve in solvating media such as ethers and amines to form blue solutions of solvated electrons. In the presence of strongly complexing ligands such as crown ethers or cryptands, electrides (complexed alkali cation and electron), or nuclides (complexed alkali cation and alkali metal anion) can be formed as shown in Scheme 7.3 [50]. Nuclides have been shown to react with monomers such as styrene and methyl methacrylate (MMA) to form intermediate dianions that are rapidly protonated by the solvent THF to form the monoanion initiating species as shown in Scheme 7.4 [51, 52]. For the nuclide-initiated polymerization of MMA, although there was good agreement between calculated and observed molecular weights, the molecular weight distributions were broad ($M_w/M_n = 1.2-1.6$) [52].

Radical Anions Many aromatic hydrocarbons react reversibly with alkali metals in polar aprotic solvents to form



Scheme 7.3 Mechanism of metal-initiated anionic polymerization.

stable, homogeneous solutions of the corresponding radical anions as shown in Equation 7.6 [4, 48]. Radical anions can be formed efficiently only in polar aprotic solvents such as THF and glymes. Aromatic radical anions such as sodium naphthalene react with monomers such as styrene by reversible electron transfer to form the corresponding monomer radical anions as shown in Scheme 7.5 (R = H).



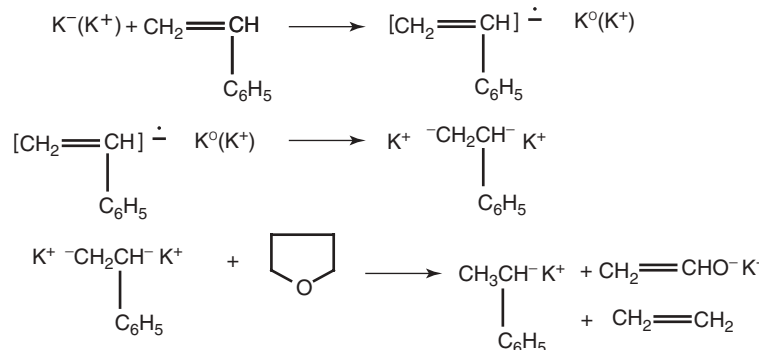
Although the equilibrium between the radical anion of the monomer and the aromatic radical anion lies far to the left because of the low electron affinity of the monomer, this is an efficient initiation process because the resulting monomer radical anions rapidly undergo head-to-head dimerization reactions with rate constants that approach diffusion control [53].

The reactions of monomers with aromatic radical anions or directly with alkali metals can be used to prepare oligomeric dianionic initiators from monomers such as α -methylstyrene which have accessible ceiling temperatures ($T_c = 61^\circ\text{C}$) as shown in Scheme 7.5 (R = CH₃) [54]. Dimers or tetramers can be formed depending on the alkali metal system, temperature, and concentration.

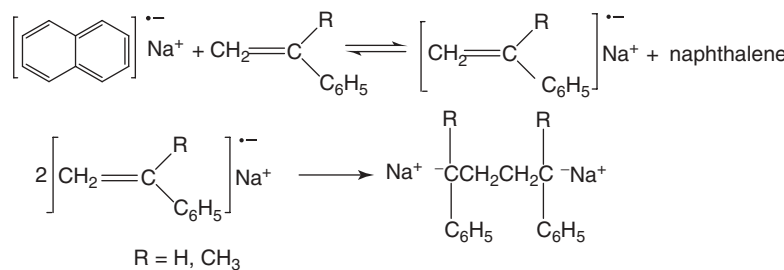
Monomers that can be polymerized with aromatic radical anions include styrenes, dienes, epoxides, thiiranes, and cyclosiloxanes. For epoxides and cyclosiloxanes, the mechanism of initiation involves nucleophilic addition of the radical anion to these monomers as shown in Scheme 7.6, in contrast to the electron transfer mechanism occurring for hydrocarbon monomers (Scheme 7.5) [45].

7.3.3.2 Initiation by Nucleophilic Addition

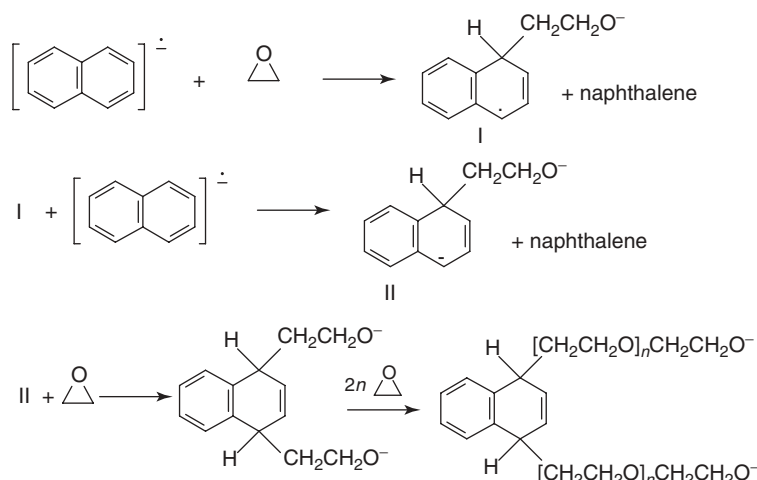
Alkyllithium Compounds Although anionic polymerization of vinyl monomers can be effected with a variety of organometallic compounds, alkyllithium compounds are the most useful class of initiators [3, 44, 46, 45, 55]. A variety of simple alkyllithium compounds are readily available commercially in hydrocarbon solvents such as hexane and



Scheme 7.4



Scheme 7.5 Initiation mechanism with aromatic radical anions by electron transfer.



Scheme 7.6 Radical anion initiation by addition.

cyclohexane. They can be prepared by reaction of the corresponding alkyl chlorides with lithium metal.

Alkyllithium compounds are generally associated into dimers, tetramers, or hexamers in hydrocarbon solution [3, 44]. The degree of association is related to the steric requirements of the alkyl group, that is, the degree of association decreases as the steric requirements of the alkyl group increase.

The relative reactivities of alkyllithiums as polymerization initiators are intimately linked to their degree of association as shown below with the average degree of association in hydrocarbon solution, where known, indicated in parentheses after the alkyllithium compound [44, 55, 56]:

Styrene Polymerization Menthyllithium (2) > *sec*-BuLi (4) > *i*-PrLi (4–6) > *i*-BuLi > *n*-BuLi (6) > *t*-BuLi (4)

Diene Polymerization Menthyllithium (2) > *sec*-BuLi (4) > *i*-PrLi (4–6) > *t*-BuLi (4) > *i*-BuLi > *n*-BuLi (6)

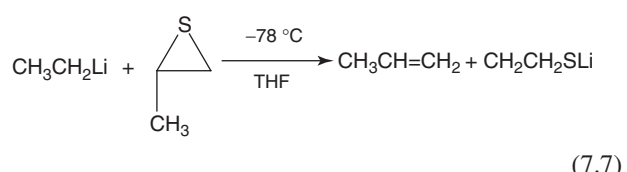
In general, the less associated alkyllithiums are more reactive as initiators than the more highly associated species.

Alkyllithium initiators are primarily used as initiators for polymerizations of styrenes and dienes. They effect quantitative living polymerization of styrenes and dienes in hydrocarbon solution. In general, these alkyllithium initiators are too reactive for alkyl methacrylates and vinylpyridines. *n*-Butyllithium is used commercially to initiate anionic homopolymerization and copolymerization of butadiene, isoprene, and styrene with linear and branched structures. Because of its high degree of association (hexameric), *n*-butyllithium-initiated polymerizations are often effected at elevated temperatures ($>50^\circ\text{C}$) and in the presence of small amounts of Lewis base to increase the rate of initiation relative to propagation and thus obtain polymers with narrower molecular weight distributions [55, 57].

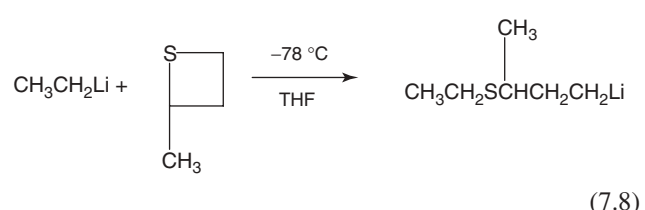
sec-Butyllithium is used commercially to prepare styrene-diene block copolymers because it can initiate styrene polymerization rapidly compared to propagation so that even polystyrene blocks with relatively low molecular weights (10,000–15,000 g/mol) can be prepared with stoichiometric control and narrow molecular weight distributions.

Alkyllithiums react quite differently with cyclic sulfides compared to the normal nucleophilic ring-opening

reaction with epoxides [58, 59]. Ethyllithium reacts with 2-methylthiacyclopropane to generate propylene and lithium ethanethiolate, Equation 7.7. The resulting lithium ethanethiolate is capable of initiating polymerization of 2-methylthiacyclopropane. In contrast, ethyllithium reacts with

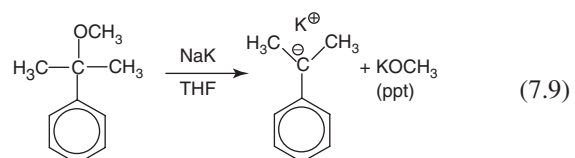


2-methylthiacyclobutane, Equation 7.8, to form an alkyl-lithium product that is capable of initiating polymerization of styrene.



Organoalkali Initiators In general, the simple organoalkali metal derivatives other than lithium are not soluble in hydrocarbon media. However, higher homologs of branched hydrocarbons are soluble in hydrocarbon media. The reaction of 2-ethylhexyl chloride and sodium metal in heptane produces soluble 2-ethylhexylsodium [60]. This initiator copolymerizes mixtures of styrene and butadiene to form styrene-butadiene copolymers with high (55–60%) vinyl microstructure [61, 62].

Cumyl potassium ($\text{p}K_a \approx 43$ based on toluene) [2] is a useful initiator for anionic polymerization of a variety of monomers, including styrenes, dienes, methacrylates, and epoxides. This carbanion is readily prepared from cumyl methyl ether as shown in Equation 7.9, and is generally used at low temperatures in polar solvents such as THF [63].



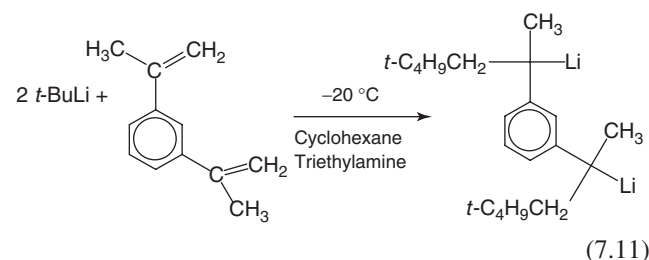
Organoalkaline-Earth Initiators Both styrene and 1,3-dienes can be polymerized by organoalkaline-earth metal compounds, specifically those of magnesium, calcium, barium, and strontium. In general, hydrocarbon-soluble benzyl, 1,1-diphenylalkyl and triphenylmethyl derivatives have been investigated. For example, the adduct of 1,1-diphenylethylene (DPE) with dibenzylbarium, that is, bis(1,1,3-triphenylpropyl)barium, is hexane-soluble and polymerizes styrene with controlled molecular

weight, but the molecular weight distribution was broad ($M_w/M_n = 1.20$) [64]. Broad molecular weight distributions are typical for these initiators for both styrene and butadiene polymerizations and has been ascribed to slow rates of initiation relative to propagation [65]. Hydrocarbon-soluble *n,s*-dibutylmagnesium is not an active initiator for styrenes and dienes in cyclohexane.

Ate Complexes Alkyllithium compounds interact with organometallic compounds of different metals (MtR'_n), most notably those of groups I, II, and II which behave like Lewis acids, to form mixed organometallic compounds, referred to as “ate” complexes, schematically represented in Equation 7.10 [66]. However, X-ray and nuclear magnetic resonance (NMR) investigations indicate the formation of more complex, stoichiometry-dependent types of structures involving bridging alkyl groups between the two types of metal centers for aluminum, magnesium, and zinc systems [67, 68]. The importance of these mixed organometallic species is that they dramatically attenuate the reactivity of the chain ends so that controlled polymerizations can be effected at higher temperatures and with higher monomer concentrations, that is, “retarded” polymerizations [69].

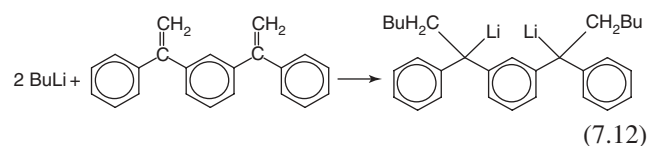


Difunctional Initiators The methodology for preparation of hydrocarbon-soluble dilithium initiators is generally based on the reaction of an aromatic divinyl precursor with two mol of butyllithium. Unfortunately, because of the tendency of organolithium chain ends in hydrocarbon solution to associate and form electron-deficient dimeric, tetrameric, or hexameric aggregates, most attempts to prepare dilithium initiators in hydrocarbon media have generally resulted in the formation of insoluble three-dimensionally associated species [70]. The reaction of *meta*-diisopropenylbenzene with 2 mol of *t*-butyllithium in the presence of 1 equivalent of triethylamine in cyclohexane at -20°C has been reported to form pure diadduct without oligomerization, Equation 7.11 [71]. This initiator in the presence of 5 vol% of diethyl ether for the butadiene block has been used to prepare well-defined poly(methyl methacrylate)-*b*-polybutadiene-*b*-poly(methyl methacrylate).



The reaction of pure *m*-divinylbenzene (DVB) with *sec*-butyllithium in toluene at -49°C in the presence of triethylamine ($[\text{Et}_3\text{N}]/[\text{Li}] = 0.1$) has been reported to produce the corresponding dilithium initiator in quantitative yield [72]. Polymerization of butadiene with this initiator in toluene at -78°C produced well-defined polybutadiene with high 1,4-microstructure (87%).

The addition reaction of 2 mol of *sec*-butyllithium with 1,3-bis(1-phenylethenyl)benzene, Equation 7.12, proceeds rapidly and efficiently to produce the corresponding dilithium species that is soluble in toluene or in cyclohexane [46, 73]. Although this dilithium initiator is useful for the preparation of homopolymers and triblock copolymers with relatively narrow molecular weight distributions, it is necessary to add a small amount of Lewis base or 2 or more equivalents of lithium alkoxide (e.g., lithium *sec*-butoxide) to produce narrow, monomodal molecular weight distributions.

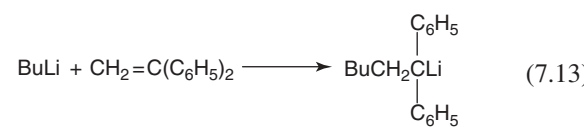


The reaction of multifunctional aryl bromides with several equivalents of *sec*-butyllithium has been reported to form multifunctional organolithium initiators that are soluble in hydrocarbon solvent as shown in Scheme 7.7 [74, 75]. It should be noted that this procedure requires 2 extra equivalents of *sec*-butyllithium to react with the 2 mol of *sec*-butyl bromide that is formed by lithium–halogen exchange. This initiator was used to prepare triblock copolymers containing polybutadiene center blocks with high 1,4-microstructure and which exhibited good tensile properties (>900% elongation, circa 30 MPa tensile strength at break). [74]

Functionalized Initiators Alkyllithium initiators that contain functional groups provide versatile methods for the preparation of end-functionalized polymers and macromonomers [76–78]. For a living anionic polymerization, each functionalized initiator molecule will produce one macromolecule with the functional group from the initiator residue at one chain end and the active anionic propagating species at the other chain end. However, many functional groups such as hydroxyl, carboxyl, phenol, and primary amine are not stable in the presence of reactive dienyllithium and styryllithium chain ends. Therefore, it is necessary to convert these functional groups into suitable derivatives, that is, protected groups, that are stable to the carbanionic chain ends and that can be removed readily after the polymerization. Examples of protected functional initiators include the hydroxyl-protected initiators, 6-lithiohexyl acetaldehyde acetal, 6-(*t*-butyldimethylsiloxy)-hexyllithium, and 3-(*t*-butyldimethylsiloxy)propyllithium

as well as a primary amine-protected initiator, 4-bis(trimethylsilyl)aminophenyllithium [76].

1,1-Diphenylmethyl Carbanions The carbanions based on diphenylmethane ($\text{p}K_a = 32$) [2] are useful initiators for vinyl and heterocyclic monomers, especially alkyl methacrylates at low temperatures [78]. 1,1-Diphenylalkyllithiums can also efficiently initiate the polymerization of styrene and diene monomers that form less stable carbanions. Diphenylmethylolithium can be prepared by the metallation reaction of diphenylmethane with butyllithium or by the addition of butyllithium to DPE as shown in Equation 7.13. This reaction can also be utilized to prepare functionalized initiators by reacting butyllithium with a substituted DPE derivative [78]. Addition of lithium salts such as lithium chloride, lithium *tert*-butoxide, or lithium 2-(2-methoxyethoxy)ethoxide with 1,1-diphenylmethylcarbanions and other organolithium initiators has been shown to narrow the molecular weight distributions and to improve the stability of active centers for anionic polymerization of both alkyl methacrylates, *tert*-butyl acrylate, and 2-vinylpyridine [79–81].



7.4 KINETICS AND MECHANISM OF POLYMERIZATION

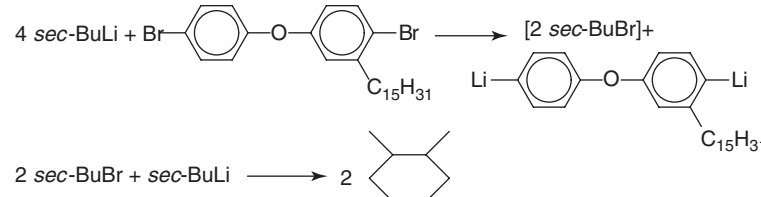
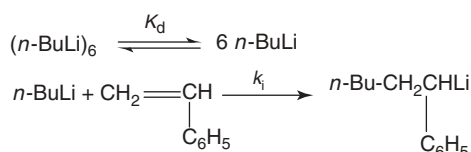
7.4.1 Styrene and Diene Monomers

7.4.1.1 Hydrocarbon Solvents

Initiation The mechanism of initiation of anionic polymerization of vinyl monomers with alkyllithium compounds and other organometallic compounds is complicated by association and cross-association phenomena in hydrocarbon solvents and by the presence of a variety of ionic species in polar media [3, 4, 45, 48, 55, 56]. The kinetics of initiation is complicated by competing propagation and the occurrence of cross-association of the alkyllithium initiator with the propagating organolithium [55]. Thus, only the initial rates provide reliable kinetic data.

Typical kinetics of the initiation reaction of *n*-butyllithium with styrene in benzene exhibits a first-order dependence on styrene concentration and approximately a one-sixth order dependence on *n*-butyllithium concentration as shown in Equation 7.14.

$$R_i = k_i \left(\frac{K_d}{6} \right)^{1/6} [\text{BuLi}]_o^{1/6} [\text{M}] \quad (7.14)$$

**Scheme 7.7** Synthesis of diaryllithium-based difunctional initiator.**Scheme 7.8** Mechanism of styrene initiation with *n*-butyllithium in hydrocarbon solution.

Since *n*-butyllithium is aggregated predominantly into hexamers in hydrocarbon solution [44], the fractional kinetic order dependency of the initiation process on the total concentration of initiator has been rationalized on the basis that unassociated *n*-butyllithium is the initiating species and that it is formed by the equilibrium dissociation of the hexamer as shown in Scheme 7.8.

The kinetic order for *sec*-butyllithium-initiated polymerization of styrene is close to 0.25 in benzene solution; this result is also consistent with initiation by unassociated *sec*-butyllithium, since *sec*-butyllithium is associated predominantly into tetramers in benzene solution [44]. The experimentally observed energy of activation (18 kcal/mol) for *n*-BuLi/styrene initiation [56] appears to be too low to include the enthalpy of complete dissociation of the aggregates, estimated to be 108 kcal/mol [82]. An alternative mechanism is the incomplete or stepwise dissociation of the aggregate [3].

The observed inverse correlation between reaction order dependence for alkylolithium and degree of alkylolithium aggregation is not observed in aliphatic solvents. The use of aliphatic solvents leads to decreased rates of initiation and pronounced induction periods. In fact, a different reaction mechanism involving the direct addition of monomer with aggregated organolithium species has been proposed for aliphatic solvents [3, 56].

The actual complexity of these initiation events has been documented by combined ¹H NMR and small-angle neutron scattering studies of the *t*-butyllithium-initiated polymerization of butadiene in heptanes at 8 °C, which revealed the presence of coexisting large-scale aggregates (*n* ≈ 100; ≤1 wt%) and smaller aggregates during all stages of the polymerization, that is, initiation and propagation [83, 84]. The average degree of aggregation decreased from *n* ≈ 140 at the beginning of initiation/polymerization process and leveled off at circa 4 with increasing chain

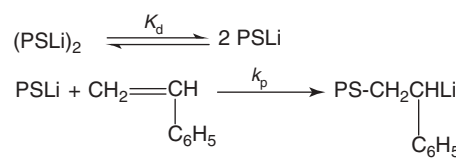
length. It was stated that for the lower aggregation numbers (circa 4) the structure of the aggregates is star-like and in agreement with the traditional mechanism (see diene propagation section) [83].

Propagation The anionic propagation kinetics for styrene (S) polymerization with lithium as counterion is relatively unambiguous. The reaction in monomer concentration is first order, as it is for polymerization of all styrene and diene monomers in heptane, cyclohexane, benzene, and toluene [3, 55, 56]. The reaction order dependence on total chain-end concentration, [PSLi]_o, is one-half as shown in Equation 7.15. The observed one-half kinetic order dependence on chain-end concentration is consistent with the fact that poly(styryl)lithium is predominantly associated into dimers in hydrocarbon solution [85, 86]. If the unassociated poly(styryl)lithium is the reactive entity for

$$R_p = -\frac{d[S]}{dt} = k_{obs}[PSLi]_o^{1/2}[S] \quad (7.15)$$

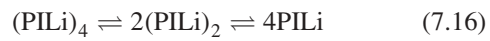
monomer addition, assuming that the aggregate is a dormant species, a simple dissociative mechanism can be invoked, Scheme 7.9. This mechanism leads to the kinetic equation (Eq. 7.15).

Elucidation of the mechanism of propagation for isoprene and butadiene in hydrocarbon solution with lithium as counterion in the past has been complicated by disagreement in the literature regarding both the kinetic order dependence on chain-end concentration and the degree of association of the chain ends, as well as by apparent changes in kinetic reaction orders with chain-end concentration [3, 56]. For butadiene and isoprene propagation, reported reaction order dependencies on the concentration of poly(dienyl)lithium chain ends include 0.5, 0.33, 0.25, and 0.167. Kinetic studies of isoprene propagation with lithium as counterion in hydrocarbon solvents showed

**Scheme 7.9** Mechanism of styrene propagation for poly(styryl) lithium.

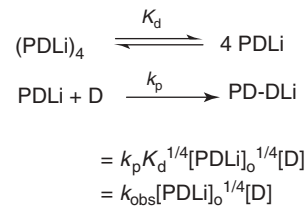
that the kinetic order dependence on chain-end concentration changed from 0.5 to either 0.25 or 0.17 as the chain-end concentration was varied from 10^{-2} to 10^{-6} mol/l [3, 87, 88]. Comparison of these kinetic orders with the degrees of association of the poly(dienyl)lithium chain ends had been complicated by the lack of agreement regarding the predominant degree of association of these species in hydrocarbon solution. However, recent evaluation of the association states of poly(dienyl)lithium chain ends in benzene by small-angle neutron scattering, as well as by dynamic and static light scattering, indicates that predominantly tetrameric aggregates are in equilibrium with small amounts of higher order aggregates ($n > 100$) [83, 89–94]. Thus, the 0.25 kinetic order dependence on poly(dienyl)lithium chain-end concentration can be interpreted in terms of the predominantly tetrameric degree of aggregation as shown by the mechanism in Scheme 7.10.

The observation of concentration dependence of the reaction order (increasing from 0.25 to 0.5 (when $[PILi] < 5 \times 10^{-5}$ mol/l) with decreasing concentration of poly(isoprenyl)lithium in benzene can be explained in terms of the intermediacy of a dimeric association state as shown in Equation 7.16 [87].

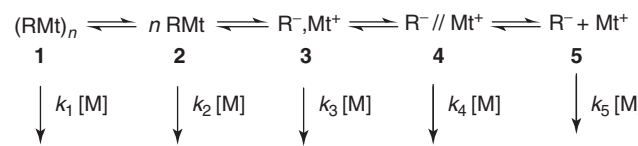


7.4.1.2 Polar Solvents A change in the reaction medium from hydrocarbon to polar solvents causes changes in the nature of the alkali metal carbanions, which can be interpreted in terms of the Winstein spectrum of ionic species as shown in Scheme 7.11 [3, 6]. Thus, in addition to the aggregated (**1**) and unaggregated (**2**) species that can exist in hydrocarbon solution, in polar solvents it is necessary to consider the intervention of free ions (**5**) and the contact (**3**) and solvent-separated (**4**) ion-paired carbanion species as propagating species as shown in Scheme 7.11.

In general, as the polarity (dielectric constant) and solvating ability of the medium increase, a transition to more ionic species (a shift in the Winstein spectrum from left to right) occurs. In weakly polar solvents such as dioxane ($\epsilon = 2.21$), the kinetics of styrene propagation exhibits pseudo-first-order behavior as illustrated in Equation 7.17,



Scheme 7.10 Kinetics and mechanism for poly(dienyl)lithium propagation.



Scheme 7.11 Possible reactive entities involved in propagation in polar solvents.

where k_{obs} is the observed pseudo-first-order rate constant, k_p is the propagation rate constant and PS^-Mt^+ represents the concentration of carbanionic chain ends that does not change for a living polymerization [48]. The values of k_p can be obtained by

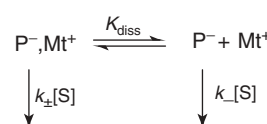
$$-\frac{d[S]}{dt} = k_{obs}[S] = k_p [PS^-Mt^+] [S] \quad (7.17)$$

plotting k_{obs} versus $[PS^-Mt^+]$. The order of reactivity (rate constants in brackets are in units of l/(mol s)) of alkali metal counterions is $Li^+ [0.9] < Na^+ [3.4–6.5] < K^+ [19–27] Rb^+ [21.5–34] < Cs^+ [15–24.5]$ [48]. The trend of increasing reactivity with increasing ionic radius, also observed in hydrocarbon solution, has been taken as evidence for contact ion pairs as the reactive propagating species. Similar behavior has been observed for isoprene polymerization in diethyl ether ($\epsilon = 4.34$) [95].

In more polar solvents such as THF ($\epsilon = 7.6$), a concentration dependence was observed for the plots of k_{obs} versus $[PS^-Mt^+]$, that is, k_p exhibits a linear dependence on $(1/[PS^-Mt^+])^{1/2}$ [48, 96–98]. This dependence has been interpreted in terms of the participation of both ion pairs and free ions as active propagating species as shown in Scheme 7.12, where k_{\pm} is the propagation rate constant for the ion pair species, k_- is the propagation rate constant for the free ion, and K_{diss} is the equilibrium constant for dissociation of ion pairs (P_{\pm}) to free ions (P_-). The corresponding rate expression for this system is shown in Equation 7.18.

$$-\frac{d[S]}{dt} = [S] (k_{\pm} [P_{\pm}] + k_- [P_-]) \quad (7.18)$$

Assuming that K_{diss} is small, then the concentration of ion-paired species can be assumed to be approximately equal to $[PMt]_{total}$ and the concentration of free ions can



Scheme 7.12 Participation of ion pairs and free ions for the mechanism of anionic propagation in polar solvents such as THF.

be calculated using the dissociation equilibrium constant as in Equation 7.19.

$$[P_-] = K_{\text{diss}}^{1/2} [PMt]_{\text{total}}^{1/2} \quad (7.19)$$

Substituting this expression for the concentration of free ions into the rate equation generates the final rate expression as shown in Equation 7.20.

$$-\frac{d[S]}{dt} = [M] \left(k_{\pm} [PMt]_{\text{total}} + k_- K_{\text{diss}}^{1/2} [Mt]_{\text{total}}^{1/2} \right) \quad (7.20)$$

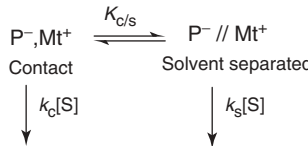
The corresponding expression for k_p is shown in Equation 7.21, recognizing that this k_p is only an apparent propagation rate constant (Eq. 7.16).

$$k_p = \frac{k_{\pm} + k_- K_{\text{diss}}^{1/2}}{[PMt]_{\text{total}}^{1/2}} \quad (7.21)$$

From plots of the apparent propagation rate constant versus $1/[P^- Mt^+]^{1/2}$, the slope corresponds to $k_- K_{\text{diss}}^{1/2}$ and the intercept is k_{\pm} ; the results are shown in Table 7.1 [48, 97–99]. It is observed that the slopes of the lines decrease as the cation size increases from lithium to cesium. Since k_- is independent of the cation, the variation of the slope with counterion reflects a decrease in K_{diss} (Scheme 7.12) as the counterion size increases. It is also observed that k_{\pm} also decreases with increasing cation size. Thus, the order of reactivity of alkali metal counterions in THF is $\text{Li}^+ > \text{Na}^+ > \text{K}^+ > \text{Rb}^+ > \text{Cs}^+$, the inverse of the order observed in the less polar solvent, dioxane, or in hydrocarbon solution. This order is in accord with expectations based on cation solvation energies, which decrease with increasing cation size. Values of the propagation rate constant for free styryl anions are relatively insensitive to solvent; the values for k_- are 6.5×10^4 and $4.0 \times 10^4 \text{ l/(mol s)}$ at 25°C in THF and in dimethoxyethane, respectively [48]. Even though free ions are present in small amounts (Table 7.1), their contribution to the overall rate of polymerization is significant because of their much higher reactivity.

TABLE 7.1 Equilibrium Dissociation Constants of Organoalkali Metal Salts of Polystyryl Carbanions and the Propagation Rate Constants for the Corresponding Ion Pairs and Free Ions in THF at 25°C [48, 97–99]

Countercation	$10^7 K_{\text{diss}}$ (mol/l)	k_{\pm} (l/(mol s))	$10^{-4} k_-$ (l/(mol s))
Li^+	1.9–2.2	160	—
Na^+	1.5	80	6.5
K^+	0.7–0.77	≈60	—
Rb^+	0.10	≈50	—
Cs^+	0.02–0.047	22	6.3



Scheme 7.13 Participation of both contact and solvent-separated ion pairs for the mechanism of anionic propagation in polar solvents such as THF.

Although normal Arrhenius behavior was observed for k_- , anomalous increases of k_{\pm} with decreasing temperature were observed in polar solvents such as THF and dimethoxyethane (glyme) [97–99]. These results have been explained in terms of a temperature-dependent equilibrium between contact and solvent-separated ion pairs as shown in Scheme 7.13. This equilibrium shifts from the less reactive contact ion pairs (k_c) to the much more reactive solvent-separated ion pairs (k_s) as temperature is decreased because the contribution from the unfavorable (negative) entropy of dissociation ($T\Delta S_{c/s}$) decreases and the enthalpy of dissociation ($\Delta H_{c/s}$) is negative. The values of k_c and k_s are not very dependent upon solvent, but the equilibrium constants $K_{c/s}$ are very dependent on the polarity of the solvent (Table 7.2). It is noteworthy that the reactivity of the solvent-separated ion pairs approaches that of the free ions. These results also provide a rationalization for the effect of counterion on k_{\pm} . Smaller cations such as lithium interact more strongly with solvent and form significant amounts of more reactive, solvent-separated ion pairs.

7.4.1.3 Termination Reactions The categorization of a given polymerization system as living is based on results obtained on the laboratory time scale, that is, the absence of chain termination or chain transfer reactions occurring within the normal time required to complete the polymerization and carry out any subsequent chemical reactions with the active carbanionic polymer chain ends [3, 1, 100]. In fact, the amount of spontaneous termination reactions in typical alkylolithium-initiated polymerizations of styrene and diene monomers depends on time, temperature, and whether polar additives are present [3, 101, 102].

Polymeric organolithium compounds exhibit good stability in hydrocarbon solutions at ambient temperatures and for short periods at elevated temperatures [101, 102]. The principal mode of decomposition is loss of lithium hydride to form a double bond at the chain end as illustrated in Equation 7.22 for poly(styryl)lithium.

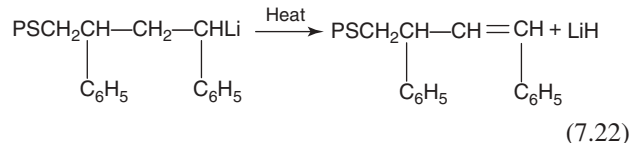


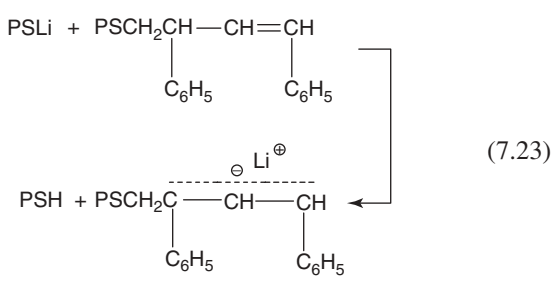
TABLE 7.2 Ion Pair Rate Constants for Anionic Polymerization of Poly(styryl)sodium in Ethereal Solvents and the Equilibrium Constant and Thermodynamic Parameters for Ion Pair Equilibrium [48]

Solvent	k_c (l/(mol s))	$10^{-4}k_s$ (l/(mol s))	$K_{c/s}$ (25 °C)	$\Delta H_{c/s}$ (kcal/mol)	$\Delta S_{c/s}$ (e.u.)
DME	12.5	5.5	0.13	-5.5	-22.5
THF	34	2.4	2.25×10^{-3}	-6.5	-34
3-Me-THF	20	12.4	5.8×10^{-4}	-5.1	-32
THP	10.7	5.3	1.3×10^{-4}	-3.0	-28
Dioxane	5.5	—	$<10^{-5}$	—	—

Abbreviations: DME, 1,2-dimethoxyethane; 3-Me-THF, 3-methyltetrahydrofuran; THP, tetrahydropyran.

Poly(styryl)lithium exhibits good stability over the duration of the polymerizations and beyond, that is, days, at ambient temperatures in hydrocarbon media. However, at elevated temperatures, it is observed that the initial UV absorption intensity at 334 nm decreases and a new absorption is observed at 450 nm, which is assigned to a 1,3-diphenylallyllithium species as shown in Equation 7.23 [101].

The rate constant for spontaneous decomposition was reported to be 40×10^{-6} s⁻¹ at 65 °C in cyclohexane [101, 103]. The rate of decomposition of PSLi in cyclohexane at 150 °C is 0.205 min⁻¹, corresponding to a 3.5-min half-life [104]. In the presence of 2 equivalents of *n*,*sec*-dibutylmagnesium at 100 °C, the rate of decomposition of PSLi is 1.9×10^{-5} min⁻¹ while it is 6.4×10^{-4} in the absence of additive, corresponding to half-lives of 102 and 3 h, respectively [105]. Similar decomposition reactions have been observed for poly(styryl)sodium [102]. The thermal stability of poly(α -methylstyryl)lithium is much lower than that of poly(styryl)lithium. The observed half-lives for spontaneous termination are 5 h and a few minutes at 25 and 60 °C, respectively [106]. The relative thermal stability of styryl carbanionic chain ends follows the order K ≫ Na > Li for the alkali metal counterions.

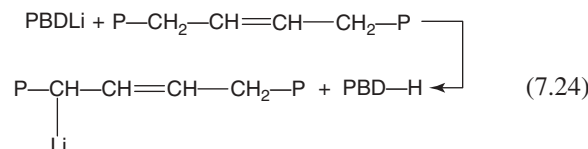


The carbanionic active centers based on 1,3-butadiene and isoprene with lithium as counterion generally possess good stability in hydrocarbon solvents at ambient temperatures. However, poly(dienyl)lithiums undergo complex decomposition reactions upon prolonged storage or heating at elevated temperatures. Poly(butadienyl)lithium in ethylbenzene exhibits an absorption maximum at 300 nm, which

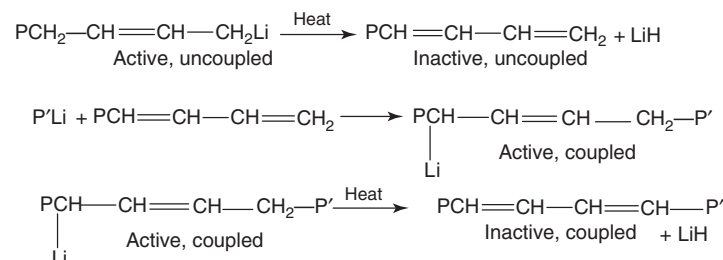
gradually decreases in intensity with the formation of absorption tails between 350 and 500 nm [101]. Approximately 20% of the active centers were destroyed in less than 3 h at 100 °C in ethylbenzene [42]. The apparent first-order rate constant for decomposition of poly(butadienyl)lithium in hexane was estimated to be 1.9×10^{-5} s⁻¹ at 93 °C and a chain-end concentration of 2.2 milliequivalents of poly(butadienyl)lithium per 100 g of solution (25 wt% polymer) [103]. The corresponding first-order rate constant for chain-end decomposition of poly(isoprenyl)lithium at 93 °C was estimated to be 6.7×10^{-5} s⁻¹ [103]. Although the differences are not large, the relative order of increasing stabilities of chain ends toward thermal degradation is poly(α -methylstyryl)lithium ≪ poly(styryl)lithium < poly(isoprenyl)lithium < poly(butadienyl)lithium as estimated by chain-end titration data.

Size-exclusion chromatography (SEC) analyses of the thermal decomposition products of poly(dienyl)lithiums in heptane at 80 °C have shown that the chain-end decomposition is accompanied by formation of species that have double and triple the molecular weight of the original living polymer [107]. After heating for 46 h at 80 °C in heptane, a 12 wt% yield of coupled products was observed for poly(isoprenyl)lithium; after heating for 27 h at 80 °C in heptane, a 19 wt% yield of coupled products was observed for poly(butadienyl)lithium. Scheme 7.14 illustrates the type of reactions proposed to explain the formation of dimeric products.

Evidence also suggests that athermal metalation of the backbone can occur as shown in Equation 7.24. It would be expected that this in-chain metalation



coupled with elimination of lithium hydride would lead to in-chain diene units which would have even more reactive allylic hydrogens for further metalation–elimination–coupling sequences that would promote thermal decomposition, branching, and ultimately gel formation.



Scheme 7.14 Proposed mechanism for thermal decomposition reactions for poly(butadienyl) lithium.

Polymeric organolithium compounds exhibit limited stability in ether solvents similar to alkylolithium compounds. Living carbanionic polymers react with ether solvents such as THF in a pseudo-first-order decay process and the rate decreases in the order $\text{Li} > \text{Na} > \text{K}$. For example, a 10^{-5} M solution of poly(styryl)lithium in THF at 25°C exhibited a rate of decay of a few percent per minute, but poly(styryl)cesium was found to be exceptionally stable [96]. Metalation and decomposition reactions can also occur in the presence of amines such as TMEDA.

7.4.1.4 Chain Transfer Reactions Chain transfer reactions to polymeric organoalkali compounds can occur from solvents, monomers, and additives that have pK_a values lower than or similar to those of the conjugate acid of the carbanionic chain end [3]. Relatively few monomers that undergo anionic polymerization exhibit chain transfer to monomer. Chain transfer has been well documented for the anionic polymerization of 1,3-cyclohexadiene. The chain transfer constant (k_{tr}/k_p) was calculated to be 2.9×10^{-2} at 20°C and 9.5×10^{-3} at 5°C in cyclohexane [29]. Although chain transfer would be expected for *p*-methylstyrene, controlled polymerizations can be effected when the temperature is maintained at room temperature or below. The observations of broad molecular weight distributions and a low molecular weight tail by SEC analysis have provided evidence for chain transfer during the anionic polymerization of *p*-isopropyl- α -methylstyrene [108]. Significant chain transfer effects have also been reported for alkylolithium-initiated polymerizations using alkenes as solvents [3].

The kinetics of chain transfer to ammonia has been investigated for potassium amide-initiated polymerization of styrene in liquid ammonia at -33.5°C . The calculated chain transfer constant (k_{tr}/k_p) was 2.34×10^{-4} [109]. The chain transfer reaction of poly(styryl)lithium with toluene at 60°C was investigated during the polymerization of styrene using ^{14}C -labeled toluene. The calculated chain transfer constant (k_{tr}/k_p) was 5×10^{-6} [41]. A much larger chain transfer constant ($k_{tr}/k_p = 1.28 \times 10^{-4}$) was found for analogous transfer from toluene to poly(styryl)sodium. In general, alkylolithium-initiated anionic polymerizations of styrenes and dienes should not be carried out in toluene as

solvent because of the occurrence of chain transfer reactions [110]. Even after one day at 20°C , 13% of the PSLi undergoes chain transfer to toluene [110]. Ethylbenzene exhibits a chain transfer rate constant to PSLi of 2.2×10^{-5} l/(mol s) [111].

Allenes and alkynes are regarded as impurities whose concentration cannot exceed certain minimum levels in monomer feed streams [112]. However, these same compounds, especially 1,2-butadiene, are also added as modifiers in alkylolithium-initiated diene polymerizations to prevent thermal branching at higher temperatures via chain termination and/or chain transfer reactions [3, 112–114]. Although these carbon acids can terminate chain growth, the ability of the resulting metalated chain transfer product to reinitiate chain growth has only been demonstrated for 1,2-butadiene [115].

Chain transfer reactions are promoted by Lewis bases. A chain transfer constant of 0.2 was reported for the telomerization of butadiene initiated by metallic sodium in a toluene/THF mixture at 40°C [116]. Such processes are used for the preparation of liquid rubbers (polybutadienes), with varying amounts of 1,2-microstructure depending on the type and amount of Lewis base, counterion, and temperature [117].

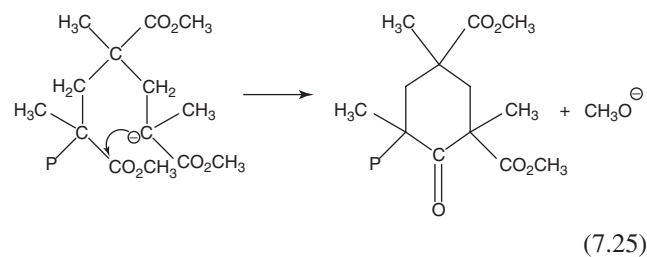
7.4.2 Polar Monomers

7.4.2.1 Polar Vinyl Monomers The anionic polymerization of polar vinyl monomers is often complicated by side reactions of the monomer with both anionic initiators and growing carbanionic chain ends, as well as chain termination and chain transfer reactions. However, synthesis of polymers with well-defined structures can be effected under carefully controlled conditions. The anionic polymerizations of alkyl methacrylates and 2-vinylpyridine exhibit the characteristics of living polymerizations under carefully controlled reaction conditions and low polymerization temperatures to minimize or eliminate chain termination and transfer reactions [118, 119]. Proper choice of initiator for anionic polymerization of polar vinyl monomers is of critical importance to obtain polymers with predictable, well-defined structures. As an example of an initiator that is too reactive, the reaction of methyl methacrylate (MMA)

with *n*-butyllithium in toluene at -78°C produces approximately 51% of lithium methoxide by attack at the carbonyl carbon [120].

7.4.2.2 Methyl Methacrylate The most generally useful initiator for anionic polymerization of MMA and related compounds is 1,1-diphenylhexyllithium which is formed by the quantitative and facile addition of butyllithium with DPE (Eq. 7.13) [121]. Using this initiator in THF at -78°C , it is possible to polymerize MMA to obtain homopolymers and block copolymers with predictable molecular weights and narrow molecular weight distributions. Controlled polymerizations are not effected in nonpolar solvents such as toluene, even at low temperatures [3, 118]. Other useful initiators for polymerization of MMA are oligomers of α -methylstyryllithium whose steric requirements minimize attack at the ester carbonyl group in the monomer. These initiators are also useful for the polymerization of 2-vinylpyridine.

The principal termination reaction in the anionic polymerization of MMA is a unimolecular back-biting reaction with the penultimate ester group to form a six-membered ring, β -keto ester group at the chain end as shown in Equation 7.25. The rate of this back-biting reaction decreases with increasing size of the counterion [118].



A dramatic development in the anionic polymerization of acrylate and methacrylate monomers was the discovery that by addition of lithium chloride it was possible to effect the controlled polymerization of *t*-butyl acrylate [122]. Thus, using oligomeric (α -methylstyryl)lithium as initiator in THF at -78°C , the molecular weight distribution (M_w/M_n) of the polymer was 3.61 in the absence of lithium chloride but 1.2 in the presence of lithium chloride ($[\text{LiCl}]/[\text{RLi}] = 5$). In the presence of 10 equivalents of LiCl, *t*-butyl acrylate was polymerized with 100% conversion and 95% initiator efficiency to provide a polymer with quite narrow molecular weight distribution ($M_w/M_n = 1.05$). More controlled anionic polymerizations of alkyl methacrylates are also obtained in the presence of lithium chloride. Other additives that promote controlled polymerization of acrylates and methacrylates include lithium *t*-butoxide, lithium (2-methoxy)ethoxide, and crown ethers [79, 80]. The addition of lithium chloride also promotes the controlled anionic polymerization of 2-vinylpyridine [81].

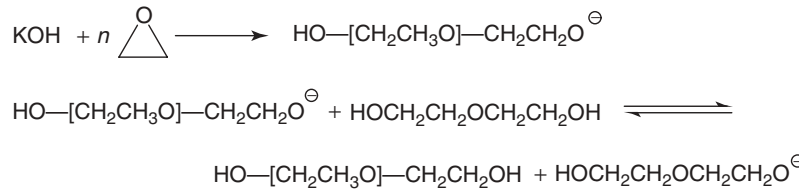
The kinetics of anionic polymerization of MMA is complicated by chain-end association effects and the

involvement of both free ions and ion pairs as propagating species. The propagating species, lithium ester enolates, are highly aggregated even in THF; association numbers range from 2.3 to 3.5 [123]. Because of chain-end association, a dependence of propagation rate constants on chain-end concentration has been observed for lithium and sodium counterions. The propagation rate constant for the free ions at -75°C in THF is $4.8 \times 10^5 \text{ l}/(\text{mol s})$ [124]. The propagation rate constant for ion pairs varies in the order Cs \approx K \approx Na \gg Li. This is consistent with the conclusion that contact ion pairs are the predominant propagating species. The ion pair rate constants for lithium and potassium as counterions in THF at -40°C are 100 and $750 \text{ l}/(\text{mol s})$, respectively [125].

The kinetic effects of lithium chloride on anionic polymerization of alkyl acrylates and methacrylates have been carefully examined [79, 80, 126, 127]. Added lithium chloride decreases the rate of propagation but has little effect on the rate of termination. In the absence of lithium chloride, free ions as well as associated and unassociated species can participate in the propagation event. By a common ion effect, the role of free ions is minimized by the addition of lithium chloride. In the absence of lithium chloride, the rate of interconversion between tetameric aggregates, dimeric aggregates, and unassociated ion pairs is slow relative to the propagation, resulting in broader molecular weight distributions. Lithium chloride decreases the amount of aggregated species and forms cross-associated complexes with the lithium ester enolate ion pairs. Most importantly, the equilibration among these lithium chloride cross-aggregated species is fast relative to propagation so that narrow molecular weight distributions can be obtained.

7.4.2.3 Heterocyclic Monomers A variety of heterocyclic monomers can be polymerized by anionic ring-opening polymerizations. The types of anionically polymerizable heterocyclic monomers include oxiranes (epoxides), thiacyclopropanes, thiacyclobutanes, lactones, lactides, lactams, anhydrides, carbonates, and silicones [128]. Among these heterocyclic monomers, the anionic polymerizations of epoxides have been examined most extensively.

Ethylene Oxide The anionic polymerization of ethylene oxide is complicated by the association phenomenon and the participation of ion-pair and free ion intermediates in the propagation reactions [129, 130]. Simple lithium alkoxides are strongly associated into hexamers and tetramers even in polar media such as THF and pyridine [130]. As a consequence, lithium alkoxides are unreactive as initiators for the anionic polymerization of oxiranes. Association effects can be minimized by effecting polymerizations in alcohol media or in dipolar aprotic solvents.

**Scheme 7.15** Reversible chain transfer in epoxide polymerizations.

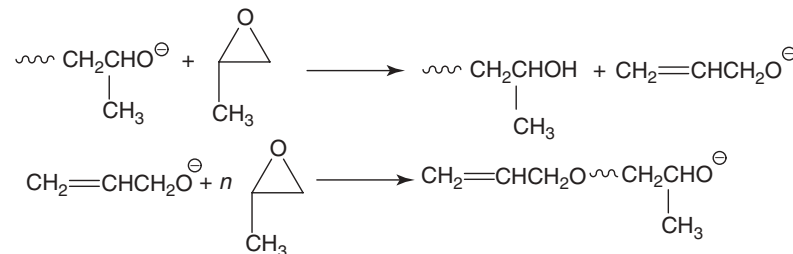
The potassium hydroxide-initiated polymerization of ethylene oxide in alcoholic solvents such as diethylene glycol produces low molecular weight polyols (MW \approx 600–700) with broad molecular weight distributions because of chain transfer reactions with alcohol that occur throughout the polymerization as shown in Scheme 7.15 [131]. “Living polymerizations with reversible chain transfer” [100] can be effected for alkoxide-initiated polymerizations of ethylene oxide in the presence of alcohol ($[\text{ROH}]/[\text{NaOR}] \approx 10$) in solvents such as dioxane [132, 133]. Narrow molecular weight distributions are obtained because, although there is formally a chain transfer reaction between HO-ended polymers and alkoxide-ended polymers, the equilibrium between these two types of chain ends is rapid and reversible such that all chains participate uniformly in chain growth as described by Flory [13].

Association phenomena and the presence of both ion pairs and free ions as propagating species complicate the kinetics of sodium alkoxide-initiated polymerizations of ethylene oxide even in dipolar aprotic solvents such as HMPA ($\epsilon = 26$). However, living polymerizations occur in dipolar aprotic solvents and in ethers such as THF, although the rates are much slower in ethers. The rates of propagation increase with increasing radius of the cation. The rates of propagation of ethylene oxide are also accelerated in the presence of cation complexing agents such as crown ethers and cryptands. Although the cryptated ion pairs are somewhat less reactive than the uncomplexed ion pairs, cryptands promote dissociation of the ion pairs to form free ions that are 70 times more reactive than the ion pairs [134]. Because of the concentrated charge on

oxygen, contact ion pairs predominate. The propagation rate constants in THF at 20°C for the cesium ion pair and the free ion are 7.3 and 100 l/(mol s), respectively [134]. An optimized living polymerization procedure utilized *N*-carbazolylpotassium as initiator in THF at 20°C in the presence of crown ether (4,7,13,16,21,24-hexaoxa-1,10-diazabicyclo[8.8.8]hexacosane); narrow molecular weight distribution polymers with controlled molecular weights as high as 266,000 g/mol could be obtained [135].

Propylene Oxide The anionic ring-opening polymerization of propylene oxide is much slower than the analogous polymerization of ethylene oxide. The propagation rate constant at 40°C in neat propylene oxide is 1.9×10^{-4} l/(mol s) [136]. The anionic ring-opening polymerization of propylene oxide using hydroxide or alkoxide initiators is not a living polymerization. Chain transfer to monomer competes with propagation to limit the maximum molecular weight attainable and to broaden the molecular weight distribution as shown in Scheme 7.16. Thus, chains are formed that have the unsaturated allyloxy end groups.

The chain transfer constant k_t/k_p is approximately 0.01; thus, the molecular weight attainable is theoretically limited to approximately 6×10^3 g/mol [137]. However, molecular weights as high as 13,000 g/mol have been obtained for polymerization of neat propylene oxide with potassium as counterion in the presence of 18-crown-6 ether. Under these conditions, chain transfer constants as low as 0.08×10^{-2} have been reported [138]. The addition of trialkylaluminum compounds to the alkali metal alkoxide/propylene oxide initiating system in hydrocarbon media accelerates the

**Scheme 7.16** Chain transfer to monomer in propylene oxide polymerization.

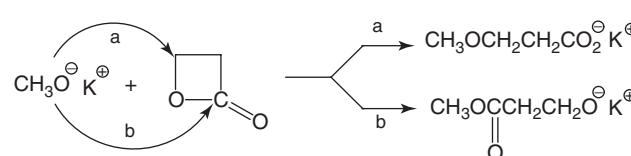
polymerization rate and reduces the rate of chain transfer reactions, with attainment of molecular weights up to 20,000 g/mol [139]. This is due to the rapid equilibration between hydroxyl-ended chains and alkoxide-ended chains, which ensures uniform growth of all chains even after chain transfer as shown in Scheme 7.15 for the analogous polymerization of ethylene oxide.

However, chain transfer to monomer will still broaden the molecular weight distribution and prevent molecular weight control even when reversible chain transfer among growing species occurs. This rapid and reversible chain transfer is used to prepare branched polypropylene oxide polymers. Initiation of propylene oxide polymerization with an alkali metal alkoxide and a triol such as glycerol will produce the corresponding polypropylene oxide with an average functionality of 3.

The anionic polymerization of propylene oxide initiated by potassium alkoxide or hydroxide occurs predominantly (95%) by cleavage of the O–CH₂ bond. For bulk polymerization at 80 °C, approximately 4% head-to-head placements occur. However, there is no stereocontrol in this alkoxide-initiated ring opening and the resulting polymer is nontactic [140].

Chain transfer reactions to monomer occur with other homologs of propylene oxide. The reactivity of higher epoxides decreases as expected based on steric hindrance effects on nucleophilic attack at the oxirane carbons.

Propylene Sulfide The anionic polymerization of propylene sulfide is a living polymerization that proceeds in the absence of termination and chain transfer [133]. The reactivity of addition corresponds to regular head-to-tail addition without detectable amounts of head-to-head or tail-to-tail additions. The polymer stereochemistry is nontactic. The kinetics of propagation of propylene sulfide initiated by carbazylsodium [pK_a (DMSO) = 1.99] [2] in THF at chain-end concentrations $<10^{-3}$ M is not complicated by chain-end association effects. The reported propagation rate constants for contact ion pairs and free ions at –40 °C are 1×10^{-3} and $1.7 \text{ l}/(\text{mol s})$, respectively [133]. The ion pair rate propagation constants increase rapidly with the size of the counterion and become higher than that of the free ion for all cryptated counterions. For example, the ion pair propagation rate constant for the corresponding [2.2.2]cryptate-solvated sodium thiolate ($11.9 \text{ l}/(\text{mol s})$) is more than 2 times larger than the corresponding free ion propagation rate constant ($5.6 \text{ l}/(\text{mol s})$) in THF at –39 °C [134]. A purportedly living anionic emulsion polymerization of propylene sulfide in water has been described [141]. Although quantitative chain-end functionalization was reported, the conversions reached limiting values and the observed M_n values were much lower than the values expected from the feed ratio. The polydispersity (M_w/M_n)



Scheme 7.17 Mechanism of initiation of β -propiolactone with methoxide anions.

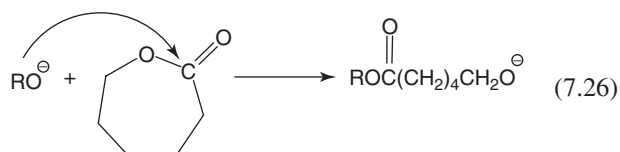
values were 1.11–1.15. The initiating system consisted of 1,3-propanedithiol and equimolar diaza[5.4.0]bicyclo[undec-7-ene] (DBU). A rather unusual initiation process, sulfur extrusion, has been reported for alkylolithium initiators; however, normal ring opening was reported for poly(styryl)lithium [142]. The low basicity but high nucleophilicity of thiolate chain ends promotes nucleophilic substitution reactions; however, dimerization readily occurs in the presence of oxygen.

Lactones

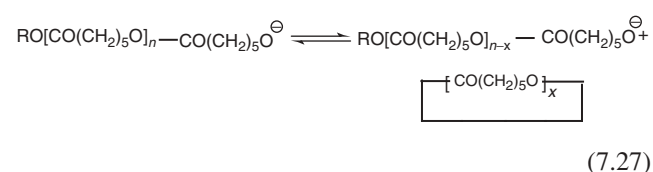
β -PROPIOLACTONE The anionic polymerizations of the β -lactones and ϵ -lactones have been extensively investigated [143]. Living characteristics are observed for the polymerization of β -propiolactone using a dibenzo-18-crown-6 ether complex of sodium acetate as the initiator in dichloromethane [144]. Depending on the reactivity of the initiator, either acyl–oxygen cleavage or alkyl–oxygen cleavage can occur to form the corresponding alkoxide or carboxylate anions, respectively, as illustrated in Scheme 7.17 for initiation with potassium methoxide, which results in both modes of ring opening. Only alkyl–oxygen cleavage is observed for initiation with potassium acetate. Regardless of the initiator, all propagating species eventually become carboxylate anions because in subsequent propagation steps a fraction of the alkoxide anions are converted to carboxylate anions. Sterically hindered anions with high basicity (e.g., *t*-butoxide) initiate with irreversible proton transfer from the ester enolate hydrogens of β -propiolactone [129, 145].

The kinetics of these polymerizations is complex. Both complexed ion pairs and free ions are involved in the propagation reactions and the free ion rate constants depend on monomer concentration. The relative reactivity of complexed ion pairs and free ions is temperature dependent. Above the inversion temperature of –35 °C, free ions are more reactive than ion pairs, but below this temperature the ion pairs are more reactive. At 30 °C in DMF, the observed (average) propagation rate constant is $0.13 \text{ l}/(\text{mol s})$ [146]. The anionic polymerization of α,α -dialkyl- β -propiolactones such as pivalolactone (α,α -dimethyl- β -propiolactone) initiated with carboxylate anions exhibits the main characteristics of living polymerizations.

ϵ -CAPROLACTONE The anionic polymerization of ϵ -lactones, especially ϵ -caprolactone, is generally complicated by intramolecular cyclization reactions and redistribution reactions which prevent control of molecular weight and lead to broader molecular weight distributions [143]. Alkoxides, but not carboxylates, are active initiators for polymerization of ϵ -caprolactone, consistent with the identification of the alkoxide anion as the propagating species as shown in Equation 7.26. Chain-end association complicates the kinetics of



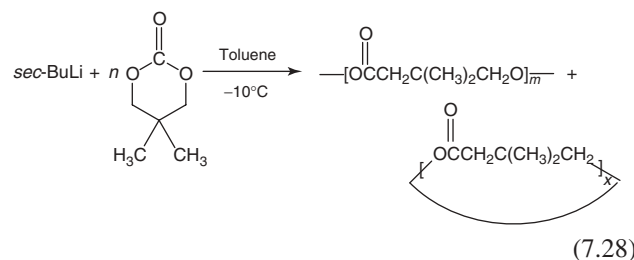
polymerization. Evidence for aggregation of lithium and sodium alkoxides, but not of potassium alkoxides, in THF has been found. The propagation rate constants in THF at 20 °C for the free ions and potassium ion pairs are 3.5×10^2 (mol s) and 4.8 l/(mol s), respectively [147]. The anionic polymerization of ϵ -caprolactone leads to the formation of a considerable amount of oligomers as by-products. In dilute solution (i.e., when the monomer unit concentration is <0.25 mol/l), no high polymer is formed [148]. In THF with potassium *t*-butoxide, the system consists of a living ring-chain equilibrium system; the monomer consumption is completed in minutes and entropy-controlled equilibrium is established quickly [148]. In bulk polymerization, more than one-third of the equilibrium distribution of products are oligomers which have been identified to be cyclic. Linear chains are formed initially and then cyclic oligomers are formed by a back-biting reaction of the active chain ends, see Equation 7.27 [143, 148]. This intermolecular transesterification leads to scrambling of the polymer molecular



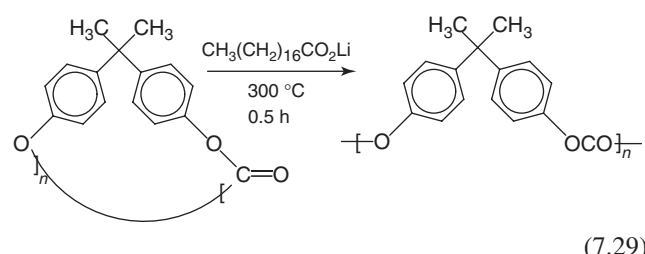
weight and a molecular weight distribution that broadens with time. Polymerizations with lithium as counterion in benzene minimize back-biting reactions at short reaction times (e.g., 3 min) [149].

Cyclic Carbonates Aliphatic cyclic carbonates such as 5,5-dimethyl-1,3-diox-2-one can be polymerized using alkylolithium compounds as initiators in hydrocarbon solution to high molecular weight polymers [150, 151]. Ring-chain equilibration is promoted at long reaction times and in THF as solvent. At -10°C in toluene,

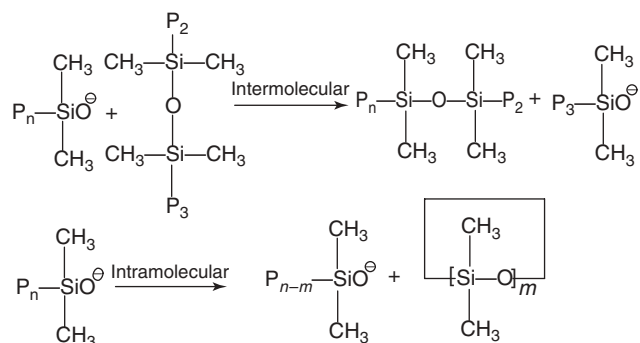
sec-butyllithium-initiated polymerization of 5,5-dimethyl-1,3-diox-2-one proceeds via a lithium alkoxide propagating species to form high molecular weight polymer ($M_n \approx 100,000$ g/mol) with only small amounts of a cyclic oligomer fraction after 1 h as shown in Equation 7.28.



Efficient methods for the synthesis of cyclic bisphenol-A polycarbonates have provided a practical technology for the rapid synthesis of high molecular weight bisphenol-A polycarbonates by anionic ring-opening polymerization as shown in Equation 7.29 [150]. A mixture of cyclic oligomers ($M_w \approx 1300$) was polymerized with lithium stearate for 0.5 h at 300 °C to yield the corresponding linear polymer with $M_w = 300,000$ g/mol and $M_w/M_n = 2.4$ [152]. Rapid chain–chain equilibration occurs under these conditions. Other useful anionic polymerization initiators include lithium phenoxide, lithium phenylacetate, and sodium benzoate. Diphenylcarbonate can be used as a chain transfer agent to control the molecular weight.



Siloxanes A variety of bases, for example, hydroxides, alkoxides, phenolates, and silanolates, are effective initiators for the anionic polymerization of hexamethyl cyclotrisiloxane (D_3) and octamethyl cyclotetrasiloxane (D_4) [153]. The heat of polymerization for the cyclic oligomers in the series from the tetramer (D_4) to the decamer (D_{10}) is approximately zero and the only driving force is a small positive entropy (circa 1.4 cal/mol (SiO groups) K) [153]. The trimer, D_3 , is unique in having a slightly exothermic heat of polymerization (3.5 kcal/mol) [154]. The growing polymer for D_4 polymerization is in equilibrium with the monomer (2% at 140 °C) as well as with various kinds of oligomers and cyclic polymers (10–15%); a Gaussian distribution of linear polymers is obtained. The concentrations of each of the various cyclics ($n > 15$) are in accord with the Jacobsen–Stockmayer cyclization theory.



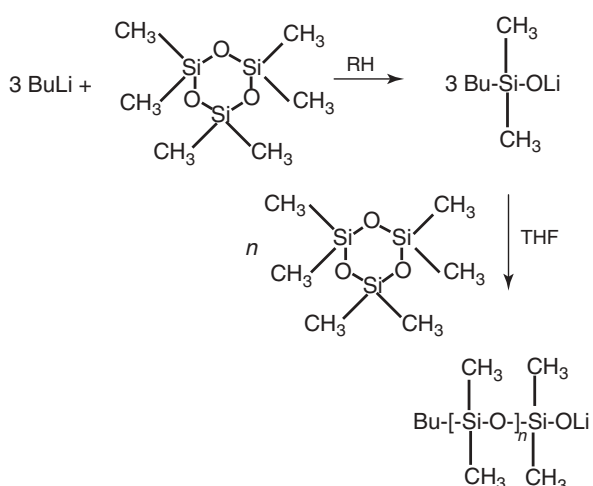
Scheme 7.18 Intermolecular and intramolecular exchange reactions in siloxane polymerizations.

20 °C, the propagation rate constants for D_3 and D_4 are 1.4 and 4×10^{-3} l/(mol s), respectively [134].

7.5 STEREOCHEMISTRY

7.5.1 Polydienes

7.5.1.1 Hydrocarbon Solvents One of the most important synthetic and commercial aspects of anionic polymerization is the ability to prepare polydienes [poly(1,3-dienes)] with high 1,4-microstructure using lithium as the counterion in hydrocarbon solutions [3, 156]. The key discovery was reported in 1956 by scientists at the Firestone Tire and Rubber Company that polyisoprene produced by lithium metal-initiated anionic polymerization had a high (>90%) *cis*-1,4-microstructure similar to natural rubber [47]. In general, conjugated 1,3-dienes [$CH_2=C(R)-CH=CH_2$] can polymerize to form four constitutional isomeric microstructures as shown below. The stereochemistry of the anionic polymerization of isoprene and

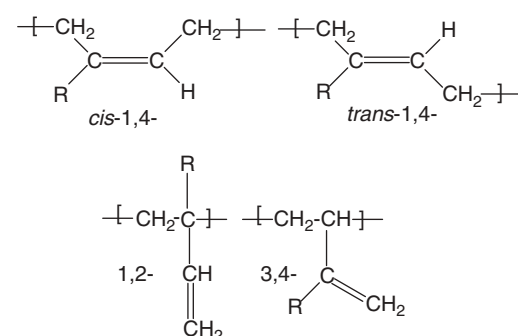


Scheme 7.19 Living polymerization of D_3 .

[155]. The mechanism of polymerization can be described as an equilibration among these various components; in addition to reaction with the monomer, the growing silanolate chain ends react with all siloxane bonds via intramolecular cyclization and intermolecular chain transfer as shown in Scheme 7.18.

In contrast to the polymerization of D_4 , the anionic polymerization of hexamethyl cyclotrisiloxane (D_3) with lithium as counterion is a living polymerization which produces polydimethylsiloxanes with well-defined structures. Useful initiators include lithium silanlates or the product from the reaction of 3 mol of butyllithium with D_3 in a hydrocarbon solvent as shown in Scheme 7.19. It is noteworthy that no polymerization occurs in the absence of a Lewis base promoter such as THF, glymes, DMSO, or HMPA.

The kinetics of polymerization of cyclosiloxanes is complicated by chain-end association. Complexation of counterions with cryptands disrupts the aggregates. For the lithium [2.1.1] cryptand complex in aromatic solvent at



R = H (butadiene, 1,2- = 3,4); R = CH₃ (isoprene)

butadiene depends on the counterion, monomer concentration, chain-end concentration, solvent, temperature, and the presence of Lewis base additives. The effect of counterion on polyisoprene stereochemistry is illustrated by the data in Table 7.3, which shows that lithium is unique among alkali metal counterions in producing polyisoprene with high 1,4 microstructure. Similar results have been reported for the stereochemistry of the anionic polymerization of butadiene except that the stereochemistry with lithium as the counterion in neat isoprene is 94% *cis*-1,4 and 6% 3,4 compared with 35% *cis*-1,4, 52% *trans*-1,4, and 13% 1,2 for analogous polymerization of butadiene. From the data in Table 7.4, it is possible to delineate the effects of monomer concentration, chain-end concentration, and solvent. The highest *cis*-1,4-microstructures are obtained in the absence of solvent, that is, with neat monomer, at low concentrations of initiator (circa 10⁻⁶ M). High *cis*-1,4 enchainment is also

TABLE 7.3 Effect of Counterion on Polyisoprene Microstructure for Neat Polymerizations [157, 158]

Microstructure	Temperature (°C)	1,4-cis	1,4-trans	1,2	3,4
Lithium	25	94	—	—	6
Sodium	25	—	45	7	48
Potassium	25	—	52	8	40
Rubidium	25	5	47	8	39
Cesium	25	4	51	8	37

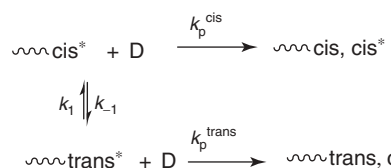
TABLE 7.4 Microstructure of Polydienes in Hydrocarbon Media using Organolithium Initiators [159–162]

Initiator Concentration (M)	Solvent	Temperature (°C)	1,4-cis	1,4-trans	3,4
<i>Polyisoprene</i>					
6 × 10 ⁻³	Heptane	-10	74	18	8
1 × 10 ⁻⁴	Heptane	-10	84	11	5
8 × 10 ⁻⁶	Heptane	-10	97	—	3
5 × 10 ⁻⁶	Heptane	25	95	2	3
9 × 10 ⁻³	Benzene	20	69	25	6
5 × 10 ⁻⁶	Benzene	25	72	20	8
1 × 10 ⁻²	Hexane	20	70	25	5
1 × 10 ⁻⁵	Hexane	20	86	11	3
3 × 10 ⁻³	None	20	77	18	5
8 × 10 ⁻⁶	None	20	96	—	4
Initiator Concentration (M)	Solvent	Temperature (°C)	1,4-cis	1,4-trans	1,2
<i>Polybutadiene</i>					
8 × 10 ⁻⁶	Benzene	20	52	36	12
5 × 10 ⁻¹	Cyclohexane	20	53*	53*	47
1 × 10 ⁻⁵	Cyclohexane	20	68	28	4
3 × 10 ⁻²	Hexane	20	30	60	8
2 × 10 ⁻⁵	Hexane	20	56	37	7
3 × 10 ⁻³	None	20	39	52	9
5 × 10 ⁻⁶	None	20	86	9	5

*Total 1,4-content (cis + trans).

favored by the use of aliphatic versus aromatic solvents at low concentrations of initiator; however, the total amount of 1,4-microstructure (cis + trans) is relatively insensitive to solvent and chain-end concentration. In general, temperature is not an important variable for polydienes prepared in hydrocarbon solutions with lithium as the counterion.

A comprehensive hypothesis has been proposed to explain the effects of the concentrations of active chain ends and monomer on polydiene microstructure [163]. Based on studies with model compounds and the known dependence of polydiene microstructure on diene monomer (D) and chain-end concentrations as shown in Table 7.4,



Scheme 7.20 Proposed mechanism for diene microstructure control.

the mechanistic hypothesis shown in Scheme 7.20 was advanced.

It was proposed that isomerization of the initially formed cis form of the active chain end occurs competitively with monomer addition at each step of the reaction [163, 159]. Thus, when the concentration of monomer is high relative to the chain-end concentration, the first-order isomerization of the cis form does not compete effectively with monomer addition. However, at low concentrations of monomer relative to chain ends, the isomerization does compete and significant amounts of the trans form will be in equilibrium with the cis form.

The kinetic order dependence on the active chain-end concentration is approximately 0.25 for diene propagation, while the kinetic order dependence on the active chain end concentration is approximately 1.0 for cis-trans isomerization of the chains ends [3, 56]. Thus, while the unassociated chain ends add monomer, isomerization of the chain ends occurs in the aggregated state. Since aggregation is favored by increasing chain-end concentrations, high 1,2-microstructure is observed (47% for butadiene) for high chain-end concentrations ([PBDLi] = circa 0.1 M) and high cis-1,4 microstructure (86% for butadiene) is obtained at low chain-end concentrations (circa 10⁻⁶M; Table 7.4).

The microstructure of anionic polymerization of other poly(1,3-diene)s with lithium as counterion in hydrocarbon media is also predominantly 1,4 microstructure [3]. However, higher amounts of cis-1,4-microstructures are obtained with more sterically hindered diene monomers. Thus, using conditions that provide polyisoprene with 70% cis-1,4, 22% trans-1,4, and 7% 3,4 microstructure, 2-i-propyl-1,3-butadiene and 2-n-propyl-1,3-butadiene provide 86% and 91% cis-1,4 enchainment, respectively. Both 2-phenyl-1,3-butadiene (92% cis-1,4) and 2-(triethylsilyl)-1,3-butadiene (100% cis-1,4) also exhibit high cis-1,4-enchainment.

7.5.1.2 Polar Solvents and Polar Additives In polar media, the unique high 1,4-stereospecificity with lithium as counterion that is observed in hydrocarbon media is lost and large amounts of 1,2-polybutadiene and 3,4-polyisoprene enchainments are obtained [3, 156]. There is a tendency toward higher 1,4-content with increasing size of the counterion in polar media. The highest 1,2-content

in polybutadiene and the highest amounts of 1,2 and 3,4 enchainments in polyisoprene are obtained with lithium and sodium [156]. In THF at 0 °C, 88% 1,2-enchainment is reported with lithium as counterion [156, 164]. The highest 1,4-enchainments are observed for cesium as counterion in polar media. Higher 1,4-contents are also obtained in less polar solvents such as dioxane. For example, with cesium as counterion, 60% 1,4-content is obtained in dioxane [156]. The use of polar solvents is generally not practical because of the instability of the polymeric carbanions in these media and because of the lack of control of diene microstructure.

It is more common to add polar modifiers as additives in anionic polymerizations.

Small amounts of Lewis base additives in hydrocarbon media can exert dramatic effects on polydiene microstructure as shown by the data in Table 7.5 [165–167]. Lewis bases that interact most strongly with lithium produce the highest amount of 1,2-microstructure. For example, there is a correlation between the enthalpies of interaction of Lewis bases with polymeric organolithium compounds and the ability of these bases to promote 1,2-enchainment [168]. The highest vinyl contents for polybutadiene are obtained with the most strongly coordinating ligands such as the bidentate bases, TMEDA and bis(piperidinoethane) (DIPIP). To obtain significant amounts of vinyl microstructure with weak donor-type bases such as diethyl ether and triethylamine, they must be present in large amounts relative to lithium. In contrast, the strongly coordinating bases produce high vinyl polybutadiene microstructure at low base to lithium atom ratios ($R = [\text{base}]/[\text{Li}] = 1 - 2$).

TABLE 7.5 Effects of Temperature and Concentration of Lewis Base on Vinyl Content of Polybutadiene in Hexane [171–173]

Base	[Base]/[Li]	% 1,2 Microstructure			
		5 °C	30 °C	50 °C	70 °C
Triethylamine	30	—	21	18	14
	270	—	37	33	25
Diethyl ether	12	—	22	16	14
	180	—	38	29	27
Tetrahydrofuran	5	—	44	25	20
	85	—	73	49	46
Diglyme	0.1	—	51	24	14
	0.8	—	78	64	40
TMEDA*	0.6	—	73	47	30
	0.4	78	—	—	—
	6.7	85	—	—	—
	1.14	—	76	61	46
DIPIP†	0.5	91	50	44	21
	1	99.99	99	68	31

**N,N,N',N'*-Tetramethylethylenediamine

†Bis(piperidinoethane)

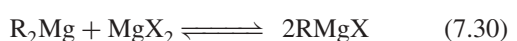
An important feature of the effect of Lewis base additives on diene microstructure is the fact that the amount of vinyl microstructure generally decreases with increasing temperature as shown in Table 7.5 [3, 165, 169]. A simple explanation for the temperature dependence of vinyl microstructure, compared to the lack of dependence of microstructure in hydrocarbon media with lithium as counterion, is that high vinyl microstructure is associated with the addition of monomer to a base-coordinated chain end (α -carbon) and this base coordination is reversed (less favorable) at higher temperatures. The sensitivity of the microstructure to polymerization temperature depends on the Lewis base and the R value ([base]/[Li]) as shown in Table 7.5. Although the strongly chelating bidentate bases promote 1,2-polybutadiene microstructure at low temperatures, they generally exhibit a dramatic decrease in their ability to promote vinyl microstructure at elevated temperatures as shown in Table 7.5. This temperature dependence presents a particular problem in high temperature processes, for example, commercial batch or continuous processes, in which medium vinyl polybutadienes are desired [3].

The ability to prepare polydienes with variable microstructures is an important aspect of alkylolithium-initiated anionic polymerization. The main consequence of the change in microstructure is that the glass transition temperatures of the corresponding polymers are higher for polymers with more side-chain vinyl microstructure. For example, the glass transition temperature of polybutadiene is an almost linear function of the percent 1,2 configuration in the chain [170]. Thus, while *cis*-1,4-polybutadiene has a glass transition temperature of -113 °C, 1,2-polybutadiene has a glass transition temperature of -5 °C [171]. This has practical consequences because polybutadienes with medium vinyl contents (e.g., 50%) have glass transition temperatures (ca. -60 °C) and properties that are analogous to those of SBR (styrene-butadiene rubber). Analogously, the glass transition temperature of *cis*-1,4-polyisoprene is circa -71 °C, while a polyisoprene with 49% 3,4-enchainment exhibited a T_g of -36 °C [172].

7.5.2 Methacrylate Stereochemistry

Like the anionic polymerization of dienes, the anionic polymerization of alkyl methacrylates, especially MMA, is dependent on the counterion, solvent, and, to a certain extent, temperature [156, 173, 121]. In general, the stereochemistry of the anionic polymerization of alkyl methacrylates in toluene solution with lithium as the counterion is highly isotactic (68–99% mm) and the isotacticity increases with the steric requirements of the alkyl ester. For example 90% mm triads are obtained for *t*-butyl methacrylate at -70 °C in toluene [174], while 68% mm triads are observed for MMA [120]. Isospecificity for polymerizations in toluene

is also observed for alkyl sodium initiators (67% mm) [175] but not for potassium or cesium alkyls in toluene [176]. Sterically hindered Grignard reagents, in particular *t*-butylmagnesium bromide or isobutylmagnesium bromide prepared in ether, provide controlled living polymerizations and highly isotactic polymers (96.7% and 92.5% mm, respectively), provided that excess magnesium bromide is present to shift the Schlenk equilibrium, Equation 7.30, in favor of RMgBr [177]. In contrast, using



di-*t*-butylmagnesium, prepared in ether, poly(methyl methacrylate) (PMMA) was obtained with predominantly syndiotacticity (79% rr) [177]. Highly isotactic PMMA is obtained for ether-free dibenzylmagnesium-initiated polymerization in toluene [178]. Ate-type complexes of *t*-butyllithium with trialkylaluminums ($[Al]/[Li] \geq 3$) effect living and highly syndiotactic ($\geq 90\%$ rr) polymerization of MMA in toluene [179]. Analogous complexes of *t*-butyllithium with (2,6-di-*t*-butyl-4-methylphenoxy)-diisobutylaluminum ($[Al]/[Li] \geq 1$) at 0°C in toluene generate PMMA with predominantly syndiotactic placements (71–75% rr) [180]. In contrast, the ate complex of *t*-butyllithium with bis(2,6-di-*t*-butylphenoxy)methylaluminum forms predominantly heterotactic PMMA (67.8% mr) and poly(ethyl methacrylate) (87.2% mr at –78°C; 91.6% mr at –95°C) [181].

In polar media, highly syndiotactic PMMA is formed for free ions and with lithium and sodium as counterions; for sodium, syndiospecificity is observed only in more polar solvents such as dimethoxyethane or in the presence of strongly solvating ligands such as cryptands [182–186]. Lithium is the smallest alkali metal cation and the most strongly solvated; the equilibrium constants for formation of free ions and solvent-separated ion pairs are largest for lithium and smallest for cesium. Since cesium and potassium have a tendency to form 52% heterotactic placements [187, 188], it is proposed that contact ion pairs result in predominantly heterotactic placements whereas solvent-separated ion pairs and free ions form predominantly syndiotactic placements in polar media. These results are general for a variety of alkyl methacrylates; even diphenylmethyl methacrylate gives 87% syndiotactic triads in THF with lithium as counterion at –78°C [173]. However, the exception is trityl methacrylate, which forms 94% isotactic triads under the same conditions and also 96% isotactic triads in toluene.

A variety of stereoregulating mechanisms have been invoked to explain the stereochemistry of anionic polymerization of alkyl methacrylates. As discussed by Pino and Suter [189], although syndiotactic diads are thermodynamically slightly more favored over isotactic diads, the free energy differences are so small that the formation of stereoregular

chains must be kinetically controlled. Since only limited tools are available to predict or understand the physical and chemical basis of such factors as solvation, particularly those associated with small energy differences of this order of magnitude, it is prudent to limit phenomenological interpretations of these stereochemical effects. Thus, any explanation of the predominantly syndiotactic polymerization stereochemistry in THF with lithium as the counterion (84% rr at –85°C) is tempered by the fact that the stereochemistry for the free-radical polymerization of MMA is also highly syndiotactic (78.5% at –55°C) [121]. Many factors such as polar monomer coordination and interaction of the counterion with the chain end with the penultimate groups have been invoked to explain the formation of isotactic polymers in nonpolar media. The coordination of the penultimate ester group with the lithium ester enolate group at the chain end would dictate a meso placement. This simple picture, however, does not take into account the fact that these lithium ester enolates are highly associated in hydrocarbon solutions and in polar media such as THF [118, 119, 123].

The control of PMMA stereochemistry is important because the glass transition temperature of PMMA strongly depends on the microstructure [121]. The measured T_g for 99% mm PMMA is reported to be 50°C, and that for PMMA with 96–98% r diads is 135°C. To obtain PMMA with higher upper use temperature, polymers with the highest syndiotactic microstructure are desired; hence the interest in developing anionic systems for MMA at higher temperatures [118, 119, 190].

7.5.3 Styrene

The stereoregularity of polystyrenes prepared by anionic polymerization is predominantly syndiotactic (racemic diad fraction ($P_r = 0.53–0.74$) and the stereoregularity is surprisingly independent of the nature of the cation, the solvent, and the temperature, in contrast to the sensitivity of diene stereochemistry to these variables [3, 156]. The homogeneous alkylolithium-initiated polymerization of styrene in hydrocarbon media produces polystyrene with an almost random (i.e., *atactic*) microstructure; for example, P_r was 0.53 for the butyllithium/toluene system [3, 191, 192]. A report on the effect of added alkali metal alkoxides showed that polystyrene stereochemistry can be varied from 64% *syndiotactic* triads with lithium *t*-butoxide to 58% *isotactic* triads with potassium *t*-butoxide [193].

When small amounts of water were deliberately added to butyllithium in hydrocarbon solutions, it was possible to prepare polystyrene with as much as 85% polymer that was insoluble in methyl ethyl ketone under reflux and identified as *isotactic* polystyrene by X-ray crystallography [194, 195]. Isotactic polystyrene (10–22% crystalline) can be prepared when lithium *t*-butoxide is

added to *n*-BuLi initiator and the polymerization in hexane (styrene/hexane = 1) is effected at -30°C [196]. This polymerization becomes heterogeneous and is quite slow (after 2–5 days, 50% monomer conversion; 20–30% conversion to isotactic polymer).

7.5.4 Vinylpyridines

The stereochemistry of anionic polymerization of 2-vinylpyridine is predominantly isotactic for most polymerization conditions [197]. The coordination of the penultimate pyridyl nitrogen with the magnesium pyridylamide at the chain end has been invoked to explain the high meso triad content for initiation by Grignard-type reagents in hydrocarbon solution. The absence of this interaction for 4-vinylpyridine results in almost *atactic* polymer stereochemistry.

7.6 COPOLYMERIZATION OF STYRENES AND DIENES

Relatively few comonomer pairs undergo anionic copolymerization to incorporate significant amounts of both monomers into the polymer chains [3, 45]. In general, the comonomer that is most reactive (lowest $\text{p}K_a$ value for the conjugate acid of the propagating anion) [2] will be incorporated to the practical exclusion of the other comonomer. Comonomer pairs that can be effectively copolymerized include styrenes with dienes and methacrylates with acrylates, that is, comonomer pairs with similar reactivity.

Anionic copolymerizations have been investigated by applying the classical Mayo–Lewis treatment which was originally developed for free-radical chain reaction polymerization [198]. The copolymerization of two monomers (M_1 and M_2) can be uniquely defined by the following the four elementary kinetic steps in Scheme 7.21, assuming that the reactivity of the chain end (M_1^- or M_2^-) depends only on the last unit added to the chain end, that is, there are no penultimate effects.

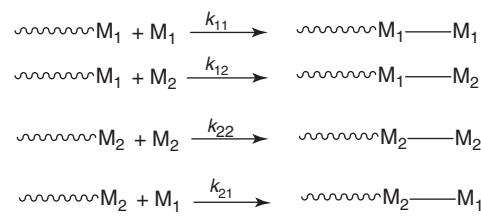
From these four basic kinetic equations, the Mayo–Lewis instantaneous copolymerization equation can be derived, Equation 7.31 (see also Chapter 6):

$$\frac{d[M_1]}{d[M_2]} = \frac{[M_1](r_1[m_1] + [m_2])}{[M_2](r_2[m_2] + [m_1])} \quad (7.31)$$

where $r_1 = k_{11}/k_{12}$ and $r_2 = k_{22}/k_{21}$, and $d[M_1]/d[M_2]$ represents the instantaneous copolymer composition. The monomer reactivity ratios r_1 and r_2 represent the relative reactivity of each growing chain end for addition of the same monomer compared to crossover to the other monomer. Representative monomer reactivity ratios for anionic copolymerizations are listed in Table 7.6. The applicability of standard copolymerization theory to anionic

TABLE 7.6 Anionic Copolymerization Parameters in Hydrocarbon Solution with Alkyllithium Initiators [45, 56, 199–205]

M_1	M_2	Solvent	${}^{\circ}\text{C}$	r_1	r_2
Butadiene	Styrene	None	25	11.2	0.04
		Benzene	25	10.8	0.04
		Cyclohexane	25	15.5	0.04
		Hexane	0	13.3	0.03
			50	11.8	0.04
		THF	-78	0.04	11.0
			25	0.3	4.0
		Diethylether	25	1.7	0.4
		Triethylamine	25	3.5	0.5
		Anisole	25	3.4	0.3
Isoprene	Styrene	Hexane	20	2.72	0.42
		THF	0	0.13	~0
Isoprene	Styrene	Benzene	30	7.7	0.13
		Toluene	27	9.5	0.25
		Cyclohexane	40	16.6	0.046
		THF	27	0.1	9



Scheme 7.21

polymerization has been considered in detail. The four equations in Scheme 7.21 represent an oversimplification since the chain ends are aggregated in hydrocarbon solution and there is a spectrum of ion pairs and free ions in polar media, see Equation 7.2.

In most copolymerizations, $r_1 \neq r_2$ and one monomer is preferentially incorporated into the initially growing polymer. This leads to a depletion of the preferentially incorporated monomer in the feed and the composition of the copolymer formed changes with conversion. For systems undergoing continuous initiation, propagation, and termination, the resulting compositional heterogeneity is intermolecular, that is, the copolymer formed initially has a different composition from the copolymer formed at the end of the reaction. However, in living anionic copolymerization, all of the compositional heterogeneity arising from the disparity in monomer reactivity ratios is incorporated into each growing polymer chain.

7.6.1 Tapered Block Copolymers

The alkylolithium-initiated copolymerizations of styrene with dienes, especially isoprene and butadiene, have been

extensively investigated, and illustrate the important aspects of anionic copolymerization. As shown in Table 7.6, monomer reactivity ratios for dienes copolymerizing with styrene in hydrocarbon solution range from approximately 9 to 15, while the corresponding monomer reactivity ratios for styrene vary from 0.04 to 0.25. Thus, butadiene and isoprene are preferentially incorporated into the copolymer initially. This type of copolymer composition is described as either a *tapered block copolymer* or a *graded block copolymer*. The monomer sequence distribution can be described by the structures below:

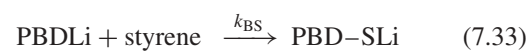


First, there is a diene-rich block; a middle block follows which is initially richer in butadiene with a gradual change in composition until eventually it becomes richer in styrene; a final block of styrene completes the structure.

For a typical copolymerization of styrene and butadiene (25/75, wt/wt), the solution is initially almost colorless, corresponding to the dienyllithium chain ends, and the rate of polymerization is slower than the homopolymerization rate of styrene. The homopolymerization rate constants for styrene, isoprene, and butadiene are 1.6×10^{-2} (l/mol) $^{1/2}$ /s, 1.0×10^{-3} (l/mol) $^{1/4}$ /s, and 2.3×10^{-4} (l/mol) $^{1/4}$ /s, respectively [56]. After approximately 70–80% conversion, the solution changes to orange-yellow, which is characteristic of styryllithium chain ends. At the same time, the overall rate of polymerization increases (inflection point). Although the percent conversion at which the inflection point is observed does not appear to depend on the solvent, the time to reach this percent conversion is quite solvent dependent. Analysis of the copolymer composition indicates that the total percentage of styrene in the copolymer is less than 5% up to approximately 75% conversion [55]; these incorporated styrene units exist predominantly as isolated sequences [206]. When these samples are analyzed by oxidative degradation by ozonolysis, polystyrene segments (corresponding to polystyrene blocks in the copolymer) are recovered only after the inflection point is reached [206]. For a 75/25 (wt/wt) feed mixture of butadiene/styrene, 72% of the styrene is incorporated into the tapered block copolymer as block styrene [207, 208].

The kinetics of copolymerization provides a partial explanation for the copolymerization behavior of styrenes with dienes. One useful aspect of living anionic copolymerizations is that stable carbanionic chain ends can be generated and the rates of their crossover reactions with other monomers measured independently of the copolymerization reaction. Two of the four rate constants involved in copolymerization correspond at least superficially to the two homopolymerization reactions of butadiene and styrene, for example, k_{BB} and k_{SS} , respectively. The other

two rate constants can be measured independently as shown in Equations 7.32 and 7.33.



Results of a number of independent kinetic studies can be summarized as follows for styrene-butadiene copolymerization [56, 209]:

$$\begin{aligned} k_{SB} &> k_{SS} > k_{BB} > k_{BS} \\ (1.1 \times 10^2 \text{l}/(\text{mol s})) &>> (4.5 \times 10^{-1} \text{l}/(\text{mol s})) \\ &> (8.4 \times 10^{-2} \text{l}/(\text{mol s})) > (6.6 \times 10^{-3} \text{l}/(\text{mol s})) \end{aligned}$$

The surprising result is that the fastest rate constant is associated with the crossover reaction of the poly(styryl)lithium chain ends with butadiene monomer (k_{SB}); conversely, the slowest reaction rate is associated with the crossover reaction of the poly(butadienyl)lithium chain ends with styrene monomer (k_{BS}). Similar kinetic results have been obtained for styrene-isoprene copolymerization [204].

In polar media, the preference for preferential diene incorporation is reduced as shown by the monomer reactivity ratios in Table 7.6. In THF, the order of monomer reactivity ratios is reversed compared to hydrocarbon media. The monomer reactivity ratios for styrene are much larger than the monomer reactivity ratio for dienes.

The counterion also has a dramatic effect on copolymerization behavior for styrene and dienes [61]. It is particularly noteworthy that the monomer reactivity ratios for styrene ($r_S = 0.42$) and butadiene ($r_B = 0.30$) are almost equal for copolymerization in toluene at 20 °C using a hydrocarbon-soluble organosodium initiator 2-ethylhexylsodium [210, 211]. Thus, an alternating-type copolymer structure ($r_S r_B = 0.126$) would be formed for this system; however, butadiene is incorporated predominantly as vinyl units (60% 1,2). In contrast, initial preferential styrene incorporation ($r_S = 3.3$; $r_B = 0.12$) is observed for an analogous organopotassium initiator, the DPE adduct of 2-ethylhexylpotassium [61].

Tapered butadiene-styrene copolymers are important commercial materials because of their outstanding extrusion characteristics, low water absorption, good abrasion resistance, and good electrical properties. Tapered block copolymers are used for wire insulation and shoe soles (after vulcanization) as well as for asphalt modification [3].

7.6.2 Random Styrene-Diene Copolymers (SBR)

Random copolymers of butadiene (SBR) or isoprene (SIR) with styrene can be prepared by addition of small

amounts of ethers, amines, or alkali metal alkoxides with alkylolithium initiators in hydrocarbon solution. Random copolymers are characterized as having only small amounts of block styrene content. The amount of block styrene can be determined by ozonolysis [206] or more simply by integration of the ^1H NMR region corresponding to block polystyrene segments ($\delta = 6.50\text{--}6.94$ ppm) [212]. Monomer reactivity ratios of $r_B = 0.86$ and $r_S = 0.91$ have been reported for copolymerization of butadiene and styrene in the presence of 1 equivalent of TMEDA, $[\text{TMEDA}]/[\text{RLi}] = 1$ [212]. However, the random SBR produced in the presence of TMEDA will incorporate the butadiene predominantly as 1,2-units. At 66°C using 1 equivalent of TMEDA, an SBR copolymer will be obtained with 50% 1,2-polybutadiene microstructure [165]. In the presence of Lewis bases, the amount of 1,2-polybutadiene enchainment decreases with increasing temperature. The use of methyl *t*-butyl ether (MTBE) as a randomizer for styrene-butadiene copolymerizations has been reported. Using a $[\text{MTBE}]/[\text{BuLi}]$ molar ratio of 15 at 50°C in cyclohexane, the monomer reactivity ratios were reported to be $r_S = 0.7$ and $r_B = 1.84$ and the vinyl microstructure amounted to 21% [213].

In general, random SBR with a low amount of block styrene and low amounts of 1,2-butadiene enchainment (<20%) can be prepared in the presence of small amounts of added potassium or sodium metal alkoxides [214, 215]. For example, at 50°C in the presence of as little as 0.067 equivalents of potassium *t*-butoxide in cyclohexane, the amount of bound styrene was relatively independent of conversion, in contrast to the heterogeneity observed in the absence of randomizer, that is, tapered block copolymer formation [214]. The polybutadiene microstructure obtained under these conditions corresponds to about 15% 1,2-microstructure [215]. Using 0.2 of hydrocarbon-soluble sodium 2,3-dimethyl-2-pentoxide in cyclohexane at 50°C , the monomer reactivity ratios for alkylolithium-initiated SBR were found to be of $r_B = 1.1$ and $r_S = 0.1$ [216]. The resulting copolymer had only 5% block styrene and 18% 1,2-vinyl microstructure. It was found that there is a very narrow compositional window ($[\text{RONa}]/[\text{RLi}]$) at which a minimum amount of styrene blockiness was obtained [217]. At both lower and higher ratios, significant and unacceptably high levels of block styrene content were formed in the copolymer. It is expected that sodium alkoxide may change the aggregation degree of the organolithium chain ends, may form cross-associated species, and may even exchange counterions with the propagating chain ends. Equilibrium among these active species obviously affects styrene incorporation and diene microstructure [217]. Recent studies have indicated the participation of multicomponent active species (complex cross-aggregates and equilibria between metal–metal exchanged species) depending on the stoichiometry of the mixed initiator [218, 219].

The effects of dibutylmagnesium and triisobutylaluminum “retarders” on the copolymerization of neat styrene and butadiene have been investigated at 25°C [220]. Although the monomer reactivity ratio for styrene was relatively constant ($r_S = 0.03$ and 0.04 at $[\text{R}_2\text{Mg}]/[\text{RLi}] = r = 1$ and 4 , respectively), the butadiene monomer reactivity ratio was sensitive to the $[\text{Mg}]/[\text{Li}]$ ratio ($r_B = 9.1$ and 1.9 at $[\text{R}_2\text{Mg}]/[\text{RLi}] = 1$ and 4 , respectively). The percentage of 1,2-units in the copolymer increased with increasing molar ratio of $[\text{Mg}]/[\text{Li}]$ from circa 12% at $r = 1$ to circa 33% at $r = 4$. These results were at 25°C , however. It would be expected that the amount of vinyl microstructure would decrease at higher temperatures [169]. For triisobutylaluminum, the monomer reactivity ratios reported were $r_S = 0.6$ and $r_B = 1.1$ and for $[i\text{-Bu}_3\text{Al}]/[\text{RLi}] = 0.85$. Thus, whereas tapered structures would be formed for the magnesium system, a random copolymer structure would be expected for the aluminum system. In addition, the presence of triisobutylaluminum did not significantly affect the polybutadiene microstructure (13% 1,2-microstructure for $[i\text{-Bu}_3\text{Al}]/[\text{RLi}] = 0.9$).

Commercial random SBR polymers (solution SBR) prepared by alkylolithium-initiated polymerization typically have 32% *cis*-1,4-, 41% *trans*-1,4-, and 27% vinyl-microstructure compared to 8% *cis*-1,4-, 74% *trans*-1,4-, and 18% vinyl-microstructure for emulsion SBR with the same comonomer composition [3, 221]. Solution SBRs typically have branched architectures to eliminate cold flow [17, 49]. Compared to emulsion SBR, solution random SBRs require less accelerator and give higher compounded Mooney, lower heat buildup, increased resilience, and better retread abrasion index [3]. Terpolymers of styrene, isoprene, and butadiene (SIBR) have been prepared using a chain of single-stirred reactors whereby the steady-state concentration of each monomer and Lewis base modifier at any degree of conversion could be controlled along the reactor chain [3, 222–224].

7.7 SYNTHETIC APPLICATIONS OF LIVING ANIONIC POLYMERIZATION

7.7.1 Block Copolymers.

One of the unique and important synthetic applications of living polymerizations is the synthesis of block copolymers by sequential monomer addition [225–228, 192]. The ability to prepare block copolymers is a direct consequence of the stability of the carbanionic chain ends on the laboratory time scale when all of the monomer has been consumed. Since a living polymerization and the ability to prepare well-defined block copolymers require the absence (or reduction to a negligible level) of chain termination and chain transfer reactions, monomer purity, and the absence of side reactions with the monomer are necessary

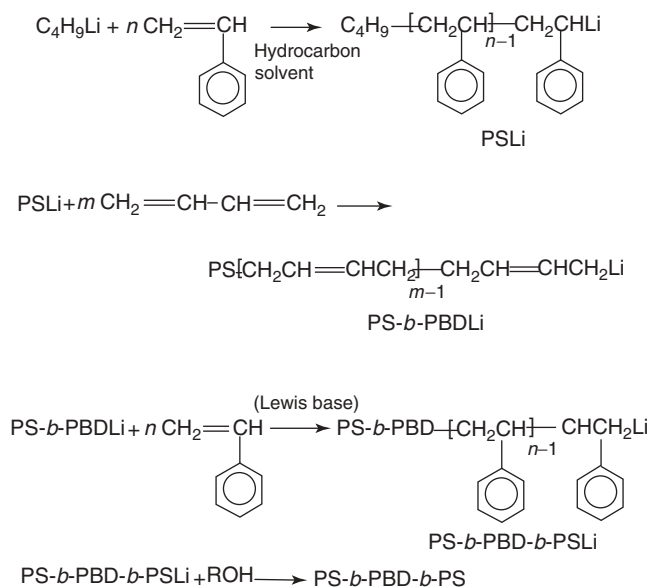
requirements [229, 37, 230]. An important consideration for successful synthesis of block copolymers is the order of monomer addition. In general, a carbanionic chain end from one monomer will crossover to form the chain end of another monomer and initiate polymerization of this monomer provided that the resulting carbanion is either of comparable stability or more stable than the original carbanion [3]. The pK_a values of the conjugate acids of carbanions provide a valuable guide to the relative stabilities of carbanions [2]. With this limitation in mind, living anionic polymerization provides a powerful synthetic method for preparing block copolymers with well-defined structures, including copolymer composition, block molecular weights, block molecular weight distributions, block sequence, and low degrees of compositional heterogeneity [226–228, 192, 229, 37, 230–232]. Organolithium initiators have been particularly useful in this regard, since they are soluble in a variety of solvents [44] and since they can initiate the polymerization of a variety of monomers, such as styrene and its homologs, the 1,3-dienes, alkyl methacrylates, vinylpyridines, cyclic oxides and sulfides, lactones, lactides, and cyclic siloxanes [3]. Utilizing these monomers, various block copolymers have been synthesized, some commercially, but the outstanding development in this area has been in the case of the ABA type of triblock copolymers, particularly polystyrene-*b*-polydiene-*b*-polystyrene (S-D-S) [233–236]. There are three general methods for anionic synthesis of triblock copolymers: (i) three-step sequential monomer addition; (ii) two-step sequential addition followed by coupling reactions; and (iii) difunctional initiation and two-step sequential monomer addition [3, 229]. Each of these methods has certain advantages and limitations.

7.7.1.1 Block Copolymer Synthesis by Three-Step Sequential Monomer Addition The preparation of block copolymers by sequential addition of monomers using living anionic polymerization and a monofunctional initiator is the most direct method for preparing well-defined block copolymers. Detailed laboratory procedures for anionic synthesis of block copolymers are available [37, 230]. Several important aspects of these syntheses can be illustrated by considering the preparation of an important class of block copolymers (Scheme 7.22), the polystyrene-*b*-polydiene-*b*-polystyrene triblock copolymers.

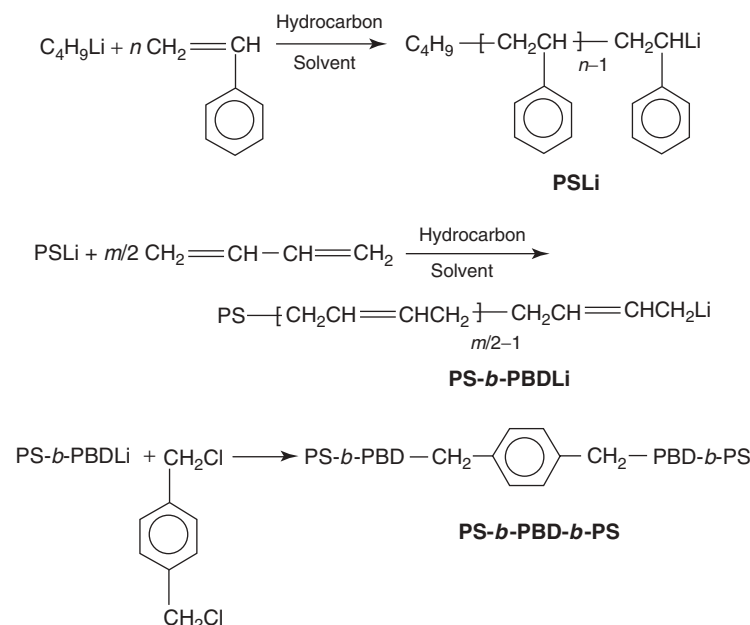
The molecular weight of each block segment is uniquely determined by the stoichiometry, that is, the ratio of the grams of monomer to the moles of initiator. In order to obtain a narrow molecular weight distribution polystyrene block in hydrocarbon solution ($k_i \geq k_p$) [3, 100], the use of a reactive initiator such as *sec*-butyllithium (tetrameric degree of aggregation) [44] is preferred; however, the less reactive but the cheaper and more thermally stable initiator *n*-butyllithium (hexameric degree of aggregation)

[44] can be used if activated by small amounts of polar modifier that will not compromise the generally desired high 1,4-polydiene microstructure (low T_g) in the elastomeric second block. The “crossover” reaction of poly(styryl)lithium with the diene is known to be very rapid, ensuring a fast initiation of the center polydiene block ($k_i > k_p$) [56, 204, 209]; this ensures that the molecular weight distribution of the polydiene block will be narrow. However, to overcome the well-known slow crossover reaction rate of poly(dienyl) lithium to styrene relative to styrene propagation [56, 204, 209] with the final styrene charge in nonpolar media, it is necessary to add a small amount of a Lewis base, for example, THF [45, 237, 238]. The limitations of this method are [3, 229] (i) the requisite addition of polar additives for the final crossover reaction to styrene; (ii) the increasing viscosity of the solution as the polymerization proceeds (poly(styryl)lithium and poly(dienyl)lithium chain ends are associated predominantly into dimers and tetramers, respectively) [83, 85, 86, 89–94]; (iii) the high monomer purity required to prevent chain termination when two subsequent monomers are added sequentially; and (iv) the undesirability of potentially contaminating the recycle solvent stream with polar materials, which affects the polydiene microstructure in commercial plants.

7.7.1.2 Block Copolymer Synthesis by Two-Step Sequential Monomer Addition and Coupling In order to avoid the problems associated with the three-step sequential monomer addition process, a two-step sequential monomer addition process followed by addition of a difunctional



Scheme 7.22 Triblock copolymer synthesis by three-step sequential monomer addition.



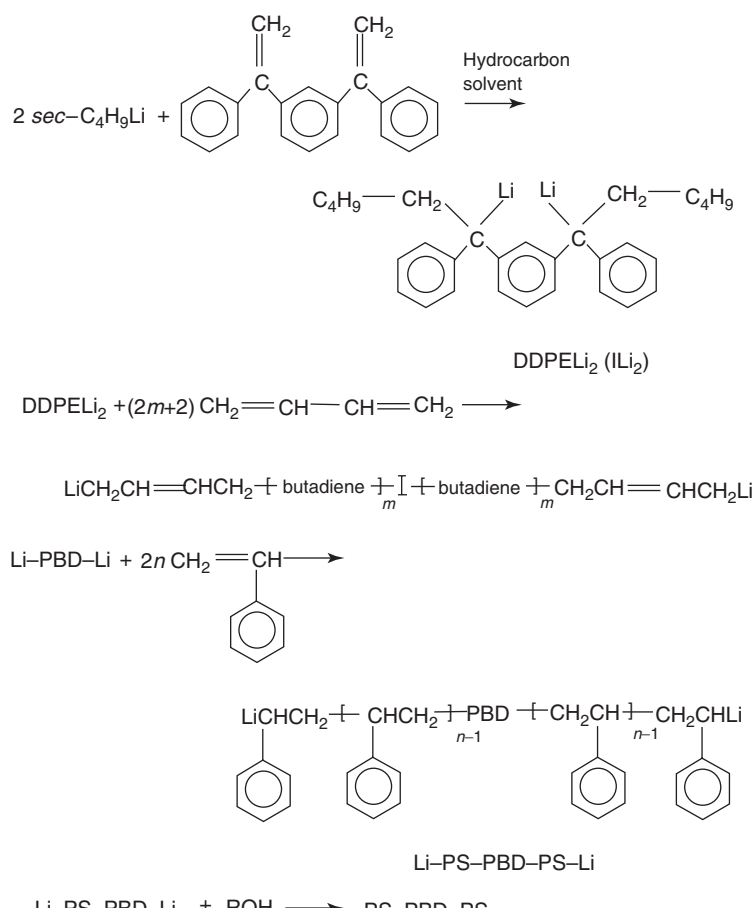
Scheme 7.23 Triblock copolymer synthesis by two-step sequential monomer addition and coupling.

coupling agent was developed as shown in Scheme 7.23 [3, 229]. This process also uses a monofunctional organolithium initiator, but the polymerization is carried only to the diblock (S-D) stage. The triblock copolymers are then formed by using a coupling agent, for example, a dihalide or an ester, to join the lithium chain ends of the diblock [3, 235, 239]. This has the advantage of involving only two monomer additions, thus reducing the possibility of introduction of impurities. However, the efficiency of the coupling reaction is dependent on the ratio of the linking agent to the chain-end concentration; any deviation from exact stoichiometry leads to the formation of free diblock impurity. The latter have been found to have a dramatic effect on the strength of the material (free chain ends in the network) [240, 241]. It is interesting to note, in this connection, that a certain amount of free polystyrene (terminated monoblock) can be easily tolerated since it is apparently incorporated into the polystyrene domains. One of the main advantages of this method is the fact that the slow crossover reaction from dienyllithium to styrene monomer is avoided, along with the necessity of adding a Lewis base to promote this crossover reaction. From a practical point of view, the polymerization time is reduced to one-half of that required for the three-step synthesis of a triblock copolymer with the same molecular weight and composition.

7.7.1.3 Block Copolymers by Difunctional Initiation and Two-Step Sequential Monomer Addition

This process requires a dilithium initiator, so that the center block (D) is

formed first, by a dianionic polymerization, followed by the addition of styrene to form the two end blocks as shown in Scheme 7.24. It, too, has the advantage of requiring only two monomer additions. However, it has several serious limitations. In the first place, it is difficult to obtain a useful dilithium initiator that is soluble in hydrocarbon media, as required for polymerization of dienes, because of the association of the chain ends to form insoluble network-like structures [3, 44, 70, 168]; however, some success in preparing hydrocarbon-soluble dilithium initiators has been reported [45, 73, 71, 242, 243]. Furthermore, any loss of functionality, either in the initiator or after the addition of the diene, leads to the formation of undesirable diblocks. However, this method can be especially useful in the case of “unidirectional” block copolymerization, that is, where monomer A can initiate monomer B but not vice versa, for example, for polar B monomers. The dilithium initiator formed by the dimerization of DPE with lithium in cyclohexane in the presence of anisole has been utilized for the synthesis of an poly(α -methylstyrene-*b*-isoprene-*b*- α -methylstyrene triblock copolymer [243]. The dilithium initiator formed by the addition of 2 mol of *sec*-butyllithium with 1,3-bis(1-phenylethenyl)benzene forms a hydrocarbon-soluble dilithium initiator which has been used in the presence of lithium alkoxide to form well-defined polystyrene-*b*-polybutadiene-*b*-polystyrene [73, 242] and poly(methyl methacrylate)-*b*-polyisoprene-*b*-poly(methyl methacrylate) triblock copolymers [244].



Scheme 7.24 Triblock copolymers by difunctional initiation and two-step sequential monomer addition.

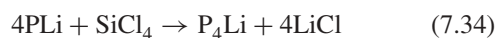
7.7.2 Star-Branched Polymers

Molecular architecture, and particularly long-chain branching, can have a profound effect on the processing and properties of polymers. The methodology of living anionic polymerization provides a variety of procedures for the synthesis of both compositionally homogeneous and compositionally heterogeneous branched polymers [3, 226, 231, 245–250]. A star-branched polymer is a particularly important type of anionically prepared branched polymer that consists of several linear chains linked together at one end of each chain by a single branch or junction point. Thus, after anionic polymerization of a given monomer is completed, the resulting living polymer with a reactive carbanionic chain end can be reacted with a variety of linking reagents to generate the corresponding star-branched polymer with uniform arm lengths. After analogous sequential polymerization of two or more monomers, linking reactions with the resulting living diblock, or multiblock, copolymers will generate star-branched block copolymers with uniform block arm length [227, 231]. It is noteworthy that, in principle, each

arm is of uniform block copolymer composition with precise block molecular weights and narrow molecular weight distributions, that is, with low degrees of compositional heterogeneity. Although various types of linking agents have been used to prepare star-branched copolymers, two of the most useful and important types of linking agents are the multifunctional silyl chlorides and DVB [251, 252].

7.7.2.1 Linking Reactions with Silyl Halides The most general methods for the preparation of regular star polymers are based on linking reactions of polymeric organolithium compounds with multifunctional electrophilic species such as silicon tetrachloride as shown in Equation 7.34 [3, 231, 239, 251]. Analogous linking reactions with multifunctional halogenated hydrocarbons are complicated by side reactions such as lithium–halogen exchange, Wurtz coupling, and elimination reactions [3, 44, 252]. In contrast, the reactions with chlorosilane compounds are very efficient and uncomplicated by similar side reactions. However, the extents and efficiencies of these linking reactions

are sensitive to the steric requirements of the carbanionic chain end [246].



In general, for a given multifunctional silicon halide, the efficiency of the linking reaction decreases in the order poly(butadienyl)lithium > poly(isoprenyl)lithium > poly(styryl)lithium. In pioneering work by Morton, Helminiak, Gadkary, and Bueche [253] in 1962, the reaction of poly(styryl)lithium ($M_n = 60.6 \times 10^3$ g/mol; $M_w/M_n = 1.06$) with a less than stoichiometric amount of silicon tetrachloride in benzene at 50°C for 48 h produced a polymer product with $M_w = 1.93 \times 10^5$ g/mol. After fractionation of this product, a four-armed star polymer ($M_w = 2.57 \times 10^5$ g/mol; $M_w/M_n = 1.09$) and a three-armed star polymer ($M_w = 1.70 \times 10^5$ g/mol; $M_w/M_n = 1.0$) were isolated in weight fraction amounts corresponding to 0.252 and 0.349, respectively. In contrast to the results of inefficient linking for poly(styryl)lithiums, the linking reactions of poly(butadienyl)lithiums with methyltrichlorosilane and silicon tetrachloride in cyclohexane at 50°C for 3 h were reported to proceed efficiently to form the corresponding three-arm and four-arm stars, respectively [254]. However, the linking efficiency of poly(isoprenyl)lithium with silicon tetrachloride is not high, as in the case of poly(styryl)lithium. The stoichiometric reaction of poly(isoprenyl)lithium with silicon tetrachloride is reported to form predominantly the three-armed star product [255]. However, high linking efficiency to form the three-armed star is obtained with methyltrichlorosilane [255].

There have been two general approaches that have been used to increase the efficiency of linking reactions of polymeric organolithium compounds with multifunctional silyl halides. The first procedure is to add a few units of butadiene to either the poly(styryl)lithium or poly(isoprenyl)lithium chain ends to effectively convert them to the corresponding less sterically hindered poly(butadienyl)lithium chain ends. For example, after crossover to butadienyllithium chain ends, the yield of four-armed star polyisoprene with silicon tetrachloride was essentially quantitative in cyclohexane [255]. The second method is to utilize a polychlorosilane compound in which the silyl halide units are more separated to reduce the steric repulsions in the linked product.

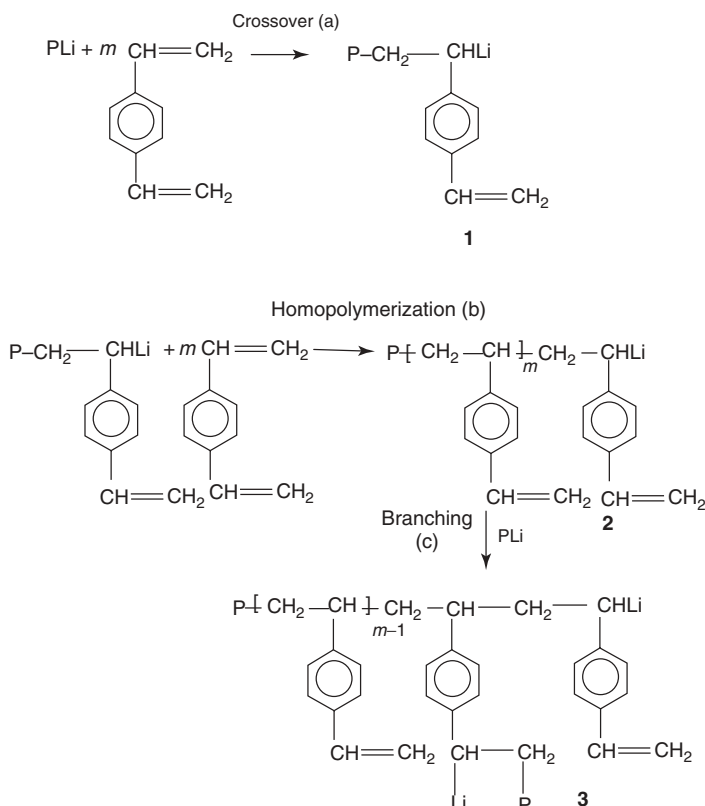
The efficiency of the linking reactions of polychlorosilanes with poly(dienyl)lithium compounds has been documented by synthesis of well-defined, narrow molecular weight distribution, 18-armed star-branched polyisoprenes, polybutadienes, and butadiene end-capped polystyrenes by linking reactions with a decaoctachlorosilane [$(\text{SiCl})_{18}$] [256, 257]. The linking reactions of poly(butadienyl)lithium ($M_n = 5.3-89.6 \times 10^3$ g/mol) with carbosilane dendrimers with up to 128 Si–Cl bonds have been reported to proceed

smoothly at room temperature but requiring periods of up to 3 weeks [258].

From a practical point of view, the effective molecular weight distribution of an anionically prepared polymer can be broadened by reaction with less than a stoichiometric amount of a linking agent such as silicon tetrachloride [239]. This results in a product mixture composed of unlinked arm, coupled product, three-arm, and four-arm star-branched polymers. Heteroarm star-branched polymers can be formed by coupling of a mixture of polymeric organolithium chains that have different compositions and molecular weights. This mixture can be produced by the sequential addition of initiator as well as monomers [3, 259, 260].

7.7.2.2 Divinylbenzene Linking Reactions The linking reactions of polymeric organolithium compounds with DVB provide a very versatile, technologically important, but less precise method of preparing star-branched polymers [251]. The linking reactions with DVB can be conceptually divided into three consecutive and/or concurrent reactions: (i) crossover to DVB; (ii) block polymerization of DVB; and (iii) linking reactions of carbanionic chain ends with pendant vinyl groups in the DVB block [poly(4-vinylstyrene)] [3, 252, 261, 262]. These reactions are illustrated in Scheme 7.25. The uniformity of the lengths of the DVB blocks depends on the relative rate of the crossover reaction (i) compared to the block polymerization of DVB (ii) and the linking reactions (iii). This block copolymerization-linking process has been described as due to the formation of a DVB microgel nodule which serves as the branch point for the star-shaped polymer [252]. In principle, j molecules of DVB could link together ($j + 1$) polymer chains [252]. Although the number of arms in the star depends on the ratio of DVB to polymeric organolithium compound, the degree of linking obtained for this reaction is a complex function of reaction variables [252, 261–263]. It should be noted that these linking reactions are effected with various technical grades of DVB which have been reported to consist of (i) 33% DVB (11% *p*-DVB, 22% *m*-DVB), and 66% *o*-, *m*- and *p*-ethylvinylbenzene (EVB) [252]; (ii) 78% DVB (meta/para = 2.6), 22% EVB isomers [262]; (iii) 56% DVB, 44% EVB isomers [263]; and (iv) 18 mol% *p*-DVB, 39 mol% *m*-DVB, 10 mol% *p*-EVB, and 33 mol% *m*-EVB [252, 264]. The purity and composition of DVB are critical since the course of the linking reaction depends on the [DVB]/[PLi] ratio; impurities can terminate the active chain ends, thus changing the effective molar ratio of DVB to active chain-end concentration.

For poly(styryl)lithium chains, the rate of crossover to DVB is comparable to the rate of DVB homopolymerization and both of these rates are faster than the rate of the linking reaction of poly(styryl)lithium with the pendant double bonds in the poly(vinylstyrene) block formed from DVB.



Scheme 7.25 Branching chemistry of polymeric organolithium compounds with divinylbenzenes.

Therefore, it would be expected that the DVB block formed by crossover from poly(styryl)lithium would be relatively uniform and that the linking reaction would generally occur after the formation of the DVB block. In general, the linking efficiency of poly(styryl)lithiums by DVB is quite high except for very low ratios of DVB/PLi [3].

For poly(dienyl)lithium chain ends, the rate of crossover to DVB is much slower than the rate of DVB homopolymerization. Therefore, it would be expected that the DVB block length would be longer for poly(dienyl)lithiums compared to poly(styryl)lithium. As a consequence, although one obtains a higher degree of branching, the linking efficiency is lower for polydiene versus polystyrene stars. However, it is possible to obtain good linking efficiencies for dienyllithium chains using ratios of $\text{DVB/PLi} \geq 3$ [3]. When small amounts of DVB are added as a comonomer during polymerization of styrenes and dienes, it is incorporated into the chain in a statistical distribution dictated by the comonomer reactivity ratios and the feed composition. Subsequent to DVB incorporation, growing chains can add to the pendant vinylstyrene units followed by further monomer addition to generate long-chain branching sites [3]. Although the resulting branch structure is not well defined, it is very effective in modifying the low and high shear viscosity characteristics of the resulting polymers.

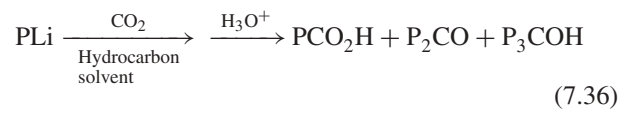
7.7.3 Synthesis of Chain-End-Functionalized Polymers

7.7.3.1 Chain-End Functionalization by Termination with Electrophilic Reagents Another unique attribute of living anionic polymerization is the ability to tailor-make well-defined polymers with low degrees of compositional heterogeneity and with functional chain-end groups [3, 265–267]. The products of living anionic polymerization are polymer chains with stable carbanionic chain ends. In principle, these reactive anionic end groups can be readily converted into a diverse array of ω -chain-end functional end groups by reaction with a variety of electrophilic species as shown in Equation 7.35, where PLi is a polymeric organolithium chain, E is an electrophilic reagent, and X represents a chain-end functional group. Unfortunately, many of these functionalization reactions have not been well characterized [3, 268]. Thus, it is generally necessary to carefully develop, analyze, and optimize new procedures for each different functional group introduced by a specific post-polymerization functionalization reaction. Two representative chain-end functionalization reactions will be described, followed by progress in the area of development of general functionalization methods.



7.7.3.2 Specific Functionalization Reactions

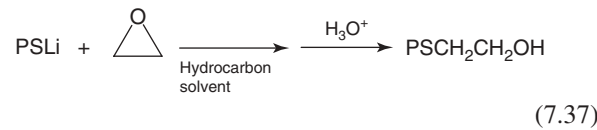
Carbonation Although the carbonation of polymeric carbanions using carbon dioxide is one of the most useful and widely used functionalization reactions, there are special problems associated with the simple reaction of polymeric organolithium compounds with carbon dioxide. Even when carbonations with high purity, gaseous carbon dioxide are carried out in benzene solution at room temperature using standard high vacuum techniques, the carboxylated polymers are obtained in only 27–66% yields for poly(styryl)lithium, poly(isoprenyl)lithium, and poly(styrene-*b*-isoprenyl)lithium [269–271]. The functionalized polymer is contaminated with dimeric ketone (23–27%) and trimeric alcohol (7–50%) as shown in Equation 7.36, where P represents a polymer chain. It was proposed that the formation of these side-products is favored relative to the desired carboxylated polymer by aggregation of the chain ends in hydrocarbon



solution [270]. Furthermore, it has been reported that the addition of sufficient quantities of Lewis bases such as THF and TMEDA can reduce or even eliminate the association of polymeric organolithium chain ends [85, 168, 272]. In accord with these considerations, it was found that addition of large amounts of either THF (25 vol%) or TMEDA ($[\text{TMEDA}]/[\text{PLi}] = 1\text{--}46$) was effective in favoring the carbonation reaction to the extent that the carboxylated polymer was obtained in yields >99% for poly(styryl)lithium, poly(isoprenyl)lithium, and poly(butadienyl)lithium [269–271].

Hydroxylation The preparation of hydroxyl-terminated polymers from polymeric organolithium compounds by reaction with ethylene oxide is one of the few simple and efficient functionalization reactions. The reaction of poly(styryl)lithium with excess ethylene oxide in benzene solution produces the corresponding hydroxyethylated polymer in quantitative yield without formation of detectable amounts of oligomeric ethylene oxide blocks, Equation 7.37 [273]. For example, ^{13}C -NMR analysis of a hydroxyethylated polystyrene ($M_n = 1.3 \times 10^3$ g/mol; $M_w/M_n = 1.08$) showed no evidence for the formation of any ether linkages expected for oligomerization of ethylene oxide, even using ^{13}C -labeled ethylene oxide [274]. No evidence for oligomerization was found by matrix-assisted laser desorption/ionization time-of-flight (MALDI-ToF) mass spectral analysis using the standard conditions of 4 equivalents of

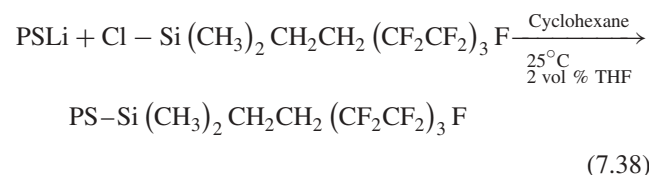
ethylene oxide after 12 h in benzene [275]. This result is surprising in view

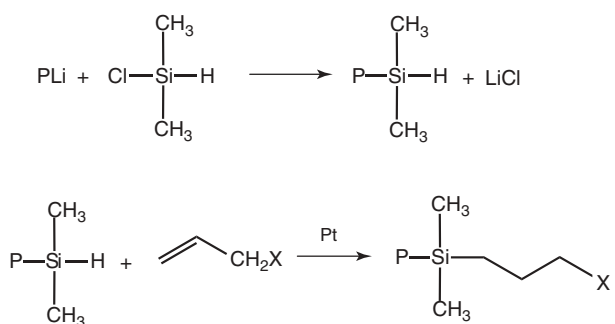


of the steric strain and intrinsic reactivity of ethylene oxide toward nucleophiles. Apparently, the high degree of aggregation of lithium alkoxides and the strength of this association even in polar solvents renders them unreactive [276]. MALDI-ToF mass spectral evidence for oligomerization detected for poly(styryl)lithium functionalization was effected with 10 equivalents of ethylene oxide for longer reaction times [275]. Quite surprisingly, oligomerization is observed for functionalization of poly(butadienyl)lithium under the standard functionalization conditions [277]. Specific functionalizations using a variety of different epoxides have been reviewed [278]. α -Chain-end, hydroxyl-functionalized polymers have also been prepared using protected alkyl-lithium initiators [77, 76].

7.7.3.3 General Functionalization Reactions General functionalization reactions are reactions of organolithium compounds that proceed efficiently to introduce a variety of different functional groups [3]. The most useful reactions can be utilized at elevated temperatures in hydrocarbon solution so that the unique characteristics of organolithium-initiated polymerizations can be preserved.

Functionalizaton Reactions with Silyl Halides The reaction of polymeric organolithium compounds with silyl halides is a very efficient reaction that is not complicated by competing side reactions [251, 252]. Therefore, these reactions provide a general functionalization methodology that can be used to prepare a variety of end-functionalized polymers by reactions with silyl halides containing either functional groups or protected functional groups [279, 280]. For example, the reaction of poly(styryl)lithium with tridecafluoro-1,1,2,2-tetrahydrooctyl)-1-dimethylchlorosilane has been used to prepare perfluoroalkyl-terminated polystyrenes ($M_n = 1000\text{--}40,000$ g/mol) as shown in Equation 7.38 [279]. This methodology was also used to prepare the analogous functionalized polybutadienes and polyisoprenes.





Scheme 7.26 General anionic functionalization using chlorosilanes and hydrosilation chemistry.

Functionalizations via Silyl Hydride Functionalization and Hydrosilation A new general functionalization method based on the combination of living anionic polymerization and hydrosilation chemistry has been developed as illustrated in Scheme 7.26 [281]. First, a living polymeric organolithium compound is quantitatively terminated with chlorodimethylsilane to prepare the corresponding ω -silyl hydride-functionalized polymer. The resulting ω -silyl hydride-functionalized polymer can then react with a variety of readily available substituted alkenes to obtain the desired chain-end functionalized polymers via efficient regioselective transition-metal-catalyzed hydrosilation reactions [282–284].

REFERENCES

- Penczek S, Moad G. Pure Appl Chem 2008;80:2163.
- Bordwell FG. Accounts Chem Res 1988;21:456.
- Hsieh HL, Quirk RP. *Anionic Polymerization: Principles and Practical Applications*. New York: Marcel Dekker; 1996.
- Szwarc M. Carbanions, Living Polymers and Electron Transfer Processes. New York: Interscience; 1968.
- Szwarc M, editor. *Ions and Ion Pairs in Organic Reactions*. Volume 1. New York: Wiley Interscience; 1972.
- Winstein S, Clippinger E, Fainberg AH, Robinson GC. J Am Chem Soc 1954;76:2597.
- Bickelhaupt FM, van Eikema Hommes JR, Guerra CF, Baerends EJ. Organometallics 1996;15:2923.
- Sapse A-M, Schleyer PR, editors. *Lithium Chemistry: A Theoretical and Experimental Overview*. New York: Wiley Interscience; 1995.
- Szwarc M. Nature 1956;178:1168.
- Szwarc M, Levy M, Milkovich R. J Am Chem Soc 1956;78:2656.
- Matyjaszewski K, Gnanou Y, Leibler L, editors. *Macromolecular Engineering: Precise Synthesis, Materials Properties, Applications*. Volume 1–4. Weinheim, Germany: Wiley-VCH; 2007.
- Worldwide Rubber Statistics/IISRP*. Houston: International Institute of Synthetic Rubber Producers; 2009.
- Flory PJ. J Am Chem Soc 1940;62:1561.
- Hirao A, Loykulnant S, Ishizone T. Prog Polym Sci 2002;27:1399.
- Hirao A, Nakahama S. Prog Polym Sci 1992;17:383.
- Fetters LJ. Monodisperse polymers. In: Kroschwitz J, editor. *Encyclopedia of Polymer Science and Engineering*. 2nd ed. Volume 10. New York: Wiley Interscience; 1987. p 19.
- Weissert FC, Johnson BB. Rubber Chem Technol 1967;40:590.
- Se K. Prog Polym Sci 2003;28:583.
- Nakahama S, Hirao A. Prog Polym Sci 1990;15:299.
- Marshall WB, Brewbaker JL, M. S Delaney. J Appl Polym Sci 1991;42:533.
- Li H, Zhang L, Wang Z-X, Hu Y. J Phys Chem 2010;114:2697.
- Penelle J. Polymerization of cycloalkanes. In: Dubois P, Coulembier O, Raquez J-M, editors. *Handbook of Ring-Opening Polymerization*. Weinheim, Germany: Wiley-VCH; 2009. p 329.
- Illy N, Boileau S, Penelle J, Barbier V. Macromol Rapid Commun 2009;30:1731.
- Gan Y, Prakash S, Olah GA, Weber WP, Hogen-Esch T. Macromolecules 1996;29:8285.
- Higashihara T, Ueda M. Macromolecules 2009;42:8794.
- Sakellariou G, Baskaran D, Hadjichristidis N, Mays JW. Macromolecules 2006;39:3525.
- Hirao A, Kitamura M, Loykulnant S. Macromolecules 2004;37:4770.
- Driva P, Pickel DL, Mays JW, Baskaran D. Macromolecules 2010;43:6915.
- Francois B, Zhong XF. Makromol Chem 1990;191:2743.
- Quirk RP, You F, Wesdemiotis C, Arnould MA. Macromolecules 2004;37:1234.
- Hong K, Mays JW. Macromolecules 2001;34:782.
- Deng S, Hassan MK, Mauritz KA, Mays JW. Polym Prepr (Am Chem Soc Div Polym Chem) 2009;54(2):433.
- Natori I, Sato H, Natori S. Polym Int 2008;57:219.
- Quirk RP, Bhatia R. Rubber Chem Technol 1989;62:332.
- Quirk RP, Gomochak DL, Bhatia RS, Wesdemiotis C, Arnould MA, Wollyung K. Macromol Chem Phys 2003;204:2183.
- Morton M, Fetters LJ. Rubber Chem Technol 1975;48:359.
- Hadjichristidis N, Iatrou H, Pispas S, Pitsikalis M. J Polym Sci A Polym Chem 2000;38:3211.
- Urig D, Mays JW. J Polym Sci A Polym Chem 2005;43:6179.
- Hublein G, Stadermann D. Prog Polym Sci 1989;14:195.
- Bywater S, Worsfold DJ. J Organomet Chem 1967;10:1.
- Gatzke AL. J Polym Sci A-1 Polym Chem 1969;7:2281.
- Schue F, Aznar R, Sledz J, Nicol P. Makromol Chem Macromol Symp 1993;67:213.
- The Merck Index*. 11th ed. Rahway (NJ): Merck & Co; 1989. p 238.

44. Wakefield BJ. *The Chemistry of Organolithium Compounds*. New York: Pergamon Press; 1974.
45. Morton M. *Anionic Polymerization: Principles and Practice*. New York: Academic Press; 1983. p 89.
46. Quirk RP, Monroy VM. Anionic polymerization. In: *Kirk-Othmer Encyclopedia of Chemical Technology*. 4th ed. Volume 14. Wiley; 1995. p 461.
47. Stavely FW, Forster FC, Binder LL, Forman LE. Ind Eng Chem 1956;48:778.
48. Szwarc M. Adv Polym Sci 1963;49:1.
49. Duck EW, Locke JM. Polydienes by anionic catalysts. In: Saltman WM, editor. *The Stereo Rubbers*. New York: Wiley Interscience; 1977. p 139.
50. Wagner MJ, Dye JL. Annu Rev Mater Sci 1993;23:223.
51. Szwarc M, Jedlinski Z, Janeczek H. Macromolecules 1997;30:4498.
52. Janeczek H, Jedlinski Z, Bosek I. Macromolecules 1999;32: 4503.
53. Szwarc M. Mechanisms of electron-transfer initiation of polymerization: a quantitative study. In: Bailey FE Jr., editor. *Initiation of Polymerization*. ACS Symposium Series. Volume 212. Washington (DC): American Chemical Society; 1983. p 419.
54. Ivin KJ, Busfield WK. Polymerization thermodynamics. In: Kroschwitz JI, editor. *Encyclopedia of Polymer Science and Engineering*. Volume 12. New York: Wiley; 1988. p 555.
55. Hsieh HL, Glaze WH. Rubber Chem Technol 1970;43:22.
56. Bywater S. Anionic polymerization of olefins. In: Bamford CH, Tipper CFH, editors. *Comprehensive Chemical Kinetics*. Volume 15. New York: Elsevier; 1976. p 1.
57. Hsieh HL, McKinney OF. Polym Lett 1966;4:843.
58. Morton M, Kammerer RF. J Am Chem Soc 1970;92:3217.
59. Morton M, Kammerer RF, Fetters LJ. Br Polym J 1971;3: 120.
60. Arest-Yakubovich AA, Pakuro NI, Zolotareva IV, Kristalnyi EV, Basova RV. Polym Int 1995;37:165.
61. Nakhmanovich BI, Arest-Yakubovich AA, Prudskova TN, Litvinenko GI. Macromol Rapid Commun 1996;17:31.
62. Arest-Yakubovich AA. Anionic polymerization of dienes induced by the group i and the group ii metals and their complexes. In: Volpin ME, editor. *Chemistry Reviews*. Volume 19. Basel: Gordon and Breach; 1994. p 1Part 4.
63. Ziegler K, Dislich H. Chem Ber 1957;90:1107.
64. Weeber A, Harder S, Brintzinger HH, Knoll K. Organometallics 2000;19:1325.
65. Harder S, Feil F. Organometallics 2002;21:2268.
66. Tochtermann W. Angew Chem Int Ed 1966;5:351.
67. Oliver JP. Adv Organomet Chem 1970;8:167.
68. Williard PG. In: Trost BM, editor. *Comprehensive Organic Synthesis*. Volume 1. Oxford, UK: Pergamon; 1991. Part 1.
69. Carlotti S, Desbois P, Warzelhan V, Deffieux A. Polymer 2009;50:3057.
70. Bandermann F, Speikamp H-D, Weigel L. Makromol Chem 2017;1985:186.
71. Yu YS, Dubois P, Jérôme R, Teissie P. Macromolecules 1996;29:2738.
72. Sanderson RD, Roediger AHA, Summers GJ. Polym Int 1994;35:263.
73. Quirk RP, Ma J-J. Polym Int 1991;24:197.
74. Matmour R, More AS, Wadgaonkar P, Gnanou Y. J Am Chem Soc 2006;128:8158.
75. Matmour R, Gnanou Y. J Am Chem Soc 2008;130:1350.
76. Patil AO, Schulz DN, Novak BM, editors. *Functional Polymers. Modern Synthetic Methods and Novel Structures*. ACS Symposium Series. Volume 704. Washington (DC): American Chemical Society; 1998. Chapters 1, 4–6, and 8.
77. Quirk RP, Jang SH, Kim J. Rubber Chem Technol 1996;69:444.
78. Quirk RP, Too T, Lee Y, Kim J, Lee B. Adv Polym Sci 2000;153:67.
79. Vlcek P, Lochmann L. Prog Polym Sci 1999;24:793.
80. Zune C, Jérôme R. Prog Polym Sci 1999;24:631.
81. Quirk RP, Corona-Galvan S. Macromolecules 2001;34:1192.
82. Graham G, Richtsmeier S, Dixon DA. J Am Chem Soc 1980;102:5759.
83. Niu AZ, Stellbrink J, Allgaier J, Wilner L, Richter D, Koenig BW, Gondorf M, Willibald S, Fettters LJ, May RP. Macromol Symp 2004;215:1.
84. Niu AZ, Stellbrink J, Allgaier J, Willner L, Radulescu A, Richter D, Koenig BW, May RP, Fettters LJ. J Chem Phys 2005;122:1.
85. Morton M, Fettters LJ, Pett RA, Meier JF. Macromolecules 1970;3:327.
86. Worsfold DJ, Bywater S. Macromolecules 1972;5:393.
87. Bywater S, Worsfold DJ. The effect of molecular weight on association in anionic polymerization. In: Hogen-Esch TE, Smid J, editors. *Recent Advances in Anionic Polymerization*. New York: Elsevier; 1987. p 109.
88. Sinn H, Lundborg C, Onsager OT. Makromol Chem 1964;70:222.
89. Gondorf M, Willibald S, Fettters LJ, May RP. Macromol Symp 2004;215:1.
90. Stellbrink J, Allgaier J, Wilner L, Richter D, Slawecki T, Fettters LJ. Polymer 2002;43:7101.
91. Miyamoto N, Yamauchi K, Hasegawa H, Hashimoto T, Koizumi D. Physica B 2006;385–386:752.
92. Matsuda Y, Sato T, Oishi Y, Watanabe H. J Polym Sci B Polym Phys 2005;43:1401.
93. Matsuda Y, Nojima R, Sato T, Watanabe H. Macromolecules 2007;40:1631.
94. Oishi Y, Watanabe H, Kanaya T, Kaji H, Horii F. Polym J 2006;38:277.
95. Dyball CJ, Worsfold DJ, Bywater S. Macromolecules 1979;12:819.
96. Bhattacharyya DN, Lee CL, Smid J, Szwarc M. J Phys Chem 1965;69:612.
97. Bohm LL, Chmelir M, Lohr G, Schmitt BJ, Schulz GV. Adv Polym Sci 1972;9:1.

98. Bohm LL, Lohr G, Schulz GV. Ber Bunsen Gesellschaft 1974;78:1064.
99. Shimomura T, Tolle KJ, Smid J, Szwarc M. J Am Chem Soc 1967;89:796.
100. Quirk RP, Lee B. Polym Int 1992;27:359.
101. Glassey MD. Prog Polym Sci 1983;9:133.
102. Fontanille M. Carbanionic polymerization: termination and functionalization. In: Eastmond GC, Ledwith A, Russo S, Sigwalt P, editors. *Comprehensive Polymer Science. Chain polymerization*. Volume 3. Elmsford (NY): Pergamon Press; 1989. p 425, Part I, Chapter 27.
103. Kern WJ, Anderson JN, Adams HE, Bouton TC, Bethea TW. J Appl Polym Sci 1972;16:3123.
104. Memoret S, Fontanille M, Deffieux A, Desbois P. Macromol Chem Phys 2002;203:1155.
105. Deffieux A, Desbois P, Fontanille M, Warzelhan V, Latsch S, Schade C. Control of active centers reactivity in the high temperature bulk anionic polymerization of hydrocarbon monomers. In: Puskas JE, editor. *Ionic Polymerizations and Related Processes*. Netherlands: Kluwer; 1999. p 223.
106. Ades D, Fontanille M, Leonard J. Can J Chem 1982;60:564.
107. Nentwig W, Sinn H. Makromol Chem Rapid Commun 1980;1:59.
108. Leonard J, Malhotra SL. J Macromol Sci Pure Appl Chem 1977;11:2087.
109. Higginson WCE, Wooding NS. J Chem Soc 1952:760.
110. Wang LS, Favier JC, Sigwalt P. Polym Commun 1989;30:248.
111. Auguste S, Edwards HGM, Johnson AF. Meszena. Polymer 1997;38:4357.
112. Tate DP, Bethea TW. Butadiene polymers. In: Kroschwitz JI, editor. *Encyclopedia of Polymer Science and Engineering*. 2nd ed. Volume 2. New York: John Wiley & Sons; 1985. p 537.
113. Adams HE, Bebb RL, Ebberly KC, Johnson BL, Kay EL. Kaut Gummi Kunstst 1965;18:709.
114. Wang Q, Liao M, Wang Y, Zhang C. Polym Int 2007;56:1021–1028.
115. Puskas JE. Makromol Chem 1993;194:187.
116. Kume S, Takahashi A, Nishikawa G, Hatano M, Kambara S. Makromol Chem 1965;84:137.
117. Luxton AR. Rubber Chem Technol 1981;54:596.
118. Baskaran D. Prog Polym Sci 2003;28:521.
119. Baskaran D, Muller AHE. Prog Polym Sci 2007;32:173.
120. Hatada K, Kitayama T, Fumikawa K, Ohta K, Yuki H. Studies on the anionic polymerization of methyl methacrylate initiated with butyllithium in toluene by using perdeuterated monomer. In: McGrath JE, editor. *Anionic Polymerization. Kinetics, Mechanisms and Synthesis*. ACS Symposium Series. Volume 166. Washington (DC): American Chemical Society; 1981. p 327.
121. Hatada K, Kitayama T, Ute K. Prog Polym Sci 1988;13:189.
122. Fay R, Forte R, Jacobs C, Jérôme R, Ouhadi T, Teyssie P, Varshney SK. Macromolecules 1987;20:1442.
123. Halaska V, Lochmann L. Collect Czechoslov Chem Commun 1973;38:1780.
124. Löhr G, Schulz GV. Eur Polym J 1974;10:121.
125. Müller AHE. Kinetics and mechanisms in the anionic polymerization of methacrylic esters. In: Hogen-Esch TE, Smid J, editors. *Recent Advances in Anionic Polymerization*. New York: Elsevier; 1987. p 205.
126. Janata M, Lochmann L, Müller AHE. Makromol Chem 1993;194:625.
127. Janata M, Lochmann L, Müller AHE. Makromol Chem 1990;191:2253.
128. Brunelle DJ, editor. *Ring-Opening Polymerization: Mechanisms, Catalysis, Structure, Utility*. New York: Hanser; 1993.
129. Penczek S, Cypryk M, Duda A, Kubisa P, Slomlowski S. Prog Polym Sci 2007;32:247.
130. Halaska V, Lochmann L, Lim D. Collect Czechoslov Chem Commun 1968;33:3245.
131. Bailey FE Jr., France HG. In: Moore JA, editor. *Macromolecular Syntheses. Collective*. Volume 1. Wiley; 1977. p 289.
132. Gee G, Higginson WCE, Merrall GT. J Chem Soc 1959:1345.
133. Boileau S. Anionic ring-opening polymerizations; epoxides and episulfides. In: Eastmond GC, Ledwith A, Russo S, Sigwalt P, editors. *Comprehensive Polymer Science. Chain polymerization*. Volume 3. Oxford: Pergamon; 1989, Part I. p 467.
134. Boileau S. Use of cryptates in anionic polymerization of heterocyclic compounds. In: McGrath JE, editor. *Anionic Polymerization. Kinetics, Mechanisms and Synthesis*. ACS Symposium Series. Volume 166. Washington (DC): American Chemical Society; 1981. p 283.
135. Eisenbach CD, Peuscher M. Makromol Chem Rapid Commun 1980;1:105.
136. Ding J, Price C, Booth C. Eur Polym J 1991;27:891.
137. Price C. Accounts Chem Res 1974;7:294.
138. Ding J, Heatley F, Price C, Booth C. Eur Polym J 1991;27:895.
139. Billouard C, Crivelli S, Desbois P, Deffieux A. Macromolecules 2004;37:4038.
140. Tsuruta T, Kawakami Y. Anionic ring-opening polymerization: stereospecificity for epoxides, episulfides and lactones. In: Eastmond GC, Ledwith A, Russo S, Sigwalt P, editors. *Comprehensive Polymer Science. Chain polymerization*. Volume 3. Oxford: Pergamon Press; 1989, Part I. p 489.
141. Rehor A, Tirelli N, Hubbell JA. Macromolecules 2002;35:8688.
142. Quirk RP, Ocampo M, Polce MJ, Wesdemiotis C. Macromolecules 2007;40:2352.
143. Jérôme R, Teyssie P. Anionic ring-opening polymerization: lactones. In: Eastmond GC, Ledwith A, Russo S, Sigwalt P, editors. *Comprehensive Polymer Science. Chain polymerization*. Volume 3. Oxford: Pergamon Press; 1989, Part I. p 501.

144. Slomkowski S, Penczek S. *Macromolecules* 1976;9:367.
145. Dale J, Schwarz JE. *Acta Chem Scand* 1986;B40:559.
146. Hofman A, Slomkowski S, Penczek S. *Makromol Chem* 1984;185:91.
147. Slomkowski S, Duda A. Anionic ring-opening polymerization. In: Brunelle DJ, editor. *Ring-Opening Polymerization: Mechanisms, Catalysis, Structure, Utility*. New York: Hanser; 1993. p 114.
148. Ito K, Hashizuka Y, Yamashita Y. *Macromolecules* 1977;10: 821.
149. Morton M, Wu M. Organolithium polymerization of ϵ -caprolactone. In: McGrath JE, editor. *Ring-opening Polymerization: Kinetics, mechanisms, and Synthesis*. ACS Symposium Series. Volume 286. Washington (DC): American Chemical Society; 1985. p 175–182.
150. Brunelle DJ. In: Brunelle DJ, editor. *Ring-Opening Polymerization: Mechanisms, Catalysis, Structure, Utility*. New York: Hanser; 1993. p 309–335.
151. Keul H, Bacher R, Höcker H. *Makromol Chem* 1986;187: 2579.
152. Brunelle DJ, Shannon TG. *Macromolecules* 1991;24:3035.
153. Carmichael JB, Winger R. *J Polym Sci* 1965;A3:971.
154. Hardman B, Torkelson A. Silicones. In: Kroschwitz J, editor. *Encyclopedia of Polymer Science and Engineering*. 2nd ed. Volume 15. New York: Wiley Interscience; 1989. p 204.
155. Jacobson H, Stockmayer WH. *J Chem Phys* 1950;18:1600.
156. Bywater S. Carbanionic polymerization: polymer configuration and the stereoregulation process. In: Eastmond GC, Ledwith A, Russo S, Sigwalt P, editors. *Comprehensive Polymer Science. Chain polymerization*. Volume 3. Oxford: Pergamon Press; 1989, Part I, Chapter 28. p 433.
157. Foster FC, Binder JL. Lithium and other alkali metal polymerization catalysts. In: *Handling and Uses of the Alkali Metals*. Advances in Chemistry Series. Volume 19. Washington (DC): American Chemical Society; 1957. p 26.
158. Tobolsky AV, Rogers CE. *J Polym Sci* 1959;40:73.
159. Gerbert W, Hinz J, Sinn H. *Makromol Chem* 1971;144:97.
160. Al-Jarrah MMF, Apikian RL, Ahmed E. *Polym Bull* 1984;12:433.
161. Morton M, Rupert JR. Factors affecting the isomeric chain unit structure in organolithium polymerization of butadiene and isoprene. In: Bailey FE Jr., editor. *Initiation of Polymerization*. ACS Symposium Series. Volume 212. Washington (DC): American Chemical Society; 1983. p 283.
162. Bywater S, Worsfold DJ, Hollingsworth G. *Macromolecules* 1972;5:389.
163. Worsfold DJ, Bywater S. *Macromolecules* 1978;11:582.
164. Bywater S, Firat Y, Black PE. *J Polym Sci Polym Chem Ed* 1984;22:669.
165. Antkowiak TA, Oberster AE, Halasa AF, Tate DP. *J Polym Sci A-1 Polym Chem* 1972;10:1319.
166. Werbowyj R, Bywater S, Worsfold DJ. *Eur Polym J* 1986;22:707.
167. Halasa AF, Lohr DF, Hall JE. *J Polym Sci Polym Chem Ed* 1981;19:1357.
168. Young RN, Quirk RP, Fetter LJ. *Adv Polym Sci* 1984;56:1.
169. Uraneck CA. *J Polym Sci A-1 Polym Chem* 1971;9:2273.
170. Aggarwal SL, Hargis TG, Livigni RA, Fabris HJ, Marker LF. Structure and properties of tire rubbers prepared. In: Lal J, Mark JE, editors. *Advances in Elastomers and Rubber Elasticity*. New York: Plenum; 1986. p 17.
171. Hargis G, Livigni RA, Aggarwal SL. Recent development in synthetic rubbers by anionic polymerization. In: Whelan A, Lee KS, editors. *Developments in Rubber Technology—4*. Essex, UK: Elsevier; 1987. p 1.
172. Widmaier JM, Meyer GC. *Macromolecules* 1981;14:450.
173. Yuki H, Hatada K. *Adv Polym Sci* 1979;31:1.
174. Yuki H, Hatada K, Niinomi T, Kikuchi Y. *Polym J* 1970;1: 36.
175. Fowells W, Schuerch C, Bovey FA, Hood FP. *J Am Chem Soc* 1967;89:1396.
176. Hatada K, Sugino H, Ise H, Kitayama T, Okamoto Y, Yuki H. *Polym J* 1980;12:55.
177. Hatada K, Ute K, Tanaka K, Okamoto Y, Kitayama T. *Polym J* 1986;18:1037.
178. Soum A, D'Accorso N, Fontanille M. *Makromol Chem Rapid Commun* 1983;4:471.
179. Hatada K, Kitayama T. *Polym Int* 2000;49:11.
180. Ballard DGH, Bowles RJ, Haddleton DM, Richards SN, Sellens R, Twose DL. *Macromolecules* 1992;25:5907.
181. Kitayama T, Hirano T, Hatada K. *Polym J* 1996;28:61.
182. Jeuck H, Müller AHE. *Makromol Chem Rapid Commun* 1982;3:121.
183. Pascault JP, Kawak J, Gole J, Pham QT. *Eur Polym J* 1974;10:1107.
184. Warzelhan V, Höcker H, Schulz GV. *Makromol Chem* 1980;181:149.
185. Kraft R, Müller AHE, Höcker H, Schulz GV. *Makromol Chem Rapid Commun* 1980;1:363.
186. Müller AHE, Höcker H, Schulz GV. *Macromolecules* 1977;10:1086.
187. Müller AHE. Present view of the anionic polymerization of methyl methacrylate and related esters in polar solvents. In: McGrath JE, editor. *Anionic Polymerization: Kinetics, Mechanisms, and Synthesis*. ACS Symposium Series. Volume 166. Washington (DC): American Chemical Society; 1981. p 441–461.
188. Erusalimskii BL. *Mechanisms of Ionic Polymerization*. New York: Consultants Bureau; 1986. p 223.
189. Pino P, Suter UW. *Polymer* 1976;17:977.
190. Jerome R, Teyssie P, Vuillemin B, Zundel T, Zune C. *J Polym Sci A Polym Chem* 1999;37:1.
191. Kawamura T, Uryu T, Matsuzaki K. *Makromol Chem Rapid Commun* 1982;3:66.
192. Tsitsilianis C. Synthesis of blocks and graft copolymers. In: Muller AHE, Matyjaszewski K, editors. *Controlled and Living Polymerizations: Methods and Materials*. Weinheim, Germany: Wiley-VCH; 2009. p 445–492.

193. Marechal J-M, Carlotti S, Shcheglova L, Deffieux A. *Polymer* 2003;44:7601.
194. Worsfold DJ, Bywater S. *Makromol Chem* 1963;65:245.
195. Makino T, Hogen-Esch TE. *Macromolecules* 1999;32:5712.
196. Cazzaniga L, Cohen RE. *Macromolecules* 1989;22:4125.
197. Soum AH, Hogen-Esch TE. *Macromolecules* 1985;18:690.
198. Mayo FR, Walling C. *Chem Rev* 1950;46:191.
199. Huang L-KPh.D. Dissertation. . Akron (OH): University of Akron; 1979. quoted in Reference 171.
200. Hill DJT, O'Donnell JH, O'Sullivan PW, McGrath JE, Wang IC, Ward TC. *Polym Bull* 1983;9:292.
201. Yuki H, Okamoto Y. *Bull Chem Soc Jpn* 1970;43:148.
202. Agarwall SL, Livigni RA, Marker LF, Dudek TJ. Block copolymers as microcomposites. In: Burke JJ, Weiss V, editors. *Block and Graft Copolymers*. Syracuse (NY): Syracuse University Press; 1973. p 157.
203. Spirin YL, Polyakov DK, Gantmakher AR, Medvedev SS. *Polym Sci USSR* 1962;3:233.
204. Worsfold DJ. *J Polym Sci A-1 Polym Chem* 1967;5:2783.
205. Korotkov AA, Mitzengendler SP, Aleyev KM. *Polym Sci USSR* 1962;3:487.
206. Tanaka Y, Sato H, Nakafutami Y, Kashiwazaki Y. *Macromolecules* 1983;16:1925.
207. Hsieh HL. Industrial applications of anionic polymerization: an introduction. In: Quirk RP, editor. *Applications of Anionic Polymerization Research*. ACS Symposium Series. Volume 696. Washington (DC): American Chemical Society; 1998. p 28–33.
208. Sardelis K, Michels HJ, Allen G. *Polymer* 1984;25:1011.
209. Ohlinger R, Bandermann F. *Makromol Chem* 1935;1980:181.
210. Arest-Yakubovich AA, Litvinenko GI, Basova RV. *Polym Prepr (Am Chem Soc Div Polym Chem)* 1994;35(2):544.
211. Arest-Yakubovich AA, Zolotareva IV, Pakuro NI, Nakhmanovich BI, Glukhovskoi VS. *Chem Eng Sci* 1996;51:2775.
212. Mochel VD. *Rubber Chem Technol* 1967;40:1200.
213. Iovu MC, Buzdugan E, Teodorescu M, Britchi AG, Hubca G, Iovu H. *Angew Makromol Chem* 1999;271:18.
214. Wofford CF, Hsieh HL. *J Polym Sci A-1 Polym Chem* 1969;7:461.
215. Hsieh HL, Wofford CF. *J Polym Sci A-1 Polym Chem* 1969;7:449.
216. Quirk RP, Lee Y, Zhou JP. *Polym Prepr (Am Chem Soc Div Polym Chem)* 2000;41(1):129.
217. Quirk RP, Zhou J-P. *Polym Mater Sci Eng* 2001;84:833.
218. Nakhmanovich BI, Zolotareva IV, Arest-Yakubovich AA. *Macromol Chem Phys* 2015;1999:200.
219. Litvinenko GI, Arest-Yakubovich AA. *Macromol Chem Phys* 2000;201:2417.
220. Carlotti S, Menoret S, Barabanova A, Desbois P, Deffieux A. *Macromol Chem Phys* 2004;205:656.
221. Hsieh HL, Farrar RC, Udupi K. *Chemtech* 1981;626.
222. Halasa AF. *Rubber Chem Technol* 1997;70:295.
223. Halasa AF, Gross B, Hsu B, Chang CC. *Eur Rubber J* 1990;172(June):36.
224. Zhao S, Zou H, Zhang X. *J Appl Polym Sci* 2004;93:336.
225. Webster OW. *Science* 1991;251:887.
226. Fetters LJ, Thomas EL. Model polymers for materials science. In: Thomas EL, editor. *Material Science & Technology*. Volume 12. Weinheim, Germany: VCH Verlagsgesellschaft; 1993. p 1.
227. Hadjichristidis N, Pispas S, Floudas G. *Block Copolymers: Synthetic Strategies, Physical Properties, and Applications*. Hoboken (NJ): Wiley Interscience; 2003.
228. Taton D, Gnanou Y. Guidelines for synthesizing block copolymers. In: Lazzari M, Liu G, Lecommandoux S, editors. *Block Copolymers in Nanoscience*. Weinheim, Germany: Wiley-VCH; 2006. p 9–38.
229. Quirk RP. Research on anionic triblock copolymers. In: Holden G, Kricheldorf H, Quirk RP, editors. *Thermoplastic Elastomers*. 3rd ed. Munchen: Hanser; 2004. p 69–91.
230. Uhrig D, Mays JW. *J Polym Sci A Polym Chem* 2005;43:6179.
231. Quirk RP, Kinning DJ, Fetters LJ. In: Aggarwal SL, editor. *Comprehensive Polymer Science. Specialty polymers and polymer processing*. Volume 7. Oxford: Pergamon; 1989. p 1.
232. Riess G, Hurtrez G, Bahadur P. Block copolymers. In: Kroschwitz J, editor. *Encyclopedia of Polymer Science and Engineering*. Volume 2. New York: Wiley; 1985. p 324.
233. Balsamo V, Lorenzo AT, Muller AJ, Corona-Galvan S, Fraga Trillo LM, Ruiz Santa Quiteria V. Structure properties and applications of ABA and ABC triblock copolymers with hydrogenated polybutadiene blocks. In: Lazzari M, Liu G, Lecommandoux S, editors. *Block Copolymers in Nanoscience*. Weinheim, Germany: Wiley-VCH; 2006. p 367–389.
234. Handlin DL Jr., Hansen DR, Wright KJ, Trenor SR. Industrial applications. In: Muller AHE, Matyjaszewski K, editors. *Controlled and Living Polymerizations: Methods and Materials*. Weinheim, Germany: Wiley-VCH; 2009. p 555–603.
235. Bening RC, Korcz WH, Handlin DL Jr., Styrenic block copolymer elastomers. In: Scheirs J, Priddy DB, editors. *Modern Styrene Polymers: Polystyrene and Styrenic Copolymers*. New York: Wiley; 2003. p 465.
236. Handlin DL Jr., Trenor S, Wright K. Applications of thermoplastic elastomers based on styrenic block copolymers. In: Matyjaszewski K, Gnanou Y, Leibler L, editors. *Macromolecular Engineering: Precise Synthesis, Materials Properties, Applications*. Volume 4. Weinheim, Germany: Wiley-VCH; 2007. p 2001.
237. Legge NR. *Rubber Chem Technol* 1987;60:G83.
238. Bywater S. Anionic polymerization. In: Kroschwitz J, editor. *Encyclopedia of Polymer Science and Engineering*. Volume 2. New York: Wiley; 1985. p 1.
239. Hsieh HL. *Rubber Chem Technol* 1976;49:1305.
240. Morton M. In: Aggarwal SL, editor. *Block Polymers*. Plenum; 1970. p 1.

241. Morton M. Styrene-diene block polymers. In: Bikales N, editor. *Encyclopedia of Polymer Science and Technology*. Volume 15. New York: Wiley; 1971. p 508.
242. Lo GY-S, Otterbacherr EW, Gatzke AL, Tung LH. *Macromolecules* 1994;27:2233.
243. Fetters LJ, Morton M. *Macromolecules* 1969;2:453.
244. Long TE, Broske AD, Bradley DJ, McGrath JE. *J Polym Sci A Polym Chem* 1989;27:4001.
245. Grest GS, Fetters LJ, Huang JS. *Adv Chem Phys* 1996;XCIV:67.
246. Hadjichristidis N, Pitsikalis M, Pispas S, Iatrou H. *Chem Rev* 2001;101:3747.
247. Ishizu K, Uchida S. *Prog Polym Sci* 1999;24:1439.
248. Pitsikalis M, Pispas S, Mays JW, Hadjichristidis N. *Adv Polym Sci* 1998;135:1.
249. Higashihara T, Inoue K, Natura M, Hirao A. *Macromol Res* 2006;14:287.
250. Kimani SM, Hitchings LR. *Macromol Rapid Commun* 2008;29:633.
251. Hadjichristidis N, Pispas S, Iatrou H, Pitsikalis M. *Curr Org Chem* 2002;6:155.
252. Bauer BJ, Fetters LJ. *Rubber Chem Technol* 1978;51:406.
253. Morton M, Helminiak TE, Gadkary SD, Bueche F. *J Polym Sci* 1962;57:471.
254. Zelinski RP, Wofford CF. *J Polym Sci* 1965;3:93.
255. Fetters LJ, Morton M. *Macromolecules* 1974;7:552.
256. Roovers J, Hadjichristidis N, Fetters LJ. *Macromolecules* 1983;16:214.
257. Toporowski PM, Roovers J. *J Polym Sci A Polym Chem* 1986;24:3009.
258. Roovers J, Zhou L-L, Toporowski PM, van der Zwan M, Iatrou H, Hadjichristidis N. *Macromolecules* 1993;26:4324.
259. Ma J-J, Nestegard MK, Majumdar BD, Sheridan MM. Asymmetric star block copolymers: anionic synthesis, characterization, and pressure-sensitive adhesive performance. In: Quirk RP, editor. *Applications of Anionic Polymerization Research*. ACS Symposium Series. Volume 696. Washington (DC): American Chemical Society; 1998. p 159–166.
260. Hartsock DL, Stacy NE. Preparation, properties and applications of high styrene content styrene-butadiene copolymers. In: Scheirs J, Priddy DB, editors. *Modern Styrenic Polymers: Polystyrenes and Styrenic Copolymers*. New York: Wiley; 2003. p 501.
261. Bywater S. *Adv Polym Sci* 1979;30:89.
262. Quack G, Fetters LJ, Hadjichristidis N, Young RN. *Ind Eng Chem Prod Res Dev* 1980;19:587.
263. Martin MK, Ward TC, McGrath JE. The reactivity of polydiene anions with divinylbenzene. In: McGrath JE, editor. *Anionic Polymerization. Kinetics, Mechanisms, and Synthesis*. ACS Symposium Series. Volume 166. Washington (DC): American Chemical Society; 1981. p 557–580.
264. Mays JW, Hadjichristidis N, Fetters LJ. *Polymer* 1988;29:680.
265. Tasdelen MA, Kahveci MU, Yagci Y. *Prog Polym Sci* 2011;36:455.
266. Jagur-Grodzinski J. *J Polym Sci A Polym Chem* 2002;40:2116.
267. Hirao A, Hayashi M. *Acta Polym* 1999;50:219.
268. Quirk RP. In: Aggarwal SL, Russo S, editors. *Comprehensive Polymer Science* First Supplement. Elmsford, NY: Pergamon Press; 1992. p 83.
269. Quirk RP, Yin J. *J Polym Sci A Polym Chem* 1992;30:2349.
270. Quirk RP, Chen W-C. *Makromol Chem* 2071;1982:183.
271. Quirk RP, Yin J, Fetters LJ. *Macromolecules* 1989;22:85.
272. Milner R, Young RN, Luxton AR. *Polymer* 1983;24:543.
273. Quirk RP, Ma J-J. *J Polym Sci A Polym Chem* 1988;26:2031.
274. Quirk RP, Mathers RT, Ma J-J, Wesdemiotis C, Arnould MA. *Macromol Symp* 2002;183:17.
275. Quirk RP, Mathers RT, Wesdemiotis C, Arnould MA. *Macromolecules* 2002;35:2912.
276. Halaska V, Lochmann L, Lim D. *Collect Czechoslov Chem Commun* 1968;33:245.
277. Ji HN, Sato N, Nonidez WK, Mays JW. *Polymer* 2002;43:7119.
278. Quirk RP, Gomochak DL. *Rubber Chem Technol* 2003;76:812.
279. Hunt MO, Belu AM, Linton RW, Desimone JM. *Macromolecules* 1993;26:4854.
280. Peters MA, Belu AM, Linton RW, Dupray L, Meyer TJ, Desimone JM. *J Am Chem Soc* 1995;117:3380.
281. Quirk RP, Kim H, Polce MJ, Wesdemiotis C. *Macromolecules* 2005;38:7895.
282. Marciniec B, editor. *Hydrosilation: A Comprehensive Review on Recent Advances*. New York: Springer; 2009.
283. Brook MA. *Silicon in Organic, Organometallic, and Polymer Chemistry*. New York: Wiley Interscience; 2000.
284. Marciniec B. *Comprehensive Handbook on Hydrosilation*. Oxford: Pergamon Press; 1992.

8

CATIONIC POLYMERIZATIONS

FILIP E. DU PREZ, ERIC J. GOETHALS, AND RICHARD HOOGENBOOM

8.1 INTRODUCTION

Since the discovery of “living” polymerizations by Swarc in 1956 [1], the area of synthesis and application of well-defined polymer structures has been developed. The livingness of a polymerization is defined as the absence of termination and transfer reactions during the course of the polymerization. If there is also fast initiation and chain-end fidelity, which are prerequisites for the so-called controlled polymerization, well-defined polymers are obtained that have a narrow molar mass distribution as well as defined end groups. Such well-defined polymers can be prepared by various types of living and controlled polymerization techniques, including anionic polymerization [2], controlled radical polymerization [3–5], and cationic polymerization [6, 7].

This chapter provides an overview of the most important living cationic polymerization methods, namely carbocationic polymerizations of vinyl monomers and cationic ring-opening polymerizations (ROPs) of heterocyclic monomers, as depicted in Scheme 8.1. In general, cationic polymerization can be regarded as chain-growth polymerizations based on positively charged propagating species. During initiation, these cationic species are formed and propagation occurs by nucleophilic attack of the monomer onto this ionic species, resulting in chain growth while the newly added monomer remains as cationic chain end. Finally, addition of another nucleophile or a second monomer can be used to introduce chain-end functionality or for the preparation of block copolymers, respectively. Despite the tremendous growth of controlled radical polymerizations in recent decades, living cationic polymerization provides access to additional defined polymer structures that cannot easily be achieved by controlled radical polymerization methods,

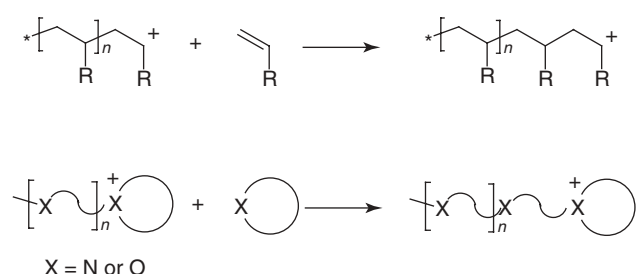
including poly(vinyl ether)s, poly(isobutene) as well as polyamines, poly(cyclic imino ether)s and poly(ethers). This additional monomer pool, which is only accessible by living cationic polymerization methods, clearly demonstrates that it is an important tool for polymer chemists.

This chapter will first discuss the living carbocationic polymerization of the three most important monomer classes: isobutene, vinyl ethers, and styrenics. The second part of the chapter will focus on living cationic ROP of cyclic ethers, cyclic imines, and cyclic imino ethers. For more detailed discussions on carbocationic polymerizations [8–14] and cationic ROPs [15–18] in general, the readers are referred to previous literature [19].

8.2 CARBOCATIONIC POLYMERIZATION

Cationic polymerization of vinyl monomers involves the highly reactive carbenium ions, which can only be formed when they are stabilized by the substituents on the vinyl group. Stabilization of the carbenium ion can be achieved by resonance structures, as is the case for vinyl ether and styrenic monomers, or by an inductive effect, which is the stabilizing mechanism for 1,1-disubstituted alkenes. Despite this stabilization, the reactivity of such carbenium ions is still very high, giving rise to the occurrence of side reactions, such as isomerization, hydride abstraction, as well as various transfer reactions. Moreover, carbocationic polymerizations are very sensitive to minor nucleophilic impurities. Nonetheless, in recent years a range of less sensitive polymerization initiators have been developed that can be used in aqueous environment [20].

The counteranion in carbocationic polymerizations is of major importance to “regulate” the reactivity of the



Scheme 8.1 Schematic representation of the propagation step, that is, monomer addition, in carbocationic polymerizations (top) and cationic ring-opening polymerizations (bottom). Counteranions have been omitted for clarity.

cationic species. Initial studies involved non-nucleophilic counteranions, such as BF_4^- , PF_6^- , SbF_6^- , or ClO_4^- , completely exposing the carbenium ions resulting in uncontrolled cationic polymerizations. In contrast, the use of strong nucleophilic counteranions, such as chloride, can lead to recombination of the carbenium ion and counteranion leading to covalently bound species, which do not propagate and, thus, terminate the polymerization. Importantly, an intermediate situation can be reached with a continuous equilibrium between cationic and covalent species by adjusting the nucleophilicity of the counteranion and the propagating carbenium ions. In this intermediate situation, the concentration of the highly reactive carbenium ions is lowered by reversibly shielding it as covalent species, which are referred to as the “dormant” species (Scheme 8.2) [21]. The main propagation reaction occurs by monomer addition to the carbenium ions which are much more electrophilic than the covalent “dormant” species. Such a polymerization mechanism, involving an equilibrium between active and “dormant” species, should be called “living” polymerization, as proposed by the

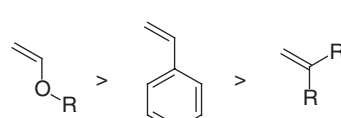
IUPAC Macromolecular Division [22], on the conditions that the exchange reactions are fast compared to the propagation rate and that transfer and termination reactions are absent. This polymerization mechanism is sometimes also referred to as “quasi-living” polymerization.

It should be noted, however, that Scheme 8.2 depicts a highly simplified mechanism for “living” carbocationic polymerizations and it is in most cases not possible to find a counteranion with intermediate reactivity that spontaneously establishes an equilibrium between cationic and covalent species. Instead, the counteranion is generally a halide that preferably forms a covalent species with the carbenium ion. The addition of a Lewis acid as co-initiator is required to activate the covalently bound halide, resulting in the cationic carbenium ion. Alternatively, a nucleophile or electron donor can be added to the cationic polymerization, to reversibly form a stable cationic addition product with the carbenium ion. Both these deactivation mechanisms are depicted in Scheme 8.3. To achieve a “living” cationic polymerization it is of critical importance to have fast deactivation equilibria. In addition, the position of the equilibria should be carefully optimized for each monomer by variation of, for example, temperature, solvent, initiator, as well as the addition of halide activators or nucleophilic deactivators.

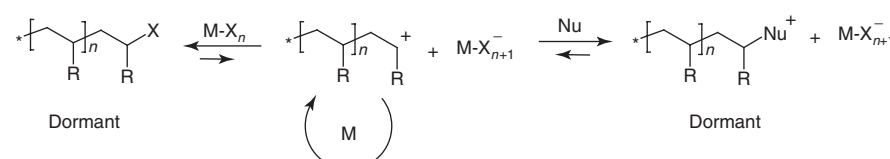
The following sections will provide an overview of the “living” carbocationic polymerizations of the three most important monomer families, namely, isobutene, vinyl ethers, and styrenics. The reactivity of the monomers for carbocationic polymerization is directly related to the stabilization of the formed carbenium ion: vinyl ethers are the most reactive monomers, followed by styrenics and, finally, 1,1-disubstituted alkenes (Scheme 8.4). As a direct consequence of this stabilization, the reactivity of the formed carbocations is opposite to that of the monomer.



Scheme 8.2 Schematic representation of the continuous equilibration between active cationic carbenium ions and covalent “dormant” species.



Scheme 8.4 Reactivity order for the most common classes of monomers for carbocationic polymerization.



Scheme 8.3 Schematic representation of the “living” carbocationic polymerization based on covalent halide species and an activator (left) or based on the addition of a nucleophilic deactivator (right). X represents a halide; M, a metal; and Nu, a nucleophile.

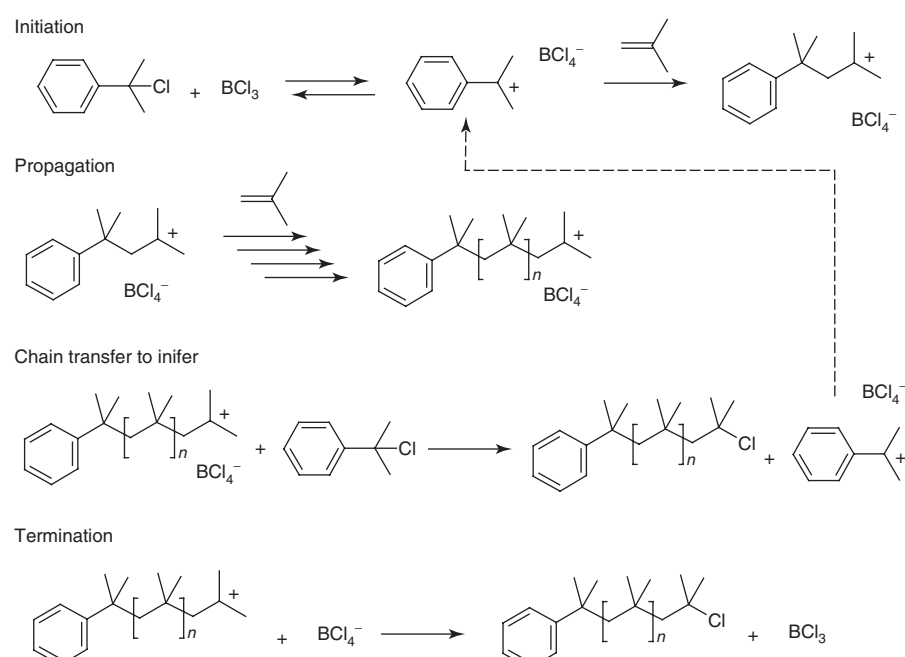
8.2.1 Isobutene

The most studied monomer for cationic polymerization is isobutene, which is related to the inductive stabilization of the formed carbocation ions. Polyisobutene (PIB) has been produced since 1943 on an industrial scale by carbocationic polymerization. PIB is an interesting polymer material with high stability and a low glass transition temperature (-70°C), and is particularly suited for low temperature elastomer applications. The majority of industrial PIB contains a diene comonomer, such as isoprene, making it suitable as “butyl rubber” that can be vulcanized by the conventional methods used in rubber industry based on the presence of a minor fraction of unsaturated bonds. The industrial, uncontrolled cationic polymerization of isobutene is performed at very low temperatures, usually -90°C , in methyl chloride using Lewis acid initiators yielding PIB with a hydrogen atom as initiating fragment and an unsaturated bond at the chain end due to various transfer and isomerization reactions [23].

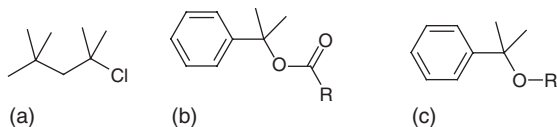
To fully exploit the beneficial properties of PIB in, for example, polyurethanes, thermoplastic elastomers, and sealants, controlled polymerization methods are required that provide access to controlled end-group functionalities. The controlled polymerization of isobutene was first reported by Kennedy, which was based on the “inifer” technique. This so-called “inifer” that is added to provide control over the polymerization is a compound that acts both as the initiator and the transfer agent. The inifer deliberately induces chain transfer to control the molecular weight of the PIB, whereby each transfer step generates

a new chain. A combination of cumyl chloride and boron trichloride was used for the inifer polymerization of isobutene, whereby the cumyl group is introduced as initiator fragment and the end group of the resulting PIB is a chloride (Scheme 8.5) [24, 25]. Initiation occurs by activation of cumyl chloride with BCl_3 followed by addition of the monomer to the formed cation (propagation). Chain transfer to cumyl chloride results in a dead polymer chain as well as a new cationic initiating fragment. In addition, termination by halogen transfer from BCl_4^- to the cationic propagating species can also occur, resulting in regeneration of BCl_3 which can activate the remaining cumyl chloride initiator. As such, the molecular weight of the PIB is not very well controlled, but the end groups of the PIB can be defined. Telechelic PIB became available via this inifer polymerization method when using bifunctional initiators. This initial controlled polymerization method does not allow reactivation of the formed covalent isobutyl halide end groups, which would be a prerequisite for a “living” polymerization.

The first hint toward a “living” cationic polymerization of isobutene was provided by Nuyken and coworkers in 1982 when they reported that the cationic polymerization of isobutene could be initiated by 2-chloro-2,4,4-trimethylpentane (Scheme 8.6), which is a low molecular weight analog of the covalent chloride-terminated PIB, in a polar solvent at -85°C [26]. This work indicated that the irreversible termination reaction in the inifer polymerization mechanism could become reversible in a more polar medium, which was indeed demonstrated by Kennedy who



Scheme 8.5 Inifer mechanism for the cationic polymerization of isobutene.



Scheme 8.6 Structures of (a) 2-chloro-2,4,4-trimethylpentane, (b) cumyl esters, and (c) cumyl ethers used as initiators for the cationic polymerization of isobutene.

reported the cationic polymerization of isobutene based on a combination of the inifer and “living” polymerization mechanisms [27]. It was proposed that, during the initial stages of the polymerization the inifer mechanism (Scheme 8.5) was dominant, whereas after complete consumption of the cumyl chloride the “living” polymerization mechanism based on reversible termination/activation was active (Scheme 8.3, left).

Already before reporting this combined inifer and “living” polymerization approach, Kennedy and coworkers developed a controlled isobutene polymerization method based on cumyl ester initiators (Scheme 8.6) with boron trichloride as activator and incremental monomer addition [28]. The “livingness” of the polymerization was demonstrated by the linear increase of number-average molar mass and the constant number of polymer chains (N) with the amount of PIB obtained (w_{PIB} , as measure for conversion) as well as the narrowing of the molar mass distribution with conversion (Fig. 8.1) [28].

Moreover, the absence of unsaturations in the resulting polymers clearly indicated the absence of chain transfer reactions. Similar “living” polymerization characteristics were reported for cationic isobutene polymerizations initiated with cumyl methyl ethers (Scheme 8.6) with BCl_3 as activator [29, 30] as well as with cumyl ethers and cumyl esters as initiators together with titanium tetrachloride as activator [31].

Originally it was proposed that these polymerizations occurred by monomer insertion into the polarized alkyl–oxygen bonds. However, this should lead to PIB with ether or ester end groups, which was not observed. Instead, the resulting PIBs contained tertiary chloride end groups, which led to the proposal of a polymerization mechanism involving rapid halogen exchange (Scheme 8.7) [32]. The initial step of the polymerization is the activation of the cumyl initiator resulting from ionization by the activator. Depending on the reactivity of the ionized complex, the monomer, and the activator, two polymerization routes can be followed separately or simultaneously. In route 1, the isobutene monomer is directly added to the ionized complex until the covalent dormant chloride PIB adduct is formed together with $\text{CH}_3\text{OCOMtCl}_{n-1}$. The latter acts as electron donor and is the key element to obtain a “living”

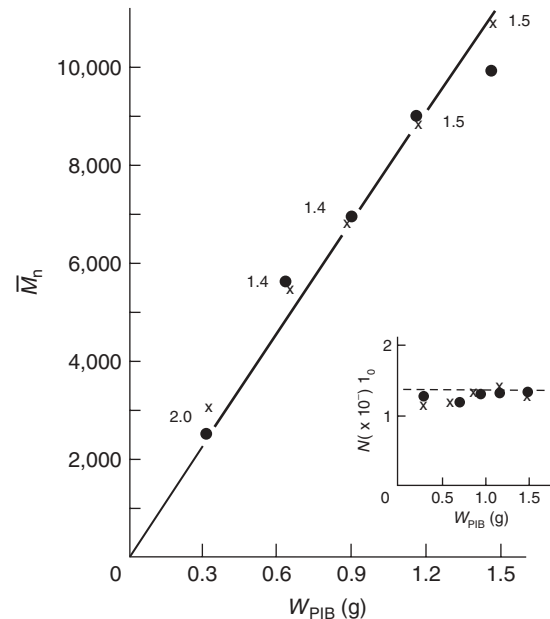
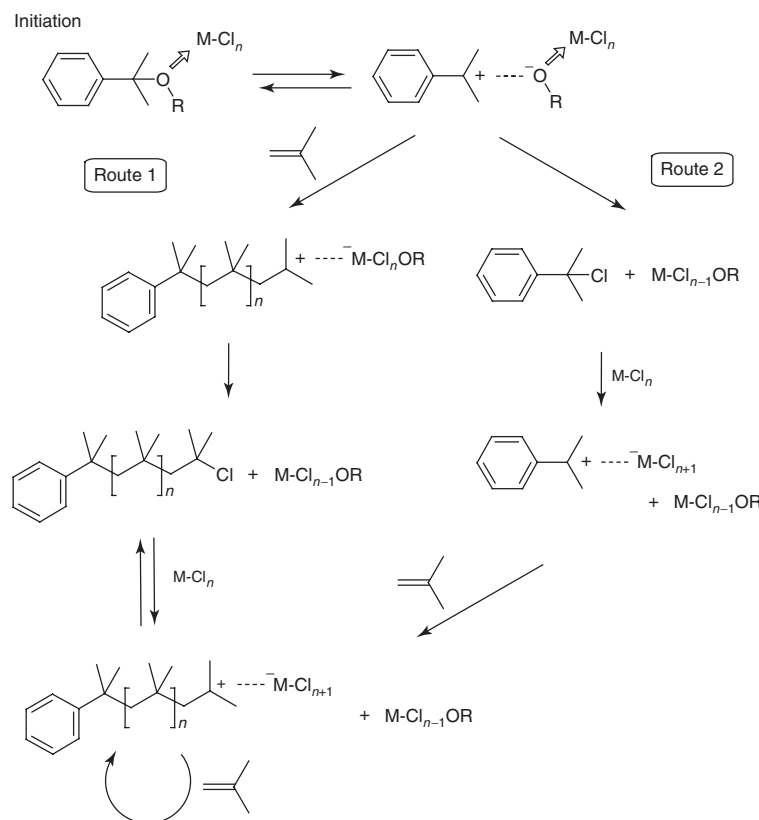


Figure 8.1 The first example of a “living” cationic polymerization of isobutene using cumyl acetate as initiator and BCl_3 as activator in dichloromethane at -30°C . Number-average molar mass, polydispersity index (numbers in the plot), and number of polymer chains (N) are reported as a function of the mass of PIB obtained. Source: Reprinted with permission from Faust R, Kennedy JP. J Polym Sci A Polym Chem 1987; 25:1847 [28]. Copyright 1987 John Wiley and Sons, Inc.

polymerization. The dormant PIB is in continuous equilibrium with the cationic species in the presence of excess activator and the electron donor, resulting in the “living” polymerization. When following route 2, the ionized complex is directly transformed into cumyl chloride and the $\text{CH}_3\text{OCOMtCl}_{n-1}$ electron donor. Subsequently, the cumyl chloride is transformed into the cationic initiating species by excess activator, which, after monomer addition, eventually results in the same “living” polymerization equilibrium between the dormant covalent species and the cationic PIB.

The “livingness” of the previously described systems is based on a complex initiation procedure involving the *in situ* formation of an electron donor complex. A simplified “living” polymerization procedure for isobutene was reported by Kennedy involving the addition of external electron donors, including amides, esters, amines, or sulfoxides [33]. The isobutene polymerization initiated by cumyl chloride or cumyl methyl ether with TiCl_4 as activator and *N,N*-dimethylacetamide or *N,N,N',N'*-tetramethyl ethylenediamine (TMEDA) as electron donor resulted in PIBs with high molar mass ($M_n > 10^5$ g/mol) and very narrow polydispersities ($M_w/M_n < 1.1$). The effect of the electron donor on the molar mass distribution is illustrated in Figure 8.2, showing



Scheme 8.7 Mechanism for the “living” polymerization of isobutene with cumyl esters or cumyl ethers as initiator and BCl_3 or TiCl_4 as activator. $\text{M} = \text{B}$ or Ti ; $\text{R} = \text{alkyl}$ or acyl .

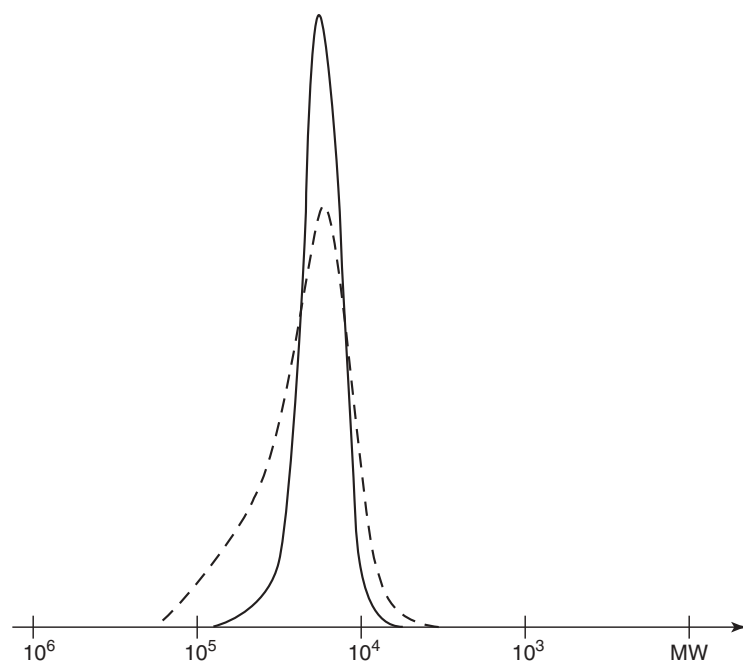


Figure 8.2 Poly(isobutene) molar mass distributions obtained using cumyl chloride as initiation and TiCl_4 as activator with (solid line) and without (dashed line) ethyl acetate as electron donor. Source: Reprinted with permission from Kaszas G, Puskas JE, Kennedy JP. Polym Bull 1988;20:413 [33]. Copyright 1988 Springer-Verlag.

the PIB molar mass distribution obtained with and without ethyl acetate as electron donor.

All these developed “living” cationic polymerization methods for isobutene provide defined tertiary chloride end groups, opening up possibilities for further end-group functionalization. A representative example was reported by Ivan and Kennedy, who described the quantitative conversion of the chloride into allyl-terminated PIB, which was converted into epoxy and hydroxyl-functional PIBs [34].

In addition to such postpolymerization modification methods, it is possible to directly include functionalities in PIB during the polymerization process by using pseudo-halide initiators, such as azide and thiocyanate, instead of halides [35]. Cheradame reported the use of cumyl azide and bifunctional 1,4-bis(1-azidomethyl)benzene initiators with AlEt_2Cl as Lewis acid activator for the polymerization of isobutene directly resulting in the mono-azido and bisazido telechelic PIBs, respectively (Scheme 8.8) [36, 37].

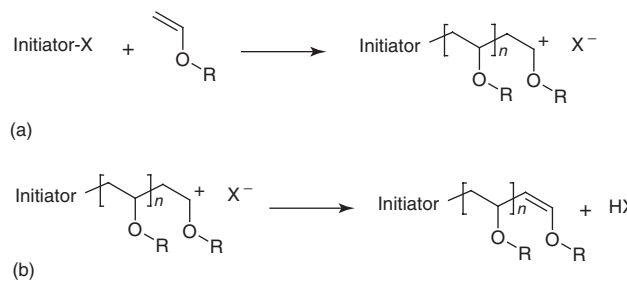
Direct end-capping of living PIB chains with a nucleophile is challenging because of the very high reactivity of the tertiary PIB carbenium ion. Faust *et al.* demonstrated that the living PIB chains react with 1,1-diphenylethylene (DPE) monomer, whereby the resulting DPE carbenium ion is more stable than the PIB carbenium ion. As a result, isobutene is not added to this relatively stable carbenium ion, while homopolymerization also does not occur because of the steric bulk of the phenyl rings [38]. Therefore, the living PIB chain ends can be quantitatively transformed into a single cationic DPE adduct, which has been utilized to couple various nucleophilic end-capping agents, including methanol, ammonia, and silanol ethers. Moreover, the less reactive DPE carbenium ion facilitates the initiation of more reactive monomers, such as styrenics [39, 40] as well as vinyl ethers [41, 42], resulting in PIB-containing block copolymers. Especially, ABA triblock copolymers with a PIB soft middle block and hard polystyrene outer blocks

are interesting thermoplastic elastomers based on the presence of hard polystyrene microdomains that act as physical crosslinks.

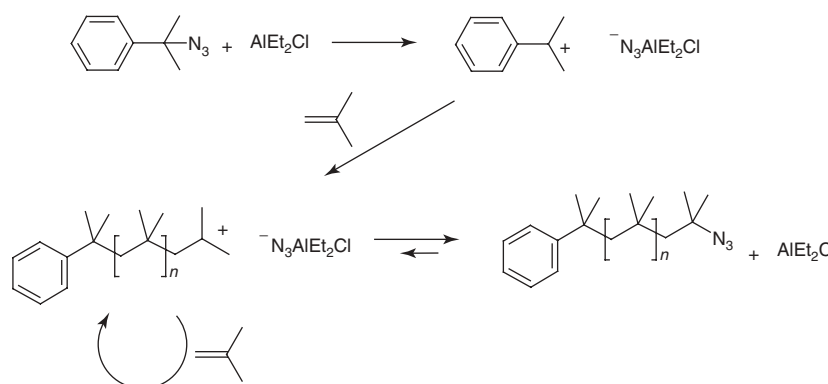
8.2.2 Vinyl Ethers

Vinyl ethers are another important class of monomers for carbocationic polymerizations that cannot be easily polymerized with radical polymerization methods because of insufficient activation of the double bond leading to very slow polymerization and low polymerization degrees. The uncontrolled cationic polymerization of vinyl ethers using strong acidic initiators, such as boron trifluoride and stannyl tetrachloride, is a well-established industrial method giving very high polymerization rates [43]. These very fast uncontrolled cationic polymerizations of vinyl ether result in carbocationic polymerization in combination with a range of chain-transfer- and termination reactions, leading to unsaturated end groups, for example, by hydrogen abstraction (Scheme 8.9).

Even though the cationic polymerization of vinyl ethers already dates back to 1878 [43], the first report on a controlled polymerization only appeared in the late 1970s by Johnson and Young [44]. They discovered that the



Scheme 8.9 (a) General polymerization mechanism for vinyl ethers and the commonly observed (b) hydrogen abstraction side reaction (X represents the leaving group).

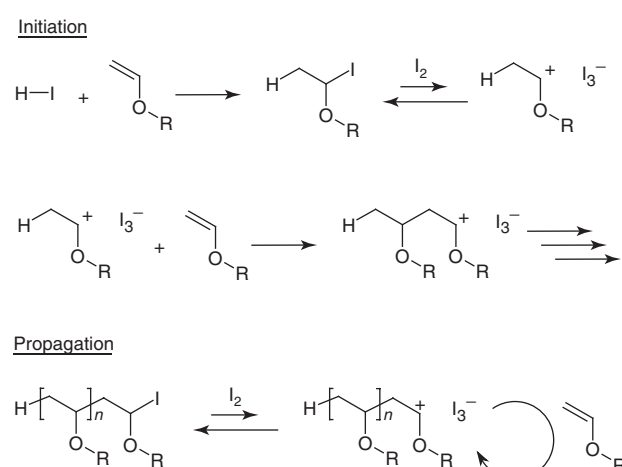


Scheme 8.8 “Living” polymerization of isobutene with a cumyl azide initiator and AlEt_2Cl as Lewis acid activator.

number-average molar mass (M_n) of polymers prepared by the iodine-initiated polymerization of butyl vinyl ether increased on sequential monomer addition after complete monomer consumption. Shortly afterward, Sawamoto and Kennedy reported a “quasi-living” carbocationic polymerization of vinyl ethers by continuous feeding of monomer to an initiator solution, whereby the M_n increased with the amount of added monomer [45]. However, in both these examples the M_n did not correlate to the theoretical value and the polydispersities were rather broad.

In 1984, the first living cationic polymerization of vinyl ethers was reported by Miyamoto et al. [46]. It was found that the polymerization of isobutylvinyl ether (IBVE) in the presence of hydrogen iodide and iodine (equimolar amounts) performed in hexane at -15°C resulted in a linear increase of M_n with conversion, whereby the amount of hydrogen iodide could be used to control the degree of polymerization. Final proof of the living character of the polymerization was provided by the successful formation of defined block copolymers by sequential monomer addition [47]. Detailed mechanistic and kinetic studies revealed that the polymerization is initiated by the addition of hydrogen iodide to the vinyl ether monomer resulting in the stable covalent α -iodo ether adduct [48]. The added iodine subsequently activates the carbon–iodine bond, leading to the cationic carbenium species. In the early days, a nonionic insertion mechanism was proposed for this hydrogen iodide/iodine-initiated polymerization [10], but nowadays it is generally accepted that there is a continuous equilibration between the “dormant” covalent iodine adduct and the active carbocation as depicted in Scheme 8.10. After this initial development of living polymerization conditions for vinyl ether monomers, various other initiating systems were reported showing similar living polymerization characteristics, whereby the combination of hydrogen iodide and zinc iodide has evolved into one of the most frequently used systems [49]. Nonetheless, a variety of other related cationic polymerization methods have been developed using, for instance, preformed α -chloro or α -bromo ethers as initiators with different zinc halides as activators, whereby the reactivity decreases in the order $\text{I} > \text{Br} \gg \text{Cl}$ [50].

Besides using preformed α -halide ether initiators, the living polymerization of vinyl ethers can be achieved with carboxylic acid/zinc halide mixtures [51, 52]. The carboxylic acid, such as trifluoro acetic acid, reacts with the vinyl ether resulting in the formation of a covalent adduct. The presence of zinc halide activates the acid bond and mediates the equilibrium between this dormant covalent adduct and the carbenium cation with trifluoroacetate as counterion (Scheme 8.11). When using a stronger Lewis acid, such as EtAlCl_2 , as activator, the equilibrium is too much shifted to the carbocationic form leading to very fast nonliving polymerization. However, upon addition of



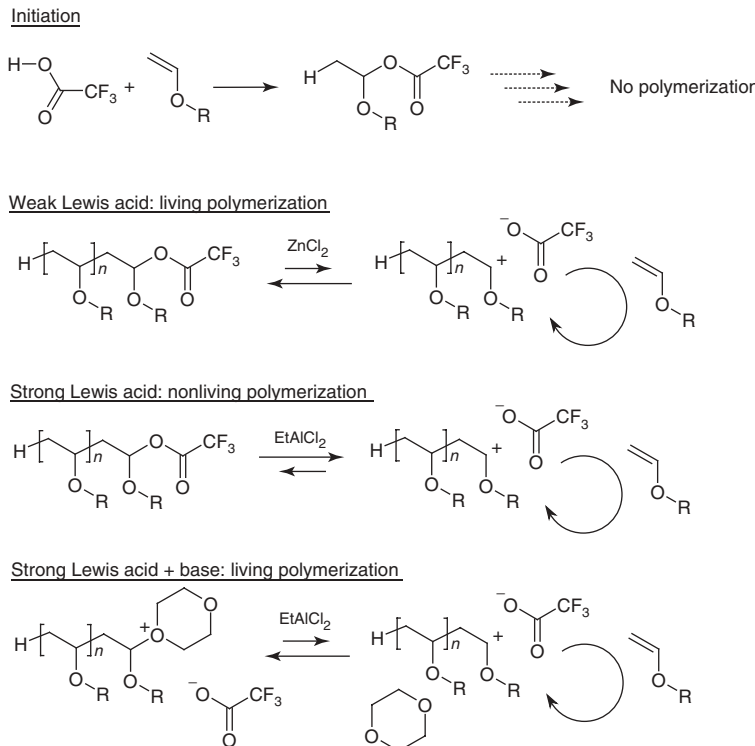
Scheme 8.10 Mechanism for the living cationic polymerization of vinyl ethers with hydrogen iodide and iodine as initiating system.

a base, such as dioxane, the polymerization with EtAlCl_2 became living again, which is due to the formation of an oxonium ion that stabilizes the dormant state and, thus, lowers the concentration of carbenium ions (Scheme 8.11).

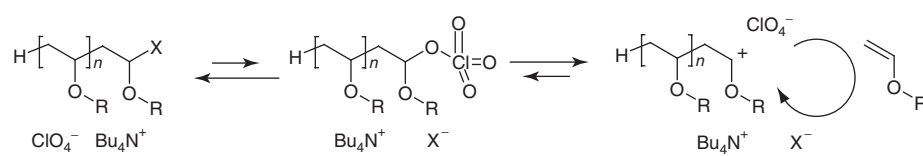
A final method to induce living polymerization of vinyl ethers is based on halide exchange reactions by the addition of a salt. The addition of a tetrabutyl ammonium salt with a nonnucleophilic counteranion, such as perchlorate, to an α -halide ether results in an exchange equilibrium between the halide and the perchlorate. The formed perchlorate adduct is also in equilibrium with the carbocationic species inducing living polymerization of various vinyl ethers as depicted in Scheme 8.12 [53–55].

Similarly, it is possible to transform the nonliving polymerization of vinyl ethers using highly reactive initiators, such as triflic acid, into a living polymerization by the addition of tetrabutyl ammonium iodide [56]. The addition of the halide salt establishes an equilibrium between the active triflate species and the dormant halide species, eventually leading to a similar overall polymerization equilibrium as depicted in Scheme 8.12.

In a recent study by Aoshima, a large variety of metal halides (Fig. 8.3) were screened for the living polymerization of isobutyl vinyl ether initiated by an α -chloro ether [57]. In the absence of added base, only zinc chloride gave rise to a controlled polymerization. By optimization of the base, namely addition of ethyl acetate, dioxane, or tetrahydrofuran, living/controlled polymerization could be achieved for all metal halides, except the metal pentachlorides and metal hexachloride. The polymerizations with SnCl_4 and FeCl_3 with the appropriate base led to very fast living polymerizations that were finished within seconds and the polymerization of isobutyl vinyl ether with NbCl_5



Scheme 8.11 Mechanism of the living polymerization of a vinyl ether with the trifluoroacetic acid using zinc chloride as weak Lewis acid activator or EtAlCl_2 as strong Lewis acid as activator, which leads to a living polymerization only in the presence of a base, for example, dioxane.



Scheme 8.12 Activation of dormant halide species by the addition of tetrabutyl ammonium perchlorate salt.

and TaCl_5 could be controlled by the addition of tetrabutyl ammonium chloride (Fig. 8.3b).

All previously discussed examples of living cationic polymerization of vinyl ethers were based on homogeneous polymerization media. In 2007, Oashima and coworkers demonstrated the living polymerization of isobutyl vinyl ether in the presence of iron(III) oxide as heterogeneous catalyst and ethyl acetate or dioxane as base [58]. The major advantage of this heterogeneous catalytic system is the easy removal of the metal oxide catalyst. In addition, it was demonstrated that the iron(III) oxide could be reused for at least five times without a decrease in activity.

The development of living cationic polymerization systems for vinyl ethers also enabled the incorporation of functional end groups as well as the control of the polymer architecture. Telechelic polymers have been prepared based on bifunctional initiating systems [59, 50, 60] while

multifunctional initiators [61–63] have been utilized for the preparation of star-shaped poly(vinyl ether)s. Larger, but less defined, star-shaped poly(vinyl ether)s have been reported based on the arm-first method; that is, living poly(vinyl ether) chains were transformed into star-shaped polymers by the addition of a bifunctional vinyl ether monomer yielding well-defined star-shaped polymers with 9–44 arms and polydispersity indices below 1.2 [64]. Such star-shaped poly(vinyl ether)s have been used as template for the preparation of gold nanoclusters in combination with a oligoethylene glycol vinyl ether monomer which results in a thermoresponsive poly(vinyl ether) that dissolves in cold water and precipitates upon heating [65]. This hybrid gold nanocluster–polymer system was applied as catalyst for aerobic alcohol oxidation, whereby the polymer phase transition enabled facile isolation of the catalyst upon heating.

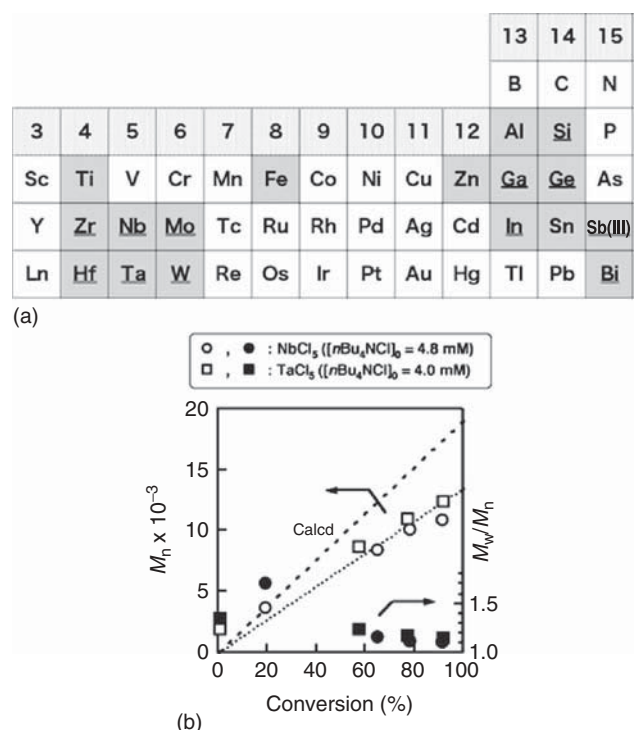
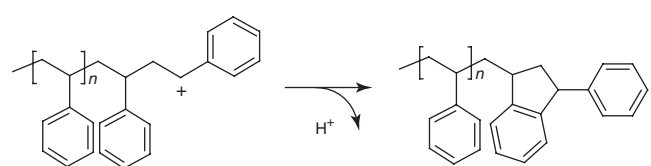


Figure 8.3 (a) All metal elements in gray were screened as metal halides for the living polymerization of vinyl ethers in the presence of added salts and bases. (b) Number-average molar mass (M_n) and polydispersity index (PDI) as function of conversion for the controlled polymerization of isobutyl vinyl ether with NbCl_5 and TaCl_5 in the presence of tetrabutyl ammonium chloride. *Source:* Reprinted with permission from Kanzawa A, Kanaoka S, Aoshima S. *Macromolecules* 2009;42:3965–3972 [57]. Copyright 2009 American Chemical Society.

8.2.3 Styrene Monomers

The cationic polymerization of styrene has been known since the 1960s using Lewis acids or strong protic acids as initiators leading to fast, uncontrolled polymerization due to extensive proton transfer reactions to, for example, counteranion, solvent, monomer, or polymer. In addition, chain transfer occurs as a result of an intramolecular Friedel–Craft reaction of the carbocation with the penultimate monomer unit, resulting in an indane chain end and the release of a proton that can reinitiate a new polymer chain as illustrated in Scheme 8.13.



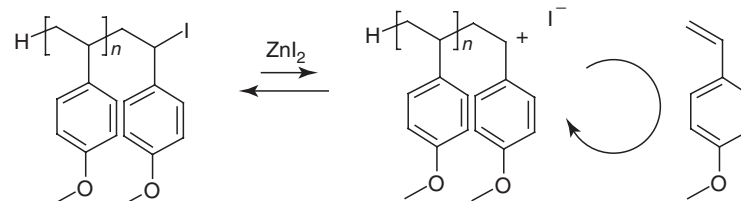
Scheme 8.13 Chain transfer by indane formation during the uncontrolled cationic polymerization of styrene.

The first step toward the development of a living cationic polymerization procedure for styrene was the observation by Pepper that the polymerization of styrene, initiated by anhydrous perchloric acid, stopped at limited conversion when performed below -80°C [66]. Upon heating, the polymerization was found to continue, which was ascribed to the formation of dormant perchlorate ester end groups at low temperatures, which dissociate into the perchlorate anion and the carbenium ion at elevated temperatures representing the first reported example of an equilibrium between dormant and active chains. The presence of a perchlorate ester end group at each polymer chain was confirmed by the successful formation of block copolymers upon the addition of *N*-*tert*-butyl aziridine to the dormant polymer chains resulting in living cationic ROP [67]. This latter report was most likely the first ever on the synthesis of block copolymers based on carbocationic polymerization utilizing a sequential monomer addition protocol.

Initially, Gandini and Plesch proposed that the perchloric acid-initiated low temperature polymerization of styrene is based on monomer insertion on the nonionic perchlorate chain ends, which was based on the observation that the polymerization mixture was not conductive [68, 69]. These nonionic polymerizations were referred to as *pseudocationic polymerizations*. However, more detailed investigations by stopped-flow UV–vis spectroscopy revealed the presence of short-lived carbocations indicating that these are the propagating species in the cationic polymerization of styrene [70, 71]. This was also confirmed for the polymerization of styrene with triflic acid for which Matyjaszewski and Sigwalt showed that the covalent triflic ester adduct was unstable even at -78°C leading to carbocationic propagating species [72].

The carbocationic polymerization of styrene involves secondary benzylic carbenium ions that are stabilized by resonance with the aromatic ring. As such, the presence of electron donating groups, such as alkoxy or alkyl, on the aromatic ring will stabilize the carbenium ion. The first report on controlled/living cationic polymerizations of styrenes involved such stabilized *p*-alkoxystyrene derivatives. Higashimura reported in 1979 that the polymerization of *p*-methoxystyrene contained long-lived propagating species when performed with iodine as initiator [73]. The same group reported the living polymerization of *p*-methoxystyrene with hydrogen iodide/zinc iodide as initiating system at -15°C in toluene (Scheme 8.14) [74]. The utilization of functional initiators and/or functional end-capping agents was explored for the synthesis of poly(*p*-alkoxystyrene)s with defined end-group functionalities [75].

The living carbocationic polymerization of styrene was reported by Kennedy using 2-chloro-2,4,4-trimethylpentane (TMPCl) with TiCl_4 as initiating system in the presence of various electron donors, such as *N,N*-dimethylacetamide



Scheme 8.14 Living carbocationic polymerization of *p*-methoxystyrene using hydrogen iodide and zinc iodide as initiating system in tetrachloromethane.

and hexamethylphosphoramide, and 2,6-di-*tert*-butyl pyridine as proton trap [76]. In the absence of these additives, ill-defined polymers with bimodal molecular weight distributions were obtained. The development of this living carbocationic polymerization method enabled the preparation of linear and three-arm star polystyrene-*b*-poly(isobutene)-*b*-polystyrene triblock copolymers as thermoplastic elastomers [77].

A rather unexpected water- and alcohol-insensitive activator, namely boron trifluoride etherate, was developed by Sawamoto for the living polymerization of *p*-hydroxystyrene in combination with the water adduct of *p*-methoxystyrene as initiator [78]. The polymerizations proceeded even in large excess of water, which is in large contrast with the absolutely dry conditions that are normally required for carbocationic polymerizations. It is proposed that acetonitrile, which is used as polymerization solvent, stabilizes the short-lived carbocationic propagating species. The same polymerization methodology could be applied for the preparation of statistical and block copolymers consisting of *p*-hydroxystyrene and *p*-methoxystyrene [79], as well as for the homopolymerizations of styrene, *p*-chlorostyrene and *p*-methylstyrene in the presence of a proton trap [80].

The controlled polymerization of *p*-methoxystyrene was also demonstrated in aqueous media using the *p*-methoxystyrene HCl adduct as initiator and $Yb(OTf)_3$ as Lewis acid activator [81]. Very recently, the aqueous living cationic suspension polymerization of styrene and methoxystyrene was reported by Ganachaud using the water adduct of *p*-methoxystyrene as initiator and $B(C_6F_5)_3$ as water tolerant Lewis acid activator [82, 83].

8.3 CATIONIC RING-OPENING POLYMERIZATION

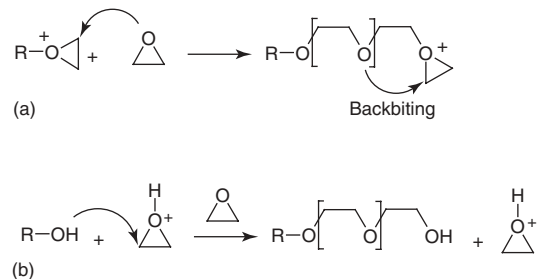
Living cationic ring-opening polymerization (CROP) techniques represent important methods for the polymerization of a wide variety of heterocyclic monomers, such as cyclic ethers, cyclic amines, and cyclic imino ethers [7, 84–87]. The main differences between carbocationic polymerization of vinyl monomers and CROP of heterocyclic monomers arise from the nucleophilic heteroatoms

in the latter monomer classes. These heteroatoms undergo cationic ring-opening and are present in the resulting polymer chains where they are prone to undergo chain transfer reactions with the cationic propagating species. So in contrast to the transfer reactions that are induced by the highly reactive carbocations present during cationic vinylic monomer polymerization, the chain transfer reactions that occur during cationic ROP are induced by the similar nucleophilicity of the monomer and the polymer. This section will discuss the living CROP of the most important monomer classes, namely cyclic ethers, cyclic amines, and cyclic imino ethers.

8.3.1 Cyclic Ethers

CROP is only reported for a limited number of cyclic ethers that exhibit enough ring strain to be readily opened. In addition, the rather similar nucleophilicity of the ether moieties in the monomers and the ring-opened polymers together with the reactive cationic oxonium species, often leads to the occurrence of transesterification reactions, complicating the development of living CROP methods. This section will focus on the living CROP of ethylene oxide, oxetane, and tetrahydrofuran.

8.3.1.1 Poly(ethylene oxide) Poly(ethylene oxide), or poly(ethylene glycol), is a popular material for personal, home, and health care applications because of its water solubility in combination with a very low toxicity and the fact that it is not easily recognized by the human immune system [88]. Well-defined poly(ethylene oxide) can be prepared by either living anionic ROP [87–90] or living CROP [87, 91], wherein the anionic polymerization method is mostly used in contemporary research since it yields well-defined polymers in a relatively straightforward manner when carefully purifying all reaction components. In contrast, the CROP of ethylene oxide in standard conditions, that is, an excess of monomer compared to the initiator, results in an uncontrolled polymerization due to the occurrence of backbiting reactions of the cationic propagating species with the polymeric ether moieties resulting in cyclic oligomers. To avoid these backbiting reactions, the CROP of ethylene oxide should be performed

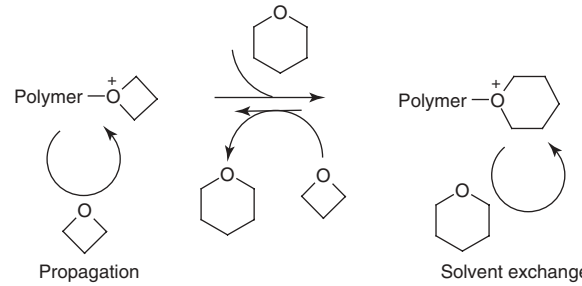


Scheme 8.15 CROP of ethylene oxide via (a) activated chain-end polymerization or (b) activated monomer polymerization.

via an activated monomer approach instead of a chain-end activation approach [87, 91]. This activated monomer polymerization procedure requires an excess of hydroxyl end groups in relation to the monomer and, thus, involves continuous feeding of the monomer to keep the monomer concentration very low (Scheme 8.15).

8.3.1.2 Poly(oxetane) The uncontrolled CROP of oxetanes, or 1,3-propylene oxide, is a commonly applied polymerization method for the fixation of coatings by crosslinking. In contrast to these widespread applications of oxetanes in coatings, only a few recent examples of the living CROP of oxetanes have been reported that are based on reversible deactivation of the living chain end by exchange with a nucleophilic nonpolymerizable solvent, such as dioxane or tetrahydropyran [92, 93]. The large excess of the solvent will induce addition of this cyclic ether onto the living polymer chain end, leading to a stable oxonium ion that does not react with the polymeric ether moieties and, thus, prevents chain transfer reactions. Continuous exchange of the oxonium end group leads mostly to solvent exchange reactions. When the oxonium solvent adduct is exchanged with oxetane, the higher reactivity enables the ring-opening of the subsequent oxetane unit leading to polymerization. This proposed polymerization mechanism is depicted in Scheme 8.16. Well-defined poly(oxetane)s could be prepared in dioxane (M_n up to 150,000 g/mol; polydispersity below 1.3), although incorporation of the dioxane into the polymers was observed above 50% monomer conversion because of activation by copolymerization. The lower nucleophilicity of tetrahydropyran could prevent the incorporation of the solvent, but a relatively slow exchange between the oxetane and tetrahydropyran adducts led to polydispersity indices of 1.4–1.5.

8.3.1.3 Poly(tetrahydrofuran) The cyclic ether monomer that has been studied in most detail with regard to living CROP is tetrahydrofuran [94]. As a result of its slightly higher nucleophilicity compared to the polymeric ether bonds, in combination with less sterical hindrance, it is relatively straightforward to develop a



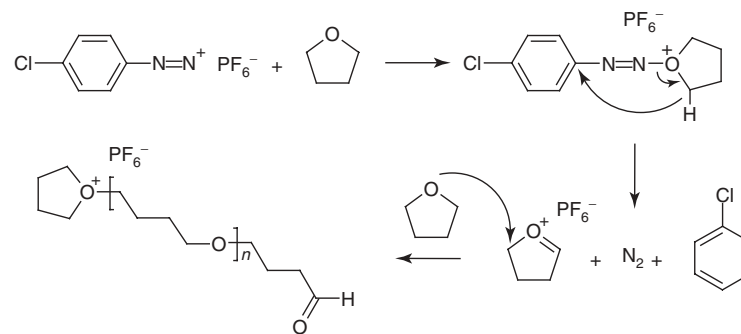
Scheme 8.16 Living cationic ring-opening polymerization of oxetane using tetrahydropyran as solvent to control polymerization.

living polymerization procedure since the propagating oxonium species do not readily attack the polymer. The first living CROP of tetrahydrofuran was reported by Dreyfuss and Dreyfuss using (*p*-chloro)benzenediazonium hexafluorophosphate as initiator [95, 96]. Detailed mechanistic investigations revealed that the chlorophenyl cation abstracts a hydrogen from tetrahydrofuran and the resulting oxonium ion initiates the polymerization leading to an aldehyde functionality at the beginning of the polymer chains as depicted in Scheme 8.17.

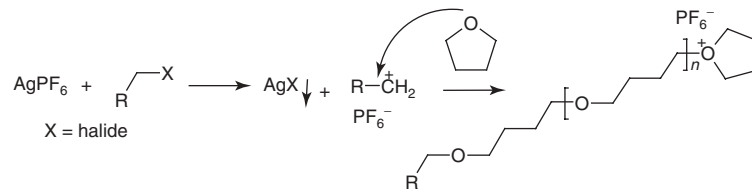
Initiation of the living CROP of tetrahydrofuran with organic halides was first reported by Thompson [97]. Both the alkyl halide and silver hexafluorophosphate were added to initiate the polymerization, whereby halide exchange results in precipitation of the silver halide salt under the formation of the carbocationic hexafluorophosphate adduct that initiates the polymerization (Scheme 8.18). This organohalide initiation method provides direct control over the polymer end groups by variation of the halide initiator, as was demonstrated using, for example, bifunctional organohalide initiators [97, 98], or initiators carrying initiating groups for controlled radical polymerizations providing direct access to poly(tetrahydrofuran) containing block copolymers [99].

In contrast to these initial reports on the living CROP of tetrahydrofuran which were performed without additional solvents, Penczek and coworkers demonstrated that the solvent plays an important role in the cationic ROP of tetrahydrofuran since it controls the proximity and stability of the ion pair at the living chain end [100, 101]. The polymerization rate increases in more polar solvents because of stabilization of the ion pair, whereby it was demonstrated that the methyl-triflate-initiated CROP of tetrahydrofuran involves an equilibrium between the cationic propagating oxonium species and the covalent triflic acid adduct, which can be shifted by the solvent choice as depicted in Scheme 8.19. Nonetheless, as a result of the much higher reactivity of the cationic propagating species, the polymerization rate is almost exclusively determined by the concentration of oxonium ions.

For the preparation of functional poly(tetrahydrofuran), a variety of other triflic esters have been prepared starting



Scheme 8.17 Mechanism for the *p*-chlorobenzenediazonium hexafluorophosphate-initiated living cationic ring-opening polymerization of tetrahydrofuran.



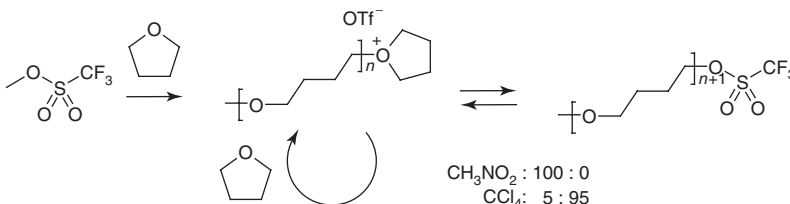
Scheme 8.18 Mechanism for the living cationic ring-opening polymerization of tetrahydrofuran initiated by the addition of both an organic halide and silver(I) hexafluorophosphate.

from the corresponding alcohols by reaction with triflic anhydride in the presence of 2,6-di-*tert*-butylpyridine as nonnucleophilic proton trap [102, 103]. Nonactivated aliphatic triflic esters resulted in slow initiation of the CROP, while the activated triflic esters of allyl alcohol and benzyl alcohol precursors afforded fast initiation, linear first-order kinetics, and poly(tetrahydrofuran) with narrow molar mass distributions. This approach has been extended to the preparation of well-defined three-arm star poly(tetrahydrofuran) using the triflic ester of 1,3,5-tris(hydroxymethyl)benzene as initiator [103].

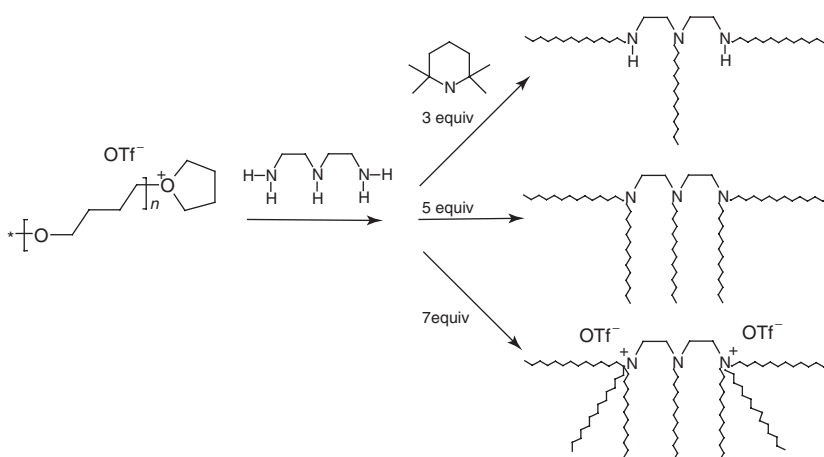
In addition to the introduction of functional groups during initiation, termination of the living chain ends by the addition of a nucleophile has been exploited. Most commonly, water is added as terminating agent, resulting in the direct formation of a hydroxyl chain-end functionality. In addition, a wide range of amine nucleophiles can be utilized as end-capping agents, including primary, secondary, tertiary amines as well as less reactive aromatic amines [104–106]. It is important to note that termination with primary amines leads to the formation of a polymeric secondary amine that can also terminate a living chain end, resulting in a polymeric tertiary amine that can react with a third living polymer chain potentially leading to star-shaped polymers. Nonetheless, this subsequent termination of living polymer chains with primary amines is partially obstructed by the release of triflic acid which protonates the formed secondary amines [106]. The multiple end-capping possibilities of primary amines

with living poly(tetrahydrofuran) chains was exploited by Goethals for the preparation of star-shaped polymers [107]. The living CROP of tetrahydrofuran was terminated by adding diethylene triamine as end-capping agent together with 2,2,6,6-tetramethylpiperidine to trap the released triflic acid. The number of polymer arms of the resulting star-shaped poly(tetrahydrofuran) could be controlled to be 3, 5, or 7 by varying the amount of proton trap that was added as depicted in Scheme 8.20. The solution and melt viscosity of the star-shaped poly(tetrahydrofuran) was significantly lower compared to the linear analogs because of reduced chain entanglements. Combination of this end-capping approach with methacrylate- or allyl-functionalized triflic ester initiators yielded star-shaped poly(tetrahydrofuran) bearing reactive double bonds at the periphery, which were successfully utilized for the preparation of crosslinked polymer networks [108, 109].

Upon termination of the living CROP of tetrahydrofuran with (strained) cyclic tertiary amines, such as 1,3,3-trimethylazetidine, *N*-phenyl-pyrrollidine, or *N*-phenyl-piperidine, the reactivity of the cationic chain end is significantly reduced making it insensitive to water while it still can react with stronger nucleophiles, such as deprotonated carboxylic acids [110–112], which has been exploited for the introduction of chain-end functionalities as well as for the formation of star-shaped poly(tetrahydrofuran) and poly(tetrahydrofuran) graft copolymers by reaction with poly(acrylic acid) sodium salt [113]. More recently, Tezuka demonstrated the formation of a wide range of



Scheme 8.19 Schematic representation of the methyl-triflate-initiated CROP of tetrahydrofuran comprising equilibration between cationic and covalent propagating species. The ratio of the cationic versus covalent propagating in different solvents is also indicated.



Scheme 8.20 Synthesis of three, five-, and seven-armed star-shaped poly(tetrahydrofuran) by end-capping with diethylene triamine in the presence of different amounts of 2,2,6,6-tetramethylpiperidine proton trap.

multicyclic polymer structures based on the combination of functional groups carrying bifunctional triflic ester initiators, *N*-phenyl-pyrrolidine end-capping, followed by cyclization with a functional group carrying bifunctional acids and coupling of these cyclic poly(tetrahydrofuran)s utilizing click chemistry methods [114]. As a representative example, the synthesis of poly(cyclic poly(tetrahydrofuran)) is schematically depicted in Scheme 8.21.

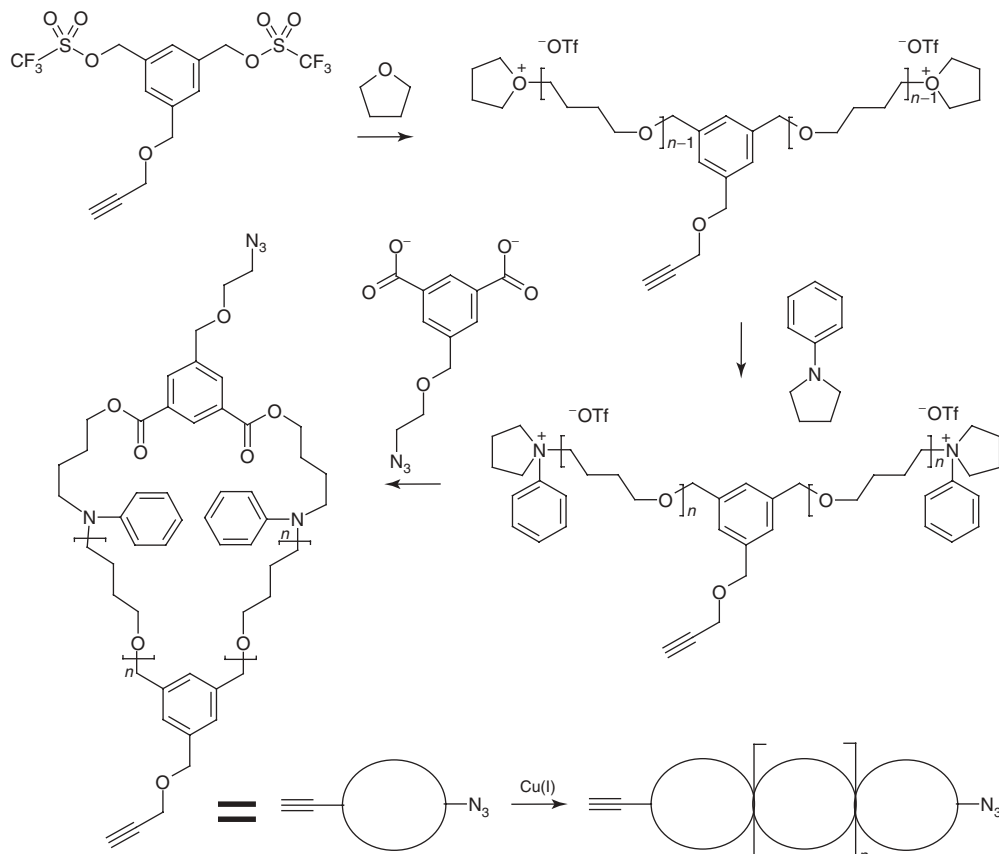
Besides first moderating the oxonium end-group activity by reaction with cyclic tertiary amines followed by termination, the living CROP of tetrahydrofuran can be also directly terminated by the addition of carboxylic acid sodium salts [99], dithiocarbamic acid sodium salts [115], or sodium alkoxides [116]. However, these direct functionalization approaches are more sensitive to traces of water or other impurities and do not allow extensive manipulation of the living polymer chains.

In contrast to these beautiful examples of poly(tetrahydrofuran) chain-end modification, the majority of studies that utilize poly(tetrahydrofuran) make use of the commercially available methyl triflate or triflic anhydride [117] initiators in combination with water as terminating agent, resulting in mono- or bis-hydroxy-functionalized

poly(tetrahydrofuran). These hydroxyl-functionalized polymers can be further used in a variety of different coupling and modification reactions. Poly(tetrahydrofuran) is a soft material with a glass transition temperature of -86°C and has been frequently used as soft block in thermoplastic elastomers [118–120]. The relatively straightforward access to well-defined poly(tetrahydrofuran)s by living CROP also stimulated their application in supramolecular polymers by incorporation of end groups capable of hydrogen bonding [121, 122] or metal–ligand complexation [123–125].

8.3.2 Cyclic Amines

Cyclic amines represent another class of monomers that can be polymerized by CROP, whereby various polymer properties can be obtained by variation of the ring-size as well as the substituents on both the carbon and nitrogen atom. Three- and four-membered cyclic amines, aziridines and azetidines, possess high ring strain and can undergo CROP, while larger cyclic amines do not have sufficient ring strain to undergo CROP. Similar to the CROP of cyclic ethers, the nucleophilicity of the amine groups in the monomers and polymers are both rather



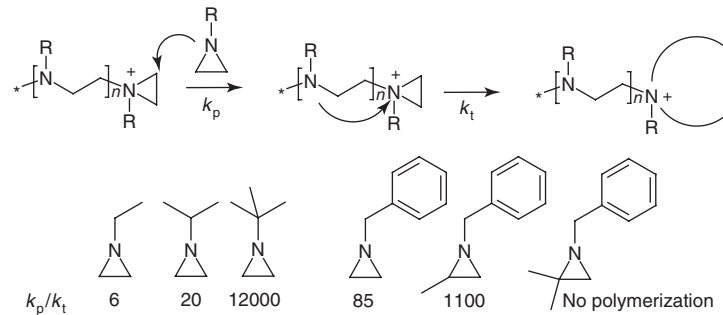
Scheme 8.21 Schematic representation of the synthesis of poly(cyclic poly(tetrahydrofuran)), bottom right, utilizing a bifunctional alkyne-modified initiator for the living CROP followed by end-capping with *N*-phenyl-pyrrolidine to moderate the end-group reactivity. Subsequent end-group modification with a bifunctional acid modified with an azide moiety yields the cyclic poly(tetrahydrofuran) comprising both alkyne and azide functionalities, which is subsequently polymerized by cycloaddition in the presence of copper(I).

high, facilitating chain transfer and/or termination reactions and, thus, complicating the development of living CROP methods. In this section, the CROP of aziridines and azetidines will be discussed.

8.3.2.1 Aziridines Ethylenimine is the simplest aziridine and its CROP is already known since 1941 [126]. Currently, poly(ethylenimine) is still produced on an industrial scale via CROP. However, the CROP of ethylenimine, that is, unsubstituted aziridine, produces a highly branched poly(ethylenimine) because of the occurrence of proton transfer reactions, chain transfer reactions as well as various termination reactions resulting in a polymer that contains a mixture of primary, secondary, and tertiary amine groups. This extensive occurrence of transfer reactions is caused by the high nucleophilicity of the secondary amine groups in the polymer that strongly compete with the monomer. The CROP of 2-methylaziridine and 2-phenylaziridine have also been reported, but are even

more complicated than the polymerization of ethylenimine because of the occurrence of the previously discussed transfer and termination reactions in combination with variations in tacticity as well as the presence of head-to-tail, tail-to-tail and head-to-head diads [127, 128].

In comparison to the previously discussed monomers, the polymerization of *N*-substituted aziridines is easier to control since the side reactions by proton transfer are eliminated because of the absence of primary and secondary amines. Nonetheless, termination by nucleophilic attack of the cationic propagating chain end into polymeric tertiary amines results in the formation of unreactive quaternary ammonium groups, that is, termination. As a result, the polymerization of *N*-substituted aziridines usually stops at limited conversion as was first demonstrated for *N*-methylaziridine by Jones [129]. Detailed evaluation of the polymerization kinetics as well as the evolution of molar mass during the polymerization revealed that termination mainly occurs via intramolecular backbiting

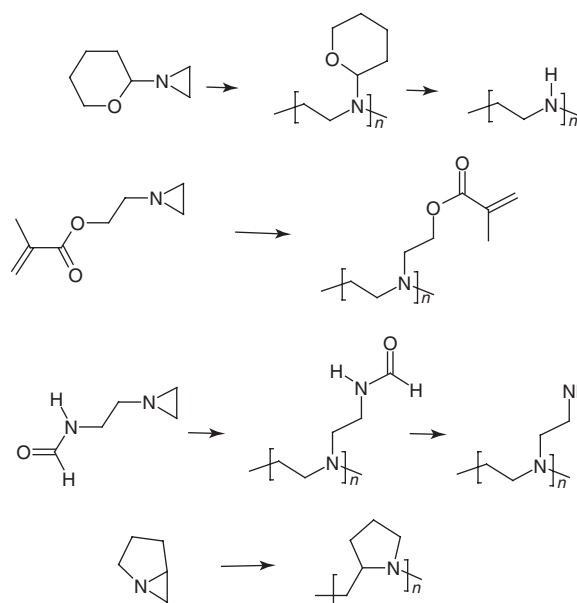


Scheme 8.22 Schematic representation of the CROP of N-substituted aziridines and the most prominent intramolecular termination reaction. At the bottom, the k_p/k_t ratio for several monomers is given as a measure for the livingness of the polymerization (performed in CH_2Cl_2 using Et_3OBF_4 as initiator at 20°C).

yielding a stable nonstrained cyclic polymer end group. The ratio of the polymerization rate constant (k_p) over the termination rate constant (k_t) can be regarded as a measure for the livingness of the polymerization of N-substituted aziridines (Scheme 8.22) [85]. By changing the N-substituent from ethyl to isopropyl and tertbutyl, the k_p/k_t ratio significantly increases, indicating that termination is more strongly suppressed by the steric bulkiness of the monomer than the polymerization, which can be understood by the fact that the polymeric amines are surrounded by multiple, flexible substituents while the end group and monomer both carry one substituent that is constrained by the cyclic aziridine structure [130]. Similarly, the introduction of a methylene substituent on the carbon atom of *N*-benzyl-aziridine significantly increases the k_p/k_t ratio while introducing two substituents on the same carbon atom completely suppresses the polymerization [85, 130, 131].

Even though termination cannot be completely eliminated for the polymerization of tertbutylaziridine, the termination rate is much slower than the propagation rate resulting in a defined end group at near-quantitative conversions, which together with the good control over the molar mass distribution are the characteristics of a controlled polymerization [132]. Since termination reactions are suppressed during the polymerization of *N*-*tert*-butylaziridine, the living cationic polymer chains can be terminated by the addition of a nucleophile to introduce a wide range of end-group functionalities [133, 134] as well as for the preparation of block and graft copolymer structures when using polymeric nucleophiles [133, 135].

Besides the most frequently studied N-substituted aziridine, *N*-*tert*-butylaziridine, a number of functional poly(N-substituted aziridine)s has been reported based on *N*-tetrahydropyryanylaziridine, 2-(1-aziridinyl)ethyl methacrylate, *N*-(ethylformamide)aziridine, and the bicyclic 1-aza-[1,3,0]-bicyclohexane as depicted in Scheme 8.23.



Scheme 8.23 Structures of less common N-substituted aziridines as precursors for functional polymers. From top to bottom: *N*-tetrahydropyryanylaziridine, 2-(1-aziridinyl)ethyl methacrylate, *N*-(ethylformamide)aziridine, and the bicyclic 1-aza-[1,3,0]-bicyclohexane.

The CROP of *N*-tetrahydropyryanylaziridine results in the tetrahydropyran-protected linear poly(ethylenimine) and, thus, provides straightforward access to linear poly(ethylenimine) by acidic removal of the tetrahydropyran groups (Scheme 8.23) [136]. As discussed previously, linear poly(ethylenimine) cannot be prepared by simply polymerizing ethylenimine because of transfer reactions resulting in branched polymers. Poly(ethylenimine)s with polymerizable methacrylate side groups have been reported based on the CROP of 2-(1-aziridinyl)ethyl methacrylate (Scheme 8.23) [137]. Subsequent radical polymerization of the methacrylate moieties results in densely crosslinked

polymer networks. Poly(*N*-(2-aminoethyl)azetidine) has been prepared by CROP of the corresponding formamide derivative since the presence of a nucleophilic amino group during the CROP would result in termination reactions [138]. Subsequent hydrolysis of the formamide groups resulted in the amino-functionalized poly(ethylenimine) as depicted in Scheme 8.23. A final example of a functional poly(aziridine) is based on the polymerization of the bicyclic 1-aza-[1,3,0]-bicyclohexane monomer resulting in a chiral polymer with a cyclic tertiary amine in the backbone (Scheme 8.23) [139, 140].

8.3.2.2 Azetidines The CROP of azetidines without the N-substituent is very similar to the CROP of ethylenimine as discussed in the previous section. As such, the CROP of azetidine is accompanied by a large number of hydrogen transfer, chain transfer, and termination reactions resulting in the formation of branched poly(propylenimine) comprising a mixture of primary, secondary, and tertiary amines [141].

The introduction of an N-substituent to the azetidine ring avoids the proton transfer reactions resulting in a polymerization that can be simply described by initiation, polymerization, and termination. Especially, the termination might give rise to branching and uncontrolled polymerizations when the living cationic chain end reacts with polymeric amines yielding a quaternary ammonium branching point. The CROP of three N-substituted azetidine monomers has been studied in detail, namely 1,3,3-trimethylazetidine, *N*-phenylazetidine, and 1-azabicyclo[4.2.0]octane (conidine) as shown in Scheme 8.24.

Kinetic investigations of the CROP of 1,3,3-trimethylazetidine with triethyloxonium tetrafluoroborate as initiator revealed that the polymerization proceeded in a living manner [142, 143]. In contrast to the living polymerization of 1,3,3-trimethylazetidine, significant termination reactions by attack of the living chain end onto polymeric amines were observed for the CROP of 1-methylazetidine, leading to branches or cyclic end groups (see Scheme 8.22) resulting from intermolecular and intramolecular termination, respectively [144]. This striking difference between the CROP of 1-methylazetidine and 1,3,3-trimethylazetidine clearly demonstrates the

importance of the two methyl groups attached to the polymer backbone, which apparently induce sufficient steric hindrance to obstruct the reaction between the azetidinium propagating species with the polymeric amines.

Similarly, the polymerization of *N*-phenylazetidine with methyl triflate as initiator shows a relatively controlled polymerization, although branching due to predominantly intermolecular termination does occur as demonstrated by the relatively low k_p/k_t ratio of 30 at 30 °C [145].

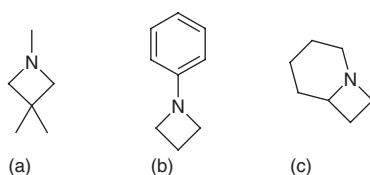
The bicyclic azetidine monomer 1-azabicyclo[4.2.0]octane can be polymerized in a living manner using the proton acid or alkylhalide adducts of the monomer as initiator, as demonstrated by the constant concentration of active species as well as the linear increase of the degree of polymerization with conversion [146, 147]. In addition, 1-azabicyclo[4.2.0]octane is a chiral monomer, and, by polymerization of an enantiomerically pure monomer, main-chain chiral polymers were obtained [148].

8.3.3 Cyclic Imino Ethers

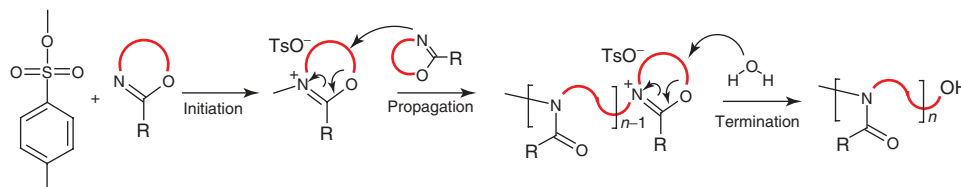
In contrast to the previously discussed cationic ROPs, the nucleophilicity of the cyclic imino ether monomers is much higher compared to the resulting poly(cyclic imino ether)s. This decrease in nucleophilicity is due to the isomerization of the imino ether moiety into an amide during the CROP as depicted in Scheme 8.25. As a result, the CROP of a wide range of cyclic imino ethers can be performed in a living manner since chain transfer to polymer side reactions are less likely to happen. Moreover, the R-group attached to the 2-position of the monomer determines the polyamide side chains and strongly influences the polymer properties.

The CROP of 2-oxazoline and 2-oxazine cyclic imino ethers was first reported in 1965 by Litt in a patent application [149]. Shortly thereafter, the CROP of various 2-oxazolines and a range of cationic initiating systems was demonstrated by four independent research groups [150–153] and the first scientific report on the CROP of 2-oxazines polymerization also appeared in 1967 [154]. The CROP of 2-oxazolines bearing chiral 4- and 5-substituents on the ring was first reported in 1974 [155, 156]. The following will focus on the living CROP of 2-oxazolines since this is the most extensively studied class of cyclic imino ethers. For an overview of the polymerization of larger cyclic imino ethers as well as 4- and 5-substituted 2-oxazoline monomers, the reader is referred to a recent review article [157].

Poly(2-oxazoline)s are attractive materials because a wide range of different monomers can be polymerized by living CROP, whereby the polymer properties can be significantly altered by changing the substituent on the 2-position of the 2-oxazoline ring. The importance of this side chain on the resulting polymer properties are evident



Scheme 8.24 Structure of the most commonly studied azetidine monomers: (a) 1,3,3-trimethylazetidine, (b) *N*-phenylazetidine, and (c) 1-azabicyclo[4.2.0]octane.



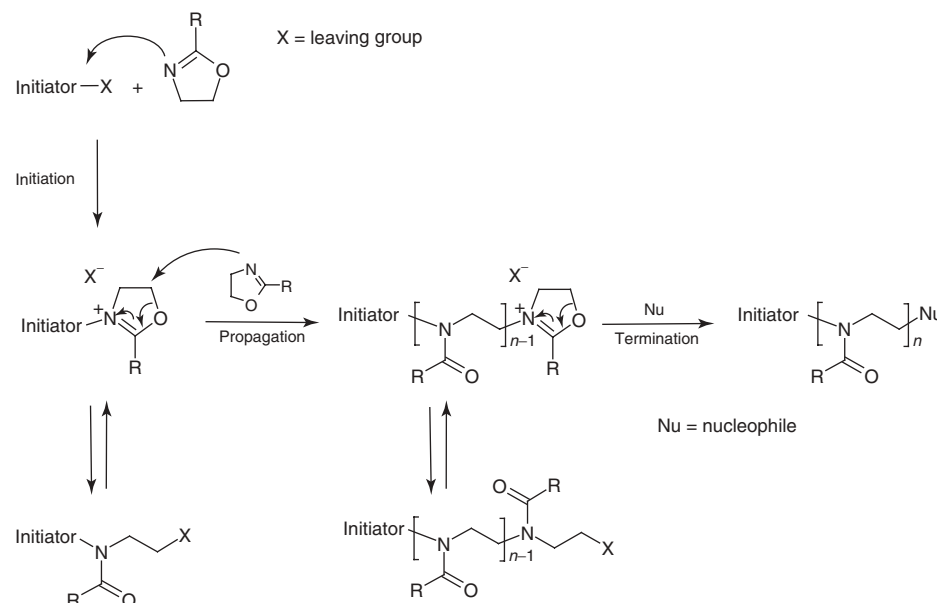
Scheme 8.25 Schematic representation of the methyl-tosylate-initiated CROP of cyclic imino ethers indicating the isomerization from an imino ether to an amide moiety during polymerization as well as the R functionality of the monomer that determines the polymer side-chain functionality.

from the water solubility of poly(2-methyl-2-oxazoline), the lower critical solution temperature (LCST) behavior of poly(2-ethyl-2-oxazoline) [158, 159], and the different analogues of poly(2-propyl-2-oxazoline) [160–162], while larger aliphatic or aromatic side chains result in hydrophobic polymers. In addition, poly(2-methyl-2-oxazoline) and poly(2-ethyl-2-oxazoline) are biocompatible and are not recognized by the immune system of living species similar to poly(ethylene oxide) [88, 163, 164]. In addition, 2-oxazolines with saturated and/or unsaturated fatty acid side chains have been prepared and polymerized by living CROP [165].

Under appropriate conditions, mostly using alkyl halides, triflates, or tosylates as initiator, the CROP of 2-oxazolines proceeds via a “living” mechanism [84, 86]. In such an ideal “living” polymerization, all polymer chains are initiated at the same time by nucleophilic attack of the imino ether onto an electrophilic initiator. Similar to the previously discussed cationic polymerizations, the CROP

of 2-oxazolines can proceed via cationic or covalent propagating species or an equilibrium between these species, as depicted in Scheme 8.26. The living CROP proceeds via nucleophilic attack of the monomer onto the C5 of the oxazolinium species, resulting in ring-opening of the oxazolinium while the newly attached monomer will be transferred into the new oxazolinium chain end. This monomer addition continues until all monomer is consumed or until a nucleophilic terminating agent is introduced into the polymerization mixture.

The type of propagating species is mainly determined by the nucleophilicity of the monomer and basicity of the leaving group of the initiator, whereby covalent propagating species are present when the basicity of the counterion is higher than the nucleophilicity of the monomer and cationic propagating species are present if the basicity of the counterion is lower than the monomer nucleophilicity. The most nucleophilic monomer, 2-methyl-2-oxazoline, polymerizes via cationic propagating species with all counterions except



Scheme 8.26 Schematic representation of the living CROP of 2-oxazolines including the equilibrium between covalent and cationic propagating species.

chloride [86, 166, 167]. In contrast, the least nucleophilic 2-perfluoralkyl-2-oxazoline monomers polymerize only via cationic propagating species with the least basic triflate counterions [86, 168]. The living CROP of the majority of monomers with intermediate nucleophilicity, such as 2-ethyl-2-oxazoline [166, 167, 169, 170], 2-unsubstituted-2-oxazoline [86, 171] and 2-phenyl-2-oxazoline [86, 166, 172], are based on an equilibrium between covalent and cationic propagating species which is determined by the basicity of the counterion and is strongly affected by the solvent polarity. The solvent stabilization effect on the ion pair proximity has been illustrated by the use of ionic liquids as extremely polar solvents, leading to a fourfold acceleration of the methyltosylate-initiated polymerization of 2-ethyl-2-oxazoline compared to using acetonitrile as solvent, despite the fact that both polymerizations proceed via cationic propagating species [173].

The large variation in polymerization rates among the various 2-oxazoline monomers has been exploited for the preparation of quasi-diblock copolymers, namely, gradient copolymers with a narrow and steep monomer gradient, by statistical copolymerization of selected monomer combinations exhibiting large differences in reactivity. Such a one-pot quasi-diblock copolymer synthesis was first demonstrated for the statistical copolymerization of 2-phenyl-2-oxazoline and a much less reactive 2-perfluoroalkyl-2-oxazoline [174]. This “living” CROP (in nitromethane at 120 °C initiated by methyl *p*-nitrobenzenesulfonate) revealed complete consumption of the 2-phenyl-2-oxazoline after 2 min with only minor incorporation of the fluorinated monomer. Continuation of the polymerization for another 40 h led to full conversion of the fluorinated monomer. The

final polymer had a narrow molar mass distribution, which, together with the monomer conversion profile, demonstrated the one-pot formation of a quasi-diblock copolymer. More recently, the one-pot statistical copolymerizations of 2-phenyl-2-oxazoline with the more nucleophilic aliphatically substituted 2-methyl-2-oxazoline, 2-ethyl-2-oxazoline, or 2-nonyl-2-oxazoline were reported to result in quasi-diblock copolymers, whereby, first, the aliphatic monomer is incorporated, followed by slow incorporation of the 2-phenyl-2-oxazoline [175, 176]. The monomer distribution along the polymer chain, which is calculated on the basis of the individual monomer conversions during the copolymerization, for statistical quasi-diblock copolymers consisting of 2-nonyl-2-oxazoline and 2-phenyl-2-oxazoline is shown in Figure 8.4.

The livingness of the CROP of 2-oxazolines allows the incorporation of chain-end functionalities using functional electrophilic initiators as well as functional nucleophilic terminating agents. Examples of reported functional initiators include allyl- [177], propargyl [178], and phtalimido [179] (as precursor for amines) functionalized tosylates. In addition, the use of multifunctional initiators has been utilized for the preparation of star-shaped poly(2-oxazoline)s with various core structures [180–183].

Besides functional initiators, a wide range of functional terminating agents have been utilized for the preparation of functional poly(2-oxazoline)s, including deprotonated carboxylic acids [184, 185], amines [185, 186], and deprotonated thiols (Scheme 8.27) [187]. The termination with primary amines can be complicated by the formation of secondary amines that can react with a second polymer chain after proton transfer to the unreacted primary amines.

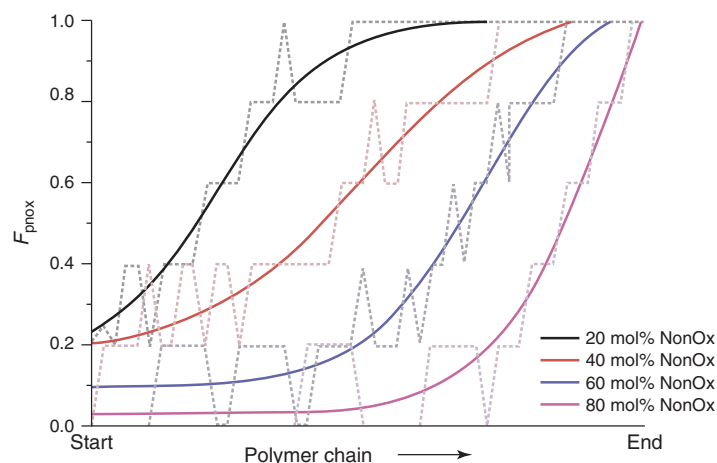
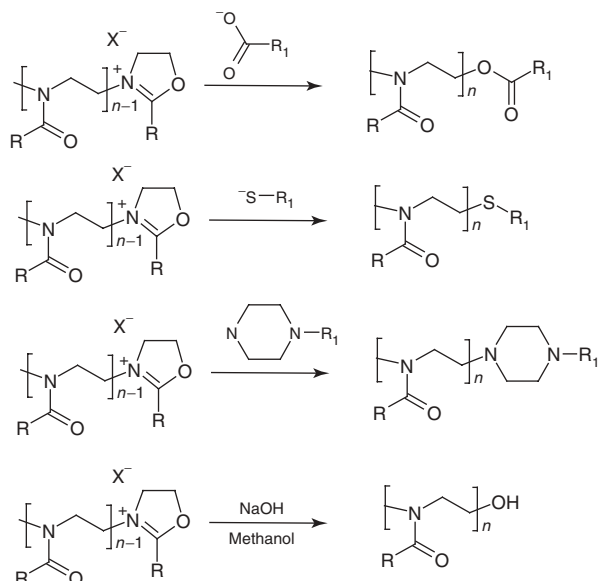


Figure 8.4 Monomer distribution along the polymer chain for statistical copolymers of 2-nonyl-2-oxazoline (NonOx) and 2-phenyl-2-oxazoline (PhOx). *Source:* Reprinted with permission Lambermont-Thijs HML, Jochems MJ, Hoogenboom R, Schubert US. *J Polym Sci A Polym Chem* 2009;47:6433 [176]. Copyright 2009 John Wiley and Sons, Inc. (See insert for the color representation of the figure.)



Scheme 8.27 Schematic representation of the functionalization of poly(2-oxazoline)s using nucleophilic terminating agents.

Therefore, the use of secondary amines might be preferable since the higher basicity of the formed tertiary amine suppresses proton transfer to the secondary amines. Piperidine has been identified as an ideal terminating agent for the living poly(2-oxazoline) chains, resulting in fast (less than 10 min) and quantitative termination [188]. Besides termination of the living chains with piperidine, a variety of monofunctionalized piperazines have been employed to introduce functional groups to the chain ends of poly(2-oxazoline)s (Scheme 8.27) [189–191]. The use of tertiary amines as terminating agents provides cationically charged end groups [185, 188], which have been demonstrated to result in antimicrobial poly(2-oxazoline)s [192]. Moreover, the introduction of a hydroxyl end group can be performed by quenching the polymerization with methanolic sodium hydroxide (Scheme 8.27) [86].

Finally, the living CROP of 2-oxazolines provides direct access to well-defined diblock copolymers by sequential monomer addition, that is, addition of a second monomer after full conversion of the first monomer [193, 194]. Further monomer addition after the second and third monomer has been demonstrated to result in defined triblock [195, 196] and tetrablock copoly(2-oxazoline)s [197].

8.4 SUMMARY AND PROSPECTS

Despite the fast development and versatility of controlled radical polymerization methods for a variety of vinyl monomers, there is still a need for cationic polymerization methods for certain important monomer classes, in

particular isobutene and vinyl ethers, which cannot be polymerized in a controlled manner using radical procedures. Poly(isobutene) is an attractive soft polymeric material for applications in, for example, thermoplastic elastomers and recently also as a biomaterial [198]. Poly(vinyl ether)s represent a versatile class of polymers with tunable properties based on the variation of the ether side chain and high hydrolytic stability, especially when compared to poly(meth)acrylates. The living CROP of mainly tetrahydrofuran and 2-oxazolines provides direct access to well-defined polymers, wherein both the initiation and termination steps provide the possibility to introduce a wide variety of functional groups. Poly(tetrahydrofuran) is a popular soft polymeric material for use as soft block in, for example, thermoplastic elastomers. The properties of poly(2-oxazoline)s can be easily tailored for certain applications by variation of the polymer side chain. This versatility of poly(2-oxazoline)s in combination with the biocompatibility, stealth behavior, and thermoresponsive behavior has led to a renewed interest in poly(2-oxazoline)s in recent years.

Therefore, it is expected that both living/controlled carbocationic polymerization and living CROP of these monomers will remain popular methods for the construction of defined macromolecular architectures for a variety of applications.

ACKNOWLEDGMENT

The author wishes to thank Ghent University for financial support via the Concerted Research Action Grant BOF11/GOA/023 on “Adaptive functional materials.”

REFERENCES

1. Swarc M. *Nature* 1956;176:1168.
2. Hadjichristidis N, Pitsikalis M, Pispas S, Iatrou H. *Chem Rev* 2001;101:3747.
3. Matyjaszewski K, Xia J. *J. Chem Rev* 2001;101:2921.
4. Hawker CJ, Bosman AW, Harth E. *Chem Rev* 2001;101:3661.
5. Perrier S, Takolpuckdee P. *J Polym Sci A Polym Chem* 2005;43:5347.
6. Webster OW. *Science* 1991;496:887.
7. Goethals EJ. *Makromol Chem Macromol Symp* 1991;42:51.
8. Plesch PH. *The Chemistry of Cationic Polymerization*. Oxford: Pergamon Press; 1963.
9. Kennedy JP, Ivan B. *Designed Polymers by Carbocationic Macromolecular Engineering: Theory and Practice*. München: Hanser; 1992.
10. Sawamoto M. *Prog Polym Sci* 1991;16:111.
11. Puskas JE, Kaszas G. *Prog Polym Sci* 2000;25:403.

12. Gandini A, Chéradame H. *Adv Polym Sci* 1987;34/35:1–289.
13. Sigwalt P, Moreau M. *Prog Polym Sci* 2006;31:44–120.
14. Goethals EJ, Du Prez FE. *Prog Polym Sci* 2007;32:220–246.
15. Penczek S, Kubisa P, Matyjaszewski K. *Adv Polym Sci* 1980;37:1–137.
16. Penczek S, Kubisa P, Matyjaszewski K. *Adv Polym Sci* 1985;68/69:1–298.
17. Ivin KJ, Saegusa T. *Ring-Opening Polymerization*. Volume I & II. London: Elsevier; 1984.
18. Allen G, Bevington JC, editors. *Comprehensive Polymer Science*. Volume III, Chapters 45–53. Oxford: Pergamon Press; 1989.
19. Matyjaszewski K, editor. *Cationic Polymerizations: Mechanism, Synthesis and Applications*. New York: Marcel Dekker Inc.; 1996.
20. Kostjuk SV, Ganachaud F. *Accounts Chem Res* 2010;43:357.
21. Matyjaszewski K, Sigwalt P. *Polym Int* 1994;35:1–26.
22. Penczek S. *J Polym Sci A Polym Chem* 2002;40:1665.
23. Toman L, Spevacek J, Vlcek P, Holler P. *J Polym Sci A Polym Chem* 2000;38:1568.
24. Kennedy JP, Smith RA. *J Polym Sci A Polym Chem* 1980;18:1539.
25. Kennedy JP et al. *J Macromol Sci Polym Chem* 1982/83; A18/19multiple contributions.
26. Nuyken O, Pask S, Vischer A. *Makromol Chem* 1982;184:553.
27. Ivan B, Kennedy JP. *Macromolecules* 1990;23:2880.
28. Faust R, Kennedy JP. *J Polym Sci A Polym Chem* 1987; 25:1847.
29. Mishra MK, Kennedy JP. *J Macromol Sci Chem* 1987;A24:933.
30. Mishra MK, Kennedy JP. *Polym Bull* 1987;17:307.
31. Kaszas G, Puskas J, Kennedy JP. *Polym Bull* 1987;18:123.
32. Kaszas G, Puskas JE, Chen CC, Kennedy JP. *Macromolecules* 1990;23:3909.
33. Kaszas G, Puskas JE, Kennedy JP. *Polym Bull* 1988;20:413.
34. Ivan B, Kennedy JP. *J Polym Sci A Polym Chem* 1990;28:89.
35. Nguyen HA, Guis C, Chéradame H. *Macromol Symp* 2000;157:121.
36. Rajabalitabar B, Nguyen AA, Chéradame H. *Macromol Chem Phys* 1995;196:3597.
37. Rajabalitabar B, Nguyen AA, Chéradame H. *Macromolecules* 1996;29:514.
38. Charleux B, Moreau M, Vairon JP, Hadjikyriacou S, Faust R. *Macromol Symp* 1998;132:25–35.
39. Fodor ZS, Faust R. *J Macromol Sci* 1995;A32:575.
40. Li D, Faust R. *Macromolecules* 1995;28:1383.
41. Hadjikyriacou S, Faust R. *Macromolecules* 1995;28:7893.
42. Hadjikyriacou S, Faust R. *Macromolecules* 1996;29:5261.
43. Schröder G. Poly(vinyl ethers). In: *Ullmann's Encyclopedia of Industrial Chemistry*. Wiley-VCH; 2000.
44. Johnson AF, Young RN. *J Polym Sci* 1976;56:211.
45. Sawamoto M, Kennedy JP. *J Macromol Sci Chem* 1982–83; A18:1275.
46. Miyamoto M, Sawamoto M, Higashimura T. *Macromolecules* 1984;17:265.
47. Miyamoto M, Sawamoto M, Higashimura T. *Macromolecules* 1984;17:2228.
48. Higashimura T, Miyamoto M, Sawamoto M. *Macromolecules* 1985;18:611.
49. Kojima K, Sawamoto M, Higashimura T. *Macromolecules* 1989;22:1552.
50. Schappacher M, Deffieux A. *Macromolecules* 1991;24:2140.
51. Kamigaito M, Sawamoto M, Higashimura T. *Macromolecules* 1991;24:3988.
52. Kamigaito M, Yamaoka K, Sawamoto M, Higashimura T. *Macromolecules* 1992;25:6400.
53. Nuyken O, Kroener H. *Makromol Chem* 1990;191:1.
54. Lubnин AV, Kennedy JP. *Polym Bull* 1992;29:9.
55. Cramail H, Deffieux A, Nuyken O. *Makromol Chem Rapid Commun* 1993;14:17.
56. Haucourt NH, Kashikar S, Goethals EJ. *Makromol Chem Rapid Commun* 1993;14:489.
57. Kanzawa A, Kanaoka S, Aoshima S. *Macromolecules* 2009;42:3965–3972.
58. Kanzawa A, Kanaoka S, Aoshima A. *J Am Chem Soc* 2007;129:2420–2421.
59. Yoshida T, Sawamoto M, Higashimura T. *Makromol Chem* 1991;192:2317.
60. Lievens SS, Goethals EJ. *Polym Int* 1996;41:277.
61. Sawamoto M, Shohi H, Sawamoto H, Higashimura T. *J Macromol Sci Pure Appl Chem* 1994;A31:1609.
62. Zhang X, Goethals EJ, Loontjens T, Derkx F. *Macromol Rapid Comm* 2000;21:472.
63. Zhang X, Goethals EJ. *J Macromol Sci Pure Appl Chem* 2001;A38:861.
64. Shibata T, Kanaoka S, Aoshima S. *J Am Chem Soc* 2006;128:7497–7504.
65. Kanaoka S, Yagi N, Fukuyama Y, Aoshima S, Tsunoyama H, Tsukuda T, Sakurai H. *J Am Chem Soc* 2007;129: 12060–12061.
66. Pepper DC, Reilly PJ. *J Polym Sci* 1962;58:291.
67. Bossaer PK, Goethals EJ, Hackett PJ, Pepper DC. *Eur Polym J* 1977;13:489.
68. Gandini A, Plesch PH. *J Chem Soc* 1965:4826.
69. Gandini A, Plesch PH. *Polym Lett* 1965;3:127.
70. Vairon JP, Rives A, Bunel C. *Makromol Chem Macromol Symp* 1992;60:97.
71. Pepper DC. *Makromol Chem* 1974;175:1077.
72. Matyjaszewski K, Sigwalt P. *Makromol Chem* 1986;187: 2299–2316.

73. Higashimura T, Mitsuhashi H, Sawamoto M. *Macromolecules* 1979;12:178.
74. Higashimura T, Kojima K, Sawamoto M. *Polym Bull* 1988;19:7.
75. Shohi H, Sawamoto M, Higashimura T. *Macromolecules* 1992;25:53.
76. Kaszas G, Puskas JE, Kennedy JP, Hager WM. *J Polym Sci A Polym Chem* 1991;29:421.
77. Kaszas G, Puskas JE, Kennedy JP, Hager WG. *J Polym Sci A Polym Chem* 1991;29:427.
78. Satoh K, Kamigaito M, Sawamoto M. *Macromolecules* 2000;33:5405.
79. Satoh K, Kamigaito M, Sawamoto M. *Macromolecules* 2000;33:5830.
80. Satoh K, Nakashima J, Kamigaito M, Sawamoto M. *Macromolecules* 2001;34:396.
81. Satoh K, Kamigaito M, Sawamoto M. *Macromolecules* 1999;32:3827.
82. Radchenko AV, Kostjuk SV, Vasilenko IV, Ganachaud F, Kaputsky FN, Guillaneuf Y. *J Polym Sci A Polym Chem* 2008;46:6928.
83. Kostjuk SV, Ganachaud F. *Macromolecules* 2006;39:3110–3113.
84. Kobayashi S. *Prog Polym Sci* 1990;15:751.
85. Goethals EJ, Schacht EH, Bruggeman P, Bossaer P. *ACS Symp Ser* 1977;59:1–12.
86. Aoi K, Okada M. *Prog Polym Sci* 1996;21:151.
87. Penczek S, Cypryk M, Duda A, Kubisa P, Slomkowski S. *Prog Polym Sci* 2007;32:247.
88. Knop K, Hoogenboom R, Fischer D, Schubert US. *Angew Chem Int Ed* 2010;49:6288–6308.
89. Flory PJ. *J Am Chem Soc* 1940;62:1561.
90. Xie H-Q, Xie D. *Prog Polym Sci* 1999;24:275.
91. Penczek S. *J Polym Sci A Polym Chem* 2000;38:1919.
92. Boucheatif H, Philbin MI, Colclough E, Amass AJ. *Chem Commun* 2005:3870.
93. Boucheatif H, Philbin MI, Colclough E, Amass AJ. *Macromolecules* 2010;43:845–855.
94. Ledwith A, Sherrington DC. *Fortsch Hochpol Forsch* 1975;19:1.
95. Dreyfuss MP, Dreyfuss P. *Polymer* 1965;6:93.
96. Dreyfuss MP, Dreyfuss P. *J Polym Sci A Polym Chem* 1966;4:2179–2200.
97. Burgess FJ, Cunliffe AV, Richards DH, Thompson D. *Polymer* 1978;19:334.
98. Hizal G, Yagci Y. *Polymer* 1989;30:722.
99. Kajiwara A, Matyjaszewski K. *Macromolecules* 1998;31:3489.
100. Matyjaszewski K, Kubisa P, Penczek S. *J Polym Sci Polym Chem Ed* 1974;12:1333.
101. Matyjaszewski K, Penczek S. *J Polym Sci Polym Chem Ed* 1905;1974:12.
102. Dubreuil MF, Goethals EJ. *Macromol Chem Phys* 1997;198:3077.
103. Oike H, Yoshioka Y, Kobayashi S, Nakashima M, Tezuka Y, Goethals EJ. *Macromol Rapid Comm* 2000;21:1185.
104. Cunliffe AV, Richards DH, Roberston F. *Polymer* 1981;22:108.
105. Hartley DB, Hayes MS, Richards DH. *Polymer* 1981;22:1081.
106. Cohen P, Abadie MJM, Schue F, Richards DH. *Polymer* 1982;22:1350.
107. Van Caeter P, Goethals EJ. *Macromol Rapid Comm* 1997;18:393.
108. Goethals EJ, Dubreuil MF, Tanghe L. *Macromol Symp* 2000;161:135.
109. Van Renterghem LM, Goethals EJ, Du Prez FE. *Macromolecules* 2006;39:528.
110. Tezuka Y, Goethals EJ. *Eur Polym J* 1982;18:991.
111. Oike H, Imamura H, Imaizumi H, Tezuka Y. *Macromolecules* 1999;32:4819.
112. Adachi K, Takasugi H, Tezuka Y. *Macromolecules* 2006;39:5585–5588.
113. Oike H, Imamura H, Tezuka Y. *Macromolecules* 1999;32:8666.
114. Sugai N, Heguri H, Ohta K, Meng Q, Yamamoto T, Tezuka Y. *J Am Chem Soc* 2010;132:14790–14802.
115. Acar MH, Gulkanat A, Seyren S, Hizal G. *Polymer* 2000;41:6709.
116. Yoshida E, Sugita A. *Macromolecules* 1996;29:6422.
117. Smith S, Hubin AJ. *J Macromol Sci Pure Appl Chem* 1973;7:1399.
118. Mumcu S, Burzin K, Feldmann R, Feinauer R. *Angew Makromol Chem* 1978;74:49.
119. Zaschke B, Kennedy JP. *Macromolecules* 1995;28:4426.
120. Petrov P, Mateva R, Dimitrov R, Rousseva S, Velichkova R, Bourssukova M. *J Appl Polym Sci* 2002;84:1448.
121. Sikova S, Bohnsack DA, Mackay ME, Suwanmala P, Rowan SJ. *J Am Chem Soc* 2005;127:18202.
122. Koevoest RA, Versteegen RM, Kooijman H, Spek AL, Sijbesma RP, Meijer EW. *J Am Chem Soc* 2005;127:2999.
123. Beck JB, Ineman JM, Rowan SJ. *Macromolecules* 2005;38:5060.
124. Hoogenboom R, Andres PR, Kickelbick G, Schubert US. *Synlett* 2004;1779.
125. Chiper M, Hoogenboom R, Schubert US. *Eur Polym J* 2010;46:260–269.
126. Kern W, Brenneisen E. *J Prakt Chem* 1941;159:193219.
127. Rivas BL, Barria B. *Polym Bull* 1996;36:157.
128. Baklouti M. *Polym Bull* 1989;21:24.
129. Jones GD, MacWilliams DC, Braxton NA. *J Org Chem* 1994;1965:30.
130. Bossaer P, Goethals EJ. *Makromol Chem* 1977;178:2983.
131. Goethals EJ, Bossaer P, Deveux R. *Polym Bull* 1981;6:121.
132. Munir A, Goethals EJ. Synthesis of living linear poly(*N*-tert butyl imino ethylene) with predictable molecular weight. In: Goethals EJ, editor. *Polymeric Amines and Ammonium Salts*. Oxford: Pergamon Press; 1980. p 19.

133. Munir A, Goethals EJ. *J Polym Sci A Polym Chem* 1981;19:1965.
134. Kazama H, Hoshi M, Nakajima H, Horak D, Tezuka Y, Imai K. *Polymer* 1990;31:2207.
135. Goethals EJ, Van de Velde M, Munir A. Synthesis of block-copolymers with polyamine segments using living poly(N-tert butyl aziridine). In: Goethals EJ, editor. *Cationic Polymerization and Related Processes*. London: Academic Press; 1984. p 387.
136. Weyts KF, Goethals EJ. *Polym Bull* 1988;19:13.
137. Ishizone T, Tanaka T, Kobayashi M. *J Polym Sci A Polym Chem* 2003;41:1335.
138. Koper GM, van Duijvenbode RC, Stam DD, Steuerle U, Borkovec M. *Macromolecules* 2003;36:2500.
139. Razvodovskii EF, Berlin AA, Nekrasov AV, Ponomarenko AT, Pushckayeva L, Puchkova NG, Enikolopyan NS. *Vysokomol Soed Ser* 1973;A15:2233.
140. Yamashita T, Nigo M, Nakamura N. *Makromol Chem* 1979;180:1145.
141. Schacht EH, Goethals EJ. *Makromol Chem* 1974;175:3447.
142. Schacht EH, Goethals EJ. *Makromol Chem* 1973;167:155.
143. Goethals EJ, Schacht EH. *J Polym Chem Lett Ed* 1973;11:497.
144. Schacht EH, Bossaer P, Goethals EJ. *Polym J* 1977;9:329.
145. Oike H, Washizuka M, Tezuka Y. *Macromol Chem Phys* 2000;201:1673.
146. Razvodovskii EF, Nekrasov AV, Berlin AA, Ponomarenko AT, Enikolopyan NS. *Dokl Akad Nauk SSSR* 1971;198:894.
147. Matyjaszewski K. *Makromol Chem* 1984;185:51.
148. Toy MS, Price CC. *J Am Chem Soc* 1960;82:2613.
149. Litt MH, Levy AJ, Bassiri TG, inventors; Allied Chemical Corporation, assignee. US patent 3483141, BE666828. 1965.
150. Tomalia DA, Sheetz DP. *J Polym Sci A Polym Chem* 1966;4:2253–2265.
151. Seeliger W, Aufderhaar E, Diepers W, Feinauer R, Nehring R, Thier W, Hellmann H. *Angew Chem* 1966;20:913–927.
152. Kagiya T, Narisawa S, Maeda T, Fukui K. *Polym Lett* 1966;4:441–445.
153. Bassiri TG, Levy A, Litt M. *Polym Lett* 1967;5:871–879.
154. Levy A, Litt M. *J Polym Sci B Polym Lett* 1967;5:881–886.
155. Saegusa T, Kobayashi S, Ishiguro M. *Macromolecules* 1974;7:958–959.
156. Saegusa T, Hirao T, Ito Y. *Macromol Commun* 1975;8:87.
157. Bloksma MM, Schubert US, Hoogenboom R. *Macromol Rapid Comm* 2011;32:1419.
158. Lin PY, Clash C, Pearce EM, Kwei TK, Aponte MA. *J Polym Sci B Polym Phys* 1988;26:603–619.
159. Christova D, Velichkova R, Loos W, Goethals EJ, Du Prez F. *Polymer* 2003;44:2255.
160. Uyama H, Kobayashi S. *Chem Lett* 1992;1643–1646.
161. Park J-S, Kataoka K. *Macromolecules* 2007;40:3599.
162. Bloksma MM, Weber C, Perevyazko IY, Kuse A, Baumgaertel A, Vollrath A, Hoogenboom R, Schubert US. *Macromolecules* 2011;44:4057–4064.
163. Zalipsky S, Hansen CB, Oaks JM, Allen TM. *J Pharm Sci* 1996;85:133.
164. Hoogenboom R. *Angew Chem Int Ed* 2009;48:7978.
165. Hoogenboom R. *Eur J Lipid Sci Technol* 2011;113:59.
166. Hoogenboom R, Fijten MWM, Schubert US. *J Polym Sci A Polym Chem* 2004;42:1830.
167. Saegusa T, Ikeda H, Fujii H. *Macromolecules* 1972;5:359.
168. Miyamoto M, Aoi K, Saegusa T. *Macromolecules* 1980;1988:21.
169. Lui Q, Konas M, Riffle JS. *Macromolecules* 1993;26:5572.
170. Hoogenboom R, Paulus RM, Fijten MWM, Schubert US. *J Polym Sci A Polym Chem* 2005;43:1487.
171. Saegusa T, Ikeda H, Fujii H. *Macromolecules* 1973;6:315.
172. Kobayashi S, Tokuzawa T, Saegusa T. *Macromolecules* 1982;15:707.
173. Guerrero-Sanchez C, Hoogenboom R, Schubert US. *Chem Commun* 2006:3797.
174. Saegusa T, Chujo Y, Aoi K, Miyamoto M. *Makromol Chem Macromol Symp* 1990;32:1.
175. Hoogenboom R, Thijs HLM, Fijten MWM, van Lankvelt B, Schubert US. *J Polym Sci A Polym Chem* 2007;45:416.
176. Lamberton-Thijs HML, Jochems MJ, Hoogenboom R, Schubert US. *J Polym Sci A Polym Chem* 2009;47:6433.
177. Chujo Y, Ihara E, Ihara H, Saegusa T. *Macromolecules* 2040;1989:22.
178. Fijten MWM, Haensch C, Hoogenboom R, Schubert US. *Macromol Chem Phys* 1887;2008:209.
179. Yang Y, Kataoka K, Winnik FM. *Macromolecules* 2043;2005:38.
180. Kobayashi S, Uyama H, Narita Y. *Macromolecules* 1992;25:3232.
181. Chang JY, Ji HJ, Han MJ, Rhee SB, Cheong S, Yoon M. *Macromolecules* 1994;27:1376.
182. Kim KM, Ouchi Y, Chujo Y. *Polym Bull* 2003;49:341.
183. Jin R-H. *Adv Mater* 2002;14:889.
184. Weber C, Becer CR, Hoogenboom R, Schubert US. *Macromolecules* 2009;42:2965.
185. Miyamoto M, Naka K, Tokumizu M, Saegusa T. *Macromolecules* 1989;22:1604.
186. Aoi K, Motoda A, Okada M. *Macromol Rapid Comm* 1997;18:945.
187. Viegas TX, Bentley MD, Harris JM, Fang Z, Yoon K, Dizman B, Weimer R, Mero A, Pasut G, Veronese FM. *Bioconjugate Chem* 2011;22:976.
188. Nuyken O, Maier G, Gross A. *Macromol Chem Phys* 1996;197:83.
189. Gross A, Maier G, Nuyken O. *Macromol Chem Phys* 1996;197:2811.
190. Meyer M, Schlaad H. *Macromolecules* 2006;39:3967.
191. Schubert US, Hochwimmer G, Heller M. *ACS Symp Ser* 2002;163.
192. Waschinsky CJ, Tiller JC. *Biomacromolecules* 2005;6:235.

193. Kobayashi S, Uyama H. *J Polym Sci A Polym Chem* 2002;40:192.
194. Wiesbrock F, Hoogenboom R, Leenen MAM, van Nispen SFGM, van der Loop M, Abeln CH, van den Berg AMJ, Schubert US. *Macromolecules* 2005;38:7957.
195. Komenda T, Jordan R. *Polymer Prepr* 2003;44:986.
196. Hoogenboom R, Wiesbrock F, Huang H, Leenen MAM, Thijs HML, van Nispen SFGM, van der Loop M, Fustin C-A, Jonas AM, Gohy J-F, Schubert US. *Macromolecules* 2006;39:4719.
197. Hoogenboom R, Wiesbrock F, Leenen MAM, Thijs HML, Huang H, Fustin C-A, Guillet P, Gohy J-F, Schubert US. *Macromolecules* 2007;40:2837.
198. Puskas JE, Chen Y, Dahman Y, Padavan D. *J Polym Sci A Polym Chem* 2004;42:3091.

9

CROSSLINKING

JULIO CÉSAR HERNÁNDEZ-ORTIZ AND EDUARDO VIVALDO-LIMA

9.1 INTRODUCTION

The concept of crosslinked polymers has already been introduced in Sections 1.1.7 and 1.2.3 of Chapter 1, as well as in Sections 3.8.1, 3.8.2, 3.8.3, 3.8.4, and 3.9.2 of Chapter 3. Brief mentions to crosslinking reactions or crosslinked polymers are also offered in other chapters of this handbook (e.g., Chapters 6 and 8). Some examples related to the modeling of network formation by free radical copolymerization (FRC) are briefly outlined in Chapters 12, 14, and 15. In Chapter 28, the chemistry of epoxy polymers and other thermosets synthesized by step-growth or chain-growth polymerizations, aimed at producing polymer networks, is described; structural transformations (gelation and vitrification) taking place during network formation are analyzed using a conversion-temperature transformation (CTT) diagram; general criteria and rules for processing the initial formulation are discussed for applications such as coatings and composites; and processing techniques are described for the production of filled or unfilled parts, and small, medium, and large series of composite materials. In this chapter, we define several terms related to polymer network formation; we also examine general aspects of some of the existing gelation theories and describe some aspects related to polymer network formation by copolymerization with crosslinking of vinyl/divinyl monomers.

A polymer network can be envisioned as a polymer molecule with an infinite molecular weight [1]. Crosslinking is a physical or chemical route by which polymers with branched or crosslinked structures are produced. The chemical route may imply a polymerization or postpolymerization stage [2–4]. Crosslinking is especially important from the commercial point of view. Polymer networks may

be undesirable for some applications; in such cases, chain transfer agents can be used to prevent or delay gelation. On the other hand, many commercial polymers owe their value to their crosslinked structures, which can range from only slightly to highly crosslinked materials. Crosslinked polymers exhibit completely different properties when compared to linear polymers with identical chemical compositions. The degree of branching/crosslinking influences polymer properties such as density, melt viscosity, and crystallinity; it also determines the flow behavior of the material. While noncrosslinked polymers are in general thermoplastic, and they can be melted and casted, extruded, or (injection) molded, highly crosslinked polymers become thermoset, and they do not flow when heated. However, polymer properties can also depend on network topology (see Fig. 9.1 for a schematic representation of two possible topologies).

9.2 BACKGROUND ON POLYMER NETWORKS

9.2.1 Types of Polymer Networks Based on Structure

9.2.1.1 Definition and Structure of Polymer Networks
A polymer network can be defined as a highly crosslinked macromolecule in which essentially all units are connected to each other in some way, either via chemical bonds or physical associations.

The structure of a polymer network can be simply depicted as a three-dimensional “mesh” formed by polymer chains interconnected by crosslink points. However, the actual structure of this “mesh” is not regular and the distribution of polymer chain length between joining points is unequal throughout the whole network. Hence, a polymer

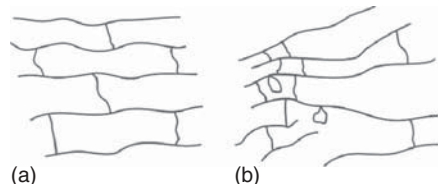


Figure 9.1 Two different topologies for a polymer network.

network represents an ensemble of regions (domains) of different structures with different crosslink densities, resulting in a heterogeneous structure. A homogeneous polymer network would be obtained if a uniform distribution of functional groups took place with the absence of structural defects. Four main types of inhomogeneities are commonly recognized in a polymer network structure: (i) chains attached to the network by only one end, yielding loose, dangling polymer chains; (ii) rings, loops, or cycles produced if a chain is joined by its two ends to the same crosslink point; (iii) permanent chain entanglements between two adjacent crosslinks; and (iv) multiple connection between two crosslink points, as shown in Figure 9.2 [5]. Inhomogeneities can be formed during both physical and chemical crosslinking. Physical networks can possess clusters of molecular entanglements, or domains of highly hydrophobic or ionic association, leading to an unequal distribution of joining points. Polymer networks formed by chemical bonding can contain regions of high crosslink density and low solvent swelling (clusters), immersed in regions of low crosslink density and high swelling index. For the case of hydrogels synthesis, for example, this may be due to hydrophobic aggregation of crosslinking agents, resulting in the formation of high crosslinked clusters [6]. The presence of unequal reactivity of the functional groups involved during network synthesis and the formation of cycles can also result in these types of clusters. According to the topology and structural level of perfection, several type of polymer network can be recognized: ideal (or perfect), model, and imperfect networks.

9.2.1.2 Ideal or Perfect Networks¹ The IUPAC Commission on macromolecular nomenclature defines a perfect network as a network composed of chains all of which are connected at both of their ends to different junction points [7]. If a perfect network is in the rubbery state, then, on macroscopic deformation of the network, all of its chains are elastically active and display rubber elasticity. An ideal or perfect network can also be defined as a collection of individual Gaussian elastic chains (linear

¹Reprinted with permission from Gérard H. Model networks based on “end-linking” processes: synthesis, structure and properties. *Prog Polym Sci* 1998;23:1019–1149 [5]. Copyright 1998 Elsevier.

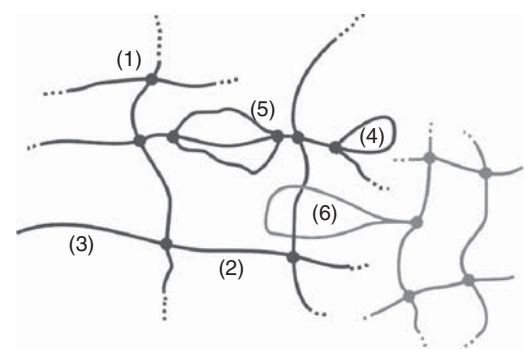


Figure 9.2 Main elements constituting the structure of a polymer network: (1) crosslink point, (2) elastically active chain, (3) dangling chain, (4) loop or cycle, (5) multiple connection between two crosslink points, and (6) permanent chain entanglements between two adjacent crosslinks.

chain elements) connecting f -functional crosslinks (junction points or branch points). This definition has several basic requirements [5]: (i) the lengths of all elastic chains of the network should be identical: all of them should be connected by one elastic chain only; (ii) the network should be Gaussian: the dimensions of each effective elastic chain should obey Gaussian statistics; (iii) the network should be macroscopically as well as microscopically homogeneous: no syneresis should have occurred during its formation; segment and crosslink densities should be identical throughout the network; and (d) the functionality f of the crosslinks should be known and constant throughout the entire network.

9.2.1.3 Imperfect Polymer Network In this network, both the elastic chain lengths and the functionality f are broadly distributed throughout the entire network. Moreover, the two major types of network defects are present at a noteworthy extent in this type of network: loose, dangling (singly attached) chains, and inactive rings or loops (cycles). For the case of a polymer network synthesized chemically with a tetrafunctional crosslinker, a junction point would be elastically active if at least three paths leading away from it are independently connected to the network. In addition, a polymer chain segment (strand) in the network would be elastically active if it is connected at each end by elastically active junctions. For a perfect tetrafunctional network, there are twice as many strands as junctions. Thus, besides causing a lack of structural order in the polymer network, free chain ends and loops also represent defects because they are not part of the network, and therefore, they do not contribute to the elasticity of the structure, thus reducing the concentration of elastically active network chains, and as a result, the shear modulus and Young’s modulus are less than their respective value expected for an ideal network [8].

9.2.1.4 Model Polymer Network² Ideal and imperfect polymer networks represent the two extremes in polymer network structures. Model networks are intermediate between these two. A model network can be prepared using a nonlinear polymerization or by crosslinking of existing polymer chains. A model network is not necessarily a perfect network. If a nonlinear polymerization is used to prepare the network, nonstoichiometric amounts of reactants or incomplete reaction can lead to networks containing loose ends. If crosslinking of existing polymer chains is used to prepare the network, then two loose ends per existing polymer chain result [7]. Rings can be present in model networks as well.

A model network should, at least, satisfy the following conditions [5]: (i) the linear chain element of a model network should exhibit known length and, if possible, a narrow molar mass distribution (D_M): each elastic chain should be connected by its two ends to two different crosslink points; (ii) a model network should be homogeneous: crosslinking density should be constant throughout the gel; and (iii) a model network should exhibit a known and constant functionality of crosslink points.

9.2.1.5 Interpenetrating and Semi-Interpenetrating Polymer Networks The void space in the structure of the polymer network can be occupied by other molecules. When this space is occupied by other polymer network, interpenetrating or semi-interpenetrating polymer networks result.

Interpenetrating Polymer Network (IPN) An interpenetrating polymer network (IPN) is an intimate combination of two or more polymer networks where at least one of which is synthesized and/or crosslinked in the presence of the other. These two polymer networks are partially interlaced on a molecular scale but not covalently bonded to each other and cannot be separated unless chemical bonds are broken. However, phase separation could limit actual interpenetration [8].

Semi-Interpenetrating Polymer Network (SIPN) A semi-interpenetrating polymer network (SPIN) is a combination of two or more crosslinked polymers with two or more linear or branched polymers, at least one of which was synthesized and/or crosslinked in the presence of the others. An SIPN is distinguished from an IPN because the constituent linear or branched macromolecules can, in principle, be separated from the constituent polymer network(s) without breaking chemical bonds; it is a polymer blend [7].

²Reprinted with permission from Gérard H. Model networks based on “endlinking” processes: synthesis, structure and properties. *Prog Polym Sci* 1998;23:1019–1149 [5]. Copyright 1998 Elsevier.

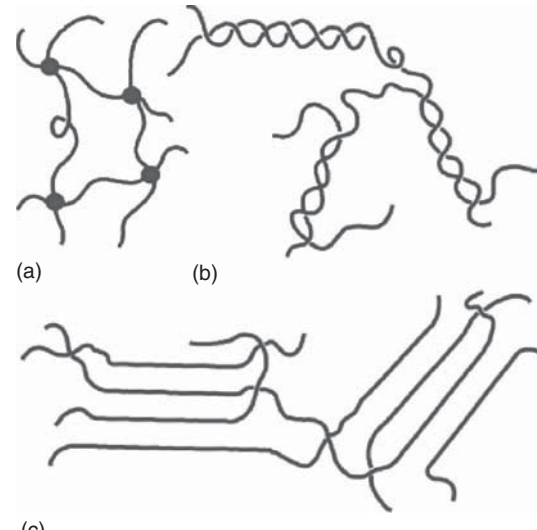


Figure 9.3 Types of links in a thermoreversible gel (a) by junction points, (b) by junction zones, and (c) by fringe micelles. Source: Reprinted with permission from Sperling LH. *Introduction to Physical Polymer Science*. 4th ed. Hoboken, Wiley Interscience; 2006 [8]. Copyright 2006 John Wiley and Sons.

9.2.2 Chemical and Physical Networks

Polymer networks can be classified as physical or chemical depending on the way of interconnection of the polymer chains that constitutes the network.

9.2.2.1 Physical Networks If the polymer chains in a polymer network are bonded via physical association, the networks are called *physical* or *reversible*. Physical interactions need not be permanent over the time scale of the observation or measurement [7]. The interaction can be due to hydrogen bonds, $\pi-\pi$ interactions, chain entanglements, etc. A physical network tends to be reversible. Reversible networks are those that form or break up as temperature is changed or under the action of a force. There are three types of links in thermoreversible gels: (i) single point bonds, called *point crosslinks*; (ii) junction zones, where interactions between chains act over a segment of their length, forming ordered secondary structures such as multiple helices; or (iii) fringe micelles, where the chains align in some regions to form small crystallite domains (Fig. 9.3). Some other weak interactions, as ion complexation, can also lead to the formation of physical networks [9].

9.2.2.2 Chemical or Covalent Networks If the interconnections that join the constituting polymer chains in a polymer network are made via chemical bonds, the networks are

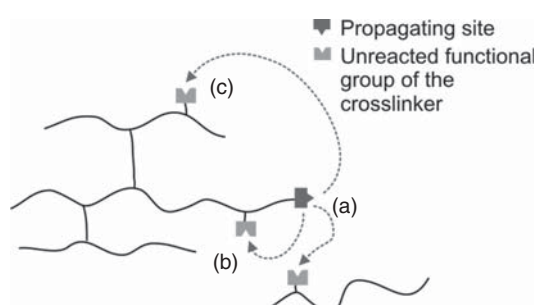


Figure 9.4 Different types of crosslinkages: (a) intermolecular, (b) intramolecular, yielding a primary cycle, and (c) intramolecular, yielding a secondary cycle.

called *chemical* or *covalent*. These polymer networks possess intermolecular or intramolecular interactions that are stable under the conditions of use of the material formed.

9.2.3 Intermolecular and Intramolecular Crosslinking

Intermolecular crosslinking involves the bonding between functional groups present on two different polymer molecules and, as a result, these two molecules link together, forming a single new macromolecule with an increased chain length. Intramolecular crosslinking occurs between two functional groups on the same polymer, causing connective loops or cycles within the macromolecule. Hence, this type of reaction is commonly referred to as *cyclization*. Similar types of intramolecular connections occur in polypeptides [10]. Typically, two different types of cycles can be distinguished. When the cycle is formed by reacting two functional groups attached to the same primary chain, a primary cycle results. On the other hand, when an extra link is formed between two primary chains that have already experienced crosslinking, a secondary cycle is formed (Fig. 9.4).

Intramolecular reactions (cyclization), in contrast to intermolecular ones, do not contribute to the growth of the molecular structure during polymerization and, therefore, they do not affect the molar mass distribution of the polymer population. However, the cyclization reaction manifests itself by a shift to a higher value of the critical conversion for onset of gelation and by a reduced amount of gel content during the formation of the polymer network. In addition, as more compact structures are produced by intramolecular crosslinking, it is also expected that some hydrodynamic volume dependant properties are affected, for instance, intrinsic viscosity [11]. Intermolecular and intramolecular crosslinking tend to occur simultaneously because both reactions involve the same functional groups. The relative reaction rates are determined by polymer concentration and chain length. Thus, at very low polymer concentrations, intramolecular crosslinking dominates, yielding

highly crosslinked particles (usually referred to as microgels) as product, whereas at higher polymer concentrations, intermolecular crosslinking is the dominant route, leading to a polymer network [12]. The presence of microgels in the network structure brings about an extremely restricted segmental mobility, while other regions of the polymer network experience a more mobile local environment, resulting in an inhomogeneous distribution of segmental mobilities and broader relaxation time distributions.

The experimental evidence reveals that the main parameters affecting the ratio intramolecular/intermolecular crosslink reaction rates are polymer concentration (degree of dilution), crosslinker content, and crosslinker structure.

9.2.4 Monomer Functionality (f)

The key parameter during the synthesis of polymer networks is the functionality f of the monomer, which is defined as the number of covalent bonds that a monomer molecule or monomeric unit in a macromolecule or oligomer molecule can form with other reactants [7]. Note that there are no monofunctional monomers, as the minimum required functionality for the backbone formation is two. When $f = 2$, only a linear chain macromolecule or a macrocycle can be formed.

9.2.5 Crosslink Density

According to the IUPAC Commission on macromolecular nomenclature, crosslink density is defined as the number of crosslinks per unit volume in a polymer network [7]. The degree of crosslinking is a fundamental property for polymer networks. A change in the level of crosslinking causes remarkable changes in the properties of the polymeric material. Crosslinking improves resistance to thermal degradation and resistance to cracking effects by liquids and other harsh environments, as well as resistance to creep, among other effects. Slight crosslink densities impart good recovery properties to polymers used as elastomers. On the other hand, high crosslink densities impart high rigidity and stability under heat and stress to polymers such as phenol-formaldehyde and urea-formaldehyde polymers.

9.2.6 Gelation and Swelling Index

During the formation of polymer networks, consecutive crosslinking brings about insolubility as a result of the remarkable increase in molecular weight. A polymer network will not dissolve in any solvent at any temperature before degradation, and it will only swell, reaching an equilibrium degree of swelling as solvent molecules diffuse into the polymer network. The formation of gel at some point of the network-forming process is characteristic when synthesizing polymer networks. A polymer gel is formed by

a polymer network expanded throughout its whole volume by its own monomer or the solvent employed during the synthesis of the network. The time of incipient network formation is referred to as *gelation point*. The mass fraction of the polymer that still remains soluble is referred to as *sol fraction*, whereas the insoluble fraction is known as *gel fraction*. Before the gelation point, the entire polymer is sol, but beyond this point, soluble polymer incorporates into the network and the amount of gel increases. The gelation point is characterized by a significant increase in the value of several properties, such as viscosity, which quickly diverges at this point, or the case of equilibrium shear modulus, which rises from zero to eventually reaching a plateau [8].

9.2.6.1 Swelling Index Swelling is defined as the increase in volume of a gel or solid associated with the uptake of a liquid or gas [7]. In fact, swelling represents the first stage in every polymer solution process, in which the solvent molecules diffuse through the polymer matrix to form a swollen, solvated mass, known as *polymer gel*. However, the gel formed after swelling polymer networks does not break up and the polymer molecules do not diffuse out of the swollen mass, and therefore, no real solution can be formed.

The swelling coefficient, Q , is defined by

$$Q = \frac{m - m_0}{m_0} \frac{1}{\rho_s} \quad (9.1)$$

where m is the weight of the swollen sample, m_0 is the dry weight, and ρ_s is the density of the swelling agent [8]. Equilibrium swelling index is determined by crosslink density and the attractive forces between solvent and polymer. The theoretical extent of swelling is predicted by the Flory–Rehner equation [13] (Eq. 9.2):

$$\ln(1 - v_2) + v_2 + \chi_1 v_2^2 = -\frac{V_1}{\bar{v}_2 M_c} \left(v_2^{1/3} - \frac{2v_2}{f} \right) \quad (9.2)$$

where v_2 is the volume fraction of polymer in the swollen mass, χ_1 is the Flory–Huggins solvent–polymer dimensionless interaction parameter, \bar{v}_2 is polymer specific volume, M_c is the average molecular weight between crosslinks, V_1 is solvent molar volume, and f the functionality of the crosslinks. The relationship between swelling index, Q , and volume fraction, v_2 , is given by

$$Q = \frac{V_H}{V_0} = \frac{1}{v_2} \quad (9.3)$$

where V_H is the volume of the swollen gel at equilibrium and V_0 the volume of the dry polymer network.

9.3 MAIN CHEMICAL ROUTES FOR SYNTHESIS OF POLYMER NETWORKS

From a general point of view, chemical crosslinking processes can be classified into four major types of reactions: step-growth polymerization, free radical polymerization, vulcanization, and end-linking of prepolymers.

9.3.1 Step-Growth Polymerization

Chapter 3 is devoted to step-growth polymerization. Here, some aspects related to crosslinking and gelation are highlighted. Nonlinear polymer molecules are obtained by step-growth polymerization when the functionality of one of the monomers is greater than two. The simplest example of such a reaction is the step-growth copolymerization of an AB monomer with a small amount of a f -functional monomer A_f (with $f > 2$). The resultant polymer has a branched structure in which f chains emanate from a branching point induced by the presence of the multifunctional monomer. However, since the reactive groups type A do not react with themselves, a crosslinked polymer will not be formed, as all growing chains coming from the branching point have functional groups type A at their ends. However, the copolymerization of AB with A_f in the presence of B_2 will lead to the formation of a crosslinked polymer. Other reacting systems that can lead to a crosslinked polymer, and eventually to gelation, are the polymerization of $A_2 + B_f$, $A_2 + B_2 + B_f$, and $A_f + B_f$, (all with $f > 2$). Many thermoset polymers of major commercial importance are synthesized by step-growth polymerization, as the case of unsaturated polyester, polyurethanes, melamines, phenolic and urea formaldehyde resins, epoxy resins, silicones, etc. In these systems, the crosslinking process, which leads to a polymer network formation, is usually referred to as *curing*.

9.3.2 Vulcanization

Vulcanization is a chemical process where linear polymer chains become crosslinked by the action of certain agents that attack some active functional groups present in the polymer backbone, thus improving the mechanical properties of the resultant polymer structure. Vulcanization by sulfur bonding is one of the main employed techniques for crosslinking of elastomers (Fig. 9.5). In vulcanization by sulfur, allylic hydrogen atoms represent the active sites. Rhombic sulfur is the most widely vulcanizing agent used for crosslinking of polymer chains with diene groups, such as natural rubber, styrene–butadiene rubber, and polybutadiene, although other chemical compounds can also be used as sulfur source, such as tetramethylthiuram disulfide (TMTD), which is also employed as an accelerator agent to speed up vulcanization rate. Some other accelerators are thiiazoles, sulfenamides, guanidines, carbamates, thiurams,

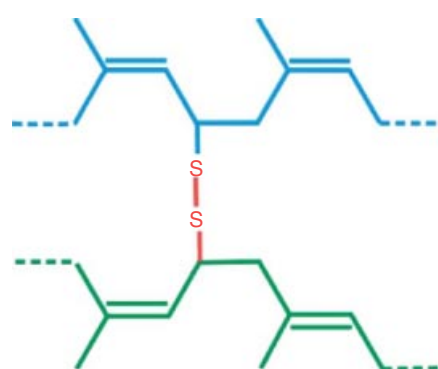


Figure 9.5 Representation of two primary chains of natural rubber (*cis*-1,4 polyisoprene) linked by vulcanization with sulfur.

xanthates, and phosphates [14]. Activators such as a zinc salt of a fatty acid or a combination of zinc oxide and a fatty acid are also used to increase the solubility in rubber of accelerators. Other broadly used vulcanizing agents are peroxides, which crosslink the polymer chains by the formation of stronger carbon–carbon bonds, instead of carbon–sulfur bonds. In fact, vulcanization by peroxides represents the route of choice for crosslinking of saturated elastomers, such as ethylene–propylene rubber (EPM), since sulfur cannot be employed for the curing of these materials because of the absence of double bonds in the polymer backbone [15]. Some metal oxides are employed as vulcanizing agents for the case of halogenated elastomers. High energy irradiation is also used [16, 17].

9.3.3 End-Linking

Model networks can be synthesized by end-linking of pre-existent linear polymer chains. In this type of network formation, two f -functional reactive groups are attached to each end of the linear prepolymer (telechelic prepolymers). The crosslinking step is then performed by bonding of the end groups. Anionic polymerization has been used for the synthesis of the well-defined macromolecules by this route. The resulting polymer networks should have crosslink points of functionality equal to that of the crosslinking agent, and the average molecular weight between crosslinks should correspond to that of the prepolymer, before crosslinking. However, this technique does not impart any control over the number of chains attached to one given crosslinking point, and fluctuations of this value can occur along the network. In addition, some network defects can be present, such as dangling ends and cyclization. The incidence of dangling-end network imperfections in model networks is reduced if the end-linking reaction is carried out under stoichiometric conditions and high conversion of

functional groups is reached. A comprehensive review on the end-linking process is available in the literature [5].

9.3.4 Free Radical Copolymerization (FRC)

FRC of a vinyl monomer with a small amount of divinyl monomer represents one of the simplest methods for synthesizing polymer networks. In these systems, the divinyl monomer acts both as a comonomer and as a crosslinker. One of the most common and studied systems of this type is the copolymerization of styrene (STY) and divinylbenzene (DVB). Poly(STY-*co*-DVB) copolymers are widely used as ion-exchange resins and separation media for size-exclusion chromatography, although several other vinyl/divinyl copolymerization systems have also been studied [18].

Polymer networks synthesized by conventional FRC present heterogeneous structures due to the inherent characteristics of this method, such as slow initiation, fast chain propagation, high termination rates, and high molar-mass dispersity (D_M) of primary chains. In these systems, primary radicals are produced gradually and constantly during the initiation step, allowing polymers of high chain length to be formed from the beginning of the reaction. At this stage, these growing polymer chains are immersed in a highly diluted environment (either by their monomers only, or by their monomers and solvent). Under these diluted conditions, polymer chains hardly ever overlap each other. Consequently, most of the pendant double bonds are consumed through intramolecular crosslinking (cyclization), undergoing gelation at a nanoscale. As the reaction and crosslinking proceeds, new polymer chains are continuously generated, promoting intermolecular crosslinking, which in turn leads to increased chain lengths. Once large polymer chains are produced and polymer concentration increases, they will react with each other through their available pendant double bonds and radical centers, and microgels will be produced. These agglomeration processes will continue until the onset of gelation is eventually reached, when all these microgels are interconnected. Therefore, gel formation by means of conventional FRC is the result of a continuous association of microgels, where each one could experience a different crosslink history, and as a result, these gels are intrinsically heterogeneous.

In the FRC of vinyl and multivinyl monomers, a drift in the instantaneous copolymer composition throughout the reaction will be undergone due to the different reactivities of the vinyl groups. This compositional drift is caused by the fact that the more reactive monomer will be consumed faster than the less reactive ones. In the simplest instance, assuming equal reactivity of the vinyl groups in mono- and divinyl monomers present in the reaction system, the reactivity of the crosslinker would be twice that of the monovinyl monomer, and therefore, the polymer chain

segments formed at early conversions would possess higher content of divinyl monomer than those formed at advanced stages of the reaction. As a consequence, the domains in the polymer network formed at early stages are more crosslinked than the domains formed later, and the resultant polymer network displays a crosslink density distribution. Some of the factors affecting the extent of compositional drift are the ratio of reactivity ratios r_1/r_2 , the initial monomer composition, and monomer conversion [19]. In addition, the pendant double bonds are less reactive, thus making the system more complex, and the polymer network more heterogeneous [20, 21]. The theory and mathematical modeling of polymer network formation by free radical copolymerization of vinyl/divinyl monomers was reviewed and analyzed by the group of Hamielec [22–25].

9.4 CHARACTERIZATION OF POLYMER NETWORKS AND GELS

In Section 16.3.9 of Chapter 16, it is mentioned that RT-FTIR is used to follow the polymerization of monomer mixtures leading to either crosslinked copolymers or IPNs. In Section 18.4.3 of Chapter 18, it is mentioned that dynamic light scattering (DLS) has been applied to study the effect of crosslinking on the dynamics of the sol–gel transition. In Section 21.2.1 of Chapter 21, it is recognized that the degree of crosslinking affects the glass transition temperature of a polymer and also affects shear modulus. Other than those just mentioned, there are no other aspects of polymer network characterization covered in other chapters of this handbook. Therefore, some additional aspects of polymer network characterization are summarized here.

9.4.1 Determination of the Gelation Point

At the onset of gelation, some physical properties of polymeric materials suffer significant changes. The change of these physical properties, such as viscosity, modulus, or dielectric properties, is the key in several methods to determine the gelation point. In general, gelation time (t_{gel}) or monomer conversion at the onset of gelation (α_{gel}) are employed to express the occurrence of the gelation point.

Measurement of steady-state viscosity represents one of the simplest methods to estimate the gelation point. According to this technique, the gelation point corresponds to the time t at which the static viscosity “goes to infinity” [26, 27]. However, it possesses some drawbacks, as the gelation point is usually found by extrapolation and the experiments are restricted to the pregel period, usually stopping the measurement before the onset of gelation to avoid overload in the equipments and sample fracture.

The gelation point can also be measured by dynamic mechanical analyses (DMA). Several criteria have been proposed for identifying the onset of gelation. One of these criteria considers the gel point as the point of crossover between the base line and the tangent, drawn from the turning point of a G' curve [28, 29]. Another criterion is to define the gelation time as the point where $\tan \delta$ is independent of frequency [30, 31]. However, the most widely employed criterion for determination the onset of gelation is the point of intersection of the storage $G'(\omega)$ and loss moduli $G''(\omega)$ (ω defined as angular frequency) [32]. It has been pointed out that this condition is only satisfied if stress relaxation at the critical gelation point follows a power law:

$$G(t) = St^{-n} \quad (9.4)$$

where S is a material constant related to the strength of the polymer chains and $n = 1/2$ [33].

As mentioned before, gelation is characterized by a notable increase in viscosity, thus greatly reducing the mobility of polymer chains. This has been employed by some authors to estimate the gelation point by differential scanning calorimetry (DSC), analyzing this phenomenon in a similar way as with polymer vitrification [34]. However, in general, the occurrence of gelation does not provoke a variation in the reaction rate profile, as the case of thermosets, in which the gelation conversion is independent of temperature [35]. Thus, gelation cannot be detected directly by DSC, which is a technique responsive only to the chemical reaction and phase transitions.

Dielectric analysis (DEA) comprises a group of methods that evaluate the response of some properties of polar materials to changes in temperature or frequency. Usually, the evaluated properties are polarization, permittivity, and conductivity. For crosslinked materials, Mangion and Johari [36–38] have demonstrated that the ionic conductivity of a polymer solution decreases at the vicinity of the gelation point, following a power law equation, and they proposed that the relationship between the ionic conductivity (σ) and the kinetics of the reaction during the pregel stage is given by

$$\sigma = \sigma_0 \left(\frac{x_{\text{gel}} - x}{x_{\text{gel}}} \right)^k \quad (9.5)$$

where σ_0 is the conductivity at $x = 0$ and k is a critical exponent that depends on temperature. Equation 9.5 is in agreement with percolation theory. In fact, the form of Equation 9.5 is similar to the one used to estimate the gelation point based on the divergence of viscosity data [39]. A plot of $\log(\sigma)$ as a function of $\log(x_{\text{gel}} - x)$ should yield a straight line with slope k . The functional form of Equation 9.5 suggests that σ approaches zero at the vicinity of gelation. The inflection point of the plot of conductivity

versus time profile has been used as an indication of the onset of gelation [40]. It has been found that the estimates of gelation time using Equation 9.5 are in good agreement with those obtained by DMA [41].

9.4.2 Measurement of Crosslink Density

Usually, crosslink density is expressed in terms of the average molecular weight between crosslinks, M_c . There are several experimental techniques available for measurement of crosslink density, such as DMA, equilibrium swelling, NMR spectroscopy, and dielectric measurements, among other methods. Reviews on these experimental techniques are available in the literature (e.g., Ref. [42]). Some aspects about three of the most important techniques are briefly highlighted here.

When a polymer network is sufficiently crosslinked so that a structure with a reasonable degree of mechanical integrity above its glass transition temperature is obtained, the molecular weight between entanglements or crosslinks can be estimated using DMA, by calculating the storage modulus. The storage modulus, either E' or G' , is a measure of the sample's elastic behavior. An important feature of the storage modulus curve is the plateau in the rubbery region, given that its value is directly related to the crosslink density of the polymer network [43, 44]. The mathematical relationship between elastic (shear) modulus G and molecular weight between crosslinks M_c (and therefore, the crosslinking density), in terms of the elementary Gaussian network theory, is given by Equation 9.6 [43, 44]:

$$G = NkT = \frac{\rho RT}{M_c} \quad (9.6)$$

where N is the number of network chains per unit volume, k represents bulk modulus, ρ is the density of the network, T is absolute temperature, and R the gas constant. Equation 9.6 is valid for polymer networks synthesized with low crosslinker content; a correction is needed for highly crosslinked polymer networks [44]. For a polymer network with loose ends (which make no contribution to the network elasticity), the corresponding shear modulus is given by Equation 9.7 [45]:

$$G = N_e kT = \frac{\rho RT}{M_c} \left(1 - \frac{2M_c}{M}\right) \quad (9.7)$$

where N_e represents the number of effective chains. Additional factors such as a distinction between different types of junction points, according to the functionality of the crosslinker, and the effect of the presence of chains not directly connected to the network (sol) have been considered [46, 47].

The extent of swelling is inversely proportional to network crosslink density and is highly dependent on the

type of solvent and temperature. The thermodynamics of the swelling network process is commonly described by the Flory–Rhener equation [13] (Eq. 9.2, based on the affine deformation model). The crosslink density for $f = 4$ can be determined by using Equation 9.8:

$$\rho = \frac{1}{2\bar{v}_2 M_c} \quad (9.8)$$

When the junctions (crosslinks) are allowed to fluctuate (phantom model), the Flory–Rhener equation takes form shown in Equation 9.9:

$$\ln(1 - v_2) + v_2 + \chi_1 v_2^2 = -\frac{V_1}{\bar{v}_2 M_c} \left(1 - \frac{2}{f}\right) v_2^{1/3} \quad (9.9)$$

The actual swollen behavior of polymer networks lies in between the extremes calculated with the affine deformation and phantom network models [48, 49]. The sources of error/uncertainties during swelling equilibrium measurements, related to the estimation of the volumetric fraction of polymer, the interaction parameter, and the selection of the Flory–Rehner model (affine deformation or phantom network model), have been reviewed recently [50].

Crosslink density can also be measured experimentally by nuclear magnetic resonance (NMR). NMR experiments provide information about the local and long-range mobility of network polymer chains. The spin–lattice relaxation time (T_1) is related to the segmental (short-range) motion in the polymer chains; it provides information regarding the elasticity and flexibility of the material. The transverse magnetization relaxation time, usually referred to as spin–spin relaxation time (T_2), is related to intersegmental (long-range) motions of the polymer chains. These types of motion are highly sensitive to the presence of crosslinks [51] and consider the dynamics of the crosslinked network, as well as of the dangling free chain ends. Therefore, this property has been widely used for the evaluation of crosslink density [52, 53]. Several models have been proposed to relate transverse relaxation time with crosslinking and/or entanglement densities [54–57].

The total transverse relaxation function $M(t)$ for inter-crosslinked chains and dangling chain ends follows an exponential correlation function [58], as shown in Equation 9.10:

$$M(t) = A \exp \left\{ -\frac{t}{T_2} - q M_2 \tau_s^2 \left[\exp \left(-\frac{t}{\tau_s} \right) + \frac{t}{\tau_s} - 1 \right] \right\} \\ + B \exp \left(-\frac{t}{T_2} \right) \quad (9.10)$$

where A and B are the fractions of proton magnetization of the inter-crosslink chains and the dangling chain ends

of the network, respectively; M_2 is the second moment of the dipolar interactions; τ_s is the correlation time for overall isotropic motion; τ_f is the correlation time for segmental motion; q is the remaining fraction of the dipolar interaction M_2 during the inter-crosslink chains motion; and $1/T_2 = M_2\tau_f$. The average molecular weight between crosslinks, M_c , can be calculated from Equation 9.11, assuming that the polymer chains behave according to a Kuhn statistical segment [59]:

$$M_c = \frac{3c_\infty M_{ru}}{5n\sqrt{q}} \quad (9.11)$$

where c_∞ is the number of backbone bonds in a Kuhn segment and M_{ru}/n is the mass of the chemical repeating unit per number of backbone bonds in this unit.

9.5 THEORY AND MATHEMATICAL MODELING OF CROSSLINKING

Historically, Carothers [1] was the first scientist who derived an expression to calculate the extent of reaction at which gelation occurs. He defined a polymer gel as a polymer network that has an infinitely large molecular weight. Consequently, his conception of the gelation point was based on the divergence of the number-average molecular weight (M_n). However, at the gelation point, there will be polymer molecules bigger than M_n and divergence in M_n would manifest itself, if at all observed, only after the actual gelation phenomenon has taken place. Later, Flory [60] gave continuity to the concept of infinite molecules by means of a statistical treatment on a weight basis, presenting the conditions for the onset of gelation in polycondensation systems. His work together with the work developed by Stockmayer [61, 62] for free radical polymerization with crosslinking set up the basis of what is known as the *classical theory* of gelation.

The formation of polymer networks by step-growth polymerization has been modeled using statistical theories, such as the Flory–Stockmayer classical theory [61–64], the Macosko–Miller conditional probability model [65–70], and Gordon’s cascade theory [71–74]. However, statistical methods have not been successful for modeling of polymer network formation in chain-growth polymerization systems.

To address polymer network formation from nonlinear chain-growth polymerization (or copolymerization), kinetic methods are more appropriate [23, 75–83]. Some of the most successful kinetic models to address this type of system are based on the method of moments [23, 75–77, 79, 80, 82, 84]. Some divergence problems at the vicinity of the gelation point are common with the method of moments, although there are practical ways to avoid this situation [80]. A more refined kinetic method to address the issue of modeling the dynamics of gelation in

chain-growth polymerization reactors, without divergence problems, is the numerical fractionation technique (NFT) of Teymour and Campbell [83]. In the NFT, the population of polymer molecules is divided into generations, with each generation having the same type of architecture. It is possible to calculate the full molecular weight distribution (MWD) with this technique, but to do that it is assumed that the MWD of each independent generation is well represented by the Flory–Schulz most probable distribution [83], or other pre-established theoretical distributions.

Percolation theory approaches have been extensively used to model possible deviations from the classical Flory–Stockmayer theory [85]. With Percolation theory, it is possible to obtain useful information on the microstructure and connectivity of the polymer chains [85], but it has not been proven useful for polymerization reactor design and dynamic analyses [83]. Percolation theory usually requires Monte–Carlo (MC)-type simulations, which are very demanding of computer time. The group of Peppas have presented interesting kinetic simulations for several polymerizations leading to gelation, including the homopolymerization of tetrafunctional monomers [86]. Tobita has also modeled branching and crosslinking in free radical polymerization using MC methods [87].

It is important to point out that every theory possesses its own advantages and disadvantages; the choice of the most suitable method depends on the type of system analyzed, the required information, the level of detail in the reaction scheme, and the computational resources available. Thus, up to now there is not a unified approach that can deal with every crosslinking system, considering all the implementation difficulties and taking into account all nonidealities present in these systems, such as cyclization. A few details about each theory are offered below.

9.5.1 Statistical Gelation Theories

Statistical theories are mean field theories, assuming equal reactivities of the functional groups (where each functional group reacts independently of one another) and absence of intramolecular (cyclization) reactions. In the so-called classical theory of gelation, Flory devised a simple treelike model, where branched and crosslinked structures are generated from monomer units or larger structural fragments under different reaction states. These reaction states are represented by the number and type of reacted functional groups and type of bonds that link one unit with its adjacent units.

Let us consider the nonlinear polymerization of a monomer bearing f functional groups, A_f . The simplest representation of such a concept is shown in Figure 9.6, for a three-functional unit. This unit can hold four reaction states, from 0 to 3, which indicates the number of reacted bonds that link this unit with its neighbor.

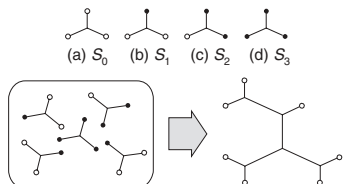


Figure 9.6 Representation of a trifunctional monomer according to the classical theory of gelation. The monomer can hold four reactive states, from 0 to 3, which indicate the number of functional groups that have been reacted, linking this unit with its neighbor. *Source:* Adapted with permission from Dusek K, MacKnight WJ. Crosslinking and structure of polymer networks. In: Labana SS, Dickie RA, Bauer RS, editors. *CrossLinked Polymers*. American Chemical Society; 1988. p. 2 [88]. Copyright 1988 American Chemical Society.

The linking process can be depicted by a tree graph in which each node represents a monomer unit. This picture is built by selecting one node at random from one polymer chain. The chosen node represents the root of the tree and, therefore, generation zero. Subsequently, the neighboring nodes linked to this node represent the first generation. Those nodes attached to this first generation represent the second generation and so on (Fig. 9.7).

In general, when a monomer unit is chosen randomly as the root of the tree in an f -functional system, the number N_r of components that can be introduced into generation g_r at conversion α is given by

$$N_r = f\alpha [(f-1)\alpha]^{r-1} \quad (9.12)$$

Once a gel is formed, the number of nodes in the rooted tree can be either finite or infinite. If it is infinite, the node chosen as the root of its tree is part of a gelled polymer chain. Flory's theory of gelation proposes that infinite network formation becomes possible when the number of units that can be added into a new generation (N_{r+1}) through branching of some of them, exceeds the value of his preceding generation (N_r). That is, if f is the functionality of the branching unit, gelation will occur when $\alpha(f-1)$ exceeds unity. Therefore, the critical value of α can be expressed by the general expression:

$$\alpha_c = \frac{1}{f-1} \quad (9.13)$$

For the case of a three-functional monomer, this will happen at $\alpha_c = 0.5$. This can be graphically expressed by means of Equation 9.12, as shown in Figure 9.8. At conversions $\alpha < \alpha_c$, $N_{r+1}/N_r = 1$ for any generation r , which represents the critical condition for the onset of gelation. For values of α greater than α_c , the values of N_{r+1} are always larger than N_r .

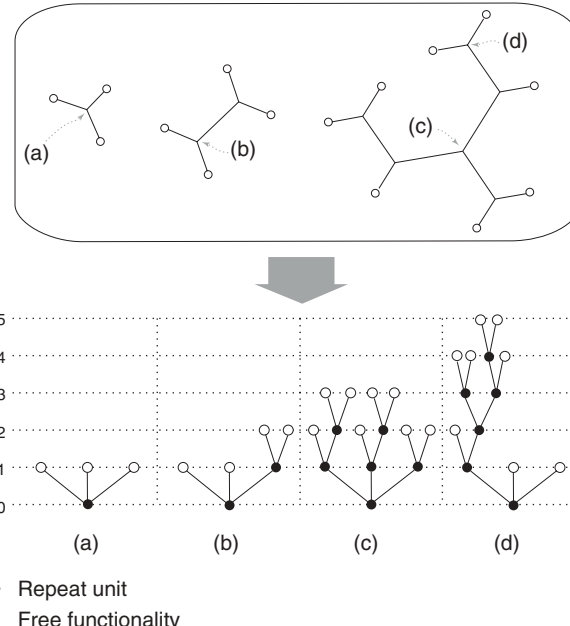


Figure 9.7 Tree plot for conceptualizing the crosslinked polymer structure, according to the classical theory of gelation. *Source:* Adapted with permission from Dusek K, MacKnight WJ. Crosslinking and structure of polymer networks. In: Labana SS, Dickie RA, Bauer RS, editors. *CrossLinked Polymers*. American Chemical Society; 1988. p. 2 [88]. Copyright 1988 American Chemical Society.

The previous observation can also be understood if we look at the expressions for the number and weight-average degrees of polymerization. For this system, these values will be respectively given by Equations 9.14 and 9.15.

$$\overline{P}_n = \frac{1}{1 - \left(\frac{f}{2}\right)\alpha} \quad (9.14)$$

$$\overline{P}_w = \frac{1 + \alpha}{1 - (f-1)\alpha} \quad (9.15)$$

Divergence of \overline{P}_w , which sets the onset of gelation, will occur at the condition expressed by Equation 9.13. The higher the functionality of the monomer A_f , the smaller the conversion required for reaching gelation. For other special cases, such as the case of $A_f + B_g$ step polymerization, the condition for gelation will be slightly different:

$$\alpha_c = \frac{1}{[r(f-1)(g-1)]^{1/2}} \quad (9.16)$$

where r is the stoichiometric imbalance ratio, defined as

$$r = \frac{A}{B} \leq 1 \quad (9.17)$$

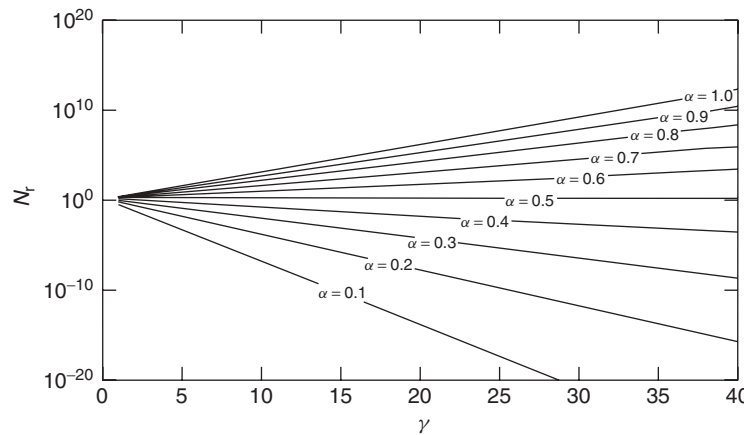


Figure 9.8 The number of components N_r that can be introduced into the generation g_r , at any given conversion α during the polymerization of a trifunctional unit. According to Flory's theory, gelation point will occur just when $N_{r+1}/N_r = 1$. In accordance with Equation 9.13, this will happen at $\alpha = 0.5$ for a trifunctional unit.

In the previous case, there is a critical stoichiometric imbalance ratio at which gelation will not occur:

$$r_c = \frac{1}{(f-1)(g-1)} \quad (9.18)$$

9.5.2 Percolation Gelation Theories

The percolation approach is a non-mean-field theory that is based on random walks in an n -dimensional space and takes spatial correlations into account. The work of Boots [89], Bansil [90], and Herrman [91] are some examples of such theory. This type of problems were first formally studied by Broadbent and Hammersley [92], but Stauffer [85] and de Gennes [2] first suggested that percolation on a three-dimensional (3D) lattice could provide a good insight into the critical phenomenon of gelation. Actually, the pioneering work of Flory and Stockmayer represents the mean field limit of percolation approaches in a Bethe lattice, a branching but loopless structure [93]. Under this approach, gel formation is visualized as a lattice model, where each lattice site with f neighbors stands for multifunctional units with f reacting sites. Two adjacent units can link each other, thus forming a bond. Let us consider, for instance, the FRC of bi- and tetrafunctional monomers producing a polymer network, as shown in Figure 9.9. Bi- and tetrafunctional monomers will be immersed within the lattice. Each monomer will occupy a lattice site. Lattice sites where a bifunctional monomer is situated can hold at most two bonds with their neighboring sites, while those sites having a tetrafunctional monomer can hold at most four bonds. Polymerization is initiated by free radicals (stars), which add to double bonds forming a growing chain that can continue this process.

During this growing process in the lattice, we can randomly select an active site and a neighboring lattice site, and examine the conditions between the two. If the adjacent site is not occupied, that is, if this site has not already undergone two or four bondings with its immediate neighbors, then the active site can be shifted to this new lattice site, thus forming a new bond. The fraction of reacted monomer will be α . At the beginning, when α is small, there will be only short chains and the entire lattice will be made out of sol. However, when a critical value of conversion, α_c , is reached, an infinite cluster is obtained. MC calculations can be performed to obtain the MWD, w_m , of this population at a certain conversion, α , which will be given by the number of clusters, each containing m sites per lattice site. Near the critical point, α_c , several properties undergo remarkable variations and the environment experienced by one molecule in one point can be noticeably different from the one experienced by any other molecule in a different point of the same system. This variation will be more evident as the system is closer to the gelation point. This non-mean-field theory allows consideration of fluctuations in chain connectivity at the vicinity of gelation. Since these fluctuations will be present during the pre- and post-gelation periods, it is useful to define a reduced conversion as

$$\varepsilon = \frac{|p_c - p|}{p_c} \quad (9.19)$$

In percolation theory, the weight-average chain length of the polymer distribution for a crosslinking system diverges according to the law:

$$\overline{P_w} \cong \varepsilon^{-\gamma} \quad (9.20)$$

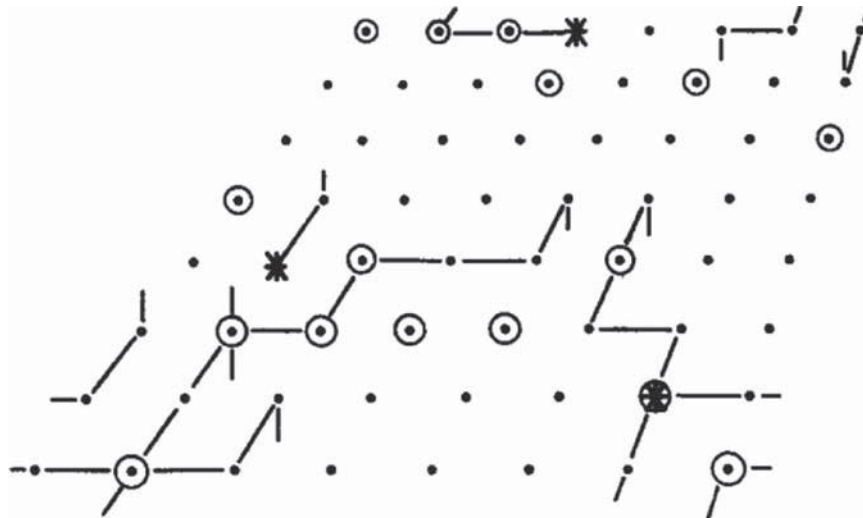


Figure 9.9 Schematic representation of a lattice considered in the percolation method. Bifunctional monomers are indicated by dots, tetrafunctional monomers by dots with circles, and active centers by stars. *Source:* Reprinted with permission from Herrmann HJ, Landau DP, Stauffer D. Phys Rev Lett 1982;49:412–415 [91]. Copyright 1982 American Physical Society.

where the exponent γ is in the order of 1.7–1.8, which differs from the critical value obtained with mean-field theories for chain connectivity $\gamma = 1$, where it is assumed that average properties are maintained throughout the whole system, even at the vicinity of gelation. However, with percolation theory, a wide range of values for γ have been obtained for several systems. For further discussion about percolation theory, the reader is referred to de Gennes [2].

9.5.3 Kinetic Theories

Kinetic approaches represent realistic and comprehensive description of the mechanism of network formation. Under this approach, reaction rates are proportional to the concentration of unreacted functional groups involved in a specific reaction times an associated proportionality constant (the kinetic rate constant). This method can be applied to the examination of different reactor types. It is based on population balances derived from a reaction scheme. An infinite set of mass balance equations will result, one for each polymer chain length present in the reaction system. This leads to ordinary differential or algebraic equations, depending on the reactor type under consideration. This set of equations must be solved to obtain the desired information on polymer distribution, and thus instantaneous and accumulated chain polymer properties can be calculated. In the introductory paragraphs of Section 9.5, we have already mentioned some of the characteristics of the kinetic theories, and mentioned some groups that have used them.

A common feature in the traditional modeling of FRC with crosslinking with kinetic theories is the use of the

“monoradical assumption”, that is, it is assumed that each polymer molecule can possess only one radical site, thus considering that polymer chains are either living or dead (in MC simulations, there is no such distinction). However, strictly speaking, this assumption is acceptable for linear polymerizations with monofunctional initiators. If cyclic multifunctional initiators are used, then multiradicals can also be present even in linear polymerizations. In nonlinear polymerizations, the presence of polymer chains with more than one radical center is expected, especially if gelation takes place.

By assuming multifunctional polymer molecules in the proposed reaction scheme for nonlinear polymerization, several imposed restrictions caused by the use of the monoradical assumption can be overcome. A single polymer population can be used instead of splitting the polymer population into classes based on functionality (i.e., labeling the polymer molecules as living, dead, or dormant, as typically done). Some important aspects of FRC with crosslinking, such as the presence of multiple living or dormant radical sites per macromolecule, the presence of multiple terminal double bonds per polymer chain, as well as the possibility of branching and crosslinking occurring not only in dead polymer molecules, but also in living or dormant ones, can be adequately modeled by using a multifunctional polymer molecule approach. In addition, when using this approach, the use of empirical closure expressions can be avoided.

Zhu and Hamielec [94] studied the FRC of vinyl monomers with chain transfer to polymer and the copolymerization of vinyl/divinyl monomers using a multiradical approach. They used the method of moments and focused on the pre-gelation period. They concluded that

the presence of multiradical macromolecules is an important feature of FRC with branching/crosslinking. However, they observed that the effect of multiradicals is not important if the propagation/terminations coefficient ratio (k_p/k_t) is smaller than 10^{-3} . Dias and Costa [95, 96] developed a kinetic model for calculation of average molecular weights based on the moment generation function (MGF). They took into account the presence of different types of radicals in the mechanism of FRC of vinyl/divinyl monomers, thus following a multidimensional approach. Korolev and Mogilevich [97] investigated the FRC with crosslinking of vinyl/divinyl monomers using MGF. They used a three-dimensional mass balance approach to take into account number of monomers, radical centers, and pendant double bonds. Recently, Iedema and Hoefsloot [98] employed the Galerkin finite-elements method (GF) to assess the importance of multiradicals on the chain length distribution (CLD) in FRC with branching by solving a set of two-dimensional balance equations. They compared their results to those obtained with a MC simulation of the same system, obtaining identical results of gelation point and evolution of the gel fraction.

9.5.4 Crosslinking and Controlled-Living Radical Polymerization

Controlled/“living” radical polymerization (CLRP) processes are well-established synthetic routes for the production of well-defined, low-molecular weight-dispersity polymers [99]. The types of CLRP processes (initiator-transfer agent-terminator (INIFERTER), atom transfer radical polymerization (ATRP), nitroxide-mediated radical (NMRP) polymerization, reversible addition-fragmentation transfer (RAFT)) and their characteristics are described in Section 3.8 of Chapter 3 and in Section 14.8 of Chapter 14.

Ide and Fukuda [100] studied the FRC of styrene with a small amount of 4,4'-divinylbiphenyl at 125°C in the presence of an oligomeric polystyryl aduct with 2,2,6,6-tetramethylpiperidinyl-1-oxyl (PS-TEMPO), with the aim of estimating the pendant double bond reactivity in such a system. They were able to mathematically describe that system by means of a simple reaction mechanism, assuming a random distribution of double bonds. They claimed that such system leads to a more homogeneous polymer network compared to those obtained by FRC. Later, they collected further experimental evidence that confirmed their initial hypothesis [101]. For the networks synthesized by regular FRC, they observed an insoluble fraction (microgels) at very low conversion, which grew up abruptly at the gelation point. In contrast, in the networks synthesized in the presence of PS-TEMPO, no microgels at low conversions were observed and the gel fraction grew gradually after the gelation point. In addition, they found that in the systems in the presence of PS-TEMPO, the critical conversion for

the onset of gelation can be described with certain degree of precision with the classical Flory–Stockmayer theory of gelation [60]. Since then, important research activity in the field of CLRP with crosslinking has emerged, addressing the INIFERTER, NMRP, ATRP, and RAFT techniques. The study of such systems has already been reviewed [102–106].

The use of CLRP as a novel approach to polymerize multifunctional monomers has gained relevance in the last few years. The reports concerning crosslinked polymers synthesized by CLRP have demonstrated that important differences exist between polymer networks synthesized by conventional free radical polymerization and those synthesized by CLRP techniques. These differences include a significant delay in the onset of the gelation point, steady increase of gel content with monomer conversion, and higher swelling ratios of the gels produced. These differences arise from the fact that the presence of CLRP reagents modifies the crosslinking process and thus, gelation occurs by a rather different mechanism. In CLRP with crosslinking, the fast and reversible equilibrium between active radicals and dormant species, coupled with fast initiation and negligible irreversible termination, results in a low and constant concentration of growing radicals. This situation reduces to some extent the heterogeneous nature of polymer gels synthesized by conventional FRC. In contrast to conventional FRC with crosslinking, the growth of polymer chains in CLRP with crosslinking is slow (in the order of hours, whereas it takes only seconds in conventional FRC), as a consequence of the activation–deactivation cycles undergone by the growing chains. During these dormant periods, the polymer molecules do not propagate but they have enough time for chain relaxation and diffusion, allowing the few radical centers to eventually and randomly react with the available pendant double bonds. Because of the high initiation rates present in CLRP, a high concentration of short polymer chains will be attained from the beginning of the reaction, thus favoring intermolecular (over intramolecular) crosslinking (Fig. 9.10). These characteristics of statistical crosslinking with low cyclization rates approximate the ideal conditions assumed in the Flory’s mean-field theory of gelation. However, it is important to point out that cyclization will unavoidably occur, and polymer gels will show certain degree of heterogeneity, irrespective of the synthetic route of gel formation. Factors such as dilution, crosslinker content, and CLRP reagent concentration will play an important role in the extent of intramolecular crosslinking and, therefore, in the homogeneity of the resultant polymer network. Moreover, the higher reactivity of the crosslinker, which causes significant compositional drift, will contribute to the heterogeneity of the produced polymer network. This situation can be minimized by implementing adequate monomer feeding policies such as those proposed by Dubé et al. [19] and Enright and Zhu [107].

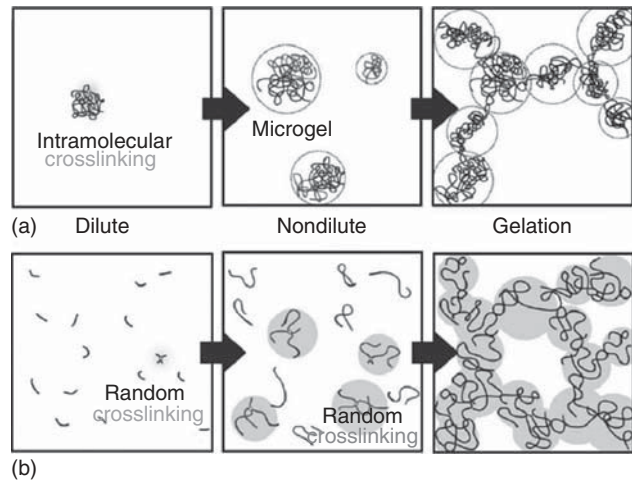


Figure 9.10 Comparison between the network formation mechanism through regular FRC and CLRP with crosslinking. (a) Conventional FRC with crosslinking; (b) CLRP with crosslinking. *Source:* Adapted with permission from Norisuye T, Morinaga T, Tran-Cong-Miyata Q, Goto A, Fukuda T, Shibayama M. Comparison of the gelation dynamics for polystyrenes prepared by conventional and living radical polymerizations: a time-resolved dynamic light scattering study. *Polymer* 2005;46:1982–1994 [108]. Copyright 2005 Elsevier.

In this system, the polymer chains bear functional groups that can be randomly linked to others by covalent bonds, thus allowing the formation of a polymer network at some point of the reaction. As the crosslinking reaction proceeds, the CLD will be modified, and therefore, it will be a function of the number of crosslink points that have been produced. Let us define $\bar{\rho}$ as the average number of crosslinked units (or crosslinking points) per polymer chain. Note that in the case of crosslinking of tetrafunctional units, as the case of vulcanization or free radical polymerization of vinyl/divinyl systems, every connection (crosslinkage) of primary chains attaches two crosslinking points and then $\bar{\rho}/2$ is the average number of crosslinkages per polymer chain. The extent of crosslinking is sometimes expressed in reduced form as the crosslink index γ (Eq. 9.A.4):

$$\gamma = \bar{\rho} \overline{P_{wp}} \quad (9.A.4)$$

According to the FS theory, the number and weight-average chain lengths of the new polymer CLD will be given by [4]:

$$\overline{P_n} = \frac{\overline{P_{np}}}{1 - \frac{\bar{\rho} \overline{P_{np}}}{2}} \quad (9.A.5)$$

$$\overline{P_w} = \frac{\bar{\rho} \overline{P_{wp}}}{1 - \bar{\rho} \overline{P_{wp}}} \quad (9.A.6)$$

$$\overline{P_z} = \frac{\overline{P_{zn}}}{(1 - \bar{\rho} \overline{P_{wp}})^2} \quad (9.A.7)$$

$$\overline{P_{z+n}} \propto \frac{1}{(1 - \bar{\rho} \overline{P_{wp}})^n}, \quad n = 1, 2, \dots \quad (9.A.8)$$

Strictly speaking, the weight-average chain length is given by $\overline{P_w} = \overline{P_{wp}} (1 + \bar{\rho}) / [1 - \bar{\rho} (\overline{P_{wp}} - 1)]$. However, since generally $\overline{P_{wp}} \gg 1$, the expression shown in Equation 9.A.6 is widely used. After successive crosslinking, the number of polymer chains will decrease constantly as they bond to each other, and polymer chains will start growing in size. These polymer chains can grow to the point where a giant molecule of remarkable molecular weight is formed. The solubility of the polymer molecules is significantly reduced, thus forming a polymer network. Hence, two clear stages can be identified: the pre- and post-gelation periods. The onset of gelation is characterized for some critical changes, as the divergence of higher order-average molecular weights. From Equation 9.A.6, the required condition for weight-average chain length to diverge is:

$$\bar{\rho} \overline{P_{wp}} = 1 \quad (9.A.9)$$

The physical meaning of Equation 9.A.9 is that an incipient polymer network will come up when, in a weight

$$w_{mp} = \frac{mN_m}{\sum_{m=1}^{\infty} mN_m} \quad (9.A.1)$$

The number and weight-average chain lengths will be given by Equations 9.A.2 and 9.A.3, respectively:

$$\overline{P_{np}} = \frac{\sum_{m=1}^{\infty} mN_m}{\sum_{m=1}^{\infty} N_m} \quad (9.A.2)$$

$$\overline{P_{wp}} = \frac{\sum_{m=1}^{\infty} m^2 N_m}{\sum_{m=1}^{\infty} mN_m} = \sum_{m=1}^{\infty} mw_{mp} \quad (9.A.3)$$

average basis, each primary chain bears one crosslinking point (or half of a crosslinkage for crosslinking with tetrafunctional monomers). Thus, during the pre-gelation period, there will be many more primary chains than crosslink points, while the opposite happens during the post-gelation period. It is worthy of attention that all higher order-average values of the resultant weight distribution after crosslinking will diverge at the same crosslink density, regardless of the primary chain distribution, as can be deduced from Equations 9.A.5–9.A.8. This derivation is of general application and applies to both nonlinear step growth and FRC and to any other crosslinking system. For instance, in the case of A_f step-growth polymerization, the crosslink density can be basically considered equal to monomer conversion, that is, $\bar{\rho} = \alpha$. This can be also applied to end-linking systems, as the copolymerization of long primary chains of B_f with a nonpolymeric crosslink agent A_g , connect randomly to form A–B bonds. In this case, $\bar{\rho} = \alpha_A \alpha_B$. This can represent, for instance, the polymerization with crosslinking of poly(vinyl alcohol) with adipic acid.

APPENDIX B CALCULATION OF SOL AND GEL FRACTIONS

Before the gelation point is reached, all polymer molecules have finite lengths and will be dissolved by any appropriate solvent. Therefore, the weight fraction of sol is equal to unity. However, at the onset of gelation, not all the polymer molecules are totally converted into an infinite molecule in a step-wise manner, but a portion of soluble low molecular weight polymer immersed in the incipient polymer network still remains. This soluble fraction will incorporate into the gels clusters just formed, increasing its molecular weight and, therefore, the amount of insoluble (gelled) polymer. If the average crosslinking density $\bar{\rho}$ is much smaller than unity, the weight fraction of sol, w_s , expresses the probability that a randomly selected unit belongs to the sol fraction. This random selection depends on chain length. Thus, the weight fraction distribution of primary chains, w_m , will be required. A primary chain will be part of the sol fraction provided that none of the units in this chain are connected to the gel. On the other hand, one chain will be part of the gel (with a probability w_g) only if it possesses crosslinking points (where the probability for this event is given by $\bar{\rho}$). Thus, the probability that a mer selected at random does not take part in a crosslink is $1 - \bar{\rho}$. The probability that it does, but that crosslinking point is not connected to the gel, is the product $\bar{\rho}(1 - w_g)$. The addition of these probabilities, namely, that one randomly selected mer is not crosslinked or it is crosslinked but it is not part of the gel, $1 - \bar{\rho} + \bar{\rho}(1 - w_g) = 1 - \bar{\rho}w_g$, represents the probability that such mer is not directly linked to the gel. Therefore, the probability that a mer in

a polymer chain with length m belongs to the sol fraction is given by $(1 - \bar{\rho}w_g)^m$. By summing the weight fraction of chains of all lengths that are not connected to the gel, the weight fraction of the sol is obtained and is given by Equation 9.B.1.

$$w_s = \sum_{m=1}^{\infty} w_m [1 - \bar{\rho}w_g]^m \quad (9.B.1)$$

Depending on the specific distribution w_m followed by the primary chains, the recursive equation for sol fraction can take several forms. If primary chains follow an exponential distribution (Flory distribution), Equation 9.B.1 can be expressed as:

$$w_s = \frac{1}{\left(1 + \frac{\bar{\rho}P_{wp}w_g}{2}\right)^2} \quad (9.B.2)$$

which can be rearranged as:

$$w_s + w_s^{1/2} = \frac{2}{\gamma} \quad (9.B.3)$$

Equation (9.B.3) represents the Charlesby–Pinner's equation [109], which is widely employed to analyze the gel curve.

If it is assumed that scission can occur with a probability $\bar{\beta}$, then Equation 9.B.3 becomes:

$$w_s + w_s^{1/2} = \frac{\bar{\beta}}{\bar{\rho}} + \frac{2}{\gamma} \quad (9.B.4)$$

On the other hand, the expression for uniform polymer chains is given by Equation 9.B.5 and represents the simplest form of Equation 9.B.1.

$$w_s = \exp(-\bar{\rho}P_{wp}w_g) \quad (9.B.5)$$

The proper knowledge of the functional form of w_m followed by every polymerization scheme would be the key factor for describing the evolution of gel content according to Equation 9.B.1. For a conventional free radical polymerization, the weight length distribution for primary chains that are formed at $x = \theta$ is given by [110]:

$$w_m(\theta) = (\tau(\theta) + \beta(\theta)) \left[\tau(\theta) + \frac{\beta(\theta)}{2} \times [\tau(\theta) + \beta(\theta)](m-1)m\Phi^{m+1}(\theta) \right] \quad (9.B.6)$$

where

$$\Phi(\theta) = \frac{1}{1 + \tau(\theta) + \beta(\theta)} \quad (9.B.7)$$

$$\tau(\theta) = \frac{R_f(\theta) + R_{td}(\theta)}{R_p(\theta)} \quad (9.B.8)$$

$$\beta(\theta) = \frac{R_{tc}(\theta)}{R_p(\theta)} \quad (9.B.9)$$

m is chain length, $R_p(\theta)$ denotes polymerization rate, $R_f(\theta)$ denotes rate of chain transfer to monomer and small molecules, $R_{td}(\theta)$ represents rate of termination by disproportionation, and $R_{tc}(\theta)$ represents rate of termination by combination. All these reaction rates are to be evaluated at conversion $x = \theta$.

Conversely, under the assumption of very low molar-mass dispersity (D_M) of primary chains, the weight-average chain length of the primary chains can be approximated by its number-average value, that is,

$$\overline{P_{wp}} \approx \overline{P_{np}} \quad (9.B.10)$$

This assumption has been proved to be a straightforward but useful mathematical expression for depicting the gel curved in reaction systems in which the molar-mass dispersity of primary chains is close to unity, as in the case of polymer networks obtained by CLRP. This equation can presumably be also applied to gels formed by living techniques, such as anionic, carbocationic, group transfer, and ring opening metathesis polymerizations. In a living polymerization, the probability that a monomer is connected to a chain end is the same for every growing chain, and therefore, the Poisson distribution can be used [111]. However, some deviations are expected to occur as a consequence of various nonideal effects.

Some other distribution functions have been proposed for living systems. For example, Müller et al. [112, 113] have reported an analytical solution for the molar mass distribution in a polymerization with degenerative transfer between active and dormant chain ends. Goto and Fukuda [114] presented a chain length distribution function based on a bivariate probability $N(x, y)$, considering that during a time t the chain experiences a number of y activation-deactivation cycles, while a total of x monomer units are added to the growing chain, as given in Equation 9.B.11:

$$N(x, y) = \frac{e^{-y_n} y_n^y}{y!} (1 - p)^y p^x \binom{x + y - 1}{x} \quad (9.B.11)$$

where y_n is the mean value of y .

Tobita [115–117] derived a fundamental weight fraction distribution represented by a hypergeometric function. He

combined the most probable and the Poisson distributions, the former expressing the CLD and the later indicating the distribution of the number of active periods of the growing chain. Nonetheless, this distribution is only applicable at constant monomer concentration. Dias and Costa [118] applied a kinetic approach based on the use of MGF for linear and nonlinear CLRP's. However, a simple kinetic scheme was considered, not taking into account termination or chain transfer reactions. They obtained a general solution for the CLD in a CLRP. Their results were similar to those described by Tobita [115–117] under similar conditions. Their treatment was generalized for nonlinear CLRP, obtaining a multimodal CLD. However, for systems considering monomer consumption, analytical solutions cannot be obtained because of the complexity of the problem; only numerical calculations can be applied in those cases.

ACKNOWLEDGMENTS

The authors acknowledge financial support from Consejo Nacional de Ciencia y Tecnología (CONACYT, México) (Project CONACYT 101682 and a Ph.D. Scholarship to J.C.H.-O., through *Beca Nacional para Estudios de Posgrado*, 202907), DGAPA-UNAM (Project PAPIIT 119510), and Instituto de Ciencia y Tecnología del Distrito Federal (ICyTDF, México) (Project PICSA11-56).

REFERENCES

1. Carothers WH. Trans Faraday Soc 1936;32:39.
2. de Gennes P-G. *Scaling Concepts in Polymer Physics*. 1st ed. Ithaca, NY: Cornell University Press; 1979.
3. Odian G. *Principles of Polymerization*. 4th ed. Hoboken, New Jersey: John Wiley & Sons; 2004.
4. Graessley WW. *Polymeric Liquids & Networks: Structure and Properties*. 1st ed. London: Garland Science; 2004.
5. Gérard H. Prog Polym Sci 1998;23:1019.
6. Hoffman AS. Adv Drug Deliver Rev 2002;54:3.
7. Alemán J, Chadwick AV, He J, Hess M, Horie K, Jones RG, Kratochvíl P, Meisel I, Mita I, Moad G, Penczek S, Stepto RFT. Pure Appl Chem 1801;2007:79.
8. Sperling LH. *Introduction to Physical Polymer Science*. 4th ed. Hoboken: Wiley Interscience; 2006.
9. Song JY, Wang YY, Wan CC. J Power Sources 1999;77:183.
10. Trester-Zedlitz M, Kamada K, Burley SK, Fenyö D, Chait BT, Muir TW. J Am Chem Soc 2003;125:2416.
11. Antonietti M, Sillescu H, Schmidt M, Schuch H. Macromolecules 1988;21:736.
12. Mecerreyes D, Lee V, Hawker CJ, Hedrick JL, Wursch A, Volksen W, Magbitang T, Huang E, Miller RD. Adv Mater 2001;13:204.

13. Flory PJ, Rehner JJ. *J Chem Phys* 1943;11:521.
14. Rodgers B, Waddell WH, Klingensmith W. Rubber compounding. In: Mark HF, editor. *Encyclopedia of Polymer Science and Technology*. New York: John Wiley & Sons, Inc; 2004.
15. Noordermeer JWM. Ethylene-propylene elastomers. In: Mark HF, editor. *Encyclopedia of Polymer Science and Technology*. New York: John Wiley & Sons, Inc; 2004.
16. Coran Y. Vulcanization. In: Eirich FR, editor. *Science and Technology of Rubber*. 2nd ed. New York: Academic Press; 1994. p 339.
17. Hofmann W. *Rubber Technology Handbook*. Revised version of the 1st edition. Munich: Hanser Publishers; 1989. p 53216.
18. Okay O. *Prog Polym Sci* 2000;25:711.
19. Dubé MA, Soares JBP, Penlidis A, Hamielec AE. *Ind Eng Chem Res* 1997;36:966.
20. Anseth KS, Goodner MD, Reil MA, Kannurpatti AR, Newman SM, Bowman CN. *J Dent Res* 1996;75:1607.
21. Dušek K, Galina H, Mikeš J. *Polym Bull* 1980;3:19.
22. Hamielec AE, MacGregor JF, Penlidis A. *Makromol Chem Macromol Symp* 1987;10/11:521.
23. Tobita H, Hamielec AE. Crosslinking kinetics in free-radical copolymerization. In: Reichert K-H, Geiseler W, editors. *Polymer Reactor Engineering*. New York: VCH Publishers; 1989. p 43.
24. Zhu S, Hamielec AE. *Macromolecules* 1992;25:5457.
25. Zhu S, Hamielec AE, Pelton RH. *Makromol Chem Theory Simul* 1993;2:587.
26. Adam M, Delsanti M, Durand D. *Macromolecules* 1985;18:2285.
27. Apicella A, Masi P, Nicolais L. *Rheol Acta* 1984;23:291.
28. Ampudia J, Larrauri E, Gil EM, Rodríguez M, León LM. *J Appl Polym Sci* 1999;71:1239.
29. Laza JM, Julian CA, Larrauri E, Rodriguez M, Leon LM. *Polymer* 1999;40:35.
30. Raghavan SR, Chen LA, McDowell C, Khan SA, Hwang R, White S. *Polymer* 1996;37:5869.
31. Scanlan JC, Winter HH. *Macromolecules* 1991;24:47.
32. Tung C-YM, Dynes PJ. *J Appl Polym Sci* 1982;27:569.
33. Winter HH. *Polym Eng Sci* 1987;27:1698.
34. Gao J, Li L, Deng Y, Gao Z, Xu C, Zhang M. *J Therm Anal Calorim* 1997;49:303.
35. Menczel JD, Judovits L, Prime RB, Bair HE, Reading M, Swier S. Differential Scanning Calorimetry (DSC). In: Menczel JD, Prime RB, editors. *Thermal analysis of polymers: Fundamentals and Applications*. 1st ed. Hoboken, NJ: John Wiley; 2009. p 7.
36. Mangion MBM, Johari GP. *Macromolecules* 1990;23:3687.
37. Mangion MBM, Johari GP. *J Polym Sci B Polym Phys* 1991;29:437.
38. Johari GP, Mangion MBM. *J Non-Cryst Solids* 1991;131–133(Part 2):921.
39. Pascault JP, Sautereau H, Verdu J, Williams RJJ. *Thermosetting Polymers*. 1st ed. New York: Marcel Dekker; 2002.
40. Bellucci F, Valentino M, Monetta T, Nicodemo L, Kenny J, Nicolais L, Mijovic J. *J Polym Sci, Part B: Polym Phys* 1995;33:433.
41. Núñez-Regueira L, Gracia-Fernández CA, Gómez-Barreiro S. *Polymer* 2005;46:5979.
42. Harrison DJP, Yates WR, Johnson JF. *J Macromol Sci C Polym Rev* 1985;25:481.
43. Treloar LRG. *The physics of rubber elasticity*. London: Oxford University Press; 1958.
44. Charlesworth JM. *Polym Eng Sci* 1988;28:230.
45. Flory PJ. *Chem Rev* 1944;35:51.
46. Case LC. *J Polym Sci* 1960;45:397.
47. Scanlan J. *J Polym Sci* 1960;43:501.
48. Flory PJ, Erman B. *Macromolecules* 1982;15:800.
49. Erman B, Flory PJ. *Macromolecules* 1982;15:806.
50. Valentín JL, Carretero-González J, Mora-Barrantes I, Chassé W, Saalwächter K. *Macromolecules* 2008;41:4717.
51. Munie GC, Jonas J, Rowland TJ. *J Polym Sci Polym Chem Ed* 1980;18:1061.
52. Charlesby A, Folland R, Steven JH. *Proc Roy Soc Lond Ser A* 1977;355:189.
53. Whittaker A. NMR Studies of Cross linked Polymers. In: Webb GA, Ando I, editors. *Annual Reports on NMR Spectroscopy*. San Diego, CA: Academic Press; 1997. p 105.
54. Brereton MG. *Macromolecules* 1989;22:3667.
55. Cohen-Addad JP. *J Chem Phys* 1974;60:2440.
56. Cohen-Addad JP. NMR and fractal properties of polymeric liquids and gels. In: Emsley JW, Feeney J, Sutcliffe LH, editors. *Progress in NMR Spectroscopy*. 3rd ed. New York: Pergamon Press; 1993.
57. Knörgen M, Menge H, Hempel G, Schneider H, Ries ME. *Polymer* 2002;43:4091.
58. Simon G, Baumann K, Gronski W. *Macromolecules* 1992;25:3624.
59. Kuhn W, Grün F. *Kolloid Z* 1942;101:248.
60. Flory PJ. *Principles of polymer chemistry*. 1st ed. Ithaca, NY: Cornell University Press; 1953. p 672.
61. Stockmayer WH. *J Chem Phys* 1943;11:45.
62. Stockmayer WH. *J Chem Phys* 1944;12:125.
63. Flory PJ. *J Am Chem Soc* 1941;63:3083.
64. Flory PJ. *J Am Chem Soc* 1941;63:3091.
65. Macosko CW, Miller DR. *Macromolecules* 1976;9:199.
66. Miller DR, Macosko CW. *Macromolecules* 1976;9:206.
67. Miller DR, Macosko CW. *Macromolecules* 1978;11:656.
68. Miller DR, Sarmoria C. *Polym Eng Sci* 1998;38:535.
69. Sarmoria C, Miller DR. *Comput Theor Polym Sci* 2001;11:113.
70. Shiau L-D. *Macromolecules* 1995;28:6273.
71. Gordon M. *Proc Roy Soc A* 1962;268:240.
72. Dušek K, Špirková M, Havliček I. *Macromolecules* 1990;23:1774.
73. Budinski-Simendič J, Petrovič ZS, Ilavsky M, Dušek K. *Polymer* 1993;34:5157.

74. Dušek K, Pascault JP, Špirková M, Somvársky J. Polyurethane networks and chemical clusters. In: Kresta JE, Eldred EW, editors. *60 Years of Polyurethanes*. Detroit: Technomic Publishing Co., Inc; 1998. p 143.
75. Mikos AG, Takoudis CG, Peppas NA. *Macromolecules* 1986;19:2174.
76. Mikos AG, Takoudis CG, Peppas NA. *Polymer* 1987;28:998.
77. Tobita H, Hamielec AE. *Makromol Chem Makromol Symp* 1988;20/21:501.
78. Zhu S. *Macromolecules* 1996;29:456.
79. Hutchinson RA. *Polym React Eng* 1992–93;1:521.
80. Vivaldo-Lima E, Hamielec AE, Wood PE. *Polym React Eng* 1994;2:87.
81. Naghash HJ, Okay O, Yağci Y. *Polymer* 1997;38:1187.
82. Luo YW, Pan ZR, Weng ZX, Huang ZM. *J Appl Polym Sci* 1995;56:1221.
83. Teymour F, Campbell JD. *Macromolecules* 1994;27:2460.
84. Tobita H, Hamielec AE. *Macromolecules* 1989;22:3098.
85. Stauffer D. *J Chem Soc Faraday Trans 2* 1976;72:1354.
86. Bowman CN, Peppas NA. *Chem Eng Sci* 1992;47:1411.
87. [a]Tobita H. *Polym React Eng* 1992–93;1:379. [b]Tobita H. *Acta Polym* 1995;46:185.
88. Dusek K, MacKnight WJ. Crosslinking and structure of polymer networks. In: Labana SS, Dickie RA, Bauer RS, editors. *CrossLinked Polymers*. American Chemical Society. Washington DC, 1988. p 2.
89. Boots HMJ, Pandey RB. *Polym Bull* 1984;11:415.
90. Bansil R, Herrmann HJ, Stauffer D. *Macromolecules* 1984;17:998.
91. Herrmann HJ, Landau DP, Stauffer D. *Phys Rev Lett* 1982;49:412.
92. Broadbent SR, Hammersley JM. *Math Proc Camb Phil Soc* 1957;53:629.
93. Sahimi M. *Applications Of Percolation Theory*. London: CRC Press; 1994.
94. Zhu S, Hamielec AE. *Macromolecules* 1993;26:3131.
95. Costa MRPN, Dias RCS. *Chem Eng Sci* 1994;49:491.
96. Costa MRPN, Dias RCS. *Chem Eng Sci* 2005;60:423.
97. Korolev GV, Mogilevich M. *Three-Dimensional Free-Radical Polymerization: CrossLinked and Hyper-Branched Polymers*. 1st ed. Berlin: Springer-Verlag; 2009.
98. Iedema PD, Hoefsloot HCJ. *Macromolecules* 2004;37:10155.
99. Davis KA, Matyjaszewski K. *Statistical, Gradient, Block and Graft Copolymers by Controlled/Living Radical Polymerizations*. Springer: Berlin; 2002.
100. Ide N, Fukuda T. *Macromolecules* 1997;30:4268.
101. Ide N, Fukuda T. *Macromolecules* 1999;32:95.
102. Gao H, Matyjaszewski K. *Prog Polym Sci* 2009;34:317.
103. Hernández-Ortiz JC, Vivaldo-Lima E, Lona LMF, McManus NT, Penlidis A. *Macromol React Eng* 2009;3:288.
104. Moad G, Rizzardo E, Thang SH. *Aust J Chem* 2006;59:669.
105. Moad G, Rizzardo E, Thang SH. *Aust J Chem* 2009;62:1402.
106. Sanson N, Rieger J. *Polym Chem* 2010;1:965.
107. Enright T, Zhu S. *Macromol Theory Simul* 2000;9:196.
108. Norisuye T, Morinaga T, Tran-Cong-Miyata Q, Goto A, Fukuda T, Shibayama M. *Polymer* 2005;46:1982.
109. Charlesby A, Pinner SH. *Proc Roy Soc Lond Ser A* 1959;249:367.
110. Hamielec AE, Tobita H. Polymerization processes, 1. fundamentals. In: *Ullmann's Encyclopedia of Industrial Chemistry*. Wiley-VCH Verlag GmbH & Co. KGaA; 2000.
111. Tobita H. *Macromolecules* 1994;27:5413.
112. Müller AHE, Zhuang R, Yan D, Litvinenko G. *Macromolecules* 1995;28:4326.
113. Müller AHE, Yan D, Litvinenko G, Zhuang R, Dong H. *Macromolecules* 1995;28:7335.
114. Goto A, Fukuda T. *Macromolecules* 1997;30:4272.
115. Tobita H. *Macromol Theory Simul* 2006;15:12.
116. Tobita H. *Macromol Theory Simul* 2006;15:23.
117. Tobita H. *Macromol React Eng* 2008;2:371.
118. Dias RCS, Costa MRPN. *Macromol Theory Simul* 2010;19:323.

10

POLYMER MODIFICATION: FUNCTIONALIZATION AND GRAFTING

JOSÉ BONILLA-CRUZ, MARIAMNE DEHONOR, ENRIQUE SALDÍVAR-GUERRA, AND ALFONSO GONZÁLEZ-MONTIEL

10.1 GENERAL CONCEPTS

The techniques for polymer functionalization and grafting are closely related. In many cases in which grafting is the ultimate goal, the generation of a reactive or functionalized polymer substrate is a preliminary step preceding the reaction of the functional groups along the polymer chain with other chemical entities (monomers or other polymers) in order to grow or attach side chains (grafts) along the primary polymer backbone. Therefore, the techniques for the generation of functionalized or functional polymers are analyzed first.

10.1.1 Methods for the Synthesis of Functional Polymers

The synthesis or modification of polymeric substrates in order to produce polymers with polar or functional groups can be carried out by several synthetic pathways. When the process starts from a previously existing nonfunctional polymer, and functional groups are introduced to the chain, the term *functionalization* is used. The techniques employed for the generation of a functionalized or functional polymer are as follows:

Direct copolymerization [1, 2]. In this case, two types of monomers react, one of them having a functional or pendant functional group; for instance, the copolymerization of maleic anhydride (MA) and styrene (St) generates the alternating copolymer poly (St-*alt*-MA) [1]. Another example is the direct copolymerization of α -olefins (polypropylene, PP, and polyethylene,

PE) with functional monomers such as MA or glycidyl methacrylate (GM); this goal remains as one of the challenges in synthetic polymer science [3]. In the latter example, the difficulty lies in the fact that the majority of this kind of polyolefins are produced by Ziegler–Natta or metallocene coordination chemistry, and both exhibit intolerance to Lewis bases because of their high oxophilic nature, which leads to deactivation of the catalysts [3b]. The most important mechanism in the catalyst deactivation is the formation of very stable complexes between the catalyst and the heteroatoms (N, O, halogens) present in the functional polar monomers [3c]. In spite of this, some advances in this field have been recently reported [4]. As a consequence, the postmodification of polyolefins with polar or functional groups, as opposed to the direct synthesis, offers the highest viability for the production of polyolefins with functional or reactive grafts.

End-functionalization [5]. Possible routes are (i) modification of the chain end of preexisting polymers; (ii) break of the growth of a polymeric chain or, (iii) break of the chain growth followed by its end-functionalization. In all cases, it is common to perform the indicated action using agents or chemical groups that contain the desirable functional group.

Functionalization-grafting [6, 7]. It consists of one of the following techniques: (i) synthesis *in situ* of grafts of homopolymers or copolymers (small or long chains) containing functional groups, starting from units located along an existing polymer backbone

(a form of the “grafting-from” technique, see next section); (ii) reaction or interchange of labile atoms of the polymeric backbone by functional monomers or reactive species; (iii) use of preexisting polymers possessing functional species and chain ends with chemical affinity to the backbone of the polymer (a form of the “grafting-onto” technique, see next section).

In several of the previous techniques, postmodification of polymers with functional groups or by grafting of polymeric chains with functional groups (polymer functionalization) is necessary. These can be generally carried out by abstraction of hydrogen atoms from the polymeric backbone by chemical methods using processes in bulk [8], solution [9], emulsion [10], or miniemulsion [11], via borane compounds [12] and in supercritical conditions (CO_2), [13] by gamma irradiations (γ) [14], ultraviolet (UV) irradiation [15], electron beam [16], or plasma [17], and by mechanical methods using high shear rate: reactive extrusion and mixing chamber [18], in the presence or absence of a peroxide-type initiator or azo-compounds; and using diverse commercial monomers or macromonomers previously synthesized. When the polymeric substrate has been previously modified, then the grafts or groups can be synthesized or attached by “grafting-from” or “grafting-onto” techniques, respectively.

10.1.2 Grafting-onto, Grafting-through, and Grafting-from

There are several ways in which structures having functional chemical groups or chains of homopolymers or copolymers grafted onto a polymeric backbone can be generated. In general, there are three common methods for the synthesis of this type of copolymers [6, 7]: “grafting-onto,” “grafting-from,” and “grafting-through.” Figure 10.1 schematically shows the synthesis of graft copolymers.

The first technique, “grafting-onto” (also called *grafting-to*), involves the reaction of an end-functional structure previously synthesized with a complementary functional monomeric unit present in the polymer backbone. Thus, grafting-onto is widely used for the synthesis of comb polymers. The “grafting-through” method uses macromonomers (polymer chains of very low molecular weight or oligomers) containing groups at their end that are capable of carrying out polymerization, particularly vinyl groups. The addition of a second monomer (comonomer) in the presence or absence (in the case of auto-initiation) of an initiator, leads to the construction of several complex topologies of graft copolymers. Indeed, depending of the reactivity ratios and the distance between adjacent grafts, brushes, regular grafts, centipede, barbwire, etc., structures can be produced [7a]. Finally, “grafting-from” is the most popular method used

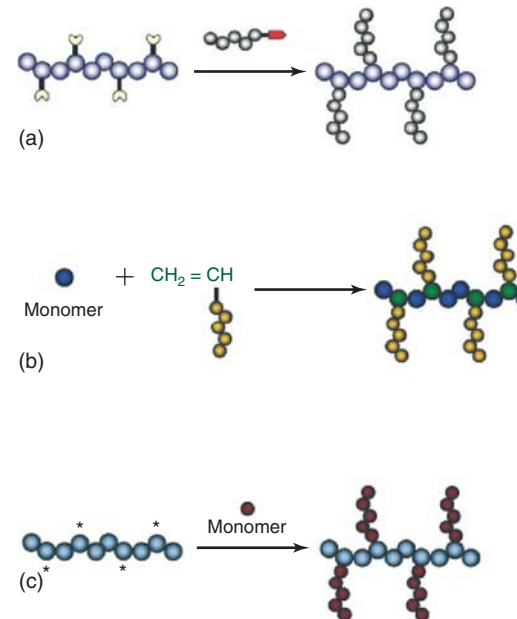


Figure 10.1 Schematic representation of (a) grafting-onto, (b) grafting-through, and (c) grafting-from methods. (See insert for the color representation of the figure.)

to obtain graft polymers, and requires a polymer containing reactive groups, functional species or initiator moieties along its backbone, which, in the presence of monomers, produce the growth of grafts from the surface of the substrate [7c–e]. Thus, the number of grafts can be controlled by the number of active sites present along the backbone.

10.1.3 Grafting on Polymeric and Inorganic Surfaces

Some applications demand only the grafting or functionalization of the surface of the polymer instead of the bulk polymer as mentioned in the previous section. In those cases some of the techniques previously discussed, such as grafting-to or grafting-from, can be applied to the surface of the polymer only, but other surface-specific techniques can be used as well. Recently, a variety of techniques have been proposed for improving or modifying surface properties of polymers, among which are graft polymerization, direct chemical modification [12], ozone and UV irradiation [15], corona and glow discharge, γ -rays [14], and electron beam [16]. Polymer surface grafting offers a versatile means for providing existing polymers with new characteristics such as hydrophilicity, adhesion, biocompatibility, conductivity, antifogging and antifouling properties, and lubrication [19].

As an illustration of the application of these techniques, the surface of poly(ethylene terephthalate) (PET) films has been modified via the grafting of polyacrylamide (PAM) by surface-initiated atom transfer radical polymerization (ATRP) and UV-initiated grafting in order to obtain a film of PET with a hydrophilic surface [15c].

On the other hand, the synthesis of hybrid materials involving polymer–inorganic interfaces has nowadays attracted much attention from the academic and industrial points of view. These materials include composites made by the dispersion of micro or nanoparticles, nanowires, or nanotubes in a polymer matrix, as well as those involving a flat interface between a polymeric and an inorganic layer. Examples of the latter are polymers grafted on flat surfaces of silicon dioxide, titanium dioxide, magnetite, carbon derivatives, ZnO, etc. In all these hybrid materials, the inorganic surface is typically modified using anchoring groups or chains of polymers, as illustrated in Figure 10.2.

In the case of composites, the surface modification leads to a good dispersion of the inorganic material in polymers matrices and, depending on the nature of the dispersed phase, imparts improved chemical and physical properties such as mechanical properties, UV attenuation, flame retardancy, thermal stability, thermal and electrical conductivity, gas barrier properties, superhydrophobicity, antimicrobial properties, etc.

Physisorption, electrostatic absorption, and covalent bonding are the most important techniques used to obtain these hybrid materials [20]. Covalent bonding offers better thermal stability between the attached group and the particle or surface than the others. Two principal approaches are widely used to produce polymer grafts covalently attached from the surface: “grafting-from” and “grafting-to.” “Grafting-to” produces a low grafting density (no. of chains/area) as a result of the diffusional effects (restriction of mobility by an increase of viscosity) of the chains into the reaction system. This problem can be overcome by the use of a solvent; however, the reaction time can increase considerably with this approach. Meanwhile, the “grafting-from” technique produces hybrid materials with high grafting density, and, similar to the polymer grafting case, it is possible to control the grafting density by controlling the number of active sites attached to the surface.

The anchoring groups covalently bonded to the surface typically are: di- or tri-(ethoxy, methoxy, chloro, etc.) silane, thiol, phosphono, and nitroxide groups [20–22]. The second moiety could be practically any chemical species, such as methyl, ethyl, vinyl, epoxy, acrylate groups, or hydrocarbon chains, as well as peroxide and azo-compounds and chemical species that, in the presence of a monomer or monomers, are capable of producing grafts on the surface by free-radical polymerization (FRP) or controlled radical polymerization (CRP) [22]. In the last case, the chemical species will be those agents used by nitroxide-mediated radical polymerization (NMRP), reversible addition-fragmentation transfer (RAFT), or ATRP.

The functionalization or modification of the particle surface with chemical groups or polymer grafts is the key to achieve excellent dispersion in polymer matrices and

to enhance the physical and chemical properties of the resulting composite; of course, in order to reach these goals the grafts must be compatible with the matrix in which the particles are dispersed.

10.1.4 Polymer Coupling Reactions

The modification of polymers can be readily conducted by chemical coupling reactions when the chain to be modified possesses groups such as vinyl, hydroxyl, or azide [23], etc. The Diels–Alder reaction between a diene and a dienophile, discovered by Otto Diels and Kurt Alder in 1928 [24], is the most important example of click chemistry.¹ These robust and efficient click coupling reactions have been widely exploited in the construction of tailor-made functional polymeric materials with complex molecular architectures [26]. Copper-catalyzed [3+2] cycloaddition reactions of azide–alkyne have also been used [23]; however, the main focus of several polymer research groups during the second half of the last decade has been the development of novel coupling reactions conducted in the absence of metal catalysts and under friendly ambient conditions [21], such as (i) metal-free [3+2] cycloaddition reaction of azide and activated alkynes, (ii) [4+2] Diels–Alder reactions, and (iii) thiol-based “click” reactions.

10.2 GRAFT COPOLYMERS

10.2.1 Commercial Polymer Grafting

The production of thermoplastics by polymer grafting synthesis techniques is widely used in the industry today. Large amounts of commercial thermoplastics, especially styrenic polymers, are nowadays produced by diverse grafting techniques, but other graft polymers are also produced commercially. Some of the most relevant examples are discussed below.

10.2.1.1 High Impact Polystyrene (HIPS) HIPS is a heterogeneous material produced by continuous bulk or bulk-suspension processes, in which a butadiene-based elastomer (polybutadiene (PB), or a block copolymer of styrene-butadiene) is first dissolved in styrene monomer (St) and the resulting mixture is then heated so that the polymerization proceeds either thermally or with the aid of a chemical initiator. At the molecular level, the product is a mixture of free polystyrene (PSt) chains and elastomer chains grafted with PSt side chains. The process yields a continuous (free) PSt matrix containing

¹The term *click chemistry* was introduced by Sharpless et al. 25 in 2001 and denotes the development of a set of powerful, highly reliable, versatile, and selective reactions for the rapid synthesis of useful new compounds and combinatorial libraries through heteroatom links.

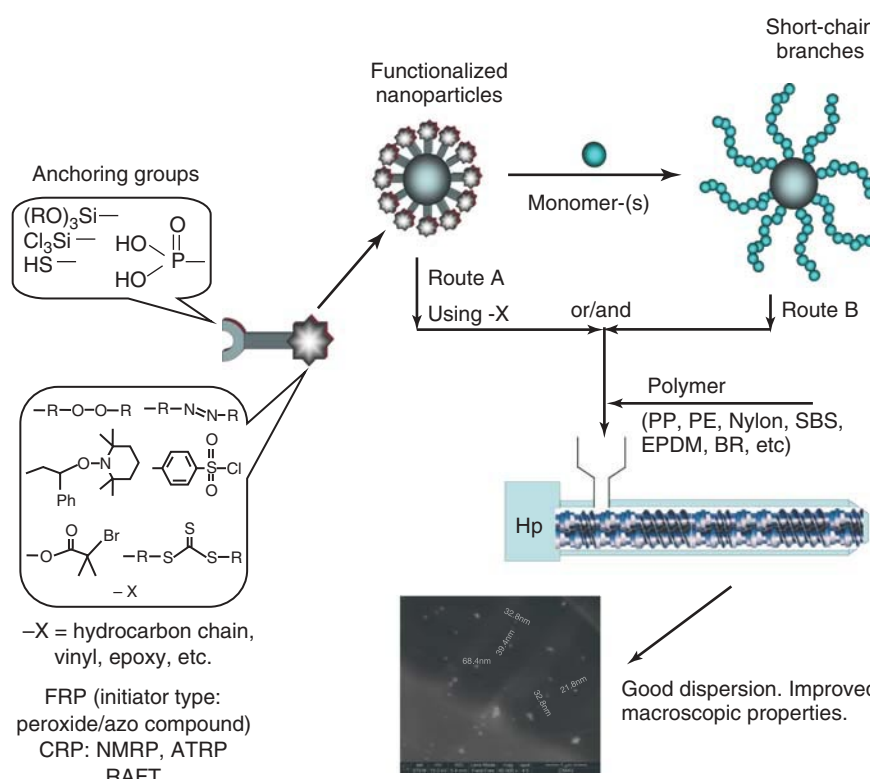
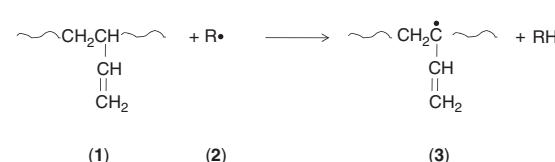


Figure 10.2 Grafting on surfaces and their dispersion in polymer matrices.

dispersed grafted PB particles of 0.5–6 µm, stabilized in the PSt matrix by the grafts of PSt which act as a compatibilizer between the matrix and the, in principle, incompatible elastomer. HIPS was born back in the 1920s when it was obvious that the versatile general-purpose polystyrene (GPPS) was too brittle for many applications. As early as 1927, Ostromislensky [27] invented HIPS by the polymerization of St in the presence of natural rubber in order to impart impact resistance to the resulting material; physical blends of rubber and PSt were also included in that pioneering patent. Later, around 1954, other companies (Shell [28], Dow [29], and Monsanto [30]) obtained patents for different versions of the synthesis process, such as the suspension and the mass-suspension processes. HIPS has become a commodity thermoplastic mainly produced by the continuous bulk process and ranks among the world's top five families of thermoplastic polymeric materials in terms of the volume of production. The world production of HIPS together with GPPS amounts to nearly 15,000,000 metric tons per year.

Technical Aspects The reaction mechanism in the synthesis of HIPS involves the basic reactions present in any FRP: initiation (thermal and chemical), propagation, transfer to monomer, and termination, mainly by combination (see Chapter 4 for the basic FRP mechanism). In addition



Scheme 10.1 Grafting mechanism by hydrogen abstraction illustrated on a 1-2 butadiene unit (**1**) of a PB chain. $R\bullet$ can be either a primary radical from the initiator or a polystyryl radical. A side chain (PSt graft) grows from (**3**) by the addition of styrene to the radical center.

to the basic scheme, some other specific reactions that lead to the grafting structures occur in the presence of PB (or butadiene units if styrene-butadiene rubber (SBR) is used); hydrogen abstraction from the PB backbone by primary or polystyryl radicals create radical centers along the PB chain from which PSt grafts (trifunctional branches in Flory's terminology) grow by propagation of the radical center with styrene monomer. Hydrogen abstraction especially occurs at the labile allylic hydrogen atoms next to unreacted double bonds of the butadiene units in the elastomer. Scheme 10.1 illustrates the grafting reaction mechanism.

Another reaction that can create grafts is addition to the double bond. Instead of abstracting the hydrogen atom in (1), species (2) can add to the double bond creating also

a radical center (tetrafunctional branch) that can propagate, but leaving R covalently bonded to the PB backbone. HIPS recipes typically consist of rubber contents of 4–8 wt% with respect to the total charge to the reactor, the rest being essentially monomer and small amounts of initiator and additives. If the process is carried out in the batch mode, the chronology of events occurring during the reaction is well known. In early stages of the process, the continuous phase is a solution of rubber in styrene and the dispersed phase is made of PSt particles swollen with monomer that precipitate out of the solution; however, at relatively low monomer conversions (15–30%), there is a phase inversion and the PSt/St solution becomes the continuous phase while the dispersed phase consists of rubber particles stabilized by the poly(butadiene-g-styrene) chains formed *in situ* during the polymerization. A complex interaction of process conditions, thermodynamic factors, and the kinetics of grafting leads to the formation of a particular rubber particle morphology known as the *salami morphology*, in which the dispersed rubber particles contain occlusions of PSt (Fig. 10.3).

Fisher and Hellmann [31], Leal and Asua [32], and Díaz de León et al. [33], among others, have published works that propose explanations for the formation of the particle morphology. Other particle morphologies are possible depending on the type of rubber used and other reaction conditions (reactor agitation, use of chain transfer agents, etc.) [34]. The particle morphology is a determining factor in the final properties of HIPS, in particular, its impact resistance and optical appearance. Fracture in HIPS occurs by the mechanism of formation of crazes, which are microcracks that propagate through the PSt matrix but initiate and terminate at rubber particles where impact energy is dissipated by particle deformation. Typical HIPS is an opaque material, but some translucent grades can be obtained by the use of styrene-butadiene block copolymers as the rubber phase.

The kinetic mechanisms [35, 36] in the HIPS polymerization process and the complete process [37–41] have been mathematically modeled to a detailed level by different groups. Diverse aspects of the HIPS technology have been extensively studied in the past by many authors; works that review several of these aspects are the texts of Scheirs and Priddy [42] (properties, applications, modeling, and later technologies), Echte [34] (particle morphology), Simon and Chapplear (industrial processes) [43], and Meira et al. [39] (process modeling and control).

10.2.1.2 Acrylonitrile-Butadiene-Styrene (ABS) Polymers Another family of important styrenic materials that are synthesized by grafting techniques, is that of acrylonitrile-butadiene-styrene (ABS) polymers. These are also thermoplastic materials like HIPS, but they exhibit improved impact and chemical resistance as well as

better appearance (gloss) than HIPS. Some grades are considered engineering polymers because of their superior properties. Worldwide production of ABS together with SAN (styrene-acrylonitrile) copolymers lies in the range of 4,000,000–5,000,000 metric tons per year during the decade 2000–2010. ABS resins show higher tensile strength and toughness as well as better solvent and heat resistance than HIPS resins. They are widely used in electrical and electronic appliances, such as telephones, radio, TV and printer cabinets, as well as automobile components [44].

ABS can be produced either by emulsion or by a bulk process. The emulsion process is more complicated but provides better flexibility than the bulk process. In the emulsion process, the first step is to generate rubber particles in a latex (aqueous dispersion) by emulsion polymerization of butadiene; since the particles produced in this way are too small, they may require an agglomeration step in order to increase their size. Next, styrene and acrylonitrile are copolymerized in the presence of the rubber latex. Part of the SAN copolymer is grafted on the rubber. Additional blending steps with SAN copolymer, either in latex form or in solid form (in an extruder), complete the synthesis process [45]. On the other hand, the continuous bulk process requires a more specialized reactor design and special pumping equipment (gear pumps) to propel the material through several reaction steps; however, the process is more cost-efficient and less contaminating, and produces a cleaner polymer than the emulsion process; so it is becoming the dominant process for massive production. In some technologies, a small amount of solvent may be used to facilitate the flow of the material.

The structure of ABS is similar to that of HIPS but with a SAN matrix instead of the PSt matrix in HIPS. PB grafted with SAN acts as a compatibilizer between the rubber particles and the SAN matrix. The rubber particle morphology in ABS can be similar to that in HIPS, with salami-type particles, but ABS particles can also be of the core–shell type, with a core of solid PB and a shell of graft copolymer, especially if the ABS is produced by the emulsion process [34]. In addition to craze formation, an important fracture mechanism in ABS polymers is shear yielding, which leads to tougher materials [46].

10.2.1.3 Other Impact-Modified Commercial Grafting-Based Polymers Typical HIPS and ABS polymers are opaque materials; however, MABS (methyl methacrylate-acrylonitrile-butadiene-styrene) polymers, which are produced by processes similar to those used in the production of ABS, are transparent materials. This property is obtained by the addition of methyl methacrylate (MMA) to the recipe in order to impart transparency to the polymer by equalizing the refracting index of the rubber particles to that of the matrix. These materials find applications

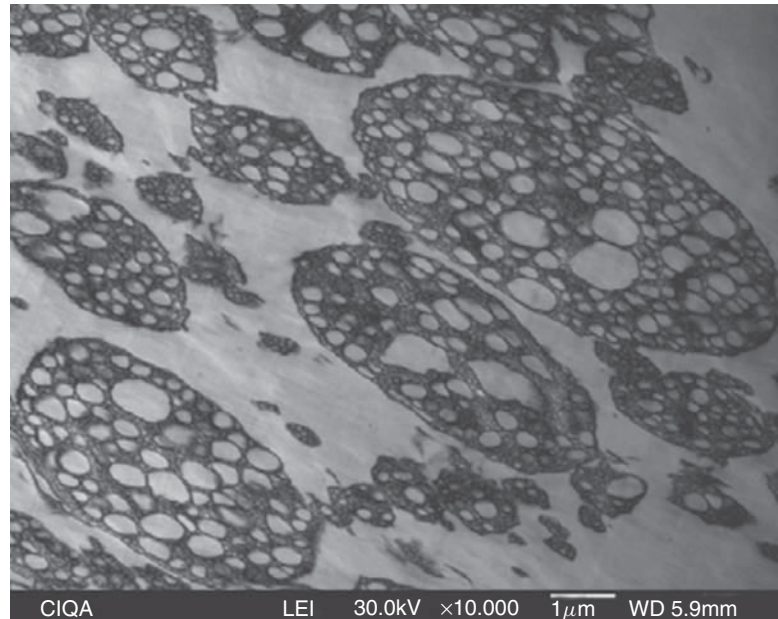


Figure 10.3 Typical salami morphology in a HIPS sample. Amplification $\times 10,000$. The sample was treated with OsO_4 . Dark areas correspond to PB segments and clear areas to PSt. Picture kindly provided by Dr. R. Díaz de León, CIQA.

in some household appliances and in electronic devices where both impact resistance and transparency are needed. A closely related family of polymers is known as *MBS* (*methyl methacrylate-butadiene-styrene*), which are based on a PB-rich backbone grafted with a copolymer of St-MMA. They can be produced by an emulsion process, and in this case they possess a core–shell morphology with a core rich in partially crosslinked elastomeric PB and a rigid shell of St-MMA copolymer. The main application of MBS is as an impact modifier for PVC resins.

Acrylonitrile-styrene-acrylate (ASA) copolymers is another family of graft-copolymer-based materials in which the rubber phase is really a copolymer of butyl acrylate (BuA) and butadiene (at least in some recipes) [47, 48], and the matrix is made of a SAN copolymer. Originally, butadiene was not present in the rubber phase [49] and perhaps those were not really graft-copolymer-based materials. The main advantage of ASA over ABS is its increased UV stability and long-term heat resistance due to the lack of residual double bonds in the acrylate part of the rubber.

10.2.1.4 Graft-Polyols Polyurethane foams are synthesized from the polycondensation reaction between a polyol and a diisocyanate. Polyols can be of two types: conventional ones (polyethers) and graft-polyols [50]. The latter are obtained by the copolymerization of SAN in the presence of a polyol polyether using a free-radical initiator. Some of the SAN chains are grafted to the polyol backbone, while others remain free. The grafting is promoted

by adding to the recipe a macromer formed by polyol polyethers functionalized with a vinyl monomer. The final result is a dispersion of SAN particles in a continuous phase of polyol polyether with the graft copolymer acting as a stabilizer. The foams formed from graft-polyols exhibit better physical and processing properties than their conventional counterparts, especially increased hardness.

10.2.2 Polyolefins

10.2.2.1 Borane Compounds A pioneering work in this field was that due to Chung and Jiang [51], who introduced a novel method to synthesize grafts along the polyolefin backbone. The chemistry is based on a “grafting-from” reaction using a borane-containing polymer. Under oxidation conditions, the borane group becomes a reactive site for FRP. With the appropriate choice of borane group and reaction conditions, the free-radical-polymerized polymers are chemically bonded to the side chains of the polyolefin with controllable compositions and molecular structures [12, 51]. The graft copolymerization of α -olefins with the monomer proceeds stepwise. The first step typically is a Ziegler–Natta or metallocene direct copolymerization of an α -olefin with a borane compound (alkyl-9-BBN, borabicyclononane); or the hydroboration [51d] of poly(ethylene-*co*-propylene-*co*-dienic monomer) (EPDM) with 9-BBN. In the next step, grafts of the polymer are produced when the copolymer is placed in the presence of monomer in THF under oxygen feed. Many grafted polyolefins have been synthesized following this novel

route [51]: for example, PE-*g*-PMMA, PP-*g*-PMMA, PP-*g*-PMA, EPDM-*g*-PMMA.

10.2.2.2 Ziegler–Natta and Metallocenes Henschke et al. [52] synthesized graft copolymers of poly(propene-*g*-styrene) by the copolymerization of propene with PSt macromonomers using the catalyst system $[\text{Me}_2\text{Si}(2\text{-Me-Benzind})_2]\text{ZrCl}_2$ and methylaluminoxane (MAO). Because of the high reactivity of allyl-terminated PSt in the metallocene-catalyzed copolymerization with propene, the application of the grafting-through method for the synthesis of polyolefin graft copolymers was possible. On the other hand, PE-*g*-silane was also synthesized by a grafting-through approach [53], copolymerizing 7-octenyldimethylphenylsilane with ethylene via $\text{Et}(\text{Ind})_2\text{ZrCl}_2$ methylaluminoxane catalyst system without loss of catalyst activity or decrease in molar mass. Finally, syndiotactic PSt-*g*-polydimethylsiloxane copolymers have also been synthesized stepwise [54].

Cationic and Anionic Graft Copolymerization Anionic and cationic polymerizations have been used in the synthesis of functionalized polyolefins. Although it is well known that living cationic polymerization has often been used in the polymerization of styrene, vinyl ethers, or isobutylene, some examples have been reported in the literature on their graft polymerization. For instance, Martini et al. [55] synthesized a copolymer of polyethylene-*g*-polystyrene (PE-*g*-PSt) using an alkylation reaction with different amounts of aluminum chloride (AlCl_3) as catalyst under near-critical conditions of n-hexane. Anionic polymerization has also been used in the synthesis of functional polyolefin-*g*-copolymers. Lu et al. [56], synthesized amphiphilic graft copolymers of polyethylene-*g*-polyethylene oxide (PE-*g*-PEO) by a new approach using anionic polymerization. The graft structure, molecular weight, as well as the molecular weight distribution of the graft copolymer could easily be controlled. The molecular weight of the side-chain PEO was proportional to the reaction time and the monomer concentration, which indicates the “living” character of the anionic polymerization of the grafts of ethylene oxide. Gohy et al. [57] reported the synthesis of well-defined poly(butadiene-*g*-*tert*-butyl methacrylate) (PB-*g*-Pt-BuMA) amphiphilic copolymers by reaction of Pt-BuMA chains end-capped with a *tert*-butyl 4-vinylbenzoate anion with the selectively hydrosilylated 1,2-units of anionically synthesized PB.

10.2.3 Modern Grafting Techniques onto Polymers

10.2.3.1 NMRP, RAFT, and ATRP Grafting functional groups (i.e., reactive monomers) onto polyolefins by means of free-radical initiators has been intensively studied and is now an established industrial process. Different kinds of

chemistry routes as well as polymerization processes have been developed to produce grafting polymers by traditional FRP. Nevertheless, FRP does not provide well-defined grafts of uniform length [58]. On the other hand, CRP has emerged as a powerful tool of synthesis in order to produce grafts of polymer with controlled architectures and narrow polydispersity for several practical applications. CRP combines the advantages of FRP—tolerance to impurities and moisture, capability of polymerization and copolymerization of a large range of monomers, smooth reaction conditions, and implementation in several polymerization process (bulk, suspension, emulsion, reactive extrusion, etc.)—with those characteristic of living polymerization chemistries (narrow polydispersities and capability for the synthesis of well-defined polymers and block copolymers). Thus, by combining the best of both worlds, CRP allows the polymerization of a large number of monomers with narrow polydispersity, as well as the synthesis of block copolymers, novel topologies, and functionalities [59]. Stable free-radical polymerization (SFRP), ATRP, and RAFT are the principal techniques employed to synthesize polymers and copolymers with controlled grafts. Refer to Chapter 4 for a brief description of CRP and each of these techniques.

10.2.3.2 Grafting and Functionalization of Polymers via CRP The synthesis of controlled grafts on polymers or the incorporation of functional/reactive entities in a controlled manner along the backbone of polymers, has been and still is one of the long-term challenges in the science and technology of polymers [58–60]. This is motivated by the potential applications of the resulting materials as compatibilizers in polymer blends with improved properties, as selective membranes to gases for food packaging, as novel polymer matrices, as nanodispersions for biomedical applications, as hybrid materials for applications in solar cells, etc. Grafting or controlled functionalization reactions have been performed or are possible in a variety of polymeric substrates such as PB, (6e, 7d,e, 13a), polyisoprene (PI) [7d], EPDM (6d, 13a), poly(styrene-*b*-isoprene-*b*-styrene) (SIS) [13a], poly(styrene-*b*-butadiene-*b*-styrene) (SBS) [61], butyl rubber (BR) (6d, 62), poly(ABS) [63], SBR [64], PP [65, 70, 80, 83, 84], PE [66, 81], and hydrogenated elastomers (SEBS) [67], among others.

Polydienes via NMRP The “grafting-from” methodology to modify polydienes by NMRP has been discussed in the patent literature; however, there are a few publications in the scientific literature that provide a deeper insight over the fundamental aspects of the modification of this kind of polymeric substrates in the presence of nitroxide groups. In the pioneering patents of Solomon et al. [68] controlled grafting of poly(methyl acrylate) along the PB backbone was described using two chemical steps. First, a multifunctional macroalkoxyamine was produced

on the basis of the functionalization of *cis*-polybutadiene (*cis*-PB, $M_n = 400,000$ Da) with nitroxide moieties (randomly distributed along the PB backbone) by using di-*tert*-butyl nitroxide and initiator (di-*t*-butylperoxyoxalate) at 50 °C in a solution process. Then, functionalized PB in the presence of tetrachloroethylene and methyl acrylate monomer at 95 °C led to well-defined grafts of poly(methyl acrylate) along the PB backbone. In 1997, Priddy and Li [69] reported the synthesis of block copolymers with controlled grafts in order to produce transparent impact polystyrene (TIPS) and HIPS. The first block copolymer (polydiene) was synthesized via anionic polymerization or by FR in the presence of peroxide or azo-type initiators and several kinds of persistent radicals (typical nitroxide radicals or initiators and comonomers previously modified with pendant nitroxide groups). The functionalized polydiene was then dissolved and heated in the presence of a vinyl monomer (bulk polymerization). The patent [69] covers the synthesis of the first block containing comonomer units with nitroxide pendant groups, which in the presence of the monomer can generate controlled grafts. Note that the dosing of comonomers with hanging nitroxide groups can produce a high density of grafting sites (brush type) in several places of the PB backbone. In 2003, Rhot et al. [70] from Ciba Spezialitätenchemie, extensively described the synthesis of controlled grafts at high temperatures (150–300 °C) by an extrusion process onto several polymeric substrates based on a variation of the strategy proposed by Solomon et al. [68]. Some examples in the patent cover the functionalization of PP and SBS with nitroxide moieties and the possibility of producing compatibilizers of α -olefins-*g*-polar monomers or SBS-*g*-polar monomers. In a 2008 patent, Saldívar-Guerra et al. [13a] disclosed the synthesis of controlled grafts of PSt or poly(butyl acrylate) (PBuA) onto both PB and SIS backbones in supercritical CO₂ (scCO₂). In a first step a multifunctional macroalkoxyamine was produced using nitroxide, initiator, and scCO₂ (swelling agent instead of organic solvents) in the presence of PB or SIS at 135 °C. Afterwards, the macroalkoxyamine in the presence of monomer in scCO₂ at 125 °C led to well-defined grafts.

In the open literature, Howell et al. [71] in 1999 described the synthesis of PB with pendant nitroxide groups to produce HIPS with high graft density by combining di-*tert*-butylperoxalate and TEMPO (2,2,6,6-tetramethyl-piperidinyl-1-oxy) in solution. The authors found that substrates possessing very high molecular weight in combination with the type of initiator used favored the formation of a gel, even in the presence of a TEMPO excess. This problem was overcome using a PB of 5000 Da. In a second step, functionalized PB was dissolved in the presence of St (5 wt%) and heated at 135 °C for 1 h to produce controlled grafts of PSt. In 2004 [64, 63], controlled grafts of PSt were synthesized

from brominated SBR [64] and brominated ABS [63], respectively, using the concept of Georges et al. [72] and the methodology developed by Hawker et al. [73] by reacting brominated sites with a functional nitroxyl compound (hydroxyl derivative of 1-benzyloxy-2-phenyl-2-TEMPO-ethane, Bz-TEMPO). The resulting macroinitiator (SBR-TEMPO) was heated in the presence of St to obtain the desired graft copolymer.

In 2008, in a detailed study using a combination of nitroxide/initiator and a model PB (5000 Da, 80/20 *cis,trans*/vinyl portion), Bonilla-Cruz et al. [7e] provided evidence on the functionalization mechanisms of polydienes with nitroxide and the influence of the side reactions during this process. The authors also demonstrated the feasibility of functionalization of PB with nitroxide only (PB-*g*-TEMPO) using an excess of nitroxide in solution under mild conditions. Finally, they showed that PB-*g*-TEMPO in the presence of St at 125 °C led to well-defined grafts of PSt along the backbone of PB. This work was further extended to the functionalization of PB, PI [7d], and EPDM [6d] using several types of nitroxide radicals and high throughput experimentation techniques, in which the grafting kinetics of the alternating copolymer of poly(styrene-*co*-maleic anhydride) (SMA) was studied in detail. More recently, in 2011 [7c] a macroinitiator of TEMPO-terminated syndiotactic polystyrene (*s*PSt-TEMPO) was prepared by reacting chloroacetylated *s*PSt with sodium 4-oxy-TEMPO derived from TEMPO-OH, which was used in the NMRP of St and *p*-methyl styrene (*p*-MSt) to yield controlled graft copolymers of *s*PSt-*g*-(PSt-*co*-*p*MSt).

Polyolefins and Other Commodities via NMRP In a pioneer work, Stehling et al. [74] in 1998 reported the copolymerization of α -olefins (propylene or 4-methylpentene) with an alkene-substituted alkoxyamine using a cationic metallocene catalyst. The functional polyolefins were used as macroalkoxyamines in the NMRP of St at 123 °C under argon in the presence of acetic anhydride. In 2000, Wiyatno et al. [75] synthesized an alkoxyamine possessing pendant polymerizable vinyl groups, which, in the presence of ethylene and 1-butene, led to terpolymers of poly(ethylene-*co*-butene-*co*-vinyl-TEMPO) using a metallocene catalyst. The terpolymer, in the presence of butadiene at 125 °C, led by NMRP to well-defined branches of PB. On the other hand, Baumert et al. [76] synthesized a novel alkoxyamine-functionalized 1-alkene which was copolymerized with ethylene using a palladium catalyst. The resulting highly branched PE with alkoxyamine-functionalized short-chain branches was used as a macroinitiator to initiate the NMRP of St and St/acrylonitrile. Mohajery et al. [77] reported the synthesis of PE-*g*-PSt copolymers via NMRP, copolymerizing first ethylene with *m,p*-MSt employing a metallocene catalyst Et(Ind)₂ZrCl₂ followed by the introduction of bromine at the benzylic position through bromination.

Macroalkoxyamines were prepared by reacting brominated copolymer with hydroxylamine. PE graft copolymers (22.6 mol% of PSt) were obtained via NMRP of St initiated from the macroalkoxyamine.

The postmodification of polyolefins in solution was studied by Park et al. [65a] PE-*g*-TEMPO and PP-*g*-TEMPO were obtained by the dissolution of the polyolefins (LDPE, $M_w = 482,000$ Da; PP, $M_w = 1,850,000$ Da) in 1,2,4-trichlorobenzene (TCB) at 170 °C in the presence of benzoyl peroxide (BPO) and TEMPO. After that, PE-*g*-PSt and PP-*g*-PSt were obtained by heating St at 120 °C in the presence of the macroalkoxyamines. Polyolefins grafted with PSt were used as coupling agents in blends of PE/PSt and PSt/PP. This idea was extended by the same group in order to polymerize controlled grafts of SMA [65b]. Lopez et al. [78] reported the preparation of a macroalkoxyamine based on PE and PE-*b*-PBuA via the NMRP of *n*-BuA, initiated by alkoxyamine-terminated PE. Finally, PVC [79] containing side-chain TEMPO (PVC-TEMPO) was prepared by reacting arylated and then brominated PVC (PVC-Ph-Br) with hydroxylamine. The macroalkoxyamine in the presence of St at 125 °C reacting during 4 h led to graft copolymers of PVC-*g*-PSt.

The chemical surface modification of polyolefin films using γ -irradiations and TEMPO has been reported by Miwa et al. [80] in a study in which peroxide groups were formed along the PP backbone by exposing isotactic PP (*i*PP, $M_v = 400,000$ Da) to ^{60}Co γ -irradiation in the presence of air. The macroinitiator PP-peroxide in the presence of TEMPO and St leads to the graft copolymer PP-*g*-PSt. Also, the same idea was utilized out by Yamamoto et al. [81] using PE ($M_n = 1.3 \times 10^4$ Da) instead of PP. In 2001, Miwa et al. [82] extended this approach to form copolymers from PP-peroxide in the presence of TEMPO, St, and a small amount of *n*-butyl methacrylate (BuMA) in order to obtain PP-*g*-poly(St-*r*-BuMA). Building upon the same approach, in 2003 Sugino et al. [83] added BPO in the copolymerization of St-BuMA under the hypothesis that, without free-radical initiators, the grafting process cannot be well controlled because of the considerably low concentration of peroxides along the polyolefin. On the other hand, polyolefins have been modified using UV irradiation. Yamamoto et al. [84] synthesized controlled grafts of MMA and BuMA onto films of *i*PP using benzophenone as initiator, toluene, and 2,2,6,6-tetramethyl-4-aminopiperidine-1-oxyl (4-amino-TEMPO) at 65 °C. Also, the synthesis of controlled grafts of PSt on silicon by NMRP atmospheric pressure plasma surface activation has been reported [85].

ATRP Techniques The synthesis of controlled grafts onto polymers by ATRP has been extensively reported in the literature (66, 86, 59a). One approach is to introduce halogen atoms along the preexisting polymeric backbone to

produce controlled grafts. For instance, Wang et al. [87] reported the synthesis of EPDM-*g*-PMMA in two steps. First, EPDM was brominated using an *N*-bromosuccinimide/azobis-isobutyronitrile system. The EPDM holding bromine groups, was then used as a macroinitiator to produce controlled grafts of MMA. Coiai et al. [88] synthesized well-defined core-shell structures polymerizing St, MMA, or ethylacrylate (EA) from brominated microparticles of ground tire rubber (GTR). On the other hand, 4-methyl-4-octene was used as a model compound of natural rubber [89], which was epoxidized to 4,5-epoxy-4-methyloctane. After that, the epoxidized compound in the presence of (a) 2-bromopropionic acid or (b) 2-bromo-2-methylpropionic acid resulted in ATRP macroinitiators, which, in the presence of MMA, produced controlled grafts of PMMA. Different kinds of graft copolymers, namely, SEBS-*g*-PMMA, SEBS-*g*-PSt, and SEBS-*g*-Pt-BuA, were recently developed by Xu et al. [90] using a stepwise procedure: (i) immobilization of ATRP initiators on the side chains of SEBS via partial chloromethylation of phenyl groups, and (ii) graft polymerization via iron-mediated activators generated by electron transfer (AGET)-ATRP. Fónagy et al. [91] synthesized thermoplastic elastomers of polyisobutylene-*g*-polystyrene (PIB-*g*-PSt) via ATRP. Functional nanoporous polymers based on nanoporous 1,2-polybutadiene with gyroid morphology were obtained by Guo et al. [92] using surface-initiated ATRP and click chemistry. Also, well-defined PB-*g*-PMMA and PB-*g*-Pt-BuA with low polydispersity and very high molecular weights were obtained by ATRP of MMA or *t*-BuA in the presence of brominated PB [93].

In the polyolefin field, controlled grafts of poly(*N*-vinyl-2-pyrrolidone) (PNVP) were synthesized onto non-woven membranes of PP [94]. In another work, using a functionalized macroinitiator derived from hydroxylated isotactic poly(1-butene), Shin et al. [95] synthesized a polar graft polyolefin, namely, isotactic poly(1-butene-*g*-poly(*tert*-butyl acrylate)) by ATRP, which was later hydrolyzed to generate some carboxylic acid functionality at the side chains. Also, an amphiphilic graft copolymer of poly((1-butene)-*g*-(acrylic acid)) was obtained from the hydrolysis of the *tert*-butoxy ester group of the graft copolymer synthesized earlier. Yamamoto et al. [96a] studied the graft polymerization of MMA from high density polyethylene (HDPE) films modified by 2,2,2-tribromoethanol or benzophenone. Also, in another approach of the same group, controlled grafts of MMA were synthesized onto PE via reverse ATRP [96b]. Liu and Sen [97] studied the synthesis of several linear PE-based copolymers with diblock grafts by ATRP. Finally, PBuA-*g*-branched PE was prepared stepwise: First, a branched PE macromonomer with a methacrylate-functionalized end group was prepared by Pd-mediated living olefin polymerization; the macromonomer was then copolymerized with *n*-BuA by ATRP [98].

RAFT Techniques Surface modification of PP microporous membranes was carried out by grafting block copolymers of poly(acrylic acid-*b*-acrylamide) using a combination of UV irradiation and the RAFT method with dibenzyl trithiocarbonate as a RAFT agent [99]. EPDM-*g*-PSt was synthesized by Joo et al. [100] stepwise. First, PSt was synthesized through the RAFT technique using trithiocarbonate as chain transfer agent. Then, a “grafting-onto” reaction of PSt onto EPDM was carried out using peroxide as a radical-generating agent. The peroxide created radical reactive sites on EPDM through hydrogen radical abstraction reaction, which were then transferred to trithiocarbonate units in PSt to afford EPDM-*g*-PSt. In another example, poly[*N,N'*-(1,4-phenylene)-3,3',4,4'-benzophenone tetracarboxylic amic acid] (PAmA) possessing controlled grafts of PMMA side chains (PAmA-*g*-PMMA) was synthesized by Fu et al. [101] via thermally induced graft copolymerization of MMA with ozone-pretreated PAmA using a RAFT process.

10.2.4 Functionalization and Grafting from Surfaces

10.2.4.1 Grafting from Nanoparticles The synthesis of grafts onto nanoparticles of silica (NPSiO₂), titanium dioxide (NPTiO₂), magnetite (NPFe₃O₄), and CdSe to obtain hybrid materials (nanoparticle-polymer) has been discussed in recent reviews and compilations [102]. As mentioned in Section 10.1.3, nanoparticle functionalization with chemical groups or grafts of polymer is the key to obtaining good dispersions of nanoparticles in polymer matrices, improving the physical and chemical properties of the resulting composite. NPSiO₂-*g*-polymer hybrids form the most studied system using FRP and CRP techniques. In general, the synthesis of grafts proceeds stepwise. In the first step, the nanoparticle surface is typically modified with organosilanes (Cl₃Si-, (RO)₃Si-; R = methyl or ethyl) or organophosphorus ((HO)₂PO-) derivative compounds used as anchoring groups containing: (i) initiating moieties (azo [103] or peroxide groups [104]), (ii) vinyl ends [105], (iii) alkoxyamines [106] (synthesized *in situ* or attached), or (iv) initiating species for ATRP [107] or RAFT [108] polymerization. In the second step, functionalized nanoparticles in the presence of monomer(s) in solution, or alternatively in bulk, led to nanoparticle-*g*-polymer composites. Prucker and Rühe [103a] were pioneers in modifying a NPSiO₂ surface with azo-chlorosilane through a base-catalyzed condensation reaction, in which PSt chains were synthesized by FRP using SiO₂-azo as a hybrid initiator at 60 °C during 6 h in the presence of St. Feng et al. [103b] introduced azo groups onto an NPSiO₂ surface via condensation between 4,4'-azobis-4-cyanopentanoic acid and alkyl-hydroxyl groups immobilized on the NPSiO₂ surface under ambient conditions. PSt chains were grafted

by FRP at 70 °C. Kasseh et al. [103c] introduced *tert*-butyl hydroperoxyde onto fumed silica, which, in the presence of St and/or BuA monomers and N-*tert*-butyl-1-diethylphosphono 2,2-dimethyl propyl nitroxide (DEPN, also known as SG1) at 120 °C in bulk, led to controlled grafts of PSt, PBuA, or poly(St-*b*-BuA). Also, controlled graft polymerization [103d-f] of BuA or ethyl acrylate (EA) can be achieved by decomposition of azo groups from NPSiO₂ functionalized with azo-triethoxysilane in the presence of SG1 and monomer at 100–120 °C. Ni et al. [104] functionalized SiO₂ particles bearing a peroxy functionality, which were used as hybrid initiators in the NMRP of St with TEMPO.

On the other hand, organosilanes with vinyl ends have also been attached to NPSiO₂ by the polymerization of vinyl monomers; thus core-shell NPSiO₂-polyacrylamide (PAM) nanospheres were synthesized by Liu and Su in 2005 [105a]. By emulsion polymerization, the vinyl ends of functionalized NPSiO₂ with γ-methacryloxypropyltri(isopropoxy)-silane were polymerized with fluorinated acrylate-siloxane monomers to obtain an organic-inorganic composite latex with an irregular core-shell structure [105b]. NPTiO₂ anatase [105c] or rutile [105d] have also been functionalized with organosilanes possessing vinyl ends, which, in the presence of St, led to grafts of PSt by FRP. Recently, in 2011, Jaymand [105e] synthesized a novel-type poly(4-chloromethyl styrene-graft-4-vinylpyridine)-*g*-TiO₂nanocomposite. First, a poly(4-chloromethyl styrene)/TiO₂nanocomposite (**1**) was synthesized by *in situ* FRP of 4-chloromethyl styrene and 3-(trimethoxysilyl) propylmethacrylate (MPS) modified nano-TiO₂. Thereafter, hydroxylamine (H-TEMPO) was covalently attached to (**1**), replacing the chlorine atoms in the poly(4-chloromethyl styrene) chains. The controlled graft copolymerization of 4-vinylpyridine was initiated by (**1**) carrying TEMPO groups as macroinitiator. Wang et al. [105f] functionalized nanosilica with vinyl-trimethoxysilane by dispersing nanosilica in the presence of vinyl-trimethoxysilane in ethanol during 2 h under ultrasonication. Functionalized nanosilica with vinyl groups in the presence of St, MA, TEMPO, and BPO led to controlled grafts of poly(SMA) at 130 °C. Magnetite (Fe₃O₄) nanoparticles with controlled grafts of 4-vinylpyridine have been obtained by polymerizing the alkoxy silane-functionalized nanomagnetite in the presence of hydroxy-TEMPO, 4-vinylpiridine, and BPO [105g].

Alkoxyamines can also be covalently bound to nanoparticles for subsequent NMRP. Thus, fumed nanosilica was functionalized with a trichlorosilane group containing an alkoxyamine initiator based on SG1 [106a]. The hybrid alkoxyamine, in the presence of BuA and sacrificial nitroxide (SG1) and N-*tert*-butyl-*N*-(1-diethylphosphono-2,2-dimethyl)propyl nitroxide (MONAMS) at 120 °C during 5–6 h, led to well-defined grafts of PBuA. Also,

Bartholome et al. [106b–d] functionalized nanosilica (diameter = 13 nm) with triethoxysilane group containing an alkoxyamine initiator based on SG1. This hybrid alkoxyamine in the presence of St leads to controlled grafts of PSt covalently attached onto nanosilica. Recently, well-defined grafts of PSt attached to both the inner and outer surfaces of ordered mesoporous silica (OMS) particles have also been generated by an NMP polymerization of St initiated from an SG1-based alkoxyamine [106e]. Sill and Emrick [106f] in 2004 functionalized cadmium–selenide nanoparticles (CdSe, 3–4 nm) with a TEMPO-alkoxyamine modified with a phosphine oxide functionality. The alkoxyamine in the presence of St at 125 °C led to controlled grafts of PSt on the CdSe surface. Kobayashi et al. (106 g) chemically modified magnetite (diameter = 10 nm) and titanium oxide nanoparticles (diameter = 15 nm) with an alkoxyamine modified with a phosphoric acid group. These hybrid alkoxyamines, in the presence of St or 3-vinyl pyridine (3VP) at 125 °C, led to controlled grafts of PSt or P3VP by NMRP.

Nanoparticle functionalization to obtain hybrid alkoxyamines is often a complicated multistep process because of the fact that it is first necessary to synthesize sophisticated alkoxyamines possessing anchoring groups that can react with -OH groups on the particle surface; therefore, new methods of functionalization involving only one step of synthesis/functionalization are highly demanded. As an example: Bartholome et al. [106c,d] synthesized a unimolecular alkoxyamine initiator (**1**) carrying triethoxysilyl end groups reactive toward the silica. This alkoxyamine was formed on the surface *in situ* by the simultaneous reaction of a polymerizable acryloxy propyl trimethoxysilane (APTMS), azobisisobutyronitrile (AIBN), and SG1 at 70 °C during 26 h. After that, (**1**) in the presence of St, toluene and sacrificial alkoxyamine, styryl-SG1, at 110 °C during 72 h led to controlled grafts of PSt on the nanosilica surface. In another work, Bonilla et al. [20b] obtained a hybrid SiO₂-TEMPO by functionalization of SiO₂ particles with TEMPO using oxoammonium salts in the presence of solvent and triethylamine by a one-step synthesis. After that, well-defined grafts of poly(St-*co*-MA) were obtained by polymerizing St and MA in the presence of SiO₂-*g*-TEMPO.

On the other hand, double-hydrophilic cylindrical polymer brushes of *t*-BuMA and oligo(ethylene glycol) methacrylate were synthesized from magnetite immobilized with poly(2-(2-bromoisobutyryloxy)ethyl methacrylate) by ATRP [107a]. Brushes of high grafting density (0.9 chains/nm²) were synthesized by combining NMRP to form PSt (8.7–8 kDa) and sequential ATRP to form Pt-BuA (18.6 kDa) from functionalized silica particles with a novel asymmetric monochlorosilane-terminated difunctional initiator [107b]. Surface-initiated ATRP with high grafting density (2 chains/nm²) of benzyl methacrylate,

MMA, and St from magnetite nanoparticles functionalized with an organophosphono initiator, was reported by Babu and Dhamodharan [107c]. Mesoporous hybrid materials made of mesoporous silica and a covalently grafted polymer with controlled chain length were successfully synthesized by surface-initiated ATRP of St and MMA [107d].

Using the RAFT technique, silica nanoparticles were functionalized by covalently attaching 3-methacryloxypropyltrimethylchlorosilane on their surface. The functional group attached had a methacrylic group at one end, which served as the initiating moiety. Thus, the polymerization of MMA in the presence of 4-cyano-4-(dodecylsulfanylthiocarbonyl) sulfanylpentanoic acid as RAFT agent and AIBN, produced PMMA–SiO₂ nanocomposites [108a] Ngo et al. [108b] synthesized hybrid TiO₂ nanoparticles of TiO₂-*g*-PMMA and TiO₂-*g*-poly(*tert*-butyldimethylsilyl methacrylate) (TiO₂-*g*-PMASi) by RAFT polymerization. First, the nanoparticles were immobilized with 3-(trimethoxysilyl) propyl methacrylate (MPS). After that, the vinyl ends of MPS were polymerized with MMA or MASI in the presence of 2-cyanoprop-2-yl dithiobenzoate (as RAFT agent) and AIBN. In this approach, the amount of free homopolymer formed was higher than that of the polymer anchored onto the surface of titania particles. On the other hand, using DDAT (*S*-1-dodecyl-*S'*-(α,α' -dimethyl- α'' -acetic acid) trithiocarbonate) as RAFT agent, Feng et al. [108c] prepared CdSe-*g*-poly(acrylonitrile) nanocomposites in the presence of a small amount of AIBN under ultrasonic radiation.

10.2.4.2 Carbon Derivatives A great number of carbon nanotube (CNT) applications are related to polymer nanocomposites. Much efforts has been focused to enhance the nanocomposite preparation methods aiming at the homogeneous dispersion of CNTs into diverse matrices to obtain novel composites with improved properties. CNT surface reactivity and polymer–nanotube interaction have been improved by functionalization [109] and surface polymer grafting [110]. The main methods to obtain hybrid CNT–polymers are (i) non-covalent attachment (i.e., polymer wrapping and absorption) and (ii) covalent attachment (i.e., “grafting-to,” “grafting-from,” and functionalization). In the case of covalent attachment, the resulting grafted polymer is usually named a polymer brush [111]. Thus, these kinds of hybrids have potential applications as cleaning, scrapping, and applying electronic contacts, among others [112]. The direct covalent functionalization of CNT preserves the nanotube structure and could favor a homogeneous and extended coverage of functionalized sites over the nanotube surface. In particular, radical reactions could be used to prepare further CNT derivatives, such as polymer-grafted nanotubes, and specifically the controlled radical polymer-grafted CNT. Several radical reactions have been performed with carbon structures (carbon black

(CB), fullerenes, and CNTs) with organic peroxides and nitroxides. Experimental results have reported the addition of radicals to carbon structures using electron spin resonance (ESR) [113]. Even more, polymer grafting has been carried out in several carbon structures, such as CB, fullerenes, CNTs, and graphene. Previous studies performed using CB and fullerenes constitute the pioneering work that evolved in the polymer grafting on CNT and graphene surfaces.

Carbon Black (CB) A permanent radical concentration [114], as well as a strong radical trapping behavior has been observed in CB [115], and also both properties have been used to graft polymers onto its surface [116]. Polymer grafting with CB has been achieved using the “grafting-from” and “grafting-onto” techniques. Cationic and anionic polymerization by azo [117], peroxyester [118], acylium perchlorate [119], and potassium carboxylated [120] groups introduced on the CB surface are examples of the “grafting-from” technique. Also, by FRP of vinyl monomers in the presence of CB under the “grafting-to” method leads to grafts of polymer onto CB with low grafting density (<10%), due to the fact that CB preferentially traps low molecular weight initiator fragments rather than polymer radicals [121]. Furthermore, when CB is treated with conventional free-radical initiators (BPO or AIBN), the corresponding radicals are bound on the surface, forming polycondensed aromatic rings and quinonic oxygen groups (115b, 122), which act as strong radical trapping agents for polymer radicals. Using this behavior as an advantage, Hayashi et al. [116a] reported the “grafting-to” reaction of CB with PSt chains polymerizing St in the presence of CB and TEMPO at temperatures above 100 °C. These experiments confirmed that CB preferentially traps more initiator fragments of low molecular weight than polymeric radicals. This behavior could be explained by the stability and the steric hindrance of the growing polymer radicals. Also, polymers having hydroxyl terminal groups could be grafted onto the CB surface in the presence of ceric ions. Complementary results by the same group determined that PEO could also be grafted onto CB without inducing gelation or crosslinking. This behavior revealed that radicals formed did not react with two CB particles.

Fullerenes Early studies on FRP of vinyl monomers in the presence of C₆₀ reported very low yields of polymer formed in solution, or even complete inhibition [123]. From these studies, it has been suggested that, in the case of St, the free radicals are trapped by fullerene, and the resulting fullerene radicals do not propagate but can terminate instead. Nevertheless, there are pieces of evidence suggesting that if the polymerization is carried out in the presence of a large excess of initiator, the radicals undergo multiple additions on the fullerene surface, changing their nature sufficiently not to inhibit polymerization [124]. Thus,

Krusic et al. [125] have shown that free-radical species can efficiently couple to the surface of C₆₀, resulting in highly functionalized fullerenes. Mehrotra et al. [123] reported that, in the presence of C₆₀, the polymerization of vinyl monomers (methyl acrylate, MMA, acrylonitrile, cyanovinyl acetate, vinyl acetate, 2-cyanoethyl acrylate, St, and N-vinylpyrrolidone) in solution was inhibited, yielding 15% or less of the polymer product. Therefore, it was concluded that the C₆₀ intercepts the initiating radicals in the polymerization reaction. Furthermore, it was observed that monomers with high reactivity could form fullerene-based radicals by their addition to the fullerene surface and could continue the polymerization process. In fact, functionalization of fullerenes with well-defined polymers by living polymerization techniques (e.g., anionic polymerization, NMRP, ATRP) has been reported recently. With these living methods, both the architecture of the polymer grafting on fullerene surfaces and, even more, the architecture of the polymer chains can be well-controlled [126].

Recently, a functionalization of carbon nano-onions (CNO, multilayer fullerenes) was carried out by [2+1] cycloaddition of nitrenes. The grafted products were prepared by the “grafting-from” method combining *in situ* ring-opening polymerization (ROP) and ATRP [127].

Carbon Nanotubes The first synthesis of polymer-grafted multiwalled carbon nanotubes (MWNTs) was reported by Jin et al. [110b] in 2000. Since then, the number of papers on this subject has increased enormously. In most of these papers, the polymer grafting of MWNTs has been achieved by one of the already mentioned techniques: “grafting-from,” “grafting-to,” and “polymer reactions with functional groups at the nanotube surface.”

POLYMER GRAFTING OF ACID-FUNCTIONALIZED CARBON NANOTUBES The first covalent attachment of PSt chains onto pretreated CNTs was reported by Shaffer in 2002 [110a]. PSt and some of their copolymers (such as poly(styrene-*co*-hydroxymethyl styrene) and poly(St-*co*-aminomethylSt) [128]) had been reported as being grafted on CNTs by one of the three previously discussed methods. In the case of acid-functionalized CNTs, the grafting of PSt could be achieved by several reactions, such as esterification [129], amidation [130], acylation [131], and Huisgen cycloaddition [132], among others. Nowadays, several polymers have been successfully grafted onto MWNTs using the “grafting-from” technique: PMMA grafted via emulsion polymerization [110c,d], sterification [133], and other methods [134]; polyethylenimine [135] and hyperbranched polyetherketones [136] via Friedel-Crafts acylation in polyphosphoric acid (PPA) [137]; PEO and PSt [138]; polyureas, polyurethanes, and poly(urea-urethane) [139]; polyethers [140], polyacetylene [141], and PSt

[142]. In all of these cases, the CNTs were chemically functionalized by acid treatment to introduce initiator molecules by chemical reaction using surface functional groups that could be used to carry out *in situ* polymerization of the different monomers.

POLYMER GRAFTING OF CARBON NANOTUBES BY CONTROLLED/LIVING RADICAL POLYMERIZATION Polymer grafting techniques that use direct covalent functionalization methods, such as radical reactions, have been developed in order to avoid the problems associated with the functionalization of CNTs using acids. These grafting techniques eliminate the need for nanotube pretreatment before the functionalization and allow attachment of polymer molecules to pristine tubes without altering their original structure.

The grafting mechanism involves free radicals from a growing or terminated polymer chain that attach themselves to the defective, doped and/or oxidized sites [110a,b], or to an aromatic ring by the inherent radical trapping mechanisms [110e] of the CNT. Both, the polymer “grafting-from” and the “grafting-to” methods on CNTs could be performed by FRP or CRP. Living polymerization methods in addition to the previously mentioned CRP include: anionic, carbocationic, and ROMP. All these methods have been used in the synthesis of polymer brushes in a “grafting-from” approach, as detailed below.

Nap et al. [143] considered how the strength and distance of the minimal interaction could be controlled by the choice of polymer chain length, surface coverage, and type of functional end group, and also how the feed ratio of monomers controlled the quantity of the grafted polymer. Like these, many other factors need to be studied to reach an understanding of the formation of polymer brushes on nanotubes. Some of the studied systems involved PMMA grafting on CNTs. Park et al. [144] reported the polymerization of PMMA over CNTs using AIBN as initiator. In this system, the radicals induced by AIBN on the outer wall of the MWNTs were found to initiate the grafting of PMMA [145]. Other authors have reported that poly(4-vinylpyridine) grafts to SWNTs during the *in situ* FRP of 4-vinylpyridine [146].

POLYMER GRAFTING OF CARBON NANOTUBES BY LIVING POLYMERIZATIONS Anionic and cationic polymerization techniques can be used to graft polymer chains on CNT surfaces. Mylvaganam et al. [147] reported, using density functional theory (DFT), that ethylene and epoxide functional groups can be grafted to CNTs using methoxy radicals and *sec*-butyl anion as initiators, leading to PE- and polyepoxide-grafted nanotubes, respectively. The theoretical study predicts that both the free-radical and the anionic functionalization methods are energetically favorable, that the resulting CNT radical and the CNT anion can react

with ethylene and epoxide functionalities, respectively, and that the resulting products have free electrons and negative charges on the carbon and oxygen atoms at the free ends of ethylene and epoxide, respectively. Hence, the *in situ* free-radical and anionic polymerizations can propagate to produce polymer-grafted CNTs. The cationic functionalization of CNTs using BF_3 as an initiator was found to be infeasible. In addition, PSt chains were grafted onto SWNTs via anionic polymerization techniques [148]. Particularly, the *in situ* surface-initiated CRP from the surface of CNT was reported by several authors using RAFT [149], ATRP [150], and NMRP [151], among others. There are only a limited number of experimental evidences of these radical polymerization techniques for the polymer grafting of CNT even after several years of work in this field. Hong et al. [149a] reported the poly(*N*-isopropylacrylamide) grafting of MWNTs via RAFT polymerization using RAFT agent-functionalized MWNT as chain transfer agents. Using the same technique, PSt chains were grafted from the surface of MWNTs [149b]. Additional examples involved the preparation of core–shell hybrid nanostructures using a RAFT agent immobilized on MWNTs. The hard phase was composed by MWNTs and the soft was a brush of poly(methacrylate) wherein the content of the polymer around carbon nanotubes could be modulated by the feed ratio [149c]. On the other hand, ATRP procedures proposed for nanotube surface polymerization are of two types: (i) the attachment of polymerization initiators via a cycloaddition reaction or the ROMP [152] and (ii) the attachment of initiator by the carboxy group generated by chemical oxidation [153]. The polymers growing over nanotubes using these techniques reported so far are principally PSt [150, 154], PMMA [155], Pt-BuA [156], PNIPAM [157], and PAA [158], as well as their copolymers [159]. Recently, a summary of the developments in nanostructured materials prepared by CRP has been given by several researchers [160]. Some advances in the understanding of the ATRP technique for the attachment of polymer on the CNT have been documented. Among these studies, Chun-Hua and Cai-Yuan [161] reported an increase in the molecular weight and a reduction of the reaction time when the *in situ* ATRP polymerization of St in the presence of silica nanoparticles and carbon nanotubes was carried out with an amount of PSt. In addition, using AGET–ATRP several amphiphilic polymers have been attached to nanoparticles forming self-assembling conjugates. Among these results, Hermant et al. [162] reported the preparation of poly(2-hydroxyethyl methacrylate)-grafted CNT. The result was an amphiphilic nanostructure. In addition, PMMA and PSt were successfully grafted over large-size pore silica under activator regenerated by electron transfer (ARGET)-ATRP conditions with control of the polymer loading and molecular weight of the grafted polymer [163]. The authors discovered that the capacity (in number, form: cylindrical or

spherical, and size) of the nanopores in the mesoporous silica defines the width of the polymer distribution. This approach, in which the polymers are degraded to convert them to carbon and the silica template is dissolved, permits the preparation of ordered arrays of hollow nanospheres and nanotubes.

Furthermore, the preparation of nanostructured carbon materials was proposed by McGann et al. [164] using the pyrolysis of films of $\text{PBuA}-b\text{-polyacrylonitrile}$ copolymers previously prepared by ATRP. Modifications of molecular weight induced changes in the final mass of the graphitic carbon films. Lee et al. [165] proposed a self-organization of aqueous droplets upon a volatile solution in order to yield macroporous polymer/carbon nanomaterial films. The materials prepared by the calcination of the polymer phase presented high conductivity and large surface area with potential applications in nanoelectronics (supercapacitors, catalytic supports) and energy storage materials (solar/fuel cell electrodes).

Recently, several authors have proposed the preparation of nanostructured materials by the use of conductive polymers and organically derived nanostructures [166]. In particular, Matyjaszewski et al. [160] have explored the use of polyaniline and polypyrrole, ionically conductive polymers, cationic poly(ethylene oxide), and various carbon nanostructures (such as graphenes), in order to generate polymers for dielectric applications. CNTs have been coated with covalently bonded polyelectrolyte brushes. Llarena et al. [167] have used poly(3-sulfopropylamino methacrylate) (PSPM) as coating by *in situ* polymerization via ATRP from initiating silanes previously attached to the CNTs. This led to the formation of hybrid nanocomposites of CNTs coated by PSPM with CdS and FeO embedded particles. The synthesis method for the hybrid nanostructures was ion exchange using sulfonate groups followed by precipitation. The reaction was followed by zeta potential measurements and TEM. Examples of metal-loaded polymer materials were developed by several researchers such as Kallitsis et al. [168] in order to add optoelectric properties to the inherent polymer properties through the presence of certain metal ions. This type of materials prepared by the use of bipyridine- and terpyridine-based ruthenium containing monomers, resulted in homo and copolymers with high Ru contents. The combination of these materials with others with electron–hole transporting properties or semiconducting properties, such as conjugated polymers or CNTs, could lead to multifunctional advanced materials (see also Chapter 29). Finally, the polymer grafting of boron nitride nanotubes (BNNT) using PSt and PMMA via ATRP has also been reported [169].

NMRP has been demonstrated on surfaces, nanoparticles and amphiphiles, and as well as very recently on CNTs by Ramirez et al. [151b]. This technique has been used in both “grafting-to” and “grafting-from” methods. In the first case, NMRP produces well-defined polymers that are

end-capped with thermally labile nitroxide functionalities; thus, this method could result in the controlled formation of polymer-centered radicals that could be utilized in the functionalization of CNT (151a, 170). In the second case, the pair initiator nitroxide could be attached to the nanotube to form a “macroinitiator,” which is susceptible to thermal initiation. The opening and closing mechanism for the free radical–controller pair favors the polymer chain growth, as described after an extensive characterization by Dehonor et al. [171]. The advantage of this functionalization is that the CNTs could be used as received and the reaction proceeds to a good extent. The available literature on the grafting of PSt to CNTs using NMRP invariably includes the functionalization of the nanotubes using strong acids to attach the initiator to the nanotube ends and defective sites. Particularly, Ramirez et al. [151a] attached an NMP initiator through carbodiimide or acid chloride chemistry to acid-functionalized nanotubes. Adronov et al. [152] proposed that the polymers could be covalently attached to SWNTs through the radical coupling of the polymer to the nanotube walls. Datsyuk et al. [151b] synthesized DWCT-polymer brushes by *in situ* nitroxide-mediated polymerization. Recently, the self-assembly of amphiphilic block copolymers of (poly(ethylene oxide)-poly(propylene oxide)-poly(ethylene oxide)) on MWNTs was studied. The polymer grafting proceeded using a nitroxide labeled PluronicTM. The presence of MWNTs changed the temperature and the dynamic behavior of the polymer and a different behavior were obtained depending on the type of CNTs used. SWNTs induced the formation of hybrid polymer–SWNT micelles, whereas the MWNTs induced the assembly of polymer aggregates at the surface of the MWNTs [172]. NMRP is the less reported CRP technique to graft polymer chains on CNT; however, the technique is promising because of the following: (i) successful functionalization is possible without any carbon nanotube surface damage like in acid-functionalized CNT and (ii) purification and separation problems are minimal (when compared to a technique such as ATRP).

10.2.5 Concluding Remarks

The development and applications of graft polymers and nano-objects (nanoparticles, carbon derivatives, etc.) possessing polymer grafts, is a scientific and technological field in continuous growth. Specifically, the CRP techniques in the synthesis of controlled grafts, have become a powerful tool to obtain new and novel materials with sophisticated architectures. As illustrated in this chapter, there are several approaches to carry out the polymer grafting of both nanoparticles and carbon nanostructures by “grafting-to” and “grafting-from” techniques. In our experience, the chemical modification (functionalization) of the surface of the nanoparticles or carbon derivatives

with grafts of polymer is the best way to achieve excellent dispersions of these nano-objects in a polymer matrix. As a consequence, the preparation of hybrid structures based on polymer grafting over solid nanostructures, is a useful tool for the design, fabrication, optimization, and eventual application of more functional nanomaterials.

In this section, a short review of the “state of the art” in the fields of synthesis of grafts over existing polymers and grafting onto different kind of nanoparticles and carbon derivatives has been presented.

REFERENCES

1. [a] Hurtgen M, Debuigne A, Fustin C-A, Jérôme C, Detrembleur C. *Macromolecules* 2011;44(12):4623. [b] Bonilla-Cruz J, Caballero L, Albores-Velasco M, Saldívar-Guerra E, Percino J, Chapela V. *Macromol Symp* 2007;248:132.
2. Cengiz U, Gencic NA, Kaya NU, Erbil HY, Sarac AS. *J Fluorine Chem* 2011;132:348.
3. [a] Kawahara N, Saito J, Matsuo S, Kaneko H, Matsugi T, Kashiwa N. *Polym Bull* 2010;64:657. [b] Marques MM, Correira SG, Ascenso JR, Ribeiro AFG, Gomes PT, Dias AR, Foster P, Rausch MD, Chien JCW. *J Polym Sci A Polym Chem* 1999;37:2457. [c] Stehling UM, McKnight AL, Stein KM, Waymouth RM. *Rapra Technology Spring* 1997;76:244–245.
4. Atiquallah M, Tinkl M, Pfaendner R, Akhtar MN, Hussain I. *Polym Rev* 2010;50:178.
5. [a] Bonilla-Cruz J, Lara-Ceniceros TE, Ramírez-Wong DG, Saldívar-Guerra E, Pérez-Rodríguez F, Márquez-Lamas U. *Macromol Chem Phys* 2011;212:1654. [b] Godoy-López R, Boisson C, D’Agosto F, Spitz R, Boisson F, Bertin D, Tordo P. *Macromolecules* 2004;37:3540. [c] Bergbreiter DE, Priyadarshani N. *J Polym Sci A Polym Chem* 2011;49:1772. [d] Thompson MR, Tzoganakis C, Rempel GL. *Polymer* 1998;39:327.
6. [a] Zdyrko B, Luzinov I. *Macromol Rapid Commun* 2011;32:859. [b] Uyama Y, Kato K, Ikada Y. *Adv Polym Sci* 1998;137:1. [c] Lei C, Li S, Chen D, Wu B, Huang W. *J Appl Polym Sci* 2011;119:102. [d] Saldívar-Guerra E, Bonilla-Cruz J, Hernández-Mireles B, Ramírez-Manzanarez G. *Macromol Symp* 2009;283–284:110. [e] Entezami AA, Abbasian M. *Iran Polym J* 2006;15(7):583.
7. [a] Sheiko SS, Sumerlin BS, Matyjaszewski K. *Prog Polym Sci* 2008;33:759. [b] Davis KA, Matyjaszewski K. *Adv Polym Sci* 2002;159:1. [c] Abbasian M. *J Elastom Plast* 2011;43(5):481. [d] Bonilla-Cruz J, Guerrero-Sánchez C, Schubert US, Saldívar-Guerra E. *Eur Polym J* 2010;46:298. [e] Bonilla-Cruz J, Saldívar-Guerra E, Torres-Lubián JR, Guerrero-Santos R, López-Carpy B, Luna-Bárcenas G. *Macromol Chem Phys* 2008;209:2268. [f] Uhrig D, Schlegel R, Weidisch R, Mays J. *Eur Polym J* 2011;47:560.
8. Gupta VK, Bhargava GS, Bhattacharyya KK. *J Macromol Sci Pure Appl Chem* 1980;A16(6):1107.
9. [a] Rahmani S, Entezami AA. *Macromol Res* 2011;19(3):221. Chandrasiri JA, Wilkie CA. *J Polym Sci A Polym Chem* 1996;34:1113.
10. Oliveira PC, Guimarães A, Cavaillé J-Y, Chazeau L, Gilbert RG, Santos AM. *Polymer* 2005;46:1105.
11. Pham TTB, Fellows CM, Gilbert RG. *J Polym Sci A Polym Chem* 2004;42:3404.
12. Chung TC. *Prog Polym Sci* 2002;27:39.
13. [a] Saldívar-Guerra E, Luna-Bárcenas G, Ramírez-Contreras JC, Bonilla-Cruz J, Pfaendner R, inventors; Ciba Holding Inc, assignee. WO patent 2009/065774A1. 2008; [b] Galia A, De Gregorio R, Spadaro G, Scialdone O, Filardo G. *Macromolecules* 2004;37:4580.
14. [a] Filho AAMF, Gomes AS. *Polym Bull* 2006;57(4):415. [b] Tsuchida A, Suda M, Otha M, Yamauchi T, Tsubokawa N. *J Polym Sci A Polym Chem* 2006;44:2972. [c] Deng J, Yang W. *Eur Polym J* 2005;41:2685.
15. [a] Yang W, Rånby B. *J Appl Polym Sci* 1996;62:533. [b] Deng J-P, Yang W-T. *J Polym Sci A Polym Chem* 2001;39:3246. [c] Zhou C, Zhang H-W, Jiang Y, Wang W-J, Yu Q. *J Appl Polym Sci* 2011;121:1254.
16. Sakurai K, Kondo Y, Miyazaki K, Okamoto T, Irie S, Sasaki T. *J Polym Sci B Polym Phys* 2004;42:2595.
17. [a] Weibel DE. *Compos Interfac* 2010;17:127. [b] Teare DOH, Schofield WCE, Garrod RP, Badyal JPS. *Langmuir* 2005;21(23):10818.
18. [a] Shao HJ, Guo JB, Li YJ, Yu J, Qin S. *Adv Mater Res* 2011;239–242:1153. [b] Cicogna F, Coiai S, Passaglia E, Tucci I, Ricci L, Ciardelli F, Batistini A. *J Polym Sci A Polym Chem* 2011;49:781. [c] Moad G. *Prog Polym Sci* 1999;24:81. [d] Moad G. *Prog Polym Sci* 2011;36(2):218. [e] Rzayev ZMO. *Int Rev Chem Eng* 2011;3(2):153. [f] Wilhelm HM, Felisberti MI. *J Appl Polym Sci* 2002;83:2953. [g] Cha J, White JL. *Polym Eng Sci* 2001;41(7):1238.
19. Uyama Y, Kato K, Ikada Y. *Adv Polym Sci* 1998;137:1.
20. [a] Wang Y, Shen Y, Pei X, Zhang W, Wei Y, Yang C. *Polym Polym Compos* 2008;16(9):621. [b] Bonilla-Cruz J, Lara-Ceniceros TE, Saldívar-Guerra E, Jiménez-Regalado E. *Macromol Rapid Commun* 2007;28:1397.
21. Kempe K, Krieg A, Remzi Bicer C, Schubert US. *Chem Soc Rev* 2012;41:176. Neouze M-A, Schubert US. *Monatsh Chem* 2008;139:183.
22. Wagner H, Brinks MK, Hirtz M, Schäfer A, Chi L, Studer A. *Chem Eur J* 2011;17(33):9107.
23. [a] Tsarevsky NV. *J Polym Sci A Polym Chem* 2010;48:966. [b] Ida S, Ouchi M, Sawamoto M. *J Polym Sci A Polym Chem* 2010;48:1449.
24. Diels O, Alder K. *Justus Liebigs Ann Chem* 1928;460:98.
25. Kolb HC, Finn MG, Sharpless KB. *Angew Chem Int Ed* 2004;2001:40.
26. Tasdelen MA. *Polym Chem* 2011;2:2133.
27. Ostromelesky JJ, inventors. US patent 1613673. 1927.
28. Haward RN, Elly J, inventors; Shell, assignee. US patent 2,668,806. 1954.

29. Amos JL, McIntire OR, McCurdy JL, inventors; The Dow Chemical Co, assignee. US patent 2,694,692. 1954.
30. Stein A, Walter RL, inventors; Monsanto Co, assignee. US patent 2,862,909. 1958.
31. Fischer M, Hellmann GP. *Macromolecules* 1996;29:2498.
32. Leal GP, Asua JM. *Polymer* 2009;50:68.
33. Díaz de León R, Morales G, Acuña P, Soriano F. *Polym Eng Sci* 2009;50(2):373.
34. Echte A. Rubber toughened styrene polymers, Chapter 2. In: Riew CK, editor. *Rubber Toughened Plastics. Advances in Chemistry Series*. Vol. 222. Washington (DC): ACS; 1989.
35. Peng FM. *J Appl Polym Sci* 1990;40:1289.
36. Chen C. *Polym React Eng* 1998;6(3–4):145.
37. Estenoz DA, Meira GR, Gómez N, Oliva HM. *AIChE J* 1998;44:427.
38. Estenoz DA, González IM, Oliva HM, Meira GR. *J Appl Polym Sci* 1950;1999:74.
39. Meira GR, Luciani CV, Estenoz DA. *Macromol React Eng* 2007;1:25.
40. Flores-Tlacuahuac A, Zavala-Tejeda V, Saldívar-Guerra E. *Ind Eng Chem Res* 2005;44(8):2802.
41. Verazaluce-García JC, Flores-Tlacuahuac A, Saldívar-Guerra E. *Ind Eng Chem Res* 1972;2000:39.
42. Scheirs J, Priddy DB. *Modern Styrenic Polymers: Polystyrenes and Styrenic Polymers*. Hoboken (NJ): John Wiley and Sons; 2003.
43. Simon RHM, Chapplear DC. Technology of styrenic polymerization reactors and processes, Chapter 4. In: Henderson JN, Bouton TC, editors. *Polymerization Reactors and Processes*. ACS Symposium Series. Vol. 104. Washington (DC): ACS; 1979.
44. McCrum NG, Buckley CP, Bucknall CB. *Principles of Polymer Engineering*. 2nd ed. New York: Oxford University Press Inc.; 1997. p 374.
45. Bouquet G. Rubber particle formation in mass ABS, Chapter 14. In: Scheirs J, Priddy DB, editors. *Modern Styrenic Polymers: Polystyrenes and Styrenic Polymers*. Hoboken (NJ): John Wiley and Sons; 2003.
46. Vu-Khanh T. Fracture behaviour of high-impact polystyrene and acrylonitrile-butadiene-styrene, Chapter 27. In: Scheirs J, Priddy DB, editors. *Modern Styrenic Polymers: Polystyrenes and Styrenic Polymers*. Hoboken (NJ): John Wiley and Sons; 2003.
47. Otto H-W, inventors; BASF, assignee. German patent DE 1182811. 1965.
48. Siebel HP, Otto H-W, inventors; BASF, assignee. German patent DE 1238207. 1967.
49. Herbig JA, Salyer IO, inventors; Monsanto, assignee. US patent 3118855. 1964.
50. Ramlow GG, Heyman DA, Grace OM. *J Cell Plast* 1983;19(4):237–242.
51. [a] Chung TC, Jiang GJ. *Macromolecules* 1992;25:4816. [b] Lu B, Chung TC. *J Polym Sci A Polym Chem* 2000;38:1337. [c] Chung TC, Rhubright D, Jiang GJ. *Macromolecules* 1993;26:3467. [d] Chung TC, Janvikul W, Bernard R, Jiang GJ. *Macromolecules* 1994;27:26. [e] Chung TC, Dong JY. *J Am Chem Soc* 2001;123(21):4871. [f] Xu G, Chung TC. *J Am Chem Soc* 1999;121:6763.
52. Henschke O, Neubauer A, Arnold M. *Macromolecules* 1997;30(26):8097.
53. Lipponen S, Seppälä J. *J Polym Sci A Polym Chem* 2004;42(6):1461.
54. Rahmani S, Entezami AA. *Macromol Res* 2011;19(3):221.
55. Martini RE, Brignole EA, Barbosa SE. *J Appl Polym Sci* 2012;123(5):2787.
56. Lu Y, Chen S, Hu Y, Chung TC. *Polym Int* 1963;2004:53.
57. Gohy J-F, Charlier C, Zhang J-X, Dubois P, Jérôme R. *Macromol Chem Phys* 1999;200(7):1630.
58. Matyjaszewski K. Radical polymerization, Chapter 3. In: Müller AHE, Matyjaszewski K, editors. *Controlled and Living Radical Polymerization*. Weinheim: Wiley-VCH Verlag GmbH&Co KGaA; 2009.
59. [a] Matyjaszewski K, Davis TP. *Handbook of Radical Polymerization*. 1st ed. Hoboken: Wiley Interscience; 2002. [b] Braunecker WA, Matyjaszewski K. *Prog Polym Sci* 2007;32:93. [c] Moad G, Solomon DH. *The Chemistry of Radical Polymerization*. 2nd ed. Oxford: Elsevier; 2006.
60. Davis KA, Matyjaszewski K. *Statistical, Gradient, Block and Graft Copolymers by Controlled/Living Radical Polymerizations*. Advances in Polymer Science. Berlin: Springer; 2002.
61. Yu P-R, Wu G-L, Peng J-Y, Hu S-A, Xiong Y-Q, Xu W-J. *J Macromol Sci A Pure Appl Chem* 2011;48(5):416.
62. Fonagy T, Ivan B, Szesztay M. *J Reinf Plast Comp* 2002;21(15):1411.
63. Bani F, Abbasian M, Taromi FA, Entezami AA. *Iran Polym J* 2004;13(6):513.
64. Abbasian M, Namazi H, Entezami AA. *Polym Adv Technol* 2004;15:606.
65. [a] Park E-S, Jin H-J, Lee I-M, Kim M-N, Lee HS, Yoon J-S. *J Appl Polym Sci* 2002;83:1103. [b] Park E-S, Yoon J-S. *J Appl Polym Sci* 2003;88:2434.
66. Zhao Y, Wang L, Xiao A, Yu H. *Prog Polym Sci* 2010;35:1195.
67. Xu W, Cheng Z, Zhang Z, Zhang L, Zhu X. *React Funct Polym* 2011;71(6):634.
68. Solomon DH, Rizzardo E, Cacioli P, inventors; CSIRO, assignee. US patent 4,581,429. 1986.
69. Priddy DB, Li IQ, inventors; The Dow Chemical Co, assignee. US patent 5,721,320. 1997.
70. [a] Roth M, Pfaendner R, Nesvadba P, inventors; Ciba Specialty Chemicals Co, assignee. US patent 6,521,710. 2003; [b] Roth M, Pfaendner R, inventors; Ciba Specialty Chemicals Co, assignee. US patent 6,525,151. 2003.
71. Howell B, Zhu Y, Zeng W, Lyons J, Meunier D, Demirors M, Priddy D. *Polym Prepr* 1999;73.
72. Veregin R, Georges M, Hamer G, Kazmaier P. *Macromolecules* 1993;26:2987.
73. [a] Hawker CJ, Hedrick JL. *Macromolecules* 1995;28:2993. [b] Hawker CJ, Barclay GG, Orellana A, Dao J, Devonport W. *Macromolecules* 1996;29:5245.

74. Stehling UM, Malmström EE, Waymouth RM, Hawker CJ. *Macromolecules* 1998;31:4396.
75. Wiyatno W, Fox PA, Fuller GG, Hawker CJ, Waymouth RM. *Polym Prepr* 2000;41(1):85.
76. Baumert M, Heinemann J, Thomann R, Mühlaupt R. *Macromol Rapid Commun* 2000;21:271.
77. Mohajery S, Rahmani S, Entezami AA. *Polym Adv Technol* 2008;19:1528.
78. [a] Lopez RG, Boisson C, D'Agosto F, Spitz R, Boisson F, Bertin D. *Macromolecules* 2004;37:3540. [b] Lopez RG, Boisson C, D'Agosto F, Spitz R, Boisson F, Gigmes D. *J Polym Sci A Polym Chem* 2007;45:2705.
79. Abbasian M, Entezami AA. *Polym Adv Technol* 2007;18:306.
80. Miwa Y, Yamamoto K, Sakaguchi M, Shimada S. *Macromolecules* 1999;32:8234.
81. Yamamoto K, Nakazono M, Miwa Y, Hara S, Sakaguchi M, Shimada S. *Polym J* 2001;33(11):862.
82. Miwa Y, Yamamoto K, Sakaguchi M, Shimada S. *Macromolecules* 2009;2001:34.
83. Sugino Y, Yamamoto K, Miwa Y, Sakaguchi M, Shimada S. *e-Polymers* 2003;7:1.
84. Yamamoto K, Kyouzuka S-J, Shimada S. *Macromolecules* 2004;37:86.
85. Lewis GT, Cohen Y. *Langmuir* 2008;24(22):13102.
86. Feng C, Li Y, Yang D, Hu J, Zhang X, Huang X. *Chem Soc Rev* 2011;40:1282.
87. Wang X-S, Luo N, Ying S-K. *Polymer* 1999;40:4515.
88. Coiai S, Passaglia E, Ciardelli F. *Macromol Chem Phys* 2006;207:2289.
89. Vayachuta L, Phinyocheep P, Derouet D, Pascual S. *J Appl Polym Sci* 2011;121:508.
90. Xu W, Cheng Z, Zhang Z, Zhang L, Zhu X. *React Funct Polym* 2011;71:634.
91. Fónagy TS, Iuán B, Szczesztay M. *J Reinf Plast Comp* 2002;21(15):1411.
92. Guo F, Jankova K, Schulte L, Vigild ME, Ndoni S. *Langmuir* 2010;26(3):2008.
93. Morandi G, Pascual S, Montembault V, Legoupy S, Delorme N, Fontaine L. *Macromolecules* 2009;42:6927.
94. Wang C, Feng R, Yang F. *J Colloid Interf Sci* 2011;357:273.
95. Shin J, Chang AY, Brownell LV, Racoma IO, Ozawa CH, Chung H-Y, Peng S, Bae C. *J Polym Sci A Polym Chem* 2008;46:3533.
96. [a] Yamamoto K, Miwa Y, Tanaka H, Sakaguchi M, Shimada S. *J Polym Sci A Polym Chem* 2002;40:3350. [b] Yamamoto K, Tanaka H, Sakaguchi M, Shimada S. *Polymer* 2003;44:7661.
97. Liu S, Sen A. *Macromolecules* 2001;34:1529.
98. Hong SC, Jia S, Teodorescu M, Kowalewski T, Matyjaszewski K, Gottfried AC, Brookhart M. *J Polym Sci A Polym Chem* 2002;40:2736.
99. Zhou J, Li W, Gu J-S, Yu H-Y, Tang Z-Q, Wei X-W. *Sep Purif Technol* 2010;71:233.
100. Joo S-I, Bae S-K, Hong SC, Cho H-C, Lee S-H, Kim Y-G. *Macromol Res* 2010;18(10):927.
101. Fu GD, Zong BY, Kang ET, Neoh KG, Lin CC, Liaw DJ. *Ind Eng Chem Res* 2004;43:6723.
102. [a] Brinks MK, Studer A. *Macromol Rapid Commun*. 2009;30(13):1043. [b] Tebben L, Studer A. *Angew Chem Int Ed* 2011;50:2. [c] Ishizu K, Lee DH. *Surface Tailoring of Polymer Nanoparticles with Living Polymerization Methods*. In: Vittal M, editor. *Advanced Polymer Nanoparticles Synthesis and Surface Modifications*. 1st ed. New York: CRC Press Taylor & Francis Group; 2011. p 223. [d] Zhang H, Han J, Yang B. *Adv Funct Mater* 2010;20:1533. [e] Barbey R, Lavanant L, Paripovic D, Schüwer N, Sugnaux C, Tugulu S, Klok H-A. *Chem Rev* 2009;109:5437. [f] Zou H, Wu S, Shen J. *Chem Rev* 2008;108:3893. [g] Tsujii Y, Ohno K, Yamamoto S, Goto A, Fukuda T. *Adv Polym Sci* 2006;197:1.
103. [a] Prucker O, Rühe J. *Macromolecules* 1998;31:592. [b] Feng L, Ye J, Qiang X, Zhang H. *J Appl Polym Sci* 2011;121:454. [c] Kasseh A, Ait-Kadi A, Riedl B, Pierson JF. *Polymer* 2003;44:1367. [d] Parvole J, Billon L, Montfort JP. *Polym Int* 2002;51:1111. [e] Parvole J, Montfort J-P, Billon L. *Macromol Chem Phys* 2004;205:1369. [f] Laruelle G, Parvole J, Francois J, Billon L. *Polymer* 2004;45:5013.
104. Ni G, Yang W, Bo L, Guo H, Zhang W, Gao J. *Chinese Sci Bull* 2006;51:1644.
105. [a] Liu P, Su Z. *J Microencapsul* 2005;22(6):683. [b] Qu A, Wen X, Pi P, Cheng J, Yang Z. *Polym Int* 2008;57:1287. [c] Zan L, Tian L, Liu Z, Peng Z. *Appl Catal Gen* 2004;264:237. [d] Xu L, Yang M. *Mat. Letter* 2008;62:2607. [e] Jaymand M. *Polymer* 2011;52(21):4760. [f] Wang Y, Shen Y, Pei X, Zhang S, Liu H, Ren J. *React Funct Polym* 2008;68:1225. [g] Chen Z, Yang Q, Peng K, Guo Y. *J Appl Polym Sci* 2011;119:3582.
106. [a] Parvole J, Laruelle G, Khoukh A, Billon L. *Macromol Chem Phys* 2005;206:372. [b] Bartholome C, Beyou E, Bourgeat-Lami E, Chaumont P, Zydownicz N. *Macromolecules* 2003;36:7946. [c] Bartholome C, Beyou E, Bourgeat-Lami E, Cassagnau P, Chaumont P, David L, Zydownicz N. *Polymer* 2005;46:8502. [d] Bartholome C, Beyou E, Bourgeat-Lami E, Cassagnau P, Chaumont P, Lefebvre F, Zydownicz N. *Macromolecules* 2005;38:1099. [e] Blas H, Save M, Boissière C, Sanchez C, Charleux B. *Macromolecules* 2011;44:2577. [f] Sill K, Emrick T. *Chem Mater* 2004;16:1240. [g] Kobayashi M, Matsuno R, Otsuka H, Takahara A. *Sci Tech Adv Mater* 2006;7:617.
107. [a] Xu Y, Yuan J, Fang B, Drechsler M, Müllner M, Bolisetty S, Ballauff M, Müller AHE. *Adv Funct Mater* 2010;20:4182. [b] Jiang X, Zhao B, Zhong G, Jin N, Horton JM, Zhu L, Hafner RS, Lodge TP. *Macromolecules* 2011;43(19):8209. [c] Babu K, Dhamodharan R. *Nanoscale Res Lett* 2009;4:1090. [d] Save M, Granvorka G, Bernard J, Charleux B, Boissière C, Gross D, Sanchez C. *Macromol Rapid Commun* 2006;27:393.
108. [a] Chinthammanipeta PS, Kobukata S, Nakata H, Shipp DA. *Polymer* 2008;49:5636. [b] Ngo VG, Bressy C, Leroux C, Margallan A. *Polymer* 2009;50:3095. [c] Feng M, Chen

- Y, Gu L, He N, Bai J, Lin Y, Zhan H. *Eur Polym J* 2009;45:1058.
109. [a] Sinnott SB. *J Nanosci Nanotechnol* 2002;2(2):113. [b] Peng H, Reverdy P, Khabashesku VN, Margrave JL. *Chem Commun* 2003;3:362. [c] Banerjee S, Hemraj-Benny T, Wong SS. *Adv Mater* 2005;17(1):17. [d] Hirsch A. *Angew Chem Int Ed* 2002;41(11):1853.
 110. [a] Shaffer MSP, Kozioł K. *Chem Commun* 2004;2002:18. [b] Jin Z, Sun X, Xu G, Goh SH, Ji W. *Chem Phys Lett* 2000;318(6):505. [c] Shieh Y-T, Liu G-L, Hwang KC, Chen C-C. *Polymer* 2005;46(24):10945. [d] Shieh Y-T, Liu G-L. *PMSE Prepr* 2004;90:437. [e] Tsubokawa N. *Polymer* 2005;37(9):637.
 111. [a] Sheiko SS, Möller M. *Chem Rev* 2001;101:4099. [b] Tasis D, Tagmatarchis N, Bianco A, Prato M. *Chem Rev* 2006;106(3):1105. [c] Schmidt G, Malwitz MM. *Curr Opin Colloid Interface Sci* 2003;8(1):103. [c] Matyjaszewski K, Miller PJ, Shukla N, Immaraporn B, Gelman A, Luokala BB, Siclovan TM, Kickelbick G, Vallant T, Hoffmann H, Pakula T. *Macromolecules* 1999;32(26):8716.
 112. Cao A, Veedu VP, Li X, Yao Z, Ghasemi-Nejhad MN, Ajayan PM. *Nature Materials*. 2005;4(7):540.
 113. [a] Walbiner M, Fischer H. *J Phys Chem* 1993;97(19):4880. [b] Morton JR, Preston KF, Krusic PJ, Hill SA, Wasserman E. *J Phys Chem* 1992;96(9):3576.
 114. Pena JM. *Polym Degrad Stabil* 2000;71(1):153.
 115. [a] Levy M, Szwarc MJ. *Chem Phys* 1954;22:1621. [b] Donnet JB. *Carbon* 1982;20:267.
 116. [a] Hayashi S, Naitoh A, Machida S, Okazaki M, Maruyama K, Tsubokawa N. *Appl Organometal Chem* 1998;12(10–11):743. [b] Donnet JB. *Rev Gen Caoutchouc* 1962;39(4):583. [c] Gessler AM. *Rubber Chem Technol* 1969;42(3):858.
 117. Fujiki K. *Polym J* 1990;22:661.
 118. Tsubokawa N. *Polym J* 1998;20:213.
 119. Tsubokawa N. *J Polym Sci A Polym Chem* 1983;21:705.
 120. Tsubokawa N. *Polym Bull* 1983;10:62.
 121. [a] Ohkita K. *Carbon* 1975;13:44328. [b] Ohkita K. *Carbon* 1978;16:41.
 122. Donnet JB. *Geldreich Comptes Rendus Physique* 1959;249:97.
 123. Mehrotra S, Nigam A, Malhotra R. *Chem Commun* 1997;463.
 124. Camp AG, Lary A, Ford WT. *Macromolecules* 1995;28(23):7959.
 125. Krusic PJ, Wasserman E, Parkinson BA, Malone B, Holler ER Jr., Keizer PN, Morton JR, Preston KF. *J Am Chem Soc* 1991;113(16):6274.
 126. Wang C, Guo Z-X, Fu S, Wu W, Zhu D. *Prog Polym Sci* 2004;29:1079.
 127. Zhou L, Gao C, Zhu D, Xu W, Chen FF, Palkar A, Echegoyen L, Kong ES. *Chem Eur J* 2009;15:1389.
 128. Hill DE, Lin Y, Allard LF, Sun Y-P. *Int J Nanosci* 2002;1(3&4):213.
 129. Hill DE, Lin Y, Rao AM, Allard LF, Sun Y-P. *Macromolecules* 2002;35(25):9466.
 130. Ham HT, Koo CM, Kim SO, Choi YS, Chung IJ. *Macromol Res* 2004;12(4):384.
 131. Huang H-M, Liu I-C, Chang C-Y, Tsai H-C, Hsu C-H, Tsiang RC-C. *J. Polym Sci A Polym Chem* 2004;42:5802.
 132. Li H, Cheng F, Duft AM, Adronov A. *J Am Chem Soc* 2005;127(41):14518.
 133. Baskaran D, Dunlap JR, Mays JW, Bratcher MS. *Macromol Rapid Commun* 2005;26:481.
 134. Liu Y, Tang J, Xin JH. *Chem Commun* 2004:2828.
 135. [a] Liu Y, Wu D-C, Zhang W-D, Jiang X, He C-B, Chung TS, Goh SH, Leong KW. *Angew Chem* 2005;44(30):4782. [b] Hu H, Ni Y, Mandal SK, Montana V, Zhao B, Haddon RC, Parpura V. *J Phys Chem B* 2005;109(10):4285.
 136. [a] Choi J-Y, Wang DH, Tan L-S, Baek J-B. *Polym Prepr* 2005;46(2):753. [b] Oh S-J, Lee H-J, Choi J-Y, Tan L-S, Baek J-B. *Polym Prepr* 2006;47(1):399.
 137. Oh S-J, Lee H-J, Keum DK, Lee S-W, Park S-Y, Lyons CB, Tan L-S, Baek J-B. *Polym Prepr* 2005;46(1):216.
 138. Baskaran D, Mays J, Bratcher M. *Polymer* 2005;46:5050.
 139. Gao C, Jin YZ, Kong H, Whitby RLD, Acquah SFA, Chen GY, Qian H, Hartschuh A, Silva SRP, Henley S, Fearon P, Kroto HW, Walton DRM. *J Phys Chem B* 2005;109(24):11925.
 140. Xu Y, Gao C, Kong H, Yan D, Jin YZ, Watts PCP. *Macromolecules* 2004;37(24):8846.
 141. Ku B-C, Kim DK, Lee JS, Blumstein A, Kumar J, Samuelson LA. *Polym Composite* 2009;30(12):1817.
 142. Hsiao C-C, Lin TS, Cheng LY, Ma C-CM, Yang AC-M. *Macromolecules* 2005;38(11):4811.
 143. Nap R, Szleifer I. *Langmuir* 2005;21(26):12072.
 144. Park SJ, Cho MS, Lim ST, Choi HJ, Jhon MS. *Macromol Rapid Commun* 2003;24:1070.
 145. Park SJ, Cho MS, Lim ST, Choi HJ, Jhon MS. *Macromol Rapid Commun* 2005;26:1563.
 146. Qin S, Qin D, Ford WT, Herrera JE, Resasco DE. *Macromolecules* 2004;37(26):9963.
 147. Mylvaganam K, Zhang LC. *J Phys Chem B* 2004;108:15009.
 148. Viswanathan G, Chakrapani N, Yang H, Wei B, Chung H, Cho K, Ryu CY, Ajayan PM. *J Am Chem Soc* 2003;125(31):9258.
 149. [a] Hong C-Y, You Y-Z, Pan C-Y. *Chem Mater* 2005;17(9):2247. [b] Cui J, Wang WP, You YZ, Liu C, Wang P. *Polymer* 2004;45(26):8717. [c] Xu G, Wang Y, Pang W, Wu W-T, Zhu Q, Wang P. *Polym Inter* 2007;56(7):847.
 150. Kong H, Gao C, Yan D. *Macromolecules* 2004;37(11):4022.
 151. [a] Ramirez SM, Sogah DY. *PMSE Prepr* 2004;91:493. [b] Datsyuk V, Guerretpiecourt C, Dagreou S, Billon L, Dupin J, Flahaut E, Peigney A, Laurent C. *Carbon* 2005;43(4):873.
 152. Adronov A, Yao Z, Liu Y. Functionalization of single-walled carbon nanotubes with polymers: New approaches to highly soluble nanotubes. In: Abstracts of Papers, 227th ACS National Meeting; 2004; Anaheim, CA.

153. Baskaran D, Mays JW, Bratcher MS. *Angew Chem* 2004;43(16):2138.
154. [a] Choi JH, Oh SB, Chang J, Kim I, Ha C-S, Kim BG, Han JH, Joo S-W, Kim G-H, Paik H-J. *Polym Bull* 2005;55(3):173. [b] Qin S, Qin D, Ford WT, Resasco DE, Herrera JE. *Macromolecules* 2004;37(3):752. [c] Cheng B, Li Y, Shen C. Polymerization of styrene from multiwall carbon nanotubes. In: Abstracts of Papers, 228th ACS National Meeting; 2004; Philadelphia, PA. POLY-075; [d] Fragneaud B, Masenelli-Varlot K, Gonzalez-Montiel A, Terrones M, Cavaille J-Y. *Chem Phys Lett* 2006;419(4–6):567.
155. [a] Gao C, Vo CD, Jin YZ, Li W, Armes SP. *Macromolecules* 2005;38(21):8634. [b] Gao C, Kong H, Yan D. Electronic properties of synthetic nanostructures. *AIP Conference Proceedings*; 2004. Melville NY, American Institute of Physics, Volume 723. pp 193.
156. [a] Li L, Lukehart CM. *Chem Mater* 2006;18(1):94. [b] Tsarevsky NV, Wu W, Hudson JL, Kowalewski T, Tour JM, Matyjaszewski K. *Polym Prepr* 2005;46(1):203–204. [c] Hong C-Y, You Y-Z, Wu D, Liu Y, Pan C-Y. *Macromolecules* 2005;38(7):2606.
157. Kong H, Li W, Gao C, Yan D, Jin Y, Walton DRM, Kroto HW. *Macromolecules* 2004;37(18):6683.
158. Kong H, Luo P, Gao C, Yan D. *Polymer* 2005;46(8):2472.
159. Kong H, Gao C, Yan D. *J Mater Chem* 2004;14:1401.
160. Matyjaszewski K, McCullough L, Yoon JA, Kowalewski T, Paik H-J. Nanostructured materials for potential energy-related applications by controlled radical polymerization. In: Abstracts of Papers, 240th ACS National Meeting; 2010; Boston, MA.
161. Liu C-H, Pan C-Y. *Polym Chem* 2011;2:563.
162. Hermant M, Kaya ZN, Vasani R, Lewis DA. Poly(2-hydroxyethyl methacrylate) grafted carbon nanotubes: A novel amphiphilic nanostructure. In: Abstracts of Papers, 241st ACS National Meeting & Exposition; 2011; Anaheim, CA.
163. Cao L, Krukn M. Synthesis of ordered mesoporous silica/polymer composites and their carbon derivatives. In: Abstracts of Papers, 239th ACS National Meeting; 2010; San Francisco, CA.
164. McGann JP, McCullough LA, Matyjaszewski K, Kowalewski T. Mass spectroscopic investigations of nanostructured carbon derived from poly(n-butyl acrylate)-b-polyacrylonitrile copolymers. In: Abstracts of Papers, 236th ACS National Meeting; 2008; Philadelphia, PA.
165. Lee SH, Park JS, Dreyer DR, Kim SO, Bielawski CW, Ruoff RS. *Polym Prepr* 2010;51(1):565.
166. McCullough LA, Matyjaszewski K. *Mol Cryst Liq Cryst* 2010;521:1.
167. Llarena I, Romero G, Ziolo RF, Moya SE. *Nanotechnology* 2010;21(5):055605.
168. Kallitsis J, Pefkianakis E, Stefanopoulos A, Merziotis A, Andreopoulou A. High metal loaded polymeric complexes for optoelectronics. In: Abstracts of Papers, 237th ACS National Meeting; 2009; Salt Lake City, UT.
169. Zhi C, Bando Y, Tang C, Kuwahara H, Golberg D. *J Phys Chem C* 2007;111(3):1230.
170. Liu Y, Yao Z, Adronov A. *Macromolecules* 2005;38(4):1172.
171. [a] Dehonor M, Masenelli-Varlot K, González-Montiel A, Gauthier C, Cavaillé J-Y, Terrones H, Terrones M. *Chem Commun* 2005;42:5349. [b] Dehonor M, Masenelli-Varlot K, González-Montiel A, Gauthier C, Cavaillé J-Y, Terrones M. *J Nanosci Nanotechnol* 2007;7(10):3450.
172. Shvartzman-Cohen R, Monje I, Florent M, Frydman V, Goldfarb D, Yerushalmi-Rozen R. *Macromolecules* 2010;43(2):606.

11

POLYMER ADDITIVES

RUDOLF PFAENDNER

11.1 INTRODUCTION

Additives are essential components of plastic formulations that provide maintenance and/or modification of polymer properties, performance, and long-term use. The extension of polymer properties by additives has been playing a substantial role in the growth of plastics, and many polymer applications are accessible only in the presence of a number of ingredients, often only in small quantities, in addition to the polymer itself.

Historically, polymer additives were decisive for the development of thermoplastic material applications. On the basis of previous findings [1], the first synthetic commercial thermoplastic, celluloid, is a success story of additives, when camphor was added to intractable cellulose nitrate to make it flexible [2–4]. Plasticized poly(vinyl chloride) (PVC) was developed in the 1930s using dialkyl phthalates. The key to processing rigid PVC was the development of heat stabilizers such as metal soaps, lead salts, and organotin compounds. There, contrary to plasticizers, small quantities were sufficient to provide the required processing performance. Light stabilizers were first used in cellulose nitrate coatings on packaging to protect packaged oil and food [5]. This was soon followed by the use of benzophenones and phenyl salicylate to protect plastics from weathering [6]. The breakthrough of polypropylene (PP), a thermally very unstable material, as well as Ziegler–Natta polyolefins was possible only through the development of efficient antioxidants. Quite logically, the growth of additives parallels the growth of plastics in the last decades [7].

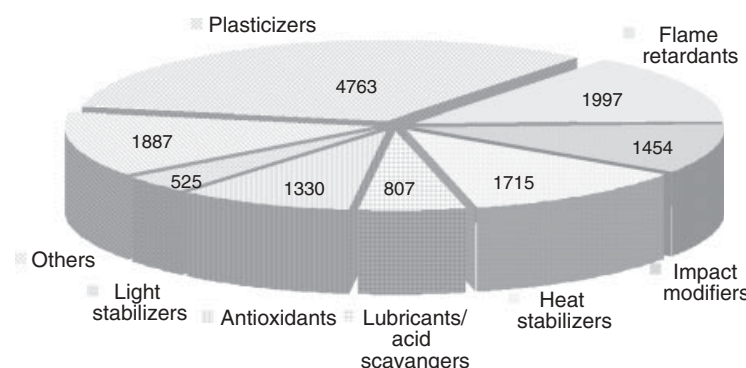
Additives embrace a wide area of different chemical structures used in plastics for many different purposes

(Fig. 11.1). They can be classified into additives to maintain polymer properties and those to extend polymer properties. The first class comprises additives to transform plastics into the desired shape and to protect the materials from degradation by heat, oxidation, as well as mechanical and chemical attack mainly during processing and thus keeping the polymer chain and the polymer molecular weight basically unchanged. Typical examples of the “maintaining” class are antioxidants, plasticizers, heat stabilizers, processing aids, and lubricants.

Additives to extend polymer properties help prolong the service life of plastic applications and/or allow the use of plastics in additional or demanding applications. Examples of these additives are UV/light stabilizers, antimicrobials, flame retardants, and also antioxidants. By using these additives, the polymer chain and polymer molecular weight remain unchanged for an extended period or under specified use conditions (e.g., outdoor, UV light) or in further application fields (e.g., microbial attack, fire risk, electrostatic discharge, high esthetics). Other additives modify polymer bulk or surface properties, again without changing the polymer chain or molecular weight. Examples comprise nucleating agents, clarifiers, surface modifiers, as well as antifogging and antistatic agents. Additives such as chain extenders or crosslinking/branching agents react with the polymer chain and may change the polymer structure/architecture fundamentally. In addition, some additives are incorporated in polymers not with the aim of influencing the polymer itself but to protect goods through the additive-incorporated polymer. Examples are UV absorbers and oxygen scavengers to protect packaged food.

The consumption of polymer additives today is estimated in the range of 5000 kt (kilotonnes) corresponding to a value

- Polymer properties retention
- Antioxidants
 - Processing stabilizers
 - Heat stabilizers
 - Lubricants
 - Acid scavengers
- Polymer properties extension
- Service life/ extended applications
 - UV / light stabilizers
 - Antioxidants
 - Flame retardants
 - Pigments
 - Optical brighteners
 - Biocides/antimicrobials
 - Scavengers
 - (Anti)odorants
 - Conductive additives
 - Repellants
 - Markers
 - Foaming agents
- Modifying bulk/surface properties
 - Antistatic agents
 - Nucleating agents
 - Clarifiers
 - Plasticizers
 - Surface modifiers
 - Slip/antiblocking
 - Antifogging
- Modifying polymer structure
 - Chain extenders
 - Crosslinking/coupling agents
 - Compatibilizers
 - Prodegradants

Figure 11.1 The world of additives.**Figure 11.2** Turnover of additives (in million dollars) in 2004 [9].

of US\$32 billion [8], without taking fillers and pigments into consideration. PVC is still the main polymer that consumes most additives because most of the plasticizers and heat stabilizers, representing together one-third of the additives production (Fig. 11.2), are used there [9]. Plasticizers still dominate the market but their growth is slow and the per kilogram value low. The class of flame retardants is the fastest growing market: about 6% annually [10]. Forty percent of the antioxidants and 45% of the light stabilizers are used in PP applications [11].

In the following part, the most important classes of additives (antioxidants, PVC heat stabilizers, light stabilizers, and flame retardants) are presented, as well as general information on chemical structures and mechanisms, on testing methods, and on use examples in selected polymer

classes. Other important additive classes are summarized afterwards. It should be mentioned that the character of an overview on additives will simplify some aspects and will focus on some selected representative examples; for more detailed information on certain additive classes, it is necessary to refer to special literature. Another aim of the chapter is to point at recently introduced products and new developments. Fillers, reinforcing agents, and impact modifiers are outside the scope of the chapter because usually large amounts of these additives are added to the polymer and composite structures with new properties formed, which deserve a more detailed description. Colorants/pigments and optical brighteners are used to provide plastics with colorful and attractive appearance, but those products are outside the scope of this chapter as well.

11.2 ANTIOXIDANTS

Polymers, like all kind of organic materials, are sensitive to oxidation. Oxidation will take place at any time of the lifetime of the polymer during thermal transformation, storage, or application. Furthermore, the combined action of light and oxygen results in photooxidation. Degradation of the polymer and irreversible changes of the polymer structure are the consequence of (photo)oxidation, resulting finally in insufficient mechanical properties, cracking, failure of the part, change in visual appearance (e.g., discoloration), etc. However, the sensitivity to oxidation depends on the chemical structure of the polymer. Polystyrene, poly(methyl methacrylate) or polyimide, and other high performance

polymers are quite stable; but PP and other polyolefins such as polybutadiene are very sensitive to oxidation (Fig. 11.3).

The so-called autoxidation of polymers starts with an initiation step forming radicals, for example, from defect structures in the polymer chain. Reaction with molecular oxygen results in peroxy radicals followed by hydroperoxide formation through H abstraction, and hydroperoxides decompose into alkoxy and hydroxyl radicals (Fig. 11.4). Furthermore, the polymer chain is modified through the formation of oxygen-containing structures (carbonyls, alcohols, carboxyls) and unsaturated groups (vinyl, vinylidene, allylic). Disproportionation and depolymerization result in low molecular weight products.

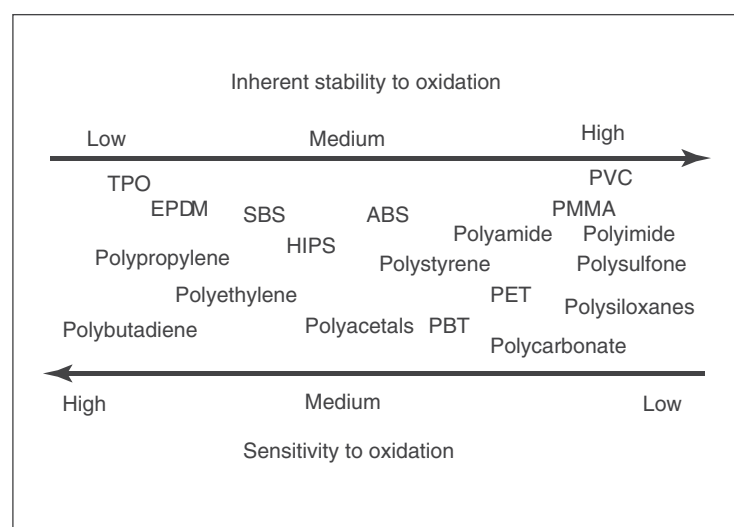


Figure 11.3 Relative sensitivity of selected thermoplastic polymers to oxidation.

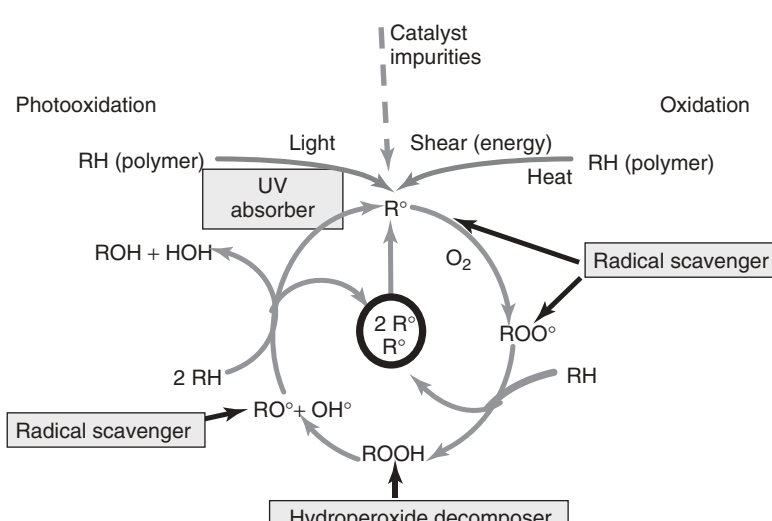


Figure 11.4 Autoxidation of polymers.

crosslinked polymer chains originate from the radical recombination of lower molecular weight fragments.

Suitable stabilizers, the so-called antioxidants, inhibit or reduce the thermo-oxidative degradation in polymers and maintain available properties during processing as well as during the product life cycle in the intended application. Antioxidants interrupt the autoxidation cycle by chemical reactions with the formed intermediates. Primary antioxidants are radical scavengers, either chain-breaking acceptors or chain-breaking donors reacting with radicals by forming thermally stable reaction products. Secondary antioxidants are hydroperoxide decomposers transforming hydroperoxides into thermally stable products.

Antioxidants are used in concentrations between 0.05% and 1% depending on the polymer structures and requirements.

11.2.1 Primary Antioxidants

Typical representatives of primary antioxidants are secondary aromatic amines and sterically hindered phenols; both classes are widely used in the protection of polymers (Figs. 11.5 and 11.6). Aromatic amines act as H donors by forming aminyl radicals, followed by coupling reactions and/or nitroxide formation and further coupling reactions.

Sterically hindered phenols react through H abstraction from the phenol group and form a phenoxy radical,

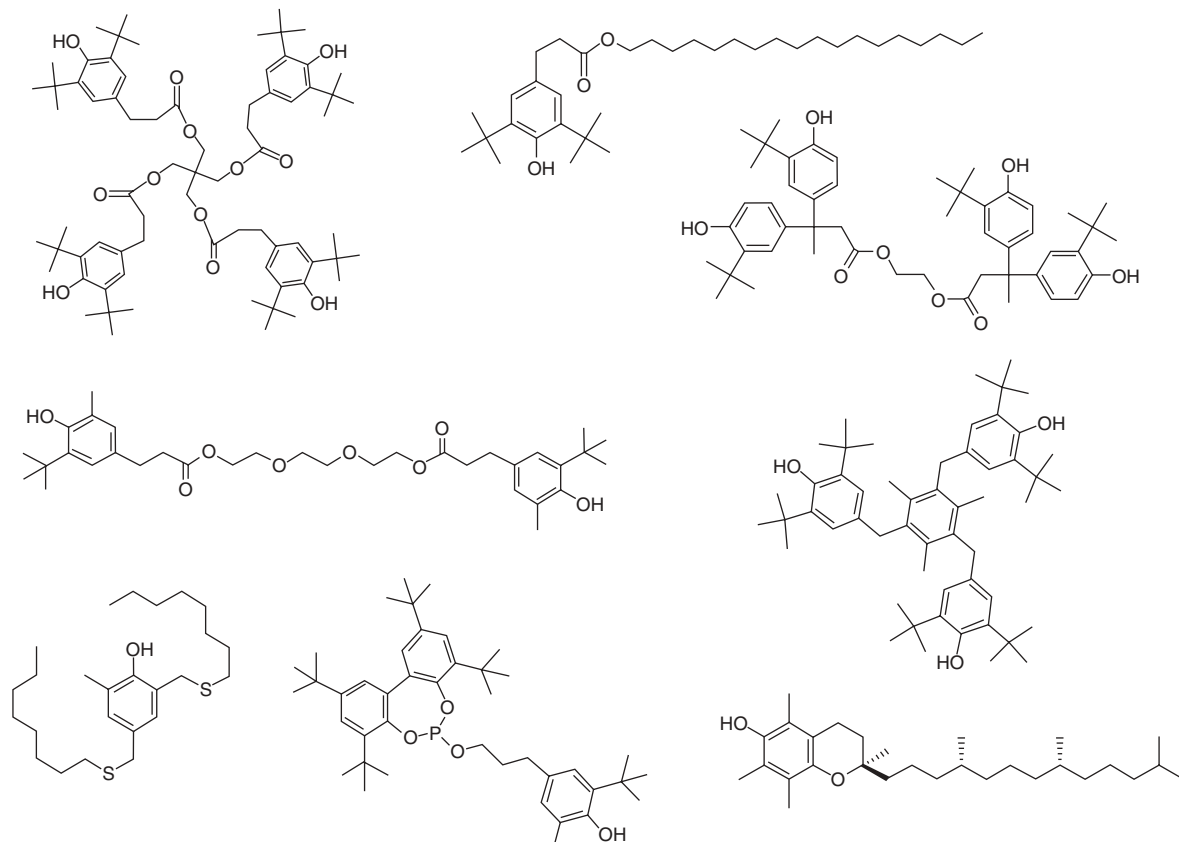


Figure 11.5 Chemical structures of phenolic antioxidants.

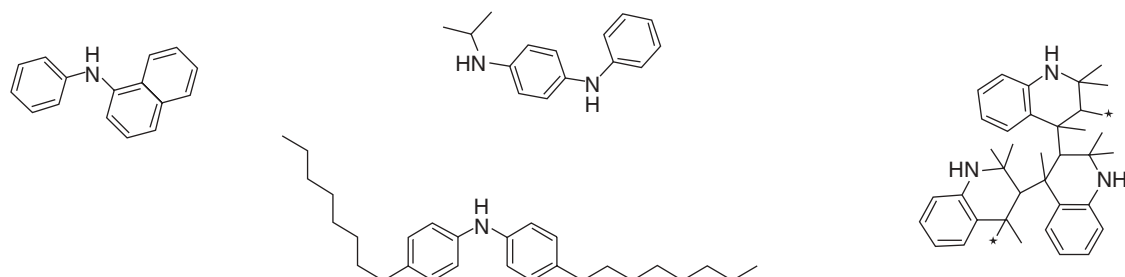


Figure 11.6 Chemical structures of aminic antioxidants.

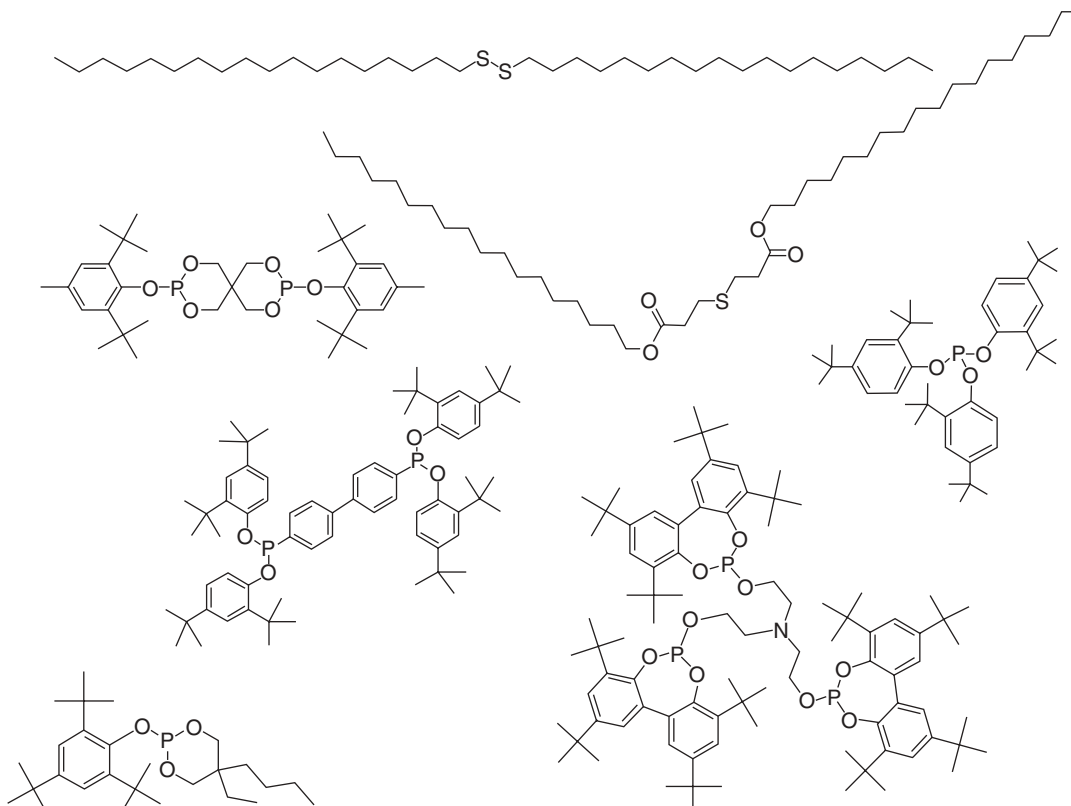


Figure 11.7 Structures of secondary antioxidants based on phosphorus and sulfur.

followed often by a disproportionation reaction to the parent compound and quinone methide, which reacts with alkyl, alkoxy, and peroxy radicals to thermally and chemically stable products.

11.2.2 Secondary Antioxidants

Examples of widely used secondary antioxidants are phosphites, phosphonites, and sulfides (Fig. 11.7). Usually, secondary antioxidants are used in combination with primary antioxidants to benefit from a synergistic effect. The main action of phosphites and phosphonites is the oxidation to the corresponding phosphates by reacting with hydroperoxides. These P compounds are mainly used as melt stabilizers during processing. Sulfur compounds act as well as hydroperoxide decomposers via sulfur oxide and sulfenic acid formation. Sulfur compounds are preferably used in combination with phenolic antioxidants to improve the long-term thermal stability of polymers at temperature ranges between 100 and 150 °C.

11.2.3 Other Antioxidative Stabilizers

Hindered amine stabilizers, popularly known as *hindered amine light stabilizers* (HALS, see below), are efficient

radical scavengers through an oxidation reaction to the nitroxyl radicals and hydroxylamines. The nitroxyl radical reacts with alkyl radicals to form stable alkoxyamines. Hydroxylamines are known *stabilizers* by themselves, whereas an intermediate product formed, nitron, scavenges C radicals. Other efficient C-radical scavengers are benzofuranone derivatives and acryloyl-modified phenols. As transition-metal ions catalyze the decomposition of peroxides resulting in reactive radicals, phenolic antioxidants modified with metal complexing groups are used as metal deactivators. Moreover, optimized blends of different antioxidants are used, and as well structures with different stabilizer functions in one molecule.

Somewhat exceptionally, aliphatic polyamides are stabilized in non-color-critical applications with small amounts (20–50 ppm) of copper in the form of halogenids, for example, CuBr or CuI, or even more efficiently in combination with metallic iron [12].

11.2.4 Testing of Antioxidants

Standard test methods to analyze the thermal stability of polymers cover multiple extrusions and accelerated heating. Multiple extrusions evaluate the melt-processing stability of a polymer or polymer formulation and determine

the efficiency of antioxidants or antioxidant combinations. The melt properties are usually characterized by melt mass flow rate (MFR) or melt volume flow rate (MVR) according to ISO 1133. The impact of processing temperature and shear can be analyzed in addition by measuring the mechanical properties, discoloration, molecular weight, or melt viscosity under different conditions and with optimized additive packages. Accelerated heat-aging simulates the long-term thermal stability. Samples are oven-aged at defined temperatures and conditions, and the change of selected properties, for example, visual appearance, color, mechanical values, molecular weight, is recorded over aging time. A simple version of long-term stability for quality control purposes is to determine the oxidation induction time (OIT, ISO 11357), whereas the induction time for the onset of the oxidation process is measured with differential scanning calorimetry (DSC) or differential thermal analysis (DTA). For some polymers, the carbonyl index is easily determined via infrared (IR) spectroscopy as an indication of the oxidative degradation of the polymer. Furthermore, the additive concentration may be analyzed directly, the consumption recorded, and the lifetime extrapolated; however, also the reaction products of the selected antioxidant may still be active as antioxidants, which are not analytically considered if only the initial molecular structure is determined.

11.2.5 Selected Examples

PP is a polymer very sensitive to oxidation. As outlined (Fig. 11.8), an unstabilized material does not survive a single processing step without deterioration of the properties. On the other side, small concentrations of phosphite or phenolic antioxidant can provide sufficient stability for several transformation steps, for example, extrusion and injection molding, however, depending on the processing conditions (temperature, shear). Furthermore, the common practice of using combinations of phosphites

and phenolic antioxidants results in improved processing stability.

Processing stabilization of other polyolefins such as high density polyethylene (HDPE), low density polyethylene (LDPE), and linear low density polyethylene (LLDPE), and styrenic polymers is achieved similarly by phosphite/phenolic antioxidant blends in the range of 0.1–0.2%. Polymers with unsaturated groups in the chain, such as polybutadiene, need higher concentrations of stabilizers. The influence of antioxidants during processing on engineering plastics such as poly(ethylene terephthalate) (PET), poly(butylene terephthalate) (PBT), or polyamide (PA) is not very pronounced; however, a certain stability improvement may be found experimentally.

In addition to processing stability, the long-term thermal stability of polymers is very important. In this case, antioxidants prolong the life of the polymer in general to an extent depending on the polymer structure and test conditions (Table 11.1). Although substantial extension of the polymer lifetime can be found in all cases, the shown values are only an indication from different experiments in order to illustrate the effect of antioxidants, as the criteria of the stabilities are not identical and the polymer grades tested may vary (manufacturing process, catalysts, testing procedure).

TABLE 11.1 Effect of Antioxidants on the Long-Term Stability of Selected Polymers

Polymer	Long-Term Thermal Stability in Days at °C, Unstabilized	Long-Term Thermal Stability in Days, 0.2% Antioxidant (AO)
Polypropylene	<1 at 135 °C	10–160
HDPE	5 at 120 °C	100 to >300
Polybutadiene	<1 at 80 °C	20–100
Polyamide-6	20 at 100 °C	40–150
PBT	3 at 160 °C	80–100

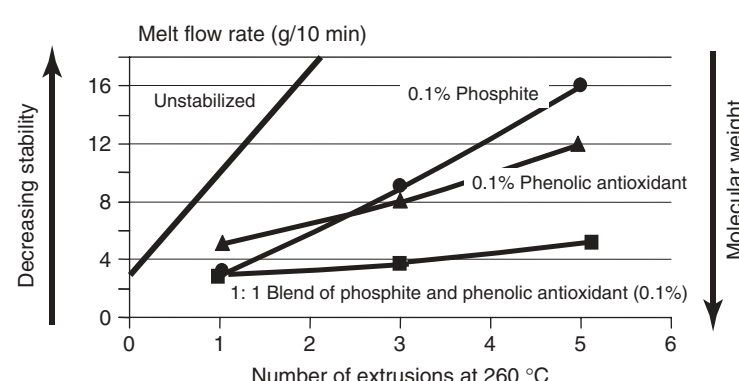


Figure 11.8 Stabilizer efficiency shown through multiple extrusion experiment.

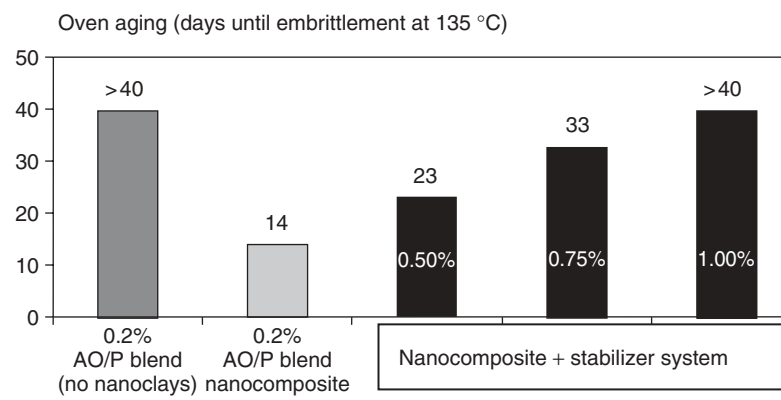


Figure 11.9 Influence of (nano)fillers on long-term thermal stability of polypropylene (P).

To select the correct stabilization package for a polymer and application further formulation ingredients have to be considered as interactions of the stabilizer with the polymer matrix and other ingredients may influence the overall stability. Fillers, pigments, carbon black, and reinforcement agents are known to interact considerably with the stabilizers. For example, a strong influence on the thermal stability is often found when fillers are added to the polymer. PP containing organically modified montmorillonite to obtain a nanocomposite degrades much faster than pure PP (Fig. 11.9). The main reason for this behavior is the adsorption of antioxidants on the filler surface [13]. To moderate the negative influence of fillers on the oxidative stability, filler deactivators or coupling agents (see below) have to be added and the overall stabilizer system concentration has to be adjusted, that is, increased [14].

11.3 PVC HEAT STABILIZERS

The principal thermal degradation reaction of halogen-containing polymers such as PVC, poly(vinylidene chloride) (PVDC), or chlorinated polyethylene (PE) is less due to autoxidation than to dehydrochlorination, that is, elimination of HCl during thermal processing. The dehydrochlorination reaction starts from polymer chain defects and results in polyene sequences and carbenium salts, both of which are responsible for the strong discoloration. Therefore, the protection of PVC by antioxidants is not very pronounced. The main mechanism to protect PVC from thermal degradation is by scavenging HCl, stabilizing initial defects of the polymer chain, as well as stabilizing the formed defects after HCl elimination. Therefore, efficient PVC heat stabilizers absorb HCl, eliminate defect structures, react with polyene sequences, and destroy carbenium salts. The compounds used today as PVC heat stabilizers are based on mixed metal salts, for example, calcium/zinc, organotin compounds, and metal-free organic-based systems. Organic

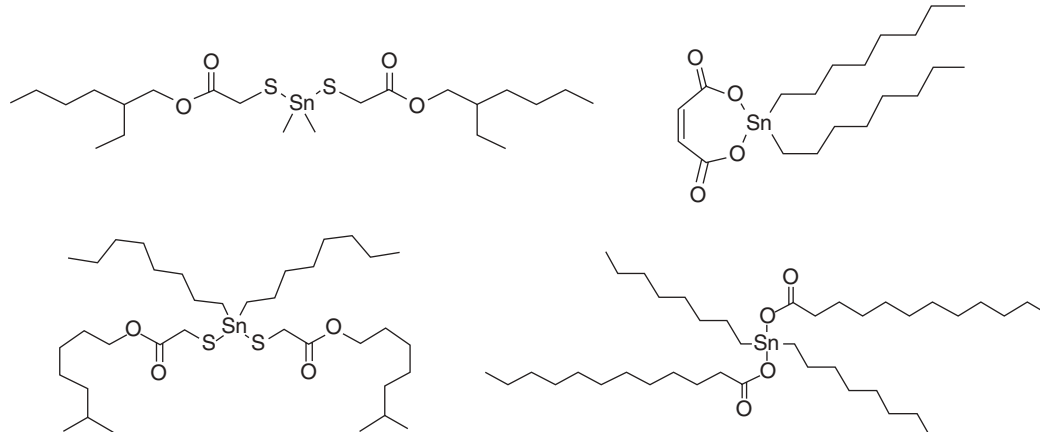
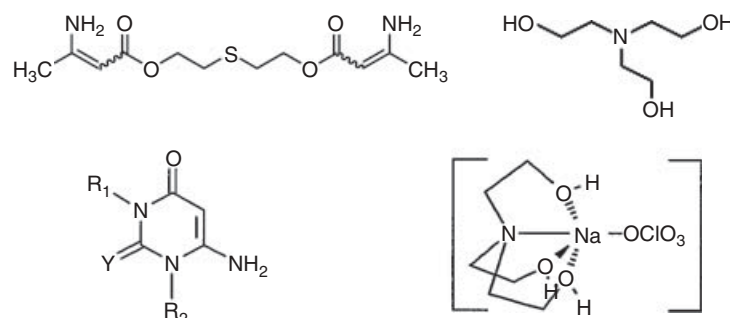
phosphites, polyols, epoxides, β -diketones, and hydroxalates are often used as costabilizers. Historically, organic and inorganic lead (Pb) compounds have been widely used as heat stabilizers; however, these are gradually phased out in many countries because of environmental and toxicity reasons. PVC heat stabilizers are used in concentrations from below 1% (tin) up to 5% (mixed metal) depending on the formulation, lubricants, plasticizers, and costabilizers.

11.3.1 Mixed Metal Salts

Calcium/zinc mixed metal salts, for example, calcium stearate and zinc stearate and barium/zinc stabilizers (or the meanwhile phased out barium/cadmium stabilizers) are used in a synergistic way. Zinc carboxylates are capable of substituting labile chlorine atoms by forming $ZnCl_2$. $ZnCl_2$ reacts with calcium carboxylates and forms again zinc carboxylates. Although Zn compounds result in very good initial color and transparency, $ZnCl_2$ itself destabilizes PVC and catalyzes the dehydrochlorination reaction. Therefore, the ratio and concentration of Ca compounds and Zn compounds, as well as of additional costabilizers, are decisive for the performance of mixed metal salts.

11.3.2 Organotin Heat Stabilizers

Organotin mercaptide, for example, dioctyltin dithioglycolate, and organotin carboxylate, for example, dioctyltin maleate (Fig. 11.10), the latter group mainly, are used for outdoor applications because of high light stability, and act as efficient heat stabilizers by reacting with HCl under formation of alkyl-substituted tin chlorides. Furthermore, there is a direct reaction with labile chlorine atoms through substitution with more stable groups. Mercaptides can add to polyene sequences and thus interrupt the conjugation. Maleic acid derivatives may act similarly in a Diels–Alder mechanism.

**Figure 11.10** Structures of selected organotin PVC stabilizers.**Figure 11.11** Structures of organic-based PVC stabilizers.

11.3.3 Metal-Free Heat Stabilizers

In recent years, metal-free stabilizer systems have been developed because of environmental concerns of traditional lead and tin stabilizers. Chemically regarded nitrogen-based molecules are used, for example, β -aminocrotonates, dihydropyrimidines [15], trialkanolamines, as well as their reaction products and salts, for example, the perchlorate salt [16], etc. (Fig. 11.11). Owing to their good compatibility with other stabilizers, organic-based stabilizers are predestinated to be used in PVC recycling in case restabilization is needed [17].

11.3.4 Costabilizers

The most important costabilizers in PVC formulations used mainly in combination with mixed metal salts are alkylarylpophosphites to improve early color. Epoxy compounds, for example, epoxidized fatty esters such as epoxidized soy bean oil, react directly with HCl or substitute labile chlorine atoms, for example, in the presence of zinc ions. Furthermore, the epoxidized fatty esters act as plasticizers. Polyols such as pentaerythritol or dipentaerythritol and β -diketones act as complexing agents and deactivate the negative effect of the formed zinc chloride. Hydrotalcites

and zeolites scavenge HCl. Contrary to tin and lead systems, mixed metal stabilizers based on Ca/Zn (or Ba/Zn) are usually complex mixtures of compounds, contributing to heat stability and optimized lubrication to provide smooth processing.

11.3.5 Testing of PVC Heat Stabilizers

The stability of PVC formulations is tested, for instance, according to ISO 305 by static heat tests, where test specimens are aged at constant temperature and mainly color changes (e.g., Yellowness Index) are recorded. Alternatively, to assess the performance of heat stabilizers, the time until the dehydrochlorination reaction takes place can be measured, for example, through pH change (ISO 182). Combined thermal and shear stress is analyzed via dynamic tests such as two-roll mill processing or multiple extrusion.

11.3.6 Selected Examples of PVC Heat Stabilization

As explained already, there is a distinct synergism between Ca/Zn stabilizers. Whereas Zn salts show a very good initial color, the time until HCl formation (discoloration) upon heating is considerably short. Ca salts offer a very

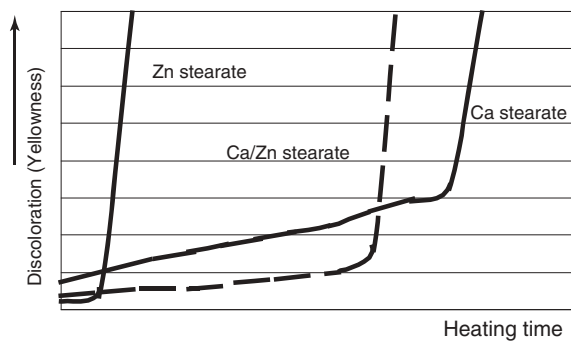


Figure 11.12 Scheme of the synergistic activity of Ca/Zn PVC heat stabilizers.

much extended stability but a less attractive initial color. Therefore, the combination of both salts is the method of choice (Fig. 11.12).

As an alternative to the widely used Ca/Zn stabilizers, organic-based stabilizers can replace technically traditional heat stabilizers. Maintenance of the initial color and transparency is supported efficiently (Fig. 11.13) [18].

11.4 LIGHT STABILIZERS

Although many polymers are sensitive to (sun)light alone, the combination of light and ubiquitous oxygen causes photooxidation. Through the action of light, free radicals are formed depending on the polymer structure and the energy of the light. These radicals can react with oxygen via peroxy radicals to form hydroperoxides (Fig. 11.4) and initiate the autoxidation cycle. Polyolefins such as PP and PE, or elastomers, are very sensitive to photooxidation, resulting in fast degradation (PP chalking) or crack formation, discoloration, and loss of mechanical properties. Polystyrene, styrene acrylonitrile polymer (SAN), antioxidant-stabilized

polyamide and polyester, and heat-stabilized PVC and poly(methyl methacrylate) are comparatively very stable. The light stability of a polymer formulation is furthermore influenced by light absorbing pigments, fillers, or carbon black, and the thickness of the parts. To protect polymers from the negative influence of light, UV absorbers, quenchers, and free-radical scavengers, namely, HALS, are used. Quenchers are based on Ni compounds and, therefore, they are phased out in many countries for environmental reasons. Light stabilizers are used in the range of 0.1–1% depending on the formulation, use area, and the required lifetime.

11.4.1 UV Absorbers

UV absorbers absorb UV radiation and dissipate it as heat in order to avoid photosensitization of the protected polymer. The UV absorber of choice should have high absorption coefficients and high inherent light stability. Chemical structures comprise mainly benzophenones, benzotriazoles, hydroxyphenyltriazines, cinnamates, diphenylcyanoacrylates, and oxanilides (Fig. 11.14).

Depending on their structure, polymers show different absorption maxima in the UV range; therefore, the UV absorber of choice should correspond to those or cover as broad a UV range as possible. Furthermore, combinations of different UV absorbers can be used or combinations of a UV absorber and HALS.

11.4.2 Hindered Amine Light Stabilizers

HALS hardly absorb UV light but act most likely as radical scavengers and hydroperoxide decomposers. Chemical structures are mainly based on piperidines. Sterically hindered piperazines are known as well (Fig. 11.15). Secondary amines are the most common structures, but alkylamines or, more recently, alkoxyamines are commercially

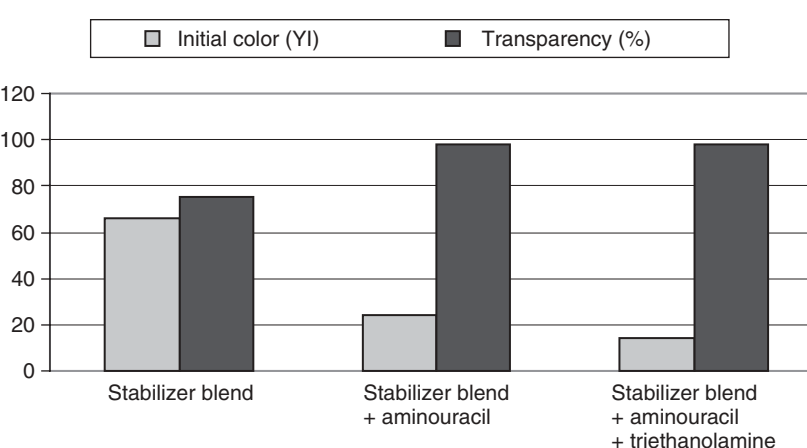
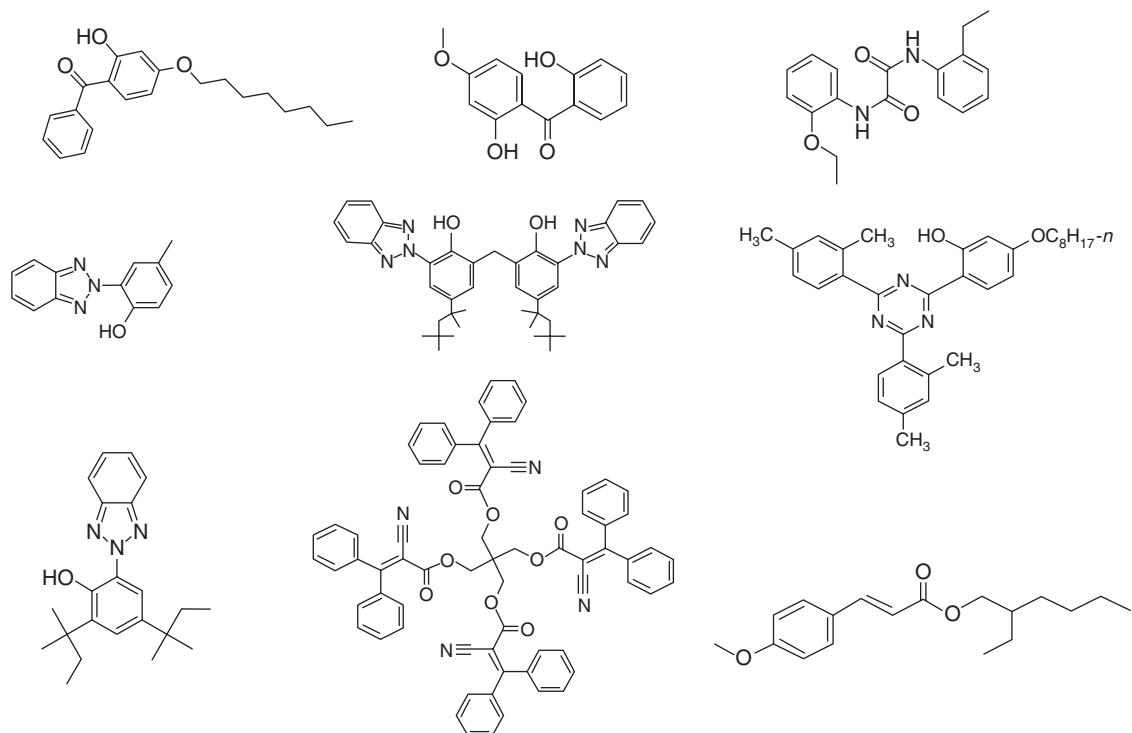
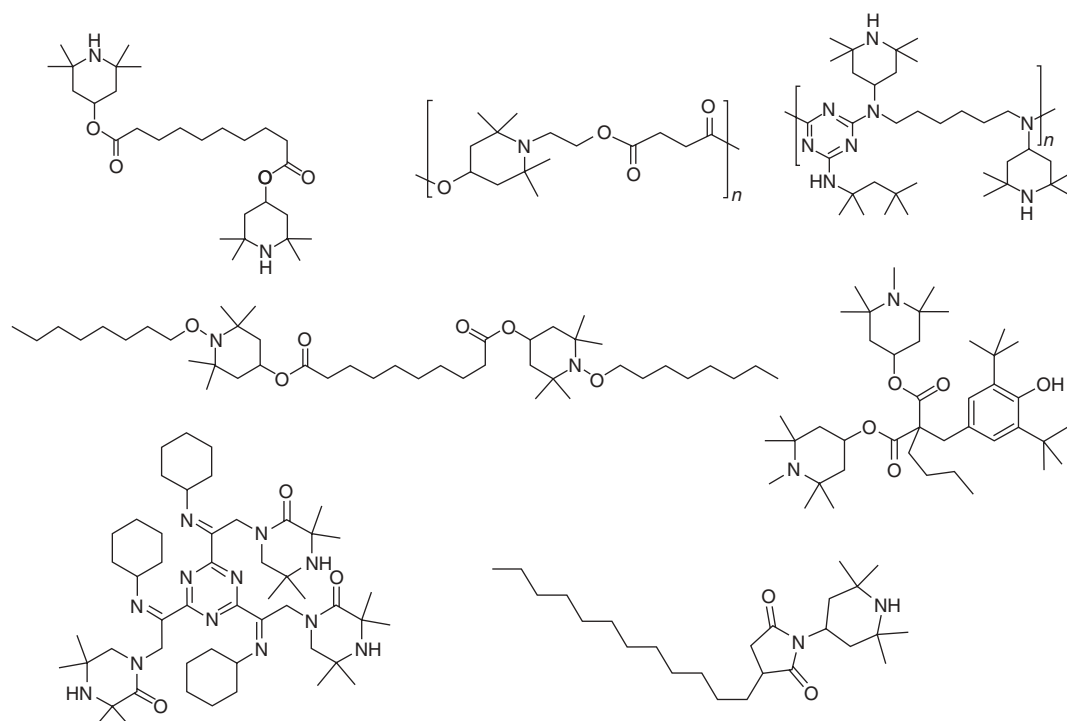


Figure 11.13 Stabilization efficiency of organic-based PVC heat stabilizers.

**Figure 11.14** Chemical structures of UV absorbers.**Figure 11.15** Chemical structures of hindered amine light stabilizers (HALS).

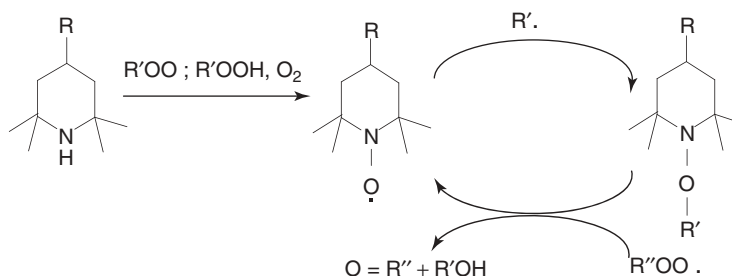


Figure 11.16 Simplified mechanism of HALS action.

available. A simplified cyclic mechanism of the stabilization through HALS starts with the oxidation to the nitroxyl radical, scavenging of an alkyl radical, reaction of the resulting alkoxyamine with a peroxyradical, and reformation of the nitroxyl radical (Fig. 11.16). To balance migration and performance, low or high molecular weight (oligomeric) products or their blends are applied.

11.4.3 Testing of Light Stabilizers

Photooxidation is tested by UV exposure or artificial or natural weathering. Natural weathering or outdoor weathering is carried out in high radiation areas to get an accelerating effect and is influenced by the season and humidity (e.g., Florida, humid or Arizona, dry). Artificial weathering is carried out in suitable devices, where light sources close to sunlight in their spectrum or lamps with high UV intensity are used. Change of the properties, for example, visual appearance such as chalking, crazes, gloss, and/or mechanical properties such as tensile strength, elongation, and impact strength are measured in relation to the exposure time or radiation energy (e.g., according to ISO 4582).

11.4.4 Selected Examples of Light Stabilization

Depending on their chemical structure, polymers show a different sensitivity to light and, therefore, a different stability with regard to maintaining mechanical or surface properties, to crack formation, and to discoloration [19]. Addition of light stabilizers shows always improvements in maintaining the properties, but to greater or lesser extents. The improvements shown (Table 11.2) can only be a rough and very general indication, as it is a compilation of different experiments, different failure criteria, and expert knowledge [19]. Although the performance of light stabilizers depends on the polymer, the grade, the application, the composition, and the exposure, there is mostly a definite relationship to the stabilizer concentration as shown for PP tapes in natural and artificial weathering (Fig. 11.17) [20]. Combination of different light stabilizers results often in a synergistic improvement as shown for different polymeric HALS (Table 11.3) [21].

11.5 FLAME RETARDANTS

With the exception of halogen-containing polymers and a few inherently flame-retarded high performance polymers, most polymers can be easily incinerated. Therefore, flame or fire retardants are added to polymer formulations in order to reduce the risk of fire, for example, for electro/electronic or construction applications. Flame retardants do not transform the polymer into a nonburning material but delay the incineration, may reduce the freed energy and decompose into easily burning gases or the damage caused by the fire. In addition to halogen-containing additives, halogen-free flame retardants are being increasingly developed. The latter are often based on inorganic hydroxides, such as Al(OH)₃ or Mg(OH)₂, or phosphorus or nitrogen compounds. Closely related to flame retardants are smoke suppressants, which are added to the polymer to reduce the generation of smoke in case of fire. Typical examples are ammonium polyphosphates and molybdates, the latter mainly used in PVC formulations. Flame retardants are often used in concentrations of 10–60% with respect to the polymer.

11.5.1 Halogenated Flame Retardants

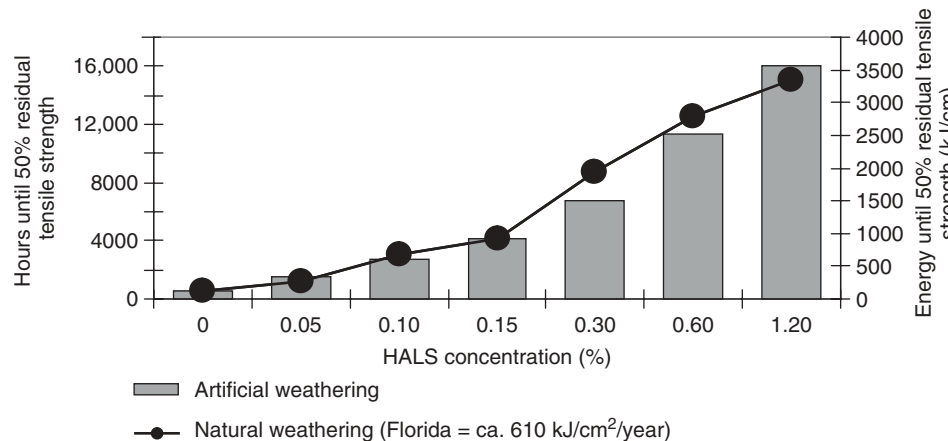
Despite some environmental concerns, halogenated flame retardants still play an important role. With the exception of a few chlorinated products (e.g., chlorinated paraffins), these flame retardants contain usually molecules with several bromo groups (Fig. 11.18). Bromo compounds are active during combustion in the gas phase, whereas HBr reacts with OH and H radicals under formation of less reactive halogen radicals. The flame retardancy of bromo compounds is often synergistically improved by the addition of antimony oxide Sb₂O₃.

11.5.2 Inorganic Flame Retardants

Aluminum trihydroxide (ATH), aluminum oxyhydroxide (boehmite), and magnesium dihydroxide (MDH) decompose at elevated temperatures endothermically with the formation of water. Therefore, these flame retardants act

TABLE 11.2 Effect of Light Stabilizers on the Lifetime of Polymers

Polymer	Polymer Degradation Induced by Light	Light Stability, Unstabilized under Artificial Weathering Conditions, h	Light Stability, 0.5% UV-A or HALS Added
Polypropylene	Loss of gloss Chalking Crazes	500	1500 h (UV-A) 1500 h (carbon black) 10,000 h (HALS)
Loss of mechanical properties			
HDPE	Crazes	1000–1500	5000 h (UV-A) >30,000 h (HALS)
LDPE/LLDPE	Crazes	>500	1500 h (UV-A) 20,000 h (HALS)
ABS	Loss of mechanical properties Yellowing	200	1500 h
PC	Yellowing	<2000	>15,000 h (5% UV-A)
PMMA	Yellowing	20,000	>20,000 h (UV-A + HALS)
Polyamide-6	Loss of transmission Loss of mechanical properties Yellowing	500	3000 h (AO) 4000 h (AO + HALS + UV)
PVC	Yellowing	500	4000–6000 h (UV-A)
PET/PBT	Loss of mechanical properties Yellowing	1000–2000	10,000 h (UV-A)
SBR/BR	Loss of mechanical properties Crack formation Yellowing	300	2000 h (UV-A)
PUR	Yellowing Crack formation	200–3000	1000–10,000 h (HALS)

**Figure 11.17** Influence of HALS concentration on the lifetime of polypropylene.

in the condensed phase by removing heat and diluting the burning gases. To generate sufficient water for this mechanism, the quantity to be used is high and mostly above 50% of the compound to be flame-retarded. More recently, nanocomposites from layered silicates [22] and carbon nanotubes (CNTs) [23] have been proposed as flame-retardant components acting through barrier formation at the surface and thus insulating the polymer from the flame source.

11.5.3 Phosphorus- and Nitrogen-Containing Flame Retardants

Red phosphorus itself can be used as an efficient flame retardant, as well as organic phosphorus compounds, for example, ammonium polyphosphate, bisphenol-A-diphenylphosphate, or resorcinol diphenylphosphate, or phosphorus-containing salts, for example, the aluminum salt of diethylphosphinate (Fig. 11.19). Phosphorus-containing

flame retardants act often through the formation of a barrier layer in the condensed phase or through P-radical species in the gas phase.

Melamine and melamine derivatives, such as melamine cyanurate or melamine polyphosphate, are representatives of nitrogen-containing flame retardants (Fig. 11.20). Melamine is an inert diluent and removes heat through decomposition; melamine polyphosphate provides an isolating barrier through an intumescence mechanism.

TABLE 11.3 Synergistic Behavior of Different HALS Structures in Light Stabilization of Polypropylene

HALS	Hours of Artificial Weathering until 50% Residual Tensile Strength
Without	450
0.3% Polymeric main chain HALS	3200
0.3% Polymeric side chain HALS	3600
0.15 + 0.15% Blend of both HALS structures	4500

More recently, alkoxyamines and azo compounds were proposed as flame retardants for thin-film PP applications [24, 25], where an activity is found already at concentrations as low as 0.5%.

11.5.4 Testing of Flame Retardancy

There are many often country- and application-specific tests to be passed for flame-retarded plastic formulations. Some standard test methods evaluate the limiting oxygen index (LOI, for example according to ISO 4589), in which a test specimen is burned in a mixture of oxygen and nitrogen. The higher the oxygen content to support burning, the more resistant the material is. LOI values range from 15% (polyoxymethylene, POM) to 95% (poly(tetrafluoroethylene), PTFE) and for most commodity polymers it ranges between 17% and 25%; above 27%, the self-extinguishing behavior can often be expected [26]. One further common test is the Underwriter Laboratory (UL) 94 test, where a sample is ignited at the bottom, burned vertically, and is classified, according to flame time, dripping, ignition of the underlying cotton, in to V-0 (best classification), V-1, V-2, and NC (not classified).

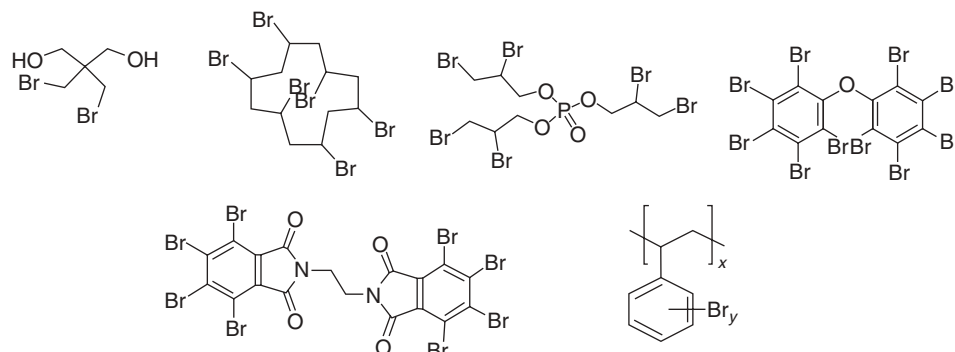


Figure 11.18 Chemical structures of brominated flame retardants.

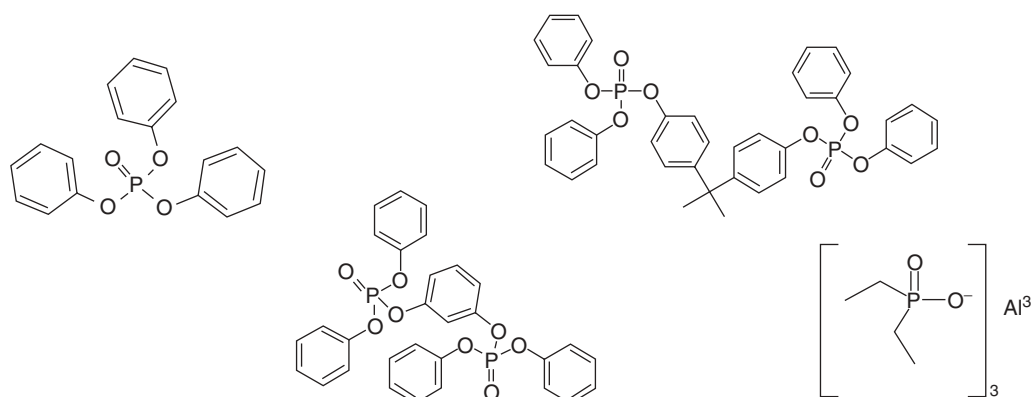


Figure 11.19 Structures of phosphorus-based flame retardants.

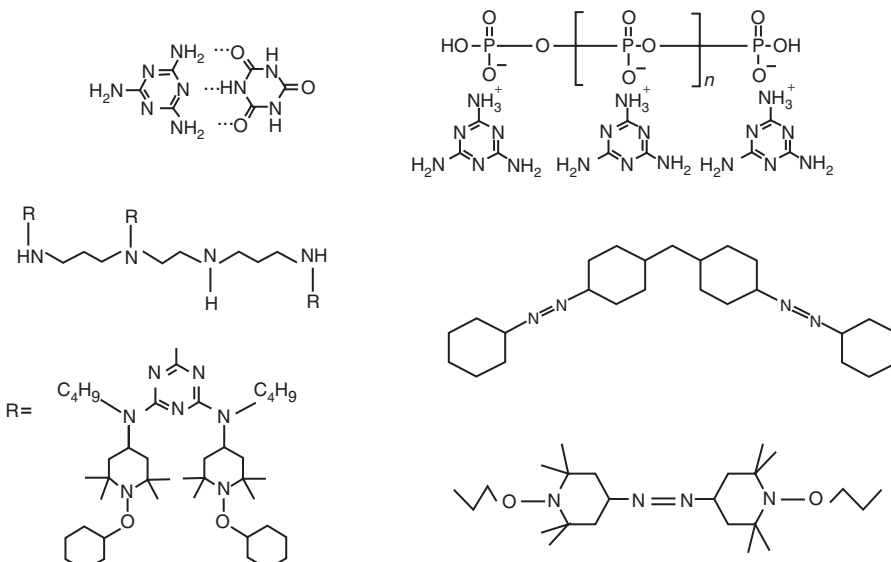


Figure 11.20 Chemical structures of nitrogen-containing flame retardants.

11.5.5 Selected Examples of Flame Retardancy

The activity of flame retardants depends on the inherent flammability of the polymer, on the degradation behavior of the polymer substrate, on the influence through further formulation ingredients, and on the degradation mechanism of the flame retardant. Moreover, the choice of a suitable flame retardant is related to the fire standards to be fulfilled. For example, unreinforced polyamide-6.6 is easily flame-retarded by adding 6–8% of melamine cyanurate to achieve a UL 94 V-0 rating. Glass-fiber-reinforced polyamide-6 achieves only a V-2 rating at around 20% of melamine cyanurate, whereas 25% of melamine polyphosphate may result in V-0. However, often synergistic combinations between different flame retardants are used from cost–performance reasons, for example, nitrogen and phosphorus compounds together. For instance, the combination of diethylaluminum phosphinate and melamine polyphosphate results in a V-0 classification of glass-fiber-reinforced polyamide 6.6 at a total concentration of 12–15% [27]. Furthermore, the combination of halogen-free flame retardants with a low concentration of halogen allows the achievement of flame retardancy at very low concentrations; for example, the combination of 0.2% aluminum hypophosphite, 0.3% melamine hydrobromide, and 0.1% 2,3-dimethyl-2,3-diphenylbutane results in a V-2 classification of PP [28]. On the other extreme, V-0 classification when using magnesium dihydroxide needs a concentration above 60% [29]. Intumescent formulations based on ammonium polyphosphate and pentaerythritol (3 : 1) achieve a V-0 classification of PP at 30% loading [30].

11.6 PLASTICIZERS

Plasticizers in the form of additives (the so-called external plasticizers) act as processing aids, reduce the melting and processing temperature of the polymer, and modify the polymer properties, for example, reducing the elastic modulus and making it more flexible and softer. PVC formulations consume most of the plasticizers. Plasticizers can be considered chemically as (weak) solvents for PVC. Phthalates such as di-2-ethylhexyl-phthalate or dibutyl phthalate represent still the major part of PVC plasticizers despite environmental concerns and bans in some applications such as children's toys in Europe. Alternative chemistries are based on phosphates, adipates, citrates, cyclohexane-1,2-dicarboxylates, terephthalates, and trimellitates (Fig. 11.21). Furthermore, oligomeric/polymeric plasticizers or plasticizers grafted to the PVC backbone via a thiol group can be seen as a new approach for plasticized PVC to cope with migration [31]. Within the trend of materials from renewable resources, plasticizers based on isosorbide esters have been introduced recently [32]. Technical performance of plasticizers is related to their gelation capacity, compatibility, volatility, water solubility, aging resistance, and light stability. Plasticizers are used in concentrations between 10% and 40%.

Technical criteria of plasticized PVC comprise the gelation behavior (measured as the temperature to fuse the plasticizer/PVC mixture), which varies between 80 and 180 °C depending on the plasticizer activity and the performance at high (processing) and low temperature. For example, adipate plasticizers allow use at lower temperatures than

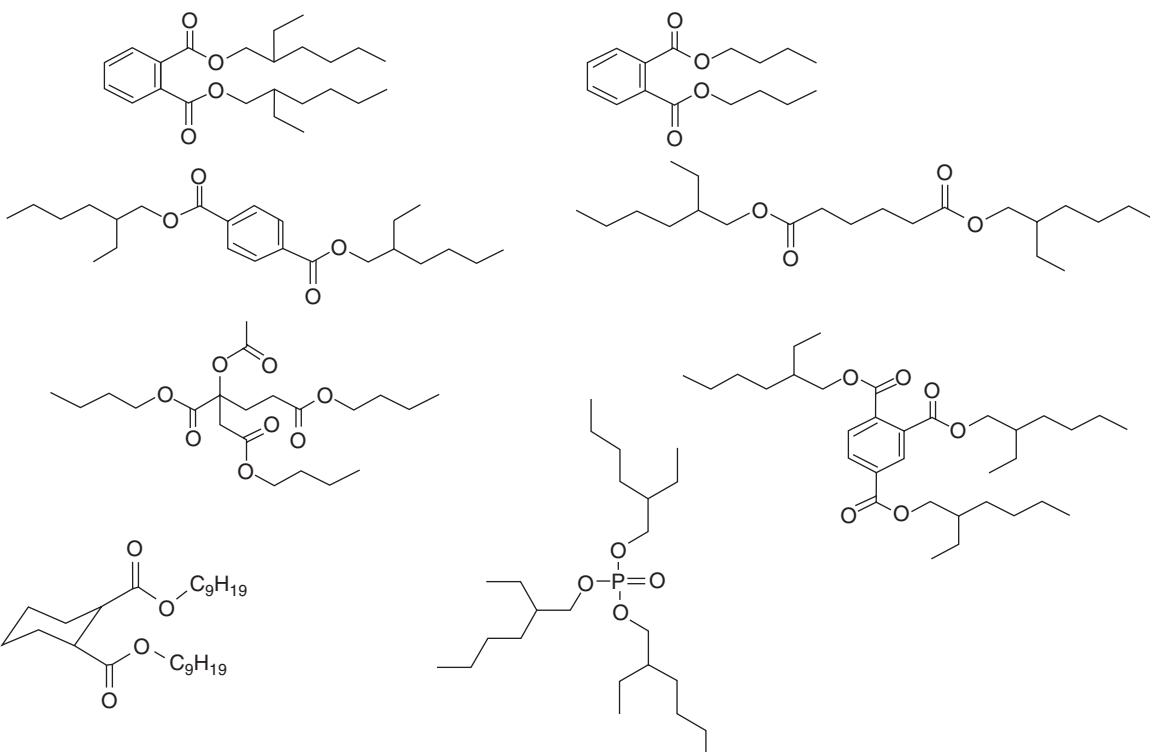


Figure 11.21 Chemical structures of plasticizers used in PVC.

phthalates. Interestingly, already rather small concentration changes show a considerable influence on properties; for example, increasing the plasticizer concentration from 37% to 42% decreases the glass-transition temperature from -7.5 to -21.5°C (unplasticized PVC: $70\text{--}90^{\circ}\text{C}$) [33].

The so-called antiplasticizers are used in PET bottle manufacturing to enhance the gas barrier. The proposed additives comprise aromatic hydroxy and carboxylic group containing benzene and naphthalene compounds, for example, methyl-4-hydroxybenzoate or 1,3-dihydroxynaphthalene [34].

11.7 SCAVENGING AGENTS

Scavenging agents are added to polymer formulations to remove unwanted byproducts, impurities, degradation products, or molecules inducing degradation of the polymer, for example, to scavenge water by reactive molecules such as carbodiimides in order to avoid hydrolytic degradation of the polymer or of other additives. The class of scavengers comprises mainly acid scavengers, aldehyde scavengers, and additives to reduce odor in recyclates.

11.7.1 Acid Scavengers

Acid scavengers or antacids are often used in base stabilization packages of polyolefins to neutralize acidic

byproducts from polymerization catalyst residues, namely, HCl. These byproducts may cause corrosion on processing equipment, reduce overall thermal stability of the polymer, and catalyze hydrolysis. Representative acid scavengers are acid salts such as calcium stearate, zinc stearate, calcium lactate, and also hydrotalcites and zinc oxide. Concentrations range mostly between 0.1% and 1%. The acid scavenger of choice depends on catalytic residues, that is, the polymerization process, acceptance of discoloration, and the required processing stability. For color-critical applications, aluminum–magnesium hydrotalcites are often preferred.

11.7.2 Aldehyde Scavenger

The main application fields of aldehyde scavengers are PET (more specifically water bottles made from PET), and polyacetals such as POM or polymers synthesized from formaldehyde such as urea–formaldehyde resins.

Any melt-processing of PET generates acetaldehyde in small concentrations caused through an elimination reaction from the terminating ethylene glycol unit. Acetaldehyde influences the taste of bottled water and, therefore, minimizing the content of acetaldehyde in the final product is mandatory. In addition to engineering approaches for optimized production, a number of molecules are known to play the role as active acetaldehyde scavengers, for example,

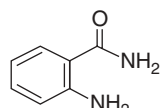


Figure 11.22 Structure of anthranilamide used as acetaldehyde scavenger in PET.

nitrogen compounds such as polyamides, amines, hydroxylamine, polyols including polyvinyl alcohol, zeolites, and cyclodextrins. Anthranilamide seems to be one of the preferred molecules (Fig. 11.22) [35, 36].

Thermal degradation of polyoxymethylene and polyacetals results in the formation of formaldehyde, which is furthermore catalyzed by oxidation of formaldehyde to formic acid. In addition to antioxidants and acid scavengers, formaldehyde scavengers are used in polyacetal formulations. Formaldehyde scavengers of choice are nitrogen compounds, for example, melamine derivatives such as benzoguanamine, urea derivatives such as allantoin, hydrazides, imides, and polyamide.

11.7.3 Odor Reduction

Some polymers, for example, recycled polymers, suffer often from odor problems caused by contaminations or degradation products. Additives that claim to reduce odor include zeolites [37] and silicates [38]. Recently, zinc ricinoleate-based additives were described to reduce odor of recyclates by absorbing low molecular weight amines and sulfuric substances [39].

11.8 ADDITIVES TO ENHANCE PROCESSING

To obtain a high production capacity of polymers processed in the melt, wear, and machine energy should be at a low level. As the polymer melt is usually of high viscosity, additives can be used to reduce the melt viscosity and internal and external friction. The most important class of additives to enhance processing is lubricants. Internal lubricants are soluble in the polymer melt and reduce the melt viscosity, whereas external lubricants are insoluble, form a film between metal surfaces of the processing equipment and the polymer melt, reduce friction, and show a slip effect. Chemically regarded lubricants are often hydrocarbons, for example, PE waxes, metal salts of long-chain acids, for example, calcium stearate or salts of montan waxes, and amide waxes, for example, erucamide or oleic acid amide. Their main use is in PVC, polyolefins, and some engineering plastics, and their concentrations may vary from below 1% up to several percentage.

Fluoropolymers (e.g., copolymers of vinylidene fluoride and hexafluoropropylene) and silicone-based (e.g., polydimethylsiloxanes) additives are often referred to as *processing aids*, preventing melt-fracture, for example, the so-called sharkskin. Fluoropolymers are applied in concentrations between 0.01% and 0.1%.

11.9 ADDITIVES TO MODIFY PLASTIC SURFACE PROPERTIES

A number of additives do not aim at modifying the properties of bulk polymers but target to influence specific surface properties. These primarily surface-active additives include slip and antiblocking agents to facilitate separation of individual films, antistatic agents to modify the surface resistivity, and antifogging agents to avoid water condensation on polymer films in the form of droplets. Other surface-modifying additives influence the roughness and the gloss of the polymer surface. Also, plasticizers and lubricants can influence the surface aspect of shaped plastic parts. Surface-active additives with hydrophilic or hydrophobic character can change the polarity of a polymer: for example, a hydrophilic surface-active agent can create a hydrophilic surface on a hydrophobic polyolefin.

11.9.1 Slip and Antiblocking Agents

Often, polymer films show a tendency to stick together, which makes it difficult to separate individual films in processing steps, for example, for packaging applications.

Slip agents are related to lubricants, as amide waxes, such as erucamide or oleamide, are typical representatives. Through migration of the slip agent to the film surface, a lubricating layer is formed that facilitates the separation of adjacent films. Antiblocking agents fulfill a similar target, but they are based on inorganic materials, for example, silica, talc, zeolites. Concentrations of slip or antiblocking agents are in the range of 0.1–0.3%.

11.9.2 Antifogging Agents

Antifogging agents help to avoid the formation of water droplets on polymer films originating from temperature differences; instead, the water droplets spread in a continuous transparent film. As the antifogging agent migrates to the surface, the surface energy of the plastic film is increased and the surface energy of the water droplet is reduced. Main applications are in agriculture/greenhouse films (to avoid reduced light transmission, burning of plant leaves through lens effect, and water drips on the plants) and in packaging films, for example, to keep esthetics of packaged food. Chemically, antifogging additives are often glycerol esters, sorbitan esters, or ethoxylated fatty alcohols, and their concentrations are in the range of 1–3%.

11.9.3 Antistatic Agents

Polymers are generally good insulators, but they can build up high electrostatic charges. Static electricity may cause handling problems of plastic goods, dust contamination, and risk of electrical discharges. Antistatic additives dissipate electrostatic charges and, therefore, reduce these potential problems. Chemically regarded, antistatic agents are based either on organic migrating compounds, on inherently antistatic polymers, or on conductive fillers. Surface migrating organic compounds cover the plastic surface and pick up water from the surrounding environment, creating a conductive pathway. Often, fatty acid esters, typically glycerol monostearate, ethoxylated alkylamines, ethoxylated alcohols, alkylsulfonates, and ammonium salts are used.

Inherently, antistatic polymers are block-copolymer elastomers, for example, block polyetheramides. These can form a permanent conductive network within the host polymer matrix, thus dissipating electrical charges, independent of water uptake [40]. Electrically, conductive fillers comprise carbon black, graphene, carbon nanotubes (CNTs), carbon nanofibers, metal powders such as copper, and conductive polymers, for example, polyaniline, polypyrrole, or polythiophene [41, 42]. In addition to the activity as antistatic agents, these molecules may be used as components for electromagnetic shielding. Concentrations of antistatic agents vary from 0.1% to 15% depending on the chemistry used, as well as the required performance and permanency.

molecular weight increase should be possible if difunctional additives are used. Higher functionalities will result in branching and crosslinking depending on the functionality and additive concentration.

Polyester chains exhibit either -COOH or -OH end groups, and polyamides either -NH₂ or -COOH end groups. In principle, any difunctional additive that reacts at the processing temperature with those chemical groups and with sufficient thermal stability may be used. The proposed chemistries include diepoxides, bis-oxazolines, di-isocyanates, dianhydrides, bis-acyllactams, bis-maleimides, dicyanates, carbodiimides, diesters, etc., sometimes combined with catalysts to accelerate the reaction. Depending on the starting polymer and careful selection and adjustment of the type and concentration of the reactive additives, the basis for manufacturing tailor-made products is provided. Concentrations vary from 0.1% up to several percent.

As an example of molecular weight increase of polyamides, the decrease of the MVR (increase in molecular weight) in relationship to the reactive additive concentration is shown for diepoxides, catalyzed by a phosphonate (Fig. 11.23) [43].

Because of a lack of functional end groups, chain extension of polymerization polymers such as polyolefins or polystyrene is limited. In case double bonds are present in the polymer, for example, in PE, these may be used for some branching and crosslinking during processing in the presence of radical generators, such as peroxides or hydroxylamine esters [44]. A limited chain extension of PP can be achieved by combining radical generators and multifunctional acrylates [45].

11.10 ADDITIVES TO MODIFY POLYMER CHAIN STRUCTURES

Some additive classes are intended to modify in a controlled way the molecular weight and/or molecular weight distribution of the polymer or to create branched or crosslinked structures often in the course of a processing step, for example, by reactive extrusion. The modification of the molecular weight can be in both directions: chain extenders and branching and crosslinking agents will increase the overall molecular weight, whereas prodegradants will decrease the molecular weight. Consequently, many polymer properties, for example, the mechanical and rheological characteristics, are influenced, as these are directly linked to the molecular weight and to the polymer architecture.

11.10.1 Chain Extenders

Polycondensation polymers such as polyesters or polyamides carry functional end groups, which can be used to build up the molecular weight by reaction with suitable additives that are capable of reacting with these end groups. As there are ideally two end groups per chain, a linear

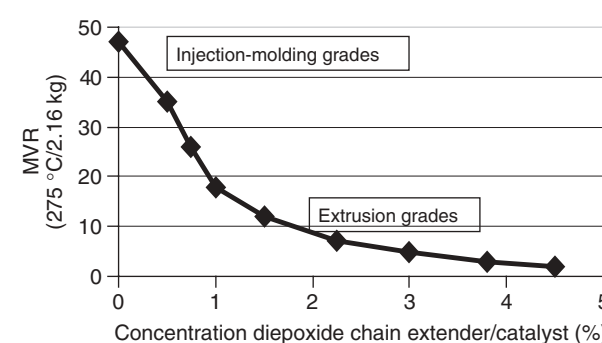


Figure 11.23 Molecular weight increase of polyamide-6,6 by chain extenders.

esters or azoalkanes have been proposed more recently for this purpose [46, 47]. The concentrations of radical generators for controlled degradation can be up to 1%.

11.10.3 Prodegradants

As an alternative to the use of biodegradable polymers, prodegradants have been developed to promote (photo)oxidative degradation of polyolefins, for example, of agricultural or packaging films, in a considerably short time, that is, after the use season. Ideally, the degradation time can be programmed. Increased photooxidative degradation is achieved by adding photosensitizers such as carbonyl-containing species, for example, diketones [48]. Additives for oxidative degradation are based on metal salts, for example, iron, cerium, or cobalt fatty acid salts [49, 50].

11.10.4 Cross-Linking Agents

Crosslinking of polymers results in a three-dimensional network and is common in thermosetting resins (curing, hardening) and in rubber processing (vulcanization). Crosslinking of thermoplastic polymers, mainly PE, is used in wire and cable insulation as well as in pipe and foam applications. Chemical compounds to achieve crosslinking are radical generators used sometimes in combination with graftable monomers. The radical generators are usually organic peroxides such as alkyl/aryl peroxides (dicumylperoxide), peroxyester, or diaroyl peroxides (dibenzoyl peroxide). By cleavage of the peroxy group, free radicals are formed, abstracting hydrogen from the polymer. The formed macroradical recombines with another macroradical, forming finally, after several reaction steps, the three-dimensional network. If reactive monomers are present, the macroradical may react with the monomer in a grafting reaction in competition to recombination. The latter is used, for example, in wire and cable insulation, when organofunctional silanes, for example, vinyltrialkoxysilanes are grafted on PE in the presence of peroxides. The silane-functionalized PE is crosslinked in a consecutive step by water. Another monomer to be grafted radically on polyolefins is maleic acid anhydride; the resulting modified polymers are used as adhesion promoters and compatibilizers between different polymers, polymer and metal, polymer and fillers, or polymer and reinforcement agents.

As an alternative to organic peroxides, carbon-carbon (CC) initiators, for example, dimethyl diphenylbutane, hydroxylamine esters [51], or unsymmetric azo compounds [47] can be used for crosslinking reactions especially at higher processing temperatures.

Concentrations of crosslinking agents depend on the required crosslinking density, the application, and the production process, and vary between 1% and 10%.

11.11 ADDITIVES TO INFLUENCE MORPHOLOGY AND CRYSTALLINITY OF POLYMERS

Some additive classes influence the overall mechanical and optical properties through inducing morphology changes. Nucleating agents, clarifiers, and antinucleation agents are used to influence the crystal growth of semicrystalline polymers. The morphology of polymer blends and the distribution of polymers, fillers, and reinforcements in a polymer matrix are adjusted with the help of compatibilizers, dispersants, and coupling agents.

11.11.1 Nucleating Agents/Clarifiers

Crystallization of semicrystalline polymers (e.g., PP, PE, PET, PBT, PA-6, and PA-6.6) can be influenced during processing through the addition of nucleating agents. Nucleating agents accelerate the crystallization rate and thereby reduce the cycle time during injection molding and increase the number of formed crystals, thus influencing the morphology as well as mechanical and optical properties. Nucleating agents that induce low haze and high transparency, for example, in PP, are called *clarifiers*. Clarifiers for PP are usually based on dibenzylidene sorbitols and its derivatives, for example, bis(3,4-dimethyl-dibenzylidene) sorbitol. Non-sorbitol structures are, for example, composed of aramides [52] or phosphates [53]. Nucleating agents for PET, PBT, and PA consist often of alkali metal salts (e.g., sodium benzoate) or phosphates (e.g., sodium 2,2'-methylene-bis-(4,6-di-*tert*-butyl-phenyl)phosphate) (Fig. 11.24); however, talc or carbon black show a nucleation effect also. The concentrations of nucleating agents used can be below 0.1% (nonsorbitol clarifiers), but are often in the range of 1–3%.

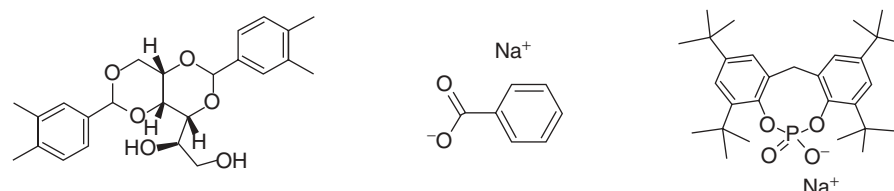


Figure 11.24 Chemical structures of nucleating agents.

Antinucleation agents reduce the crystallization rate of polymers: for example, addition of 1% SAN or polystyrene to PET reduces haze during blow-molding [54, 55].

11.11.2 Coupling Agents/Compatibilizers

Polymers of different structures are in general not miscible thermodynamically and, therefore, do not form homogeneous blends. The polymer in the highest concentration forms a continuous phase, and the polymer with a lower concentration is dispersed in the continuous matrix. The intermolecular adhesion between the continuous and the dispersed phases is very weak, resulting in insufficient mechanical properties of such a blend. Compatibilizers modify polymer interphases by reducing the interfacial tension in the melt, stabilizing the dispersed phase against growth during annealing (“morphology stabilizers”), and increasing the adhesion at phase boundaries, resulting finally in improved overall properties. Compatibilizers are polymers with structures similar to those the polymers to be compatibilized. They can be reactive, that is, carrying functional groups, or nonreactive [56, 57]. Examples of reactive compatibilizers include acrylic acid-grafted or maleic acid anhydride-grafted PE or PP or glycidyl(meth)acrylate copolymers. A typical nonreactive compatibilizer is styrene-(ethylene/butylene) styrene triblock copolymer. The concentrations of compatibilizers have to be in the range of 5–15% to show the requested effects.

Like compatibilizers, coupling agents are used to improve the adhesion of fillers and reinforcements, for example, glass fibers or carbon fibers to the polymer matrix [58]. The coupling agent consists of a part that is compatible to the polymer and another part that is reactive to the filler or reinforcement. Examples of coupling agents are fatty acids (e.g., stearic acid), calcium, zinc, or magnesium stearate, and amino-, epoxy-, methacryl-functionalized silanes. More sophisticated coupling agents are based on complex titanates and zirconates [59]. Optimized concentrations of coupling agents depend on the filler/reinforcement surface area and are in the range of 0.2–5%.

11.12 ANTIMICROBIALS

Antimicrobials or biocides protect plastics from attack on the surface by microorganisms, for example, fungi, yeasts, bacteria, and algae, and are used in outdoor applications in public areas (e.g., wood–plastic composites, liners for pools, bath mats, appliances), in hygienic household and consumer applications such as textiles, and in medical devices [60, 61]. Biocides are based on organic, often surface migrating, molecules, or inorganic compounds releasing silver, copper or zinc ions. Examples

for organic biocides are 10,10'-oxybisphenoxyarsine, 2-*n*-octyl-4-isothiazolin-3-one, both mainly used as antifungals in flexible PVC, 2,4,4'-trichloro-2'-hydroxy-diphenylether (Triclosan), and quaternary ammonium salts, for example, polysiloxanes with functional ammonium groups [62]. Silver-releasing antimicrobial compounds include silver salts, colloidal silver, nanosilver, silver complexes such as Ag zeolite sometimes in combination with Zn, and silver glasses. The concentrations used of antimicrobials are in the range of 0.2–2%.

11.13 ADDITIVES TO ENHANCE THERMAL CONDUCTIVITY

Thermally conductive compounds are mainly used in the electronic industry to remove heat from electronic components. Additives to be used are ceramics (e.g., aluminum nitride, or boron nitride) or carbon-based additives (e.g., graphite, carbon fibers, or CNTs) or even metal fibers [63, 64]. The concentrations used are quite high and can easily be in the 50% range.

11.14 ACTIVE PROTECTION ADDITIVES (SMART ADDITIVES)

Some additives are incorporated in polymers not to protect or influence the polymer itself but to act on the surroundings in an active way: protection of packaged goods, plant growth in greenhouses, or heat management in buildings.

11.14.1 Content Protection

The incorporation of additives in packaging to protect packaged goods is a technique often called *active packaging*. Examples include the use of UV absorbers to protect food from discoloration and food ingredients, for example, vitamins, from degradation and to extend the shelf-life. The UV absorbers are based on the same chemical classes as used for protecting plastics as described above.

Oxygen scavengers remove oxygen residues from the packaging by a chemical reaction and transform them into stable products. Therefore, the packaged good is protected from oxidation, and undesirable taste, odor, or appearance caused by oxidation of the food is eliminated. Chemical compounds to act as oxygen scavengers include polybutadiene or copolymers with cyclohexene or with allylic groups in combination with transition-metal catalysts based on cobalt or zinc (e.g., cobalt acetate or zinc acetate) or photocatalytic initiation [65]. Alternative oxygen scavengers are based on the oxidation of iron activated by moisture.

Other additives to be used in food packaging include ethylene scavengers (e.g., potassium permanganate) on silica, CO₂ scavenger (e.g., calcium hydroxide reacting to calcium carbonate), and CO₂- generating additives (e.g., ferrous carbonate). Further additives to be used for content protection incorporated in plastics provide antimicrobial effects, for example, silver or ethanol release, antioxidant release, flavor release, flavor absorption, and moisture control [66].

11.14.2 Productivity Enhancer

The growth of plants in greenhouses and some potential plant diseases caused by pests and fungi may be controlled by incorporating fluorescent dyes or pigments in greenhouse films. These dyes are able to modify the spectrum of outside solar radiation and convert UV light into visible red light. The changes in the radiation transmission can result in significant modification of plant architecture and shape, as the photosynthetic process strongly depends on the total amount of light that plants receive in photosynthetic active radiation (400–700 nm). For example, the yields of tomatoes and the number of rose flowers were significantly increased when a film with a red fluorescent dye was used in the greenhouse [67].

11.14.3 Heat Control

IR absorbers and reflectors are used to limit the heat development in rooms (e.g., in greenhouses) and are incorporated in agricultural films or in glazing. Typical materials range from kaolin (aluminum silicate) or other silicates and hydrotalcites [68] in agricultural films to dyes (e.g., phthalocyanines or anthraquinones). Furthermore, dyes with near-IR absorption are added to enhance laser welding of polymers.

11.15 ODOR MASKING

Odor from contaminants or degradation products, instead of being scavenged (see above), may be masked by

fragrance-releasing agents, for example, with fruit or flower scent. In some cases, to manage odor it may be advantageous to use combinations of maskants, odor absorbers, and/or neutralizers.

11.16 ANIMAL REPELLENTS

Plastic application materials such as cables are destroyed by animals and especially by rodents. Therefore, additives may be incorporated to eliminate potential damage to these materials. Additives of choice to repel rodents are substances with a bitter taste, for example, denatonium benzoate, with a spicy taste (capsaicin, hot pepper), and/or with an unpleasant odor for animals (Fig. 11.25). Other substances repel birds, for example, natural oils or methyl salicylate [69].

11.17 MARKERS

Identification of polymers may be important for the manufacturer to establish the identity and the source and to differentiate own products from those of other suppliers (e.g., in the case of identifying the cause of damage) or to separate different polymers for recycling reasons. Target is the use of very small quantities of additives as markers or tracers. Proposed additives of choice may be fluorescent dyes [70], haptens compounds [71], or rare-earth metals [72] in the ppm range.

11.18 BLOWING AGENTS

Blowing agents are used in manufacturing foams. Chemical blowing agents are additives that decompose thermally within the foam production process, liberate gases, and create the foamed structure. Product classes comprise azo compounds (e.g., azodicarbonamide, hydrazides, tetrazoles), monosodium citrate, but also inorganic carbonates, for example, sodium hydrogen carbonate (Fig. 11.26).

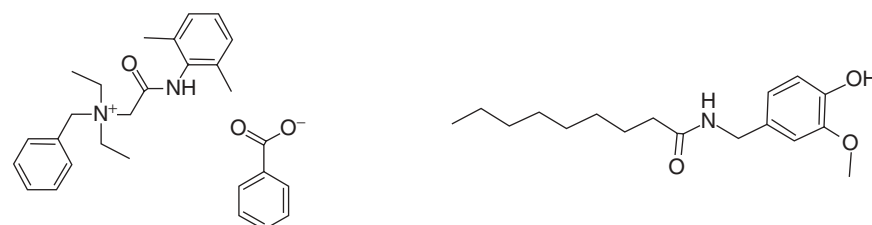


Figure 11.25 Chemical structures of animal repellents.

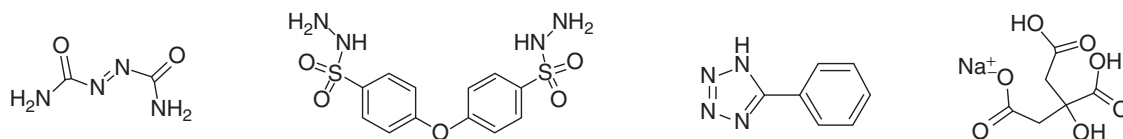


Figure 11.26 Chemical structures of blowing agents.

11.19 SUMMARY AND TRENDS IN POLYMER ADDITIVES

Additives are essential components in polymer formulations to maintain and to extend polymer properties. Many additive classes, for example, antioxidants, heat stabilizers, and light stabilizers, are seen today as commodities and standard products, available from different manufacturers and applied in many use areas. These additives will grow in parallel to the growth of plastics. New additive developments in the traditional areas address more stringent or new requirements, mainly in niche applications. Optimized combinations of different additives acting through different mechanisms result often in an optimized solution for a specific requirement. The art of formulation is in the knowledge on the synergisms and antagonisms of the considered additives.

Furthermore, modification of polymer properties through additives contributes decisively to the use of commodity plastics in demanding applications that have been the traditional field of engineering plastics.

A further driver for developing new additives is the increasing awareness of the environment, of carbon footprint, and of energy savings, resulting in environmentally friendly additive solutions shown, for example, through the developments of halogen-free flame retardants and metal-free PVC stabilizers as well as green manufacturing processes. Moreover, (bio)additives based on renewable resources may grow in the future.

Owing to the trend in plastics to be produced in larger volumes and fewer grades, the importance of additives in plastics will not only sustain but also increase. Typical additive examples comprise surface or interphase modifiers, nucleating agents, and reactive additives, providing tailor-made molecular weight, polymer structures, morphologies, as well as rheological and/or surface behavior. Smart additives allow plastics to enter new applications, new effects, and new functionalities of high value.

In a nutshell, plastic additives are and will be essential components in polymer formulations to support the further growth of plastics. Also they do and will provide innovative solutions for the resin producer and the plastic converter, and better value for the user of the plastic article.

REFERENCES

1. Available at <http://www.answers.com/topic/alexander-parkes>. Accessed 2010 July 6.
2. Hyatt JW, Hyatt IS, inventors. US patent 156,353. 1874.
3. Hyatt IS, Hyatt JW, inventors. US patent 156,352. 1874.
4. Hyatt JW, Hyatt IS, inventors. US patent 105,938. 1870.
5. Hunter AS, inventor. US patent 2,129,131. 1938.
6. Klemchuk PP. History of stabilizing additives for polymers. In: Pospisil J, Klemchuk PP, editors. *Oxidation Inhibition in Organic Materials*. Volume 1. Boca Raton: CRC Press; 1990. p 11.
7. Pfaendner R. Polym Degrad Stab 2006;91:2249.
8. Available at www.townsendpolymer.com/publications/plastic-additives-globalstudy. Accessed 2010 July 6.
9. Widmer A. Chem Rundsch 2004:5.
10. Available at <http://www.bccresearch.com/report/plastics-additives-global-markets-pls022b.html>. Accessed 2012 Oct 12
11. Zweifel H, editor. *Plastics Additives Handbook*. 5th ed. Munich: Hanser Publisher; 2001. p 3 and p 142.
12. Gijsman P, Sour WJM, Rulkens R, Janssen RHC, inventors; DSM IP Assets B.V., assignee. WO 2006/074912. 2006.
13. Allen NS, Edge M, Corrales T, Childs A, Liauw CM, Catalina F, Peinado C, Minihan A, Aldcroft D. Polym Degrad Stab 1998;61:183.
14. Pfaendner R. Polym Degrad Stab 2010;95:369.
15. Hopfmann T, Wehner W, Ryningen A, Stoffelsma JU, Clucas P, Pfaendner R. Plast Rub Compos Pro 1998;27:442.
16. Beck R, Hacker P, Wehner W, Dave T, Scholz S, inventors; Catena Additives GmbH & Co KG, assignee. WO 2009/053000. 2009.
17. Dave T. Plastics, Additives and Compounding 2004 Nov/Dec:44.
18. Hopfmann T, Friedrich HH, Kuhn KJ, Wehner W, inventors; Crompton Vinyl Additives GmbH, assignee. US patent 7,358,286. 2008.
19. Gugumus F. Light stabilisers. In: Zweifel H, editor. *Plastic Additives Handbook*. 5th ed. Munich: Hanser Publisher; 2001. p 141.
20. Gugumus F. Light stabilisers. In: Zweifel H, editor. *Plastic Additives Handbook*. 5th ed. Munich: Hanser Publisher; 2001. p 251.

246 POLYMER ADDITIVES

21. Gugumus F, inventor; Ciba Geigy Corp., assignee. US patent 4,863,981. 1989.
22. Kiliaris P, Papaspyrides C. *Progr Polymer Sci* 2010;36:902.
23. Beyer G. *Fire Mater* 2002;26:291.
24. Aubert M, Nicolas RC, Pawelec W, Wilen CE, Roth M, Pfaendner R. *Polymer Adv Tech* 2011;22:1529.
25. Aubert M, Wilen CE, Pfaendner R, Kniesel S, Hoppe H, Roth M. *Polym Degrad Stab* 2011;96:328.
26. Schartel B. Uses of fire tests in materials flammability development. In: Wilkie CA, Morgan AB, editors. *Fire Retardancy of Polymers*. Boca Raton: CRC Press; 2010. p 391.
27. Schlosser E, Nass B, Wanzke W, inventors; Clariant GmbH, assignee. EP 1070754. 2000.
28. Costanzi S, inventor; Italmatch Chemicals S.P.A., assignee. EP 1907473. 2005.
29. Hornsby PR. *Fire Mater* 1994;18:269.
30. Bourbigot S, Bras ML, Duquesne S, Rochery M. *Macromol Mater Eng* 2004;289:499.
31. Reade L. *Pipe and Profile Extrusion* 2010 Oct:23.
32. Yin B, Hakkarainen M. *J Appl Polymer Sci* 2011;119:2400.
33. Persico P, Ambrogi V, Acierno D, Carfagna C. *J Vinyl Add Techn* 2009;15:146.
34. Mehta S, Roodvoets MR, inventors; Invista Technologies S.A.R.L., assignee. WO 2007/106302. 2007.
35. Rule M, Shi Y, Huang X, inventors; Coca Cola Co, assignee. WO 2001/62838. 2001.
36. Mahiat B, Waeler J, inventors; Polyone Corp., assignee. WO 2006/086365. 2006.
37. Gioffre AJ, Marcus Bk, inventors; Union Carbide Corp., assignee. US patent 4795482. 1989.
38. Heberer S, Kunz FR, Lotz BM, Maier HJ, Wartusch R, inventors; Degussa, assignee. DE 10062558. 2002.
39. Markarian J. Available at <http://www.specialchem4polymers.com/resources/articles/article.aspx?id=4226>. Accessed 2012 Oct 12.
40. Hund MC. *Kunststoffe* 2010;100:50.
41. Markarian J. *Plastics, Additives and Compounding* 2008 Sept/Oct:22.
42. Sherman L. *Injection World* 2011 Feb:28.
43. Pfaendner R. Additives for mechanical recycling of plastics. In: Zweifel H, editor. *Plastics Additives Handbook*. 5th ed. Munich: Hanser Publisher; 2001. p 1006.
44. Roth M, Pfaendner R, Nesvadba P, Zink MO, inventors; Ciba Specialty Chemicals Corp., assignee. US patent 7,358,365. 2008.
45. Pfaendner R. *Compt Rendus Chem* 2006;9:1338.
46. Roth M, Pfaendner R, Nesvadba P, Zink MO, inventors; Ciba Specialty Chemicals Corp., assignee. US patent 7,030,196. 2006.
47. Aubert M, Roth M, Pfaendner R, Wilen CE. *Macromol Mater Eng* 2007;292:707.
48. Poyner WR, Chakraborty KB, inventors; Robinson Broth. Ltd., assignee. US patent 5,274,019. 1993 Dec 28.
49. Maennle F, Beylich J, Lecerf N, Olafsen K, Hauge R, Roedseth KR, Kleppe EA, inventors; NOR X Industry A.S., assignee. WO 2004/094516. 2004.
50. Pablos JL, Abrusci C, Marin I, Lopez-Marin J, Catalina F, Espi E, Corrales T. *Polym Degrad Stab* 2057; 2010:95.
51. Roth M, Pfaendner R, Nesvadba P, Zink MO, inventors; Ciba Specialty Chemicals Corp., assignee. US patent 7,579,411. 2009.
52. Abraham F, Ganzleben S, Hanft D, Smith P, Schmidt HW. *Macromol Chem Phys* 2010;211:171.
53. Sherman L. *Compounding World* 2011 Feb:41.
54. Wellen RMR, Rabello MS. *J Appl Polymer Sci* 2009; 114:1884.
55. Wellen RMR, Rabello MS. *J Appl Polymer Sci* 2010; 116:1077.
56. Makarian J. *Plastics, Additives and Compounding* 2004 Feb:25.
57. Feldman D. *J Macromol Sci Part A* 2005;42:587.
58. DeArmitt C. *Compounding World* 2011 Feb:28.
59. Monte SJ. *Polymer Polymer Compos* 2002;10:1.
60. Sherman L. *Compounding World* 2009 Sept:28.
61. Simoncic B, Tomsic B. *Textil Res J* 2010;80:1721.
62. Getman GD, Bootman M, Wagner D, Ward T, inventors; Biosafe Inc., assignee. WO 2006/102366. 2006.
63. Janssen RHC, Douven IL, van Dijk HK. *Compounding World* 2010 Feb:38.
64. Sherman L. *Compounding World* 2010 Feb:28.
65. Schiraldi DA, Sekelik DJ, Smith BL, inventors; Arteva Tech. S.A.R.L., assignee. EP 1283234. 2003.
66. Vermeiren L, Devlieghere F, van Beest M, de Kruijf N, Debevere J. *J Food Tech Af* 2000;5:6.
67. Novoplansky A, Sachs T, Cohen D. *Sol Energ Mater* 1990;21:17.
68. Takahashi H, Okada A, inventors; Kyowa Chem. Ind. Ltd., assignee. US patent 6,418,661. 2002.
69. Gerritsen CPA, inventor; Nedap N.V., assignee. WO 2010/011139. 2010.
70. Luttermann K, Claussen U, Sayed AE, Riess R, inventors; Bayer AG, assignee. EP 0476416. 1992.
71. Garner RC, Phillips DJ, Wilkinson TG, Angella FG, Dorland ER, Stow MW, inventors; Biocide Ltd., assignee. US patent 5,776,713. 1998.
72. Kolbe A, Markwitz H, inventors; Thüringisches Institut für Textil- und Kunststoff-Forschung e.V., assignee. WO 2008/049414. 2008.

FURTHER READING

- Ash M, Ash I, editors. *Handbook of Plastics and Rubber Additives*. 2nd ed. Shropshire: Rapra Technology; 2005.
- Datta S, Lohse D. *Polymeric Compatibilizers*. Munich: Hanser; 1996.

- Horrocks AR, Price D, editors. *Advances in Fire Retardant Materials*. Cambridge: Woodhead; 2008.
- Hull RT, Kandola BK, editors. *Fire Retardancy of Polymers*. Cambridge: RSC Publishing; 2009.
- Murphy J, editor. *Additives for Plastics Handbook*. 2nd ed. New York: Elsevier; 2001.
- Pionteck J, Wypych G. *Handbook of Antistatics*. Toronto: ChemTec Publishing; 2007.
- Pospisil J, Klemchuk PP, editors. *Oxidation Inhibition in Organic Materials* Volumes 1 and 2. Boca Raton: CRC Press; 1989.
- Weil ED, Levchik SV, editors. *Flame Retardants for Plastics and Textiles*. Munich: Hanser; 2009.
- Wilkie CA, Morgan AB, editors. *Fire Retardancy of Polymeric Materials*. 2nd ed. Boca Raton: CRC Press; 2010.
- Wypich G. *PVC Degradation and Stabilization*. Toronto: ChemTec Publishing; 2008.
- Wypich G. *PVC Formulary*. Toronto: ChemTec Publishing; 2009.
- Wypich G, editor. *Handbook of UV Degradation and Stabilization*. Toronto: ChemTec Publishing; 2011.
- Wypich G. *Handbook of Plasticizers*. Toronto: ChemTec Publishing; 2004.
- Zweifel H, Maier RD, Schiller M, editors. *Plastic Additives Handbook*. 6th ed. Munich: Hanser; 2009.

PART III

POLYMERIZATION PROCESSES AND ENGINEERING





12

POLYMER REACTION ENGINEERING

ALEXANDER PENLIDIS, EDUARDO VIVALDO-LIMA, JULIO CÉSAR HERNÁNDEZ-ORTIZ, AND ENRIQUE SALDÍVAR-GUERRA



12.1 INTRODUCTION

If a definition of polymer reaction engineering (PRE) was sought, a good approach would be to use the definition of chemical engineering [1], but applied to large macromolecules, instead of small molecules. Therefore, one may state that PRE is the branch of engineering that deals with the technology of large-scale *polymer* production and the manufacture of *polymer* products through *polymerization* processes. PRE is a broad and multidisciplinary area, relatively young and developing fast, which combines polymer science, chemistry, and technology with principles of process engineering [2].

The practical history of PRE started and evolved during the first half of the twentieth century as the everyday effort of the industrial pioneers in charge of polymer production facilities to keep businesses running: polymer chemists with little or no training in chemical engineering, or chemical engineers with little or no training in polymer science. From the scientific/academic perspective, once Staudinger's concept of polymer molecules had been accepted, progress accelerated in all areas of polymer science.

The 1930s were rich with theoretical findings in polymer science and engineering and with the commercial production of several new polymers. These investigations would transform our understanding of polymer manufacture and culminate in the development of several continuous polymerization processes and the establishment of PRE as a new area of research in the 1940s [3]. The period from 1950 to 1990 saw the continued growth and evolution of process technologies, largely stimulated by the combination of PRE principles with the fundamental understanding of polymerization kinetics developed in the earlier years [3].

It is roughly in the last 30–40 years that PRE has become a scientific discipline of its own, thanks to “forerunners” such as Böhm, Hamielec [4], Ray, Reichert, and Sinn [5]. It would take a single book to revisit the history and development of PRE. Instead, the interested reader is referred to a few selective yet representative reviews or editorial papers [2–13]. The importance of this area can also be sensed and monitored by following the contents of the dedicated journals to PRE [*Polymer Reaction Engineering* [14], from 1992 to 2003, the *Macromolecular Reaction Engineering* regular section in *Macromolecular Materials & Engineering* [15], from 2004 to 2006, and *Macromolecular Reaction Engineering* [16], from 2007 to present], and two major international conferences (the *International Workshop on Polymer Reaction Engineering*, usually held in Germany and organized by DECHEMA every three years and the conference series “*Polymer Reaction Engineering*,” organized by Engineering Conferences International (ECI), usually held in North America, also every three years, but one year apart from each other). At present, PRE research can be classified in process-oriented, product-oriented, and enabling research (which comprises kinetics, thermodynamics, process observation and control, modeling, and simulation tools) [5]. However, different classifications can be proposed, the bottom line being that every new key discovery in any area of polymer science (e.g., nanomaterials, biomaterials, green and sustainable processes, etc.) will need the application of PRE principles to turn it into a useful commercial application.

In this chapter, we do not cover all the topics studied in PRE. Instead, we provide some basic background sometimes overlooked in the PRE literature, a very useful collection of tips on PRE and modeling, and some

samples of polymerization schemes and the resulting kinetic equations, which are the bases of much of the research published in PRE. The reader will recognize the relationship and connections between this chapter and other chapters from this handbook (e.g., Chapters 6, 9, 13, and 15).

12.2 MATHEMATICAL MODELING OF POLYMERIZATION PROCESSES

12.2.1 Chemical Reactor Modeling Background

Polymerization reactors are a specific kind of chemical reactors in which polymerization reactions take place; therefore, in principle, they can be analyzed following the same general rules applicable to any other chemical reactor. The basic components of a mathematical model for a chemical reactor are a reactor model and rate expressions for the chemical species that participate in the reactions. If the system is homogeneous (only one phase), these two basic components are pretty much what is needed; on the other hand, for heterogeneous systems formed by several phases (emulsion or suspension polymerizations, systems with gaseous monomers, slurry reactors or fluidized bed reactors with solid catalysts, etc.), additional transport and/or thermodynamic models may be necessary to build a realistic mathematical representation of the system. In this section, to illustrate the basic principles and components needed, we restrict ourselves to the simplest case, that of homogeneous reactors; in other sections, additional components and more complex cases are discussed.

The rate expressions will be ideally derived from our knowledge of the reaction or kinetic mechanism. If this is not available, then empirical expressions obtained from experimentation will have to be used. Several techniques have been developed by statisticians and/or chemical engineers to find adequate rate expressions from experimental data. Fortunately, in the polymerization field, there is a good level of knowledge of the reaction mechanism for the most common polymerization chemistries: polycondensation, free radical, ionic coordination, etc.; therefore, whenever possible, to derive rate expressions, it is recommended to start from the accepted reaction mechanism for the type of polymerization of interest.

Reaction mechanisms consist of a set of so-called elementary reactions that describe the chemical steps that occur at the molecular level. Once a kinetic mechanism is postulated, all the relevant chemical species should be listed: these will be those that participate as reactants and/or products in at least one of the elementary reactions of the mechanism. Note that intermediate species, not appearing as reactants entering the reactor or products leaving it in the global reaction stoichiometry, are often relevant chemical species that must be considered (such as growing radicals or ionic propagating species).

For each of the chemical species participating in the mechanism, a mass balance equation must be written. The appropriate form of the mass balance for the specific type of reactor at hand must be used. Two of the most common types of reactors used in industry are the CSTR (continuous stirred tank reactor) and the tubular reactor. The corresponding mathematical models for their idealized forms, based on transport phenomena equations and available in any standard chemical reactor text [17, 18], are the ideal CSTR and the ideal model for the plug flow tubular reactor (PFR). The ideal CSTR model is given by Equation 12.1:¹

$$\frac{dM_i}{dt} = W_{i,\text{in}} - W_{i,\text{out}} + R_i, \quad i = 1, 2, \dots, n \quad (12.1)$$

where M_i is the instantaneous value of mass of species i in the reactor, expressed in moles; $W_{i,\text{in}}$ and $W_{i,\text{out}}$ are the molar flows of species i at the reactor entrance and exit, respectively; and R_i represents the reaction rate expressions for production of species i by elementary chemical reactions in molar units.

While for a CSTR it is possible to apply a macroscopic mass balance, since the spatial distribution of the species inside the reactor is assumed uniform, for a PFR this is not applicable and it is necessary to resort to a microscopic [19] (or differential) mass balance, in which axial diffusion of the chemical species is neglected. Assuming constant density, the following balance equation is obtained for a species A in the PFR:

$$\frac{\partial[A]}{\partial t} + v \frac{\partial[A]}{\partial z} = R_A \quad (12.2)$$

where $[A]$ is the molar concentration of species A , v is the velocity of the stream throughout the reactor, and z is the axis parallel to the reactor length.

Note that because of the microscopic nature of the balance in Equation 12.2, an intensive variable (concentration) must be used in this case, instead of absolute moles. Equations 12.1 and 12.2 are given for the more general non-steady-state operation (including start-ups or grade changes). The steady-state operation is a particular case of these general equations and can be obtained making the time derivative equal to zero in the corresponding equation.

The simplest reactor type, in which only non-steady-state operation is possible, is the batch reactor, for which the mass balance is simply given by

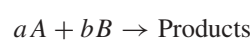
$$\frac{d[A]}{dt} = R_A \quad (12.3)$$

¹In writing the term R_i it has been supposed that the units are mole per unit time. It is customary that the rate expression is given per volume unit; in that case this term must be multiplied by the volume of reaction.



A beaker used at the laboratory level by the synthetic polymer chemist corresponds to this reactor type.

Once the mass balances for each chemical species are written using the corresponding reactor type model, it is necessary to write an explicit expression for the reaction rate (production and consumption) of each chemical species R_i . This is done by the application of the mass action law. This law, in one of its versions, establishes that for an elementary reaction



the reaction rate is given by

$$R_A = k[A]^a[B]^b \quad (12.4)$$

where k is the kinetic rate coefficient or rate constant (temperature and pressure dependent), and $[A]$ and $[B]$ are the molar concentrations of A and B , respectively.

12.2.2 The Method of Moments

To explain this technique, let us consider as an illustration a simple kinetic model for free radical polymerization, which contains only a subset of the possible reactions in these systems (Table 12.1). The application of the technique to a batch reactor, which is the simplest one, will be used to illustrate the method; extension to other reactor types is straightforward.

Mass balances for a batch reactor yield the following equations:

$$\frac{dI}{dt} = -k_d I \quad (12.5)$$

$$\frac{dR}{dt} = 2fk_d I - k_i \frac{RM}{V} \quad (12.6)$$

$$\frac{dM}{dt} = \frac{-\left(k_p M \sum_{n=1}^{\infty} P_n + k_i RM\right)}{V} \quad (12.7)$$

where P , the zeroth moment of the live polymer, is defined as

$$P = \sum_{n=1}^{\infty} P_n \quad (12.8)$$

The equations for indexed variables (live and dead polymer) result in

$$\frac{dP_1}{dt} = \frac{\left(k_i RM - k_t P_1 \sum_{i=1}^{\infty} P_i - k_p P_1 M\right)}{V} \quad (12.9)$$

$$\frac{dP_n}{dt} = \frac{\left(k_p P_{n-1} M - k_t P_n \sum_{i=1}^{\infty} P_i - k_p P_n M\right)}{V}, \quad n > 1 \quad (12.10)$$

$$\frac{dD_n}{dt} = \frac{\left(k_{td} P_n \sum_{i=1}^{\infty} P_i\right)}{V}, \quad n \geq 1 \quad (12.11)$$

To apply the method of moments, the definitions of the K th moments of the chain length distributions (CLDs) for live and dead polymer, respectively, are invoked:

$$\mu_K = \sum_{i=1}^{\infty} i^K P_i, \quad \lambda_K = \sum_{i=1}^{\infty} i^K D_i \quad (12.12)$$

From the first moments of the CLD, it is possible to calculate the number and weight-average molecular weight as follows.

$$\bar{M}_n = \frac{\mu_1 + \lambda_1}{\mu_0 + \lambda_0} W_m \quad (12.13)$$

$$\bar{M}_w = \frac{\mu_2 + \lambda_2}{\mu_1 + \lambda_1} W_m \quad (12.14)$$

where W_m is the molecular weight of the monomeric unit. The method of moments converts the system of Equations 12.8, 12.9 and 12.10 into a finite dimension system in which, instead of describing the full CLD (equivalent to the molecular weight distribution, MWD, if Equation 12.12 is defined in terms of molar mass M_i , instead of chain length i), equations for the moments (0, 1, 2, ...) are obtained. It is sufficient to calculate the first few moments of these distributions to obtain average molecular weights. To apply the method of moments, the following steps must be performed:

1. Multiplication of the equation for the species “ n ” of each polymer distribution by n^K ($n = 1, 2, \dots, \infty$).
2. For each distribution (live and dead polymer in this case), summation of the equations resulting from the first step, varying n from 1 to infinity.

To illustrate the technique, the method is applied to Equations 12.9 and 12.10 (live polymer CLD) and Equation 12.11 (dead polymer CLD). By applying steps 1 and 2, the result is, for live polymer:

$$\begin{aligned} \sum_{n=1}^{\infty} n^K \frac{dP_n}{dt} &= \frac{d \sum_{n=1}^{\infty} n^K P_n}{dt} = \frac{k_i RM}{V} + k_p M \sum_{n=2}^{\infty} n^K \frac{P_{n-1}}{V} \\ &- k_p M \sum_{n=1}^{\infty} n^K \frac{P_n}{V} - k_{td} P \sum_{i=1}^{\infty} n^K \frac{P_i}{V} \end{aligned} \quad (12.15)$$



TABLE 12.1 Simple Kinetic Mechanism for Free Radical Polymerization

Reaction Step	Kinetic Expression
Initiator decomposition	$I \xrightarrow{k_d} 2R$
First propagation	$R + M \xrightarrow{k_i} P_1$
Propagation	$P_n + M \xrightarrow{k_p} P_{n+1}$
Termination by disproportionation	$P_n + P_m \xrightarrow{k_{td}} D_n + D_m$

I is initiator; M , the monomer; R , the primary radicals; P_n , the living polymer of length n ; and D_m , the dead polymer of length m . (Note that it is also customary in the PRE literature to denote primary radicals as R_{in} or R_0 , living polymer as R_n^* and dead polymer as P_m).

which can subsequently be written as

$$\frac{d\mu_K}{dt} = \frac{k_i RM}{V} + k_p M \sum_{n=2}^{\infty} n^K \frac{P_{n-1}}{V} - k_p \frac{M \mu_K}{V} - k_{td} \frac{\mu_0 \mu_K}{V}, \\ K = 0, 1, 2, \dots \quad (12.16)$$

where the identity $\mu_0 = P = \sum_{n=1}^{\infty} P_n$ has been used. To write the second term on the right-hand side in terms of moments, a change of variable for the length subscript m is made, by setting: $m \equiv n - 1$, resulting in

$$\sum_{n=2}^{\infty} n^K P_{n-1} = \sum_{m=1}^{\infty} (m+1)^K P_m = \sum_{m=1}^{\infty} (m+1)^K P_m \quad (12.17)$$

Using the binomial theorem $(m+1)^K = \sum_{R=0}^K \binom{K}{R} m^{K-R}$ where the binomial coefficients are defined as

$$\binom{K}{R} = \frac{K!}{R!(K-R)!} \quad (12.18)$$

Equation 12.17 turns into Equation 12.19:

$$\begin{aligned} \sum_{n=1}^{\infty} n^K P_{n-1} &= \sum_{m=1}^{\infty} \sum_{R=0}^K \binom{K}{R} m^{K-R} P_m \\ &= \sum_{R=0}^K \sum_{m=1}^{\infty} \binom{K}{R} m^{K-R} P_m \\ &= \sum_{R=0}^K \mu_{K-R} \end{aligned} \quad (12.19)$$

Substituting this result into Equation 12.16, the final expression becomes

$$\frac{d\mu_K}{dt} = k_i \frac{RM}{V} + k_p M \sum_{R=0}^K \binom{K}{R} \frac{\mu_{K-R}}{V} - k_p M \frac{\mu_K}{V} \\ - k_{td} \frac{\mu_0 \mu_K}{V}, \quad K = 0, 1, 2, \dots \quad (12.20)$$

Applying the technique to Equation 12.11 for the dead polymer CLD, the result is

$$\sum_{n=1}^{\infty} n^K \frac{dD_n}{dt} = \frac{d \sum_{n=1}^{\infty} n^K D_n}{dt} = k_{td} P \sum_{i=1}^{\infty} n^K \frac{P_n}{V} \quad (12.21)$$

which is equivalent to

$$\frac{d\lambda_K}{dt} = k_{td} \frac{\mu_0 \mu_K}{V}, \quad K = 0, 1, 2, \dots \quad (12.22)$$

Expansion of the binomial coefficients in Equation 12 allows the derivation of one equation for each of the K th moments. The integration of Equations 12.20 and 12.22 for as many moments as required (usually the first three) yields information on the evolution of the CLD (or the associated MWD) in terms of its averages.

12.2.3 Bivariate Distributions

In some cases, it is necessary to use more than one subscript for the description of distributions in polymerization systems. One of such cases is the modeling of the bivariate distribution of chain length and number of branches resulting from polymerizations involving branched polymers. The extension of the method of moments to bivariate distributions is straightforward. Let us consider the bivariate distribution of live polymer of length n and number of branches b : $P_{n,b}$, for the sake of illustration of the method of moments, consider only the kinetic steps of propagation and transfer to polymer (see Table 12.2 for the reduced kinetic mechanism).

For a batch reactor, the application of the mass action law considering only these two kinetic steps results in

$$\begin{aligned} \frac{dP_{n,b}}{dt} &= \dots - k_p (P_{n,b} M + P_{n-1,b} M) \\ &\quad - k_{trp} P_{n,b} \left(\sum_{m=1}^{\infty} \sum_{c=0}^{\infty} m D_{m,c} \right) \\ &\quad + k_{trp} n D_{n,b-1} \sum_{h=1}^{\infty} \sum_{e=0}^{\infty} P_{h,e} + \dots, \\ n &= 1, \dots, \infty; b = 0, \dots, \infty \end{aligned} \quad (12.23)$$



TABLE 12.2 Reduced Kinetic Mechanism for Transfer to Polymer

Reaction Step	Kinetic Expression	
Propagation	$P_{n,b} + M \xrightarrow{k_p} P_{n+1,b}$	$n = 1, \dots, \infty$ $b = 0, \dots, \infty$
Transfer to polymer	$P_{n,b} + D_{m,c} \xrightarrow{k_{trp}} D_{n,b} + P_{m,c+1}$	$n, m = 1, \dots, \infty$ $b, c = 0, \dots, \infty$

Note that in the transfer to polymer reaction there are as many possible sites of reaction as monomeric units in the dead polymer chain participating in the reaction.

The bivariate moments for live and dead polymer are defined respectively as follows:

$$\mu_{G,H} = \sum_{n=1}^{\infty} \sum_{b=0}^{\infty} n^G b^H P_{n,b} \quad (12.24)$$

$$\lambda_{G,H} = \sum_{n=1}^{\infty} \sum_{b=0}^{\infty} n^G b^H D_{n,b} \quad (12.25)$$

From these definitions, the number and weight-average molecular weights, as well as the number average of branches can be written, respectively, as

$$M_n = \frac{\mu_{1,0} + \lambda_{1,0}}{\mu_{0,0} + \lambda_{0,0}} W_m \quad (12.26)$$

$$M_w = \frac{\mu_{2,0} + \lambda_{2,0}}{\mu_{1,0} + \lambda_{1,0}} W_m \quad (12.27)$$

$$B_n = \frac{\mu_{0,1} + \lambda_{0,1}}{\mu_{0,0} + \lambda_{0,0}} \quad (12.28)$$

The application of the method of moments to the live polymer requires the application of the summation operator defined by Equation 12.24 on both sides of Equation 12.23, resulting in

Left-hand side:

$$\sum_{n=1}^{\infty} \sum_{b=0}^{\infty} n^G b^H \frac{dP_{n,b}}{dt} = \frac{d \sum_{n=1}^{\infty} \sum_{b=0}^{\infty} n^G b^H P_{n,b}}{dt} = \frac{d\mu_{G,H}}{dt} \quad (12.29)$$

Right-hand side:

$$\dots - k_p M \mu_{G,H} + k_p M \sum_{n=1}^{\infty} \sum_{b=0}^{\infty} n^G b^H P_{n-1,b} \\ - k_{trp} \mu_{G,H} \lambda_{1,0} + k_{trp} \mu_{0,0} \sum_{n=1}^{\infty} \sum_{b=0}^{\infty} n^{G+1} b^H D_{n,b-1} + \dots \quad (12.30)$$

Some of the terms are directly written as a function of moments; for others, some algebraic manipulation is needed. The positive term for propagation can be treated using the change of variable $m \equiv n - 1$, as in the univariate case, resulting in

$$\begin{aligned} \sum_{n=1}^{\infty} \sum_{b=0}^{\infty} n^G b^H P_{n-1,b} &= \sum_{m=1}^{\infty} \sum_{b=0}^{\infty} b^H (m+1)^G P_{m,b} \\ &= \sum_{m=1}^{\infty} \sum_{b=0}^{\infty} \sum_{R=0}^G \binom{G}{R} m^{G-R} b^H P_{m,b} \\ &= \sum_{R=0}^G \binom{G}{R} \mu_{G-R,H} \end{aligned} \quad (12.31)$$

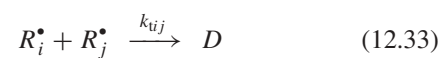
where the binomial theorem has already been applied. A similar change of variable ($r \equiv b - 1$) can be applied to the positive transfer to polymer term. The final result for the moment expression is

$$\begin{aligned} \frac{d\mu_{G,H}}{dt} &\dots - k_p M \mu_{G,H} + k_p M \sum_{R=0}^G \binom{G}{R} \mu_{G-R,H} \\ &- k_{trp} \mu_{G,H} \lambda_{1,0} + k_{trp} \mu_{0,0} \sum_{K=0}^H \binom{H}{K} \lambda_{G+1,H} + \dots \end{aligned} \quad (12.32)$$

Other kinetic steps can be treated in a similar manner.

12.2.4 Pseudo-Homopolymer Approach or Pseudokinetic Rate Constants Method (PKRCM)

In multimonomer polymerizations, the number of possible reactions increases rapidly with the number of monomers. For example, for the copolymerization of two monomers under the assumption of terminal model kinetics, four propagation steps must be considered (see Eq. 6.1). Similarly, for the termination step (chemically controlled), three reactions are possible:



where D stands for dead polymer and $k_{t12} = k_{t21}$.



When the MWD is to be modeled, there are two possibilities: (i) One is to use $c + 1$ subscripts for a c comonomer system, one for the radical type, and c for the number of monomer units of each type in the polymer chain. For example, $R_{1,r,m}$ could represent a type 1 radical having “ r ” monomer-1 units and “ m ” monomer-2 units already in the chain. The treatment for any number of monomers using this approach is possible via the method of moments or generating functions [6], but as the number of monomers increases, the algebra becomes more intricate. (ii) The second approach is to use only two subscripts, without regard to the number of monomers involved, one of the subscripts defining the monomer type and the second one defining the total number of units in the chain, regardless of their chemical nature. In this second case, and following the example given before, the quantity to be modeled would be $R_{1,q}$ ($q = r + m$). Although some information on the composition is lost using this approach, simple mass balances on each monomer (which are necessary anyways) can provide the evolution of the average composition with reaction time; the only information lost is the (stochastic) broadening of the composition distribution. Besides, if the chains are long, all the chains formed instantaneously will have similar composition.

The second approach implies that the MWD equations for a multicomponent monomer system are treated as those of a homopolymer. These ideas appeared in the literature under slightly different names but around the same period, when more researchers started studying copolymerization systems (e.g., Ballard et al. [20]). Hamielec’s group formalized this approach under the name of *pseudokinetic rate constants method* (PKRCM) and illustrated its use for linear, branched, and crosslinked copolymerization systems [21], as well as for batch, semibatch, and continuous reactors [22]. Ray’s group also made use of what they referred to as *apparent rate constants* [23]. The group of Morbidelli used a similar idea that they termed as *pseudo-homopolymer* approach [24].

Li et al. [25] validated the use of the PKRCM for the case of MMA/EGDMA (methyl methacrylate) with gelation. Tobita and Hamielec used this method to model gelling systems, at both the pre- and postgelation regimes [26]; they also showed that this method could be used equally well for copolymerization systems described by higher order Markov chain statistics such as the penultimate model [27]. Zabisky et al. used it to model olefin copolymerization in high pressure tubular reactors [28]. Finally, Xie and Hamielec further extensively evaluated the use of the PKRCM for the calculation of molecular weight development in linear [29] and nonlinear (with long-chain branching (LCB) [30]) copolymerization systems. Ever since the PKRCM has become a standard tool in PRE.

In any of the forms mentioned above, the approach requires the use of the long-chain hypothesis (LCH), which assumes that the monomer consumption is essentially due to propagation reactions and the quasisteady-state approximation (QSSA) for radicals, by virtue of which the rates of radical generation and consumption are instantaneously equated. The basis of the pseudo-homopolymer approach is introduced here using as an example of the modeling of the MWD for a multicomponent (c monomers) system, following the terminal model. Table 12.3 lists the kinetic mechanism for this system. In this table, P_i^n stands for polymeric radicals of type i and length n , and D^n is dead polymer of length n .

To describe the MWD for live polymer, mass balances for polymeric radicals are written:

$$\frac{dP_i^1}{dt} = k_i RM_i - P_i^1 \sum_{j=1}^c k_{pij} M_j - P_i^1 \sum_{m=1}^{\infty} \sum_{j=1}^c k_{ujj} P_j^m, \\ i = 1, \dots, c \quad (12.34)$$

$$\begin{aligned} \frac{dP_i^n}{dt} &= \sum_{j=1}^c k_{pj} P_j^{n-1} M_i - P_i^n \sum_{j=1}^c k_{pij} M_j \\ &\quad - P_i^n \sum_{m=1}^{\infty} \sum_{j=1}^c k_{ujj} P_j^m, \quad i = 1, \dots, c; \\ n &= 2, \dots, \infty \end{aligned} \quad (12.35)$$

Note that in this representation an equation is needed for each type of polymeric radical of a given length. By taking the summation of Equations 12.34 and 12.35 from $n = 1$ to ∞ , using the LCH and the QSSA (the time derivative is set to zero), and the definition $P_i = \sum_{n=1}^{\infty} P_i^n$, the result is

$$\sum_{j=1}^c k_{pj} P_j M_i = \sum_{j=1}^c k_{pj} P_j M_i, \quad i = 1, \dots, c \quad (12.36)$$

TABLE 12.3 Kinetic Mechanism for Molecular Weight Distribution in Multicomponent Copolymerization

Reaction Step	Kinetic Expression
Initiation	$I \xrightarrow{k_d} 2R$ $i = 1, \dots, c$
Propagation	$R + M_i \xrightarrow{k_i} P_i^1$ $i = 1, \dots, c$
	$P_i^n + M_j \xrightarrow{k_{pij}} P_i^{n+1}$ $j = 1, \dots, c$
	$n = 1, \dots, \infty$
Termination	$P_i^n + P_j^m \xrightarrow{k_{ujj}} D^{n+m}$ $i = 1, \dots, c$
	$n, m = 1, \dots, \infty$

Using the definition for the fraction of radical types,

$$P_i = \frac{[P_i]}{\sum_{j=1}^c [P_j]} \quad (12.37)$$

dividing Eq. 12.36 by the product $\sum_{j=1}^c [P_j] \sum_{j=1}^c [M_j]$, and expressing it in terms of p_i and f_i (mole fraction of monomer i), Equation 12.38 is finally obtained:

$$\sum_{j=1}^c k_{pji} p_j f_i = \sum_{j=1}^c k_{pij} p_i f_j \quad (12.38)$$

As discussed in Chapter 6 (see discussion of Equation 6.48, Section 6.3.6), only $c - 1$ out of the c equations represented by Equation 12.38 are linearly independent. An additional independent equation for the p_i terms is

$$\sum_{i=1}^c p_i = 1 \quad (12.39)$$

The solution of Equations 12.38 and 12.39 (which is a linear algebraic system for the p_i 's) provides the instantaneous radical-type distribution. Once a procedure to explicitly calculate this distribution has been made available, it is possible to apply the pseudo-homopolymer approach by performing the following steps:

1. By application of the ergodic hypothesis, by which the average radical type over the whole population of growing chains at a given instant is the same as the time average of the radical type of each growing chain, every instance of P_i^n (in Equations 12.34 and 12.35) is replaced by $P^n p_i$ ($n = 1, \dots, \infty$) where $P^n = \sum_{i=1}^c P_i^n$.
2. For each one of Equations 12.34 and 12.35, a summation over $i = 1, \dots, c$ is calculated.

The result on Equations 12.34 and 12.35 is, respectively,

$$\begin{aligned} \frac{dP^1}{dt} &= R \sum_{i=1}^c k_i M_i - P^1 \sum_{j=1}^c \sum_{i=1}^c k_{pji} p_i M_j \\ &\quad - P^1 \sum_{m=1}^{\infty} \sum_{i=1}^c \sum_{j=1}^c k_{uij} p_i p_j P^m \end{aligned} \quad (12.40)$$

$$\begin{aligned} \frac{dP^n}{dt} &= \sum_{i=1}^c \sum_{j=1}^c k_{pji} P^{n-1} p_j M_i - P^n \sum_{i=1}^c \sum_{j=1}^c k_{pji} p_i M_j \\ &\quad - P^n \sum_{m=1}^{\infty} \sum_{i=1}^c \sum_{j=1}^c k_{uij} p_i p_j P^m \end{aligned} \quad (12.41)$$

TABLE 12.4 Pseudokinetic or Apparent Rate Constants

Reaction	Apparent Rate Constant
Initiation	$\bar{k}_i = \sum_{i=1}^c f_i k_i$
Propagation	$\bar{k}_p = \sum_{i=1}^c \sum_{j=1}^c p_i f_j k_{pji}$
Termination	$\bar{k}_t = \sum_{i=1}^c \sum_{j=1}^c p_i p_j k_{uij}$

Finally, replacing M_i by $f_i M$, Equations 12.40 and 12.41 can be written as:

$$\begin{aligned} \frac{dP^1}{dt} &= RM \sum_{i=1}^c k_i f_i - \left(\sum_{j=1}^c \sum_{i=1}^c p_i f_j k_{pji} \right) P^1 M \\ &\quad - \left(\sum_{i=1}^c \sum_{j=1}^c p_i p_j k_{uij} \right) P^1 \sum_{m=1}^{\infty} P^m \end{aligned} \quad (12.42)$$

$$\begin{aligned} \frac{dP^n}{dt} &= \left(\sum_{i=1}^c \sum_{j=1}^c p_j f_i k_{pji} \right) P^{n-1} M \\ &\quad - \left(\sum_{i=1}^c \sum_{j=1}^c p_i f_j k_{pji} \right) P^n M \\ &\quad - \left(\sum_{i=1}^c \sum_{j=1}^c p_i p_j k_{uij} \right) P^n \sum_{m=1}^{\infty} P^m \end{aligned} \quad (12.43)$$

Note that by defining the terms in parenthesis as pseudokinetic or apparent rate constants (Table 12.4) Equations 12.42 and 12.43 are identical to those describing the MWD of the live polymer in a homopolymerization.

12.3 USEFUL TIPS ON POLYMER REACTION ENGINEERING (PRE) AND MODELING

These tips are useful so that one does not use mathematical equations (models) blindly. Almost anybody can write equations for reaction systems, especially these days with the proliferation of computer modeling and other numerical packages and tools. These practical tips will help make the input to and output from these equations more meaningful. Each tip can be considered independently of the others. However, put all of them together and one will see a beautiful "PRE painting." Several hints and food-for-thought questions/points will add more color to the picture. Instead of a title, each tip is related to several key words that provide an overview of the topic(s) covered under the specific tip.

Tip 1: Initiators, initiator data, and initiator decomposition. Several books on polymer science and engineering cite information about commercial initiators (decomposition rate constants, activation energies, and half-lives). It should be noted that these initiator data may not be accurate for a particular monomer–polymer system. Commercial manufacturers usually report initiator decomposition data determined in organic solvents (toluene or benzene). These values are, at best, starting values for certain kinetic parameters. Published initiator decomposition data measured in the specific monomer–polymer environment are very rare, if at all available.

Tip 2: Chain stereoregularity and active sites. In free radical polymerization, polymer chain configuration and MWD are often independent of initiator type and initiation mechanism, depending strongly on reaction temperature, initiation rate, and monomer concentration. One can, therefore, often predict chain stereoregularity and MWD without a detailed knowledge of the initiation mechanism.

This is usually not possible with ionic polymerization. Here, the modes of propagation, transfer, and termination reactions are influenced significantly by the initiation stage. For example, a heterogeneous coordination catalyst has reactive sites with a distribution of activities for propagation and produces a polymer with a very broad MWD. For polymer reactor calculations, it is sufficient to realize that there is a small but finite time for the development of active sites on addition of the ionic catalyst system to the monomer solution. The number of active sites remains relatively constant thereafter, with a slow reduction in number due to some site decay or poisoning. During calculations of polymer production rate (productivity) and molecular weights (quality), the number of active sites is usually introduced as an adjustable parameter in the reactor model.

Tip 3: Radical lifetime. The lifetime of a radical is of the order of 0.1–1 s. How can one calculate/verify this quickly? The number of monomer units added to a radical center per second is simply equal to the product ($k_p[M]$). Consider a typical value for k_p of 500 l/mol/s and a typical $[M]$ of 10 mol/l, yielding 5000 monomer units added to a radical in one second. Hence, a polymer chain with a molecular weight of 500,000 was a polymer radical for about one second, considering a typical molecular weight for a monomer to be 100 g/mol.

Tip 4: Chain microstructure and propagation reactions. Propagation reactions are mainly responsible for the development of polymer chain microstructure (and control chain composition and sequence length distribution in copolymerizations). In free radical polymerization, the stereoregularity of a high molecular weight homopolymer chain depends on polymerization temperature almost exclusively. It is usually independent of initiator type and monomer concentration. Calculations on stereoregularity

are not usually done for reactors producing polymers via radical polymerization. To achieve high degrees of regularity in chain microstructure, one must resort to ionic polymerizations.

Tip 5: Transfer reactions, branching, effects on molecular weight averages, and effects on polymerization rate. During free radical polymerization (in fact, with some slight changes in the mechanism, accordingly, in any chain growth polymerization), transfer reactions may take place between the growing radical and initiator (not often nowadays due to better understanding of the initiator molecule chemistry), monomer (an important reaction), solvent (if the solvent has labile hydrogens or halogens), impurity (often, but equally often neglected), chain transfer agent (CTA, usually the preferred transfer reaction for molecular weight reduction and control), any small molecule present in the polymerizing mixture and polymer (a large molecule). The last reaction essentially “resurrects” the usually “dead” polymer molecules and makes them behave as reactants again. The transfer radical usually reacts rapidly with monomer to generate a new radical.

These transfer reactions, with the exception of transfer to polymer, cause a shift in the MWD of the polymer to lower molecular weights. Transfer to (dead) polymer leads to (trifunctional) branching, causing a shift to higher molecular weights. Transfer to polymer does not change the total number of polymer molecules and hence the number-average molecular weight is unaffected. In contrast, the weight-average molecular weight increases appreciably, thus increasing molecular weight dispersity (polydispersity) as well. The number of labile atoms (hydrogens or chlorines) in a polymer chain is usually equal to the number of monomer units in the chain; therefore, the rate of transfer to polymer will be proportional to the mass of polymer (weight fraction of polymer in the polymerizing mixture) rather than to the number of polymer molecules. Transfer to polymer will be promoted at high conversion levels and will increase with temperature.

Transfer reactions do not change the total number of radicals in the mixture and therefore usually (ideally) do not influence the rate of polymerization (nor copolymer composition). However, there might be indirect effects on the rate (especially in systems with strong diffusional limitations, where a lowering of the rate may be observed with increased concentrations of CTA or solvent). If the transfer radicals have low activity, then retardation may be observed.

Tip 6 (related to Tip 5): Impurities, transfer to monomer, and terminal double bonds. The role of impurities should not be neglected, especially in emulsion/dispersion systems. See the case studies described in Penlidis et al. [31], Chien and Penlidis [32], and Dubé and Penlidis [33], for both homopolymerization and multicomponent polymerization systems, in both bulk/solution and emulsion. Transfer to

monomer is important in controlling the molecular weights of the polymer produced in many commercial polymerizations. The characteristic here is that the monomer radicals obtained from transfer to monomer, on propagation and, eventually, termination, will yield dead polymer chains having a terminal double bond (TDB) (this will have interesting repercussions to be discussed shortly; see Tips 8, 10, and 14).

Tip 7: Glass transition temperature, limiting conversion, methyl methacrylate polymerization, and depropagation. Special conditions are satisfied when the polymerization temperature is below the glass transition point of the polymer being synthesized. With increasing conversion of monomer, a point will be reached where the polymer-in-monomer mixture will become a “glass.” In a glass, even small molecules have low mobility and, for all practical purposes, polymerization rate will tend to zero (for typical polymerization time scales).

Hint 1. Observe conversion versus time data for the bulk polymerization of MMA at 70 °C. At a conversion level of about 90% the polymerization rate will be zero. The conversion versus time curve will “level off.” This will give the “limiting conversion.” The glass transition point (or temperature) of poly(MMA) is in the range of 105–110 °C and apparently a mixture of MMA with poly(MMA) containing 10% monomer has a glass transition point of 70 °C. A mixture containing about 80% poly(MMA) and 20% MMA exhibits a glass transition temperature of about 22.5 °C. One can thus construct a plot of polymerization temperature versus limiting conversion.

Hint 2. An increase in temperature will increase the limiting conversion. Following the MMA polymerization example, polymerizing isothermally at 80 °C will give a limiting conversion about 93%. At 100 °C, the limiting conversion will go up to about 97–98%. If the temperature is 120 °C, the polymerization will almost go to completion, that is, there is no limiting conversion (within experimental error).

Hint 3. We stated in Hint 2, following the MMA polymerization case, that if the polymerization temperature is 120 °C, conversion will “almost” go to completion (no limiting conversion). If temperature keeps on increasing, conversion will become lower. This is not a limiting conversion, but rather an upper “conversion limit” (a thermodynamic equilibrium limit, at that). This conversion limit is related to depropagation reactions (depolymerization). For case studies with depropagation, both in copolymerization and terpolymerization, and with experimental confirmations of mathematical modeling results, see Palmer et al. [34, 35], McManus et al. [36], and Leamen et al. [37, 38].

Food for thought. What temperature does one obtain from a plot of polymerization temperature versus limiting conversion (see Hint 1, Tip 7), if one extrapolate the curve to 100% conversion? In fact, the temperature estimate will

compete in accuracy with any such temperature determination from DSC (differential scanning calorimetry).

Tip 8: Terminal double bond polymerization. Transfer to monomer and termination by disproportionation lead to dead polymer molecules with a TDB. This TDB may react with a polymer radical, thus forming a radical center somewhere along the chain of the combined molecules. This radical center, on propagation with monomer, will eventually form a trifunctionally branched chain.

TDB polymerization reduces the number of dead polymer molecules. Therefore, it causes an increase in both number- and weight-average molecular weights. A practical corollary is that an isothermal batch polymerization yielding a number-average molecular weight that does not change with conversion would rule out the importance of TDB polymerization.

Tip 9: Radical stationary state hypothesis. A few practical steps to check for the validity of the (quasi-) stationary (steady-) state hypothesis (QSSH or simply SSH) for radicals are as follows: (i) determine the rate of change (with time) of the total radical concentration; (ii) find the maximum rate in (i); (c) divide (ii) by the rate of initiation; and (iv) if the ratio is much less than unity, the QSSH (or QSSA, A here stands for assumption) is valid.

Hint 1. One can plot the ratio versus conversion or crosslinker concentration or mole fraction of a comonomer or weight fraction of polymer, and observe how it behaves with respect to unity.

Hint 2. One can also check the ratio of the propagation rate constant over the termination rate constant, evaluated at different times (conversion levels). If this ratio is less than 0.001, then the QSSH is valid.

Food for thought. Does it make sense that we scrutinize the (k_p/k_t) ratio? Where else does this ratio appear (slightly modified) and why is it important for a polymerization?

Tip 10: Troubleshooting with molecular weight data and detection of branching. For an isothermal polymerization, a significant increase in (cumulative) weight-average molecular weight (\bar{M}_w) with conversion (and usually, a corresponding broadening of the MWD) can be the result of diffusion-controlled termination (with most of the chains produced by termination reactions; for an additional discussion on diffusion-control or “gel effect” issues, see Section 4.4.1), LCB reactions (transfer to polymer and/or TDB polymerization), or due to both classes of reactions occurring simultaneously as polymerization proceeds. How do you differentiate among these events?

One experimental approach that has proven to be effective is to measure \bar{M}_w (and plot it vs conversion) by size exclusion chromatography (SEC) or gel permeation chromatography (GPC) and light scattering (LS, usually, low angle laser light scattering, these days). For linear or branched polymer chains, LS gives the correct \bar{M}_w , while SEC/GPC

would underestimate \bar{M}_w , if the polymer chains were branched. Another fact to note is that diffusion-controlled termination and TDB polymerization cause the (cumulative) number-average molecular weight (\bar{M}_n) to increase with conversion, while transfer to polymer has no effect on \bar{M}_n .

Hint 1. Another way to check for the presence of LCB (and hence, reactions in the mechanism that give rise to LCB) is to add a previously synthesized relatively narrow MWD polymer sample (say, from low conversion levels) to its monomer and then initiate polymerization. The previously synthesized polymer will hopefully be clearly separated from the new polymer by SEC/GPC. If the previously synthesized polymer mode (GPC response) has shifted toward larger hydrodynamic volumes, then this is an indication for LCB (say, due to reactions with the backbone polymer molecules via transfer to polymer).

Hint 2. For a detailed discussion on the important topic of branching detection and determination, see Scorah et al. [39, 40].

Hint 3. Check also Tip 14.

Tip 11: Long-chain approximation, density/volume of polymerizing mixture, ideal vs diffusionaly limited kinetics. The long-chain approximation (LCA) is valid in polymerizations producing high molecular weight chains. In other words, monomer consumed in reaction steps other than propagation reactions is negligible in the calculation of total monomer consumption and polymer production rate.

The density of the polymerizing mixture increases with monomer conversion and hence the volume of the polymerizing mixture undergoes shrinkage. These form the bases of determining conversion via densitometry and dilatometry.

For isothermal cases, an “ideal” polymerization would show a decrease in polymerization rate with increasing conversion. This is hardly the picture in typical polymerizations due to diffusional limitations. A solution polymerization with a large volume fraction of solvent would tend to exhibit “ideal” polymerization kinetics.

Tip 12: Copolymerization, reactivity ratios, and estimation of reactivity ratios. In a binary copolymerization of monomers M_1 and M_2 , reactivity ratios r_1 and r_2 are important parameters for calculating polymerization rate, copolymer composition, and comonomer sequence length indicators (see Chapter 6 for basic equations and further information).

The tendency of two monomers to copolymerize is noted by the relative values of r_1 and r_2 . If r_1 is greater than 1, then the M_1 radical (i.e., radical ending in M_1 unit) preferentially adds M_1 over M_2 . If r_1 is less than 1, then the M_1 radical preferentially adds M_2 . An r_1 value very close to zero would indicate that M_1 is incapable of homopolymerizing.

The literature is full of values for reactivity ratios fraught with inconsistencies of varying degrees. When dealing with

reactivity ratio estimates, pay attention to the following points: (i) reactivity ratios are rather weak functions of temperature over typical polymerization temperature ranges and changes (emphasis on typical); (ii) use nonlinear regression techniques to estimate reactivity ratios (even better, use the error-in-variables model (EVM) nonlinear regression technique); (iii) reactivity ratios coming from linear regression (based on linearized models) are highly suspect (linear regression is simply incorrect to employ); they can, at best, be used as starting parameter values for the class of nonlinear regression techniques described, for example, in Polic et al. [41]; (iv) it is not only important to obtain point estimates for reactivity ratios but also estimates of their uncertainty in the form of joint confidence regions (contours); see again Polic et al. [41]; (v) the larger the difference between reactivity ratios (i.e., two widely differing reactivity ratio values would be 10 and 0.03, for example), the more interesting the comonomer system behavior will be (in terms of polymerization rate, copolymer composition, and molecular weights) and the trickier the reactivity ratio estimation problem is (from both perspectives of reliable experimental data collection and numerical estimation); see, for instance, Dubé et al. [42].

Tip 13 (related to Tip 12): Copolymerization, copolymer composition, composition drift, azeotropy, semibatch reactor, and copolymer composition control. Most batch copolymerizations exhibit considerable drift in monomer composition because of different reactivities (reactivity ratios) of the two monomers (same ideas apply to terpolymerizations and multicomponent cases). This leads to copolymers with broad chemical composition distribution. The magnitude of the composition drift can be appreciated by the vertical distance between two items on the plot of the instantaneous copolymer composition (ICC) or Mayo–Lewis (model) equation: item 1, the ICC curve (ICC or mole fraction of M_1 incorporated in the copolymer chains, F_1 , vs mole fraction of unreacted M_1 , f_1) and item 2, the 45° line in the plot of F_1 versus f_1 .

For example, in the absence of an azeotrope (the 45° line is the azeotropic line for which $F_1 = f_1$), and when M_1 is more reactive than M_2 (i.e., r_1 greater than 1 and r_2 less than 1), the ICC will decrease in M_1 with an increase in conversion. The extent of composition drift depends on the ratio (r_1/r_2), the initial monomer composition, and the monomer conversion level.

Hint 1. Plot F_1 versus f_1 in a batch copolymerization for different combinations of r_1 and r_2 and observe the composition drift. Is the direction of composition drift always the same? Are azeotropic points stable or unstable to small perturbations in monomer concentration?

Hint 2. One can also appreciate the composition drift picture by plotting the cumulative mole fraction of M_1 in the copolymer chains, \bar{F}_1 , versus conversion.

Food for thought. Another, yet equivalent, way of representing composition drift is to plot the mole fraction of copolymer chains (i.e., mole fraction of monomer incorporated (bound) into the copolymer) with composition in the range between F_{10} and F_{1x} versus F_1 . F_{10} is the initial mole fraction of M_1 in the copolymer, corresponding to f_{10} (the initial mole fraction of M_1 in the comonomer feed at time or conversion zero). F_{1x} is the copolymer composition at some conversion level x corresponding to f_1 . With some algebra and using the definition of conversion, what one is essentially plotting on the y-axis is the ratio (x/x_f) , where x_f is some final conversion level that one would like to achieve in the polymerization. The x-axis of the plot is F_1 . This plot is the cumulative copolymer composition distribution (CCD) and requires a combination of the ICC equation (relating F_1 to f_1) with the Meyer–Lowry equation (relating conversion x to f_1).

(Additional food for thought. What does the plot indicate if the curve one obtains is almost a vertical line?)

Hint 3. Semibatch or continuous reactors involve the continuous (over a certain period or periods of time) or intermittent flow of monomer (or other ingredients, like components of an initiator system, solvent or CTA) into the polymerizing mixture. This flow may in general have several beneficial effects, ranging from extra cooling to more flexibility for molecular weight and branching control, all the way to polymerization rate and composition control.

There are two basic monomer feed policies (and several modifications of the basic ones) that may be used in semibatch polymerization to minimize compositional drift (or optimize other properties). See Hamielec et al. [22] and Fujisawa and Penlidis [43] for more details.

Tip 14: Instantaneous vs cumulative properties, troubleshooting with molecular weight data. What differentiates polymerizations from conventional petrochemical processes (small molecules of the same molecular weight) is the existence of many distributional properties for the polymer product (copolymer composition or sequence length or molecular weight or branching or other property distribution). When a distributional property exists, we can make a distinction between an instantaneous (differential) property and a final, accumulated (or cumulative) property. The cumulative property is the accumulation (integration or sum) of instantaneous properties over a finite period of time or interval of conversion using as appropriate weights how many of the (chains) molecules (with the property in question) have been produced.

In batch polymerizations, we often find that the instantaneous molecular weights vary with time or conversion, and that the cumulative polymer product is made up of chains produced under a variety of conditions. This might be due to local variations or changes in temperature, monomer concentration, initiator concentration, or other recipe ingredient concentration.

Hint 1. If what controls the instantaneous MWD is independent of reaction time or conversion, then the final product will have the most probable (or Flory–Schulz) distribution with a molecular weight dispersity (polydispersity) of 2 (for isothermal operation).

Hint 2. Should transfer to monomer control the molecular weight development, then polymer (cumulative) molecular weight averages would be independent of monomer conversion for isothermal polymerizations. Poly(vinyl chloride) polymerization is an example of this case. Large variations in initiation rate will have little (or no detectable) influence on cumulative molecular weights. The product molecular weight dispersity (polydispersity) will be close to 2. In such a case, to produce a higher molecular weight polymer, we must lower the polymerization temperature (there is no other effective alternative). In fact, in the absence of a CTA, \bar{M}_n and \bar{M}_w depend only on temperature and will be the same in all process types (e.g., bulk, suspension, etc.) and reactor types (e.g., batch, continuous, etc.) operating at the same temperature level.

Hint 3. A considerable increase in number-average molecular weight with conversion is mainly due to TDB polymerization. It is of great interest to compare the growth of the (cumulative) weight-average molecular weight (\bar{M}_w) due to LCB and its growth due to diffusion-controlled termination reactions. With diffusion control, an explosive growth in \bar{M}_w occurs at lower conversions. \bar{M}_w varies almost linearly with conversion but eventually the change decelerates at high conversions or near complete conversion. With LCB (transfer to polymer and TDB polymerization), on the other hand, the growth in \bar{M}_w is initially rather gradual, but \bar{M}_w continues to grow at an accelerated rate in mid- to high conversions, approaching almost infinite molecular weight values at near complete conversion. These observations are useful and practical in differentiating between different events (see also Tip 10).

Tip 15: Expressions for rate of polymerization. The expression for the rate of chain growth polymerization in homogeneous (single phase) polymerization systems (e.g., regular bulk/solution) is given by (for the free radical case)

$$R_p = k_p[M][R] \quad (12.44)$$

R_p is the rate of polymerization (rate of monomer consumption) in moles per liter per second, k_p is the propagation rate constant in liters per mole per second, $[M]$ is the monomer concentration at the reaction site in moles per liter, and $[R]$ is the total concentration of radicals (indicated as P in Section 12.2.1) in moles per liter.

Duality between processes in general tells us that we can express the rates of many other polymerizations in an analogous way, as long as we evaluate the variables involved properly, based on the polymerization at hand. For instance, for anionic polymerization, the general expression

in Equation 12.44 is the same, with $[R]$ being replaced by $[LE]$, the concentration of living ends.

For regular emulsion polymerization (or often referred to as macroemulsion, a heterogeneous multiphase system), a widely used expression for the rate is

$$R_p = k_p [M_p] \frac{(N_p n)}{N_A} \quad (12.45)$$

$[M]$ in Equation 12.44 has been replaced by $[M_p]$ in Equation 12.45. This makes sense, since the monomer concentration that “feeds” the radicals in emulsion polymerization (at the appropriate reaction site) is indeed the monomer concentration in the polymer (latex) particles. Since $[R]$ in Equation 12.44 represents total radical concentration, it has been replaced by the product $(N_p n)$, which represents the total number of radicals present at the reaction site (the main locus of polymerization, which is inside the monomer-swollen polymer particles). N_p is the total number of particles (usually per lit of water) and n represents the average number of radicals per particle. N_A , Avogadro’s number, appears in the equation simply for unit conversion. Needless to say, Equation 12.45 is completely analogous to Equation 12.44.

Hint. Use Equation 12.44 and try to “fit” other types of polymerizations into the general polymerization rate formula. How about suspension polymerization? How about precipitation-type polymerization? How about Ziegler–Natta polymerizations? How about controlled radical polymerizations (CRPs)?

Food for thought. Consider emulsion polymerization again, but now one is interested in describing the rate of polymerization in the water (aqueous) phase only. Are we going to use Equation 12.44 or 12.45? How are we going to modify the terms involved and where are the different concentrations going to be evaluated at?

Tip 16: Polymerization of methyl methacrylate, styrene, and vinyl acetate. MMA, when polymerized, exhibits termination by both combination and disproportionation (in fact, disproportionation is promoted at higher temperatures). Termination by disproportionation leads to the formation of radicals and, eventually, polymer molecules with a TDB. We also know that TDBs will become competitive with the monomer vinyl bonds for radicals as conversion increases. TDB polymerization (characterized by rate constants close (in value) to propagation rate constants) leads to trifunctional LCB. Yet, upon analysis, poly(MMA) chains are linear. How come? What is the explanation/reasoning for this observation? We also know that styrene terminates predominantly via combination. Styrene also exhibits transfer to monomer, which is enhanced at higher temperature levels. Transfer to monomer generates chains with TDBs. Yet, polystyrene is linear. What is the explanation?

Vinyl acetate, another common monomer, is known for producing polymer with high levels of LCB. There might be several independent reasons for this outcome. What are these reasons? Which event contributes more to branching formation?

Tip 17: Termination in homopolymerization and copolymerization, initiation rate in homopolymerization, and copolymerization. Cope with the statement: “Termination reactions are almost always diffusion-controlled right from the outset of polymerization.” *Food for thought (and additional investigation).* How important is the chain length dependence of the termination rate constant in polymer reactor modeling?

Cope with the statement: “In copolymerization, the chemically controlled termination rate constant (i.e., the termination rate constant at time or conversion zero; in essence, the value at very low conversion levels) is a function of both temperature (albeit, weak) and comonomer composition.”

Food for thought. Can one show that in copolymerization (two types of radicals) the initiation rate is given by the exact same expression as in homopolymerization, that is,

$$R_I = 2 f k_d [I] \quad (12.46)$$

R_I represents initiation rate (units of any rate expression), f is the initiator efficiency factor, k_d is the initiator decomposition rate constant (per second), and $[I]$ is the initiator concentration in moles per liter.

Therefore, the expression for the total radical concentration is exactly the same as in homopolymerization.

Tip 18: Internal double bond polymerization. We know that transfer to polymer and TDB polymerization produce trifunctional (long) branches, in addition to increasing the weight-average molecular weight and broadening the MWD (see also Tips 5 and 8). A reaction “similar” to TDB polymerization is the polymerization with internal (pendant) double bonds [double bonds “internal” in dead polymer chains, appearing therein due to (co)polymerization of di-functional (divinyl) monomers (e.g., buta-di-ene)]. Internal double bond (IDB) polymerization produces tetrafunctional (long) branches and leads eventually to the formation of crosslinked polymer (gel). Needless to say, both molecular weight averages increase due to IDB polymerization and the MWD broadens considerably.

In general, monomer addition to a backbone radical center (“internal radical” as opposed to a radical center at the end of a chain) leads to the formation of trifunctional branch points. In addition, b-scission at backbone radical centers can also produce polymer chains with TDBs. IDB polymerization leads to the formation of tetrafunctional branch points. In addition, termination by combination of two backbone radicals also leads to the formation of a tetrafunctional branch point (crosslinking again, leading to

the production of crosslinked gel, i.e., polymer molecules effectively insoluble and hence, of infinite molecular weight due to their interconnected network structure), but swellable by an appropriate solvent (which is a good solvent for the corresponding linear chains or sol).

Tip 19: Intramolecular chain transfer, backbiting, and short-chain branching. Backbiting reactions (intramolecular chain transfer) can account for the high short-chain branching (SCB) frequencies (and often for the excess methyl groups in polymer chains, above and beyond the expected number of end groups). This type of chain transfer is believed to occur by a backbiting reaction between the radical on the terminal carbon atom and a hydrogen atom located on the same chain but five or six carbon atoms away from the radical center (i.e., the radical end “curls” backward and abstracts a hydrogen, thus forming a SCB). This SCB formation is important when studying the kinetics of high pressure low density poly(ethylene), poly(vinyl chloride), and poly(butyl acrylate) at high temperatures.

Tip 20: Polymerization heat effects and energy balances. Polymerizations are highly exothermic reactions. The higher the rate of polymerization, the higher the instantaneous heat generation rate (heat release), and, in principle, the higher the productivity. The main limitation in productivity will be the heat removal rate (i.e., limitations in reactor cooling capabilities). Permitting a temperature increase during polymerization gives higher productivity. The highest productivity could be obtained using adiabatic polymerization (no heat removal from the reactor). However, adiabatic temperature rises are excessive (hence, a very broad MWD with a low molecular weight tail would be obtained) and, hence, the need for good temperature control and/or optimal temperature programming (see also Chapter 13 for more details on energy balances and related model equations). An approximate calculation of the adiabatic temperature rise for bulk (mass) polymerization of styrene would give 300–350 °C. This temperature rise would be much smaller in emulsion or suspension or solution, due to the presence (and high heat capacity) of the water or solvent. The high polymerization heat release allows one to monitor monomer conversion (online or offline) by exploiting reliable heat balances around a reactor and its jacket.

To run a batch reactor at its optimum (minimum) batch time, the heat generation rate at any point during polymerization should equal the heat removal rate, with some allowance for a safety factor. This would translate to a monomer conversion profile varying almost linearly with time.

Heat removal is most commonly achieved through jacket cooling, but with large reactors, additional heat removal sources may be employed, such as reflux condensers, internal cooling coils, etc.

Hint 1. The overall heat transfer coefficient can fall significantly during polymerization (viscosity increase of the polymerizing mixture and scale formation (polymer build-up) on the reactor walls).

Hint 2. As a reactor increases in size, the available heat transfer area (via its walls) increases with reactor volume raised to the 0.67 power. On the other hand, the heat generation rate is proportional to reactor volume raised to the first power.

Hint 3. When heat removal is through reactor walls, it is unsafe to polymerize at temperature levels where the derivative of the heat generation rate becomes large (since in such a case, a very small increase in temperature would require a large decrease in heat transfer fluid temperature in order to avoid a reactor thermal runaway).

Hint 4. In many cases, polymer molecular weights are largely independent of polymerization rate because transfer reactions control (or may be made to control, via the use of a CTA) molecular weight averages and/or other polymer quality indicators. Temperature gradients (and/or “hot spots” in the polymerizing mixture) could in general lead to polymer quality deterioration (as manifested by uncontrolled broadening of the MWD).

Hint 5. In general, it is possible to operate a CSTR at a higher production rate than a comparable batch (or tubular) process (the beneficial effect of cold inlet (monomer) feed allows for a higher specific polymerization rate than in batch). Typical calculations with the energy balance equations of Chapter 13 would indicate that for the same operating conditions, one can run a CSTR at about twice the rate of a batch reactor of the same volume (and heat removal capacity).

Hint 6. In polymer reactor design, polymerization temperature is most often dictated by desired specifications on polymer molecular weight and distribution, rather than polymerization rate.

Tip 21: Crosslinking, gelation, gel formation, and sol versus gel. Experimental data clearly show that once gel (insoluble polymer network, crosslinked polymer) is formed, it grows very rapidly at the expense of the soluble polymer chains (soluble part or sol). Gel acts like a “sponge,” “sucking” in the (linear) polymer chains from the sol. Radical centers located on polymer chains in the gel are longer lived, because of their greatly reduced mobility. These radical centers terminate mainly by reaction diffusion. The greatly reduced termination rates of radical centers located on chains in the gel result in a very high concentration of these radical centers, and this in part is the cause of the rapid growth of gel at the expense of the sol. The more active (reactive) the double bonds bound in copolymer chains, and the greater the number of these double bonds, then the onset of gelation occurs at lower monomer conversion levels. At the same time, the more transfer to a small molecule (such as monomer or CTA),

the further in conversion is the onset of gelation (i.e., a more delayed onset of gelation is observed).

Hint 1. The cumulative number-average molecular weight will increase (sometimes only slightly at higher conversions) with increasing monomer conversion, but it will remain finite. The number-average molecular weight increases with increasing reactivity of pendant double bonds because of the decrease in the total number of dead polymer chains due to the crosslinking reactions. On the other hand, higher order molecular weight averages (weight- and z -average) will increase significantly with increasing monomer conversion and will eventually diverge at the gelation point (i.e., go to infinity). Overall, the molecular weight development of crosslinking copolymerizations is very sensitive to the reactivity of pendant double bonds. If the reactivity of pendant double bonds is assumed to be the same as that of the divinyl monomer (crosslinker), then higher order molecular weight averages will likely be overestimated.

Hint 2. More details on crosslinking systems and their mathematical modeling are given in Section 12.4 and also in Chapter 9.

12.4 EXAMPLES OF SEVERAL FREE RADICAL (CO)POLYMERIZATION SCHEMES AND THE RESULTING KINETIC AND MOLECULAR WEIGHT DEVELOPMENT EQUATIONS

12.4.1 Modeling Linear and Nonlinear Homo- and Copolymerizations Assuming Monofunctional Polymer Molecules and Using the PKRCM

The modeling of homopolymerization as well as linear and nonlinear (chain transfer to polymer and crosslinking) copolymerizations can be represented with the same polymerization scheme shown in Figure 12.1. The kinetic

equations obtained from this polymerization scheme are shown in Figures 12.2 and 12.3.

I , M , T , R_{in}^* , P_r , and D_r in Figures 12.1–12.3 are initiator, monomer, small molecule (e.g., a CTA, an inhibitor, etc.), primary free radicals, polymer radicals, and dead polymer, respectively. (Note that P_r , D_r , and p_i (fraction of radicals type “ i ”) as defined in this chapter are usually termed R_r^* , P_r , and ϕ_i^* in most of the papers from Hamielec’s group). k_d , k_i , k_p , k_{tc} , k_{td} , k_{fT} , k_{fp} , and k_p^{*0} are pseudokinetic rate constants for initiator decomposition, first propagation step (part of the initiation reaction), propagation, termination by combination, termination by disproportionation, transfer to a small molecule T , transfer to polymer, and intrinsic crosslinking (propagation through pendant double bonds). The pseudokinetic rate constants are defined below, in Table 12.5. k_{cp} and k_{cs} represent primary and secondary cyclizations, respectively. Y_i and Q_i are i th-order moments for living and dead polymer populations, respectively (denoted by μ_K and λ_K in the nomenclature of Section 12.2).

By proper selection of initial conditions or parameter values, the equations of Figures 12.2 and 12.3 can represent linear homopolymerization, linear copolymerization, or nonlinear copolymerization. Examples for the specific case of conventional (noncontrolled) copolymerization with crosslinking can be found in Vivaldo-Lima et al. [44–46]. As a matter of fact, the simulation profiles for homogeneous linear copolymerization of TFE and VAc in supercritical carbon dioxide (sc-CO₂) shown in Chapter 15 (Fig. 15.6) were obtained with this model by setting $k_p^{*0} = k_{cs} = k_{cp} = 0$. So was the case of the heterogeneous linear homopolymerization of MMA in sc-CO₂, also addressed in Chapter 15 (Figs 15.7, 15.8, and 15.9), and copolymerization with crosslinking in sc-CO₂ (Fig. 15.10). The only change in those heterogeneous cases was that additional equations

Initiation	$I \xrightarrow{k_d} 2R_{in}^*$ $R_{in}^* + M \xrightarrow{k_i} P_1$
Propagation	$P_r + M \xrightarrow{k_p} P_{r+1}$
Propagation through double pendant bonds (Crosslinking)	$P_r + D_s \xrightarrow{k_p^{*0}} P_{r+s}$
Transfer to small molecule “ T ”	$P_r + T \xrightarrow{k_{fT}} D_r + T^\bullet$
Transfer to polymer	$P_r + D_s \xrightarrow{k_{fp}} D_r + P_s$
Termination by disproportionation	$P_r + P_s \xrightarrow{k_{td}} D_r + D_s$
Termination by combination	$P_r + P_s \xrightarrow{k_{tc}} D_{r+s}$

Figure 12.1 Polymerization scheme for nonlinear copolymerization with crosslinking under PKRCM and monofunctional polymer molecules.

Initiator consumption	$\frac{d[I]}{dt} = -k_d [I]; R_i = 2 f k_d [I]$
Overall monomer consumption	$\frac{d[M]}{dt} = -k_p [M] [P]; \frac{dx}{dt} = k_p [P] (1-x)$
Small molecule consumption	$\frac{d[T]}{dt} = -k_{fT} [T] [P]$
Monomer composition	$\frac{df_i}{dt} = \frac{f_i - F_i}{1-x} \frac{dx}{dt}, i = 1, 2, \dots, N$
Instantaneous copolymer composition	$F_j = \frac{\sum_{i=1}^N k_{ij} p_i f_i}{k_p}, N = \text{number of monomers}$
Accumulated copolymer composition	$\bar{F}_j = \frac{f_{j0} - f_j (1-x)}{x}$
Crosslink density	$\frac{d[x \rho_a]}{dt} = \frac{k_p^* [\bar{F}_2 (1 - k_{cp} - \bar{\rho}_a (1 + k_{cs}))] x}{k_p (1-x)} \frac{dx}{dt}$

Figure 12.2 Kinetic equations for small molecules, copolymer composition, and average additional crosslinking density derived from the polymerization scheme of Figure 12.1.

- Mass balance for polymer radicals:

$$\begin{aligned} \frac{d[P_r]}{dt} &= R_i - k_{fT}[T][P_r] - (k_{tc} + k_{td})[P_r][P] + k_p[M]\{[P_{r-1}] - [P_r]\} \\ &\quad - (k_{fp} + k_{p}^*)[P_r]Q_1 + k_{fp}Y_0rD_r + k_p^*\sum_{s=1}^{r-1}s[D_s][P_{r-s}] \end{aligned}$$

- Mass balance for dead polymer:

$$\begin{aligned} \frac{d[D_r]}{dt} &= k_{td}[P_r][P] + k_{fT}[T][P_r] + \frac{1}{2}k_{tc}\sum_{s=1}^{r-1}[P_s][P_{r-s}] - (k_{fp} + k_p^*)Y_0r[D_r] \\ &\quad + k_{fp}[P_r]Q_1 + k_p^*\sum_{s=1}^{r-1}[P_{r-s}]s[D_s] \end{aligned}$$

Figure 12.3 Kinetic equations for living and dead polymer molecules derived from the polymerization scheme of Figure 12.1.

had to be used for partition of components among the phases.

12.4.2 Modeling Linear and Nonlinear Homo- and Copolymerizations Assuming Multifunctional Polymer Molecules and Using the PKRCM

In Section 12.2.4, it was mentioned that one possibility to address the calculation of the MWD in copolymerization systems was to use $c + 1$ subscripts for a c comonomer

TABLE 12.5 Pseudokinetic Rate Constants (Pseudo-Homopolymer Approach)

Propagation	$k_p = \sum_{i=1}^3 \sum_{j=1}^2 k_{ij} \phi_i^* f_i$
Propagation through pendant double bonds (crosslinking)	$k_p^* = \sum_{i=1}^3 k_{i3p}^* \phi_i^* (\bar{F}_2 - \bar{\rho}_a - \bar{\rho}_c)$
Transfer to a small molecule	$k_{fT} = \sum_{i=1}^3 k_{fTi} \phi_i^*$
Transfer to polymer	$k_{fp} = \sum_{i=1}^3 \sum_{j=1}^2 k_{fp(i,j)} \phi_i^* \bar{F}_j$
Termination by disproportionation	$k_{td} = \sum_{i=1}^3 \sum_{j=1}^3 k_{td(i,j)} \phi_i^* \phi_j^*$
Termination by combination	$k_{tc} = \sum_{i=1}^3 \sum_{j=1}^3 k_{tc(i,j)} \phi_i^* \phi_j^*$

system, one for the radical type, and c for the number of monomer units of each type in the polymer chain. When one deals with bivariate (e.g., MWD and CCD) or multivariate (e.g., MWD, CCD, and distribution of branching and crosslinking points), one approach is to use polymer molecules with several subscripts. In the treatment of copolymerization of vinyl/divinyl monomers in the presence of nitroxide-mediated radical polymerization

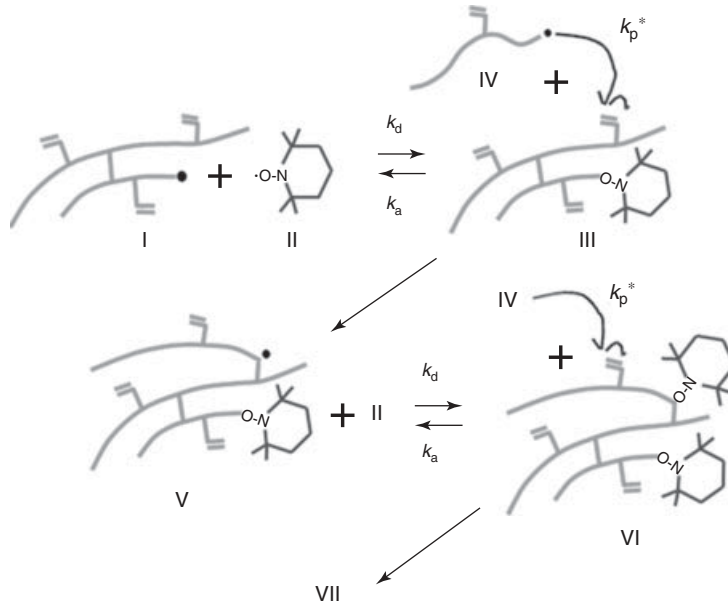


Figure 12.4 Polymer species formed from crosslinking and activation/deactivation reactions in NMRP of vinyl/divinyl monomers. Source: Reprinted with permission from Hernández-Ortiz JC, Vivaldo-Lima E, Lona LMF, McManus NT, Penlidis A. Macromol React Eng 2009;3:288 [48]. Copyright 2009 Wiley-VCH Verlag GmbH & Co. KGaA, Weinheim.

(NMRP) type of controllers, which is one case of CRP (see Chapter 4 for background on CRP and NMRP), Hernández-Ortiz et al. [47] used a multidimensional type of approach. Instead of using subscripts for every monomer type (multicomponent copolymerization), as mentioned in Section 12.2.4, they used three subscripts to count the number of total monomer units, total number of active (free radical) centers, and total number of dormant centers, namely, they have dealt with a “multifunctional” type of model.

Figure 12.4 shows a schematic representation of the system studied by Hernández-Ortiz et al. [47, 48]. The polymerization scheme for that case is listed in Table 12.6. On the basis of that polymerization scheme, the kinetic equations summarized in Table 12.7 and Equation 12.46 were derived. The pseudokinetic rate constants used are summarized in Table 12.8. The reader is referred to the paper by Hernández-Ortiz et al. [47] for more details. What is interesting here is to point out, as listed in Table 12.9, that simpler cases can be adequately described by simplifying that complex model:

$$\begin{aligned} \frac{1}{V} \frac{d(V[P_{m,r,d}])}{dt} \\ = k_p [M] r [P_{m-1,r,d}] - k_p [M] r [P_{m,r,d}] \\ + k_{da} (r+1) [P_{m,r+1,d-1}] [\bullet ON_x] - k_{da} r [P_{m,r,d}] [\bullet ON_x] \\ + k_a (d+1) [P_{m,r-1,d+1}] - k_a d [P_{m,r,d}] \end{aligned}$$

$$\begin{aligned} & + k_{td} (r+1) [P_{m,r+1,d}] \sum_{n=1}^{\infty} \sum_{s=1}^{\infty} \sum_{e=0}^{\infty} s [P_{n,s,e}] \\ & - k_{td} r [P_{m,r,d}] \sum_{n=1}^{\infty} \sum_{s=1}^{\infty} \sum_{e=0}^{\infty} s [P_{n,s,e}] \\ & + \frac{1}{2} k_{tc} \sum_{n=1}^{m-1} \sum_{s=1}^r \sum_{e=0}^d (s+1)(r-s+1) [P_{n,s+1,e}] \\ & \times [P_{m-n,r-s+1,d-e}] \\ & - k_{tc} r [P_{m,r,d}] \sum_{n=1}^{\infty} \sum_{s=1}^{\infty} \sum_{e=0}^{\infty} s [P_{n,s,e}] \\ & + \frac{1}{2} k_p^* \sum_{n=1}^{m-1} \sum_{s=1}^r \sum_{e=0}^d (s)(m-n) [P_{n,s,e}] [P_{m-n,r-s,d-e}] \\ & - k_p^* r [P_{m,r,d}] \sum_{n=1}^{\infty} \sum_{s=1}^{\infty} \sum_{e=0}^{\infty} n [P_{n,s,e}] \\ & + \frac{1}{2} k_p^* \sum_{n=1}^{m-1} \sum_{s=1}^r \sum_{e=0}^d (n)(r-s) [P_{n,s,e}] [P_{m-n,r-s,d-e}] \\ & - k_p^* m [P_{m,r,d}] \sum_{n=1}^{\infty} \sum_{s=1}^{\infty} \sum_{e=0}^{\infty} s [P_{n,s,e}] \\ & + k_{fp} (r+1) [P_{m,r+1,d}] \sum_{n=1}^{\infty} \sum_{s=1}^{\infty} \sum_{e=0}^{\infty} n [P_{n,s,e}] \end{aligned}$$

$$\begin{aligned}
& -k_{fp}r [P_{m,r,d}] \sum_{n=1}^{\infty} \sum_{s=1}^{\infty} \sum_{e=0}^{\infty} s [P_{n,s,e}] \\
& + k_{fp}m [P_{m,r-1,d}] \sum_{n=1}^{\infty} \sum_{s=1}^{\infty} \sum_{e=0}^{\infty} n [P_{n,s,e}] \\
& - k_{fp}m [P_{m,r,d}] \sum_{n=1}^{\infty} \sum_{s=1}^{\infty} \sum_{e=0}^{\infty} s [P_{n,s,e}] \\
& + k_{fm}(r+1) [P_{m,r+1,d}] [M] - k_{fm}r [P_{m,r,d}] [M] \\
& + k_{fd}(r+1) [P_{m,r+1,d}] [D] - k_{fd}r [P_{m,r,d}] [D] \\
& + k_{fin}(r+1) [P_{m,r+1,d}] [I] - k_{fin}r [P_{m,r,d}] [I] \\
& + k_{fs}(r+1) [P_{m,r+1,d}] [S] - k_{fs}r [P_{m,r,d}] [S] \\
& + k_{decomp}(d+1) [P_{m,r,d+1}] - k_{decomp}d [P_{m,r,d}]
\end{aligned} \tag{12.47}$$

TABLE 12.6 Elementary Reactions in the Nitroxide-Mediated Radical Copolymerization of Vinyl/Divinyl Monomers

Process	Equation
Initiator decomposition	$I \xrightarrow{k_d} 2R_{in}$
Dimerization	$M + M \xrightarrow{k_{dim}} D$
Thermal initiation	$M + D \xrightarrow{k_{thi}} P_{1,1,0} + D^\bullet$
<i>First Propagation</i>	
Primary radicals	$M + R_{in} \xrightarrow{f k_i} P_{1,1,0}$
Dimeric radicals	$M + D^\bullet \xrightarrow{k_i} P_{1,1,0}$
Solvent radicals	$M + S^\bullet \xrightarrow{k_i} P_{1,1,0}$
Propagation	$P_{m,r,d} + M \xrightarrow{(r)k_p} P_{m+1,r,d}$
<i>Reversible Deactivation of</i>	
Primary radicals	$R_{in} + \cdot ON_x \xrightleftharpoons[k_{a3}]{k_{da3}} R_{in}ON_x$
Dimeric radicals	$D^\bullet + \cdot ON_x \xrightleftharpoons[k_{a3}]{k_{da3}} DON_x$
Solvent radicals	$S^\bullet + \cdot ON_x \xrightleftharpoons[k_{a3}]{k_{da3}} SON_x$
Polymer radicals	$P_{m,r,d} + \cdot ON_x \xrightleftharpoons[(d+1)k_a]{(r)k_{da}} P_{m,r-1,d+1}$
<i>Chain Transfer to</i>	
Initiator	$P_{m,r,d} + I \xrightarrow{(r)k_{fi}} P_{m,r-1,d} + R_{in}$
Monomer	$P_{m,r,d} + M \xrightarrow{(r)k_{fm}} P_{m,r-1,d} + P_{1,1,0}$
Dimer	$P_{m,r,d} + D \xrightarrow{(r)k_{fd}} P_{m,r-1,d} + D^\bullet$
Solvent	$P_{m,r,d} + S \xrightarrow{(r)k_{fs}} P_{m,r-1,d} + S^\bullet$
Polymer	$P_{m,r,d} + P_{n,s,e} \xrightarrow{(rn)k_{fp}} P_{m,r-1,d} + P_{n,s+1,e}$
Propagation with pendant double bound	$P_{m,r,d} + P_{n,s,e} \xrightarrow{(rn)k_{p*}} P_{m+n,r+s,d+e}$
Termination by disproportionation	$P_{m,r,d} + P_{n,s,e} \xrightarrow{(rs)k_{td}} P_{m,r-1,d} + P_{n,s-1,e}$
Termination by combination	$P_{m,r,d} + P_{n,s,e} \xrightarrow{(rs)k_{tc}} P_{m+n,r+s-2,d+e}$
Dimer proton abstraction by nitroxide	$D + \cdot ON_x \xrightarrow{k_h3} D^\bullet + HON_x$
Alkoxyamine decomposition	$P_{m,r,d} \xrightarrow{(d)k_{decomp}} P_{m,r,d-1} + HON_x$
Addition of nitroxide to monomer	$M + \cdot ON_x \xrightarrow{k_{INO}} P_{1,1,0}$
Promoted dissociation of BPO	$I + \cdot ON_x \xrightarrow{k_{pr}} R_{in} + B + N$

Source: Adapted with permission from Hernández-Ortiz JC, Vivaldo-Lima E, Penlidis A. Macromol Theory Simul 2012;21:302 [47]. Copyright 2012 Wiley-VCH Verlag GmbH & Co. KGaA, Weinheim.

TABLE 12.7 Balance and Moment Equations in the Nitroxide-Mediated Radical Copolymerization of Vinyl/Divinyl Monomers

Component	Equation
Chemical initiator	$\frac{1}{V} \frac{d(V[I])}{dt} = -k_d[I] - k_{fin}Y_{010}[I] - k_{pr}[I][\bullet ON_x]$
Monomer conversion	$\frac{dx}{dt} = 2k_{dim}[M]_0(1-x)^2 + k_{thi}[D](1-x) + k_i([R_{in}] + [D^\bullet] + [S^\bullet])(1-x)$ $+ (k_p + k_{fm})(1-x)Y_{010} + k_{INO}[\bullet ON_x](1-x)$
Dimer	$\frac{1}{V} \frac{d(V[D])}{dt} = k_{dim}[M]^2 - k_{thi}[M][D] - k_{fd}Y_{010}[D] - k_{h3}[D][\bullet ON_x]$
Solvent	$\frac{1}{V} \frac{d(V[S])}{dt} = -k_{fs}Y_{010}[S]$
Primary radical	$\frac{1}{V} \frac{d(V[R_{in}])}{dt} = 2fk_d[I] - k_i[R_{in}][M] + k_{fin}Y_{010}[I] + fk_{pr}[I][\bullet ON_x] - k_{da3}[R_{in}][\bullet ON_x] + k_{a3}[R_{in}ON_x]$
Dimer radical	$\frac{1}{V} \frac{d(V[D^\bullet])}{dt} = k_{thi}[D][M] - k_i[M][D^\bullet] + k_{fd}Y_{010}[D] + k_{h3}[D][NO_x] - k_{da3}[D^\bullet][\bullet ON_x] + k_{a3}[DON_x]$
Solvent radical	$\frac{1}{V} \frac{d(V[S^\bullet])}{dt} = -k_i[M][S^\bullet] + k_{fs}Y_{010}[S] - k_{da3}[S^\bullet][\bullet ON_x] + k_{a3}[SON_x]$
Dormant primary radical	$\frac{1}{V} \frac{d(V[R_{in}ON_x])}{dt} = k_{da3}[R_{in}][\bullet ON_x] - k_{a3}[R_{in}ON_x]$
Dormant dimer radical	$\frac{1}{V} \frac{d(V[DON_x])}{dt} = k_{da3}[D^\bullet][\bullet ON_x] - k_{a3}[DON_x]$
Dormant solvent radical	$\frac{1}{V} \frac{d(V[SON_x])}{dt} = k_{da3}[S^\bullet][\bullet ON_x] - k_{a3}[SON_x]$
Nitroxyl radical	$\frac{1}{V} \frac{d(V[\bullet ON_x])}{dt} = k_aY_{001} - k_{da}Y_{010}[\bullet ON_x] + k_{a3}([R_{in}ON_x] + [DON_x] + [SON_x]) - k_{da3}([R_{in}] + [D^\bullet]$ $+ [S^\bullet])[ON_x] - k_{h3}[D][\bullet ON_x] - k_{pr}[I][\bullet ON_x] - k_{INO}[\bullet ON_x][M]$
Zeroth-order moment	$\frac{1}{V} \frac{d(VY_{000})}{dt} = k_{thi}[M][D] + k_i[M]([R_{in}] + [D^\bullet] + [S^\bullet]) - \frac{1}{2}\bar{k}_{tcn}Y_{010}^2$ $- k_p^*Y_{100}Y_{010} + k_{fm}Y_{010}[M] + k_{INO}[\bullet ON_x][M]$
First-order moments	$\frac{1}{V} \frac{d(VY_{100})}{dt} = k_p[M]Y_{010}$ $\frac{1}{V} \frac{d(VY_{010})}{dt} = k_{thi}[M][D] + k_i[M]([R_{in}] + [D^\bullet] + [S^\bullet]) - (\bar{k}_{tcn} + \bar{k}_{tdn})Y_{010}^2 - k_{da}Y_{010}[\bullet ON_x] + k_aY_{001}$ $+ k_{INO}[\bullet ON_x][M] - (k_{fin}[I] + k_{fd}[D] + k_{fs}[S])Y_{010}$
Second-order moments	$\frac{1}{V} \frac{d(VY_{001})}{dt} = k_{da}Y_{010}[\bullet ON_x] - k_aY_{001} - k_{decomp}Y_{001}$ $\frac{1}{V} \frac{d(VY_{200})}{dt} = 2k_p[M]Y_{110} + k_p[M]Y_{010} + \bar{k}_{tcw}Y_{110}^2 + 2k_p^*Y_{110}Y_{200}$ $\frac{1}{V} \frac{d(VY_{020})}{dt} = k_{thi}[M][D] + k_i[M]([R_{in}] + [D^\bullet] + [S^\bullet])$ $- 2\bar{k}_{tdw}Y_{020}Y_{010} + \bar{k}_{tdw}Y_{010}^2 + 2\bar{k}_{tcw}Y_{010}^2 - 4\bar{k}_{tcw}Y_{020}Y_{010} + \bar{k}_{tcw}Y_{020}^2$ $+ 2k_p^*Y_{020}Y_{110} + k_{da}(Y_{010} - 2Y_{020})[\bullet ON_x] + k_a(Y_{001} + 2Y_{011})$ $+ k_{fp}(2Y_{010}Y_{100} + 2Y_{010}Y_{110} - 2Y_{020}Y_{100}) + k_{INO}[\bullet ON_x][M]$ $+ k_{fm}[M]Y_{010} + (k_{fm}[M] + k_{fin}[I] + k_{fd}[D] + k_{fs}[S])(Y_{010} - 2Y_{020})$
	$\frac{1}{V} \frac{d(VY_{002})}{dt} = \bar{k}_{tcw}Y_{011}^2 + 2k_p^*Y_{011}Y_{101} + k_{da}(Y_{010} + 2Y_{011})[\bullet ON_x] + k_a(Y_{001} - 2Y_{002}) + k_{decomp}(Y_{001} - 2Y_{002})$
	$\frac{1}{V} \frac{d(VY_{110})}{dt} = k_p[M]Y_{020} - \bar{k}_{tdw}Y_{110}Y_{010} + \bar{k}_{tcw}Y_{110}Y_{020} - 2\bar{k}_{tcw}Y_{110}Y_{010}$ $+ k_p^*Y_{020}Y_{110} + k_p^*Y_{110}^2 - k_{da}Y_{110}[\bullet ON_x] + k_aY_{101} + k_{fp}(Y_{010}Y_{200} - Y_{100}Y_{110})$ $- (k_{fm}[M] + k_{fin}[I] + k_{fd}[D] + k_{fs}[S])Y_{110}$
	$\frac{1}{V} \frac{d(VY_{101})}{dt} = k_p[M]Y_{011} + \bar{k}_{tcw}Y_{110}Y_{011} + k_p^*Y_{200}Y_{011} + k_p^*Y_{110}Y_{101}$ $+ k_{da}Y_{110}[\bullet ON_x] - k_aY_{101} - k_{decomp}Y_{101}$
	$\frac{1}{V} \frac{d(VY_{011})}{dt} = -\bar{k}_{tdw}Y_{011}Y_{010} + \bar{k}_{tcw}Y_{011}Y_{020} - 2\bar{k}_{tcw}Y_{011}Y_{010}$ $+ k_p^*Y_{011}Y_{110} + k_p^*Y_{020}Y_{101} + k_{da}(Y_{020} - Y_{010} - Y_{011})[\bullet ON_x]$ $+ k_a(Y_{002} - Y_{001} - Y_{011}) - k_{decomp}Y_{011} + k_{fp}(Y_{010}Y_{101} - Y_{011}Y_{100})$ $- (k_{fm}[M] + k_{fin}[I] + k_{fd}[D] + k_{fs}[S])Y_{011}$

Source: Adapted with permission from Hernández-Ortiz JC, Vivaldo-Lima E, Penlidis A. Macromol Theory Simul 2012;21:302 [47]. Copyright 2012 Wiley-VCH Verlag GmbH & Co. KGaA, Weinheim.

TABLE 12.8 Definition of the PseudoKinetic Rate Constants Needed in the Model

Pseudokinetic Rate Constant	Mathematical Expression
Dimerization	$k_{\text{dim}} = k_{\text{dim}11} f_1^2 + \frac{1}{2}k_{\text{dim}12} f_1 f_2 + \frac{1}{2}k_{\text{dim}21} f_2 f_1 + k_{\text{dim}22} f_2^2$
Thermal initiation	$k_{\text{thi}} = \sum_{j=1}^M k_{\text{thij}} f_j$
Propagation	$k_p = \sum_{i=1}^R \sum_{j=1}^M k_{ij} p_i f_j$
Crosslinking	$k_p^{*\circ} = \sum_{i=1}^R k_{pi3} p_i$
Deactivation	$k_{\text{da}} = \sum_{i=1}^R k_{\text{dai}} p_i$
Activation	$1k_a = \sum_{i=1}^R k_{\text{ai}} q_i$
Chain transfer to initiator	$k_{\text{fin}} = \sum_{i=1}^R k_{\text{fini}} p_i$
Chain transfer to monomer	$k_{\text{fm}} = \sum_{i=1}^R \sum_{j=1}^M k_{\text{fmi}j} p_i f_j$
Chain transfer to dimer	$k_{\text{fd}} = \sum_{i=1}^R k_{\text{fdi}} p_i$
Chain transfer to solvent	$k_{\text{fS}} = \sum_{i=1}^R k_{\text{fSi}} p_i$
Chain transfer to polymer	$k_{\text{fp}} = \sum_{i=1}^R k_{\text{fp}ij} p_i F_j$
Number-average termination by disproportionation	$\overline{k_{\text{tdn}}} = \sum_{i=1}^R \sum_{j=1}^R \overline{k_{\text{tcn}ij}} p_i p_j$
Weight-average termination by disproportionation	$\overline{k_{\text{tdw}}} = \sum_{i=1}^R \sum_{j=1}^R \overline{k_{\text{tcw}ij}} p_i p_j$
Number-average termination by combination	$\overline{k_{\text{tcn}}} = \sum_{i=1}^R \sum_{j=1}^R \overline{k_{\text{tc}ij}} p_i p_j$
Weight-average termination by combination	$\overline{k_{\text{tcw}}} = \sum_{i=1}^R \sum_{j=1}^R \overline{k_{\text{tcw}ij}} p_i p_j$

TABLE 12.9 Specific Cases That Can be Analyzed with the General Model Presented in Tables 12.6 and 12.7

Conventional Systems	Conventional homopolymerization Required initial conditions: $[M]_0, [I]_0, [S]_0$ Fixed initial conditions: $f_{20} = 0, [\text{NO}_x]_0 = 0$ Comments: pseudokinetic rate constants method not required.	Conventional copolymerization (without crosslinking) Required initial conditions: $[M]_0, [I]_0, f_{20}, [S]_0$ Fixed initial conditions: $[\text{NO}_x]_0 = 0$ Comments: pseudokinetic rate constants method required. If two monomers are employed, $M = 2, R = 2$ in the definitions.
Controlled Systems	Homopolymerization in the presence of NMRP controllers Required initial conditions: $[M]_0, [I]_0, [\text{NO}_x]_0, [S]_0$ Fixed initial conditions: $f_{20} = 0$ Comments: pseudokinetic rate constants method not required	Copolymerization in the presence of NMRP controllers (without crosslinking) Required initial conditions: $[M]_0, [I]_0, [\text{NO}_x]_0, f_{20}, [S]_0$ Comments: pseudokinetic rate constants method required. If two monomers are employed, $M = 2, R = 2$ in the definitions.
Crosslinked Systems (With or Without Controller)	Copolymerization of vinyl/divinyl monomers Required initial conditions: $[M]_0, [I]_0, f_{20} = 0, [S]_0$ Fixed initial conditions: $[\text{NO}_x]_0 = 0$ Comments: pseudokinetic rate constants method required. $M = 2, R = 3$ in the definitions.	Copolymerization of vinyl/divinyl monomers in the presence of NMRP controllers Required initial conditions: $[M]_0, [I]_0, [\text{NO}_x]_0, f_{20}, [S]_0$ Comments: pseudokinetic rate constants method required. $M = 2, R = 3$ in the definitions.

ACKNOWLEDGMENTS

The authors acknowledge financial support from Consejo Nacional de Ciencia y Tecnología (CONACYT, México) (Project CONACYT 101682 and a Ph.D. Scholarship to J.C.H.-O., through *Beca Nacional para Estudios de Posgrado*, 202907), DGAPA-UNAM (Project PAPIIT 119510), and Instituto de Ciencia y Tecnología del Distrito Federal (ICyTDF, México) (Project PICSA11-56).

REFERENCES

1. The American Heritage® Dictionary of the English Language. 4th ed., Houghton Mifflin Company; 2000. Available at <http://www.thefreedictionary.com/chemical+engineering>. Accessed 2012 Apr 6.
2. Penlidis A. Can J Chem Eng 1994;72:385.
3. Ray WH, Soares JBP, Hutchinson R. Macromol Symp 2004;206:1.
4. Hrymak A, Pelton R, Zhu S. 2005. Compilers, Collected Works of Archie Hamielec. McMaster University, Hamilton, Ontario, Canada. Available at <http://chemeng.mcmaster.ca/departmentnews/Collected%20Works%20of%20Archie%20Hamielec.pdf>. Accessed 2012 Apr 6.
5. Hungenberg K-D. Macromol React Eng 2009;3:220.
6. Ray WH. J Macromol Sci Rev Macromol Chem 1972; C8:1.
7. Penlidis A, MacGregor JF, Hamielec AE. AlChE J 1985;31:1547.
8. Kiparissides C. Chem Eng Sci 1996;51:1637.
9. Dubé MA, Soares JBP, Penlidis A, Hamielec AE. Ind Eng Chem Res 1997;36:966.
10. Yoon WJ, Kim YS, Kim IS, Choi KY. Korean J Chem Eng 2004;21:147.
11. Asua J. *Polymer Reaction Engineering*. Hoboken: Wiley-Blackwell; 2007.
12. Bausa J. Macromol Symp 2007;259:42.
13. Mueller PA, Richards JR, Congalidis JP. Macromol React Eng 2011;5:261.
14. Penlidis A, editor. *Polymer Reaction Engineering*. Taylor & Francis. ISSN 1054-3414 (Print), 1532-2408 (Online). Available at http://www.tandfonline.com/loi/lree20?open=10#vol_10. Accessed 2012 Apr 6.
15. Spiegel S, editor. *Macromolecular Materials & Engineering*. Weinheim: Wiley-VCH Verlag GmbH & Co. KGaA. Online ISSN 1439-2054. Available at [http://onlinelibrary.wiley.com/journal/10.1002/\(ISSN\)1439-2054](http://onlinelibrary.wiley.com/journal/10.1002/(ISSN)1439-2054). Accessed 2012 Apr 6.
16. Spiegel S, editor. *Macromolecular Reaction Engineering*. Weinheim: Wiley-VCH Verlag GmbH & Co. KGaA. Online ISSN 1862-8338. Available at [http://onlinelibrary.wiley.com/journal/10.1002/\(ISSN\)1862-8338](http://onlinelibrary.wiley.com/journal/10.1002/(ISSN)1862-8338). Accessed 2012 Apr 6.
17. Hill CG Jr. *Chemical Engineering Kinetics and Reactor Design*. New York: John Wiley & Sons; 1977.
18. Smith JM. *Chemical Engineering Kinetics*. 3rd ed. New York: McGraw Hill; 1981.
19. Bird RB, Stewart WE, Lightfoot EN. *Transport Phenomena*. 2nd ed. New York: John Wiley & Sons; 2007.
20. Ballard MJ, Napper DH, Gilbert RG. J Polym Sci Polym Chem Ed 1981;19:939.
21. Hamielec AE, MacGregor JF. In: Reichert KH, Geiseler W, editors. *Polymer Reaction Engineering, Modelling Copolymerizations*. Munich: Hanser Publishers; 1983. p 21ff.
22. Hamielec AE, MacGregor JF, Penlidis A. Makromol Chem Macromol Symp 1987;10/11:521.
23. [a] Arriola DJ. Modeling of addition polymerization systems [Ph. D. thesis]. Madison (WI): University of Wisconsin; 1989; [b] Saldívar E, Dafniotis P, Ray WH. J Macromol Sci Rev Macromol Chem Phys 1998;C38:207.
24. Storti G, Carrá S, Morbidelli M, Vita G. J Appl Polym Sci 1989;37:2443.
25. Li W-H, Hamielec AE, Crowe CM. Polymer 1989;30: 1518.
26. Tobita H, Hamielec AE. Macromolecules 1989;22:3098.
27. Tobita H, Hamielec AE. Polymer 1991;32:2641.
28. Zabisky RCM, Chan WM, Gloor PE, Hamielec AE. Polymer 1992;33:2243.
29. Xie T, Hamielec AE. Makromol Chem Theory Simul 1993;2:421.
30. Xie T, Hamielec AE. Makromol Chem Theory Simul 1993;2:455.
31. [a] Penlidis A, MacGregor JF, Hamielec AE. J Appl Polym Sci 1988;35:2009. [b] Penlidis A, MacGregor JF, Hamielec AE. J Appl Polym Sci 1988;35:2023.
32. [a] Chien DCH, Penlidis A. Polym React Eng 1994;2:163. [b] Chien DCH, Penlidis A. Chem Eng Sci 1994;49:1855.
33. Dubé MA, Penlidis A. J Polym Sci A Polym Chem 1997;35:1659.
34. Palmer DE, McManus NT, Penlidis A. J Polym Sci A Polym Chem 2000;38:1981.
35. Palmer DE, McManus NT, Penlidis A. J Polym Sci A Polym Chem 2001;39:1753.
36. McManus NT, Hsieh G, Penlidis A. Polymer 2004;45: 5837.
37. Leamen MJ, McManus NT, Penlidis A. J Polym Sci A Polym Chem 2005;43:3868.
38. Leamen MJ, McManus NT, Penlidis A. Chem Eng Sci 2006;61:7774.
39. Scorah MJ, Dhib R, Penlidis A. Branching level detection in polymers. In: Lee S, editor. *Encyclopedia of Chemical Processing (ECPH)*. London: Taylor & Francis; 2005. p 251ff.
40. Scorah MJ, Tzoganakis C, Dhib R, Penlidis A. J Appl Polym Sci 2007;103:1340.
41. Polic AL, Duever TA, Penlidis A. J Polym Sci A Polym Chem 1998;36:813.

42. [a] Dubé MA, Penlidis A. *Polymer* 1995;36:587. [b] Dubé MA, Penlidis A. *Macromol Chem Phys* 1995;196:1101. [c] Dubé MA, Penlidis A. *Polym Int* 1995;37:235.
43. Fujisawa T, Penlidis A. *J Macromol Sci Pure Appl Chem* 2008;45:115.
44. Vivaldo-Lima E, Hamielec AE, Wood PE. *Polym React Eng* 1994;2(1&2):87.
45. Vivaldo-Lima E, García-Pérez R, Celedón-Briones OJ. *Rev Soc Quím Mex* 2003;47:22.
46. Quintero-Ortega IA, Vivaldo-Lima E, Luna-Bárcenas G, Alvarado JFJ, Louvier-Hernández JF, Sanchez IC. *Ind Eng Chem Res* 2005;44:2823.
47. Hernández-Ortiz JC, Vivaldo-Lima E, Penlidis A. *Macromol Theory Simul* 2012;21:302.
48. Hernández-Ortiz JC, Vivaldo-Lima E, Lona LMF, Manus NT, Penlidis A. *Macromol React Eng* 2009;3: 288.



13

BULK AND SOLUTION PROCESSES

MARCO A. VILLALOBOS AND JON DEBLING

13.1 DEFINITION

Bulk and solution polymerizations refer to polymerization systems where the polymer produced is soluble in the monomer. This is in contrast to heterogeneous polymerization where the polymer phase is insoluble in the reaction medium. In bulk polymerization, only monomer provides the liquid portion of the reactor contents, whereas in solution processes, additional solvent can be added to control viscosity and temperature. In both processes, small amounts of additional ingredients such as initiators, catalysts, chain transfer agents, and stabilizers can be added to the process, but in all cases, these are also soluble in the reactor medium. As described in more detail below, the viscosity of the reaction medium and managing the energetics of the polymerization pose the most significant challenges to operation of bulk and solution processes.

13.2 HISTORY

Given its formulation simplicity, bulk polymerization was the preferred laboratory and commercial polymerization method in the early days of polymer synthesis when scientists discovered that certain liquid substances turned into hard solids by effects of temperature, sunlight, or in the presence of other substances acting as *accelerators*. Anecdotal and documented evidence suggest that the first synthetic bulk polymer ever purposely made was poly(vinyl chloride) (PVC), first synthesized by the German chemist Eugen Baumann in 1872. A method to polymerize PVC under sunlight was first patented in 1913 by Friedrich Klatte also from Germany and in 1926,

the American Waldo Semon, working for B.F. Goodrich, invented plasticized PVC [1–3].

In 1839, the German apothecary Eduard Simon first isolated polystyrene (PS) from a natural resin. More than 85 years later, in 1922, German organic chemist Hermann Staudinger realized that Simon's material comprised long chains of styrene molecules. He described that materials manufactured by the bulk thermal processing of styrene were polymers. The first commercial bulk polymerization process for the production of PS is attributed to the German company Badische Anilin & Soda-Fabrik (BASF) working under trust to IG Farben in 1930. In 1937, the Dow Chemical company introduced PS products to the US market [1, 4–5].

Between 1930 and the onset of World War II (WWII) in 1939, several polymer families were invented and commercially developed through bulk processes. The most important ones include low density polyethylene (LDPE), poly(methyl methacrylate) (PMMA), polyurethanes (PU), poly(tetra-fluoro ethylene) (PTFE), polyamides (PAs), and polyesters (PEs). The last three are attributed to Dupont's scientists Roy Plunkett and Wallace Carothers, respectively. During WWII, bulk polymerization was still instrumental in the development and commercialization of new families of PEs such as polyethylene terephthalate (PET) developed by ICI and Dupont and unsaturated polyester resins (UPRs) [1, 6–8].

From the 1940s, the bulk polymerization technique led way to other polymerization processes suitable for the commercial production of new polymer families. The inclusion of inert solvents into the reaction mix allowed for lower viscosity operation with the consequent improvements in reactor control, turning bulk processes into solution ones.

While other polymerization processes such as emulsion, suspension, gas phase, precipitation, and interfacial polymerization were being developed, bulk polymerization evolved from its early processes of the 1930s where monomers and catalysts were loaded into a batch polymerization reactor operating at semiadiabatic conditions to temperature-programmed semicontinuous reactors and to continuous batteries of stirred and plug flow reactor trains developed in the 1970s and 1980s. Since then, advanced process control strategies, and novel stirred and plug flow reactor geometries have maintained bulk polymerization as one of the preferred manufacturing processes for a wide variety of commodity, engineering, and high performance plastics [1, 4].

13.3 PROCESSES FOR BULK AND SOLUTION POLYMERIZATION

13.3.1 Reactor Types

13.3.1.1 Batch/Semibatch Reactor The simplest and arguably the oldest process vessel for polymerization and a natural extension of laboratory glassware equipment is the batch reactor. In this configuration, a reactor equipped with an agitator is charged with all of the ingredients (monomer, solvent, initiator, catalyst, etc.), heated to the desired temperature and the polymerization is allowed to proceed until completion. Safe operation of these processes requires judicious *a priori* selection of the appropriate feed formulation, batch size and cooling system to prevent uncontrollable reaction runaway and potential safety issues. A “semibatch” reactor is simply a “batch reactor” operated with a continuous or intermittent feed to the reactor instead of charging all of the material at the beginning. Often the same vessel can be used for “batch” or “semibatch” modes of operation. Metering the feed to the reactor over sufficient time allows control of the desired product quality as well as controlling the temperature from the heat of polymerization. In “semibatch” mode, it is common to stage different feeds to the process at chosen intervals over the reaction time as product needs dictate. In both the batch or semibatch processes, the product is not withdrawn until the “batch” is finished and the residence time is simply defined by the “batch” time or total process time in the “kettle.”

For both batch and semibatch processes, the reactor “kettle” is often provided with heating or cooling as needed by external sources such as cooling water, tempered water, steam, oil, or electric or reflux condensers. The reaction vessel may also be put under vacuum to remove undesired volatile material. In many cases, the removal of volatiles is not simply a requirement to achieve regulatory requirements, but rather to drive the reaction to completion. For example, in condensation polymerization

where equilibrium often exists, the extent of reaction is controlled by removal of a condensate; vacuum removal is critical to achieving final product molecular weight and end group concentration [9].

13.3.1.2 Continuous Stirred Tank Reactor (CSTR) The continuous stirred tank reactor (CSTR) is a continuous process that is ideally fully back mixed such that the product leaving the reactor has the same composition and properties as the material inside the reactor. The CSTR may be considered a well-mixed “semibatch” reactor with continuous feed and product withdrawal. In many cases, the same reactor vessel used for batch/semibatch may be used as a CSTR with little modification. Figure 13.1 shows different internal configurations of CSTRs. Multiple CSTRs operating at different temperatures can be linked in a cascade of two or more in series, to achieve desired conversion of monomer and molecular weight. In between each CSTR, additional feed may be added to form unique polymers. CSTRs may also be used in combination with other reactors, such as tube reactors, to enhance monomer conversion.

Unlike batch/semibatch reactors, the mean residence time of a CSTR at steady state is defined by the ratio of volume inside the reactor to volumetric feed rate, which at equal density of feed and reactor contents is equal to the reactor space time. The advantage of the CSTR over the batch or semibatch reactor is that it is ideally suitable for long runs of continuous production of a polymer product. Once the reactor process is brought to steady state, uniform quality and consistent product is made. However, the CSTR requires several reactor turnovers (at least 3–4) before the process is at steady state and uniform product is made [10].

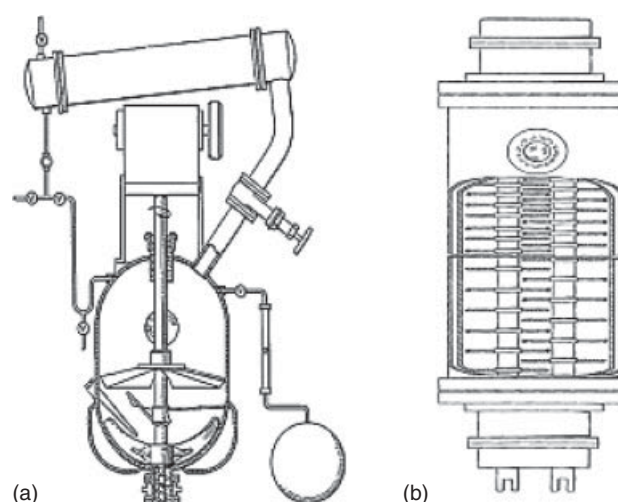


Figure 13.1 Different CSTR configurations: (a) pressure tank with condenser system and (b) vertical or horizontal intermeshing paddle mixing reactor [16, 66].

13.3.1.3 Autoclave Reactor An autoclave reactor is a batch or continuous reactor usually operating at moderate-to-high pressures > 1 bar and a pressurized liquid or gaseous environment.

13.3.1.4 Tubular Reactor A tubular reactor is a continuous process where the monomer feed is charged to the inlet of a tube and the product withdrawn at the other end. The reactor has the advantage of high surface area to volume and thus good heat transfer. On the other hand, plugging and fouling must be managed as does high pressure drop. Flow through the tube is “plug flow” without significant axial mixing and thus the conversion and molecular weight of the polymer changes over the length of the tube. Sometimes axial mixing can be improved by the addition of static mixers at various places through the tube. The residence time of the reactor is defined as the tube volume divided by the volumetric feed rate. Different types of tubular reactors are shown in Figure 13.2.

13.3.1.5 Loop Reactor A loop reactor, as shown in Figure 13.3, is a tubular reactor wound around itself and operated under high recycle. It has the advantages of good heat transfer and residence time distribution of a fully back-mixed CSTR. However, loop reactors require high recycle ratios and hence significant pumping systems to provide sufficient mixing. At high recycle ratios, a loop reactor operates with the same residence time distribution as a CSTR. At low recycle ratios, it has been shown that the loop reactor residence time distribution is oscillatory [11].

13.3.1.6 Casts and Molds Polymerizations may also be carried out in molds or casts. In this process, the monomer is added to a mold and allowed to heat up to the point of self-polymerization. The resultant polymer product is removed from the pans and cooled. While this more manual process appears slightly archaic, its simplicity allows the production of a number of specialty products still in commercialization today.

13.3.2 Processes for Free Radical Polymerization

Free radical polymerization is a subset of the chain growth polymerization addition mechanisms between two

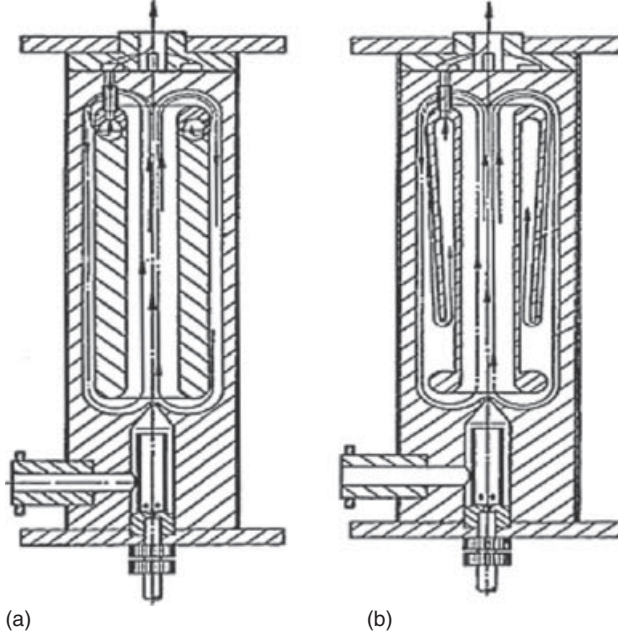


Figure 13.3 Different loop reactor configurations: (a) outlet flow is guided by a hollow ring and (b) outlet flow is guided by double walls [99].

molecules (monomers) bearing $C=C$ double bonds. The term *homopolymerization* refers to cases where a single monomer is employed, whereas *copolymerization* refers to polymerizations where more than one monomer is present in the reaction mix. Suitable monomers for free radical polymerization include those unsaturated monomers bearing a $C=C$ double bond of the general structure shown in Figure 13.4.

This includes α -olefins, vinyl monomers, dienes, mono- and polyunsaturated organic compounds such as alkenyl derivatives of fatty acids and alcohols. Exemplary

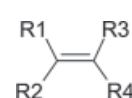


Figure 13.4 Suitable monomers for free radical polymerization.

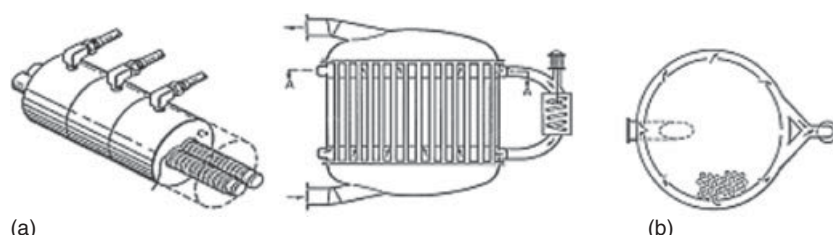


Figure 13.2 Different PFR configurations: (a) detailed of wiped surface reactor and (b) side and top view of tube bundle and shell reactors [22, 98].

monomers include styrene, α -methyl styrene, acrylic acid, and its esters (acrylates), as well as methacrylic acid and its esters (methacrylates). The chemistry of free radical polymerization is described elsewhere in this book (Chapter 4) and other references [12, 13]. The most commonly polymerized monomers and resulting polymers produced by bulk and solution processes are described below.

13.3.2.1 Polystyrene One of the largest volume products made today through bulk addition polymerization is PS. PS repeat unit structure is shown in Figure 13.5. Developed in the 1950s, bulk polymerization of styrene monomer to make general purpose polystyrene (GPPS) originally took place in molds. In this process, styrene monomer was charged into individual molds that were assembled in a filter press like array and closed under mechanical pressure. Heating oil or steam was circulated through the individual molds, which heated the monomer about 70 °C to sustain polymerization. Isothermal polymerization (thermal or catalyzed) took 5–14 h by progressive heating of the reaction mix at temperatures between 80 and 150 °C. Semiadiabatic polymerization was completed much faster ($t < 60$ min) with temperatures approaching 300 °C. At the end of the polymerization, the molds were cooled and opened to remove GPPS blocks, then the polymer ground into pellets. In spite of its simplicity and relatively high reactor productivity, mold processes were abandoned in the late 1970s due to high residual styrene levels (>1 wt%), poor M_w reproducibility (due to temperature variability), and high dispersity (M_w/M_n) that affect product properties (melt flow index, tensile and impact strength, heat deformation temperature (HDT), and Vicat softening point) [14, 15].

Modern GPPS is produced by continuous bulk and solution processes developed in the mid-1950s by major PS producers, BASF, Dow Chemical, Monsanto, Union Carbide, and others. In the modern continuous GPPS process, as the one shown in Figure 13.6, styrene monomer is continuously fed to a packed column (normally alumina, silica gel, or clay) to remove moisture, impurities, and inhibitor, blended with recycled styrene monomer, peroxide initiator (normally dialkyl or diacyl peroxides, such as di-*tert*-butyl peroxide, dicumyl peroxide, or *tert*-butyl peroxibenzoate utilized at low concentrations; $[I] < 0.5\%$ w/w in the feed), chain transfer agent (normally aliphatic

or aromatic thiols, such as *t*-dodecyl mercaptan and *n*-dodecyl mercaptan used in small concentrations [CTA] <1% w/w) and fed to a CSTR. Reactor residence times are approximately 1–3 h and typical reactor sizes in the range of 20–100 m³ to achieve reasonable economics of scale. Normally the CSTR operates partially full (~90 %) with a vapor headspace under moderate pressure of <10 bar and isothermally at temperatures below 150 °C. At steady state, the reaction mix in the CSTR consists of a single phase comprised of 30–40% PS in monomer with small amounts of impurities, initiator, and chain transfer agents. Conversion is purposely limited so as to achieve a manageable reactor mix viscosity and maintain isothermal conditions for high molecular weight PS (normally $M_w < 300,000$ Da). In the end, the three variables (T , θ , and $[I]$) define the monomer conversion, reaction rate (and thus heat generation), and molecular weight of the PS. New process advances include adding reflux condensers, external heat exchangers, chilled jacket cooling fluids, cooling baffles, and extended area internal cooling coils and diperoxide initiators to allow an increase in reactor productivity and higher monomer conversions [16–18].

The product from the CSTR is continuously metered to a second reactor in series. Usually the second reactor is a PFR operating at higher temperature than the CSTR (up to 200 °C) in isothermal or semiadiabatic mode. Typical residence times are between 5 and 50 min. A temperature profile may be prescribed in the PFR by segmenting the reactor jacket and allowing heating oil of different temperatures to circulate through each jacket. Semiadiabatic operation in PFRs is also possible by allowing the heat generation rate to approach the heat removal rate, thus causing the reaction mix to vary along the reactor coordinate. In any operation mode, the heat generation rate should always be less than the heat removal capacity at any point in the reactor to prevent a runaway. The higher reaction temperatures in the PFR lead to much higher reaction rates ($d[M]/dt = 1–10\%/\text{min}$) than the CSTR and Trommsdorff and glassy effects are limited at these high reaction temperatures [18–20]. Therefore, the conditions in the PFR can be tuned to tailor the MWD of the product thus defining different GPPS grades [21–23].

The hot reaction mix leaving the second reactor is continuously pumped through a preheater operating at $T_{PH} < 300$ °C, and then to an evaporator to separate molten polymer (up to 80% of the mixture) from the unreacted volatile components. A variety of types of equipment have been used including wiped film evaporators (WFEs), wiped surface evaporators (WSEs), falling strand evaporators (FSEs), and filmtruders, described in Section 13.5.6. For PS, evaporators typically operate at high temperatures $T_{wall} \approx 250–300$ °C and moderate vacuum ($P \approx 1–50$ torr) with residence times in the evaporator of the order of $\theta = 2–10$ min. They are designed to minimize residual

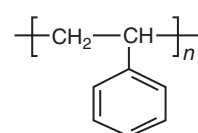


Figure 13.5 Polystyrene structure.

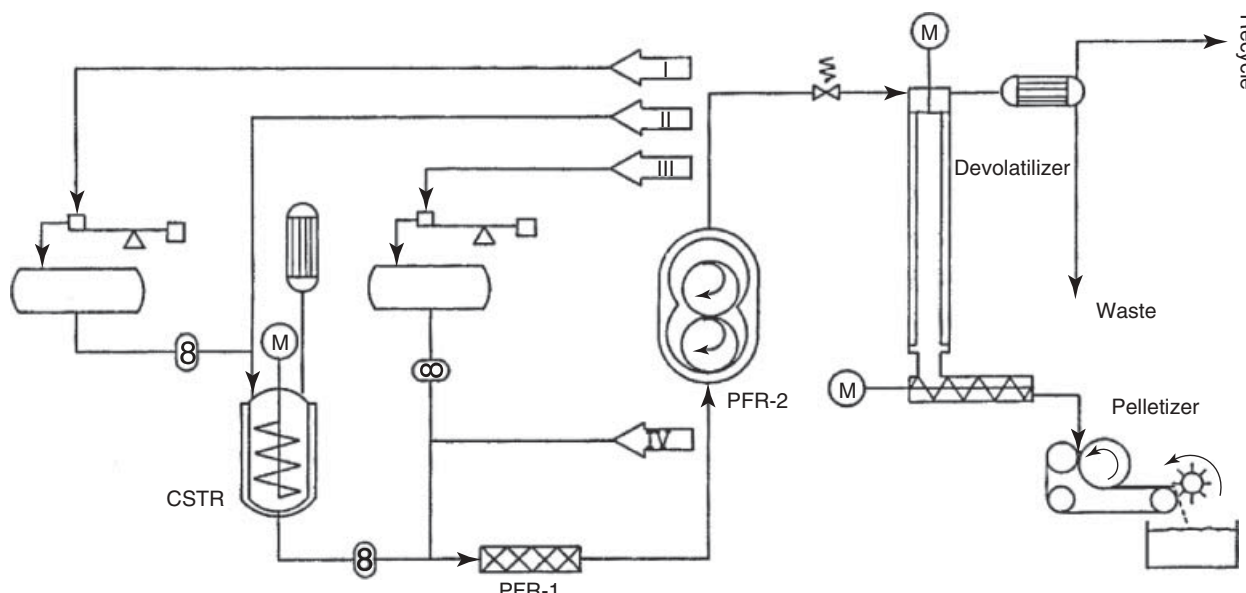


Figure 13.6 Schematic bulk continuous process for high molecular weight styrenic polymers showing a CSTR and two different PFRs in series, evaporation unit, and pelletization unit. I: monomer(s) or monomer–rubber solutions feed stream, II: initiator and additives feed, III: continuous recycled stream from evaporators, and IV: additional initiator/additives feed [21].

styrene to less than 500 ppm, but some processes include two or more evaporator stages in series to reduce volatiles to under 50 ppm. The volatile material leaving the evaporator section is recovered in a liquid separation operation, most often single- or multistage distillation and recycled to the first reactor. The molten PS leaving the evaporator is pumped to a pelletizing line where it is finally bagged as a solid pellet product [16, 21, 23].

Solution GPPS processes differ from bulk processes in that an inert solvent (normally ethyl benzene) is fed with the monomer. The purpose of the solvent, normally 10–30% of the reaction mix, is to reduce viscosity and aid in reactor temperature control. By reducing reactor viscosity, higher monomer conversions are possible and higher molecular weight polymer can be produced in each reactor. In addition, higher polymerization rates are possible since solvent decreases the total heat generation rate per unit mass in proportion to its content in the reaction mix. The use of solvents in sufficient levels also allows the use of multiple CSTR's in series in lieu of CSTR/PFR combinations. On the negative side, the use of solvents decreases monomer concentration and polymer production rate. For GPPS, however, the reduced monomer concentration is usually offset by higher temperature, and thus for a given reactor size, polymer productivity in bulk and solution processes is similar. Except for the presence of solvent in ppm amounts in the solution product, GPPS made through solution or bulk processes are virtually undistinguishable from one another [23–25].

A special grade of PS that is also produced commercially is low molecular weight PS. Often referred to as *oligomeric polystyrene*, this grade of material typically has an M_w from 1800 to 25,000 Da and is used for specialty applications such as additives for plastics. Low molecular weight PS can be conveniently made by a high temperature polymerization process [26–28]. At high temperatures, reaction rates and monomer conversions are extremely high and ideal for making low molecular weight oligomers. The kinetics of styrene polymerization at high temperatures has been thoroughly described by Campbell who has shown that at elevated temperatures the dominant mode of chain termination in styrene polymerization is by back biting and scission [29].

13.3.2.2 Styrene Acrylonitrile (SAN) Copolymers
Styrene–acrylonitrile copolymers are produced either by batch or continuous bulk or solution processes. SAN copolymers produced in a CSTR are clear, but in batch processes they may be hazy due to compositional drift and some degree of incompatibility between copolymers of different compositions. To prevent or minimize compositional drift, commercial batch SAN is polymerized at compositions approaching the azeotropic copolymerization condition for this monomer pair (77/23 S/AN % mol, acrylonitrile), where the instantaneous copolymer composition equals the comonomer mix composition. Around these conditions, the batch or continuous SAN processes closely follow those described for GPPS [23, 30].

13.3.2.3 High Impact Polystyrene (HIPS) (see also Section 10.2.1.1) High impact polystyrene (HIPS) is a composite material comprising the polymerization product of styrene monomer in which 3–15% of polybutadiene (PB) rubber has been dissolved before polymerization. Designed in the 1950s to obtain ductile PS, it was originally manufactured by a suspension polymerization process. As demand for this ductile plastic grew during the 1960s and 1970s, continuous bulk and solution GPPS plants were redesigned to accommodate the PB dissolution step and to handle the normally higher reaction mix viscosities of HIPS [25].

PB, the polymerization product of 1,3-butadiene ($\text{CH}_2=\text{CH}-\text{CH}=\text{CH}_2$), is not an inert component but a reactive one in the HIPS system. Both its total content and its vinyl (1,2-addition unit) to linear (1,4-addition unit) ratio are fundamental in the process design and product characteristics. Depending on the polymerization process, PB can be stereospecific with varying contents of cis- and trans isomers. Normally high *cis*-PB contents are more than 80% of the *cis* adduct and more than 85% of 1,4-addition units. Free radical PB is nonstereo specific. Either one can be used to make HIPS. Typically, high *cis*-PB leads to products with higher ductility and enhanced mechanical performance. PB bales are ground in cold to pebble size particles and added into a tank containing cold styrene monomer and agitated at low RPM. The dissolution is carried out below room temperature to prevent onset of styrene polymerization [25, 31].

As in the bulk GPPS process, the single-phase solution of PB in styrene is continuously fed into a series of CSTRs or CSTR-PFR arrays, depending on whether the process runs as solution or bulk. Dialkyl and diacyl peroxide initiators are selected to optimize polymerization rate and degree of PB grafting. Mercaptan molecular weight regulators are added in similar proportions in the PS process described. Prevention of extensive PB crosslinking requires the use of antioxidant, normally hindered phenols and hindered amines, used in <0.3% w/wp. Styrene conversion in the first reactor is about 20–35% and 65–80% in the second and further reactors. In this sense, HIPS and PS are very similar processes. The major process differences arise due to the additional reactions involving PB, noticeably PB–PB crosslinking reactions, and PB–S copolymerization or PB–PS grafting reactions. The higher solubility of the styrene/PS pair than PB/styrene one causes the PB to become insoluble in the mix and precipitate in the form of discrete dispersed particles at conditions dependent on styrene conversion and molecular weight, temperature, and PB content in the mix. In this manner, the single-phase PB/styrene solution fed to a CSTR finds at steady state as a two-phase system where PB particles have formed a separate phase. The PB particle formation process is still poorly understood. The forming spherical rubber particles

are themselves composite particles with a PB continuous phase and dispersed spherical occlusions of a polymerizing mix of styrene and PS, and PS grafts forming on the available S/PB internal and external interfaces [31–33].

The rubber particle size distribution (PSD) and occluded and grafted PS fraction in HIPS are mostly controlled by optimizing reactor agitation parameters and target reactor conversion, solids, and viscosity. Higher agitation rates may lead to smaller rubber particle sizes due to droplet shear breakage. In the first reactor, the reaction mix consists of a styrene/PS continuous phase and a PB/styrene/PS dispersed phase. While extensive PB crosslinking renders the PB phase ineffective to the desired toughening of the PS matrix, total lack of crosslinking also fails to maximize reinforcing properties. It is still an art in HIPS polymerization to carefully craft the reactor design and process conditions (T profile, RTD, conversion profile, and [I]) to generate the most effective PB rubber PSD for reinforcement (0.5–10 μm). This includes an optimal level of PB crosslinking, measured as both swelling index and percent gel in the product, amount of PS occluded in the composite rubber phase (1–3 parts of PS per PB part), and optimal degree of PS grafting in the internal PS occlusions, and onto the PS matrix, to maximize interfacial adhesion, and thus particle stability and HIPS mechanical performance at a given PB content. After the second reactor, whether a CSTR or PFR, the product is devolatilized and separated as described before in the PS process [31, 33–36].

13.3.2.4 Acrylonitrile/Butadiene/Styrene (ABS) Acrylonitrile/butadiene/styrene (ABS) polymers are not true terpolymers. As HIPS they are multipolymer composite materials, also called *polyblends*. Continuous ABS is made by the copolymerization of styrene and acrylonitrile (SAN) in the presence of dissolved PB rubber. It is common to make further physical blends of ABS with different amounts of SAN copolymers to tailor product properties. Similar to the bulk continuous HIPS process, in the ABS process, high *cis*-PB (>50%, >85% 1,4-addition) is dissolved in styrene monomer, or in the process solvent, and fed continuously to a CSTR where streams of AN monomer, recycled S/AN blends from the evaporator and separation stages, peroxide or azo initiators, antioxidants and additives are continuously metered according to the required mass balance to keep the copolymer composition constant over time at steady state.

Two or three CSTRs in series or a CSTR–PFR array can be used in mass processes. In the most common two CSTR or CSTR/PFR arrays, the PB solution is added to the first CSTR that operates between 20% and 40% solids at steady state. The second CSTR operates at solid contents between 50% and 80% depending on reactor volume and design. In the three-CSTR array, the first reactor operates at low conversions, $X_m < 20\%$, and the second CSTR operates

at a total solid contents of 25–40%. This process allows the choice to feed the PB rubber solution to either the first or second reactor. The addition of the PB solution to the second reactor changes the rubber PSD, the amount of SAN occluded in the PB phase, as well as the extent of SAN grafting onto the rubber particles, all instrumental parameters in defining the properties of the resulting ABS product. Ideally, a rubber content of 3–15% is desired, depending on the required impact resistance of the ABS; 3–6% PB for mid-impact grades, 6–10% for high impact grades, and 10–15% for ultrahigh impact grades, or for mid- and high impact grades that will be obtained by further dilution with bulk or suspension SAN. To maximize impact resistance, rubber particle size must be distributed between 0.5 and 10 μm . Research studies suggest that narrow rubber particle size distributions centered about 2 μm yield a better balance of impact and gloss at a given PB content. The fraction of grafted and occluded SAN in the rubber particles is also instrumental in maximizing the impact properties of ABS, with maximum properties observed at 1 : 1 to 1 : 3 ratios of PB to SAN. As in HIPS processes, minimizing PB crosslinking is also instrumental to maximize impact properties. Normally, stereospecific high *cis*-PB is preferred for high performance grades.

In ABS production, the first reactor operates at temperatures between $T_{r1} = 90$ – 150°C . The second reactor may be an isothermal CSTR operating a $T_{r2} = 110$ – 170°C , or a PFR operating on a prescribed raising temperature profile within these same limits. The far end process resembles that of PS or HIPS previously described [23, 37, 38]. The use of high T_g comonomers such as Maleic anhydride, α -methyl styrene, and *n*-phenyl maleimide in the monomer mix (<15% w/wm) has been successfully employed to increase the T_g of ABS product by 3–10 $^\circ\text{C}$, producing the so-called high heat ABS grades [37–39].

13.3.2.5 Acrylics Acrylic polymers form a broad class of materials ranging from viscous liquids to hard, transparent resins. They find many applications including additives for plastics, dispersants for pigments in coatings and printing inks, overprint varnishes, adhesives, and additives for coatings, to name a few [40]. The family of acrylic monomers comprises a broad variety of vinyl monomers based on acrylic and methacrylic acid and their esters. They include acrylic and methacrylic acid and the corresponding esters of both. Functional monomers bearing hydroxyl, epoxy, and amino groups, for example, are also included in this category. Acrylic polymers range from homopolymers to copolymers containing two or more monomers. Often comonomers include styrene, and the compounds may still be referred to as *acrylics*.

PMMA is a transparent thermoplastic with high glass-transition temperature ($T_g \sim 105^\circ\text{C}$), commonly used as glass replacement in windows and in colored thermoformed

parts where deep profiles, mechanical and chemical resistance is required, such as bathtubs and sinks. The cast polymerization process was developed by Rohm & Haas, and Chimey in the 1960s to make Plexiglass™ plastic windows. Although partially replaced by continuously polymerized PMMA extruded into transparent sheet, the cast process is still in use today for panels requiring thicknesses in excess of one half inch. In the PMMA cast process, MMA monomer is first polymerized slowly to low conversion (<25 wt%) in the presence of azo initiators (typically AIBN), dyes, chain transfer agents, and plasticizers, at relatively low temperatures ($T_{rx} < 100^\circ\text{C}$) to produce a viscous syrup [13]. The chemical structure of PMMA repeat unit is shown in Figure 13.7. Comonomers such as acrylic acid, methacrylic acid, and their alkyl esters are often employed in low proportions (<10% mol). The syrup is then transferred to a mold, sealed, and immersed in an open water pool where slow polymerization occurs over a period of hours. Slow polymerization is required to avoid self-acceleration due to the autoacceleration or Trommsdorff effect, which can lead to overheating, monomer boiling, and deterioration in product quality [19]. The mold polymerization stops when the product mixture glassifies as its T_g approaches the polymerization temperature; however, further processing is required to increase monomer conversion above 90%. The molds are therefore emptied and the product placed in convection ovens, heated above the T_g , and slowly (<1–2 %/h) polymerized to conversions above 99.9%. More recent modifications of the mold process include prepolymerization in a continuous plug flow reactor, followed by a high temperature pressurized autoclave and the use of initiator mixtures to optimize the reaction rate [41–43].

Semibatch solution polymerization is a well-established method for producing acrylic resins. In the semibatch solution process, solvent is commonly charged to the reactor and heated to the desired reaction temperature, typically 100–140 $^\circ\text{C}$. Monomer, initiator, and other ingredients are slowly fed to the reactor over a period of 4–6 h to achieve a desired solids content (typically up to 70% by weight solids). During polymerization, the solvent may be refluxed to help remove the heat of polymerization [40]. At the end of the polymerization, a hold time and post charge of initiator solution are common to techniques designed to reduce

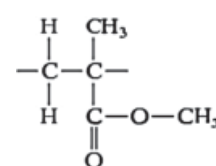


Figure 13.7 Poly(methyl methacrylate) (PMMA) repeat unit structure.

the free monomer remaining in the reactor. Many acrylic polymers, such as acrylic polyols for isocyanate cured coating, are sold as solutions in solvent. In this case, the solution is simply cooled to room temperature, additives added, and the material drummed or charged into a tanker car for shipment. Low T_g acrylic polymers can be sold as 100% solids if the reaction solvent can be removed from the vessel by vacuum distillation. In such cases, low boiling point solvents, such as acetone or isopropanol, are usually used in the polymerization process.

A wide variety of initiators may be used in the solution polymerization of acrylics and the choice depends on reaction temperature, final end-use applications, process capability (some initiators emit gaseous by-products upon decomposition), and cost. One usually selects an initiator with a suitable half-life decomposition time appropriate for the polymerization temperature and residence time to maximize initiator usage effectively. Generally, liquid initiators are used, although solid ones exist. Ideally, the initiator requires no special handling such as refrigeration; however, initiators with low half-lives temperatures usually require more extensive storage. A wide variety of Azo and organic peroxides initiators are commonly used in solution polymerization processes [44, 45]. There are more than 50 organic peroxides available including families of diacyl peroxides, *t*-alkyl peroxyesters, monoperoxycarbonates, di(*t*-alkyl) peroxides, and *t*-alkyl hydroperoxides, to name a few. The selection of the appropriate initiator can also have an impact on the final properties of the produced polymer. Choosing initiators that are “hot” or “active” can abstract hydrogen from the polymer backbone and lead to broader molecular weight distributions [46].

Producing high molecular weight acrylics in solution polymerization presents many of the challenges described previously for GPPS relating to heat transfer, solution viscosity, temperature control, and productivity. Making a high molecular weight acrylic often means reducing temperature and initiator content, but this requires long batch times and low solution solids. A constant trend in the market, however, is for lower VOC systems, which has resulted in a growing demand for lower molecular weight acrylic polymers. Producing low molecular weight acrylics by solution polymerization has some challenges. As temperature is raised, the pressure in the reactor increases and limits the use of volatile solvents. Making a very low molecular weight polymer by a solution process often means adding significant levels of initiator or chain transfer agents, which can add cost, regulatory hurdles, color, and odor to the final product.

To overcome the challenges described above, associated with the production of low molecular weight acrylic polymers by solution processes, a high temperature continuous polymerization processes was developed in the early 1980s by the S.C. Johnson Co. Several US patents disclose

a processes for continuous bulk polymerization of acrylic monomers with styrene at elevated temperatures $>180^{\circ}\text{C}$ in a CSTR at high conversions and low residence times [26–28]. At high temperatures in the presence of styrene, acrylic copolymers require little to no initiator, as styrene undergoes thermal decomposition to form free radicals. In addition, the high reaction temperatures result in low reactor viscosities and thus little or no solvent is required in these processes.

At high temperatures, the main mechanism of chain termination of styrenic and acrylate polymers is not by the classical methods of disproportionation and combination but rather by backbiting and scission [29]. This results in termination unsaturation in the final product and the presence of oligomers [47, 48]. Some monomers may be difficult to polymerize at high reaction temperatures due to depropagation. Debling and Villalobos have shown that methacrylates undergo significant depropagation at temperatures above 180°C but can achieve high conversion by copolymerization with acrylates or styrene [49]. At very high temperatures, acrylic acid is also prone to decarboxylation and anhydride formation reactions, which must be carefully controlled. Recent advances in understanding the kinetic mechanisms of acrylate and methacrylate polymerization at high temperatures and the modeling of these systems have been recently published [50–55].

High reaction temperatures not only favor low molecular weights at high polymerization rates but also enable slower reactions, normally not significant at lower reaction temperatures. Condensation reactions, for example, can proceed concurrently with free radical polymerization to provide uniquely modified specialty copolymers [56–59]. At the same time, deleterious side reactions that form gel can also occur and must be controlled by proper selection of solvent systems in some chemistries [60].

13.3.2.6 Water-Soluble Polymers A number of polymers useful for such applications as diaper absorbents, detergents, dispersants, thickeners, and water treatment applications are water soluble and thus may be made by aqueous polymerization processes [61–63]. Poly(methacrylic acid) and its high acid copolymers and salts, as well as poly(*N*-vinyl pyrrolidone), are some examples. Typically initiators include water-soluble azo compounds, hydroperoxides, persulfates, and redox systems [64]. Often, if the solubility is not complete in water, alcohol solvents are sometimes added.

13.3.3 Processes for Step-Growth Polymerization

Step-growth polymerization chemistry is based on reacting molecules having complementary reactive moieties A and B, where these react with one another to form a new chemical species given by $\text{A} + \text{B} \rightarrow \text{C}$, wherein species

A and B contain functional groups that may react with each other to form a linkage. Sometimes, a small molecule or “condensate” is formed in the process. The most commonly functional groups in step-growth polymerization are carboxyl acids, hydroxyl, primary and secondary amines, isocyanate, oxirane, esters, and anhydride.

In contrast to addition polymerization, in step-growth polymerization, the molecular weight buildup progresses slowly with conversion and depends on the stoichiometry of the reactants. In step-growth polymerization, the monomer disappears at low conversions, and high molecular weights are achieved only at high conversions. In condensation step growth, the reactions are often reversible and thus, the removal of the condensation product becomes instrumental in reaching high group conversions and therefore high molecular weights. It is common in these systems, then, to design the reactor and operating conditions such that removal of the condensation product is facilitated. Reflux condensers with tailored fractionation separation of volatile condensates and vacuum operation are common in the step-growth commercial reactors. It should be noted that many monomers used in step-growth polymerization are solid at room temperature or form polymers with high glass-transition temperatures ($T_g > 100^\circ\text{C}$) and/or are semicrystalline, exhibiting high melting points ($T_m > 200^\circ\text{C}$). This requires processes to be run at high temperatures to avoid polymer glassification in the reactor and to deal with increasing reaction mix viscosity [65].

The use of catalyst to accelerate chain propagation steps is well documented in the art. It is important to note that the use of catalysts does not substitute the need to eliminate condensation products and impurities from the system, when present. For instance, some esterification catalysts, such as Lewis acids, are known to also catalyze hydrolysis reactions when the accumulation of moisture in the system is high.

13.3.3.1 Polyesters In general, PEs are the high molecular weight condensation product of an aliphatic or aromatic dicarboxylic acid of general formula (HOOC-R-COOH) and an aliphatic or aromatic diol of general formula (HO-R'-OH). Because of their superior thermal, optical, and mechanical properties, the most commercially important thermoplastic PEs manufactured today are polyalkylene terephthalates, specifically PET, the condensation product of ethylene glycol (EG) with terephthalic acid (TPA) shown in Figure 13.8, and poly(butylene terephthalate) (PBT), the condensation product of butanediol with TPA, both semicrystalline polymers. Poly(ethylene naphthalate) (PEN) and poly(trimethylene terephthalate) (PTT) have gained commercial interest in the last decade [65].

PEs are produced by a variety of batch and continuous bulk processes. PET and PBT are commercially made by both continuous processes, in a series of CSTRs of varying

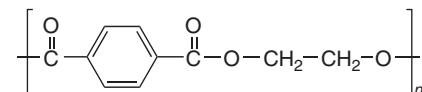


Figure 13.8 Poly(ethylene terephthalate) (PET) structure.

geometries and stirring arrays, or in batch processes. In the continuous process, the first CSTR is used to form a “prepolymer” or oligomer of 2–10 units long. In the second stage, the “prepolymer” is grown to higher molecular weight in the “melt polymerization stage.” The final, “finishing” stage, often employs a long residence time reactive zone to drive off the condensate under vacuum and build molecular weight to useful levels. This is the so-called solid-state polymerization stage, which conducted while the polymer remains in the solid state.

During the prepolymerization stage, direct esterification of the diol, either EG for PET, or 1,4-butanediol (BD) for PBT, onto TPA or most commonly transesterification of the diol onto dimethyl terephthalate (DMT), is carried out to form the corresponding diol-ester. DMT is produced separately as the esterification product of TPA with methanol. The DMT route is sometimes preferred because DMT is more soluble in the reaction mix and easier to purify than TPA. Additionally, TPA is known to catalyze the cyclization of BD and is largely avoided in PBT manufacturing [65–69].

The transesterification reaction is typically carried out in a CSTR by continuously feeding a “paste” of premixed DMT/diol into a diol-ester prefilled reactor operating between 160 and 240 °C. Typically DMT/diol molar ratios of 1 : 2 to 1 : 2.2 are used for PET and 1 : 1.1 to 1 : 1.5 for PBT. The reaction for PET is catalyzed by a metal acetate. Zinc acetate is commonly used, but antimony, barium, calcium, and magnesium acetates may also be used. For PBT titanium orthoesters, such as tetra-butyl titanate, are employed as catalysts. The CSTR operates at low pressures, 0.1 to 1.0 bar, allowing the condensation product (methanol) and the excess diol to be distilled out of the reactor through a system of overhead condensers and distillation columns. Typical residence times in the reactor are between 60 and 240 min. The reaction product consists of a mix of the diol-ester and some low molecular weight oligomers. This first step is shown for PET in Figure 13.9 [65].

The product of the prepolymerization stage is continuously fed into the melt polymerization reactor, where the condensation reaction of the diol-ester to form the corresponding polyalkylene terephthalate (PAT) (either PET or PBT), shown in Figure 13.10. In this self-trans-esterification, the ester-diol is the source of both ester and alcohol functionalities. Since these PE products are semicrystalline, the reaction must be carried out above their melting point (T_m) to prevent solidification of the

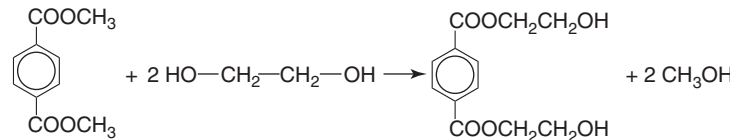


Figure 13.9 DMT transesterification (first stage).

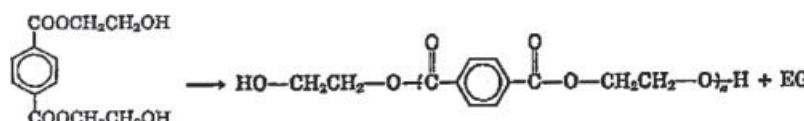


Figure 13.10 Self-trans-esterification to produce PET.

reaction mass (T_m of PBT = 222–232 °C and T_m of PET = 255–265 °C). As with any equilibrium condensation reaction, attaining high reactive group conversions, and thus high PE molecular weights, requires the effective elimination of the diol condensation product.

Given the current high plant throughputs (50,000–300,000 tons/year), and the need for high reaction temperatures and low pressures to attain the required product molecular weight, these continuous reactor systems are complex. Reactor designs approaching plug flow performance are common. Among these, compartmentalized horizontal or vertical stirred reactors, with local stirring moving the reacting mass continuously between compartments and allowing for continuous removal of the diol by-product, are prominent in the art. Single compartmentalized reactors, or a series of reactors with enhanced ability to handle high viscosities, are common [65–68].

Melt polymerization reactors normally operate either isothermally or in prescribed upward temperature profiles at temperatures for PET between 260 and 290 °C and 230 and 260 °C for PBT. The reaction is catalyzed most commonly by antimony trioxide for PET and by titanium orthoesters for PBT, and operated at reactor pressures between 1 and 100 mbar. Temperature profile, reactor pressure, and catalyst concentration are set to minimize the residence time needed to attain a target M_w (usually 15,000 to 25,000 Da). Minimizing product exposure to extreme temperatures in these ranges is important to minimize thermal degradation, which leads to impurities and color. This is particularly important in PET used for food packaging, where small amounts of a particular degradation product, acetaldehyde (AA), may affect its organoleptic performance even at concentrations under 10 ppm. In this regard, the undesired presence of residual antimony compounds in PET food packaging is also pushing the industry toward antimony catalyst replacement. Different organo-metal compounds are being developed as suitable replacements.

The difficulty in eliminating the diol at high viscosities, the high energy requirements needed to stir and pump the

viscous mass, and the need to eliminate degradation by-products set a practical limit for the maximum M_w that can be achieved in these reactors (about M_n = 15,000–20,000 Da for PET and M_n = 25,000–40,000 Da for PBT). Normally, these melt polymerization product molecular weights are measured in the industry as intrinsic viscosity, I.V. = 0.5–0.6 dl/g for PET and I.V. = 0.8–1.2 dl/g for PBT corresponding to the M_n ranges above. These molecular weights confer PET and PBT PEs with sufficient mechanical properties for a wide variety of applications. More commonly, PET of this I.V. range is used in extrusion applications of fiber, film, and sheet, and PBT in injection molding applications such as electrical connectors [65–68]. Figure 13.11 shows a simplified process diagram for continuous PBT.

The molten PET or PBT products leaving the melt polymerization reactor are quenched, pelletized, and then crystallized by exposing the solid amorphous pellets to temperatures slightly under their T_g (120–140 °C and 30–50 °C, respectively) in crystallization silos. Normally, PBT crystallization rate is so high that the crystallization step can be avoided by controlled quenching of the melt polymerization product [65, 67, 68].

Demanding applications for PET, such as injection-blow molding of bottles and other food containers, and PBT-molded engineering parts, require higher molecular weights not attainable through melt polymerization. In these cases, solid-state polymerization (SSP) is employed. In a simple manner, SSP requires crystallized pellets of the melt polymerization to be exposed to high temperatures without melting, under high vacuum, and for long residence times, to remove residual diol molecules, thus allowing the equilibrium condensation reaction to proceed in the forward direction. Typically, SSP proceeds at measurable rates when temperatures approach $T_m - 10$ °C and pressures reach 1 to 50 mbar [70].

In batch SSP processes, crystallized PE pellets are loaded into rotating drum reactors heated to the required temperature under dry N_2 , and subjected to extremely low

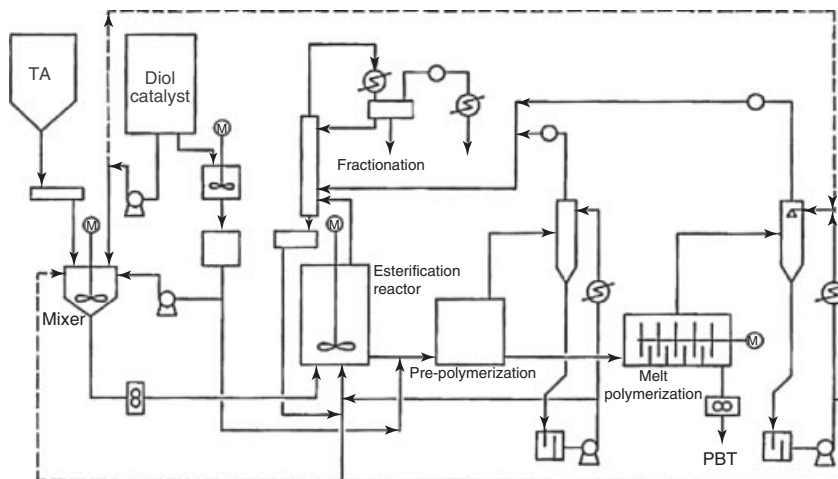


Figure 13.11 Schematic of bulk continuous polymerization process for high molecular weight PBT [67].

pressures (<50 mbar) to slowly eliminate diol promoting further polymer–polymer condensation. At these conditions, the molecular weight of PET can increase from $M_n = 20,000\text{--}50,000$ Da (I. V. = 0.6–1.0 dl/g) within 10–24 h residence time. This M_n allows PET to be used in food bottles and engineering applications such as tire cords. The M_w of PBT can be also increased via SSP to levels exceeding $M_n = 100,000$ Da for demanding engineering applications [65, 70].

Continuous SSP is carried out nowadays at throughputs relevant to the high melt polymerization rates so that it can be done in series to obtain high I.V. grades in a single continuous process train. Most high throughput plants are designed in this manner. In this case, the SSP reactor consists of plug flow large vertical continuous vessels where crystallized pellets are maintained under a vigorous stream of dried hot nitrogen as they slowly flow from top to bottom of the vessel. By controlling the flow and temperature of the nitrogen stream close to T_m , the SSP proceeds at rates requiring only a few hours residence time to get to the target I.V. [70, 71].

13.3.3.2 Polyamides PAs are the polycondensation reaction product of diamines, of general formula $\text{NH}_2\text{-R-NH}_2$ with dicarboxylic acids of general formula HOOC-R'-COOH . Batch and continuous processes for PAs have been used over the last 70 years, since Carothers synthesized the first materials in the 1930s. Nylon 6,6 is made by a multistage process by bulk polymerization of hexamethylene diamine and adipic acid. In this process, 2 CSTRs + last stage + vacuum are employed.

Nylon-6, on the other hand, is made by the ring opening polymerization of caprolactam with water in a tubular VK column reactor [6–8]. The process consists of two main stages: (i) caprolactam hydrolysis to aminocaproic

acid (ACA) and (ii) linear self-condensation polymerization of ACA and ring opening addition of caprolactam. The reaction scheme is shown in Figure 13.12 [72].

Molten caprolactam at about 80–100 °C is continuously fed into a steam-pressurized CSTR operating at temperatures between 90 and 125 °C for 30–180 min residence time. At these conditions, caprolactam hydrolyzes to ACA until equilibrium is reached at about 10 mol% of caprolactam in the mix. At these conditions, the reaction mix starts incipient A-R-B linear polycondensation of the amine and carboxylic acid moieties. A blend of ACA, caprolactam, and oligomers of polyaminocaproic polymerization and H_2O from the hydrolysis reactor, is continuously fed into a series of 2–3 CSTRs operating at temperatures between 220 and 300 °C, at very low pressures (<10 torr) under nitrogen. The average residence time in each reactor is about 1–3 h. Reactors are fitted with continuous head space purging designed to eliminate condensation water and low molecular weight oligomers from the reactor, so that reaction can proceed to high functional group conversions and high molecular weights. Catalysts, commonly phosphites, allow the polymerization to proceed toward high conversions. Molecular weight is often controlled at the right target by adding small amounts of monofunctional acids or amines. The molten PA 6 product is quenched, pelletized, and washed in a leaching tower operating with water at about 100 °C. Pellets are then dried [72–75]. The process diagram is shown in Figure 13.13.

13.3.3.3 Polycarbonates Polycarbonates are linear PEs of carbonic acid, the vast majority of which are based on bisphenol A diol, as shown in Figure 13.14. Modern polycarbonates have a high T_g ranging from 140 to 155 °C, are tough, transparent, and thermally stable. Two important and distinct commercial manufacturing routes are used in

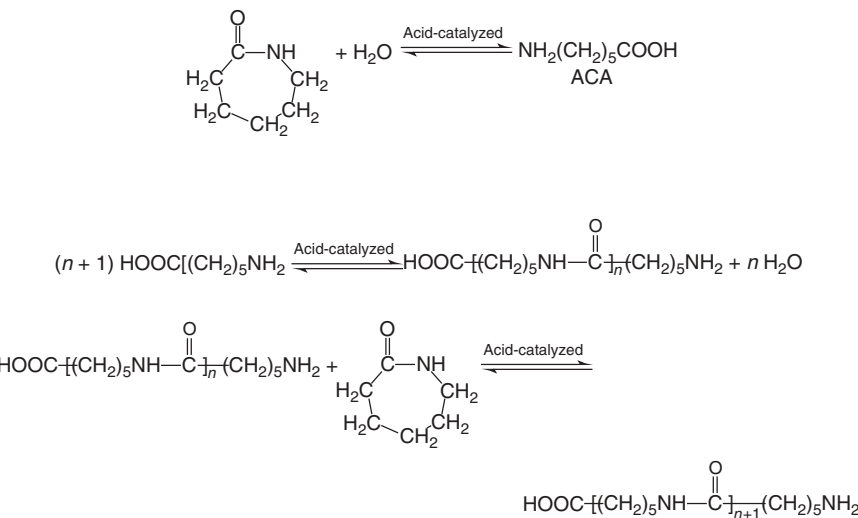


Figure 13.12 Polyamide 6, reaction scheme.

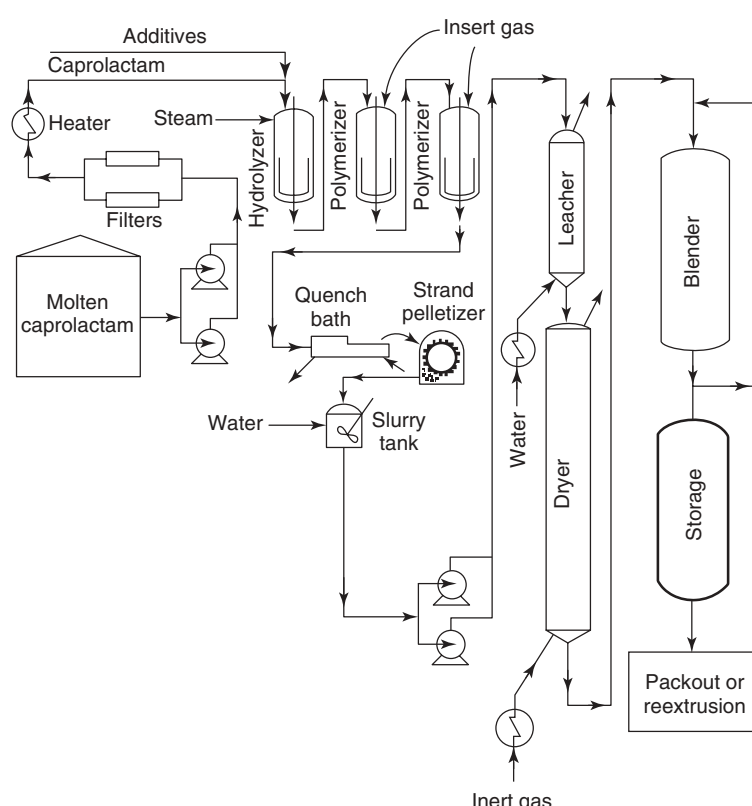


Figure 13.13 Schematic of bulk continuous polyamide 6 process. *Source:* Reproduced with permission from Welgos RJ. Polyamides, plastics. In: Kroschwitz JI, editor. High performance polymers and composites. John Wiley & Sons; 1991. p 519–527 [72]. Copyright 1991 John Wiley & Sons.

polycarbonate manufacture today. The first is an interfacial polymerization involving a Schotten–Baumann reaction of phosgene with an aromatic diol such as bisphenol A in an amine-catalyzed reaction [76]. An alternative bulk polymerization process for making polycarbonates is based

on the melt transesterification of bisphenol A with diphenyl carbonate [12]. Early patents for this technology were issued to GE in 1964 [77].

In the melt transesterification process, bisphenol A and diphenyl carbonate are heated to high temperatures

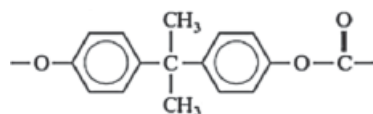


Figure 13.14 Polycarbonate (PC) repeat unit structure.

(200–300 °C) under vacuum to remove phenol under equilibrium. The reaction is generally catalyzed by basic materials such as Na, Li, and K hydroxides. During the final stages of the polymerization, the polymer melt becomes viscous, and thus, additional equipment such as WFEs or extruders are needed to remove residual phenol. Claimed advantages of the melt transesterification process for polycarbonate include stable molecular weight with thermal processing and lower oligomers [76].

13.3.3.4 Polysulfones Polysulfones are aromatic PEs made usually by the reaction of bisphenol A and bis(4-chlorophenyl) sulfone in a nucleophilic substitution condensation reaction. The first polysulfones produced by Union Carbide in the early 1960s involved the reaction of bisphenol with and bis(4-chlorophenyl) sulfone in the presence of an alkali base (NaOH, KOH, and K carbonate) in a dipolar aprotic solvent such as NMP, DMSO, sulfolane, or dimethyl acetamide [78]. Typical temperatures are in the range of 130–160 °C. The reaction of the base with bis A generates water, which must be removed.



13.3.4 Processes for Ionic/Anionic Polymerization

Ionic polymerization systems of commercial importance employ mostly batch and continuous solution polymerization processes. Suitable monomers for ionic polymerization include conjugated dienes and vinyl aromatic. Among these, the anionic polymerization of styrene–butadiene (SB) and styrene–isoprene (SI) copolymers and the cationic polymerization of styrene are the most commercially important systems.

13.3.4.1 Anionic Polystyrene (PS), Styrene–Butadiene (SB), and Styrene–Isoprene (SI) Copolymers Anionic addition polymerization requires monomers bearing carbon–carbon double bonds ($C=C$) able to form stable propagating carbanions ($C-C^-$) after their formation through an electron transfer reaction with an organo-metal compound, most commonly *n*-butyl-lithium, *s*-butyl-lithium, and *t*-butyl-lithium initiators. The list of monomers meeting these conditions is relatively short, yet some commercially important addition monomers like styrene, butadiene, and isoprene are part of this list.

Although stable carbanions propagate at comparable rates as their free radical counterparts, anionic polymerization presents two main mechanistic differences

over free radical polymerization: (i) pseudo-instantaneous initiation, resulting in virtually all polymer chains undergoing initiation simultaneously and (ii) the absence of polymer–polymer bimolecular termination reactions. The direct result of these is that living quasi-monodispersed polymer chains of stoichiometric D_n (=moles of reacted monomer/moles of initiator) are present at any time in the reaction mix, with the final $M_n \approx M_w =$ (total moles of monomer in the mix/total moles of initiator in the mix). Importantly, the lack of polymer–polymer termination confers a living character to the polymer–lithium propagating chains allowing for the addition of comonomers to the reaction mix in manners that allow control of the copolymer microstructure. For instance, in addition to the random copolymers obtained by simultaneous addition of monomers A and B, fast addition of monomer A followed by an increased addition of a monomer B from low to high A/B ratios allows for compositionally tapered polymer chain microstructures rich in one end of monomer A and of monomer B in the other end. Moreover, the addition of monomer B to the reaction mix after monomer A has been consumed allows for nearly perfect AB block formation in every chain. The addition of monomer A after B is exhausted would further allow for ABA triblock copolymer formation. This ability gives anionic polymerization its synthetic advantages over other addition polymerization methods that do not allow for MW monodispersed or controllable block formation [23, 79].

As main disadvantages, anionic polymerization requires the use of completely dry (moisture free) and high purity raw materials, since moisture and other impurities (acids, alcohols) deactivate anions via proton transfer destroying the living character of the chains, and requires a relatively large concentration of solvent (30–70% w/w) to control the high heat evolution caused by the instantaneous initiation. The fact that the final M_w of the polymer product is independent of the reaction rate allows for high product reproducibility in a broad range of reaction conditions of temperature ($T_{rx} = -70$ –130 °C) and monomer concentration ([M] = 0.5–5 mol/l), as long as the initiator-to-monomer mole ratio is maintained the same in the initial reaction mix. This allows for highly nonisothermal conditions (semi-adiabatic conditions) to be used in anionic reactors as the temperature profile is unimportant for the final MWD of the product [79, 80].

With this in mind, the anionic polymerization of styrene (PS), styrene–butadiene (SB), or SI is typically carried out by feeding distilled and dried monomer and solvent and purified *n*-butyl-lithium to a CSTR operating in semicontinuous mode. The reaction mix is heated to the reaction temperature and the second monomer is fed at a programmed feed rate that allows the desired copolymer microstructure to be built, whether a block SB or SI, or tapered or random copolymers. Solution SBR is commonly



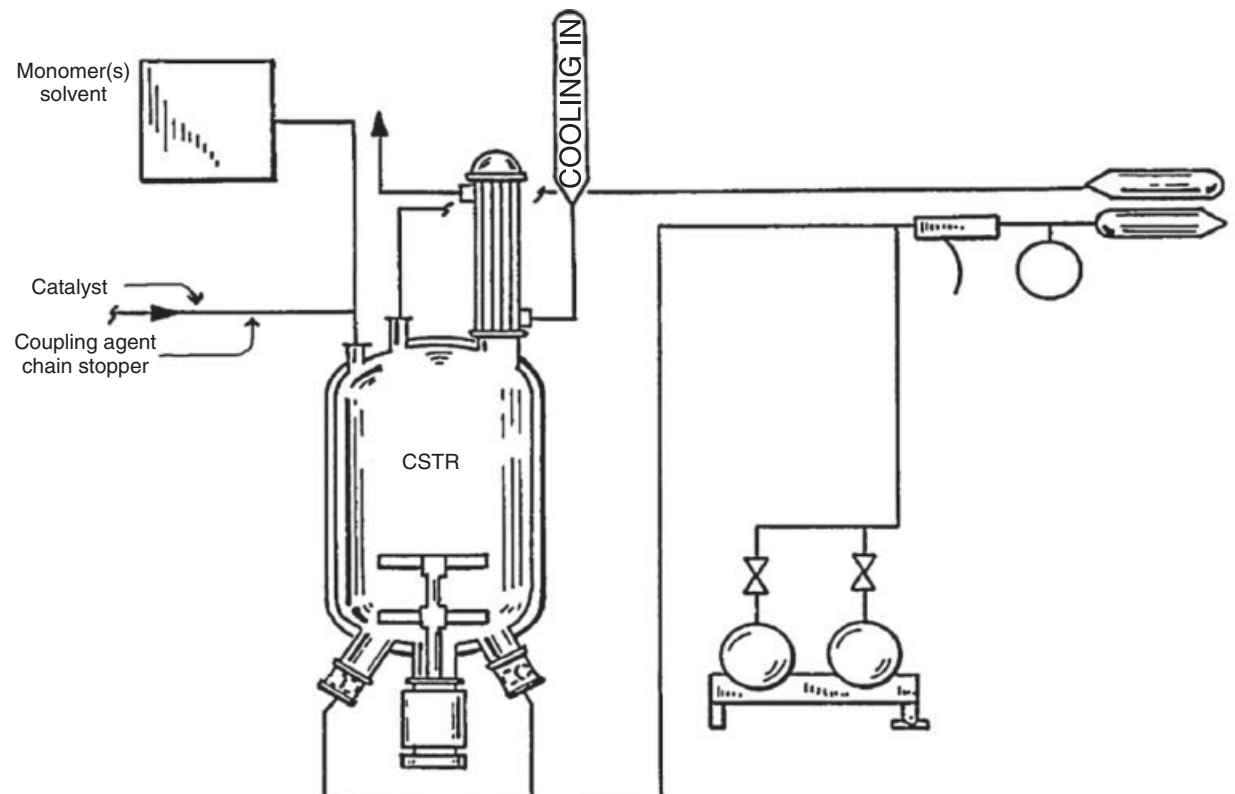


Figure 13.15 Reactor and termination stage in batch and semicontinuous anionic polymerization.
I: Recycle stream from fractionator; and II: polymer product stream to devolatilization fractionation [100].

made as a random or tapered copolymer in a variety of compositions (butadiene >70% w/w/p). Thermoplastic elastomers (TPEs) normally require SB or SI blocks and a butadiene or isoprene content >50% w/w. Transparent and ductile PS grades are made as block or tapered blocks with butadiene contents under 40% (w/wp). PS is often manufactured for specialty applications such as HPLC column standards. Figure 13.15 shows a typical reaction array for batch or semicontinuous anionic polymerization.

Solvent type plays a very important role in the reactivity ratios of anionic copolymerization pairs. Hydrocarbon solvents, such as C4–C10 alkanes and cycloalkanes, are commonly used. *n*-Hexane and cyclohexane are employed in many commercial processes. Except for some SBRs with very specific microstructures made at very low temperatures ($T_{rx} < -20^{\circ}\text{C}$), the so-called cold rubbers, most anionic polymerization processes occur at relatively high temperatures ($T_p > 30\text{--}100^{\circ}\text{C}$), isothermally or semiadiabatically. Number average molecular weights for the blocks vary widely but may be most commonly maintained between 30,000 and 100,000 Da. Once all monomer has been consumed via propagation reactions, a short stopper reactant, typically alcohol or water, is added to the mix to kill the living character of the anion and

complete the polymerization process. In some instances, coupling agents such as polyepoxides, PEs, and polyhalides are added to terminate the anions, SB and SI star polymers with 2, 4, 6, or 8 SB arms, or combinations thereof are formed by adding bi-, tetra-, hexa-, or octofunctional coupling agents, respectively [23, 79–81].

SBS and SIS triblock copolymers are alternatively made by using bifunctional initiators that create two growing anions, one on each end of the polymer chain. In these cases, the central block (PB or polyisoprene) is grown first, followed by an addition of the right ratio of styrene monomer. Owing to the need for high purity and dry monomer and solvent, the polymer separation part of the process is complex. First, the polymer is coagulated into large agglomerates (crumbs) via a solvent exchange process in a large agitated tank and then separates via centrifugation prior to be sent to dryers. Elastomers and SBRs are bagged as crumbs, and TPEs and thermoplastics as powder or pelletized particles. The solvents, unreacted monomers, by-products, and impurities from the additives system (antioxidants, stabilizers, etc.) are separated by a series of distillation columns that recover solvent and any residual monomer to be used in the next polymerization [23, 80, 81].

13.3.5 Processes for Homogenous Catalyzed Polymerization

13.3.5.1 Polyethylene Polyethylene is produced by several commercial processes including gas-phase fluidized bed, liquid slurry CSTR or loop reactors, autoclaves, and tubes. LLDPE and HDPE grades of polyethylene have been and are still produced in a continuous solution process by companies such as Dow and DuPont using homogenous Ziegler–Natta or Metallocene catalysts. Ethylene, comonomers (1-octene, 1-hexene, and 1-butene), solvent (e.g., cyclohexane, iso-octane, and isopar E), and catalyst (Ti, V, and Cr) are provided to a CSTR operating at high temperatures (150–250 °C) and pressures from 35 to 140 bar [82]. The product is continuously charged to a flash separator to remove solvent and the polymer is subsequently pelletized [83, 84]. Compared to older processes, modern processes with high efficiency catalysts no longer require a catalyst separation stage and thus are more economical than older plants [85]. Solution processes for polyethylene have relatively small reactors, short residence times (~10 min), and fast transitions, but there are limitations on molecular weight due to solution viscosity [86]. They are ideal for the production of rubber materials, such as EPR and other tacky copolymers that cannot be produced in traditional slurry or gas-phase polymerizations. The process is well suited for making copolymers of ethylene with higher α -olefins such as 1-octene that are difficult to make in gas phase, due to low comonomer vapor pressures.

13.4 ENERGY CONSIDERATIONS

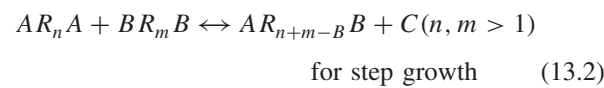
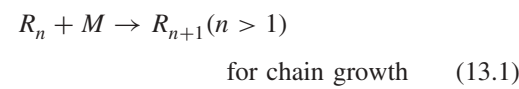
Historically, the emergence of different polymerization methods has been the result of dealing with basic engineering principles of mass and energy balances. While mass balances define the desired amounts and ratios of chemical reactants in a polymerization reactor (monomers, catalysts, initiators, etc.), the energy balance defines our ability to control the reactor operating temperature. As other chemical processes, polymerization processes can be designed to operate in batch, semicontinuous, or continuous modes. In turn, each one of these processes can be designed to operate isothermally, (semi)adiabatically, or under a prescribed temperature path. Given that elemental polymerization reactions, as many other chemical reactions, exhibit an Arrhenius-type exponential rate dependency with temperature ($k_p = A \exp(-E/RT)$), the outcome of a given polymerization recipe, namely, the extent of reaction, reaction rate, and the molecular weight distribution of the polymer, will be strongly influenced by the ability to control the reaction temperature in the prescribed manner. The simultaneous solution of mass and energy balances defines the type and size of reactor necessary to achieve the desired throughput and polymer characteristics.

TABLE 13.1 Heat of Reaction for Some Common Monomers

	kcal/mol at 25 °C
Ethylene	21.2
Propylene	19.5
Butadiene	17.6
Styrene	16.7
Vinyl chloride	22.9
Vinylidene chloride	18.0
Vinyl acetate	21.2
Methyl acrylate	18.5
Methyl methacrylate	13.2
Acrylonitrile	18.4
Formaldehyde	7.4

13.4.1 Heat of Polymerization

The elementary propagation steps for chain growth and step-growth polymerizations are shown below:



The heats of polymerization for both of these steps are considerably different. For additional polymerization through the $C=C$, heats of reaction are in the order of 100–200 kJ/mol. While the energy on a molar basis is rather consistent, as shown in Table 13.1, on a mass balance this implies that small monomers often are more energetic than larger monomers, for example, acrylic acid versus stearyl acrylate. On the other hand, the heats of polymerization for condensation reactions are quite low because the bond energies of the monomer and products are similar. A consequence of this is that for addition polymerizations, the heats of polymerization are quite high, and thus, removing sufficient heat from the process is often the problem. On the other hand, in step polymerizations, the issue is rarely removing heat; however, adding heat to maintain a high reaction temperature can be an issue. We explore these aspects further below.

13.4.2 Adiabatic Temperature Rise

A useful way to depict how highly energetic polymerization reactions are is the computation of their adiabatic temperature rise. Adiabatic temperature rise, ΔT_a , is defined as the maximum temperature rise achieved during an exothermic chemical reaction when all heat generated by the reaction is adsorbed by the reacting mass in a closed system with

zero heat transfer to the surroundings. It can be related to the heat of polymerization, ΔH_p , and the average heat capacity of the system over the temperature interval, \hat{C}_p , and simply equal to the difference in the final, T_f , and initial, T_0 , temperature of the system. For many materials, the heat capacity at room temperature is roughly 2 kJ/kg and decreases moderately over temperature. An average heat capacity calculated or measured with techniques such as modulated differential scanning calorimetry (MDSC) can be used to measure heat capacity with temperature:

$$\Delta T_a = T_f - T_0 = \frac{-\Delta H_p}{\hat{C}_p} \quad (13.3)$$

$$\hat{C}_p = \frac{\int_{T_0}^{T_f} C_p dT}{(T_f - T_0)} \quad (13.4)$$

Adiabatic temperature rise for free radical polymerizations can be substantial (hundreds of degrees Celsius). If allowed to polymerize adiabatically, many of these monomers would first yield high reactor pressures during the polymerization, followed by decomposition to gases. Thus, extremely large increases of temperature must be anticipated during adiabatic polymerization conditions. Taking into account the changes in rate of reaction, heat generation rate, and monomer vapor pressure associated with these large changes in polymerization temperature, it is clear that polymerization reactions approaching adiabatic conditions will operate in a self-accelerating mode, extremely challenging to control [87–89].

One method of handling the high adiabatic temperature rise is to provide a solvent in the formulation. In this case, some of the heat is absorbed by the solvent during the polymerization. The adiabatic temperature rise is thus a function of the solid fraction, x , in the original formulation, and the average heat capacity of the polymer + solvent:

$$\Delta T_a = \frac{-x \Delta H_p}{\hat{C}_p} \quad (13.5)$$

13.4.3 Self-Accelerating Temperature

The temperature at which a polymerization can be self-sustaining is termed *self-accelerating temperature* (SAT). It can be conveniently measured by a calorimeter run such as a vent sizing package (VSP) or reactive safety screening tool (RSST). For polymerizations, the SAT should be measured on the feed used in the polymerization. In cases where initiator is charged to the feed, measurements must be done on the initiated feed. VSP or RSST instruments are important safety tools for studying the exothermic polymerization systems and for evaluating appropriate relief devices [90].

13.4.4 Reactor Energy Balance

The general energy balance for a reactor element can be simply expressed as

$$\text{Accumulation} = \text{In} - \text{Out} + \text{Generation} - \text{Losses} \quad (13.6)$$

Accumulation terms generally reflect the change in temperature of the process. Inflow and outflow terms measure the enthalpy of the feeds, product, and by-products leaving or entering a reactor element. The generation terms are the heats of polymerization but may include power added from mechanical equipment, such as agitators. Losses include transport of energy to the reactor surface, heat transfer to a fluid via jacket, walls or coils, and losses through uninsulated surfaces. Balances may be written at steady state when the accumulation term disappears or dynamically. We explore these further for the different chemistries and reactive systems.

13.4.4.1 CSTR For a CSTR, the energy balance for material in the reactor can be written as follows, where we have assumed heat transfer to both a jacket and losses to the atmosphere. In the case of additional coils in the reactor, a further term can be added:

$$\frac{d}{dt} (m \hat{C}_p T) = Q_{in} \hat{C}_{pin} T_{in} - Q_{out} \hat{C}_p T + m R_p \Delta H_p - UA_t (T - T_{Amb}) - UA_j (T - T_j) \quad (13.7)$$

In Equation 13.7, m is the mass in the reactor; t is time; T , T_{in} , T_{Amb} , T_j are reactor, inlet, ambient, and jacket temperatures; \hat{C}_p , \hat{C}_{pin} are reactor and inlet feed heat capacities; Q_{in} , Q_{out} are mass flow rates into and out of the reactor; R_p is rate of polymerization; ΔH_p is heat of polymerization; and UA_t , UA_j are heat transfer coefficients for ambient and jacket heat transfer.

In the case where the mass flows in and out of the reactor are constant and assuming average heat capacity in the reactor and the feed and constant density, we can simplify the above equation, resulting in Equation 13.8:

$$\frac{dT}{dt} = \frac{(T_{in} - T)}{\theta} + \frac{m R_p \Delta H_p - UA_t (T - T_{Amb}) - UA_j (T - T_j)}{m \hat{C}_p} \quad (13.8)$$

At steady state, the change in temperature is zero and we can rearrange the equation into a more useful form, as expressed in Equation 13.9:

$$T = T_{in} + \frac{\frac{\theta}{m\hat{C}_p} (mR_p \Delta H_p + UA_t (T_{Amb}) + UA_j (T_j))}{\left(1 + \frac{\theta}{m\hat{C}_p} (UA_t + UA_j)\right)} \quad (13.9)$$

The careful reader will note that in addition to heat losses from jacket or ambient losses, heat is consumed by sensible heat of raising the temperature of the feed to the reactor temperature:

$$Q_{in} \hat{C}_p (T_{in} - T) \quad (13.10)$$

As reactor temperature increases, the heat load from heating the feed becomes significant. At very high operation temperatures, the process can operate at net endothermic and require heat addition. The energy balance of the system is such that at low temperatures, the CSTR operates in exothermic mode, that is, net heat must be removed from the process jacket or sometimes internal coils. At elevated process conditions, the system becomes net endothermic as a result of the considerable heat required to raise the feed to reactor temperature. The total heat of polymerization is dependent on both the energetics of the system and the conversion of monomer to polymer. This in turn is defined by the kinetics of the system [50, 91, 92].

The solvents added to the system reduce the heat load of the reactor because energy is needed to increase the temperature of the solvent to the reactor conditions (sensible heat), yet no heat of polymerization is released by the solvent. This can be an effective measure to reduce heat load at the expense of reduced polymer productivity. When the reactor system operates at elevated temperatures, the additional solvent can pose a challenge to the heating system. Because of the sensible heat effect, some processes use chilling of the monomer, as long as the chilled temperature is not too low to freeze any component.

The heat transfer coefficient UA_t for ambient temperature loss is a function of how well insulated the reactor is. Jacket heat transfer coefficient, UA_j , is a function of the reactor geometry, agitator blade design and RPMs, the viscosity of the medium, and relative amount of fouling in the reactor. The viscosity of the reaction medium as discussed before is dependent on solids level, M_w , and T_g of the polymer as well as reactor temperature. In general, removing heat from the CSTR becomes more difficult as the reactor size increases due to the surface to volume ratios.

13.4.4.2 Cascade of CSTRs In several processes, a cascade of CSTRs may be used to obtain the desired polymer properties and maximize monomer conversion. Conversion of monomer increases from reactor to reactor and thus the solids content and viscosity would increase and heat transfer coefficients decrease for each progressive reactor. For each reactor, an energy balance can be performed using Equation 13.9 by replacing the temperature

of the inlet feed with that of the exit temperature of the prior CSTR. An immediate observation is that the sensible heat available for cooling or heating (which depends on the operating temperatures of the reactors) the downstream reactor is less than available to the first reactor (51, 92). On the other hand, as one progresses from reactor 1 to 2 to 3, etc., less monomer is available to convert to polymer and less polymerization heat is given off. The overall heat load and heat removal technical challenges are thus dependent on the specific product made. Commonly, the second and third reactors in a process experience “bumps” in temperature, which are less severe than the first CSTR.

13.4.4.3 Tubular Reactors Tubular reactors can also be used for polymerizations. In general, these have high surface to volume ratios and commonly the temperature in the center of the reaction medium is higher than the outside. Larger tube diameters increase productivity but reduce heat transfer effectiveness and sometimes static mixing elements are added to increase axial mixing. Without static mixing, tubular reactors can approach zero slip at the wall surface and thus polymer may deposit over time, gel and foul the surface of the unit, thus causing a decline in heat transfer coefficient. The reader is referred to the following good references for more information [93, 94].

13.5 MASS CONSIDERATIONS

13.5.1 Reactor Size

Bulk and solution processes range from small laboratory scale vessels smaller than 100 ml to large industrial processes capable of manufacturing millions of kilograms per year of product. At the pressure rated laboratory vessels can be conveniently purchased as “off the shelf” products from a variety of suppliers. Often the reactors are certified for pressures and temperatures well above the expected manufacturing process and serve amply for research and development purposes. However, a major challenge for small-scale polymerization vessels is maintaining adequate heating and insulation on bare metal surfaces. For bulk and solution polymerization, the polymer may be ultimately separated from the unreacted monomers and solvent and thus the viscous resin must be maintained hot and flowing to avoid solidification and plugging.

Bulk and solution polymerization pilot plants are designed to mimic the manufacturing plants to facilitate accurate scale-up to the manufacturing process. Often in the liter to tens of liters sizes, they are usually built with the same quality and safety standards of a manufacturing process with Class 1, Div. 1 or Class 1 Div. 2 rated areas. The number and sizes of the pilot reactors is a function of the development activity load and the sample sizes needed for application testing.

Commercial manufacturing plants are sized to provide sufficient volume of product to satisfy market demand with provisions for reasonable growth. Maximizing the benefits of economies of scale while minimizing inventories, waste, and energy demands are key for a cost effective process. Often, the same reactor is used for multiple products and consideration of strategies for efficient product transitions, often in between chemistries is important [86]. For batch/semibatch processes, the yearly production volume is highly dependent on the reactor size and total batch time. However, it should be noted that total batch time must take into consideration all process steps such as precleaning, preheating, precharges, polymerization time, postreaction hold time, solvent stripping, cool down, product discharge, postcleaning, etc. Batch processes are generally built to be as large as possible but practical constraints such as mechanical equipment fabrication, heat and mass transfer effects, controllability, and safety limit the maximum effective reactor size. Thus, often, a batch/semibatch plant will be composed of several reactors operating independently for manufacturing the entire line of products. Continuous bulk and solution processes are ideal for making long runs of a given product grade; however, because of capital cost, they commonly produce multiple grades in a given process train. Reactor sizes are much smaller than batch/semibatch reactors and heat transfer often better. As with batch processes, many of the same issues of inventory management, grade transitions, reactor cleaning, and maintenance apply. However, the consequences of a process upset are more severe with a continuous process, which is designed to “keep running” when started up.

13.5.2 Process Residence Time, Conversion, Transients, and Steady State

The influence of the various feed flows, process kinetics, and reactor geometry on reactor productivity and product properties is complex and beyond the scope of this chapter. The interested reader is encouraged to read the other chapters of this book, or the references provided in those chapters, for more details on process modeling, kinetic mechanisms and the prediction of polymer properties. In this section, key implications of these are briefly discussed.

In Section 13.3.1, the concept of batch/reactor residence time was presented. For batch/semibatch processes, batch time is often simply dictated by the maximum polymerization rate possible for a given piece of equipment and the time required to reduce monomer residuals or end groups to within specification. For a continuous bulk or solution process, reactor residence time is simply a function of the size of the vessel and how fast monomer can be pumped

through it. Monomer conversion to polymer increases with residence time but the returns are usually diminishing. Polymer properties, such as molecular weight, may also be dependent on residence time. The task of the chemical engineering is to balance reactor productivity with properties within the range of residence times practical for the continuous process. This implies consideration of the maximum and minimum capabilities of upstream and downstream process equipment.

Process residence time has a major impact on the time required to bring a continuous process to steady state and thus making on specification product. For plug flow type processes such as tubular reactors, changes to the process take on the order of one residence time to make good product. However, for CSTRs, at least 3–4 residence times is needed during a transition before the system is at steady state. Thus, a CSTR with 5 min residence time can come to steady state in 15–20 min, whereas a CSTR with a 2 h residence time would take 6–8 h. In either case, the amount of intermediate “waste” material would equal several reactor turnovers [95].

13.5.3 Reactor Pressure

Continuous bulk and solution polymerization processes often operate at moderate-to-high pressures. Predicting the expected pressure in the reactor is critical to designing safe processes. In a closed reactor vessel, the equilibrium pressure is a function of the vapor pressure of the material in the vessel plus condensable gases. A first estimate of the vapor pressure is a simple Raoult’s law summation of the vapor pressure of each remaining ingredient in the reactor such as solvent and unreacted monomer and should include any small molecules formed during polymerization such as water, alcohol condensate, and initiator by-products. Simple Antoine-type expressions usually suffice for individual vapor pressure predictions, but often a Flory–Huggins expression is needed to account for the interaction between the polymer in solution and solvents. Noncondensable gases contribute additively to the total reactor pressure. These may include precharged gases such as nitrogen and gases generated during the polymerization. Examples include nitrogen generated from azo initiators or CO₂ generated from some peroxides or by decarboxylation of monomer [95].

13.5.4 Viscosity

In bulk and solution polymerizations, the reaction mixture is homogenous (single phase) and thus the viscosity at any time is given by the viscosity of polymer solution at the given reactor temperature. During the polymerization, high solution viscosity can constrain mixing, heat and mass

transfer, and product flow from the vessel. Therefore, to maintain a manageable viscosity in the reactor, polymer solids are often limited, minimum temperature guidelines are established, or the final product properties (T_g , M_w) constrained. Consideration must also be given to the final solution viscosity after cool down if the product is supplied in solvent or the molten polymer viscosity at process temperature if the solvent is to be stripped from the resin during processing.

For amorphous polymers, the viscosity at a given temperature is a function of the T_g and M_w of the material. For many polymers, the Williams–Landry–Ferry (WLF) equation provides a good estimate of melt viscosity where η_T is melt viscosity, η_{T_g} polymer viscosity at T_g , T is the melt temperature, T_g the polymer glass-transition temperature, and b and f_g are parameters:

$$\ln\left(\frac{\eta_T}{\eta_{T_g}}\right) = \frac{\left(\frac{b}{f_g}\right)(T - T_g)}{\left(\frac{b}{f_g}\right) + (T - T_g)} \quad (13.11)$$

The WLF equation is based on the Doolittle relationship between viscosity and free volume and the assumption of a linear relationship between free volume and temperature difference from T_g , that is, the so-called iso-free volume ($T - T_g$) condition. For many polymers, $b = 1$ and $f_g = 0.025$. Below the entanglement molecular weight, the viscosity of a linear polymer in the melt state generally follows a slope of 1 on a log scale with M_w and 3.4 above the entanglement molecular weight. The WLF equation has great utility for a given polymer and has recently been cast in a generic form for amorphous polymer to account for the T_g dependence on M_n for oligomers and also the molecular weight of the polymer [96].

In nonaqueous solvents, the viscosities of polymer solutions is often well described by a simple relationship with temperature, solids and M_w and T_g can be fit to a general semiempirical expression as described by Pezzin [97]. Essentially, higher solids, M_w and T_g and lower temperatures yield higher viscosity solutions. Secondary factors such as hydrogen bonding can also impact the solution viscosity and this must be taken into consideration when using functional monomers. Solutions in water are much more difficult to predict as neutralized polymer solutions often go through a maximum in viscosity with neutralization degree then decrease.

13.5.5 Mixing

Adequate mixing during polymerization is critical to achieving uniform product quality, heat transfer, and efficient use of initiator systems. A variety of blade designs have been used for polymerization systems ranging from pitched blade multiflight arrays to helical screws. The

choice of mixing system depends on viscosity and shear requirements, power to volume ratios, as well as heat transfer needs. Often baffles can be added to the reactors to improve mixing and flow patterns in the reactor, but postcleaning must always be factored into the design.

Mixing times should be relatively short compared to reaction times. In free radical polymerization, poor mixing can lead to inefficient utilization of the initiator if it is not dispersed adequately before decomposition, which can lead to molecular weight broadening. In condensation processes, sufficient mixing is important to ensure dispersion of all ingredients and the removal of condensate by-products. Concurrent with impeller design is the proper placement of feed injection tubes. These must be placed appropriately to ensure adequate distribution of the monomer, initiators, and additives. In modern polymerization technology, the use of fluid dynamics modeling software is extremely useful in predicting flow patterns and optimizing mixing designs.

13.5.6 Polymer Purification

In bulk and solution processes, the polymer product may often need removal of unreacted monomer and solvent. Several technologies are available that use high vacuum and temperature to strip the unreacted monomer and solvent from the resin. In most cases, the unreacted material can be condensed and recycled back to the process for further use or optionally burned as fuel.

Flash devolatilization is a simple and effective method to remove the majority of solvent and unreacted monomers from the polymer solution. Product from the reactor is charged to a flash vessel and throttled to vacuum conditions whereby the volatile solvent and monomers are recovered and condensed. In the process, the polymer melt cools, sometimes considerably, due to the evaporation of volatiles. The polymer product is pumped from the bottom of the flash vessel with a gear pump or other suitable pump for viscous materials. Critical to operation of the flash devolatilization unit is prevention of air back into the unit that reduces “stripping” ability and potentially allows oxygen into the unit that can discolor products or pose a safety hazard if low autoignition temperature solvents are used. Often one flash devolatilization unit is insufficient to reduce the residual material to a sufficient level and thus additional units can be added in series [61]. In each vessel, the equilibrium concentration of volatile material in the polymer melt, is a function of the pressure and temperature the flash unit operates at, with consideration for the polymer solvent interaction effects described by the Flory–Huggins equation. Flash devolatilization units, while simple to operate, may be prone to foam development as the superheated volatiles rapidly escape from the polymer melt. Viscous polymers or polymers with mixed functionalities

can adhere to the surfaces of the vessel and discolor or form gels upon exposure to heat.

An alternative to a flash devolatilization unit is the oil heated thin film or WFE. In this equipment, the molten polymer/solvent solution is throttled to the WFE comprising a rotating set of blades that draws the melt into a thin film. In this manner, very good heat transfer from the oil heated surface is obtained and the thin film minimizes diffusion distances and allows rapid mass transfer of volatiles out of the melt. Both vertical and horizontal WFE units are in commercial production and are effective for small-to-medium-sized plants with moderate viscosity melts. Larger units require very large motors to strip viscous resins. Like flash devolatilization units, bubble formation and collapse are essential to effective mass transport of solvent from the polymer melt.

Commercial polymerization plants often use FSEs (23, 62). Often these are used as a secondary stripping stage whereby molten resin from a prior evaporation stage is preheated and then forced through a tray containing small holes. The polymer extrudes through the holes and falls by gravity into a vessel under pressure. The thin spaghetti-like strands provides good surface area for residual removal, and there are no costly moving parts in this unit. FSEs are particularly useful for high molecular weight, and high viscosity melts that have some mechanical integrity to them to prevent spattering on the vessel walls. As in other devolatilization equipment, the injection of a noncondensable gas such as nitrogen can enhance volatile stripping by reducing the partial pressure of the monomer and solvents.

Polymer devolatilization can also be accomplished by the use of single and twin screw extruders [61]. Extruders are well suited for high viscosity materials and, when equipped with appropriate vents, allow the discharge of volatiles.

Polymers made by batch and semibatch processes can also be stripped of unreacted solvents and monomers by processing through equipment described above, but commonly they are purified by vacuum stripping. In vacuum stripping, volatile solvents are pulled out at the end of the batch as much as possible. Initially the amount of solvent recovered is high; however, as the solids content increases, the melt viscosity increases and the rate of solvent recovered declines.

In all cases of polymer purification, care must be taken to avoid overheating the polymer during purification. Most polymers will discolor to a slightly amber color on extended heating especially in the presence of oxygen. Furthermore, many polymers are thermally sensitive and can degrade with excessive overheating. PS, for example, is known to degrade back to monomer upon extensive overheating [23]. Thus, increasing devolatilization temperature in PS first decreases and then increases free monomer.

REFERENCES

1. Mark HF. *Chem Eng News* 1976;54:176.
2. Semon WL, inventor; B.F. Goodrich, assignee. US patent 1,929,453. 1933.
3. Semon WL, inventor; B.F. Goodrich, assignee. US patent 2,188,396. 1940.
4. Dubois JH. *Plastics History - USA*. Boston: Cahners; 1971.
5. Schimidt F, inventor; Hopff H, I.G. Farbenindustrie, assignee. US patent 2,102,179. 1937.
6. Carothers WE, inventor; E.I. DuPont de Nemours, assignee. US patent 2,012,267. 1935.
7. Carothers WE, inventor; E.I. DuPont de Nemours, assignee. US patent 2,071,250. 1938.
8. Carothers WE, inventor; E.I. DuPont de Nemours, assignee. US patent 2,130,523. 1938.
9. Takamatsu T, Shioya S, Okada Y. *Ind Eng Chem Res* 1988;27:93.
10. Platzer N. *Ind Eng Chem* 1970;62:6.
11. Zacca J, Debling J, Ray WH. *Chem Eng Sci* 1996;51:4859.
12. Rudin A. *The Elements of Polymer Science and Engineering*. New York: Academic Press; 1982.
13. Matyjaszewski K, Davis TP. *Handbook of Radical Polymerization*. Hoboken: John Wiley and Sons; 2002.
14. Semple RB, inventor; Monsanto Chemical Co, assignee. US patent 2,367,805. 1945.
15. Glick SE, inventor; Monsanto Chemical Co, assignee. US patent 2,456,558. 1948.
16. Allen I Jr., Marshall WE, inventors; Union Carbide and Carbon Co, assignee. US patent 2,496,653. 1950.
17. Britton EC, LeFevre WJ, inventors; The Dow Chemical Co, assignee. US patent 2,359,196. 1944.
18. Villalobos MA, Hamielec AE, Wood PE. *J Appl Polym Sci* 1991;42:629.
19. Trommsdorff E, Kohle H, Lagally P. *Makromol Chem* 1947;1:169.
20. Friis N, Hamielec AE. *Polymer Prepr* 1975;16:192.
21. Wingler F, Schmidt A, Liebig L, Wassmuth G, inventors; Bayer, assignee. US patent 4,141,934. 1979.
22. Kotnur TA, Barber RL, Krueger WL, inventors; Minnesota Mining and Manufacturing Co, assignee. US patent 4,619,979. 1986.
23. Scheirs J, Priddy D. *Modern Styrenic Polymers: Polystyrenes and Styrenic Copolymers*. West Sussex, England: John Wiley and Sons; 2003.
24. Wallis JPA, Ritter RA, Andre H. *AIChE J* 1975;21:691.
25. Doak KW, Erchak M Jr., Toekes B, inventors. US patent 3,311,675. 1967.
26. Hamielec A, Lawless G, Schultz H, inventors; S. C. Johnson, assignee. US patent 4,414,370. 1983.
27. Schmidt R, Schultz H, Wilson D, inventors; S. C. Johnson, assignee. US patent 4,529,787. 1985.
28. Brand J, Morgan L, inventors; S. C. Johnson, assignee. US patent 4,546,160. 1985.

29. Campbell D. The kinetics of high temperature polymerization of styrene [dissertation]. Zurich: Swiss Federal Institute of Technology Zurich (ETHZ); 2003.
30. Melacini P, Patron L, Moretti A, Tedesco R, inventors; Montelibre S.p.H, assignee. US patent 3,839,288. 1974.
31. Peng FM. *J Appl Polym Sci* 1990;40:1289.
32. Anzaldi SL, Bonifaci E, Malaguti MV, Ravanetti GP. *J Mater Sci Lett* 1994;13:1555.
33. Huang NJ, Sundberg DC. *J Appl Polym Sci* 1995;33:2571.
34. Sosa JM, Morris J, inventors; Fina Technology Inc., assignee. US patent 4,857,587. 1989.
35. Fryling CF, inventors; Koppers Company, assignee. US patent 3,144,420. 1964.
36. Estonoz DA, Meira GR, Gomez N, Oliva HM. *AIChE J* 1998;44:427.
37. Simon RHM, inventors; Monsanto Co., assignee. US patent 4,252,911. 1981.
38. Preti D, Rossi AG, Nocci R, Vecchini N, inventors; Enichem S.P.A., assignee. US patent 5,807,928. 1998.
39. Shinmura T, Konishi K, inventors; Denki Kagaku Kogyo Kabushiki Kaisha, assignee. US patent 5,532,317. 1996.
40. Balbour M, Clarke J, Fone D, Hoggan A, James R, Jones Grad P, Lam P, Langham C, O'Hara K, Oldring P, Raynor G, Royston I, Tuck N, Usher R. *Waterborne & Solvent Based Acrylics and Their End User Applications*. London: SITA Technology Limited; 1996.
41. Krieg M, inventor; Rohm GmbH, assignee. US patent 5,324,802. 1994.
42. Shimada K, Maeda T, Nishizawa T, Narisada T, Anzai H, Sasaki Y, inventors; Mitsubishi Rayon Co., assignee. US patent 3,900,453. 1975.
43. Van Acker EM, Bijl JM, inventors; Shell Oil Co., assignee. US patent 4,062,908. 1977.
44. Archema Peroxide Initiators. Available at <http://www.arkema-inc.com>. Accessed 2012 Mar.
45. Dupont Vazo Initiators. Available at http://www2.dupont.com/Vazo/en_US/. Accessed 2012 Mar.
46. Callais P, Moskal M. Higher solids higher quality acrylic coatings resins. Available at www.arkema-inc.com/literature/pdf/304.pdf. Accessed 2012 Mar.
47. Spychaj T, Hamielec A. *J Appl Polym Sci* 1991;42:2111.
48. Campbell D, Teymour F, Morbidelli M. *Macromolecules* 2003;36:5502.
49. Debling J, Villalobos M. Modelling and simulation of continuous free radical polymerization with multiple monomers exhibiting reversible propagation. DECHEMA 7th International Workshop on Polymerization Reaction Engineering; 2001; Hamburg, DE.
50. Wang W, Hutchinson RA. *AIChE J* 2011;57:227.
51. Leamen M, McManus N, Penlidis A. *Chem Eng Sci* 2006;61:7774.
52. Nising P. High temperature radical polymerization of methyl methacrylate in a continuous pilot scale process [dissertation]. Lausanne: Ecole Polytechnique Federale de Lausanne; 2006.
53. McManus N, Penlidis A, Dube M. *Polymer* 2002;43:1607.
54. Peck ANF, Hutchinson RA. *Macromolecules* 2004;37:5944.
55. Webb S. Bulk thermal copolymerization of styrene and acrylic acid in continuous flow reactors [dissertation]. Hamilton: McMaster University; 1985.
56. Andrist K, Campbell JD, Chylla R, Debling J, DeYoung D, Kaai M, Kimura T, Wilson D, inventors; S. C. Johnson Commercial Markets, assignee. US patent 6,255,403. 2001.
57. Campbell JD, Debling J, DeYoung D, Giannakitsas I, Hellwig D, Schatz D, Teymour F, Villalobos M, inventors; S. C. Johnson Commercial Markets, assignee. US patent 6,346,590. 2002.
58. Campbell JD, Debling J, DeYoung D, Giannakitsas I, Hellwig D, Schatz D, Teymour F, Villalobos M, inventors; S. C. Johnson Commercial Markets, assignee. US patent 6,689,853. 2004.
59. Andrist K, Blasko J, Calhoun G, Hansen F, Hellwig D, Hessenius K, Hurley S, Jayasuriya S, Lee M, Maccani S, Mills T, Peterson G, Sandwick P, Wilson D, Wiruth J, inventors; Johnson Polymer LLC, assignee. US patent 6,858,678. 2005.
60. Andrist K, Campbell JD, Chylla R, Popli R, inventors; S. C. Johnson and Sons, assignee. US patent 5,508,366. 1996.
61. Grulke E. *Polymer Process Engineering*. Englewood Cliffs, NJ: PTR Prentice Hall; 1994.
62. McCormick C, Ayres N, Lowe A and Herman F. Mark. Water soluble polymers. In: *Encyclopedia of Polymer Science and Technology*. John Wiley & Sons [ONLINE]; Volume 1. p 79–96; 2002.
63. Scott R, Peppas N. *AIChE J* 1967;43:135.
64. Swift G and Herman F. Mark. Acrylic (and methacrylate) acid polymers. In: *Encyclopedia of Polymer Science and Technology*. John Wiley & Sons [ONLINE]; Volume 1. p 79–96; 2002.
65. Jadhav YJ and Kantor SW. Polyesters, thermoplastic. In: Kroschwitz JI, editor. *High Performance Polymers and Composites*. New York: John Wiley & Sons; 1991. p 730–747.
66. Vodonik JL, inventor; Du Pont de Nemours and Co., assignee. US patent 2,758,915. 1956.
67. Heinze H, Karben W, inventors; Davy McKee A.G., assignee. US patent 4,680,376. 1987.
68. Van Endert ES, Hagen R, Atlas C, Thiele U, inventors; Inventa-Fischer GmbH & Co., assignee. US patent 7,115,701. 2006.
69. Burkhardt R, Meyer G, Schmidt R, Thewaklt K, inventors; Dynamit Nobel A.G., assignee. US patent 4,289,895. 1981.
70. Moore LD, Rule M, Wicker TH, inventors; Eastman Kodak Company, assignee. US patent 4,446,303. 1984.
71. Cavaglia G, inventor; Cavaglia G, assignee. US patent 7,557,180. 2009.
72. Welgos RJ. Polyamides, plastics. In: Kroschwitz JI, editor. *High performance polymers and composites*. New York: John Wiley & Sons; 1991. p 519–527.

294 BULK AND SOLUTION PROCESSES

73. Howell TJ, inventor; Rohm and Haas Company, assignee. US patent 3,923,749. 1975.
74. Kharkov BA, inventor; Kharkov BA, assignee. US patent 3,607,102. 1971.
75. Smith HA, inventor; The Dow Chemical Company, assignee. US patent 4,366,306. 1982.
76. Brunelle D and Herman F. Mark. Polycarbonates. In: *Encyclopedia of Polymer Science and Technology*. John Wiley & Sons [ONLINE]; 2006. p 1–33.
77. Fox D, inventor; General Electric Co., assignee. US patent 3,153,008. 1964.
78. El-Hibri J, Weinberg S, and Herman F. Mark. Polysulfones. In: *Encyclopedia of Polymer Science and Technology*. John Wiley & Sons [ONLINE]; 2006.
79. Stevens MP. *Polymer Chemistry, an Introduction*. 2nd ed. p 54–176.
80. Gunesin BZ, Nelson PJ, inventors; BASF Corporation, assignee. US patent 5,602,206. 1997
81. Warfel DR, inventor; Atlantic Richfield Company, assignee. US patent 4,346,193. 1982.
82. Jaber IA, Ray WH. *J Appl Polym Sci* 1993;50:217.
83. Simpson D, Vaughan G, Herman F. Mark. Ethylene polymers, LLDPE. In: *Encyclopedia of Polymer Science and Technology*. John Wiley & Sons [ONLINE]; Volume 2. p 441–482.
84. Benham E, McDaniel M, and Herman F. Mark. Ethylene polymers, HDPE. In: *Encyclopedia of Polymer Science and Technology*. John Wiley & Sons [ONLINE]; 2010. p 1–30.
85. Jaber IA, Ray WH. *J Appl Polym Sci* 1993;49:1695.
86. Deblng J, Han C, Kuijpers F, VerBurg J, Zaccia J, Ray WH. *AIChE J* 1994;40:506.
87. Abel O, Helbig A, Marquardt W, Zwick H, Daszkowski T. *J Process Contr* 2000;10:351.
88. Jacobsen LL, Ray WH. *AIChE J* 1992;38:911.
89. Chylla RW, Haase DR. *Comput Chem Eng* 1993;17: 257.
90. Balchan AS, Paquet D, Klein J. *Process Saf Progr* 1999; 18:71.
91. Henderson LS III, Cornejo RA. *Ind Eng Chem Res* 1989;28: 1644.
92. Lopez-Negrete R, Lopez-Rubio J, Flores-Tlacuahuac A, Saldivar-Guerra E. *Ind Eng Chem Res* 2006;45: 1689.
93. Hill C. *An Introduction to Chemical Engineering Kinetics and Reactor Design*. New York: John Wiley and Sons; 1977.
94. Bird B, Stewart W, Lightfoot E. *Transport Phenomena*. New York: John Wiley and Sons; 1960.
95. Villa CM. *Ind Eng Chem Res* 2007;46:5815.
96. Kim SH, Teymour F, Deblng J. *J Appl Polym Sci* 2006;103: 2597.
97. Pezzin G. *J Appl Polym Sci* 1966;10:21.
98. Neudstadt FL, inventor; BASF, assignee. US patent 3,566,961. 1971.
99. Burger H, inventor. US patent 4,037,825. 1977.
100. Moore ER, Dalke BD, Malanga MT, Poinexter GM, inventors; The Dow Chemical Company, assignee. US patent 4,883,846. 1989.

14

DISPERSED-PHASE POLYMERIZATION PROCESSES

JORGE HERRERA-ORDÓÑEZ, ENRIQUE SALDÍVAR-GUERRA, AND EDUARDO VIVALDO-LIMA

14.1 INTRODUCTION

In dispersed-phase polymerization processes, one or more of the ingredients may be partially or completely insoluble in the continuous phase. The continuous phase is typically water, but this is not always the case. Nowadays, supercritical carbon dioxide (scCO_2) or other compressed fluids can be used as continuous phase (Chapter 15). The polymerization usually takes place or proceeds at a faster rate in the dispersed phase. Dispersed-phase polymerization processes have the advantage of producing a reaction mass of low enough viscosity as to be carried out in reactors or equipments with conventional mixing. Another key advantage of these processes is the good heat release rate that allows for adequate temperature control. One major disadvantage is a reduced productivity, compared to bulk polymerization processes. Depending on the solubility of the ingredients (monomer and initiator, mainly) in the continuous phase and the droplet/particle size range of the dispersed droplets or particles, the processes are classified as dispersion, precipitation, suspension, or emulsion polymerizations (or variations of the latter). The differences and major issues associated with these processes are explained in the following subsections. An emphasis is placed on emulsion polymerization, given its complexity and commercial importance. In particular, this chapter provides the fundamentals of the emulsion polymerization process as well as an overview of related subjects such as particle morphology, control of particle size dispersity, characterization of latexes, micro- and miniemulsion polymerization, controlled free-radical polymerization (CRP) in aqueous systems, and applications of polymer latexes. A section on suspension polymerization is also included.

14.2 EMULSION POLYMERIZATION

14.2.1 Historical Developments

The word *latex* has become a generic term that applies to all kinds of polymer colloidal dispersions, including those found in nature and those obtained by emulsion polymerization. Latex obtained from the sap of certain trees was used around 1600 BC by the Mayas in the ancient Mesoamerica for medicines, paints, manufacturing of rubber balls, waterproof cloths, and other rubber artifacts [1]. At present, there are a vast number of applications of polymer latexes, some of which are mentioned below. The growing variety of applications and environmental concerns has constituted the driving force for the development of this field.

For a long time, natural rubber covered the demand of this kind of material; however, eventually the need for producing synthetic rubber arose (specifically during the Second World War) and the effort focused to mimic natural latex. It seems to be accepted [2–4] that the earliest reports regarding polymerization of monomers in the form of an aqueous emulsion are some patents by Farbenfabriken Bayer in 1909–1915. Toward the end of the 1940s, Harkins' theory was published [5], which is considered the most important qualitative theory of emulsion polymerization; for previous works, see References 2, 4, 6, and 7. Harkins' work was the precursor of the Smith and Ewart's quantitative theory [8]. These pioneering theories have been the starting point or the base of many studies for several decades, which reflect the difficulties and successes in advancing the understanding of this complex heterogeneous process. There are several reviews in the literature regarding the advances and controversial issues in

the field of emulsion polymerization [4, 9–16]. For the sake of clarity and given the colloidal nature of the latex, before starting with the analysis of the emulsion polymerization topic, some aspects of colloid science relevant to emulsion polymerization are treated in this chapter. For a deeper insight on this topic, readers can refer to colloid science textbooks [17–19], or chapters devoted to colloid stability in emulsion polymerization textbooks [20–22].

It is worth mentioning that it is not intended here to provide an exhaustive review of the area but to highlight only those references that can be useful as starting points for further reading.

14.2.2 Principles of Colloid Science

Colloid Science is the science of both large molecules and finely subdivided multiphase systems whose characteristic dimension is between ~ 1 nm and ~ 1 μm [18]. Such dimensions are large in comparison with atomic dimensions [23], and so we use the terms *continuous phase* and *dispersed phase* to refer to the medium and to the particles in the colloidal size range, respectively.

Emulsions, *suspensions*, and *dispersions* are examples of colloidal systems. It is important to mention that these terms are not always used consistently in the literature and that this situation may be confusing for students and nonpolymer scientists [24]. From the point of view of polymer science and engineering, these terms refer to heterogeneous polymerizations, particularly polymerizations in aqueous/alcoholic dispersed media. Thus, the aforementioned terms have connotations that have to do with the initiator, monomer, and polymer solubility in each phase as well as with particle size and the main locus of polymerization. These aspects are treated in detail later; for the moment, let us assume that there are no chemical reactions and that such terms are used in the context of colloid science.

14.2.2.1 Colloid Stability In most cases, the fine dispersion of one phase into another is not a thermodynamically favored process, and hence interfacial area tends to be minimized. However, there are lyophobic colloids that notwithstanding they are thermodynamically unstable exhibit *kinetic* stability. Many two-phase mixtures do not undergo interfacial area changes over very long periods of time. The process by which the interfacial area is reduced is called *coagulation*, which refers to the fusion of two or more small particles to form a single larger particle. In the *aggregation* process, on the other hand, the small particles come together but they do not fuse, and they retain their identities instead; the aggregates look like a bunch of grapes. The greater the difficulty for the particles to coagulate or aggregate, the greater their kinetic stability. Unless

otherwise stated, in this chapter, the term *colloid stability* means kinetic stability, a usual practice in the literature.

Colloid stability comes from the interaction forces between neighbor particles. Such interactions are the result of repulsive (electrostatic and/or steric) and attractive (van der Waals) forces. The net potential energy is the sum of both kinds of interactions, and its height is analogous to the activation energy in ordinary reaction chemistry. This energy barrier serves as an obstacle along the path to coagulation. Quantitative description of such interaction forces constitutes what is known as the Derjaguin–Landau–Verwey–Overbeek (DLVO) theory formulated in the 1940s. For more details about this theory, the reader is referred to textbooks [18, 19] and references cited therein.

14.2.2.2 Surfactants in Aqueous Solution A very important component that is usually present in the lyophobic colloids is the surfactant. These molecules are amphiphilic, that is, a part of the molecule is much more polar than the other part. On the basis of the nature of the polar groups in the surfactant molecule, they are classified as ionic (anionic or cationic) and nonionic. When ionic-type surfactants are adsorbed onto polymer particles, they provide stabilization by electrostatic repulsion between them and when the non-ionic type are adsorbed instead the mode of stabilization is by steric repulsion. Electrosteric stabilization is provided by polyelectrolyte chains that give place to both modes of repulsion: electrostatic and steric.

When a relatively small amount of surfactant is added to water, part of it is dissolved; the dissolved molecules move freely in the aqueous phase. The other part is reversibly adsorbed on the interfaces present. The free and adsorbed surfactant molecules are subject to an adsorption/desorption equilibrium. The greater their affinity to the substrate, the stronger their adsorption. The well-known Langmuir equation is often used to quantitatively describe the adsorption of surfactants, particularly in the case of anionic surfactants. For other types of surfactants or mixtures of them, other equations may apply; for details in this regard, the reader is referred to specialized textbooks [25, 26] and articles [27–29].

If more surfactant is added to water such that its concentration exceeds the *critical micelle concentration* (CMC), then solute molecules aggregate to form clusters, known as *micelles* [30], of roughly spherical shape and the interfacial concentration reaches its saturation value, which is equal to $1/a_s$, where a_s is the specific area of a given surfactant adsorbed onto a given substrate. Surfactant molecules aggregate with their hydrophobic tails pointing to the center of the sphere (the core of the micelle) and their hydrophilic part at the micelle surface, in contact with the water phase.

For the case of ionic surfactants, the attainment of the *CMC* is not the only necessary condition to form micelles; the *Kraft point* (T_k) of the surfactant has also to be taken into account. If the temperature is below T_k , a given surfactant is not soluble enough to reach the CMC and thus micelles are not formed. T_k values for several surfactants are reported in Reference 25 and in manufacturers' technical sheets.

For the case of nonionic surfactants, such as polyoxyethylenated surfactants, their aqueous solutions become turbid if they are heated to a temperature known as *cloud point* [25].

14.2.2.3 Emulsions When a relatively small amount of a hydrophobic liquid is added to a surfactant aqueous solution containing micelles, part of it is dissolved in the aqueous phase and the other part is solubilized inside the micelles, leading to an increment of the aggregation number and micelle size as well [31]. There is an upper limit to the amount of hydrophobic liquid that can be solubilized in a given surfactant solution. Below this limit, a microemulsion is obtained and beyond this limit a macroemulsion is formed if the mixture is subject to agitation. In the latter case, the excess solubilizate leads to the formation of droplets (diameter $\sim 1\text{--}10^3 \mu\text{m}$), which are much larger than micelles (diameter $\sim 10^4 \text{ nm}$ for ionic surfactants). In the absence of agitation phase-separation occurs forming what is known as a *Windsor I system*, where the lower layer is an oil in water microemulsion and the upper layer is formed by the hydrophobic liquid [19, 32, 33].

The droplet average size (DS) and droplet size distribution (DSD) of the macroemulsion so obtained depend on the volume fraction of the dispersed phase, the geometry of the vessel and impeller, stirring speed, as well as on physical properties of the continuous and dispersed phases, such as density and viscosity, and on interfacial properties [34–39].

The addition of co-stabilizers and the use of high efficient homogenization devices produce miniemulsions [40] where the droplet size (diameter $\sim 10^1\text{--}10^3 \text{ nm}$) is intermediate between that of swollen micelles and the droplets present in a macroemulsion [41]. Besides the size of the droplets, another major distinction among macroemulsions, miniemulsions, and microemulsions is the stability that they exhibit.

In macroemulsions the DSD is determined by a droplet breakup-coalescence process. Breakup occurs only in the region very near the impeller, while coalescence occurs in the rest of the reactor, which is used to recirculate material back to the impeller [37]. Microemulsions, on the other hand, are thermodynamically (permanently) stable. Stability of miniemulsions lies in between those of macroemulsions and microemulsions.

14.2.2.4 Monomer Partitioning and Swelling in Polymer Colloids

Given the biphasic nature of the polymerization systems we are interested in, it is basic to know how their different components are distributed between the phases and the colloidal entities present in such systems. This distribution of components determines the contribution of the continuous phase and of the different colloidal entities to the overall rate of polymerization (R_p). For the case of copolymerizations, monomer partitioning defines the copolymer composition obtained because this depends on the concentration of monomers in the polymerization site, which can be different from the composition feed. Several models have been reported in the literature to quantitatively describe monomer partitioning in aqueous heterophase polymerizations. These approaches can be classified in two groups: those based on partition coefficient models [42–46] and those based on more fundamental thermodynamic considerations [47–52]. A simplified thermodynamic approach has been investigated by German and coworkers [53–58]. Dafniotis and Saldívar [52] and Gugliotta et al. [59] have compared the results of monomer partition models of different levels of complexity and have pointed out that selection of the model to be used is based on a good balance of simplicity, accuracy, and data availability.

Morton, Kaizerman, and Altier (MKA) [60] made the first contribution to the problem of describing the thermodynamics of partitioning and swelling. They obtained an equation for equilibrium swelling of polymer particles by a solvent. Such equation is commonly referred in the literature as *Morton or MKA equation*. According to this equation, when the polymer (subscript P) is in equilibrium with free solvent (subscript A), the following condition exists:

$$\left(\frac{\Delta G}{RT} \right)_A = [\ln(1 - \phi_P) + (1 - m_{AP})\phi_P + \chi_{AP}\phi_P^2] + \frac{2\gamma\bar{V}_A}{rRT} \quad (14.1)$$

The terms between the brackets correspond to the osmotic contribution to the Gibbs free energy (ΔG), and they also constitute the standard expression for ΔG of the Flory–Huggins theory of polymer solutions [61], where ϕ_P is the volume fraction of polymer and m_{AP} the ratio of the equivalent number of molecular segments of solvent to polymer (usually expressed as the ratio of molar volumes of solvent and polymer). χ_{AP} is the Flory–Huggins interaction parameter of solvent and polymer and the last term of Equation 14.1 is the interfacial free energy contribution where γ is the interfacial tension, V_A the molar volume of solvent, and r the particle radius. T is temperature in Kelvin and R is the universal gas constant.

Modifications to the MKA equation have been proposed to take into account the swelling pressure and the dependence of the interfacial tension (γ) and the Flory–Huggins interaction parameter (χ) on particle size [62, 63] as well as the presence of adsorbed surfactant on particle swelling [64, 65]. These modifications have allowed to obtain better agreement between theory and experimental data for the swelling of polystyrene particles using reasonable parameter values.

14.2.3 Formulation Components in Emulsion Polymerization

There are several formulation components that can be present in an emulsion polymer (latex) formulation, which can be added before, during, or after the polymerization reaction. This section is intended to provide the reader with an overview on the role of each component, as well as their impact the process and/or the product.

14.2.3.1 Monomers The solid (essentially polymer) content of most of the commercial latexes is in the range of 45–55%, although for special applications and kinetic studies lower overall monomer concentrations are used.

One of the most important bulk property variables of polymers is the glass transition temperature T_g , which must be well below the use temperature to allow the interdiffusion and entanglement of polymer chains when the particles get in contact, once the aqueous phase has been evaporated. Thus, the monomer(s) used have to be selected such that the desired T_g is obtained. Useful tables showing T_g and other physical and chemical properties of homopolymers are available in the literature [66–68]. The well-known Fox equation [69] can be used to estimate the T_g of a copolymer as a function of monomer composition and T_g 's of the component monomers. It is important to take into account that polar polymers tend to hydroplasticize, reducing the T_g in the film formation process [70]. Several commercial latexes are terpolymers that contain two of the monomers present in major amounts to grossly obtain the basic desired properties, with the third monomer present in a minor amount for fine tuning of a special property [71–73].

14.2.3.2 Water Most modern emulsion polymerization processes use deionized water because the ionic species naturally present in water affect colloid stability. Ion exchange and inverse osmosis are the most common water deionization methods [74].

Oxygen content is important because this element is a free-radical scavenger that can act as an inhibitor or a retardant in emulsion polymerizations depending on the water solubility of the monomer(s) [75] and stirring [76–78].

14.2.3.3 Water-Soluble Initiator There are two types of water-soluble initiator systems used in emulsion polymerization: dissociative and redox initiators [2, 79–89]. Inorganic persulfates are by far the most widely used class of dissociative initiators for emulsion polymerization reactions, in which the persulfate ion undergoes (thermal) homolytic dissociation into two sulfate radical anions. Redox initiators, on the other hand, are systems comprising a reducing agent and an oxidizing agent whose mutual interaction produces free radicals. Dissociative initiators are used in the temperature range of 50–90 °C, while redox initiators produce free radicals even at low temperatures, such as 5 °C. Low polymerization temperatures are used when crosslinking is to be avoided, as in the production of random styrene–butadiene rubber copolymer.

14.2.3.4 Surfactants These substances are also known as *emulsifiers* or *soaps* and are typically used in the range 1–6% by weight with respect to monomer. Extensive practical testing is likely to be required to determine the least expensive emulsifying system that will give good performance during and after the polymerization process, as well as acceptable results in a given application.

Concerning performance during emulsion polymerizations, the surfactant should provide stability to the latex particles protecting them from mechanical coagulation, avoiding N (the number of particles per unit volume) to decrease [76] and minimizing the formation of macroscopic flocs or coagulum in the latex, or over the surfaces of the process equipment.

Nonionic surfactants enhance freeze-thaw, shear and electrolyte stability, but, on the other hand, they can reduce the free radical entry into particles [90–95] and R_p [96]. Thus, they are not normally used as the sole emulsifying agent in emulsion polymerization [96–101]. Sometimes the reaction is started in the presence of only an anionic surfactant, and a steric stabilizer is added at a higher conversion or as a poststabilizer.

A system named HLB (hydrophilic–lipophilic balance) constitutes a useful guide to the selection of a suitable surfactant for a given dispersed phase [2, 25, 97, 102].

14.2.3.5 Chain Transfer Agents Chain transfer agents (CTAs) are used in free-radical emulsion polymerization to reduce the molecular weight of the produced polymer. For this purpose, mercaptans of high molecular weight are often used [103–107], which are alkyl compounds containing from 7 to 14 carbon atoms. A review of substances used as CTAs is provided in chapter 8 of Blackley's book [2]. The usage of surfactants with chain transfer agent properties ("transurfs") [108, 109] and catalytic CTAs [110] has also been studied.

14.2.3.6 Other Components Other components of emulsion polymerization systems include electrolytes and sequestering agents. Sometimes electrolytes are added to act as buffers and to avoid the hydrolysis of monomers containing the ester group or the acceleration of persulfate initiators decomposition as well [79, 111]. It has to be kept in mind that the addition of electrolytes has an influence on the colloidal stability of the latex, CMC, micellar aggregation number, and adsorption of surfactant, as well as on other physicochemical phenomena [25].

It is common industrial practice to add very small amount of compounds such as ethylenediamine tetra-acetic acid to sequester traces of calcium and magnesium ions [2].

14.2.4 Overall Description of Emulsion Polymerization

As explained before, when surfactant, water, and monomer(s) are mixed, the colloidal system obtained consists of monomer-swollen micelles (if the surfactant concentration exceeds its CMC) and monomer droplets dispersed in an aqueous phase that contains dissolved molecules of surfactant and a small amount of the sparingly water-soluble monomer(s). When free radicals are generated in the aqueous phase by action of an initiator system, then the emulsion polymerization takes place. Its evolution is such that the colloidal entities initially present tend to disappear and new colloidal entities (polymer latex particles) are born by a process called *nucleation*. For convenience, we first focus on the particle nucleation mechanisms, a very important aspect of emulsion polymerization.

14.2.4.1 Nucleation Mechanisms Particle formation can occur by homogeneous nucleation, micellar nucleation, or both mechanisms. In any case, the process begins with the generation and subsequent propagation and side reactions of free radicals in the aqueous phase [81, 112–114]. Most of these free radicals are amphiphilic in nature because they are formed by a hydrophobic propagating tail that has in its extreme a hydrophilic group that comes from the initiator. As the oligoradicals add more monomeric units in the aqueous phase, they become more hydrophobic until they reach a critical degree of polymerization, j_{cr} , at which these molecules are no longer water soluble and they separate from the solution forming a new particle called *primary* or *precursor particle*. This mechanism is known as *homogeneous nucleation* [115–117].

The initiator-derived radicals can undergo other events during their diffusion in the aqueous phase. If the surfactant concentration is above its CMC, they can penetrate into monomer-swollen micelles. If the time they remain in the micelles is long enough to propagate before they desorb back to the aqueous phase, then a primary particle is

formed. This mechanism is known as *micellar nucleation* [5, 8].

The initiator-derived radicals can also undergo bimolecular termination in the aqueous phase or enter into a pre-existing polymer particle, preventing the formation of a new particle. In other words, homogenous nucleation, micellar nucleation, termination of radicals in the aqueous phase, and free-radical capture in particles are competing processes.

Obviously, below the CMC of the surfactant, there are no micelles and hence in these conditions homogeneous nucleation is the only possible nucleation mechanism. Nowadays, it is widely accepted that well above the CMC, micellar nucleation is the dominant mechanism of primary particle formation. Experimental evidences, arguments, and theoretical results supporting this idea are reported elsewhere [46, 90, 118–126].

If the surfactant concentration is just slightly above the CMC, homogeneous nucleation could compete effectively with the micellar nucleation depending on the water solubility of the monomer. Homogeneous nucleation becomes more important as the surfactant concentration approaches the CMC. The experimental and theoretical results of Nomura et al. [127] on the emulsion polymerization of vinyl acetate (a partially water-soluble monomer) are also consistent with this idea.

A controversial issue related to the nucleation mechanism has been the colloidal stability of the primary particles when the surfactant concentration is above the CMC [10, 11, 128]. Below this value, there is no doubt that, to greater or lesser extent, limited coagulation occurs because of the low availability of surfactant. Coagulation of primary particles leads to particles with higher surface charge density because of the redistribution of the adsorbed surfactant onto a smaller surface. The interfacial area of a mature particle is smaller than the total interfacial area of the primary particles from which the former was formed; thus, surface charge density (and therefore stability) increases. Coagulation occurs, or it is limited to the moment at which polymer particles are stable and their growth is mainly propagative. This is called *limited coagulation*.

For the case of styrene emulsion polymerization above CMC, there are experimental results [129, 130] suggesting that if limited coagulation occurs, it is not as extensive as it was believed to be according to calculations based on the coagulative-nucleation mechanism [131]. It is by this mechanism that the primary particles formed either by homogeneous or micellar nucleation undergo limited coagulation to form mature particles.

Recently, the formation of a significant population of nanodroplets under conditions of a conventional emulsion polymerization has been reported; hence, it has been claimed that these nanodroplets might become the main locus of particle formation [16, 132]. This issue is still a subject of debate, but the generally accepted mechanism

of particle formation above the CMC continues to be the micellar nucleation.

Smith and Ewart [8] proposed the following equation to estimate the final value of the total number of polymer particles per unit volume, N , on the basis of micellar nucleation:

$$N = k \left(\frac{R_i}{\mu} \right)^{0.4} (a_s S)^{0.6} \quad (14.2)$$

where μ is the (constant) rate of particle volume growth, R_i the rate of radical generation, a_s the specific area of the surfactant, and S the surfactant concentration. The constant k is 0.53 for the case in which all the generated radicals give place to new particles, and 0.37 for the case in which polymer particles compete with micelles for the capture of radicals. Deviations from Equation 14.2 observed for monomers with higher water solubility than styrene are ascribed to the higher probability of desorption of monomeric radicals that can contribute very significantly to micellar nucleation [125, 127, 133]. These monomeric radicals are produced within the particles by chain transfer to monomer. Desorption of these species has been recently studied by Brownian dynamic simulation [134, 135]. In the Smith and Ewart theory, nucleation by this kind of radicals and limited coagulation are not considered.

Those emulsion polymerizations for which initially polymer latex particles are not present, but in which particles are formed by some of the mechanisms described above, are known as *ab initio. Seeded* emulsion polymerizations are those in which at the beginning of the process there are preformed (and usually characterized) polymer latex particles; this kind of polymerizations are commonly used in industry to avoid the variability of the process associated with the nucleation stage.

14.2.4.2 Intervals of an Emulsion Polymerization

Taking as a reference the evolution of the colloidal entities present in an emulsion polymerization system, Gardon [136] proposed to distinguish three intervals in isothermal batch emulsion homopolymerization as follows:

- Interval I. Nucleation takes place, and so N increases; monomer droplets are present.
- Interval II. If coagulation of particles does not occur, then N is constant; monomer droplets are present.
- Interval III. N is constant, but there are no monomer droplets present.

The evolution from interval I to interval II and from this to interval III are a consequence of the simultaneous and interrelated events associated with radical polymerization and the colloidal and physicochemical behavior of the species present in the system.

At the beginning of an emulsion polymerization performed above the CMC, the free radicals generated in the aqueous phase promote the nucleation of particles by the homogeneous and micellar mechanisms explained previously. The fact that the surface area of all monomer droplets is by far much smaller than that of all the other colloidal species makes it unlikely that the radicals existing in the aqueous phase enter and polymerize into monomer droplets. Thus, the droplets play the role of monomer reservoirs. The diffusion of this component through the aqueous phase provides the monomer needed to replace that consumed by reaction and to swell the polymer produced in the particles.

The growth of polymer particles constitutes the driving force not only for mass transport of monomer to the main reaction site, but also for adsorption of surfactant onto the growing surface of the particles. Hence, micelles (if present) disaggregate and their concentration diminishes with time until they eventually disappear, that is, when the surfactant concentration falls below CMC; at this point, micellar nucleation ceases. Only about 1/1000th of the micelles initially present act as nucleation sites, and the rest disaggregate to stabilize the growing particles.

Concerning homogeneous nucleation, strictly speaking, the formation of primary particles by this mechanism should not cease provided there is dissolved monomer and generation of radicals in the aqueous phase. However, eventually particle formation by this mechanism becomes nonsignificant because the number and size of particles is such that they capture most of the radicals produced in the aqueous phase. Interval I finishes when N does not increase anymore, independently of the mechanism(s) of nucleation involved.

During interval II, N is usually constant and the polymer particles are still growing at the expense of the monomer present in droplets. Eventually, monomer droplets disappear, marking the end of interval II. During this interval, the surface concentration of surfactant on the interfaces diminishes because this component has to be redistributed over a larger area as this interval proceeds (recall that there are not micelles anymore to keep the interfaces saturated).

During interval III, N is usually constant as well and the monomer concentration in particles diminishes because there are no remaining droplets to replace the monomer consumed in the polymerization. Nearly total monomer conversion is reached.

In emulsion polymerizations performed below CMC, limited coagulation of mature particles might occur so that the transition from interval I to interval II might not be obvious. The end of interval II is the same as in polymerizations above CMC.

14.2.4.3 Rate of Polymerization R_p

The rate of polymerization is important not only because it determines the

productivity of the process but also because it is a macroscopic manifestation of phenomena occurring at the microscopic and submicroscopic levels. Gardon's description of the intervals in emulsion polymerization has been complemented with the behavior of the rate of polymerization (R_p). On the basis of the idea that $R_p \propto N$, several authors have considered that R_p increases, remains constant, and diminishes in intervals I, II, and III, respectively. The notion that R_p is constant during interval II is also supported by the fact that at intermediate conversions statistical analysis of gravimetric data leads to conclude that monomer conversion varies linearly with time. However, Gardon [137] has questioned this concept on the basis that the nonlinear nature of the conversion-time curve can be hidden if the conversion range studied is too narrow. The nonconstant behavior of R_p during interval II in emulsion polymerization above the CMC has been confirmed by quasicontinuous calorimetric measurements [138–141]. These results also show that R_p does not necessarily decrease during interval III but often exhibits a maximum as a consequence of the autoacceleration effect [142–145]. R_p is given by

$$R_p = \frac{K_p C_{Mp} \bar{n} N}{N_A} \quad (14.3)$$

where K_p , C_{Mp} , and \bar{n} , are the propagation kinetic rate coefficient, the monomer concentration in particles, and the average number of radicals per particle, respectively. N_A is Avogadro's number. The effect of each one of these parameters on R_p is discussed next.

K_p is constant during most of the polymerization, but it may diminish toward the end of interval III, at high monomer conversions, due to diffusion limitations.

C_{Mp} maintains its saturation value during intervals I and II provided that the interfacial area of monomer droplets is high enough to allow the monomer transport to the growing particles where it replaces the monomer consumed swelling the polymer formed [146]. However, on the basis of Monte-Carlo simulations, Tauer and Hernandez [147] have claimed that latex particles in emulsion polymerization never experience either a period of saturation with monomer or a constant monomer concentration during interval II, as frequently assumed.

C_{Mp} evolution is affected to certain extent by the evolution of γ . As explained before, during intervals I, II, and III in an emulsion polymerization above CMC, γ is constant, increasing, and practically constant, respectively. During interval II, the increases in γ and in r approximately compensate each other in such a way that the average C_{Mp} in all the particles tends to be constant [118] or slightly decreases [148, 149].

During interval III, C_{Mp} monotonically diminishes according to the conversion of monomer to polymer.

Concerning \bar{n} , three scenarios can exist, which are known as the Smith-Ewart (S-E) cases [8]:

Case 1: $\bar{n} < 0.5$. In this scenario, the radicals produced by chain transfer to monomer inside the particles have high probability of being desorbed to the aqueous phase. Small particle sizes and low rates of free-radical capture in particles favor this scenario.

Case 2: $\bar{n} \geq 0.5$. If the rate of chain transfer-desorption of radicals is negligible compared to the rate of free-radical capture in particles, and the mutual termination rate of two radicals is so high that only particles with zero and one radicals can exist, then approximately one-half of the particles contain a single free radical. Small particle sizes and high rates of free-radical capture in particles favor this scenario.

Case 3: $\bar{n} > 0.5$. In this scenario, there is not instantaneous termination as in cases 1 and 2; thus, two or more radicals can coexist in a particle. Large particle sizes, high rates of free-radical capture in particles, and the Trommsdorff effect (Chapter 4) favor this scenario.

S-E cases 1 and 2 correspond to what is known as zero-one systems, in which the radicals grow in isolated compartments, reaching very high molecular weights; hence, this characteristic feature of emulsion polymerization is known as *compartmentalization*. In case 3, this characteristic is relaxed so that radicals in a given particle grow in the presence of other radicals. As more radicals coexist within the particles, the system approaches the behavior of a bulk polymerization (or pseudobulk system).

Regarding N , it has been reported [116] that this parameter reaches a maximum during the nucleation stage if the polymerization is performed below the CMC, because the low availability of surfactant causes limited coagulation. On the other hand, N tends to increase in this stage when the surfactant concentration is above the CMC. During interval II, N is typically assumed to be constant, but some authors have reported that this parameter increases in this period [138, 150–152]. The subject is still a matter of debate due to the limitations of certain particle sizing techniques [125, 129, 130].

Next, the effect of the simultaneous evolution of the parameters involved in Equation 14.3 on R_p is discussed.

In intervals I and II, R_p is mainly determined by the products $\bar{n} C_{Mp} N$ and $\bar{n} C_{Mp}$, respectively.

According to theoretical results [125], \bar{n} exhibits a minimum at early times of emulsion polymerizations above CMC. This minimum is explained in terms of the competition between micelles and particles for the capture of radicals and has been characterized as an

evolution from case 1 toward case 2 during the early stages of the polymerization. \bar{n} , C_{Mp} , and N increase, and consequently R_p does so. N rises from zero to typically 10^{12} – 10^{13} and 10^{14} particles/cm³ water, for emulsion polymerizations performed below and above the CMC, respectively. Therefore, any decrease of other parameter(s) can be overcompensated and consequently R_p increases in interval I. In interval II, N is usually constant; hence, R_p depends on the product $\bar{n}C_{Mp}$. As it was explained before, C_{Mp} tends to be constant or to slightly diminish in this interval. Therefore, the R_p evolution depends on how \bar{n} counterbalances the C_{Mp} evolution. In interval III, N is also usually constant and K_p eventually becomes diffusion-controlled; hence, R_p depends on the product $K_p\bar{n}C_{Mp}$. The maximum of the R_p evolution curve, characteristic of the autoacceleration (Trommsdorff) effect in free-radical polymerization systems, can also be observed in emulsion polymerization. Considering that the parameters defining R_p can evolve in different ways in different polymerization systems, it is not plausible to establish a general R_p profile.

14.2.4.4 Molecular Weight Molecular weight determines many end-use properties of polymers. Thus, it is very important to know the events that control it. The relative importance of such events is highly system dependent; hence, the molecular weight obtained in heterogeneous systems like emulsion polymerization can be very different from that obtained in homogeneous systems like bulk and solution polymerizations. In homogeneous systems, the generation, propagation, and termination of free-radicals occur in the same phase so that any radical has access to any other. However, in an emulsion polymerization, the generation of radicals takes place in the aqueous phase and their propagation and termination occur predominantly within the polymer particles. In this way, a radical in one particle does not have direct access to radicals in another particle so that they grow isolated in their own compartments. Termination events occur when another radical enters a particle that previously contains a growing chain or when this latter undergoes a chain transfer reaction. Bimolecular termination occurs instantaneously for relatively small particle sizes, as those present during interval I of emulsion polymerization above the CMC, so that only particles containing zero or one radicals exist (i.e. a 0–1 system). As particles become bigger, the probability that two or more radicals can coexist in the same particle is higher, that is, the system tends to behave like a bulk polymerization from the point of view of molecular weight. Compartmentalization has a profound effect on the kinetics of emulsion polymerization. Polymerization rates and molecular weights are usually higher than in the corresponding bulk or pseudobulk systems because the termination rate is reduced [153–155].

14.2.5 Batch, Semibatch, and Continuous Processes

In *batch processes*, all the formulation components are completely added to a stirred-tank reactor (STR) at the start of the polymerization, while in *semibatch* operation only certain part is initially added and the rest is continuously fed over some period of time. *Continuous* reactors are operated with continuous input flow of components and output flows of products.

Most polymers produced by emulsion polymerization are copolymers; therefore, it is important to consider the effect of the reactor operation mode on copolymer composition. Moreover, because of the heterogeneous nature of the system, partition of the monomers between the phases during the polymerization as well as monomer reactivities have to be taken into account.

A difference in monomer reactivity causes that the more reactive monomer is consumed preferentially leading to a drift in copolymer composition. In batch polymerization, the copolymer may exhibit a broad composition distribution because all the monomers are added at the beginning, and so there is no chance to control the concentration of monomers in the polymerization sites that, together with the reactivity ratios, determine the copolymer composition. In contrast, in the semibatch mode, the polymerization can be performed under monomer-starved conditions. Under these conditions, the copolymer formed has the same overall composition as that of the comonomer mixture added. Thus, in the latter process, if a comonomer mixture of constant composition is fed, copolymers of uniform composition are produced. Otherwise, if the monomer feed is such that polymer latex particles are swollen at their equilibrium value, then monomer-flooded conditions are present and the semibatch polymerization is essentially indistinguishable from the equivalent batch reaction. To ensure colloidal stability as particles grow, it is usually necessary to feed more surfactant during the period of monomer addition. This is done by adding the monomer mixed with water and surfactant (as an emulsion) or by adding the surfactant as a separate input stream. It is also possible to feed the monomers in a calculated manner, such that the drift in composition is compensated by the composition of the monomer feed (time dependent). A number of works have been published in the literature regarding composition control in semibatch emulsion polymerizations [156–160]. Continuous stirred-tank reactors (CSTRs) are economically advantageous when high production rates are required or when product grades differ slightly [161–163]. Monomer conversion in CSTRs might exhibit sustained oscillations [164] leading to product quality problems. These oscillations have been ascribed to on–off nucleation phenomena coupled with particle growth; thus, the use of seed significantly enhances reactor stability. Another alternative is the use of tubular reactors that exhibit stable

operation [165]. Wall fouling and plugging are potential disadvantages of this kind of reactors; however, these can be avoided by using a pulsation source [165].

Free-radical polymerizations are exothermic, and so the heat produced during polymerization must be removed. This is not a significant problem in a laboratory scale; however, heat transfer problems constitute a restriction for batch processes in an industrial scale. In the case of semibatch and CSTR, the cold monomer and water feed are beneficial for heat removal so that much higher production rates are feasible than for a batch reactor of the same volume. For tubular reactors, their large heat transfer area is advantageous for the strongly exothermic polymerizations.

The reactor type and operation mode also influence the particle size distribution (PSD). This aspect is treated next in the context of PSD control.

14.2.6 Control of Number and Size Distribution of Particles

PSD is one of the most important characteristics of latexes. For some applications, a very low particle size dispersity is required [166], while in others [167, 168] a multimodal PSD is necessary.

Latex particles are not strictly monodisperse. The reason is that particles are not born at the same time, but they are formed during a period of time (i.e., the nucleation stage) in which they simultaneously grow. Thus, particles formed toward the end of the nucleation stage will be smaller than those formed at early times of the polymerization. Therefore, the longer the nucleation stage, the wider the PSD. In general, polymerizations carried out at or below the CMC will lead to the formation of bigger particles with more uniform sizes. Occurrence of limited coagulation during the nucleation stage tends to homogenize by itself the particle sizes.

The reason why some kind of anionic surfactants leads to lower particle size dispersities was studied recently by Farias et al. [65].

If polydisperse latexes are desired in batch emulsion polymerizations above CMC, high S_0 values and low initial initiator concentrations (I_0) prolong interval I enhancing the formation of negatively skewed [169] or even bimodal PSDs [127].

Secondary nucleation can also be used to produce bimodal or multimodal PSDs. This can be done in several ways by means of seeded [170] or *ab initio* polymerizations [171–178]. Miniemulsion polymerization can also be used to produce broad PSDs [179, 180].

14.2.7 Particle Morphology

Composite latexes, that is, those with particles containing different phases, are used for many applications such as

adhesives and coatings [181], impact modifiers [182], and other high value-added products [73]. They are prepared by a series of consecutive emulsion polymerizations with different monomer types where the monomer(s) is/are added under conditions such that polymerization occurs in the pre-existing particles. As the concentration of newly formed polymer chains increase, phase separation occurs, leading to the formation of clusters that migrate in such a way that the interfacial energy of the system tends to be minimized. The final morphology strongly depends on the kinetics of such cluster migration whose driving force comes from the balance between van der Waals and viscous forces [183–185]. Equilibrium morphologies such as core–shell or inverted core–shell may be attained if the internal viscosity of the particle is low, and the polymers are very incompatible. If the morphology is kinetically controlled, then the different phases are not fully consolidated and nonequilibrium-type structures such as salami-, raspberry-, and octopus like are obtained [186–188].

14.2.8 Latex Characterization

Characterization of polymer latexes can be performed by techniques available for polymers in general and by other techniques specific for emulsions.

Monomer Conversion. Off-line methods such as gravimetric analysis and gas chromatography as well as several online methods can be used to determine monomer conversion throughout polymerization [116, 138, 149, 189–195].

Particle Size and PSD. According to the basic principles that they are based on, the techniques for measuring these important characteristics of the latexes are classified into four major groups [196]: (i) microscopy, (ii) light scattering, (iii) particle movement (e.g., capillary hydrodynamic chromatography and field flow fractionation methods), and (iv) acoustics.

The choice of the method depends on several factors, such as the size range of interest, the accuracy desired, and the time required for a measurement. Availability, cost, and method limitations of the instrument have to be considered as well. Useful guidelines to instrument selection are given by Collins [196] and Schoenmakers [197].

Particle Morphology. It can be observed by means of transmission electron microscopy, scanning electron microscopy, and atomic force microscopy. Useful information about particle morphology can also be obtained by means of other techniques [198–203].

14.3 MICROEMULSION POLYMERIZATION

As mentioned above, micelles have a limited capability to solubilize hydrocarbons within them; thus, *swollen micelles*

is another term for microemulsions [18]. Microemulsions are thermodynamically stable and transparent dispersions containing oil, water, and surfactant(s). A useful guide to their formulation is given by Candau [204].

The term *microemulsion polymerization*, as is the case with some other polymerization processes in aqueous dispersed media, refers to the initial state of the system before polymerization.

When a water-soluble initiator is added to a microemulsion, polymer particles are nucleated mainly by the micellar mechanism. The role of the monomer-swollen micelles in microemulsion polymerization is not only to act as nucleation loci and surfactant reservoir but also as monomer reservoir. The fast nucleation rate leads to the initial increment of R_p . As the monomer is polymerized, its concentration in micelles diminishes and eventually monomer concentration within polymer particles decreases as well [205]. As a consequence, the nucleation and polymerization rates tend to decrease, explaining in this way the maximum in the R_p evolution curve experimentally observed. The final latex consists of surfactant-stabilized polymer particles that typically contain only polymer and empty micelles formed by excess surfactant.

The utility of microemulsion polymerization comes from its capability of producing smaller particles than those obtained by emulsion polymerization and of forming porous solid materials (by inverse microemulsion polymerization). This process has also been found to be suitable for performing CRP [206]. More particularities on microemulsion polymerization can be found in References 188, 204, 207, and 208.

14.4 MINIEMULSION POLYMERIZATION

The size of the colloidal entities and their stability in *miniemulsions* lies between those of *macroemulsions* and *microemulsions*. The diameter of miniemulsion droplets ranges from 50 to 500 nm and their stability vary from days to months [41]. A typical formulation consists of water, monomer(s), surfactant, initiator system, and co-stabilizer. The main function of the latter is to retard the Ostwald ripening effect. Hexadecane and cetyl alcohol are typically used as co-stabilizers. Miniemulsions are formed by subjecting the mixture to high shear and/or cavitation to break the oil phase into submicron size droplets [209]. This can be done by means of devices such as high pressure homogenizers, rotor stators, and ultrahigh sonifiers [210–212].

The droplet size distribution, DSD, and the presence of swollen micelles in miniemulsions depend on the formulation, homogenization procedure, and storage time [40]. Assuming that a water-soluble initiator is used, a key difference between miniemulsion and conventional

emulsion polymerizations is that, in the former, monomer (mini) droplets compete with monomer-swollen micelles for capturing the oligoradicals generated in the aqueous phase. The goal in this regard is to maximize the fraction of particles generated by minidroplet nucleation, by adjusting the amount of surfactant and the homogenization procedure. Nucleation in minidroplets can be enhanced by pre-dissolving 1% polymer into the monomer before homogenization [213, 214]. Other hydrophobic species such as oil-soluble initiators [215, 216], CTA [217], and other reactive species [218] have been evaluated as co-stabilizers.

The R_p curves of miniemulsion and conventional emulsion polymerization obtained by calorimetry show the same general behavior [219]. In contrast to conventional emulsion polymerization, in miniemulsion polymerization, the monomer concentration in polymer particles diminishes throughout the polymerization. At the beginning, the nucleation rate overcompensates the decrease of monomer concentration leading to the first rise in the R_p . The number of droplets decreases and the remaining droplets shrink in size due to monomer loss by molecular diffusion to the polymer particles. As a consequence, the nucleation rate diminishes and eventually it may not be fast enough to compensate the decrease of the monomer concentration. Thus, R_p may reach a maximum and decrease before the end of the nucleation period [219]. In conventional emulsion polymerization, the nucleation period ends before the first maximum in R_p , which is ascribed to the disappearance of monomer droplets [125].

Applications of miniemulsion polymerization come from taking advantage of the droplet nucleation mechanism. Some examples are production of high solid content latexes [179], encapsulation of inorganic solids [220], encapsulation of fragrances [221], production of hybrid polymer particles [222–224], step polymerization [225–228], CRP [229–233], and so on.

14.5 APPLICATIONS OF POLYMER LATEXES

Emulsion polymers have been used in a broad range of applications because of their environment-friendly nature and the versatility of the process for adjusting both macromolecular and colloidal properties of the latex. Out of the worldwide demand of emulsion polymers, 23% is used for surface sizing and coating of paper and paper board, 20% for paints and coatings, 25% for adhesives and sealants, and 9% for carpet backing [234]. References 234 and 235 and several chapters of the book edited by Lovell and El-Aasser are devoted to the major industrial uses of emulsion polymerization and polymer latexes.

Besides these large-volume applications of latexes, there are specialty applications, such as some in the

optoelectronics and biotechnology fields, for which high added-value latexes are produced at a smaller scale. This kind of products requires fine control of composition, particle size, PSD, morphology, surface chemistry, and functionalities [236].

14.6 DISPERSION AND PRECIPITATION POLYMERIZATIONS

A free-radical dispersion polymerization is a heterogeneous process where particles are formed in the presence of an adequate stabilizer, with a reaction mixture homogeneous at the beginning of the polymerization. This process can be described as proceeding in three stages [237–239]. In “Stage 1,” primary radicals are formed from thermally promoted fragmentation of the initiator. These primary radicals rapidly react with monomer molecules to produce polymer chains that upon fast growth become insoluble in the continuous phase. The aggregation of polymer chains results in the formation of unstable polymer microdomains. The reaction mixture consists primarily of pure monomers, initiator, primary radicals, and oligomer radicals, since the polymer concentration is lower than its solubility limit. Therefore, in this stage, the polymerization can be described as a solution polymerization process. In “Stage 2,” because of the very limited stability of the microdomains, they rapidly aggregate to form primary polymer particles, also called *domains*. From this point on, the polymerization proceeds in two phases, namely, the polymer-rich phase and the continuous, monomer-rich phase. This stage goes from the time of appearance of the dispersed polymer phase to a fractional overall monomer conversion, x_c , at which the monomer concentration in the continuous phase is negligible and eventually disappears. The overall polymerization rate is given by the sum of the polymerization rates in each phase. Finally, in “Stage 3,” at higher overall monomer conversions ($x_c < x \leq 1$), the polymerization proceeds mainly in the polymer-rich phase. The polymer particles are swollen with monomer and solvent; thus, the monomer mass fraction in the polymer phase decreases as the total monomer conversion approaches a final limiting value.

The mathematical modeling of the polymerization kinetics and molecular weight development in dispersion polymerization processes (using scCO₂ as continuous phase), using the approach described above, has been reported in the literature [237–239]. Besides the kinetics and molecular weight development equations that describe the polymerization in each phase (similar to those described in Chapter 12), it is necessary to account for species partitioning among the phases. The equations for species partitioning can go from simple partition coefficients [237–239] to elaborate thermodynamic equations for polymer solutions

(e.g., the Sanchez–Lacombe equation of state) [240, 241] (Section 14.2.2.4).

Representing the dispersion polymerization process as proceeding in three stages has some implications regarding its mathematical treatment. If the system is modeled as starting as a single-phase polymerization, the rigorous modeling of the formation of the second phase will not be an easy issue to handle, since fulfillment of the initial conditions may lead to numerical difficulties. Moreover, the three-stage representation suggests imposing a second discontinuity (when going from stage 2 to 3), which may not be necessary, since a continuous model should be able to capture the behavior of the system when monomer in the continuous phase has been fully consumed. Although Kiparissides et al. [237] first proposed and used this three-stage approach, which implied using two discontinuous transitions, a later contribution from the same group [240] and the model approach used by Mueller et al. [241] treat the system as consisting of a two-phase polymerization from the very beginning, which is reasonable due to the very fast formation of high molecular weight polymer, which will phase-separate.

Precipitation polymerization is similar to dispersion polymerization. They both start as a solution polymerization (homogeneous phase). However, in the case of precipitation polymerization, there is no colloidal stabilizer present, and so the polymer formed precipitates as a completely separate phase, while in dispersion polymerization, the polymer particles are stabilized by a colloidal stabilizer.

14.7 SUSPENSION POLYMERIZATION

14.7.1 Generalities¹

The topic of suspension polymerization has been reviewed by several authors at different times, with different emphases [24, 242–248]. In a suspension polymerization process, the monomer (or monomers in the case of a copolymerization), which is relatively insoluble in water, is (are) dispersed as liquid droplets. Dispersion stability is maintained with the help of a stabilizer and vigorous stirring. The final product, once the continuous (usually aqueous) phase has been removed, consists of solid polymer particles (beads). The initiators used in this process are usually soluble in the liquid monomer. The terms *pearl* and *bead polymerization* are also used for the suspension polymerization process when particle porosity is not required. The major aim in suspension polymerization is the formation of an, as uniform as possible, dispersion of monomer droplets in the aqueous phase, with controlled

¹ Adapted with permission from Zhu D-W. Macromolecules 1996;29:2813 [249]. Copyright 1997 American Chemical Society.

coalescence of these droplets during the polymerization process. The interfacial tension, the degree of agitation, the design of the stirrer/reactor system, the amount of dispersed phase, and the evolution of the polymer molecular weight distribution govern the dispersion of monomer droplets, typically with diameters in the range of 10 μm –5 mm. The presence of suspending agents (e.g., stabilizers) hinder the coalescence of monomer droplets and the adhesion of partially polymerized particles during the course of the polymerization, so that the solid beads may be produced in the same spherical form in which the monomer was dispersed in the aqueous phase. Many important commercial suspension polymers yield bead sizes above 10 μm , and so these relatively large particles (compared to emulsion particles) are simply isolated by centrifugation, filtration, and/or sedimentation [244].

Nonaqueous suspension agents such as paraffin oils have been developed to polymerize polar monomers, such as acrylic acid. The so-called water-in-oil (W/O) suspension polymerization (reversed phase suspension polymerization) comprises an aqueous solution containing the hydrophilic monomer(s) and initiator(s), which are dispersed in a liquid paraffin oil or other nonpolar hydrocarbon media and polymerized. The use of perfluorocarbon fluids has extended the scope of the suspension polymerization method to monomers and initiators that cannot be used, due to their high solubility and reactivity, in conventional suspension media [249].

The reactor vessel is usually a stirred tank. The monomer phase is subjected either to turbulent pressure fluctuations or to viscous shear forces, which break it into small droplets that assume a spherical shape under the influence of interfacial tension. These droplets undergo constant collisions (collision rate $\geq 1 \text{ s}^{-1}$), with some of the collisions resulting in coalescence. Eventually, a dynamic equilibrium is established, leading to a stationary mean particle size. Individual drops do not retain their unique identity, but undergo continuous breakup and coalescence instead. In some cases, an appropriate dispersant can be used to induce the formation of a protective film on the droplet surface. As a result, pairs of clusters of drops that tend to coalesce are broken up by the action of the stirrer before the critical coalescence period elapses. A stable state is ultimately reached in which individual drops maintain their identities over prolonged periods of time [247].

In the case of a polymer that is miscible in all proportions with its monomer (e.g., styrene and methyl methacrylate), a very large variation of the range of the dispersed-phase viscosity is observed during the course of polymerization. The initially low viscosity liquid monomer is transformed gradually into an increasingly viscous polymer in monomer solution and, as conversion increases, the dispersed phase acquires the characteristics of a solid particle. Rapid polymerization during the sticky stage minimizes the

number of effective collisions among polymer particles and thus should reduce coagulation [247] (which may lead to catastrophic coagulation with reaction runaway and loss of the batch). The most important issue in the practical operation of suspension polymerization is the control of the final PSD. The size of the particles will depend on the monomer type, the viscosity change of the dispersed phase with time, the type and concentration of stabilizer, and the agitation conditions in the reactor. The particle morphology is an important characteristic for the application of the polymer product, particularly in the cases of expandable polystyrene (EPS), ion-exchange resins, and poly(vinyl chloride) [246]. The polymerization kinetics and the mechanism of primary particle aggregation in the polymerization of vinyl chloride are rather different to the ones present in bead polymerization. The differences are mainly due to the insolubility of polyvinyl chloride in vinyl chloride. Modeling of the polymerization kinetics and PSD (using a population balance equation) in vinyl chloride polymerization has been addressed by the group of Kiparissides [250].

Suspension polymerization has the following advantages compared to the other polymerization processes (bulk, solution, and emulsion): easy heat removal and temperature control; low dispersion viscosity; low levels of impurities in the polymer product (compared to emulsion); low separation costs if the polymer is to be used as a solid (compared to emulsion); and final product in particle form. On the other hand, among the disadvantages of suspension polymerization one may refer to the following: lower productivity for the same reactor capacity (compared to bulk); wastewater problems (contamination); polymer build-up on the reactor wall, baffles, agitators, and other surfaces; no commercial continuous process operable yet; and difficulty to produce homogeneous copolymer composition during batch suspension polymerization [246]. Semibatch operation is more difficult with suspension versus emulsion polymerization because of the lower interfacial area (particle/water).

A number of important commercial resins are manufactured by suspension polymerization, including poly(vinyl chloride) and copolymers, styrene resins [general purpose polystyrene, EPS, high impact polystyrene (HIPS), poly(styrene-acrylonitrile) (SAN), poly(acrylonitrile-butadiene-styrene) (ABS), styrenic ion-exchange resins], poly(methyl methacrylate) and copolymers, and poly(vinyl acetate). However, some of these polymers rather use a mass-suspension process, in which the polymerization starts as a bulk one and, at certain conversion, water and suspending agents are added to the reactor to form a suspension and continue the polymerization in this way up to high conversions. No continuous suspension polymerization process is known to be employed on a

commercial scale, but such processes have been carried out in the laboratory and on pilot-plant scale [246].

The step of scaling up a reactor from pilot plant to industrial scale is an issue where much empiricism is still used and where expensive and time-consuming experimental programs are usually required. Complete geometric, kinematic, dynamic, chemical, and thermal similarity cannot be simultaneously achieved in a scale up procedure, and so some differences should be allowed at some point [251].

14.7.2 Some Issues about the Modeling of PSD in Suspension Polymerization

Although the suspension polymerization process has been widely studied over more than 60 years, the present situation is that its understanding is still limited and a lot of experimental effort and empirical knowledge are still used to design new resins and to scale their production up from a pilot scale reactor to an industrial level one. The least developed issues in the suspension polymerization process are related to the changing rheological behavior of the reacting mass during polymerization, the nonhomogeneous flow and rate of energy dissipation field distributions within the tank reactor, and the relationship among them and the polymerization kinetics with the breakage/coalescence phenomena that ultimately determine the PSD [248]. The PSD in suspension polymerization is affected by many factors. There have been many studies related to the study of the effects of these parameters on the PSD, although few of them have been complete and systematic. These factors, listed in the first column of Table 14.1, can be classified into four categories: polymerization kinetics, surface phenomena, intensity of mixing, and dispersion concentration.

Some of the responses that can be related to the PSD in suspension polymerization are listed in the second column of Table 14.1. The values of some of these factors can be fixed *a priori*. It is known that the kinetics of polymerization strongly affects the PSD, but this dependence goes in only one direction (namely, the PSD does not affect the kinetics of polymerization in bead suspension polymerization). The link between the polymerization kinetics and the PSD is the zero shear viscosity of the disperse phase, which depends on the molecular weight of the polymer. The effects of the kinetic factors on molecular weight development are reasonably well understood and can be studied independently. This means that by changing the values of the kinetic factors it is possible to generate different molecular weight evolution profiles (thus, different viscosity evolution profiles). A known and adequate evolution profile can be obtained by choosing adequate values for crosslinker concentration, temperature, initiator concentration, and concentration of CTA.

TABLE 14.1 Important Factors and Responses in Suspension Polymerization

Factors	Responses
<i>Polymerization Kinetics</i>	<i>Main Responses</i>
Monomer type	Mean diameter
Monomer concentration	Particle size distribution
Crosslinker concentration (comonomer concentration)	Identity point
Temperature	<i>Secondary Responses</i>
Initiator type (mono- or bifunctional)	Conversion
Initiator concentration	Dispersed-phase viscosity
Presence or absence of chain transfer agent (CTA)	Viscoelasticity
CTA concentration	Molecular weight averages
Inhibitor type	Interfacial tension
Inhibitor concentration	
<i>Intensity of Mixing</i>	
Gravity effect (Froude number)	
Agitator design	
Impeller diameter	
Agitation speed	
Agitation time	
Off-bottom clearance	
Distance of separation between impellers	
Presence or absence of baffles	
Vessel configuration (geometry of the tank)	
Reactor volume	
<i>Surface Phenomena</i>	
Stabilizer type (protective colloid or inorganic powder)	
Stabilizer concentration	
<i>Dispersion Concentration</i>	
Disperse phase holdup	

Although many studies on PSD in suspension polymerization have been published in the last few decades, the understanding of the influence and importance that the known key factors have on the shape and spread of the PSD is still unclear and incomplete. In the critical review on suspension polymerization presented by Vivaldo-Lima et al. [248], a systematic approach to the study of PSD in suspension polymerization was proposed, which was aimed at providing an adequate framework for the development of an effective mathematical model for the calculation of the PSD. Some of the stages of that approach included the selection of the polymerization conditions using a mechanistic model-based experimental design technique [252], and the development of a preliminary mathematical model for the PSD using a compartment-mixing (CM) model approach to

account for the nonhomogeneous mixing in the tank reactor [253]. The original idea of using a CM modeling approach for the calculation of the PSD in suspension polymerization, calculating the intensity of mixing for each compartment from rigorous computational fluid dynamics (CFD) simulations of the actual tank reactor, first proposed [248] and used [253] by the group of Hamielec, has also been used by others since then [254–257]. The homogeneous mixing approach (single CM model) is still used in the context of proposal or evaluation of different variations of the breakage-coalescence models, or evaluation of numerical techniques to solve the population balance equations [258–260].

A Bayesian experimental design technique has been used to determine the relative importance that the different factors of the process have on the PSD [261]. The information obtained served as a measure of how much greater a degree of complexity is needed about the different phenomena that affect the PSD to improve the mathematical model.

14.8 CONTROLLED RADICAL POLYMERIZATION (CRP) IN AQUEOUS DISPERSIONS

Once the basic synthesis techniques and mechanisms of CRP were established (around 2000), a significant part of the research effort in this field has been focused on the development of processes in aqueous dispersions (mostly emulsion and miniemulsion), given the industrial advantages of these processes. In spite of these efforts, there are still important challenges to overcome. The most successful results fall in the category of miniemulsion processes [262–265], but true emulsion processes, which are preferable from the industrial point of view, are still in the development stages.

The basic CRP techniques and mechanisms are discussed in Chapter 4; here only those issues associated with the presence of water in the system are dealt with. The subject has been reviewed by several authors [206, 266, 267]. Perhaps the most important challenge in this field is the development of a robust and general *ab initio* emulsion process (without using a seed). An essential problem in this endeavor is to avoid the nucleation in monomer droplets, which causes colloidal instability.

Two phenomena are behind the complex interaction between the controlled/living character of the polymerization, the particle nucleation phenomenon and the latex stability. One is the superswelling [206] of polymer particles with low molecular weight species. This phenomenon was reported by Ugelstad et al. [268], who revealed that, in the presence of strong hydrophobes, oligomers can swell the polymer particles in a volume ratio as high as 100. In the initial stages of CRP, because of the controlled nature of the

process, only oligomers are generated; these favor the superswelling, which provokes unusual growth of the polymer particles and latex destabilization due to increasing buoyant forces acting on the particles, altering also the partitioning of controlling agent among the phases and reducing the living/controlled character of the polymerization. The second phenomenon, *Ostwald ripening* [206], described above, also promotes excessive growth of particles leading to latex instability and/or bimodalities in the PSD.

In miniemulsion polymerization, the presence of a cosurfactant (highly hydrophobic) inhibits the Ostwald ripening and favors the latex (kinetic) stability; however, this process has the drawback of requiring intense stirring to disperse the monomer droplets in the aqueous phase, consuming high energy, and demanding the use of special mechanical devices.

14.8.1 Nitroxide Mediated Radical Polymerization (NMRP) in Aqueous Dispersions

In general, it is possible to perform stable and reproducible NMRP processes in miniemulsion [262–264]; however, *ab initio* emulsion processes usually exhibit either colloidal stability problems or poor living/controlled character [269–271]. An additional technical requirement is to achieve sufficiently high concentration of the nitroxide in the particle phase. Two or the most successful techniques that can be considered *ab initio* are described next. In the nanoprecipitation process [270], seed particles are generated dispersing an acetone solution of polymeric (polystyrene) macroinitiator containing alkoxyamine groups in a surfactant aqueous solution. Then the acetone is evaporated, and the particles are swelled with more monomer to continue with the polymerization. Good colloidal stability and controlled character have been demonstrated. Self-assembly is a second successful group of techniques [272]. In general, they use a water-soluble alkoxyamine that avoids the nucleation in monomer droplets by different strategies. In a variation of this technique, which is the closest one to an *ab initio* process, a water-soluble SG1 macroalkoxyamine, together with monomer and surfactant-free water, are heated to form block copolymers that self-assemble into nanoparticles dispersed in the aqueous phase. After a slightly unstable period, the latex becomes more stable as the reaction progresses. On the other hand, seeded emulsion polymerizations are simpler due to their lack of a nucleation period with its inherent instability [269, 271, 273, 274].

14.8.2 Atom Transfer Radical Polymerization (ATRP) in Aqueous Dispersions

The subject has been reviewed in the literature [275, 276]. There are some literature reports on successful miniemulsion ATRP reactions; [277] however, side reactions owing

to the presence of water tend to hinder the controlled character. The Cu^{2+} deactivator complex can be dissociated in the presence of protic substances, losing effectiveness and resulting in an excess of the active species, which leads to poor control. Ligand selection is important in order to keep the Cu complexes mostly in the organic phase. In addition, Cu^{1+} is easily oxidized during the emulsification stage due to the presence of oxygen, and therefore some variations of ATRP (e.g., Activators Generated by Electron Transfer (AGET) ATRP), less sensitive to oxygen, are preferred in this case [278]. The surfactant should be nonionic or cationic, since anionic surfactants can deactivate the copper complexes. Truly emulsion ATRP systems usually fail because the initiator tends to migrate to the organic phase leading to excessive nucleation and colloidal instability.

14.8.3 Reversible Addition Fragmentation chain-Transfer (RAFT) in Aqueous Dispersions

RAFT chemistry is probably the most versatile and robust one for polymerization in aqueous dispersions amongst the different CRP techniques. The RAFT agent is bonded to the polymeric chains and therefore does not tend to partition back to the aqueous phase. However, this type of systems also exhibits problems of colloidal stability. In miniemulsion systems, these are attributed to nucleation in monomer droplets and superswelling and can be

minimized by adding more cosurfactant and using oligo- or polymeric RAFT agents. A number of homopolymers have been synthesized by miniemulsion RAFT polymerization: styrene, acrylates, methacrylates, vinyl acetate, acrylic acid, as well as block and gradient copolymers using several of these monomers [279]. Some of these systems show the rate retardation phenomenon, which is also observed in solution or bulk RAFT polymerizations using some CTAs (dithiobenzoates) [280]. In addition to the possible causes of rate retardation reported for bulk and solution systems (slow fragmentation of the adduct and intermediate radical cross-termination with live polymer), it is likely that in aqueous systems the leaving R group desorbs from the particles reinforcing the retardation phenomenon [281, 282].

As for other CRP systems, *ab initio* RAFT emulsion polymerization is difficult to perform due to colloidal stability problems. The use of xanthates (Macromolecular Design via Inter-exchange of Xanthate (MADIX) process) [283] as transfer agents diminishes this problem due to the low transfer constant of these species, leading to relatively high molecular weights at low conversions and reducing the superswelling phenomenon. A drawback of these systems is that they result in relatively large polydispersities.

14.8.4 Controlled Radical Suspension Polymerization

The first CRP carried out in suspension was reported by Georges et al. [284]. They copolymerized styrene and

TABLE 14.2 Controlled Radical Suspension Polymerizations (in chronological order)

Type of CRP	Monomers	Controller	Initiator	Comments	References
NMRP	STY/Butadiene	TEMPO	BPO	$M_w/M_n = 1.35$	[284]
	MMA/DVB	TMTD and <i>p</i> -XDC		Narrow PSD microspheres	[285]
NMRP	STY	TEMPO	BPO & DCP	$M_n > 100,000$ and $M_w/M_n < 1.5$	[286]
ATRP	MMA	RuCl ₂ (PPh ₃) ₃	B	High $M_n (\sim 10^5)$ and $M_w/M_n = 1.1$	[287]
NMRP	STY/AN/BMA	TEMPO	BPO & DCP	Block copolymers with $M_w/M_n \sim 1.5$	[288]
ATRP	MMA	dNbpy	EBiB	$M_w/M_n = 1.18 - 1.33$ at high conversions, using different stabilizers	[289]
ATRP	BA/STY	Fe(Cp)I(CO) ₂	A	$M_w/M_n = 1.25$ for poly(<i>n</i> -BA) and 1.2 for Polystyrene	[290]
NMRP	VC	TEMPO	C	$M_w/M_n = 1.9$	[291]
ATRP	VAc	Co(acac) ₂	V-70	Satisfactory particles of P(VAc) with $M_w/M_n = 1.35$	[292]
ATRP	BMA	Cu(I)Br and Cu(I)Cl	EBiB	M_n and M_w/M_n depend on ligands	[293]
NMRP	STY/BA	TEMPO	BPO	$M_n = 4793$ and $M_w/M_n = 1.14$ for PSTY	[294]
RAFT	MMA	2-Cyane-2-propyl dithiobenzoate	AIBN	$M_w/M_n \sim 1.25$	[295]
RAFT	VND/EGDMA	Xhantates		Similar microsphere distributions as in RP for poly(VND-EGDMA)	[296]
RAFT	MMA	2-Cyane-2-propyl dithiobenzoate		$M_w/M_n \sim 1.25$	[266]

dNbpy, copper halide/4,4'-di(5-nonyl)-2,2'-bipiridine; EBiB, ethyl-2-bromoisobutirate; VND, vinyl neodecanoate; EGDMA, ethylene-glycol-dimethacrylate; V-70, 2,2'-azobis(4-methoxy-2,4-dimethyl valeronitrile); Fe(Cp)I (CO)₂ dicarbonylcyclopentadienylidoiron(II) Co(acac)₂, copper acetylacetone; A, (CH₃)₂C(CO₂-Et)I; B, dichloroacetophenone; C, 1,1-dimethyl-2-ethylhexanperoxoate; TMTD, tetramethylthiuram disulfide; *p*-XDC, dimethylldithiocarbamate-*p*-xylene; DCP, dicumyl peroxide; and AIBN, 2,2'-azobisisobutyronitrile; DVB, divinyl benzene; STY, styrene; MMA, methyl methacrylate; AN, acrylonitrile; BMA, butyl methacrylate; BA, butyl acrylate; VC, vinyl chloride; VAc, vinyl acetate.

butadiene in the presence of BPO (benzoyl peroxide) as initiator and TEMPO (2,2,6,6-tetramethylpiperidin-1-yl)oxyl) as controller. They obtained reasonably low molecular weight dispersities (~ 1.35). Other CRP cases carried out in suspension are listed in Table 14.2.

REFERENCES

- Hosler D, Burkett SL, Tarkanian MJ. *Science* 1999;284:1988.
- Blackley DC. *Emulsion Polymerization Theory and Practice*. London: Applied Science Publishers LTD; 1975.
- Antonietti M, Tauer K. *Macromol Chem Phys* 2003;204:207.
- Hansen FK. Historic Overview. In: van Herk A, editor. *Chemistry and Technology of Emulsion Polymerisation*. Oxford: Blackwell Publishing; 2005. p 3.
- Harkins WD. *J Am Chem Soc* 1947;69:1428.
- Hohenstein WP, Mark H. *J Polym Sci* 1946;1:127.
- Hohenstein WP, Mark H. *J Polym Sci* 1946;1:549.
- Smith WV, Ewart RH. *J Chem Phys* 1948;16:592.
- Sudol ED, Daniels ES, El-Aasser MS. *ACS Symp Ser* 1992;492:1.
- Hansen FK. *ACS Symp Ser* 1992;492:12.
- Herrera-Ordonez J, Olayo R, Carro S. *J Macromol Sci – Polym Rev* 2004;C44:207.
- Nomura M, Tobita H, Suzuki K. *Adv Polym Sci* 2005;175:1.
- Vale HM, McKenna TF. *Prog Polym Sci* 2005;30:1019.
- Chern C-S. *Prog Polym Sci* 2006;31:443.
- Thickett SC, Gilbert RG. *Polymer* 2007;48:6965.
- Tauer K, Hernández H, Kozempel S, Lazareva O, Nazaran P. *Colloid Polym Sci* 2008;286:499.
- Buscall R, Corner T, Stageman JF. *Polymer Colloids*. England: Elsevier Applied Science Publishers; 1985.
- Hiemenz PC, Rajagopalan R. *Principles of Colloid and Surface Chemistry*. 3rd ed. New York: Marcel Dekker Inc.; 1997.
- Adamson AW, Gast AP. *Physical Chemistry of Surfaces*. 6th ed. New York: John Wiley & Sons; 1997.
- Ottewill RH. The stability and instability of polymer latices. In: Piirma I, editor. *Emulsion Polymerization*. New York: Academic Press; 1982. p 1.
- Ottewill RH. Stabilization of polymer colloids dispersions. In: Lovell PA, El-Aasser MS, editors. *Emulsion Polymerization and Emulsion Polymers*. England: John Wiley & Sons; 1997. p 59.
- Vincent B. Colloidal aspects of emulsion polymerisation. In: van Herk A, editor. *Chemistry and Technology of Emulsion Polymerisation*. Oxford: Blackwell Publishing; 2005. p 140.
- Verwey EJW, Overbeek JTG. *Theory of the Stability of Lyophobic Colloids*. Amsterdam: Elsevier; 1948.
- Arshady R. *Colloid Polym Sci* 1992;270:717.
- Rosen MJ. *Surfactants and Interfacial Phenomena*. New York: John Wiley & Sons; 1978.
- Fainerman VB, Möbius D, Miller R. *Surfactants: Chemistry, Interfacial Properties, Applications*. Amsterdam: Elsevier; 2001.
- Olayo R, Garcia E, Garcia-Corichi B, Sanchez-Vazquez L, Alvarez J. *J Appl Polym Sci* 1998;67:71.
- Colombie D, Landfester K, Sudol ED, El-Aasser MS. *Langmuir* 2000;16:7905.
- Ramirez JC, Herrera-Ordonez J, González VA. *Polymer* 2006;47:3336.
- Cui X, Mao S, Liu M, Yuan H, Du Y. *Langmuir* 2008;24:10771.
- Almgren M, Swarup S. *J Phys Chem* 1982;86:4212.
- Ruckenstein E. Thermodynamics of microemulsions II. In: Kumar P, Mittal KL, editors. *Handbook of Microemulsion Science and Technology*. New York: Marcel Dekker; 1999. p 45.
- Salager J-L, Antón RE. Ionic microemulsions. In: Kumar P, Mittal KL, editors. *Handbook of Microemulsion Science and Technology*. New York: Marcel Dekker; 1999. p 247–280.
- Sprow FB. *AIChE J* 1967;13:995.
- Sprow FB. *Chem Eng Sci* 1967;22:435.
- Janssen JJM, Boon A, Agterof WGM. *AIChE J* 1994;40:1929.
- Dotson NA, Galván R, Laurence RL, Tirrel M. *Polymerization Process Modeling*. New York: Wiley-VCH Verlag GmbH; 1996.
- Maaß S, Zaccione A, Paschedag AR, Kraume M. *Trans I Chem E Part A – Chem Eng Res Des* 2007;85(A5):703.
- Razzaghi K, Shahrazi F. *Chem Eng Res Des* 2010;88:803.
- Asua JM. *Prog Polym Sci* 2002;27:1283.
- Sudol ED, El-Aasser MS. Miniemulsion polymerization. In: Lovell PA, El-Aasser MS, editors. *Emulsion Polymerization and Emulsion Polymers*. England: John Wiley & Sons; 1997. p 699.
- Hamielec A, MacGregor JF, Penlidis A. Modeling copolymerizations – control of composition, chain microstructure, molecular weight distribution, long chain branching and crosslinking. In: Reichter KH, editor. *Polymer Reaction Engineering*. Heidelberg: Hunthig & Wepf Verlag; 1983. p 21.
- Dougherty E. *J Appl Polym Sci* 1986;32:3051.
- Guillot J. Computer Simulation of Emulsion Copolymerization Processes for Monomers of Different Water Solubility. In: Reichter KH, editor. *Polymer Reaction Engineering*. Heidelberg: Hunthig & Wepf Verlag; 1986. p 147.
- Armitage PD, de la Cal JC, Asua JM. *J Appl Polym Sci* 1994;51:1985.
- Saldívar E, Dafniotis P, Ray WH. *J Macromol Sci – Rev Macromol Chem Phys* 1998;C38(2):207.
- Gardon JL. *J Polym Sci A Polym Chem* 1968;6:2859.
- Vanzo E, Marechessault RH, Stannett V. *J Colloid Sci* 1965;20:65.
- Guillot J. *Makromol Chem Rapid Commun* 1980;1:697.
- Guillot J. *Acta Polym* 1981;32:593.

51. Ugelstad J, Mork PC, Nordhuus I, Mfutakamba H, Soleimany E. *Makromol Chem Suppl* 1985;10/11:215.
52. Dafniotis P, Saldívar E. Modeling emulsion copolymerization reactors. Kinetics and monomer partition [Term Project: Che 730 *Chemical Reactor Principles*]. Madison: Department of Chemical Engineering, University of Wisconsin; May 1990.
53. Maxwell IA, Kurja J, van Doremale GHJ, German AL, Morrison BR. *Makromol Chem* 1992;193:2049.
54. Maxwell IA, Kurja J, van Doremale GHJ, German AL. *Makromol Chem* 1992;193:2065.
55. Aerdt AA, Boei MMWA, German AL. *Polymer* 1993;34: 574.
56. Noel LFJ, Maxwell IA, German AL. *Macromolecules* 1993; 26:2911.
57. Noel LFJ, Vanzon JMAM, Maxwell IA, German AL. *J Polym Sci A Polym Chem* 1994;32:1009.
58. Schoonbrood HAS, van den Boom MAT, German AL, Hutovic J. *J Polym Sci A Polym Chem* 1994;32:2311.
59. Gugliotta LM, Arotcarena M, Leiza JR, Asua JM. *Polymer* 1995;36:2019.
60. Morton M, Kaizerman S, Altier MW. *J Colloid Interface Sci* 1954;9:300.
61. Flory PJ. *Principles of Polymer Chemistry*. New York: Cornell University Press; 1953.
62. Antonietti M, Kaspar H, Tauer K. *Langmuir* 1996;12:6211.
63. Tauer K, Kaspar H, Antonietti M. *Colloid Polym Sci* 2000;278:814.
64. Farias-Cepeda L, Herrera-Ordonez J, Saldívar-Guerra E. *Colloid Polym Sci* 2009;287:1215.
65. Farias-Cepeda L, Herrera-Ordonez J, Saldívar-Guerra E. *Colloid Polym Sci* 2010;288:1401.
66. Klein A, Daniels ES. Formulation components. In: Lovell PA, El-Aasser MS, editors. *Emulsion Polymerization and Emulsion Polymers*. England: John Wiley & Sons; 1997.
67. Lesko PM, Sperry PR. Acrylic and styrene-acrylic polymers. In: Lovell PA, El-Aasser MS, editors. *Emulsion Polymerization and Emulsion Polymers*. England: John Wiley & Sons; 1997. p 619.
68. Hagiopol C. *Copolymerization, Toward a Systematic Approach*. New York: Kluwer Academic/Plenum Publishers; 1999.
69. Fox TG. *Bull Am Phys Soc* 1956;1:123.
70. Sperry PR, Snyder BS, O'Dowd ML, Lesko PM. *Langmuir* 1994;10:2619.
71. Ceska GW. *J Appl Polym Sci* 1974;18:427–437.
72. Sakota K, Okaya T. *J Appl Polym Sci* 1977;21:1035.
73. Kawaguchi H. *Prog Polym Sci* 2000;25:1171.
74. Liu DHF. Quality criteria of water for processing areas in typical emulsion polymerization processes. In: Cecil LK, editor. *Complete WaterReuse. Ind. Opportunity, Pap. Nat. Conf.* New York: AIChE; 1973. p 328.
75. De Bruyn H, Gilbert RG, Hawkett BS. *Polymer* 2000; 41:8633.
76. Nomura M, Harada M, Eguchi W, Nagata S. *J Appl Polym Sci* 1972;16:835.
77. López de Arbina L, Gugliotta LM, Barandarian MJ, Asua JM. *Polymer* 1998;39:4047.
78. Krishnan S, Klein A, El-Aasser MS, Sudol ED. *Ind Eng Chem Res* 2004;43:6331.
79. Kolthoff IM, Miller IK. *J Am Chem Soc* 1951;73:3055.
80. Berhman EJ, Edwards JO. *Rev Inorg Chem* 1980;2:179.
81. Okubo M, Mori T. *Makromol Chem Makromol Symp* 1990; 31:143.
82. Okubo M, Fujimura M, Mori T. *Colloid Polym Sci* 1991;269:121.
83. Santos AM, Vindevoghel PH, Graillat C, Guyot A, Guillot J. *J Polym Sci A Polym Chem* 1996;34:1271.
84. Sarkar S, Adhikari MS, Banerjee M, Konar RS. *J Appl Polym Sci* 1996;62:1509.
85. Henton DE, Powell C, Reim RE. *J Appl Polym Sci* 1997; 64:591.
86. Lamb DJ, Fellows CM, Gilbert RG. *Polymer* 2005;46:7874.
87. Boutti S, Zafra RD, Graillat C, McKenna TF. *Macromol Chem Phys* 2005;206:1355.
88. van Berkel KY, Russel GT, Gilbert RG. *Polymer* 2006; 47:4667.
89. Kohut-Svelko N, Pirri R, Asua JM, Leiza JR. *J Polym Sci A Polym Chem* 2009;47:2917.
90. Hansen FK. *Chem Eng Sci* 1993;48:437.
91. Coen EM, Lyons RA, Gilbert RG. *Macromolecules* 1996; 29:5128.
92. Leemans L, Jerome R, Teyssié P. *Macromolecules* 1998; 31:5565.
93. Colombie D, Sudol ED, El-Aasser MS. *Macromolecules* 2000;33:4347.
94. Vorwerg L, Gilbert RG. *Macromolecules* 2000;33:6693.
95. Thickett SC, Gilbert RG. *Macromolecules* 2006;39:6495.
96. Copek I. *Adv Colloid Interface Sci* 2002;99:77.
97. Dunn AS. Effects of the choice of emulsifier in emulsion polymerization. In: Piirma I, editor. *Emulsion Polymerization*. New York: Academic Press; 1982. p 221.
98. Colombie D, Sudol ED, El-Aasser MS. *Macromolecules* 2000;33:7283.
99. Suzuki K, Wakatuki Y, Shirasaki S, Fujita K, Kato S, Nomura M. *Polymer* 2005;46:5890.
100. Schneider M, Graillat C, Guyot A, McKenna TF. *J Appl Polym Sci* 2002;84:1916.
101. Schneider M, Graillat C, McKenna TF. *Polymer* 2005; 46:1211.
102. Okubo M, Chaiyasat A, Yamada M, Suzuki T, Kobayashi H. *Colloid Polym Sci* 2007;285:1755.
103. Nomura M, Fujita K. *Polym React Eng* 1994;2(4):317.
104. Harelle L, Pith T, Hu G-H, Lambla M. *J Appl Polym Sci* 1994;52:1105.
105. Barudio I, Guillot J, Fovotte G. *J Polym Sci A Polym Chem* 1998;36:157.

312 DISPERSED-PHASE POLYMERIZATION PROCESSES

106. Cunningham MF, Ma JW. *J Appl Polym Sci* 2000;78:217.
107. Mendoza J, de la Cal JC, Asua JM. *J Polym Sci A Polym Chem* 2000;38:4490.
108. Vidal F, Guillot J, Guyot A. *Colloid Polym Sci* 1995;273:999.
109. Guyot A, Tauer K, Asua JM, Van Es S, Gauthier C, Hellgren AC, Sherrington DC, Montoya-Goni A, Sjoberg M, Sindt O, Vidal F, Unzue M, Schoonbrood H, Shipper E, Lacroix-Desmazes P. *Acta Polym* 1999;50:57.
110. Smeets NMB, Jansen TGT, Sciarone TJ, Heuts JPA, Meuldijk J, Van Herk AM. *J Polym Sci A Polym Chem* 2010;48:1038.
111. Lock MR, El-Aasser MS, Klein A, Vanderhoff JW. *J Appl Polym Sci* 1990;39:2129.
112. Casey BS, Morrison BR, Gilbert RG. *Prog Polym Sci* 1993;18:1041.
113. Tauer K, Deckwer R. *Acta Polym* 1998;49:411.
114. Goicochea M, Barandarian MJ, Asua JM. *Macromolecules* 2003;36:6245.
115. Priest WJ. *J Phys Chem* 1952;56:1077.
116. Fitch RM, Tsai CH. Particle formation in polymer colloids, III: Prediction of the number of particles by a homogeneous nucleation theory. In: Fitch RM, editor. *Polymer Colloids*. New York: Plenum Press; 1971. p 73.
117. Fitch RM, Tsai CH. Homogeneous nucleation of polymer colloids, IV: The role of soluble oligomeric radicals. In: Fitch RM, editor. *Polymer Colloids*. New York: Plenum Press; 1971. p 103.
118. Harada M, Nomura M, Kojima H, Eguchi W. *J Appl Polym Sci* 1972;16:811.
119. Hansen FK, Ugelstad J. *J Polym Sci Polym Chem Ed* 1979;17:3047.
120. Hansen FK, Ugelstad J. Particle formation mechanisms. In: Piirma I, editor. *Emulsion Polymerization*. New York: Academic Press; 1982. p 51.
121. Morbidelli M, Storti G, Carra S. *J Appl Polym Sci* 1983;28:901.
122. Nomura M, Satpathy US, Kouno Y, Fujita K. *J Polym Sci, Part C: Polym Lett* 1988;26:385.
123. Morrison BR, Maxwell IA, Gilbert RG, Napper DH. *ACS Symp Ser* 1992;492:28.
124. Herrera-Ordonez J, Olayo R. *J Polym Sci A Polym Chem* 2000;38:2201.
125. Herrera-Ordonez J, Olayo R. *J Polym Sci A Polym Chem* 2000;38:2219.
126. Herrera-Ordonez J, Olayo R. *J Polym Sci A Polym Chem* 2001;39:2547.
127. Nomura M, Harada M, Eguchi W, Nagata S. *ACS Symp Ser* 1976;24:102.
128. Giannetti E. *AIChE J* 1993;39:1210.
129. Carro S, Herrera-Ordonez J. *Macromol Rapid Commun* 2006;27:274.
130. Carro S, Herrera-Ordonez J, Castillo-Tejas J. *J Polym Sci A Polym Chem* 2010;48:3152.
131. Coen EM, Gilbert RG, Morrison BR, Leube H, Peach S. *Polymer* 1998;39:7099.
132. Shastry V, García-Rubio LH. *J Appl Polym Sci* 2006;100:2847.
133. Hansen FK, Ugelstad J. *Makromol Chem Phys* 1979;180:2423.
134. Hernandez HF, Tauer K. *Macromol Theory Simul* 2010;19:249.
135. Hernandez HF, Tauer K. *Ind Eng Chem Res* 2008;47:9795.
136. Gardon JL. *J Polym Sci A Polym Chem* 1968;6:623.
137. Gardon JL. *J Polym Sci A Polym Chem* 1968;6:687.
138. Varela de la Rosa L, Sudol ED, El-Aasser MS, Klein A. *J Polym Sci A Polym Chem* 1996;34:461.
139. Varela de la Rosa L, Sudol ED, El-Aasser MS, Klein A. *J Polym Sci A Polym Chem* 1999;37:4054.
140. Varela de la Rosa L, Sudol ED, El-Aasser MS, Klein A. *J Polym Sci A Polym Chem* 1999;37:4066.
141. Varela de la Rosa L, Sudol ED, El-Aasser MS, Klein A. *J Polym Sci A Polym Chem* 1999;37:4073.
142. Friis N, Hamielec AE. *ACS Symp Ser* 1976;24:82.
143. Vivaldo-Lima E, Hamielec AE, Wood PE. *Polym React Eng* 1994;2(1–2):17.
144. O'Shaughnessy B, Yu J. *Macromolecules* 1994;27:5067.
145. O'Neil GA, Torkelson JM. *Macromolecules* 1999;32:411.
146. Brooks BW. *Br Polym J* 1971;3:269.
147. Tauer K, Hernández H. *Macromol Rapid Commun* 2010;31:419.
148. Van der Hoff BME. *Adv Chem Ser* 1962;34:6.
149. Hawkett BS, Napper DH, Gilbert RG. *JCS Faraday Trans 1980;76:1323*.
150. Robb ID. *J Polym Sci A Polym Chem* 1969;7:417.
151. Chatterjee SP, Bandopadhyay M, Konar RS. *Indian J Chem* 1976;14A:836.
152. Emelie B, Pichot C, Guillot J. *Makromol Chem Suppl* 1985;10/11:43.
153. Gilbert RG. *Emulsion Polymerization: A Mechanistic Approach*. London: Academic Press; 1995.
154. Miller CM, Clay PA, Gilbert RG, El-Aasser MS. *J Polym Sci A Polym Chem* 1999;35:989.
155. Clay PA, Christie DI, Gilbert RG. *ACS Symp Ser* 1998;685:104.
156. Guyot A, Guillot J, Pichot C, Ríos L. *ACS Symp Ser* 1981;165:415.
157. Urretabizkaia A, Arzamendi G, Unzué MJ, Asua JM. *J Polym Sci A Polym Chem* 1994;32:1779.
158. Canu P, Canegallo S, Morbidelli M, Storti G. *J Appl Polym Sci* 1994;54:1899.
159. Saldívar E, Ray WH. *AIChE J* 1997;43:2021.
160. Sáenz de Buruaga I, Armitage PD, Leiza JR, Asua JM. *Ind Eng Chem Res* 1997;36:4243.
161. Poehlein GW. Emulsion polymerization in continuous reactors. In: Piirma I, editor. *Emulsion Polymerization*. New York: Academic Press; 1982. p 357.

162. Poehlein GW. Continuous processes. In: Lovell PA, El-Aasser MS, editors. *Emulsion Polymerization and Emulsion Polymers*. England: John Wiley & Sons; 1997. p 277.
163. Poehlein GW. Reaction engineering for emulsion polymerization. In: Asua JM, editor. *Polymeric Dispersions: Principles and Applications*. The Netherlands: Kluwer Academic Publishers; 1997. p 305.
164. Saldívar E, Ray WH. Ind Eng Chem Res 1997;36:1322.
165. Paquet DA, Ray WH. AIChE J 1994;40:73.
166. Wohlleben W, Bartels FW, Altmann S, Leyrer RJ. Langmuir 2007;23:2961.
167. Do Amaral M, Van Es S, Asua JM. J Polym Sci A Polym Chem 2004;42:3936.
168. Tzitzinou A, Keddie JL, Geurts JM, Peters ACIA, Satguru R. Macromolecules 2000;33:2695.
169. Gerrens H. Fortschr Hochpolym - Forsch 1959;1:234.
170. Morrison BR, Gilbert RG. Macromol Symp 1995;92:13.
171. Özdeger E, Sudol ED, El-Aasser MS, Klein A. J Polym Sci A Polym Chem 1997;35:3813.
172. Guyot A, Chu F, Schneider M, Graillat C, McKenna TF. Prog Polym Sci 2002;27:1573.
173. Boutti S, Graillat C, McKenna TF. Polymer 2005;46:1211.
174. Flores-Cerrillo J, MacGregor JF. Ind Eng Chem Res 1805;2002:41.
175. Park M-J, Dokucu MT, Doyle FJ III. Ind Eng Chem Res 2004;43:7227.
176. Rajabi-Hamanea M, Engellb S. Chem Eng Sci 2007;62:5282.
177. Alamir M, Sheibat-Othman N, Othman S. AIChE J 2010;56:2122.
178. Ohmura N, Kitamoto K, Yano T, Kataoka K. Ind Eng Chem Res 2001;40:5177.
179. Do Amaral M, Asua JM. J Polym Sci A Polym Chem 2004;42:4222.
180. Ouzineb K, Graillat C, McKenna TF. J Appl Polym Sci 2005;97:745.
181. Urban D, Takamura K. *Polymer Dispersions and Their Industrial Applications*. Weinheim: Wiley-VCH Verlag GmbH; 2002.
182. Lovell PA, Pierre D. Rubber-toughened plastics. In: Lovell PA, El-Aasser MS, editors. *Emulsion Polymerization and Emulsion Polymers*. England: John Wiley & Sons; 1997. p 657.
183. González-Ortíz LJ, Asúa JM. Macromolecules 1995;28: 3135.
184. González-Ortíz LJ, Asúa JM. Macromolecules 1996;29:383.
185. González-Ortíz LJ, Asúa JM. Macromolecules 1996;29: 4520.
186. Dimonie V, Daniels ES, Shaffer O, El-Aasser MS. Control of particle morphology. In: Lovell PA, El-Aasser MS, editors. *Emulsion Polymerization and Emulsion Polymers*. New York: John Wiley & Sons Ltd.; 1997.
187. Stubbs JM, Sundberg DC. J Appl Polym Sci 2006;102:945.
188. Chern C-S. *Principles and Applications of Emulsion Polymerization*. New Jersey: John Wiley & Sons; 2008.
189. Shork J, Ray WH. J Appl Polym Sci 1983;28:407.
190. Storti G, Morbidelli M, Carra S. J Appl Polym Sci 1993;47: 961.
191. Canegallo S, Apostolo M, Storti G, Morbidelli M. J Appl Polym Sci 1995;57:1333.
192. Moritz H-U. Polymerization calorimetry - A powerful tool for reactor control. In: Reichert KH, Geiseler W, editors. *Polymer Reaction Engineering*. Weinheim: Wiley-VCH Verlag GmbH; 1989. p 248.
193. Elizalde O, Azpeitia M, Reis MM, Asua JM, Leiza JR. Ind Eng Chem Res 2005;44:7200.
194. Alb AM, Drensk MF, Reed WF. Polym Int 2008;57:390.
195. Alb AM, Drensk MF, Reed WF. Macromol React Eng 2010;4:470.
196. Collins EA. Measurement of particle size and particle size distribution. In: Lovell PA, El-Aasser MS, editors. *Emulsion Polymerization and Emulsion Polymers*. England: John Wiley & Sons; 1997. p 385.
197. Schoenmakers P. Analysis of polymer molecules: Reaction monitoring and control. In: van Herk A, editor. *Chemistry and Technology of Emulsion Polymerisation*. Oxford: Blackwell Publishing; 2005. p 160.
198. Guillot J. ACS Symp Ser 1992;492:145–162.
199. Landfester K, Spiess HW. Acta Polym 1998;49:451.
200. Stubbs JM, Durant YG, Sundberg DC. Langmuir 1999;15: 3250.
201. Kawahara S, Bushimata S, Sugiyama T, Hashimoto C, Tanaka Y. Rubber Chem Technol 1999;72:844.
202. Stubbs JM, Sundberg DC. J Polym Sci B Polym Phys 2005;43:2790.
203. Colombini D, Ljungberg N, Hassander H, Karlsson OJ. Polymer 2005;46:1295.
204. Candau F. Polymerization in microemulsions. In: Kumar P, Mittal KL, editors. *Handbook of Microemulsion Science and Technology*. New York: Marcel Dekker Inc; 1999. p 679.
205. Guo JS, Sudol ED, Vanderhoff JW, El-Aasser MS. ACS Symp Ser 1992;492:99.
206. Zetterlund PB, Kagawa Y, Okubo M. Chem Rev 2008;108: 3747.
207. Puig JE. Microemulsion polymerization (oil-inwater). In: Salamone JC, editor. *Polymeric Materials Encyclopedia*. Boca Raton: CRC Press; 1996.
208. O'Donnell J, Kaler E. Macromol Rapid Commun 2007;28: 1445.
209. do Amaral M, Bogner A, Gauthier C, Thollet G, Jouneau P-H, Cavaillé J-Y, Asúa JM. Macromol Rapid Commun 2005;26:365.
210. Tang PL, Sudol ED, Adams ME, Silebi CA, El-Aasser MS. ACS Symp Ser 1992;492:72.
211. Manea M, Chemtob A, Paulis M, de la Cal JC, Barandiaran MJ, Asúa JM. AIChE J 2008;54:289.
212. Goikoetxea M, Beristain I, Minari RJ, Paulis M, Barandiaran MJ, Asúa JM. Chem Eng J 2011;170:114.
213. Blythe PJ, Morrison BR, Mathauer KA, Sudol ED, El-Aasser MS. Macromolecules 1999;32:6944.

314 DISPERSED-PHASE POLYMERIZATION PROCESSES

214. Blythe PJ, Morrison BR, Mathauer KA, Sudol ED, El-Aasser MS. *Macromolecules* 1999;32:6952.
215. Alduncin JA, Forcada J, Asua JM. *Macromolecules* 1994;27:2256.
216. Reimers JL, Schork FJ. *Ind Eng Chem Res* 1997;36:1085.
217. Mouran D, Reimers J, Schork FJ. *J Polym Sci A Polym Chem* 1996;34:1073.
218. Chern C-S, Liou YC. *J Polym Sci A Polym Chem* 1999;37:2537.
219. Miller CM, Sudol ED, Silebi CA, El-Aasser MS. *J Polym Sci A Polym Chem* 1995;33:1391.
220. Landfester K, Weiss CK. *Adv Polym Sci* 2010;229:1.
221. Theisinger S, Schoeller K, Osborn B, Sarkar M, Landfester K. *Macromol Chem Phys* 2009;210:411.
222. Guyot A, Landfester K, Schork FJ, Wang C. *Prog Polym Sci* 2007;32:1439.
223. Weiss CK, Landfester K. *Adv Polym Sci* 2010;233:185.
224. Lopez A, Degrandi-Contraires E, Canetta E, Creton C, Keddie JL, Asua JM. *Langmuir* 2011;27:3878.
225. Tiarks F, Landfester K, Antonietti M. *J Polym Sci A Polym Chem* 2001;39:2520.
226. Barrere M, Landfester K. *Polymer* 2003;44:2833.
227. Crespy D, Landfester K. *Macromolecules* 2005;38:6882.
228. Li C-Y, Li Y-H, Hsieh K-H, Chiu W-Y. *J Appl Polym Sci* 2008;107:840.
229. Li M, Matyjaszewski K. *J Polym Sci A Polym Chem* 2003;41:3606.
230. Monteiro MJ, Charleux B. Living radical polymerisation in emulsion and miniemulsion. In: van Herk A, editor. *Chemistry and Technology of Emulsion Polymerisation*. Oxford: Blackwell Publishing; 2005. p 111.
231. Tobita H. *Macromol Theory Simul* 2009;18:108.
232. Guo Y, Liu J, Zetterlund PB. *Macromolecules* 2010;43:5914.
233. Tobita H. *Macromol React Eng* 2010;4:643.
234. Urban D, Schuler B, Schmidt-Thümmes J. Large-volume applications of latex polymers. In: van Herk A, editor. *Chemistry and Technology of Emulsion Polymerisation*. Oxford: Blackwell Publishing; 2005. p 226.
235. DeFusco AJ, Sehgal KC, Bassett DR. Overview of uses of polymer latexes. In: Asua JM, editor. *Polymeric Dispersions: Principles and Applications*. NATO ASI Series. The Netherlands: Kluwer Academic Publishers; 1997. p 379.
236. Pichot C, Delair T. Specialty applications of latex polymers. In: van Herk A, editor. *Chemistry and Technology of Emulsion Polymerisation*. Oxford: Blackwell Publishing; 2005. p 257.
237. Kiparissides C, Pagalos N, Chatzidoukas C, Mantelis C. Mathematical modeling of dispersion polymerization of vinyl monomers in supercritical fluids. International Conference of High Pressure Chemical Engineering; 1999 Mar 3–5; Karlruhe, Germany.
238. Quintero-Ortega IA, Vivaldo-Lima E, Luna-Bárcenas G, Alvarado JFJ, Louvier-Hernández JF, Sanchez IC. *Ind Eng Chem Res* 2005;44:2823.
239. Quintero-Ortega IA, Jaramillo-Soto G, García-Morán PR, Castellanos-Cárdenas ML, Luna-Bárcenas G, Vivaldo-Lima E. *Macromol React Eng* 2008;2:304.
240. Chatzidoukas C, Pladis P, Kiparissides C. *Ind Eng Chem Res* 2003;42:743.
241. Mueller PA, Storti G, Morbidelli M. *Chem Eng Sci* 2005;60: 377.
242. Mitchel GB. Effect of agitator geometry and speed on suspension polystyrene particle formation [M. Eng. Thesis]. Hamilton, Ontario: Department of Chemical Engineering, McMaster University; 1986.
243. Villalobos MA. Suspension polymerization of styrene through bifunctional initiators [M. Eng. Thesis]. Hamilton, Ontario: Department of Chemical Engineering, McMaster University; 1989.
244. Dawkins JV. Aqueous suspension polymerizations, chain polymerization, II, Chapter 14. In: Geoffrey A, Bevington JC, editors. *Comprehensive Polymer Science. The Synthesis, Characterization & Applications of Polymers*. Volume 4. Oxford: Pergamon Press; 1989.
245. Brooks BW. *Makromol Chem Macromol Symp* 1990;35/36: 121.
246. Yuan HG, Kalfas G, Ray WH. *J Macromol Sci Rev Macromol Chem Phys* 1991;C31(2–3):215.
247. Hamielec AE, Tobita H. Polymerization processes. In: Elvers B, Hawkins S, Schultz G, editors. *Ullmann's Encyclopedia of Industrial Chemistry*. Volume A21. Weinheim: Wiley-VCH Verlag GmbH; 1992. p 305 ff.
248. Vivaldo-Lima E, Wood PE, Hamielec AE, Penlidis A. *Ind Eng Chem Res* 1997;36:939.
249. Zhu D-W. *Macromolecules* 1996;29:2813.
250. Kiparissides C, Daskalakis G, Achilias DS, Sidiropoulou E. *Ind Eng Chem Res* 1997;36:1253.
251. Okufi S, Pérez de Ortiz ES, Sawistowski H. *Can J Chem Eng* 1990;68:400.
252. Vivaldo-Lima E, Wood PE, Hamielec AE, Penlidis A. *J Polym Sci A Polym Chem* 1998;36:2081.
253. Vivaldo-Lima E, Wood PE, Hamielec AE, Penlidis A. *Can J Chem Eng* 1998;76:495.
254. Maggioris D, Goulas A, Alexopoulos AH, Chatzi EG, Kiparissides C. *Comput Chem Eng* 1998;22:S315.
255. Maggioris D, Goulas A, Alexopoulos AH, Chatzi EG, Kiparissides C. *Chem Eng Sci* 2000;55:4611.
256. Alexopoulos AH, Maggioris D, Kiparissides C. *Chem Eng Sci* 2002;57:1735.
257. Kiparissides C, Alexopoulos A, Roussos A, Dompazis G, Kotoulas C. *Ind Eng Chem Res* 2004;43:7290.
258. Chen Z, Pauer W, Moritz HU, Pruss J, Warnecke HJ. *Chem Eng Technol* 1999;22:609.
259. Machado RAF, Pinto JC, Araujo PHH, Bolzan A. *Braz J Chem Eng* 2000;17:395.
260. Hounslow MJ, Ni X. *Chem Eng Sci* 2004;59:819.
261. Vivaldo-Lima E, Penlidis A, Wood PE, Hamielec AE. *J Appl Polym Sci* 2006;102:5577.

262. Farcet C, Nicolas J, Charleux B. *J Polym Sci A Polym Chem* 2002;40:4410.
263. Lin M, Hsu JCC, Cunningham MF. *J Polym Sci A Polym Chem* 2006;44:5974.
264. Saka Y, Zetterlund PB, Okubo M. *Polymer* 2007;48:1229.
265. Oh JK, Perineau F, Charleux B, Matyjaszewski K. *J Polym Sci A Polym Chem* 2009;47–7:1771.
266. Cunningham MF. *Prog Polym Sci* 2008;33:365–398.
267. Kwon OH J. *J Polym Sci A Polym Chem* 2008;46:6983–7001.
268. Ugelstad J, Mork PC, Kaggerud KH, Ellingsen T, Berge A. *Adv Colloid Interface Sci* 1980;13:101.
269. Nicolas J, Charleux B, Guerret O, Magnet S. *Macromolecules* 2005;38:9963.
270. Szkurhan AR, Georges MK. *Macromolecules* 2004;37:4776.
271. Simms RW, Hoidas MD, Cunningham MF. *Macromolecules* 2008;41:1076.
272. Charleux B, Nicolas J. *Polymer* 2007;48:5813.
273. Bon SAF, Bosveld M, Klumperman B, German AL. *Macromolecules* 1997;30:324.
274. Nicolas J, Charleux B, Guerret O, Magnet S. *J Polym Sci A Polym Chem* 2006;44:4142.
275. Min K, Matyjaszewski K. *Cent Eur J Chem* 2009;7–4:657.
276. Li M, Matyjaszewski K. *J Polym Sci A Polym Chem* 2003;41–22:3606.
277. Tsarevsky N, Matyjaszewski K. *Chem Rev* 2007;107:2270.
278. Kagawa Y, Zetterlund PB, Minami H, Okubo M. *Macromolecules* 2007;40:3062.
279. Rizzardo E, Moad G, Thang SH. *RAFT polymerization in bulk monomer or in (organic) solution*, Chapter 6. In: Barner-Kowollik C, editor. *Handbook of RAFT Polymerization*. Weinheim: Wiley-VCH Verlag GmbH; 2008.
280. Barner-Kowollik C, Buback M, Charleux B, Coote ML, Drache M, Fukuda T, Goto A, Klumperman B, Lowe AB, Mcleary JB, Moad G, Monteiro MJ, Sanderson RD, Tonge MP, Vana P. *J Polym Sci A Polym Chem* 2006;44:5809.
281. Monteiro MJ, Hodgson M, de Brouwer H. *J Polym Sci A Polym Chem* 2000;38:3864.
282. Rivera MR, Rodríguez-Hernández AA, Hernández N, Castillo P, Saldívar E, Ríos L. *Ind Eng Chem Res* 2005;44:2792.
283. Taton D, Destarac M, Zard SZ. *Macromolecular design by interchange of xanthates: Background, design, scope and applications*, Chapter 10. In: Barner-Kowollik C, editor. *Handbook of RAFT Polymerization*. Weinheim: Wiley-VCH Verlag GmbH; 2008.
284. Georges M, Veregin R, Kazmaier H, Hamer G. *Macromolecules* 1993;26:2987.
285. Saito R, Ni X, Ichimura A, Ishizu K. *J Appl Polym Sci* 1998;69:211.
286. Schmidt-Naake G, Drache M, Taube C. *Die Angew Makromol Chem* 1999;265:62.
287. Nishikawa T, Kamigaito M, Sawamoto M. *Macromolecules* 1999;32:2204.
288. Taube C, Schmidt-Naake G. *Macromol Mater Eng* 2000;279:26.
289. Jousset S, Qiu J, Matyjaszewski K. *Macromolecules* 2001;34:6641.
290. Fuji Y, Ando T, Kamigaito M, Sawamoto M. *Macromolecules* 2002;35:2949.
291. Wannemacher T, Braun D, Pfaendner R. *Macromol Symp* 2003;202:11.
292. Debuigne A, Caille J, Detrembleur C, Jérôme R. *Angew Chem Int Ed* 2005;44:3439.
293. Limer A, Heming A, Shirley I, Haddleton D. *Eur Polym J* 2005;41:805.
294. Kaminski M, Cunningham M, Lima E, Pinto J. *Ind Eng Chem Res* 2005;44:2568.
295. Biasutti J, Davis T, Lucien F, Heuts J. *J Polym Sci A Polym Chem* 2005;43:2001.
296. Nguyen U, Farrugia B, Davis T, Barner-Kowollik C, Stenzel M. *J Polym Sci A Polym Chem* 2007;45:3256.

15

NEW POLYMERIZATION PROCESSES

EDUARDO VIVALDO-LIMA, CARLOS GUERRERO-SÁNCHEZ, CHRISTIAN H. HORNUNG,
IRAÍS A. QUINTERO-ORTEGA, AND GABRIEL LUNA-BÁRCENAS

15.1 INTRODUCTION

As the environmental policies for reduction of emissions of different chemical substances become more restrictive, the idea of developing new and alternative (more sustainable) methods for producing polymeric materials has gained considerable interest in recent years. In this context, the reduction in the consumption of volatile organic compounds (VOCs) as well as the use of alternative energy sources and reaction configurations during polymer manufacturing has become a priority in research development. The design of new polymerization processes must be carried out on the basis of promoting both energy savings and reduction of VOCs, and implementing the principles of green chemistry whenever possible [1].

The best way to avoid using organic solvents is to develop solvent-free processes, but problems associated with the high viscosities attained in polymerization processes make this route impractical in most instances. The second best choice is then to replace organic solvents with environmentally benign ones, such as water, ionic liquids (ILs), fluorous phases, and compressed (e.g., supercritical) fluids. Each one of these approaches has advantages and disadvantages [2, 3]. Solvent-free processes may be considered as the “ideal” and the cleanest way of chemical manufacture. However, in polymer industry, bulk processes require an enormous amount of energy and high temperatures to overcome the problems related to the transportation of highly viscous polymer melts, which in some cases may provoke side-reactions and/or degradation of the products (Chapter 1).

The use of water, as a readily available, inexpensive, and harmless solvent, is a well-established approach in polymer

synthesis. In this regard, one can mainly find radical polymerizations performed via emulsion, suspension, and dispersion processes (Chapter 14). Even though water would be the most suitable selection for developing green polymerization processes, this approach cannot be used in moisture-sensitive systems, such as ionic polymerizations (Chapters 7 and 8).

This chapter provides an overview of the state of the art on emerging technologies with potential use in the production of polymeric materials. The addressed technologies in this chapter include the use of alternative solvents for polymer synthesis (e.g., supercritical CO₂ (scCO₂) and ILs), the preparation of polymer composites based on ILs, as well as the use of alternative reactor and energy technologies. Given the fact that some of the new polymerization processes emphasized in this chapter involve the use of compressed fluids, a subsection of this chapter is devoted to expand some of the key concepts of phase behavior of polymer systems presented in Chapter 25, but emphasizing high pressure systems (mainly associated with scCO₂).

15.2 POLYMERIZATIONS IN BENIGN OR GREEN SOLVENTS

15.2.1 Polymerizations in Compressed and Supercritical Fluids (SCF)

15.2.1.1 Phase Behavior of Polymer Systems in High Pressure Fluids The basic description and definitions of the different phenomena associated with phase equilibria in polymer solutions are described in Section 25.2.5. Topics such as construction and interpretation of binary

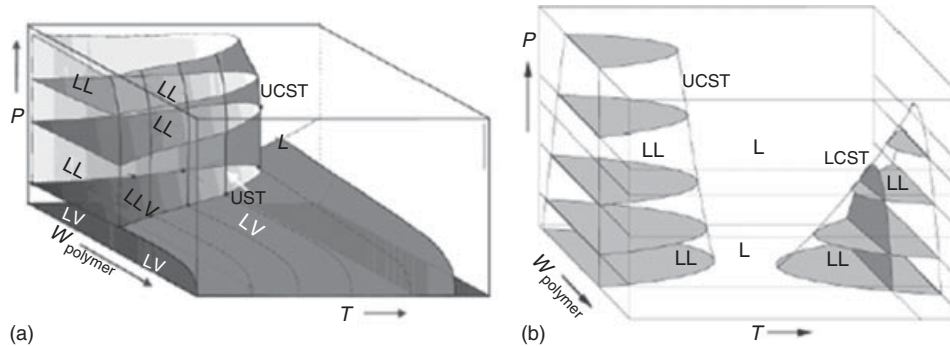


Figure 15.1 Schematic three-dimensional temperature–pressure–composition phase diagrams of polymer–solvent system: (a) UCST-LLE, VLE, and VLLE; (b) UCST- and LCST-LLE. *Source:* Adapted with permission from Seiler M, Rolker J, Arlt W. *Macromolecules* 2005;2003:36 [4]. Copyright 2003 American Chemical Society.

phase diagrams, the definition of upper critical solution temperature (UCST) and lower critical solution temperature (LCST), miscibility regions, and the basic theoretical treatment for phase separation are covered there.

To obtain a more general insight, both $P-w$ and $T-w$ diagrams are transferred into the three-dimensional phase diagram, which is illustrated in Figure 15.1.

In Figure 15.1a, only UCST behavior is illustrated. Vapor–liquid equilibrium as well as vapor–liquid–liquid equilibrium, where two liquid phases are in equilibrium with one vapor phase, can be distinguished. In Figure 15.1b, one can recognize the two LLE regions in the $T-w$ plain. With increasing pressure, the two-phase regions become smaller. Usually, the slope of the UCST line is steeper than that for LCST.

Another projection of the three-dimensional $T-P-w$ diagram is the illustration of pressure versus temperature at critical concentration, shown in Figure 15.2, and reveals some further insights into the behavior of polymer–solvent systems.

One can see again that the miscibility of the system becomes better with increasing pressure since the temperature difference between the UCST and LCST curve becomes larger. The points where the UCST and LCST curve settle on the VLE line are called *upper critical equilibrium point* (UCEP) and *lower critical equilibrium point* (LCEP), respectively (sometimes, one can find “end point” instead of “equilibrium point” in the literature). At these points, two liquid phases and one vapor phase are in equilibrium.

It is worthy to emphasize that Figure 15.2 illustrates the solution behavior at the critical concentration. However, in the literature, one often finds the terms UCST and LCST in pressure–temperature diagrams that describe the phase separation behavior of a solution at any constant concentration. If this concentration is different from the critical concentration, which is even not always necessarily known, strictly speaking, the correct designation should be UST (upper solution temperature) and LST (lower solution

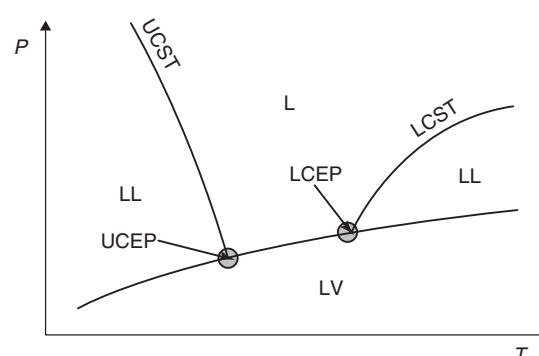


Figure 15.2 Schematic pressure–temperature phase diagram at the critical concentration of a polymer–solvent system with UCST and LCST phase separation. *Source:* Adapted with permission from Kiamos AA, Donohue MD. *Macromolecules* 1994;27(2):357 [5]. Copyright 1994 American Chemical Society.

temperature), respectively. Consequently, the end points of the curves should be named UEP (upper end point) and LEP (lower end point) instead of UCEP and LCEP, respectively. The terms UCST and LCST are used here, however, just keeping in mind that the actual critical concentration is not usually known.

The addition of a compressed or supercritical gas to a polymer–solvent system, which acts as an antisolvent because of the introduction of free volume, has various effects [6]: (i) all phase transition curves shift to higher pressure, which is needed to keep the gas in solution, and (ii) the LCST curve shifts to lower temperatures since the free-volume effect is enhanced.

Eventually both UCST and LCST curves can merge to a single curve. Figure 15.3 shows the qualitative influence of gas on the phase behavior of polymer–solvent systems in a $P-T$ diagram at constant concentration and a $T-w$ diagram at constant pressure.

If the UCST and LCST curves are merged, the so-called hour glass shape is formed as can be seen in the

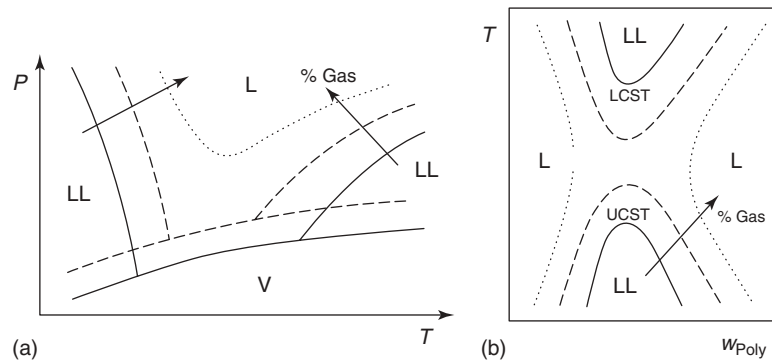


Figure 15.3 Effect of gas content on phase behavior of a polymer–solvent system: (a) pressure–temperature diagram at constant concentration and (b) temperature–composition diagram at constant pressure. *Source:* Adapted with permission from ter Horst MH, Behme S, Sadowski G, de Loos TW. *J Supercrit Fluids* 2002;14:181 [7]. Copyright 2002 Elsevier.

$T-w$ diagram. In that case, there exists no temperature at which the system is completely miscible over the whole concentration range.

The phase behavior of polymers in supercritical fluid (SCF) solvents has been reviewed by Kirby and McHugh [8]. The effect of supercritical carbon dioxide on polymer–solvent mixtures is addressed elsewhere [5].

The effect of the variation of the molecular mass of the polymer on the equilibrium lines is comparable to the effect of gas concentration. This is due to the fact that small solvent molecules dissolve small molecules better than bigger ones. Thus, by increasing the molecular weight of the polymer, the immiscibility region is expanded. UCST and LCST move toward each other until they eventually merge to the hour glass shape. The effect of several variables on the location of the UCST and LCST is qualitatively illustrated in Figure 15.4.

A monodisperse polymer population is an idealization. Rather, one has to consider the polymer as a multicomponent mixture of many species with identical molecular

structure but different molecular masses. This complicates the illustration of phase diagrams.

To explain the behavior of a polymeric multicomponent system, the polymer is considered as a mixture of two polymer species, P1 and P2. By doing this, the polymer–solvent system can be illustrated using a ternary Gibbs triangular diagram. It is assumed that one species of the polymer, P1, has a lower molecular mass than P2 and is completely miscible with the solvent, whereas P2 exhibits an immiscibility region (Figure 15.5).

Adding solvent to a polymer mixture F at T_1 , the immiscibility region is entered at point C1, where the solution turns cloudy. This is why this point is also called *cloud point*. At this moment, a second phase appears whose concentration is given by S1. Since the amount of the second phase is so small, its concentration is experimentally not accessible and this point is named *shadow point*. Adding more solvent, the two-phase region is finally left at the other side at the cloud point C2 with the corresponding shadow point S2.

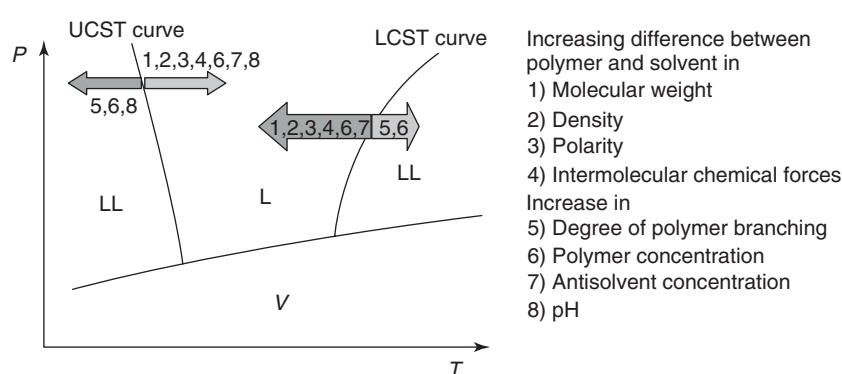


Figure 15.4 Effect of various variables on LCST and UCST shown schematically in a pressure–temperature diagram. *Source:* Adapted with permission from Seiler M. *Chem Eng Tech* 2002;2:237 [9]. Copyright 2002 Wiley-VCH Verlag GmbH & Co. KGaA.

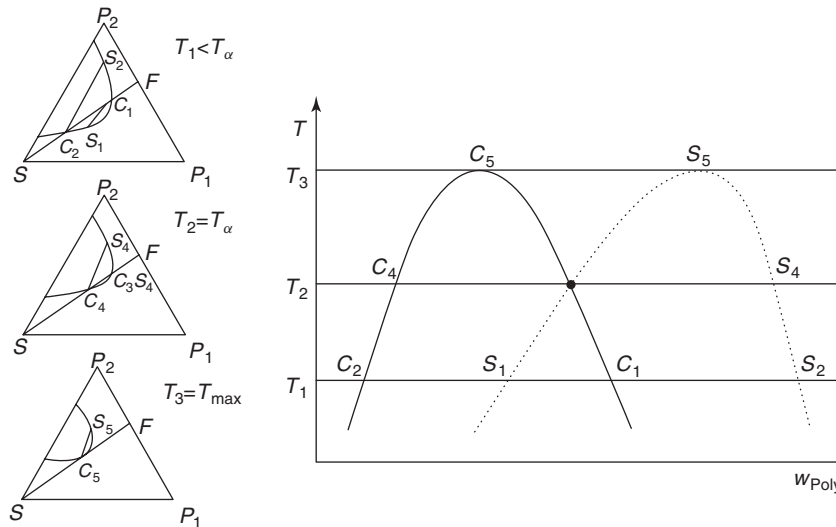


Figure 15.5 Effect of molecular weight dispersity (\mathcal{D}) (formerly known as polydispersity) using schematic Gibbs triangle diagrams for polymer–solvent system, generation of cloud point curve and shadow curve in temperature–composition diagram.

At other temperatures, the shape of the immiscibility region differs. For example, at a higher temperature T_2 , it could be that the two-phase region is entered at its critical point, and so both phases have the same concentration. However, they can still be distinguished by their different densities. Or, at an even higher temperature T_3 , the two-phase region is tangented at only one point. This would be the UCST.

One can illustrate these circumstances in the usual (pseudobinary) T – w diagram, w_{Poly} being the summarized weight fraction of both polymer species. By doing this, information about the distribution of the polymer species in the different phases is not available. However, it is known that along the cloud point curve, the concentration is always equal to the initial polymer distribution F, whereas it differs strongly along the shadow curve. Usually, there is an enrichment of longer polymer chains in the shadow phase.

Typically, in literature, one can only find data of cloud point curves since the shadow phase is experimentally not accessible. This data can be obtained using different methods. Usually, a temperature- and pressure-controlled autoclave is used. The polymer solution of known concentration is charged into the autoclave and is then tempered and pressurized. By varying either temperature or pressure, holding the other property constant, the cloud point pressure or cloud point temperature can be determined. Often the cloud point is defined as a rather subjective change of color of the solution, which becomes turbid when the second phase appears. By repeating this formalism for a broad range of initial solution concentrations, cloud point curves can be created over a large range of temperature, pressure, and concentration.

15.2.1.2 Earlier High Pressure Polymerization Processes

The use of high pressures in polymerization processes, where the monomer is compressed but not necessarily in its supercritical region, is not new. Strange and Bliss polymerized butadiene and its substituted derivatives by applying a pressure of 300–400 MPa (much higher than the critical pressure of butadiene of 4.322 MPa) [10, 11]. In 1936, ICI patented a process for ethylene polymerization using free radical initiators in the presence of benzaldehyde at 170 °C and 190 MPa, clearly in the supercritical region of ethylene ($T_{\text{cr}} = 9.25$ °C, $P_{\text{cr}} = 5.04$ MPa), and small-scale production started in 1939 [12]. However, the motivation for high pressure applications in the early processes was not from environmentally benign grounds. High pressures were used to polymerize monomers that would not polymerize at atmospheric pressure, to increase polymerization rate, to increase molecular weight, and to obtain some additional information about the processes [11].

15.2.1.3 Polymerization in Supercritical Carbon Dioxide (scCO_2)

Background and Overview CO_2 is an attractive alternative to organic solvents for various applications because it is nontoxic, nonflammable, inexpensive, and environmentally relatively benign [6, 13]. An extensive review about the potential of CO_2 -based technology was presented by the group of DeSimone [14]. Its critical conditions can be easily be obtained ($T_{\text{cr}} = 31.1$ °C, $P_{\text{cr}} = 7.38$ MPa). Because of its low value of polarizability per volume, compressed or supercritical CO_2 is able to dissolve most small nonpolar molecules, but just a few polymers that have low cohesive

densities, for example, fluoroacrylates, fluorocarbons, fluoroethers, and siloxanes [6, 14–17]. However, besides these few “CO₂-philic” polymers, CO₂ rather behaves like an antisolvent in polymer solutions, which is the basis for many industrial processes.

As all SCFs, scCO₂ offers interesting properties that lie between those of a gas and a liquid. As liquids, they exhibit high density and can swell polymers [6, 14, 18–20]. As gases, they have low viscosity and relatively high diffusivity. scCO₂ is highly compressible; its density and, therefore, solvent properties, such as viscosity and dielectric constant, can be tuned by varying the temperature and pressure of the system [6, 15]. Its solvent power can thus be controlled precisely.

Compressed gases exhibit various effects that can be exploited in industrial processes [6, 21]: (i) tunability of the solvent power of a solvent by addition of a fluid antisolvent and pressure variation; (ii) controllability of phase transition kinetics by variation of the gas content and system pressure; (iii) swelling of polymers and decreasing of the glass transition temperature (transition of a polymer from a viscous melt to a hard noncrystalline glassy state) by dissolution of compressed gases; and (iv) decrease of viscosity and higher diffusion and transition coefficients by dissolution of compressed gases.

Polymerizations in scCO₂ Many polymers have been synthesized in scCO₂, including fluoropolymers, polysiloxanes, poly(methyl methacrylate), polystyrene, and polycarbonates, as reviewed elsewhere [22–24]. The literature on polymer chemistry in scCO₂ is extensive and keeps growing, as evidenced from the review by Kendall et al. [23]. Specifically, the homopolymerizations of styrene [25–30] and methyl methacrylate (MMA) [15, 31–41] in scCO₂ have been studied in some depth in the literature, from an experimental perspective. In this section, we emphasize the modeling of polymerization processes in scCO₂. To do so, three case studies are considered: (i) the modeling of homogeneous (single-phase) systems [42]; (ii) the modeling of heterogeneous free radical homopolymerizations [43]; and (iii) the modeling of heterogeneous free radical copolymerization with crosslinking [44]. All these cases were addressed using the principles and modeling tools described in Chapter 12.

CASE STUDY 1: HOMOGENEOUS HOMO- AND COPOLYMERIZATIONS IN scCO₂ The first case analyzed [42] was the homogeneous homopolymerization of dihydroperfluorooctyl acrylate (FOA) in supercritical carbon dioxide at the same conditions reported by DeSimone et al. [45]. Once the model was implemented, parameter sensitivity analyses were carried out. The first objective was to test the model implementation, namely, to verify that the expected trends were predicted by the model. The second objective of these

sensitivity analyses was to determine bounds on the values of the propagation and termination kinetic rate constants, k_p and k_t , respectively, in case it was necessary to use them as fitting parameters to the experimental data from the literature that were available. The second system modeled for this case study was the surfactant-free precipitation copolymerization of TFE/VAc (approximated as homogeneous) in supercritical carbon dioxide. This is a reasonable assumption, since the copolymerization proceeds mostly in a single phase because the monomer acts as a cosolvent, enhancing the solubility of the produced polymer during the reaction [46]. In that study, the initial composition of fluoromonomer was increased from 13.1% to 83.3%, on a molar basis, in five cases (13.1%, 34.5%, 50%, 67.7%, and 83.3%). The five cases were simulated with the model, which for this case consisted of a conventional homopolymerization (even the copolymerization was described with the same model equations, but considering the kinetic rate constants as pseudokinetic rate constants, as explained in Chapter 12). Although not enough experimental information was available, nor reported kinetic rate constants for these monomers at such conditions, fairly good agreement was obtained by using reasonable kinetic rate constants, as it can be observed in Figure 15.6 for the case of copolymer composition in the copolymerization of TFE/VAc.

CASE STUDY 2: COMPARISON OF MATHEMATICAL MODELS FOR FREE RADICAL HOMOPOLYMERIZATION OF VINYL MONOMERS IN scCO₂ In this case study, a comparison of performance of the different kinetic models proposed in the literature for dispersion polymerization of styrene and MMA in scCO₂ is presented. The models used by Quintero-Ortega et al. [43] (models 1 and 2) and those presented by the groups of Kiparissides [47] (model 3) and Morbidelli [48] (model 4) for MMA homopolymerization are used for the comparison. The differences among these models are related to the calculation of the partition of components between the two phases and are summarized in Table 15.1.

Figure 15.7 shows that models 1–3 perform equally well for the prediction of polymerization rate (Fig. 15.7a) and molecular weight development (Fig. 15.7b). However, the predictions of monomer and solvent concentrations in both phases differ significantly (Fig. 15.8). Moreover, when interpolating the parameters of these three models to consider a system with lower pressure, and now comparing models 1, 2, and 4, it is observed that models 1 and 2 perform poorly, and model 4 reproduces reasonably well the behavior of this system (Fig. 15.9).

Although the overall performance of the models compared in this case study, measured in terms of predictions of polymerization rate and molecular weight development, can be considered acceptable if adequate and reliable parameters are used, it is clear that important differences exist, and that the study of component partitioning between the

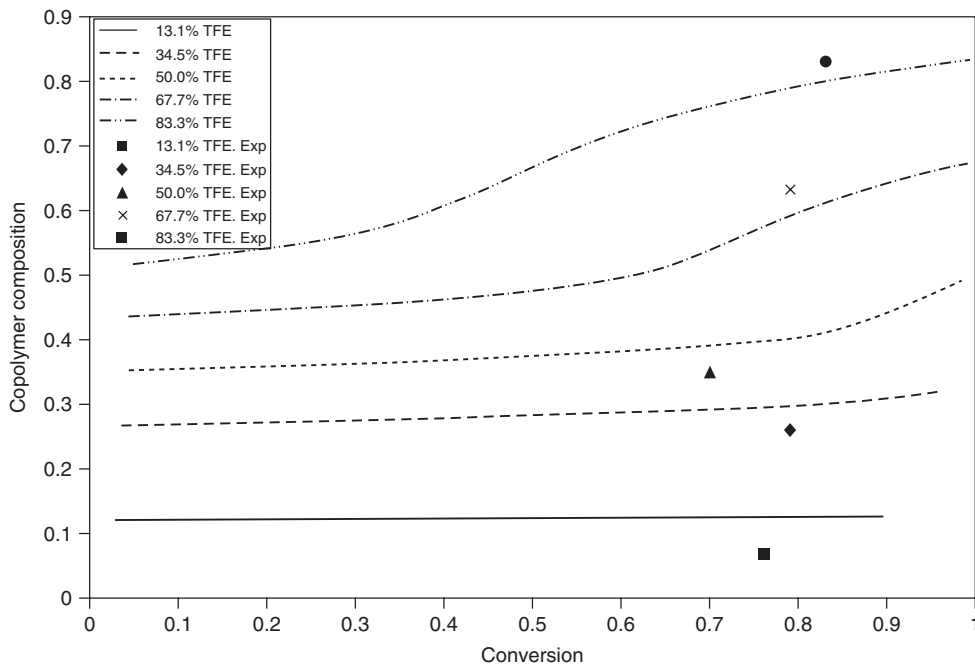


Figure 15.6 Effect of fluoromonomer composition on copolymer composition in copolymerization of TFE and VAc at the experimental conditions of Baradie and Shoichet [46]. *Source:* Reprinted with permission from Quintero-Ortega IA, Vivaldo-Lima E, Gupta RB, Luna-Bárcenas G, Penlidis A. *J Macromol Sci Pure Appl Chem* 2007;44:205 [42]. Copyright 2007 Taylor & Francis Group, LLC.

phases in dispersion polymerization of vinyl monomers is still far from complete. The disagreement observed in some of the dispersion polymerization cases seems to be related to inadequate estimates or inadequate modeling of the partition of components between the two phases.

CASE STUDY 3: MODELING OF COPOLYMERIZATION OF VINYL/DIVINYL MONOMERS IN scCO_2 . A mathematical model for the free radical copolymerization kinetics with crosslinking of vinyl/divinyl monomers in carbon dioxide at supercritical conditions was developed by Quintero-Ortega et al. [44]. The copolymerization of styrene and divinylbenzene was analyzed as case study. The effects of the kinetic and physical parameters on monomer conversion, molecular weight development, copolymer composition, appearance of the gelation point, gel fraction, and average crosslink density were studied. Model predictions showed the expected trends, although the system was quite sensitive to pressure, which makes an interesting and promising way to tailor some of the polymer properties. The model corresponds to the case with crosslinking explained in Chapter 12 of this handbook, but considering a two-phase situation, using the modeling approach called *model 1* of the preceding case study for calculation of the partition of the recipe components between the two phases. Figure 15.10 shows the remarkable effect of pressure on the polymerization kinetics, molecular weight development,

and evolution of network formation. Calculations were carried out using parameters for a styrene/divinylbenzene copolymerization at 65°C .

15.2.1.4 Polymerization in Other Compressed Green Solvents

Supercritical water ($T_{\text{cr}} = 374.15^\circ\text{C}$, $P_{\text{cr}} = 22.1 \text{ MPa}$) is a very effective reaction medium for oxidation reactions [3, 50, 51]. However, corrosion and elevated investment costs are adverse issues that make the intense use of this technology difficult [3].

Besides supercritical water and scCO_2 , another compressed fluid successfully used in the development of green polymerization processes is 1,1,1,2-tetrafluoroethane (R134a, $T_{\text{cr}} = 101.1^\circ\text{C}$, $P_{\text{cr}} = 4.06 \text{ MPa}$). Some advantages/characteristics of R134a are [52] as follows: (i) it is nontoxic and nonflammable and is widely regarded as having zero ozone depletion potential; (ii) it has found widespread use as a CFC replacement in refrigeration and auto air conditioning systems; in addition, its low toxicity has led to approval for use in metered dose inhalers; (iii) its global warming potential is estimated to be 1300 times that of CO_2 , but a widely held view is that HFCs will have a very small impact on overall climate change, which will arise mostly from the accumulation of CO_2 in the atmosphere from the burning of fossil fuels; (iv) although it is more expensive than CO_2 , and any HFC-based process would likely require effective recycling of the solvent,

TABLE 15.1 Differences between the Four Models*

	Model 1 [44]	Model 2 [43]	Model 3 [47]	Model 4 [48]
Assumptions	Homogeneous at the beginning; appearance of second phase at solubility limit	Two phases from the beginning of the reaction	Two phases from the beginning of the reaction	Two phases from the beginning of the reaction
Reaction loci	Homogeneous up to x_s , then heterogeneous. At x_c polymerization proceeds only in the dispersed phase	Both, continuous and dispersed phases	Both, continuous and dispersed phases	Both, continuous and dispersed phases
Reactions considered	Initiation, propagation, chain transfer to monomer and termination, in both phases	Initiation, propagation, chain transfer to monomer and termination, in both phases	Initiation, propagation, chain transfer to monomer and termination, in both phases	Initiation, propagation, chain transfer to monomer and termination, in both phases
Diffusion-controlled (DC) effects	DC propagation and termination only in the dispersed phase	DC initiation, propagation, chain transfer to monomer and termination, in both phases	DC propagation and termination, in both phases	DC initiation, propagation and termination, in both phases
Partition of low molecular weight species between the phases	Semiempirical expressions that relate solubility and conversion are used	Phase transfer and concentrations in each phase are controlled by partition coefficients and equilibrium considerations	Monomer, initiator, and solvent are at equilibrium concentrations, which are calculated using the Sanchez–Lacombe EOS	Monomer, initiator, and solvent are at equilibrium concentrations, which are calculated using the Sanchez–Lacombe EOS
Polymeric species concentrations	Living oligoradicals in the continuous phase; living and dead polymer in the dispersed phase	The propagating radicals transfer to the dispersed phase as soon as they reach the critical chain length	The polymer is at interphase equilibrium. Concentrations are evaluated using the Sanchez–Lacombe EOS	A chain-length-dependent equilibrium partition coefficient for polymer chains between continuous and dispersed phases is considered. Radical partition (RP) model [48]
Calculation of the MWD	The averages M_n and M_w are calculated from the moments of the MWD	The full MWD is calculated using Galerkin's method [49]	The averages M_n and M_w are calculated from the moments of the MWD	Full MWD calculated using the discretization method of Kumar and Ramkrishna [48]

*Source: Adapted with permission from Quintero-Ortega IA, Jaramillo-Soto G, García-Morán PR, Castellanos-Cárdenas ML, Luna-Bárcenas G, Vivaldo-Lima. E. Macromol React Eng 2008;2:304 [43]. Copyright 2008 Wiley-VCH Verlag GmbH & Co. KGaA.

energy-efficient recycling of R134a may be practical since it was developed originally as a refrigerant; and (v) regarding its degree of polarity, CO₂ is symmetrical and has no permanent dipole moment (although it does possess a substantial quadrupole moment), while R134a is moderately polar and has a significant dipole moment (2.1 D).

Wood and Cooper [53] successfully synthesized crosslinked polymer microspheres by dispersion polymerization of MMA and trimethylolpropane trimethacrylate (TRIM) in R134a using perfluoropolyether stabilizers and moderate pressures (10–20 bar). However, the authors reported that the production of linear homopolymers from MMA, styrene, acrylonitrile, and acrylic acid using the same stabilizers was not successful, since low yields

and modest molecular weights, as well as nonuniform latex particles were observed with these monomers. In a subsequent study by the same group [52], successful production (yields up to 95%, molecular weights as high as 42,000.00 g/mol and microspheres of 4–5 μm in diameter) of polystyrene in R134a using poly(vinyl acetate) macromonomer stabilizers was reported.

More recently, López-Luna et al. [54] reported the successful enzyme-mediated syntheses of polyester structures in scCO₂ and R-134a. Lipase-mediated synthesis of relatively high molecular weight poly(δ-valerolactone) (PVL) was reported in scCO₂ and liquid R-134a solvent media. However, they found that polymers and copolymers

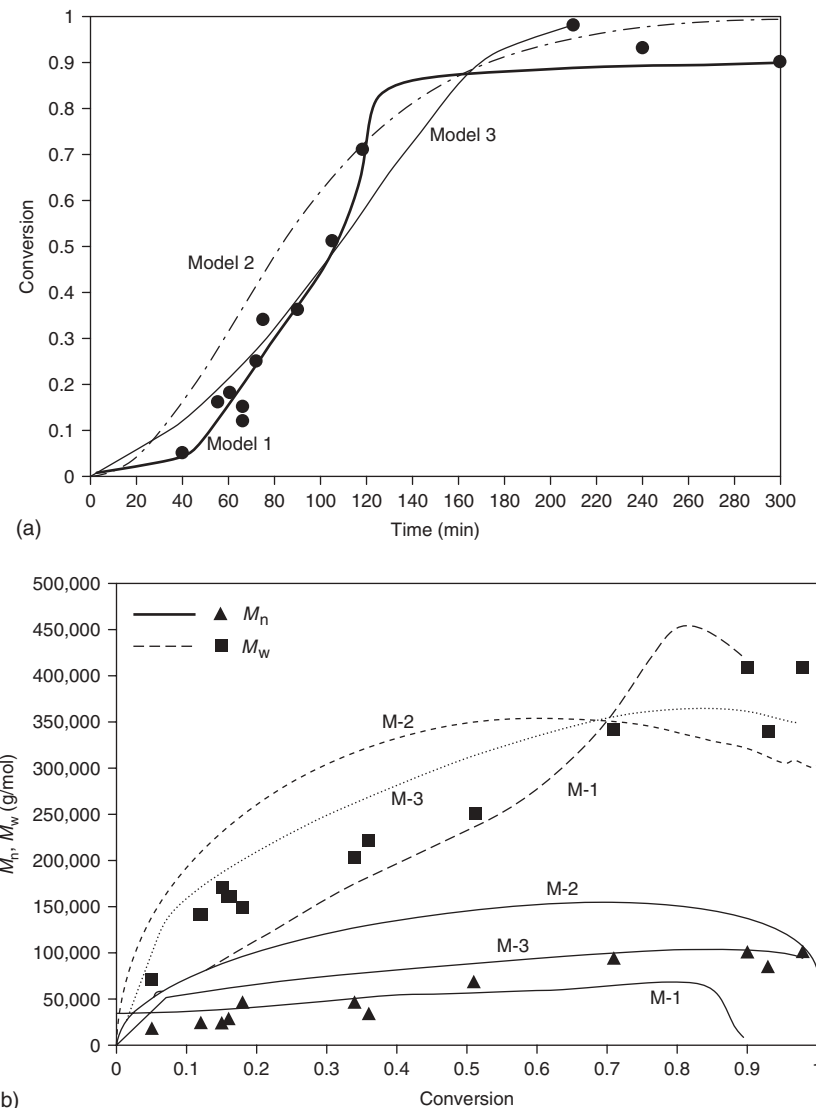


Figure 15.7 Polymerization of MMA in scCO_2 at 65°C and 206.8 bar: comparison of experimental data [39] of (a) monomer conversion versus time and (b) number- and weight-average molecular weights, M_n and M_w , versus conversion, against predicted profiles obtained with models 1–3. Source: Reprinted with permission from Quintero-Ortega IA, Jaramillo-Soto G, García-Morán PR, Castellanos-Cárdenas ML, Luna-Bárcenas G, Vivaldo-Lima E. Macromol React Eng 2008;2:304 [43]. Copyright 2008 Wiley-VCH Verlag GmbH & Co. KGaA.

from 2,2-bis(hydroxymethyl)butyric acid (BHB) and ϵ -caprolactone (CL), aimed at achieving hyperbranched polyesters, presented low solubility in compressed CO_2 and good solubility in liquid R134a. Lipase-mediated hyperbranched poly(VL-*co*-BHB), as well as poly(CL-*co*-BHB), were successfully synthesized in liquid R134a.

15.2.2 Polymerizations in Ionic Liquids

ILs, a new class of substances composed entirely of ions that are in liquid state at temperatures below 100°C , have

been proposed for different applications [55, 56]. In polymer chemistry, ILs have been investigated as reaction media, initiators, monomers, catalysts and exothermic moderators [2, 57, 58], as well as additives to polymers (flame retardants, plasticizers, electrolytes, as well as gelling and porogenic agents) [59–61] and self-assembly processes [60, 62]. This is mainly due to the fact that, unlike conventional substances, the properties of ILs (e.g., viscosity, solubility, miscibility, ionic conductivity, and melting point) can be readily tuned in a wide range by varying the composition of their respective ions [55]. Moreover, ILs are considered

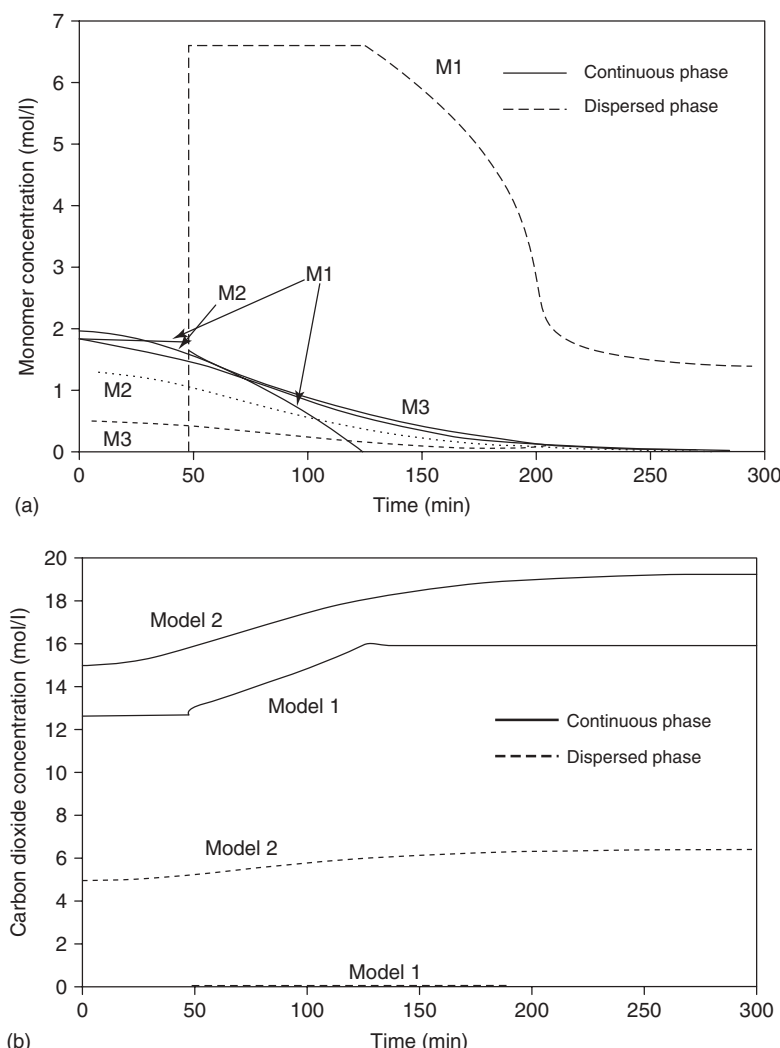


Figure 15.8 Polymerization of MMA in scCO₂ at 65 °C and 206.8 bar: (a) monomer and (b) solvent (CO₂) calculated concentration using models 1–3. *Source:* Reprinted with permission from Quintero-Ortega IA, Jaramillo-Soto G, García-Morán PR, Castellanos-Cárdenas ML, Luna-Bárcenas G, Vivaldo-Lima E. *Macromol React Eng* 2008;2:304 [43]. Copyright 2008 Wiley-VCH Verlag GmbH & Co. KGaA.

as stable and “environmentally friendly” compounds due to their negligible vapor pressure and flammability, and liquid state in a broad temperature range [55]. Recently the use of ILs as new solvent systems has also triggered unprecedented possibilities for the design of advanced materials [63–65] and polymer-based physical–chemical systems [66, 67].

As addressed in the literature [2, 57], the use of ILs as solvents in polymerization processes can be advantageous in certain cases. For instance, the rate of the propagation reaction in radical polymerizations can be enhanced in the presence of ILs, while the rate of termination decreases as compared to polymerizations performed in conventional solvents, resulting in polymers with higher molar masses.

Because of the fact that ILs are able to dissolve many organometallic and inorganic catalysts used in some polymerizations [e.g., in atom transfer radical polymerization (ATRP)], these reactions can be homogeneously performed in ILs without the inconvenience of a multiphase reaction; an additional advantage is the feasibility of recycling solutions of expensive catalysts. The high charge density of ILs can also have a significant influence on the stereochemistry of polymers synthesized in chiral ILs and on the reaction mechanisms of ionic polymerizations, which are not commonly observed in polymerizations reactions in conventional organic solvents. The remarkable thermal stability and nonvolatility of ILs can be very suitable to perform polycondensation reactions, where the removal of

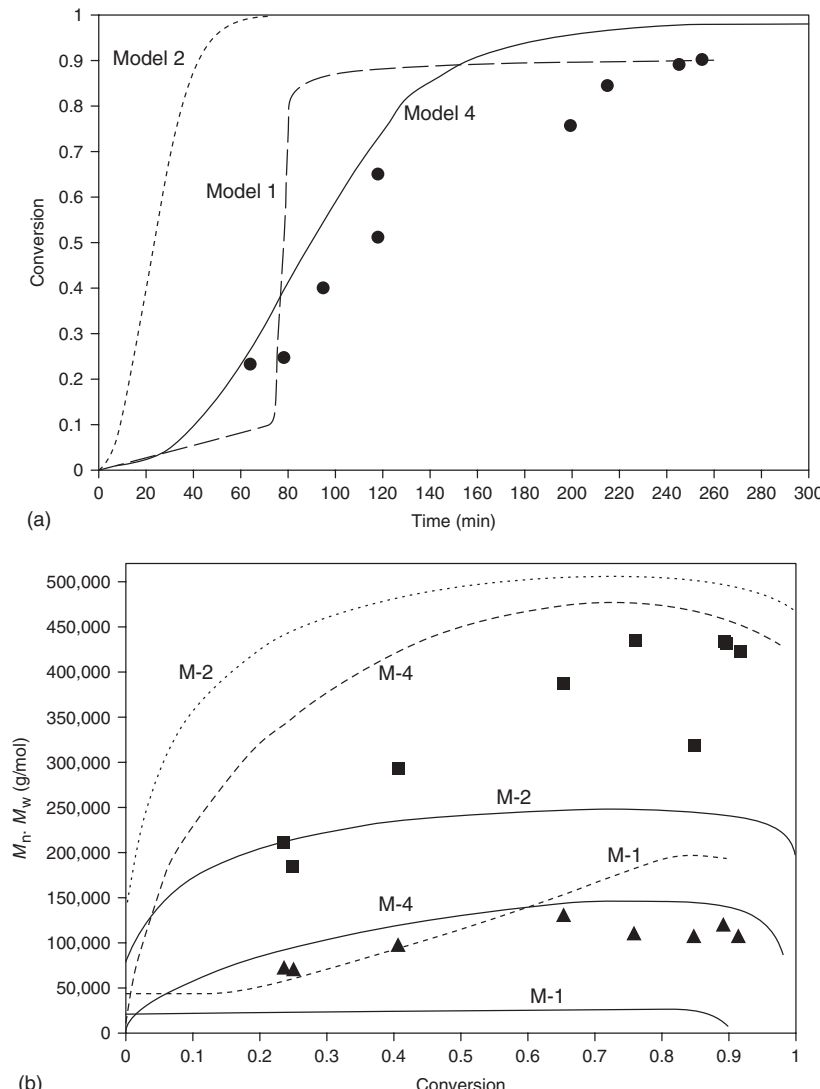


Figure 15.9 Polymerization of MMA in scCO_2 at 65°C and 140 bar (initial pressure): comparison of experimental data [48] of (a) monomer conversion versus time and (b) number- and weight-average molecular weights, M_n and M_w , versus conversion, against predicted profiles obtained with models 1, 2, and 4. *Source:* Reprinted with permission from Quintero-Ortega IA, Jaramillo-Soto G, García-Morán PR, Castellanos-Cárdenas ML, Luna-Bárcenas G, Vivaldo-Lima E. *Macromol React Eng* 2008;2:304 [43]. Copyright 2008 Wiley-VCH Verlag GmbH & Co. KGaA.

bystproducts at high temperatures is required for obtaining polymer with high molar masses. ILs have also been proposed as moderators in exothermic polymerization reactions and related processes to avoid thermal runaways [2]. Other reactions such as coordination, electrochemical, enzymatic polymerizations, depolymerizations at high temperatures, and dissolution and modification of cellulose can be favorably carried out in ILs [2, 57]. For instance, the use of milder reaction conditions, reuse of catalysts without loss of activity (or even polymerizations in the absence of catalyst), higher yields, high conductive polymer films, and longer enzymatic activities have been reported. It is also

worth noting that ILs are not always inert when used as reaction media, which can lead to undesired side reactions in some cases [2, 57]. This implies a meticulous selection of ILs for specific reactions.

Nevertheless, the replacement of VOCs by ILs does not necessarily imply that polymeric materials and their related processes will become automatically more efficient and “cleaner.” For instance, in far too many investigations in the literature where ILs are used as reaction media in polymer synthesis [2, 57], suitable approaches for the isolation and purification of the obtained polymers, and the recycling of the used ILs are not addressed since

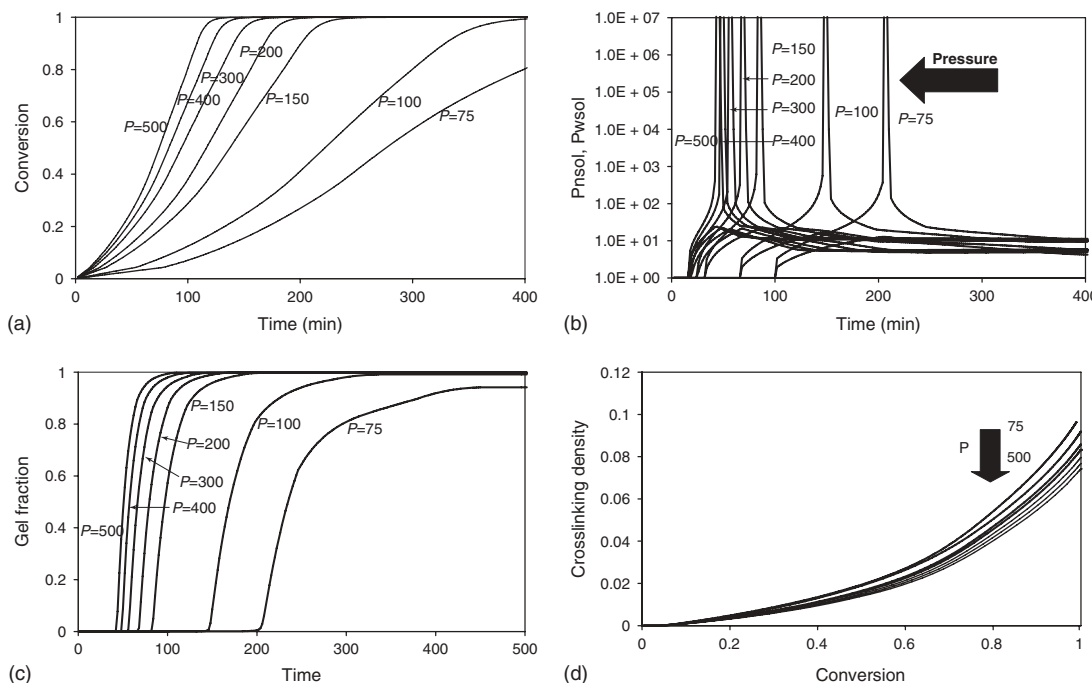


Figure 15.10 Effect of the operating pressure, P , on (a) polymerization rate, (b) number- and weight-average chain lengths, (c) gel fraction, and (d) crosslink density. *Source:* Reprinted with permission from Quintero-Ortega IA, Vivaldo-Lima E, Luna-Bárcenas G, Alvarado JFJ, Louvier-Hernández JF, Sanchez IC. Ind Eng Chem Res 2005;44:2823 [44]. Copyright 2005 American Chemical Society.

the use of conventional organic solvents to recover the product is commonly necessary. These approaches obviate the advantages of ILs as replacements of VOCs. From this point of view, the “green” properties of ILs are in many cases exaggerated, and it is not always clear what the advantages of replacing conventional chemical compounds with ILs are. Moreover, the improvement of synthetic methods and commercial availability of most ILs are still required since they are more expensive than conventional solvents. Hence, the use of ILs as reaction media for polymerization processes can be only justified in specific cases where the properties of ILs show significant positive effects, which would be difficult to obtain in conventional solvents. All these aspects together open up possibilities to envision a real application of ILs as solvents in large-scale industrial processes.

Moreover, the entire life cycle of ILs in any application must be integrally considered including energy use, demand of nonrenewable resources, transportation, health, safety, biodegradability, and (eco-)toxicity [2, 57]. In this regard, conventional solvents or chemical compounds such as CO_2 , water, and alcohols (e.g., methanol and ethanol) may be more suitable than ILs. For instance, the production of ILs requires a considerable amount of energy, and additional manufacturing and purification steps, which might hinder their aforementioned advantages. In addition, the (eco-)

toxicity of ILs is not fully known, and suitable strategies for their disposal still have to be determined, which further limits their application.

To overcome the current drawbacks of ILs in polymeric materials, it is mandatory to develop suitable and efficient recycling strategies. In addition, the use of ILs coupled with alternative and efficient energy sources may provide “cleaner” and more energetically integrated polymerization processes. For instance, this vision could, indeed, be achieved by combining ILs as reaction media with microwave energy as a heating source, both applied to different stages of polymer manufacturing. This approach is addressed in the following section.

15.3 ALTERNATIVE ENERGY SOURCES FOR POLYMERIZATION PROCESSES

15.3.1 Microwave-Activated Polymerization

Microwave energy is a form of electromagnetic radiation with wavelengths between 1 mm and 1 m (located between infrared radiation and radio frequencies). Microwave irradiation was first proposed as a heating method several decades ago, but it was during the last decade that it rapidly became a well-established technique for different chemical reactions

and processes, especially in organic synthesis [68–70]. Microwave irradiation is an alternative, efficient, selective, and fast volumetric heating method, which increases the energy of molecules by directly interacting with their dipole moments. In general, the principle of microwave heating is based on the ability of polar substances to absorb and transform microwave irradiation into heat. In this regard, the permanent dipoles of a molecule rapidly try to align to the direction of a constantly changing electric field, which provokes the rotation of the molecule and friction with other molecules, and subsequently, the energy of the entire system is lost in the form of heat [68–70]. Microwave irradiation can offer some advantages as compared to convective and conductive heating methods (e.g., higher heating rates, selective heating, homogeneous heating without temperature gradients, higher yields for a certain reaction time, and energy savings) [68–70].

Microwave energy has also been extensively used as an efficient heating method for different types of polymerization reactions (e.g., free- and controlled radical polymerizations, polycondensations, and ring-opening polymerizations) and polymer processing (e.g., curing processes, recycling of plastics, and polymer modification methods) [71–76]. Regarding the theoretical understanding of microwave irradiation on free radical polymerizations, the group of Vivaldo-Lima has proposed a “microwave promoted initiation step” (similar to thermal self-initiation) in the reaction scheme and successfully modeled microwave irradiated emulsion polymerizations [77], as well as controlled radical polymerizations (nitroxide-mediated radical polymerization (NMRP) [78] and reversible addition-fragmentation chain transfer (RAFT) [79]).

The use of ILs as reaction media for microwave assisted chemical modifications can result advantageous [80–82]. In general, most of conventional organic solvents are flammable and volatile, which can become a serious limitation for chemical reactions performed at high temperature due to the fact that the pressure in the reactors can increase considerably. In this regard, ILs possess extremely low vapor pressure, high thermal stability, high dielectric constant, and rather low heat capacity [56]. These properties enable ILs to interact very efficiently with microwave irradiation through an ionic conduction mechanism, which results in an extremely fast heating without any significant pressure increase in the reactions vessels (at least not due to the presence of ILs). In fact, it has been demonstrated that the use of small amounts of ILs can have a significant effect on the heating profiles of solvents and monomers under microwave irradiation [83]. Moreover, microwave irradiation has also been proposed for the synthesis of ILs themselves as an alternative to increase their purity and to reduce the organic waste related to these processes [84, 85]. Due to these advantages, ILs have been proposed as reaction media for different microwave-assisted polymerizations. For instance,

the microwave-assisted ring opening polymerizations of ϵ -caprolactone and trimethylene carbonate was significantly enhanced in the presence of suitable ILs [86, 87].

The microwave-assisted cationic ring opening polymerization of 2-ethyl-2-oxazoline performed in ILs can show higher polymerization rates (i.e., lower activation energies) and lower molecular weight dispersities (D) as compared to the polymerization performed in acetonitrile [88]. It was suggested that the presence of additional ionic moieties (ILs) can have a significant influence on the association constant between the living polymer chain ends and their respective counterions, which can have a positive or negative effect on the polymerization kinetics depending on the type of IL used [88]. Additional homogeneous microwave-assisted polymerizations of other oxazoline monomers and the free radical polymerization of MMA using water-soluble ILs as reaction media have also been investigated [83]. Other microwave-assisted free radical homo- and copolymerizations using ILs as reaction media have been investigated and directly compared with conventional heating and conventional organic solvents [89–91]. For these later cases, it was found that certain combinations of ILs with microwave irradiation can also have positive and negative effects on the polymerization rates as compared to the reaction systems performed under conventional heating or conventional organic solvents.

Microwave-assisted polycondensation reactions in ILs have also allowed the enhanced synthesis of polyamides and polyurethanes; the comparison between microwave synthesis conditions in ILs with conventional heating methods and conventional organic solvents has also been addressed [92, 93]. Pretreatment methods combining microwave irradiation and ILs for cellulose dissolution and modification have been also proposed [94, 95]. Microwave irradiation can enhance the solubility of cellulose in ILs and decrease the degree of polymerization of regenerated cellulose after IL dissolution, which can be beneficial for improving cellulose hydrolysis [95].

In spite of the numerous advantages that ILs and microwave irradiation can offer to perform polymerization reactions as described above, only few reports in the literature adequately address the problems of polymer isolation and IL recycling, avoiding entirely the use of VOCs, and the efficient use of microwave irradiation as an alternative energy source when combined with ILs [83]. For instance, a polymerization reaction where the monomer is soluble in a water soluble IL, but not its polymer, was described for the cationic ring opening polymerization of 3-ethyl-3-hydroxymethyloxetane, whereby the polymerization starts as a homogeneous system but the polymer then precipitates during the course of the reaction [96]. Afterward, the polymer can be isolated from the reaction mixture by filtration or decantation and the water-soluble IL recovered. Other

examples describe the heterogeneous free radical polymerizations in aqueous solutions of ILs or pure ILs (under conventional heating), where ILs can perform as reaction media and/or as surfactants to stabilize the heterogeneous reaction systems (monomers and polymers insoluble in IL) [97–99]. In these latter cases, it was shown that the polymer can be obtained as a precipitate, which is washed with water to remove the remains of IL and isolated by a simple filtration; thereafter, the IL is recovered from the resulting aqueous solution by distillation, or the IL aqueous solution itself can be used directly to carry out further polymerization reactions [97–99]. Following a similar approach, in the homogeneous (monomers and polymers soluble in IL) microwave-assisted cationic ring opening polymerization in ILs of hydrophilic polymers (2-ethyl-2-oxazoline) it was demonstrated that the use of hydrophobic ILs is convenient since it facilitates the isolation of the hydrophilic polymer by a simple extraction with water and the IL can also be easily recovered and used in further reaction cycles [88]. In this last example, in the homogeneous (monomers and polymers soluble in IL) microwave-assisted synthesis of hydrophobic polymers in water soluble ILs as a reaction media, it was shown that IL recycling was possible by adding water to the reaction mixture, subsequent filtration for the recovery of the polymer, and followed by a microwave-assisted distillation of the remaining solution to remove the water from the IL before usage in additional reaction cycles [83]. Microwave-assisted distillations in this type of integrated processes may give room to additional energy savings [83, 100]. Thus, it is believed that these and other similar synthetic hybrid techniques, combining ILs as reaction media with microwave irradiation to perform polymer synthesis could open up possibilities for the development of “greener” and more efficient polymerization processes allowing for depletion VOCs emissions as well as for energy savings.

15.3.2 Polymerization under Irradiation of Other Wavelengths

The last two decades brought along the renaissance of sonochemical research so that ultrasound has become a more common laboratory tool to enhance chemical synthesis. The use of ultrasound in chemical systems increases rates, improves yields and selectivities, prevents catalyst deactivation, and improves heat and mass transfer [101].

Radiation-induced polymerization (photopolymerization) is an efficient method for fast generation of highly crosslinked polymer networks from liquid resin systems.

Various types of radiation such as ultraviolet (UV) radiation, and electron beams can be used for initiation of polymerization reactions. Curing of polymer matrices by UV irradiation can be applied to a variety of processes in the production of composite components, as long

as the component can be directly irradiated. Wet lay-up techniques, vacuum infusion-type processes with UV-transparent membranes, filament winding, and prepreg processes have been adapted to UV curing. Unlike thermal curing, the curing time is in the order of minutes rather than hours, which means a significant reduction in cycle time. The radiation can be generated by a variety of sources suitable for various specific applications and different curing strategies. The most frequently used radiation sources are mercury arc lamps. Because of the absorption of radiation passing through matter, the thickness of laminates for efficient application of UV curing is limited. The curing mechanism is either radical polymerization for acrylate-based resins or cationic polymerization for epoxies and vinyl ethers. The properties of the UV-cured polymer matrix are determined by the crosslinking density. This depends on the type and concentration of the photoinitiator and of the (optional) diluents, the intensity and the duration of the irradiation, and the temperature at which the curing process takes place [102].

Radiation crosslinked engineering plastics are low-cost materials, which can be tailored to suit specific applications and can be readily adapted and processed for use in mass production. Until recently, radiation crosslinking was limited to only a few applications: the manufacture of rubber for tyres, cables, pipes (for underfloor heating systems), and heat-shrinkable tubes. Crosslinking was then performed with electron accelerators of low energies (0.1–3 MeV), allowing only surface treatments (limited to a few millimetres of depth). High energy electron accelerators (10 MeV) and γ -plants (strong capacity of penetration of the radiation) were developed since, allowing treatments of thicker parcels and pallets (1 m deep), enabling the radiation crosslinking of molded plastic parts, directly in their packaging [103].

15.4 POLYMERIZATION IN MICROREACTORS

Microreactor technology for chemical processing is currently an area of rapid growth with many application fields. The last two decades have seen the development of a large variety of different microstructured devices for chemical reactions. An overview of the research in microreactor technology can be found in numerous journal reviews and books [104–112]. Microreactors are devices containing fluidic pathways in the submillimeter range. Most designs have a single or multiple parallel channels with diameters between 10 and 1000 μm , where the chemical reaction takes place. The most common microreactor types are tubular, chip-based, or platelet-type designs, but there is a large number of different devices, many of which are tailored for specific applications. They can be fabricated from a variety of different materials, including glass, metal, polymers,

ceramics, and others and, depending on design, temperature and solvent stability of the material, they are used for gas phase, liquid phase, or heterogeneous processes. Microreactors have a very large surface area to volume ratio, which leads to high heat and mass transfer rates for any transfer process involving the channel walls. Liquid flow in microchannels is generally laminar, and mixing is often based on molecular diffusion processes, which for most applications is very efficient because of the small channel geometries. These characteristics lead to a series of process benefits in many reaction systems, such as increased conversion and selectivity or enhanced process control and safety. A key benefit of microreactor technology over classical batch processing is the ability to increase the reactor throughput by a simple “numbering-up” of the basic flow components, as opposed to a classical scale-up approach, which often requires several design steps, ranging from normal laboratory scale through a pilot-plant stage to the final production scale. A major problem of microfluidic channels are blockages caused by fouling or scaling. For this reason, most particle-containing or precipitate-forming reaction systems are not suitable for use in these devices. Most applications of microreactors lie within the wider field of organic chemistry [113–118], ranging from the laboratory synthesis of drug-like molecules or natural products in milligram quantities to the production scale processing of speciality chemicals or renewable fuels.

Microreactor technology has also been adopted for the use in polymer synthesis, for various reasons, such as the excellent heat transfer properties of the reactors and the resulting improvement of temperature control of the process. Compared to many other areas of organic chemistry, where reaction takes place in simple mono- or biphasic systems, the highly viscous nature of many solution phase polymerizations makes it more challenging to perform them in a microreactor system, as pressure drop is large in miniaturized flow channels. General reviews on polymerization in microstructured reactors were published by Hessel et al. [119] and Wilms et al. [120]; the article by Schork and Guo [121] gives an overview on miniemulsion polymerizations in continuous microreactor systems. One of the first investigations on solution phase polymerization in a specialized microreactor system was conducted by Iwasaki and Yoshida [122]. This work describes the free radical polymerization (FRP) of five different monomers in a steel reactor system containing capillaries with 500 μm inner diameter. The results were compared to macroscale batch processing and advantages of the microreactor system were identified in particular for exothermic reactions using acrylate monomers. Later work by the same group demonstrated the numbering-up of a continuous flow microreactor system to the pilot plant scale for the use in free radical polymerization of MMA [123]. Here, a stainless steel shell and tube microreactor was developed consisting

of 94 microtubes (500 μm i.d.) with a total volumetric hold-up of 9.6 ml. The shell was divided into two sections, accounting for the different temperatures in the two stages of the process. Hot oil was introduced in the first section of the shell to carry out the polymerization at 100 °C, and coolant in the second for fast termination. The authors concluded that precise temperature control by effective heat transfer, which is an inherent advantage of microreactor systems, was responsible for the effective control of the molecular weight distribution of the polymer. Serra et al. [124, 125] have conducted numerical simulations of FRP in multilamination microreactors, using a multiphysics model that simultaneously takes into account hydrodynamics, heat, and mass transfer (convection, diffusion, and chemical reaction).

Within the field of radical polymerization, special attention was recently drawn to the use of microreactors for controlled radical polymerization techniques, namely, ATRP, NMRP and RAFT. Shen and Zhu [126] have devised a column reactor packed with silica-gel-supported copper bromide-hexamethyltriethylenetetramine (HMTETA) for the continuous ATRP of homo- and block copolymers of MMA. Wu et al. [127] report the use of microfluidic chips made from thiolene polymer for continuous ATRP of 2-hydroxypropylmethacrylate. Control over the molecular properties of the product was achieved by varying either the flow rate or the relative concentrations of reactants. Enright et al. [128] conducted continuous nitroxide-mediated miniemulsion polymerizations in a steel tubular reactor to prepare a latex of polystyrene homopolymer dispersed in water. The authors report that by chain extension of the polystyrene latex it was possible to synthesize polystyrene-*block*-poly(butyl acrylate) diblock and polystyrene-*block*-poly(butyl acrylate)-*block*-polystyrene triblock copolymers. Rosenfeld et al. [129, 130] described the continuous NMRP of styrene and *n*-butyl acrylate at high temperature in a steel microtube reactor. The authors state that the main advantage of their microreactor system is its ability to handle highly exothermic chemical reactions because of its high surface to volume ratio and the possibility to carry out the polymerization process in homogeneous conditions, ultimately resulting in lower D values when compared to a conventional lab-scale batch reactor. This work was then extended to investigate the influence of mixing characteristics of an additional interdigital multilamination micromixer on monomer conversions, molecular weights, and D for the synthesis of block copolymers inside the reported microreactor platform. Russum et al. [131, 132] conducted RAFT polymerizations in a continuous miniemulsion using a tubular steel reactor. Comparative batch polymerizations were carried out, and it was found that in general the two reaction systems behaved similarly, from a kinetic point of view. Hornung et al. [133–135] investigated solution phase RAFT polymerizations in tubular stainless steel reactors.

The continuous flow process was automated further by including inline degassing of the monomer stock solution prior to reaction, and post-polymerization stages, such as RAFT end group removal.

Microreactors have also been used for ionic polymerization or polycondensation processes. Nagaki et al. [136] have synthesized polystyrene-poly(alkyl methacrylate) block copolymers by butyllithium initiated anionic polymerization in an integrated flow microreactor system. A high level of control of molecular weight was achieved at temperatures between -28 and $+24^\circ\text{C}$ due to fast mixing, fast heat transfer, and residence time control. Santos and Metzger [137] have studied a cationic ethane polymerization in a microfluidic device using a Ziegler–Natta catalyst system. The polymerization intermediates were studied directly from the solution using an inline mass spectrometer and their catalytic activity was proved. Honda et al. [138] have developed a microfluidic system for the synthesis of poly(amino acid) using an anionic ring-opening polycondensation. The authors found that the microreactor produced polymers with narrower molecular weight distribution in comparison to polymers obtained from a batch process. Kessel et al. [139] performed the polycondensation of trialkoxysilanes to poly(silsesquioxane)s in a microreactor setup. Wilms et al. [140] have used a slit-interdigital micromixer system for the synthesis of hyperbranched polymers, employing the ring-opening multibranching polymerization of glycidol. The characteristics of the microstructured reactor were used to engineer a continuous flow process for the preparation of well-defined hyperbranched polyglycerols with molecular weights up to 1000 g/mol.

Besides the synthesis of bulk polymers, microreactor technology is also used for more specialized polymerization applications such as the formation of polymer membranes or particles [119, 141–146]. Bouqey et al. [142] synthesized monodisperse and size-controlled polymer particles from emulsions polymerization under UV irradiation in a microfluidic system. By incorporating a functional comonomer, polymer microparticles bearing reactive groups on their surface were obtained, which could be linked together to form polymer beads necklaces. The ability to confine and position the boundary between immiscible liquids inside microchannels was utilized by Beebe and coworkers [145] and Kitamori and coworkers [146] for the fabrication of semipermeable polyamide membranes in a microfluidic chip via interfacial polycondensation.

The use of microreactor technology for polymer chemistry presents an interesting alternative to conventional processing methods, in both batch and macroscale continuous flow. Microreactors offer a better process control of many exothermic polymerization processes, leading to increased product quality such as narrower polydispersity, and they allow for the synthesis of novel polymeric materials for a range of new applications.

ACKNOWLEDGMENTS

E.V.-L. acknowledges financial support from Consejo Nacional de Ciencia y Tecnología (CONACYT, México) (Project CONACYT 101682), DGAPA-UNAM (Project PAPIIT 119510), and Instituto de Ciencia y Tecnología del Distrito Federal (ICyTDF, México) (Project PICSA11-56). G. L.-B. acknowledges the help from Sebastian Stolz in the preparation of some of the figures and analyses of Section 15.2.1.1.

REFERENCES

1. US Environmental Protection Agency. Green Chemistry. Available at <http://www.epa.gov/greenchemistry/>. Accessed 2012 April 4.
2. Erdmenger T, Guerrero-Sanchez C, Vitz J, Hoogenboom R, Schubert US. *Chem Soc Rev* 2010;39:3317.
3. Kemmere MF. Chapter 1: Supercritical carbon dioxide for sustainable polymer processes. In: Kemmere MF, Meyer T, editors. *Supercritical Carbon Dioxide in Polymer Reaction Engineering*. Weinheim: Wiley-VCH; 2005. p 1 ff.
4. Seiler M, Rolker J, Arlt W. *Macromolecules* 2003;36:2085.
5. Kiamos AA, Donohue MD. *Macromolecules* 1994;27(2): 357.
6. McHugh MA, Krukonis VJ. *Supercritical Fluids Extraction: Principles and Practice*. 2nd ed. Stoneham (MA): Butterworth-Heinemann; 1994.
7. ter Horst MH, Behme S, Sadowski G, de Loos TW. *J Supercrit Fluids* 2002;14:181.
8. Kirby CF, McHugh MA. *Chem Rev* 1999;99:565.
9. Seiler M. *Chem Eng Tech* 2002;2:237.
10. Strange EH, Bliss HGW, inventors. British patent 3,045. 1913.
11. Sivergin YM. Chapter 6: Polymerization under pressure. In: Kovarskii AL, editor. *High-Pressure Chemistry and Physics of Polymers*. Boca Raton: CRC Press, Inc; 1994. p 195 ff.
12. Whiteley KS, Heggs TG, Koch H, Mawer RL, Immel W. Polyolefins. In: Elvers B, Hawkins S, Schulz G, editors. *Plastics, Properties and Testing of Polyvinyl Compounds*. 5th ed. Vol. A21. New York: VCH Publishers; 1992. p 487 ff.
13. McHugh MA, Guckes TL. *Macromolecules* 1985;18:674.
14. Taylor DK, Carbonell R, DeSimone JM. *Annu Rev Environ Resour* 2000;25:115.
15. Hsiao YL, Maury EE, DeSimone JM, Mawson M, Johnston KP. *Macromolecules* 1995;28:8159.
16. Mawson SM, Johnston KP, Combes JR, DeSimone JM. *Macromolecules* 1995;28:3182.
17. Luna-Barcenas G, Mawson S, Takishima S, DeSimone JM, Sanchez IC, Johnston KP. *Fluid Phase Equilib* 1998;146: 325.
18. Kamiya Y, Mizoguchi K, Terada K, Fujiwara Y, Wang JS. *Macromolecules* 1998;31:472.
19. Li D, Han B. *Macromolecules* 2000;33:4506.

332 NEW POLYMERIZATION PROCESSES

20. Lee CT, Ryoo W, Smith PG, Arellano J, Mitchell DR, Lagow RJ, Webber SE, Johnston KP. *J Am Chem Soc* 2003; 125:3181.
21. Bungert B, Sadowski G, Arlt W. *Ind Eng Chem Res* 1998;37:3208.
22. Canelas DA, DeSimone JM. *Adv Polym Sci* 1997;133:103.
23. Kendall JL, Canelas DA, Young JL, DeSimone JM. *Chem Rev* 1999;99:543.
24. Charpentier PA, Kennedy KA, DeSimone JM, Roberts GW. *Macromolecules* 1999;32:5973.
25. Wang R, Cheung HM. *J Appl Polym Sci* 2004;93:545.
26. Beuermann S, Buback M, Isemer C, Lasik I, Wahl A. *Macromolecules* 2002;35:3866.
27. Shiho H, DeSimone JM. *J Polym Sci A Polym Chem* 2000; 38:1146.
28. Shiho H, DeSimone JM. *J Polym Sci A Polym Chem* 1999; 37:2429.
29. Canelas DA, DeSimone JM. *Macromolecules* 1997;30:5673.
30. Canelas DA, Betts DE, DeSimone JM. *Macromolecules* 1996;29:2818.
31. Hwang HS, Gal Y-S, Johnston KP, Lim KT. *Macromol Rapid Commun* 2006;27:121.
32. Woods HM, Nouvel C, Licence P, Irvine DJ, Howdle SM. *Macromolecules* 2005;38:3271.
33. Deniz S, Baran N, Akgün M, Uzun IN, Dincer S. *Polym Int* 2005;54:1660.
34. Rosell A, Storti G, Morbidelli M. *Macromolecules* 2004;37: 2996.
35. Wang W, Griffiths RMT, Giles MR, Williams P, Howdle SM. *Eur Polym J* 2003;39:423.
36. Fehrenbacher U, Ballauff M. *Macromolecules* 2002;35:3653.
37. Christian P, Howdle SM. *Macromolecules* 2000;33:237.
38. Beuermann S, Buback M, Schmaltz C, Kuchka F-D. *Macromol Chem Phys* 1998;199:1209.
39. O'Neill ML, Yates MZ, Johnston KP, Smith CD, Wilkinson SP. *Macromolecules* 1998;31:2838.
40. van Herk AM, Canelas DA, Quadir MA, DeSimone JM, Manders BG. *Macromolecules* 1997;30:4780.
41. Shaffer KA, Jones TA, Canelas DA, DeSimone JM. *Macromolecules* 1996;29:2704.
42. Quintero-Ortega IA, Vivaldo-Lima E, Gupta RB, Luna-Bárcenas G, Penlidis A. *J Macromol Sci Pure Appl Chem* 2007;44:205.
43. Quintero-Ortega IA, Jaramillo-Soto G, García-Morán PR, Castellanos-Cárdenas ML, Luna-Bárcenas G, Vivaldo-Lima E. *Macromol React Eng* 2008;2:304.
44. Quintero-Ortega IA, Vivaldo-Lima E, Luna-Bárcenas G, Alvarado JFJ, Louvier-Hernández JF, Sanchez IC. *Ind Eng Chem Res* 2005;44:2823.
45. DeSimone JM, Guan Z, Elsbernd CS. *Science* 1992;257:945.
46. Baradie B, Shoichet MS. *Macromolecules* 2002;35:3569.
47. Chatzidoukas C, Pladis P, Kiparissides C. *Ind Eng Chem Res* 2003;42:743.
48. Mueller PA, Storti G, Morbidelli M. *Chem Eng Sci* 2005;60: 377.
49. Wulkow M. *Macromol Theor Simul* 1996;5:393.
50. Modell M, inventors. US patent 4338199. 1982.
51. Thomason TB, Modell M. *Hazard Waste* 1984;1:453.
52. Wood CD, Cooper AI. *Macromolecules* 2003;36:7534.
53. Wood CD, Senoo K, Martin C, Cuellar J, Cooper AI. *Macromolecules* 2002;35:6743.
54. López-Luna A, Gallegos JL, Gimeno M, Vivaldo-Lima E, Bárcana E. *J Mol Catal B Enzym* 2010;67:143.
55. Deetlefs M, Seddon KR. *Chim Oggi* 2006;24,16.
56. Plechkova NV, Seddon KR. *Chem Soc Rev* 2008;37:123.
57. Kubisa P. *Prog Polym Sci* 2009;34:1333.
58. Winterton N. *J Mater Chem* 2006;44:4281.
59. Brazel CS, Rogers RD, editors. *Ionic Liquids in Polymer Systems-Solvents, Additives and Novel Applications. ACS Symposium Series*. Vol. 913. Washington: American Chemical Society; 2005.
60. Ueki T, Watanabe M. *Macromolecules* 2008;41:3739.
61. Lui J, Yan F, Texter J. *Prog Polym Sci* 2009;34:431.
62. Greaves TL, Drummond CJ. *Chem Soc Rev* 2008;37:1709.
63. Guerrero-Sánchez C, Lara-Ceniceros T, Jimenez-Regalado E, Rasa M, Schubert US. *Adv Mater* 2007;19:1740.
64. Casamada Ribot J, Guerrero-Sánchez C, Hoogenboom R, Schubert US. *J Mater Chem* 2010;20:8279.
65. Casamada Ribot J, Guerrero-Sánchez C, Hoogenboom R, Schubert US. *Chem Commun* 2010;46:6971.
66. Guerrero-Sánchez C, Gohy JF, D'Haese C, Thijss HML, Hoogenboom R, Schubert US. *Chem Commun* 2008;44: 2753.
67. Guerrero-Sánchez C. *Ionic Systems in Materials Science: New Materials and Processes Based on Ionic Liquids and/or Ionic Polymerizations*. Saarbrücken: VDM Verlag Publisher; 2008.
68. Tierney JP, Lidstrom P, editors. *Microwave Assisted Organic Synthesis*. Oxford: Blackwell Publishing; 2005.
69. Kappe CO. *Angew Chem Int Ed* 2004;43:6250.
70. Kappe CO, Dallinger D, Murphree S. *Practical Microwave Synthesis for Organic Chemists*. Weinheim: Wiley-VCH; 2008.
71. Bogdal D, Penczek P, Pieliowski J, Prociak A. *Adv Polym Sci* 2003;163:193.
72. Wiesbrock F, Hoogenboom R, Schubert US. *Macromol Rapid Commun* 2004;25:1739.
73. Hoogenboom R, Schubert US. *Macromol Rapid Commun* 2007;28:368.
74. Zhang C, Liao L, Gong S. *Green Chem* 2007;9:303.
75. Bogdal D, Prociak A. *Microwave Enhanced Polymer Chemistry and Technology*. Oxford: Blackwell Publishing; 2007.
76. Mallakpour S, Rafiee Z. *Iran Polym J* 2008;17:907.
77. Aldana-García MA, Palacios J, Vivaldo-Lima E. *J Macromol Sci Pure Appl Chem* 2005;42:1207.

78. Hernández-Meza JJ, Jaramillo-Soto G, García-Morán PR, Palacios-Alquisira J, Vivaldo-Lima E. *Macromol React Eng* 2009;3:101.
79. Hernández-Ortiz JC, Jaramillo-Soto G, Palacios-Alquisira J, Vivaldo-Lima E. *Macromol React Eng* 2010;4:210.
80. Hoffmann J, Nuechter M, Ondruschka B, Wasserscheid P. *Green Chem* 2003;5:296.
81. Martinez-Palou R. *J Mex Chem Soc* 2007;51:252.
82. Martinez-Palou R. *Mol Divers* 2009;14:3.
83. Guerrero-Sánchez C, Lobert M, Hoogenboom R, Schubert US. *Macromol Rapid Commun* 2007;28:456.
84. Varma RS, Namboodiri VV. *Chem Commun* 2001:643–644.
85. Deetlefs M, Seddon KR. *Green Chem* 2003;5:181.
86. Liao L, Liu L, Zhang C, Gong S. *Macromol Rapid Commun* 2006;27:2060.
87. Liao LQ, Zhang C, Gong S. *J Polym Sci A Polym Chem* 2007;45:5857.
88. Guerrero-Sánchez C, Hoogenboom R, Schubert US. *Chem Commun* 2006;25:3797.
89. Schmidt-Naake G, Woecht I, Schmalfuss A, Gluck T. *Macromol Symp* 2009;275–276:204–218.
90. Woecht I, Schmidt-Naake G. *Macromol Symp* 2009;275–276:219–229.
91. Gluck T, Woecht I, Schmalfuss A, Schmidt-Naake G. *Macromol Symp* 2009;275–276:230–241.
92. Mallakpour S, Kowsari E. *Iran Polym J* 2006;15:239.
93. Mallakpour S, Rafiee Z. *Polymer* 2007;48:5530.
94. Zhang Z, Zhao ZK. *Bioresour Technol* 2010;101:1111.
95. Ha SH, Mai NL, An G, Koo YM. *Bioresour Technol* 2011;102:1214.
96. Biedron T, Bednarek M, Kubisa P. *Macromol Rapid Commun* 2004;25:878.
97. Guerrero-Sánchez C, Erdmenger T, Sereda P, Wouters D, Schubert US. *Chem Eur J* 2006;12:9036.
98. Yan F, Texter J. *Chem Commun* 2006;25:2696.
99. Guerrero-Sánchez C, Wiesbrock F, Schubert US. *ACS Symp Ser* 2005;913:37.
100. Gamallo-Lorenzo D, Barciela-Alonso MC, Moreda-Pineiro A, Bermejo-Barrera A, Bermejo-Barrera P. *Anal Chim Acta* 2005;542:287.
101. Toukonen B, Mikkola J-P, Murzin DY, Salmi T. *Appl Catal Gen* 2005;279:1.
102. Endruweit A, Johnson MS, Long AC. *Polym Compos* 2006;27:119.
103. Rouif S. *Nucl Instrum Methods Phys Res B* 2005;236:68.
104. Hessel V, Renken A, Schouten JC, Yoshida J, editors. *Micro Process Engineering: A Comprehensive Handbook*, 3 Volume Set. Weinheim: Wiley-VCH; 2009.
105. Wirth T, editor. *Microreactors in Organic Synthesis and Catalysis*. Weinheim: Wiley-VCH; 2008.
106. Kockmann N, editor. *Micro Process Engineering: Fundamentals, Devices, Fabrication, and Applications*. Weinheim: Wiley-VCH; 2006.
107. Hessel V, Hardt S, Löwe H, Müller A, Kolb G, editors. *Chemical Micro Process Engineering*, 2 Volume Set. Weinheim: Wiley-VCH; 2005.
108. Ehrfeld W, Hessel V, Löwe H. *Microreactors: New Technology for Modern Chemistry*. Weinheim: Wiley-VCH; 2000.
109. Kiwi-Minsker L, Renken A. *Catal Today* 2005;79:2.
110. Kolb G, Hessel V. *Chem Eng J* 2004;98:1.
111. Jähnisch K, Hessel V, Löwe H, Baerns M. *Angew Chem Int Ed* 2004;43:406.
112. Löwe H, Ehrfeld W. *Electrochim Acta* 1999;44:3679.
113. Seeberger PH, Blume T, editors. *New Avenues to Efficient Chemical Synthesis, Emerging Technologies*. Berlin: Springer; 2007.
114. Ley SV, Baxendale IR. *Chimia* 2008;62:162.
115. Kirschning A, Solodenko W, Mennecke K. *Chem Eur J* 2006;12:5972.
116. Zhang XL, Wiles C, Painter SL, Watts P, Haswell SJ. *Chim Oggi* 2006;24:43.
117. Ley SV, Baxendale IR. *Nat Rev Drug Discov* 2002;1:573.
118. Fletcher PDI, Haswell SJ, Pombo-Villar E, Warrington BH, Watts P, Wong SYF, Zhang XL. *Tetrahedron* 2002;58:4735.
119. Hessel V, Hardt S, Löwe H, Serra C, Hadzioannou G. *Chem Ingen Technik* 2005;77:1693.
120. Wilms D, Klos J, Frey H. *Macromol Chem Phys* 2008;209:343.
121. Schork FJ, Guo J. *Macromol React Eng* 2008;2:287.
122. Iwasaki T, Yoshida J. *Macromolecules* 2005;38:1159.
123. Iwasaki T, Kawano N, Yoshida J. *Org Process Res Dev* 2006;10:1126.
124. Serra C, Sary N, Schlatter G, Hadzioannou G, Hessel V. *Lab Chip* 2005;5:966.
125. Serra C, Schlatter G, Sary N, Schönfeld F, Hadzioannou G. *Microfluid Nanofluidics* 2007;3:451.
126. Shen Y, Zhu S. *AIChE J* 2002;48:2609.
127. Wu T, Mei Y, Cabral JT, Xu C, Beers KL. *J Am Chem Soc* 2004;126:9880.
128. Enright TE, Cunningham MF, Keoshkerian B. *Macromol React Eng* 2010;4:186.
129. Rosenfeld C, Serra C, Brochon C, Hadzioannou G. *Chem Eng Sci* 2007;62:5245.
130. Rosenfeld C, Serra C, Brochon C, Hadzioannou G. *Lab Chip* 2008;8:1682.
131. Russum JP, Jones CW, Schork FJ. *Macromol Rapid Commun* 2004;5:1064.
132. Russum JP, Jones CW, Schork FJ. *Ind Eng Chem Res* 2005;44:2484.
133. Hornung CH, Guerrero-Sánchez C, Brasholz M, Saubern S, Chiefari J, Moad G, Rizzardo E, Thang SH. *Org Process Res Dev* 2011;15:593.
134. Hornung CH, Nguyen X, Dumsday G, Saubern S. *Macromol React Eng* 2012; published online. DOI: 10.1002/mren.201200029.
135. Hornung CH, Postma A, Saubern S, Chiefari J. *Macromol React Eng* 2012;6:246.

334 NEW POLYMERIZATION PROCESSES

136. Nagaki A, Miyazaki A, Yoshida J. *Macromolecules* 2010;43:8424.
137. Santos LS, Metzger JO. *Angew Chem Int Ed* 2006;45:977.
138. Honda T, Miyazaki M, Nakamura H, Maeda H. *Lab Chip* 2005;5:812.
139. Kessler D, Löwe H, Theato P. *Macromol Chem Phys* 2009;210:807.
140. Wilms D, Klos J, Frey H. *Chem Eng Technol* 2007;30: 1519.
141. Serra CA, Chang Z. *Chem Eng Technol* 2008;31:1099.
142. Bouquey M, Serra C, Berton N, Prat L, Hadzioannou G. *Chem Eng J* 2008;135(Suppl. 1):S93.
143. Karnik R, Gu F, Basto P, Cannizzaro C, Dean L, Kyei-Manu W, Langer R, Farokhzad OC. *Nano Lett* 2008;8:2906.
144. Huang S, Khoo H, Chang Chien S, Tseng F. *Microfluid Nanofluidics* 2008;5:459.
145. Zhao B, Viernes NOL, Moore JS, Beebe DJ. *J Am Chem Soc* 2002;124:5284.
146. Hisamoto H, Shimizu Y, Uchiyama K, Tokeshi M, Kikutani Y, Hibara A, Kitamori T. *Anal Chem* 2003;75:350.

PART IV

POLYMER CHARACTERIZATION

16

POLYMER SPECTROSCOPY AND COMPOSITIONAL ANALYSIS

GLADYS DE LOS SANTOS-VILLARREAL AND LUIS E. ELIZALDE

16.1 INTRODUCTION

The molecular structure plays an important role in determining the characteristics, properties, and behavior of any polymer during its end use. The elucidation of a polymer structure can be conducted in several ways. Since many years ago, several characterization techniques have been used to analyze basically aspects such as the composition, configuration, and conformation of the chemical groups within the polymer.

By analyzing the composition of a polymer molecule, the nature of the atoms in the polymer chain and the type of bonding can be inferred. Then, the configuration gives an idea about the chemical state of the polymer, the spatial order of the chemical groups, and the optical characteristics and possible behavior of the whole molecule. The conformation characterizes the geometrical state of a polymer.

Polymer chains are made up of sequences of chemical repeating units that may be arranged regularly or irregularly along the backbone conforming the microstructure and morphology of the polymer molecule. Chain alignments, orientation, and entanglements in the molecule play an important role in providing valuable information during qualitative and quantitative analyses.

Ideally, a polymer chain can be represented as in Figure 16.1.

From the composition, the polymer structure can also be inferred if detected differences between two structural elements in the polymer are used. For example, signals for an initiator fraction can be compared with the monomer structure or the functionalizing end group; that is, it

is possible to measure the individual number of any component in the polymer chain [1].

Characterization of polymers can be conducted in several ways, from the oldest and simplest techniques to the most sophisticated and complete spectroscopic characterization techniques.

The older methods of noninstrumental chemistry, which still possess high informational value, are those dealing with the chemical analysis of polymers based on searching the number and kind of elements that can occur in a given sample of an unknown polymer.

This chapter is a brief summary of spectroscopic characterization techniques that can be used to identify the polymer structure.

16.2 ELEMENTAL ANALYSIS

16.2.1 General Principles

Combustion techniques, such as pyrolysis, are one of the most common analytical methods of identification of the constituents of any sample; the structure of the monomers or any other added molecules used during the polymer synthesis can then be subsequently confirmed by spectroscopic techniques.

Analytical methods usually involve, for example, burning of a sample in an oxygen-containing atmosphere, in order to determine amounts of carbon, hydrogen, nitrogen, sulfur, halogens, and oxygen (the last one by difference). Also, dry-ashing, fusion, bomb, and acid digestion can be used to remove organic material and trace metal

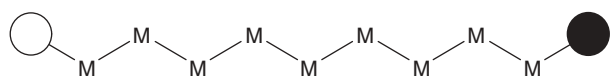


Figure 16.1 Representation of a linear polymer chain. M represents the repeating unit or the monomer that will be repeated n number of times. Clear and black circles can both be either the initiator fragment remaining on each side of the molecule or an end group deliberately added to functionalize the polymer.

TABLE 16.1 Elemental Composition of Some Common Polymers

Polymer	C	H	O	N
Polyethylene	85.63	14.37	—	—
Polypropylene	85.63	14.37	—	—
Polyisoprene	86.88	13.12	—	—
Polybutadiene	88.82	11.18	—	—
Poly(vinylmethylketone)	68.55	8.63	22.83	—
Poly(ethyleneterephthalate)	64.90	6.30	28.00	—
Poly(methyl methacrylate)	59.98	8.05	31.96	—
Poly(vinyl acetate)	55.81	7.02	37.17	—
Nylon 6, 10	68.04	10.71	11.33	9.92
Nylon 6, 6	63.69	9.80	14.14	12.38
Polyacrylamide	50.69	7.09	22.51	19.71

residues, which can be further analyzed by spectroscopic techniques.

Elemental composition of some common polymers used to manufacture several products is presented in Table 16.1.

Elemental composition and content of some specific elements is an important analytical tool for polymer characterization, mainly for the characterization of copolymers and polymer blends and the determination of molecular weight of homopolymers [2, 3].

The knowledge of the elemental composition of a polymer can be a useful indicator of the identity of the polymer.

16.2.1.1 Determination of Copolymer Composition

Elemental analysis (EA) is a convenient method for determination of copolymer and blend composition if one homopolymer contains an element not present in the second one. For example, EA can be properly used to quantify nitrogen in copolymers containing acrylonitrile units and oxygen in polymeric surfactants such as poly(oxyalkylene). Therefore, for a binary system, every element can be balanced according to the following equation:

$$f_1 + f_2 = 1 \quad (16.1)$$

$$W_{X1}f_1 + W_{X2}f_2 = W_{Xm} \quad (16.2)$$

where f_1 and f_2 are the weight fractions of components 1 and 2, respectively; W_X is the weight fraction of a given

element in the copolymer or polymer blend; and 1, 2, and m denote component 1, component 2, and their mixture, respectively. For every element X,

$$f_2 = \frac{W_{Xm} - W_{X1}}{W_{X2} - W_{X1}} \quad (16.3)$$

If only one of the homopolymers in the copolymer or polymer blend contains the element X, then

$$f_2 = \frac{W_{Xm}}{W_{X2}} \quad (16.4)$$

The values of W_{Xm} are obtained by EA, while those of W_{X1} and W_{X2} are calculated according to the chemical formula of the respective component in the mixture or copolymer.

In this way, EA can be applied to determine monomer composition in copolymers and polymer blends and any other composite material. Although results from EA are comparable to those obtained from spectroscopic techniques such as IR and NMR (nuclear magnetic resonance) spectroscopies, developments in EA are needed to improve the accuracy and precision of the method.

16.2.1.2 Determination of Molecular Weight Commonly used techniques to determine molecular weight of polymers are osmometry, viscosimetry, light scattering, gel permeation chromatography, NMR, etc. (Chapter 17). In all of them, the sample must be soluble in organic solvents or water. However, several kinds of polymers, such as the new and intelligent materials, especially highly thermostable or conductive polymers such as poly(phenylene sulfides), poly(*p*-xylylidene), or polypyrrole, are barely soluble or even insoluble in typical solvents. In such cases, EA is a promising and useful method.

The molecular weight of polymers could be obtained from the analysis of some elements present in the polymer chain; for example, heavy metal salts from the analysis of the metal content.

For polymers with high molecular weight, the results obtained from EA should be consistent with the formula of the repeating unit; however, also for oligomers, molecular weight must be calculated from the formula:

$$M = K1 - (AaBb \dots Yy \dots) - nK2 \quad (16.5)$$

where M represents the molecular weight and $K1$ and $K2$ denote atoms or groups of atoms at the ends of the macromolecules; therefore, the equation for calculation of degree of polymerization is derived from the simple percentage formula of a given element Y, that is, from the ratio of the weight of element Y contained in a polymer to the total molecular weight, M , of a polymer.

The calculation of M depends on structural factors of a given polymer, and the result depends on the correct

estimation of the type of end groups as well as on the choice of the analyzed element Y. Then, the content of the element Y is taken directly from the EA value; hence, the result depends on the precision in the analysis of Y.

16.3 INFRARED SPECTROSCOPY

16.3.1 General Principles

Infrared spectroscopy is a technique based on the vibrations of atoms of a molecule. In order to get a spectrum, the sample is placed in a sample holder and then an infrared ray is passed through the sample. The signals or peaks that can be appreciated in an IR spectrum correspond to the energy absorbed by the sample at specific frequencies that depend on the molecule's structure. To detect a signal, molecules must change their electric dipole during irradiation, which implies the generation of specific movements between atoms and chemical bonds [4].

Interactions between IR radiation and molecules involve changes in molecular dipoles associated with vibrations and rotations. The atoms in molecules can move and bond lengths can vary; also, one atom can move out of its present plane in stretching and bending movements. Vibrations can involve a change in either bond length (stretching) or bond angle (bending). Depending on the type of movement, there are also symmetric and asymmetric stretchings; each of them is represented as an individual absorption signal in Figure 16.2.

Even for simple molecules, there will be many vibrational signals. A simple molecule can generate a complex spectrum. In a polymer, the repeating unit represents the simple molecule that will be generating a pool of signals or bands. Bands of vibrations associated with the presence of characteristic functional groups are called *skeletal vibrations*, and these skeletal vibrations are likely to constitute a pattern or fingerprint of the molecule as a whole.

16.3.2 Instrumentation

During the 1940s, the first IR spectrometers were commercially available and they relied on prisms to achieve the dispersion of IR irradiation. After 1950, the most significant advances in IR spectroscopy were related to the appearance of Fourier transform (FT) spectrometers. This type of equipment processes the obtained results with an interferometer using the well-established mathematical equation of the FT. Once FT-IR spectroscopy was developed, it was possible to get high quality spectra with minimal data acquisition time. To get spectra, an interferogram is generated. This is a collection of the signals produced by the change of path length between two beams by the use of a moving mirror in the apparatus.

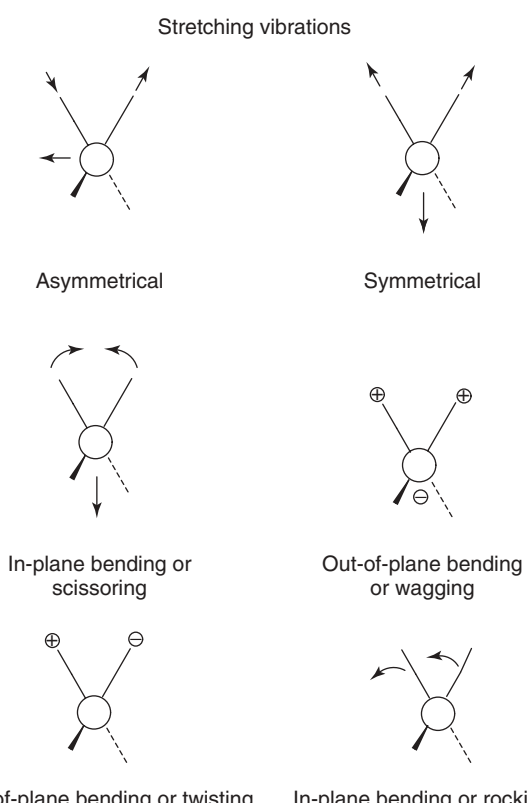


Figure 16.2 Symmetrical and asymmetrical stretching and bending movements in chemical bonds.

In practice, the radiation emerging from a source is passed through an interferometer and then through the sample before reaching the detector. On amplification of the signal, in which high frequency contributions have been eliminated by a filter, the data are converted and processed by FT. The most common interferometer used in FT-IR is the Michelson interferometer, which consists of two perpendicularly plane mirrors, one of which can travel in a direction perpendicular to the plane. A semireflecting film, the beam splitter, bisects the planes of these two mirrors. The beam splitter material has to be chosen according to the infrared region to be examined.

16.3.3 Qualitative Analysis of Polymers

Most organic molecules (including polymers) show absorption bands from the interaction between the IR radiation and the atoms in a chemical bond in the mid-IR region. Most IR studies are related to the analysis of vibrations in the mid-IR region, but near- and far-IR regions also provide important information about certain materials.

Figure 16.3 represents the whole infrared region and its divisions into near-, mid-, and far-infrared spectroscopy.

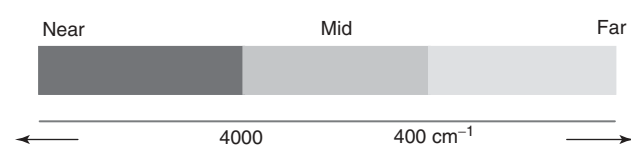


Figure 16.3 Regions for the study of IR: near, middle, and far. (See insert for the color representation of the figure.)

The mid-IR spectrum ($4000\text{--}400\text{ cm}^{-1}$) can be divided into four main regions, and the nature of a group frequency may generally be determined by the region in which it is located. In Table 16.2, the fundamental vibrations of some common chemical bonds in the mid region are presented and the wavelength and region for each vibration are included.

More details are given in Table 16.3 for each region to identify the main functional groups attached to the polymer backbone.

Each band in an IR spectrum can be assigned to a particular movement in a molecule or group of atoms in a chemical bond. If this is applied to any bond in a molecule, there will be multiple bands even for similar molecules. A spectrum may have a hundred or more absorption bands

and there is no need to assign the vast majority; this can be regarded as the “fingerprint” of the molecule.

16.3.4 Quantitative Analysis of Polymers

The Lambert–Beer law is used to relate the amount of light transmitted by a sample to the thickness of the sample. The absorbance of a solution is proportional to the sample concentration:

$$A = lce \quad (16.6)$$

where A is the absorbance; c , the sample concentration; l , the length of the cell; and ε , the constant of proportionality, which is referred as the molar absorptivity. The absorbance can be defined as

$$A = \log_{10} \left(\frac{I_0}{I} \right) \quad (16.7)$$

where I_0 corresponds to the light entering the sample and I is the light transmitted by the sample. Since the absorbance is dimensionless, the transmittance T can be defined as

$$T = \frac{I}{I_0} \quad (16.8)$$

In order to quantify the amount of an analyte or molecule in a given sample, absorbance against concentration must be plotted and the resulting graph should be linear. To analyze a solution of unknown concentration, a calibration procedure must be followed. Solutions of known concentration need to be prepared, a suitable band must be chosen, and the absorbance at this wavenumber can be measured. Then, a calibration graph must be prepared that relates the measured absorbance of an unknown sample to its concentration.

For quantification of a functional group present in a sample or a polymer, several factors need to be considered. The first factor relates to the absorbance value of the band to be quantified, this must be neither too weak nor too intense. The second one refers to the choice of a suitable absorption peak that does not overlap any other peak. Another problem can be the presence of asymmetric shapes of the bands; in this case, peak heights cannot be used because the baseline will vary from sample to sample and peak area measurements must be used instead. Quantitative measurements need to be carried out on absorbance spectra.

IR spectroscopy can be used to measure the number of functional groups in a molecule or polymer backbone since absorptivity of the bands corresponding to the groups is proportional to the number of groups that are present in the sample. This approach can be used, for example, to measure the number of methylene groups in polyethylene (PE), determining molecular weight by measuring the stretching in the C–H bond at 1467 cm^{-1} . Quantification usually is

TABLE 16.2 Fundamental Vibrations for the Four Major Regions in the Mid-IR

Chemical Bond	Wavelength Region (cm^{-1})	Region Name
X–H	4000–2500	Stretching
C≡X	2500–2000	Triple bond
C=X	2000–1500	Double bond
C–X	1500–600	Fingerprint

TABLE 16.3 Comments for the Most Common Chemical Transitions during IR Analysis

Wavelength (cm^{-1})	Chemical Bond	Comments
3700–3600	O–H	Broad band
3400–3300	N–H	Sharp band
3000–2850	C–H	Several stretching bands
2300–2050	C≡C	Sharp but weak band
2300–2200	C≡N	Sharp band with medium intensity
2400–2200	P–H, Si–H	—
2000–1500	C=C, C=O, C=N	Carbonyl stretching is one of the easiest absorptions to recognize in an IR spectrum
3000–1700	C–H, N–H, O–H	Stretching bands usually weak in intensity

performed for samples in solution because analysis of solid samples results in more errors due to scattering of radiation.

16.3.5 Sampling Methods

There are several types of methods to obtain an IR spectrum depending on the nature of the sample to be analyzed. Transmission spectroscopy is based on the absorption of IR radiation at specific wavelengths as the radiation passes through a sample. With this technique, it is possible to analyze liquids, solids, or gaseous samples. This is the most common method; the samples can be placed in a cell in solution, dispersed in NaCl, KBr, CaF₂ (for water-soluble samples), or CsBr. Liquid thin films can also be analyzed using a drop of the sample, which will be sandwiched between two IR KBr cells and placed in a holder. When samples are analyzed in a solvent solution, several factors must be considered: the solvent has to dissolve the whole sample with a minimum of solvent–solute chemical interactions and it should not strongly absorb IR radiation.

16.3.6 Attenuated Total Reflectance (ATR)

When the sample to be analyzed is a solid or liquid, the intensity of the spectral features is determined by the thickness of the sample, which cannot be more than a few tens of micrometers. An attenuated total reflection accessory operates by measuring the changes occurring in a totally reflected IR beam when it comes into contact with a sample. An IR beam is directed onto an optically dense crystal with high refractive index at a certain angle, creating an evanescent wave that extends beyond the surface of the crystal into the sample held in contact with the crystal. This evanescent wave protrudes only a few micrometers (0.5–5 μm) beyond the crystal surface and into the sample. Consequently, there must be good contact between the sample and the crystal surface. The attenuated energy from each evanescent wave is passed back to the IR beam, which then exits at the opposite end of the crystal and is passed to the detector in the IR spectrometer. The system then generates an IR spectrum as shown in Figure 16.4.

16.3.7 Diffuse Reflection IR Fourier Transform Spectroscopy (DRIFT)

As a nondestructive method, DRIFT has been used to map the millimeter-scale of some surfaces, giving some mapping data that require geometric corrections for quantitative interpretation [5].

16.3.8 FT-IR Microscopy

To study very small samples, it is possible to pass an IR beam through a sample holder where the sample has been fixed by a microscope. This technique can be used to characterize samples with particle size less than 10 μm. IR radiation is focused onto a sample placed in a microscope and then collected by an objective that produces an image within the barrel of the microscope. In addition, by switching mirrors in the optical train, the microscope can be converted from transmission mode to reflectance mode.

16.3.9 Real-Time IR Spectroscopy

The final IR spectrum observed by a user for any sample (organic molecule or polymer) consists of a series of scans. An IR spectrum is composed generally of at least 20 scans. However, the combination of multiple scans with FT-IR provides a powerful real-time (RT) method for monitoring chemical changes, such as an *in situ* polymerization reaction. The rate of UV curing and photopolymerization, for example, can be easily calculated by analyzing the quantitative appearance or disappearance of a specific absorption band.

RT-FTIR spectroscopy has been a valuable technique to monitor reaction yields during UV curing processes, since IR spectra can be acquired before, during, and after exposure to the light without moving or changing the sample. In cases where an infrared feature corresponds to a chemical bond involved in the photopolymerization process, obtaining multiple spectra each second during the curing process can provide an accurate measure of the kinetics involved in the reaction and the extent of conversion [6].

RT-FTIR is used most of the times for photopolymerization reactions as a well-suited methodology to follow the

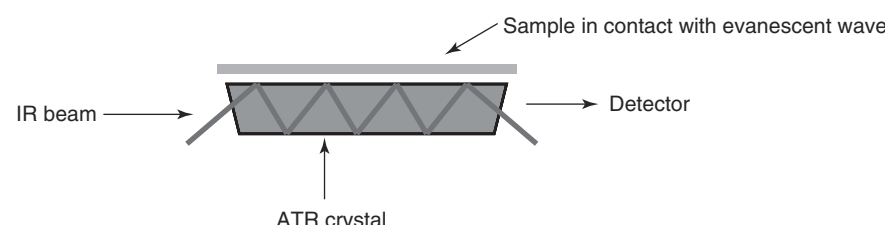


Figure 16.4 Mechanism of IR analysis by attenuated total reflectance. (See insert for the color representation of the figure.)

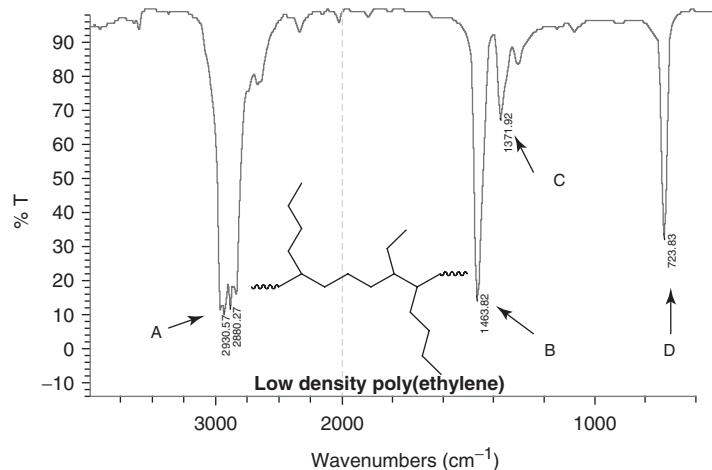


Figure 16.5 IR spectrum for low density polyethylene.

polymerization of monomer mixtures leading to the formation of either crosslinked copolymers or interpenetrating polymer networks. Analysis can be performed following the disappearance of a specific band on UV light exposure [7]. This technique provides RT analysis with high sensitivity, short response time, and versatility, giving as a result a powerful tool of investigation [8].

16.3.10 Discussion of IR Spectra for Polyethylene

The IR spectrum for low density PE in Figure 16.5 shows four high intensity absorption bands. The first band (A) corresponds to the symmetric and asymmetric stretchings of methyl and methylene groups. Then, symmetrical bending of methyl (B) and methylene (C) groups of the polymer

is observed, and the last band (D) corresponds to the stretching movement of the methylene groups in the backbone of the polymer chain.

However, the IR spectrum for high density PE in Figure 16.6 shows some differences, since there are three main signals for a molecule having the same chemical composition. Band (A) represents the symmetrical stretching for methyl and methylene groups, and band (B) corresponds to the symmetric methylene bending. The last one (C) is ascribed to the absorption of the methylene groups.

16.3.11 Conclusions

FT-IR spectrometry is an instrumental technique of analysis that presents significant advantages over other analytical

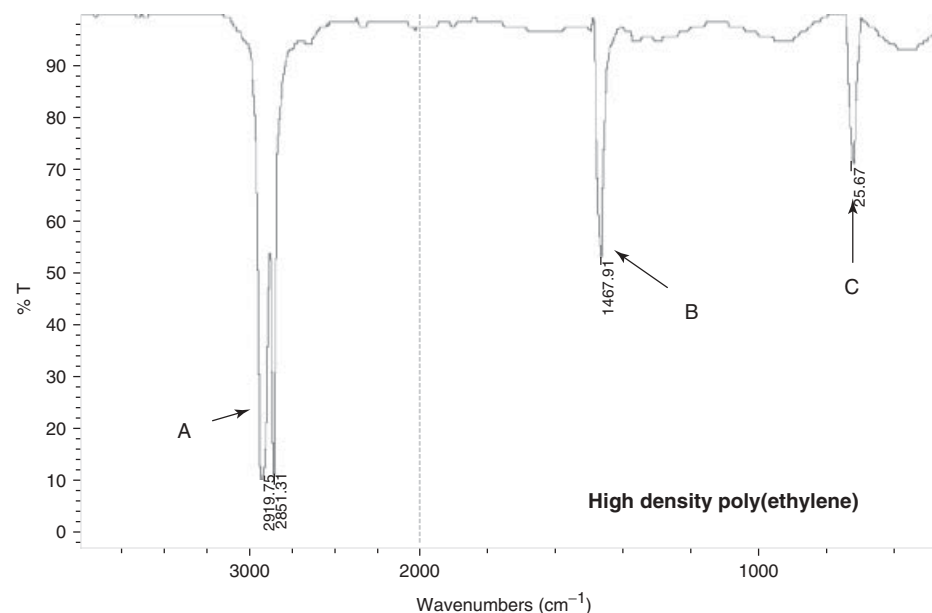


Figure 16.6 IR spectrum for high density polyethylene.

techniques; it has good signal-to-noise ratio, good capacity of obtaining absorption spectra of low energy, and, therefore, also bands of absorption of weak intensity.

IR has been used in addition to many other techniques to analyze polymer and copolymer compositions, either by itself or in addition to other techniques. Recently, the characterization by spatial differentiation of submicrometer domains in poly(hydroxyalkanoate) copolymer by the combination of atomic force microscopy (AFM) and IR spectroscopy was reported [9, 10]. This new capability resulting from the combination of two single instruments enables the spectroscopic characterization of microdomain-forming polymers at levels not previously possible.

16.4 NUCLEAR MAGNETIC RESONANCE OF POLYMERS IN SOLUTION

NMR is now a powerful analytical technique that has widespread applications in all areas of chemistry, including polymer characterization. Using NMR for elucidating the molecular structure of an unknown sample of polymer, accurate information can be obtained for qualitative and quantitative analyses of polymeric materials.

NMR is basically another form of absorption spectrometry that can be used in addition to IR, or UV, spectrometries. It is based on the absorption of electromagnetic radiation under appropriate conditions in the radio-frequency region at frequencies defined by the nature of the sample. Absorption is a function of each nucleus in the molecule. The main purpose of this technique is to provide information for the identification of organic molecules by studying the magnetic properties of nuclei.

All nuclei carry a charge. In some nuclei, this charge spins on the nuclear axis, and this circulation of nuclear charge generates a magnetic dipole along the axis (Fig. 16.7).

The angular momentum of the spinning charge can be described in terms of spin numbers, having the values of 0, 1/2, 1, 3/2, etc., where 0 denotes "no spin" like in ^{12}C , ^{16}O , ^{32}S , etc. For these elements, NMR experiments cannot be conducted since there is no spin angular moment and thus no magnetic moment to be analyzed. Several nuclei, however, such as ^1H , ^3H , ^{13}C , ^{15}N , ^{19}F , ^{29}Si , and ^{31}P have spin numbers I of 1/2 and a uniform spherical charge distribution, so all of them can be studied by NMR. Because of the abundance of the ^1H isotope (of about 100%) in all types of organic molecules, ^1H is obviously the most studied nucleus, resulting in relevant information for the proper determination of molecular structures. In quantum mechanical terms, the spin number I determines the number of orientations that a nucleus may assume in an external uniform magnetic field in accordance to the formula $2I + 1$. For example, considering the proton whose spin number

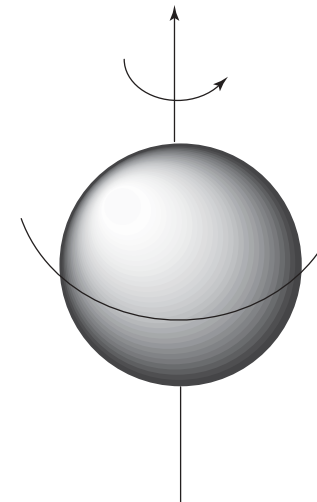


Figure 16.7 Magnetic dipole generated by the spinning charge of a proton nucleus.

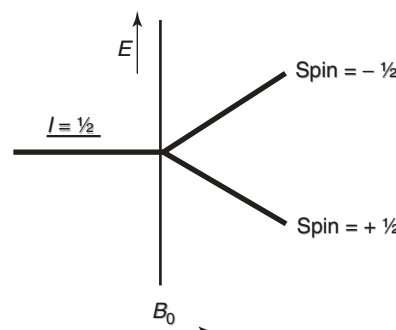


Figure 16.8 Two energy levels for a proton in a magnetic field B_0 .

I is 1/2, there are two energy levels as can be seen in Figure 16.8.

The nuclear magnetic moment, μ , is given as

$$\mu = \frac{\gamma I h}{2\pi} \quad (16.9)$$

where h is the Planck's constant and γ is the gyromagnetic ratio, which is a constant for each particular nucleus.

The most observed nuclei by NMR are ^1H and ^{13}C , both of them having spin number $I = 1/2$ and two magnetic states, characterized by a set of magnetic quantum numbers.

An irradiation with a frequency of 100 MHz is needed at a magnetic field B_0 of 2.33 tesla (T) for the proton to be excited from the lower energy state to the higher energy state.

16.4.1 Chemical Shift

Considering the hydrogen atom as an example, the electron shielding process, when the nucleus of the observed atom is placed in a magnetic field, can be analyzed.

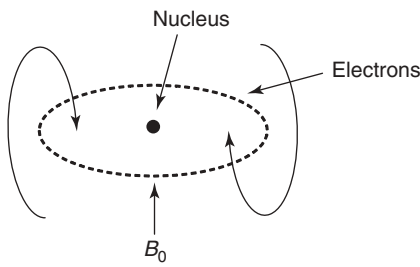


Figure 16.9 Motion of electrons by a magnetic field and around a nucleus.

In the presence of the magnetic field, the electron circulates in anticlockwise direction to B_0 . The motion of the electron is similar to an electric current flowing in a closed loop, and as such, it is associated with a secondary magnetic field that opposes the applied field B_0 . Thus, the observed resonance frequency of a proton appears to be slightly less than that predicted from the value of B_0 and the gyromagnetic ratio of a proton (Fig. 16.9).

Therefore the chemical shift, δ , is defined as the nuclear shielding divided by the applied field, and thus is only a function of the nucleus and its environment. It is always measured from a suitable reference compound:

$$\delta = \frac{B_{\text{ref}} - B_{\text{sample}}}{B_{\text{ref}}} \times 10^6 (\text{ppm}) \quad (16.10)$$

where B_{ref} is the magnetic field at the reference nuclei and B_{sample} is the field at the sample nuclei. Chemical shift δ in parts per million (ppm) is a molecular parameter depending only on the measurement conditions and not on the magnetic field or frequency applied for the determination.

According to the previously described equation, tetramethylsilane (TMS) is usually the recommended reference compound for analyses of ^1H and ^{13}C NMR. This has several advantages: it is chemically inert, symmetrical, and

soluble in most organic solvents; it gives a single sharp signal and absorbs at higher field than almost all protons from organic molecules. Usually, the absorption peak of TMS is fixed at 0.00 Hz or ppm.

The methyl protons of sodium 2,2-dimethyl-2-silapentane-5-sulfonate (DSS), acetonitrile, and dioxane have been sometimes used as external standards.

Extensive tables and charts of chemical shifts have been published in the literature, providing useful information about the region where specific groups of protons appear in the spectrum. Figure 16.10 shows the chemical shifts observed for the most common functional groups in organic molecules.

As previously mentioned, ^{12}C nucleus is not magnetically active for NMR analyses, but ^{13}C with $I = 1/2$ can be detected by this technique. However, since the natural abundance of ^{13}C is about 1.1% that of ^{12}C , and its sensitivity is only about 1.6% that of ^1H , the overall sensitivity of ^{13}C compared with ^1H is about 1/5700. Even when this characteristic can be considered as a disadvantage in comparison to ^1H NMR, ^{13}C NMR is being extensively used with excellent results for characterization of plenty of samples and their molecular arrangement.

The same transient and local magnetic fields affect both nuclei in the same way with respect to chemical shift: carbon as well as proton. The presence of equivalent carbon atoms in a molecule results in a discrepancy between the number of peaks and the actual number of carbon atoms in the molecule. ^{13}C shifts are related to the hybridization and substituent electronegativity and are affected by substitutions as far removed as the δ position. In the benzene ring, for example, pronounced shifts for ^{13}C are caused by substituents in the ortho, meta, and para positions.

The range of shifts generally encountered in routine ^{13}C studies is about 240 ppm, and, as mentioned for ^1H NMR, the location of regions for particular absorption

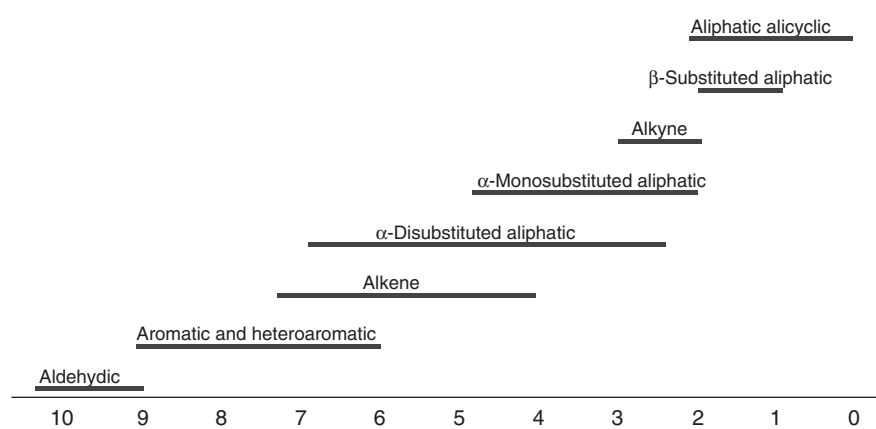


Figure 16.10 ^1H NMR, general regions of chemical shifts in organic molecules.

peaks depend on the type of substituents and adjacent carbon atoms in the studied molecule.

The chemical shift for usual polymers lies in the range of 0–200 ppm and provides the possibility of observing detailed structural differences.

16.4.2 Spin-Spin Coupling

NMR spectra consist not only of individual lines but also of groups of lines termed *multiplets*. The splitting of a peak into a multiplet arises from nuclear interactions called *spin-spin coupling*.

It has been suggested that the mechanism involves the bonding electrons. The discussion about two adjacent atoms can be centered in the spin state of the nucleus of atom A, which is coupled to the nucleus of spin state of atom B, via the bonding electrons. The energy level of spin A depends on the orientation of spin B, so two spectral lines are generated. The magnitude of the interaction is given by the spin-spin coupling constant J_{AB} , which is expressed in hertz and is independent of the applied field.

^{13}C NMR spectra are usually obtained under ^1H decoupling conditions because in this way the spectra become much simpler. The low abundance of ^{13}C nuclei results in a low possibility of observing ^{13}C – ^{13}C spin-spin coupling. This makes the spectra simpler, but information on C–C connectivity in the chains is scarcely obtainable.

Besides ^1H and ^{13}C nuclei, several other NMR observable nuclei have been utilized in polymer analysis, because ^{15}N , ^{19}F , ^{29}Si , and ^{31}P nuclei are found in some important polymers.

16.4.3 Instrumentation

High resolution NMR spectrometers can be categorized into continuous wave (CW) and pulsed FT, both of them requiring a radio-frequency source and a magnetic field. As

illustrated in Figure 16.11, which shows an FT-NMR spectrometer, the tube containing the sample solution is placed in a probe that is set in the magnetic field. Then, the sample tube is rotated about its axis using an airflow. The radio-frequency radiation is transmitted by a coil on the probe and detected either by the same coil or by a separate one. When the resonance condition has been achieved, the sample absorbs energy from the radio-frequency radiation and the resulting signal is detected on the receiver coil, amplified, and recorded. Using this procedure, the spectrum is obtained.

After the excitation pulse is turned off, the spin system emits the energy, returning to thermal equilibrium of the spin states. The signal observed in this process is called the *FID (Free Induction Decay) signal*, which is a spectrum recorded in the time domain.

16.4.4 Sample Preparation

Analysis of polymers involves dissolving a polymer sample in a suitable solvent and introducing the polymer solution in an NMR sample tube. The sample solution must be clear and free of suspended dust and impurities.

For ^1H and ^{13}C NMR experiments, the samples must be prepared in totally or partially deuterated solvents to avoid the interference created by solvent signals. In most of the modern NMR instruments, the deuterium signal from the solvent is used by an NMR lock system to avoid fluctuation of the magnetic field strength. Recent advances in NMR provide spectra with high resolution and high signal-to-noise ratio. This enables one to take the spectrum of the sample solution at very low concentrations.

A routine sample for proton NMR consists of about 5–20 mg of the sample in 0.4 ml of deuterated solvent in a 5 mm o.d. NMR test tube. ^{13}C NMR spectra are obtained under the same experimental conditions than proton analyses, but with a sample amount of 100–200 mg.

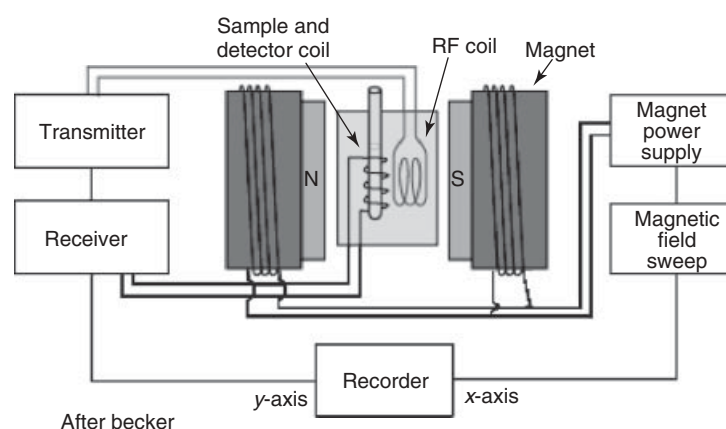


Figure 16.11 Diagram of an FT-NMR spectrometer. (See insert for the color representation of the figure.)

16.4.5 Qualitative Analysis of Polymers

NMR spectroscopy is an analytical tool extremely useful to follow the synthesis of polymers or supramolecular systems, from starting materials, intermediates, to products, and their three-dimensional conformation. The rapid development of advanced techniques has substantially broadened the application of NMR to the study of polymers [11–13].

Examples of ^1H NMR spectra of polystyrene (PS) and its monomer styrene (S) are shown in Figure 16.12a and b, respectively. The faster decay of the signal from PS than

that from the monomer is due to faster relaxation of the spins or shorter relaxation times. The difference is reflected as a difference in peak width.

Several characteristic signals appear in the ^1H NMR spectra for styrene: the doublet at 5.25 ppm corresponding to one of the methylene protons from the vinyl fraction of the molecule and the doublet at 5.8 ppm for the other proton of the same group. Then, a pair of doublets is also observed at 6.65–6.75 ppm, corresponding to the proton of the carbon atom directly attached to the aromatic ring. The signals at 7.2–7.4 ppm can be attributed to the five aromatic protons in the monomer molecule.

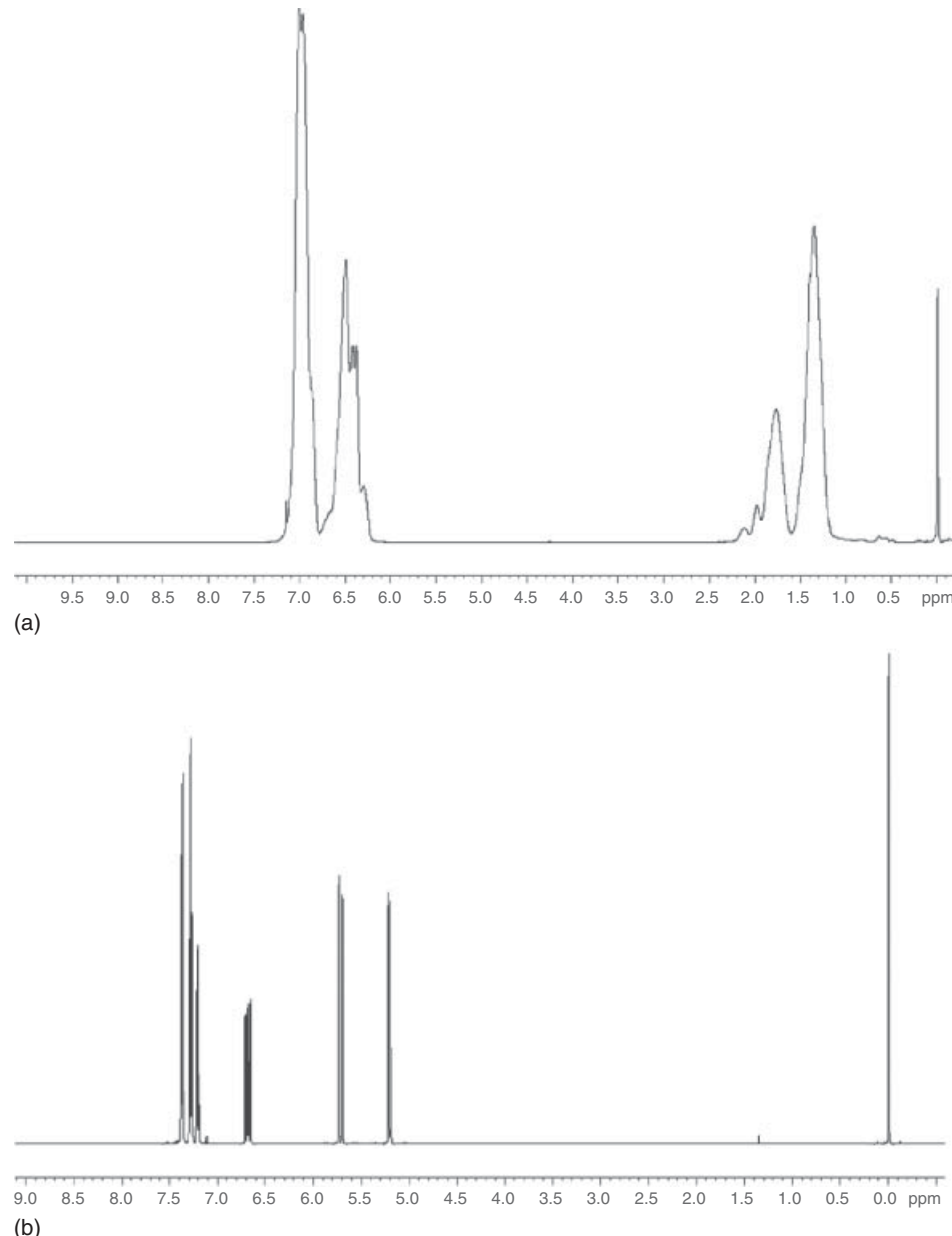


Figure 16.12 (a) ^1H NMR spectrum for polystyrene. (b) ^1H NMR spectrum for styrene.

By comparing this spectrum with that of the corresponding polymer, in the PS spectrum, the disappearance of the signals for the vinylic protons can be clearly detected and a new broad band for aliphatic protons is observed. As mentioned, broad peaks can be attributed to the relaxation time of the atoms in the molecule and the high concentration of protons in the observed region of the polymer chain.

As an additional example, for the structure in Figure 16.13, Figure 16.14 shows the ^1H NMR spectrum for a sample of poly(dimethylsiloxane) (PDMS-H) obtained by anionic polymerization of hexadimethyl-trisiloxane (D_3) initiated by butyl-lithium in the presence of chlorodimethylsilane [14].

In Figure 16.13, the chemical structure of the obtained polymer can be appreciated, while Figure 16.14 shows the ^1H NMR spectrum for PDMS-H.

For this polymer, a complex broad peak corresponding to the methyl protons (d) placed over the silicon atom in the polymer chain is observed at 0–0.2 ppm. Then, at approximately 0.5 ppm, there is a peak assigned to the methylene group (c) belonging to the butyl fraction from the initiator and next to the first silicon atom in the polymer chain. Protons (b), represented as a multiplet, have been assigned to the methylene groups from the butyl fraction. The last signal (a) is a triplet that corresponds to the methyl group, also from the initiator fraction, in the PDMS-H chain. Since the PDMS-H synthesized in this experiment has low molecular weight (<10,000 g/mol), the proton from the silane functionalizing group (e) placed at the end of the polymer chain can be easily detected.

Plenty of applications of NMR in polymer structure elucidation research can be found in the literature; the

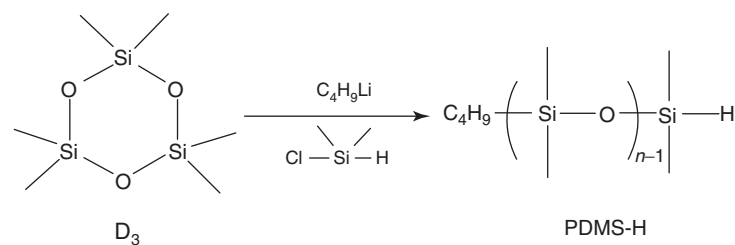


Figure 16.13 Chemical structure representation of the synthesized poly(dimethylsiloxane) (PDMS-H).

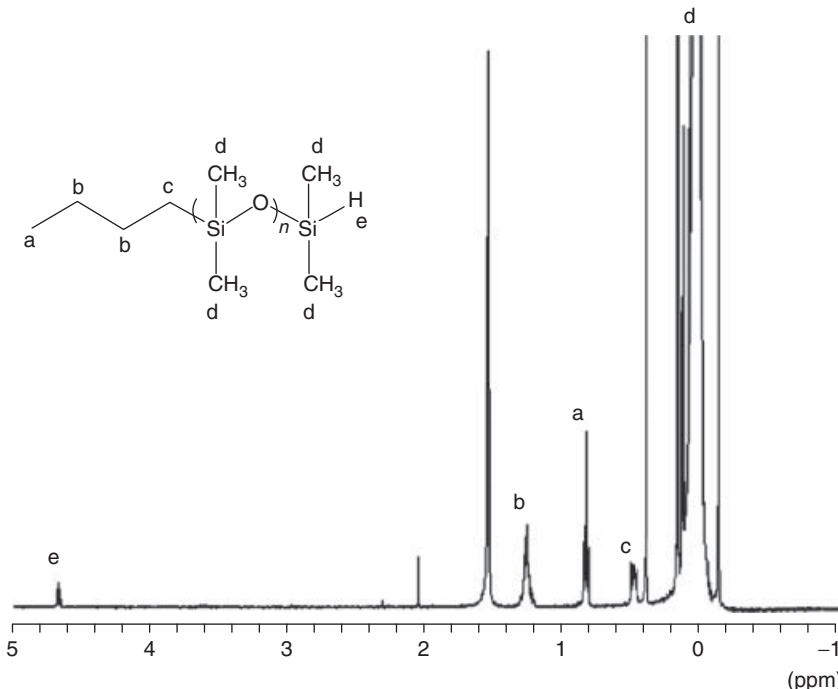


Figure 16.14 ^1H NMR (300 MHz, CDCl_3 , δ in ppm) for synthetic poly(dimethylsiloxane) (PDMS-H).

reports cover a broad range of polymeric systems, including copolymers [15].

There are three sources of interference with sample analysis via ^1H NMR: residual protons in deuterated solvents, water solubilized in the sample solution, and any other impurity present at the moment of the analysis. Sometimes the content of water represents an important problem to solve, particularly in the case of diluted samples in which the absorption peaks will have low intensity.

Deuterated chloroform is one of the most commonly used NMR solvents since it is the cheapest one due to the presence of only one deuterium atom in its molecule. However, besides water, some impurities dissolved in chloroform can sometimes occur, such as trichloroethane, dichloromethane, dibromomethane, acetonitrile, acetone. Water can also be introduced in the solvent during storage and its content increases gradually with time.

Solutions of polymer samples sometimes contain small amounts of low molecular weight impurities, including unreacted monomer and the solvent used for polymerization or purification.

Elucidation of the polymer structure depends on the nature of the chemical bonds between the atoms in the polymer chain. Sometimes, bonding can be inferred from the ^1H and ^{13}C chemical shifts and from the spin-spin coupling between nuclei. The first step in an NMR study of a polymer is to assign NMR to specific structural features of the polymer. Observing the following clues, it is possible to get the exact or the most approximate molecular structure of an unknown polymer via NMR analysis.

- Whenever possible, chemical shifts of low and high molecular weight of the same polymer must be compared.
- It is important to estimate the polymer chemical shifts using additivity relationships.
- It is easier to assign a structural model when the synthesized polymer has known structural or compositional features that establish chemical shift resonance–structure relationships.
- To highlight specific sites on the polymer chain, the polymer can be enriched with ^{13}C or with deuterium sites instead of protons.
- Computer simulation and comparison with spectra reported in the literature can be done in order to predict chemical shifts and multiplicity of some peaks, calculated on the basis of assumed polymerization kinetics and statistical models.
- Two-dimensional techniques revealing correlations between nuclei can be employed.

Two-dimensional NMR techniques can be satisfactorily used to determine the coupling between nuclei and to reveal the chemical shifts of these nuclei.

16.4.6 Two-Dimensional NMR Analysis

For many years, researchers have been using NMR in addition to other analytical techniques, such as IR or MS (mass spectrometry), to characterize and to quantitate organic molecules. In that sense, an NMR spectrum is normally obtained under standard conditions. In science, molecular complexity in organic synthesis has increased and normal experiments have been run at an increasingly higher magnetic field strength, resulting in the overlapping of signals.

Multidimensional NMR experiments offer a new way to resolve even highly overlapping resonances into readily interpretable multiplets and permits chemical shift assignments to be made in a simple manner [16–18].

Homonuclear correlation spectroscopy (COSY) offers a way to identify spin-coupled pairs of nuclei, even when structural information for the specific molecule under study is completely lacking. Correlation is established using homonuclear coupling, so the technique essentially shows the same information in one plot as in 1D homonuclear decoupling experiments. A potentially useful application for this class of analysis is the spin–spin correlation of ^{13}C – ^{13}C , but there are two main problems with this approach. The first one is related to the need of the presence of ^{13}C nuclei in two adjacent atoms. In natural abundance, this probability is too low, so the experiment is highly insensitive and suitable only for concentrated samples rich in carbon content. The second one relates to the relative weakness of the spin-coupled peaks from ^{13}C – ^{13}C pairs when compared with the peaks from isolated ^{13}C nuclei.

It is also possible through selective heteronuclear single-frequency decoupling to correlate bonded carbons and protons (HETCOR, Heteronuclear Correlated Spectroscopy) as an alternative to identify all directly bonded and long-distance carbon–proton pairs in a molecule.

In addition, a common experiment in NMR is the study of the relaxation behavior of nuclei, such as the nuclear Overhauser effect (NOE), to identify the local neighborhood of the nucleus and to infer information about the distances between atoms. From this, NOESY (nuclear Overhauser and exchange spectroscopy) and ROESY (rotating-frame Overhauser spectroscopy) methods are derived. The NOESY experiment correlates peaks by means of the nuclear Overhauser enhancement and identifies pairs of nuclei that are sufficiently close together in space to relax by their dipole–dipole interaction. This technique is not applicable in determining stereochemical assignments but may be extremely useful in determining the chain conformation in a study of an alternating copolymer such as that formed by styrene and methyl methacrylate [19].

Multidimensional NMR techniques, such as 2D-INADEQUATE, can allow the direct tracing out of carbon

skeletons of molecules, even without any prior partial knowledge of the structure of the molecule [20].

16.4.7 Quantitative and Compositional Analyses

NMR is a very useful technique in organic synthesis, not only as a method for characterization but also as an analytical tool that offers the capability of providing information about molecular architecture particular of each polymer, which cannot be obtained by any other technique [21].

Using NMR, it is possible to quantify the following.

16.4.7.1 Functional Groups and Compositions in Polymers, Copolymers, or Polymer Blends

The chemical shifts observed in an NMR spectrum characterize the environment of the nucleus under observation. The identification and quantification of functional groups such as pendant groups can be performed following the ratio between a characteristic peak for a proton or a carbon of that group and the proton or carbon of a known group in the polymer [22].

A specific example illustrates this point [23, 24]. The composition of the product copolymer in Figure 16.15 was determined by the relationship between the integrals of the two hydrogen atoms having a chemical shift of 8.0 ppm, which corresponds to the photochromic monomer, and the three hydrogen atoms at 3.25, 2.93, and 2.78 ppm of the oxirane ring (Fig. 16.16).

In addition, NMR can be used to determine the composition of a mixture by measuring the intensities of peaks belonging to each component in it. The components

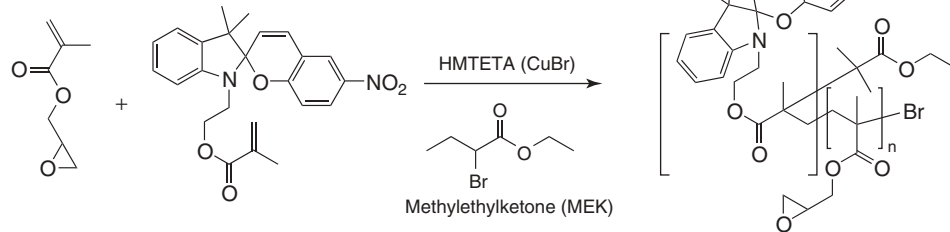


Figure 16.15 Chemical structure of poly(glycidyl methacrylate-*r*-1'-(2-methacryloxyethyl)-6-nitro-3',3'-dimethylspiro-[2H-1]-benzopyran-2,2'-indoline). HMTETA: 1,1,4,7,10,10-Hexamethyltriethylenetetramine; MEK: Methyl ethyl ketone.

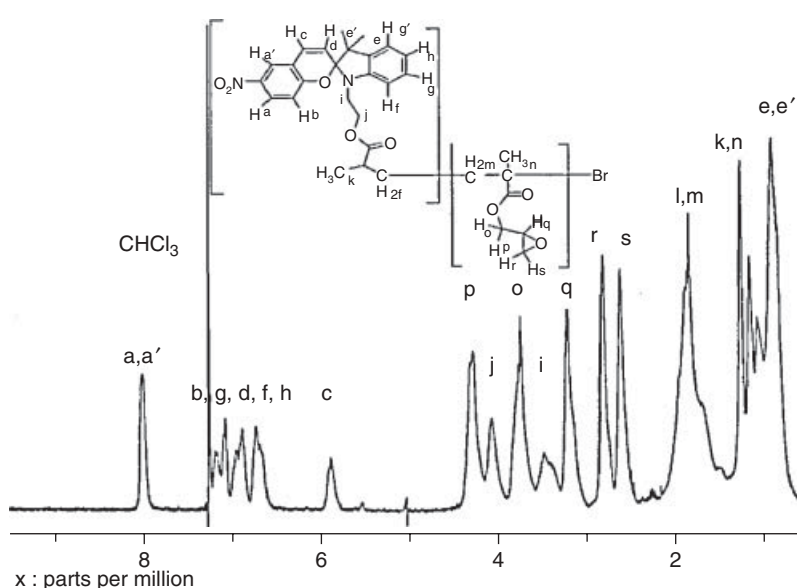


Figure 16.16 ^1H NMR of the copolymer poly(glycidyl methacrylate-*r*-1'-(2-methacryloxyethyl)-6-nitro-3',3'-dimethylspiro-[2H-1]-benzopyran-2,2'-indoline). Source: Reprinted with permission from Flores M, Elizalde LE, de los Santos G. *J Macromol Sci Pure Appl Chem* 2009;46:223 [23]. Copyright 2009 Taylor & Francis.

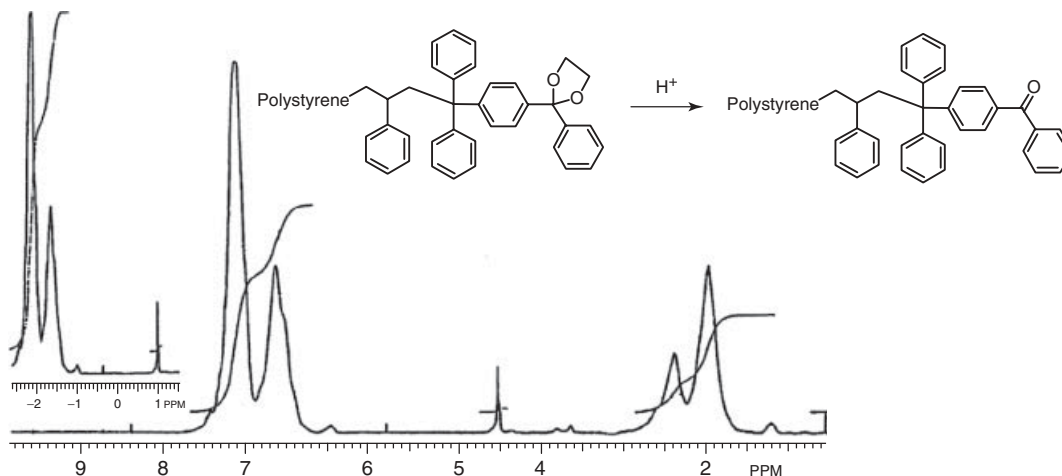


Figure 16.17 1H NMR for benzophenone (before deprotection) end-functionalized polystyrene synthesized by anionic polymerization. *Source:* Reprinted with permission from Kalyuzhnaya E, de los Santos G, Elizalde LE, Guerrero R. *J Appl Polym Sci* 1996;61:1055 [25]. Copyright 1996 John Wiley and Sons.

may be different chains in a polymer blend, different monomer units in a copolymer, or a polymer included in small amounts as an additive.

16.4.7.2 End Groups The end groups of a chain are determined by all the chemical steps in a polymerization reaction. The determination of the end-group structures is often extremely valuable in studying those processes. As an example, Figure 16.17 shows the resulting polymer from the anionic polymerization of styrene. During this addition polymerization, the growth of the PS chain was conducted as a living process, which was then terminated by a benzophenone derivative [25]. Monofunctional PSs were prepared by this anionic polymerization. The 1H NMR spectra of the prepared polymers contain, besides ordinary signals of PS, a signal at 4.03 ppm belonging to the methylene of the 1,3-dioxolane ring. The amount of the end group was calculated from the ratio between these two signals [26].

Quantitatively, the end-group intensity relative to the main-chain intensity gives the number-average degree of polymerization directly.

16.4.7.3 Stereochemistry (Tacticity) Vinyl polymers were the first to be classified stereochemically and studied by NMR. When the relative configuration of neighboring units among carbons in a polymer chain is considered, several stereochemically different diastereomers are possible. The first two diastereomers shown in Figure 16.18 are termed (i) *isotactic* and (ii) *syndiotactic*.

In isotactic polymers, all the groups have the same configuration, while in the second one, the syndiotactic stereoisomer, the pending groups in the polymer chain are alternating.

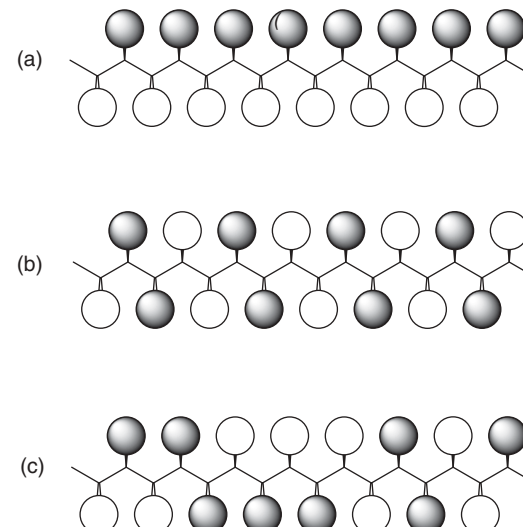


Figure 16.18 Schematic representation of (a) isotactic, (b) syndiotactic, and (c) atactic polymers.

There also exists the possibility of having a polymer with an irregular arrangement of the pending groups, which is termed *atactic*.

Examples of these three types of structural arrangements are known; in general, stereoregular polymers are synthesized by the use of coordination catalysts, whereas atactic polymers are formed by uncoordinated catalysts such as free radicals or free ions. Stereoregular polymers are often partially crystalline, and usually, even the isotactic and syndiotactic isomers have different properties. For example, isotactic poly(methyl methacrylate) (PMMA) has a glass-transition temperature of 35 °C, while that of the syndiotactic polymer is 105 °C.

In most NMR spectra of stereoregular polymers, the key factor for the analysis is the methylene group in the polymer chain. In an isotactic molecule, the two methylene protons are not identical, and therefore, two resonances must be observed. For a syndiotactic chain, the two protons in the methylene group are identical by symmetry, so only one resonance is observed [27].

The ^{13}C spectra of stereoregular polymers show a single sharp line for each chemically distinct carbon because, within each type of chain, each monomer residue is identical. However, the chemical shifts for isotactic and syndiotactic chains are not the same.

16.5 MASS SPECTROMETRY

16.5.1 General Principles

MS is a useful analytical technique to analyze and determine the molecular structure of an organic compound by observing its fragmentation pattern. This can be applied to qualitative or quantitative analysis.

In a common experimental routine, an organic sample is introduced to the instrument through the gas phase of a gas chromatograph that is kept in contact with an ion source resulting in the ionization of the sample molecules. At this point, positive ions are selected by particle size and conducted to the mass analyzer. Then, the resulting fragments are analyzed and the data processed. Finally, through the analysis of the sharp lines observed in the spectrum, there will be enough information to determine the molecular structure.

A mass spectrum is a two-dimensional representation of signal intensity of a fragment and the ratio between mass (m) and charge (z) of the fragment (m/z). The intensity of the peak correlates with the abundance of the corresponding ion.

Often but not always, the molecular ion peak can be appreciated in the mass spectrum, resulting from the detection of the intact ionized molecule. It is usually accompanied by several peaks at lower m/z caused by fragmentation of the molecular ion to yield fragment ions.

The peak showing the highest intensity in a mass spectrum is called the *base peak*. In most cases, this signal is normalized to 100% relative intensity.

There are several aspects about the performance of the mass spectrometer that must be considered:

Sensitivity This term refers to the overall response of the instrument to the investigated analyte when the apparatus is operated under well-defined methods. The sensitivity is defined as the slope of a plot of analyte concentration versus signal strength.

Detection Limit This term is often confused with sensitivity since it defines the smallest flow or the lowest amount of analyte necessary to obtain a signal that can be distinguished from the background noise.

Signal-to-Noise Ratio This parameter describes the uncertainty of an intensity measurement and provides a quantitative measure of a signal's quality by quantifying the ratio of the intensity of a signal relative to noise. Noise can be obtained from different sources: impurities due to sample handling, impurities from previous samples run by gas chromatography, column bleed, and the electronics in the instrument. Consequently, signals and their intensities can be influenced by noise.

16.5.2 Electron Ionization

The fundamental principle of MS is based on the impact of electrons onto neutral gaseous molecules that are usually obtained from the transfer line placed at the end of a gas chromatograph. These neutral gaseous molecules undergo ionization (electron ionization (EI)), generating positive, negative, and neutral charged fragments. Electron impact ionization or electron impact is still an important technique to analyze molecules with low to medium polarity and also organic nonionic compounds.

16.5.3 Sample Introduction

There are different types of instruments that can be attached to the EI source for MS analysis. The most commonly used technique consists of the analysis of a gaseous sample obtained from the gas chromatograph. However, other introduction systems, such as reservoir inlets and direct insertion probes, are also frequently used.

Table 16.4 summarizes existing sample introduction systems for EI-MS.

16.5.4 Other Ionization Processes

As mentioned before, MS is a useful technique to analyze unknown organic molecules by studying their fragmentation pattern. However, since there are several requirements for samples to be analyzed, when an organic molecule is unsuitable to be studied by gas chromatography, another suitable analytical technique can be chosen, for example, liquid chromatography (LC), direct injection probe (DIP), and direct exposure probe (DEP).

A specific problem in MS analysis of polymers, which can make it difficult to be performed by normal techniques, is related to the fact that the most common procedure to introduce the sample in the ionization chamber is to take it from the gaseous stream at the end of a gas chromatograph; however, the usually high molecular weight and covalent

TABLE 16.4 Sample Introduction Systems for EI-MS

Inlet System	Principle	Types of Analytes
Reservoir inlet	Sample is vaporized in a heated reservoir	Liquids with low to medium boiling points
Direct insertion probe (DIP)	Sample is heated directly into the ionization chamber without the use of GC	Solids, waxes, thermally unstable molecules, liquids with high boiling temperature
Direct exposure probe (DEP)	Sample particles are heated on a metal filament	Solids of extremely low volatility and that are thermally unstable
Gas chromatograph (GC)	Sample is obtained from the eluent gas stream and injected directly into the ion source	Most volatile organic compounds and volatile mixtures of organic molecules
Liquid chromatograph (LC)	Connected via particle beam interface	Used for analytes that cannot be separated by GC due to its high polarity

bonding in the polymer makes the material prone to be degraded before entering the ionization chamber. This translates into clogging of the chromatographic column. To avoid such circumstances, several techniques associated to MS, which also analyze the fragmentation pattern, have been developed and some of them are described in the following sections.

16.5.4.1 Matrix-Assisted Laser Desorption/Ionization (MALDI)

This topic has received much attention since several years ago, especially with regard to its application to polymer analysis.

In MALDI (matrix-assisted laser desorption/ionization), the ionization process occurs in two steps: an initial primary ionization followed by a secondary reaction [28]. During primary ionization, the ions are formed after the sample has absorbed the energy from the laser beam, and then, upon continuing laser beam irradiation, the analyte undergoes secondary neutralization reactions with free electrons until they become singly charged. Meanwhile, neutral analyte molecules evaporate and are charged by secondary protonation reaction. In this way, they can be detected.

Since its introduction by Karas and coworkers in 1987 [29], MALDI has become a powerful analytical technique for the study of thermolabile or unstable molecules and nonvolatile samples such as polymers.

A MALDI mass spectrum can be very useful when applied to polymers, because important structural information

can be obtained, such as the nature of the repeating unit; the presence of end groups; molecular weights; molecular weight distributions; some information about branching; information on the nature of random, ordered, and block copolymers; and the presence and nature of some additives in the polymer [30].

From 1987 up to now, there are many reports in the literature related to the satisfactory use of MALDI to characterize polymer chains [31]. The first reports of polymer characterization by MALDI were published by Tanaka et al. [32] in 1988 describing the characterization of poly(propylene) and poly(ethylene glycol) (PEG) using MALDI.

The mass spectrometer most widely used with MALDI is the TOF-type (time of flight) mass spectrometer, mainly due to its large mass range. MALDI-TOF is equipped with an ion mirror to reflect ions, which uses an electric field, doubling the ion flight path and increasing thus the resolution [33, 34].

In the field of living radical polymerization, MALDI-TOF has been highly useful for characterization of polymers prepared by nitroxide-mediated radical polymerization (NMRP) [35, 36], atom transfer radical polymerization (ATRP) [37], and reversible addition-fragmentation chain transfer polymerization (RAFT) [38, 39]. The modern MALDI-TOF-MS permits fast and accurate determination of a variety of polymer characteristics [40].

16.5.4.2 Analysis of Nonpolar Polymers MALDI analysis of hydrocarbon polymers is a challenging task since they are chemically inert due to the absence of functional groups in their chains, making their characterization somewhat difficult. In that sense, PS is one of the most common synthetic polymers analyzed by MALDI-MS due to the presence of the phenyl functionality in PS that facilitates its easier ionization compared to other nonpolar nonfunctional polymers such as poly(butadiene), poly(isoprene), polyethylene, or poly(propylene).

16.5.4.3 Tandem Mass Spectrometry Tandem MS is an early technique that involves the isolation of a specific ion followed by its fragmentation, which occurs in a collision cell, resulting in a fragment ion spectrum. This technique has been satisfactorily used for the study of peptide sequences [41], but it can also be used for the analysis of synthetic polymers.

In 2009, Crecelius et al. [42] reported the characterization of homopolymers, copolymers, and star-shaped polymers by tandem MS. The main aim of the work was the analysis of end-group functionalization, which can be determined faster by this technique.

In polymer analysis by MALDI-related techniques (such as tandem MS), there are two possibilities to obtain fragment ion spectra. The first one uses the traditional MALDI

instrument equipped with a reflector to collect metastable fragments that are formed during ion acceleration out of the ion source in the field-free region. This fragmentation is termed *postsource decay* (PSD). The main disadvantage of a PSD spectrum is the long acquisition times, since recording a mass spectrum can take up to 1 h, after which unresolved peaks still remain. The other possibility is the collision-induced dissociation (CID), which requires the placement of a collision cell in the field-free region of the analyzer. This last technique has been successfully used in polymer characterization in recent years. There are many published works related to the investigation of structural features and end-group determination for a variety of polymers. Homopolymers such as PMMA, linear and branched [43]; PEGs [44, 45]; and PSs [46] have been characterized by MALDI-CID analysis.

REFERENCES

- Koenig JL. *Spectroscopy of Polymers*. 2nd ed. New York: Elsevier Science Inc.; 1999. p 12.
- Dobkowski Z. *Appl Polym Anal Charact* 1992;2:363.
- Rabindranath M, Sukumar M. *J Polymer Mater* 1993; 10(3):183.
- Silverstein RM, Bassler GC, Morrill TC. *Spectrometric Identification of Organic Compounds*. 5th ed. New York: John Wiley & Sons, Inc.; 1991. p 91.
- Leue M, Gerke H, Ellerbrock R. *Soil Sci Soc Am J* 2011;75(5):1626.
- Lowry S, Weesner F. *Spectroscopy Solutions for Materials Analysis*. Special Issue, Aug 1, 2011 (e-journal). <http://www.spectroscopyonline.com/spectroscopy/FT-IR+Spectroscopy/Using-Real-Time-FT-IR-to-Characterize-UV-Curable-O/ArticleStandard/Article/detail/735157>.
- Decker C. *Polymer News* 2005;30(2):34.
- Pereira HL, Machado F, Lima LE, Pinto JC. *Macromol Symp* 2011;299/300:1.
- Curtis M, Lo M, Kjoller K, Prater C, Noda I. *Appl Spectros* 2011;65(10):1145.
- Prater C, Kjoller K, Shetty R, Dazzi A. *Laser Focus World* 2011;47(3):52.
- Matyjaszewski K, Gnanou Y, Leibler L. Macromolecular engineering. In: Matyjaszewski K, Gnanou Y, Leibler L, editors. *Macromolecular Engineering: Precise Synthesis, Materials Properties, Applications*, Volume 3. Weinheim, Germany: Wiley VCH; 2007. p 1937.
- Ibett RN. *NMR Spectroscopy of Polymers*. 1st ed. Glasgow, UK: Blackie Academic & Professional; 1993.
- Hatada K, Kitayama T. *NMR Spectroscopy of Polymers*. Berlin, Germany: Springer; 2004.
- González M, Elizalde LE, Saldívar E. Synthesis of block copolymer poly(dimethylsiloxane-*b*-methylmethacrylate) by anionic ring opening polymerization and ATRP. 2nd US – México Meeting Advanced Polymer Science and XXIV SPM National Congress; 2011 Dec 7–11: Cancún, Q. Roo.
- Shu J, Li P, Chen Q, Zhang S. *Macromolecules* 2010; 43(21):8993.
- Croasmun WR, Carlson RMK. *Two-Dimensional NMR Spectroscopy*. 2nd ed. Hoboken NJ: John Wiley & Sons; 1994.
- Hatcher P, Bialk H, Sleighter R, McKee G, Liu Z, Byrne C. 234th American Chemical Society National Meeting, David J. Clifford Memorial Symposium; 2007 Aug 19–23; Boston, MA, USA.
- Webb G. *Int J Plast Technol* 2004;8(2):371.
- Mirau PA, Bovey FA, Tonelli AE, Heffner SA. *Macromolecules* 1987;20:1701.
- Webb G. *Macromolecules* 2005;38(7):2775.
- Webb G. *J Polym Sci A Polym Chem* 2005;43(5):1100.
- Webb G. *Polym J* 2007;39(2):118.
- Flores M, Elizalde LE, de los Santos G. *J Macromol Sci Pure Appl Chem* 2009;46:223.
- Webb G. MACRO 2004, International Conference on Polymers for Advanced Technologies; 2004 Dec 15–17, Thiruvananthapuram, India.
- Kalyuzhnaya E, de los Santos G, Elizalde LE, Guerrero R. *J Appl Polym Sci* 1996;61:1055.
- Webb G. *Eur Polym J* 2006;42(6):1455.
- Webb G, editor. *Modern Magnetic Resonance*. Volume 1. Heidelberg: Springer; 2006. p 553.
- Batoy SMAB, Akhmetova E, Miladinovic S, Smeal J, Wilkins CL. *Appl Spectros Rev* 2008;43:485.
- Karas M, Bachman D, Bahr U, Hillenkamp F. *Int J Mass Spectrom Ion Process* 1987;78:53.
- Hercules DM. *Anal Bioanal Chem* 2008;392:571.
- Pasch H. *Polymer Preprint* 1996;37(1):319.
- Tanaka K, Waki H, Ido Y, Akita S, Yoshida Y, Yoshida T, Matsuo T. *Rapid Comm Mass Spectrom* 1988;2:151.
- Ladaviere C, Lacroix-Desmazes P, Delolme F. *Macromolecules* 2009;42(1):70.
- Nonaka H, Ouchi M, Kamigaito M, Sawamoto M. *Macromolecules* 2001;34(7):2083.
- Farce C, Belleney J, Charleux B, Pirri R. *Macromolecules* 2002;35(13):4912.
- Dourges M, Charleux B, Vairon J, Blais J, Bolbach G, Tabet J. *Macromolecules* 1999;32(8):2495.
- Shen X, He X, Chen G, Zhou P, Huang L. *Macromol Rapid Comm* 2000;21(16):1162.
- England RM, Rimmer S. 238th American Chemical Society National Meeting, Stimuli-Responsive Polymer Materials and Composites; 2009 Aug 16–20; Washington, DC, USA.
- Wang D, Zhou Q, Pu H, Yang G. *J Polym Sci A Polym Chem* 2008;46(11):3756.
- Dempwolf W, Flakus S, Schmidt-Naake G. *Macromol Symp* 2009;275–276:166.
- Nesvizhskii AI, Vitek O, Aebersold R. *Nat Methods* 2007;4:787.

354 POLYMER SPECTROSCOPY AND COMPOSITIONAL ANALYSIS

42. Crecelius AC, Baumgaertel A, Schubert US. *J Mass Spectrom* 2009;44:1277.
43. Jackson AT, Bunn A, Chisholm MS. *Polymer* 2008;49:5254.
44. Miladinovic S, Robotham SA, Wilkins CL. *Anal Bioanal Chem* 2008;392:585.
45. Jackson AT, Slade SE, Thalassinos K, Scrivens JH. *Anal Bioanal Chem* 2008;392:643.
46. Polce MJ, Ocampo M, Quirk RP, Leigh AM, Wesdemiotis C. *Anal Chem* 2008;80:355.

17

POLYMER MOLECULAR WEIGHT MEASUREMENT

MARÍA GUADALUPE NEIRA-VELÁZQUEZ, MARÍA TERESA RODRÍGUEZ-HERNÁNDEZ, ERNESTO HERNÁNDEZ-HERNÁNDEZ, AND ANTELMO R. Y. RUIZ-MARTÍNEZ

17.1 INTRODUCTION

Gel permeation chromatography (GPC), also known as *size-exclusion chromatography* (SEC), is a chromatographic technique that employs specialized columns to separate natural and synthetic polymers, biopolymers, or proteins on the basis of their size. GPC is the most widely used technique for the analysis of polymers, in relation to other techniques of molecular weight (MW) measurement; the analysis is very fast (compared to older techniques) and can be carried out in a couple of hours. It can be used for samples soluble in organic and aqueous eluents, and for MWs from approximately 100 to several million daltons (Da). With GPC, it is also possible to obtain the MW of polymers that are soluble only at high temperatures. Besides, in contrast to traditional techniques, it yields all MW averages and the molecular weight distribution (MWD).

17.2 HISTORICAL BACKGROUND

The word chromatography was used for the first time in 1906 by a Russian botanist, Mikhail Tswett, who described it as a new technique to separate the components of complex mixtures [1, 2]. His work was published in the Proceedings of the German Botanical Society; there he described a technique based on the partition of solutes between a stationary solid adsorbent and a moving liquid phase. The experiment consisted in pouring a small quantity of the solution of pigments, such as green leaf pigments, on the top of a vertical column of absorbent, followed by a flow of pure solvent, whereupon a series of colored bands formed

down the length of the column in a sequence determined by mass relationships and absorption coefficients [3].

Despite the tremendous potential impact of his discovery, chromatography was not revived until 1931, under the stimulus of widespread research on the separation of carotenoids from several natural sources by adsorption analysis on fibrous alumina [4]. Since the cited work was published, chromatography application has been extended over practically all areas of chemistry. In polymer science, chromatography was used for the first time by Moore in 1963 to determine the MWD of polymers [5].

The technique was really invented by Lathe and Ruthven [6], who were working at Queen Charlotte's Hospital in London. They received the John Scott Award for their invention. In 1964 Moore, from the Dow Chemical Company, prepared GPC columns using crosslinked polystyrene with controlled pore size [7]; after publishing his results, there was a rapid increase of research activity in the field of measurement of the MW of polymers.

James Waters, industry pioneer and entrepreneur, had founded Waters Associates (WA) in 1958 in order to invent instruments for others. He worked with five employees in the rented basement of a police station. In 1961 John Moore required from WA to develop a 0.1 ml volume flow cell, which would enable him to develop an instrument using gel columns to analyze the MW of polymers (natural and synthetic macromolecules). After experimental work by Moore, followed by negotiations between Dow and WA and additional hard work to scale up the synthesis of the polymeric gel used in the columns, the invention of the GPC was completed, becoming a major breakthrough for WA.

In 1963, Waters obtained an exclusive license to Dow's patent [5] for GPC and introduced Waters' first liquid chromatography (LC) system, the GPC 100, which was larger than a refrigerator.

17.3 PRINCIPLES OF GPC

17.3.1 Principle of Separation

The fundamental principle of separation by size exclusion in a column is represented in Figure 17.1. The column is packed with semisolid particles of a polymer whose structure is crosslinked to form a gel and whose pore distribution has been controlled during the synthesis of the polymer. Molecules that are smaller than the pore size can enter inside the pores and therefore have a longer path and a longer transit time than larger molecules which cannot enter the pores. Molecules larger than the pore size cannot enter the pores and elute before smaller molecules. This condition is called *total exclusion* because of the fact that the largest molecules are rejected from entering the pores, as shown in Figure 17.1. Molecules that can enter the pores will have an average residence time in the particles that depends on the molecular size and shape.

The separation parameters in GPC are obtained by the distribution coefficient k_d , related to the internal volume according to

$$k_d = \frac{V_{i,acc}}{V_i} = \frac{V_e - V_0}{V_0} \quad (17.1)$$

where $V_{i,acc}$ is the accessible internal volume, V_i is the internal volume, V_e is the elution volume, and V_0 is the external volume or interparticle volume. When $k_d = 0$, it means that the molecules are excluded; $0 < k_d < 1$ indicates that the molecules are retained in the gel pores; $k_d = 1$ suggests that the molecules occupy the total inner volume [8].

The fundamental principle of separation by SEC was described by Benoit and coworkers in 1967. They found an excellent correlation between the elution volume and a dynamically based molecular size, the hydrodynamic volume V_H ¹ for a wide range of species and large-scale molecular architectures [9]. Their theory assumed a thermodynamic separation principle considering that the elution volume is independent of the flow rates. Recently, it has been proved that the radius of gyration is more appropriate than the hydrodynamic volume [10]. The radius of gyration R_g is defined as the mean square distance away from the center of gravity [11]. Its mathematical definition is:

$$R_g^2 = \left(\frac{1}{N} \right) \sum_{i=1}^N r_i^2 \quad (17.2)$$

¹The hydrodynamic volume is proportional to the product of the molecular weight M and the intrinsic viscosity $[\eta]$; that is, $V_H \propto [\eta]M$.

which is the radius of gyration of N scattering points located at distances r_i . In mechanical terms, R_g can be interpreted as the radius of a thin ring that has the same mass and same moment of inertia as the body when this is centered around the same axis [12]. Furthermore, calculations indicate that the morphology of polymers in solution is not spherical in overall shape, but rather ellipsoidal [13]. In terms of their overall shape, branched polymers are more symmetric than linear ones [14]. This explains some of the differences between linear and branched polymers with respect to size exclusion. Similar arguments have been used to explain the failure of R_g to provide an appropriate size measure for the SEC of oligomers of polyethylene and polystyrene [15, 16].

GPC is the technique of choice for rapid and reliable characterization [17] of MW averages, MWD, and molecular structure for all types of macromolecules—proteins, oligomers, natural polymers, and synthetic polymers.

The polymer characteristics that can be measured by GPC can be listed as

- absolute MW;
- MWD;
- MW averages (see below) and dispersity of the MWD (formerly called *polydispersity*);
- branching and structure;
- molecular size;
- copolymer composition.

17.3.2 Average Molecular Weight of Polymers

The following MW averages can be obtained by GPC:

- \overline{M}_n , number-average MW;
- \overline{M}_p , peak-average MW;
- \overline{M}_v , viscosity-average MW;
- \overline{M}_w , weight-average MW;
- \overline{M}_z , Z-average MW;
- \overline{M}_{z+1} , Z+1-average MW.

The different MW averages can also be measured by the techniques shown in Table 17.1. The main disadvantage of other techniques to measure average MW in polymers is that they are very time consuming. In some cases, just one of these MWs is obtained in a week. On the other hand, by using GPC the different averages of MW can be obtained in about 2 h.

The MW averages \overline{M}_n , \overline{M}_w , \overline{M}_z , \overline{M}_{z+1} , and \overline{M}_v , are mathematically defined in Section 1.5 of Chapter 1. For any MWD, the various average MWs always rank in the order $\overline{M}_n < \overline{M}_v < \overline{M}_w < \overline{M}_z < \overline{M}_{z+1}$. If all the average MWs are the same, then we have a monodisperse polymer.

\overline{M}_n and \overline{M}_w are the most commonly used average MWs; in industry, it is usually enough (although not always) to

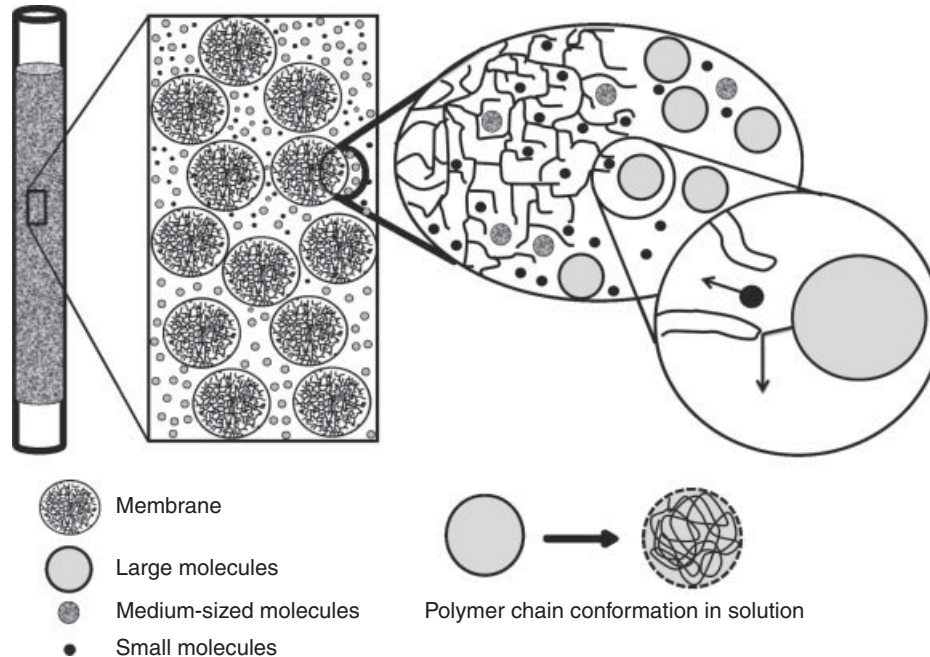


Figure 17.1 Illustration of the separation of polymer molecules by size exclusion.

TABLE 17.1 Techniques for Measuring Different Molecular Weight Averages

Average Molecular Weight	Technique
M_n	Vapor pressure osmometry End-group titration Proton NMR Boiling point elevation Freezing depression (cryoscopy) GPC
M_w	Light scattering Small-angle neutron scattering (SANS) X-ray scattering Sedimentation velocity GPC
M_v	Viscometry GPC
M_z	Ultracentrifugation GPC
M_{z+1}	Ultracentrifugation GPC

know them to describe the main features of the MWD of a polymer.

Osmotic pressure and vapor pressure methods are used to determine absolute values of M_n , while light scattering and sedimentation velocity are used to determine M_w . However, if the GPC equipment is coupled with different detection techniques, such as light scattering, viscometry, refractive

index, etc., then it is possible to obtain absolute MWs of polymers. Table 17.1 shows the different techniques used to measure different average MWs of polymers. It can be appreciated that GPC measures all MW averages. The different average MWs obtained by GPC can be represented in a MWD curve, as appreciated in Figure 17.2.

The MW dispersity had been already defined in Section 1.5 of Chapter 1, and is the ratio M_w/M_n . Polymers with a narrow distribution (low MW dispersity) are more suitable for injection molding, whereas polymers with

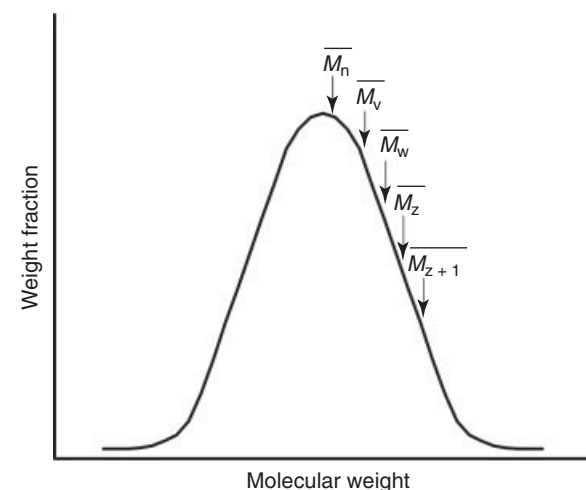


Figure 17.2 Schematic plot of a distribution of MWs showing the different averages of MW.

TABLE 17.2 Various Average Molecular Weights and their Relation with Polymer Properties

Molecular Weight	Polymer Properties
Number-average molecular weight (M_n)	Tensile strength, impact strength, and hardness
Weight-average molecular weight (M_w)	Brittleness
Z-average molecular weight (\overline{M}_z)	Deflection and rigidity

a high MW dispersity are more suitable for extrusion. Polymers with a MW dispersity of 1.0 can be produced only by biological systems. Many physical properties can be affected by the MW dispersity.

The physical and chemical properties of the polymers in general are directly related to the MW, MWD, MW dispersity, and long-chain branching [18, 19]. Table 17.2 shows the relationship between the average MWs and some physical properties of polymers. There is also a relationship between the MW and the viscoelastic properties of polymers [20, 21] and thus it is possible to predict some properties of the polymer with a simple determination of the MW by GPC. Polymers with high MWs have higher viscosity, they also present low melt flow index, and are more difficult to dissolve, since they present higher chemical resistance; polymers with very high MW are more difficult to process and require higher temperatures.

17.3.3 GPC Systems

A GPC system consists of various instruments. Injectors are used to introduce the polymer solution into the columns of separation. Pumps deliver the sample and solvent through the columns and the system. Detectors record the exit of fractions of the sample and count the number of molecules of a certain MW. The computer controls the test automatically, records the results, and calculates the different MW averages. The GPC system contains a number of different instruments that work together to provide the optimum system performance. Figure 17.3 shows a schematic of a gel permeation chromatograph with the basic components.

17.3.3.1 Injector The injector introduces the polymer solution into the mobile phase. It must be capable of injections of small and large volumes. It should not interfere with the continuous mobile phase flow. It should be capable of multiple sample injection and should be capable of self-cleaning between injections. In the past, the injections were carried out manually, but this is not the case at present, since most of the GPC instruments have automatic injectors.

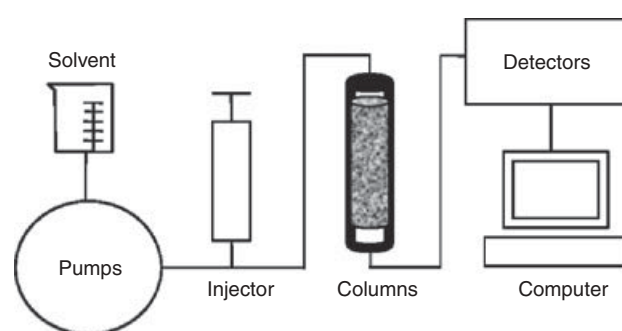


Figure 17.3 Schematic representation of the components of a GPC system.

17.3.3.2 Pumps These are piston-type precision pumps. They pump the polymer in solution through the system. The pump must deliver the same flow rates throughout the time in order to maintain the same pressure inside the system. Any variation in flow rates affects directly the results. The pump also has to deliver the same flow rates independently of the viscosity differences. In addition, some detectors are highly sensitive to the solvent flow rate precision. Such constant flow is a critical feature of the instrument.

17.3.3.3 Columns They are considered the heart of the equipment. The separation of the macromolecules takes place in their interior. They are filled with a porous crosslinked polymer, and the macromolecules to be separated interact with the polymer pores depending on their size in solution. It is highly recommended to use at least a set of three columns in order to obtain good results. Columns are available at different pore sizes. Columns with very small pores sizes are used for polymers of low MW, while columns packed with material containing large pore sizes are used for polymers with high MW. High efficiency columns give maximum separating capability and rapid analyses. Every column must provide reproducible information over extended periods for both analytical and fraction-collection purposes. There are columns for different types of applications. For example, there are columns that can stand high temperatures, which are used to fractionate polymers that are soluble only at high temperatures, such as polyethylene or polypropylene. There are also columns suitable to work with aqueous solvents, those columns are packed with a material known as *ultrahydrogel*, which is basically a crosslinked hydroxylated polymethacrylate; these columns are used with polymers that are soluble in water, such as poly(acrylic acid), poly(vinyl alcohol), poly(ethylene glycol), etc.

17.3.3.4 Detectors The detectors used in a GPC system monitor the separation and respond to the components and/or fractions as they elute from the column.

Detectors must be sensitive and must have a wide linear range in order to respond to both trace amounts and large quantities of material, if necessary. They must be nondestructive to the eluting components if they are to be collected for further analysis. There are different types of detectors for GPC, the most common ones being the refractive index (RI) detector, the UV detector, viscometer detector, as well as light scattering and infrared detectors.

Since all compounds refract light, the RI is known as a "universal" detector. It is the most widely used detector to monitor the MWD. The refractive index of polymers is constant above approximately 1000 Da. Therefore, the detector response is directly proportional to the concentration.

In addition to the information about MW averages and distribution obtained with the RI detector, UV absorbance detectors may provide information about composition. UV detectors are used for polymers containing chromophore groups.

Online light scattering detectors and viscometers provide information about the polymer structure. If a light scattering detector is used together with an RI, then it is not necessary the use of polymer standards to calibrate the equipment, since light scattering gives the absolute weight-average MW (\overline{M}_w). Light scattering detectors also measure the radius of gyration. Viscometer detectors also provide information about the intrinsic viscosity of the polymer and the level of branching (index of branching) of the polymeric chains. The more the number of detectors coupled to the GPC equipment, the more detailed is the structural and chemical information of a polymer that can be obtained.

17.3.3.5 Computer The computer automatically calculates, records, and report numerical values for \overline{M}_n , \overline{M}_w , M_v , M_z , M_{z+1} , and the MWD. It can also provide complete control of GPC systems so that large numbers of samples can be run unattended and raw data can be automatically processed. Nowadays, the software used in GPC should be capable of providing special calculations for multidetection processing, special calibration routines, polymer branching, and intrinsic viscosity determination, etc.

SEC can be used as a measure of both the size and the MW dispersity of a polymer; that is, it has the capability of finding the distribution of the sizes of polymer molecules. If standards of a known size are run previously, then a calibration curve can be created to determine the sizes of polymer molecules of interest in the solvent chosen for analysis often tetrahydrofuran (THF). Alternatively, techniques such as light scattering and/or viscometry, which do not rely on the calibration using standards of known MW, can be used online with SEC to yield absolute MWs. Because of the difference in size of two different polymers

with identical MWs, the absolute determination methods are, in general, more desirable.

17.3.3.6 Calibration In order to obtain the MW and the MWD of a polymer sample it is necessary to calibrate the equipment. To achieve this, solutions of some polymer standards of known MW and very narrow MWD are prepared by dissolving them in a suitable solvent; it is common to prepare the solution of polymer standards ("standards" for short) at a concentration of 0.1% (w/v). Two or more standards can be prepared in the same vial. In order to obtain a good calibration curve, it is recommended to run at least 10 polymer standards of MWs between 100 and 15,000,000 Da. Once the standards are injected into the GPC, the calibration curve is built plotting on the y-axis the log(MW) and on the x-axis the elution volume. The calibration curve has to be linear and is used by the equipment to obtain the different MWs of the unknown sample as well as the MWD (Fig. 17.4).

The following are the most popular narrow polymer standards for GPC: polystyrene, poly(methyl methacrylate), and poly(acrylonitrile). For samples soluble in water, the ones recommended are poly(acrylic acid), poly(ethylene glycol), poly(ethylene oxide), and poly(vinyl alcohol), among others.

17.3.3.7 Universal Calibration In the conventional calibration (described above), there is a problem when a sample that is chemically different from the standards used to calibrate the column is analyzed. However, this is a common situation; for instance, a polyethylene sample is run by GPC while the calibration curve is constructed with polystyrene standards. In this case, the MW obtained with the conventional calibration is a MW related to polystyrene, not to polyethylene. On the other hand, it is very expensive to construct calibration curves of every polymer that is analyzed by GPC. In order to solve this problem, a universal calibration technique, based on the concept of hydrodynamic volume, is used. As mentioned before, the basic principle behind GPC/SEC is that macromolecules are separated on the basis of their hydrodynamic radius or volume. Therefore, in the universal calibration a relationship is made between the hydrodynamic volume and the retention (or, more properly, elution volume) volume, instead of the relationship between MW and elution volume used in the conventional calibration. The universal calibration theory assumes that two different macromolecules will have the same elution volume if they have the same hydrodynamic volume when they are in the same solvent and at the same temperature. Using this principle and the constants K and α from the Mark-Houwink-Sakurada equation (Eq. 17.18), it is possible to obtain the absolute MW of an unknown polymer. The universal calibration principle works well with linear polymers; however, it is not applicable to branched polymers.

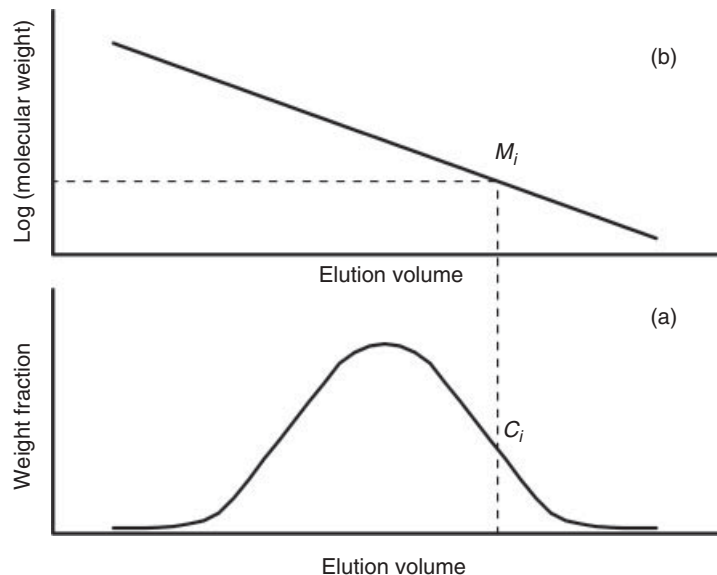


Figure 17.4 MW determination of (a) an unknown sample using (b) the calibration curve.

17.3.3.8 High Temperature Gel Permeation Chromatography (HT-GPC)

HT-GPC measures the average MW and MWD of polymers requiring higher analysis temperatures.

Typically, GPC is performed at room temperature, using THF or chloroform as solvents, demanding simple separation hardware requirements. However, there are many polymers, some of high commercial importance, such as polyolefins, nylons, or polyesters, that exhibit limited solubility at room temperature because of their high crystallinity, and therefore, their MWs can be assessed only at high temperatures, making them soluble in certain solvents, such as toluene, xylene, and 1,2,4-trichlorobenzene [22, 23]. New parameters need to be introduced in HT-GPC including polymer configuration, retention volume, MW calibration errors, solvent, polymer degradation, and column efficiency as a function of separation temperature [22–26]. Nevertheless, it is accepted that HT-GPC has the advantages of reduced analysis time and increased separation efficiency. Polymers that cannot dissolve at room temperature, especially those with a high level of crystallinity, generally require the use of high temperature and stirring in order to destroy the crystals. On cooling, the polymer will recrystallize and precipitate from the solution. For this reason, high temperature is required throughout the entire analysis to ensure that the samples remain in solution during the experiment. Thus, it is necessary that the GPC system is equipped with a column heater in order to keep the polymer in solution and to obtain reliable and reproducible results. In general, all different sections of the equipment have to be kept at high temperature to avoid the precipitation of the polymer and the blockage of the tubing due to an increase of the pressure of the system. The equipment

for HT-GPC is specially made to stand high temperatures. HT-GPC allows the measurement of average MWs and MWDs of polymers that will not dissolve in GPC solvents at conventional GPC temperatures. For analysis at high temperature, it is necessary to prepare standards at the same experimental conditions as used to prepare the normal samples; the standards commonly used for high temperatures are polystyrene and polybutadiene, among others.

The effect of the temperature on the elution peak position is presented in Figure 17.5 for eight PS standards at three different temperatures [27]. When the samples are analyzed above room temperature, the elution peak presents a shift to lower values, which is indicative of the fact that the volume of the pore is also reduced as a result of the thermal expansion of the eluent and the packing materials. As can be seen, the elution time diminishes as the temperature increases in the column, an effect which is larger for a lower MW. The magnitude of the peak gets relatively small for the higher MW samples.

It is usually reported that the width of the elution peak decreases significantly as the column temperature increases, which is attributed to the facilitated mass transfer of the polymer chains. As a result of the reduced width, a better resolution is obtained in the chromatograms when high temperature SEC is used.

Polymers Characterized by HT-GPC A number of polymers can be characterized by GPC in 1,2,4-trichlorobenzene at an elevated temperature: polyethylene, polypropylene, poly(ethylene-vinyl acetate), poly(ethylene-methyl acrylate), polyethylene propylene diamine rubber, different types of butyl rubber, and poly(phenylene oxide). In Table 17.3 are presented some common polymers, as well

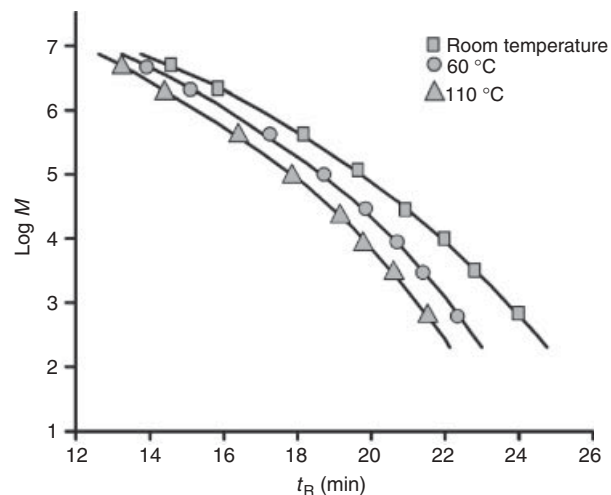


Figure 17.5 Effect of column temperatures on calibration curves of eight PS standards. *Source:* Reprinted with permission from Cho H, Park S, Ree M, Chang T, Jung JC, Zin WC. *Macromol Res* 2006;14(3):383 [27]. Copyright 2006 The Polymer Society of Korea.

as the solvents used to dissolve them; as can be observed some of them require high temperature in order to be run by GPC. Most of the rubbers can be dissolved in toluene at 75 °C. Most of the amorphous polymers can be prepared at room temperature, but semicrystalline polymers require high temperatures to be dissolved.

Branching High temperature GPC equipment generally counts with different types of detectors such as refractive index, light scattering, and viscometer, among others; using these detectors it is possible to obtain the absolute MW, and in most cases it is not necessary to construct a calibration curve. A viscometer detector also provides information about the level of branching of a polymer; in fact, using this it is possible to obtain the index of branching (g'), which is defined by the following equation [28]:

$$g' = \frac{\eta_1}{\eta_b} \quad (17.3)$$

where η_1 is the intrinsic viscosity of the linear polymer and η_b is the intrinsic viscosity of the branched polymer (of the same chemical nature and same molecular weight).

Sample Preparation A small sample of polymer is weighed (10 mg) and placed in a 15-ml stainless steel vial. Then, 10 ml of 1,2,4-trichlorobenzene is added to the vial and the sample is placed in an oven at 120 °C for 3 h. A stabilizing agent, such as Irganox 1010, should be added to the solvent to avoid degradation of the polymer during the dissolution period. Once the polymer is solubilized, a stainless steel filter is placed on top of the stainless steel vial; the filter is pushed down, thus the solution is filtered; in this step, any contaminants are removed from the solution.

TABLE 17.3 Polymers Commonly Characterized by GPC and Conditions Used in the Analysis

Solvent	Polymer
Chloroform 30 °C	ABS PB PC Poly(ethyl acrylate) PS
Chloroform/hexa-fluoroisopropanol (98/2%) 25 °C	PET PBT
Tetrahydrofuran 25 °C	PB SBR TFA
Tetrahydrofuran 30 °C	Alquidalic resins Poly(acrylonitrile-methyl methacrylate) Cellulose acetate butyrate Cellulose acetate propionate Cellulose nitrate Cellulose propionate Cellulose triacetate Epoxy resins Phenolic resins Phenol formaldehyde resins PB Polybutene Poly(butadiene-styrene) PMMA Poly(propylene glycol) PS
Toluene 75 °C	SAN Poly(styrene- α -methylstyrene) SBS PVA PVB PVC Polyisobutylene Chlorinated rubber Silicone PDMS
Toluene 30 °C	PB Polyisobutylene Polyisoprene Poly(methyl acrylate) PE Chlorinated polyethylene EVA Acid methacrylic polyethylene
1,2,4-Trichlorobenzene 140 °C	UHMWPE
1,2,4-Trichlorobenzene 145 °C	PP

Abbreviations: ABS, acrylonitrile-butadiene-styrene terpolymer; PB, polybutadiene; PC, polycarbonate; PS, polystyrene; PET, poly(ethylene terephthalate); PBT, poly(butylene terephthalate); SBR, styrene-butadiene rubber; TFA, *N*-trifluoroacetylated polyamides; PMMA, poly(methyl methacrylate); SAN, poly(styrene-acrylonitrile); SBS, poly(styrene-butadiene-styrene); PVA, poly(vinyl acetate); PVB, poly(vinyl butyral); PVC, poly(vinyl chloride); PDMS, poly(dimethyl siloxane); PE, polyethylene; EVA, poly(ethylene-vinyl acetate); UHMWPE, ultra high molecular weight polyethylene; PP, polypropylene.

After this, the sample is ready to be injected into the GPC column. The filtration of the sample can be carried out by the equipment itself (automatically) or manually by the technician. The filtered solution has to be kept at high temperature to avoid the precipitation of the polymer. Once the sample is filtered, it is ready to be run by GPC. Samples must be injected at least four times to obtain statistically valid results of the MW.

17.4 MEASUREMENT OF INTRINSIC VISCOSITY

17.4.1 Introduction

The measurement of intrinsic viscosity is simple and inexpensive when compared with other measurements related to the polymer MW. However, it can be time consuming, even if modern semiautomatic instruments are used for that purpose. As mentioned in Chapter 1, measurements of intrinsic viscosity were historically important in establishing the concept of macromolecules [29].

The determination of the intrinsic viscosity of a polymer essentially requires the measurement of the flow time of a polymer solution through a glass capillary at different solution concentrations. A polymer solution passing through a capillary obeys the Poiseuille's law for laminar flow through capillaries, which indicates that the pressure drop ΔP is directly proportional to the viscosity η of the fluid [29, 30].

$$\Delta P = k\eta \quad (17.4)$$

where $k = 8Ql/\pi r^4$. Then, the viscosity can be expressed as

$$\eta = \frac{\pi \Delta P r^4}{8lQ} \quad (17.5)$$

where η is the viscosity of the polymer solution (poise), ΔP is the pressure difference of the fluid in the capillary

(dyn/cm²), r is the capillary radius (cm), l is the capillary length (cm), and Q is the volumetric flow rate through the capillary (cm³/s).

In order to get a simpler equation, some considerations are made. The bulb volume in the viscometer is fixed; therefore, the flow rate Q is inversely proportional to the time between marks. Since ΔP is usually the hydrostatic pressure, which is proportional to the density ρ of the fluid, we have

$$\eta \propto t\rho \Rightarrow \eta = At\rho \quad (17.6)$$

where A is a constant for a particular viscometer, which may be evaluated using liquids of known viscosity; t is time, and ρ is the density of the liquid.

The above equation is valid if the whole pressure difference applied across the capillary is used in overcoming viscous forces. However, the potential energy of the liquid column imparts kinetic energy to the fluid. In order to correct the contribution of the kinetic energy, as the length of the capillary increases, the radius decreases [31, 32].

Several methods exist for characterization of the solution viscosity or, more specifically, the capacity of the solute to increase the viscosity of the solution. That capacity is quantified by using one of several different measures of solution viscosity.

17.4.2 The Ubbelohde Capillary Viscometer

The Ubbelohde viscometer is the most common type of viscometer used for the determination of the intrinsic viscosity. It was originally introduced in 1937 [33] and is shown in Figure 17.6.

For the operation of the viscometer, a polymer solution of known concentration is put in the reservoir and aspirated to the upper bulb, usually by creating some vacuum in that chamber; then air is admitted so the solution flows down the capillary by gravity. The time for the liquid to flow between

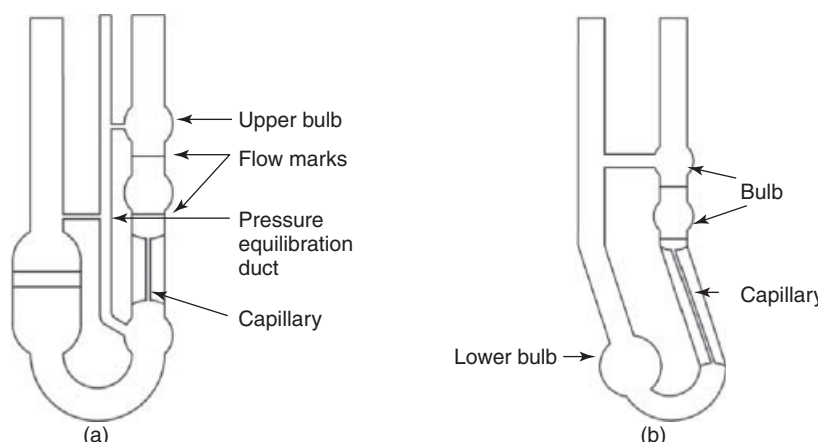


Figure 17.6 Illustration of two types of viscometers: (a) Ubbelohde and (b) Cannon–Fenske.

the two marks is recorded. This operation is repeated for increasingly dilute solutions of the same polymer/solvent. A duct parallel to the capillary allows pressure equilibration, so the flow of the fluid is only due to the hydrostatic head. Notice that the Cannon–Fenske viscometer [34] does not have the pressure equilibration duct, so it is not appropriate for accurate measurements of the intrinsic viscosity.

17.4.2.1 Measurement of the Intrinsic Viscosity The principle behind capillary viscometry is the Poiseuille's law, which states that the time of flow of a polymer solution (ps) through a thin capillary is proportional to the viscosity of the solution. The latter increases with increasing solution concentration. From Equation 17.6, the time of flow of the solvent (solv) or of the polymer solution will be proportional to the viscosity, and inversely proportional to the density:

$$t_{\text{solv}} = \frac{\eta_{\text{solv}}}{\rho_{\text{solv}}} \quad (17.7)$$

$$t_{\text{ps}} = \frac{\eta_{\text{ps}}}{\rho_{\text{ps}}} \quad (17.8)$$

It is convenient to define some terms related to the viscosity of polymer solutions:

η_r is the relative viscosity (or viscosity ratio according to the IUPAC), defined as the ratio

$$\eta_r = \frac{\eta_{\text{ps}}}{\eta_{\text{solv}}} \quad (17.9)$$

η_{sp} is the specific viscosity, which is defined as the ratio

$$\eta_{\text{sp}} = \frac{\eta_{\text{ps}} - \eta_{\text{solv}}}{\eta_{\text{solv}}} = \eta_r - 1 \quad (17.10)$$

η_{red} is the reduced viscosity (or viscosity number according to the IUPAC), which is defined as

$$\eta_{\text{red}} = \frac{\eta_{\text{sp}}}{c} \quad (17.11)$$

where c is the polymer solution concentration.

At the low polymer concentrations used in viscometry, $\rho_{\text{ps}} \approx \rho_{\text{solv}}$, therefore, from Equations 17.7–17.9, the relative viscosity becomes

$$\eta_r = \frac{t_{\text{ps}}}{t_{\text{solv}}} \quad (17.12)$$

By similar arguments, the specific viscosity can be expressed by the following equation:

$$\eta_{\text{sp}} = \eta_r - 1 = \frac{t_{\text{ps}} - t_{\text{solv}}}{t_{\text{solv}}} \quad (17.13)$$

Both η_r and η_{sp} depend on the polymer concentration. In fact, Flory proposed that the ratio η_{sp}/c (reduced viscosity) is a measure of the specific capacity of the polymer to increase the relative viscosity [35]. By extrapolating the reduced viscosity to zero concentration, the inherent properties of the polymer at hand are captured. Therefore the intrinsic viscosity is found as stated by Equation 17.14:

$$[\eta] = \lim_{c \rightarrow 0} \frac{\eta_{\text{sp}}}{c} \quad (17.14)$$

17.4.2.2 Intrinsic Viscosity The intrinsic viscosity $[\eta]$, defined by Equation 17.14, as the limiting value of the ratio of the solution's specific viscosity to the concentration of the solute as the concentration approaches zero, reflects the capability of a polymer in solution to increase the viscosity of the solution.

Kraemer defined the intrinsic viscosity as [36]

$$\frac{\ln \eta_r}{c} = [\eta] + k_1 [\eta]^2 c \quad (17.15)$$

where k_1 is known as the *Kraemer constant*.

The intrinsic viscosity (or limiting viscosity number) can be obtained by measuring the relative viscosity at different concentrations and then taking the limit of the specific viscosity when the concentration is extrapolated to zero (Fig. 17.7). The behavior of the intrinsic viscosity with concentration depends on the nature of both the specific polymer molecule and the solvent. Since the intrinsic viscosity of linear polymers is related to the MW, for linear macromolecules intrinsic viscosity measurements provide a simple method for the determination of MW when the relationship between viscosity and MW is known.

Additionally, Huggins described the relation η_{sp}/c (reduced viscosity) as [37]

$$\eta_{\text{red}} = \frac{\eta_{\text{sp}}}{c} = [\eta] + k_2 [\eta]^2 c \quad (17.16)$$

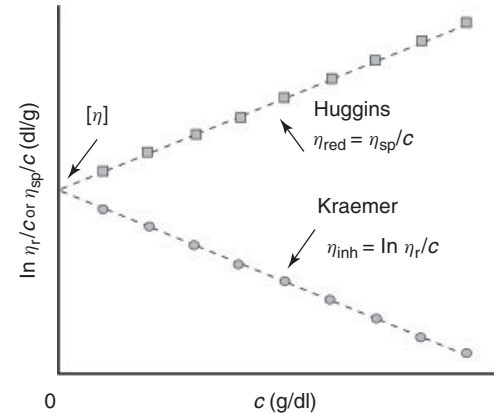


Figure 17.7 The Kraemer–Huggins plot to obtain the intrinsic viscosity, where the inherent viscosity is defined as $\eta_{\text{inh}} = \ln \eta_r/c$.

where k_2 is called the *Huggins viscosity constant* and is derived from the slope of the plot of reduced viscosity with c . This constant can be understood as a measure of solvent quality. For example, for polymers in a good solvent $k_2 \approx 1/3$, while in poor solvents k_2 values are in the range 0.5–1. Details of the values of this constant can be found in the literature [29].

The lines in Figure 17.7 come from plotting η_{red} from Equation 17.11, using Equation 17.13, for η_{sp} or plotting $[\ln(\eta_r)]/c$. The latter is also called *inherent viscosity*, η_{inh} , or logarithmic viscosity number (IUPAC). Both lines have the same intercept, which gives an estimation of $[\eta]$, the intrinsic viscosity.

Conventionally, the most common units used for concentrations in this type of measurements is g/dl (grams per deciliters, which is rather uncommon units in other fields), so $[\eta]$ is usually expressed as dl/g (units of inverse concentration according to Equation 17.14, since η_{sp} is dimensionless).

The intrinsic viscosity reflects the average interactions of single polymer molecules with the solvent and, if the molecule is considered to be spherical, $[\eta]$ is proportional to the volume of the molecule. In most of the cases, the configuration of polymer molecules in dilute solution roughly resembles a ball, whose size is characterized by the radius of gyration R_g . For polymers having a random-coil configuration, it is calculated that $R_g \propto M^{1/2}$, where M is the molar mass of the polymer. Thus, the relationship between intrinsic viscosity and molar mass is given by [38]

$$[\eta]_\theta = K_\theta M^{1/2} \quad (17.17)$$

This equation applies for polymeric solutions under “theta” conditions. Theta conditions are those at which excluded volume effects (expansion of the dimensions of the ideal coil) are exactly compensated by polymer solvent interactions (Chapter 25). The dependence between intrinsic viscosity and MW is given by the Mark-Houwink-Sakurada equation (see also Chapter 1):

$$[\eta] = K \overline{M}_v^\alpha \quad (17.18)$$

where K and α are two parameters that depend on the solvent, polymer, and temperature. Values of these coefficients for several polymers and solvents are presented in Table 17.4. More complete tables are reported in different polymer handbooks [39]. Thus, given an experimental measurement of the intrinsic viscosity in the laboratory, and the values of K and α reported in tables from the literature, one can obtain the viscosity-average molar mass of a polymer, \overline{M}_v .

The MW obtained in this way, \overline{M}_v , is higher than \overline{M}_n and lower than \overline{M}_w ; sometimes \overline{M}_v can reach values very close to \overline{M}_w . An advantage of obtaining this average MW with capillary viscosimetry is that the equipment used (the viscometer) is very inexpensive in comparison to those used in other sophisticated techniques, and the measurements of flow time are very simple; the only drawback is the time consumed to prepare the samples at different concentrations and to run the samples in the glass viscometer, repeating the measurements a certain number of times.

The constant α in the Mark-Houwink-Sakurada equation can take values between 0.5 and 0.8, depending of the

TABLE 17.4 The Mark-Houwink-Sakurada Constants for Various Polymers in Selected Solvents

Polymer	Solvent	Temperature (°C)	$K \times 10^4 [\eta]$ (dl/g)	α	References
Polybutadiene (cis/trans ≈ 0.8), 8% vinyl	Tetrahydrofuran	25	4.57	0.693	[40]
Butyl rubber	Tetrahydrofuran	25	0.85	0.75	[40]
Nylon 66	<i>m</i> -Cresol	130	0.40	1.00	[40]
Nylon 6	<i>m</i> -Cresol	25	32	0.62	[40]
Polyethylene (LDPE)	<i>o</i> -Dichlorobenzene	138	5.06	0.70	[40]
Poly(ethylene terephthalate)	<i>m</i> -Cresol	135	1.75	0.81	[40]
Poly(methyl methacrylate) atactic	Acetone	25	0.96	0.69	[39]
Poly(methyl methacrylate) isotactic	Acetone	30	2.30	0.63	[39]
Poly(dimethyl siloxane)	<i>o</i> -Dichlorobenzene	138	3.83	0.57	[40]
Polypropylene	<i>o</i> -Dichlorobenzene	135	1.30	0.78	[40]
Polypropylene atactic	Benzene	25	2.7	0.71	[39]
Polypropylene isotactic	Biphenyl	125.1	15.2	0.50	[39]
Polypropylene syndiotactic	Heptane	30	3.12	0.71	[39]
Poly(acrylic acid)	Aq. NaCl (1 M)	25	4.15	0.63	[39]
Poly(methyl acrylate)	Acetone	25	1.98	0.66	[39]
Polystyrene atactic	Benzene	25	2.27	0.72	[39]
Polystyrene isotactic	Benzene	30	0.95	0.77	[39]
Poly(vinyl acetate)	Tetrahydrofuran	25	3.50	0.63	[40]
Poly(vinyl chloride)	Tetrahydrofuran	25	1.63	0.766	[40]
SBR (25% styrene)	Tetrahydrofuran	25	4.10	0.693	[40]

configuration that the macromolecule adopts in solution. Values closer to 0.8 indicate that the polymer is in a good solvent. If constants for a specific polymer–solvent system are not reported in the literature, they can be obtained experimentally using monodisperse polymers of known MW.

If Equation 17.18 is plotted in the log–log scale, the intercept will give the value of $\log(K)$ while the slope will provide an estimate of α . The slope is related to the shape of the polymer molecules and the polymer–solvent interactions. For a polymer under theta conditions (unperturbed random coil), $\alpha = 0.5$. For a polymer in a good solvent, $\alpha = 0.8$; while for rodlike polymers $\alpha = 2$ [41]. van Krevelen [41] also provides some criteria to estimate α , which is based on the solubility parameters of the polymer and the solvent.

It is important to point out that the Mark–Houwink–Sakurada equation does not apply to polymers with low MWs, as indicated in the literature [29].

Nowadays, the new GPC hardware can have different detectors coupled, such as viscosity detectors, which allow measurements *in situ* of the intrinsic viscosity of polymers as well as the constants K and α . Using this advanced equipment, one can obtain the MW and intrinsic viscosities of polymers in a very short time.

17.4.2.3 Detailed Sample Preparation and Measurement of Intrinsic Viscosity In order to obtain the intrinsic viscosity of a polymer in a dilute solution, different concentrations of a polymer in a solvent are prepared. A small amount of polymer is weighed and dissolved in a solvent during a few hours using a stirrer in order to improve the solubility of the polymer. It is recommended to prepare at least six different concentrations of a polymer in a solvent. The highest concentration could be in the order of 30 mg in 10 ml of solvent and the rest of the concentrations should be more dilute; however, the concentrations will depend on the type of polymer. There are different ASTM (American Society for Testing and Materials) methods recommended to measure the intrinsic viscosity of different polymers.

The solutions prepared, as well as the pure solvent, should be filtered to remove any impurities that could affect the results. The filters used are generally made of Nylon, Teflon, or cellulose acetate with a pore size of less than 5 μm .

Once the solutions are prepared, a thoroughly clean capillary viscometer is introduced into a bath of water or oil at controlled temperature. The viscometer containing the pure solvent is left at least for 20 min in the bath in order to reach thermal equilibrium. Once the temperature is stable, a chronometer is used to measure the time it takes for the solvent to flow between the two marks of the viscometer. This measurement is carried out at least seven times in order to obtain the average time of flow. Once the time of the

solvent flow is measured, the solvent is removed from the viscometer and the previous procedure is repeated for the solution with the highest polymer concentration. Again, the sample is left for at least 20 min in the bath at controlled temperature and, upon reaching thermal equilibrium, the flow time measurements are carried out at least seven times in order to obtain the average flow time. The procedure is followed for all the polymeric solutions prepared. Once the flow times of the solvent and of the different solutions are registered, the data are plotted as described in the previous section. The inherent or reduced viscosity is plotted against concentration, and from the linear plot obtained, the intrinsic viscosity is obtained using the Huggings or Kraemer equations. Intrinsic viscosity is obtained by the extrapolation of the curve obtained to zero concentration (intercept with the y -axis). The plot obtained should be a straight line; if the curve obtained is not a straight line, more dilute solutions of the polymer should be prepared and the measurements repeated to obtain a linear behavior.

The intrinsic viscosity is commonly used in several polymer industries for estimation of the MW of certain polymers, especially poly(ethylene terephthalate) (PET) or Nylon. Once the intrinsic viscosity is known, the viscosimetric MW (\overline{M}_v) of the polymer can be obtained using the values of K and α reported in the literature [39].

REFERENCES

1. Tswett M. Ber Deutsch ot Ges 1906;24:316.
2. Abraham MH. J Chromatogr A 2004;1061:113.
3. Mainhard JE. Science 1949;110:387.
4. Kuhn R, Lederer E. Naturwissenschaften 1931;19(14):306.
5. Moore JC, inventors; The Dow Chemical Company, assignee. US patent 3326875. 1963.
6. Lathe GH, Ruthven CRJ. Biochem J 1956;62:665.
7. Moore JC. J Polym Sci A 1964;2(2):835.
8. Schroder E, Muller G, Arndt KF. *Polymer Characterization*. 1st ed. New York: Hanser Verlag; 1989. p 167.
9. Grubisic Z, Benoit H, Rempp P. J Polym Sci Polym Lett 1967;5(9):753.
10. Sun T, Chance RR, Graessley WW, Lohse DJ. Macromolecules 2004;378(11):4304.
11. Sperling LH. *Introduction to Physical Polymer Science*. 2nd ed. New York: John Wiley and Sons Inc.; 1992. p 91.
12. Bender M. J Chem Educ 1952;29(1):15.
13. Rubin RJ. J Chem Phys 1972;56:5747.
14. Wei G. Macromolecules 1997;30(7):2125.
15. Chance RR, Banluklewickz SP, Mintz D, Strate GV, Hadjichristidis N. Int J Polym Anal Charact 1995;1(1):3.
16. Boyd RH, Chance RR, Strate GV. Macromolecules 1996; 29(4):1182.
17. Otocka EP. J Chromatogr A 1973;76(1):149.

366 POLYMER MOLECULAR WEIGHT MEASUREMENT

18. McCormick HW, Brower FM, Kin L. *Polym Chem* 1959; 39(135):87.
19. Gehman SD. *Ind Eng Chem* 1952;44(4):730.
20. Montfort JP, Marin G, Monge P. *Macromolecules* 1986; 19(7):1979.
21. Fetters LJ, Lohse DJ, Richter D, Witten TA, Zirkel A. *Macromolecules* 1994;27(17):4639.
22. Sadao M, Susuki T. *Anal Chem* 1980;52(11):1625.
23. Holding SR, Vlachogiannis G, Barker PE. *J Chromatogr A* 1983;261:33.
24. Yamamoto S, Nomura M, Sano Y. *J Chromatogr A* 1987; 394(2):363.
25. Renn CN, Synovec RE. *Anal Chem* 1992;64:479.
26. Antia FD. Csaba Horváth. *J Chromatogr A* 1988;435:1.
27. Cho H, Park S, Ree M, Chang T, Jung JC, Zin WC. *Macromol Res* 2006;14(3):383.
28. Zimm BH, Stockmayer WH. *J Chem Phys* 1949;17: 1301.
29. Barth HG, Mays JW. *Modern Methods of Polymer Characterization*. 1st ed. New York: Wiley; 1991. p 2321.
30. Striegel AM, Yau WW, Kirkland JJ, Bly DD. *Modern Size-Exclusion Liquid Chromatography*. 1st ed. New York: John Wiley & Sons; 1979. p 163.
31. Cannon MR, Manning RE, Bell JD. *Anal Chem* 1960;32(3): 355.
32. Wagner RH. *Anal Chem* 1948;20(2):155.
33. Ubbelohde L. *Ind Eng Chem Anal Ed* 1937;9(2):85.
34. Cannon MR, Fenske MR. *Ind Eng Chem Anal Ed* 1938; 10(6):297.
35. Flory PJ. *Principles of Polymer Chemistry*. New York: Cornell University Press; 1953. p 309.
36. Kraemer EO. *Ind Eng Chem* 1938;30(10):1200.
37. Huggins ML. *J Am Chem Soc* 1942;64:2716.
38. Flory PJ. *Principles of Polymer Chemistry*. New York: Cornell University Press; 1953. Chapter 10.
39. Brandrup J, Immergut EH, Grulke EA, editors. *Polymer Handbook*. 4th ed. New York: Wiley; 1999.
40. Evans JM. *Polym Eng Sci* 1973;13(6):401.
41. van Krevelen DW, te Nijenhuis K. *Properties of Polymers*. 4th ed. Amsterdam: Elsevier; 2009.

18

LIGHT SCATTERING AND ITS APPLICATIONS IN POLYMER CHARACTERIZATION

ROBERTO ALEXANDER-KATZ

18.1 INTRODUCTION

Electromagnetic scattering phenomena occur when an electromagnetic field interacts with a medium that is heterogeneous at a scale of the wavelength of the incident field; that is, a material might look perfectly homogenous to the eye, however, when a laser beam goes across it, light will scatter in all directions other than those given by the refraction and reflection laws. Examples of this can be found in simple liquids such as highly clarified benzene or carbon disulfide, where density fluctuations at the scale of the wavelength of visible light give rise to scattering that is observable by the naked eye. In the case of polymer solutions or particle suspensions, the local fluctuations in the dielectric constant take place due to fluctuations in local concentration as well as the density fluctuations. The analysis of such fluctuations gave rise to two popular applications of this technique: the determination of molecular weights and sizes of macromolecules by static light scattering (SLS) and particle sizing by dynamic light scattering (DLS). However, light scattering together with its sister techniques, namely, small-angle X-ray scattering (SAXS), small-angle neutron scattering (SANS), and inelastic neutron scattering (INS), can give more information about the structure of the scattering objects, the thermodynamics, and the dynamic processes taking place in complex systems.

In this chapter, we emphasize on the principles in which light scattering methods are founded and apply these to different systems. We also stress the importance of a solid

theoretical framework in the field of polymers or other complex systems in expanding the scope of applications of these tools beyond the standard applications.

Unfortunately, because of space, we have not covered important new developments in light scattering for the study of nontransparent systems such as diffusion wave spectroscopy (DWS), fiber-optic quasi-elastic light scattering (FOQELS), dual-color cross-correlation, 3D cross-correlation DLS, and improved techniques followed from these techniques [1–4].

In the first section, we introduce the general theory of light scattering. The second section is devoted to SLS, and we give some examples of its application. In the third section, we discuss the principles of DLS and we apply these to the study of the dynamics of different systems, whether dilute or concentrated solutions.

18.2 PRINCIPLES OF STATIC AND DYNAMIC LIGHT SCATTERING

Let us consider an electromagnetic field incident on a small volume element on the order of λ^3 , where λ is the wavelength of light in the material (solution, particle suspension, etc.); due to the imbalance of the molecules that enter and leave such volume, there will be fluctuations in density, concentration, and others that concomitantly will produce fluctuations in the local dielectric constant. Let us denote by $\Delta\epsilon(\mathbf{R}, t)$ the deviation of the dielectric constant from its mean $\langle\epsilon\rangle$ at \mathbf{R} and time t . Since these

fluctuations are in most cases very small, we can assume that the scattered electric field E_s will be proportional to $\Delta\epsilon$ and to the incident electric field E_0 ; that is,

$$E_s \approx \Delta\epsilon(\mathbf{R}, t) E_0 \quad (18.1)$$

However, in the scattering volume V , there are a great number of volume elements that contribute to the total scattered electric field. If $\Delta\epsilon(\mathbf{R}, t)$ is very small, we can consider that each molecule in V is sensing the same incident field, and therefore, we can write the scattering field just as a superposition of the fields coming from all elements of our scattering volume. This approximation is called the *Rayleigh-Debye-Gans approximation (RDGA)* and is valid when $\Delta\epsilon \ll 1$ and the phase shifts induced by the fluctuations are very small [5]. This is the case of any simple fluid or solution away from its critical point (or critical line). However, there are cases where these conditions are not met, such as a suspension of latex particles where the refractive index of the particles differs substantially from that of the suspending fluid. In the latter case, the internal field at any point in the domain is not the same as the applied field, and one has to consider the contribution of all elements in the domain. There are several approaches to this end, some analytical, such as Mie's theory for spheres and cylinders, and others numerical for particles with no particular symmetries, such as the T-matrix theory [6, 7]. However, for most of the classical light scattering applications to polymer characterization in solution, the RDGA is fully satisfied, and therefore, we discuss it thoroughly in what follows. In any case, we will point out along the chapter whenever a Mie-type calculation is required.

The measured quantity is the intensity of the scattered field, that is, the square of the scattered field,

$$I_s = E_s \cdot E_s^* \quad (18.2)$$

Therefore, the total scattered intensity will be the sum of the cross products of the scattered electric fields from different volume elements. Yet, these fields can interfere between each other in view that they might be out of phase, due to the difference in optical paths, and the motion of the molecules can induce frequency changes. This leads finally to an expression for the scattered intensity

$$I_s(\mathbf{q}, \Delta\omega) \approx I_0 \iint \langle \Delta\epsilon(\mathbf{R}, t) \Delta\epsilon^*(\mathbf{R}', 0) \rangle \exp(-i[\mathbf{q}(\mathbf{R} - \mathbf{R}') + (\omega - \omega_0)t]) d\mathbf{R} d\mathbf{R}' dt \quad (18.3)$$

where I_0 is the incident intensity and

$$\mathbf{q} = \mathbf{k} - \mathbf{k}' \quad (18.4)$$

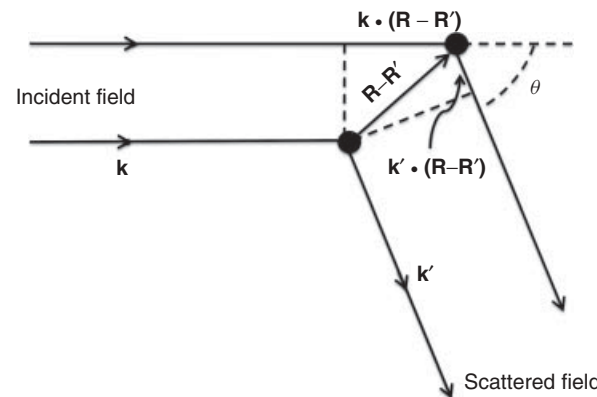


Figure 18.1 Schematics of the changes in optical paths.

while \mathbf{k} and \mathbf{k}' are the wave vectors of the incident and scattered fields, respectively, as shown in Figure 18.1. From this figure, it can be seen that $\mathbf{q} \cdot (\mathbf{R} - \mathbf{R}')$ corresponds to the difference in optical paths between the fields that are scattered by two molecules that are $\mathbf{R} - \mathbf{R}'$ apart. We have added average brackets to the product of the local dielectric constant differences (dielectric constant correlation function) since these are varying randomly, and therefore, we only observe an average in a typical measurement.

A formal derivation of Equation 18.3 leads to [8]

$$I_s(\mathbf{q}, \Delta\omega) = \frac{I_0 V k^4 \sin^2 \alpha}{32\pi^3 \epsilon_0^2 r^2} \iint \langle \Delta\epsilon(\mathbf{R}, t) \Delta\epsilon^*(\mathbf{R}', 0) \rangle \exp(-i[\mathbf{q} \cdot \mathbf{R} + \Delta\omega t]) d\mathbf{R} dt \quad (18.5)$$

where it has been made use of translational invariance; k is the wavenumber ($2\pi/\lambda$) in the medium, ϵ_0 is the vacuum dielectric constant, r is the distance from the scattering volume to the observer, and α is the angle of observation relative to the linearly polarized incident field, as shown in Figure 18.2. The r dependence arises because any element of the scattering volume is a source of spherical waves, and the irradiance of a point source decays as $1/r^2$. The $\sin^2 \alpha$ factor comes from the transversal nature of the electromagnetic waves; that is, for a vertically polarized incident beam, the only component of the field that will propagate in the direction shown in Figure 18.2 will be $\approx \sin \alpha$, and therefore, the scattered intensity will be $\approx \sin^2 \alpha$. Finally, Rayleigh has shown that the light scattered by any small volume element (as compared to λ) should scale as $1/\lambda^4 \approx k^4$ [9]. All these front factors are related to the instrument and not to the optical properties of the sample. For a given instrument, we will only vary the scattering angle θ .

If the detecting system does not have any device that can resolve the frequency (or time) dependence of I_s , such as

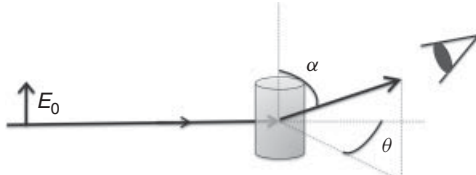


Figure 18.2 Scattering geometry.

a correlator, Fabry–Perot interferometer, or, as discussed later, if the setup of the detecting system is not appropriate to observe the intensity fluctuations with time, then this will be equivalent to integrating over all frequencies, and Equation 18.5 reduces to

$$I_s(\mathbf{q}) = \frac{I_0 V k^4 \sin^2 \alpha}{16\pi^2 \epsilon_0^2 r^2} \int \langle \Delta\epsilon(\mathbf{R}) \Delta\epsilon^*(\mathbf{0}) \rangle \exp(-i\mathbf{q} \cdot \mathbf{R}) d\mathbf{R} \quad (18.6)$$

In this case, we will be speaking of SLS since time is not involved any more. Equation 18.6 actually represents the point of departure of the classical light scattering applications: the determination of molecular weights and radius of gyration of polymer molecules. Since

$$|\mathbf{q}| = \frac{4\pi}{\lambda} \sin \frac{\theta}{2} \quad (18.7)$$

this means that varying the angle is equivalent to changing the wavelength. This fact makes scattering a unique technique because we can change the scale of our probe (wavelength) by simply observing our sample at a different angle. As we approach the incoming beam, θ becomes very small, and this is equivalent to having a large effective wavelength of

$$\lambda_{\text{eff}} = \frac{\lambda}{\sin(\theta/2)} \quad (18.8)$$

If instead of light we use an X-ray source, the only difference from the previous discussion is that we will substitute the fluctuations in the dielectric constant by the fluctuations in the electronic density. X-ray wavelength is typically on the order of 1.5 Å. However, if we perform SAXS at angles of the order of 2 min from the incoming beam, it would be equivalent to change the scale of our probe by more than 3400 times! This means that using the *same* wavelength, the scale of our probe can change from 1.5 to 5100 Å, overlapping the visible region of the electromagnetic spectrum. This allows us to explore our material in a wide range of scales without having absorption effects, as is the case with spectroscopic techniques. All this can be extended to neutron sources with the difference that instead of electron clouds, neutrons interact with the nucleus of the atoms and the magnetic fields of their impaired electrons. Thermal neutron sources have equivalent wavelength as X-rays, and therefore, neutron

scattering at small angles (SANS) is a powerful tool to explore condensed matter in a wide range of scales. Neutrons, X-rays, and light scattering are complementary techniques very much used in the study of polymers in solution or in solid state [10, 11].

Since both Equations 18.5 and 18.6 depend on instrumental variables, it is customary to introduce the so-called Rayleigh ratio R_θ , so that the results are independent of the geometry and intensity of the light source used; that is,

$$R_\theta = I_s(\mathbf{q}) \frac{r^2}{V I_0 \sin^2 \alpha} = \frac{k^4}{16\pi^2 \epsilon_0^2} \int \langle \Delta\epsilon(\mathbf{R}) \Delta\epsilon^*(\mathbf{0}) \rangle \exp(-i\mathbf{q} \cdot \mathbf{R}) d\mathbf{R} \quad (18.9)$$

In Equation 18.9, we observe two competing factors: $\langle \Delta\epsilon(\mathbf{R}) \Delta\epsilon^*(\mathbf{0}) \rangle$ and the interference factor $\exp(-i\mathbf{q} \cdot \mathbf{R})$. The dielectric constant correlation function will tend to be zero for distances greater than the correlation length ξ . For dilute systems, this length is related to a characteristic length of the heterogeneities in the system, such as the particle size or the radius of gyration of a macromolecule. On the other hand, $|\mathbf{q}|^{-1}$ is proportional to the effective scale ($\lambda/\sin(\theta/2)$) with which we are probing our system. The ratio between these two lengths defines differences between the theoretical approaches for the calculation of Equation 18.9. In the limiting case of $q^{-1}/\xi \gg 1$ that corresponds to $\theta \rightarrow 0$, the particles or macromolecules will appear as points without structure since the scale of observation is much larger than their own size, as shown schematically in Figure 18.3. We will call this as the *thermodynamic limit* because the excess of light scattered is due to the imbalance between the incoming and exit of the macromolecules or particles *as a whole* in a volume element of the order of q^{-3} , that is, due to the local fluctuations in the number of molecules in the system, which is a thermodynamic variable.

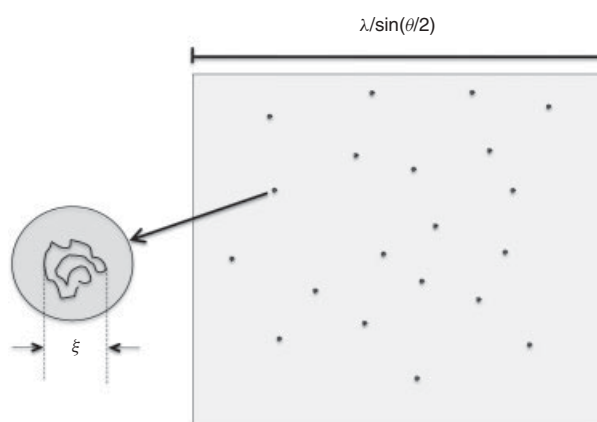


Figure 18.3 Small-angle limit. In this limit, all macromolecules appear as point particles compared to the volume probed.

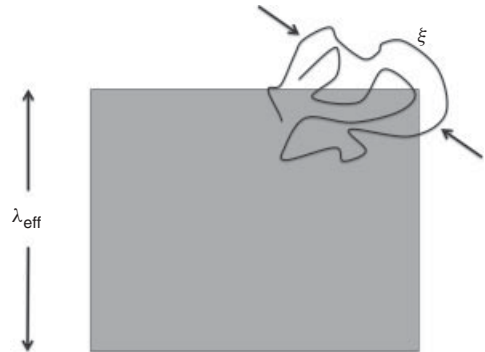


Figure 18.4 When ξ is of the order of magnitude of or greater than the effective wavelength, the *partial* entrance of the macromolecule or particle will produce fluctuations in the scattered intensity.

On the other hand, if $q^{-1} \approx \xi$, the excess in the fluctuations is due to the imbalance between the entrance and exit of a *fraction* of a macromolecule (or particle) as shown schematically in Figure 18.4. The latter is not a thermodynamic variable, and for these values of q , the scattering will be sensitive to the *structure* of the macromolecule.

In the next two sections, we discuss the SLS by dilute polymer solutions in both cases: in the limit of small angles and when q^{-1} is of the order or smaller than ξ .

The theory of thermodynamic fluctuations in the context of light scattering was introduced first by Smoluchowski and Einstein [12, 13]. Einstein considered that the scattering of light in a solution arises from local density and concentration fluctuations. However, it was only till the late 40s and early 50s that Brinkman and Hermans [14], Stockmayer [15], and Kirkwood and Goldberg [16] adopted this approach in the context of light scattering by polymer solutions. Here, we summarize only the basic results for a binary mixture.

In a binary mixture, there are 3 degrees of freedom and it can be proved that the fluctuations in the dielectric constant can be reduced to the sum of the fluctuation in the density of the pure solvent plus the fluctuations in the molar concentration of macromolecules,

$$\langle(\Delta\epsilon)^2\rangle = \left(\frac{\partial\epsilon}{\partial\rho_s}\right)^2 \langle(\Delta\rho_s)^2\rangle + \left(\frac{\partial\epsilon}{\partial N_1}\right)^2 \langle(\Delta N_1)^2\rangle \quad (18.11)$$

where ρ_s is the density of the pure solvent and N_1 is the number of moles of the solute. However, the first term corresponds to the contribution of the light scattered by the solvent and can be measured independently. Therefore, if we subtract this term from $\langle(\Delta\epsilon)^2\rangle$, we will obtain the excess in the fluctuation in the dielectric constant due to the fluctuation in concentration of the solute, that is,

$$\langle(\Delta\epsilon)^2\rangle_{\text{ex}} = \left(\frac{\partial\epsilon}{\partial N_1}\right)^2 \langle(\Delta N_1)^2\rangle = \left(\frac{\partial\epsilon}{\partial N_1}\right)^2 \frac{k_B T}{(\partial\mu_1/\partial N_1)}_{\text{TP}} \quad (18.12)$$

where μ_1 is the chemical potential of the solute and k_B is the Boltzmann constant. If we write this expression in terms of the solute weight concentration c_1 (in g/cc), then

$$\begin{aligned} \langle(\Delta\epsilon)^2\rangle_{\text{ex}} &= \frac{M_1}{N_A V} \left(\frac{\partial\epsilon}{\partial c_1}\right)^2 \frac{k_B T}{(\partial\mu_1/\partial c_1)}_{\text{TP}} \\ &= \frac{k_B T c_1}{N_0 V_0} \left(\frac{\partial\epsilon}{\partial c_1}\right)^2 \frac{1}{(\partial\pi/\partial c_1)}_{\text{TP}} \end{aligned} \quad (18.13)$$

where N_0 is the number of moles of the solvent, V_0 is the molar volume of the solvent, and π is the osmotic pressure. Hence, the excess Rayleigh factor will be

$$R_\theta^{\text{ex}} = \frac{k^4 k_B T c_1}{16\pi^2 \epsilon_0^2} \left(\frac{\partial\epsilon}{\partial c_1}\right)^2 \frac{1}{(\partial\pi/\partial c_1)}_{\text{TP}} \quad (18.14)$$

where we have made the approximation $N_0 V_0 \approx V$ since we are in the limit of dilute solution. Equation 18.14 establishes a relation between light scattering and the osmotic pressure, valid in the limit $\theta \rightarrow 0$. This relation constitutes the basis for the determination of the molecular weight and other thermodynamic properties by light scattering.

$$R_\theta = \frac{k^4 V}{16\pi^2 \epsilon_0^2} \langle(\Delta\epsilon)^2\rangle \quad (18.10)$$

Using the virial expansion for the osmotic pressure, we can write π as

$$\pi = RTc_1 \left(\frac{1}{M} + A_2 c_1 + A_3 c_1^2 + \dots \right) \quad (18.15)$$

where A_2, A_3, \dots are the virial coefficients. Then,

$$R_\theta^{\text{ex}} = \frac{k^4 c_1}{16\pi^2 \varepsilon_0^2} \left(\frac{\partial \varepsilon}{\partial c_1} \right)^2 \frac{1}{N_A (1/M + 2A_2 c_1 + \dots)} \quad (18.16)$$

It is common to regroup all constants into one constant as¹

$$K = \frac{4\pi^2}{\lambda^4 N_A} \left[n_0 \left(\frac{\partial n}{\partial c_1} \right) \right]^2 \quad (18.17)$$

where n and n_0 are the refractive indexes of the solution and the solvent, respectively, and we have used the relation $n = \sqrt{(\varepsilon/\varepsilon_0)}$. Equation 18.16 then takes the form

$$\frac{K c}{R_\theta^{\text{ex}}} = \frac{1}{M} + 2A_2 c_1 + 3A_3 c_1^2 + \dots \quad (18.18)$$

The generalization of Equation 18.18 to polydisperse homopolymers is

$$\frac{K c}{R_\theta^{\text{ex}}} = \frac{1}{\langle M \rangle_w} + 2 \langle A_2 \rangle_w c + \dots \quad (18.19)$$

where c is the polymer concentration (in g/cc) and $\langle M \rangle_w$ and $\langle A_2 \rangle_w$ are given by

$$\langle M \rangle_w = \sum_i M_i w_i \quad (18.20)$$

and

$$\langle A_2 \rangle_w = \frac{1}{\langle M \rangle_w^2} \sum_i \sum_j M_i M_j A_{ij} w_i w_j \quad (18.21)$$

where w_i and M_i are the weight fraction and molecular weight of species i , respectively. The difference between a direct determination of the molecular weight by osmometry and that with light scattering is that they average differently. The former averages number wise while the latter does it by weight. This also applies to the virial coefficients. Furthermore, in Equation 18.16, there is a front factor $(\partial \varepsilon / \partial c_i)^2$ for each species, which in the case of homopolymers are the same, independently of molecular weight, and can be

¹This expression for K is valid for vertically polarized light. In what follows in this chapter, we assume that the incident field is vertically polarized and that we are observing in the plane of incidence, that is, $\sin \alpha = 1$. For light that is polarized horizontally, Equation 18.17 should have a factor $\cos^2 \theta$, and for unpolarized light, the factor should be $(1 + \cos^2 \theta)/2$.

factored out as in Equation 18.19. However, if the species in question differ also in composition, the $(\partial \varepsilon / \partial c_i)^2$ term will be different for each species and cannot be factored out, giving rise to an apparent molecular weight as in the case of copolymers. The same occurs when we have a solution of mixed solvents and a homopolymer; again the extrapolation at $c \rightarrow 0$ and $\theta \rightarrow 0$ will give rise to an apparent molecular weight because of the preferential sorption of each solvent component in the polymer molecule [17]. In these cases, different authors have proposed alternative methodologies to determine the weight-average molecular weight [18–20]. To illustrate this, let us consider the case of copolymers. If we define the K_i as

$$K_i = K^* \left(\frac{\partial n}{\partial c_i} \right)^2 \Big|_{c=0} = K^* v_i^2 \quad (18.22)$$

where

$$K^* = \frac{4\pi^2 n_0^2}{N_A \lambda^4} \quad (18.23)$$

and

$$v_i = \left(\frac{\partial n}{\partial c_i} \right) \Big|_{c=0} \quad (18.24)$$

Then,

$$\frac{K^* v^2 c}{R_\theta^{\text{ex}}} \Big|_{\substack{c \rightarrow 0 \\ \theta \rightarrow 0}} = \frac{1}{\frac{1}{v^2} \sum_i \frac{c_i}{c} M_i v_i^2} = \frac{1}{M_{\text{app}}} \quad (18.25)$$

where c is the concentration of the copolymer in the solution and v is the specific increment in the refractive index of the copolymer solution extrapolated to $c \rightarrow 0$. This means that if we followed the same procedure as with homopolymers, we are actually measuring a molecular weight given by

$$M_{\text{app}} = \frac{1}{v^2} \sum_i \frac{c_i}{c} M_i v_i^2 \quad (18.26)$$

Since v_i depends of the solvent used, the molecular weight determined in this way is necessarily apparent.

If we assume that the specific refractive index increments follow a weight sum rule, then for copolymers made of two monomers A and B, the relationship between M_{app} and $\langle M \rangle_w$ can be expressed as

$$M_{\text{app}} = \left(\frac{v_A v_B}{v^2} \right) \langle M \rangle_w + \left[\frac{v_A (v_A - v_B)}{v^2} \right] W \langle M_A \rangle_w + \left[\frac{v_B (v_B - v_A)}{v^2} \right] (1 - W) \langle M_B \rangle_w \quad (18.27a)$$

$\langle M_A \rangle_w$ and $\langle M_B \rangle_w$ being the weight averages of the components A and B of the copolymer, respectively, while v_A and v_B are the specific refractive index increments of the solution with homopolymer types A and B, respectively. W is the average weight fraction of A in the copolymer. The relationship can alternatively be expressed as

$$M_{\text{app}} = \langle M \rangle_w + 2P \left(\frac{v_A - v_B}{v} \right) + Q \left(\frac{v_A - v_B}{v} \right)^2 \quad (18.27b)$$

P and Q are given by

$$P = \sum_i \frac{c_i}{c} M_i \delta W_i \quad (18.28)$$

$$Q = \sum_i \frac{c_i}{c} M_i (\delta W_i)^2 \quad (18.29)$$

with $\delta W_i = W_i - W$, where W_i is the weight fraction of monomer A in the copolymer of the species i .

According to Equation 18.27b, the molecular weight measured depends on $\langle M \rangle_w$ as well as on the first two moments of the distribution in composition. In principle, by index matching with a single solvent, we could obtain $\langle M \rangle_w$, $\langle M_A \rangle_w$, $\langle M_B \rangle_w$, and Q .

A common procedure to determine $\langle M \rangle_w$ is to perform several light scattering experiments to measure M_{app} with different solvents with a reasonably range of values of $(v_A - v_B)/v$ and finally obtain by regression methods the parameters of the parabola in Equation 18.27b. The latter procedure will provide not only $\langle M \rangle_w$ but also P and Q , which give us information about the first two moments of the distribution in composition. However, to have a reasonable accuracy, at least v_A or v_B should be large in order to increase the overall intensity of the scattered light. Unfortunately, it is difficult to find a one-component solvent to index match or fulfill the requirements of the regression method. Therefore, we are forced to use mixed solvents, which in turn will add an extra complication due to preferential sorption. Casassa and Eisenberg have shown that in the case of mixed solvents, we can use one-component solvent light scattering relationships if we substitute the conventional refractive index increment measured at constant composition of the mixed solvents by v 's measured at constant chemical potential (v_μ) for all diffusible components of the solvent, that is, after the establishment of osmotic equilibrium between the polymer solution and the polymer-free mixed solvents [21, 22]. The experimental procedures to determine v_μ 's are described by Tuzar et al. [23, 24]. A thorough test of the Bushuk–Benoit theory was conducted by Podešva et al. [25].

On the other hand, since, in the case of mixed solvent, light scattering is sensitive to preferential sorption by polymers, it has been used as a tool in the study of

such important phenomena [26–33]. An elegant example of the study of preferential sorption by light scattering is that of Marchal and Strazielle who studied the thermal transitions from coil to helix of poly(L-benzyl glutamate) in a mixture of dichloro acetic acid (DCA) and heptane; they found an unusual variation in the apparent molecular weight (Fig. 18.5) as the conformation changed from coil to helix, indicating that the helical structure adsorbed fewer DCA molecules than the coiled form [32].

Finally, as per Equation 18.27b, if a copolymer has a very narrow composition distribution, M_{app} will be very close to $\langle M \rangle_w$ using a single solvent; the same applies to mixed solvents if we follow the procedure mentioned earlier. This can be the case, for instance, of a radical copolymerization in a true azeotrope composition or of a block copolymer synthesized by a controlled anionic or living radical polymerization.

18.3.2 Application of SLS for the Determination of Structure When $|q \xi| \geq 1$

In this section, we discuss the application of the RDGA for arbitrary q 's. When the scale with which we are probing our system is on the order of the radius of gyration of our macromolecule (Fig. 18.4), the calculation of $\langle \Delta\epsilon(\mathbf{R})\Delta\epsilon(\mathbf{0}) \rangle$ will not reduce to the thermodynamic fluctuations since the number of monomers in a volume element is not a thermodynamic variable and, additionally, in this case, $\exp(-i\mathbf{q} \cdot \mathbf{R})$ is an oscillating function in the probing volume element.

However, we can still follow the steps from the previous section if we assume that the dielectric constant depends on \mathbf{R} through the local volume fraction occupied by the solvent $\varphi(\mathbf{R})$, the number of monomers in that volume element $N_1(\mathbf{R})$, and the local temperature $T(\mathbf{R})$, that is,

$$\varepsilon(\mathbf{R}) = \varepsilon [\varphi(\mathbf{R}), N_1(\mathbf{R}), T(\mathbf{R})] \quad (18.30)$$

Here, $\varphi(\mathbf{R})$ and $T(\mathbf{R})$ are the thermodynamic variables, while $N_1(\mathbf{R})$ is not. However, we can still assume that $N_1(\mathbf{R})$ is not correlated with $\varphi(\mathbf{R})$ and $T(\mathbf{R})$ and thus calculate the excess in the fluctuations in the dielectric constant as

$$\langle \Delta\epsilon(\mathbf{R})\Delta\epsilon(\mathbf{R}') \rangle_{\text{ex}} = \left(\frac{\partial \varepsilon}{\partial N_1} \right)^2 \langle \Delta N_1(\mathbf{R})\Delta N_1(\mathbf{R}') \rangle \quad (18.31)$$

We can write Equation 18.31 in terms of the number density of monomers $\rho_1 = N_1/V$ as

$$\langle \Delta\epsilon(\mathbf{R})\Delta\epsilon(\mathbf{R}') \rangle_{\text{ex}} = \left(\frac{\partial \varepsilon}{\partial \rho_1} \right)^2 \langle \Delta\rho_1(\mathbf{R})\Delta\rho_1(\mathbf{R}') \rangle \quad (18.32)$$

The Fourier transform of correlation function of the local number densities of monomers can be written in terms of

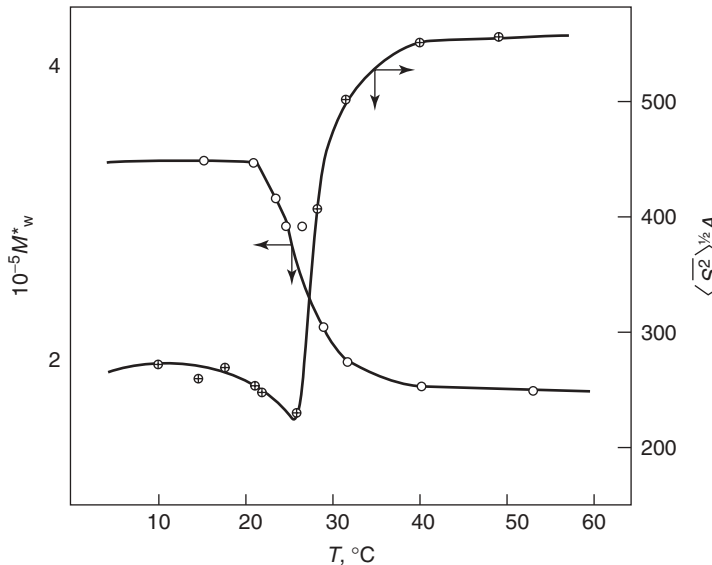


Figure 18.5 Helix–coil transitions of poly(L-benzyl glutamate) in a mixture of dichloroacetic acid and heptane showing the variation of the apparent molecular weight (M_w^* in their notation) and the radius of gyration. Source: Reprinted with permission from Cowie JMG. *Pure Appl Chem* 1970;23:355 [33]. Copyright 1970 International Union of Pure and Applied Chemistry (after Marchal E, Strazielle C. *Compt Rendu* 1968;C267:135. Academie Française de Science).

$G(\mathbf{R}, c)$, the joint probability of finding any monomer at \mathbf{R} when any other is at the origin, as

$$\begin{aligned} & \iint \langle \Delta\rho_1(\mathbf{R}) \Delta\rho_1(\mathbf{R}') \rangle \exp(-i\mathbf{q}[\mathbf{R} - \mathbf{R}']) d\mathbf{R} d\mathbf{R}' \\ &= nN_p \int (G(\mathbf{R}, c) - \langle \rho_1 \rangle) \exp(-i\mathbf{q} \cdot \mathbf{R}) d\mathbf{R} \quad (18.33) \end{aligned}$$

where n is the number of monomers per chain, N_p is the number of polymer chains, and $\langle \rho_1 \rangle$ is the average number density of monomers. We have explicitly written the dependence of $G(\mathbf{R}, c)$ on polymer concentration because the average $\langle \Delta\rho_1(\mathbf{R}) \Delta\rho_1(\mathbf{R}') \rangle$ depends on the actual polymer concentration. It is common to divide $G(\mathbf{R}, c)$ in terms of the intramolecular and the intermolecular contributions, $G_{\text{intra}}(\mathbf{R}, c)$ and $G_{\text{inter}}(\mathbf{R}, c)$, respectively, as

$$G(\mathbf{R}, c) = G_{\text{intra}}(\mathbf{R}, c) + G_{\text{inter}}(\mathbf{R}, c) \quad (18.34)$$

where $G_{\text{intra}}(\mathbf{R}, c)$ is the joint probability of finding any monomer at \mathbf{R} when any other of the *same* macromolecule is at the origin, while $G_{\text{inter}}(\mathbf{R}, c)$ is the joint probability of finding any monomer at \mathbf{R} when any monomer of a *different* macromolecule is at the origin.

Substituting Equations 18.32, 18.33 and 18.34 into Equation 18.9, we obtain a generalization of the Rayleigh ratio of a monodisperse sample for an arbitrary q and

polymer concentration as

$$\begin{aligned} \frac{R_\theta^{\text{ex}}}{Kc} &= M \left\{ \frac{1}{n} \int G_{\text{intra}}(\mathbf{R}, c) \exp(-i\mathbf{q} \cdot \mathbf{R}) d\mathbf{R} \right\} \\ &+ N_A c \left\{ \int (g_{\text{inter}}(\mathbf{R}, c) - 1) \exp(-i\mathbf{q} \cdot \mathbf{R}) d\mathbf{R} \right\} \quad (18.35) \end{aligned}$$

where $g_{\text{inter}}(\mathbf{R}, c) = G_{\text{inter}}(\mathbf{R}, c) / \langle \rho_1 \rangle$ and c is the concentration in g/ml of the polymer in the solution. In dilute solutions, the only relevant correlation length is related to the size of a single polymer chain, and therefore, the only surviving correlation function will be $G_{\text{intra}}(\mathbf{R}, c)$. In the dilute limit, to first order in concentration, Equation 18.35 reduces to the well-known result [34]

$$\frac{Kc}{R_\theta^{\text{ex}}} = \frac{1}{M P(\theta)} + 2A_2 c + \dots \quad (18.36)$$

where $P(\theta)$ is the normalized Fourier transform of $G_{\text{intra}}(\mathbf{R}, c)$,

$$P(\theta) = \frac{1}{n} \int G_{\text{intra}}(\mathbf{R}) \exp(-i\mathbf{q} \cdot \mathbf{R}) d\mathbf{R} \quad (18.37)$$

usually called the *form factor*. Equation 18.36 contains information on solution properties (polymer molecular weight, second virial coefficient, and so on) as well as structural information contained in $P(\theta)$, such as size

(radius of gyration), shape, and even internal structure of the macromolecule depending on how large is ξ relative to q^{-1} . In the limit of $\theta \rightarrow 0$ and $P(\theta) = 1$, Equation 18.36 reduces to Equation 18.18 for a monodisperse dilute polymer solution.

Writing $G_{\text{intra}}(\mathbf{R})$ in terms of the distribution of polymer segments $P_{ij}(\mathbf{R})$ (the probability of finding monomer j in \mathbf{R} when i is at the origin), we can rewrite Equation 18.37 as

$$P(\theta) = \frac{1}{n^2} \sum_i^n \sum_j^n \int_V P(R_{ij}) e^{-i\mathbf{q} \cdot \mathbf{R}_{ij}} d\mathbf{R}_{ij} \quad (18.38)$$

Integrating, we arrive at the famous Debye expression for $P(\theta)$ [35]:

$$P(\theta) = \frac{1}{n^2} \sum_i^n \sum_j^n \left\langle \frac{\sin q R_{ij}}{q R_{ij}} \right\rangle \quad (18.39)$$

Debye introduced this in the context of X-ray scattering where the RDGA is commonly valid; he derived the general expression for the intensity of X-rays scattered by an ensemble of randomly oriented particles. Later on, Debye himself applied it to the scattering by polymer solutions [36, 37]. If the particle is rigid then distance between the elements that conforms to the object a_{ij} will be constant and Equation 18.39 reduces to

$$P(\theta) = \frac{1}{n^2} \sum_i^n \sum_j^n \frac{\sin q a_{ij}}{q a_{ij}} \quad (18.40)$$

This expression applies to any rigid object independent of its shape. The only assumption made was that $P_{ij}(\mathbf{R}) = P(R_{ij})$.

Instead, we can write $P(\theta)$ in terms of the moments of the distribution polymer segments as

$$P(\theta) = \sum_{p=0}^{\infty} \frac{(-1)^p}{(2p+1)!} q^{2p} \left[\frac{1}{n^2} \sum_{i < j}^n \left\langle R_{ij}^{2p} \right\rangle \right] \quad (18.41)$$

If q is small compared with the inverse of the term in brackets, we can only recover up to the second moment of the distribution polymer segments, that is,

$$P(\theta) \cong 1 - \frac{1}{3} q^2 \left[\frac{1}{n^2} \sum_{i < j}^n \left\langle R_{ij}^2 \right\rangle \right] = 1 - \frac{1}{3} q^2 \langle R_g^2 \rangle \quad (18.42)$$

where $\langle R_g^2 \rangle$ is the mean square radius of gyration of the polymer chain (or particle). As q becomes larger, we can recover in addition higher moments of the distribution and therefore more information about the scattering object.

Substituting Equation 18.42 into Equation 18.36, we get in terms of the scattering angle

$$\frac{Kc}{R_\theta^{\text{ex}}} = \frac{1}{M} \left[1 + \frac{16\pi^2 n_s^2}{3\lambda^2} \langle R_g^2 \rangle \sin^2 \left(\frac{\theta}{2} \right) + \dots \right] + 2A_2 c + \dots \quad (18.43)$$

where n_s is the refractive index of the medium.

The generalization to polydisperse polymer solutions is straightforward, leading to

$$\frac{Kc}{R_\theta^{\text{ex}}} = \frac{1}{\langle M \rangle_w} \left[1 + \frac{16\pi^2 n_s^2}{3\lambda^2} \langle R_g^2 \rangle_z \sin^2 \left(\frac{\theta}{2} \right) + \dots \right] + 2 \langle A_2 \rangle_w c + \dots \quad (18.44)$$

where

$$\langle R_g^2 \rangle_z = \frac{\sum_i N_i M_i^2 \langle R_g^2 \rangle_i}{\sum_i N_i M_i^2} \quad (18.45)$$

Equation 18.44 constitutes the main expression of classical light scattering polymer characterization. This suggests the form of plotting scattering data named after Zimm [38], the *Zimm plot*, 18.37 an example of which is shown in Figure 18.6 [39]. However, there are other forms to plot scattering data depending on the form and size of the particle and the type of information that has to be extracted from the experiments. Examples of some of these will be given later in the chapter. Using either Equation 18.37 or 18.39, we can derive the form factor for different geometries, as shown in Table 18.1² [40].

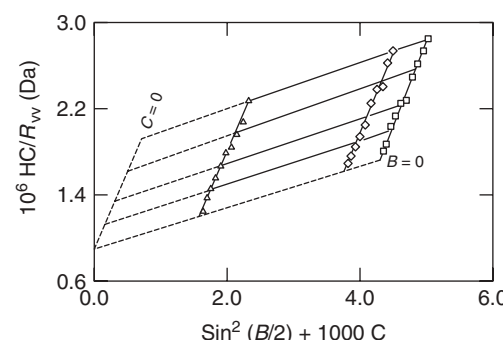


Figure 18.6 Zimm's plot of an alternating copolymer of ethylene and tetrafluoroethylene (PETFE) in diisobutyl adipate at 240 °C.
Source: Reprinted with permission from Chu B, Wu C. *Macromolecules* 1987;20:93–98. Copyright 1987 American Chemical Society.

²For a sphere, the conditions of the RDGA might not be matched because the refractive index of the sphere could be substantially different from that of the suspension medium. If so, $P(\theta)$ should be calculated by Mie's theory. This is the case of PS (polystyrene) latex spheres in water.

TABLE 18.1 Form Factors for Different Geometries in the RDGA

Sphere	Rod	Gaussian Coil
$x = qa$ $P(\theta) = \left[\frac{3}{x^3} (\sin x - x \cos x) \right]^2$	$x = \frac{qL}{2}$ $P(\theta) = \frac{1}{x} \int_0^{2x} \frac{\sin y}{y} dy - \left(\frac{\sin x}{x} \right)^2$	$x = q^2 \langle R_g^2 \rangle$ $P(\theta) = (2/x^2)(x - 1 + e^{-x})$

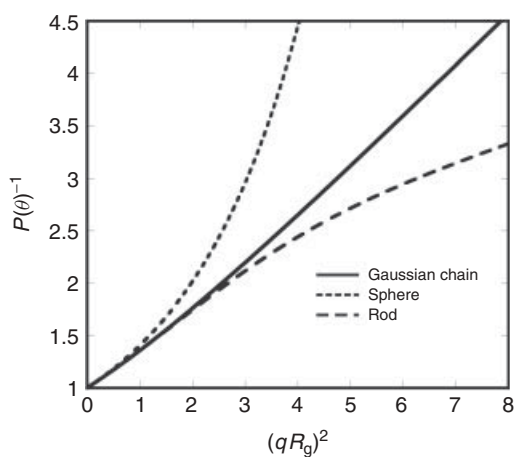


Figure 18.7 Calculated form factors for a Gaussian chain, sphere and a rod. The R_g 's used were: for a homogenous sphere of radius a , $R_g^2 = 3/5 a^2$ and for a rod of length L , $R_g^2 = L^2/12$.

Figure 18.7 shows the effects of structure on $P(\theta)^{-1}$. In the case of a rod, $P(\theta)^{-1}$ tends to grow slower with $q^2 \langle R_g^2 \rangle$. Therefore, for a wormlike chain, $P(\theta)^{-1}$ will lie between a flexible Gaussian chain and a rod. A similar effect occurs for a polydisperse sample of flexible chains because light scattering from the large molecules decays more rapidly with increasing angle than the scattering from small molecules, and therefore, their contribution becomes more significant at larger angles; hence, polydispersity and rigidity have qualitatively equivalent effects. The same applies to solvent effects; in good solvents, chains tend to swell and deviate from the Gaussian distribution and this concomitantly will make $P(\theta)^{-1}$ grow slower with $q^2 \langle R_g^2 \rangle$. The opposite happens for a homogenous sphere where $P(\theta)^{-1}$ tends to grow faster with $q^2 \langle R_g^2 \rangle$. Chain branching tends to give, for the same molecular weight, more compact structures, and therefore, $P(\theta)^{-1}$ will have a shape between a linear Gaussian chain and a sphere [41]. The influence of such factors on $P(\theta)^{-1}$ does not allow a unique interpretation of the structure of the macromolecule or the particle shape; one should have additional information from complementary independent characterization methods. It is interesting to note that independently of the shape, the initial slope is always 1/3.

In the opposite limit, for $q\xi \gg 1$, Benoit proved, for a Gaussian chain, that $P(\theta)^{-1}$ is still linear with q^2 . In fact, in this limit, $P(\theta)^{-1} = 1/2 (1 + q^2 \langle R_g^2 \rangle)$ [42]. For a polydisperse sample, in the limit $q \langle R_g^2 \rangle^{1/2} \gg 1$, Equation 18.44 becomes

$$\left[\frac{Kc}{R_\theta^{\text{ex}}} \right] c = 0 = \frac{1}{2 \langle M \rangle_n} (1 + Bq^2) \quad (18.46)$$

where $B = \langle N \rangle_n \ell^2/6$, with ℓ and $\langle N \rangle_n$ being the monomer size and the number-average degree of polymerization, respectively, and $\langle M \rangle_n$ is the number-average molecular weight, defined as $\sum N_i M_i / \sum N_i$. This result was extended to rods by Holtzer, except that instead of q^2 dependence, he found a linear behavior with q [43]. In principle, this implies that for large q 's one can obtain also the first moment of the distribution in molecular weight. However, in practice, for the wavelengths used in light scattering experiments, in the majority of the cases, this asymptotic limit will never be reached. Nevertheless, if instead, we do a scattering experiment with X-rays (with enough electron density contrast) or neutrons, using a deuterated polymer in solution, then we will certainly reach this asymptotic limit.

As an illustration of SLS, in what follows, we give some interesting examples of the application of this technique to study the structure of complex systems. Figure 18.8 shows the experimental results of Galinsky and Burchard [44] on the determination of $P(\theta)$ for a collection of seven samples of branched macromolecules in a solution of 0.5 N NaOH, prepared from potato starch by controlled acid degradation. Previously, Burchard [45] had derived a form factor for trifunctional polycondensation model without excluded volume effects, namely,

$$P(q) = \frac{1 + (C/3) (q R_g)^2}{\left[1 + ((1+C)/6) (q R_g)^2 \right]^2} \quad (18.47)$$

The parameter C increases with the molar mass and is related to the branching probability p . For self-similar structures, one expects that the particle topology does not vary with molar mass, that is, the form factor should be independent of molar mass. These nonrandomly branched

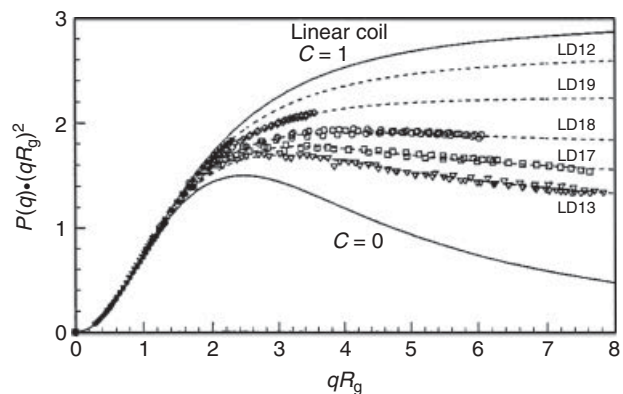


Figure 18.8 Kratky's plot of the form factor of samples of branched polymers derived from potato starch by controlled acid degradation. The upper continuous line corresponds to a linear chain ($C = 1$) while the lower one to a homogenously branched polymer ($C = 0$). Source: Reprinted with permission from Galinsky G, Burchard W. *Macromolecules* 1997;30:4445 [44]. Copyright 1997 American Chemical Society.

samples show only very limited intermediate range power law behavior. Furthermore, the various samples of different molar masses are not self-similar to each other, but each sample exhibits its own exponent in the asymptotic region. The Kratky representation of the data emphasizes the behavior at large qR_g and shows how well Equation 18.47 fits the experimental data with a single parameter.

Another interesting application, relevant to controlled drug release, is the determination of the outer diameter d and the membrane thickness δ as a function of pH of a sample of large polydisperse microcapsules ($\sim 10 \mu\text{m}$) made of poly(L-lysine-*alt*-terephthalic acid). Dobashi et al. [46] showed that it is possible to measure $P(\theta)$ for individual particles with a new design of the sample cell (capillary tubing cell) and detecting system that could cover a range of q 's from 0.5 to $6 \mu\text{m}^{-1}$. By comparing the experimental $P(q)$ with the form factor for a spherical thin shell, they determined the values of d and δ as illustrated in Figure 18.9. The authors found that the lowest values for d and δ corresponded to pH 4 and increase as the pH differs from 4. They also established that d and δ change approximately proportional to each other suggesting an isotropic volumetric phase transition.

In the previous example, the microspheres were far greater than q^{-1} , and therefore, Dobashi et al. were able to resolve fine details. However, this is not always the case and we have to use complementary techniques such as SAXS or SANS to cover a wider range of q 's.³ An example of

³The theoretical framework of both techniques is the same as the one discussed for light scattering except for the front factor. For SAXS or SANS, the intensity will be related to the correlation of electron densities or nuclei densities, respectively.

this is the study by Lonetti et al. [47] of wormlike micelles of a block copolymer of poly(butadiene-*co*-ethylene oxide) (PB-PEO) in water; these structures have a very broad range of length scales ranging from the contour and persistence length to the core/corona diameter and aggregation number per unit length (number of copolymer molecules per PB-core length of the worm). For the weight fraction of PEO w_{PEO} between 0.47 and 0.59, this system self-assembles in water as wormlike micelles with a core of PB and a corona of PEO, while for $w_{\text{PEO}} > 0.6$ and $w_{\text{PEO}} < 0.47$, they form spherical micelles and bilayers, respectively. However, a different way of tuning these morphological transitions is through solvent selectivity using a mixture of solvents. Lonetti et al. used in their work a mixture of N, N-dimethylformamide (DMF) and water and studied the relation between the smallest relevant length scale, as the diameter and aggregation number per unit length, to changes in the mesoscopic structure, that is, the contour and persistent lengths of the wormlike micelles; they also analyzed the transition from wormlike to spherical micelles. Figure 18.10 shows the experimental scattering intensities as a function of q for different solvent compositions of d-DMF and D_2O . The filled symbols correspond to SLS data, while the open symbols refer to SANS. For high water content, at low q values, the scattering intensity scales as q^{-1} (SLS region), corresponding to rigid rods, independent of the micelle length, polydispersity, and flexibility. No sign of q^{-2} dependence typical of wormlike micelles is observed in view that the persistence length is larger than 500 nm. At d-DMF mole fraction, $f_{\text{d-DMF}} > 0.09$, the low q data shows a change in q dependence allowing to obtain information about the persistence length. We also observe that as the DMF content increases, the minima of the oscillation in the form factor move toward larger q 's indicating a smaller overall cylinder diameter. From Figure 18.10, they could infer qualitatively a transition to spherical micelles. By adding DMF until $f_{\text{d-DMF}} = 0.5$, a 50% decrease in the scattering intensity is reported, with no change in slope. From $f_{\text{d-DMF}} = 0.7$, the intensity becomes independent of q forming a plateau, representative of the scattering by spherical objects. Using the Kholodenko model to fit the data and other complementary techniques, Lonetti et al. were able to obtain information about the core/corona diameter, the aggregation number per unit length, the density gradient of the shell, the contour, and the persistence length [48].

These examples show the potential that scattering techniques have in determining thermodynamic and structural features of rather complex polymeric systems. However, they also show that if we want to go beyond the determination of molecular weight and average radius of gyration, theoretical modeling is necessary to interpret the scattering data and obtain more information about the system. More examples of the application of SLS and DLS, including a

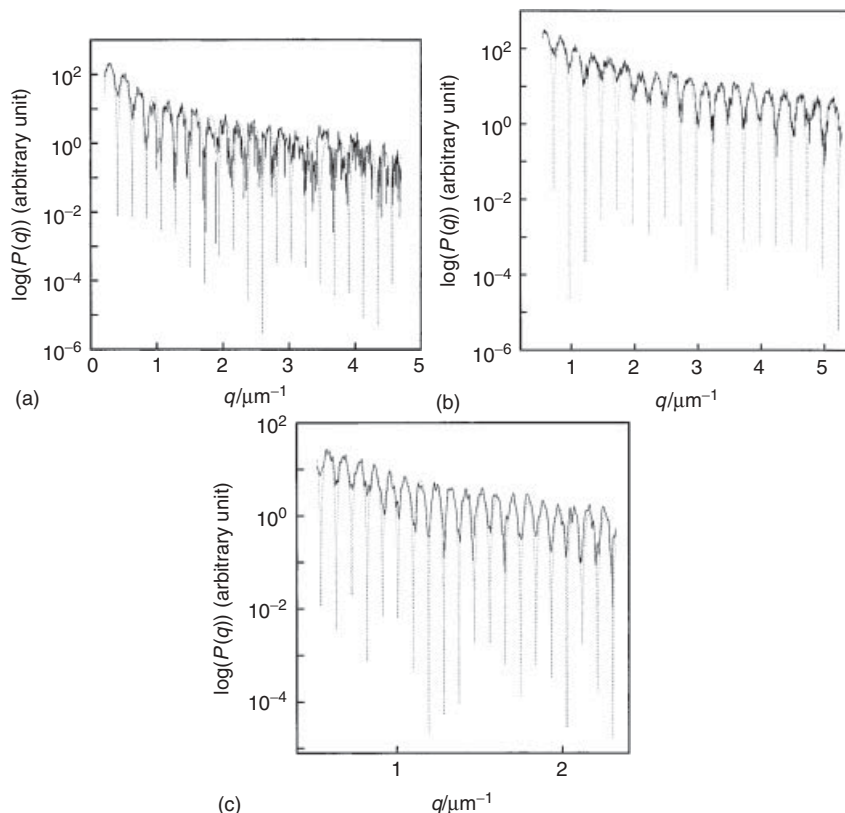


Figure 18.9 Observed (solid curve) and calculated (dotted curve) scattering pattern of microcapsules with (a) pH = 2, (b) pH = 4, and (c) pH = 10. *Source:* Reprinted with permission from Dobashi T, Narita T, Masuda J, Makino K, Mogi T, Ohshima H, Takenaka M, Chu B. *Langmuir* 1998;14:745 [46]. Copyright 1998 American Chemical Society.

discussion of experimental details, can be found in Schärtl's book [49].

18.4 DYNAMIC LIGHT SCATTERING

18.4.1 General Concepts: Determination of Particle Sizes in Dilute Solutions

In order to observe the time dependence of the scattered intensity, certain experimental conditions must be met. First, the characteristic time of a fluctuation is rather short and therefore requires special detectors that can respond to such timescale. Second, the scattering volume should be small and the angle subtended on the detector should also be small so that the area seen by the detector is on the order of one coherence area (which is the zone where the light is almost in phase producing constructive interference). Rephrasing the previous statements, if we illuminate with a laser a cell filled with a sample of a suspension of scattering particles, we will observe a "speckle pattern" (bright spots) that is constantly changing due to the motion of the particles; experimentally, we

should observe a volume on the order of a single "speckle." The timescale of the fluctuations depends on the time that takes a particle to move a distance of the probing effective wavelength ($\lambda/\sin(\theta/2)$). This time depends on the size and geometry of the scattering objects, the fluid viscosity, the temperature, and the concentration.

There are basically two approaches for the measurement of the time dependence of the scattered intensity. The first one is addressed to processes that are rather fast, which require the Fabry–Perot interferometers or diffraction gratings to obtain the spectral decomposition of the scattered light. These devices are placed in between the scattering cell and the detecting system and act as a filter. By varying the spacing or other setting parameter, we can make a spectral decomposition of the scattering intensity and obtain $I(\mathbf{q}, \Delta\omega)$, as in Equation 18.5. However, these techniques do not have the resolution to study processes slower than 10^{-6} s. Diffraction gratings resolve adequately when the dynamics is faster than 10^{-10} s, while Fabry–Perot interferometer is the right choice for the process in between 10^{-6} and 10^{-10} s. On the other hand, in common applications, the timescale ranges from

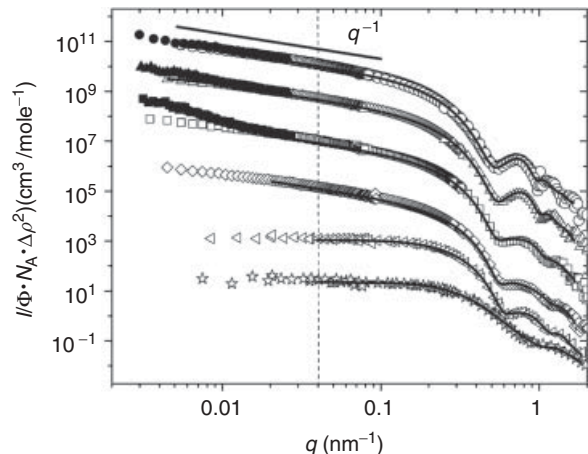


Figure 18.10 Experimental and fitted lines as a function of q of the scattered intensity by PB-PEO block copolymer in different solvent whose compositions go from d-DMF to D₂O. (open symbols SANS, filled symbols SLS). Circle, pure D₂O; up triangle, $f_{\text{d-DMF}} = 0.09$; square, $f_{\text{d-DMF}} = 0.36$; diamond, $f_{\text{d-DMF}} = 0.5$; left triangle, $f_{\text{d-DMF}} = 0.7$; star, pure d-DMF. The dashed line indicates the range of fit of SANS data. For the sake of clarity, data were shifted by arbitrary factors. Source: Reprinted with permission of Lonetti B, Tsigkri A, Lang PR, Stellbrink J, Willner L, Kohlbrecher J, Lettinga MP. Macromolecules 2011;44:3583 [47]. Copyright 2011 American Chemical Society.

10^{-7} to 1 s. If this is the case, we use the so-called optical mixing techniques (OMTs), also called *photon correlation spectroscopy* (PCS). In PCS, the scattered light is directly collected by the detector; if the previously discussed experimental conditions are met, then we will have a highly fluctuating scattered intensity with time as the output. In the homodyne (or self-beat) method, only the scattered light is collected, while in the heterodyne method, we mix in the detector the scattering light with another nonscattered light, normally a small portion of the incident beam. Furthermore, the statistical analysis of the fluctuating scattered intensity is done by means of a digital correlator. For the homodyne arrangement, the final output will be then the correlation function between intensities

$$G_2(\mathbf{q}, \tau) = \lim_{T \rightarrow \infty} \frac{1}{T} \int_0^T I_s(\mathbf{q}, t) I_s(\mathbf{q}, t + \tau) dt \quad (18.48)$$

If the process is stationary and ergodic, the time average can be replaced by an ensemble average, $G_2(\mathbf{q}, \tau) = \langle I_s(\mathbf{q}, \tau) I_s(\mathbf{q}, 0) \rangle$. Experimentally, $G_2(\mathbf{q}, t)$ is determined by recording $I_s(t)$ at time intervals much shorter than the timescale of typical fluctuations and accumulating the products of the intensities as a function of the sampling time τ . The sampling can be chosen to be linear or exponential. Actually, the exponential sampling is the best choice.

If we assume the scattered electric field as a superposition of a large number of statistically independent random electric fields, then according to the central limit theorem, the scattered field will be a random field with a Gaussian distribution. This is called the *Gaussian approximation*, which is valid in many cases. However, this will not be satisfied, for example, in strongly interacting particles, or in nonergodic systems such as gels. Within the Gaussian approximation, $G_2(\mathbf{q}, t)$ can be written in terms of the autocorrelation function between the scattered fields $G_1(\mathbf{q}, t) = \langle E_s(\mathbf{q}, \tau) E_s(\mathbf{q}, 0) \rangle$ as

$$G_2(\mathbf{q}, t) = B + f |G_1(\mathbf{q}, \tau)|^2 \quad (18.49)$$

which is known as the *Siegert relationship*. Here, B is the baseline $\langle I_s(\mathbf{q}) I_s(\mathbf{q}) \rangle$ and f is the spatial coherent factor that depends on the number of coherent areas in the detector and will be equal to 1 for a single coherent area or less [50–52].

Although homodyne is the most used method in PCS, we describe shortly also the heterodyne method, which is widely used for Doppler velocimetry experiments or when the Siegert relation is not applicable. Heterodyning means that we mix in the detector the scattered light with a strong nonscattered signal (named commonly as the *local oscillator*), that is,

$$\langle I_s(\mathbf{q}, t) I_s(0) \rangle = \langle |E_{\text{LO}} + E_s(\mathbf{q}, t)|^2 |E_{\text{LO}} + E_s(\mathbf{q}, 0)|^2 \rangle \quad (18.50)$$

Since $E_{\text{LO}} \gg E_s$, we can approximate $\langle I_s(t) I_s(0) \rangle$ as

$$\langle I_s(\mathbf{q}, t) I_s(0) \rangle \cong [I_{\text{LO}}^2 + 2I_{\text{LO}} \text{Re}G_1(\mathbf{q}, t)] \quad (18.51)$$

This means that in most applications, we can relate $G_2(\mathbf{q}, t)$ to $G_1(\mathbf{q}, \tau) = \langle E_s(\mathbf{q}, \tau) E_s(\mathbf{q}, 0) \rangle$ by either homodyne or heterodyne methods. Proceeding in the same way as in the SLS, we can relate $\langle \Delta\varepsilon(\mathbf{R}, t) \Delta\varepsilon(\mathbf{0}, \mathbf{0}) \rangle$ with the dynamic joint probabilities $G_{\text{intra}}(\mathbf{R}, t)$ and $G_{\text{inter}}(\mathbf{R}, t)$ and write Equation 18.5 as

$$I_s(\mathbf{q}, \Delta\omega) \cong \left\{ \frac{1}{n} \int G_{\text{intra}}(\mathbf{R}, t) e^{(-i(\mathbf{q} \cdot \mathbf{R} + \Delta\omega t))} d\mathbf{R} dt \right\} \\ + N_A c \left\{ \int (g_{\text{inter}}(\mathbf{R}, t) - 1) e^{(-i(\mathbf{q} \cdot \mathbf{R} + \Delta\omega t))} d\mathbf{R} \right\} \quad (18.52)$$

Equation 18.52 becomes the dynamic equivalent of Equation 18.35 where $G_{\text{intra}}(\mathbf{R}, t)$ is the probability of finding any monomer at \mathbf{R} at time t when any other of the *same* macromolecule is at the origin at $t = 0$, while $G_{\text{inter}}(\mathbf{R}, t)$ is the joint probability of finding any monomer at \mathbf{R} at time t when any monomer of a *different* macromolecule is at the origin at $t = 0$. In Equation 18.52,

$g_{\text{inter}}(\mathbf{R}, t) = G_{\text{inter}}(\mathbf{R}, t)/\langle \rho_1 \rangle$. For a dilute solution, this reduces to

$$I_s(\mathbf{q}, \Delta\omega) \cong \int G_{\text{intra}}(\mathbf{R}, t) e^{(-i(\mathbf{q} \cdot \mathbf{R} + \Delta\omega t))} d\mathbf{R} dt \quad (18.53)$$

We have omitted all the front factors since they are not relevant for the time dependence of the scattering intensity.

Let us now consider the simplest case, a system consisting of diluted suspension of spheres, such as a latex particle suspension. As with any rigid body, there will be only two dynamic modes: a translation of the center of mass and the rotation around the center of mass. For a sphere, the only mode that participates in the fluctuations in concentration will be the translational one since a rotation around the center of mass will have no effect on mass transfer in a scattering volume element. This means that in the case of a sphere, we can factorize $G_{\text{intra}}(\mathbf{R}, t)$ as

$$G_{\text{intra}}(\mathbf{R}, t) = G_{\text{intra}}(\mathbf{R}') P(\mathbf{r}_{\text{cm}}, t) \quad (18.54)$$

where \mathbf{r}_{cm} is the position vector of the center of mass and \mathbf{R}' is the position vector of any point in the sphere relative to the center of mass ($\mathbf{R} = \mathbf{R}' + \mathbf{r}_{\text{cm}}$). Substituting Equation 18.54 into Equation 18.53, we can factorize $I_s(\mathbf{q}, \Delta\omega)$ as

$$I_s(\mathbf{q}, \Delta\omega) \approx P(\theta) \left[\int P(\mathbf{r}_{\text{cm}}, t) e^{-i(\mathbf{q} \cdot \mathbf{r}_{\text{cm}} + \Delta\omega t)} d\mathbf{r}_{\text{cm}} dt \right] \quad (18.55)$$

$P(\theta)$ is the form factor for a sphere already discussed and $P(\mathbf{r}_{\text{cm}}, t)$ is the probability that the center of mass of a sphere is at \mathbf{r}_{cm} at time t when at $t = 0$ was at the origin.

To illustrate, let us assume that the particles all move at constant velocity \mathbf{v}_0 . Then $P(\mathbf{r}_{\text{cm}}, t)$ is given by

$$P(\mathbf{r}_{\text{cm}}, t) \approx \delta(\mathbf{r}_{\text{cm}} - \mathbf{v}_0 t) \quad (18.56)$$

and spectral decomposition of the scattered intensity is

$$\begin{aligned} I_s(\mathbf{q}, \Delta\omega) &\approx P(\theta) \left[\int e^{i(\pm \mathbf{q} \cdot \mathbf{v}_0 - \Delta\omega t)} dt \right] \\ &\approx P(\theta) [\delta(\Delta\omega + \mathbf{q} \cdot \mathbf{v}_0) + \delta(\Delta\omega - \mathbf{q} \cdot \mathbf{v}_0)] \end{aligned} \quad (18.57)$$

that is, in frequency space, we will observe two sharp spikes at $\omega_0 \pm \mathbf{q} \cdot \mathbf{v}_0$, as shown in Figure 18.11. This means that if we illuminate with a frequency ω_0 , the scattered light will suffer a Doppler shift from the incident frequency by $\pm \mathbf{q} \cdot \mathbf{v}_0$. Since we know \mathbf{q} , we can determine \mathbf{v}_0 by DLS.

Now, let us consider the case of spherical particles diffusing in a medium; the equation governing $P(\mathbf{r}_{\text{cm}}, t)$ will be Fick's law

$$\frac{\partial P(\mathbf{r}_{\text{cm}}, t)}{\partial t} = D \nabla^2 P(\mathbf{r}_{\text{cm}}, t) \quad (18.58)$$

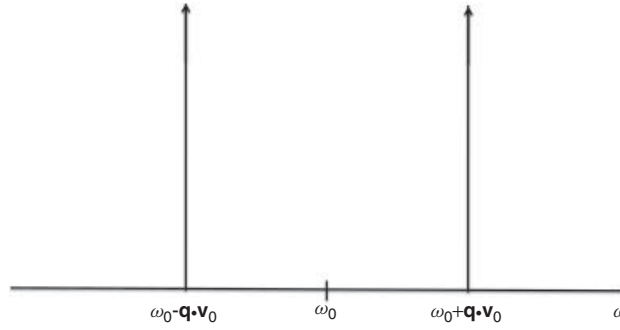


Figure 18.11 Spectral decomposition of the scattered light by spheres moving at constant velocity.

where D is the diffusion coefficient. The solution in q space is

$$P(\mathbf{q}, t) \approx e^{-q^2 D t} \quad (18.59)$$

Therefore, the time dependence of the scattered intensity is

$$I_s(\mathbf{q}, t) \approx e^{-q^2 D t} \quad (18.60)$$

This is probably the most emblematic expression in DLS (Fig. 18.12).

As we can see, the decay time $\tau = 1/(q^2 D)$ is nothing else than the time that it takes for a Brownian particle to cross a distance $\sqrt{6/q}$.

Equation 18.60 is valid for any object that follows a *translational* diffusion no matter what its actual form is. If the object is not a rigid sphere then will have other dynamical modes that contribute to the fluctuations in the scattered field, such as rotational diffusion, elastic modes, which will also contribute to the scattered intensity, as discussed later.

The decay constant can be written in terms of the particle size using the Stokes–Einstein relationship

$$D = \frac{k_B T}{\zeta} \quad (18.61)$$

where ζ is the friction coefficient. In the case of a sphere $\zeta = 6\pi\eta R$, where R is the radius of the sphere and η is the viscosity of the medium. When the diffusing particles are not hard spheres, it is common to introduce the concept of the hydrodynamic radius R_h that is the radius of an equivalent hard sphere with the same translational diffusion as the scattering object, whether this is a macromolecule, a rod, or any other form.

Thus, the decay time of the normalized correlation function $g_1(\mathbf{q}, t) = \langle E(\mathbf{q}, t) E(\mathbf{q}, 0) \rangle / I_s(\mathbf{q})$ for a monodisperse sample of spheres is

$$\tau = \frac{1}{q^2 D} = \frac{6\pi\eta R}{q^2 k_B T} \quad (18.62)$$

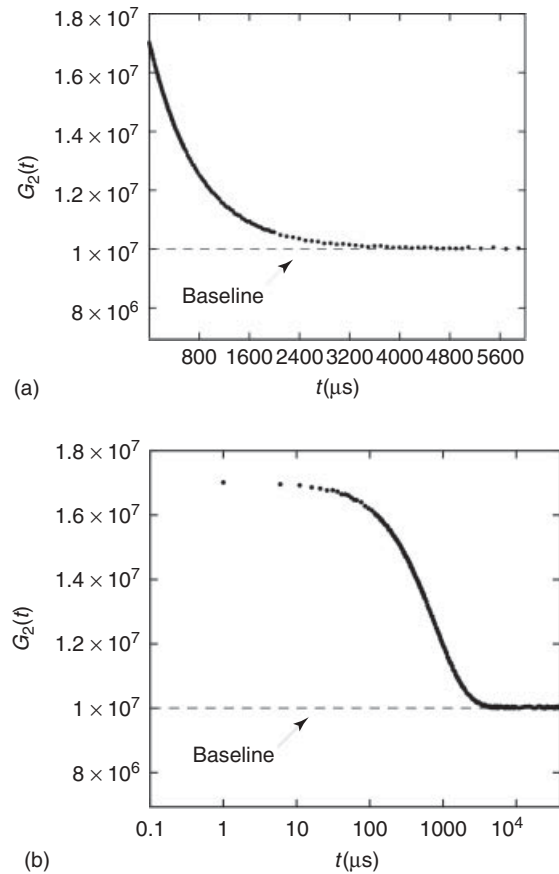


Figure 18.12 Typical $G_2(t)$ display for a monodisperse latex sample of 400 nm particle diameter. (a) Linear plot and (b) logarithmic plot.

Since q , T , and η are known, we determine R from the measurement of τ . Actually, most commercial software calculate the size assuming that the object is spherical. As mentioned before, the digital correlator gives directly $G_2(\mathbf{q}, t)$, and therefore, after subtracting the baseline and dividing by baseline, we get by the Siegert relationship a correlation function $C(t)$ given by

$$C(t) = \frac{G_2(t) - B}{B} = f e^{-2q^2 D t} \quad (18.63)$$

Notice that in a homodyne experiment the decay time is *twice* of that in a heterodyne experiment. This means that when we perform a homodyne experiment, we must be sure that no stray light reaches the detector, otherwise we might have a mixture of homodyne–heterodyne output. A thorough discussion of the instrumental considerations to be followed when using DSL is found in Reference 52.

In the case of a polydisperse sample of spheres, each particle size contributes to the scattered intensity following the time dependence shown in Equation 18.60, giving

rise to a superposition of exponential decays; the specific contribution of each species to the total light scattered is proportional to the scattered intensity by the particles of the species, that is,

$$I_s(\mathbf{q}, t) \approx \sum_i I_{si}(\mathbf{q}) e^{-q^2 D_i t} \quad (18.64)$$

Writing Equation 18.64 in terms of $g_1(\mathbf{q}, t)$ we have

$$g_1(\mathbf{q}, t) = \frac{\sum_i I_{si}(\mathbf{q}) e^{-q^2 D_i t}}{\sum_i I_{si}(\mathbf{q})} \quad (18.65)$$

To simplify the notation, we omit in the following discussion the explicit \mathbf{q} dependence in I_s and g_1 and use a single parameter $\Gamma = q^2 D$ to identify the species; in that case, we can rewrite Equation 18.65 as:

$$g_1(t) = \int_0^\infty G(\Gamma) e^{-\Gamma t} d\Gamma \quad (18.66)$$

which is the Laplace transform of $G(\Gamma)$ that is given by

$$G(\Gamma) = \frac{\sum_i I_{si} \delta(\Gamma - \Gamma_i)}{\sum_i I_{si}} \quad (18.67)$$

All the information on the distribution is in G , while $g_1(t)$ is experimentally determined using the Siegert relation. To extract from $g_1(t)$ the size distribution, one has to invert Equation 18.66; however, this type of linear transformations are known to be ill-conditioned, that is, if the experimentally measured $g_1(t)$ contains any noise, the solution for $G(\Gamma)$ is not unique. We can only expect to have a poor-resolution picture of $G(\Gamma)$ and we will never retrieve the fine details of the distribution. The mathematical reasons for this were studied by McWhirter and Pike [53] who solved the eigenvalue problem of the Fredholm equation of the first class with the Laplace kernel. They prove that the eigenfunctions are mutually orthogonal and form a complete set; they also obtained the eigenvalue spectrum for the Laplace transform λ_μ^\pm and found that they decay exponentially with μ . The latter is the fundamental reason why it is impossible to recover a high resolution $G(\Gamma)$; any small noise in $g_1(t)$ will give rise to a large noise in $G(\Gamma)$. In such circumstances, it is not possible to obtain a complete and unique result.

In spite of the ill-conditioned inversion problem, there are a good number of approaches that try to overcome the inherent limitations by proposing schemes that can provide some information about the distribution function. The simplest and oldest of all DSL data analysis methods is

the method of cumulants [54]. The essence of this method lies in expanding $\exp(-\Gamma t)$ in Equation 18.66 about the mean value $\langle \Gamma \rangle$, where $\langle \Gamma \rangle$ is defined as

$$\langle \Gamma \rangle = \int_0^\infty \Gamma G(\Gamma) d\Gamma \quad (18.68)$$

Then,

$$g_1(t) = \exp(-\langle \Gamma \rangle t) \left[1 + \frac{\mu_2 t^2}{2!} - \frac{\mu_3 t^3}{3!} + \dots \right] \quad (18.69)$$

where

$$\mu_i = \int_0^\infty (\Gamma - \langle \Gamma \rangle)^i G(\Gamma) d\Gamma \quad (18.70)$$

are the i th moments about the mean (cumulants) of $G(\Gamma)$. $\langle \Gamma \rangle$ can be obtained directly from $g_1(t)$ as

$$\langle \Gamma \rangle = - \left[\frac{dg_1(t)}{dt} \right]_{t=0} \quad (18.71)$$

Since the weighting factors in $G(\Gamma)$ are the I_{si} 's, we know from the SLS discussion that $I_{si}(\mathbf{q}) \approx N_i M_i^2 P_i(q)$, where N_i and M_i are the number and mass of species i , respectively, while $P_i(q)$ is its form factor. Substituting the expression for I_{si} in Equation 18.68 leads to

$$\frac{\langle \Gamma \rangle}{q^2} = \frac{\sum_i N_i M_i^2 P_i(q) D_i}{\sum_i N_i M_i^2 P_i(q)} \quad (18.72)$$

This is sometimes called the *apparent diffusion coefficients* $D_{app}(q)$ since it depends on q . If the particle sizes are small compared to λ , or if we observe at very small angles, then $P(q) \rightarrow 1$ and Equation 18.72 reduces to

$$\frac{\langle \Gamma \rangle}{q^2} = \frac{\sum_i N_i M_i^2 D_i}{\sum_i N_i M_i^2} = \langle D \rangle_z \quad (18.73)$$

Normally, $\langle D \rangle_z$ is obtained by taking several measurements of $D_{app}(q)$ at different angles and extrapolating to zero angle. In terms of the hydrodynamic radius, Equation 18.73 implies that in the limit of $q \rightarrow 0$, $\langle \Gamma \rangle / q^2 = (k_B T / 6\pi\eta) \langle R_h^{-1} \rangle_z$.

From Equation 18.70, μ_2 can be written as the variance of Γ : $\mu_2 = \langle \Gamma^2 \rangle - \langle \Gamma \rangle^2$. In the limit of small angles, we can write the so-called polydispersity index (PI), $\mu_2 / \langle \Gamma \rangle^2$ as

$$\frac{\mu_2}{\langle \Gamma \rangle^2} = \frac{\langle D^2 \rangle_z - \langle D \rangle_z^2}{\langle D \rangle_z^2} \quad (18.74)$$

In view of McWhirter and Pike's work, noise will limit the number of cumulants that we can actually measure. In most cases, only $\langle \Gamma \rangle$ and μ_2 can be determined. Cumulants are used for monomodal size distributions that have a PI not larger than 0.3. In bimodals or other more complex distributions, cumulant analysis will be meaningless and will only give some type of rough screening of the data. Even more, $D_{app}(q)$, which is what is usually determined, is also dependent on the type of correlator, whether linear or nonlinear correlator, and the number of channels used [55].

Ostrowsky et al. [56] proposed one of the first methods of inverting Equation 18.66. On the basis of the previous work of McWhirter and Pike, mentioned before, they suggested replacing Equation 18.66 by a sum of exponentials whose Γ 's are spaced exponentially according to

$$\Gamma_{n+1} = \Gamma_n \exp\left(\frac{\pi}{\omega_{\max}}\right) \quad (18.75)$$

where ω_{\max} is a parameter determined by the noise level of the correlation function. The number of exponentials used in the reconstruction depends also on the noise level.

The amplitudes of the histogram of the distribution function are calculated by a non-negative least square method. This procedure is known as the *exponential sampling method* and is applicable to both monomodal and bimodal distributions. However, in view of the limitations of the Laplace inversion, it is difficult to resolve bimodal distributions with a ratio between the two particle species below 2.

Provencher has developed an effective inversion software package, CONTIN, which is a generalized inverse Laplace transform with constraints. CONTIN also turns $g_1(t)$ into a discrete sum of exponentially spaced set of exponential; however, it includes additional constraints in order to suppress artificial oscillations. For that purpose, it uses a constraint regularization term, which limits solutions with high curvatures (constraints on the second derivatives) [57, 58]. This software is included in all commercial instruments. Other approaches that have been used are maximum entropy, Regularized Positive Exponential Sum (REPES), single value decomposition, multiangle constrained inversion, Bayesian inversion method together with multiangle DSL (MDSL), to mention some [59–65].

A general comment that applies to all the inversion methods is that when they are used as a black box (as they are normally used), one should take the result only as indicative of the distribution. The ill-conditioned nature of the inversion problem together with uncontrolled factors and artifacts of the inversion method used can lead to false particle size distributions. In any case, in spite of the inherent limitations of any of these methods, a well-trained researcher in DLS can profit from these methods as optimized inversion tools.

18.4.2 Dynamic Light Scattering by a Dilute Solution of Thin Rods

Let us consider now a system consisting of thin rods suspended in a fluid at a concentration regime where the rods do not interact between each other. This particular geometry is important since there are many biological molecules, which, as a first approximation, can be described as rigid rods, such as helical polypeptides, some proteins, and tobacco mosaic virus (TMV). Also, important new nanotechnological products such as organic or inorganic nanotubes or nanorods with a large aspect ratio are good examples of rodlike particles. For this geometry, two types of motions contribute to the fluctuations in the scattered intensity. The first one is again related to the translational motion of the rod, while the second dynamic mode is associated with the rotation of the rod around the center of mass of the rod.

The first to calculate the time dependence of the scattering intensity of thin rods was Pecora [66, 67]. He introduced some simplifications assuming that the translational and the rotational dynamics were not coupled and that the thickness of the rod is negligible compared with the wavelength. The mathematical details of his derivation can be found in Berne and Pecora's book [50]. His final result for the scattered intensity time dependence for a VV configuration is⁴

$$I_s^{\text{VV}}(\mathbf{q}, t) \approx S_0(qL) \exp[-q^2Dt] + S_1(qL) \exp[-(q^2Dt + 6D_r t)] + \dots \quad (18.76)$$

where L is the length of the rod, D is the translational diffusion coefficient of the center of mass, and D_r is the rotational diffusion coefficient. $S_0(qL)$, $S_1(qL)$, ... are the sums of the Bessel functions. What is interesting from his result is that for $qL \leq 3$, $S_0(qL)$ is much greater than any other terms and therefore we can neglect them. This implies that at very small angles or L small compared with λ , the time dependence of the scattered intensity will be fully dominated by the translational diffusion. On the other hand, for $qL \geq 5$, $S_1(qL)$ becomes relevant; its contribution to $I_s^{\text{VV}}(\mathbf{q}, t)$ for $qL = 5.2$ is 12% and is 57% for $qL = 10$. The rest of the terms in the series are negligible up to $qL \leq 8$. This means that we can determine the translational diffusion, extrapolating $D_{\text{app}}(q)$ to zero angle. At higher angles, the second term becomes relevant and using the value of D previously determined we can measure the rotational diffusion coefficient D_r .

⁴VV stands for an incident beam vertically polarized, and we observe the vertically polarized component of the scattered field. In the VH configuration, we observe the cross-polarized component of the scattering field for a vertical polarization of the incident beam.

In general, the diffusion equation for a rod with finite thickness contains the coupling of translational and rotational motions. A lucid account of this topic can be found in Doi and Edwards' book [68]. Wilcoxon and Schurr [69] and, independently, Maeda and Fujime [70] have studied the theory of DLS by thin rodlike particles. Although the explicit autocorrelation function can only be obtained numerically, the first cumulant can be derived readily

$$\frac{\langle \Gamma \rangle}{q^2} = D - \Delta \left[\frac{1}{3} - f_2 \left(\frac{qL}{2} \right) \right] + \frac{L^2}{12} D_r f_1 \left(\frac{qL}{2} \right) \quad (18.77)$$

where $D = (1/3)(D_{\parallel} + 2D_{\perp})$ is the translational diffusion coefficient of the center of mass; D_{\parallel} and D_{\perp} are the translational diffusion coefficients parallel and perpendicular to the axis of the rod, respectively; and $\Delta = D_{\parallel} - D_{\perp}$. The functions $f_1(qL/2)$ and $f_2(qL/2)$ are given numerically by Maeda and Fujime and analytically by Hammouda [71]. When $qL \ll 1$, $f_1(qL/2)$ and $f_2(qL/2)$ tend to be 0 and 1/3, respectively, and we recover Pecora's result for small qL values where translational diffusion of the center of mass is the dominant dynamical mode. In contrast, for $qL \gg 1$, $f_1(qL/2)$ and $f_2(qL/2)$ approach 1 and 0, respectively, and $\langle \Gamma \rangle/q^2 \rightarrow D_{\perp} + (L^2/12)D_r$.

D_{\parallel} and D_{\perp} and D_r are related to the length L and the diameter d of the rod as

$$D_{\parallel} = \left(\frac{k_B T}{2\pi\eta L} \right) [\ln(p) + v_{\parallel}(p)] \quad (18.78)$$

$$D_{\perp} = \left(\frac{k_B T}{4\pi\eta L} \right) [\ln(p) + v_{\perp}(p)] \quad (18.79)$$

$$D_r = \left(\frac{3k_B T}{\pi\eta L^3} \right) [\ln(p) + v_r(p)] \quad (18.80)$$

where p is the aspect ratio of the rod $p = L/d$, η is the viscosity of the solvent, and the functions v 's are end-effect corrections and have been calculated by several authors [72]. This implies that for thin rods that have a length comparable to the wavelength, it is possible to determine by DLS all diffusion coefficients and their geometrical dimensions.

Throughout this discussion, we have implicitly assumed that the rod is optically homogenous with a single index of refraction and that the Rayleigh-Debye-Gans theory is valid, which basically restricts the theory to thin rods, unless the refractive index of the cylinder is close to that of the solvent used [73].

In a depolarized dynamic light scattering (DDLS) experiment in the VH configuration, we observe the cross-polarized component of the scattering field produced by a vertically polarized incident beam with respect to the scattering plane. In this case, the purely translational

particle motion does not contribute to I_{SVH} and for small qL values, the only term that survives will be

$$I_{\text{SVH}}(\mathbf{q}, t) \approx S_{\text{VH}}(qL) \exp[-(q^2 D + 6D_r)t] \quad (18.81)$$

Therefore, by plotting $\langle \Gamma \rangle$ against q^2 and extrapolating to $q = 0$, we can determine D_r , whereas the slope of the linear regression of the fitted data gives us the value of D .

A drawback of DDLS experiments is the low intensity of the depolarized signal that requires the use of high power lasers; however, heating of the sample will be the limiting factor on how intense the primary beam can be. Therefore, special care must be taken to avoid all types of possible extra signals that could enter the detecting system. DDLS experiments can have very short decay times, depending on the timescale of the motion of the particles in solution. For timescales of 50 ns and faster, which is usually valid for molecules with a molecular weight of less than 50,000 Da, interferometric methods are recommended. For larger particles, the usual homodyne photon correlation techniques can be applied.

Lehner et al. [74] have compared DLS and DDLS methods in the determination of D , D_r , and Δ for TMV, a well-characterized biological model for these types of techniques. TMV is a rigid cylinder of 300 nm length and 18 nm diameter with a molecular weight of 4×10^{-7} Da and it is highly uniform in size with a normalized variance (PI) much less than 0.1. In a dilute concentration sample (0.245 g/l of TMV in pure water), it is necessary to add a small concentration of salt (2×10^{-3} M NaCl solution) to screen out the surface charges of TMV. Figure 18.13 shows a comparison of the DDLS results with and without the addition of salt. While the D_r value remains almost unchanged after addition of salt, a significant increase in the slope, and hence in D , is observed. With the added salt solution, the authors obtained values of 299 ± 9 s⁻¹ and $(4.05 \pm 0.09) \times 10^{-12}$ m²/s for D_r and D , respectively.

Furthermore, they compared the DDLS results with a DLS measurement fitting the experimental data with Equation 18.77. Figure 18.14 shows a plot of $\langle \Gamma \rangle/q^2 (=D_{\text{eff}})$ against q^2 ; the solid line corresponds to a fit where they fixed D_r to the value obtained by DDLS and left D and Δ as free-fitting parameters. Following this procedure, they found D to be around 5% higher than the value obtained by DDLS and Δ was close to the value reported by Wilcoxon and Schurr by DLS [69]. They also followed a different procedure where D and D_r were taken from the DDLS measurements and only left Δ as a free-fitting parameter (dashed line); however, in this case, the Δ obtained was 40% lower than that obtained by the first method. Hydrodynamic theories lead to a Δ of approximately 1.8×10^{-12} m²/s, which is close to the value obtained by the first method (1.79×10^{-12} m²/s) [72]. They attributed this difference to the lowest angle considered in the second

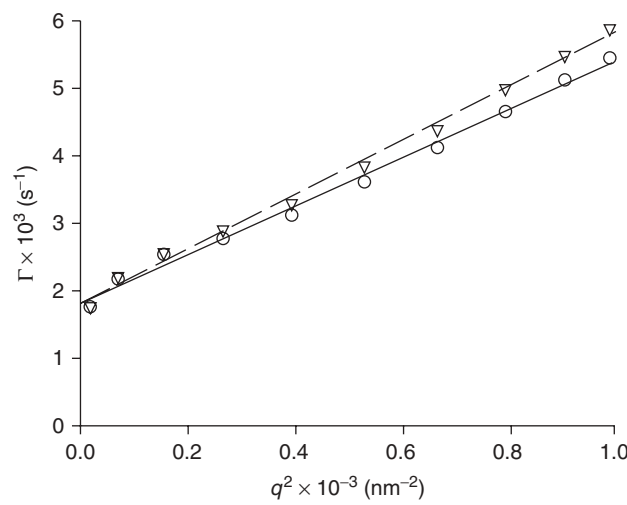


Figure 18.13 Comparison of the decay rate Γ with q^2 from DDLS data of a 0.245 g/l TMV solution in pure water (○) and in 2×10^{-3} M NaCl solution (▽) at 20 °C. Source: Reprinted with permission from Lehner D, Lindner H, Glatter O. *Langmuir* 2000;16:1689 [74]. Copyright 2000 American Chemical Society.

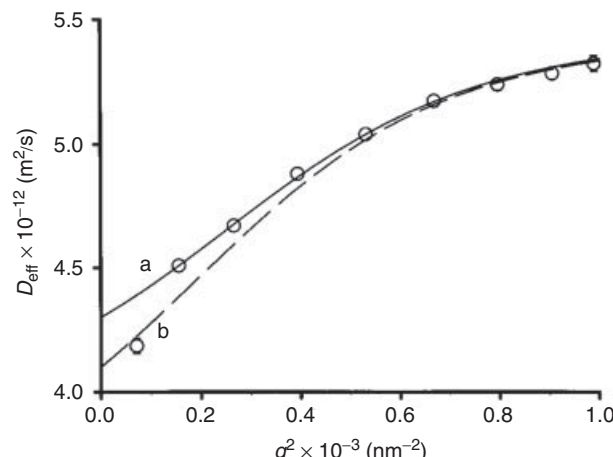


Figure 18.14 DLS data ($D_{\text{eff}} = \langle \Gamma \rangle/q^2$ vs q^2) of a 2×10^{-3} M NaCl solution of TMV at a concentration of 0.245 g/l at 20 °C (○). (a) $D = 4.3 \times 10^{-12}$ m²/s, $D_r = 300$ s⁻¹, and $\Delta = 0.41 D$ (full line); (b) $D = 4.1 \times 10^{-12}$ m²/s, $D_r = 300$ s⁻¹, and $\Delta = 0.25 D$ (dashed line). Source: Reprinted with permission from Lehner D, Lindner H, Glatter O. *Langmuir* 2000;16:1689 [74]. Copyright 2000 American Chemical Society.

procedure (20°) and suspected that some stray light coming from dust could contaminate the detected signal.

18.4.3 Dynamic Light Scattering by Flexible Polymers

Following the line of discussion, the next step is to consider a system with more degrees of freedom, such as a deformable body, which besides the translational and

rotational “modes,” can also have elastic modes. This can be a gel, a polymer melt, or a single polymer chain to mention some. As in the previous sections, in order to understand the nature of the time dependence of the scattered intensity we must understand the dynamics of the objects that scatter light. The polymer dynamics at different concentration regimes or in constrained systems such as permanent gels is beyond the scope of this chapter; the reader interested in this field can consult a classical modern treatise on the subject such as Doi and Edwards’ [75] or de Gennes’ books [76]. In any case, in what follows, we illustrate the main results as far as DLS is concerned, from the single chain (dilute solutions) to cooperative diffusion process at higher concentrations and other diffusion processes that occur in polymers with a microstructure, such as block copolymers.

Let us consider a dilute polymer solution of flexible macromolecules. The dynamics of a single Gaussian chain has been around for many years in the context of the molecular theory of transport phenomena in polymer solutions and has been fully reviewed in textbooks or articles in this subject [77]. Rouse’s theory is about the simplest of all them and helps understand the basic ingredients of the theory [78]. Rouse proposed a simplification of the problem by representing a polymer chain as a collection of beads connected by springs (the bead and spring model). The solvent interacts with the chain through the beads and it is assumed to freely drain through the chain. The only interaction between the beads is through the springs. The spring constant will be given as an effective entropic elastic constant produced by a collection of monomers whose end-to-end distance is the bead size b , that is, $k = 3k_B T/b^2$. The total friction exerted by the fluid on the chain is $\zeta_R = N\zeta$, where N is the number of beads and ζ is the friction coefficient of each bead. Since the model is already a coarse-grained picture of the chain, it can only give a reasonable answer for the slow long “wavelength” motions. In summary, the Rouse model reduces the problem to the dynamics of Brownian motion of coupled oscillators. The solution to the dynamics problem is well known and can be expressed as a superposition of normal modes.⁵ The correlation function of these modes decays exponentially with time, and the relaxation time of the p -mode is given by

$$\tau_p = \frac{\tau_1}{p^2} \quad \text{for } p = 1, 2 \dots \quad (18.82)$$

where

$$\tau_1 \cong \frac{\zeta N^2 b^2}{3\pi^2 k_B T} \quad (18.83)$$

⁵A normal mode is an independent collective motion. The equation that describes the dynamics of a normal mode is not coupled to the other modes. A general motion of the chain can be written as a superposition of its normal modes.

The zero mode is the self-diffusion of the center of mass whose diffusion coefficient is given by the Stokes–Einstein relation $D = k_B T/N\zeta$. The time τ_1 will be proportional to the time required for a chain to diffuse an end-to-end distance, that is, $\approx \langle R^2 \rangle / D = \zeta N^2 b^2 / k_B T$. This means that for time scales longer than τ_1 the motion of the chain will be purely diffusive. On timescales shorter than τ_1 , it will exhibit viscoelastic modes. However, the dynamics of a single chain in a dilute solution is more complex due to long-range forces; hydrodynamic interactions between distant monomers through the solvent are present and, in good solvents, excluded volume interactions also have to be taken into account. The correction of the Rouse model for hydrodynamic interaction was done by Zimm [79]. From a mathematical point of view, the problem becomes harder and requires approximations to arrive at some useful results. In this case, the translational diffusion coefficient obtained is

$$D \approx \left(\frac{k_B T}{\eta b} \right) N^{-\nu} \approx \frac{k_B T}{\eta R_g} \quad (18.84)$$

where ν in good solvents is close to 3/5 and in θ -solvents is 1/2. The relaxation time of mode p is

$$\tau_p = \tau_1 p^{-3\nu} \quad (18.85)$$

where

$$\tau_1 \cong \frac{\eta \langle R^2 \rangle^{3/2}}{k_B T} \cong \frac{\eta b^3}{k_B T} N^{3\nu} \quad (18.86)$$

which is close to the experimentally observed molecular weight dependence for D and τ_1 in both θ -solvents and good solvents. If we compare the Rouse models with those of Zimm for θ -solvents, we see that while in the former, D and τ_1 scale with M as $D \approx M^{-1}$ and $\tau_1 \approx M^2$ and in Zimm’s theory D and τ_1 scale as $D \approx M^{-1/2}$ and $\tau_1 \approx M^{3/2}$. From these results, we can conclude that the Rouse chain suffers a larger frictional force than the corresponding Zimm chain. In fact, according to Equation 18.84, the chain moves as a solid sphere of radius R_g , which means that the chain is dragging the solvent within the chain, whereas in the Rouse model, the chain is fully free draining and all the beads suffer the same friction.

Pecora analyzed $g_1(\mathbf{q}, t)$ for the Rouse model and found that this could be written in the form

$$\begin{aligned} g_1(\mathbf{q}, t) \approx & S_0 (q^2 R_g^2) \exp(-q^2 D t) \\ & + S_2 (q^2 R_g^2) \exp\left[-\left(q^2 D + \frac{2}{t_1}\right)\right] + \dots \end{aligned} \quad (18.87)$$

He arrived at the conclusion that for small qR_g values, the first term was fully dominant and only the

diffusion of the center of mass (D) could be observed [80]. However, for $qR_g \geq 1.73$, the first relaxation time starts to influence $g_1(\mathbf{q}, t)$. A simple calculation tells us that in order to observe the first internal relaxation mode, the polymer chain must have an extremely high molecular weight. In fact, most dynamic light experiments in the dilute regime that tried to observe the first internal relaxation mode were performed with very high molecular polymers on the order of several million Daltons [81, 82]. In the intermediate q region defined as $qR_g \gg 1$ but $q\ell < 1$ where ℓ is an effective monomer length, Dubois-Violette and de Gennes [83] showed that $g_1(\mathbf{q}, t)$ scaled as $g_1(\mathbf{q}, t) \approx \exp(f[\omega_c(q)t])$ where $\omega_c(q)t$ is a dimensionless time. They obtained explicitly the form of f for the case of an unperturbed Gaussian chain and found that $\omega_c(q) \approx (k_B T/\eta)q^3$. Akcasu and Benmouna [84] obtained the first cumulant $\langle \Gamma(q) \rangle$ for all q regions, including the transition zone, for different models of chain and without preaveraging the hydrodynamic interactions. They found, in the intermediate region, the same scaling law for $\omega_c(q)$ than Dubois-Violette and de Gennes. For $qR_g \ll 1$, they recovered the usual diffusive behavior. Lodge et al. (82b) confirmed experimentally this scaling law in the intermediate q region in a temperature range going from θ -solvent to a good solvent. However, the authors found a small and systematic deviation of the experimentally found $\langle \Gamma(q) \rangle$ with that predicted by Akcasu and Benmouna without preaveraging approximation. Recently Li et al. (82c) found experimentally that for temperatures below the θ temperature, this scaling law no longer holds.

As the concentration increases and reaches the local concentration of a single chain c^* , the chains start to overlap each other. The limiting concentration c^* can vary depending on solvent quality and temperature. Concentration higher than c^* but lower than the entanglement concentration c_e is called the *semidilute regime*. When $c > c_e$, we refer it as a *concentrated solution*. When $c > c_e$, all chains entangle with each other. Each chain could be visualized as being for a short time within a tube made of the surrounding chains and whose diameter depends on concentration. In fact, at a particular instant we can picture the entangled mesh, with an average mesh size ξ (the correlation length) and therefore the tube diameter will be on the order of ξ and will only depend on concentration. In an athermal solvent, a portion with average size ξ (blob) of the chain inside the tube will not interact with other chains. So we can imagine the chain inside the tube as formed of a collection of blobs of g monomers each. Since the first cumulant is only related to the short time dynamics, the motion that we will be concerned at high concentrations is that produced by the thermally excited monomers inside the blobs that will concomitantly produce Brownian motion of their center of mass.

At higher concentrations, besides a fast mode (cooperative diffusion), other modes are present by DLS even for lower molecular weight polymers, since other cooperative phenomena occur that involve more chains or aggregates of these.

Recently, Li et al. [85] reexamined the slow relaxation mode and found that in dust-free samples of monodisperse PS, the solvent quality was a definitive factor in observing or not observing the slow mode. For athermal solvents for PS such as benzene, they showed that even at concentrations as high as 20% only one fast diffusive mode was observed (Fig. 18.15a). In contrast, they showed that the slow mode for $c > c^*$ is enhanced as the solvent quality decreases. In cyclohexane, in which solvent quality for PS decreases when temperature decreases from 50 to 32 °C, they observed a slow mode, in addition to the cooperative diffusion (fast mode). In Figure 18.15b, $G_2(\mathbf{q}, t)$ shows a single fast mode for a PS with $M_w = 1.83 \times 10^6$ Da in cyclohexane at 50 °C for $c/c^* \approx 1$; however, when $c/c^* > 1$, a second mode appears. All samples in this study were prepared in the same way, except the solvent used and the concentration. Cyclohexane is a good solvent of PS at 50 °C, but it is not athermal. They concluded that if c is only a few times larger than the overlap concentration (c^*) but lower than the entanglement concentration (c_e), the slow mode is related to transient interchain segment-segment interaction induced clusters. Actually, for $c/c^* = 1.4$, they were able to observe the slow mode with molecular weights as low as 4.6×10^{-4} Da; reinforcing their conclusion was the fact that this mode was more notorious at *small angles*. For $c > c_e$, it is attributed to the confinement of each chain inside an inhomogeneous tube with a “band”-like structure due to relatively stronger segment-segment interaction near the entanglement points.

In fact, having all chains entangled with each other they form a large cluster and, at short times, only the blobs can jiggle around in the tube; their motion will depend on how close they are to an entanglement point. In contrast with the semidilute regime, for $c > c_e$, the slow mode is most pronounced when observed at *large angles*, implying that it is not related to the scattering of some large object. They also pointed out that in the athermal solvent, there is no interaction between the chain blobs and the tube so that they experience the same microenvironment resulting in only a diffusive relaxation mode. Finally, in their study, the scaling law of $\langle \Gamma \rangle_{\text{slow}}$ with q depended on the concentration, going from q^3 for dilute solutions to q^0 at high concentrations, suggesting that the origin of the slow mode is different for each concentration regime.

Following the same line of thought, Yuan et al. [86] applied DLS to thermally responsive systems such as poly(N-isopropylacrylamide) (PNIPAM) or poly(ethylene oxide)-b-poly(propylene oxide)-b-poly(ethylene oxide) (PEO-PPO-PEO) in water. Similar to the PS/cyclohexane

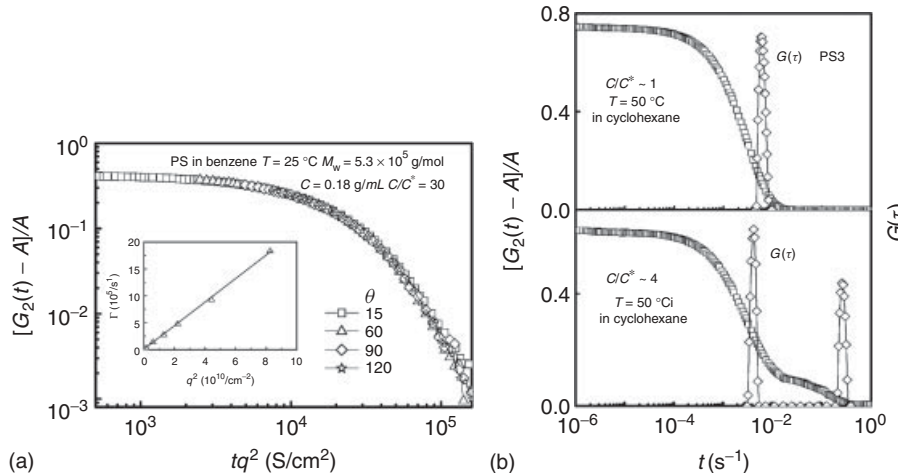


Figure 18.15 Intensity–intensity time correlation function for a solution of PS in benzene and cyclohexane. (a) A highly concentrated athermal solution of PS in benzene: only a single diffusive mode is present. The inset shows the q^2 dependence of $\langle \Gamma \rangle$. (b) $G_2(\mathbf{q}, t)$ and the distribution of time relaxation ($G(\tau)$) for a solution of a 1.83×10^6 PS in cyclohexane at 50°C at concentrations $c \approx c^*$ and $c \approx 4 c^*$. Source: Reprinted with permission from Li J, Li W, Huo H, Luo S, Wu C. *Macromolecules* 2008;41:901 [85]. Copyright 2008 American Chemical Society.

system, they were able to use the temperature dependence of the solvent–polymer interaction in both systems to investigate the temperature-induced shrinkage of polymer chains. The difference in nature of the slow mode in these two systems is that as the solvent becomes poorer, PNIPAM/H₂O aggregates, whereas PEO-PPO-PEO/H₂O forms micelles.

Another interesting application of DLS is the work by Pan et al. [87] on the dynamics of block copolymers in the vicinity of an order–disorder transition (ODT). Motivated by the phenomena encountered near the ODT, such as chain stretching and large amplitude concentration fluctuations, Pan et al. studied the polymer dynamics of solutions of symmetric block copolymers of poly(styrene-*b*-isoprene) (PSI) from dilute, semidilute, and concentrated regimes. Previously, Benmouna and coworkers [88] had predicted two dynamical modes: a cooperative diffusion, with a diffusion coefficient D_C (C-mode) corresponding to the relaxation of fluctuations in polymer concentration, and an internal mode (Γ_I), reflecting relative motion of the centers of mass of the two blocks on a single chain. Semenov et al. [89], in addition, predicted a third mode: the heterogeneity mode (H-mode) due to chain-to-chain fluctuations in composition and that relaxes by translational diffusion with a diffusion coefficient D_H . They assumed that these modes are uncoupled, and therefore, $g_1(\mathbf{q}, t)$ can be written as a sum of exponentials. The decay constants for the cooperative diffusion and heterogeneity mode are of the form $q^2 D$, given their diffusive character, as we shall see, whereas the internal mode has a decay constant $\Gamma_I \approx \tau_1^{-1}$, where τ_1 is the longest viscoelastic relaxation time of the chain.

In semidilute and concentrated solutions, D_C and D_H are cleanly resolved; however, in these concentration regimes, the internal mode Γ_I was only observed in the higher molecular weight blocks used in the study (3.4×10^5 Da and referred to as SI(170-170) with a number fraction of 0.5 for the PS block). In all the systems used in this study, $qR_g < 1$. In the semidilute regime, they confirmed that D_C scaled with concentration as $\approx c^{0.70}$, independent of the molecular weight (M). It was also observed that translational diffusivity was unaffected by the ODT. The relative amplitudes of D_C and D_H also scaled with c , M , and the refractive index of the solvent, n_s , as predicted by the theory. Figure 18.16a shows a representative intensity correlation function at 90° for the SI(170-170) copolymer at various weight fractions (w). For this block copolymer, the limiting concentration c^* between the dilute and semidilute regimes corresponds to $w = 0.0169$. Using the Siegert relation to obtain $g_1(\mathbf{q}, t)$ and CONTIN to perform the Laplace inversion, they resolved the modes’ contribution to $g_1(\mathbf{q}, t)$, as shown in Figure 18.16b. In dilute solutions, as expected, only one diffusive mode is present and is attributed to a superposition of D_C and D_H . As we reach the semidilute regime, the H- and C-modes are clearly resolved, with the C-mode being dominant. As we increase the concentration furthermore ($w = 0.049$), an intermediate mode appears, which was assigned to the internal mode, and the contribution of H-mode overpasses that of the C-mode as predicted by the theory. At higher concentrations only the H-mode is well resolved; this data correspond to a solution close to the ordered state. As stated above, the Laplace inversion methods do not give us a high resolution $G(\Gamma)$,

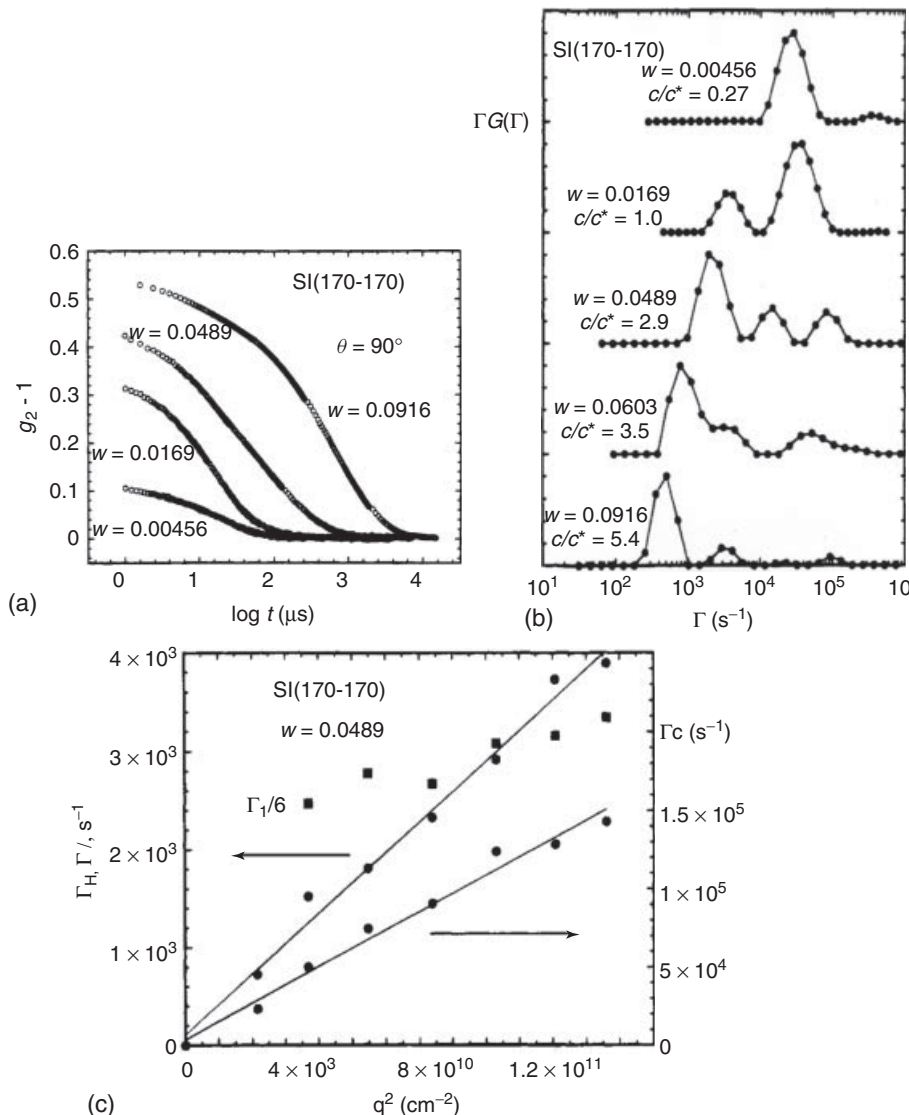


Figure 18.16 Intensity–intensity correlation functions for a symmetric PS-PI block copolymer with $M_w = 3.4 \times 10^5$ Da in benzene at different weight concentrations. (a) $G_2(q, t)$ versus w ; (b) the Laplace inversion time decay rate distribution $G(\Gamma)$; (c) Γ versus q^2 for the three modes. Source: Reprinted with permission from Pan C, Maurer W, Liu Z, Lodge TP, Stepanek P, von Meerwall ED, Watanabe H. *Macromolecules* 1995;28:1643 [87]. Copyright 1995 American Chemical Society.

and if two modes are not well separated, as is the case with Γ_I and Γ_C , then they might appear as a single mode; this is even worse if one of the modes has comparatively a smaller contribution to $G(\Gamma)$ such as Γ_I . Finally, Figure 18.16c shows the q^2 dependence of Γ_H and Γ_C , proving their diffusive character, whereas Γ_I has a mild q dependence for $qR_g < 0.5$.

The study of internal modes by DLS has led to many interesting applications, for example, the effect of crosslinking on dynamics during sol–gel transition [90], the study of the apparent diffusion coefficient on hyperbranched

starch samples [55], structural relaxation in glassy polymers [91], diffusion in concentrated colloidal suspensions and glasses [92], and many more that we cannot review in this chapter because of space constraints.

REFERENCES

- [a] Maret G, Wolf PE. *Z Phys B* 1987;65:409. [b] Pine DJ, Weitz DA, Chaikin PM, Herbolzheimer E. *Phys Rev Lett* 1988;60:1134. [c] Weitz DA, Pine DJ. Diffusing-wave spectroscopy. In: Brown W, editor. *Dynamic Light Scattering*.

- New York: Oxford University Press; 1993. p 652. [d] Scheffold F, Romer S, Cardinaux F, Bissig H, Stradner A, Rojas-Ochoa LF, Trappe V, Urban C, Skipetrov SE, Cipelletti L, Schurtenberger P. *Progr Colloid Polymer Sci* 2004;123:141.
2. [a] Brown RGW. *Appl Opt* 1987;26:4846. [b] Wiese H, Horn D. *J Chem Phys* 1991;94:6429. [c] Auweter H, Horn D. *J Colloid Interface Sci* 1985;105:399.
 3. [a] Phillips GDJ. *Phys Rev A* 1981;24:1939. [b] Schätzel K. *J Mod Opt* 1991;38:1849. [c] Segré PN, Van Megen W, Pusey PN, Schätzel K, Peters W. *J Mod Opt* 1995;42:1929. [d] Stieber F, Richtering W. *Langmuir* 1995;11:4724.
 4. [a] Aberle LB, Hulstede P, Wiegand S, Schroer W, Staude W. *Appl Opt* 1998;37:6511. [b] Urban C, Schurtenberger P. *J Colloid Interface Sci* 1998;207:150. [c] Pusey PN. *Curr Opin Colloid Interface Sci* 1999;4:177. [d] Block I, Scheffold F. *Rev Sci Instrum* 2010;81:123107.
 5. van de Hulst HC. *Light Scattering by Small Particles*. New York: John Wiley; 1957.
 6. [a] Kerker M. *The Scattering of Light and Other Electromagnetic Radiation*. New York: Academic Press; 1969. [b] Bohren C, Huffman D. *Absorption and Scattering of Light by Small Particles*. New York: John Wiley; 1983.
 7. Mishchenko MI, Travis LD, Lacis AA. *Scattering, Absorption, and Emission of Light by Small Particles*. Cambridge: Cambridge University Press; 2002.
 8. Landau LD, Lifshitz EM, Pitaevskii LP. *Electrodynamics of Continuous Media*. 2nd ed. Vol. 8. Oxford, UK: Butterworth-Heinemann; 1984.
 9. [a] Lord Rayleigh (Strutt JW), Philos Mag 1871;41:107. [b] Lord Rayleigh (Strutt JW), Philos Mag 1881;12:81.
 10. Glatter O, Kratky O, editors. *Small Angle X-ray Scattering*. New York: Academic Press; 1982.
 11. [a] Lovesey SW. *The Theory of Neutron Scattering from Condensed Matter*. Vol. 1 & 2. Oxford: Oxford University Press; 1984. [b] Hammouda B. *J Macromol Sci Polymer Rev* 2010;50:14.
 12. von Smoluchowski M. *Ann Phys* 1908;25:205.
 13. Einstein A. *Ann Phys* 1910;33:1275.
 14. Brinkman HC, Hermans JJ. *J Chem Phys* 1949;17:574.
 15. Stockmayer WH. *J Chem Phys* 1950;18:58.
 16. Kirkwood JG, Goldberg RJ. *J Chem Phys* 1950;18:54.
 17. Strazielle C. Light Scattering in Mixed Solvents In: Huglin MB, editor. *Light Scattering by Polymer Solutions*. London: Academic Press; 1972. p 633.
 18. Stockmayer WH, Moore LD Jr., Fixman M, Epstein BN. *J Polym Sci* 1955;16:517.
 19. Bushuk W, Benoit H. *Can J Chem* 1958;36:1616.
 20. Benoit H and Froelich D. Application of Light Scattering to Copolymers In: Huglin MB, editor. *Light Scattering by Polymer Solutions*. London: Academic Press; 1972. p 467.
 21. Casassa EF, Eisenberg H. *J Phys Chem* 1960;64:753.
 22. Casassa EF, Eisenberg H. *J Phys Chem* 1961;65:427.
 23. Tuzar Z, Kratochvil P, Straková D. *Eur Polym J* 1970;6:1113.
 24. Tuzar Z, Kratochvil P, Colin Czech Chem Commun 1967;32:3358.
 25. Podešva J, Stejskal J, Kratochvíl P. *Macromolecules* 1987;20:2195.
 26. Read BE. *Trans Faraday Soc* 1960;56:382.
 27. Vrij A, Overbeek JT. *J Colloid Sci* 1962;17:570.
 28. [a] Strazielle C, Benoit H. *J Chim Phys* 1961;58:675. [b] Strazielle C, Benoit H. *J Chim Phys* 1961;58:678.
 29. Lange H. *Makromol Chem* 1965;86:192.
 30. Stockmayer WH, Chan L-L. *J Polym Sci A* 1966;4:437.
 31. Mauss Y, Chambron J, Daune M, Benoit H. *J Mol Biol* 1967;27:579.
 32. Marchal E, Strazielle C. *Compt Rendu* 1968;C267:135.
 33. Cowie JMG. *Pure Appl Chem* 1970;23:355.
 34. Zimm BH. *J Chem Phys* 1948;16:1093.
 35. Debye P. *Ann Phys* 1915;46:809.
 36. Debye P. *J Phys Colloid Chem* 1947;51:18.
 37. Debye P, Anacker EW. *J Phys Colloid Chem* 1951;55:644.
 38. Zimm BH. *J Chem Phys* 1948;16:1099.
 39. Chu B, Wu C. *Macromolecules* 1987;20:93.
 40. Kratochvíl P. Particle Scattering Functions In: Huglin MB, editor. *Light Scattering by Polymer Solutions*. London: Academic Press; 1972. p 333.
 41. [a] Burchard W. *Adv Polym Sci* 1983;48:1. [b] Burchard W. *Adv Polym Sci* 1999;143:113.
 42. [a] Benoit H. *J Polymer Sci* 1953;11:507. [b] Benoit H, Holtzer AM, Doty P. *J Phys Chem* 1954;58:635.
 43. Holtzer A. *J Polymer Sci* 1955;17:432.
 44. Galinsky G, Burchard W. *Macromolecules* 1997;30:4445.
 45. Burchard W. *Macromolecules* 1977;10:919.
 46. Dobashi T, Narita T, Masuda J, Makino K, Mogi T, Ohshima H, Takenaka M, Chu B. *Langmuir* 1998;14:745.
 47. Lonetti B, Tsikri A, Lang PR, Stellbrink J, Willner L, Kohlbrecher J, Lettinga MP. *Macromolecules* 2011;44:3583.
 48. Kholodenko AI. *Macromolecules* 1993;26:4179.
 49. Schärtl W. *Light Scattering from Polymer Solutions and Nanoparticle Dispersions*. Berlin, Heidelberg: Springer-Verlag; 2007.
 50. Berne BJ, Pecora R. *Dynamic Light Scattering*. New York: John Wiley & Sons; 1976.
 51. Siegert AJF, Massachusetts Institute of Technology, Boston, MA. 1943. M.I.T. Rad. Lab. Rep., No. 465.
 52. Ford NC. Theory and practice of photon correlation spectroscopy. In: Dahneke BE, editor. *Measurement of Suspended Particles by Quasi-elastic Light Scattering*. New York: Wiley-Interscience; 1983. p 31.
 53. [a] McWhirter JG, Pike ER. *J Phys A Math Gen* 1978;11:1729. [b] McWhirter JG. *Opt Acta* 1980;27:8.
 54. Koppel DE. *J Chem Phys* 1972;57:4814.
 55. Galinsky G, Burchard W. *Macromolecules* 1997;30:6966.
 56. Ostrowsky N, Sornett D, Parker P, Pike ER. *Opt Acta* 1981;28:1059.

57. Provencher SW, Hendrix J, De Maeyer L, Paulusen N. *Chem Phys* 1978;69:4273.
58. [a] Provencher SW. *Makromol Chem* 1979;180:201. [b] Bryant G, Abeynayake C, Thomas J. *Langmuir* 1996;12:6224.
59. Gull SF. Developments in maximum entropy data analysis. In: Skilling J, editor. *Maximum Entropy and Bayesian Methods*. Dordrecht: Kluwer Academic Publishers; 1989. p 53–71.
60. Jakes J. *Czech J Phys* 1988;38:1305.
61. De Vos C, Deriemaeker L, Finsy R. *Langmuir* 1996;12:2630.
62. Finsy R. *Adv Colloid Interface Sci* 1994;52:79.
63. Bryant G, Thomas J. *Langmuir* 1995;11:2480.
64. [a] Vega JR, Gugliotta LM, Gonzalez VDG, Meira GR, J Colloid Interface Sci 2003;261:74. [b] Gonzalez VDG, Gugliotta LM, Vega JR, Meira GR. *J Colloid Interface Sci* 2005;285:581. [c] Gugliotta LM, Stegmayer GS, Clementi LA, Gonzalez VDG, Minari RJ, Leiza JR, Vega JR. *Part Part Syst Char* 2009;26:41.
65. Clementi LA, Vega JR, Gugliotta LM, Orlande HRB. *Chemometr Intell Lab Syst* 2011;107:165.
66. Pecora R. *J Chem Phys* 1964;40:1604.
67. Pecora R. *J Chem Phys* 1968;48:4126.
68. Doi M, Edwards SF. *The Theory of Polymer Dynamics*. Oxford: Clarendon Press; 1988. Chapter 8.
69. Wilcoxon J, Schurr JM. *Biopolymers* 1983;22:849.
70. Maeda T, Fujime S. *Macromolecules* 1984;17:1157.
71. Hammouda B. *Macromolecules* 1985;18:293.
72. [a] Broersma S. *J Chem Phys* 1960;32:1626. [b] Broersma S. *J Chem Phys* 1981;74:6989. [c] Tirado MM, García de la Torre J. *J Chem Phys* 1979;71:2581. [d] Tirado MM, García de la Torre J. *J Chem Phys* 1986;1980:73. [e] Tirado MM, López Martínez C, García de la Torre J. *J Chem Phys* 1984;81:2047.
73. Buitenhuis J, Dhont JKG, Lekkerkerker HNW. *J Colloid Interface Sci* 1994;162:19.
74. Lehner D, Lindner H, Glatter O. *Langmuir* 2000;16:1689.
75. Doi M, Edwards SF. *The Theory of Polymer Dynamics*. Oxford: Clarendon Press; 1988.
76. de Gennes PG. *Scaling Concepts in Polymer Physics*. Ithaca, NY: Cornell University Press; 1979.
77. [a] Yamakawa H. *Modern Theory of Polymer Solutions*. New York: Harper & Row; 1971. Chapter 6. [b] Doi M, Edwards SF. *The Theory of Polymer Dynamics*. Oxford: Clarendon Press; 1988. Chapter 4. [c] Stockmayer WH. Dynamics of chain molecules. In: Balian R, Weill G, editors. *Molecular Fluids*. New York: Gordon and Breach; 1976.
78. Rouse PEJ. *J Chem Phys* 1953;21:1272.
79. Zimm BH. *J Chem Phys* 1956;24:269.
80. Pecora R. *J Chem Phys* 1968;49:1032.
81. Huang WN, Frederick JE. *Macromolecules* 1974;7:34.
82. [a] Han CC, Akcasu AZ. *Macromolecules* 1981;14:1080. [b] Lodge TP, Han CC, Akcasu AZ. *Macromolecules* 1983;16:1180. [c] Li J, Lu Y, Zhang G, Wu C. *Chin J Polym Sci* 2008;26:775.
83. Dubois-Violette E, de Gennes PG. *Physics* 1967;3:181.
84. Akcasu AZ, Benmouna M, Han CC. *Polymer* 1980;21:866.
85. Li J, Li W, Huo H, Luo S, Wu C. *Macromolecules* 2008;41:901.
86. Yuan G, Wang X, Han CC, Wu C. *Macromolecules* 2006;39:3642.
87. Pan C, Maurer W, Liu Z, Lodge TP, Stepanek P, von Meerwall ED, Watanabe H. *Macromolecules* 1995;28:1643.
88. [a] Benmouna M, Duval M, Borsali R. *J Polym Sci Polym Phys Ed* 1987;25:1839. [b] Benmouna M, Benoit H, Borsali R, Duval M. *Macromolecules* 1987;20:2620.
89. Semenov AN, Fytas G, Anastasiadis SH. *Polymer Prepr* 1994;35:618.
90. [a] Ngai T, Wu C, Chen Y. *J Phys Chem B* 2004;108:5532. [b] Ngai T, Wu C, Chen Y. *Macromolecules* 2004;37:987. [c] Ngai T, Wu C. *Macromolecules* 2003;36:848. [d] Li J, Ngai T, Wu C. *Polym J* 2010;42:609.
91. [a] Patterson GD. *Adv Polym Sci* 1983;48:125. [b] Forrest JA, Svanbera C, Revesz K, Rodahl M, Torell LM, Kasemo B. *Phys Rev E* 1998;58:R1226.
92. [a] Bartsch E. *Curr Opin Colloid Interface Sci* 1998;3:577. [b] Cipelletti L, Weeks ER. Glassy dynamics and dynamical heterogeneity in colloids. In: Berthier L, Biroli G, Bouchaud J-P, Cipelletti L, editors. *Dynamical Heterogeneities in Glasses, Colloids, and Granular Media*. Oxford, UK: Oxford University Press; 2011.



19

SMALL-ANGLE X-RAY SCATTERING OF POLYMER SYSTEMS

CARLOS A. AVILA-ORTA AND FRANCISCO J. MEDELLÍN-RODRÍGUEZ

19.1 INTRODUCTION

Semicrystalline thermoplastic polymers are widely used for a number of applications in food packaging, automotive parts, textiles, medical devices, etc., because of their excellent physical and chemical properties. In turn, these properties depend on the morphology developed by these crystalline systems. Unit cell, lamellar structure, and microstructure show different morphological features at different scales. In the nanoscale, the lamellar structure formed by alternating crystalline and amorphous layers predominates. Because of the length scale and the electron density difference between the crystalline and amorphous phases, this type of morphology is well suited to be studied by means of small-angle X-ray scattering (SAXS). This technique is useful to determine the crystalline and amorphous thicknesses and their distributions, as well as the crystal perfection. In this chapter, we describe the fundamentals of polymer morphology, one-dimensional data analysis in the reciprocal space as well as their possibilities in real space, and an application example.

19.2 POLYMER MORPHOLOGY

Polymers are considered macromolecular chains of high molecular weight formed by monomers bonded covalently. They can be obtained from natural sources or from synthetic processes through different polymerization routes [1]. A number of both natural and synthetic polymers are able to form regular arrangements, that is, crystalline entities, under either quiescent or deformed states. Cellulose and natural

rubber are examples of natural polymers, while polyethylene (PE), isotactic polypropylene (iPP), and poly(ethylene terephthalate) (PET) are common synthetic polymers that can crystallize. The size, shape, and organization of the crystals depend on the chemical and molecular structure (stereoregularity, tacticity, molecular weight, chain flexibility) and crystallization conditions (quiescent, deformed, melt, solution). Although thermosets and rubbers can show crystalline behavior, thermoplastic polymers offer a wide range of possibilities, and so we focus our attention on this type of polymers.

Thermoplastic polymers are synthetic polymers that become plastic on heating and harden on cooling. PE, iPP, PET, and polyamides, among others, are typical examples of this type of polymers. Depending on the chemical and molecular structure and processing variables, they may or may not crystallize. Thermoplastic polymers that are able to crystallize have a significant amount of amorphous material, and therefore they are known as *semicrystalline thermoplastic polymers*.

The study of polymer morphology aims to elucidate the organization of crystalline domains [2]. Polymer morphology depends on the intrinsic properties of the polymer (chemical and molecular structure) as well as on the processing conditions (crystallization conditions, temperature, pressure, deformation, state). Besides, polymer morphology has a hierarchical structure. Polymer single crystals, spherulites, and shish kebabs are common polymer morphologies on the micrometer size, formed of lamellae on the nanometer scale (thickness), with unit cells in angstroms. These entities are the dimensional levels for the morphology of crystalline polymers.

19.2.1 Single Crystals, Spherulites, and Shish Kebabs

Polymer crystals can be obtained from either dilute solutions or amorphous states (glassy or molten) [2, 3]. Crystallization from dilute solutions usually gives polymer single crystals. Fischer, Keller, and Till reported the formation of polymer single crystals from dilute solutions [4]. On the other hand, three-dimensional polycrystalline structures named *spherulites* are usually obtained during polymer crystallization from the glassy or the molten state [5]. Bunn and Alcock and Keller found that polymers show this type of organization [6]. Finally, when the polymer solution or the amorphous state is under stress, long chains extend, serving as nuclei (shish), whereas smaller chains crystallize (kebab), usually in the form of a disk. Shish kebab structures were first observed by Mitsuhashi, Pennings, and Binsbergen [7].

19.2.2 Lamellae

Polymer chains form regular arrangements while extended (extended chain crystals) or when they fold (chain-folded crystals or lamellae). The former is usually observed when crystallization conditions are near the thermodynamic conditions (near the equilibrium melting point), while the latter is governed by the kinetics at temperatures far away from the equilibrium conditions, where most industrial processes take place. In this case, polymer chains fold, forming thin lamellae with thicknesses ranging from 5 to 20 nm and widths in the range of micrometers. Keller inferred the existence of a chain-folded molecular conformation within polyethylene single crystals obtained from dilute solutions (4b). These thin crystals are known as *chain-folded crystals* when polymers are crystallized from dilute solutions, while they are named *chain-folded lamellae* or *lamellae* when they are crystallized from the amorphous (glassy or molten) state [8]. A scheme of a chain-folded crystal is shown in Figure 19.1, where the crystal thickness is denominated l_c .

The lamella is recognized as the component that imparts texture to most semicrystalline polymers. Besides, the surface regions of lamellae combine two different characteristics [2]. On one hand, there is evidence of order, and on the other, disorder. Both characteristics must be accommodated in the space of a crystalline unit. Therefore, the amorphous material alternates with lamellar crystals, resulting in the formation of lamellar structures (Fig. 19.2). Under quiescent conditions, lamellar crystals grow from a common radiating center forming spherulites, while for stressed melts cylindrical crystals alternate with amorphous material along an elongated nucleus to form shish kebab structures. Even when lamellar and spherulitic morphologies of crystallized polymers are different, lamellae should be inside spherulites, as is schematized in Figure 19.3 [8].

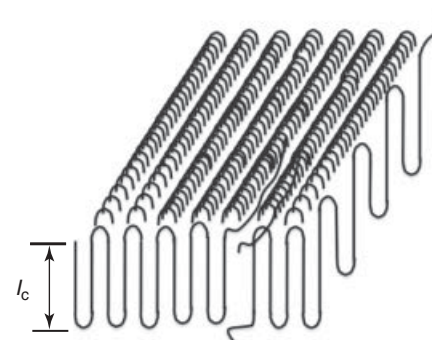


Figure 19.1 Scheme of unique crystal of folded chain for PE. Source: After Hoffman JD, Davis GT, Lauritzen JI. The rate of crystallization of linear polymers with chain folding. In: Hannay NB, editor. Treatise Solid State Chemistry, Volume 3, p 418, 508, 520 [8]. Copyright 1976 Plenum Press.

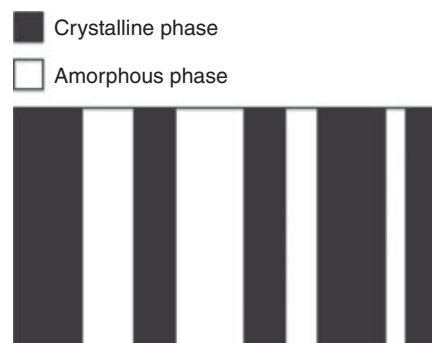


Figure 19.2 Scheme of lamellar structure.

19.2.3 Unit Cells

Chain-folded molecules ordered in a regular arrangement are three-dimensional crystals. A three-dimensional crystal is formed by a large number of smaller, hypothetical, three-dimensional crystals with sizes a , b , and c , named *unit cells*. Each unit cell contains a complete representation of the entire crystalline structure and gives the information needed to describe the whole arrangement. Depending on the conformation of the molecular chains and its own arrangement, any structure can be assigned to one of the six systems characterized by the ratios of the unit cell edges (a , b , and c) and their angles (α , β , and γ). The values of the unit cell constants are in general in the range of angstroms, which make them suitable to be studied by wide-angle X-ray scattering (WAXS). Semicrystalline polymers produce a mixed interference pattern, sharp and diffuse at the same time, when analyzed by WAXS [9]. This evidences the existence of a two-phase system, that is, a three-dimensional crystalline network with amorphous zones.

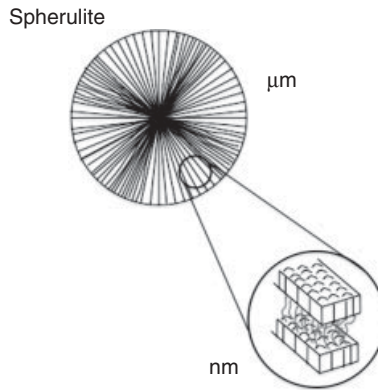


Figure 19.3 Spherulitic structure model. Note the growth direction and points of lamellar ramification, to fill void space with crystals in a uniform way. Source: After Hoffman JD, Davis GT, Lauritzen JI. The rate of crystallization of linear polymers with chain folding. In: Hannay NB, editor. Treatise Solid State Chemistry, Volume 3, p 418, 508, 520 [8]. Copyright 1976 Plenum Press.

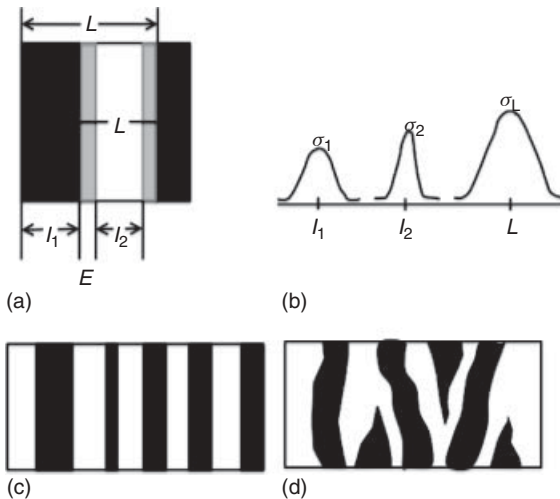


Figure 19.4 Physical representation of morphological parameters: (a) characteristic distances, (b) statistical features, (c) stacking size, and (d) interfaces planarity.

19.3 SMALL-ANGLE X-RAY SCATTERING

SAXS is a powerful tool to study the morphology of semicrystalline systems. The application of this technique is based on the electron density difference between the crystalline and amorphous phases (lamellar structure) in polymer systems. The crystalline (l_c) and amorphous (l_a) thicknesses can be obtained using this technique. Besides, the distance from one crystalline region to the next provides the size of a lamellar structure, also known as *the long period* (L). Other morphological features are the interface thickness (E), the thickness distribution (σ_c , σ_a , σ_L), the size of the lamellar stacking (t), and the dispersion capacity or invariant (Q). A schematic representation of some of these parameters is shown in Figure 19.4. Lamellar thicknesses l_c and l_a correspond to the average size of each phase. Since the technique cannot differentiate which thickness corresponds to the crystalline phase and which one to the amorphous phase, we denote them as l_1 and l_2 . The long period L is the distance between phases of the same type. Each of these thicknesses has a size distribution, typically Gaussian. The interface thickness E is the distance when the interface is not sharp, that is, the interface is finite. The lamellar stacking size can be finite or infinite.

19.3.1 Interaction of X-Rays with Matter

SAXS is determined by interference phenomena, where the waves are coherent and therefore their amplitudes can be added even if the emerging waves are not in phase as in the case of WAXS [10]. SAXS intensity is given by the absolute square of the resulting amplitude, which is obtained by summing all secondary waves. All amplitudes have the

same magnitude and differ only in their phase ϕ , which depends on the electron position in space. The secondary scattering wave can be represented as $e^{i\phi}$, where ϕ is $2\pi/\lambda$ times the optical path δ and a reference point. Considering the number of electrons implied in the dispersion process, and the fact that an electron cannot be localized exactly, it becomes convenient to introduce the concept of electron density as described next.

19.3.2 Electron Density Function

Electron density function is defined as the number of electrons per unit volume and it is denoted as $\rho(r)$. Electron density function of a semicrystalline polymer consists of a series of alternating steps, positive ρ_1 and negative ρ_2 , which represent phases, and fluctuate around an average value ρ_m . If, for example, an r vector is passed along the semicrystalline structure (Fig. 19.5), it can be seen that $\rho(r) = \rho_1$ if $\rho(r) > \rho_m$. On the other hand, $\rho(r) = \rho_2$ if $\rho(r) < \rho_m$, where ρ_1 is a high density region (crystalline) and ρ_2 is a low density region (amorphous).

19.3.3 Scattering Vector

Because of the inverse relation existing between the size of the scatterer and the distance of incidence of the source, experimental effects are observed in reciprocal space. Therefore, in order to obtain estimates in the reciprocal space, the geometry of a system with two dispersion centers which is impacted by X-ray beam is defined, determining a scattering vector in the reciprocal space, q .

In order to calculate the scattering vector q , it is necessary to calculate the phase ϕ . As previously mentioned,

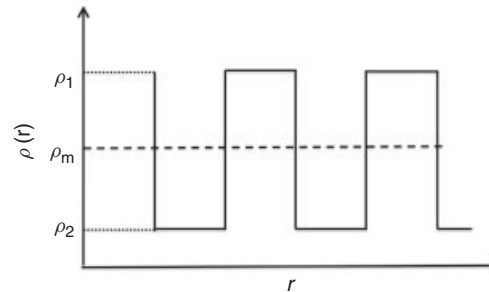


Figure 19.5 Schematic representation of the electron density function.

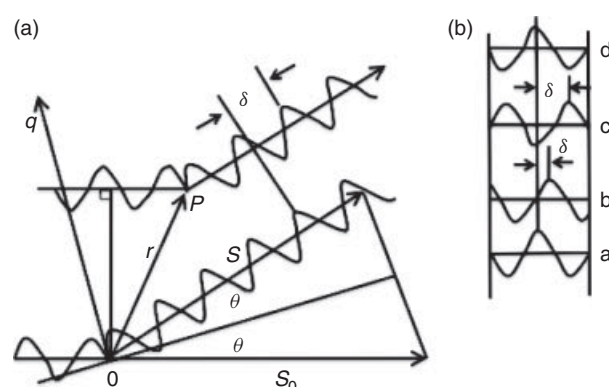


Figure 19.6 A (left). Geometry to obtain the scattering vector q . B (right). Wave enlargement: a, Reference wave; b, wave displaced δ ($0 < \delta < 1$); c, wave displaced 1π ($\delta < 1/2$); and d, wave displaced 2π ($\delta = 1$).

$\phi = 2\pi/\lambda \cdot \delta$. The distance from one dispersion center to another is called r , as shown in Figure 19.6A, where the unit vector s_0 has the direction of the incident beam and the unit vector s represents the vector of the dispersed wave. Bearing in mind this idea, $\delta = -r(s - s_0)$ can be defined, and therefore $\phi = -2\pi/\lambda \cdot r(s - s_0)$. The magnitude $(s - s_0) = 2 \cdot \sin\theta$, where θ is the angle of the scattering vector. A new q vector can be defined with direction $(s - s_0)$ and magnitude $4\pi/\lambda \cdot \sin\theta$ as

$$q = \frac{4\pi}{\lambda} \cdot \sin\theta \quad (19.1)$$

for which the phase $\phi = q \cdot r$. Then, the representation of a dispersed secondary wave in the complex form is e^{-iqr} . The vector product qr means that only the component of r in q is relevant for the phase, so that all the points in a plane perpendicular to q will have the same phase [10].

When the emergent waves of a scattering center in small angles are displaced in the range ($0 < \delta > 1$, $\delta \neq 1/2$) with respect to a reference wave, a dispersion phenomenon occurs (Fig. 19.6B, case b). If the emergent wave is

displaced by $\delta = 1/2$, then widths of the waves cancel out and dispersion does not take place (Fig. 19.6B, case c). These two cases do not produce diffraction (WAXS) since the condition for the diffraction phenomenon to take place is that the waves must be in phase, thus is, $\delta = 1$, as illustrated in case (d) of Figure 19.6B.

Additionally, this condition is also necessary in order to produce the phenomenon of scattering. In short, WAXS and SAXS techniques depend on the value of δ . In the range ($0 < \delta \leq 1$, $\delta \neq 1/2$) this condition is fulfilled, so that the scattering phenomenon (SAXS) is produced; the diffraction phenomenon (WAXS) is produced if and only if $\delta = 1$.

19.3.4 Scattering Intensity

Assuming a unique dispersion process and the applicability of the theory of kinematic dispersion, the intensity of dispersion $I(q)$ is given by

$$I(q) = \Im[\Delta p^{*2}(r)] \quad (19.2)$$

where $\Delta\rho(r)$ is the difference between the local and the average electronic densities ($\rho(r) - \rho_m$), \Im represents the three-dimensional Fourier transform, and the term *2 indicates an autoconvolution or autocorrelation [11]. Then Equation 19.2 can be rewritten as

$$I(q) = \int_V \Delta p^{*2}(r) \cdot e^{-iqr} dV \quad (19.3)$$

In Equation 19.3, it is observed that the real space (r) and the reciprocal space (q) are connected by the phase qr , and naturally q will diminish when r increases, and vice versa, with the same factor. In this way, large particles will give a concentrated scattering pattern in small angles. Especially with particles or heterogeneities of colloidal dimensions, and with a wavelength of 1.5 \AA , the dispersion pattern is limited to 1° or 2° of the scattering angle. This is the typical domain of SAXS.

In SAXS, two restrictions are generally present which simplify the analysis of scattering:

1. The system is statistically isotropic. Because of this restriction, the distribution $\rho^{*2}(r)$ depends only on the magnitude of the distance r . Additionally, the phase factor e^{-iqr} can be replaced by its average taken in all directions and it is expressed as [12]

$$\langle e^{-iqr} \rangle = \frac{\sin(qr)}{qr} \quad (19.4)$$

Then Equation 19.3 can be written as

$$I(q) = \int_V 4\pi r^2 \Delta p^{*2}(r) \cdot \frac{\sin(qr)}{qr} dr \quad (19.5)$$

2. Long-range order does not exist [12]. This means that correlation between two widely separated points does not exist. In accordance with the above, at large values of r , the electron densities would be independent, and they could be replaced by the average value ρ_m . In this way, the structure is represented by the finite region where $\rho^*(r)$ deviates from the mean value, and therefore values of r widely separated do not provide information.

19.4 ANALYSIS IN RECIPROCAL SPACE

An experimental intensity curve as a function of the scattering vector is produced in SAXS. From the isotropic patterns of a melt-crystallized polymer, a slice is taken and, when projected in the plane $I(q)$ against q , it shows a scattering maximum with a wide statistical distribution. The evaluation of structural parameters from the intensity curve requires the whole scattering curve. Nonetheless, the lower and upper ends of the curve cannot be determined because of the nature of the scattering process. Therefore, mathematical approximations are used to access both ends of the curve. According to the characteristics of the dispersion function measured experimentally, the intensity curve is divided into three parts, which are described in the following sections.

19.4.1 Scattering Intensity when $q \rightarrow 0$

As previously mentioned, it is not possible to obtain the experimental intensity data for q values near zero; therefore, it is desirable to extrapolate the obtained data down to $q = 0$. This can be done by means of models or using arbitrary extrapolations (straight lines, polynomials, etc.). When using models in this region, it is possible to obtain information about the average radius of gyration and the radius for a spherical domain, as well as the size of the inhomogeneities [13]. For a system of isolated domains at high dilutions, Guinier and Fournet (13a) proposed

$$I(q) \underset{q \rightarrow 0}{=} K_G e^{[-R^2/3]q^2} \quad (19.6)$$

where K_G is a constant and R is the average radius of gyration, given by $R = (3/5)^{1/2}R_d$ for a spherical domain of radius R_d . Then, by means of a plot of $\ln[I(q)]$ versus q^2 , it will be possible to obtain the parameters K_G and R .

Debye et al. (13b) developed a model for random scatterers, which is given by the expression

$$I(q) \underset{q \rightarrow 0}{=} \frac{A}{(1 + \varepsilon^2 q^2)^2} \quad (19.7)$$

where A is a constant and ε is the length of the inhomogeneity. By means of a plot of $1/I(q)^{1/2}$ versus q^2 , it will then be possible to obtain the parameters A and ε . Equations 19.6 and 19.7 can be used for extrapolating the intensity $I(q)$ at $q = 0$ if there is enough data near $q = 0$.

19.4.2 Scattering Intensity at Intermediate Angles

Most semicrystalline polymers give rise to SAXS patterns that are characterized by one or more maxima in the dispersion curve. These patterns have been interpreted in terms of a simple model of crystalline and amorphous regions that alternate regularly [14]. The angular position of the maximum of diffraction (Bragg's law) and its correction for time of collection (the Lorentz factor) can be interpreted to provide the average structural period (periodicity L) of the polymer. In the following paragraphs, the possibilities for this region are given.

19.4.2.1 Bragg's Law In the analysis of semicrystalline polymers, in a first approach, it can be assumed that L is associated with the distance between the lamellar planes. These distances can be related through the Bragg's law with the diffracted waves that are in phase and are reinforced in certain directions (angles) [15]. This analysis give values that qualitatively coincide with the structure observed by means of electron microscopy and with sizes of crystals indicated by means of WAXS [16]. The periodicity L is related to the vector q in the maximum of dispersion according to [17]

$$L = \frac{2\pi}{q_{\max}} \quad (19.8)$$

However, in most cases the structural sizes inferred from this treatment do not agree with the structures observed by means of electron microscopy [18]. For instance, polymers crystallized from the molten state rarely have orders of multiple dispersion (as required by diffraction) and, moreover, they present a wide first-order peak as shown in Figure 19.7 [19]. Then, when applying the Bragg's law, the obtained period will be distorted considerably from the average period of the structure [14]. This discrepancy of values can decrease, but not vanish, when applying the Lorentz factor to the curve of observed intensity.

19.4.2.2 The Lorentz Factor L_0 The factors that rule the diffraction intensity $I(hkl)$ are the structure factor for atomic dimensions $F(hkl)$, the polarization factor P , the Lorentz factor L_0 , and the multiplicity factor j . However, in studies of SAXS, all factors except the Lorentz factor can be omitted [9].

In diffraction, the Lorentz factor depends basically on the reflection time, that is, the time during which a family of planes reflects X-rays under certain experimental

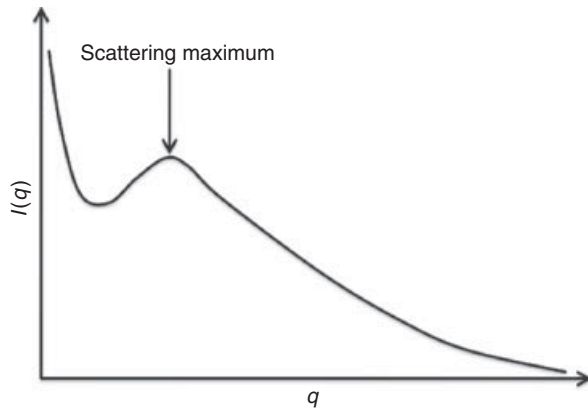


Figure 19.7 Scheme of a typical SAXS curve of $I(q)$ versus q of a semicrystalline polymer.

conditions. The time of reflection originates partly because of the lack of parallelism and monochromaticity of the incident beam [9].

In SAXS studies of a real sample, all the lamellar layers or stacks are oriented at random with respect to the incident beam; therefore the intensity function $I(q)_{\text{obs}}$ which corresponds to the measured intensity shows spherical symmetry [20]. However, when using theoretical one-dimensional models (where the lateral width of the lamellae is much greater than the periodicity), the dispersion intensity is calculated assuming that the lamellar stacks are correctly oriented (perpendicular) with respect to the incident beam [21]. This implies that the observed intensity (with spherical symmetry) should be corrected to a perpendicular intensity to the lamellar stacks. Because of this, the Lorentz factor that is described for lamellar systems is also used.

The nature of the inhomogeneities of semicrystalline polymers can be expressed for spherically symmetric dispersion by means of a structure factor $F(q)$. For X-ray dispersion, this can be represented as

$$I_{\text{obs}}(q) = \overline{|F(q)|^2} \cdot L_0 \quad (19.9)$$

where L_0 plays a similar role as the Lorentz factor in classical X-ray crystallography.

The form of L_0 in Equation 19.9 depends on the experimental conditions used, the form of the scatterers, and the searched parameters. For instance, it is proportional to q^{-2} for point collimation and to q^{-1} when collimation is made through a grid [9]. On the other side, independent of the collimation system utilized, L_0 is proportional to q^{-1} when the section of a cylindrical particle is determined, while it is proportional to q^{-2} when the thickness of a laminar particle is determined [22].

On the other hand, it is well known that the ideal intensity generated by the structure with a factor $F(q)$

is given by the absolute square of this factor [9, 10], that is,

$$I_{\text{id}}(q) = |F(q)|^2 \quad (19.10)$$

Considering that the factor L_0 for point collimation and for laminar particles (one-dimensional model) is q^{-2} , substituting Equation 19.10 in Equation 19.9 and rearranging gives

$$I_{\text{id}}(q) = I_{\text{obs}}(q) \cdot q^2 \quad (19.11)$$

Equation 19.11 means that the observed intensity must be multiplied by a factor q^2 to obtain a better estimation of the periodicity in lamellar systems of semicrystalline polymers. The factor q^2 is related to the change from the scatterers oriented at random to dispersers perfectly aligned (Fig. 19.8). This correction is implied, for instance, in the use of models of one-dimensional stacking [19]. As $I_{\text{id}}(q)$ has been obtained from a one-dimensional model, it can be written as $I_1(q)$ [19].

In summary, the purpose of the Lorentz factor is to allow the comparison of an anisotropic intensity (in reciprocal space) calculated from a model with the obtained experimental intensities of samples whose symmetry (due to static or time-averaged disorientations) is generally different from that of the model [22]. It also takes into account the fact that only the intensity in reciprocal space that intersects the Ewald sphere can be observed experimentally [23]. Also, the time-averaged orientations may be related to the collimator type and the particle shape. This region in general has a well-defined shape, therefore only polynomial adjustments are made if necessary in order to avoid experimental noise.

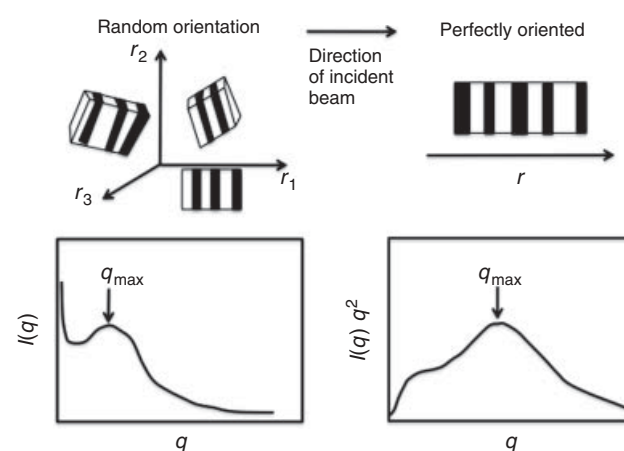


Figure 19.8 Rearranging of scatterers from random orientation to perfectly oriented with respect to the incident beam.

19.4.3 Scattering Intensity when $q \rightarrow \infty$

The third region of the scattering intensity curve is known as *Porod's region* and it contains information on the phase limits. This region is located at large scattering angles and after the first-order maximum for semicrystalline polymers. By analyzing this region, it is possible to determine the interface thickness between the phases and whether the polymer has fluctuations of electronic density inside the phases [11]. The possible types of calculation in this region are described below.

19.4.3.1 Ideal System without Interface (Porod's Law)

According to the Equation 19.2, the intensity of dispersion for an ideal structure will be the Fourier transform of the autoconvolution of the difference between the local and the average electronic densities, that is,

$$I_{\text{id}}(q) = \Im[\Delta\rho_{\text{id}}^{*2}(r)] \quad (19.12)$$

Porod predicted that, for an ideal lamellar system of two phases (Fig. 19.5) in which neither fluctuations of density within phases nor interfacial thickness of finite width are present, the intensity of dispersion diminishes proportionally to the reciprocal of the fourth power of q , which is mathematically expressed as

$$\lim_{q \rightarrow \infty} I_{\text{id}}(q) = \frac{K_p}{q^4} \quad (19.13)$$

where K_p is the Porod constant, and Equation 19.13 is called *Porod's law* [24]. The determination of K_p is important because of the fact that it is related to certain structural parameters of the system, that is,

$$K_p = \left(\frac{S}{V}\right) \left(\frac{Q}{8\pi^3 \phi_1 \phi_2}\right) = \frac{Q}{2\pi^3 l_p} \quad (19.14)$$

where Q is known as the *three-dimensional Porod invariant* and it is given by

$$Q = \int_0^\infty q^2 I(q) dq = V \phi_1 \phi_2 (\rho_1 - \rho_2)^2 \quad (19.15)$$

S/V is the area of the interface per unit volume, ϕ_1 and ϕ_2 are the volume fractions of the phases ρ_1 and ρ_2 , respectively, and l_p is the longitude of the Porod inhomogeneity, a parameter that serves as a measure of the average size of the phases in all the directions of densities ρ_1 and ρ_2 .

If the interfaces of the lamellae are totally flat and the lateral dimensions are very large compared to the thickness of the lamellae, the total interfacial area S_0/V is given by

$$\frac{S_0}{V} = \frac{2}{L} \quad (19.16)$$

where the parameter L is called *periodicity* or *long period*. If the interfaces are not flat, the obtained interfacial area S obtained from l_p is larger than S_0 obtained from L . Therefore, the relationship

$$\frac{S}{S_0} = \frac{2\phi_1\phi_2 L}{l_p} = \frac{2l_1 l_2}{L l_p} \quad (19.17)$$

is a measure of the planarity of the interfaces.

19.4.3.2 System with Finite Interface (Negative Deviations of Porod's Law) Tsvaskin and Blundell were the first to consider that polymers show a transition area between the crystalline and amorphous phases of length E , which was taken into account in theoretical models [21, 25]. This finite thickness (E) of the amorphous-crystalline interface causes semicrystalline polymers to exhibit deviations from the ideality dictated by the Porod's law [11]. This thickness can be represented through a smoothing function in real space, that is, $h(r)$. According to Ruland (1971), this function convolutes with the Fourier transform of the autoconvolution of the difference between the local and the average electronic densities to reproduce the gradient profile of the interfacial density of a structure with finite thickness, that is,

$$\Delta\rho_E(r) = \Delta\rho_{\text{id}}(r) * h(r) \quad (19.18)$$

where $\Delta\rho_E(r)$ is the difference between the local and the average electronic densities for a structure with finite thickness [11]. The Fourier transform of a convolution product in real space is equivalent to the product of those Fourier transforms in reciprocal space. From Equations 19.2 and 19.18, one can obtain the scattering intensity for this particular case as

$$I_E(q) = \Im[\Delta\rho_{\text{id}}^{*2}(r)] \Im[h^{*2}(r)] \quad (19.19)$$

or

$$I_E(q) = I_{\text{id}}(q) * H^2(q) \quad (19.20)$$

$I_E(q)$ is the intensity of dispersion for a structure with finite thickness, and $H^2(q)$ is the Fourier transform of $h^{*2}(r)$ in the reciprocal space. Because the width of the function $h(r)$ should be small compared to the average regions of constant density (for a two-phase system), the width of the function $H(q)$ will be considerably larger than that of the intensity. In this way, the intensity of dispersion is affected essentially only at large q values, that is, in the Porod's region. As a consequence, and using Equation 19.13, the result is

$$I_E(q) = \frac{K_p}{q^4} * H^2(q) \quad (19.21)$$

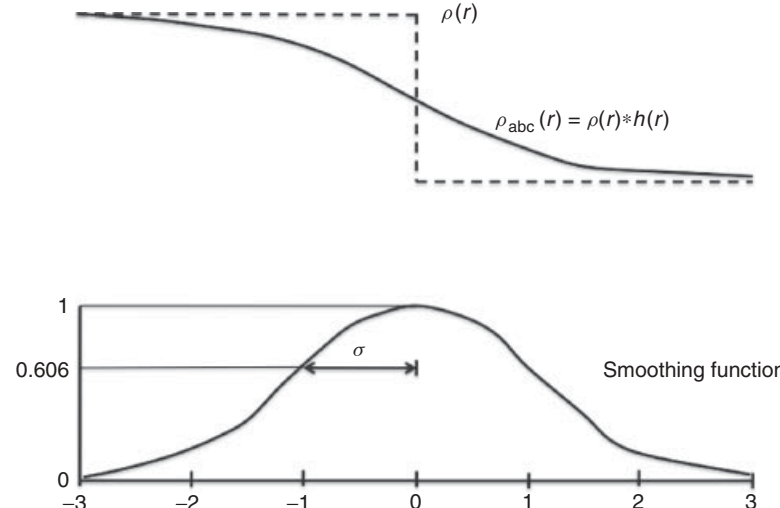


Figure 19.9 Sigmoidal model of gradient of interface. *Source:* Reproduced with permission from Koberstein JT, Morra B, Stein RS. J Appl Crystallogr 1980;13:34 [27]. Copyright 1980 IUCr (International Union of Crystallography) (<http://dx.doi.org/10.1107/S0021889880011478>).

where the shape of the smoothing function is defined by the geometric model used for the interfacial gradient.

The sigmoidal model for the interfacial gradient was introduced by Ruland and consists of a Gauss-type change of the electron density, as shown in Figure 19.9 [11]. The smoothing function is then Gaussian and $H(q)$ is given by

$$H(q) = e^{-\frac{(\sigma^2 q^2)}{2}} \quad (19.22)$$

where σ is the standard deviation of the smoothing Gaussian function related to the finite thickness [26]. Inserting Equation 19.22 into Equation 19.21, the resulting scattering intensity is given by

$$I_E(q) = \frac{K_p}{q^4} \cdot e^{-\frac{(\sigma^2 q^2)}{2}} \quad (19.23)$$

The value of σ can be defined using the curve of $\ln[I_E(q)q^4]$ versus q^2 . This represents a linear relationship with negative slope where Porod's law is fulfilled (negative deviation of Porod's law). By expanding the exponential function, the intensity can be approximately calculated by

$$I_E(q) = \frac{K_p}{q^4} \cdot e^{1-\frac{(\sigma^2 q^2)}{2}} \quad (19.24)$$

Therefore, in a curve of $I_E(q)q^4$ versus q^2 , a linear region with negative slope should be located where Porod's law is fulfilled. The slope obtained by Equations 19.23 and 19.24 is related to the structural parameters through the expression [11]

$$\text{Slope} = -\frac{Q\sigma^2 q^2}{2\pi^3 l_p} \quad (19.25)$$

The straight line extrapolated to $q = 0$ intersects the $I_E(q)q^4$ axis at $Q/(2\pi^3 l_p)$, which enables the calculation of the value of K_p . On the other hand, σ and E are related by [26]

$$E = (2\pi)^{1/2}\sigma \quad (19.26)$$

Another model for the electron density gradient was proposed by Blundell and analyzed by Vonk; it consists of a linear density change in the interface [21, 28]. In this model, called the *geometric linear model*, the smoothing function is of rectangular type (Fig. 19.10) and its Fourier transform is given by

$$H(q) = \frac{\sin(Eq)}{Eq} \quad (19.27)$$

where E is the interfacial thickness. The dispersion of intensity is given by

$$I_E(q) = \frac{K_p}{q^4} \cdot \frac{\sin^2(Eq)}{(Eq)^2} \quad (19.28)$$

A drawback of this equation is that it cannot be treated in graphical form. However, by expanding the sine function in a power series truncated after the second term, a more manageable form can be obtained as follows:

$$I_E(q) = \frac{K_p}{q^4} \cdot \left[1 - \frac{E^2 q^2}{3} \right] \quad (19.29)$$

From this, by plotting $I_E(q)q^4$ versus q^2 , a linear region of negative slope can be located where the Porod's law is fulfilled if the thickness is finite.

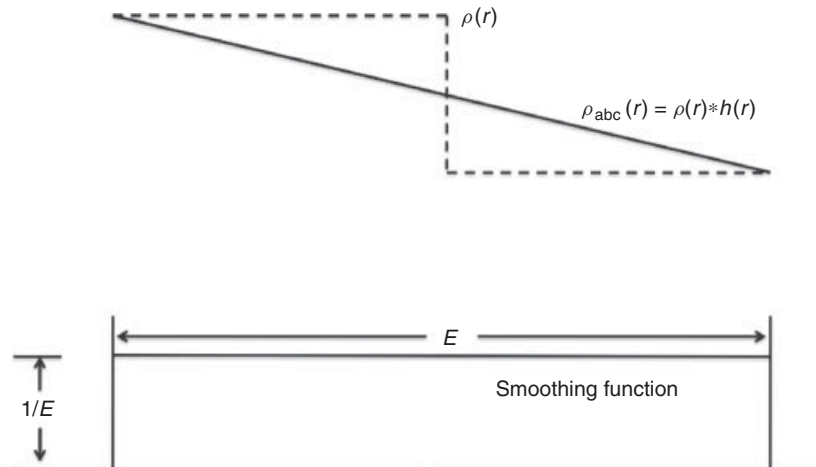


Figure 19.10 Linear model of the interface gradient. Source: Reproduced with permission from Koberstein JT, Morra B, Stein RS. J Appl Crystallogr 1980;13:34 [27]. Copyright 1980 IUCr (International Union of Crystallography) (<http://dx.doi.org/10.1107/S0021889880011478>).

19.4.3.3 System with Fluctuations within the Phases (Positive Deviations of Porod's law) Besides presenting interfacial thicknesses of finite width, semicrystalline polymers generally have electron density fluctuations inside the phases denoted FL [11]. Such electron density fluctuations are associated with thermal and density fluctuations. These fluctuations cause a global increment in the scattering intensity, which is denoted I_{FL} . This effect is different from that exhibited at high values of the dispersion vector where it is also observed that the intensity curve grows because of the beginning of the WAXS region [27]. The increment in the scattering intensity caused by the presence of fluctuations inside the phases, which is limited by the beginning of the WAXS region, is known as the *background intensity* $I_B(q)$ [29].

With the aim of determining the value of $I_B(q)$, Vonk proposed that the function $I_B(q)$ can be expanded in a power series truncated at the first or second term, according to

$$I_B(q) = I_{FL} + b_1 q^n \quad (19.30)$$

where b_1 is a constant, n is an integer, and I_{FL} is the value of the intensity extrapolated to $q = 0$ [28].

According to Ruland, $I_B(q)$ can also be approximated by an exponential function, which is expressed as

$$I_B(q) = I_{FL} \cdot e^{b_2 q^2} \quad (19.31)$$

where b_2 is a constant and I_{FL} is the value of the intensity extrapolated to $q = 0$ [30].

If the background intensity $I_B(q)$ is added to the intensity produced by systems with interfacial thickness, $I_E(q)$, the following expression can be obtained:

$$I_{EXP}(q) = I_{id}(q) \cdot H^2(q) + I_B(q) \quad (19.32)$$

which is the fundamental equation that describes the experimental intensity in semicrystalline polymers [11]. As a good approximation, it is possible to consider $I_B(q)$ a constant and equal to I_{FL} . In this case, it is possible to evaluate $I_B(q)$ from the positive slope of a plot of $I_{EXP}(q)$ versus q^4 (positive deviation of Porod's law) if it is assumed that $H^2(q)$ is constant as a first approximation [11, 31].

Equation 19.32 can be modified to outline the intensity of an ideal system, $I_{id}(q)$:

$$I_{id}(q) = \frac{I_{EXP}(q) - I_B(q)}{H^2(q)} \quad (19.33)$$

where $I_B(q)$ can be a constant, an exponential, or a power series, $H^2(q)$ can be unity ($E = 0$; $\sigma = 0$), geometric sigmoidal, sigmoidal expanded, linear geometric, or linear expanded. The ideal intensity curve can be produced by different ways. Siemann and Ruland proposed a method of trial and error adjusting the parameters K_p , σ , and I_B ; Medellin and Avila applied a technique of numerical parameter fitting using the quasi-Newton method for PET [26, 32].

19.5 ANALYSIS IN REAL SPACE

19.5.1 Correlation Function, $\gamma(r)$

Debye and Bueche introduced the correlation function when studying porous solids [33]. The correlation function is based on the fluctuations of local densities with respect to an average value ($\eta_1 = [\rho_1(r) - \rho_m]$) where $\rho_1(r)$ is a local value and ρ_m is the average value. Since this function depends only on density fluctuations, it can be used for semicrystalline polymers where strong density

deviations exist [20]. The correlation function can be seen in the following way: consider two neighboring points in the system, located at a distance r [33, 34]. Take the product of both fluctuations $\eta_1 = \rho_1(r) - \rho_m$ and $\eta_2 = \rho_2(r) - \rho_m$, the first taken at point 1 and the second taken at point 2. Move points 1 and 2 through the material, maintaining a fixed distance r . If a large number of values of the product $\eta_1\eta_2$ are obtained, then the average value of this product indicated by $\langle\eta_1\eta_2\rangle_m$ can be found. According to this discussion, this product depends on the distance r . If $r = 0$ then $\eta_2(0) = \eta_1(0)$, and therefore, the previous product is given by $\langle\eta_1\eta_2\rangle_m = \eta_2^2$. For large r values, the product will be zero because the fluctuations will vary independently. In general, $\langle\eta_1\eta_2\rangle_m$ will be a function of the distance r , starting at η^2 for $r = 0$ and decaying to zero when increasing the value of r . Then, it can be concluded that the average extension of the heterogeneities is given by the relationship $\langle\eta_1\eta_2\rangle_m/\eta^2$, which is known as the *correlation function* and does not have physical dimensions; that is, it is a dimensionless number that varies with the distance and indicates the average extension of the heterogeneities.

$$\gamma(r) = \frac{\langle\eta_1\eta_2\rangle_m}{\eta^2} \quad (19.34)$$

19.5.1.1 Experimental Correlation Function $\gamma(r)$ Following a similar process, Vonk and Kortleve introduced the correlation function for semicrystalline polymers, but in a single dimension (Fig. 19.8) [20]. If the cosine Fourier transform of the correlation function is obtained, then

$$\gamma_1(r) = \frac{\int_0^\infty I_1(q) \cos(qr) dq}{\int_0^\infty I_1(q) \cos(0) dq} \quad (19.35)$$

where $\cos 0 = 1$. Replacing the value of $I_1(q)$ by its equivalent in $I(q)$ (Eq. 19.11), the function $\gamma_1(r)$ becomes

$$\gamma_1(r) = \frac{\int_0^\infty q^2 I(q) \cos(qr) dq}{\int_0^\infty q^2 I(q) dq} \quad (19.36)$$

where $\gamma_1(r)$ is the one-dimensional correlation function and the denominator is the invariant Q (Eq. 19.15). In this way, the correlation function $\gamma_1(r)$ is normalized by the invariant Q , having an initial value of 1. This function shows a series of maxima and minima of diminishing height, which finally become zero at large values of r . This behavior suggests a periodicity in the structure; the position of the first maximum corresponds to the average value of the distance of periodicity, in other words, the long period L .

In many cases, $\gamma(r)$ depends only on the distance r and not on the direction in the space of this vector; therefore, integration over all directions can be done [33]. In the cases

of polyethylene and polytetramethylene, Fulcher *et al.* used the following relation [35]:

$$\gamma_3(r) = \frac{\int_0^\infty q^2 I(q) \left(\frac{\sin(qr)}{qr}\right) dq}{\int_0^\infty q^2 I(q) dq} \quad (19.37)$$

where $\gamma_3(r)$ is the three-dimensional correlation function which depends only on the magnitude of the distance r . The form of this function is similar to the one shown for the function $\gamma_1(r)$, but the information that they provide is not the same.

From the previous paragraph, it follows that r is a vector perpendicular to the layers of the crystalline and amorphous regions for $\gamma_1(r)$ or in any direction for $\gamma_3(r)$. In a medium in which γ depends originally on r and not on their directions, under stress, γ will begin to depend also on the direction of r [33]. In this case, the scattering intensity does not have a symmetry center around the direction of the primary beam. The same thing happens if the heterogeneities are aligned along a common axis. Therefore, when carrying out the analysis of the morphology of lamellar systems, it is advisable to meditate in an appropriate way the required information for the system under study.

19.5.1.2 Form and Properties of the One-Dimensional Correlation Function A periodic structure with a given electron density function $\rho(r)$ can be described by means of the long period L , the crystalline thickness l_c , and the difference of electronic densities $\Delta\eta = \rho_c - \rho_a$. The effect of different lamellar systems on the form and properties of the one-dimensional correlation function was discussed by Strobl and Schneider [36]. Next, systems of two phases and their impact are presented, giving the form and characteristics of the correlation function $\gamma_1(r)$, in accordance with these authors.

19.5.1.3 Ideal Lamellar System of Two Phases In an ideal lamellar system, the interface thickness and the density fluctuations within the phases are negligible, and the structure can be described by the long period L , the crystalline thickness l_c , and the electron density distribution, as shown in Figure 19.11a with their corresponding function $\gamma_1(r)$ for the irradiated volume. In this case, the form of the function $\gamma_1(r)$ consists of a series of autocorrelation triangles which show a periodicity L . The autocorrelation triangle centered in the origin has a number of important characteristics. The value of $\gamma_1(r)$ at $r = 0$ is the invariant Q . The line between the triangles is known as the *baseline*. Its negative coordinate is given by

$$-A = -\phi_c^2 (\rho_c - \rho_a)^2 \quad (19.38)$$

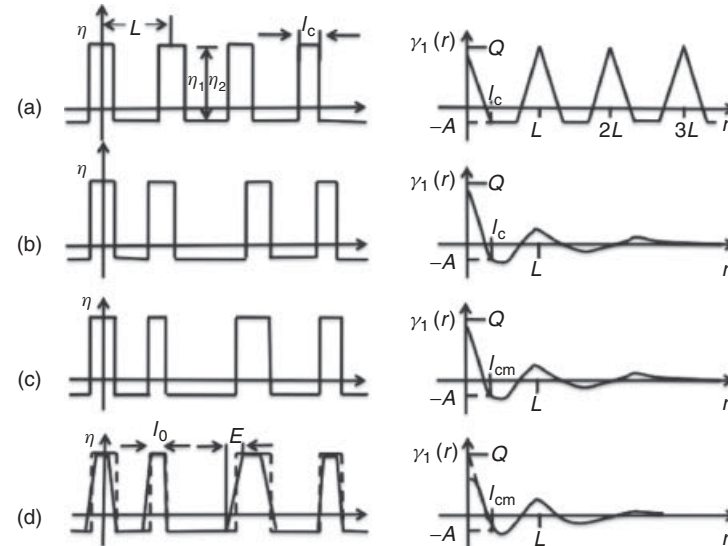


Figure 19.11 Representation of a system of two phases and their impact in the function $\gamma_1(r)$.
(a) Periodic system of two phases, (b) effect of variations in the period L , (c) effect of additional thickness fluctuations, (d) effect of the introduction of diffuse frontiers (interface thickness).
Source: Reproduced with permission from Strobl GR, Schneider M. J Polym Sci Polym Phys Ed 1980;18:1343 [36]. Copyright 1980 Wiley Periodicals, Inc.

Therefore, the height of the triangle becomes

$$Q + A = \phi_c (\rho_c - \rho_a)^2 \quad (19.39)$$

Hence, the slope $d[\gamma_1(r)/dr] = -S_0/2(\rho_c - \rho_a)^2$ (Eq. 19.17). The first intersection of the function $\gamma_1(r)$ with the axis $r[\gamma_1(r) = 0]$ occurs at

$$r_0 = I_c (I - \phi_c) \quad (19.40)$$

The function $\gamma_1(r)$ intersects the baseline at $r_1 = l_c$.

19.5.1.4 Ideal Lamellar System of Two Phases with Variation in the Interlamellar Space Because the autocorrelation part remains the same, in this case the only consequence is an enlargement in the width of the peak due to the closer correlations (Fig. 19.11b). Additionally, the position of the maximum provides the periodicity, which denotes the most probable spacing.

19.5.1.5 Ideal Lamellar System of Two Phases with Variation in the Interlamellar Space and Thickness If ϕ_c and S_0 are kept constant, then the invariant Q , the slope $d[\gamma_1(r)/dr]$, and the baseline A are not affected. Nonetheless, a change occurs near the base of the triangle where $\gamma_1(r)$ becomes curved (Fig. 19.11c). The straight section of $\gamma_1(r)$ will intersect the axis r at

$$r_0 = \frac{-Q}{d\gamma/dr} = (1 - \phi_c) \frac{\phi_c}{S_0/2} = (1 - \phi_c) I_{cm} \quad (19.41)$$

and the baseline at

$$r_1 = \frac{Q + A}{d\gamma/dr} = \frac{\phi_c}{S_0/2} = I_{cm} \quad (19.42)$$

In these equations, I_{cm} denotes the average (in number) lamellar thickness and can be defined as

$$I_{cm} = \phi_c L \quad (19.43)$$

19.5.1.6 Ideal Lamellar System of Two Phases with Variation in the Interlamellar Space, in the Lamellar Thickness, and in the Presence of Interface Thickness

The presence of a transition zone changes the shape of the correlation function near the origin (Fig. 19.11d). However, the original straight line does not change. This happens because the thickness of the transition area E is smaller than the average thickness for all the lamellae, I_{c0} . In this case, the original straight line is located between $r = E$ and $r = I_{c0,min}$, where $I_{c0,min}$ denotes the average thickness of the thinnest lamellae of the system.

It is possible to directly derive the parameters of this system. The extrapolation of the linear section to $r = 0$ corresponds to its invariant Q , which is generally larger than the fluctuation of the square average electron density $\gamma_1(0)$ of the real structure. All the basic

structural parameters of this type of system are obtained by means of

$$\phi_c = \frac{A}{A + Q} \quad (19.44)$$

$$l_{cm} = r_1 \quad (19.45)$$

$$l_{cm} = \frac{r_0}{1 - \phi_c} \quad (19.46)$$

$$S_0 = \frac{2\phi_c}{l_{cm}} \quad (19.47)$$

$$(\eta_c - \eta_a)^2 = \frac{Q}{\phi_c(1 - \phi_c)} \quad (19.48)$$

In another method of graphic analysis, proposed by Vonk, the average thickness of the lamellae, l_{cm} , is evaluated from the following equation:

$$l_{cm} = Qr_1 + \frac{E}{3} \cdot \frac{\phi_c}{1 - \phi_c} \quad (19.49)$$

In this way, the analysis has been restricted to the autocorrelation in $\gamma_1(r)$ [28].

Because of the usual experimental ranges of crystallinity, the appearance of the baselines in the study of semicrystalline polymers is not very frequent [36, 37]. Therefore, the crystalline volume fraction should be obtained by other alternative techniques such as, for example, differential scanning calorimetry. In this way, if the crystallinity in volume is known, it is possible to obtain the lost baseline [37, 38]. However, if the crystallinity is either low or high, it is possible to directly obtain the baseline for which it is foreseen that the morphology is solved [36]. For example, Vonk and Pijpers and Vonk and Koga worked at high crystallinities and they observed the aforementioned baselines [39].

The presence of thermal and density fluctuations, ($I_B(q)$), causes waves in the function $\gamma_1(r)$ as reported by Defoor and Avila [40]. After extrapolating both sides of the intensity curve, the fluctuations that could not be eliminated using ($I_B(q)$) are suppressed. Also, Avila (40b) and Medellín and Avila (41) determined that the use of a two-distance sample detector when recording intensity data provides more detailed information than when data are taken with a single-distance sample detector. This is because a greater range of values of q is accessed, which allows a better estimation, particularly of ($I_B(q)$) and E .

19.5.2 Interface Distribution Function $g(r)$

A more detailed analysis of data from SAXS can be carried out by means of the interface distribution function $g_1(r)$, introduced by Ruland [30]. This function is the second derivative of the one-dimensional correlation function and

is the correlation function derived from the first derivative of the local electron density function, that is,

$$g_1(r) = \gamma_1''(r) = -[\rho'(r)]^{*2} \quad (19.50)$$

The previous function $g_1(r)$ requires the determination of the region in which Porod's law is valid in the reciprocal space. According to Ruland, since $\rho(r)$ consists of a sequence of positive and negatives steps located at the interfaces of the lamellae (Fig. 19.5), its first derivative is a series of positive and negative Dirac delta functions weighted by means of the height of the step (Fig. 19.12a) [30]. The correlation function of the first derivative consists of a series of distribution of distances with positive and negative values that correspond to the neighboring interfaces (Fig. 19.12b).

19.5.2.1 Experimental Interface Distribution Function $g(r)$ When the second derivative of $\gamma_1(r)$ with respect to r is calculated for one-dimensional two-phase systems, the result is

$$\frac{\partial^2}{\partial r^2} \gamma_1(r) = -\frac{2Q}{d_p} \delta(r) + g_1(r) \quad (19.51)$$

where Q is the invariant, d_p is the average one-dimensional longitude parameter, $\delta(r)$ is the Dirac delta function at the origin, and $g_1(r)$ contains the values for $r \neq 0$. From the Fourier transform of this equation

$$q^4 I(q) = \frac{2Q}{d_p} - G_1(q) \quad (19.52)$$

where $G_1(q)$ is known as the *interference function* and is given by

$$G_1(q) = \Im[g_1(r)] = K_p - q^4 I(q) \quad (19.53)$$

From Equation 19.53, one can obtain

$$g_1(r) = \frac{t}{V} \frac{1}{2\pi^2} \int_0^\infty G_1(q) \cos(qr) dq \quad (19.54)$$

where t is the thickness and V is the volume occupied by the lamellar stacks. When experimental $I(q)$ data versus q are collected in an ideal lamellar system without a finite interface, it is possible to apply this equation to obtain information about the nature of the system.

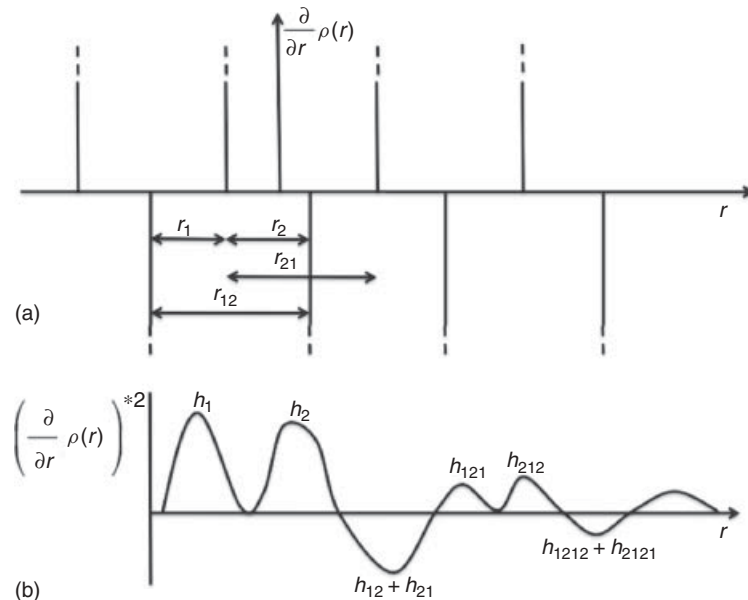


Figure 19.12 Schematic representation of (a) first derivative from $\rho(r)$ and (b) its correlation function. Source: Reproduced with permission from Ruland W. Colloid Polym Sci 1977;255:417 [30]. Copyright 1977 Springer.

19.5.2.2 Form and Properties of the Interface Distribution Function According to Stribeck and Ruland [42], the first distribution $h_1(r)$ of distances r_1 is positive and is related to the spacing between adjacent interfaces corresponding to the thickness of lamellae of the phase with the smaller volume concentration. The second distribution $h_2(r)$ of distances r_2 is also positive and is related to the distances between adjacent interfaces that correspond to the thickness of the lamellae of the phase with the greatest volume concentration. The following distribution $h_3(r)$ for distances r_3 is negative, and is related to the spaces of the following second interface, for example, that extending from the beginning of a region of density ρ_1 to the following region with the same density. Following the sequence, the fourth distribution $h_4(r)$ for distances r_4 will be positive and will be related to the distance of the third following interface with the lowest volume concentration and lamellae of the phase of maximum volume concentration, etc.

For the evaluation of the functions $g_1(r)$, the distributions $h_1(r)$, $h_2(r)$, $h_3(r)$, etc. should be separated from the adjacent distributions, and their statistical weights and momenta should be determined. The weights w of the distributions contain, through the weighting functions $(1 - r/t)$, the information of the size of the stacking, t . Because the signs of the weights are alternated, serious errors can be introduced when the distributions of opposite signs overlap. This effect is more severe at large distances, so that only values of w for the distributions near the origin will be significant. The same occurs with the determination of

the momenta of the distributions where only the first and second momenta can be obtained with reasonable accuracy. However, an exact determination of the weights and the first and second momenta of the distributions until h_4 will allow the determination of an average value of t , and of the characteristics of the thickness of lamellae and its variation. The centers of $h_1(r)$ and $h_2(r)$ correspond to the average thicknesses l_{1m} and l_{2m} of the lamellae of density ρ_1 and ρ_2 , respectively; a comparison of the variances σ_1^2 and σ_2^2 obtained from the second momenta of h_1 and h_2 with those of h_3 and h_4 can be used to study the type of statistic present in the lamellar stacking. If the distributions of the distances are overlapped even for short distances, so that an unambiguous evaluation in terms of w_i , l_i , and σ_i is difficult, then the use of theoretical models for the simulation of lamellar systems is required in order to adjust them to experimental curves.

19.5.2.3 Simulated Interface Distribution Function $g(r)$ If Gaussian distributions are assumed to represent the variation of the interface distances, then theoretical functions $g_1(r)$ can be obtained. In this case, the function $g_1(r)$ is given by

$$g_1(r) = \sum_{i=1}^{\infty} w_i h_i \quad (19.55)$$

where w_i are the weights for the Gaussian distributions of distance h_i centered at r_i . When considering normalized

distributions, h_i is given by

$$h_i = \frac{1}{\sigma_i \sqrt{2\pi}} \exp \left[-\frac{(r - r_i)^2}{2\sigma_i^2} \right] \quad (19.56)$$

where σ_i is the standard deviation of the n th distribution of the distance. The distances r_i are given by

$$\begin{aligned} r_i &= n(r_1 + r_2) && \text{for } i = 3n \\ r_i &= n(r_1 + r_2) + r_1 && \text{for } i = 3n + 1 \\ r_i &= n(r_1 + r_2) + r_2 && \text{for } i = 3n + 2 \end{aligned} \quad (19.57)$$

In these equations, n is an ascending integer that begins with 1.

For the size of infinite stacking, the weighting functions are given by

$$\begin{aligned} w_{i1} &= 1 && \text{for } i \neq 3n \\ w_i &= -2 && \text{for } i = 3n \end{aligned} \quad (19.58)$$

and a first approximation for finite stacking is given by

$$\begin{aligned} w_i &= \exp \left(\frac{-r_i}{t} \right) && \text{for } i \neq 3n \\ w_i &= -2 \exp \left(\frac{-r_i}{t} \right) && \text{for } i = 3n \end{aligned} \quad (19.59)$$

The statistics by which the phases are related depend on the theoretical model used. In general, three theoretical models are considered and these are the homogeneous lamellar model, the network model, and the lamellar stacking model. In the following paragraphs, the particular distribution relationships are presented depending on the index of the distance.

Homogeneous Lamellar Model (HLM) In this model, the variation of parameters of the lamellar structure from one stacking to another is perfectly periodic and contains the same volume fractions of the two phases. In this case σ_i/r_i are constant; for that

$$\frac{\sigma_1}{r_1} = \frac{\sigma_2}{r_2} = \frac{\sigma_3}{r_3} \dots \sigma_i = r_i \quad \text{for every } i \quad (19.60)$$

where a single variance and two distances can be fixed in order to obtain the other related parameters.

Lattice Model (LM) This model consists of the independent variation of the thickness l_1 and the distance L ($L = r_3$) between the centers of the lamellae of the same phase within a given stacking. The change of σ_i is given by

$$\sigma_i = n \left(\frac{\sigma_1^2}{2} + \sigma_L^2 \right) \quad \text{for } i = 3n \text{ and } i = 3n \pm 1 \quad (19.61)$$

Lamellar Stacking Model (LSM) In this case, the function $g_1(r)$ results from the independent variation of the quantities σ_1 and σ_2 of the distances r_1 and r_2 , respectively (equivalent to the thickness l_1 and l_2 of the lamellae of phases 1 and 2), within a given stacking. The change of σ_i is given by

$$\begin{aligned} \sigma_i^2 &= n(\sigma_1^2 + \sigma_2^2) && \text{for } i = 3n \\ \sigma_1^2 &= n(\sigma_1^2 + \sigma_2^2) + \sigma_1^2 && \text{for } i = 3n + 1 \\ \sigma_1^2 &= n(\sigma_1^2 + \sigma_2^2) + \sigma_2^2 && \text{for } i = 3n + 2 \end{aligned} \quad (19.62)$$

APPENDIX A PROCEDURE TO OBTAIN MORPHOLOGICAL DATA FROM 1D SAXS PROFILES

This procedure outlines the main steps used to obtain morphological data from 1D SAXS patterns of polymer samples. As an example, an isothermally crystallized sample of a copolymer containing ethylene/hexane and ethylene/butene was characterized using time-resolved synchrotron radiation at the Advanced Polymers Beamline, X27C, National Synchrotron Light Source, Brookhaven National Laboratory. The X-ray beam wavelength was 1.366 Å, and the size was circa 0.4 mm in diameter. The SAXS pattern was collected using a linear position-sensitive detector (European Molecular Biological Laboratory) with a sample-to-detector distance of 1788 mm. SAXS scattering angle was calibrated using silver behenate. Calculations were performed by the authors using Mathcad™ by the routine developed for this purpose.

19.A.1 Data Analysis

19.A.1.1 Corrections to the Experimental Data Qualitative analysis of SAXS data requires the extrapolation to both 0 and ∞ of the scattering intensity as a function of the scattering vector q . In the first case, SAXS data was extrapolated to $q \rightarrow 0$ using Debye's equation (Eq. 19.7). On the other hand, the density profile as a function of a space vector r for an ideal two-phase system resembles a squared function because the boundaries are assumed to be sharp and the density within the phases is considered as constant. In this case, Porod established that the intensity decays as the inverse of the fourth power of the scattering vector at large q values, mathematically expressed as the Porod's law, Equation 19.13. However, two-phase polymer systems often deviate from the ideality due to the presence of a density gradient between the phases as well as density variations within the phases. The latter is often associated with a background scattering I_B , which produces a positive deviation of the Porod's law, while the former corresponds to a negative deviation associated with the interface thickness

E. Assuming finite boundaries, $E = 0$, Equation 19.13 becomes

$$I(q) = \frac{K_p}{q^4} + I_B \quad (19.A.1)$$

If enough data is acquired at large q values, K_p and I_B can be determined using nonlinear least-squares fitting and, therefore, the ideal intensity. However, the problem arises in the selection of q limits, since the choice of both the lower and upper limits significantly affects the validity of the Porod's law. In this case, the upper limit was set to $q_{\text{upp}} = 2$, and the lower limit q_{low} was varied until the minimum area of the interference function $G_1(q)$ was obtained (Eq. 19.53). Once this criterion is achieved, the interface distribution function $g_1(r)$ (Eq. 19.54) is calculated from the Fourier transform of $G_1(q)$.

19.A.1.2 Correlation Distances and Distributions The characteristic distances between each interface, as well as their statistical distributions, were obtained by means of a lamellar stacking model with infinite size to Lorentz data (I_q^2)

$$I_{\text{ideal}}(q) \cdot q^2 = \frac{K_p}{q^2} \cdot \text{Re} \left[\frac{H_1 \cdot H_2}{1 - H_1 \cdot H_2} \right] \quad (19.A.2)$$

where

$$H_i = 1 - \exp \left(i \cdot r_i \cdot q - \frac{\sigma_i^2 \cdot q^2}{2} \right) \quad (19.A.3)$$

r_i corresponds to the i th interface distance, and σ_i to its corresponding standard deviation. Interface distances and their distributions were obtained by means of a nonlinear least-squares fitting of the $I_{\text{ideal}}(q) \cdot q^2$ to Equation (19.A.2). A weight factor of $1/I_{\text{ideal}}(q) \cdot q^2$ was used. The periodicity or long period L is the sum of $r_1 + r_2$. The resulting parameters are shown in Tables 19.A.1 and 19.A.2. Finally, the ideal intensity, the Lorentz intensity, the interference function, and the interface distribution function were

TABLE 19.A.1 Experimental Parameters Obtained in Reciprocal-Space Analysis

$q \rightarrow 0$		$q \rightarrow \infty$		Whole Range			
A	e	K_p	E (nm)	I_B	Q	Area $G_1(q)$	
1280	7.91	18.676	0.000	5.709	36.41	0.343	

TABLE 19.A.2 Experimental Parameters Obtained in Real-Space Analysis

Correlation Distance (nm)			Standard Deviation (nm)		
r_1	r_2	L	s_1	s_2	s_L
6.59	2.06	8.64	2.731	1.472	3.102

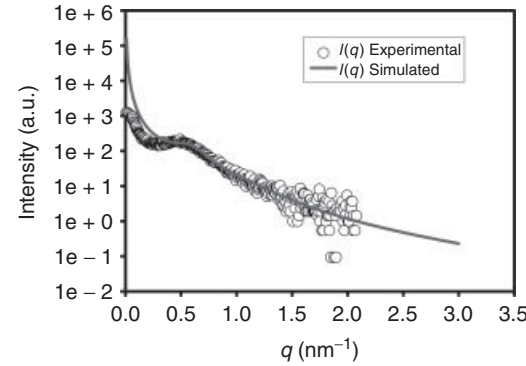


Figure 19.A.1 Intensity plot. (See insert for the color representation of the figure.)

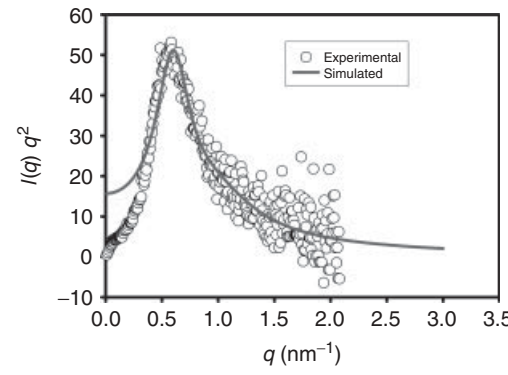


Figure 19.A.2 The Lorentz plot. (See insert for the color representation of the figure.)

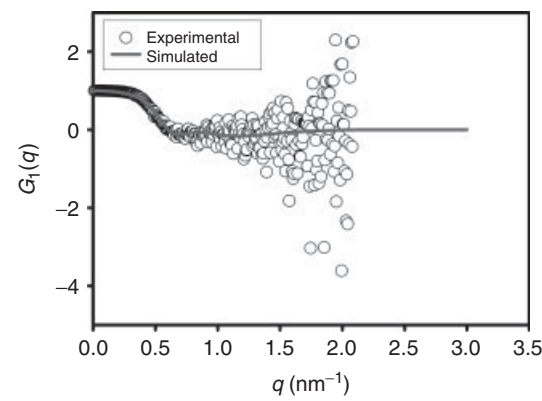


Figure 19.A.3 Interference function. (See insert for the color representation of the figure.)

simulated and compared with the experimental data to check for validity of the results (Figs. 19.A.1, 19.A.2, 19.A.3, and 19.A.4).

Finally, and only to show the effect of the statistics, simulations where performed using different standard deviations keeping the correlation distances shown in

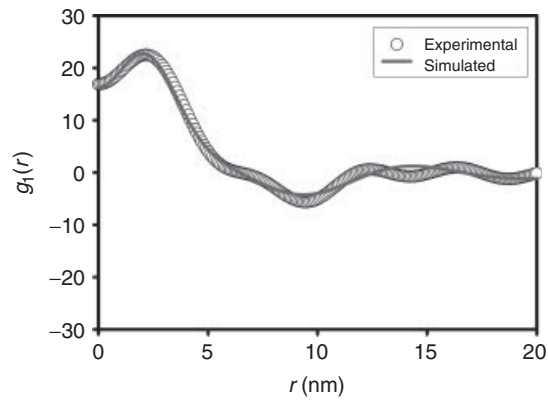


Figure 19.A.4 Interface distribution function. (See insert for the color representation of the figure.)

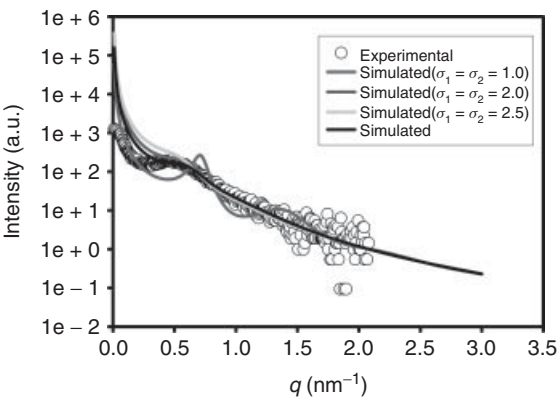


Figure 19.A.5 Statistical effect on the intensity plot. (See insert for the color representation of the figure.)

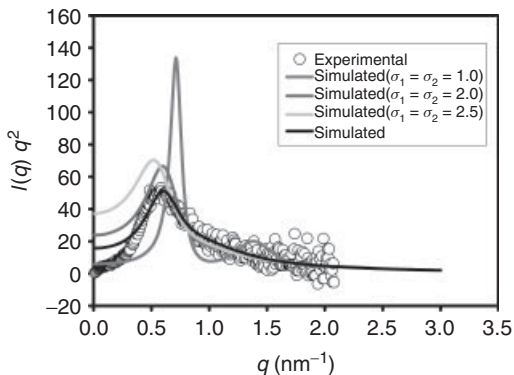


Figure 19.A.6 Statistical effect on the Lorentz plot. (See insert for the color representation of the figure.)

Table 19.A.2. The results are presented in Figures 19.A.5, 19.A.6, 19.A.7, and 19.A.8. These results indicate that the statistical variation in the distances can have a profound effect in the shape of the different functions in both reciprocal and real space.

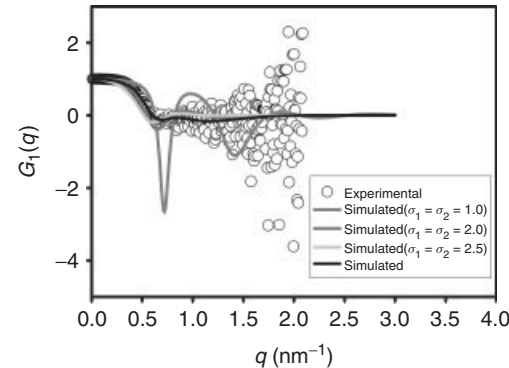


Figure 19.A.7 Statistical effect on the interference function. (See insert for the color representation of the figure.)

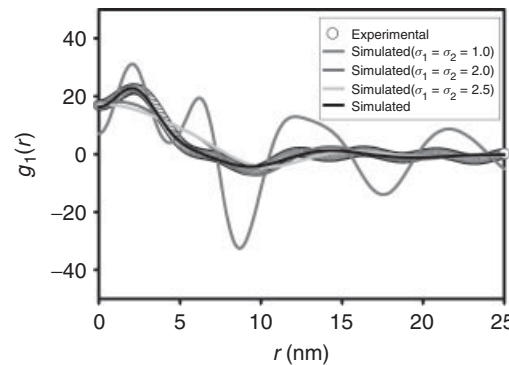


Figure 19.A.8 Statistical effect on the interface distribution function. (See insert for the color representation of the figure.)

REFERENCES

1. Sperling LH. *Introduction to Physical Polymer Science*. Hoboken: John Wiley and Sons; 1999. p 845.
2. Bassett DC. *Principles of Polymer Morphology*. Cambridge: Cambridge University Press; 1981. p 251.
3. Schultz J. *Polymer Materials Science*. Upper Saddle River: Prentice-Hall; 1974. p 524.
4. [a] Fischer EW, Z. Z. Naturforsch. 1957;12a, 753; [b] Keller A. Philos Mag 1957;2:1171–1175. [c] Till PH. J Polym Sci 1957;24:301.
5. Keith HD, Padder FJ. J Appl Phys 1963;34:2409.
6. [a] Bunn CW, Alcock TC. Trans Faraday Soc 1945;41:317. [b] Keller A. J PolymSci 1955;17:291.
7. [a] Mitsuhashi S. Bull Text Res Inst 1963;66:1. [b] Pennings AJ, Kiel AM. Kolloid Z Z Polym 1965;205:160–162. [c] Binsbergen FL. Nature 1966;211:516.
8. Hoffman JD, Davis GT, Lauritzen JI. The rate of crystallization of linear polymers with chain folding. In: Hannay NB, editor. *Treatise Solid State Chemistry*. Volume 3. New York: Plenum Press; 1976. p 418508, 520.

9. Alexander LE. *X-Ray Diffraction Methods in Polymer Science*. New York: Wiley Interscience; 1969. p 582.
10. Porod G. *General Theory in: Small-angle X-ray Scattering*. London: Academic Press; 1982. p 515.
11. Ruland W. *J Appl Crystallogr* 1971;4:70.
12. Debye P. *Ann Phys* 1915;351:809.
13. [a] Guinier A, Fournet G. *Small Scattering of X-Rays*. New York: Wiley; 1955. p 268. [b] Debye P, Anderson HR, Brumberger H. *J Appl Phys* 1957;28:679.
14. Crist B. *J Polym Sci Polym Phys Ed* 1973;11:635.
15. Bragg WL. *Camb Philos Soc* 1913;17:43.
16. [a] Geil PH. *Polymer Single Crystal*. Rockland: Interscience; 1962. [b] Fischer EW, Goddar H, Schmidt GF. *Kolloid Z Z Polym* 1968;226:30. [c] Davis HA, VanVeld RD, Billica HR. *Bull Am Phys Soc* 1971;16. [d] McHugh AJ, Schultz JM. *Philos Mag* 1971;24:155. [e] Bassett DC, Phillips JM. *Polymer* 1971;12:730. [f] Statton WO. *J Polym Sci* 1959;41:143.
17. Baltá-Calleja FJ, Vonk CG. *X-ray Scattering of Synthetic Polymers*. Amsterdam: Elsevier; 1989. p 317.
18. Geil PH. *Small-angle Scattering from Fibrous and Partially Oriented Systems*. New York: Interscience; 1966. p 149.
19. Brundell DJ. *Polymer* 1978;19:1258.
20. Vonk CG, Kortleve G. *Kolloid Z Z Polym* 1967;220:19.
21. [a] Blundell DJ. *Acta Crystallogr Sect A: Found Crystallogr* 1970;26:476. [b] Blundell DJ. *Acta Crystallogr Sect A: Found Crystallogr* 1970;26:472.
22. Crist B, Morosoff N. *J Polym Sci Polym Phys Ed* 1973;11:1023.
23. Atkins EDT. *Comprehensive Polymer Science*. New York: Pergamon; 1989.
24. [a] Porod G. *Kolloid-Z* 1951;124:83–114. [b] Porod G. *Kolloid-Z* 1952;125:51.
25. [a] Tsvankin DY. *Vysokomol Soyed* 2078;1964:11. [b] Tsvankin DY. *Vysokomol Soyed* 2083;1964:11.
26. Siemann U, Ruland W. *Colloid Polym Sci* 1982;260:999.
27. Koberstein JT, Morra B, Stein RS. *J Appl Crystallogr* 1980;13:34.
28. Vonk CG. *J Appl Crystallogr* 1973;6:81.
29. [a] Rathje J, Ruland W. *Colloid Polym Sci* 1976;254:358. [b] Wiegand W, Ruland W. *Colloid Polym Sci* 1979;66:355.
30. Ruland W. *Colloid Polym Sci* 1977;255:417.
31. Bornschlegl E, Bonart R. *Colloid Polym Sci* 1980;258:319.
32. [a] Medellín-Rodríguez FJ, Avila-Orta CA. *Av Ing Química* 1996;6(2):152. [b] Medellín-Rodríguez FJ, Avila-Orta CA. *Av Ing Química* 1996;6(2):156.
33. Debye P, Bueche AM. *J Appl Phys* 1949;20:518.
34. Chalkley HW, Cornfield J, Park H. *Science* 1949;110:295.
35. Fulcher KU, Brown DS, Wetton RE. *J Polymer Sci C* 1972;38:315.
36. Strobl GR, Schneider M. *J Polym Sci Polym Phys Ed* 1980;18:1343.
37. Strobl GR, Schneider MJ, Voigt-Martin IG. *J Polym Sci Polym Phys Ed* 1980;18:1361.
38. Medellín-Rodríguez FJ, Phillips PJ, Lin JS. *Macromolecules* 1995;28:7744.
39. [a] Vonk CG, Pijpers AP. *J Polym Sci Polym Phys Ed* 1985;23:2517. [b] Vonk CG, Koga Y. *J Polym Sci Polym Phys Ed* 1985;23:2539.
40. [a] Defoor F. Molecular, Thermal and Morphological Characterization of Narrowly Branched Fractions of 1-Octene LLDPE, Ph.D. Thesis, Katholieke Universiteit Leuven, Belgium 1992; [b] Avila-Orta CA. Contribución al estudio de la morfología de polímeros semicristalinos a través de dispersión de rayos-X en ángulos bajos, BSc Thesis, Universidad Autónoma de San Luis Potosí, Mexico 1994.
41. Medellín-Rodríguez FJ, Avila-Orta CA. *Av Ing Química* 1995;5(2):191.
42. Stribeck N, Ruland W. *J Appl Crystallogr* 1978;11:535.

20

MICROSCOPY

MARIAMNE DEHONOR, CARLOS LÓPEZ-BARRÓN, AND CHRISTOPHER W. MACOSKO

20.1 INTRODUCTION

Polymer and polymer-related materials are characterized by scanning electron microscopy (SEM), transmission electron microscopy (TEM), scanning transmission electron microscopy (STEM), high resolution transmission electron microscopy (HRTEM), energy-dispersive X-ray (EDX) analysis, electron diffraction energy-loss spectroscopy (EELS), and energy-filtered transmission electron microscopy (EFTEM), among others. The information that these techniques provide is related to the structure, morphology, topology, structure, elemental composition, and chemical bonding of the materials.

This chapter includes a review of the recent literature on polymer microscopy. The basic principles and current challenges of the techniques, as well as the experimental aspects of sample preparation and observation are reviewed elsewhere [1–8]. Specific techniques are surveyed in other reviews; for instance: TEM [9], SEM [10], Field emission SEM [11], and high angle annular dark field (HAADF)-STEM [12].

20.2 TRANSMISSION ELECTRON MICROSCOPY

The characterization of materials using TEM can give information about their structure and morphology. Allied techniques from TEM, such as EDX, EELS, EFTEM, and electron diffraction (ED), can complement the information obtained for a specific material. Several reviews and compilations of the studies on TEM and related techniques

are available [13]. In this chapter, some of the most recent applications of TEM and allied techniques to polymer materials have been compiled from 2000 to the present. The focus is on nonconventional techniques such as electron holography, *in situ* TEM, STEM, EELS, cryo-TEM, Z-contrast, etc. In addition, a very detailed section is devoted to 3D imaging.

20.2.1 Conventional Transmission Electron Microscopy

There are several applications of conventional transmission electron microscopy (CTEM), including study of the morphology of polymers and their crystallization behavior. Some reports include studies on the branched crystal morphology of linear polyethylene [14]; the morphology of nucleation and crystallization of polyethylene/carbon nanotubes composites, making evident the behavior of carbon nanotubes as nucleating agents [15]; and the formation of supramolecular polymeric systems as well as the effect of polymer rigidity and the reversibility of self-assembly processes [16].

HRTEM has also been used in the study of polymer crystallinity. A high resolution image is an interference image of the transmitted and diffracted beams. It has been reported that changes in weight-average molecular weight lead to structural changes [17].

Some of the observed changes are related to lamellar thicknesses, disorder in the crystalline packaging of the chains, interconnectivity between crystalline lamellae, as well as tilt angles of the polymer chains.

20.2.2 Transmission Electron Microscopy Allied Techniques

20.2.2.1 Electron Holography Electron holography is an imaging technique that records the interference pattern of an object on a film or detector, forming a hologram [18]. Electron holography was invented by Dennis Garbor in 1948. He developed the technique to improve the resolution of electron microscopes, by solving the spherical aberration problem of the primary lens that affects the phase components of the electron beam. The method is based on the combination of two waves in the electron microscope, namely, the image wave and the undeviated wave. If the electron optical geometry is correctly set up, these two waves can be made to interfere. The interference pattern would then be processed using optical techniques to form optical holograms. The hologram is a Fresnel diffraction image of the object [2]. Several electron optical geometries have been developed to produce holograms; among them electron holography is an inline scheme and high energy electron holography is an off-axis scheme [19]. Detailed description of both modes can be found elsewhere [20, 21]. In this technique, the phase image can be referred to the variations in the sample thickness due to the change in phase of the electron wavefront in comparison with the original wave. Phase contrast can be carried out by an imaging defocus or by the off-axis holography.

Electron holography is used in several applications, such as in biological samples, for example, bacterial surfaces [22]; in nanocrystals of metallic catalysts to determine the shapes from the 3D structure and to extract details from the structure and morphology on an atomic scale; in thin films to study electrical and magnetic fields, as magnetic and electric fields can shift the phase of the interfering wave passing through the sample [23]; in ferroelectric materials to enhance contrast between regions of different polarizations [24]; in semiconductor devices [25]; and in polymer nanoparticles to give phase-contrast imaging to avoid the use of a staining procedure [26]. Even though there are many applications using electron holography in materials characterization, only a limited number of scientific reports are found in the polymer field. Specific materials characterized by electron holographic techniques include arborescent graft polystyrene (PS) nanoparticles [26]. Chou et al. [26] have reported that electron holography could provide higher contrast than generated by the traditional method of transferring information to amplitude via defocusing. Electron holography is thus capable of recovering significant phase contrast from the PS particles despite the fact that they provide negligible amplitude contrast. This technique has the advantage of avoiding heavy element staining that induces amplitude contrast but has difficulties in the preparation the analysis of the structures at the nanometer scale.

Polymers are being used as holographic recording material, as reported by Lawrence et al. [27]. According to the authors, photopolymers present several advantages such as ease of production and high efficiencies, even though they have low ability to record high spatial frequency gratings compared to dichromated gelatin and silver halide photographic emulsions. In the same way, Garcia et al. [28] have studied a photopolymer based on acrylamides, consisting of acrylamide as monomer, yellowish eosin as sensitizer, and triethanolamine as radical generator, all on a matrix of poly(vinyl alcohol).

Gölzhäuser et al. [29] studied the optimal conditions (electron energy, width of the electron beam, and the detector size) for low electron point source microscopy using holograms of phthalocyaninato polysiloxane (PcPS), a rodlike macromolecule.

Binh et al. [30] have reported the electron holography of carbon and polymer fibers.

20.2.2.2 *In situ* Transmission Electron Microscopy

Nowadays, electron microscopy has evolved to allow the determination of polymer morphology and composition to be mapped as a function of time in several physical conditions. In particular, *in situ* microscopy can provide morphological structure and also information on the dynamic changes in properties present in microstructures during synthesis, phase transformations, and physical tests [31].

In general, *in situ* microscopy can be performed by using SEM, TEM, and atomic force microscopy (AFM). By using SEM and environmental scanning electron microscopy (ESEM) techniques, several studies on the deformation, crack propagation, and fracture processes can be carried out. In addition, TEM enables the study of the same processes but at the nanoscale. Finally, AFM images give information about the micromechanical deformation at atmospheric pressure and in the absence of electron irradiation. In general, in addition to mechanical studies, the *in situ* techniques that can be performed over materials using microscopy techniques are heating and cooling, electron irradiation, application of electric and magnetic fields, and application of different ambient atmospheres, among others [2]. It is also common to use a combination of *in situ* techniques, such as deformation tests using temperature variations. In all cases, microscopy images can be observed in real time but the sample preparation varies depending on the technique.

In situ TEM can be performed to study the optical, electrical, and mechanical properties of materials. The instrumentation involved considers several types of specimen holders. At present, the main types of specimen probes used in industry are electrical probing (TEM–STM) [32], micro-force (TEM–nanoindenter) [33], nano-force (TEM–AFM) [34, 35], optical, scanning fiber, multiple electrical wire,

and some of their combinations [36–39]. In all cases, very thin samples (100–500 nm) are required.

In general, the applications of *in situ* TEM involve the understanding of the relationship between the physical properties and the structure of nanomaterials.

In addition to the electrical and mechanical properties that can be directly extrapolated from macro-sized experiments, it has been reported that it is possible to bring optical signals into TEM and position them on selected areas of the specimen using an external laser beam, or to acquire optical emission from a specimen to analyze it externally. Regarding external laser illumination with simultaneous TEM imaging, the reported applications are (i) sintering of powder specimens; (ii) heating to induce phase or structural changes in specimens; (iii) illumination of photovoltaic specimens with simultaneous electrical current measurement; and (iv) illumination of photocatalytic materials with simultaneous electrical current measurement. The applications that involve acquiring emitted light from specimens include (i) cathodoluminescence used to investigate photonic materials and (ii) temperature determination.

Heating of specimens followed by the study of changes in TEM images allows the observation of phase transformation, alloying, sintering, element diffusion, grain size changes, defect motion, etc.

Specific reports on the applications of *in situ* TEM in polymer materials are described in the following paragraphs.

Synthesis Crozier et al. [40] have reported the gas-phase polymerization of polypropylene using Ziegler–Natta catalysis performed in an *in situ* environmental TEM. In this case, the monomer was introduced into the microscope and the probability of polymerization when the monomer strikes an active site was calculated using the available area of the catalyst.

Crystal Morphology Crystal morphology determines the mechanical properties, the biodegradability, and the biocompatibility of polymers. Thus, it is necessary to understand the mechanism of polymer crystallization in order to control the polymer microstructure and, thereby, its properties. The crystallinity and cavitation of polymers have been studied using optical and *in situ* electron microscopy as complementary techniques, among many others.

Mechanical Strength Stress measurements can be conducted using SEM and TEM. A report on the mechanical properties of polyethylene under deformation and fracture was presented [41]. Three types of fractures depending on the molecular weight and linearity, namely, crazing, elongation, and the “interfacial splitting” of spherulites were described.

It is well known that the main mechanisms of inelastic deformation are shear yielding and multiple crazing in the rigid matrix phase, as well as cavitation in the soft dispersed phase in rubber-toughened plastics and multiphase polymers [42]. For many years, these mechanisms have been studied using microscopy techniques.

Garcia Gutierrez et al. [43] studied the crazing behavior of linear and long-chain branched polystyrene (PS) as function of temperature. The changes of temperature around the glass-transition temperature favor the disentanglement that consequently modifies the characteristics of the crazes (in this case from homogeneous to fibrillated). Using this technique, the deformation rate could also be analyzed.

Rubber-modified amorphous polymers and butadiene-styrene block copolymers have been observed to enhance the plastic yielding of the amorphous glassy components PS and poly(methyl methacrylate) (PMMA). These materials were analyzed using deformed samples or by *in situ* deformation tests of thin sections using TEM and scanning force microscopy (SFM) [44]. Toughening studies in rubber-modified polymers have been performed by Michler and Bucknall [45]. Their experiments on the deformation mechanisms in various rubber-modified polymers were carried out using microscopy techniques. From these studies, two new mechanisms of energy absorption were found. In particular, *in situ* mechanical tests were carried out using *in situ* TEM.

Studies from the composite deformation mechanism and interfacial bonding between nanofillers and the polymer matrix have been performed [46–48]. In these reports, the authors performed straining studies to determine the load transfer between carbon nanotubes and the polymer and observed the phenomena of crack propagation and polymer debonding. In some cases, the mechanical deformation processes were followed over the electrospun composite fibers. Microscopic images revealed information on the dispersion and orientation of nanotubes within the fiber and their impact in the mechanical performance regarding strain at break and stress concentration at the pores of the nanotubes.

Other types of nanocomposites have been studied, such as PMMA/montmorillonite [49]. In this system, tensile tests were performed using TEM to obtain information on the deformation process.

Processing Polymer processing properties that affect the crystallization stages can be studied in detail using *in situ* probes. Several reports on this application have been published. Among them, the rheology of polyethylene and polyethylene blends was studied by *ex situ* TEM to determine their crystallization process and its effect on the shear behavior. The obtained information at different length scales (during shear flow and flow during crystallization) was used to construct a crystallization process model [50].

The relationship between shear history and the subsequent anisotropic crystal growth is of particular interest.

Additional applications of *in situ* TEM include *in situ* measurement of the interfacial adhesive forces in nanoparticles and biological samples [51].

20.2.2.3 Scanning Transmission Electron Microscopy

STEM is a type of TEM. In this type of microscopy, the electron beam is focused to a narrow spot, which is scanned over the sample. The scanned electrons traverse the samples as in CTEM. Using this technique, several analyses such as mapping by EDX spectroscopy, EELS, and annular dark-field (ADF) imaging can be performed. Both types of information, image and quantitative data, can be obtained. It is noteworthy that STEM imaging provides information from a volume of the material, and therefore in the case of films, it provides information on the membrane thickness [49].

Biological Samples Some studies of biological architectures from tissues and cells have been performed by combining confocal light microscopy, TEM, STEM, and focused ion beam (FIB). The images from the STEM technique were used to explore the morphology of the materials as 3D relationships for a range of length scales and materials [52].

Specific examples using STEM include structural studies over chitin gels used to produce chitin films. The results of the tests performed revealed that shrinkage resulted in a coarser microstructure. This morphology affected the tensile properties. It was also observed that shrinkage was proportional to the ductility and roughness of the material [53].

Polymers Regarding polymer particulate systems, it has been reported that SEM has been employed to examine particle size and shape, and STEM has been used to characterize the internal structure of multilayer particles [54]. Thus, it was possible to follow the synthesis of particles by STEM. In fact, particles from different morphologies have been studied by several groups.

Particles from polyisoprene (PI) and PMMA were prepared in solution. The obtained lamella-structured block copolymer particles and their cross-sectional images were observed by a staining procedure using STEM [55]. The authors reported that the lamellar phase changed to disordered structures when the suspension of nanoparticles was annealed. In addition, they followed the particle versus the planar film stability.

Polymer particles have been observed using STEM in order to find the differences in their internal structures. Examples include particles of poly(styrene-*b*-sodium acrylate), poly(styrene-*b*-4-vinylpyridine), and poly(styrene-*b*-isoprene) prepared by solvent evaporation [56]. In these systems, the differences between amphiphilic (hollow

structures) and hydrophobic block copolymer nanoparticles (lamellar microphase separation structures) were analyzed. Poly(styrene-*ran*-styrenesulfonate) (P(S-SS_x)) ionomers have also been analyzed [57, 58].

A latex used for coating applications and made from an acrylic phase and an alkyd phase contains surfactant particles that stabilize the phases after the film-forming process. Using STEM, the imaging of these surfactant molecules was carried out in order to understand the influence of the surfactant–polymer affinity on the surfactant location after film formation [59].

The grafting process of polymer chains over particles or fibers can be analyzed using STEM, among other techniques. The aspects that can be studied by STEM are the distribution of the polymer chains obtained at different particle/fiber concentrations and the effect of the surface rugosity and composition on the distribution of the polymer, among others [14]. Other examples involving polymeric chains grafted on macroporous silica gel were analyzed using a procedure involved staining, embedding in epoxy, and ultrathin slicing [58].

The synthesis of carbon nanotubes with metal hybrids has been studied using STEM and ED. The carbon nanotubes could be functionalized (or not) with a polymer. Gao et al. [60] have reported particle sizes of 2–20 nm and a metal deposition of 82 wt%.

Additional applications of STEM include (i) the imaging of multilayer particles, considering PS and poly(trifluoroethyl methacrylate) (PTFEMA) particles [54], as well as the distribution of polymer layers covalently grafted on the inner and outer surfaces of macroporous silica gel particles; (ii) the nucleation of spherulites in crystalline and semicrystalline polymers filled with particles, observing that the nucleating efficiency of the filler depends on the size and on the crystallographic orientation of the facet [61]; (iii) the miscibility of polymers in a blend as a way to observe the interface of materials [62]; (iv) the penetration (diffusion) of poly(ethylene glycol) (PEG) chains into wood cell walls [63]; (v) the morphologies of cured epoxy/brominated-phenoxy blends [64]; and (vi) the confirmed presence of quantum dots of (CdSe)ZnS surrounded by protein oligomers [65].

Polymer Nanocomposites The morphology and dispersion state of a filler-like sepiolite (lamella and fiber type) were determined using STEM [66].

Some improvements in the analysis of the morphology by STEM have been reported. In one study, the authors used the deconvolution of the ionomer images by the Pixon method with a simulated electron probe in order to enhance the overall image quality and the detection of subnanometer-scale features (in size and shape) compared to the original ones. The use of deconvoluted images instead of the original ones makes it possible to follow the

distribution of ions in the aggregate, discriminating overlapping particles. Studies of ionic aggregate distributions have been reported in polymer matrix systems [67, 68].

20.2.2.4 Wet-STEM Gai [69] proposed in 2002 the development of wet environmental scanning transmission electron microscopy (wet-ESTEM) experiments in order to perform direct probing of controlled liquid–catalyst reactions. The first nanoscale images from dynamic liquid hydrogenation and polymerization reactions of polyamides were then reported.

Furthermore, Bogner et al. [70] proposed experiments using a STEM imaging system to make transmission observations of wet samples in an ESEM without poor contrast or drifting of objects, as obtained in the ESEM of particles that are embedded in a liquid medium. The proposed system was based on ADF imaging conditions and considers specific features to allow slow-scan, high definition imaging of particles below tens of nanometers. The applications of wet-STEM include the studies of emulsion samples of latex polymer-grafted particles [70], polymer-grafted natural rubber particles [71], and clay platelets [72], among others. In several cases, the images acquired showed good resolution and contrast, without staining. In particular, Wet-STEM images provide important information about grafted particles in their native state in solution. Additional applications involve solution-solid and solution-gas-solid reactions in the chemical and biological sciences, as well as thin polymer and biological films.

Theoretical studies of this technique were carried out by Barkay [73]. In this study, wettability (aqueous nanodroplet shape and contact angle) at the nanoscale was quantified using Monte Carlo simulation. The technique was based on the measurement of transmitted electrons through nanodroplets of water.

In nanoclay composites, particularly from montmorillonite, the shape and dimensions of platelets after extrusion process were observed using TEM and wet-STEM. The differences in the size observed between platelets using TEM and STEM techniques were attributed to the preparation by ultramicrotomy and the effect of projection [72]. Thus, in this case, the combination of microscopy techniques revealed the effect of each step of the process.

20.2.2.5 Cryogenic Transmission Electron Microscopy Cryogenic transmission electron microscopy (Cryo-TEM) or cryogenic high resolution transmission electron microscopy (Cryo-HRTEM) involves the observation of samples of vitrified macromolecules.

Some of the Cryo-TEM and Cryo-HRTEM applications in polymer materials are (i) studies of crystal transformation, for example, the nucleation process and shape of crystals in lamellar crystals of polybutene-1 [74]; (ii) studies of the morphology of several materials, such as polypeptides

[75]; investigations on the degradation and erosion of polymers, for example, studies of random copolymers of DTE (desaminotyrosyl-tyrosine ethyl ester) and PEG [76]; and (iv) studies of the spatial structure of polymer brushes, such as poly(styrenesulfonate) chains grafted to core particles of PS latex [77].

The technique is under development. Studies on specimen thickness dependence during cryo-TEM of hydrated soft materials were proposed by Yakovlev et al. [78]. The authors found a way to obtain higher spatial resolution using thin specimens and higher electron doses.

20.2.2.6 High Angle Annular Dark Field (HAADF)-STEM A high angle detector can be added to STEM to obtain atomic resolution images where the contrast is directly related to the atomic number (Z-contrast image). These images are therefore directly interpretable, in contrast to conventional HRTEM which uses phase contrast and needs simulation for interpretation. HAADF-STEM is an incoherent imaging technique whose characteristics include high signal-to-noise ratio, linearity of the signal intensity, and a reduced number of imaging artifacts. Thus, information on the nanoscale organization of polymeric materials, which is not accessible by CTEM, can be obtained by HAADF-STEM.

There are important advantages of this technique compared to CTEM, such as the possibility to use different values of the camera length in HAADF-STEM imaging to enhance the contrast between crystalline and amorphous compounds through diffraction contrast [79], as well as the use of low convergence angles for imaging HAADF-STEM tomography, which allows to obtain information from micrometer-thick samples [80]. Some of the reported applications are described below.

Loos et al. [12] have explored several polymer systems using HAADF-STEM, such as a rubber blend, a carbon-filled conductive nanocomposite, a functional blend, semicrystalline polyethylene, and template-grown nanotubes (polymer and liquid-crystalline material) [81]. The authors discussed the advantages of HAADF-STEM for the morphology characterization of polymer systems. For carbon-based (carbon black (CB)) functional polymer systems HAADF-STEM can provide high contrast between the CB agglomerates and the polymer matrix, revealing details of the interface and permitting a clear assignment of the phases [79].

Additional reports [82] revealed that the volume concentrations of CB can be precisely determined using HAADF-STEM. In another study, the same authors reported that the filler distribution in polymer nanocomposite systems could be clearly determined [83]. They also observed the nanoscale organization in a photoactive layer of a polymer solar cell that could not be seen with CTEM [79].

Phase separation of poly(vinylidene fluoride) (PVDF) and sulfonated PS within a poly(vinylidene fluoride)-*graft*-poly(styrenesulfonic acid) (PVDF-*g*-PSSA) system and ionic sulfonic aggregates could be determined using HAADF-STEM [84].

Finally, significant contrast increase of stained samples was reported when the HAADF-STEM technique was used for several systems, such as cellulose microfibers and whiskers within poly(lactic acid) [85].

20.2.2.7 Z-Contrast Several studies of particle formation using different methods were performed using Z-contrast STEM [86, 87]. Some of the reports involved the study of the dispersion of colloidal CdSe semiconductor nanocrystals embedded in poly[2-methoxy-5-(2-ethylhexyloxy)-1,4-phenylene-vinylene] (MEH-PPV) polymer films [88]. In another report, the authors [89] discussed the possibility of measuring absolute thicknesses of atomic columns if the crystal structure was known. In fact, Z-contrast STEM can have a resolution of atomic and subnanometer order. Thus, the technique is able to provide the three-dimensional shape profile reconstructed from the atomic columns. Another application of Z-contrast involved the study at atomic resolution of the structures exhibited by polymer-capped Pt and Pd nanoclusters used as a model of an electrocatalyst [90]. The advantages of subnanometer resolution and the atomic number contrast make it possible to study atomic structures in detail.

Z-contrast has been used to distinguish between two phases using the differences in the atomic number of the particular phase of the analyzed material. Some of the applications reported involved distinguishing a liquid crystal from polymer nanotubes [81].

20.2.2.8 Low and High Voltage Transmission Electron Microscopy Low voltage transmission electron microscopy (LV-TEM) allows to obtain high contrast images of samples from a variety of polymer and organic molecules [91]. LV-TEM has been applied to obtain images of the phase structure of polymer blends without a prior staining procedure [92]. The instrument used in the technique combines light and electron sources (voltage of 5 kV) and charge-coupled device (CCD) imaging. Some of the reported studies are related to the phase structure of polycarbonate/poly(styrene-*co*-acrylonitrile) (PC/SAN), polystyrene/polypropylene (PS/PP), and polyethylene/polypropylene (PE/PP, ADFLEX). The authors have compared the results with LV-STEM at 25 kV. Additional studies have used LV-TEM to identify the morphology of polymers such as PEDOT [93] and polyethylene [91].

Several studies have been carried out in order to understand the relief of ultrathin sectioning and the effect of the imaging at low voltages [94, 95]. The studied polymers

involved hard matrixes and soft particles, such as high impact PS, and polymer blends (e.g., PC/SAN blend). From these studies, the authors showed the correspondence between mechanical behavior and morphology of polymers, thus surface relief and phase structure.

In contrast to LV-TEM, studies on the morphology and microdeformation behavior of PP-wood composites modified with high amounts of maleated poly(propylene) as a coupling agent were carried out using high voltage transmission electron microscopy (HV-TEM) [96]; the authors reported the effect of using coupling agents on the adhesion properties between matrix and wood fillers and the resulting increase of the composite's mechanical properties.

20.2.2.9 Electron Energy-Loss Spectroscopy Elemental mapping (EDX) and EELS by EFTEM allows the characterization of interfaces with low spatial resolutions (<10 nm) and high elemental detection sensitivity. EELS, in addition, has the ability to reveal different forms of the same element. Thus, EELS solves important application-oriented problems associated with hetero interfaces, nanoscale mixing, and nanoparticle separation. Several applications have been reported on the basis of the fact that each polymer has a different EELS fingerprint. Thus, EELS can be a way to differentiate one phase from another. Many studies have been performed in order to improve the information obtained from polymer characterization using EELS. In the following, some research in the field will be briefly described.

Yakovlev and Libera [97] studied the dose-limited imaging of soft materials in STEM as a way of controlling the spatial resolution and avoiding chemical or structural damage. The authors used the low loss of an EELS spectrum to provide a guide to enhance the dose-limited spatial resolution for soft-materials imaging. Also, it has been reported [98] that the spatial resolution is limited by the dose constraints in order to avoid radiation damage. As a consequence, it is necessary to use fine electron probe sizes that reduce counts in the energy-loss spectra.

Libera [99] has presented an alternative for the study of polymer morphology avoiding the staining procedure as a way to induce amplitude contrast. He proposed the use of EELS to study different polymer systems to obtain several levels of resolution (related to the radiation sensitivity of the material) when studying interfaces, such as those in polystyrene-poly(2-vinyl pyridine) homopolymer blends, epoxy-alumina interfaces, and hydrated polymers. Polymers could be distinguished from each other on the basis of the energy-loss spectra in their low loss (valence) and core loss (elemental composition).

A detailed study on the influence of fast secondary electrons from a 200 keV incident electron beam on the characteristic 7 eV $\pi-\pi^*$ peak in PS was carried out using EELS with STEM. Siangchaew and Libera [100] found a relation between the π -bond degradation, the total radiation

dose, and the dose rate. At higher rates, the π bond was less damaged. Cryo and room temperatures did not affect the damage behavior. The authors concluded that damage to the valence bonds was at least partly due to core excitations.

Regarding applications, nanoscale morphology could be studied in soft materials such as polymers and biological tissue using EELS [101–104].

A combination of cryo-STEM and EELS allowed the study of the spatial distribution of water in frozen hydrated polymers. Because of the reduced information spectra due to the sensitivity of the samples, Sousa et al. [98] reported a method to identify the water in the sample. The problem was studied using theoretical and experimental approaches. They considered hydrophilic poly(vinyl pyrrolidone) (PVP) dispersed in a hydrophobic matrix of PS.

Spatially resolved EELS in STEM was used to examine the size, structure, and composition of material interphases. In particular, the aliphatic bis(*p*-aminocyclohexyl)methane (PACM20) curing agent and the aromatic diglycidyl ether of bisphenol-A (DGEBA) epoxy resin were used in getting spatially resolved $\pi-\pi^*$, carbon, and thickness profiles in the epoxy phase near the interphase area [105].

Polymer composites are being studied by HRTEM, EELS, scanning tunneling spectroscopy (STS), Raman spectroscopy, and allied techniques. In addition, polymer grafting on carbon nanotubes has been studied using EELS. In particular, the covalent attachment of polymer chains onto nanotube surfaces could be successfully proved using low loss EELS [106, 107]. In addition, the propagation of concentric cracks around carbon fibers was observed using EELS, paying special attention to plasmons [108].

An extensive list of applications includes spatial distribution of several elements in a matrix using EELS [108], for example, in a natural rubber [109]; study of the interfaces between a polymer and an adhesive, as in the case of poly(butylene terephthalate) (PBT) and an epoxy adhesive, to correlate the nanoscale interfacial structure with the adhesion strength by EFTEM [110]; characterization of the coating of nanosized particles [111]; studies on the accelerated vulcanization process with regard to the interactions between rubber and ZnO particles [112]; multilayer films of polymers [113]; intercalation of barium atoms in poly(*p*-phenylene) matrixes in atoms per molecules [114]; and studies on the rate and mechanism of hydrolytic degradation and erosion in bioresorbable polymers by EELS and cryo-STEM to determine morphological changes [76].

20.2.2.10 Energy-Filtered Transmission Electron Microscopy EFTEM uses the low electron energy-loss spectroscopy (LEELS) to generate spectral images and enables the search of the spatial distribution of molecules, ions, and particles within nanostructured solids, which could be differentiated by small changes. Thus, as reported, EFTEM provides a molecular map resolution near the

bright-field resolution of the same instrument. It is also observed that slight changes in the molecules produce intensity variations in the molecular spectra [115]. Some examples of the application of this technique to polymer materials are described next. Also, there is a review by Ribbe [116] focusing on the advances in EFTEM imaging techniques applied to polymeric materials.

EFTEM by EELS in the image-spectrum mode was used in several applications to polymeric materials such as the following:

1. *In Copolymers and Polymer Blends.* EFTEM was applied to differentiate the phases using the energy transitions due to chemical bondings [117], colloidal dispersions of natural rubber, and styrene-acrylic latex with inorganic particles [118]. The spatial distribution of clay platelets in polymer nanocomposites was investigated using TEM images; nevertheless, this is more difficult than the case of polymer blends. Linares et al. [119] proposed the use of EFTEM crossover region to clearly observe clay nanoplatelets within a polymer blend matrix. The materials studied were natural rubber and poly(styrene-Bu acrylate), poly(styrene-Bu acrylate) and poly(vinyl chloride), as well as natural rubber and starch.
2. *In Polymer-Functionalized Nanoparticles and Nanocomposites.* EFTEM was used to evaluate the covalent bonding of polymer coating on nanoparticles and the nanoparticle dispersion, as in a polycarbonate/alumina nanocomposite [120].
3. *In Polymer-Polymer Interfaces.* EFTEM was used to analyze the effect of annealing temperature on the interfacial structures of copolymers, such as poly(methyl methacrylate)/polystyrene-*co*-polyacrylonitrile (PMMA/SAN) random copolymer [121] and PMMA/SAN random copolymer bilayer films [112]; to study the interface between a polymer and an adhesive, looking for a relationship between the nanoscale interfacial structure and the adhesion strength [110]; and to understand the effect of annealing temperature on the interphase by annealing at different temperatures and using elemental mapping and image-EELS on EFTEM.
4. *Inorganic Polymers.* To study the morphology of polymers [122] and polymer brushes [123].
5. *Conductive Polymers.* EFTEM was used to follow the distribution of ions inside the polymer and the ion-exchange processes as well as to study the elemental distributions in the polymer nanofibers [124], the distribution of lithium ions in solid copolymer electrolytes for lithium batteries [125] and the particle morphology of copolymers [116].

20.3 THREE-DIMENSIONAL MICROSCOPY

20.3.1 Introduction

2D imaging techniques (including optical microscopy, SEM, TEM, and AFM) have been widely used for several decades to study multicomponent polymeric materials (e.g., polymer blends, block copolymers, and polymer composites) [1]. However, 2D micrographs do not fully display the 3D morphological complexity, as they are just cross sections, thin sections, or projections of the bulk specimens. Consequently, qualitative interpretation of 2D images is not always easy. For instance, transversely cut rods can be confused with isolated droplets [126]. When it comes to quantitative assessment of a geometrical parameter, the situation is even more complicated because 2D images generally give only limited pieces of structural information with low statistical accuracy. For some applications, stereological methods (i.e., mathematical relations between 2D and 3D geometrical parameters) can be used to extract 3D information from 2D micrographs [127–130]. However, this approach is limited to a number of geometrical parameters and is contingent on the statistical significance of the micrographs [126, 131].

Scattering techniques (i.e., small angle light, X-ray, or neutron scattering) give statistically averaged structural information of the scattering volume. However, scattering methods do not provide an intuitive morphological insight (i.e., real-space images) as microscopy does. Hence, some knowledge of the morphologies as well as the use of models is usually required to obtain structural parameters. A typical protocol for a complete morphological characterization includes 2D microscopy followed by a hypothesized 3D structure which is tested by scattering measurements. This protocol carries the latent misinterpretation of 2D micrographs, especially for the case of complex interfaces (e.g., bicontinuous structures [126, 132, 133]).

To overcome the above drawbacks, a new technique, namely, 3D microscopy has emerged and rapidly evolved in recent years [132–134]. Obtaining 3D images involves specialized microscopes or attachments (as described below) as well as additional image processing [135] and 3D-rendering algorithms [136]. The reward for this extra equipment and image processing effort is direct 3D information and the computation of parameters not available from any other technique (e.g., local curvature distributions, and local topology).

20.3.2 Methods to Obtain 3D Micrographs

There are two ways to generate 3D images: (mechanical or optical) serial sectioning and tomography. Mechanical sectioning has been used to image metal alloys [137–139] and is in principle applicable to polymeric materials.

However, this technique is destructive and requires extra steps to align the 2D micrographs [137]. In optical sectioning, a system with a small depth of field (DOF) is used to image a series of sections of the bulk specimen. Optical sectioning has the advantage of filtering the stray scattered light originated from outside the section. This “gating” property allows imaging through moderately low scattering media (e.g., biological tissue or blends of polymers with similar refractive indices). The most popular technique that uses this approach is confocal microscopy (described in the following section). In tomography, a system with a large DOF is used to record projections of the object at different angles. Transmission electron microtomography (TEMT) and X-ray microtomography (μ -CT) have been used to image multiphase polymer-related materials. These techniques are described below.

20.3.2.1 Laser Scanning Confocal Microscopy (LSCM)

In confocal microscopy, the object is illuminated with a focused laser spot, and the light from the object is refocused onto a small pinhole placed in front of the light detector [140, 141]. Images are acquired point by point and reconstructed with a computer algorithm, allowing 3D reconstructions of topologically complex objects. For opaque specimens, this is useful for surface profiling, while for nonopaque specimens interior structures can be imaged. LSCM is a very attractive technique because it does not require time-consuming sample preparation and the image acquisition is fast and nondestructive. However, it has two major drawbacks: one is that at least the first of the phases has to be fluorescent in order to attain a good contrast in the images; and the second is that to image internal structures, the sample has to be transparent in order to provide an adequate DOF [140]. Figure 20.1 shows the basic setup of a confocal microscope. In order to obtain very high intensities, a laser is used to provide the excitation light. The light (blue lines) reflects off a dichroic mirror, which directs it to an assembly of vertically and horizontally scanning mirrors (not shown). These motor-driven mirrors scan the laser across the specimen. The dye in the specimen is excited by the laser light and fluoresces. The fluorescent (green lines) light is descanned by the same mirrors that are used to scan the excitation light from the laser. This light is then passed through the dichroic mirror and is focused onto the pinhole. The light that passes through the pinhole is measured by a photomultiplier. The lateral and axial resolutions in LSCM (r_{xy} and r_z , respectively) are on the order of 1 μm . They can be calculated with $r_{xy} = 0.61\lambda_{\text{exc}}/\text{NA}$ and $r_{xy}/r_z = 3.28n/\text{NA}$, where λ_{exc} is the excitation wavelength, n is the refractive index of the object medium, and NA is the numerical aperture of the objective lens [141]. In confocal microscopy, one can never get a complete image of the specimen because at any instant, only one point is observed. Thus, for visualization,

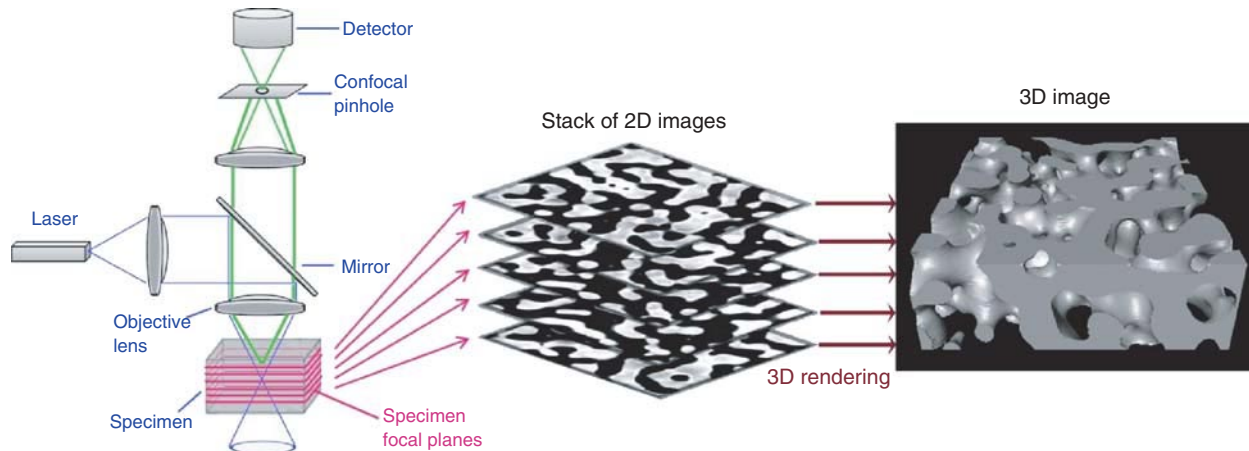


Figure 20.1 Schematic of LSCM. A stack of 2D images is recorded at different focal planes in the specimen and subsequently reconstructed in three dimensions using the marching cubes algorithm [136]. (See insert for the color representation of the figure.)

the detector is attached to a computer, which builds up the image one pixel at a time.

Verhoogt et al. pioneered the use of LSCM to visualize polymeric materials [142]. They compared images of the microstructure of the blend made of styrene (ethylene/butylene) styrene (SEBS) block copolymer and poly(ether ester) from LSCM and SEM. Jinnai and coworkers have extensively used LSCM to visualize bicontinuous structures generated during the late stage of spinodal decomposition of binary mixtures of polybutadiene with deuterated polybutadiene [134, 143, 144] and of polybutadiene with poly(styrene-*ran*-butadiene) [134, 145, 146]. Recently, Lopez-Barron and Macosko made 3D images of immiscible polymer blends of polystyrene/styrene-*ran*-acrylonitrile (PS/SAN) copolymer with cocontinuous morphologies during structural coarsening [126, 147–150].

20.3.2.2 X-Ray Microtomography X-ray μ -CT has similar spatial resolution as LSCM ($\sim 1 \mu\text{m}$) but the big advantage is its stronger penetration power. This is particularly useful to image opaque materials. For instance, Montminy and coworkers [151] used a commercial desktop μ -CT to image and analyze 3D structures of polyurethane foams (Fig. 20.2). They developed an image analysis algorithm to measure and quantify the number of struts and windows in the foam structure. However, the main limitation of this technique in pure polymer samples is the poor contrast because of the low X-ray absorption in polymers. Therefore, the use of laboratory X-ray sources allows the imaging of only high contrast samples, including polymer foams [151, 152], biopolymer scaffolds [153], and polymer composites [154–156].

By using a higher X-ray flux (i.e., a synchrotron source), distinct polymer phases can be detected using phase contrast. The interaction of electromagnetic radiation (X-rays)

with matter depends on the complex refractive index of matter, $n = 1 - \delta + \beta i$ [134]. The real part δ is associated with phase contrast, which is due to edge-enhancement effects based on diffraction, refraction, and interference, whereas the imaginary part β underlies absorption contrast. Different polymer regions have different refractive indices and thus produce different lateral displacements of a collimated X-ray beam (which is provided by synchrotron X-ray sources). The interference between the transmitted and displaced beams that occurs near the boundary regions of the two polymers gives rise to dark and bright fringes, resulting in edge enhancement. Elmouataouakkil et al. [157] used synchrotron X-ray μ -CT to analyze the 3D structure of polymer foams. This high X-ray flux enabled quantitative measurements of cell wall thicknesses. Weiss et al. [158] obtained better spatial resolution in bone by using synchrotron X-ray μ -CT. Pyun et al. [159] imaged the cocontinuous structure of a blend of PS and high density polyethylene with X-ray μ -CT. They showed that, as the coarsening proceeded, the specific interfacial area obtained from the analysis of the reconstructed 3D images exceeded that calculated from 2D images, even after applying a stereological correction [126].

20.3.2.3 Transmission Electron Microtomography TEMT is an emerging technique used for characterization of 3D nanostructures, (e.g., self-assembled block copolymers). The first tomographic reconstructions date from 1968 [160–162]. A large amount of theoretical and technical developments followed these pioneering works. The history, theory, and recent developments in TEMT can be found in two excellent reviews by Jinnai and coworkers [132, 133]. A typical TEMT procedure consists in recording projections at different angles by tilting the specimen with respect to the electron beam in the TEM column. During tilting, misalignments due to

the eccentricity of the specimen stage are unavoidable. Hence, alignment of the digitalized image is necessary before 3D reconstruction. Another problem is the loss of resolution due to the restricted tilt range in TEM, which produces a wedge-shaped region in the Fourier space. This limitation, known as the *missing wedge*, is challenging and is discussed elsewhere [133, 163].

The first report of TEMT on block copolymer nanostructures, by Spontak [164], appeared in 1988. This was followed by three morphological studies carried out in the 1990s [165–167]. Only recently has TEMT become more popular in characterizing polymer nanostructures, including block copolymers [134, 164, 167–173], nanocomposites [174, 175], and polymer nanocomposites [176]. Kawase et al. [177] recently presented a protocol to perform complete rotation (i.e., 90°) on a ZrO₂/polymer nanocomposite, by which they achieved truly quantitative TEMT for the first time.

This technique has been particularly useful to characterize complex (bicontinuous) nanostructures, for example, gyroid (G) and perforated lamellar (PL). 2D projections of these structures, acquired by regular TEM, give inconclusive identification because they appear identical along several projection axes. For instance, the “wagon wheel” pattern in TEM projections associated with the double Gyroid (DG) formed in triblock copolymers (Fig. 20.2a) [178], was once believed to be a Schurtz D surface with *Pn3_m* symmetry [179]. Small-angle X-ray scattering and self-consistent field theory calculations allowed the correct interpretation of the G surface [180]. However, the first direct observation of the 3D DG was recently achieved by Jinnai and coworkers using TEMT on a poly(styrene-*b*-isoprene-*b*-polystyrene) (SIS) triblock copolymer (Fig. 20.2b) [132, 168]. The authors were also able to compute the local curvature distributions of the gyroid interface (using the methods described in the following section) and use them to infer details of the nanostructure stability in terms of packing constraints.

Studying topological transformations during order-order transitions (OOTs) in block copolymer systems is challenging with CTEM because of the complexity of the interface between the two evolving structures. TEMT is ideal to study these transitions. An example is shown in Figure 20.3, which shows the reconstructed 3D micrograph of poly(styrene-*b*-isoprene) (SI) block copolymer during the OOT from hexagonally packed cylinder (HEX) phase to DG [181]. OOTs between DG and hexagonal PL domains and between single helix to DG were also studied with TEMT [182, 183]. Another complex interface that was experimentally ascertained with TEMT is the lamellar twist grain boundary (in SI block copolymer), in which two lamellar nanodomains intersect forming the Scherk’s first surface [145].

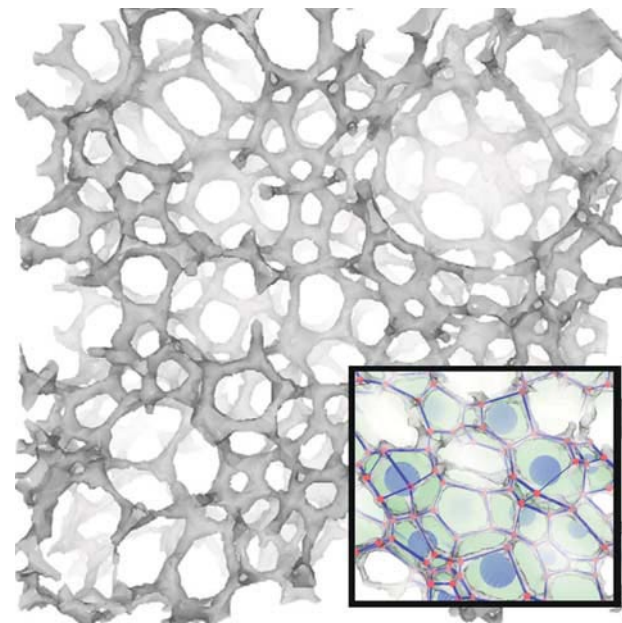


Figure 20.2 3D-rendered image of a polyurethane foam obtained via X-ray μ -CT. The black voxels within this image represent the locations of foam struts, while the white areas represent void space. The inset show a close-up of the foam structure showing the correlation between the detected strut, vertex, and cell locations and the original foam volume. The large blue spheres in the image indicate the centers of detected foam cells. Source: Reprinted with permission from Journal of Colloid and Interface Science, Vol. 280, M.D. Montminy, A.R. Tannenbaum, C.W. Macosko, The 3D structure of real polymer foams, Journal of Colloid and Interface Science 2004, 280, pages 202–211 [152]. Copyright 2004 Elsevier. (See insert for the color representation of the figure.)

20.3.3 3D Image Analysis

One of the key advantages of 3D images is that they contain rich structural information (not available using any other technique) which can be extracted using cutting-edge quantitative image analysis. Even some basic structural parameters, such as volume fractions or interfacial area per unit volume, can be inaccurately estimated from 2D images. These parameters are directly and easily measured from 3D images. Moreover, 3D microscopy is the only experimental technique capable of evaluating local curvatures, normal vector fields, and genus (interconnectivity) [134, 148, 150]. Some of the methods to evaluate these parameters are summarized below.

Typical 3D reconstruction from 2D sections or projections involves the generation of a triangular mesh describing the interface between the phases via nonstructuring meshing methods based on the marching cubes algorithm [136]. Geometrical parameters are then obtained by applying differential geometry on the mesh. For instance, the interfacial area per unit volume (Q) is simply obtained

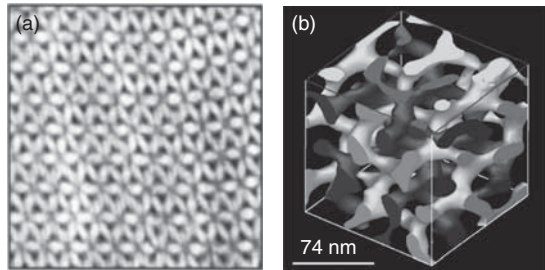


Figure 20.3 (a) TEM projection of a thin section of poly(isoprene-*b*-styrene-*b*-dimethylsiloxane) (ISD) triblock copolymer. The poly(dimethylsiloxane) (D) domains appear dark, while the poly(isoprene) (I) and poly(styrene) (S) domains appear white. The “wagon wheel” pattern is associated with the two D networks arranged in a gyroid morphology. *Source:* Reprinted with permission from Reference [178]. Copyright 1999 American Chemical Society. (b) 3D reconstructed TEMT image of the gyroid morphology in a SIS triblock copolymer. The nonintersecting light and dark channels correspond to the minority styrene microphases, while the majority (isoprene) microphase is transparent. The edge of each cube equals twice the periodic length. *Source:* Reprinted with permission from Jinnai H, Spontak RJ, Nishi T. Transmission Electron Microtomography and Polymer Nanostructures. *Macromolecules* 2010, 43, 1675–1688 [132]. Copyright 2010 American Chemical Society.

by adding the areas (A_i) of all the triangles in the mesh and dividing by the total volume (V), that is, $Q = \sum_{i=1}^N A_i / V$, where N is the total number of triangles.

The shape of the interface can be locally determined by the values of the principal curvatures (κ_1 and κ_2) or alternatively by the values of the mean (H) and the Gaussian (K) curvatures defined as $H = (\kappa_1 + \kappa_2)/2$ and $K = \kappa_1 \cdot \kappa_2$, respectively. H and K are very useful to characterize biphasic systems. H is directly related to the interfacial energy of systems containing an interface; hence it is a measure of the microstructure stability [149, 184, 185]. The Gaussian curvature is particularly useful to characterize the local shape of surfaces. The sign of K gives the type of points on a surface: hyperbolic if $K < 0$, elliptic if $K > 0$, parabolic if $K = 0$ but $H \neq 0$, and planar if $K = H = 0$. Additionally, the area integral of K is directly proportional to the Euler characteristic χ , which is a measure of the surface topology, via the Gauss–Bonnet theorem [186].

Jinnai and coworkers developed two methods to quantify the curvature between the two phases by applying differential geometry to the 3D reconstructed images [149]: (i) using a parallel surface method, they measured the area-average of H [187] and (ii) using a sectioning and fitting (SF) method, they were able to measure the local values of H and K [144]. More recently, Lopez-Barron and Macosko [148] presented a simplified method to calculate the local values of H and K , which was based on a surface patch parameterization algorithm. This method uses the coordinate transformation method proposed by Sander and

Zucker [188]. Figure 20.4a shows the details of a triangular mesh, with the mean curvature of each triangle represented by a color scale map for an immiscible blend of PS and styrene-*ran*-acrylonitrile (SAN) copolymer with cocontinuous morphology [149]. The red- and blue-colored triangles represent regions of high interfacial energy, which supply the driving force for coarsening these structures.

The probability densities of the mean curvature, $P_H(H)$, and the Gaussian curvatures, $P_K(K)$ at different annealing times provide a great deal of information about the dynamics of coarsening of biphasic materials. $P_H(H)$ and $P_K(K)$ for PS/SAN cocontinuous blend are shown in Figure 20.4b [148]. The fact that $P_H(H)$ is symmetric and centered at zero indicates that the area-averaged mean curvature, $\langle H \rangle$, is zero and hence the coarsening progresses along a path of minimal energy. Both distributions narrow down with time, which confirms that the interfacial energy is minimized by minimizing the interfacial curvature. The values of $P_K(K)$ are mostly negative at all times, indicating that the surface is predominantly hyperbolic (i.e., saddle shaped) during the whole coarsening process. Topological transformations of bicontinuous structures can also be determined from the computed values of χ via the area integral of local K , as described elsewhere [148, 189–191].

Interface anisotropy is another important parameter in multiphase fluids. This is mostly relevant to relate rheological properties with microstructure [192]. The interface anisotropy can be quantified using the interface tensor q_{ij} , defined as $q_{ij} = \frac{1}{V} \int_S (n_i n_j - \frac{1}{3} \delta_{ij}) dS$ where n_i is the i th component of the interface unit normal vector, δ_{ij} is the Kronecker delta, and the integration is performed on the surface S contained in the volume V . Hence, the unit normal vector is required in order to compute q_{ij} .

The three components of the normal vector cannot be computed from 2D micrographs without previous knowledge (or assumption) of the interface shape. For simple shapes with axial symmetry that can be described with simple functions, such as ellipsoidal droplets and cylindrical threads, analytical expressions for n_i (and q_{ij}) have been obtained from 2D images [193–195]. However, for complex interfaces (e.g., cocontinuous structures), which are not axisymmetric and cannot be described by any analytical equation, this approach is not applicable.

Recently, Lopez-Barron and Macosko [150] introduced the local cross-product method (LCPM) to compute n_i and q_{ij} from 3D images. The method is applicable to any kind of interface, regardless of its complexity, provided that 3D images are available. The method is based on a simple geometric principle: given a triangular polygon, with vertices, $p_n(x_n, y_n, z_n)$ (with $n = 1, 2, 3$), the normal to that triangle can be obtained by first describing two directional vectors in the same plane, for example, $\mathbf{d}_1 = (x_2 - x_1, y_2 - y_1, z_2 - z_1)$ and $\mathbf{d}_2 = (x_3 - x_2, y_3 - y_2, z_3 - z_2)$ (Fig. 20.5a). The

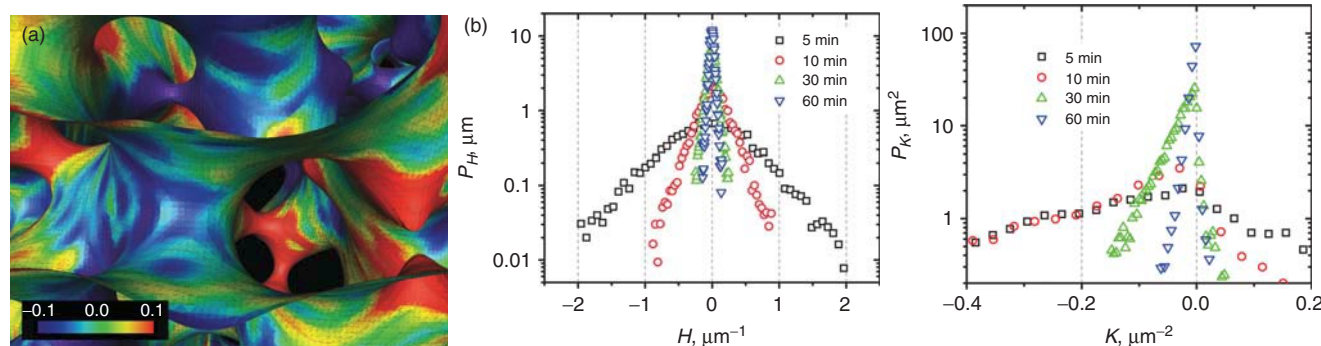


Figure 20.4 (a) 3D-rendered interface of 50/50 PS/SAN cocontinuous blend. The color in each triangle represents the value of the mean curvature given by the color bar scale. *Source:* Reproduced with permission from López-Barrón C, Macosko CW. A new model for the coarsening of cocontinuous morphologies. *Soft Matter* 2010;6:2637–2647 [149]. Copyright 2010 The Royal Society of Chemistry. (b) Probability densities of the mean and the Gaussian curvatures of the 50/50 PS/SAN interface at different annealing times. *Source:* Reprinted with permission from Lopez-Barron C, Macosko CW. Characterizing interface shape evolution in immiscible polymer blends via 3D image analysis. *Langmuir* 2009;25:9392–9404 [148]. Copyright 2009 American Chemical Society. (See insert for the color representation of the figure.)

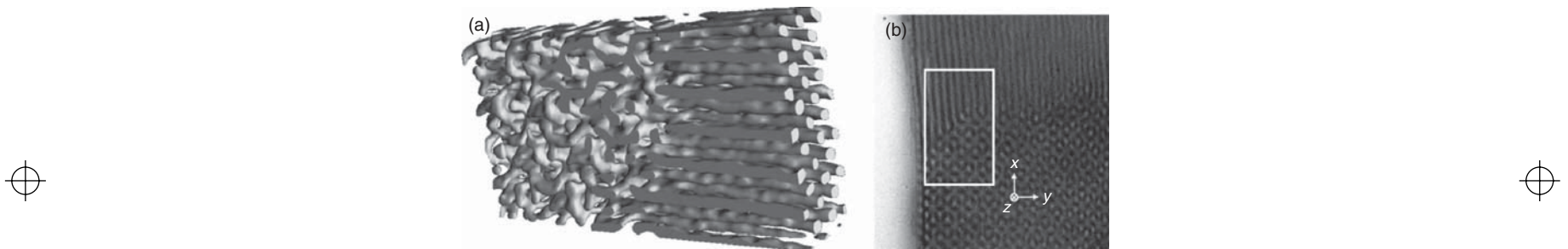


Figure 20.5 (a) 3D reconstructed image of coexisting DG and HEX phases in a SI block copolymer. Only the PS domain is shown. The dimensions of the hexahedron are $400 \text{ nm} \times 200 \text{ nm} \times 80 \text{ nm}$ (X, Y, Z). (b) TEM image of the sample region from which the 3D image was reconstructed (boxed area). Here, z is the direction of the incident electron beam and xz is the film plane. *Source:* Reprinted with permission from Park H-W, Jung J, Chang T, Matsunaga K, Jinnai H. New Epitaxial Phase Transition between DG and HEX in PS-*b*-PI. *J. Am. Chem. Soc.* 2009, 131, 46–47 [181]. Copyright 2009 American Chemical Society.

cross product $d_1 \times d_2$ gives a vector perpendicular to the polygon. Therefore, the unit normal vector is given by $n = d_1 \times d_2 / |d_1 \times d_2|$. Accordingly, given a surface that can be represented with a triangular mesh, the normal vector field is readily obtainable by performing the cross-product on each triangle in the mesh. Figure 20.5b shows the details of the normal vector field for a cocontinuous interface computed with the LCPM. Lopez-Barron and Macosko tested the LCPM with the gyroid surface, and found good agreement between the anisotropy computed with LCPM and that computed analytically as well as with the predictions from Doi–Ohta’s theory [192]. They also applied the method to measure the anisotropy evolution of a cocontinuous PS/SAN blend during uniaxial elongation and subsequent relaxation (Fig. 20.6) [150].

20.3.4 Summary

LSCM, X-ray μ -CT, and TEMT have been progressively evolved into mature techniques to visualize and quantify microstructures of polymer-related materials in three dimensions. These techniques currently allow the accurate evaluation of basic geometrical parameters (such as interfacial area per unit volume) and of more specific parameters (such as local curvatures and normal vector fields). Topology (network connectivity) is also important and achievable with 3D image analysis. Moreover, 3D microscopy is actively branching out into more sophisticated techniques such as four-dimensional microscopy, where a time sequence of x, y, z, t images is treated as a single object in the x, y, z, t space. Combination of 3D microscopy with other techniques (such as self-consistent field theory calculations

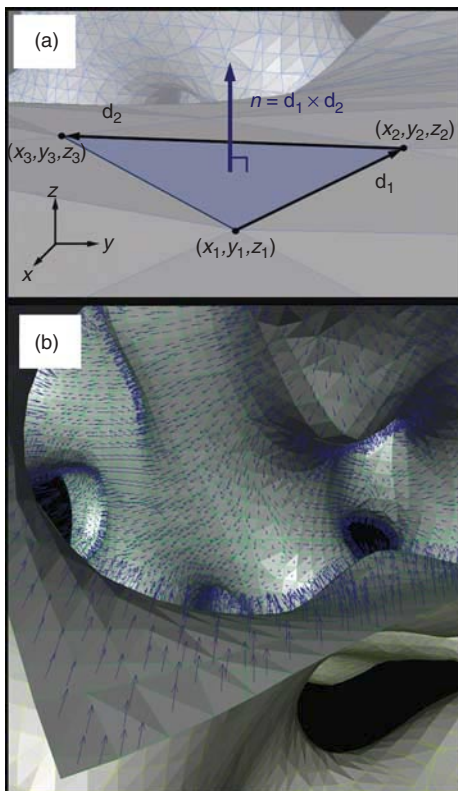


Figure 20.6 (a) Schematic of the computation of the vector normal to a triangle. (b) Detail of the normal vector field generated with the LCPM on a cocontinuous interface. *Source:* Reprinted with permission from López-Barrón CR, Macosko CW. Direct measurement of interface anisotropy of bicontinuous structures via 3D image analysis. *Langmuir* 2010;26 (17):14284–14293 [150]. Copyright 2010 American Chemical Society. (See insert for the color representation of the figure.)

[172] and neutron reflectometry [173]) has yielded basic understanding of block copolymer self-assembly from the molecular level or in confined geometries.

REFERENCES

1. Sawyer LC, Grubb DT, Meyers GF. *Polymer Microscopy*. Springer: New York; 2008.
2. Michler GH. *Electron Microscopy of Polymers*. Springer-Verlag Berlin Germany; 2008.
3. Bosco G. *Trend Anal Chem: TRAC* 2011;30:1189.
4. Drummy LF, Kübel C. *Polym Rev* 2010;50:231.
5. Buschow, K.H.J., Cahn, Robert, Flemings, Merton, Ilshner, Bernhard, Kramer, Edward, Mahajan, Subhash, Veyssiére, Patrick. *Encyclopedia of materials: Science and Technology*. Elsevier Sci. The Netherlands. 2001. p. 7654.
6. Michler GH. *Appl Spectrosc Rev* 1993;28:327.
7. Martin DC, Thomas EL. *Polymer* 1995;36:1743.
8. Kunz M, Shull K. *Polymer* 1993;34:2427.
9. Libera MR, Egerton RF. *Polym Rev* 2010;50:321.
10. Bar G, Tocha E, Garcia-Meinhardt E, Todd C, Blackson J. *J Macromol Symp* 2009;282:128.
11. Osten EF, Smith MS. *Microsc Microanal* 1998;4:814.
12. Loos J, Soury E, Lu K, de With G, Bavel SV. *Macromolecules* 2009;42:2581.
13. Berry VK. In: Gupta RK, Kennel E, Kim K-J, editors. *Polymer Nanocomposites Handbook*. CRC Press. FL, USA. Eds: R. K. Gupta, E. Kennel, K.-J. Kim. USA. 2010. p 309.
14. Zhang F, Liu J, Huang H, Du B, He T. *Eur Phys J E Soft Matter* 2002;8:289.
15. He L, Xu Q, Song R, Hua C. *Polym Compos* 2010;31:913.
16. Aprahamian I, Mendes P, Leung KC-F, Benitez D, Stoddart JF. The functionalization of polymers with gold nanoparticles using reversible supramolecular self-assembly processes. Abstracts of Papers In: 232nd ACS National Meeting; 2006 Sept 10–14; San Francisco (CA).
17. Brinkmann M, Rannou P. *Macromolecules* 2009;42:1125.
18. Tonomura A. *Electron Holography*. Springer; New York, USA. 1942.
19. Cowley JM. *Ultramicroscopy* 1992;41:335.
20. Gabor D. *Nature* 1948;161(4098):777–778.
21. Haine ME, Mulvey T. *J Opt Soc Am A* 1952;42. pp. 763–769.
22. Simon P, Lichte H, Wahl R, Mertig M, Pompe W. *BBA – Biomembranes* 2004;1663:178.
23. McCartney MR, Agarwal N, Chung S, Cullen DA, Han M-G, He K, Li L, Wang H, Zhou L, Smith DJ. *Ultramicroscopy* 2010;110:375.
24. Lichte H, Reibold M, Brand K, Lehmann M. *Ultramicroscopy* 2002;93:199.
25. Barton KE, Boettcher SH, Gaudiello JG, Kimball LJ, Wang YYF. US Patent. US Patent Number 7560692. 2008.
26. Chou T-M, Libera M, Gauthier M. *Polymer* 2003;44:3037.
27. Lawrence JR, O'Neill FT, Sheridan JT. *Optik – Int J Light Electron Opt* 2001;112:449.
28. García C, Fimia A, Pascual I. *Optik – Int J Light Electron Opt* 2002;113:111–116.
29. Götzhäuser A, Völkela B, Grunze M, Kreuzer HJ. *Micron* 2002;33:241.
30. Binh VT, Semet V, Garcia N. *Ultramicroscopy* 1995;58. p. 307.
31. Crozier PA, *In situ* nanoscale observation of polymer structures with electron microscopy. Abstracts of Papers In: 224th ACS National Meeting; 2002 Aug 18–22; Boston (MA).
32. Ertz D, Löhnus A, Löhnus R, Olin H. *Appl Phys A Mater Sci Process* 2001;72. pp. S71–S74.
33. Nafari A, Ghavanini FA, Bring M, Svensson K, Enoksson P. *J Micromech Microeng* 2007;17:2102.
34. Jiang N, Gao S, Wei XL, Liang XL, Chen Q. *J Phys Chem C* 2008;112:15631.
35. Nafari A, Karlen D, Rusu C, Svensson K, Olin H, Enoksson P. *J Microelectromech Syst* 2008;17. p. 328.
36. Golberg D, Costa PMFJ, Mitomea M, Bandoa Y. *J Mater Chem* 2009;19:909.

37. Golberg D, Costa PMFJ, Lourie O, Mitome M, Bai X, Kurashima K, Zhi C, Tang C, Bando Y. *Nano Lett* 2007;7:2146.
38. Lu Y, Huang JY, Chao Wang SSaJL. *Nat Nanotechnol* 2010;5. p. 218–224.
39. Nafari A, Angenete J, Svensson K, Sanz-Velasco A, Enoksson P. *J Micromech Microeng* 2010;20. pp. 064017.
40. Crozier PA, Oleshko VP, Westwood AD, Cantrell RD. *In situ* environmental transmission electron microscopy of gas phase Ziegler-Natta catalytic polymerization of propylene. Presented at Institute of Physics Conference Series; 2001.
41. Tatsuya K, Yoshiyuki A. Effect of long-chain branching on mechanical strength of polyethylenes. In: KEK Proceedings; 2002.
42. Bucknall CB. *J Microsc* 2001;201:221.
43. Garcia Gutierrez MC, Henning S, Michler GH. *J Macromol Sci Phys* 2003;B42:95.
44. Michler GH. *J Macromol Sci Phys* 2001;B40:277.
45. Michler GH, Bucknall CB. *Plast Rubber Compos* 2001;30:110.
46. Qian D, Dickey EC, Andrews R, Rantell T. *Appl Phys Lett* 2000;76:2868.
47. Qian D, Dickey EC. *J Microsc* 2001;204:39.
48. Kim GM, Michler GH, Poetschke P. *Polymer* 2005;46:7346.
49. Kim G-M, Lach R, Michler GH, Chang Y-W. *Macromol Rapid Commun* 2005;26:728.
50. Mitchell GR, Holt JJ, Thornley SA, Chai CK. X-ray and neutron scattering rheology: Crystallization from sheared melts. Abstracts of Papers. In: 222nd ACS National Meeting; 2001 Aug 26–30; Chicago (IL).
51. Castillo J, Dimaki M, Svendsen WE. *Integr Biol* 2009;1:30.
52. Stokes DJ, Morrissey F, Lich BH. *J Phys Conf Ser* 2005;26:50.
53. Yusof NLBM, Lim LY, Khor E. *Adv Chitin Sci* 2003;7:7.
54. Wei Z, Gourevich I, Field L, Coombs N, Kumacheva E. *Macromolecules* 2006;39:2441.
55. Tajima A, Higuchi T, Yabu H, Shimomura M. *Colloids Surf A Physicochem Eng Asp* 2008;313,314:332.
56. Higuchi T, Yabu H, Shimomura M. *J Nanosci Nanotechnol* 2007;7:856.
57. Zhou NC, Chan CD, Winey KI. *Macromolecules* 2008;41:6134.
58. Rueckert B, Kolb U. *Micron* 2005;36:247.
59. Faucheu J, Chazeau L, Gauthier C, Cavaille J-Y, Goikoetxea M, Minari R, Asua JM. *Langmuir* 2009;25:10251.
60. Gao C, Li W, Jin YZ, Kong H. *Nanotechnology* 2006;17:2882.
61. Vesely D, Ronca G. *J Microsc* 2001;201:137.
62. Madbouly SA, Otaigbe JU, Hassan MK, Mauritz KA. *PMSE Preprints* 2006;94:831.
63. Jeremic D, Cooper P, Brodersen PH. *Holzforschung* 2007;61(3):272.
64. Yokoyama N, Nonaka Y, Kurata T, Sakai S, Takahashi S, Kasemura T. *J Appl Polym Sci* 2007;104:1702.
65. Ding S-Y, Rumbles G, Jones M, Tucker MP, Nedeljkovic J, Simon MN, Wall JS, Himmel ME. *Macromol Mater Eng* 2004;289:622.
66. Xie S, Zhang S, Wang F, Yang M, Seguela R, Lefebvre J-M. *Compos Sci Technol* 2007;67:2334.
67. Taubert A, Wind JD, Paul DR, Koros WJ, Winey KI. *Polymer* 1881;2003:44.
68. Benetatos NM, Winey KI. *J Polym Sci B Polym Phys* 2005;43:3549.
69. Gai PL. *Microsc Microanal* 2002;8:21.
70. Bogner A, Thollet G, Basset D, Jouneau P-H, Gauthier C. *Ultramicroscopy* 2005;104:290.
71. Bogner A, Guimaraes A, Guimaraes RCO, Santos AM, Thollet G, Jouneau PH, Gauthier C. *Colloid Polym Sci* 2008;286:1049.
72. Vermogen A, Masenelli-Varlot K, Vigier G, Sixou B, Thollet G, Duchet-Rumeau J. *J Nanosci Nanotechnol* 2007;7:3160.
73. Barkay Z. *Appl Phys Lett* 2010;96:183109/1.
74. Tosaka M, Kamijo T, Tsuji M, Kohjiya S, Ogawa T, Isoda S, Kobayashi T. *Macromolecules* 2000;33:9666.
75. Pakstis LM, Ozbas B, Hales KD, Nowak AP, Deming TJ, Pochan D. *Biomacromolecules* 2004;5:312.
76. Sousa A, Schut J, Kohn J, Libera M. *Macromolecules* 2006;39:7306.
77. Wittemann A, Drechsler M, Talmon Y, Ballauff M. *J Am Chem Soc* 2005;127:9688.
78. Yakovlev S, Misra M, Shi S, Libera M. *J Microsc* 2009;236:174.
79. Sourty E, van Bavel S, Lu K, Guerra R, Bar G, Loos J. *Microsc Microanal* 2009;15:251.
80. Kangbo L, Erwan S, Joachim L. *J Electron Microsc* 2010;59:S39.
81. Schaper AK, Kurata H, Yoshioka T, Masaki T. *Microsc Microanal* 2007;13:336.
82. Lu K, Erwan S, Joachim L. *J Electron Microsc* 2010;59:S39.
83. Lu K, Sourty E, Guerra R, Bar G, Loos J. *Macromolecules* 2010;43:1444.
84. Huang HS, Chen CY, Lo SC, Lin CJ, Chen SJ, Lin LJ. *Appl Surf Sci* 2006;253:2685.
85. Tanem BS, Kvien I, van Helvoort ATJ, Oksman K. *ACS Sym Ser – Cell Nanocompos* 2006;938:48.
86. Vaughn JM, Gao X, Yacaman M-J, Johnston KP, Williams RO 3rd., *Eur J Pharm Biopharm* 2005;60:81.
87. Reyes-Reyes M, Lopez-Sandoval R, Arenas-Alatorre J, Garibay-Alonso R, Carroll DL, Lastras-Martinez A. *Thin Solid Films* 2007;516:52.
88. Kadavanich AV, Kippeny TC, Erwin MM, Pennycook SJ, Rosenthal SJ. *J Phys Chem B* 2001;105:361.
89. Kadavanich AV, Kippeny T, Erwin M, Rosenthal SJ, Pennycook SJ. Nanocrystal thickness information from Z-STEM: 3-D imaging in one shot. Presented at Materials Research Society Symposium Proceedings; 2001.
90. Sanchez SI, Small MW. *J.-m. G. Nuzzo. J Am Chem Soc* 2009;131:8683.

91. Martin DC, Drummy LF, Coufalova E. Mater Res Soc Sym Proc – Adv Biomater: Characterization, Tissue Eng Compl 2002;711:107.
92. Lednicky F, Coufalova E, Hromadkova J, Delong A, Kolarik V. Polymer 2000;41:4909.
93. Martin DC, Wu J, Shaw CM, King Z, Spanninga SA, Richardson-Burns S, Hendricks J, Yang J. Polym Rev 2010;50:340.
94. Lednicky F, Pientka Z, Hromadkova J. J Macromol Sci Phy 2003;B42:1039.
95. Lednicky F, Hromadkova J, Pientka Z. Polymer 2001;42:4329.
96. Hristov V, Krumova M, Michler G. Macromol Mater Eng 2006;291:677.
97. Yakovlev S, Libera M. Micron 2008;39:734.
98. Sousa A, Aitouchen A, Libera M. Ultramicroscopy 2006;106:130–145.
99. M. R. Libera, Imaging unstained polymer morphology using electron energy-loss spectroscopy. Abstracts of Papers. In: 224th ACS National Meeting; 2002 Aug 18–22; Boston (MA).
100. Siangchaew K, Libera M. Philos Mag A: Phys Condens Matter: Struct, Defects Mech Properties 2000;80:1001.
101. Francoise W, Genevieve V, Jaafar G, Patricia G, Jean-Claude P. Biology of the cell / under the auspices of the European Cell Biology Organization 2002;94:55.
102. Sung-Hee P, Seong-Geun O, Ji-Young M, Sung-Sik H. Colloids Surf B Biointerfaces 2005;44:117.
103. Sousa A, Sengonul M, Latour R, Kohn J, Matthew L. Langmuir 2006;22:6286.
104. Bockelmann U, Lunsdorf H, Szewzyk U. Environ Microbiol 2007;9:2137.
105. Arayasantiparb D, McKnight S, Libera M. J Adhes Sci Technol 2001;15:1463–1484.
106. Dehonor M, Masenelli-Varlot K, Gonzalez-Montiel A, Gauthier C, Cavaille J-Y, Terrones M. J Nanosci Nanotechnol 2007;7:3450.
107. Chiang LY, Anandakathir R, Hauck TS, Lee L, Canteenwala T, Padmawar PA, Pritzker K, Bruno FF, Samuelson LA. Nanoscale 2010;2:535.
108. Reznik B, Fotouhi M. Compos Sci Technol 2008;68:1131.
109. Rippel MM, Leite CAP, Galembeck F. Anal Chem 2002;74:2541.
110. Horiuchi S, Hamanaka T, Aoki T, Miyakawa T, Narita R, Wakabayashi H. J Electron Microsc 2003;52:255.
111. Shen Y, Gokhale A, Wei D, Dave R, Pfeffer R. Coating of ultra-fine particles using supercritical fluids. In: AIChE Spring National Meeting, Conference Proceedings; 2006 Apr 23–27; Orlando (FL).
112. Horiuchi S, Dohi H. Langmuir 2006;22:4607.
113. Chernev B, Belegratis MR, Ingolic E. Macromol Symp–Modern Polym Spectrosc 2008;265:272.
114. Dubois M, Dailly A, Ghanbaja J, Merlin A, Billaud D. Polymer 2002;44:801.
115. Linares EM, Leite CAP, Valadares LF, Silva CA, Rezende CA, Galembeck F. Anal Chem 2009;81:2317.
116. Ribbe AE. Recent Res Dev Macromol 2003;7:171.
117. Varlot K, Martin JM, Quet C. Polymer 2000;41:4599.
118. Fonseca VL, Fabio d C B, Aparecida d S C, Paula LCA, Fernando G. J Colloid Interface Sci 2007;309:140.
119. Linares EM, Rippel MM, Galembeck F. ACS Appl Mater Interfaces 2010;2:3648.
120. Chandra A, Turng L-S, Gopalan P, Rowell RM, Gong S. Compos Sci Technol 2008;68:768.
121. Horiuchi S, Yin D, Ougizawa T. Macromol Chem Phys 2005;206:725.
122. Trabelsi S, Janke A, Haessler R, Zafeiropoulos NE, Fornasieri G, Bocchini S, Rozes L, Stamm M, Gerard J-F, Sanchez C. Macromolecules 2005;38:6068.
123. Horiuchi S, Hanada T, Ebisawa M, Yasuhiro M, Kobayashi M, Takahara A. ACS Nano 2009;3:1297.
124. Rubino S, Razaq A, Nyholm L, Stromme M, Leifer K, Mihranyan A. J Phys Chem B 2010;114:13644.
125. Gomez ED, Panday A, Feng EH, Chen V, Stone GM, Minor AM, Kisielowski C, Downing KH, Borodin O, Smith GD. Nano Lett 2009;9:1212.
126. López-Barrón CR, Macosko CW. J Microsc 2010;242:242.
127. Miles RE. J Microsc 1981;121:21–27.
128. Russ JC. *Practical Stereology*. New York: Plenum Press; 1986.
129. Howard V, Reed MG. *Unbiased Stereology: Three-Dimensional Measurement in Microscopy*. Oxford, New York: Scientific Publishers/Springer; 1998.
130. Underwood EE. *Quantitative Stereology*. Reading (MA): Addison-Wesley Pub. Co; 1970.
131. Exner HE. Image Anal Stereol 2004;23:73–82.
132. Jinnai H, Spontak RJ, Nishi T. Macromolecules 2010;43:1675.
133. Jinnai H, Spontak RJ. Polymer 2009;50:1067–1087.
134. Jinnai H, Nishikawa Y, Ikebara T, Nishi T. Adv Polym Sci 2004;170:115–167.
135. Russ JC. *The Image Processing Handbook*. CRC Press; 2007. Boca Raton, FL.
136. Lorensen WE, Cline HE. SIGGRAPH Comput Graph 1987;21:163–169.
137. Alkemper J, Voorhees PW. J Microsc 2001;201:388–384.
138. Alkemper J, Voorhees PW. Acta Mater 2001;49:897–902.
139. Wilson JR, Kobsiriphat W, Mendoza R, Chen H, Hiller JM, Miller DJ, Thornton K, Voorhees PW, Adler SB, Barnett SA. Nat Mater 2006;5:541.
140. Sheppard C, Shotton D. *Confocal Laser Scanning Microscopy*. Oxford, New York: Springer; 1997.
141. Inoue S. In: Pawley JB, editor. *Handbook of Biological Confocal Microscopy*. New York: Springer; 2006.
142. Verhoogt H, Van Dam J, Posthuma de Boer A, Draaijer A, Houpt PM. Polymer 1993:34.
143. Jinnai H, Nishikawa Y, Hashimoto T. Phys Rev E 1999;59:R2554.
144. Nishikawa Y, Koga T, Hashimoto T, Jinnai H. Langmuir 2001;17:3254.

145. Jinnai H, Nishikawa Y, Koga T, Hashimoto T. *Macromolecules* 1995;28:4782.
146. Jinnai H, Koga T, Nishikawa Y, Hashimoto T, Hyde ST. *Phys Rev Lett* 1997;78:2248–2251.
147. Lopez-Barron CR, Macosko CW. *Macromol Symp* 2009;283–284:348.
148. Lopez-Barron C, Macosko CW. *Langmuir* 2009;25:9392.
149. López-Barrón C, Macosko CW. *Soft Matter* 2010;6:2637.
150. López-Barrón CR, Macosko CW. *Langmuir* 2010;26:14284.
151. Montminy MD, Tannenbaum AR, Macosko CW. *J Colloid Interface Sci* 2004;280:202.
152. B. E. Pangerle, N. P. Hammer, M. L. Bidault, R. E. Listemann, R. E. Stevens, X. D. Zhang, C. W. Macosko, In: Proc. Soc. Plast. Ind. Polyurethanes; 1998; Dallas (TX).
153. Donath T, Beckmann F, Heijkants RGJC, Brunke O, Schreyer A. Proc SPIE Int Soc Opt Eng 2004;5535:775.
154. Conner WC, Webb SW, Spanne P, Jones KW. *Macromolecules* 1990;23:4742.
155. Schilling PJ, Karedla BR, Tatiparthi AK, Verges MA, Herrington PD. *Compos Sci Technol* 2005;65:2071–2078.
156. Schell JSU, Renggli M, van Lenthe GH, Müller R, Ermanni P. *Compos Sci Technol* 2006;66:2016.
157. Elmoutauakkil A, Fuchs G, Bergounhon P, Peres R, Peyrin F. *J Phys D: Appl Phys* 2003;36:A37.
158. Weiss P, Obadia L, Magne D, Bourges X, Rau C, Weitkamp T, Khairoun I, Bouler JM, Chappard D, Gauthier O, Daculsi G. *Biomaterials* 2003;24:4591.
159. Pyun A, Bell JR, Won KH, Weon BM, Seol SK, Je JH, Macosko CW. *Macromolecules* 2007;40:2029.
160. Hoppe W, Langer R, Knesch G, Poppe C. *Naturwissenschaften* 1968;55:333.
161. De Rosier DJ, Klug A. *Nature* 1968;217:130.
162. Hart RG. *Science* 1968;159:1464.
163. Bates RHT, McDonnell MJ. *Image Restoration and Reconstruction*. Oxford, Oxfordshire; New York: Oxford University Press; 1986.
164. Spontak RJ, Williams MC, Agard DA. *Polymer* 1988;29:387.
165. Spontak RJ, Fung JC, Braunfeld MB, Sedat JW, Agard DA, Kane L, Smith SD, Satkowski MM, Ashraf A, Hajduk DA, Gruner SM. *Macromolecules* 1996;29:4494.
166. Laurer JH, Hajduk DA, Fung JC, Sedat JW, Smith SD, Gruner SM, Agard DA, Spontak RJ. *Macromolecules* 1997;30:3938.
167. Radzilowski LH, Carragher BO, Stupp SI. *Macromolecules* 1997;30:2110.
168. Jinnai H, Nishikawa Y, Spontak RJ, Smith SD, Agard DA, Hashimoto T. *Phys Rev Lett* 2000;84:518.
169. Yamauchi K, Takahashi K, Hasegawa H, Iatrou H, Hadjichristidis N, Kaneko T, Nishikawa Y, Jinnai H, Matsui T, Nishioka H, Shimizu M, Furukawa H. *Macromolecules* 2003;36:6962.
170. Wilder EA, Braunfeld MB, Jinnai H, Hall CK, Agard DA, Spontak RJ. *J Phys Chem B* 2003;107:11633.
171. Dobriyal P, Xiang H, Kazuyuki M, Chen J, Jinnai H, Russell TP. *Macromolecules* 2009;42:9082.
172. Morita H, Kawakatsu T, Doi M, Nishi T, Jinnai H. *Macromolecules* 2008;41:4845.
173. Niihara K, Matsuwaki U, Torikai N, Atarashi H, Tanaka K, Jinnai HA. *Macromolecules* 2007;40:6940.
174. Nishioka H, Niihara K, Kaneko T, Yamanaka J, Nishikawa Y, Inoue T, Nishi T, Jinnai H. *Compos Interface* 2006;13:589.
175. Zhao Y, Thorkelsson K, Mastrianni AJ, Schilling T, Luther JM, Rancatore BJ, Matsunaga K, Jinnai H, Wu Y, Poulsen D, Frechet JMJ, Paul Alivisatos A, Xu T. *Nat Mater* 2009;8:979.
176. Jinnai H, Shinburi Y, Kitaoka T, Akutagawa K, Mashita N, Nishi T. *Macromolecules* 2007;40:6758.
177. Kawase N, Kato M, Nishioka H, Jinnai H. *Ultramicroscopy* 2007;107:8.
178. Shefelbine TA, Vigild ME, Matsen MW, Hajduk DA, Hillmyer MA, Cussler EL, Bates FS. *J Am Chem Soc* 1999;121.
179. Thomas EL, Alward DB, Kinning DJ, Martin DC, Handlin DL, Fetters LJ. *Macromolecules* 1986;19:2197.
180. Hajduk DA, Harper PE, Gruner SM, Honeker CC, Thomas EL, Fetters LJA. *Macromolecules* 1995;28:2570.
181. Park H-W, Jung J, Chang T, Matsunaga K, Jinnai H. *J Am Chem Soc* 2009;131:46.
182. Jung J, Park H, Lee S, Lee H, Chang T, Matsunaga K, Jinnai H. *ACS Nano* 2010;4:3109.
183. Chen C, Hsueh H, Chiang Y, Ho R, Akasaka S, Hasegawa H. *Macromolecules* 2010;43:8637.
184. Helfrich W. *Z Naturforsch C Biosci* 1973;28:693.
185. Scholten E, Sagis LMC, van der Linden E. *J Phys Chem B* 2004;108:12164.
186. Gray A, Abbena E, Salamon S. *Modern Differential Geometry of Curves and Surfaces with Mathematica*. Boca Raton: Chapman & Hall, CRC; 2006.
187. Nishikawa Y, Jinnai H, Koga T, Hashimoto T, Hyde ST. *Langmuir* 1998;14:1242.
188. Sander PT, Zucker SW, Tracing surfaces for surfacing traces. In: Proceedings of the 1st International Conference on Computer Vision; 1987; London.
189. Jinnai H, Kajihara T, Watashiba H, Nishikawa Y, Spontak RJ. *Phys Rev E* 2001;64:010803.
190. Jinnai H, Kajihara T, Watashiba H, Nishikawa Y, Spontak RJ. *Phys Rev E* 2001;64:069903/1.
191. Jinnai H, Watashiba H, Kajihara T, Takahashi M. *J Chem Phys* 2003;119:7554.
192. Doi M, Ohta T. *J Chem Phys* 1991;95:1242.
193. Vinckier I, Mewis J, Moldenaers P. *Rheol Acta* 1997;36:513.
194. Wetzel ED, Tucker CL III, *Int J Multiphase Flow* 1999;25:35.
195. Almusallam AS, Larson RG, Solomon MJ. *J Nonnewton Fluid Mech* 2003;113:29.

21

STRUCTURE AND MECHANICAL PROPERTIES OF POLYMERS

MANUEL AGUILAR-VEGA

21.1 STRUCTURE OF POLYMER CHAINS

A good reason for the widespread use of polymeric materials is that they present physical and chemical properties that are well tuned for different applications at a cost that is quite reasonable. Polymers, as a group of materials, present a wide range of properties, perhaps the largest of all known materials, since they can be found in the form of liquids, soft viscoelastic (rubbery) materials, or rigid solids. The wide variety of properties found in polymers are the result of their macromolecular structure since, by definition, they are molecules resulting from the covalent bonding of at least hundreds and up to thousands or millions of basic units. Properties of polymers, as in the case of any chemical compound, are highly dependent on the structure of the polymer chains and the molecular weight resulting from the number of units covalently bonded. Polymer chemical structure affects polymer properties due to the nature of the repeating units that form the macromolecule, the branching and number or crosslinks, as well as differences in the order of the macromolecular units in the case of copolymers (see also Chapter 6). The molecular weight and the molecular weight distribution determine the molecular size and give a description of the distribution of the different molecular sizes in a polymer [1, 2]. The behavior of polymers in terms of processing depends on the number-average molecular weight, M_n , and on the shape of the molecular weight distribution, measured by the molecular weight dispersity (D). Mechanical properties such as tensile strength are limited by short macromolecules, while long chains control the melt flow and elasticity of the

processed polymer. Figure 21.1 shows the graph of a typical molecular weight distribution with the four main molecular weight averages commonly determined in a polymer.

For a precise definition of the molecular weight averages shown in Figure 21.1, see Section 1.5.1.

D is calculated as the ratio of M_w/M_n ; a value of 1 indicates that the polymer is monodisperse. Depending on the synthetic route, D can be as large as 2 in step-growth polymers and as narrow as 1 for anionic polymerization [3]. When branching is present, the value can be much larger (up to 20 or more).

Mechanical properties such as strength under tension are related to M_n , while the melt viscosity is determined by M_w . M_z is related to the viscoelastic properties or melt elasticity during processing.

It is well known that the interactions between atoms in a chemical molecule with neighboring molecules of the same or different type determine its macroscopic properties. Other physical properties are dependent on short- and long-range interactions between the atoms that constitute the molecule with other neighboring molecules. Thus, physical properties such as density, volume, and boiling or freezing points are the result of the interactive forces between molecules. On the other hand, the interactions with other chemical molecules, which have also been studied by thermodynamics, give rise to the determination of other parameters, for example, the solubility parameters, that measure the interaction energy between molecules. The interactions between different chemical molecules of low molecular weight (nonpolymers) and their properties have been estimated, and equations that relate them

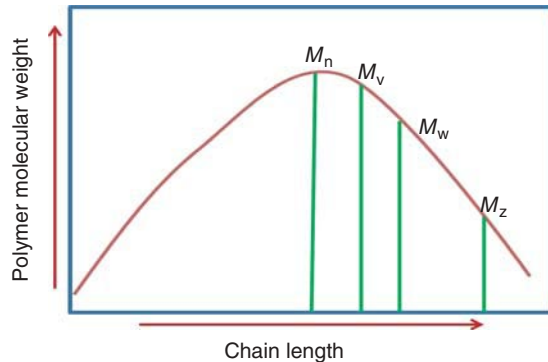


Figure 21.1 Polymer molecular weight distribution with the most common average molecular weights.

have been already developed; these properties and correlations to estimate them have been tabulated to a large extent [4].

In the specific case of polymers, the chemical structure is also quite important, since the atoms present in the polymer chain determine, as in low molecular weight structures, the interactions with other molecules; however, as polymers are synthesized from covalently bonded molecules that are repeated hundreds to thousands of times, their physical properties are different, since they do not depend on the properties of the short-range interactions of a few atoms as in simple, small molecules. Structural features, such as polymer morphology, are also affected by the configuration of the chains due to the stereoregularity in the pendant groups or in the double-bond position. Natta [5] realized the importance of tacticity and developed the nomenclature for polyolefins, for example, polypropylene, which reflects that, depending on the position of the pendant CH_3 group along the chain, polypropylene could be isotactic, syndiotactic, or atactic, as described in Figure 21.2.

Polymer stereoregularity is important since the morphology of the macromolecule depends on crystallization and the degree of crystallinity determines, in the end, several physical properties such as density, mechanical properties, as well as thermal properties. Atactic polymers have difficulties in crystallizing; they are amorphous or show a low degree of crystallinity, while the degree of crystallinity in isotactic and syndiotactic polymers is high.

The determination of the physical and chemical interaction properties of a polymer, or even better, their prediction from the simple knowledge of the polymer structure has been successfully achieved using the concept of molar additivity of the groups forming the polymer molecule by the so-called group contribution methods. These are extensively treated in the book by Van Krevelen and Nijsenhuys [6], where the prediction of physical properties such as density, T_g and other physical transitions, heat

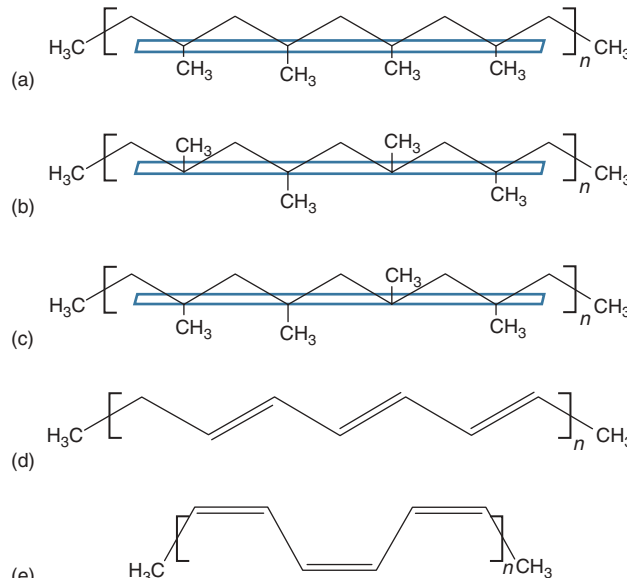


Figure 21.2 PP configurations involving pendant group position: (a) isotactic; (b) syndiotactic; (c) atactic, the dark gray line is a reference plane for symmetry distribution of atoms in the chain, and configurations of double bond in dienes; (d) 1,4-*trans*, and (e) 1,4-*cis*.

capacities, solubility parameters, optical properties, magnetic, acoustic, transport, and mechanical properties among others can be found. Another approach that has been successful for the prediction of the polymer properties starting from the knowledge of their molecular structure, is the topological index approach developed by Bicerano and coworkers, which uses a connectivity index and is the basis for commercial simulation packages that predict polymer properties [7].

21.2 MECHANICAL PROPERTIES OF POLYMERS

Depending on the final polymer application, mechanical properties are considered to be the most important in everyday use where the polymer product is subjected to all kinds of external forces such as pressure, tension, vibration, or traction. The large number of polymers available allows a wide spectrum of mechanical properties to choose from, including very soft liquid-like, elastic or rigid materials.

Mechanical properties, as in the case of other properties, can be organized in terms of their relationship to polymer structure, depending on the functional groups present in the polymer backbone and the side groups from the main chain. Other factors that affect the mechanical properties of a polymer, besides its chemical composition, are molecular weight and molecular weight distribution,

degree of branching in addition polymers, and degree of crosslinking in thermoset polymers. The mechanical properties of a polymer will also be affected by the ability of the polymer to crystallize and the size and distribution of the crystals in the bulk of the polymer (morphology), which, together with molecular orientation, has a strong influence on its mechanical properties.

It is also possible to manipulate the structure by introducing other monomers into the polymer chain, changing the mechanical properties of the final material by copolymerization. It is also common, for economic reasons or to increase mechanical properties, to add particulate solids to the polymer, such as wood flour or other additives, that will affect the final mechanical properties. Another common approach is the preparation of blends of two different polymers, which are commonly nonsoluble in each other, as a strategy to increase some mechanical properties such as impact strength, as in the well-studied case of nylon toughening by butyl rubber [8, 9].

External factors that will influence polymer mechanical properties are temperature or thermal treatment, temperature history, large differences in pressure, and environmental factors such as humidity, solar radiation, or other types of radiation. The mechanical properties of polymer are also sensitive to the methods and variables used for testing, such as strain deformation as well as the rate at which the strain is performed. Finally, the mechanical behavior of polymeric materials and the values of their mechanical properties will be sensitive to the kind of strain that is imposed by the applied force, namely, tension, compression, biaxial, or shear.

Polymers are also unique in their viscoelastic nature, a behavior that is situated between that of a pure elastic solid and that of a pure viscous liquid-like material; their mechanical properties present a strong dependence on time and temperature. Given all the factors that have to be taken into account to determine the mechanical properties of polymers, their measurement would appear to be very complex. However, there is a series of general principles that determine the different mechanical properties and that give a general idea of the expected results in different mechanical tests. These principles can be organized in a systematic manner to determine the interrelation of polymer structure and the observed mechanical properties, using equations and characteristic parameters of polymeric materials.

In the following section, the role of some of these structural and external factors on the mechanical properties of polymers is discussed. Figure 21.3 shows an example of the most common methods used to apply an external force to a polymeric material.

In general, the elastic or Young's modulus M , a characteristic property of a material, is a measure of the

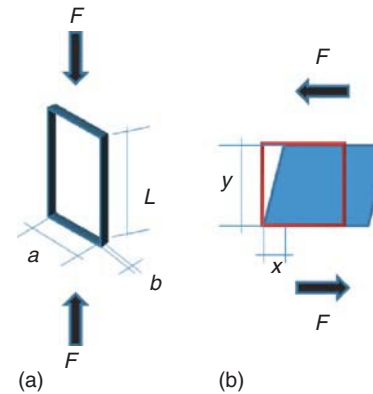


Figure 21.3 Common force fields for applied forces in a material (a) tension and (b) shear. (See insert for the color representation of the figure.)

resistance to strain (ε) of a material under an external force F . It is defined by the following expression:

$$\sigma = M\varepsilon \quad (21.1)$$

where M stands for modulus and σ is the stress or force applied per unit area (F/A) of the material. There are three types of moduli: elastic or Young's modulus, E ; shear modulus, G ; and bulk modulus, K . If a material is isotropic, as in the case of amorphous polymers, it is only needed to know two moduli to describe the elastic behavior of the material. The moduli are related by

$$E = \frac{9GK}{3K + G} \quad (21.2)$$

The relationship between moduli can be also calculated using Poisson's ratio, $\nu = \varepsilon_T/\varepsilon_L$ (where ε_T and ε_L are transverse and axial strains, respectively), which measures contraction in a material subject to tension, in order to compensate for the strain:

$$E = 2G(1 + \nu) = 3K(1 - 2\nu) \quad (21.3)$$

For elastic solids $\nu = 0.5$, while for glassy polymers $0.3 < \nu < 0.44$

If the materials are anisotropic, they will present different properties in the different directions. Examples of these polymeric materials are polymer fibers, such as polyethylene terephthalate, PET, nylon fibers, injection-molded polymers, fiber-reinforced composites with a polymeric matrix, and crystalline polymers where the crystalline phase is not randomly oriented. A typical method for measuring the modulus in tension is the stress-strain test, in which the modulus corresponds to the initial slope of the stress-strain curve. Figure 21.4 shows typical stress-strain curves for different types of polymeric materials.

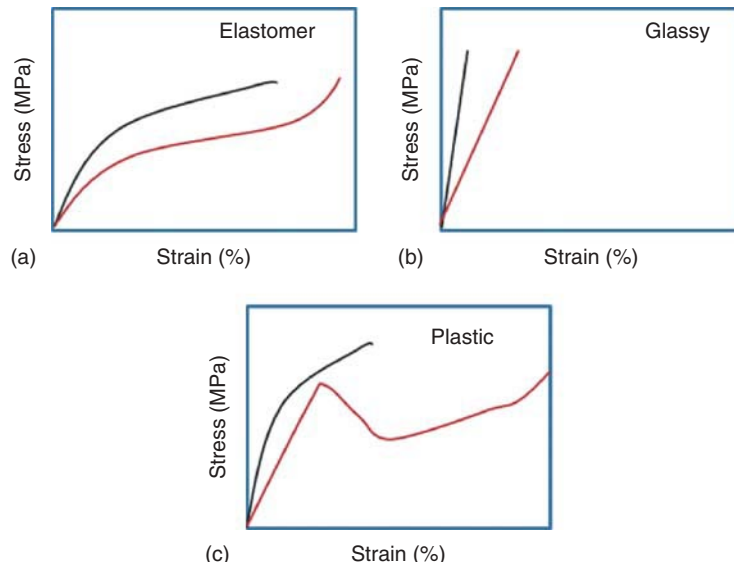


Figure 21.4 Typical stress-strain curves for different types of polymers: (a) elastomer, (b) glassy, and (c) plastic. (See insert for the color representation of the figure.)

From these experimental curves, it is possible to determine the modulus as

$$E = \left(\frac{d\sigma}{d\varepsilon} \right)_{\varepsilon \rightarrow 0} = \left(\frac{F/A}{(L - L_0)/L_0} \right)_{L \rightarrow L_0} \quad (21.4)$$

which involves the definition of stress as $\sigma = F/A$ and simple strain as $= (L - L_0)/L_0$ where L is the length of the specimen after the stress has been applied and L_0 is its original length. Values of modulus for shear or compression experiments can also be calculated using their stress-strain curves.

21.2.1 Molecular Structure and Mechanical Properties

There are a large number of tests to determine mechanical properties of polymers as well as instruments to perform them. A large number of these tests are already standardized by the American Society for Testing and Materials, ASTM. From the point of view of their structure, the large majority of polymers are either completely amorphous or partially crystalline. This implies that a polymer can be mechanically rigid below certain temperature, the glass-transition temperature, T_g . Above T_g , at moderate strain rates, amorphous polymers are soft and flexible and their physical appearance is that of an elastomer or a liquid-like viscous material. In the region where the glass transition occurs, polymers show a drastic change in their mechanical behavior. Their elastic modulus E or shear modulus G , at tension or shear, respectively, diminishes by a factor of 10^3 as it goes across T_g . For this reason, the T_g of polymer can

be considered the most important characteristic transition in terms of its mechanical properties. Other properties that change drastically in the glass-transition range are the thermal expansion coefficient α , refractive index n , heat capacity at constant pressure C_p , as well as some electrical properties, and, as the modulus changes, the strain ε for measurements under shear and the ultimate strength σ_u also change drastically in the glass-transition region.

In general, considering the T_g value of a polymeric material, and taking into account that most polymers are used at room temperature, it is possible to roughly classify the mechanical behavior of a polymer according to its glass-transition temperature, T_g . Thus, rubbers and elastomers have T_g values below room temperature, while for brittle and rigid polymers, T_g is above room temperature. Polymer T_g can span a large interval of temperatures, from -110°C for polyethylene to temperatures above 300°C for aromatic polyamides and thermoset resins. The value of T_g also depends on the timescale of the mechanical tests and its value can vary depending on factors such as the heating rate or frequency used for the test in dynamic mechanical analysis (DMA) measurements.

Since T_g depends on the structure of the polymer, it is possible to identify three factors that affect T_g . First, the rigidity or flexibility of the polymer chain; it is known that the presence of aliphatic $-\text{CH}_2-\text{CH}_2-$, ether, $-\text{CH}_2-\text{CH}_2-\text{O}-$, or siloxane chains with methyl substitutions, such as dimethyl siloxane, $-\text{Si}(\text{CH}_3)_2-\text{O}-$, comprises flexible polymer chains that decrease T_g . It is also known that the length of lateral aliphatic groups also diminishes T_g as in the case of the methacrylic polymers (see Table 21.1) [10].

TABLE 21.1 Glass-Transition Temperature, T_g , of Methacrylate Polymers

Acrylic Polymer	T_g (°C)
<chem>CC(=O)C(C)C</chem> MMA	105
<chem>CC(=O)C(CC)C</chem> Ethyl MA	65
<chem>CC(=O)C(CC)CC</chem> Propyl-MA	21
<chem>CC(=O)C(CC)CCC</chem> Butyl-MA	-5
<chem>CC(=O)C(CC)CCCC</chem> Hexyl-MA	-20
<chem>CC(=O)C(CC)CCCCC</chem> Octyl-MA	-65
<chem>CC(=O)C(CC)CCCCCCCC</chem> Decyl-MA	

Second, T_g is also affected by the polarity of the polymer chain moieties. As a general rule, as the polarity increases, T_g increases (Table 21.2) [10].

T_g also increases with molecular weight, M_n , until it reaches a limiting value, T_g^o for $M_n \rightarrow \infty$. The change in T_g due to the increase in molecular weight can be approximated using the following equation:

$$T_g = T_g^o - \frac{K}{M_n} \quad (21.5)$$

where K is a characteristic constant for each polymer [11].

T_g can also be affected by the degree of crosslinking, an increase of which is equivalent to an increase in the polymer molecular weight toward infinity. This is due

TABLE 21.2 Effect of Polymer Polarity on T_g

Polymer Repeating Unit	T_g (°C)
<chem>CC</chem> PP	-10
<chem>CCCl</chem> PVC	85
<chem>CC#N</chem> PAN	101

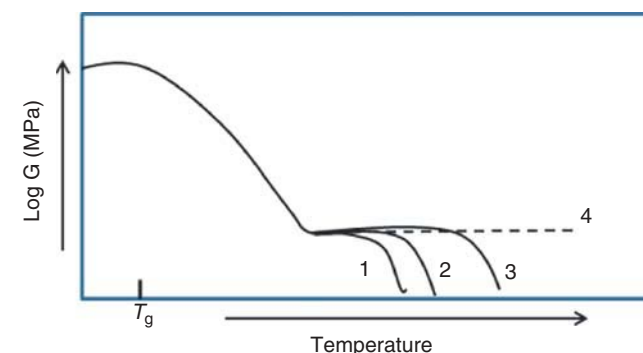


Figure 21.5 Schematic representation of shear modulus behavior as a function of temperature for a polymer with (1) low M_n , (2) medium M_n , (3) high M_n , and (4) a crosslinked polymer.

to an increased restriction in polymer chain mobility. An empirical equation derived by Nielsen from reported experimental data allows the calculation of T_g as function of the degree of crosslinking as follows:

$$T_g = T_g^o + \frac{3.9 \times 10^4}{M_c} \quad (21.6)$$

where T_g^o is the T_g of the non-crosslinked polymer and M_c is the molecular weight between crosslink points. This equation allows the estimation of T_g of the polymer due to structural variations. A schematic representation of changes in the shear modulus, G , due to the effect of increasing molecular weight in the polymer or crosslinking is depicted in Figure 21.5.

21.2.2 Viscoelastic Properties and Temperature

One of the main characteristics of polymers is that polymer chains can rearrange when they are subjected to an induced stress and the strain will not be constant, but it will increase with time due to the high molecular weight and the large number of entanglements between chains. If the strain is removed, then the polymer will slowly recover its original shape if the strain was small enough. This is due to a slow

recovery of the original shape of the long entangled molecular chains that make up the polymer bulk. Furthermore, polymers show viscoelastic behavior at all temperatures, because they are not perfect elastic solids or perfect liquid-like viscous materials. A difference with respect to metals is that polymers show a dependence of mechanical properties with time at small and large strains. If a polymer sample is suddenly subjected to a given stress, σ , in tension, the strain will increase with time, $\varepsilon(t)$; if after certain time the sample is allowed to recover toward its original shape, a recovery curve can be obtained that implies a dynamic value $1/(E(t)) = D(t) = \varepsilon(t)/\sigma$, where $D(t)$ is sometimes called the *compliance of the polymer*, a quantity that measures its ability to recover its original shape.

Another test that shows the viscoelastic behavior of a polymeric material is the stress relaxation test, in which a sudden strain is imposed on the polymer sample at $t = 0$, and the stress, σ , required to maintain the strain is recorded as a function of time. As time increases, the stress, $\sigma(t)$, necessary to maintain the constant strain, ε , decreases due to relaxation of the entangled polymer chains that try to reach an equilibrium conformation. If the strain is released at short times, the sample will recover its original shape; on the other hand, long relaxation times will produce permanent deformation on the sample. If the stress, which is a function of time, is divided by the strain, a modulus value as a function of time can be defined:

$$E(t) = \frac{\sigma(t)}{\varepsilon} \quad (21.7)$$

Although these simple experiments show the viscoelastic nature of polymers due to the large number of polymer molecules with different lengths, a more quantitative expression has been suggested by Maxwell, considering the system as a combination of a spring, a pure elastic element, and a dashpot, a purely viscous element, as represented in Figure 21.6:

$$\sigma_1 = E\varepsilon_1 \quad (21.8)$$

$$\sigma_2 = \eta \frac{d\varepsilon_2}{dt} \quad (21.9)$$

In the Maxwell simple combination of mechanical elements, the stress σ and the strain ε are measured using subscript 1 for the spring element and subscript 2 for the viscous dashpot element. Given the way in which the stress is applied to the whole element, the stress on each element is the same, while the strain in each element is different:

$$\sigma = \sigma_1 = \sigma_2 \text{ and } \varepsilon = \varepsilon_1 = \varepsilon_2$$

Using these facts,

$$\frac{d\varepsilon}{dt} = \frac{\sigma}{\eta} + \frac{1}{E} \frac{d\sigma}{dt} \quad (21.10)$$

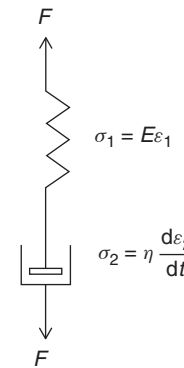


Figure 21.6 Maxwell's simple mechanical element combination of the spring and a dashpot in series as a representation of the viscoelastic behavior of a polymer.

Equation (21.10) is the general equation for the Maxwell mechanical model analogy for viscoelastic behavior.

If the creep experiment described before is performed on the basis of this model, with a constant stress applied to the Maxwell mechanical element, the strain will be function of time, as indicated in Equation (21.11).

$$\varepsilon(t) = \varepsilon_0 \left(\frac{t}{\eta} + \frac{1}{E} \right) \quad (21.11)$$

Sometimes it is desirable to express the strain as the compliance $J(t)$:

$$J(t) = \frac{\varepsilon(t)}{\sigma_0} = \frac{t}{\eta} + \frac{1}{E} \quad (21.12)$$

The response of the model indicates that as the stress is removed, the spring immediately recovers the deformation, but the dashpot deformation is permanent or recovers very slowly. This behavior is frequently seen in polymers subjected to a sudden and permanent stress that is later removed.

In the case of a stress relaxation experiment using the Maxwell mechanical model, if an initial strain ε_0 is imposed and the change in the stress is followed as a function of time, the resulting expression is as follows:

$$\sigma(t) = \sigma_0 e^{-Et/\eta} \quad (21.13)$$

where η/E is the relaxation time, λ , which is a measure of the rate at which the stress decays in the polymer sample.

It is also common that polymers are subjected to forces, or stresses, such as mechanical vibration; in that case, the strain will also be sinusoidal in the same frequency but not in the same phase. In that sense, it is possible to model the responses to a periodic strain using the Maxwell mechanical model analogy. The response to an applied sinusoidal strain

as a function of time is $\varepsilon = \varepsilon_m \sin \omega t$ and, using the values of E and $\lambda = \eta/E$, is the expression for the stress, is given by:

$$\sigma = \varepsilon_m E \frac{\omega \lambda}{(1 + \omega^2 \lambda^2)^{1/2}} \sin(\omega t + \delta) \quad (21.14)$$

The stress is proportional to the modulus E , and will be ahead of the strain by an angle $\delta = \cot^{-1} \omega \lambda$.

These equations are often used in terms of complex variables such as the complex dynamic modulus, $E^* = E' + iE''$, where E' is called the *storage modulus* and is related to the amount of energy stored by the viscoelastic sample. E'' is termed the *loss modulus*, which is a measure of the energy dissipated because of the internal friction of the polymer chains, commonly as heat due to the sinusoidal stress or strain applied to the material. The ratio between E'/E'' is called $\tan \delta$ and is a measure of the damping of the material. The Maxwell mechanical model provides a useful representation of the expected behavior of a polymer; however, because of the large distribution of molecular weights in the polymer chains, it is necessary to combine several Maxwell elements in parallel to obtain a representation that better approximates the true polymer viscoelastic behavior. Thus, the combination of Maxwell elements in parallel at a fixed strain will produce a time-dependent stress that is the sum of all the elements:

$$\sigma(t) = \sum \sigma_i = \varepsilon \sum E_i e^{-t/\lambda} \quad (21.15)$$

The modulus as a function of time, $E(t)$, for the parallel arrangement of elements will be given as

$$E(t) = \frac{\sigma(t)}{\varepsilon} = \sum E_i e^{-t/\lambda_i} \quad (21.16)$$

This model indicates that the modulus of the polymer is the result of the individual moduli of each element, E_i , and the stress depends on the relaxation times, λ_i , of each element. This equation is a better approximation to the behavior of polymers. To model the viscoelastic behavior of polymers, other models have been proposed, such as the Kelvin model [12].

21.3 MECHANICAL PROPERTIES OF POLYMER COMPOSITES

Polymer composites have received widespread attention due to the large combination of materials and properties that are possible using the wide variety of different polymers and loads available. There is a large variety of composite materials that can be obtained by the combination of a polymer, usually as a matrix material, and some type of "loading." The loading can be very elaborate, such as a mat

of continuous carbon fibers with a geometry that takes into account all the possible angles to reinforce an epoxy resin matrix. This can be used in high performance applications, such as aircraft critical parts, due to its low weight and high tensile and load resistance, or in race car bodies or brakes where protection or temperature performance is critical. Other similar materials for not so critical performance are continuous glass-fiber-reinforced polyester resins, which are used in boats and more common molded products.

These long-fiber-reinforced materials present mechanical properties that can be tailored by orientation of the fibers in the desired directions. The preparation and properties of these materials has been studied by several authors [11, 13–15].

A more common and widely used process involves the preparation of short-fiber polymer composite materials and particulate composite polymeric materials, where the fibers or particles act as reinforcement of the polymer. In this particular case, when a polymer matrix is filled with fibers or particles, which in general possess higher mechanical properties than the polymer matrix, the resultant composite material presents properties that are between those of the soft polymer matrix and the rigid filler.

For polymer composites filled with small particles, either micro- or nanoparticles, mechanical properties have been extensively studied because of their versatility and importance [16–20]. The elastic modulus of polymer composite materials with particles that present an aspect ratio about 1 (spherical or near-spherical particles) improves with the use of inorganic particles that have large moduli and strength compared to the polymer matrix. To improve stress transfer between the matrix and the polymer, it is also important to increase the interfacial adhesion between the polymer and the particles. The bonding between different particles and the polymer is often obtained by the use of a coupling agent that improves the interaction within the particles and the polymer matrix. The concentration of particles in the polymer matrix is also important since they impart increased rigidity (elastic modulus) to the composite, as the concentration, usually expressed as a volume fraction, ϕ_p , increases in the polymer matrix. Several empirical and semiempirical equations have been proposed to predict the moduli of polymer composites filled with particles. The elastic modulus for particulate-filled composites can be calculated using Einstein's equation:

$$\frac{E_c}{E_m} = 1 + 2.5\phi_p \quad (21.17)$$

where E_c and E_m are the elastic moduli of the composite material and the matrix, respectively, and ϕ_p is the volume fraction of particles. This equation was obtained for a very dilute suspension of spheres and, therefore, it is only valid in the range of low particle-filled polymer. It is also

assumed that the adhesion between the polymer matrix and the solid spheres is good. A more realistic equation is the semiempirical one proposed by Halpin and Tsai:

$$\frac{E_c}{E_m} = \frac{1 + A_1 B_1 \phi_p}{1 - B_1 \phi_p} \quad (21.18)$$

where A_1 is a constant related to particle shape and matrix Poisson ratio, and B_1 is related to the moduli of the particle and the polymer matrix. An improved equation for prediction of the elastic modulus was proposed by Nielsen [11], which takes into account the particle packing fraction in the matrix:

$$\frac{E_c}{E_m} = \frac{1 + A_1 B_1 \phi_p}{1 - \Psi B_1 \phi_p} \quad (21.19)$$

where Ψ is the particle packing fraction parameter which is given by:

$$\Psi = 1 + \left[\frac{1 - \phi_{p \max}}{\phi_{p \ max}^2} \right] \phi_p \quad (21.20)$$

where $\phi_{p \ max}$ is the maximum packing fraction of particles.

There are a number of modified equations that correlate well with different experimental data. A recent review on particulate composites lists many of them [21].

The tensile strength is usually taken as the maximum stress that a material can bear under a tensile loading. In polymer composite materials filled with particles, the stress transfer between the particles and polymer matrix affects the final tensile strength of the composite. Expressions for the prediction of tensile strength in polymer composites are difficult to find because they are associated with parameters that are difficult to measure, such as stress concentration, interfacial adhesion, and particle distribution. However, some semiempirical equations are sometimes used to model and try to predict the tensile strength of the composite material. The simplest model assumes that the stress is not transferred from the matrix to the particles; therefore, the strength of the composite is given by the amount of polymer matrix present:

$$\sigma_c = \sigma_m (1 - \phi_p) \quad (21.21)$$

where σ_c and σ_m are the composite and matrix strengths, respectively, and ϕ_p is the volume fraction of particles. An improved equation that still considers no stress transfer between particles and matrix was proposed by using geometrical considerations by Nicolais and Nicodemo [22], which improves on the above equation:

$$\sigma_c = \sigma_m (1 - 1.21 \phi_p^{2/3}) S_r \quad (21.22)$$

where S_r is a reduction factor that takes values between 0.2 and 1 for high and low volume fractions. If some

degree of stress transfer between the particles and the matrix exists because of a better adhesion between them, a simple general semiempirical equation, given by Equation (21.23), is proposed:

$$\sigma_c = \sigma_m (1 - a \phi_p^b + c \phi_p^d) \quad (21.23)$$

where a , b , c , and d are constants that can be obtained by experimental data fitting. In general, the strength in particulate-filled composite materials and in fiber-filled materials is that of the matrix, and only in the cases of successful surface treatment of the particles, is it possible to transfer part of the load to the filler to improve strength.

There has been an increased interest in the preparation of polymer–short natural fiber composite materials, particularly with high volume polyolefins, polypropylene, and polyethylene. The attractiveness of short-fiber natural reinforced polymers lies in the wide availability of mainly cellulosic materials from different renewable resources (Chapter 26). There are reports of hose cellulose fiber-reinforced materials [23], cellulosic fiber composites from wood pine and birch [24], or cellulosic fiber composites from henequen cellulose [25]. Some advantages of cellulosic fibers are that they do not break during processing either by milling or extrusion as rigid short fibers do, maintaining their length constant; however, their main drawback is their poor adhesion with the polyolefin matrix. Several treatments have been proposed such as *o*-hydroxybenzenediazonium salt for coir fibers in a polypropylene matrix [26], oxidation of jute fibers in PP composites post-treated with urotropine [27], and bamboo flour–HDPE composites using a maleic anhydride ethylene/propylene elastomer [28]. The use of a silane coupling agent with cellulosic fibers extracted from henequen whole fibers [25] proved to be very effective in increasing the tensile strength and increasing the surface adhesion between cellulosic fibers and the LPDE matrix (Fig. 21.7).

In general, natural fiber treatment improves the adhesion between the fiber and the polymer matrix, increasing the elastic modulus and the tensile strength under tension [29, 30]. Figure 21.8 shows micrographs of the differences in fiber treatment and the surface interaction of LDPE matrix with cellulosic fibers extracted from henequen. In the figure, the enhanced interfacial adhesion using the silane agent that increases the tensile strength of the materials is denoted by the coating of the matrix and also by the fact that the composite failed by shear yielding and tearing from the fiber.

Carbon nanotubes and carbon nanofibers have been studied lately as reinforcement materials for several different polymers because their high modulus and stiffness bear the promise of levels of reinforcement not found with micron-size particles or fibers. This performance can be achieved with concentrations

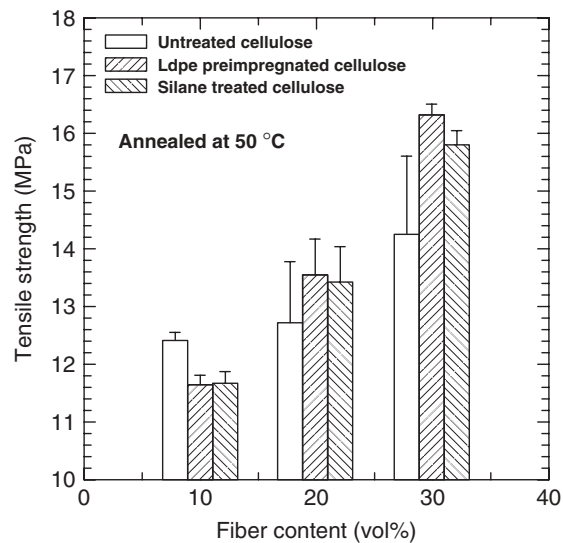


Figure 21.7 Effect of surface treatment of henequen cellulosic fibers on tensile strength of LDPE–henequen cellulosic fiber composites. Source: Reproduced with permission from Herrera-Franco PJ, Aguilar-Vega M. *J Appl Polym Sci* 1997;65:197 [25]. Copyright 1997 John Wiley and Sons.

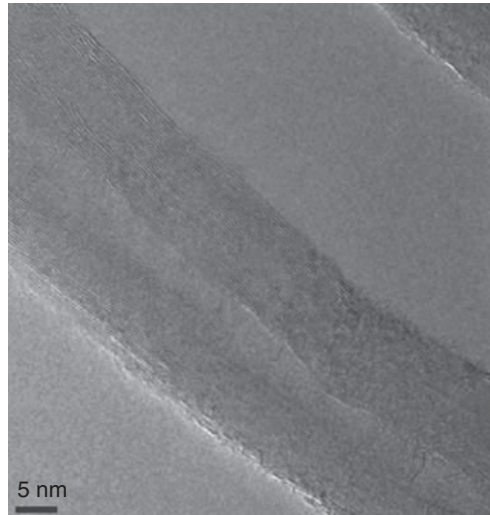


Figure 21.9 TEM micrograph of multiwalled carbon nanotube, Baytubes C150P. (Courtesy of Dr. Francis Aviles.)

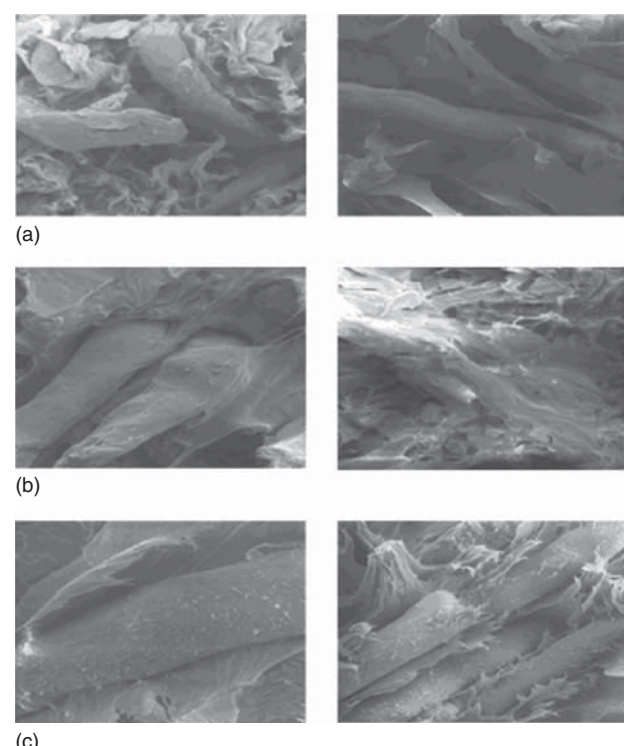


Figure 21.8 Micrographs of the failure surface by shear of LDPE–henequen cellulosic fiber composite with 20 and 30% by volume of cellulosic fiber: (a) untreated cellulose; (b) LDPE preimpregnated cellulose; and (c) silane-treated cellulose. Source: Reproduced with permission from Herrera-Franco PJ, Aguilar-Vega M. *J Appl Polym Sci* 1997;65:197 [25]. Copyright 1997 John Wiley and Sons.

below 10% of fibers [31, 32]. Single-walled carbon nanotubes are reported to have tensile strengths between 50 and 500 GPa and tensile moduli about 1500 GPa, while multiwalled nanotubes present tensile strengths between 15 and 60 GPa and tensile moduli about 1000 GPa. Figure 21.9 is a micrograph of a multiwalled carbon nanotube.

It is also known that polymers containing nanofillers present better surface finishing and reinforcement than those prepared using microfillers owing to the small size of the filler [33]. One of the drawbacks in the preparation of nanotubes and nanofibers filled polymer composites is the difficulty found to disperse them in the polymer matrix without breaking them, which in the end may affect the L/d aspect ratio of the nanotube (where L is the length and d the diameter of the fiber or nanotube). At the nanoscopic level, the forces between nanotubes and nanofibers tend to agglomerate them into bundles. If the filler is not properly dispersed in the matrix, the polymer composite will have poor mechanical properties because the agglomerates will act as stress concentration centers. Nanotubes and nanofibers can be dispersed by *in situ* polymerization, solution and evaporation of the solvent [34], melt spinning, spin casting, or melt mixing. From these techniques, melt mixing seems to be the easiest one to use; the dispersion can be facilitated by using grafted maleic anhydride, PP or PE [32]. Maleic anhydride can also improve the interfacial adhesion between the nanotubes or nanofibers with the matrix.

As in the case of microfillers, stress transfer between the matrix and the nanotubes increases with an increase in nanofiber or nanotube aspect ratio (L/d). Nanotubes can be considered as hollow cylinders, and their critical length

for reinforcement, l_c , can be calculated from the following equation:

$$l_c = \frac{\sigma_f D}{2\tau} \left[1 - \frac{D_i^2}{D^2} \right] \quad (21.24)$$

Here, σ_f is the fiber tensile strength, τ is the interfacial shear stress, and D and D_i are the external and internal diameters of the cylinder, respectively. Out of these parameters, τ is the critical factor that measures the stress transfer from the matrix to the polymer.

Elastic moduli of polymer composite materials filled with nanotubes and nanofibers can be estimated from Cox's equation [32]:

$$E_c = (1 - \phi_f)E_m + n\phi_f(\eta_f E_f) \quad (21.25)$$

where E_c is the composite elastic modulus, ϕ_f is the filter volume fraction, E_m is the elastic modulus of the polymer matrix, η_f is the filler efficiency factor, E_f is the filler elastic modulus, and n is a constant that takes into account the orientation of the nanotubes or nanofibers. This equation takes into account the filler aspect ratio and has been used successfully for the prediction of short-fiber composite materials. Halpin-Tsai's equation (Eq. 21.18) has also been used [32].

Particulate polymer composites with fibers are a very active area of development, particularly carbon nanotubes and nanofiber composites, and the new graphite and polymer composites [35]. This fact, combined with the continued interest in nanocomposites based in nanometric clays [36], suggests that improvements in mechanical properties of particulate and short-fiber polymer composite materials will continue to be reported.

REFERENCES

1. Flory PJ. *Principles of Polymer Chemistry*. Ithaca, NY: Cornell University Press; 1953.
2. Odian G. *Principles of Polymerization*. New York: John Wiley and Sons; 1991.
3. Stevens MP. *Polymer Chemistry, an Introduction*. New York: Oxford University Press; 1990.
4. Reid RC, Prawnsitz JM, Poling BE. *The Properties of Gases and Liquids*. 4th ed. New York: McGraw Hill; 1987.
5. Natta G, Pino P, Corradini P, Danusso F, Manica E, Mazzanti G, Moraglio G. *J Am Chem Soc* 1955;77:1708.
6. van Krevelen DW, te Nijenhuis K. *Properties of Polymers*. 4th ed. Amsterdam, The Netherlands: Elsevier; 2009.
7. Bicerano J. *Prediction of Polymer Properties*. 2nd ed. New York: Marcel Dekker, Inc.; 1996.
8. Oshinski AJ, Keskkula H, Paul DR. *Polymer* 1992;33:284.
9. Oshinski AJ, Keskkula H, Paul DR. *Polymer* 1996;37:4919.
10. Kauffman HS, Falcetta JJ. *Introduction to Polymer Science and Technology, an SPE Textbook*. New York: Wiley-Interscience; 1977.
11. Nielsen LE, Landel RF. *Mechanical Properties of Polymers and Composites*. 2nd ed. New York: Marcel Dekker; 1994.
12. McCrum NG, Buckley CP, Bucknall CB. *Principles of Polymer Engineering*. New York: Oxford University Press; 1988.
13. Jones MR. *Mechanics of Composite Materials*. Tokyo: McGraw HillKogakusha; 1975.
14. Chawala KK. *Composite Materials*. New York: Springer Verlag; 1987.
15. Adams DF, Carlsson LA, Pipes RB. *Experimental Characterization of Advanced Composite Materials*. Boca Raton, FL: CRC Press; 2003.
16. Cho JW, Paul DR. *Polymer* 2001;42:1083.
17. Fornes TD, Yoon PJ, Keskkula H, Paul DR. *Polymer* 2001;42:9929.
18. Yoon PJ, Hunter DL, Paul DR. *Polymer* 2003;44:5323.
19. Chavarria F, Paul DR. *Polymer* 2004;45:8501.
20. Stretz HA, Paul DR, Li R, Keskkula H, Cassidy PE. *Polymer* 2005;46:2621.
21. Fu SY, Feng XQ, Lauke B, Mai YW. *Composites B* 2008;39:933.
22. Nicolais L, Nicodemo L. *Int J Polym Mater* 1974;3:229.
23. Goetler L, Lambrigh AJ, Leib RI, DiMauro PI. *Rubber Chem Technol* 1981;54:277.
24. Karlsson O, Blachot JF, Pegury A, Gatenholm P. *Polym Compos* 1996;17:300.
25. Herrera-Franco PJ, Aguilar-Vega M. *J Appl Polym Sci* 1997;65:197.
26. Islam MN, Rahman MR, Haque MM, Huque MM. *Composites A* 2010;41:192.
27. Rahman MR, Huque MM, Islam MN, Hasan M. *Composites A* 2008;39:1739.
28. Liu H, Wu Q, Han G, Yao F, Kojima Y, Suzuki S. *Composites A* 2008;39:189.
29. Loría-Bastarrachea MI, Carrillo-Escalante HJ, Aguilar-Vega MJ. *J Appl Polym Sci* 2002;83:386.
30. Toledano-Thompson TT, Loria-Bastarrachea MI, Aguilar-Vega MJ. *Carbohydr Polym* 2005;62:67.
31. Kanagaraj S, Varanda FR, Zhil'tsova TV, Oliveira MSA, Simoes JAO. *Composites Sci Technol* 2007;67:3071.
32. Al-Saleh MH, Sundaraj U. *Composites A* 2011;42:2126.
33. Paul DR, Robeson LM. *Polymer* 2008;49:3187.
34. Avilés F, Llanes L, Oliva AI, Corona JE, Aguilar-Vega M, Loría-Bastarrachea MI. ASME International Mechanical Engineering Congress and Exposition; 2008.
35. Sengupta R, Bhattacharya M, Bandyopadhyay S, Bhowmick AK. *Prog Polym Sci* 2011;36:638.
36. Moreno M, Quijada R, Santa Ana MA, Benavente E, Gomez-Romero P, Gonzalez G. *Electrochim Acta* 2011;58:112.

PART V

POLYMER PROCESSING



22

POLYMER RHEOLOGY

ESTANISLAO ORTÍZ-RODRÍGUEZ

22.1 INTRODUCTION TO POLYMER RHEOLOGY FUNDAMENTALS

The term *rheology* comes from the Greek words *ροή* (flow) and *λόγος* (study) and as such it is the science that studies the relationships between forces applied to a material and the resulting deformations. The mathematical form of these relationships is called *constitutive equation* or *rheological equation of state*. Depending on the rheological properties, which are described by the relationship between the applied force and its resulting deformation, materials can be classified as shown in Figure 22.1.

The limiting cases shown in Figure 22.1 are those of solids with constant deformation modulus (Hookean solids) and liquids with constant viscosity (Newtonian liquids). Viscoelastic materials (solids or liquids) exhibit a rheological behavior that is a combination of the behavior of elastic solids and viscous liquids. There is a wide variety of materials with viscoelastic behavior, but this type of behavior is particularly relevant for both solid and molten thermoplastic polymers. Understanding the viscoelastic nature of polymeric materials is of particular importance when dealing with polymer processing operations, such as extrusion, injection molding, film blowing, and blow molding.

22.1.1 Deformation Response of Polymeric Solids¹

Solid synthetic polymers can exhibit a wide variety of mechanical behaviors depending on physical aspects such as crystallinity and architectural characteristics such

as molecular weight (M_w), branching, or degree of crosslinking. Polymeric materials can be classified as fibers, elastomers, flexible plastics, or rigid plastics depending on their mechanical behavior, which is determined by the relationship between the applied force or stress and the resulting deformation or strain [1]. In what follows in this section, a brief overview of the deformation behavior of polymeric solids under uniaxial loading is discussed. Under this loading condition, fibers exhibit very low deformations, and elastomers present relatively high deformations and they fully recover their initial shape on removal of the force that caused deformation. On the other hand, rigid plastics present very low deformations at break, whereas flexible plastics can exhibit large deformations, but their elastic recovery is generally very small. The deformation behavior of elastomers and flexible plastics is relatively different from one another. This is briefly illustrated by means of the general stress-strain curve shown in Figure 22.2.

As observed in Figure 22.2, the tangent modulus of elastomers (rubberlike materials) has initially low values, the tangent modulus being defined as the slope of the stress-strain curve. However, after a certain value of deformation (strain) experienced by the elastomer, the modulus increases. An important characteristic of this type of materials is the fact that their deformation behavior is reversible. For flexible plastics, from low to moderate strains, relatively constant values of the tangent modulus can be observed. However, as the strain is increased, a change in the behavior of the modulus versus deformation profile is observed. The convex region of the stress-strain profile shown in Figure 22.2 is associated with necking due to the plasticity of flexible plastics. For these types of materials, only the deformation observed before yield and necking is reversible.

¹This section was adapted with permission of John Wiley & Sons, Inc., from section 1.6 of Odian G. Principles of Polymerization. 4th ed. New York: Wiley-Interscience; 2004 [1].

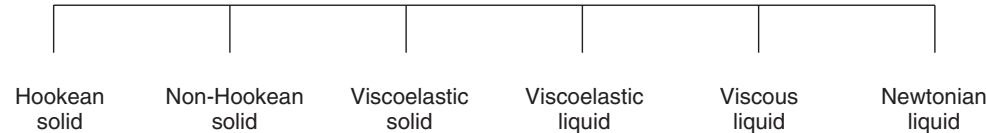


Figure 22.1 Classification of solids and liquids depending on their observed rheological behavior.

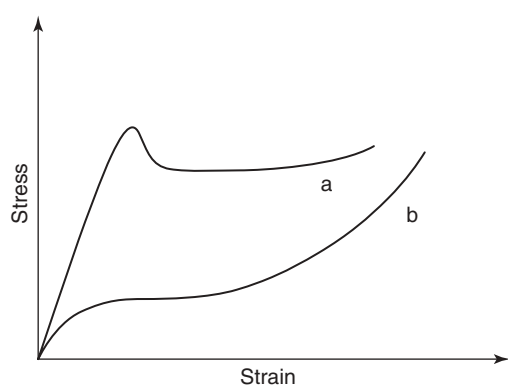


Figure 22.2 General description of the uniaxial load/deformation behavior for: (a) flexible plastics and (b) elastomers. Source: Adapted with permission of John Wiley & Sons, Inc., from Odian G. Principles of Polymerization. 4th ed. New York: Wiley-Interscience; 2004 [1].

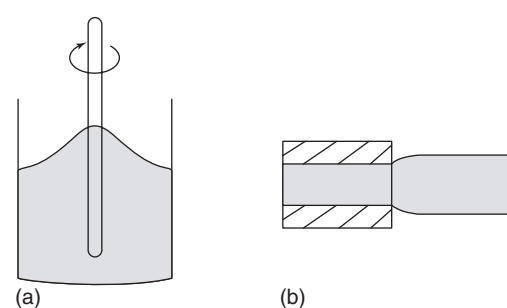


Figure 22.4 Illustration of (a) the Weissenberg effect and (b) extrudate swelling.

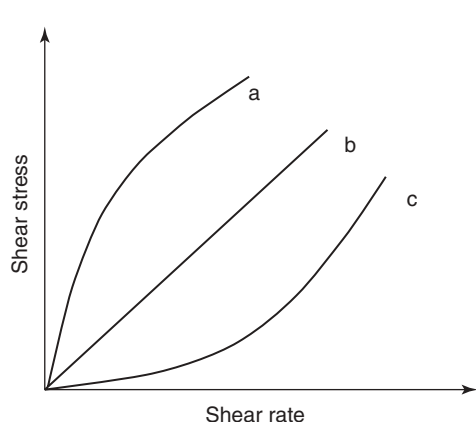


Figure 22.3 Stress versus shear rate behavior for (a) shear thinning, (b) Newtonian, and (c) shear thickening materials.

22.1.2 Rheology of Polymeric Liquids

Different types of liquid-like behavior can be related to polymeric liquids. In some cases, polymers are just dispersed in the bulk of another material, for instance, in polymeric suspensions such as some types of liquid paints. In some other cases, the polymer forms the bulk, as in the case of polymer melts. Models describing the rheology of the latter type of liquid polymers are needed to perform numerical analysis of processing operations and

sizing of equipment, such as extruders and dies used in the manufacturing of extruded products.

Different types of polymer fluid rheological behaviors are shown in Figure 22.3. In general, polymeric materials exhibit non-Newtonian behaviors, meaning that their viscosities are not constant. It is observed in Figure 22.3 that the viscosity of some materials, given by the slope of the stress versus shear rate curve, decreases as the stress to which they are subjected increases. Materials exhibiting this rheological behavior are termed *pseudo-plastic* or *shear thinning materials*. Some other materials called *dilatants* exhibit a shear thickening behavior. The viscosity of such materials increases as the stress increases. This type of behavior can be found in some ionic polymer solutions [2]. Shear thinning describes well the rheology of molten polymers for practical engineering purposes.

There are several aspects of rheological behavior exhibited by polymeric liquids that set these materials apart from Newtonian fluids. An excellent summary of the differences in fluid response between Newtonian liquids and non-Newtonian polymeric liquids under various scenarios has been given by Bird and Curtis [3]. Two very well-known “atypical” phenomena exhibited by polymeric liquids are the Weissenberg effect (a polymer melt or solution tends to climb a rotating rod) and extrudate swelling, which are illustrated in Figure 22.4.

In general terms, both of the aforementioned rheological phenomena can be related to the viscoelastic nature of polymeric materials and more specifically to the development of normal stresses and the deformation history of such materials. Extrudate swelling has direct implications

in industrial polymer extrusion operations where extrusion dies have to be designed to minimize extrudate swelling effects, for instance, in profile extrusion. For a particular polymer, its molecular characteristics, such as M_w and molecular weight distribution (MWD) [4, 5] and type of branching [6], are related to the extent of extrudate swelling observed at a particular shear rate. In general terms, extrudate swelling increases as shear rate increases, up to a certain value [6]. Some of the implications of the viscoelastic nature of polymer melts in polymer processing are addressed in Reference 7.

22.1.3 Mathematical Relationships for Polymer Rheology

A great deal of the mathematical background for understanding rheology is related to vectors and tensors. A comprehensive discussion of these subjects is out of the scope of this work. However, in what follows in this section, a brief summary of some of the mathematical relationships and quantities of common use in polymer rheology is presented. The reader interested in more details may refer to rheology, fluid, and solid mechanics textbooks [8–13].

The mathematical description of the rheological behavior of materials can be traced back to the description of solids and liquids by means of the equations of fluid motion, for liquids, or the implementation of equations describing the deformation behavior of solids with continuum mechanics relationships. To illustrate the type of mathematical relationships of general use when dealing with the deformation of solids and liquids, let us consider a linear uniaxial deformation and the deformation resulting from the shearing of a rectangular material element, as illustrated in Figure 22.5.

A measure of the uniaxial deformation is the linear strain, which relates the amount of stretching of the material to its initial length, as stated in the following equation:

$$\gamma_1 = \frac{\Delta L}{L} = \frac{du_1}{dx_1} \quad (22.1)$$

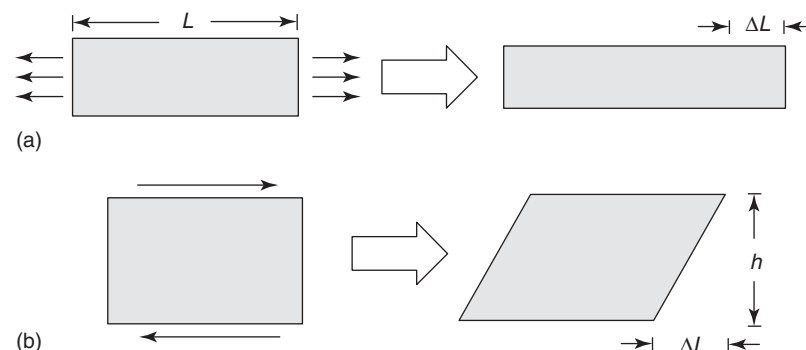


Figure 22.5 (a) Linear uniaxial deformation and (b) shearing of a material.

In this equation, L is the initial length; ΔL , the change in length due to stretching; and u_1 , the displacement of a material point in the stretching direction (x_1).

On the other hand, a measure of the shear deformation of the rectangular material element shown in Figure 22.5 is given in terms of shear strain, which is given in the following equation:

$$\gamma_{12} = \frac{\Delta L}{h} = \frac{du_1}{dx_2} \quad (22.2)$$

In this case, the shear strain relates the displacement (u_1) in the shearing direction (x_1) to a reference length (h) in the direction (x_2), perpendicular to the shearing direction of the material.

For a three-dimensional deformation, a generalization of the strain as a measure of deformation when a material is subjected to deformation is the strain tensor. There are several ways to express the strain tensor, based on linear and nonlinear representations of the strain components. In Equation 22.3, the strain tensor is written by using a linear representation of the strain components:

$$\boldsymbol{\gamma} = \nabla \mathbf{u} + (\nabla \mathbf{u})^T \quad (22.3)$$

where

$$\nabla \mathbf{u} = \begin{bmatrix} \frac{\partial u_1}{\partial x_1} & \frac{\partial u_2}{\partial x_1} & \frac{\partial u_3}{\partial x_1} \\ \frac{\partial u_1}{\partial x_2} & \frac{\partial u_2}{\partial x_2} & \frac{\partial u_3}{\partial x_2} \\ \frac{\partial u_1}{\partial x_3} & \frac{\partial u_2}{\partial x_3} & \frac{\partial u_3}{\partial x_3} \end{bmatrix}$$

When one is following the deformation experienced by solid or liquid materials with respect to time, one deals with the rate of deformation. As a generalization of the above results, the strain rate tensor can be written as indicated in the following equation:

$$\dot{\boldsymbol{\gamma}} = \nabla \mathbf{v} + (\nabla \mathbf{v})^T \quad (22.4)$$

where $\dot{\gamma}$ is the strain rate tensor and \mathbf{v} is the velocity vector.

Taking into consideration the forces that cause the deformation of a given material, one invokes the relationships for the stresses developed in that solid or liquid material. Following the generalizations of the strain and strain rate to express such quantities in terms of tensorial expressions, the stress tensor is expressed as in Equation 22.5 (index and symbolic notations, Eq. 22.5a and 22.5b, respectively):

$$\tau_{ij} = \frac{F_j}{A_i}, \quad i, j = 1, 2, 3 \quad (22.5a)$$

$$\boldsymbol{\tau} = \frac{\mathbf{F}}{\mathbf{A}} \quad (22.5b)$$

where $\boldsymbol{\tau}$ is the stress tensor, F_j is the force acting in the j th direction on an area element A_i , which is perpendicular to the i th direction.

Another important quantity of general use in fluid mechanics and polymer rheology is the total stress tensor. This tensor is defined in terms of the stress tensor and the hydrostatic pressure, as indicated in the following equation:

$$\boldsymbol{\sigma} = \boldsymbol{\tau} - P\mathbf{I} \quad (22.6)$$

where $\boldsymbol{\sigma}$ is the total stress tensor; \mathbf{I} , the identity tensor; and P , the hydrostatic pressure.

22.2 LINEAR VISCOELASTICITY

Linear viscoelasticity is the simplest type of viscoelastic behavior observed in polymeric liquids and solids. This behavior is observed when the deformation is very small or at the initial stage of a large deformation. The relationship between stress and strain may be defined in terms of the relaxation modulus, a scalar quantity. This is defined in Equation 22.7 for a sudden shear deformation:

$$G(t, \gamma) = \frac{\tau(t, \gamma)}{\gamma} \quad (22.7)$$

where $G(t, \gamma)$ is the shear relaxation modulus; t , the experimental time; and γ , the shear strain. Under linear viscoelastic conditions, the relaxation modulus is independent of the magnitude of the strain. This leads to a linear relationship between stress and strain:

$$\tau(t) = G(t) \gamma \quad (22.8)$$

For a solid material, the typical difference in deformation behavior between a Hookean solid and a viscoelastic solid can be explained in terms of an applied constant load.

For a Hookean solid, say a metal, the load will produce a deformation that stays constant over time. On the other hand, for a polymeric material the same load will produce an initial deformation, followed by a slow and constant deformation up to a certain value (creep). This is an illustration of a retardation process, where the final response of the material to the load is retarded. On the other hand, one can also visualize an experiment where a constant strain is imposed to both, a Hookean solid and a viscoelastic solid. Under these experimental conditions, a constant stress is developed in the first case, whereas in the second case, the stress is nonconstant; it starts at an initial value and then decreases up to a zero value. This experimental behavior constitutes a relaxation process.

To illustrate what happens in the case of polymeric liquids with respect to linear viscoelasticity, let us consider the following equation, which is a general relationship between stress and strain rate:

$$\tau(\dot{\gamma}) = \eta(\dot{\gamma}) \dot{\gamma} \quad (22.9)$$

where $\eta(\dot{\gamma})$ is the viscosity of the material as a function of shear rate, $\dot{\gamma}$.

The time dependency of the stress-strain rate relationship can be omitted for polymeric liquids in many practical situations. Now, let us consider Figure 22.6, which is a typical plot for viscosity in terms of shear rate for a polymer melt. Two different regions can be observed in the figure. In the first region, which occurs at moderate low shear rate values, there is a smooth variation of polymer viscosity. In the second region, there is a more pronounced decrease of viscosity as shear rate is further increased. This section of the curve is often described mathematically by a power-law model that expresses the relationship between shear rate and the viscosity stated in Equation 22.9, as discussed in

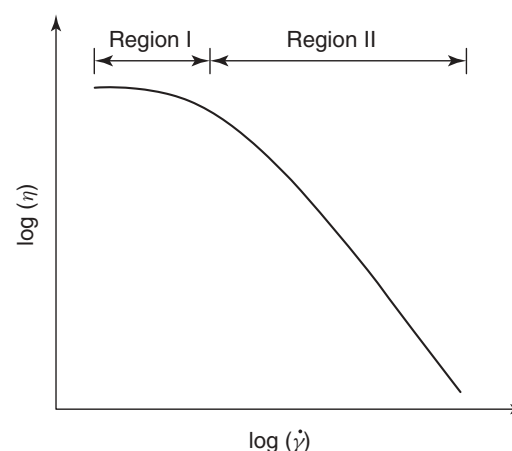


Figure 22.6 Variation of viscosity as a function of shear rate for polymeric melts.

Section 22.3.1. Polymer processing is generally achieved at shear rates lying in the shear thinning region of the viscosity curve (the second region of the curve shown in Fig. 22.6). Regarding the first region of the curve shown in Figure 22.6, it can be seen that the viscosity approaches a plateau at low shear rate values. The value of viscosity at this plateau is known as the *zero-shear-rate viscosity* η_0 , and it is usually determined by means of experiments in the linear viscoelastic region [5, 9].

As shown in Figure 22.6, the determination of viscosity at low shear rates corresponds to measurements in the linear region of viscoelasticity (additional information regarding the measurement of viscosity in the linear viscoelastic regime is presented in Section 22.3.2). In the work by Meissner [5], several methods used in the evaluation of linear viscoelasticity are outlined. Measurement of melt viscosity in the linear viscoelastic region is of great importance in the characterization of thermoplastics. These measurements provide information about long branching, M_w , or filler content of thermoplastic melts [5, 6, 14].

22.3 VISCOMETRIC TECHNIQUES FOR POLYMER MELTS

As stated earlier, polymer rheology is not confined to the study of liquid polymers. However, this section is focused on the analysis of polymer melts, since these materials have a great relevance in polymer processing. The viscometric techniques to be discussed in this section may apply not only to polymer melts but also to other polymeric liquid systems, such as solutions and suspensions.

22.3.1 The Capillary Rheometer

Different experimental techniques for the evaluation of the relationship between the shear rate experienced by a polymeric material and the corresponding polymer viscosity have to be implemented to determine the flow behavior of a polymer melt. Figure 22.6 shows the rheological behavior (shear thinning) of a polymer melt under typical processing conditions. A very useful and yet relatively easy-to-understand expression used to describe the shear thinning behavior of polymer melts is the power-law model, as given in the following equation:

$$\eta(\dot{\gamma}) = K\dot{\gamma}^{n-1} \quad (22.10)$$

where K is the consistency index and n is the power-law index. This equation describes the second region of the curve shown in Figure 22.6. The description of this region of the curve with viscometric techniques is performed with the capillary rheometer. With this instrument, the viscosity

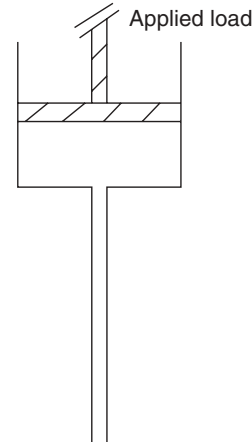


Figure 22.7 Schematic representation of a capillary rheometer.

of a polymer melt is evaluated from the flow inside a long- and small-diameter capillary tube. In a typical way of operation, the polymer in the solid state is fed to a cylindrical reservoir where it is melted and forced through the capillary tube by a piston. A graphical representation of the capillary rheometer is depicted in Figure 22.7. The viscosity measurements obtained from the capillary rheometer are very important as they help to establish a relationship between shear rate and viscosity of melted polymers under typical operating conditions in polymer processing equipment.

There are two main corrections that have to be applied to the information obtained from the capillary rheometer. First, there is an entrance pressure drop when the molten polymer enters the capillary, which is taken into account through the entrance or Bagley correction. This pressure drop is related to elastic deformations of the melt at the entry of the capillary [15]. Secondly, the non-Newtonian shear rate is expressed in terms of an apparent viscosity (defined in terms of a Newtonian flow). The relationship between the non-Newtonian and Newtonian shear rates, expressed as in the following equation, is known as the *Rabinowitch correction* [13, 16]:

$$\dot{\gamma}_w = \frac{3n+1}{4n}\dot{\gamma}_{app} \quad (22.11)$$

where

$$\dot{\gamma}_{app} = \frac{4Q}{\pi R^3}$$

Here, $\dot{\gamma}_w$ and $\dot{\gamma}_{app}$ are the shear rate at the wall of the capillary and the apparent shear rate, respectively; n is the power-law index; Q is the volumetric flow rate; and R is the radius of the capillary.

The Bagley correction is further explained considering the following equations:

$$\tau_w = \frac{R(\Delta P_c)}{2L} \quad (22.12a)$$

$$\tau_w = \frac{R(\Delta P_c)}{2(L + L_{\text{ent}})} \quad (22.12b)$$

$$\tau_w = \frac{\Delta P_c}{2(L/R + |e|)} \quad (22.12c)$$

$$\tau_w = K' (\dot{\gamma}_{\text{app}})^n \quad (22.13a)$$

$$\ln(\tau_w) = \ln(K') + n \ln(\dot{\gamma}_{\text{app}}) \quad (22.13b)$$

where

$$K = K' \left(\frac{4n}{3n+1} \right)^n$$

In these equations, τ_w is the shear stress at the capillary wall, ΔP_c is the total pressure drop in the capillary, L is the capillary length, L_{ent} is an apparent length, and e is the Bagley entrance correction.

Equation 22.12a represents the shear stress at the wall of the capillary in the absence of the pressure drop due to entrance effects. On the other hand, Equation 22.12b and 22.12c correspond to the corrected equation when the entrance pressure drop is taken into account. The correction parameter e given in Equation 22.12c can be calculated as the x -intercept in a plot of ΔP_c versus L/R at constant $\dot{\gamma}_{\text{app}}$. The experimental data needed to generate this plot are obtained from capillary rheometer measurements, using capillaries of different lengths and constant diameter. The pressure drop is dependent on the value of $\dot{\gamma}$, or $\dot{\gamma}_{\text{app}}$; therefore, different correction factors are needed for different values of $\dot{\gamma}_{\text{app}}$ [15]. After performing both the Bagley and Rabinowitch corrections, the consistency and power-law indexes can be obtained from a regression analysis of the experimental data using Equation 22.13a and 22.13b. Because of the significant amount of experimental work associated with the Bagley correction, it is a common practice to avoid performing this correction when long L/D diameter capillaries are used in the capillary rheometer. In this way, negligible flow entrance effects to the die can be assumed. Although capillaries with $L/D \geq 20$ [4, 9, 17, 18] have been used for such purposes, Macosko [9] points out that in some cases this approach is not as accurate as expected.

A variation of a capillary rheometer as the one previously described can be used to determine the melt flow index (MFI) of thermoplastic melts. The MFI is the amount of polymer flowing through a capillary of specific dimensions under a given weight and at a given temperature as those are described by international standards, such as the American Standards for Testing and Materials (ASTM).

The MFI represents one point on the viscosity curve and it is widely used as an industrial indicator of the processability of thermoplastic polymers and for quality control purposes. Although the MFI is not a rigorous indicator of viscosity, Shenoy et al. [19–21] have proposed and implemented a methodology for determining the complete viscosity curve from individual MFI measurements and a reference viscosity curve.

22.3.2 Rotational Rheometers

The cone-and-plate and parallel-plate rheometers are rotational devices used to characterize the viscosity of molten polymers. The type of information obtained from these two types of rheometers is very similar. Both types of rheometers can be used to evaluate the shear rate–viscosity behavior at relatively low values of shear rate; therefore, allowing the experimental determination of the first region of the curve shown in Figure 22.6 and thus the determination of the zero-shear-rate viscosity. The rheological behavior observed in this region of the shear rate–viscosity curve cannot be described by the power-law model. On the other hand, besides describing the polymer viscosity at low shear rates, the cone-and-plate and parallel-plate rheometers are also useful as dynamic rheometers and they can yield more information about the structure/flow behavior of liquid polymeric materials, especially molten polymers.

In a dynamic experiment, a small-amplitude oscillatory shear is imposed to a molten polymer confined in the rheometer. The shear stress response of the polymeric system can be expressed as in Equation 22.14. In this equation, G' and G'' are dynamic moduli related to the elastic storage energy and dissipated energy of the system, respectively. For a viscoelastic fluid, two independent normal stress differences, namely, first and second normal stress differences can be defined. These quantities are calculated in terms of the differences of the components of the stress tensor, as indicated in Equation 22.15a and 22.15b, and can be obtained, for instance, from the radial pressure distribution in a cone-and-plate rheometer [5]. Some other experiments used in the determination of the normal stress differences can be found elsewhere [9, 22]:

$$\tau_{12} = G' \gamma_0 \sin \omega t + G'' \gamma_0 \cos \omega t \quad (22.14)$$

where $\gamma = \gamma_0 \sin \omega t$

$$\tau_{11} - \tau_{22} = \psi_1 \dot{\gamma}^2 \quad (22.15a)$$

$$\tau_{22} - \tau_{33} = \psi_2 \dot{\gamma}^2 \quad (22.15b)$$

The terms on the left-hand side of Equation 22.15a and 22.15b are the first and second normal stress differences, respectively. ψ_1 and ψ_2 are the first and second normal stress difference coefficients, respectively, and $\dot{\gamma}$ is the shear rate.

22.3.3 Temperature and Pressure Effects on Viscosity

For a polymer of constant composition, it is a common practice to determine its viscosity curve, as the one shown in Figure 22.6. The obtained curve is valid for a given set of experimental conditions, that is, for a given pressure and temperature. In general terms, the viscosity increases as temperature decreases or pressure increases. According to Reference 23 at lower values of shear rate, a decrease of temperature has a similar effect to an increase of pressure. There is a method that makes use of a semiempirical relationship to take into account the effects of temperature and pressure on the viscosity curve. This method is based on the concept of a master curve and essentially it allows for the construction of a viscosity curve from a reference curve and a single viscosity value [15].

A master curve can be constructed as indicated in Figure 22.8, where the zero-shear-rate viscosity η_0 has to be evaluated for each one of the indicated viscosity curves. Both, the effect of temperature and pressure on the viscosity versus shear rate curve can be addressed by considering a shift factor that may be related, for instance, to the free volume of the system by means of the Williams, Landel, and Ferry (WLF) equation [9, 15, 23, 24]. With the aid of this shift factor, the new viscosity curve can be constructed from known viscosity values and the reference curve at the prescribed values of temperature and a pressure. The use of shift factors to take into account the temperature dependence on the viscosity curve was also used by Shenoy et al. [19–21] in their methodology for producing viscosity curves from MFI measurements.

22.3.4 Other Viscometric Determinations

In this section, only measurements of shear viscosity have been addressed. However, some other devices are available that can assist in the characterization of the rheology of polymer melts under different types of deformation, other than shear. For instance, extensional viscosities can

be evaluated from such different experimental devices [5, 9, 13]. In addition, in some instances, optical determinations are used to complement the information of melt rheology in relation to the molecular orientation of polymer systems under flow [5, 16, 25–27].

Optical measurements are applied for both polymeric melts and molded plastics. In the latter case, polarized light microscopy (POM) can be used, for example, in performing analyses of residual stresses [16]. POM analyses of polymer melts and solids are based on light birefringence caused by optical anisotropy of oriented polymer systems that can be characterized by means of this optical technique. In the case of molten polymers, experimental techniques such as POM, infrared spectroscopy, and small angle laser light scattering (SALLS) have been used to investigate the flow behavior of polymer melts or to correlate experimental results to rheological parameters [25].

A complementary use of polymer viscometry is the indirect evaluation of the MWD of a polymer from dynamic viscosity measurements [28–30]. The methods used to correlate the MWD of polymers to rheological data are based on the previous determination of the polymer relaxation spectrum from linear oscillatory shear experiments [31, 32]. MWDs obtained from viscometric data analysis can help in the determination of the MWD curve from online measurements, or in cases where this curve cannot be easily determined from size exclusion chromatography (SEC) [30, 31].

22.4 OVERVIEW OF CONSTITUTIVE EQUATIONS

As previously indicated, the mathematical relationships describing the stress–deformation behavior of viscoelastic polymeric materials are known as constitutive equations. Different classifications have been given for these types of equations [12, 33–36]. Here, a classification is given from a mathematical point of view, similar to that

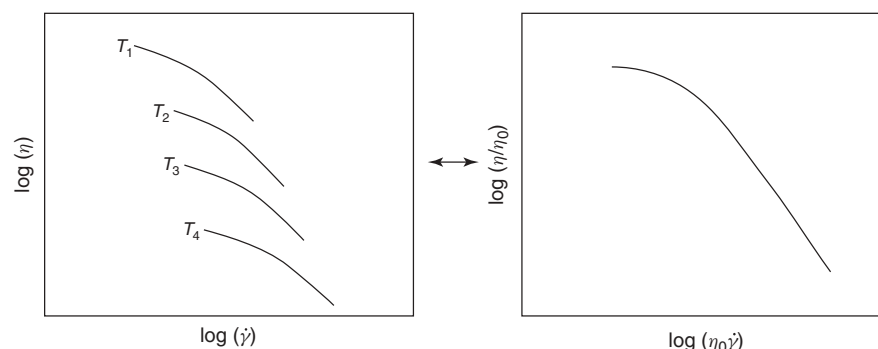


Figure 22.8 Construction of a viscosity versus shear rate master curve. *Source:* Adapted with permission from Michaeli W. Extrusion Dies for Plastics and Rubber. 3rd ed. Munich: Hanser; 2003 [15].

used by Nassehi [35]. Only constitutive models based on continuum mechanics principles are addressed in this chapter, and no equations derived from molecular considerations [34, 37, 38] are discussed.

22.4.1 The Generalized Newtonian Fluid

Newton's law of motion for liquids describes a linear relationship between the deformation of a fluid and the corresponding stress, as indicated in Equation 22.16, where the constant of proportionality is the Newtonian viscosity of the fluid. The generalized Newtonian fluid (GNF) refers to a family of equations having the structure of Equation 22.16 but written in tensorial form, in which the term corresponding to viscosity can be written as a function of scalar invariants of the stress tensor (τ) or the strain rate tensor ($\dot{\gamma}$). For the GNF, no elastic effects are taken into account [12, 33]:

$$\tau = \eta \dot{\gamma} \quad (22.16)$$

where η is the Newtonian viscosity.

The GNF represents a relatively simple relationship between the stress and strain rate tensors, which can account for viscous effects of polymeric flows, such as temperature increase due to viscous dissipation. Because of its simplicity, the GNF can be readily incorporated into the momentum equation, which may be solved by means of numerical techniques in computational fluid dynamics (CFD) simulations. In general terms, since the processing temperature is not constant during a processing operation, an Arrhenius-type relationship can be assumed for some of the parameters of the models used to describe the viscosity of the system. In addition, here it is important to note that the parameters of the power-law and similar models are dependent on the M_w of a given polymer. An interesting case in the description of polymer processing operations occurs in reactive extrusion. In a reactive extrusion process, the parameters of the power-law, or similar model, change during the course of the reaction due to the variation of both M_w and temperature of the reacting system [39, 40].

Since viscosity can be expressed in terms of strain rate for the GNF, the stress tensor can be written in terms of the strain rate tensor and some constant parameters, as given in Equation 22.17. A power-law relationship for viscosity in terms of the strain rate has been assumed in Equation 22.17. In the case of flow between two parallel plates where one plate is fixed and the other one is moving with a given velocity, Equation 22.17 reduces to Equation 22.18, a familiar fluid mechanics equation:

$$\tau = K (\Pi_{\dot{\gamma}})^{n-1} \dot{\gamma} \quad (22.17)$$

Here, $\Pi_{\dot{\gamma}}$ represents the second invariant of the strain rate tensor, $\Pi_{\dot{\gamma}} = |\dot{\gamma}| = \sqrt{\frac{1}{2} (\dot{\gamma} : \dot{\gamma})}$.

$$\tau = K \dot{\gamma}^n \quad (22.18)$$

Note that in this case all the components of the strain rate tensor, except the one describing shearing of the material (the shear rate), are zero.

Other equations have been developed to describe the shear thinning behavior of polymer melts, for instance, the Yasuda–Carreau equation, which is written here as Equation 22.19 [41]. In this equation, as in the power-law model, the effect of temperature on viscosity of the system can be taken into account by means of an Arrhenius-type relationship:

$$\eta(\dot{\gamma}) = \frac{\eta_0}{(1 + (\lambda \dot{\gamma})^a)^{(1-n)/a}} \quad (22.19)$$

where $\eta(\dot{\gamma})$ stands for viscosity; η_0 is zero-shear-rate viscosity; n the power-law index; a is a fitting parameter related to the transition between the zero-shear-rate viscosity and the shear thinning regions in the viscosity curve; λ is a characteristic flow time; and $\dot{\gamma}$ is shear rate.

22.4.2 Differential Equations

Mechanical analog models based on a combination of spring and dashpot elements can be mathematically described by means of differential equations. These models can be used to represent viscoelastic phenomena, such as relaxation and creep. Two of such models are the Maxwell and the Voigt models. In particular, the first one of these models is very suitable to explain stress relaxation. Here, a brief explanation of the Maxwell model is presented omitting the somehow elegant mathematical formalities used to provide a more complete explanation of the model [16, 42]. A physical representation of this model is depicted in Figure 22.9. This physical model is a series arrangement of a spring element and a dashpot. For small deformations, the stress–strain behavior of this composed element may be given in terms of a linear response of its components, according to Equation 22.20. The explanation of stress relaxation in terms of the Maxwell model can be given as follows. First, when the composed element is subjected to an initial strain, its stress response is mainly associated with the spring element, producing an initial stress. However, as time passes, the initial deformation of the spring decreases gradually at the expense of viscous dissipation because of the movement of the piston of the dashpot. This process

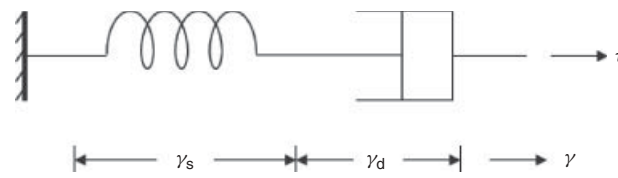


Figure 22.9 Physical representation of the Maxwell fluid element.

continues until the spring is no longer subjected to any deformation and the stress has completely relaxed.

$$\dot{\gamma}_s = -\frac{\tau}{G} \quad (22.20a)$$

$$\dot{\gamma}_d = -\frac{\tau}{\eta} \quad (22.20b)$$

$$\dot{\gamma} = \dot{\gamma}_s + \dot{\gamma}_d \quad (22.20c)$$

$$-\eta\dot{\gamma} = \lambda \frac{d\tau}{dt} + \tau \quad (22.20d)$$

where $\lambda = \frac{\eta}{G}$ is the relaxation time.

Unlike simple differential constitutive equations as the one previously addressed, constitutive equations may present special types of derivatives such as the substantial derivative, or other types of derivatives in which a hypothetical frame of observation of the flow is allowed to translate, rotate, and/or deformate [33]. The Criminale-Ericsen-Filbey (CEF) equation, written here as Equation 22.21, is an example of this type of equations. The CEF equation is relatively simple, and it is explicit in the stress tensor. The latter is a feature not shared by all rheological relationships belonging in the category of equations with special types of derivatives [35].

$$\tau = -\eta\dot{\gamma} - \left(\frac{1}{2}\psi_1 + \psi_2 \right) \{\dot{\gamma} \cdot \dot{\gamma}\} + \frac{1}{2}\psi_1 \frac{d\dot{\gamma}}{dt} \quad (22.21)$$

Here, Ψ_1 and Ψ_2 are the first and second stress difference coefficient functions, and the derivative of the strain rate is the Jaumann derivative, which is related to a frame of reference that translates and rotates with the local velocity of the fluid (this relationship can be numerically evaluated from the deformation and vorticity tensors).

22.4.3 Integral Constitutive Equations

Integral constitutive equations are explicit in the stress tensor [35], but unlike those equations describing stress only in terms of strain, for example, GNF type of equations, these equations involve functions that in general terms relate to the viscoelastic nature of the flow. Integral constitutive equations are often said to be related to the flow history of the fluid. This principle very well applies to the effect of extrudate swelling observed in polymer extrusion, whose association with the flow history of a material can be readily understood from practical experience. A simple relationship that has the form of a more general integral constitutive equation known as the Goddard-Miller (G-M) equation [33, 36] is presented here as Equation 22.22. After some mathematical manipulation, Equation 22.20d can be analytically integrated yielding a relationship of the form of Equation 22.22 [12]; therefore, the latter equation

can be used to address the linear viscoelastic response of polymeric melts.

$$\tau = - \int_{-\infty}^t G(t-t')\dot{\gamma}(t') dt' \quad (22.22)$$

Here t is actual time, t' refers to previously elapsed times, related to the flow history of the fluid, and $G(t-t')$ is relaxation modulus.

CFD software has been used to implement integral constitutive equations in the evaluation of viscoelastic responses in different polymer flow situations such as calendering, extrusion die swelling, and blow molding. In the work by Tadmor and Gogos [36], some applications of integral viscoelastic models, more specifically of the Kaye-Bernstein-Kearsly-Zapas (K-BKZ) type, are addressed. This type of model has been extensively used by Mitsoulis and coworkers to simulate different polymer flow situations (see for instance References 43 and 44). A simplified form of the K-BKZ equation used by Mitsoulis [44] is written here as follows:

$$\tau = \frac{1}{1-\theta} \int_{-\infty}^t \sum_{k=1}^N f(t-t', a_k, \lambda_k, M) \times \left[C_{t'}^{-1}(t') + \theta C_{t'}(t') \right] dt' \quad (22.23)$$

In this equation, θ is a material parameter related to the first and second normal stress differences of the polymer; N is the number of relaxation modes; a_k and λ_k are relaxation modulus and times, respectively; and C stands for the Cauchy-Green tensor.

22.5 BRIEF OVERVIEW ON OTHER RELEVANT POLYMER RHEOLOGY ASPECTS

In this section, some other relevant aspects of the rheology of polymer melts are addressed in some detail. The case of filled systems is discussed first. These types of systems are of significant importance in industrial applications. In addition, molecular dynamic and fluid dynamic simulations that have greatly benefited from the significant advances in computer power are discussed to some extent.

22.5.1 Rheology of Filled Polymeric Melts

In the previous sections, nothing has been said about the rheology of polymeric melts containing fillers. The latter type of materials are commonly used in industrial polymer processing operations and are aimed, for instance, to reinforce polymers, to improve processability [17], or to obtain

polymers with enhanced physical properties, such as higher electrical and thermal conductivities [18]. Among polymer fillers, one can find carbon black, glass fibers, and some other types of inorganic materials. Some materials that are becoming more common as polymer loads are natural fibers and nanocomposites. For some fillers, such as glass fibers, a surface treatment is needed for technical reasons [45].

Some modifications of the melt flow behavior of thermoplastics that can be observed depending on filler concentration are a yield-like behavior (i.e., in these cases, there is no flow until a finite value of the stress is reached), a reduction in die swell, a decrease of the shear rate value where nonlinear flow takes place, and wall slip or near-wall slip flow behavior [14, 27, 46]. Other reported effects of fillers on the rheology of molten polymers are an increase of both the shear thinning behavior and the zero-shear-rate viscosity with the filler loading and a decrease in the dependence of the filler on viscosity near the glass transition temperature [18, 47–49].

In filled polymer systems, it has been observed that the effect of filler content on viscosity decreases as shear rate increases [14, 49]. In the case of nanocomposite fillers, this effect has been explained in terms of a detachment/reattachment mechanism [49]. With respect to the dimensions of the fillers, it has been observed that as the surface area of the filler increases so does the viscosity of the filled polymer melt [18, 48]. For particles with similar shapes, an increase in the surface area means a reduction in particle size. In this sense, nanofillers are expected to significantly increase the viscosity of polymer melts in relation to fillers with sizes in the range of micrometers. An analysis of filler shape and other relevant aspects of polymer fillers can be found in the work by Shenoy [50].

22.5.2 Molecular Dynamic Simulations in Polymer Rheology

On the basis of the length scale of a simulation, one traditionally deals with micro- or macrosystems, and the simulations related to these systems are referred to as *micro-* or *macrosimulations*. Macrosimulations relate to the bulk behavior of materials, while microsimulations are referred to simulations of systems or parts of a system with length scales in the order of micro- or nanometers. Going down in the length scale of physical systems, an area of increasing interest that has also been facilitated by the improvement in computational power is the modeling and simulation at molecular and atomistic length scales for both low and high M_w materials. In addition, the modeling and simulation of physical systems involving models addressing different length scales of the same system (multiscale modeling), for example, molecular and macromodels, has been performed [51–56].

Molecular dynamic simulations seem to be very suitable to address polymer rheology in systems where the characteristic dimensions of the polymer chains are of the same range as some other characteristic lengths of the system under study. Examples of this latter scenario are flow through very thin gaps and the study of interactions between polymer melts and nanofillers [48, 57]. On the other hand, molecular dynamic simulations have been used to evaluate the accuracy of rheological models based on molecular considerations [58]. Since the goals in the implementation of the latter type of models may include the synthesis or design of polymeric materials with tailor-made processing properties [58, 59], their verification or improvement is of significant importance.

22.5.3 A CFD Perspective on Polymer Rheology

In CFD problems, the geometry of a physical system is subdivided into small elements, and discretized versions of the governing differential equations describing the physics of the system are applied to such elements. The discretized forms of the differential equations may be obtained, for instance, by means of Taylor series. The goal of CFD simulations is the determination of field variables in the physical geometry of interest. Two numerical methods widely used in this type of simulations are the finite element method (FEM) and the finite volume method (FVM).

A practical application of polymer rheology is the implementation of rheological models in CFD simulations to address different polymer flow problems. The simulation of a flow situation, in the case of processing operations, for example, the flow within an extruder, may present some geometrical challenges. In some cases, some considerations to simplify the complexity of the flow problem to provide reasonable good engineering predictions without involving the use of CFD techniques can be implemented. On the other hand, in some cases, especially those dealing with complex flow geometries, the flow can only be adequately described by using CFD algorithms. In the following, a brief overview focused on the application of CFD simulations in addressing polymer flows is presented.

A convenient way of determining the deformations experienced by fluid elements, in a particular flow situation, is the use of the Lagrangian reference frame. In such reference frame, the position of a material element is described as a function of time and the initial position of the material element, as indicated in Equation 22.24. From the latter equation, the deformation tensor, which, as stated by Ottino [60], is the basic measure of deformation with respect to the reference configuration, \mathbf{X} , can be obtained. The relationship between \mathbf{x} , \mathbf{X} , and the deformation tensor has been written as Equation 22.25. In general, the solution of the flow field is determined numerically and, then, the deformation tensor can be calculated as the fluid element

travels through the flow field. To perform such calculation, numerical techniques for solving differential equations are used [61]. Note here that, in general, in CFD simulations, the latter statement refers to the evaluation of the flow field by means of say FEM or FVM software:

$$\mathbf{x} = \mathbf{x}(\mathbf{X}, t) \quad (22.24)$$

Here, \mathbf{x} is the position of a material element at a time t and \mathbf{X} is the initial position of the material element.

$$\begin{aligned} \mathbf{F} &= (\nabla_x \mathbf{x})^T \\ F_{ij} &= \left(\frac{\partial x_i}{\partial X_j} \right) \end{aligned} \quad (22.25)$$

Where \mathbf{F} is the deformation tensor, and ∇_x indicates differentiation with respect to \mathbf{X} .

With the use of CFD algorithms, once the flow field has been determined, some other important characteristics of a flow system, for instance, an evaluation of distributive mixing, can be performed, as indicated by the following equations:

$$\eta = \lim_{|dA| \rightarrow 0} \left(\frac{|da|}{|dA|} \right) \quad (22.26)$$

$$\eta = (\det \mathbf{F}) (\mathbf{C}^{-1} \mathbf{N} \mathbf{N})^{1/2} \quad (22.27)$$

where η stands for the area stretch ratio; $\mathbf{C} \equiv (\mathbf{F}^T \cdot \mathbf{F})$ is the Cauchy–Green tensor; and \mathbf{M} and \mathbf{N} (the orientation vectors) are defined by

$$\mathbf{M} \equiv \frac{d\mathbf{X}}{|d\mathbf{X}|} \quad \mathbf{N} \equiv \frac{d\mathbf{A}}{|d\mathbf{A}|}$$

Some other predictions such as the amount of dissipated energy of the system, residence time distributions, and indications of dispersive mixing can be obtained from similar calculation procedures to those previously addressed.

In flow systems analyzed by means of CFD, other relevant information can be obtained from numerical visualization experiments. In this type of experiments, for instance, a number of particles can be seeded at a particular position of the flow geometry and their position is tracked as a function of time. Particle tracking has been used to analyze the transient behavior (time periodic flow) taking place in the screw elements of corotating intermeshing twin screw extruders. In particle tracking analysis, the path of specific particles is obtained by integrating the Eulerian velocity field according to the relationship given in the following equation [62, 63]:

$$\mathbf{X}(t) = \mathbf{X}(t_0) + \int_{t_0}^t \mathbf{V}(t) dt \quad (22.28)$$

Here, $\mathbf{X}(t)$ and $\mathbf{X}(t_0)$ are the positions of a particle \mathbf{X} at times t and t_0 , respectively, and $\mathbf{V}(t)$ is the velocity vector of the particle.

A schematic representation of the tracking of color particles is shown in Figure 22.10. The flow situation being described in this figure corresponds to the flow in fully filled conveying elements of a corotating intermeshing twin screw extruder. In essence, what happens in the depicted flow problem is that a polymeric flow takes place in

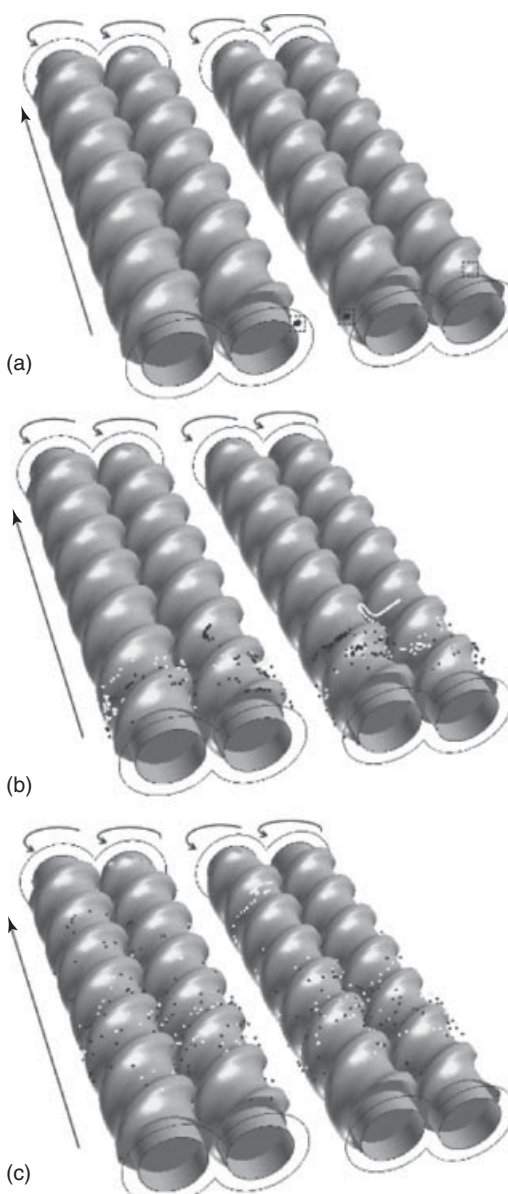


Figure 22.10 (a) Initial position of around 400 black and 400 white particles located in rectangular boxes near the entrance of the screw elements and their positions after (b) 2.5 and (c) 7.5 screw revolutions for a screw speed of 100 rev/min. The rotation and flow directions are indicated by the arrows.

the indicated screw elements due to the corotating action (rotation in the same direction) of the shafts of a twin screw extruder. In the discussion below, only a few of the conditions for the flow problem presented in Figure 22.10 are addressed. A more detailed description of this flow problem is discussed in the work by Ortiz-Rodriguez [64]. For the screw elements depicted in Figure 22.10, black and white particles were seeded on imaginary two-dimensional boxes near the entrance to the flow geometry. The corresponding CFD simulations were performed by means of the commercial FEM based software POLYFLOW®. To have a better perspective of the visualization experiment shown in Figure 22.10, the same screw elements are presented twice with a 180° rotation along the coordinate axis parallel to screws axes. In this case, isothermal Newtonian flow conditions were used for the simulations. The use of nonisothermal non-Newtonian flow conditions is also possible with commercial CFD software, but the computational time is greatly increased with respect to the Newtonian case, because the momentum equations become highly nonlinear due to the non-Newtonian viscosity used in the GNF model.

REFERENCES

1. Odian G. *Principles of Polymerization*. 4th ed. New York: Wiley-Interscience; 2004.
2. Marrucci G. *J Phys Condens Matter* 1994;6:A305–A309.
3. Bird RB, Curtiss CF. *Phys Today* 1984;36.
4. Racine R, Bogue DC. *J Rheol* 1979;23:263.
5. Meissner J. *Pure Appl Chem* 1984;56:369.
6. Nakajima N. *J Elastom Plast* 2000;32:46.
7. Hatzikiriacos SG, Migler KB. *Polymer Processing Instabilities: Control and Understanding*. New York: Marcel Dekker; 2005.
8. Aris R. *Vectors, Tensors, and the Basic Equations of Fluid Mechanics*. New York: Dover Publications Inc.; 1989.
9. Macosko CW. *Rheology: Principles, Measurements and Applications*. New York: Wiley-VCH; 1994.
10. Dealy JM, Wissbrun KF. *Rheometers for Molten Plastics: A Practical Guide to Testing and Property Measurement*. New York: Van Nostrand Reinhold; 1982.
11. Spencer AJM. *Continuum Mechanics*. New York: Dover Publications Inc.; 2004.
12. Bird RB, Stewart WE, Lightfoot EN. *Transport Phenomena*. 2nd ed. New York: Wiley; 2007.
13. Han CD. *Rheology and Processing of Polymeric Materials: Volume 1: Polymer Rheology*. New York: Oxford University Press; 2007.
14. Lakdawala K, Salovey R. *Polym Eng Sci* 1987;27:1035.
15. Michaeli W. *Extrusion Dies for Plastics and Rubber*. 3rd ed. Munich: Hanser; 2003.
16. Lenk RS. *Polymer Rheology*. London: Applied Science Publishers Ltd.; 1978.
17. Liu X, Xie M, Li H. *J Appl Polym Sci* 1824;2005:96.
18. King JA, Via MD, Keith JM, Morrison FA. *J Compos Mater* 2009;43:3073.
19. Shenoy AV, Saini DR, Nadkarni VM. *Polymer* 1983;24:722.
20. Shenoy AV, Chattopadhyay S, Nadkarni VM. *Rheol Acta* 1983;22:90.
21. Saini DR, Shenoy AV. *J Elastom Plast* 1985;17:189.
22. Mezger TG. *The Rheology Handbook: For Users of Rotational and Oscillatory Rheometers*. 2nd ed. Hannover: Vincentz Network GmbH & Co KG; 2006.
23. Driscoll PD, Bogue DC. *J Appl Polym Sci* 1990;39:1755.
24. Williams ML, Landel RF, Ferry JD. *J Am Chem Soc* 1955;77:3701.
25. Fuller GE. *Optical Rheometry of Complex Fluids*. New York: Oxford University Press; 1995.
26. Ylitalo CM, Kornfield JA, Fuller GG, Pearson DS. *Macromolecules* 1991;24:749.
27. Malkin AY. *Polym Sci Ser A* 2009;51:80.
28. Lavallée C, Berker A. *J Rheol* 1997;41:851.
29. Kunamaneni S, Buzzia DMA, Parker D, Feast WJ. *J Mater Chem* 2003;13:2749.
30. Borg T, Pääkkönen EJ. Proceedings of the XIVth International Congress on Rheology; The Korean Society of Rheology, Korea; 2004.
31. Mavridis H, Shroff R. *J Appl Polym Sci* 1993;49:299.
32. Kiparissides C, Pladis P, Moen Ø. From Polyethylene Rheology Curves to Molecular Weight Distributions. In: Laso M, Perpète EA, editors. *Multiscale Modelling of Polymer Properties, Computer-Aided Chemical Engineering*. Volume 22. Amsterdam: Elsevier; 2006.
33. Bird RB, Armstrong RC, Hassager O. *Dynamics of Polymeric Liquids, Volume I, Fluid Mechanics*. New York: Wiley; 1977.
34. Larson RG. *Constitutive Equations for Polymer Melts and Solutions*. Boston: Butterworths; 1988.
35. Nassehi V. *Practical Aspects of Finite Element Modeling of Polymer Processing*. West Sussex: Wiley; 2002.
36. Tadmor Z, Gogos CG. *Principles of Polymer Processing*. Hoboken: Wiley-Interscience; 2006.
37. Bird RB, Armstrong RC, Hassager O, Curtiss CF. *Dynamics of Polymeric Liquids, Volume II, Kinetic Theory*. New York: Wiley; 1977.
38. McLeish TCB, Larson RC. *J Rheol* 1998;42:8.
39. Tzoganakis C, Vlachopoulos J, Hamielec AE. *Int Polym Proc* 1988;3:141.
40. Zhu L, Narh KA, Hyun KS. *Int J Heat Mass Tran* 2005;48:3411.
41. Yasuda P, Armstrong RC, Cohen RE. *Rheol Acta* 1981;20:163.
42. Shaw MT, MacNight WJ. *Introduction to Polymer Viscoelasticity*. 3rd ed. Hoboken: Wiley; 2005.
43. Mitsoulis E, Hatzikiriacos SG. *Rheol Acta* 2003;42:309.
44. Mitsoulis E. *Comput Meth Mater Sci* 2010;10(3):1.
45. Eberle APR, Baird DG, Wapperom P. *Ind Eng Chem Res* 2008;37(10):3470.

46. Chan Y, White JL, Oyanagi Y. *Polym Eng Sci* 1978;18:268.
47. Hsich HS-Y. *J Mater Sci* 1982;17:438.
48. Kairn T, Davis PJ, Ivanov I, Bhattacharya N. *J Chem Phys* 2005;123:194905.
49. Kabanemi KK, Hétu J-F. *J Non-Newtonian Fluid Mech* 2010;165:866.
50. Shenoy AV. *Rheology of Filled Polymer Systems*. Dordrecht: Kluwer Academic Publishers; 1999.
51. Harmandaris VA, Mavrantzas VG, Theodorou DN. *Macromolecules* 1998;31:7934.
52. Yamamoto R, Onuki A. *J Chem Phys* 2002;117:2359.
53. Hung FR, Gubbins KE, Franzen S. *Chem Eng Ed* 2004;38:242.
54. Laso M, Muneta LM, Müller M, Alcazar V, Chinesta F, Ammar A. Hierarchical approach to flow calculations for polymeric liquid crystals. In: Laso M, Perpète EA, editors. *Multiscale Modelling of Polymer Properties, Computer-Aided Chemical Engineering*. Volume 22. Amsterdam: Elsevier; 2006.
55. De S, Fish J, Shephard MS, Kebinski P, Kumar SK. *Phys Rev E Rapid Communication* 2006;74:030801(R).
56. Wood BD. *Chem Eng Ed* 2009;43:29.
57. Khare R, de Pablo JJ, Yethiraj A. *Macromolecules* 1996; 29:7910.
58. Larson RG, Zhu Q, Shanbhag S, Park SJ. *AIChE J* 2007;53:542.
59. Leonardi F, Derail C, Marin G. *J Non-Newtonian Fluid Mech* 2005;128:50.
60. Ottino JM. *The Kinematics of Mixing: Stretching, Chaos, and Transport*. Cambridge: Cambridge University Press; 1989.
61. Bigio DI, Conner JH. *Polym Eng Sci* 1995;35:1527.
62. Yao C-H, Manas-Zloczower I. *Int Polym Proc* 1997;12:92.
63. Bravo VL, Hrymak AN, Wright D. *Polym Eng Sci* 2004;44:779.
64. E. Ortiz-Rodriguez. Numerical simulations of reactive extrusion in twin screw extruders [PhD Dissertation]. Ontario: University of Waterloo; 2009.

23

PRINCIPLES OF POLYMER PROCESSING

LUIS F. RAMOS-DE VALLE

23.1 GENERAL

Most polymeric raw materials are available in the solid state as granules, flakes, or powders. Solid raw materials have to be transformed into a fluid or plastic state, which is accomplished by heating. Once in the plastic or fluid state, the material is shaped, after which the resulting shape is fixed by cooling (thermoplastics), or by a chemical reaction (thermosets). During processing, heat is supplied either from the outside, via electric heaters (extrusion or injection molding), infrared (IR) radiation (thermoforming), or direct flame (rotomolding), or generated by internal friction as the polymer mass is transported along the machine, first in the solid state and eventually in the highly viscous liquid state (extrusion or injection molding).

Two important polymer characteristics that affect processing are their low thermal conductivity, either in the solid or in the fluid state and their very high viscosity in the fluid state.

The low thermal conductivity makes heating and eventually cooling slow processes.

The high viscosity makes processing to require of powerful machines, capable of pumping a fluid (e.g., molten polyethylene at 180 °C) that is circa 1 million times more viscous than water; $[\eta]_{\text{water at } 20^\circ\text{C}} \sim 1 \text{ mPa s}$ vs $[\eta]_{\text{PE at } 180^\circ\text{C}} \sim 1 \text{ kPa s}$.

With respect to viscosity, it decreases with increasing temperature (Fig. 23.1). But in addition, considering that molten polymers are shear-thinning non-Newtonian fluids, their viscosity decreases with increasing shear rate, that is, increases the flow rate [1–3] (see Fig. 23.2).

Notwithstanding this fact, high pressures are required to transport the fluid mass through the transport channels or into the mold of a processing machine with an acceptable speed. Pressure levels of 50–150 MPa (500–1500 bars) are normal, so the machines have to be very robust.

The choice of the process depends, *inter alia*, on the requirements of the end product; with injection molding, narrower tolerances can be achieved than with thermoforming or rotomolding, for example. The nature of the polymer also plays a role; it depends, for instance, on the stability of the polymer at the high temperatures in a process. The length of the rubbery region on the temperature scale determines the ease of vacuum forming; too brittle a polymer is difficult to machine, for example.

A very important factor in the choice of a process is the *economy*. The manufacturing costs of the various processing techniques are very different and are strongly dependent on the number of articles to be made.

23.2 COMPOUNDING

Before the actual forming process, often the raw material has to be compounded, that is, blended with a number of other components.

To obtain a better dispersion, a blending process in the fluid state is necessary. To achieve this, various types of mixing devices are available, such as internal mixers and mixing extruders [4–8].

Internal mixers, such as the *Banbury* mixer (Fig. 23.3), and the laboratory *Brabender* or *Haake* mixers contain two connecting chambers, in which blades rotate in opposite directions with a narrow clearance to the walls, resulting

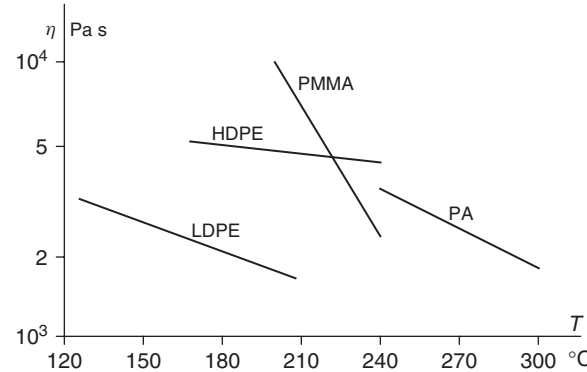


Figure 23.1 Melt viscosity as a function of temperature.

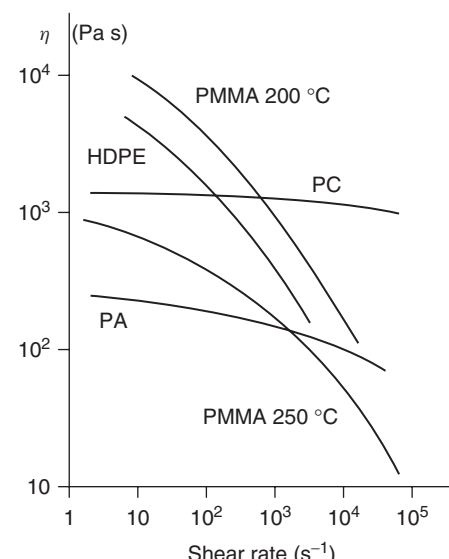


Figure 23.2 Melt viscosity as a function of shear rate.

in high shear rates. The chamber walls can be cooled or heated. After mixing, the material is removed from the chambers, milled into a sheet, and cut into ribbons or granulated for storage or further processing.

The other type of compounding device is the extruder. In addition to its use in fabrication, it is also used as a mixer. In essence, it is a screw pump in which the mass to be mixed is transported in a heated cylinder by a screw or, with twin-screw extruders, by two parallel screws. During this transport, melting and intensive mixing take place. At the end of the screw, the blend is forced through a die with a number of holes to produce spaghetti-like ribbons, which are then cooled down and cut into granules.

Most manufacturers of end products do not make the compounds by themselves but obtain them from the material supplier. In the bigger industries, compounding is sometimes carried out in-house, with the advantages

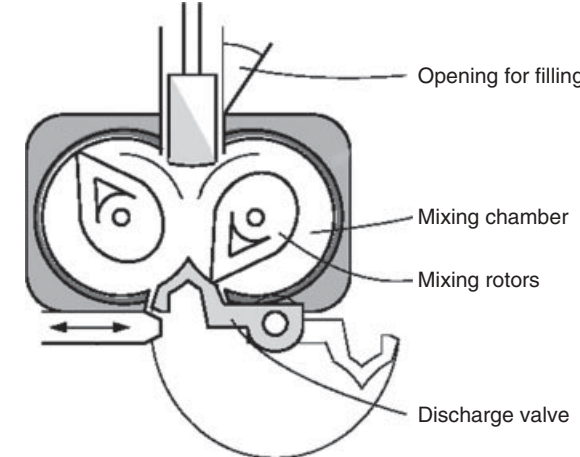


Figure 23.3 Simple sketch of a Banbury mixer.

of economy and of flexibility to tune their products to reach the best compromise of processability on the machines available and the desired properties of the end product.

23.3 EXTRUSION

The extruder is schematically represented in Figure 23.4. Its most essential part is the screw, which fits in a cylinder, provided with heating elements and cooling channels, so that a desired temperature profile can be established. At one end of the screw, there is the feed section for the raw material supply and, at the other end, the molten polymeric compound leaves the machine via the forming die [9–11].

In *extrusion*, the material is heated, molten, pressurized, and forced through a die, all along one and the same screw.

The controlling geometric parameters that characterize the extruder are the screw diameter D and the length to diameter ratio L/D . Extruders are categorized according to diameter, from which the output and the power demand for a given rotating speed of the screw are derived.

The diameters in use fall in the range of 2.5–30 cm, but most fall in the range of 5–15 cm. The ratio of the length to the diameter L/D is ~24, but has been moving to larger values (longer screws) of 36–42 in order to improve melt homogeneity.

The screw performs the following tasks:

- transport of raw material (granules, flakes, or powder);
- melting and thereby increasing the apparent density;
- mixing and homogenizing the polymer;
- pumping of the molten polymeric compound to the die and generating sufficient pressure to pass through the die.

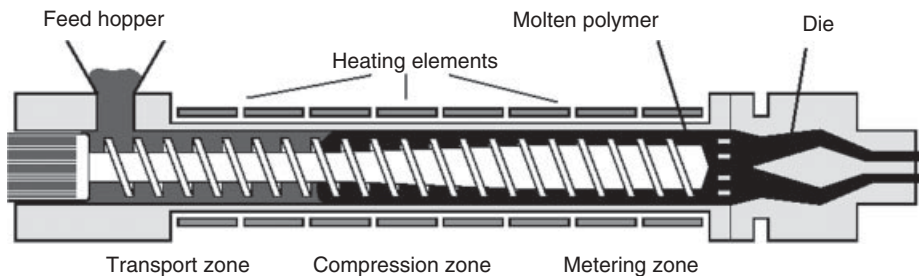


Figure 23.4 Simplified diagram of an extruder.

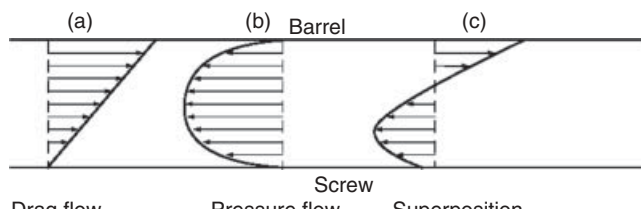


Figure 23.5 Velocity distribution in the screw channel of an extruder.

Each polymer has its own demands in relation to the granule size, L/D ratio, compression ratio,¹ melting behavior, risks of degradation, etc.

In the final part of the screw, where the fluid consists entirely of the molten polymer, the forward flow occurs as a result of the drag of a moving surface in contact with the molten polymer, and this can be visualized most easily by first imagining the screw at rest in a rotating cylinder and then unrolling the screw channel into a straight channel with a rectangular cross section. The cylinder wall then forms a lid on the channel, moving at a certain angle. Assuming the end of the channel is open, a velocity distribution along the direction of the channel would occur as depicted in Figure 23.5a. That is, $V = 0$ at the bottom of the channel, and $V = U$ (the component of the cylinder speed in the length direction).

But with a flow restriction at the end of the channel (the die), a backpressure P is built up. This will produce a backward flow along the last part of the screw channel as a result of the difference in pressure ΔP between the final part of the screw (high P) and the initial part of the screw (low P). This backward pressure flow would look as depicted in Figure 23.5b.

The combination of these two distributions is depicted in Figure 23.5c; a net flow results that governs the volumetric flow of the extruder. This flow Q can be estimated as follows: The drag flow to the right, Q_d , is proportional to

¹Compression ratio = H/h , where H is the channel depth in the first, deepest, part of the screw and h is the channel depth in the last, shallowest, part of the screw.

the velocity V , that is, the rpm of the screw N , and is also dependent on the geometry of the screw channel, but not on the viscosity of the melt. So

$$Q_d = aN \quad (23.1)$$

The pressure flow in the opposite direction, Q_p , is proportional to the pressure P , inversely proportional to the viscosity η , and, again, dependent on the screw geometry. So

$$Q_p = b\Delta P/\eta \quad (23.2)$$

The net flow $Q = Q_d - Q_p$ is

$$Q = aN - b\Delta P/\eta \quad (23.3)$$

(which represents a straight line with a negative slope).

The flow through the die (after the tip of the screw) is solely dependent on the high pressure at the entrance of the die and the low pressure at the die exit (circa 1 bar).

The flow through the die would then be

$$Q_p = c\Delta P/\eta \quad (23.4)$$

(which represents a straight line with a positive slope and intersection at the origin).

A plot of the flow Q as a function of the pressure P is given in Figure 23.6. For a given screw geometry, the first equation, the screw characteristic, is given for two values of the rpm N , while the second equation, the die characteristic, is shown for two levels of the flow resistance in the die, $1/c$. Each combination gives rise to an intersection of the two lines, which is the working point of the extruder, from which the values of Q and P can be read.

In other words, the flow rate for a given screw/die combination is proportional to the rpm of the screw and independent of the pressure and viscosity. This treatment is valid only for a Newtonian fluid. In reality, polymers deviate from this simplified picture, though the general conclusions are not affected.

Besides the single-screw extruder (SSE), there is the twin-screw extruder (TSE), that is, two parallel screws rotating within the same cylindrical housing [8].

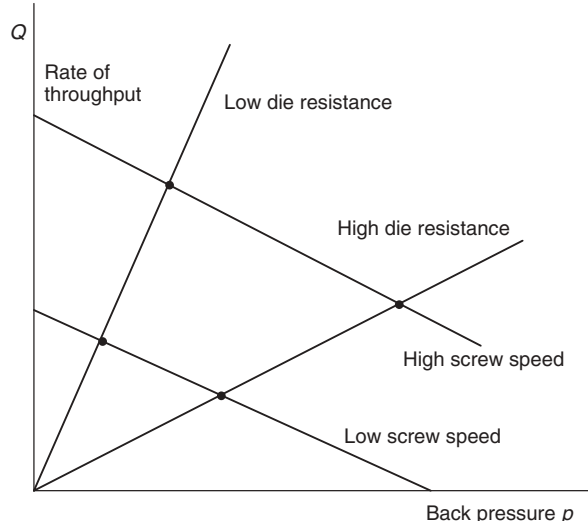


Figure 23.6 Variation of throughput versus backpressure at different rpms and die resistance.

TSE can either be **corotating**, that is, both screws rotating in the same direction, or **counter-rotating**, that is, each rotating in opposite directions.

In addition, TSE can either be **intermeshing** (Fig. 23.7), when the interaxis (I) is less than the sum of the radii of the two screws, that is, when the flights of one screw penetrate into the channel of the other screw and vice versa; or **nonintermeshing**, when the interaxis is equal to the sum of the radii of the two screws, that is, when the tip of the flights of one screw just touches the tip of the flights of the other screw.

In this respect, a high level of intermeshing will produce the maximum positive pumping action but minimum mixing and homogenizing. On the contrary, a low level of intermeshing will produce a diminished pumping action but a much better mixing and homogenization.

The mixing and homogenizing capacity of TSE is much greater than that of a SSE. They are preferred in the compounding industry.

The range of products that can be made by extrusion is very large: rods, pipes, hoses, sheets, films, profiles, filaments and fibers, wire coatings, etc.

Filaments and rods can be formed quite easily by using a die with a circular orifice.

Pipes and hoses require an annular orifice. After leaving the die, while still hot and malleable, the pipe/hose is fed into a calibrator (which is a cylinder with an inner diameter identical to the required pipe/hose outside diameter) in which, either by internal pressure or by vacuum suction, the pipe/hose is pressed against the highly polished inside surface of the calibrator.

Sheet extrusion requires a broad, slit die, in which an even distribution of the flowing polymer along its width

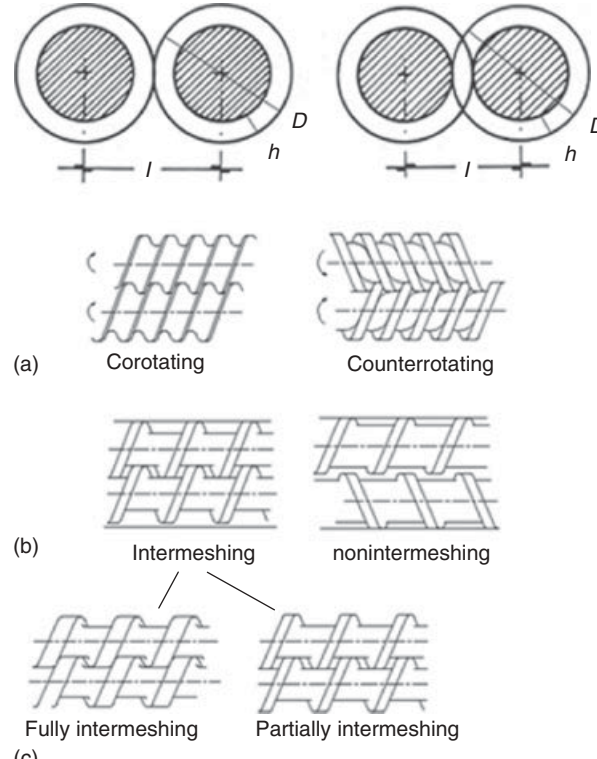


Figure 23.7 Simplified diagrams of twin-screw extruder configurations. I = interaxis = separation (distance) between the screw axes; D = screw diameters; h = screw channel depth.

and an equal flow resistance at each point has to be taken care of. Sheets are being extruded up to a width of 3–4 m and up to 3 cm thickness. If desired, sheets can be produced with a wave shape by passing the still-malleable extrudate between two profiled rolls.

Film extrusion can be done in a similar way, with a narrower die gap. After extrusion, sheets and films are cooled in a water bath or on polished cooling rolls.

Another application of extrusion is the coating of metal wires or profiles with a plastic layer. This is done on a large scale in the manufacture of electric wires and cables. For this purpose, a cross-head die is needed (Fig. 23.8). The same principle is used for plastic profiles containing a metal core.

An alternative way of producing a film is by the **blown film** process. An annular die is used from which the material emerges as a thin-walled tube, which is immediately blown up by internal pressure to a much larger diameter (Fig. 23.9).

The tubular film thus formed is laid flat and reeled, and can, by cutting and welding, easily be formed into plastic bags.

Coextrusion is a process variant in which two or more extruders feed a single die. A laminar flow of two or more

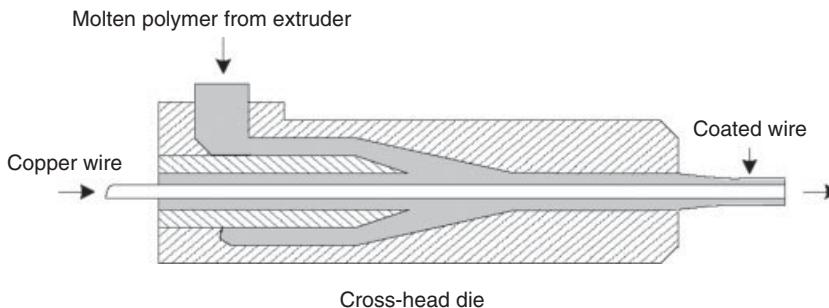


Figure 23.8 Wire coating.

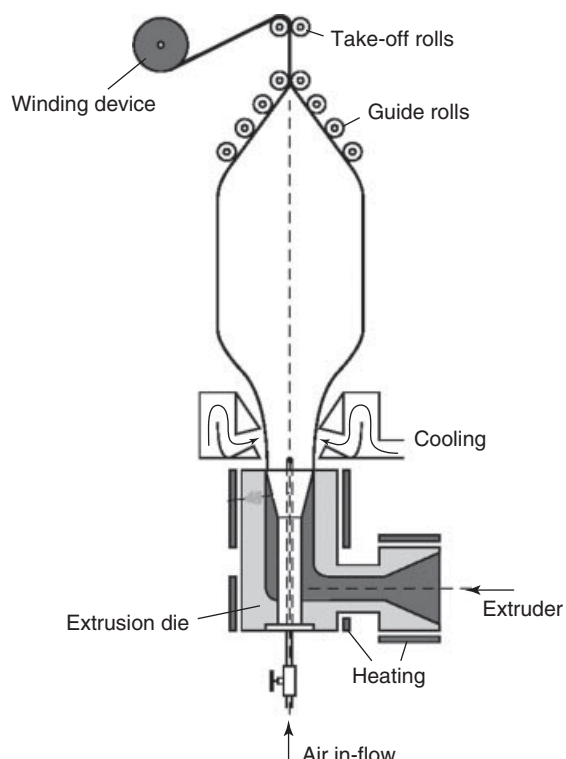


Figure 23.9 Film blowing.

adjacent polymer currents flow through the die to produce a multilayer film or laminate, for example, or a multilayer rod or pipe. Multilayer products can be composed of different polymers. For each polymer, a separate extruder is used.

A laminated film can be made by coextrusion, for example, in which one of the layers provides the strength, another acts as a gas barrier, and yet other layers promote adhesion, etc.

23.4 BOTTLE BLOWING

Blowing of *hollow articles* such as bottles and containers can be carried out online with the extrusion process.

A thermoplastic tube emerging from the extruder die is, while still malleable, blown up against the inside of a mold comprising two halves, the walls of which are cooled [12, 13]. The neck of the bottle is calibrated with the aid of a mandrel and the bottom is sealed by the mold parts. The principle is indicated in Figure 23.10. Since the cooling time largely governs the cycle time, a series of moving molds are used. When the bottle has cooled down sufficiently, the mold is opened and moved back to the extruder to be filled again.

The blowing process, though simple, has a few disadvantages: the wall thickness is uneven and the weld at the bottom is deformed. These drawbacks are partly taken care of by a variant of the process, that is, the injection-molding blowing process. Here, a preform is made by injection molding, comparable to the extruded portion, but now more adjusted to the ultimate shape of the bottle. This preform is transported to a second part of the mold, in which it is blown up under pressure.

When using poly (ethyleneterephthalate) PET, the preform is injection molded and rapidly cooled in the mold so that it remains amorphous (PET crystallizes very slowly). By heating it above its T_g (65°C), it passes into the rubbery state and can then be blown up and, simultaneously, longitudinally stretched. The biaxial orientation thus obtained accelerates the crystallization and, at the same time, results in a very fine crystalline texture so that a thin-walled, strong, transparent, and heat-resistant bottle is obtained.

23.5 INJECTION MOLDING

Injection molding is the most used technique for manufacturing end products directly from a thermoplastic raw material. In this process, articles are formed by injecting the molten polymer into a mold. This method is also used on rubbers and thermosets, though in these cases the mold is heated rather than cooled in order to promote the vulcanization or curing reaction [14–16].

Here, the material is heated by heat transfer from the cylinder wall as well as by internal friction. The material

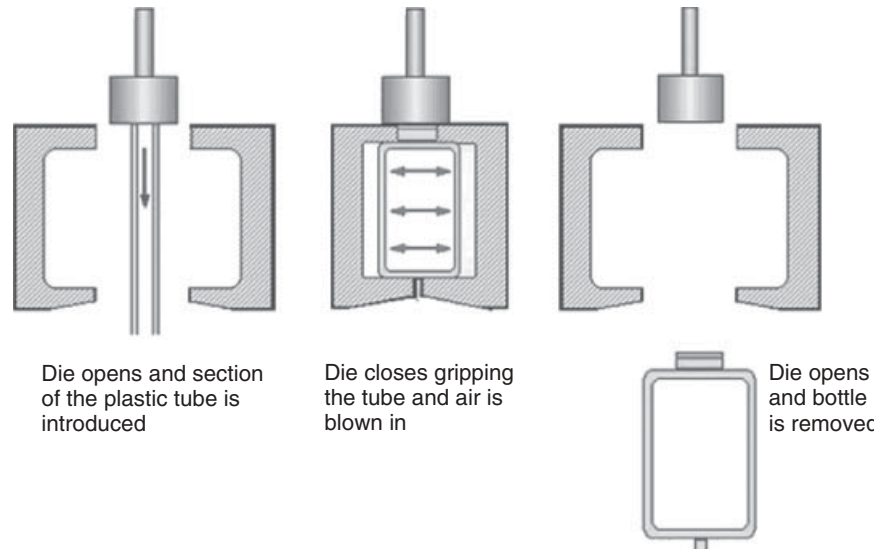


Figure 23.10 Bottle blowing.

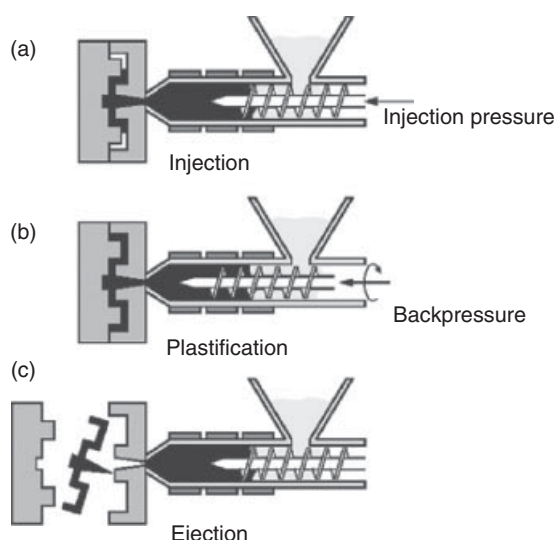


Figure 23.11 Reciprocating-screw injection-molding machine.

is transported and homogenized by an extrusion screw and, after reaching the screw tip, is injected into the mold at a very high pressure (sometimes up to 1500 bar) by the same screw, which now acts as a plunger (Fig. 23.11a). After the mold is filled, the transport channel is closed; the screw continues rotating, but now it transports the molten material to the front side while itself moving backwards (Fig. 23.11b). This takes place while the polymer in the mold cools down sufficiently to be demolded (Fig. 23.11c). In the mold, the product cools down under pressure. After complete solidification, the mold is opened and the product is ejected from it (Fig. 23.11c). The high injection pressure would push away the backside of the mold if this is not

be pressed against the front side by a closing force, which has to be very high, for instance, for small machines 10–50 tons (100–500 kN) and for very big machines up to 10,000 tons (100,000 kN).

The *mold* is a very complicated tool. It comprises two halves: a fixed half attached to the stationary platen and a moving half attached to the moving platen. With complicated shapes, or with long flow paths, injection has to take place at several points. For the transport of the melt to these injection points, channels are present that are mostly heated ("hot runners") in order to prevent cooling of the melt before it enters the cavity. The mold cavity is surrounded by thick metal walls through which cooling channels run (with rubbers and thermosets, these channels are used for heating). The mold contains an ejection mechanism to remove the molding after opening.

The melt should be present at the appropriate temperature and pressure at each injection point to enable the desired flow pattern in the cavity. Unwanted phenomena such as poor welding lines, frozen-in orientations, or cooling stresses should be avoided.

The mold is kept closed during injection by a heavy hydraulically controlled closing mechanism. The magnitude of the required forces can be estimated as follows: With an injection pressure of, for example, 1000 bars, the pressure in the mold may, on average, amount to one-third of this value, say 300 bars. When the projected area of the mold is 500 cm², the maximum closing force is 1500 kN (150 tons). The size of an injection-molding machine is often characterized by its closing force; for smaller machines, this amounts, for example, to 200 kN, and for bigger ones 3000 kN and even up to 100,000 kN.

23.5.1 Limitations

A first requirement for a good injection-molding process is, of course, that the mold be completely filled. The pressure at which the molten polymer is injected should be sufficient not only to transport the melt through the injection channels at the desired speed but also to continue this transport within the mold through narrow channels with cooled walls. During this transport, the melt is cooled, so that the viscosity increases. Eventually, it solidifies, starting from the walls. If solidification has proceeded through the whole cross section of the channel, then further flow is impossible and incomplete molding results. The dimensions of the end product are limited by this phenomenon; the flow path, that is, the ratio of the maximum distance over which the melt is able to flow and the thickness of the channel, has an upper value. A practical rule of thumb is that, for well-flowing materials this ratio should not exceed about 300. When the length to diameter ratio of the object to be formed is higher, or when the polymer flows less well, then the solution could be to increase the number of injection points.

When the injection pressure is too high to be withstood by the closing mechanism of the mold, the mold halves will be pushed apart, allowing a small quantity of the melt to escape, which results in a very thin extension of the product ("flash"). At higher temperatures, that is, with lower viscosities, flash occurs at lower injection pressures as a result of better pressure transfer.

23.5.2 Defects

Shrinkage during solidification always tends to reduce the dimensions to values lower than those of the mold. The magnitude of this shrinkage is shown in Figure 23.12. It appears that for amorphous polymers a reduction in volume of circa 10% occurs when the polymer is cooled from the processing temperature to the ambient; for crystalline polymers, this reduction may amount to 20–25% (Fig. 23.12).

However, cooling and solidification take place under pressure; that is, the melt is compressed and, as a consequence, has undergone a decrease in volume because of its compressibility (Fig. 23.13). This compressibility facilitates the forced introduction of an additional small amount of polymer which will be able to compensate part of the normal shrinkage that occurs as a result of cooling and solidification and, in such a case, because of crystallization.

Figure 23.14 presents the relation between the volume and temperature at several pressure levels, showing the competition between compressibility and shrinkage for amorphous and semicrystalline polymers. These figures are valid for a certain rate of cooling. The effect of cooling rate and pressure are of importance. Higher pressures

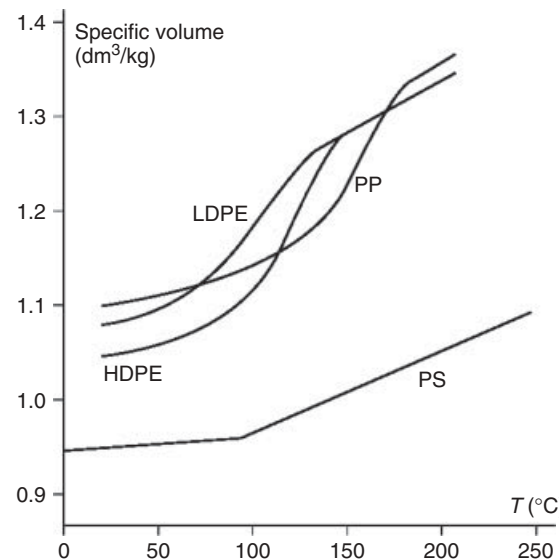


Figure 23.12 Relation between specific volume and temperature (no pressure applied).

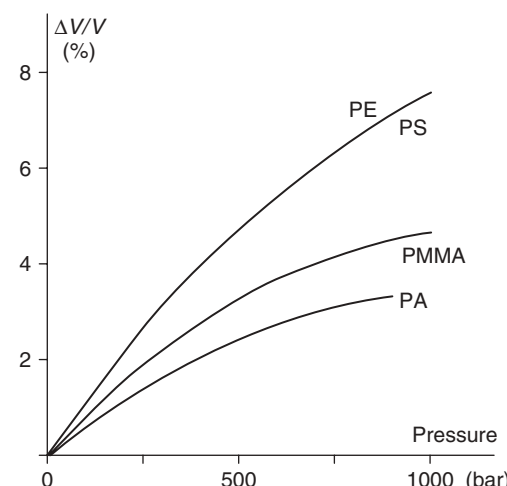


Figure 23.13 Compressibility of molten polymers.

increase the glass transition temperature (T_g) as well as the crystallization temperature (T_c).

Further reduction of shrinkage in injection molding is reached by maintaining the injection pressure for some time on the mold cavity, the so-called afterpressure. While the outer layers solidify and shrink, an extra amount of melt is pressed into the cavity, which further reduces the final overall shrinkage (Fig. 23.15). A rapid decrease in pressure down to zero (i) indicates a considerable final shrinkage when the end-pressure is high, and (ii) the afterpressure has been too high or applied for too long; the shrinkage is negative and the molding will be tightly clamped in the mold. The ultimate shrinkage is, for amorphous polymers,

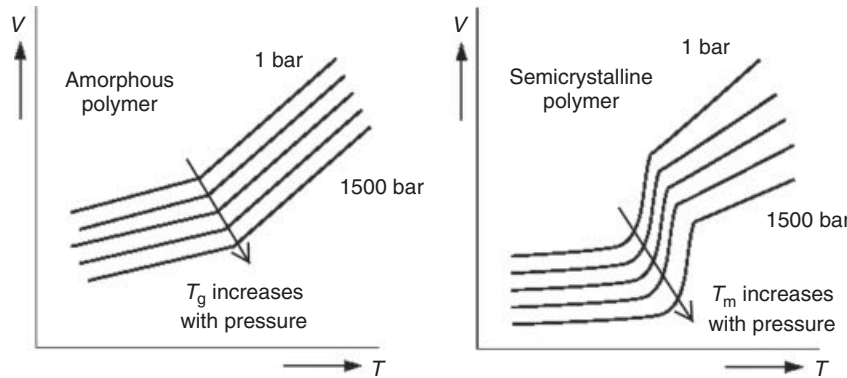


Figure 23.14 p, V, T diagrams for an amorphous and a semicrystalline polymer.

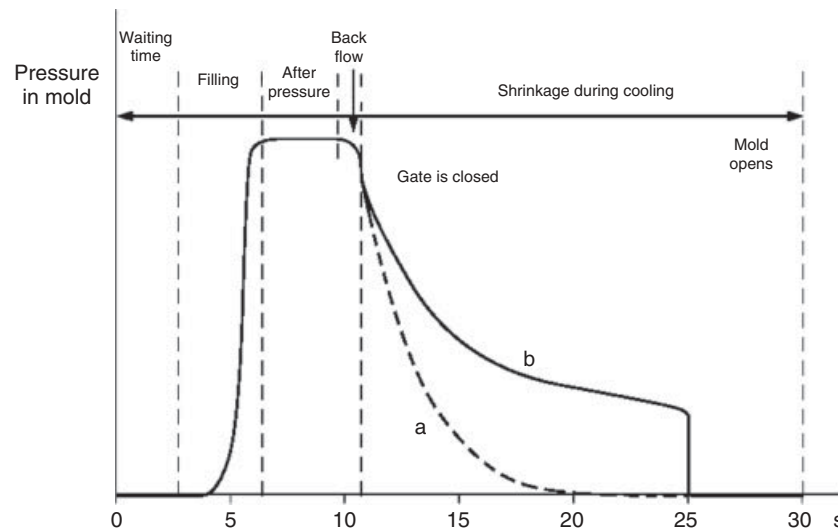


Figure 23.15 Variation of pressure within the mold during the molding cycle.

mostly between 0.3% and 0.7% and for semicrystalline polymers between 1% and 3%.

The shrinkage may vary from place to place depending on the rate of solidification. The simplest example is a solid block that solidifies rapidly on the outside; the hard skin formed this way prevents further shrinkage of the inner part. This results in internal stresses which may lead to tearing and void formation.

Another source of uneven shrinkage is a thickness difference in the molding. A thicker part cools more slowly and attains a higher density than a thin part. These shrinkage differences may give rise to warping of the molding. Also, at the opposite sides of a thicker part, sink marks may occur as a result of a higher local shrinkage.

Shrinkage may also be anisotropic, for example, when chain orientation is present. This orientation is found in parts where the melt has been rapidly cooled under a high rate of strain. Shrinkage is higher in the orientation direction than across, so that, for instance, a flat disk injected from its center tends to deform into a saddle-like shape (warping).

The choice of the polymer plays a role, for instance, in the chain length and distribution, in orientations, and in the various process variables (injection pressure and temperature, afterpressure, mold temperature).

23.5.3 Rotational Molding

Molding of hollow articles is possible by rotation. Rotation about two perpendicular axes enables the formation of a hollow article (Fig. 23.16).

The starting material in these process is not necessarily in the liquid state; also polyvinyl chloride (PVC) pastes (plastisols) can be used, as well as even a well-flowing thermoplastic powder [17]. The particles will melt when in contact with the heated wall and will form a compact layer of material. The softened powder sticks to the wall, and other particles gradually complete the shaping process. Only the outer surface of an article made this way will be smooth, which is not objectionable for many applications.

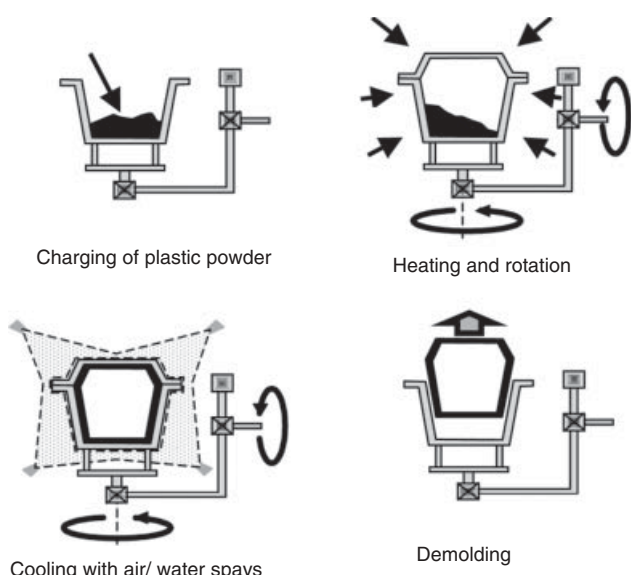


Figure 23.16 Rotational molding with two rotating axes.

This method is eminently suited for the manufacture of large objects such as containers and also nonclosed articles such as furniture, dashboard, etc. The material thickness in these articles varies between 1.5 and 15 mm, depending on the type of article.

Wall thickness fluctuations of up to 5% may occur as a result of the uneven temperature in the molten polymer during rotation. Also, because of rate of cooling which is not always reproducible, deviations in the dimensions of the finished product may amount to 5%. Requirements for this process are that the material can be molten completely, that the melt is of sufficiently low viscosity, and that the molten polymer does not degrade too rapidly. Besides plasticized PVC, high and low density polyethylene (HDPE and LDPE) are often used, as well as copolymers of PE such as EVA (ethylene-vinyl acetate). Cycle times vary between 3 and 40 min, depending on the wall thickness. Cycle time is predominantly controlled by the heating and cooling time.

A very promising development is the combination of the *in situ polymerization* mentioned earlier with the principle of rotational molding. This method is, in particular, used for the manufacture of large-sized polyamide-6 articles, starting with caprolactam. The big advantage compared with centrifugal casting is that one starts off with a low-viscous liquid and ends with a solid material. During the whole process, the temperature does not exceed the melting point of the polyamide (PA) formed. The article, therefore, does not need a cooling cycle before it can be taken out of the mold. An example is an oil tank of 1200 l with a wall thickness of around 4.5 mm, which requires 33 kg of caprolactam. The cycle time for heating, rotating, and simultaneous polymerization is around 13 min.

The molds are mostly made of steel or aluminum. Since the forces during rotational molding are relatively small, wall thicknesses of ~1.5 mm will be sufficient.

23.5.4 Compression Molding

Compression molding is the simplest technique to transform a raw polymeric material from the solid state into an end product. The material, as granules, flakes, or powder, is put between the two heated halves of the mold, which are then pressed together [18].

Thermoplastics, thermosets, and rubbers can be processed by compression molding. For thermoplastics, this technique is an exception.

Compression molding of thermoplastics is, in general, unattractive because the mold has to be heated (so the polymeric material melts and takes the mold form) and cooled (so the polymer part solidifies and can be taken out of the mold).

With thermosets, compression molding is commonly applied. The starting material is a molding powder comprising the resin, curing agent, and filler.

The powder is heated in the mold; it becomes a fluid and fills the mold completely, after which the curing reaction takes place.

In this case, if T is low (the curing reaction rate will be low), then η will be high and the material will require a high pressure to fill the mold or will probably not flow to fill the mold. On the contrary, if T is high (the curing reaction rate will be high), then η will be low but curing will probably start before the material fills the mold completely. When these effects coincide, the process fails. If the reaction time is longer than the time needed for flow, then a perfect molding is obtained, but the cycle time may be too long. Therefore, care must be taken in preparing an adequate formulation.

Molding powders cure, in general, at temperatures between 140 and 180 °C, under pressures between 200 and 600 bars. A substantial part of the temperature increase comes from the reaction heat, which may raise the temperature to above the temperature of the wall. This effect will be stronger with thicker articles.

A simple compression molding device is sketched in Figure 23.17.

In the case of thermosets, numerous articles are made by compression molding, such as bulb fittings, switches, wall plugs, crockery, and many other technical and household articles. The process is very economical because no expensive machines and molds are required and the cycle times are short (the finished article can be taken out of the mold without cooling down).

Compression molding of rubbers is not essentially different. The starting material is a blend of a rubber, vulcanization additives, and fillers. The compound is heated

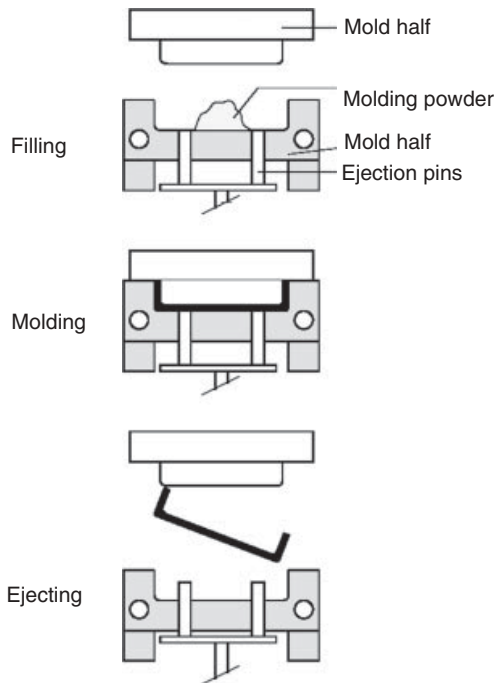


Figure 23.17 Simplified diagram of compression molding.

to become malleable, and is forced to flow into a mold, where it is kept at a high temperature until the vulcanization reaction is completed. Also here, there is a competition between flow and curing; premature vulcanization interferes with good processing. Tires are made this way.

23.6 THERMOFORMING

The starting material usually comes from extrusion, for instance as a laminate or a film.

When starting with a laminate, this is first heated to above its softening temperature, then formed, and finally cooled [19]. The technique most frequently applied for forming is vacuum forming; the force required for deformation is brought about by a vacuum below the heated laminate, which sucks the laminate onto the mold. This

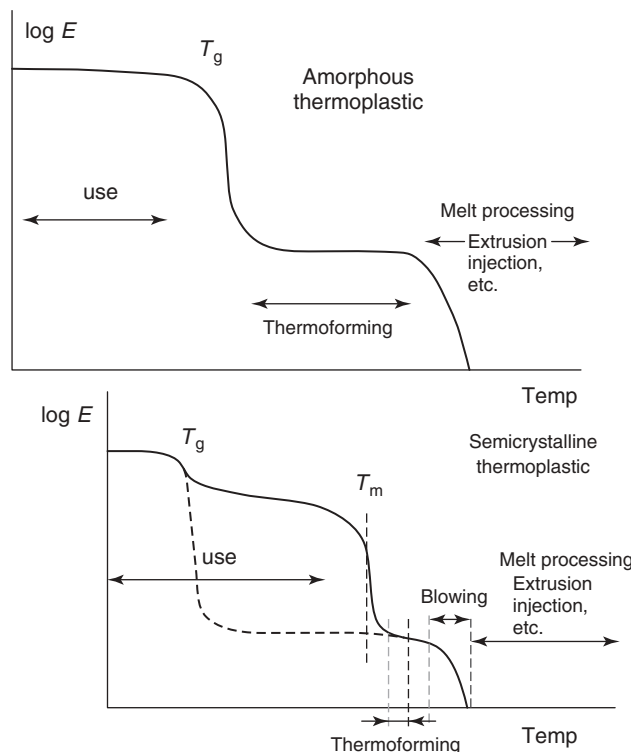


Figure 23.19 Temperature regions in which various processing techniques can be applied.

process is depicted in Figure 23.18. Heating is mostly achieved with infrared radiation and cooling is achieved with air or water sprays.

An important factor with thermoforming is that the polymer should show a pronounced *rubbery region* on the temperature scale. For this reason, amorphous polymers such as PVC, PS, poly(methyl methacrylate) (PMMA), polycarbonate (PC), acrylonitrile butadiene styrene (ABS), etc. are well suited for thermo forming. With semicrystalline polymers, the rubbery region is largely masked by the crystallinity (Fig. 23.19). With PE and polypropylene (PP), thermo forming is, therefore, a critical operation, in which the processing conditions should be very carefully controlled.

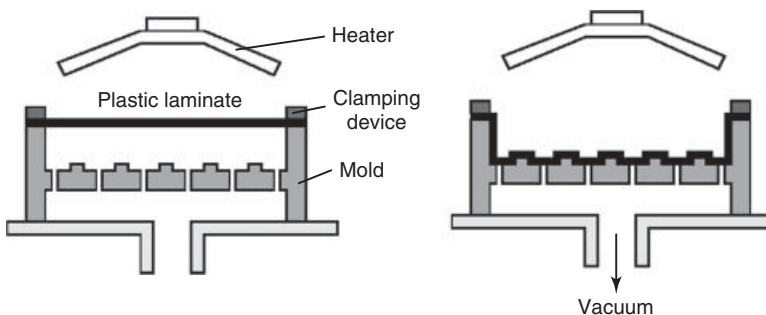


Figure 23.18 Simplified diagram of thermoforming.

Only high-molecular grades show sufficient rubbery behavior above their melting point to enable a thermoforming process. PA, PET, and poly(butylene terephthalate) (PBT), however, will be very difficult to shape using this technique.

With thicker articles or with complex shapes, vacuum does not always provide a sufficiently high force to produce the required deformation. Therefore, air pressure or plugs are sometimes applied, either simultaneously or consecutively. Typical areas of application are cups and trays for food packaging, articles with a larger area such as lighting ornaments, casings for appliances and machines, kitchen dressers, bath tubs, rowing boats, etc. The molds for thermoforming are simpler and cheaper than for injection molding. Cast aluminum is excellently suited for thermoforming molds; experimental molds can be made from timber or gypsum.

Thermoforming shows two important drawbacks. First, the pattern of deformation results in highly uneven wall thicknesses in the finished article. In a cup, for example, the lower brim may be half as thin as the middle or the upper rim. Second, the fact that deformation takes place in the rubbery condition. In this condition, straining is accompanied by chain orientation, which is frozen in upon rapid cooling. When the article is heated to above its T_g , it tends to recover its original shape and deforms, but at lower temperatures it shows a strong tendency to shrink.

REFERENCES

1. Malkin AY, Isayev AI. *Rheology: Concepts, Methods, and Applications*. Toronto: ChemTec; 2006.
2. Gupta BR. *Applied Rheology in Polymer Processing*. Delhi, India: Asian Book Pvt Ltd; 2005.
3. Macosko CW. *Rheology, Principles, Measurements and Applications*. New York: Wiley-VCH; 1994.
4. Zloczower IM. *Mixing and Compounding of Polymers, Theory and Practice*. 2 ed. Munich: Hanser Publisher; 2009.
5. White JL, Coran AL, Moet A. *Polymer Mixing Technology and Engineering*. Munich: Hanser Publishers; 2001.
6. Rauwendaal C, editor. *Mixing in Polymer Processing*. New York: Marcel Dekker; 1991.
7. Mathews G. *Polymer Mixing Technology*. London: Applied Science; 1984.
8. Kohlgrüber K. *Co-Rotating Twin-Screw Extruders; Fundamentals, Technology, and Applications*. Munich: Hanser Publishers; 2007.
9. Rauwendaal C. *Polymer Extrusion*. 4 ed. Munich: Hanser; 2001.
10. Chung CI. *Extrusion of Polymers: Theory and Practice*. Munich: Hanser; 2000.
11. Ramos-deValle LF. *Extrusión de Plásticos: Principios Básicos*. Mexico: Limusa; 1993.
12. Lee N. *Blow Molding Design Guide*. Munich: Hanser Publishers; 1998.
13. Fischer EG. *Blow Molding of Plastics*. London: Butter Worths; 1976.
14. Kamal MR, Isayev AI, Liu S-J, White JL. *Injection Molding: Technology and Fundamentals*. Cincinnati: Hanser; 2009.
15. Osswald T, Turng L, Gramann P. *Injection Molding Handbook*. 2 ed. Munich: Hanser; 2007.
16. Rubin II. *Injection Molding: Theory and Practice*. 1 ed. Hoboken (NJ): Wiley-Interscience; 1973.
17. Crawford RJ. *Rotational Molding*. Taunton, England: Research Press Ltd.; 1996.
18. Davis B, Gramann P, Osswald T, Rios A. *Compression Molding*. Munich: Hanser; 2003.
19. Throne JL. *Technology of Thermoforming*. Munich: Hanser; 1996.

FURTHER READING

- McKelvey JM. *Polymer Processing*. New York: Wiley; 1962.
 Middleman S. *Fundamentals of Polymer Processing*. New York: McGraw-Hill Company, Inc.; 1977.
 McCrum NG, Buckley CP, Bucknall CB. *Principles of Polymer Engineering*. Oxford: Oxford University Press; 1988.
 Cheremisinoff NP. *Advanced Polymer Processing Operations*. Westwood (NJ): Noyes Publications; 1998.
 Berins ML. *Plastics Engineering Handbook of the Society of the Plastics Industry*. 5 ed. Dordrecht, The Netherlands: Kluwer Academic Publishers; 2000.
 Harper CA. *Handbook of Plastics, Elastomers and Composites*. 4 ed. New York: McGraw-Hill Company, Inc.; 2000.
 Hatzikiriakos SG, Migler KB. *Polymer Processing Instabilities: Control and Understanding*. New York: Marcel Dekker; 2005.

24

BLOWN FILMS AND RIBBONS EXTRUSION

JORGE R. ROBLEDO-ORTÍZ, DANIEL E. RAMÍREZ-ARREOLA,
DENIS RODRIGUE, AND RUBÉN GONZÁLEZ-NÚÑEZ

24.1 INTRODUCTION

Sheet and bag manufacturing by blown film and ribbon extrusion represents a large segment of the plastics industry. A recent review on the situation and outlook of plastic films was presented by Pardo [1]. This chapter covers various aspects of polymer materials and/or their applications in specific end-products. In general, for most films, the main end-user is the packaging industry. A wide variety of plastic materials are used to produce films, essentially polyolefin, poly(ethylene terephthalate) (PET) for magnetic and optical applications, poly(vinyl chloride) (PVC) for consumer goods and medical applications, and poly(vinyl butyral) (PVB) for automobile applications [1]. An approach to improve film properties is to directly use blends of commercial polymers. These blends are generally easier to process, require lower investments, and do not require the development of new molecules for each specific application. The final film properties of such blends depend on the individual component properties, morphology, interphase, composition, and processing method [2]. The process consists of the following steps: extrusion of a polymer melt through a die, stretching, and cooling in air or water. In general, cooling occurs at a short distance from the die exit and the process is considered isothermal. Nevertheless, depending on the cooling distance, nonisothermal conditions can prevail. Blow extrusion and ribbon extrusion vary in the design of die used and in the type of cooling. The design and operation of the extruder up to the die is the same for both methods. The basic extrusion process is designed to continuously shape a thermoplastic material into a specific form.

This chapter includes, first, a general description of blown film and ribbon extrusion, including the most important parameters that need to be controlled. In

section 24.3, the equations used to calculate the final dimensions of films and ribbons are presented. In that section, nonisothermal and non-Newtonian flow behavior is considered. A historical development of the different models available in the literature is also included. The relationship between the cooling process and the stretching forces is discussed in section 24.5. Section 24.6 deals with the relationships between morphology and mechanical properties for immiscible polymer blends.

24.2 EXTRUSION PROCESSES FOR BLOWN FILMS AND RIBBONS

The blown film process involves the extrusion of a polymer melt through an annular die and the subsequent blowing of the tube shaped. The materials used to produce films can be neat components, blends of two or more polymers, virgin materials, recycled materials, or blends of those. Additives such as slip, antiblock, antistatics, or pigments can also be added into the extruder feed.

The extrusion process is usually carried out in single- or twin-screw extruders. The molten polymer flows through an annular die in the following stage of the process. The flow through the die must be uniform across the exit plane; however, this gets complicated because of the nonlinear dependence of polymer viscosity on temperature and shear rate in the die. In this sense, a good die design is essential for optimal processing. The polymer tube is inflated by introducing air through a duct in the center of the die, maintaining a constant pressure. The bubble is pulled upward by means of a roller system at a specific rate to obtain the desired thickness and diameter.

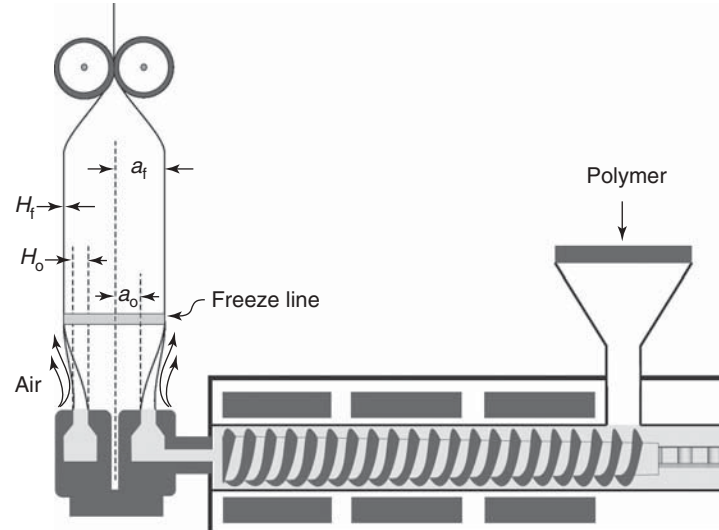


Figure 24.1 Schematic representation of the blown film process.

The cooling process is carried out through a ring placed on the die that provides air at high speed. Thickness and bubble diameter can also be controlled by changing, in addition to the take-up roller velocity, the cooling rate and pressure inside the bubble.

There are some characteristic parameters in the blown film process (see Fig. 24.1): the blow-up ratio (BUR), which is the ratio between the final radius (a_f) and the radius at the die exit (a_0); the thickness ratio (TR) calculated as the ratio of thickness at the die exit (H_0) and the final film thickness (H_f); and the draw ratio (DR) defined as the ratio of take-up roller velocity (V_f) to the extrusion velocity (V_0). The stretching force (F_z) is the force needed to take up the bubble by the roller system (Fig. 24.1).

A relationship among TR, DR, and BUR for stable bubble operation can be obtained from a mass conservation analysis as:

$$\frac{1}{\text{TR}} = \frac{(a_0 + H_0)^2 - R_0^2}{2a_0 H_0} \left(\frac{\rho_m}{\rho_s} \right) \frac{1}{\text{DR} \times \text{BUR}} \quad (24.1)$$

where ρ_m and ρ_s are the melt and solid polymer densities, respectively. This equation shows a linear relationship between TR^{-1} and $(\text{DR} \cdot \text{BUR})^{-1}$.

On the other hand, the ribbon extrusion process consists of the following steps: extrusion of a polymer melt through a small rectangular die, stretching, and cooling with air or water. Depending on the cooling distance, nonisothermal or isothermal conditions can be considered.

The ribbon extrusion process is studied using the following assumptions: steady state, incompressible flow, the velocity component in the stretching direction is the only function of this direction, each cross section remains

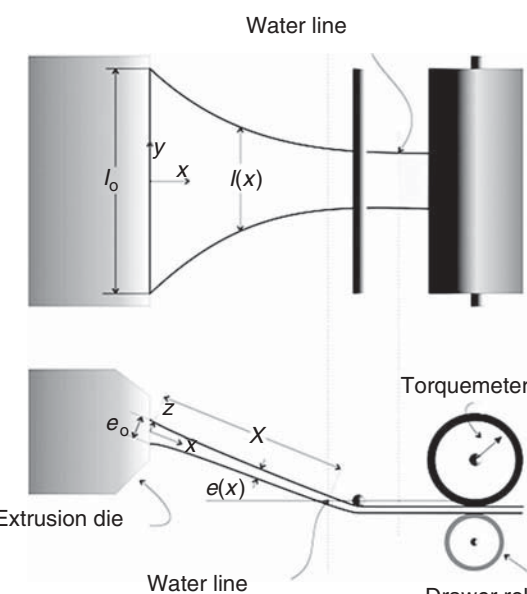


Figure 24.2 Schematic representation of the ribbon extrusion process.

rectangular, and temperature is assumed constant on a cross section.

There are also characteristic parameters of the process (see Fig. 24.2): distance in the stretching direction (x); total cooling length (X); cooling length in air (X_a); cooling length in water (X_w); ribbon width (l); die and initial ribbon widths (l_0); ribbon thickness (e); and die gap and initial ribbon thickness (e_0). DR is defined in the same way as in blown film processes and the stretching force (F) is the force needed to take off the ribbon by the roller system.

TABLE 24.1 Blown Film Modeling

Author(s)	Description
Pearson and Petrie [3, 4]	Newtonian model, isothermal
Han and Park [5, 6]	Power-law model, nonisothermal
Petrie [7]	Newtonian, nonisothermal, gravity effects included
Luo and Tanner [8]	Maxwell and Leonov models, nonisothermal
Kanai and White [9]	Newtonian model, nonisothermal including the effect of polymer crystallization
Cao and Campbell [10]	Nonisothermal Maxwell model extended past the freeze line with the Hookean elastic behavior
Sidiropoulos et al. [11]	Modified nonisothermal Newtonian model
Doufas and McHugh [12]	Model including flow-induced crystallization in the blown film
Muke et al. [13]	Nonisothermal, Kelvin viscoelastic model
Zatiloukal and Vlcek [14, 15]	Variational principles to describe bubble shapes
Rao and Rajagopal [16]	Simulation for semicrystalline polymers
Robledo-Ortiz et al. [17]	Describes a correction factor to predict more precisely stretching force values
Shin et al. [18]	Multiplicity, bifurcation, stability, and hysteresis in dynamic solutions, nonisothermal viscoelastic model
Pirkle et al. [19]	Parameter estimation to characterize convective heat transfer
Pirkle and Braatz [20, 21]	Two-phase microstructural constitutive equation combined with the thin-shell model and dynamic model including the effect of crystallization
Housidas [22]	Model including the aerodynamic effect of the air jet
Lee et al. [23]	Nonlinear dynamic behavior, nonisothermal film blowing with constant bubble pressure

24.3 EQUATIONS

24.3.1 Blown Film Equations

The blown film process has been studied analytically since the early 1970s (Table 24.1). The first analysis was proposed by Pearson and Petrie [3, 4], who followed a fluid mechanics approach. However, this model is restricted to Newtonian fluids under isothermal conditions. This first model has been modified several times to consider different aspects of the process, such as temperature variation and rheological behavior of the system.

The majority of the studies presented in Table 24.1 focus on the final dimensions of the blown films. However, the calculated stretching forces are not in close agreement with the reported experimental values.

It is possible to model the deformation of film bubbles with a system of dimensionless equations that is derived according to the following assumptions [13]: steady-state and axisymmetrical flow (z -axis) of an incompressible fluid; thin and flat film; external forces on the bubble are neglected; Newtonian, pseudoplastic, or viscoelastic fluids; and linear temperature profiles between die exit and freeze-line position. The system of dimensionless fundamental equations can be represented, irrespective of the rheological constitutive equation used, as shown in the following equations:

$$L = \frac{(A + Br^2)(1 + r'^2)^{1/2}}{rh} \quad (24.2)$$

$$r'' = \frac{[h C (1 + r'^2)^{1/2} - 2r B (1 + r'^2)]}{A + Br^2} \quad (24.3)$$

Each dimensionless quantity in these equations is defined as [3, 4]:

$$L = \frac{a_0 \sigma_{11}}{V_0 \eta_0} \quad (24.4a)$$

$$C = \frac{a_0 \sigma_{33}}{V_0 \eta_0} \quad (24.4b)$$

$$r = \frac{a}{a_0} \quad (24.4c)$$

$$h = \frac{H}{H_0} \quad (24.4d)$$

$$A = \frac{F_z a_0}{\eta_0 Q} - B (\text{BUR})^2 \quad (24.4e)$$

$$\text{BUR} = \frac{a_f}{a_0} \quad (24.4f)$$

$$B = \frac{\pi a_0^3 \Delta P}{\eta_0 Q} \quad (24.4g)$$

where σ_{11} and σ_{33} are the main normal stresses, V_0 is initial velocity, a is radius, a_0 is initial radius, H is film thickness, H_0 is initial film thickness, F_z is stretching force, η_0 is Newtonian viscosity evaluated at T_0 , Q is volumetric flow rate, ΔP is pressure difference, G_0 is elastic modulus, T_0 is extrusion temperature (die), and T is temperature.

For the Kelvin model, second-order and first-order equations for radius and thickness, respectively, are obtained. Rewriting the second-order equation as two first-order equations the system is transformed into the following equations [13]:

$$r'_1 = r_2 \quad (24.5)$$

$$r'_2 = \frac{1}{2r_1^2(A + Br_1^2)} \left[2\alpha r_1^2 h (1 + r_2^2)^{1/2} \ln(r) + 6\beta r_2 + r_1 (1 + r_2^2) (A - 3Br_1^2) \right] \quad (24.6)$$

$$h' = h \left[-\frac{r_2}{2r_1} + \frac{\alpha}{4\beta} r_1 h (1 + r_2^2) \ln\left(\frac{1}{r_1^2 h^4}\right) - \frac{(A + Br_1^2)(1 + r_2^2)}{4\beta} \right] \quad (24.7)$$

where α is dimensionless shear modulus and β is dimensionless zero shear viscosity, defined as follows:

$$\alpha = \frac{a_0 G_0(T)}{v_0 \eta_0(T_0)} \quad (24.8a)$$

$$\beta = \frac{\eta_0(T)}{\eta_0(T_0)} \quad (24.8b)$$

For the Newtonian case, $\alpha = 0$, and for the pseudoplastic case,

$$\beta = \frac{\eta(T, \dot{\gamma})}{\eta_0} \quad (24.9)$$

An extended mathematical development is presented by Muke et al. [13]. The dependence of viscosity on temperature is represented by an Arrhenius equation, as shown in the following equation:

$$\eta(T) = \eta(T_{\text{ref}}) \exp\left[\frac{E_a}{R} \left(\frac{1}{T} - \frac{1}{T_{\text{ref}}}\right)\right] \quad (24.10)$$

The rate of deformation is calculated as shown in the following equation:

$$\dot{\gamma} = \frac{Q}{2\pi(1+r'^2)^{1/2} rha_0^2 H_0} \left[\left(\frac{r'}{r}\right)^2 + \left(\frac{h'}{h}\right)^2 + \left(\frac{h'r'}{hr}\right)^2 \right]^{1/2} \quad (24.11)$$

In the case of blown film simulations, a linear temperature profile can be used to obtain a greater stability in the solution of the system. The set of boundary conditions imposed on the system is given as shown in the following equation:

$$\text{for } x = X, \quad \begin{cases} r_1 = \text{BUR} \\ r_2 = 0 \\ h = h_f \end{cases} \quad \text{and for } x = 0, \quad \begin{cases} r_1 = 1 \\ h = h_0 \end{cases} \quad (24.12)$$

24.3.2 Ribbon Extrusion Equations

The physical and mathematical description of the ribbon extrusion process was first given by Pearson [24], who simplified the conservation equations by using a one-dimensional, isothermal, Newtonian fluid approach, and neglected the effects of polymer solidification. As in the case of blown film processes, several modifications and models have been proposed for the ribbon extrusion process (Table 24.2).

Considering the assumptions previously mentioned for the study of ribbon extrusion and the fact that the flow is mostly elongational, which means that the shear components are neglected, the velocity gradient ($\dot{\epsilon}$) and the volumetric flow rate (Q) are given by the following equations:

$$[\dot{\epsilon}] \approx \begin{bmatrix} \frac{\partial u}{\partial x} & 0 & 0 \\ 0 & \frac{\partial v}{\partial y} & 0 \\ 0 & 0 & \frac{\partial w}{\partial z} \end{bmatrix} \quad (24.13)$$

$$\frac{dQ}{dx} = \frac{d(uel)}{dx} = 0 \quad (24.14)$$

For a Newtonian polymer, the stress tensor (τ) becomes

$$[\tau] = 2\eta[\dot{\epsilon}] - p[I] \quad (24.15)$$

where p is the hydrostatic pressure, given by the following equation:

$$p = -\frac{1}{3} [\tau_{xx} + \tau_{yy} + \tau_{zz}] \quad (24.16)$$

TABLE 24.2 Ribbon Extrusion Modeling

Author(s)	Description
Pearson [24]	Newtonian model, isothermal
Cotto et al. [25]	The isothermal restriction was eliminated for biaxial deformation
Iyengar and Co [26]	Giesekus constitutive equation
Silagy et al. [27]	Viscoelasticity effects included
Acierno et al. [28]	Newtonian model, nonisothermal
Lamberti et al. [29]	Cross viscosity model including the effect of polymer crystallization
Satoh et al. [30]	Nonisothermal flow, viscoelastic fluid by the Larson model
Ramirez et al. [31]	Stretching force calculated using the nonisothermal Kelvin–Voigt model
Hallmark [32]	New method to measure polymer deformation during film casting
Lamberti [33]	Flow-induced crystallization

From the boundary conditions and neglecting the friction with air,

$$\mathbf{v} \cdot \mathbf{n} = 0 \quad (24.17)$$

$$[\tau] \cdot \mathbf{n} = 0 \quad (24.18)$$

The following set of equations results from the conservation of momentum for a Newtonian fluid [29]:

$$\frac{dF}{dx} = 0 \quad (24.19)$$

$$\frac{dl}{dx} = \frac{6Q\eta_0}{Fl} - \sqrt{\left(\frac{6Q\eta_0}{Fl}\right)^2 + 2} \quad (24.20)$$

$$\frac{du}{dx} = \frac{u}{4} \left(\frac{F}{\eta_0 Q} - \frac{2}{l} \frac{dl}{dx} \right) \quad (24.21)$$

$$\frac{de}{dx} = -\frac{e}{ul} \left(u \frac{dl}{dx} - l \frac{du}{dx} \right) \quad (24.22)$$

Neglecting viscous dissipation and assuming steady state, the conservation of energy can be written as [28, 29]

$$\frac{dT}{dx} = \frac{2h_c l}{\rho C_p Q} (T_a - T) \quad (24.23)$$

where h_c is the convective heat transfer coefficient, C_p is the polymer heat capacity, and T_a is air temperature. Once the temperature profile is known, the change of viscosity with temperature is related to an Arrhenius expression (Eq. 24.10). To solve the set of ordinary differential Equations 24.17–24.23, the following boundary conditions are used:

$$\begin{aligned} \text{for } x = 0, \quad & \left\{ \begin{array}{l} e = e_0 \\ l = l_0 \\ u = u_0 \\ T = T_0 \end{array} \right\} \text{ and} \\ \text{for } x = X, \quad & \left\{ \begin{array}{l} u = u_X \\ T = T_M \equiv \text{Melt temperature} \end{array} \right\} \quad (24.24) \end{aligned}$$

To eliminate the Newtonian simplification, a rheological constitutive equation is replaced in the equations that require it. Or, in the case where viscoelasticity effects are required, the simple Kelvin–Voigt model can be used. In this case, the stress is decomposed into its viscous and elastic components, as shown in the following equation:

$$\tau = G\varepsilon + \eta\dot{\varepsilon} \quad (24.25)$$

The Kelvin–Voigt model has the advantage of not needing the derivative of the stress, which is difficult to obtain experimentally, as in the Maxwell model.

24.4 RIBBON AND FILM DIMENSIONS

From numerical solution of the set of equations that represent both processes, it is possible to predict the ribbon and film dimensions and temperature profiles from the die to the freeze line. Figure 24.3 shows two-dimensional simulations of a PA6/LDPE blown film (extruded at 250 °C and DR = 20) and a PS/HDPE ribbon (extruded at 200 °C and DR = 4).

The numerical prediction of film and ribbon dimensions is strongly affected by the rheological model used. In general, in the case of blown film processes, good predictions of radius and curvature (angle) profiles can be obtained with any model because they mainly obey volume conservation. However, in several occasions not all the models give the same results for film thickness and stretching force. Figure 24.4 shows the predicted radius and angle profiles obtained from viscoelastic simulations, which are in agreement with experimental data for an LDPE blown film process. Similar predictions are obtained from Newtonian and pseudoplastic simulations. It is also observed that the bubble radius decreases and the freeze-line position increases with increasing values of DR.

As shown in Figure 24.5, similar results are observed for numerical simulations of ribbon dimensions (in dimensionless form). It is clear that all the rheological models tested (Newtonian, pseudoplastic, and viscoelastic) perform equally well in predicting thickness and width of the ribbon. As expected, once again the dimensions of the ribbon decrease with increasing DR.

24.5 COOLING PROCESS AND STRETCHING FORCE

The stretching force (F_z) highly affects the final dimensions, morphology, and stability of both processes. On the other hand, the position (from the die exit) at which molten polymer is solidified is defined as the freeze-line height (FLH) for the blown film process and as total cooling length for ribbon extrusion. The FLH can be controlled by the cooling process, increasing or decreasing the air velocity in film blowing or in the case of ribbon extrusion the cooling length is modified by increasing or decreasing the distance between the die exit and the cooling water bath.

The stretching force is a direct consequence of the distance of polymer solidification (DPS) in both processes (i.e., FLH in film blowing processes or cooling length in ribbon extrusion). In this sense, controlling DPS offers the possibility to control the final properties of films and ribbons. Table 24.3 lists typical values of stretching force as function of FLH and DR for blown films of LDPE.

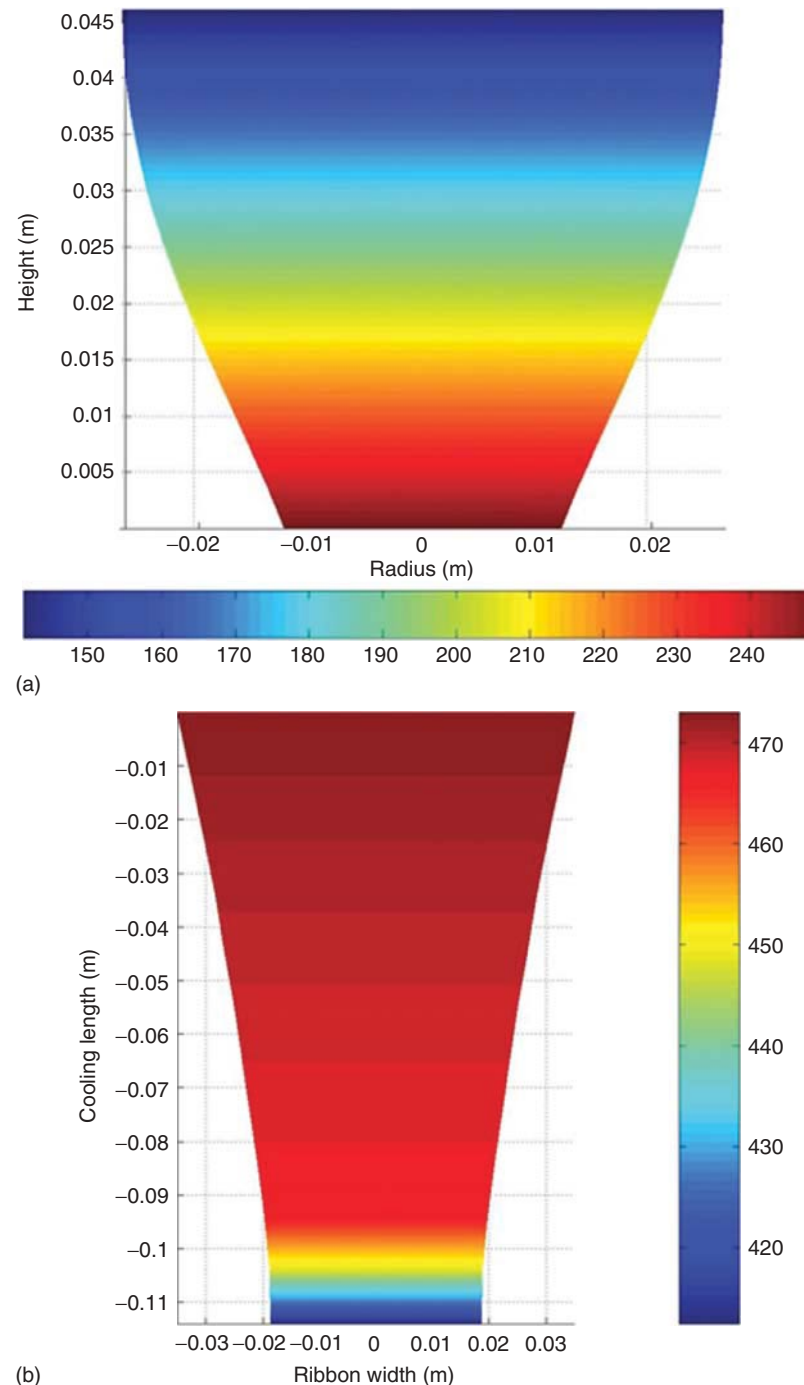


Figure 24.3 Simulated (a) bubble radius, (b) ribbon width, and temperature profiles. (See insert for the color representation of the figure.)

The stretching force and FLH increase with DR and, for a fixed DR, the stretching force decreases with increasing FLH.

In the same way, Figure 24.6 presents the stretching force (F) as a function of DR for different total cooling lengths (X). The stretching force increases with increasing

DR, but decreases with increasing X . This behavior is attributed to the rheological properties of the polymer melt and a relaxation process for long water contact distances (in all the cases after a value of $DR \approx 6$). There is also a maximum DR value that can be used before the ribbon breaks, which indicates limiting operation conditions.

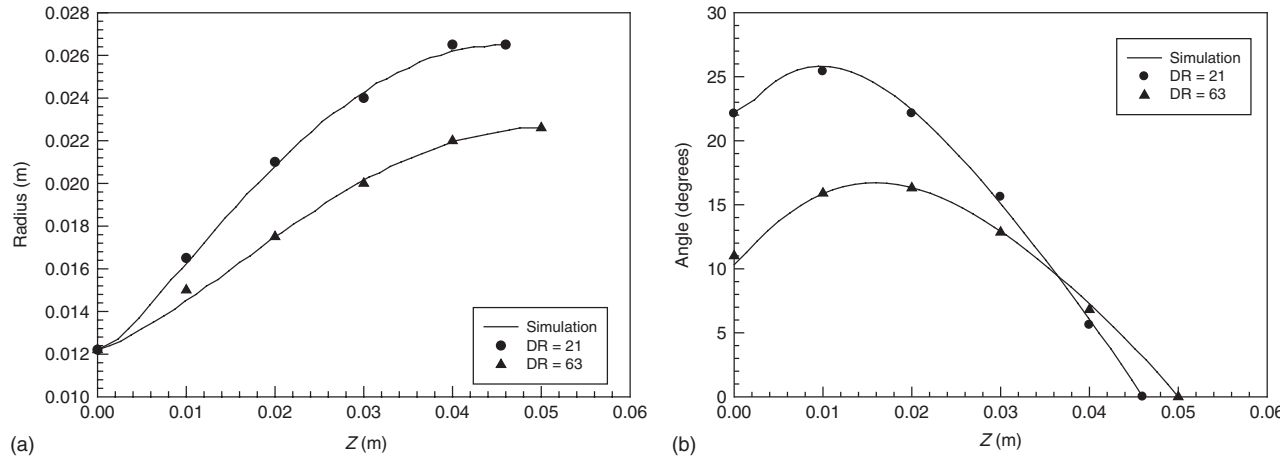


Figure 24.4 (a) Bubble radius and (b) curvature as function of DR.

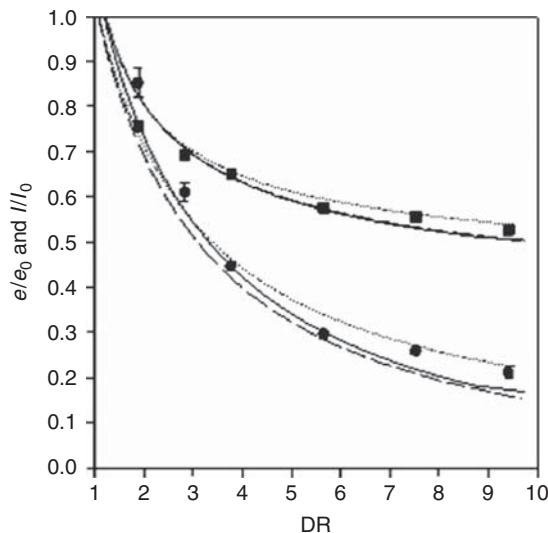


Figure 24.5 Dimensionless width (l/l_0) and thickness (e/e_0) of the ribbon as function of DR. Symbols are experimental data (●, thickness; ■, width) and lines are the predictions. Newtonian (.....), pseudoplastic (----), and viscoelastic (—).

24.6 MORPHOLOGY AND MECHANICAL PROPERTIES

Several studies focused on the hot stretching postextrusion of polymer blends and their effect on mechanical properties to obtain specific final products characteristics have been reported [34–37]. The morphology of a dispersed phase in a matrix is strongly affected by the processing conditions and it is reflected on the final physical and mechanical properties. Figure 24.7 shows longitudinal micrographs of blown films obtained with a blend of 6% of PA6 with LDPE. It is clear that the deformation of the dispersed phase is greater when the position of the cooling line is

TABLE 24.3 Experimental Stretching Force (F_z) as Function of Freeze-Line Position (Z) and Draw Ratio (DR) for LDPE Films

Z(m)	DR = 14	DR = 21	DR = 27		
	F_z (N)	$Z(m)$	F_z (N)	$Z(m)$	F_z (N)
0.046	1.388	0.052	1.452	0.058	1.516
0.052	1.310	0.055	1.390	0.059	1.460
0.056	1.220	0.057	1.310	0.060	1.390

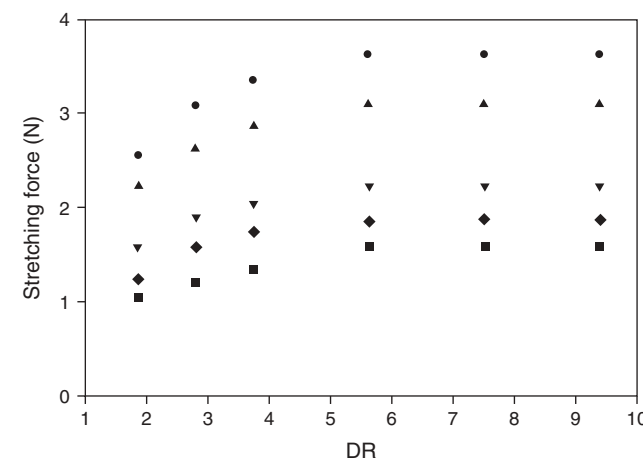


Figure 24.6 Experimental data for the stretching force (F) as function of DR under different water contact distances (X) values for HDPE ribbons: ●, 3.5 cm; ▲, 5 cm; ▼, 10 cm; ♦, 15 cm; and ■, 20 cm.

lower, as the stretching force is greater when the position of the cooling line is lower. In the same way, the deformation increases with higher DR values. On the other hand, in the case of the transverse direction (TD), negligible changes in particle deformation are observed.

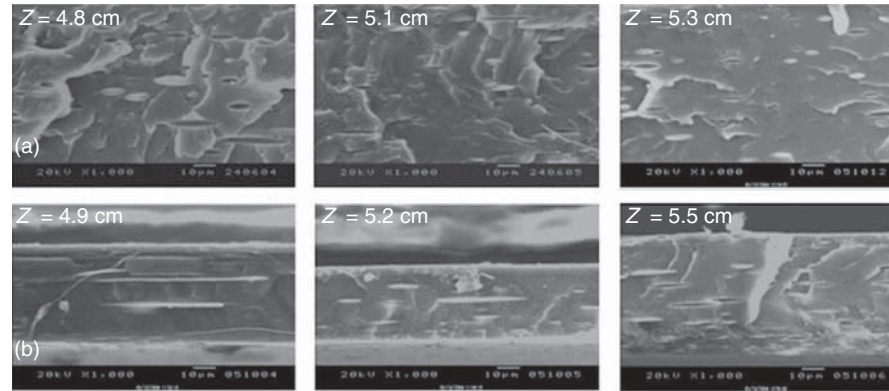


Figure 24.7 Longitudinal micrographs of 6% PA6-/LDPE films for (a) DR = 14 and (b) DR = 21 at different FLH.

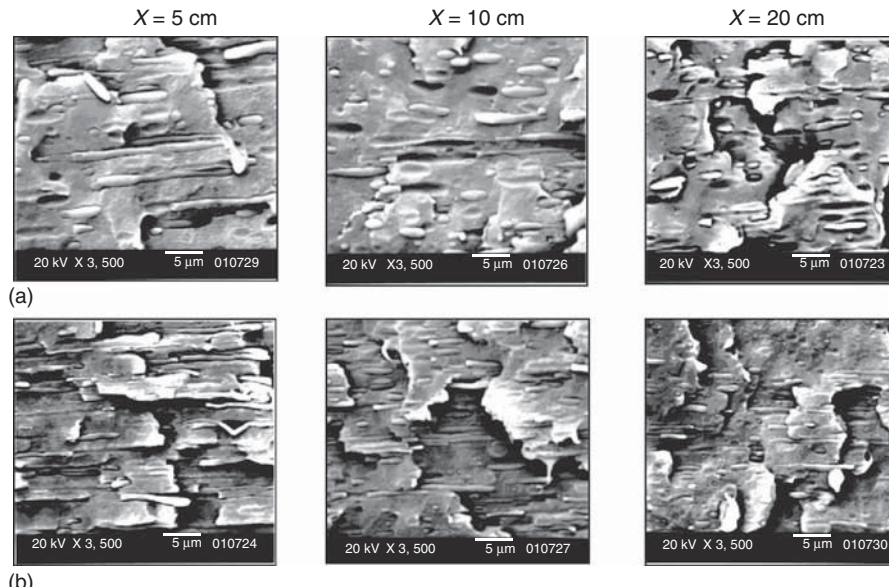


Figure 24.8 Micrographs of 9% PS/HDPE ribbons for (a) DR = 3.76 and (b) DR = 5.64.

Figure 24.8 shows SEM micrographs for ribbons of 9% PS in HDPE under different DR and X values. Similar to blown films, it is observed that deformation increases with increasing DR, but decreases with increasing X . This behavior is attributed to a larger stretching force, F , which increases with increasing DR and decreasing water contact distance. Similar behavior is observed for different contents of PS in HDPE.

It is well known that the mechanical properties of polymer blends strongly depend on the raw materials and on their final morphologies, which are controlled by interfacial adhesion, properties of the neat materials, and processing conditions, among others [2, 37–39].

Because of biaxial deformations in the blowing process, the tensile modulus is usually determined in both the machine direction (MD) and TD. Results obtained from

tensile tests have been used to determine the tensile strength (nominal), elongation at break, and elastic modulus of the films. Table 24.4 lists the mechanical properties of LDPE and PA6/LDPE (with and without compatibilizer, Surlyn 9020, DuPont) films [40]. Mechanical properties are greatly affected by polymer molecular chain orientation [41].

For DR values between 10 and 50, a decrease in elastic modulus with DR is observed. In the case of a polymer blend, such as PA6/LDPE, there is an almost independent behavior of the tensile properties in the MD of noncompatibilized blends as a function of the dispersed phase concentration. However, in the TD, a clear dependence of the elastic modulus is observed. It is also observed that compatibilized films have higher modulus compared to noncompatibilized films. For the films presented in Table 24.4, PA6 particulate fibers

TABLE 24.4 Mechanical Properties of PA6/LDPE Films

Film (%PA6)	DR	σ_p (MPa)		ε_b (%)		E (MPa)	
		MD	TD	MD	TD	MD	TD
LDPE (0%)	18.4	11.5	7.7	298	166	133	122
	29.0	15.6	9.1	187	224	122	110
	50.5	31.9	20.1	151	300	107	96
10% Without Surlyn	19.9	21.7	6.1	410	99	174	162
	25.4	10.6	3.2	199	74	158	153
	32.3	7.1	2.7	127	36	156	126
30% Without Surlyn	12.6	22.0	8.4	504	11	187	146
	20.3	18.1	4.1	458	36	171	123
	36.2	22.8	—	469	—	137	—
10% With Surlyn	10.6	12.7	10.3	449	350	192	177
	25.5	15.1	9.3	359	210	185	164
	36.6	12.8	7.8	212	120	170	154
30% With Surlyn	12.3	15.7	7.0	365	48	238	194
	19.2	13.5	5.3	407	27	230	185
	34.5	12.4	6.7	258	24	224	168

Abbreviations: σ_p , tensile strength (nominal); ε_b , elongation at break; E , elastic modulus; MD, machine direction; TD, transverse direction; and DR, draw ratio.

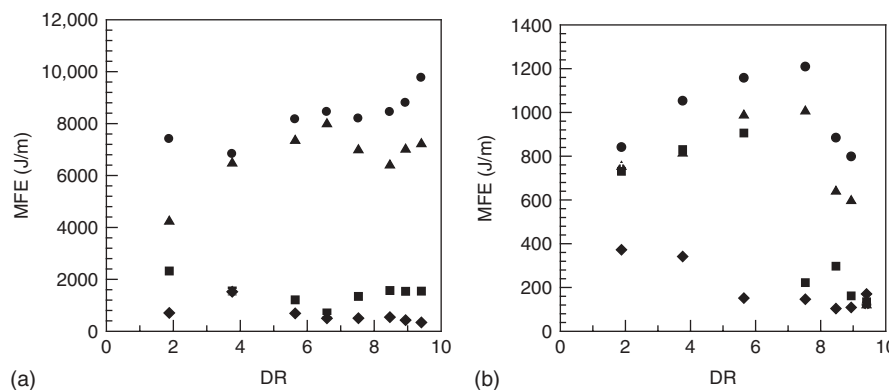


Figure 24.9 Mean failure energy for (a) 3% and (b) 9% PS in HDPE at different cooling lengths
(X): ◇, 5 cm; ■, 10 cm; ▲, 15 cm; and ●, 20 cm.

(or lamellas) formed in the LDPE matrix during the deformation process are oriented in the flow direction (MD), which produces better mechanical properties than neat LDPE. This is also the reason properties in the TD are lower than in the MD.

Figure 24.9 shows the effect of cooling length (X) and DR on mean failure energy (MFE) for PS in HDPE. At low PS concentrations (3%), the variation of MFE with DR is relatively small but MFE varies substantially when the cooling length is changed. In the first case, the HDPE matrix sustains the impact energy mostly alone; whereas in the case where the cooling length increases, the relaxation process restraining further crystallization progresses. This makes the ribbons more stretchable, with better MFE properties. At low DR thicker samples are obtained. This facilitates the segregation of the crystalline part of the polymer on its amorphous part, creating failure points where fractures can

propagate (low MFE values). Increasing DR, on the other hand, produces thinner ribbons and increased MFE values are observed due to greater MD orientation [42].

Another parameter influencing MFE is the blend morphology. By increasing DR, higher hydrodynamic stresses are transferred from the matrix to the dispersed phase, leading to increased deformation and MFE values. At low X values, the polymer is rapidly cooled down from the die exit and the particles do not have much time to relax because the morphology is frozen quickly. Depending on the concentration of the dispersed phase, a transition in the blend morphology from deformed spheroid and elongated particles to fiber formation is produced as DR increases. Particles may also coalesce. In general, it is observed that deformed particles increase MFE, whereas the formation of long fibers has the reverse effect. For high concentrations of the dispersed phase, increasing further DR decreases MFE,

which is attributed to fiber breakup. This behavior is observed in Figure 24.8 for DR = 5.64 and X = 5 cm. The corresponding MFE is presented in Figure 24.9.

REFERENCES

1. Pardo F. *Plastic Films; Situation and Outlook; A Rapra Market Report*. 1st ed. Shawbury: Rapra Technology Ltd; 2004. p 7.
2. Paul DR, Bucknall CB, editors. *Polymer Blends*. Volume 2. New York: Wiley; 2000. p 360.
3. Pearson JR, Petrie CJS. J Fluid Mech 1970;40:1.
4. Pearson JR, Petrie CJS. J Fluid Mech 1970;42:609.
5. Han CH, Park JY. J Appl Polym Sci 1975;19:3257.
6. Han CH, Park JY. J Appl Polym Sci 1975;19:3277.
7. Petrie CJS. AIChE J 1975;21:275.
8. Luo XL, Tanner RI. Polym Eng Sci 1985;25:620.
9. Kanai T, White JL. J Polym Eng 1985;5:135.
10. Cao B, Campbell GA. AIChE J 1990;36:420.
11. Sidiropoulos V, Tian JJ, Vlachopoulos J. J Plast Film Sheet 1996;12:107.
12. Doufas AK, McHugh AJ. J Rheol 2001;45:1085.
13. Muke S, Connell H, Sbarski I, Bhattacharya SN. J Non-Newt Fluid Mech 2003;116:113.
14. Zatloukal M, Vlcek J. J Non-Newt Fluid Mech 2004;123:201.
15. Zatloukal M, Vlcek J. J Non-Newt Fluid Mech 2006;133:63.
16. Rao IJ, Rajagopal KR. Mech Adv Mater Struc 2005;12:129.
17. Robledo-Ortiz JR, Ramírez-Arreola D, González-Núñez R, Rodrigue D. J Plast Film Sheet 2006;22:287.
18. Shin DM, Lee JS, Jung HW, Hyun JC. J Rheol 2007;51:605.
19. Pirkle JC, Fujiwara M, Braatz RD. Ind Eng Chem Res 2010;49:8007.
20. Pirkle JC, Braatz RD. J Rheol 2010;54:471.
21. Pirkle JC, Braatz RD. J Process Contr 2011;21:405.
22. Housidas KD. Polym Eng Sci 2011;51:1301.
23. Lee JS, Jung HW, Hyun JC. AIChE J 2011;57:3565.
24. Pearson JRA. *Mechanical Principles of Polymer Melt Processing*. 1st ed. New York: Pergamon Press; 1966. p 1.
25. Cotto D, Saillard P, Agassant JF, Haudin JM. *Interrelations Between Processing Structure and Properties of Polymeric Materials*. 1st ed. Amsterdam: Elsevier Science Ltd; 1984. p 1.
26. Iyengar VR, Co A. Chem Eng Sci 1996;51:1417.
27. Silagy D, Demay Y, Agassant JF. Polym Eng Sci 1996;36:2614.
28. Acierno D, Di Maio L, Ammirati CC. Polym Eng Sci 2000;40:108.
29. Lamberti G, Titomanlio G, Brucato V. Chem Eng Sci 2001;56:5749.
30. Satoh N, Tomiyama H, Kajiwara T. Polym Eng Sci 2001;41:1564.
31. Ramírez-Arreola D, Padilla-Lopez H, González-Núñez R, Rodrigue D. Int Polym Proc 2006;21:121.
32. Hallmark B. Polym Eng Sci 2008;48:37.
33. Lamberti G. Polym Eng Sci 2011;51:851.
34. Iñiguez CG, Michel E, González-Romero VM, González-Núñez R. Polym Bull 2000;45:295.
35. Li ZM, Yang MB, Xe BH, Feng JM, Huang RW. Polym Eng Sci 2003;43:615.
36. Quan H, Zhong GJ, Li ZM, Yang MB, Xie BH, Yang SY. Polym Eng Sci 2003;45:1303.
37. Fasce L, Seltzer R, Frontini P, Rodriguez-Pita VJ, Pacheco EBAV, Dias ML. Polym Eng Sci 2005;45:354.
38. Huang HX, Huang YF, Li XJ. Polym Test 2007;26:770.
39. Dhoble A, Kulshreshtha B, Ramaswami S, Zumbrunnen DA. Polymer 2005;46:2244.
40. Lopez-Barron CR, Robledo-Ortiz JR, Rodrigue D, Gonzalez-Núñez R. J Plast Film Sheet 2007;23:149.
41. Patel RM, Butler TI, Walton KL, Knight GW. Polym Eng Sci 1994;34:1506.
42. Ramírez-Arreola DE, Robledo-Ortiz JR, Moscoso F, González-Núñez R, Rodrigue D. Polym Eng Sci 2008;48:1600.

25

POLYMER SOLUTIONS AND PROCESSING

DÁMASO NAVARRO RODRÍGUEZ

25.1 INTRODUCTION

In simple terms, a polymer solution is a mixture of polymer and solvent molecules. The combination of these two chemical species, so different in size and properties, involves complex phenomena that have posed major challenges to engineers and scientists over the last 70 years. The difference in size is in fact the main origin of many dissimilar properties. A good illustration is the low viscosity of the majority of solvent liquids [1, 2] compared to the high viscosity of most polymer melts [3, 4]. In polymer solutions such a difference reflects in a large increase in viscosity with small increments in solute concentration [5]. The formation of a one-phase homogeneous polymer solution depends on the capacity of the solvent to dissolve the polymer [6]. In good solvents, polymers absorb, swell, disentangle, and finally disperse as individual molecules, except for crosslinked polymers or gels that absorb and swell as well, but to a limited degree without dissolution [7–11]. Thermodynamic parameters such as change in entropy (ΔS) and enthalpy (ΔH) of mixing play a crucial role in the formation of a polymer solution as well as in phase equilibria when phase separation occurs [12–14]. The entropy term describes the number of arrangements that the chains adopt in the system, whereas the enthalpy term accounts for the interactions between adjacent molecules [15]. Important factors are concentration, temperature, nature of both solvent and polymer, molecular weight of the polymer, among others [16–21].

Polymer solutions can be classified into five regimes (dilute, semidilute not entangled, semidilute entangled, concentrated not entangled, and concentrated entangled) [22] according to the polymer concentration and molar mass; however, it is much common to classify them into only

three regimes of concentration (expressed in terms of polymer volume fraction, φ): dilute ($\varphi < \varphi^*$), semidilute ($\varphi \geq \varphi^*$), and concentrated ($\varphi^* \ll \varphi < 1$) solution [23]. The overlap concentration φ^* is not sharp, but it is rather a region at which polymer coils come close together and begin to overlap each other; experimentally, this could correspond to the condition where the concentration of the solution equals the average local concentration in the inside of the polymer coils [15, 24]. In a semidilute regime, the macromolecules are substantially overlapped, even though the solvent volume fraction is by far dominant. A more quantitative definition of these three concentration regimes can be found in various reports [25, 26]. Many studies on the physical and chemical properties of polymers have been conducted in dilute solutions, where the isolated polymer coils are relatively far apart from each other, and therefore the interchain perturbation may be negligible [27]. Under this low concentration regime, characteristics such as molecular weight, radius of gyration, number and frequency of long-chain branching, and some other structural parameters of the macromolecules can be readily determined [28–32]. Also, without difficulty, interactional parameters can be measured from dilute solutions [17, 33, 34]. On the other hand, semidilute and concentrated polymer solutions have also been very promising for the thermodynamic characterization of polymers [23, 35], although for these two regimes rheological studies have resulted particularly valuable to determine both structural and interactional characteristics [3, 5, 36]. It is to point out that, even though semidilute and concentrated polymer solutions are no longer appropriate to evaluate macromolecules individually, structure–property relationships in these regimes provide important information on these coiled molecules [23, 37].

At present, polymers are almost everywhere and, for many of their applications, particularly as fibers and films, they are processed from solution [38–41]. Dilute, semidilute, and concentrated polymer solutions are required for a wide variety of manufacturing processes, from the deposition of thin films over a substrate [spin coating, spraying, epitaxy, Langmuir–Blodgett (LB) deposition, etc.] to the processing of viscous polymer solutions or high polymer load dispersions (dip coating, wet and dry spinning, electrospinning, etc.) to obtain films and fibers with specific characteristics and properties.

In this chapter, a brief description on the fundamental aspects of polymer solution thermodynamics is given. Only some very basic or primary theories and their corresponding equations (simple approaches) are presented and discussed. For rigorous approaches and related advanced theories adequate references are given. As already mentioned, polymer solutions are required for a wide variety of processing techniques and even though most of such techniques were implemented on the basis of practical experience, much further work was done by engineers and scientists to refine them on the basis of polymer solution thermodynamics and rheology. There is abundant theoretical and empirical literature on the processing of polymers from solution; here, only some common processing techniques are briefly presented making special emphasis on spin coating, which at present time is extensively used for the deposition of thin films of a wide variety of polymers over a substrate.

25.2 POLYMER SOLUTION THERMODYNAMICS AND CONFORMATION OF POLYMER CHAINS: BASIC CONCEPTS

25.2.1 Change in Enthalpy, Entropy and Gibbs Free Energy of Mixing

In terms of thermodynamics, the solubility of a polymer in a solvent is determined from the free energy of mixing [42, 43]. In making a mixture, the internal energy (U) of a system changes from an initial to a final state. According to the first law of thermodynamics, a change in internal energy (ΔU) involves a flow heat from (or released to) the surroundings of the system and a work done on (or by) the system [44, 45]. At constant pressure P , the change in the enthalpy of mixing ΔH is

$$\Delta H = \Delta U + P\Delta V \quad (25.1)$$

where ΔV is the change in the volume of mixing.

On the other hand, the second law of thermodynamics stipulates that, in a spontaneous or nonreversible process, the entropy increases and the system moves toward a

thermodynamically stable lower energy state, namely, state of equilibrium [46]. For binary systems the change in the entropy of mixing depends on the number of mixed molecules as follows:

$$\Delta S = k_B \ln \Omega_{1,2} \quad (25.2)$$

where k_B is the Boltzmann constant and $\Omega_{1,2}$ is the number of configurations or spatial arrangements that N_1 solvent molecules and N_2 solute molecules can adopt in the system (lattice) [47]. In contrast to a molecular solution (high ΔS value), in which both solvent and solute molecules are small, a polymer solution shows a much lower ΔS value because the number of configurations the joined mers (repeating units) can adopt in the lattice is much less important compared to that adopted by the same number of free mers [48]. In a spontaneous transformation, at constant pressure, the amount of heat a system (ΔH_{sys}) gives or receives is the same that the surroundings (ΔH_{surr}) receives or gives, respectively: $\Delta H_{sys} = -\Delta H_{surr}$. Thus, at constant temperature

$$\Delta S_{surr} = \frac{\Delta H_{surr}}{T} = -\frac{\Delta H_{sys}}{T} \quad (25.3)$$

According to the second law of thermodynamics, the entropy increases in spontaneous changes, $\Delta S_{sys} + \Delta S_{surr} > 0$, then

$$\Delta H_{sys} - T\Delta S_{sys} < 0 \quad (25.4)$$

The Gibbs free energy of mixing (ΔG) is the driving force for the composition of the mixture to change until the equilibrium is reached. The Gibbs free energy of mixing for a system is then defined as [44]

$$\Delta G_{sys} = \Delta H_{sys} - T\Delta S_{sys} \quad (25.5)$$

For a spontaneous process $\Delta G < 0$, for a nonspontaneous process $\Delta G > 0$, and for a system at equilibrium $\Delta G = 0$. Therefore, ΔG becomes an essential parameter that determines if a polymer will be spontaneously dissolved in a solvent or not.

At this point it is necessary to examine some basic concepts related to the polymer chain conformation that will certainly change in solution. In the solid state (amorphous or/and crystalline), the macromolecules contract and interpenetrate (entangle/co-crystallize) into the others, but once the solvent diffuses, they start to swell and eventually (high dilution) they disentangle to be finally dispersed in the solvent. In this process the polymer coils gradually expand reaching a conformational equilibrium dictated by thermodynamic laws. It was suggested that many properties of polymer solutions depend on the conformation of the chain, rather than on the nature of the chain atoms [45].

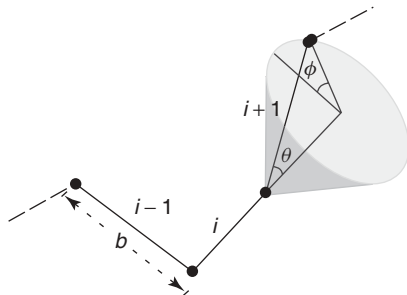


Figure 25.1 Basic geometrical parameters of a polymer chain.

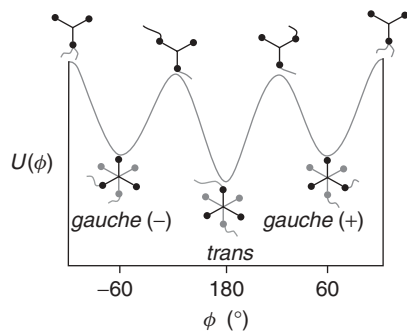


Figure 25.2 Energy diagram for the bond rotation.

25.2.2 Conformation of Polymer Chains

Statistical chain parameters can be readily determined from three geometrical parameters: the bond length (b), the angle (θ) between two successive bonds, and the bond rotation angle (ϕ) between the $i + 1$ and $i - 1$ bonds, projected on a disk generated by the 360° rotation of the i bond (Fig. 25.1) [48]. For a linear polymer chain, represented by a random coil, ϕ is normally restricted to just three values of minimal energy, 180° , 60° , and -60° , known as *trans*, *gauche+*, and *gauche-*, respectively (Fig. 25.2). There are also eclipsed positions at 0° , 120° , and -120° , which are energy barriers for the i bond to rotate. In surpassing one of these energy barriers (partial rotation) the relative position of the adjacent chain substituent groups changes, altering the local conformation. It is to point out that most thermal and mechanical properties of polymers are related to the extent of these energy barriers. If the energy barriers are not much larger than the thermal energy, the *trans-gauche* isomerization takes place easily, indicating that the chain is dynamically flexible [15].

One of the characteristic dimensions of polymer coils is the root-mean-square end-to-end distance ($\langle r^2 \rangle^{1/2}$), which for a linear chain of n bonds is calculated by considering the backbone bonds as vectors (\mathbf{b}_i) [49].

$$r_{ij}^2 = nb^2 + 2 \sum_{i < j}^n \mathbf{b}_i \cdot \mathbf{b}_j \quad (25.6)$$

For a freely joined chain that consists of n' successive chain segments of fixed average length l' and bond angles between neighbor segments (uncorrelated), assuming all values with equal probability, the root-mean-square end-to-end distance is [50]

$$\langle r^2 \rangle_0 = n'l'^2 \quad (25.7)$$

The subscript zero indicates an unperturbed state and the angle brackets denote a statistical mechanical average. The length of a fully extended chain is nb or $n'l'$.

Another characteristic dimension is the radius of gyration ($\langle R_g^2 \rangle^{1/2}$), which is a root-mean-square distance calculated from the distances (s_i) joining all segments of the chain to a center of gravity [48],

$$R_g^2 = \frac{1}{n} \sum_i^n s_i^2 \quad (25.8)$$

The radius of gyration is related to r_{ij} through the *Lagrange theorem*,

$$\langle R_g^2 \rangle = \frac{1}{2n^2} \sum_i^n \sum_j^n \langle r_{ij}^2 \rangle \quad (25.9)$$

$$\langle R_g^2 \rangle_0 = \frac{\langle r^2 \rangle_0}{6} \quad (25.10)$$

The parameters $\langle r^2 \rangle_0^{1/2}$ and $\langle R_g^2 \rangle_0^{1/2}$ correspond to an ideal chain. For the calculation of parameters of real chains, short- and long-range interactions may be considered. The former are related to local geometrical and interactional parameters such as fixed bond angles and potentials perturbing bond rotations, whereas the latter are mainly related to interactions involving remote units in the chain. As is discussed later, the long-range interactions can be eliminated through experimental procedures; the unperturbed dimensions thus obtained may be interpreted only in terms of short-range features [49].

The dimensions $\langle r^2 \rangle^{1/2}$ and $\langle R_g^2 \rangle^{1/2}$ are single-average distances of a very large number of possible conformations. By means of probability tools, the distribution function $W(r)$ of all possible r^2 can be deduced [45, 49]. For ideal polymer chains this function is Gaussian,

$$W(r) = \left(\frac{3}{2\pi \langle r^2 \rangle} \right)^{3/2} e^{-3r^2/2\langle r^2 \rangle} \quad (25.11)$$

It should be said that a Gaussian coil is not appropriate for the representation of real polymer chains because it does not take into account volume effects produced by long-range interactions. A polymer chain in a random walk cannot cross its own path. In other words, a real

polymer chain has excluded volume, which disallows a number of chain conformations. As a consequence, the polymer coil swells reaching a larger dimension than that normally calculated for a Gaussian coil. Exact numerical and analytical self-avoiding walk models were developed for a more accurate calculation of the chain parameters [51–53]. It was demonstrated that the radius of gyration of real chains scales as N^v (v is approximately 3/5) and not as $N^{0.5}$, as deduced for ideal chains. Experimental and theoretical approaches were proposed to determine the value of v [54, 55]. One approach is the exact enumeration of self-avoiding walk models, which considers a limited number of computed walks, but is accurate when precise and refined extrapolation methods are used [56]. Another approach is through Monte Carlo methods in which quite long walks can be sampled, but the data are necessarily subjected to statistical uncertainty [55]. By considering excluded volume effects, an acceptable value of 0.588 (for $d = 3$ dimensions) was estimated by Monte Carlo methods.

25.2.3 Flory–Huggins Lattice Theory and Related Theories

When a number of polymer molecules (N_2) are mixed with a number of molecules of a good solvent (N_1) they disperse and at the same time they expand from a constricted dimension. Hereafter, in this section the subscripts 1 and 2 refer to the solvent and the polymer in the mixture, respectively. The resulting polymer solution can be examined from the Flory–Huggins theory, in which a 3D lattice of sites is filled with solvent and polymer molecules; each site of the lattice being occupied either by a solvent molecule or by a polymer segment whose size or volume is similar to that of the solvent molecule [42, 43]. Under this consideration, the volume of a polymer chain (V_2) is r times the volume of a solvent molecule (V_1). The volume fraction of the polymer (φ_2) in the lattice is then $N_2 r/(N_1 + N_2 r)$. Compared to a solution in which both solvent and solute molecules are small, the combinatorial calculated number of configurations for a polymer solution may be much smaller due to the fact that the contiguous segments of a polymer chain are constrained to occupy only adjacent sites. The logarithm of the number of calculated configurations for a polymer solution in terms of volume fraction is $\ln \Omega_{1,2} = -(N_1 \ln \varphi_1 + N_2 \ln \varphi_2)$ [45]. For an ideal or athermal solution ($\Delta H = 0$), the intermolecular interaction energy between mixed species is the same ($\varepsilon_{11} = \varepsilon_{22} = \varepsilon_{12}$), then

$$\Delta G = -T \Delta S = k_B T (N_1 \ln \varphi_1 + N_2 \ln \varphi_2) \quad (25.12)$$

In this relation, ΔG is always negative, because the mole fractions are always less than unity.

Polymer solutions are in general considered as regular solutions for which the intermolecular interaction energy between the mixed species is different from one another ($\varepsilon_{11} \neq \varepsilon_{22} \neq \varepsilon_{12}$) and then $\Delta H \neq 0$ [47]. In these solutions the change in the entropy of mixing is considered similar to that calculated for ideal solutions. This simplification may be acceptable for polymer solutions of low polar character. The change in the enthalpy of mixing for regular solutions is

$$\Delta H = N_1 \varphi_2 z \Delta \varepsilon \quad (25.13)$$

where z is the lattice coordination number and $\Delta \varepsilon$ is the energy of mixing for each contact. So, the change in the Gibbs free energy of mixing for a regular solution is [48]

$$\Delta G = k_B T (N_1 \ln \varphi_1 + N_2 \ln \varphi_2 + N_1 \varphi_2 \chi_{1,2}) \quad (25.14)$$

where $\chi_{1,2}$ is a dimensionless parameter known as the *Flory interaction parameter*.

From this equation, the chemical potential of mixing per moles of component i ($\Delta \mu_i$) can be calculated [48]. For a binary mixture,

$$\Delta \mu_1 = \left(\frac{\partial \Delta G}{\partial N_1} \right)_{T, P, N_2} \quad (25.15)$$

$$\Delta \mu_1 = k_B T \left[\ln \varphi_1 + \left(1 - \frac{1}{r} \right) \varphi_2 + \chi_{1,2} \varphi_2^2 \right] \quad (25.16)$$

In this equation, $\chi_{1,2}$ is independent of composition and enthalpic nature; however, experiments have demonstrated that this is not necessarily true [16, 20, 57].

For a dilute solution $\ln(1 - \varphi_2) \approx -\varphi_2 - \varphi_2^2/2$, and taking into account that $V_2/V_1 = r$ and $\varphi_2 = CV_2/M_2$

$$\Delta \mu_1 = -RT \left[\frac{CV_1}{M_2} + \left(\frac{1}{2} - \chi_{1,2} \right) \left(\frac{CV_2}{M_2} \right)^2 \right] \quad (25.17)$$

where C is the concentration of the solution, R is the gas constant, M_2 is the molecular weight of the polymer, and V_1 and V_2 are the partial molar volumes of the solvent and polymer, respectively.

It is to note that this simple equation was deduced assuming a random mixing process, a volume change upon mixing that vanishes, and an interaction parameter $\chi_{1,2}$ independent of composition, among others [58, 59]. In spite of these simplification criteria, and others of subtle nature, the equation gives a qualitative insight into the nature of polymer solutions.

The change in the chemical potential of the solvent is related to the osmotic pressure (π) through a simple expression $\Delta \mu_1 = -\pi V_1$ [17], then

$$\pi = RT \left[\frac{C}{M_2} + \left(\frac{1}{2} - \chi_{1,2} \right) \left(\frac{V_2}{M_2} \right)^2 \left(\frac{1}{V_1} \right) C^2 \right] \quad (25.18)$$

This second-degree polynomial equation can be simply represented as

$$\frac{\pi}{RT C} = \frac{1}{M_2} + A_2 C \quad (25.19)$$

where A_2 is the osmotic second virial coefficient. A_2 and M_2 can then be deduced by measuring the osmotic pressure of a series of diluted polymer solutions. The value of A_2 can be either positive or negative depending on the experimental temperature [17]. The temperature at which $A_2 = 0$ is known as the Flory temperature or *theta* temperature. $A_2 = 0$ for $\chi_{1,2} = 0.5$, which is a critical value of miscibility of a polymer in a solvent [16]. In most cases, $\chi_{1,2}$ is positive because interactions are mainly van der Waals attractions [15]. For good solvents $\chi_{1,2}$ is much smaller than 0.5. For $\chi_{1,2} = 0.5$ it is supposed that the attractive and repulsive forces between the polymer and the solvent are completely compensated and the polymer chains are considered to be under unperturbed conditions (ideal chains) [35].

Light scattering measurements can also be used to determine the molecular weight (M_2) of solute molecules as well as interactional (second and third virial coefficients) and structural parameters (radius of gyration) [60, 61]. The reader is referred to Chapter 18 for more information on light scattering methods. The dependence of A_2 and $\langle R_g^2 \rangle$ on M have been the subject of many research studies in polymer solution thermodynamics [29, 62]. Many other experimental techniques can be used to determine these and other related parameters [28, 35, 63].

The Flory–Huggins lattice theory has been considered the basis of the polymer solution thermodynamics and many of further theories on this subject have been either simple or complex modifications, aiming to overcome deficiencies that have arisen from simplifications used in the original equation. Flory and Krigbaum developed the Flory–Huggins theory by taking into account alternate regions of pure solvent and solvated polymer domains, and introduced the concepts of excluded volume and *theta* temperature [27]. Heil and Prausnitz [16] have derived a semiempirical equation containing two adjustable parameters, which is a compromise between the relatively simple one-adjustable parameter equation of Flory–Huggins and the complex multiparameter theories of later authors. Their so-called segment-interaction equation, which makes use of the local volume fraction concept, first stipulated by Wilson [64], was successfully applied to a variety of polymer solutions including polymer-mixed solvent systems having specific interactions such as hydrogen bonding. Renuncio and Prausnitz have proposed an approximation introducing non-randomness to the Flory–Huggins equation [65]. For that purpose they have also used the Wilson local composition concept. The residual entropy calculated under this assumption was different from that of the Flory–Huggins equation.

The calculated change in the enthalpy of mixing and activity data that they applied to a few binary polymer–solvent systems was consistent with experimental results. Alternative expressions of this model were later proposed making the theory more realistic [66]. Sanchez–Lacombe developed a molecular theory on pure fluids of variable geometry and size that was later generalized to mixtures [67, 68]. Their model, which considers occupied and vacant lattice sites (holes), makes a complete thermodynamic description of the fluid that is useful to predict liquid–vapor transitions and the effect of chain length on the critical and boiling point of normal alkanes, among others. A similar model, which introduces a nonrandom distribution of mixing to pure-hole components and polymer solutions, was later proposed [69]. Examples of other approaches and refinements of the Flory–Huggins theory can be found in the literature, all of them aiming at improving predictions on the polymer solution properties [21, 70–72].

25.2.4 The Solubility Parameter

The choice of an appropriate solvent to dissolve a polymer is frequently based on experience or guided by literature and technical reports on some solvent characteristics such as solvent “strength,” rate of evaporation, and solvent/nonsolvent mixture effects, among others; some of these characteristics may have strong effects on both the polymer processing from solution and the properties of the final product. Theories on polymer–solvent mixtures are of essential importance and could be developed to understand the thermodynamics of the system but, sometimes, they can be extremely complex to be developed and applied in ordinary polymer solutions that are going to be processed. Alternatively, numerous simple and practical methods reported in the literature can be used for the prediction of the solubility behavior in polymer solutions [13, 19]. One of the most practical methods uses the Hildebrand solubility parameter (δ), which is a numerical value related to the intermolecular interactions (van der Waals) that hold together the molecules in a solvent or in a solid. For a small amount of a solid (solute) in a solution those interactions are disrupted by the solvent in such a way that the individual solute molecules separate from one another. Such a disruption seems to be optimal when the solute–solute and solvent–solvent molecular interactions are of similar “strength.” Thus, solvents and solids (polymers) showing similar δ values may dissolve in the other and form miscible mixtures; through this simple rule the solubility of a polymer in a solvent can be practically predicted [70].

The solubility parameter is defined as the square root of the cohesive energy density per unit volume and for a solvent it can be obtained from the heat of vaporization (ΔE_i^{vap}), which is the energy supplied to vaporize a fluid [70]. This property is particularly helpful because it is

supposed that the same intermolecular forces should be overcome to vaporize a liquid and to dissolve it.

$$\delta_i = \left(\frac{\Delta E_i^{\text{vap}}}{V_i} \right)^{1/2} \quad (25.20)$$

There is no way to determine the solubility parameter of polymers by means of the heat of vaporization; instead, swelling experiments, methods involving cloud-point determinations, and some others are used to determine it [13].

The Flory interaction parameter is related to the solubility parameter through the following equation:

$$\chi_{1,2} = \frac{V_1}{RT} (\delta_1 - \delta_2)^2 \quad (25.21)$$

where δ_1 and δ_2 are the solubility parameters of the solvent and the polymer, respectively, and V_1 is the partial molar volume of the pure solvent.

This equation takes into account only enthalpic contributions; however, for a best calculation of the Flory parameter $\chi_{1,2}$, the entropic contributions, χ_s , should be considered as well [70, 73].

$$\chi_{1,2} = \chi_s + \frac{V_1}{RT} (\delta_1 - \delta_2)^2 \quad (25.22)$$

In terms of solubility parameters, the change in the enthalpy of mixing is

$$\Delta H = n_1 V_1 \varphi_2 (\delta_1 - \delta_2)^2 \quad (25.23)$$

This equation clearly shows that ΔH tends to zero when δ_1 and δ_2 approach each other. In this case, $\Delta G < 0$ is expected, and good solubility properties will be observed with small mixing heats. It has been reported that miscibility should occur for values of δ_1 and δ_2 within 2 or 3 $\text{J}^{1/2} \text{cm}^{-3/2}$ of one another [74].

An extension of the Hildebrand parameter to estimate the relative miscibility of polar and hydrogen bonding systems has been proposed: $\delta^2 = \delta_d^2 + \delta_p^2 + \delta_h^2$. The components of this equation are the dispersion (δ_d^2), electrostatic (or polar) (δ_p^2), and hydrogen bond (δ_h^2) Hansen solubility parameters [75, 76].

Numerous sources with compiled solubility parameters are available for commercial solvents [1, 2] and polymers [2, 73]. Although their use affords qualitative results, they are commonly used in industry to predict the miscibility of polymers in solvents [39, 77]. For solvents ranked according to their solubility parameter, those in close proximity may show a comparable solubility behavior, whereas those that are far apart may show substantial differences.

25.2.5 Phase Equilibria in Polymer Solutions

Phase separation is frequently observed in polymer solutions and it is mainly due to their low entropy of mixing. At a state of equilibrium each species of the mixture is partitioned between two phases, namely, the supernatant (extremely dilute) and precipitated (moderately dilute) phases [78]. Theoretical models and experimental techniques have been developed to predict the solubility behavior of polymer solutions, polymer blends, and other related systems [79, 80]. Simple theories only permit a rather qualitative description of this phenomenon [78]. Refined and improved theoretical and semiempirical models allow a more accurate prediction of the demixing phenomena and related thermodynamic properties [57, 81].

At a given pressure and temperature, the total Gibbs free energy of mixing of a one-phase polymer–solvent system of composition φ_2 should be necessarily minimum, otherwise the system will separate into two phases of different composition, as it is represented in a typical ΔG versus φ phase diagram of a binary solution (Fig. 25.3). The volume fractions at the minima ($\partial \Delta G / \partial \varphi = 0$), φ' , and φ'' , will vary with temperature (*binodal*) up to critical conditions (T_c and φ_c) where $\varphi' = \varphi''$ (Fig. 25.3b).

According to the type of T versus φ diagram (Fig. 25.4), the binary solution can exhibit an upper critical solution temperature (UCST), a lower critical solution temperature (LCST), or both (close-loop phase behavior). Above the UCST or below the LCST the system is completely miscible in all proportions [82]. Below the UCST and above LCST a two-phase liquid can be observed between φ' and φ'' . The two-phase liquid can be subdivided into unstable (spontaneous phase separation) and metastable (phase separation takes some time). These two kinds of mixtures are separated by a *spinodal*, which is outlined by joining the inflection points ($\partial^2 \Delta G / \partial \varphi^2 = 0$) of successive ΔG versus φ phase diagrams, obtained at different temperatures (Fig. 25.3b). Thus, the binodal and spinodal touch each other at the critical points φ_c and T_c .

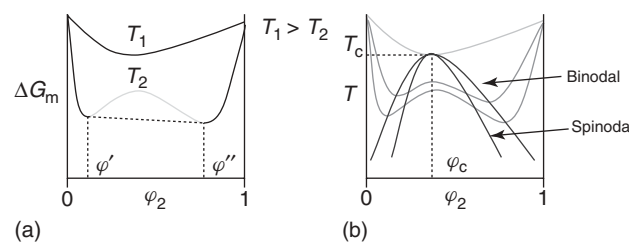


Figure 25.3 Binary phase diagrams. (a) At T_1 the mixture is miscible at all composition and at T_2 the mixture shows phase separation (between φ' and φ''). (b) Binodal and spinodal curves, and critical temperature (T_c) and concentration (φ_c).

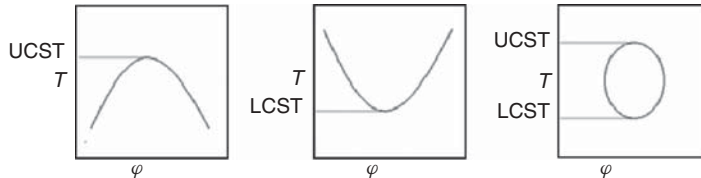


Figure 25.4 Temperature–volume fraction diagrams for binary polymer solutions.

From Equation 25.16 the conditions for incipient phase separation are [12, 45]

$$\left(\frac{\partial \mu_1}{\partial \varphi_2}\right)_{T,P} = 0 \quad \text{and} \quad \left(\frac{\partial^2 \mu_1}{\partial \varphi_2^2}\right)_{T,P} = 0 \quad (25.24)$$

The combination of the resulting expressions gives [48]

$$\varphi_c = \frac{1}{1 + \sqrt{r}} \quad (25.25)$$

and

$$\chi_c = \frac{1}{2} \left(1 + \frac{1}{\sqrt{r}}\right)^2 \cong \frac{1}{2} + \frac{1}{\sqrt{r}} \quad (25.26)$$

Then, the critical concentration (φ_c) depends on the relative size (molecular weight) of the components of the mixture. For mixtures involving small molecules ($\sqrt{r} = 1$), φ_c takes a value of around 0.5; however, for polymer solutions the phase diagram (Fig. 25.5) becomes highly asymmetric with φ_c essentially confined to the solvent-rich regime ($\varphi_c \rightarrow 0$ for $r \rightarrow \infty$).

Flory has proposed that

$$\frac{1}{2} - \chi_{1,2} = \psi \left(1 - \frac{\theta}{T}\right) \quad (25.27)$$

where ψ is the entropy of dilution parameter.

At the temperature where phase separation occurs $T = T_c$, then

$$\frac{1}{T_c} = \frac{1}{\theta} \left(1 + \frac{1}{\psi \sqrt{r}}\right) \quad (25.28)$$

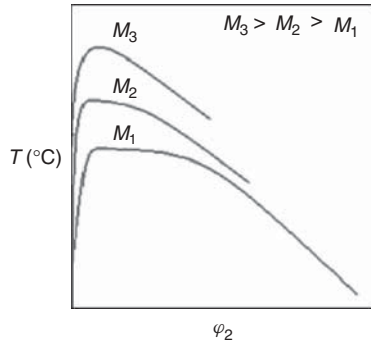


Figure 25.5 Phase diagrams for polymer/solvent mixtures.

This equation shows that the critical temperature (T_c) is also dependent on the molecular weight of the polymer [82]. Thus, for a UCST diagram this critical parameter moves toward higher temperatures as the chain length increases (Fig. 25.5). This dependence is particularly useful for the fractionation of most synthetic polymers, which are seldom molecularly uniform [83].

At equilibrium, the two-phase coexistence is conditioned to an identical chemical potential of components (*i*) between phases ($\Delta\mu'_i = \Delta\mu''_i$). The chemical potential is a valuable parameter because it is directly related to experimentally accessible properties, as is the case of the osmotic pressure, $\pi = -\Delta\mu_1/V_1$.

Initial works on the phase equilibrium of polymer solutions were concerned with nonpolar solutions using carefully prepared quasi-monodisperse polymer fractions [78]. The theory and practice was later extended to molecularly heterogeneous polymers [84], multicomponent solutions (ternary mixtures) such as polymer/solvent mixture [16, 85] and polymer mixture/solvent [86], and polymer blends [79, 80], among others [87]. Improvements on predicting thermodynamic properties were particularly proposed for polymer solutions of industrial importance, including those having polar and hydrogen-bonded components [16].

25.2.6 Characterization of Polymers Using Thermodynamic-Based Techniques

Characterization of polymers in solution has posed unique challenges owing to their inherent complexity, primarily associated to their high molecular weight, chemical structure, and composition. Such complexity is accentuated by the fact that most polymers exhibit a molecular weight distribution and structural defects. For the characterization of polymers in solution there exist well-developed instrumentation and methodologies. The most common techniques are as follows:

- NMR, FTIR, UV-vis—chemical and structural characterization (see Chapter 16)
- GPC (or SEC), MALDI-TOF—molecular weight and MWD (see Chapters 17 and 16, respectively)
- LS, Neutron scattering—molecular weight, structural and interactional parameters (see Chapter 18)
- Viscometry—molecular weight, flow properties, and structural and interactional parameters

MO, VPO, Eb., Cry.¹ —molecular weight and interactional parameters.

All these techniques use different principles of measurement. Here, only two methods based on colligative properties are described.

The number-average molecular weight (M_n) of polymers can be easily determined from methods based on colligative properties, which are dependent on the number of molecules in the solution [28]. Thus, the addition of a number of solute molecules to a solvent produces a change in the chemical potential ($\Delta\mu_1$) of the solvent from which the molecular and interactional parameters can be deduced.

Among the different techniques based on colligative properties, the most practical ones to determine M_n (number-average molecular weight) are the MO [17, 28] and the VPO [88], both performed in dilute solution.

25.2.6.1 Membrane Osmometry In this technique a dilute polymer solution and a pure solvent are separately placed in two different chambers that are divided by a tightly held semipermeable membrane through which only solvent molecules can move across. Because the chemical potential of pure solvent is higher than that of the solvent in the solution, the solvent will diffuse across the membrane from the pure solvent to the solution chamber up to the point in which the osmotic pressure equals the hydrostatic pressure created by the volume imbalance between the liquids of the two chambers. The osmotic pressure ($\pi = \rho gh$) at equilibrium (static method) can be calculated from the difference in height (h) between the liquids in the capillaries connected to each chamber. In practice, a dynamic method is used in which a pressure (P) is applied to counterbalance (at $t = 0$) the osmotic pressure (π) exerted by the pure solvent. This later method is known as *dynamic osmometry* and allows an instantaneous determination of π [17, 89].

For a series of dilute solutions ($C_1, C_2, C_3, C_4 \dots$) at constant temperature [60],

$$\frac{\pi}{C} = RT \left(\frac{1}{M_n} + A_2 C + A_3 C^2 + \dots \right) \quad (25.29)$$

The first term of this equation is the van't Hoff expression ($\pi/C_{c \rightarrow 0} = RT/M_n$) for osmotic pressure at infinite dilution and the second term is related to the second virial coefficient (A_2). Thus, M_n and A_2 can be, respectively, determined from the intercept and the slope from a π/C versus C plot (the third and higher virial coefficient terms are normally ignored) [90]. Compared to other experimental techniques (SEC and light scattering), MO is limited

¹MO, membrane osmometry; VPO, vapor pressure osmometry; Eb., ebullometry; Cry., cryoscopy.

to the study of a relatively narrow molar mass range $10^3 - 5 \times 10^5$ g/mol, which depends on the membrane permeability (low molar mass limit) and on the smallest osmotic pressure that can be reliably measured (upper molar mass limit). As mentioned above, A_2 is a measure of polymer–solvent interactions and its value is an indication of the capacity of the solvent to dissolve a polymer at determined conditions. Good solvents show positive values typically in the order of $10^{-4} - 10^{-3}$ (ml mol)/g². At *theta* conditions $A_2 = 0$, where polymer molecules are supposed to be under unperturbed conditions. It is common to build $(\pi/C)^{0.5}$ versus C plots because they are normally linear over broader ranges of concentration compared to those of π/C versus C plots. The main advantage of this technique is that calibration with standards is not required, yielding an absolute number-average molecular weight (M_n).

25.2.6.2 Vapor Pressure Osmometry The VPO became a popular method for the determination of the number-average molecular weight of nonvolatile solutes of less than about 20,000 g/mol and that tend to diffuse across the membrane in MO experiments [91]. This method operates on the principle that the vapor pressure of a solution is lower than that of a pure solvent (P_1^0) at constant pressure and temperature. This vapor pressure lowering (ΔP) is proportional to the molar mass of the solute (polymer) for dilute solutions. As it is known, the vapor pressure of a solvent in dilute solutions obeys the Raoult's law, $P_1 = P_1^0 x_1$, where P_1 is the partial vapor pressure of the solvent whose mole fraction in the solution is x_1 . In terms of the mole fraction of the solute, $P_1 = P_1^0 (1 - x_2)$ or $\Delta P/P_1^0 = -x_2$.

As measuring vapor pressure depression using VPO requires extreme sensitivity, a thermoelectric method is used based on the following principle. One drop of pure solvent is placed on one of two matched temperature-sensitive thermistors located in a chamber saturated with vapor solvent, at constant temperature. On the other thermistor, a drop of polymer solution is placed. The solvent condensation on the solution drop will heat it up until its vapor pressure matches that of the pure solvent drop [35].

From thermodynamics,

$$\Delta T = \frac{RT^2 x_2}{\Delta H_{\text{vap}}} \quad (25.30)$$

For dilute solutions $x_2 \approx n_2/n_1$, and, if the polymer concentration (C_w) is expressed in grams of solute per 1000 g of solvent (molality),

$$\Delta T = \frac{RT^2}{\Delta H_{\text{vap}}} \times \frac{C_w}{M_n} \times \frac{m_1}{1000} \quad (25.31)$$

where m_1 is the molar mass of the solvent.

The temperature change causes a resistance change (ΔR) in the thermistor and for practical reasons ΔR measurements are preferred instead of direct measurements of ΔT . ΔR is directly proportional to ΔT for small changes in temperature ($\Delta R \propto \Delta T$) [92]. In this method substances of known molecular weight are used to determine the calibration constant of the instrument. A calibration curve relates the change in resistance to the molal concentration of the solution. The molecular weight of the polymer can then be determined from the resistance measurements through the following equation [91]:

$$\left(\frac{\Delta R}{C} \right)_{C \rightarrow 0} = \frac{K}{M_n} \quad (25.32)$$

Details on the methodologies and instruments for MO and VPO can be found elsewhere [17, 28, 90].

25.3 SEMIDILUTE POLYMER SOLUTIONS

The thermodynamic behavior of semidilute polymer solutions is substantially different from that of dilute solutions [15]. In the semidilute regime ($\varphi > \varphi^*$), the chains interpenetrate each other reducing their overall motion. Under this condition, viscosity and the osmotic pressure of the solution rapidly increase with small changes in concentration [26, 93]. The overlap concentration (φ^*) decreases as the chain length (or N) increases and, consequently, the range of the semidilute regime widens, although the upper limit is ambiguous to define.

The mean field theory seems to be helpful in explaining the behavior of semidilute solutions, but it fails in explaining various experimental results [35]. Alternative theories such as the blob concept and the scaling theory, both introduced in the 1970s, have been successfully applied to determine the thermodynamic behavior of these solutions [15].

25.3.1 The Blob Model

Between two neighboring entanglement points of the same chain there is a segment that occupies a domain or sphere (blob) and that adopts its conformation independently of other segments (Fig. 25.6). The chain segment within the blob takes a similar conformation to that of the whole chain. As this concept applies to all chain segments, the entire solution is implicitly composed of blobs.

At the overlap concentration φ^* , in a good solvent ($v = 3/5$), the overall monomer density (ρ^*) is [15, 26]

$$\rho^* \cong N R_g^{-3} \cong b^{-3} N^{-4/5} \quad (25.33)$$

A blob of size ξ has g monomers of size b , then $\xi \cong bg^v$. Also, the density of monomers within the blob is $\rho \cong g\xi^{-3}$.

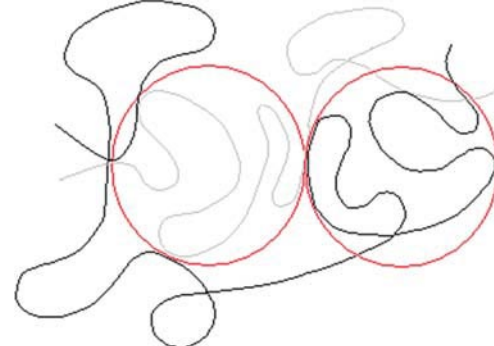


Figure 25.6 Representation of blobs in a polymer chain. (See insert for the color representation of the figure.)

The combination of these two relations ($\xi \cong b^{-5/4} \rho^{-3/4}$) indicates that the blob size decreases with concentration. It can also be noticed that ξ is determined only by the monomer density and not by N .

The blob size relative to the mean-square radius of gyration is

$$\xi \cong R_g \left(\frac{\rho}{\rho^*} \right)^{-3/4} \quad (25.34)$$

and the number of monomers in the blob is

$$g \cong N \left(\frac{\rho}{\rho^*} \right)^{-5/4} \quad (25.35)$$

For $\rho = \rho^*$, $\xi = R_g$ and $g = N$. At $\rho > \rho^*$ both ξ and g decrease (Fig. 25.7) because the chains become more densely overlapped with each other.

In ideal solutions, the polymer chain moves as a unit. The osmotic pressure for this solution is

$$\pi_{C \rightarrow 0} = \frac{\rho}{N} k_B T \quad (25.36)$$

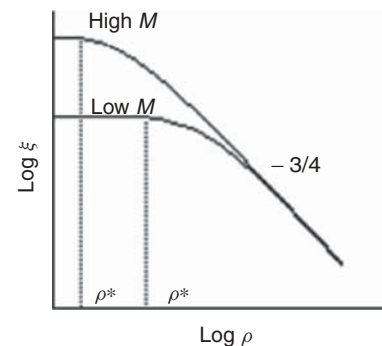


Figure 25.7 Blob size as a function of monomer density for two different chain lengths.

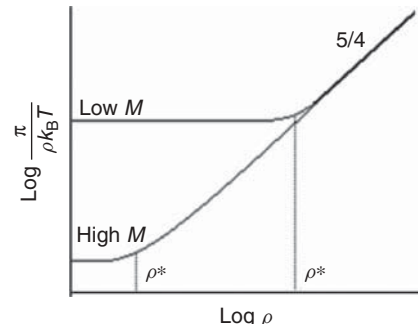


Figure 25.8 Osmotic pressure reduced by $\rho k_B T$ as a function of monomer density for two different chain lengths.

For semidilute solutions the segment of a blob moves as a unit. The osmotic pressure for this solution depends on the number of blobs per unit volume ($1/\xi^3$).

$$\pi \approx k_B T \xi^{-3} \approx k_B T b^{-15/4} \rho^{-9/4} \quad (25.37)$$

This relation indicates that in a semidilute regime π is the same for solutions of polymers of different chain length or molecular weight (Fig. 25.8); thus, at $\rho > \rho^*$ the osmotic pressure is independent of M , contrasting with the behavior of a dilute solution, in which π is strongly dependent on M .

$$\frac{\pi}{k_B T} = \frac{\rho}{N} f_{II}(x) = \frac{\rho}{N} \text{const} \left(\frac{\rho R_g^3}{N} \right)^m \quad (25.38)$$

where f_{II} is the scaling function. As $R_g = bN^{3/5}$,

$$\frac{\pi}{k_B T} = \text{const} b^{3m} \rho^{m+1} N^{(4m/5)-1} \quad (25.39)$$

For $m = 5/4$, π is independent of N and dependent on $\rho^{9/4}$ [17, 26]. The dependence of π on ρ in the mean field theory (ρ^2) is different from that in the scaling theory ($\rho^{9/4}$) by a factor of $\rho^{1/4}$. Such difference is related to a correlation effect given by the number of contacts between monomers. The reduced osmotic pressure (π/π_{ideal}) plotted as a function of the reduced concentration (ρ/ρ^*), in a double logarithm scale, displays a curve that shows the change in slope to $5/4$ for $\rho/\rho^* > 1$ (Fig. 25.9).

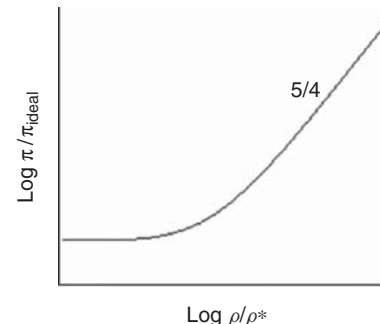


Figure 25.9 Reduced osmotic pressure as a function of reduced concentration.

25.4 PROCESSING OF POLYMER SOLUTIONS

A large number of solution-based processing methods have been used for manufacturing films and fibers from a wide variety of commercial polymers [94–96]. These methods are in fact ideal for the processing of nonmelting but soluble polymers or for the processing of thermally sensitive polymers. Also, they are often the most appropriate methods for the fabrication of very thin films and fibers that cannot be produced by melt extrusion, and they are particularly useful to deposit functional thin and ultrathin films over a wide variety of substrates.

25.4.1 Film Forming Processes via Polymer Solution

25.4.1.1 Solvent Casting Solvent casting is a method for manufacturing films from a solution or dispersion [96]. In a standard process, the polymer and other components are dissolved in a solvent and the resulting solution is poured into a mold (usually an open vessel) where the solvent evaporates leaving a residual film [97, 98]. Two main technologies, the wheel and the belt (or band) casting processes are used in the industry to cast continuous polymer films from solution (Fig. 25.10; 94, 99). The essential elements of these processes are the dope preparation, the film deposition, and the film drying. The dope is a polymer solution or dispersion normally prepared using low vapor pressure solvents; it may contain some other components like plasticizers, ultraviolet absorbers, antistatic compounds, and release agents [100]. Standard mixers are used to disperse the polymer and other solids (or liquids) in the solvent or mixture of solvents to form a homogenous dispersion that should be stable before and during the film forming process [101]. The rheological properties of the solution depend, among others, on the concentration of solids, which typically ranges between 5% and 40%, and on the temperature, which can vary between room temperature and the boiling point of the solvents [96, 102]. The dope is normally degassed to prevent the

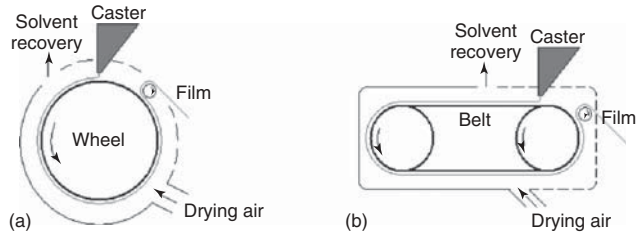


Figure 25.10 Schematic representation of the (a) wheel and (b) belt casting processes.

formation of air bubbles during the film forming process [103]. A filtration or clarification system is required to eliminate gels, agglomerates, or some other undesirable particles. The dope is continuously deposited as a thin film of uniform thickness over an endless moving surface (wheel or belt) that requires an accurate speed control. The surface finish of the casting support is critical, taking into account that the surface is accurately replicated onto the contact surface of the casted film. Specially designed casters or dies are used to homogeneously distribute the dope across the moving surface. For best results, the flow rate in the die may not exceed that corresponding to laminar flow. The film drying can be performed through different methods, including airstream and radiation heating, at relatively soft conditions. The solvent evaporates all along the film forming process while it is evacuated and conducted up to a solvent recovery system. The evaporation rate of the solvent depends on the solids' content, which continuously increases as the solvent evaporates [104]. Solvent evaporation takes place in essentially two stages: in the first stage it is governed by the vapor pressure, but as long as the polymer solidifies the solvent is retained within the film and it is lost in the second stage by a diffusion-controlled process [105]. Before the takeoff point, the film is cooled down to reduce tackiness and to increase its mechanical strength. Once detached from the support, the semifinished film is air dried at both open surfaces in further steps to be finally wound.

25.4.1.2 Coating Coating is a process of deposition of a thin film over a surface or substrate to change its characteristics and properties [39, 106]. Also, the term coating describes any material applied as a thin continuous layer to a surface. A wide variety of coating processes can be performed from solution, the choice of one of them depends on the characteristics and/or properties of the solution, the substrate, the polymer and other components, the solvent, and the final film, among others [107]. More recent influences on the choice of the coating process are environmental considerations, health and safety legislations, and cost/benefit relationships [39]. Of primary importance are solvents, which play a crucial role as diluents of the polymer and other nonvolatile components [108].

Most diluents are organic solvents, although for specific applications or for environmental reasons diluents such as water are preferred [109, 110]. The flow properties are highly dependent on the polymer/solvent characteristics and their relative amounts in the solution [111]. Once the solution is deposited, the solvent evaporates leaving a regular film adhered to the substrate, which is composed solely of the nonvolatile components. In general, deposited films are soluble if they were solidified by evaporation of the solvent, but they become insoluble if they are cured (crosslinked) through chemical reactions [112, 113]. The film thickness depends on the solution concentration (density), viscosity, polymer characteristics, and deposition speed, among others [114–117]. Multilayer films can be deposited from the same or different coating solution by means of successive coatings [118, 119].

The most important coating processes for the deposition of polymer films from solution are spreading, spraying and flow coating. Spreading (e.g., brush and roller) and spraying (e.g., air spray) are the most extensively used methods for the application of architectural and industrial coatings or paints [39]. Flow coating processes are automated methods for the application of industrial liquids (coatings) over a moving surface. They may be broadly classified into two categories: self-metered and premetered [120]. Self-metered ones include dip as well as roll and blade coating, while premetered ones comprise slot, slide, and curtain coating [121]. In self-metered coating methods a reservoir is normally used for direct or indirect coating. A blade often serves as a metering flow element. In premetered coating methods, a coating die delivers and distributes the desired amount of one or more coating flows. The following are simple schematic configurations of various common coating processes used for the deposition of polymer films (Fig. 25.11).

Following are the important steps in coating processes: preparation of the coating solution, deposition of the solution over a substrate, and finally the solidification of the deposited film (drying or curing). Most industrial coating processes use automated coaters, although for some specific coating needs hand application methods are still preferred.

In relatively recent years, singular coating processes have emerged to comply with specific application needs, especially for the deposition of functional or advanced thin and ultrathin films. In these processes, the thickness of deposited films can vary from one molecular layer to thousands, depending on specific applications or end-use requirements that can vary from simple protective coatings to functional films as, for instance, patterned films of π -conjugated polymers for electronic applications [122, 123]. One of these processes is spin coating, which is a simple and effective method to deposit thin and ultrathin homogenous films across planar substrates. Compared with other film forming processes, spin coating is perhaps the

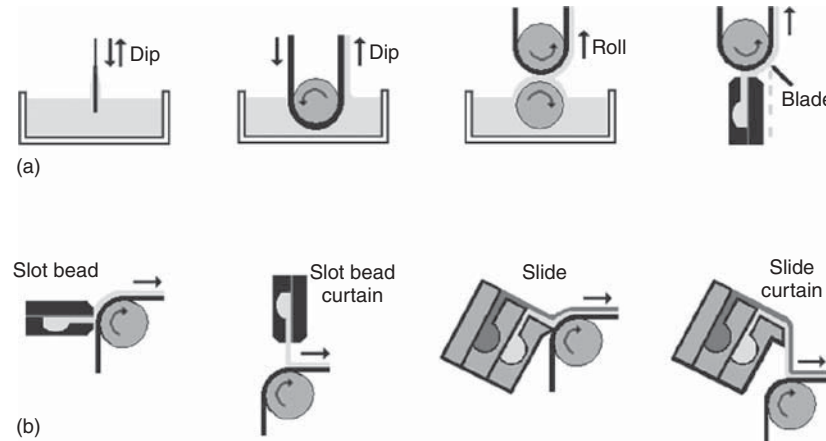


Figure 25.11 Schematic representation of (a) self-metered and (b) premetered coating processes.

simplest method to deposit thin films over a substrate, although small changes in the process parameters can greatly affect the final film characteristics and properties. Other techniques, including LB deposition, layer-by-layer (LbL) deposition, spraying, and epitaxy can be used for the deposition (from solution) of films as thin as one single molecular layer [118, 124–126].

25.4.1.3 Spin Coating Spin coating is a procedure which involves the deposition of uniform thin coating—typically having a thickness in the micron (thin) and submicron (thin > 200 nm > ultrathin) ranges and a total thickness variation of few nanometers—over a rotating flat substrate (or wafer) [127, 128]. In a few words, it is accomplished by flooding the substrate with a solution and rotating it at a constant speed (1000–8000 rpm) [117]. Curved, patterned, and many other specific surfaces can also be covered by this process [129–131]. Fluids of different nature, including sol–gel colloidal suspensions [132], polymer solutions [133], and hybrid materials [134], can also be processed by spin coating following similar procedures. The spin coating method is extensively used in microelectronics and related areas for the deposition of photoresists [135, 136], protective coatings [137], active layers in light emitting diodes [123], among others. This is also a common choice of method for research on thin and ultrathin functional films mainly due to the high quality of deposited films along with additional benefits when combined with various external fields [130].

The basic stages of the spin coating process are as follows:

1. Deposition of an excess volume of a solution onto the center of a substrate that might be held in a perfect horizontal position, either immobile (static dispense) or rotating at a relatively low speed (dynamic dispense). Other modes of deposition can be implemented [138].

2. Acceleration of the rotational speed of the substrate (spin-up).
3. Rotation of the substrate at a rotational speed that typically falls in the 10^3 – 10^4 rpm range (spin-off).
4. Evaporation of volatile components while the substrate is still rotating.

In standard practice, stages 1 and 2 take a minor fraction of time compared to that consumed in stages 3 and 4. A schematic representation of the spin coating stages is depicted in Figure 25.12.

As established long time ago, the film thinning arises basically from two distinct and quasi-simultaneous effects: spreading of the fluid caused by radial forces and evaporation of the solvent [128]. The spin coating process is not sensitive to the deposited volume as long as this suffices to cover the substrate; excess volume is ejected off the edge of the substrate [127, 139]. Most part of the solvent is evaporated during spinning at a rate that depends basically on the volatility of the solvent, the rotation rate, and the ambient conditions at the immediate film surroundings [114]. A postprocess drying treatment helps to eliminate the remaining volatile components and allows the film to equilibrate [140, 141]. In some cases the surrounding air phase is saturated with solvent vapor during film formation providing in this way sufficient time for chain mobility. This strategy has been used for instance for the recognition of the topology of prepatterned substrates and for fully developing a phase-separated microstructure in block copolymers in the film [130]. It has been also used to prevent film defects resulting from a rapid drying of highly volatile solvents [136]. The thickness and quality of the final free-solvent film (dry film) depends on multiple factors associated with the spin coating process, the solution and substrate characteristics, and the ambient conditions [117, 142]. In general, the higher the angular speed of spinning and the lower the concentration of the solution,

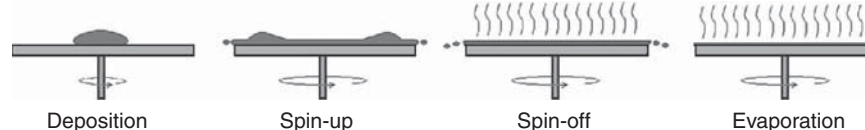


Figure 25.12 Basic stages in the spin coating process.

the thinner the film [123, 127, 128, 143]. The solvent and polymer characteristics are also key parameters in determining the film thickness [123, 133]. It is to point out that a minor variation in one of these and some other parameters can result in important deviations from the desired film characteristics; therefore, the repeatability is one of the most important challenges of spin coating. Commercial spin coaters are currently available for extensive production and experimental research. Technical details of commercial spin coaters are fairly accessible in the web.

Theory Because of its wide usage, the spin coating process has been much investigated from both the experimental and the theoretical points of view. There exist extensive experimental data on the process that has permitted not only to set up the process conditions for many specific polymer/solvent systems, but it has also permitted to understand the correlation of involved parameters and, therefore, to improve the spin coating process to comply with specific applications and research needs [114]. On the other hand, the theoretical or mathematical modeling of the spin coating process has been especially challenging due to the intricate coupling between fluid rheology and solvent evaporation, both having strong effects on the film thinning process [123].

Pioneering works on the mathematical modeling were very simple models in which flow and evaporation were decoupled. In a first approach by Emslie et al. [129], the film thinning (dh/dt) of a viscous flow of density ρ , deposited onto a flat substrate that rotates at constant angular velocity ω , was exclusively analyzed from the rheological point of view. The problem was simplified assuming Newtonian behavior (η_0), regular initial film thickness (h_0), no significant gravitational effects, no significant Coriolis forces, among others. The resulting equation (in cylindrical polar coordinates r, θ, z) allows the calculation of the film thickness (h) after a time t , starting with a liquid having a uniform initial thickness h_0 (Eq. 25.40). These authors have also modeled the case of liquids having irregular initial surface contours, demonstrating that thick layer regions thin out much more rapidly than thin ones, meaning that deposited fluids having a nonuniform initial surface profile tend to homogenize with time, confirming the utility of the spin coating process for producing uniform films of desired thickness [138]. Although not suitable for actual physical flow situations presented by most spin-coated fluids, this mathematical

model has captured the essentials of the flow characteristics of liquids deposited onto a spin coater, and for this reason it has been frequently taken as the starting point of the film thinning modeling driven by centrifugal forces.

$$h = \frac{h_0}{\left[1 + 4 \left(\frac{\rho\omega^2}{3\eta_0}\right) h_0^2 t\right]^{1/2}} \quad (25.40)$$

The work of Emslie et al. [129] was later extended by Acrivos et al. [144] to the case of power law non-Newtonian fluids, typical of concentrated polymer solutions. Contrary to the behavior observed in centrifuged Newtonian fluids, the non-Newtonian ones showed no tendency to form uniform films, even those having a uniform initial surface profile. The authors have thus concluded that spin-coated films of Newtonian fluids have a much better chance to be uniform. This is usually the case for sufficiently low concentrated polymer solutions.

In the second approach, Meyerhofer [128] introduced the film thinning (dh/dt)–evaporation rate (e) dependence to the Emslie, Bonner, and Peck model. In contrast to Equation 25.40, where h tends to vanish with time, Equation 25.41 predicts the formation of a solid film, which attains a finite final thickness (h_f) at time t_f . In this case, the hydrodynamic analysis should consider the viscosity–concentration dependence, but the problem has been simplified considering two separated subprocesses that omit such dependence, assuming that in the first stage the outflow dominates (concentration changes are neglected), but, once a specific thickness is attained, the flow stops and from this point on the second stage starts where the film thins only by evaporation. The mathematical expression for calculating the resulting final thickness for this model is as follows:

$$h_f = \frac{S_0}{L_0} \left(\frac{3\eta e}{2\rho_0\omega^2} \right)^{1/3} \quad (25.41)$$

where S_0 and L_0 are the initial volumes of the solute and solvent, respectively, $C_0 = S_0/(S_0 + L_0)$ and η is a power law function of concentration ($\eta = \eta_{\text{solvent}} + \eta_{\text{solute}} C^\gamma$). From this equation, it is clear that the film thickness is greatly influenced by the evaporation rate, as confirmed by Chen in an investigation on the solvent–evaporation effect on the spin coating of thin films of poly(vinyl butyryl) and cellulose acetate [114].

Bornside et al. [138] have developed a model for spin coating in which evaporation has been analyzed in terms of the mass flux (or mass transfer) from the liquid phase into the adjacent gas phase. Such a mass flux is controlled by a convection–diffusion process that depends on the solution concentration that increases as the solvent leaves the liquid phase. The characteristics of the gas phase in the close vicinity may also have a specific effect on the evaporation process. A modified model based on the equations of Meyerhofer and Bornside was used by Chang et al. [123] to predict the film thickness of spin-coated polymers. In their model, two equations were used: one to predict the wet film thickness, h_w , after spin coating but before drying and another to determine the final film thickness (h_f). The film thicknesses that they have theoretically predicted agree well with those experimentally determined, especially in solutions of low polymer concentration.

More recently, it was proposed that the flow dominates only for a short period before the “onset” of a relatively long intermediate flow/evaporation stage that culminates at high concentration when evaporation becomes dominant. The time interval for each one of these three stages was calculated by Cregan and O’Brien using a formal asymptotic approach [139]. These authors demonstrated that in the first stage (from t_0 to t') the flow dominates while the layer thickness decreases rapidly, then, in the second stage (from t' to t''), the flow and evaporation are equally important from an asymptotic point of view, and in the third stage the flow practically stops and the evaporation dominates letting the film to thin linearly. Figure 25.13 shows a schematic representation of different models of film thinning in a spin coating process.

SOLUTION THERMODYNAMICS IN SPIN COATING. A polymer solution confined between two surfaces (thin film) may show substantial differences in thermodynamic properties when compared to those in bulk [145]; this is because surface effects (important in thin films) may influence the phase equilibrium as well as the kinetics of demixing. Surface effects are important because they lead to

a specific lateral-phase segregation, to a surface-oriented phase separation, to the formation of a wetting layer or to the breakup of a surface layer, among others [146, 147].

The preparation of polymer films from spin coating involves rapid evaporation of the solvent along with the formation of segregated domains that grow until their size reaches the thickness of the film. Further growth of segregated domains is then limited by the geometrical constraints imposed by the film that thins continuously during the spin coating process. The lateral growth of segregated domains is determined by the complex interplay between different time-dependent processes such as elongational flow under a shear field, chain mobility, and solvent diffusion; therefore, the resulting morphology may be far from thermodynamic equilibrium. In this concern, Walheim et al. [141] studied polystyrene (PS)/solvent/poly(methyl methacrylate) (PMMA) solutions, which are interesting systems because PS and PMMA are strongly incompatible, show substantial differences in solubility in common solvents, and interact differently with substrates of different polarity. In addition, one of the two phases can be easily removed by using a selective solvent to obtain information from inside the film. These authors have reported microscopic images of thin films prepared from PS/solvent/PMMA solutions that exhibit a lateral-phase-separated morphology consisting of islands (PS or PMMA) whose composition differs from that of the surrounding continuous phase (PMMA or PS). They also examined the role of the substrate by using substrates of different surface energy. In substrates of high surface energy (polar) the PMMA forms a homogeneous layer and on top of this layer a phase-segregated domain structure is formed. A different polymer distribution may occur when the solution is deposited onto a substrate of low surface energy (nonpolar). In this hydrophobic surface the bottom layer consists mainly of PS rather than PMMA. The formation of a wetting PMMA (or PS) layer indicates the occurrence of a surface-oriented segregation process [148]. Segregation in thin films of PMMA–PS di-block copolymers has also been studied, showing some structural similarities driven by surface effects [149].

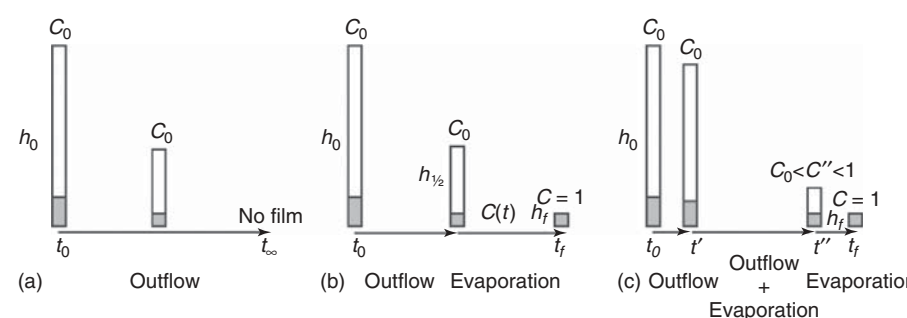


Figure 25.13 Graphical representation of (a) Emslie, Bonner and Peck, (b) Meyerhofer, and (c) Cregan and O’Brien models for the spin coating process.

25.4.1.4 Langmuir–Blodgett Deposition In the LB film deposition technique, a one-molecule-thickness (monolayer) film formed at an air–liquid interface is transferred onto a substrate [150]. The monolayer film (also known as *Langmuir film*) is built up with molecules partially ejected from the liquid (usually water) subphase as a result of polar/nonpolar interactions. This gas-like phase is then slowly compressed up to the formation of a floating two-dimensional solid film that may have the molecules laterally packed and with their polar head pointing toward the water side. This process is normally monitored through a surface pressure versus molecular area plot (or isotherm), which shows the transitions occurring from the less compressed gas-like phase to the solid phase, where molecules are closely packed [151]. Defects such as holes, collapsed regions, and grains can occur but they are, in general, reduced by taking extreme care during film preparation [152]. The monolayer films can be transferred onto hydrophilic or hydrophobic substrates. Most reported works on LB film deposition have been conducted with fatty-acid-type materials (soaps), for which a wealth of information on experimental data exist; however, the preparation of thin films with polymeric materials is of increasing interest, particularly for polymers showing appropriate amphiphilic properties to form monolayer and multilayer films [152, 153].

25.4.1.5 Layer-by-Layer Deposition The LbL deposition is performed by using alternating oppositely charged materials dissolved in an appropriate solvent [154, 155]. Other functionalities, such as hydrogen bonding, can also be used as the driving force for film assembly [156]. Different methods including dip coating, spin coating, and spray coating can be used for LbL deposition of thin films, although dip coating is the most preferred method [157]. One of the main advantages of the LbL deposition method is the high degree of control over the film thickness, which increases linearly as the number of deposited layers increases [155].

25.4.1.6 Epitaxy Epitaxial crystallization is a method of deposition of thin solid films from a solution. In this process a substance crystallizes (guest crystal) on the surface of a crystalline substrate (host crystal) of similar or different nature [126]. Examples of epitaxial crystallization range from single atom arrangements up to the deposition of complex synthetic and biological high molecular weight molecules [158]. In fact, many investigations have been devoted to the epitaxial crystallization of polymers to obtain thin crystalline films, particularly from a dilute polymer solution. Under this regime and favorable conditions, single polymer molecules are trapped on the substrate surface following a segmental contact that nucleates the formation of crystal overgrowths. The resulting molecular order of such overgrowths depends on different parameters

including temperature, solution concentration, polymer characteristics (molecular weight, molecular architecture, etc.), solvent nature, and substrate type. Epitaxy can induce molecular arrangements that are not observed under ordinary crystallization conditions. A number of techniques of polymer film preparation by epitaxy on selected substrates have been employed [158–161]. One of the simplest techniques involves the preparation, at high temperature, of a dilute polymer solution using a high melting temperature substance that will act as a diluent and as a substrate [159, 161]. On cooling, the diluent crystallizes, providing surface substrates for the subsequent crystallization of the polymer. The substrate is then dissolved in an appropriate solvent and the remaining crystalline polymer is recuperated. Other simple method is the isothermal immersion method in which a substrate is first introduced into a slowly boiling polymer solution [162]. Then, this system is rapidly transferred to a thermostated bath heated at a desired crystallization temperature to induce the epitaxial growth. Next, the crystallization is stopped by dilution using the same solvent previously heated at the crystallization temperature. Finally, the substrate is dissolved at room temperature using a suitable solvent and the crystallized polymer is recuperated. Inorganic salts such as the NaCl-like alkali halides single crystals have been frequently used as templates [163], although organic substrates also induce well-developed epitaxial crystallization [126]. Polymer substrates have been successfully used as templates as well [126, 164]. Numerous examples of epitaxial crystallization from a polymer solution are reported in the literature [165, 166].

25.4.2 Fiber Forming Processes from Solution

Polymer fibers are normally manufactured through spinning processes in which a viscous liquid (melt or solution) is forced through multiple tiny holes (spinneret) to emerge as continuous filaments. The principal spinning processes from polymer solutions are wet, dry, and gel spinning. All three methods involve the formation of continuous filament strands by forcing the material through dies of specific geometry and the subsequent removal of the solvent to form solid filaments. A completely different method, the electrospinning process, has been developed to obtain nanoscale diameter filaments from polymer solutions.

25.4.2.1 Wet Spinning Wet spinning is a process in which a polymer solution is forced through a spinneret submerged in a coagulation bath (or wet bath), allowing the filaments to precipitate (solidify) as soon as they come out of the spinneret holes [167, 168]. These filaments are removed from the bath by a rotating roll and then collected in bundles, which are concurrently washed in successive extraction baths to eliminate residual solvent, and finally

dried. The solvent is selected according to the particular fiber to be spun, and the nonsolvent (coagulant), which is normally chemically inert to the film forming material, is selected according to both the film forming material and the extrusion solvent [169]. The as-spun fibers are drawn under specific conditions to obtain final dimensions. The morphology and final properties of filaments are highly dependent on coagulation [40, 170–172] and also on the drawing process that induces molecular orientation [173]. Acrylic [172], cellulose [40], aramid [174], spandex [175], among others [168], can be produced by this process.

25.4.2.2 Dry Spinning In this process a polymer solution is pumped through a spinneret and the emerging filaments are dried (solvent evaporation) by using a high temperature inert gas flow [176]. Solidified filaments are grouped into bundles before being collected on a take-up wheel. Dry spun fibers are normally drawn (stretched) either during or subsequent to spinning to effect orientation of polymer chains, increasing in this way the tensile strength of the material and other properties [177, 178]. Owing to environmental and safety reasons the use of this process is limited. This process may be used for the production of fibers of polymers such as acetate [179], acrylic [180], polyamides [177], polybenzimidazole (PBI) [181], and spandex [182].

25.4.2.3 Gel Spinning This is a process in which a gel is spun into fibers and then ultradrawn to reach final dimensions and strength [183, 184]. This process is also known as dry–wet spinning because the fibers are first air dried, then cooled in a liquid bath. The gel is a semidilute solution with partially crystallized chains (liquid crystalline state) showing entanglement of low density that allows the polymer molecules to reach high orientation in the drawing process. The high orientation of molecules gives rise to the formation of high performance fibers normally showing an outstanding tensile strength property. Some high-strength polyethylene and aramid fibers are produced by gel spinning [183, 185].

25.4.2.4 Electrospinning Electrospinning is a method for the production of nanofibers. Although molten polymers have been successfully electrospun [186], electrospinning is above all a process for polymer solutions. In this process high voltage is applied to a polymer solution to create an electrically charged jet, which is continuously ejected from the tip of a capillary tube by the effect of an applied electric field [187]. Before reaching a collector, the jet loses the solvent by evaporation and the polymer molecules come close to each other to form nanoscale diameter fibers. The applied voltage induces electrical charges on the surface of the fluid (at the tip), which initially elongates up to the formation of a Taylor cone, and once the induced repulsive electrostatic force surpasses the surface tension of the fluid,

an electrically charged jet is suddenly ejected toward an oppositely charged screen. This primary charged jet may split into multiple jets of different diameter.

Solution characteristics such as concentration, elasticity, viscosity, surface tension, nature of the solvent (or solvents), and conductivity, along with processing variables such as applied voltage, capillary tip to collector distance, and processing temperature, are important parameters in electrospinning [187]. All these characteristics may be considered to get free-defect continuous nanofibers of determined average diameter. In general, the fiber diameter is proportional to concentration and viscosity. As the viscosity of solutions is significantly reduced by heating, high concentrated solutions can be electrospun at high temperatures.

Electrospinning has been conducted with a variety of polymer solutions in different solvents at concentrations ranging from 0.5 to 30 wt%, although most reports indicate concentrations ranging from 10 to 20 wt%. Electrospinning is applicable to a wide range of polymers such as polyamides, polyester, and PBI [188], as well as to polymers such as DNA [189], polypeptides [190], or others like π -conjugated (or conducting) polymers [191].

REFERENCES

- Parrish CF. Solvent, industrial. In: Grayson M, Eckroth D, editors. *Kirk-Othmer Encyclopedia of Chemical Technology*. 3rd ed. Volume 21. New York: John Wiley & Sons; 1983. p 377.
- Fleischer D. Physical constants of the most common solvents. In: Brandrup J, Immergut EH, editors. *Polymer Handbook*. 3rd ed. New York: Wiley-Interscience Pub.; 1989. p III/29.
- Rubin II. Injection molding of thermoplastics. In: Berins ML, editor. *SPI Plastics Engineering Handbook*. 5th ed. Boston: Kluwer Academic Publishers; 1991. p 133.
- Wang JS, Porter RS. *Rheol Acta* 1995;34:496.
- Berry GC, Fox TG. *Adv Polym Sci* 1968;5:261.
- Patterson GB. *Physical Chemistry of Macromolecules*. 1st ed. New York: CRC Press, Taylor & Francis Group; 2007. p 43.
- Erman B, Flory JP. *Macromolecules* 1982;15:806.
- Daoud M, Bouchaud E, Jannik G. *Macromolecules* 1986;19:55:19.
- McKenna GB, Flynn KM, Chen Y. *Polymer* 1990;1937:31.
- Yamauchi A. Gels: Introduction. In: Osada Y, Kijiwara K, editors. *Gels Handbook, I. Fundamentals*. 1st ed. San Diego: Academic Press; 2001. p 4.
- Russ T, Brenn R, Geoghegan M. *Macromolecules* 2003;36:127.
- Sebille B. Solubilité des Polymères. In: Champetier G, editor. *Chimie Macromoléculaire II*. Paris: Hermann; 1972. p 65.

13. Blanks RF. *Polym Plast Technol Eng* 1977;8:13.
14. Kurata M. *Thermodynamis of Polymer Solutions*. MMI Press Polymer Monograph Series. 1st ed. New York: Harwood Academic Publishers; 1982. p 3.
15. De Gennes PG. *Scaling Concepts in Polymer Physics*. 1st ed. New York: Cornell University Press; 1979. p 19, 69.
16. Heil JF, Prausnitz JM. *AICHE J* 1966;12:678.
17. Candau F, Strazielle C, Benoit H. *Eur Polym J* 1976;12:95.
18. Hsu JP, Lin SH. *Polymer* 2003;44:8201.
19. Miller-Chou BA, Koenig JL. *Prog Polym Sci* 2003;28:1223.
20. Bercea M, Wolf BA. *Macromol Chem Phys* 2006;207:1661.
21. Krenz RA, Laursen T, Heidemann RA. *Ind Eng Chem Res* 2009;48:10664.
22. Graessley WW. *Polymer* 1980;21:258.
23. Daoud M, Cotton JP, Farnoux B, Jannink G, Sarma G, Benoit H, Duplessix R, Picot C, de Gennes PG. *Macromolecules* 1975;8:804.
24. Amirzadeh J, McDonnell ME. *Macromolecules* 1982;15:927.
25. Ying Q, Chu B. *Macromolecules* 1987;20:362.
26. Teraoka I. *Polymer Solutions: An Introduction to Physical Properties*. 1st ed. New York: John Wiley & Sons Inc.; 2002. p 63, 277.
27. Flory PJ, Krigbaum WR. *J Chem Phys* 1950;18:1086.
28. Barth HG, Mays JW. *Modern Methods of Polymer Characterization*. 1st ed. New York: John Wiley and Sons Inc.; 1991. p 201.
29. Nakamura Y, Akasaka K, Katayama K, Norisuye T, Teramoto A. *Macromolecules* 1992;25:1134.
30. Pfefferkorn P, Beister J, Hild A, Thielking H, Kulicke WM. *Cellulose* 2003;10:27.
31. Yu Y, DesLauriers PJ, Rohlfing DC. *Polymer* 2005;46:5165.
32. Sun T, Brant P, Chance RR, Graessley WW. *Macromolecules* 2001;34:6812.
33. Sanchez IC, Lacombe RH. *Macromolecules* 1978;11:1145.
34. Castells RC, Romero LM, Nardillo AM. *Macromolecules* 1996;29:4278.
35. Karimi M, Albrecht W, Heuchel M, Weigel T, Lendlein A. *Polymer* 2008;49:2587.
36. Kelley FN, Bueche F. *J Polym Sci* 1961;50:549.
37. Chatterjee AP, Schweizer KS. *Macromolecules* 1998;31:2353.
38. Chen X, Burger C, Wan F, Zhang J, Rong L, Hsiao BS, Chu B, Cai J, Zhang L. *Biomacromolecules* 2007;1918:8.
39. Lambourne R, Strivens TA. *Paint and Surface Coatings. Theory and Practice*. 2nd ed. Cambridge: Woodhead Publishing Ltd; 1999. p 1, 169.
40. Ruan D, Zhang L, Zhou J, Jin H, Chen H. *Macromol Biosci* 2004;4:1105.
41. Romdhane IH, Price PE, Miller CA, Benson PT, Wang S. *Ind Eng Chem Res* 2001;40:3065.
42. Flory PJ. *J Chem Phys* 1942;10:51.
43. Huggins ML. *Ann New York Acad Sci* 1942;43:1.
44. Kamide K, Dobashi T. *Physical Chemistry of Polymer Solutions: Theoretical Background*. 1st ed. Amsterdam: Elsevier Science B.V; 2000. p 1.
45. Sun SF. *Physical Chemistry of Macromolecules: Basic Principles and Issues*. 2nd ed. New Jersey: John Wiley & Sons Inc.; 2004. p 67, 96.
46. Pitzer KS, Brewer L. *Thermodynamics*. 2nd ed. New York: McGraw-Hill Inc; 1961. p 75.
47. Munk P. *Introduction to Macromolecular Science*. 1st ed. New York: John Wiley & Sons; 1989. p 217.
48. Flory PJ. *Principles of Polymer Chemistry*. 1st ed. Ithaca (NY): Cornell University Press; 1953. p 399, 495.
49. Flory PJ. *Statistical Mechanics of Chain Molecules*. New York: Hanser Publishers; 1989. p 1, 30.
50. Mattice WL, Suter UW. *Conformational Theory of Large Molecules: The Rotational Isomeric State Model in Macromolecular Systems*. 1st ed. New York: John Wiley & Sons Inc.; 1994. p 5.
51. de Gennes PG. *Phys Lett* 1972;A 38:339.
52. Edwards SF. *Proc Phys Soc* 1965;85:613.
53. Duxbury PM, de Queiroz SLA, Stinchcombe RB. *J Phys Math Gen* 1984;17:2113.
54. des Cloizeaux J, Noda I. *Macromolecules* 1982;15:1505.
55. Ottinger HC. *Macromolecules* 1985;18:1348.
56. Fisher ME, Sykes MF. *Phys Rev* 1959;114:45.
57. Hashizume J, Teramoto A, Fujita H. *J Polym Sci Polym Phys Ed* 1981;19:1405.
58. Huggins ML. *J Am Chem Soc* 1964;86:3535.
59. Patterson D. *Rubber Chem Technol* 1967;40:1.
60. Li J, Wan Y, Xu Z, Mays JW. *Macromolecules* 1995;28:5347.
61. Duval M, Coles HJ. *Rev Phys Appl* 1980;15:1399.
62. Fujita H, Norisuye T. *Macromolecules* 1985;18:1637.
63. Mitchell J Jr., *Applied Polymer Analysis and Characterization*. Volume II. Munich: Hanser; 1992. p 3.
64. Wilson GM. *J Am Chem Soc* 1964;86:127.
65. Renuncio JAR, Prausnitz JM. *Macromolecules* 1976;9:898.
66. Rubio RG, Renuncio JAR. *Macromolecules* 1980;13:1508.
67. Sanchez IC, Lacombe RH. *J Phys Chem* 1976;80:2352.
68. Lacombe RH, Sanchez IC. *J Phys Chem* 1976;80:2568.
69. Panayiotou C, Vera JH. *Polym J* 1982;14:681.
70. Danner RP, High MS. Fundamentals of polymer solution thermodynamics. In: Danner RP, High MS, editors. *Handbook of Polymer Solution Thermodynamics*. 1st ed. New York: Design Institute for Physical Property Data AIChE; 1993. p 3.
71. Kumar SK, Suter UW, Reid RC. *Ind Eng Chem Res* 1987;26:2532.
72. Mansouri GA. *Condens Mater Phys* 2005;8:389.
73. Blanks RF, Prausnitz JM. *Ind Eng Chem Fundamentals* 1964;3:1.
74. Orwoll RA. Solubility of polymers. In: Kroschwitz JI, editor. *Concise Encyclopedia of Polymer Science and*

- Engineering.* 1st ed. New York: John Wiley & Sons; 1990. p 1066.
75. Hansen CM. The three dimensional solubility parameter and solvent diffusion coefficient. Their importance in surface coating formulation [PhD thesis]. Technical University of Denmark Copenhagen; 1967.
 76. Belmares M, Blanco M, Goddard WA, Ross RB, Caldwell G, Chou S-H, Pham J, Olofson PM, Thomas C. *J Comput Chem* 2004;1814:25.
 77. Chanda M, Roy SK. *Plastics Technology Handbook.* 2nd ed. New York: Marcel Dekker Inc.; 1993. p 40.
 78. Schultz AR, Flory PJ. *J Am Chem Soc* 1952;74:4760.
 79. Utracki LA. *Polymer Alloys and Blends: Thermodynamics and Rheology.* 1st ed. New York: Hanser Publishers; 1990. p 29.
 80. Rauwendaal C. *Polymer Mixing: A Self Study Guide.* 1st ed. Munich: Hanser; 1998. p 25.
 81. Van der Haegen R, Kleintjens LA. *Pure Appl Chem* 1989;61:159.
 82. Saeki S, Kuwahara N, Konno S, Kaneko M. *Macromolecules* 1973;6:246.
 83. Schouterden P, Groeninckx G, Van der Heijden B, Jansen F. *Polymer* 1987;2099:28.
 84. Okamoto H, Sekikawa K. *J Polym Sci* 1961;55:597.
 85. Favre E, Nguyen QT, Clement R, Neel J. *Eur Polym J* 1996;32:303.
 86. Sariban A, Binder K. *Macromolecules* 1988;21:711.
 87. Lutz JT Jr.. *Thermoplastic Polymer Additives: Theory and Practice.* 1st ed. New York: Marcel Dekker Inc.; 1989. p 1.
 88. Sabadini E, Assano EM, Atvars TDZ. *J Appl Polym Sci* 1997;65:595.
 89. Moses CL, Robelo LPN, Van Hook WA. *J Polym Sci B Polym Phys* 2003;41:3064.
 90. Striolo A, Prausnitz JM, Bertucco A, Kee RA, Gauthier M. *Polymer* 2001;42:2579.
 91. Wachter AH, Simon W. *Anal Chem* 1969;41:90.
 92. Meeks AC, Goldfarb IJ. *Anal Chem* 1967;39:908.
 93. Berry GC. *J Phys Chem* 1966;70:1194.
 94. Law PW, Longdon A, Willins GG. *Macromol Symp* 2004;208:293.
 95. Reinehr U, Herbertz T. inventors; Bayer Aktiengesellschaft. US patent 4,650,624. 1987.
 96. Siemann U. *Progr Colloid Polym Sci* 2005;130:1.
 97. Schruben DL, Gonzalez P. *Polym Eng Sci* 2000;40:139.
 98. Tang ZG, Black RA, Curran JM, Hunt JA, Rhodes NP, Williams DF. *Biomaterials* 2004;25:4741.
 99. Tsujimoto T, inventors; Fujifilm Corporation. US patent 7,390,434. 2008.
 100. Tsujimoto T, inventors; Fujifilm Corporation. US patent 7,361,295 B2. 2008.
 101. Abiru D, inventors; Fujifilm Corporation. US patent 7,891,861 B2. 2011.
 102. Li Z, Jiang C. *J Appl Polym Sci* 2001;82:283.
 103. Schruben DL, Kumble D. *Polym Eng Sci* 1996;36:2494.
 104. Kunst B, Sourirajan S. *J Appl Polym Sci* 1983;1970:14.
 105. Hansen CM. *Ind. Eng Chem Prod Res Dev* 1970;9:282.
 106. Bierwagen GP. Corrosion and its control by coatings. In: Bierwagen GP, editor. *Organic Coatings for Corrosion Control.* ACS Symposium Series. 1st ed. Volume 689. Washington (DC): Oxford University Press; 1998. p 1.
 107. Wicks ZW Jr., Jones FN, Pappas SP. *Organic Coatings Science and Technology.* 2nd ed. New York: Wiley-Interscience; 1999. p 1.
 108. Smith RL. *Environ Health Perspect* 1984;57:1.
 109. Athawale VD, Nimbalkar RV. *J Am Oil Chem Soc* 2011;88:159.
 110. Bourtoom T. *Int Food Res J* 2008;15:237.
 111. Isono Y, Nagasawa M. *Macromolecules* 1980;13:862.
 112. Moore JE, inventors; General Electric Company. US patent 4,902,725. 1990.
 113. Bongiovanni R, Montefusco F, Priola A, Macchioni N, Lazzeri S, Sozzi L, Ameduri B. *Progr Org Coating* 2002;45:359.
 114. Chen BT. *Polym Eng Sci* 1983;23:399.
 115. Ton-That C, Shard AG, Bradley RH. *Langmuir* 2000;16:2281.
 116. Cisneros-Zevallos L, Krochta JM. *J Food Sci* 2003;68:503.
 117. Weill A, Dechenaux E. *Polym Eng Sci* 1988;28:945.
 118. Krogman KC, Zacharia NS, Schroeder S, Hammond PT. *Langmuir* 2007;23:3137.
 119. Jiang X, Hammond PT. *Langmuir* 2000;16:8501.
 120. Ruschak KJ. *Annu Rev Fluid Mech* 1985;17:65.
 121. Weinstein SJ, Ruschak KJ. *Annu Rev Fluid Mech* 2004;36:29.
 122. Kobayashi A, Saiki Y, Watanabe K. Nanocapacitor: new tantalum capacitor with conducting polymer. In: Rupprecht L, editor. *Conductive Polymers and Plastics in Industrial Applications.* 1st ed. New York: Plastic Design Library; 1999. p 167.
 123. Chang CC, Pai CL, Chen WC, Jenekhe SA. *Thin Solid Films* 2005;479:254.
 124. Kolasinska M, Krastev R, Gutberlet T, Warszynski P. *Langmuir* 2009;25:1224.
 125. Chen W, McCarthy TJ. *Macromolecules* 1997;30:78.
 126. Wittmann JC, Lotz B. *Prog Polym Sci* 1990;15:909.
 127. Hall DB, Underhill P, Torkelson JM. *Polym Eng Sci* 2039;1998:38.
 128. Meyerhofer D. *J Appl Phys* 1978;49:3993.
 129. Emslie AG, Bonner FT, Peck LG. *J Appl Phys* 1958;29:858.
 130. Lee G, Sung Jo P, Yoon B, Hee Kim T, Acharya H, Ito H, Kim HC, Huh J, Park C. *Macromolecules* 2008;41:9290.
 131. Kim S, Lee J, Jeon SM, Lee HH, Char K, Sohn BH. *Macromolecules* 2008;41:3401.
 132. Britten JB, Thomas IM. *J Appl Phys* 1992;71:972.
 133. Schubert DW, Dunkel T. *Mat Res Innovat* 2003;7:314.
 134. Beek WJE, Wienk MM, Kemerink M, Yang X, Janssen RAJ. *J Phys Chem B* 2005;109:9505.

135. Chandrasekhar P. *Conducting Polymers: Fundamentals and Applications*. 1st ed. Boston: Kluwer Academic Publishers; 1999. p 591.
136. Gurer E, Litvak H, Savage R, inventors. US patent 6,027,760. 2000.
137. Washo BD. IBM J Res Dev 1977;21:190.
138. Bornside DE, Macosko CW, Scriven LE. J Imag Technol 1987;13:122.
139. Cregan V, O'Brien SBG. J Colloid Interface Sci 2007;314:324.
140. Frank B, Gast AP, Russell TP, Brown HR, Hawker C. Macromolecules 1996;29:6531.
141. Walheim S, Böltau M, Mlynek J, Krausch G, Steiner U. Macromolecules 1997;30:4995.
142. Gupta SA, Gupta RK. Ind Eng Chem Res 1998;37:2223.
143. Affrossman S, Henn G, O'Neill SA, Pethrick RA, Stamm M. Macromolecules 1996;29:5010.
144. Acrivos A, Shah MJ, Petersen EE. J Appl Phys 1960;51:963.
145. Reich S, Cohen Y. J Polym Sci Polym Phys Ed 1981;19:1255.
146. Geoghegan M, Jones RAL, Payne RS, Sakellariou P, Clough AS, Penfold J. Polymer 1994;20:1935.
147. Vaynzof Y, Kabra D, Zhao L, Chua LL, Steiner U, Friend RH. ACS Nano 2011;5:329.
148. Winesett DA, Ade H, Sokolov J, Rafailovich M, Zhu S. Polym Int 2000;49:458.
149. Mayes AM, Russel TP, Bassereau P, Baker SM, Smith GS. Macromolecules 1994;27:749.
150. Reitzel N, Greve DR, Kjaer K, Howes PB, Jayaraman M, Savoy S, McCullough RD, McDevitt JT, Björnholm T. J Am Chem Soc 2000;122:5788.
151. de Boer B, van Hutton PF, Ouali L, Grayer V, Hadzioannou G. Macromolecules 2002;35:6883.
152. Somanathan N, Pandiyarajan CK, Goedel WA, Chen WC. J Polym Sci B Polym Phys 2009;47:173.
153. Wijekoon WMKP, Wijaya SK, Bhawalkar JD, Prasad PN, Penner TL, Armstrong NJ, Ezenyilimba MC, Williams DJ. J Am Chem Soc 1996;118:4480.
154. Lee SH, Balasubramanian S, Kim DY, Viswanathan NK, Bian S, Kumar J, Tripathy SK. Macromolecules 2000;33:6534.
155. Smith RR, Smith AP, Stricker JT, Taylor BE, Durstock MF. Macromolecules 2006;39:6071.
156. Stockton WB, Rubner MF. Macromolecules 1997;30:2717.
157. Zucolotto V, He JA, Constantino CJL, Barbosa Neto NM, Rodrigues JJ Jr., Mendoza CR, Zilio SC, Li L, Aroca RF, Oliveira ON Jr., Kumar J. Polymer 2003;44:6129.
158. Sun LH, Xu CY, Yu F, Tao SX, Li J, Zhou H, Huang S, Tang L, Hu J, He JH. Cryst Growth Des 2010;10:2766.
159. Wittmann JC, Lotz B. J Polym Sci Polym Phys Ed 1981;19:1837.
160. Wittmann JC, Lotz B. J Polym Sci Polym Phys Ed 1981;19:1853.
161. Lotz B, Wittmann JC. J Polym Sci Polym Phys Ed 1986;24:1559.
162. Sano M, Sandberg MO, Yoshimura S. Langmuir 1994;10:3815.
163. Fujita M, Hamada N, Tosaka M, Tsuji M, Kohjiya S. J Macromol Sci Phys 1997;36:681.
164. Petermann J, Xu Y, Loos J, Yang D. Polymer 1992;33:1096.
165. Shen Y, Yang D, Feng Z. J Mater Sci 1991;26:1941.
166. Cartier L, Okihara T, Ikada Y, Tsuji H, Puiggali J, Lotz B. Polymer 2000;41:8909.
167. Watthanaphanit A, Supaphol P, Furuike T, Tokura S, Tamura H, Rujiravant R. Biomacromolecules 2009;10:320.
168. Yan J, Zhou G, Knight DP, Shao Z, Chen X. Biomacromolecules 2010;11:1.
169. Hoxie HM, inventors; American Viscose Corporation. US patent 2,577,763. 1951.
170. Oh SC, Wang YS, Yeo YK. Ind Eng Chem Res 1996;35:4796.
171. Hirano S. Macromol Symp 2001;168:21.
172. Ji BH, Wang JH, Wang CG, Wang YX. J Appl Polym Sci 2008;108:328.
173. Um C, Ki CS, Kweon HY, Lee KG, Ihm DW, Park YH. Int J Biol Macromol 2004;34:107.
174. Jassal M, Ghosh S. Indian J Fibre Textil Res 2007;22:290.
175. Martin KE, Bing-Wo RD, Lock RL, inventors; In-Vista Technologies S.A.R.L. WO 2010/111088. 2010.
176. Gogolewski S, Pennings AJ, inventors; Medtronic Inc. US patent 4,915,893. 1990.
177. Gogolewski S, Pennings AJ. Polymer 1985;26:1394.
178. Smith P, Lemstra PJ, inventors; Stamicarbon B. V. US patent 4,344,908. 1982.
179. Brazinsky I, Williams AG, LaNieve HL. Polym Eng Sci 1975;15:834.
180. Reinehr U, Uhlemann H, inventors; Bayer Aktiengesellschaft. US patent 4,457,884. 1984.
181. Tan M, inventors; Celanese Corporation. US patent 4,263,245. 1981.
182. Houser NE, Bakker W, Dreibelbis RL, inventors; E. I. Du Pont de Nemours and Company. US patent 5,362,432. 1994.
183. Barham PJ, Keller A. J Mater Sci 1985;20:2281.
184. Hoogsteen W, van der Hooft J, Postema AR, ten Brinke G, Pennings AJ. J Mater Sci 1988;23:3459.
185. Pennings AJ, van der Hooft RJ, Postema AR, Hoogsteen W, ten Brinke G. Polym Bull 1986;16:167.
186. Larrondo L, St John Manley R. J Polym Sci Polym Phys Ed 1981;19:909.
187. Huang ZM, Zhang YZ, Kotaki M, Ramakrishna S. Comp Sci Technol 2003;63:2223.
188. Kim JS, Reneker DH. Polym Eng Sci 1999;39:849.
189. Fang X, Reneker DH. J Macromol Sci Phys 1997;36:169.
190. Khadka DB, Cross MC, Haynie DT. Appl Mater Interfaces 2011;3:2994.
191. Srivastava Y, Marquez M, Thorsen T. J Appl Polym Sci 2007;106:3171.

26

WOOD AND NATURAL FIBER-BASED COMPOSITES (NFCs)

JORGE R. ROBLEDO-ORTÍZ, FRANCISCO J. FUENTES-TALAVERA, RUBÉN GONZÁLEZ-NÚÑEZ, AND
JOSÉ A. SILVA-GUZMÁN

26.1 INTRODUCTION

Customer preferences for recycled products have encouraged a more efficient use of wood and natural fibers. One potential approach to preserve wood and use natural fibers is the development of commodity-engineered composites that blend wood and natural fibers with other materials, such as plastic. The idea of combining wood and plastic is to produce a product with performance characteristics that combine the positive attributes of both materials. Wood and other natural fibers have been used as fillers and/or reinforcement to improve the mechanical properties of a variety of products. The combination of wood and plastic creates the ability to develop diverse products using many different manufacturing processes.

This chapter includes several technical topics associated with natural fiber composites. First, a background is provided that briefly discusses the historical development of natural fiber-based composites (NFCs). Key points related to the success of NFCs are discussed. In the following section, the types of natural fibers are outlined as well as the factors that promote their increasing use in commercial products. The types of polymers and additives used are also described in this section. Only plastics that melt below 200 °C (392 °F) are commonly used in NFCs because wood and natural fibers cannot withstand higher extrusion temperatures. The effects of the polymer/natural fiber interface, natural fiber/polymer mass ratio, particle size, and moisture content on the composites' performance are also addressed. Next, the processes used to manufacture natural fiber composites are described. Molding and injection processes are the most common

processes used and are emphasized in that section. The properties and durability of natural fiber composites are discussed afterwards. Durability is a major concern because of the natural fiber component in the composite. Natural fibers remain susceptible to moisture uptake in spite of the presence of a polymer barrier, thus limiting applications on exterior environments where moisture could be a potential problem. The factors that influence durability and performance of these materials along with the methods used for testing durability are discussed in detail. Finally, current and future uses of NFCs are overviewed. Figure 26.1 shows the typical components present in an NFC.

26.2 BACKGROUND

Wood and natural fibers have been used as fillers or reinforcement materials in order to improve the mechanical properties of a variety of products. The combination of wood and plastic allows the development of products with enhanced properties by using many different manufacturing processes, such as injection and molding, as well as the ability to create an infinite array of products that vary in wood content as well as type of plastic.

Combining lignocellulosic materials with thermoplastics is not new. The first wood–thermoset composites date to the early 1900s [1]. Wood/plastic composites (WPCs) were widely investigated in the 1960s. Substantial amounts of wood/plastic flooring were produced for airport terminals and office buildings in the 1960s [2].

The term *wood/plastic composite* refers to any composite material that contains wood and thermosets (plastic that



Figure 26.1 Typical composite components: (a) fiber, (b) polymer and additives. (See insert for the color representation of the figure.)

does not melt by reheating) or thermoplastics (plastic that can be repeatedly melted). WPCs are also known as *natural fiber composites*, *wood fiber plastic composites*, *wood fiber thermoplastic composites*, *polymer/wood composites*, and *wood-filled plastics* [3]. Because wood is by far the raw material most used to manufacture natural fiber composites, in this chapter the term *WPC* (for wood/fiber composite) is used more frequently than NFC. The objective in the development of WPCs is to produce a product with performance characteristics that combine the positive attributes of both wood and plastics [4]. The addition of wood significantly improves the thermal stability as well as mechanical (stiffness) and working properties of WPCs. The disadvantages of using wood fibers are their low bulk density, high tendency to absorb moisture, and susceptibility to fungal attack [1]. Plastic coating of wood particles in a WPC can reduce moisture uptake while enhancing dimensional stability and protection against fungal attack [4]. Furthermore, wood particles also reduce the need to use more costly thermoplastics [5].

In the mid-1980s, high lumber prices and the desire of customers for recycled products stimulated the production of lumber substitutes produced from recycled thermoplastics. However, the totally thermoplastic lumber exhibited limited applications and suffered from poor thermal stability, high heat retention, poor creep resistance, and low fastener-holding properties [4]. These problems stimulated the interest in using wood as filler or reinforcement in combination with thermoplastics because of the advantages offered by wood fibers over inorganic fillers (calcium carbonate and mica) and reinforcements (glass or carbon fibers) in thermoplastics. In contrast to the glass and carbon fiber fillers, wood fibers are abundant, renewable, strong (high stiffness), lightweight (low density), less abrasive to processing equipment, nonhazardous, nontoxic to mammals, relatively inexpensive, easy to process, and available from a variety of sources [6].

Perhaps the most likely reason for the historically low use of these natural fibers in thermoplastics was unfamiliarity. The birth of the wood plastic industry involved the interfacing of two industries that historically had little in

common [1]. Initial failures in the early stages of WPC development occurred because thermoplastic manufacturers were unaware of the effects of the high hygroscopicity and thermal degradation of wood on composite production [7]. WPCs are currently produced for commercial purposes in many countries [2]; however, production has been limited because of poor interfaces between wood and plastic, low thermal resistance of plastics, high thickness swelling, and thermal degradation of wood fibers at high temperatures [8].

Plastics are generally resistant to fungal attack; however, a major concern with these materials is that wood in the composite remains susceptible to biological degradation. Many manufacturers avoid this risk by producing products for interior uses where little or no water is present, thereby minimizing the risk of fungal attack. There is little data on decay patterns or effects of fungal attack on the physical and mechanical properties of WPCs, although new reports are emerging in this rapidly expanding area. Initially, it was presumed that plastic encapsulated the wood fibers, protecting them from wetting and further decay, but a number of tests suggest that wood encapsulation by plastic is incomplete [9]. As a result, the wood component in these materials reaches moisture levels suitable for fungal attack [8, 10].

The expanding commercial production and marketing of WPCs for use in exterior applications has encouraged research on the durability and service life of WPCs.

26.3 RAW MATERIALS

26.3.1 Natural Fibers

According to Mohanty et al. [11], natural fibers could be classified into the following categories:

- Straw—rice, wheat, cornstalks, sugar cane, etc.
- Bast—flax, hemp, jute, and kenaf
- Leaf—sisal, henequen, pineapple, and banana
- Seed/Fruit—cotton, kapok, and coir (from coconut husks)
- Grass—bamboo, switch, elephant
- Wood

By far, wood particles are the major raw material source used for manufacturing WPCs. Wood particles can originate from sawdust, planer shavings, short solid pieces of lumber, conventional wood composite scrap [6], and scrap pallets [12]. Both softwoods and hardwoods can be used for WPC production. Currently, most WPCs using softwoods are made with southern yellow pine, while WPCs produced with hardwoods are made with oak, maple, or aspen. The anatomical features as well as physical, mechanical, and chemical properties of softwoods and hardwoods differ considerably among species, and may affect the wood–polymer interface, and, as a consequence, the composite's properties and performance.

The effect of wood species on the wood–polymer interface and on properties of WPCs has received little attention in the literature. Stark and Berger [13] evaluated the effect of ponderosa pine, loblolly pine, maple, or oak on the mechanical properties of polypropylene WPCs. In general, WPCs made with maple or oak exhibit slightly better tensile and flexural properties and heat deflection temperatures than either of the pines. Composites elaborated with coconut fiber and polyurethanes have shown good results. Coconut fiber acts as reinforcement and active part of the matrix system, improving the interface [14]. Composites were prepared using waste tire powder, sugar bagasse cane, high density polyethylene (HDPE), and a coupling agent in order to obtain value-added products. Results indicate that these composites accomplish similar values as the standards for using in diverse exterior environments. It is an interesting opportunity for recycling of waste tires and the use of agricultural fibers [15].

26.3.2 Types of Polymers Used in Wood/Plastic Composites Manufacturing

Thermoplastic linear or branched polymers become rigid when cooled, and soften at varying elevated temperatures (depending on the polymer). Only thermoplastics that melt below 200°C (392°F) are commonly used in WPCs because wood cannot withstand higher extrusion temperatures. Several thermoplastic polymers including polypropylene, polyethylene, and poly(vinyl chloride) are currently used to produce WPCs [16]. The polymer contained in WPCs transfers stress between reinforcement fibers, acts as a glue to hold fibers together, protects fibers from mechanical and environmental damage, and improves durability. Both virgin and recycled polymers can be used to produce WPCs. This flexibility creates the potential for using recycled plastics, although care must be taken to ensure reasonable uniformity in the recycled products in order to avoid plastics with higher melting temperatures because of concerns about cellulose decomposition. One great advantage of WPCs is that they can be melt-processed or extruded for further processing. This feature creates the potential to

recycle the material by grinding or beadling for later heating and extrusion.

26.3.3 Additives

There are several important reasons for using additives when producing WPCs. Additives improve the manufacturing process and/or enhance composite performance, durability, and aesthetics [17]. Susceptibility to ultraviolet (UV) light degradation and fungal attack remain the two primary reasons for additive use in WPCs for exterior applications. Additives include adhesives, lubricants, and/or surfactants. Other additives used in WPCs include colorants, fungicides, foamers, and UV light stabilizers, which are essential for exterior applications since they prevent crazing (development of ultrafine cracks) as well as disintegration due to UV absorption and improve aesthetics. Additionally, additives can modify surface energy, improve fiber dispersion and orientation, and increase interfacial adhesion through mechanical interlocking (see also Chapter 11 for a general discussion on additives) [2, 5, 18].

26.3.4 Polymer–Natural Fiber Interface

One key factor for producing acceptable WPCs is the interaction between the wood and thermoplastic components (wood–polymer interface). It is difficult to achieve wood/plastic interaction because the hydrophobic thermoplastic (nonpolar) and hydrophilic wood (polar) are energetically different [2, 4]. During wood/plastic mixing, the thermoplastic must first coat or spread over the wood fiber surface to interact [4]. It is observed in Figure 26.2 that the polymer–fiber interface and a poor surface adhesion lead to fiber slipping from the matrix.

Sanadi et al. [2] indicate that there is no evidence of chemical reaction at the interface between wood and polymer; the interfacial adhesion between both materials appears to be solely through mechanical interlocking. However, according to Wålinder and Gardner [19], there are five main adhesion mechanisms recognized in the interface between wood particles and plastic: (i) adsorption (also referred to as *wetting*), (ii) mechanical interlocking, (iii) diffusion, (iv) electrostatic forces, and (v) weak boundary layers and interfaces. These mechanisms may contribute to the intrinsic adhesion forces acting across the interface between wood fibers and plastics. Adsorption appears to be the most likely adhesion mechanism for WPC [20], where “adsorption” is defined as “macroscopic manifestations of molecular interaction between liquids and solids in direct contact at the interface between them” [18]. The dominance of adsorption as an adhesion mechanism helps to explain why wood particle geometry affects the wood–polymer interface.

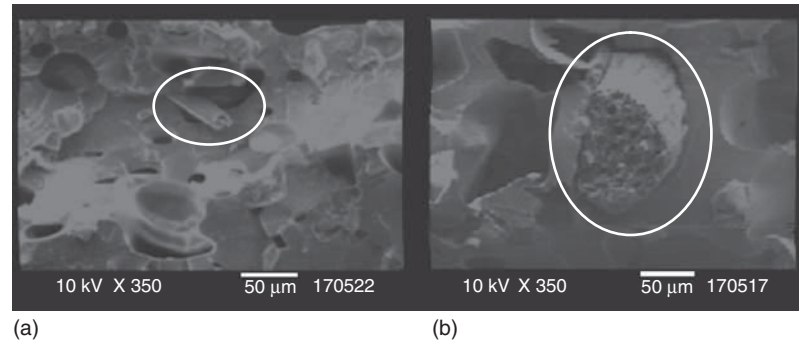


Figure 26.2 SEM micrographs of an LDPE–agave fiber interface for 10 wt% (a) and 20 wt% (b) of fiber composition.

Large wood particles tend to be associated with the formation of voids at the interface between wood fiber and polymer [10], while small particles improve the interface between wood fibers and polymer, limiting void formation on the interface and reducing fiber–fiber surface contact [20]. Large particles are less likely to be uniformly coated or wetted, leading to voids in the resulting WPC. There are a few reports describing the nature of the interface between the wood particles and the plastic. According to Tze et al. [21], the interfacial properties of cellulose fiber–polymer composites can be evaluated by the micro-Raman (Raman spectroscopy) technique. This technique identifies the strain distribution along the cellulose fiber/plastic interface by using a frequency of 895 cm^{-1} (corresponding to a cellulose mode) with applied strain to map the local tensile strain.

Thermoplastic composite manufacturing is often a two-step process, wherein the raw materials are mixed in a process called *compounding*, where fibers and additives are dispersed in the molten polymer. This process may be carried out in either batch or continuous mixers. The molten product is then either extruded or injection-molded into its final shape [1]. Thermal degradation of wood during extrusion and the presence of excessive moisture in wood have major effects on subsequent WPC properties. The temperatures required for many low melting point plastics are still too high for wood, and, as a consequence, some thermal degradation of wood is expected during processing [3]. New equipment has been developed for processing, including material handling, drying and feeding systems, extruders, die designs, and downstream equipment (after extrusion equipment), making the manufacturing process more efficient and versatile and improving the final quality of the resulting composite [1]. Typically, the melt temperatures (temperature of molten material) used for processing WPCs are below 204°C (400°F). Degradation (smoke, odor, discoloration) becomes evident above this limit. In general, polyethylene-based formulations are successfully compounded at temperatures of 180°C (356°F) or less,

whereas polypropylene-based materials work well at temperatures near 190°C (374°F) [6].

26.3.5 Wood/Polymer Ratio, Particle Size, and Moisture Content

Since the plastic is largely immune to fungal attack, the amount of wood and plastic (wood/plastic ratio) has a direct effect on WPC decay resistance. Currently, the most common wood/plastic ratio used to manufacture WPCs is 50 : 50 wood/polymer, but 40 : 60 and even 70 : 30 ratios are also used [1, 22]. The optimal wood/plastic ratio depends on the end use of the composite, and represents a delicate balance between the lower cost of using wood versus the increased risk of wetting as the wood/plastic ratio rises. High wood contents are associated with faster water uptake because more lignocellulosic material is available for moisture sorption [1, 22]. The wood/plastic ratio also affects processing parameters and the physicomechanical properties of WPCs. Increased wood flour content improves flexural and tensile modulus, density, heat deflection temperature, and notched impact energy (energy required for crack propagation) [20]. Increasing the plastic content improves flexural and tensile strength, tensile elongation, mold shrinkage, and melt flow index, while the unnotched impact energy (minimum energy needed to initiate a crack) decreases [20].

A variety of wood particle sizes are used to produce WPCs depending on the type of product. The dimensions of wood particles are usually measured in mesh size as the particles resulting from passing through a mesh with a given number of mesh squares in a square inch. The wood used in WPCs is most often in particulate form (wood flour) or very short fibers rather than longer individual fibers. Commonly, mesh sizes 20, 40, 60, and 80 are used in WPC production.

Particle size can affect the stiffness, moisture resistance (ability to withstand water uptake), wood/plastic interactions, and susceptibility to fungal attack of the resulting WPC [13, 23]. WPCs produced from smaller particle sizes

tend to exhibit increased water resistance and modulus of rupture (MOR) [24]. Stark and Rowlands [20] found that aspect ratio, not particle size, had the greatest effect on strength and stiffness. Particle size affects the formation of the wood–polymer interface. Large wood particles have been associated with the formation of voids on the wood fiber–polymer interface. These voids can serve as pathways for moisture movement and fungal colonization [10]. In contrast, small particles improve the interface between the wood fibers and the polymer, and decrease the fiber–fiber contact and voids in the interface area by increasing the probability of a particle getting coated by the plastic. These characteristics limit the potential for moisture uptake as well as fungal growth. Small, well-dispersed particles are also associated with better composite properties; however, wood particles are often difficult to disperse because of their tendency to agglomerate [5]. Early WPC manufacturers tended to use larger wood particles (10–30 mesh) owing to their lower processing costs, but the industry has reduced particle sizes to as small as 80 mesh. These changes appear to produce a material with better performance and more fungal resistance [1].

The moisture content in air-dry wood fibers ranges from 6% to 7%, but the processes for plastics manufacturing tolerate little or no water. Even 1% or 2% moisture is considered too high [1, 6]. Removal of water is critical because any moisture remaining in the wood–plastic blend turns to steam and manifests itself in the form of foam, disrupting processes, resulting in poor surface quality, weak wood–plastic interface, and voids that are unacceptable for final sale [3, 25]. As a result, particles must be predried for blending.

26.4 MANUFACTURING PROCESS

Profile extrusion is the most common process for WPC production. The composite material is first heated so that the thermoplastic component can flow; then it is pumped and forced through a die of a given cross-sectional configuration. The material is supported as it cools, usually in a cold-water bath, and then cut to a given length. Pipes, tubing, furniture, moldings, and sheet goods are the common products made using profile extrusion [26]. WPCs tend to be produced by extrusion because of the process throughput that is possible with this approach.

In the injection-molding process, the material is heated and pumped into a permanent mold, where it takes its final shape and cools. The mold is then opened and the finished part discharged [26]. WPCs produced by injection-molding have been extensively studied, showing that the final properties are strongly affected by the processing conditions, composition, and the presence of coupling and dispersion agents [27]. Adding fibers to low density

polyethylene (LDPE) increased flexural and tensile moduli and strength for samples without weld lines [18].

Currently, rotational molding (or rotomolding) processes have been used for WPC production. In this process, the material is charged in a mold and afterwards taken to a heated chamber and rotated at controlled speed around two perpendicular axes. The rotational movement produces the material to melt and stick to the inner surface of the mold. When the material has built a uniform layer, the mold is cooled maintaining constant rotation. The raw materials can be used in powder or liquid forms. Polyethylene powders with sisal, wood, or flax fibers are some examples of WPCs produced by rotomolding [28–30]. Calendering, thermoforming, and compression molding are also processing methods used in the production of WPCs [31].

26.5 PROPERTIES OF COMPOSITE MATERIALS

26.5.1 Water Absorption in Natural Fiber Plastic Composites

Wood plastic composites tend to have better dimensional stability than solid wood when exposed to moisture [1]. WPCs with higher wood/plastic ratios (>50%) experience water uptake when exposed to moisture sources. WPCs have a higher resistance to moisture absorption and thickness swelling (<1%) than wood-based panels such as plywood and laminated veneer lumber or oriented strand board (>40%) [32]. The plastic covering the wood particles in a WPC tends to reduce moisture uptake; however, a number of tests suggest that wood fiber encapsulation by the polymer is incomplete, especially near the surface. As a result, the wood component in these materials absorbs water when exposed to moisture sources [8]. According to Wälinder and Gardner [19], the wood substrate interacts with water during prolonged exposure to moisture, resulting in debonding of the wood/polymer interface by the intrusion of water. Water movement through WPCs generally takes longer than through solid wood before reaching equilibrium, and cannot be directly achieved by vacuum/pressure cycles [8, 33]. The slow moisture uptake by WPCs creates moisture gradients between the surface and the core. Apparently, moisture levels nearest the surface are more suitable for fungal growth, while moisture levels in the core are too low to support microbial activity [34]. This wetting pattern will ultimately affect the mode and patterns of subsequent fungal attack.

Higher levels of water uptake are associated with poor wood–fiber interfaces. Water sorption by WPCs can severely weaken wood adhesion to thermoplastic matrices, decreasing the mechanical properties of WPCs [35]. Low moisture uptake was observed in composites made with sugar bagasse cane, HDPE, and a coupling agent [36].

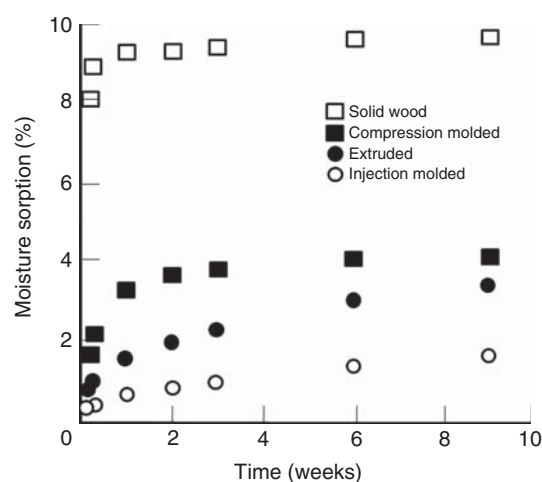


Figure 26.3 Moisture sorption for solid wood and NFCs produced by different manufacturing processes (Clemons [1]).

Swelling by moisture absorption of WPCs exposed in external environments is associated with an increase in UV degradation, as swelling develops new surfaces, exposing more polymer to degradation [37]. Moisture sorption in WPCs is associated with permanent reductions in strength and stiffness (modulus of elasticity (MOE) and MOR), proportional to the moisture content of the wood in the composite [1, 38]. As shown in Figure 26.3, the processing methods and additives used have a significant influence on moisture diffusion in WPCs, and, as result, on the potential for further effects on composite properties [1, 38].

26.5.2 Mechanical Properties

Most commercial WPCs are considerably more flexible than solid wood. WPCs creep more than solid wood, are less tough, and can handle less fatigue before failure [5, 38]. The use of wood fibers as reinforcing agents rather than just as fillers increases MOE, MOR, and the ultimate tensile strength (UTS) [39] as well as the unnotched energy [12]. Composites manufactured using sugar bagasse cane, recycled HDPE, and a coupling agent exhibited good properties (MOE and MOR) according to standards [40]. These mechanical properties are strongly influenced by the amount, size, and type of wood particles added to the matrix, and also by the additives incorporated during processing [12]. Despite the potential improvements, the MOEs of most WPCs are less than half those of solid wood [6]. In contrast, the tensile strength of WPCs is significantly reduced when wood fiber is added to the plastic matrix [32].

The processes used to produce WPCs may influence the mechanical performance of the material. Extruded materials have higher stiffness and strength than materials produced by injection molding [38]. Polypropylene blends

tend to perform better than polyethylene blends [6]. As noted previously, the mechanical properties can be greatly improved by using additives to enhance wood/plastic adhesion [5, 18]. Table 26.1 shows the mechanical properties for neat polypropylene and composites produced with wood flour and fibers. It is observed that adding fibers rather than flour increases mechanical properties such as strength, elongation, and unnotched Izod impact energy [1].

26.6 DURABILITY

26.6.1 Decay

The resistance of conventional plastics to fungal attack is due primarily to the low surface area and relative impermeability of plastics, as well as to the very high molecular weight of the plastic material [8]. Microorganisms tend to attack the ends of large molecules. Because the number of ends is inversely proportional to the molecular weight, it would be necessary to break large molecules into very small fragments with a large surface area in order to make the plastic degradable [7]. In addition, fungi tend to lack the enzymes capable of degrading these materials. Polyethylene, polystyrene, and poly(vinyl chloride) are not susceptible to fungal attack [8].

The perceived resistance of WPCs to fungal attack is based on the belief that plastic encapsulates the individual wood fibers in a continuous plastic matrix and acts as a barrier to protect wood fibers from wetting. However, a number of tests suggest that wood fiber is not completely encapsulated by the polymer, especially near the surface. As a result, the wood component in these materials does reach moisture levels suitable for fungal attack (>30%) [1, 8, 10]. For example, WPC specimens exposed for 16 weeks to decay fungi in laboratory tests experienced weight loss exceeding 40% [23, 41]. Morris and Cooper [42] found WPCs manufactured from recycled wood and plastic that were attacked by brown-rot, white-rot, and blue stain fungi in the Everglades National Park, Florida, USA. According to Naghipour [8], the brown-rot fungus *Gloeophyllum trabeum* was able to grow on WPC samples, whereas pure polyethylene and polypropylene were immune to fungal attack. Weight losses were less than 5% at the 60% wood level, while WPCs with wood levels of 50% or less showed good resistance to fungal attack [8].

Decay activity in WPCs is concentrated on the exterior surfaces of the composite, resulting in gradual roughening of the composite surface [22]. Breakdown on the polymer surface leads to more wood particles being exposed, thereby increasing moisture uptake [43]. Surface wood particles exposed directly to fungal attack are generally totally decayed [41]. This decay mechanism is similar to that observed for microbial degradation of polyethylene-starch composites [22].

TABLE 26.1 Mechanical Properties of Wood-Polypropylene Composites*

Composite [†]	Tensile			Flexural			Izod Impact Energy			Heat Deflection Temperature (°C [°F])
	Density (g/cm ³ [pcf])	Strength (MPa [psi])	Modulus (GPa [psi])	Elongation (%)	Strength (MPa [psi])	Modulus (GPa [psi])	Notched (J/m [ft-lb/in])	Unnotched (J/m [ft-lb/in])		
Polypropylene	0.9 [56.2]	28.5 [4130]	1.53 [221,000]	5.9	38.3 [5550]	1.19 [173,000]	20.9 [0.39]	656 [12.3]	57 [135]	
PP + 40% wood flour	1.05 [56.2]	25.4 [3680]	3.87 [561,000]	1.9	44.2 [6410]	3.03 [439,000]	22.2 [0.42]	73 [1.4]	73 [1.4]	89 [192]
PP + 40% hardwood fiber	1.03 [64.3]	28.2 [4090]	4.20 [609,000]	2.0	47.9 [6950]	3.25 [471,000]	26.2 [0.49]	91 [1.7]	91 [1.7]	100 [212]
PP + 40% hardwood fiber + 3% coupling agent	1.03 [64.3]	52.3 [7580]	4.23 [613,000]	3.2	72.4 [10,500]	3.22 [467,000]	21.6 [0.41]	162 [3.0]	162 [3.0]	105 [221]

PP, polypropylene.

*Ref. 1.

†Percentages based on weight.

Microscopic observations of decayed WPC specimens showed mycelium concentrated in the interfacial voids between the wood and the thermoplastic component. This observation supported the premise that the primary mode of fungal degradation was via hyphal penetration through the voids on the wood/polymer interfaces [10, 22]. The materials used in these studies tended to have large wood particles, which resulted in lesser wood/plastic adhesion and more voids for fungal entry.

Resistance to fungal attack of WPCs could be evaluated using agar tests. Both, malt extract agar (MEA) and potato dextrose agar (PDA) are suitable media for accelerated WPCs decay. Both media could produce acceptable results in a relatively short period [9]. The traditional soil block method used for testing durability of solid wood is generally less effective for evaluating WPCs than solid wood. This test produces low weight losses on WPCs in comparison to solid wood. While the soil block test can provide valuable information, it is evident that a new method will be required for assessing the decay resistance of WPCs which accounts for the characteristics and properties of this composite.

The American Society for Testing and Material (ASTM) subcommittee composed of materials scientists, wood scientists, and polymer scientists attempted to develop standards for performance ratings for WPC deck boards, but there is little published on actual method development.

The absence of definitive information on decay resistance of WPCs ultimately will limit the ability to reliably and rapidly assess the durability of new materials.

26.7 FACTORS THAT AFFECT DECAY OF WOOD-PLASTIC COMPOSITES

26.7.1 Moisture

Moisture is essential for fungal colonization and decay of lignocellulosic materials. Water absorption on the surface is the key parameter because this is where fungal attack is initiated [8]. WPCs with high wood contents (>50%) clearly absorb water [8, 10]. Naghipour [8] showed that WPCs had slower moisture uptake than plastic composites, but were permeable and, as a consequence, subject to fungal decay, particularly at high wood/polymer ratios (>50% wood). Polyethylene composites absorbed more water than those made with polypropylene at comparable wood/plastic ratios [8]. Surface deterioration and delamination in WPCs have been associated with weathering [8, 43]. Moisture sorption can lead to void formation at wood/polymer interfaces [8]. The voids and cracks that are present before water exposure will expand after exposure. These voids could create pathways for entry by water and fungal hyphae. Short-term boiling can be used to rapidly increase moisture

absorption [8, 33]; however, care needs to be taken to avoid altering the wood/plastic interface or leaching of any fungicides. Ibach and Clemons [33] reported that chemical modification of the wood cell wall would reduce WPC moisture uptake below the level required for fungal attack. They evaluated the resistance to fungal attack of WPCs made with chemically modified fiber or flour and polypropylene. Overall, weight losses were consistent with the lower moisture absorption of the composite. According to Ibach et al. [44], moisture contents of WPCs above 15% lead to significant weight losses, but these levels must be viewed cautiously because they do not appear to be favorable for inducing fungal attack. Wang and Morrell [34] exposed samples to water for long periods and found that the conditions on the surface of commercial WPCs were suitable for fungal attack, while moisture levels 5 mm below the surface had changed only slightly. Clearly, test specimen sizes that maximize the surface to volume ratios will result in conditions more suitable for decay development.

26.7.2 Wood Particle Size and Wood/Plastic Ratios

WPCs containing large particles tend to experience more severe decay at similar wood ratios (>50% wood) [23]. Large wood particles create more pathways into the plastic matrix, exposing more surface area to water and fungal hyphae. Simonsen et al. [45] noted similar effects using polyethylene and polypropylene. While small particles are preferable for slow moisture uptake, they are more costly to produce and therefore increase the final cost of the product.

Mankowski and Morrell [10] examined the influence of the wood/plastic ratio and wood particle size on the decay of commercial WPCs made with pine and HDPE. A 20% wood weight loss was observed in the WPCs made with 70% wood (small wood particles) after exposure to a brown-rot fungus. In contrast, little or no degradation was observed in two samples of WPCs made with 50% wood content, despite the use of larger wood particles. These results suggest that the amount rather than size of the wood particles may have a greater effect on WPC durability [13, 22].

26.7.3 Wood/Polymer Interface

Differences between the hydrophilic wood and the hydrophobic thermoplastic during processing can limit bond development, resulting in poor adhesion between wood fibers and the plastic polymer. Without chemical or physical bonding, failures on the wood–polymer interface and interfacial voids can develop because of poor processing or as a result of external factors, such as moisture uptake or UV degradation. These failures in the wood–polymer interface

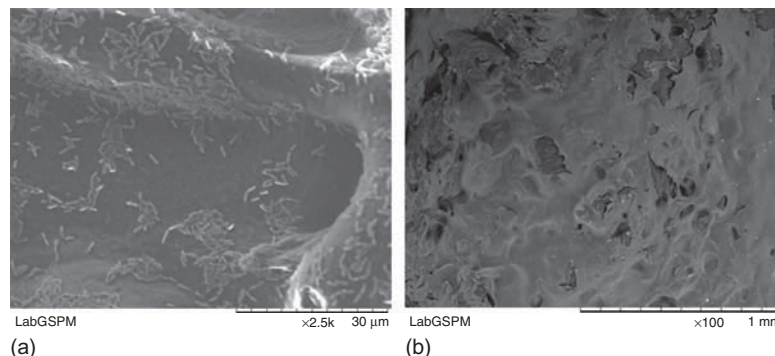


Figure 26.4 Composite surface with adhered bacteria (a) and coated with chitosan (b).

are of critical importance for assessing the WPC performance [22]. Nearly all WPCs contain additives designed to produce some chemical interaction at the wood/plastic interface, but most are proprietary and their effects on decay resistance of the final product are poorly understood.

26.8 USES OF WOOD-PLASTIC COMPOSITES

By far, the most noted marketplace for WPCs in North America is the outdoor decking market [46], followed by windows, door framing, and railings. Roofing, fencing, sea walls, garden structures, and patio furniture are emerging applications for these composites [47]. The largest market segment for natural fiber composites in Europe is automotive parts, agricultural fibers being the norm. Legislation in Europe requires the recyclability of automobiles and other products [46], thus promoting the use of natural fibers. Although WPC decking is more expensive than pressure-treated wood, manufacturers promote its lower maintenance, lack of cracking, and high durability. The actual lifetime of WPC lumber is currently being debated, but most manufacturers offer a 10-year warranty [1].

The automotive industry has long used natural fibers in combination with plastics [1, 48, 49]. Currently, WPCs are primarily used for exterior decking, window and door framing, decorative trim, and railings [7, 47]. Roofing, fencing, sea walls, garden structures, and patio furniture are emerging applications for these composites [47]. Significant markets are also emerging for railroad ties, flowerpots, furniture, and marine piers [7, 47]. The lower creep resistance, stiffness, and strength compared to solid wood and other structural materials severely limit the use of WPCs in applications that require considerable structural performance [1]. Although much work is being done on assessing the durability of WPCs, the methods remain less than ideal. Industry has the potential to produce an array of WPCs with properties tailored to meet specific use conditions. However, these developments are limited by

the slow rate of biological testing. For example, process laboratories capable of producing 50 test materials per day must wait 4–6 months to learn whether these materials are durable. Clearly, methods must be developed or refined that accelerate both moisture uptake and decay potential.

Recently, WPCs have been used as carriers for biopolymers and microorganisms (Fig. 26.4). Robledo-Ortíz et al. [50] used a composite material of recycled HDPE and agave fibers for bacterial immobilization. According to the results reported, the natural adhesion of *Pseudomonas putida* F1 onto the composite surface is strongly affected by temperature, pH, ionic strength, and initial biomass concentration. Vázquez et al. [51] coated the same material (agave fibers/HDPE) with chitosan to be applied in heavy-metal adsorption. These studies showed that composite materials represent an attractive low-cost recycled support for bacterial and biopolymers with potential applications in biotechnological and environmental cleanup processes.

Until 2008, there was an explosive growth in wood and natural fiber composites in the United States. Because of the crisis in the building-products market, the demand for these composites dropped sharply. However, it is expected that economics, environmental concerns, and improved properties in the coming years will increase the demand for natural fiber composites.

REFERENCES

1. Clemons CM. Forest Prod J 2002;52(6):10.
2. Sanadi A, Caulfield DF, Rowell RM. Lignocellulosic/plastic composites. The fibril angle, Spring 1998 Newsletter. American Chemical Society; Dallas, TX: 1998. p 8.
3. Forest Products Laboratory. Wood handbook: Wood as an engineering material. Gen. Tech. Rep. FPL-GTR-113. U.S. Department of Agriculture, Forest Service, Forest Products Laboratory; Madison (WI): 1999.
4. Wolcott M, editor. The role of thermoplastics in conventional wood composites. 30th International Particleboard/Composite Materials Symposium; 1996; Pullman (WA): Washington State University; 1996.

5. Oksman K, Clemons C. *J Appl Polym Sci* 1998;67(9):1503.
6. English B. Wood fiber-reinforced plastics in construction. Proceedings No. 7286, The use of recycled wood and paper in building applications; Madison, WI. Wisconsin: USDA Forest Service and The Forest Products Society; 1996. p 79–81.
7. Clemons CM. Wood fiber-plastic composites in the United States – History and current and future markets. Proceedings 3rd International Wood and Natural Fibre Composites Symposium; Kassel, Germany: 2000. p 1.1.
8. Naghipour B. Effects of extreme environmental conditions and fungal exposure on the properties of wood-plastic composites [dissertation]. Toronto (ON): University of Toronto; 1996.
9. Silva A. Development of an Accelerated Method for Assessing Decay of Wood Plastic Composites (WPC's) [dissertation]. Corvallis (OR): College of Forestry Science and Forestry, Oregon State University; 2004.
10. Mankowski M, Morrell JJ. *Wood Fiber Sci* 2000;32(3):340.
11. Mohanty AK, Misra M, Drzal LT, editors. *Natural Fibers, Biopolymers and Biocomposites*. Boca Raton (FL): CRC Press; 2005.
12. Stark N. *Forest Prod J* 1999;49(6):39.
13. Stark N, Berger MJ. Effect of species and particle size on properties of wood-flour-filled polypropylene composites. Proceedings of the Functional fillers for thermoplastics & thermosets; 1997; Madison, WI. Wisconsin: USDA Forest Service. Forest Products Laboratory; 1997. p 1.
14. Trujillo M. Desarrollo de un material compuesto de fibras naturales entrecruzadas con poliuretano [dissertation]. Guadalajara, México: Universidad de Guadalajara; 2005.
15. Rodríguez AR. Elaboración de materiales compuestos utilizando residuos de llanta, bagazo de caña y polietileno de alta densidad [dissertation]. Guadalajara, México: Universidad de Guadalajara; 2004.
16. Patterson J. *J Vinyl Addit Technol* 2001;7(3):138.
17. Fulmer MS. Compounding and processing additives for woodfiber-plastic composites. Proceedings of the 5th International Conference on Woodfiber-Plastic Composites; Madison, WI. Wisconsin: Forest Products Society; 1999. p 23.
18. Leduc S, Galindo JR, Gonzalez-Nunez R, Ramos-Quijarte J, Riedl B, Rodrigue D. *Polym Polym Comp* 2008;16(2):115.
19. Wålinder MEP, Gardner DJ. Surface energy and acid-base characterization of components used for wood-polymer composites. Proceedings of the 6th International Conference on Woodfiber-Plastic Composites; 2001; Madison, WI. Wisconsin: Forest Products Society; 2002. p 185.
20. Stark NM, Rowlands RE. *Wood Fiber Sci* 2003;35(2):167.
21. Tze WTY, Gardner DJ, Tripp CP, Shaler SM, O'Neill SC. Interfacial adhesion studies of cellulose-fiber/polymer composites using a Micro-Raman technique. Proceedings of the 6th International Conference on Woodfiber-Plastic Composites 2001; Madison, WI. Wisconsin: Forest Products Society; 2002. p 177.
22. Pendleton DE, Hoffard TA, Addock T, Woodward B, Wolcott MP. *Forest Prod J* 2002;52(6):21.
23. Verhey SA, Lacks PE, Richter DL. The effect of composition on the decay resistance of model woodfiber-thermoplastic composites. Proceedings of the 6th International Conference on Woodfiber-Plastic Composites; 2001; Madison, WI. Wisconsin: Forest Products Society; 2002. p 79.
24. Takatani M, Ito H, Ohsugi S, Kitayama T, Saegusa M, Kawai S, Okamoto T. *Holzforschung* 2000;54(2):197.
25. English B, Clemons CM, Stark N, Schneider JP. Wastewood-derived fillers for plastics. Gen. Tech. Rep. FPL-GTR-91. Madison, (WI): U. S. Department of Agriculture, Forest Service, Forest Products Laboratory; 1996.
26. B E, P C, D SB. Processing into composites. In: RM R, RA Y, JK R, editors. *Paper and Composites from Agro-Based Resources*. Boca Raton (FL): CRC Lewis Publishers; 1997. p 269.
27. Sun SY, Hai SH, Gan CD. *J Reinf Plast Compos* 2010;29(5):637.
28. Ward J, Panigrahi S, Tabil LG, Crerar WJ, Powell T. Rotational molding of flax fiber reinforced thermoplastics. Proceedings 2002, The Society for Engineering in Agricultural, Food and Biological Systems; Chicago, IL; 2002. Paper No: MBSK 02-209.
29. Torres FG, Aragon CL. *Polym Test* 2006;25(4):568.
30. Jayaraman K, Lin R, Bose D, Maarouf M. *Adv Mater Res* 2007;29-30(4):307.
31. Youngquist JA. Wood-based composites and panel products. Wood handbook: wood as an engineering material. Gen. Tech. Rep. FPL-GTR-113. U.S. Department of Agriculture, Forest Service, Forest Products Laboratory; Madison (WI); 1999.
32. Falk RH, Lundin T, Felton C. The effects of weathering on wood-thermoplastic composites intended for outdoor applications. Proceedings of the 2nd Annual Conference on Durability and Disaster Mitigation in Wood-Frame Housing, Madison, WI. Wisconsin: Forest Products Society; 2001. p 175.
33. Ibach RE, Clemons CM. Biological resistance of polyethylene composites made with chemically modified fiber or flour. Proceedings of the 6th Pacific Rim Bio-based Composites Symposium and Workshop on the Chemical Modification of Cellulosics; 2002 Nov 10–13; Portland, OR. Portland (OR): Oregon State University; 2002. p 574.
34. Wang W, Morrell JJ. *Forest Prod J* 2004;54(12):209.
35. Uerkanrak K. High density polyethylene/wood fiber composites: measuring the effect of processing parameters on their physical and mechanical properties [dissertation]. East Lansing (MI): School of Packaging, Michigan State University; 2001.
36. Fuentes TF, Silva GJ, Richter HG, Sanjuán DR, Ramos QJ. *Indust Crops Prod* 2007;26(1):1.
37. Lange SE, Rowell RM. Weathering performance of aspen-polypropylene composites. Proceedings of the 7th International Conference on Woodfiber-Plastic Composites, 2003; Madison, WI. Wisconsin: Forest Products Society; 2004. p 317.

38. Rangaraj S. Durability assessment and modeling of wood-thermoplastic composites [dissertation]. Pullman (WA): School of Mechanical and Materials Engineering, Washington State University; 1999.
39. Simonsen WJ. Forest Prod J 1997;47(1):74.
40. Fuentes FJ, Silva A, Sanjuán R, Ramos J. Properties of composite materials manufactured with sugar cane bagasse particles and recycled plastic. Proceedings 8th International Conference on Woodfiber-Plastic Composites. Madison, WI. Wisconsin: Forest Products Society; 2006. p 355.
41. Silva A, Gartner B, Morrell J. J Test Eval 2007;35(2):203.
42. Morris PI, Cooper P. Forest Prod J 1998;48(1):86.
43. Peyer S, Wolcott MP. Damage in woodfiber-plastic composites: a look-up close and personal. Proceedings of the 6th International Conference on Woodfiber-Plastic Composites; 2001; Madison, (WI). Wisconsin: Forest Products Society; 2002. p 280.
44. Ibach RE, Clemons CM, Stark NM. Combined UV and water exposure as a preconditioning method in laboratory fungal durability testing. Proceedings of the 7th International Conference on Woodfiber-Plastic Composites; 2003 May 19–20; Madison, WI. Wisconsin: Forest Products Society; 2004. p 61.
45. Simonsen J, Freitag CM, Morrell JJ. The effect of wood-plastic ratio on the performance of borate biocides against brown-rot fungi. Proceedings of the 6th International Conference on Woodfiber-Plastic Composites; 2001, Madison, WI. Wisconsin: Forest Products Society; 2002. p 69.
46. Hansen E. Market and innovation considerations in development of natural/wood fibre composites. In: Pickering K, editor. *Properties and Performance of Natural-Fibre Composites*. Cambridge, England: Woodhead Publishing; 2008. p 356.
47. Morton J, Quarley J, Rossi L. Current and emerging applications for natural and woodfiber composites. Proceedings of the 7th International Conference on Woodfiber-Plastic Composites; 2003; Madison, WI. Wisconsin: Forest Products Society; 2004. p 3.
48. Rowell R. The state of the art and future development of bio-based composites science and technology towards the 21st century. Proceedings: The Fourth Pacific Rim Bio-Based Composites Symposium; 1998; Bogor, Indonesia. Indonesia: Bogor Agricultural University; 1998. p 1.
49. Lee EC, Baldwin K. Material damping characteristics of natural fiber reinforced plastics by DMTA and modal analysis. Proceedings of the 6th International Conference on Woodfiber-Plastic Composites; 2001; Madison, WI. Wisconsin: Forest Products Society; 2002. p 6.
50. Robledo-Ortíz JR, Ramírez-Arreola DE, Gómez C, González-Reynoso O, González-Núñez R. Bacterial immobilization by adhesion onto agave fiber/polymer foamed composites. Bioresour Technol 2010;101(4):1293.
51. Vázquez MO, Herrera VS, Gómez C, Gómez-Salazar S, Rodrigue D, González-Núñez R, Luna-Bárcenas JG, Mani-González PG, Herrera-Gómez A. J Appl Polym Sci 2010;115(5):2971.

27

POLYMER BLENDS

SAÚL SÁNCHEZ-VALDES, LUIS F. RAMOS-DE VALLE, AND OCTAVIO MANERO

27.1 INTRODUCTION

The modification of already existing polymers is more economically viable than the development of new monomers for the production of new types of polymers. High-value-added materials can be obtained either by new polymerization methods or by alloying or blending, and reinforcing existing polymer materials. Polymer modification processes based on simple mechanical mixtures of two or more polymers originated a new class of materials called *polymer blends*. A polymer blend, analogous to metal alloys, is the mixture of at least two different polymers to create a new type of material with different physical properties. The first polymer blend was patented in 1846 by Parkes [1]. This blend of natural rubber with gutta-percha resulted in a partially crosslinked material whose modulus was controllable by the composition of each isomer. The performance of polymer blends depends on the properties of each polymer in the blend, their content, and morphology. The cost of the blend depends on the material, compounding method, and blend morphology, which can be tailored for a specific application. Most blends have been developed for the improvement of a specific property such as impact strength, or extending the performance of an engineering resin, improving the processability or recycling facility, etc.

Polymer blends can be classified into the following categories:

1. *Immiscible Polymer Blends*. These blends have large-size domains of dispersed phase and poor adhesion between them. If the blend is formed by two polymers, two glass transition temperatures will be observed.

2. *Miscible Polymer Blends*. These are homogeneous blends with a single-phase structure. In this case, one glass transition temperature will be observed.
3. *Compatible Polymer Blends*. These are immiscible polymer blends that exhibit macroscopically uniform physical properties caused by sufficiently strong interface interactions between the polymer blend components.
4. *Compatibilized Polymer Blends*. Immiscible blends in which the microstructure and physical properties can be stabilized by adding surface-active species called *compatibilizers*. These compatibilizers will influence various morphological processes, such as deformation, breakup, and coalescence of droplets.

27.2 MISCIBILITY IN POLYMER BLENDS

Miscibility is similar to the thermodynamic solubility, that is, two or more polymers are miscible in each other if the free energy of mixing is negative. This is a function of the structural characteristics of the polymers, such as molecular weight, molecular weight distribution, copolymer composition, as well as of temperature, pressure and blend composition. Polymer blends can exhibit miscibility or phase separation and various levels of mixing in between the extremes. The most important factor leading to miscibility in low-molecular-weight materials is the combinatorial entropy contribution, which is very large compared to high-molecular-weight polymers. This contribution is the reason solvent–solvent mixtures offer a much broader range of miscibility than polymer–solvent combinations. The range

of miscible combinations involving polymer–polymer mixtures is even much smaller.

Miscibility in polymer blends is not a requirement; however, interfacial adhesion between the polymer components is highly desirable for enhancing specific properties of the blend.

One of the most important relationships that governs the behavior of dissimilar components is given by the change of free energy of mixing (ΔG_m), given by:

$$\Delta G_m = \Delta H_m - T \Delta S_m \quad (27.1)$$

where ΔG_m is the free energy of mixing; ΔH_m , the enthalpy of mixing or heat of mixing; T , the absolute temperature; and ΔS_m , the entropy of mixing.

If two polymers are mixed, the most frequent result is a system that exhibits complete phase separation due to the repulsive interaction between the components (i.e., the chemical incompatibility between the polymers). A necessary condition for miscibility to occur is that ΔG_m must be negative ($\Delta G_m < 0$). This is a necessary requirement, but not a sufficient one, as the following expression must also be satisfied in order to obtain a stable one-phase system. The expression that describes the criteria for phase stability of binary mixtures of composition φ at fixed temperature T and pressure P is [2]:

$$\left[\frac{\partial^2 \Delta G_m}{\partial \varphi^2} \right]_{T,P} > 0 \quad (27.2)$$

Figure 27.1 shows a schematic phase diagram for binary blends showing the relationship between free energy of mixing (ΔG_m) and blend composition (φ). For sample A, an immiscible system is obtained ($\Delta G_m > 0$), for sample B a fully miscible system is obtained in which $\Delta G_m < 0$, and C represents a partially miscible system that satisfies $\Delta G_m < 0$ for all compositions, but $\partial^2 \Delta G_m / \partial \varphi^2$ is lower than 0 at certain compositions, indicating that at these compositions the blend will be immiscible.

A miscible polymer blend is a polymer blend that is homogeneous down to the molecular level and associated with negative values of the free energy of mixing, and whose domain size is comparable to the dimensions of the macromolecular statistical segment. The value of $T \Delta S_m$ is always positive because there is an increase in entropy when mixing takes place. Therefore, the sign of ΔG_m always depends on the value of the enthalpy of mixing ΔH_m that can be negative or positive but very small.

Traditionally, the thermodynamics of polymer mixtures was developed in terms of a lattice model, with each monomer unit of the polymer chains occupying a single lattice site. The free energy of mixing of polymers in solution can be described by the Flory–Huggins equation:

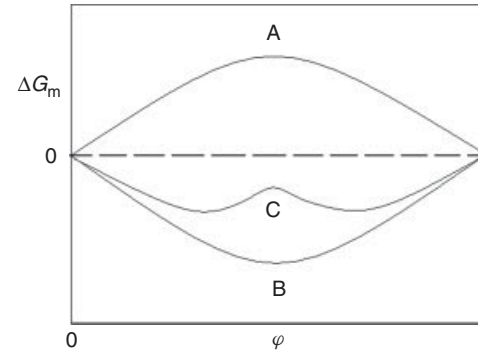


Figure 27.1 Schematic phase diagram for binary blends.

$$\Delta G_m = RTV \left[\frac{\varphi_A \ln \varphi_A}{V_A} + (1 - \varphi_A) \frac{\ln(1 - \varphi_A)}{V_B} + \chi_{AB}^* \varphi_A (1 - \varphi_A) \right] \quad (27.3)$$

where V is the total volume of the sample, R is the gas constant, T is the absolute temperature, φ_i is the volume fraction of each component, V_i is the molar volume of each specimen, and $\chi_{AB}^* = \chi_{AB}/V$ is the Flory binary interaction parameter.

The first two logarithmic terms give the combinatorial entropy of mixing, whereas the third term gives the enthalpy of mixing. For blends of polymers of high molecular weight, the volume (V_i) is quite large; thus, the combinatorial entropy is very small and the entropic stabilization is vanished. Hence, the negative value of ΔG_m required for mutual miscibility of the system will strongly depend on the value of the enthalpy of mixing or interaction contribution [$\chi_{AB}^* \varphi_A (1 - \varphi_A)$].

From this equation, it is clear why blends of high-molecular-weight polymers are different from small molecule mixtures. As most polymers have degrees of polymerization higher than 1000, the entropy of mixing is generally quite small. The interactions between two polymers are quite small compared to those between their small molecule monomers, and so the enthalpy of mixing will not depend on the molecular weight of the components. The enthalpy of mixing is positive for most mixtures and the rule of “like prefers like” always applies. Enthalpy will be negative and favorable to mixing if the two components interact through specific interactions, such as charge transfer or hydrogen bonding.

The entropy of mixing of small molecules can be so large that it overwhelms the positive mixing enthalpy and forces the components to mix under a wide range of temperature and compositions. This is why polyolefins,

such as polypropylene (PP) and polyethylene (PE), are immiscible under all conditions, whereas monomers of low molecular weight are miscible over a large range of conditions, which is simply due to the near absence of mixing entropy for the two high-molecular-weight polymers.

The enthalpy of mixing (ΔH_m) can be expressed in terms of solubility parameters:

$$\Delta H_m = V (\delta_A - \delta_B)^2 \varphi_A (1 - \varphi_A) \quad (27.4)$$

where δ_i are the Hildebrand solubility parameters.

Miscibility can be estimated by using solubility parameters, which are tabulated for many different polymers and solvents. Hildebrand solubility parameters have been used to predict the solubility of solvents in polymers [3]. If the exact solubility of a solvent is unknown, the Hildebrand parameters are useful to obtain an indication of the solubility and swelling behavior of the polymer under the load of a specific solvent. This parameter (δ) is a result of the following intermolecular forces: dispersion (δ_d), dipole–dipole (δ_p), and hydrogen bonding (δ_h). When a solvent and a polymer have a similar solubility parameter, the solubility of the solvent in the polymer is high. Table 27.1 lists typical values of solubility parameters for several polymers and solvents [4]. From Equations 27.1 and 27.4, it can be seen that the consumption of heat or enthalpy of mixing is small when the difference between solubility parameters is small. Thus, the entropy of mixing (a measure of chaos) from Equation 27.1, which is negative, will promote a favorable negative energy of mixing ($\Delta G_m < 0$). When the heat of mixing is high, only high temperatures will drive the entropy to a sufficient level that can compete with the heat of mixing. Therefore, solubility usually increases with temperature.

As a miscible polymer blend shows very low or even negative values of the Flory–Huggins interaction parameter (χ_{AB}), some reports relate the miscibility of a polymer blend with polymer interactions in terms of intermolecular forces. Table 27.2 lists the bond energy and relative strength of different intermolecular forces. From this table, we can classify a miscible polymer blend with van der Waals interactions as one having weak interactions, and a miscible polymer blend with other types of interactions as one having strong interactions.

TABLE 27.2 Bond Energy and Relative Strength of Different Intermolecular Forces

Type of Interaction	Bond Energy (kJ/mol)	Relative Strength
Ionic attraction	850–1700	1000
Hydrogen bonding	50–170	100
Dipole–dipole interaction	2–8	10
van der Waals interaction	1	1

In polymer blends, different phase behaviors can be observed as shown in Figure 27.2. It is possible to calculate the compositions at which the blend will always separate into more than one phase (two-phase region), and also those compositions in which the blend may either form a single phase or will separate into several phases by different mechanisms, either in the metastable or in the spinodal regions. The binodals separate the miscible (one phase) and the metastable regions; the metastable region is

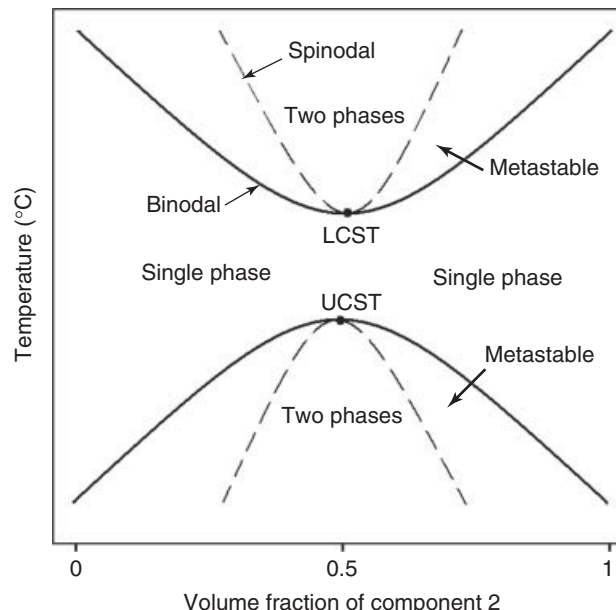


Figure 27.2 Phase diagram for binary blends showing the different phase regions and the upper and lower critical solution temperatures (UCST and LCST).

located between the binodal and spinodal curves and the two-phase separated region of immiscibility is bordered by the spinodal curve. This figure also shows the lower critical solution temperature (LCST) and the upper critical solution temperature (UCST). Blends that have positive entropies and mixing heats (endothermic mixtures) usually tend to exhibit UCST, whereas blends that have negative values of entropies and enthalpies of mixing usually exhibit LCST. In other words, if the enthalpic interactions between polymer components are unfavorable, the blend will exhibit a UCST and it will be immiscible at lower temperatures, mainly due to weak interactions between them [5].

Phase separation takes place when a single-phase system suffers a change of temperature, pressure, or composition that forces it to enter either the metastable or the spinodal regions. Phase separation occurs by different mechanisms. When the system enters from a single-phase region (Fig. 27.2), uniform in composition, into the spinodal region of immiscibility where the mixture is unstable, phase separation occurs by a spontaneous and continuous process. This spontaneous process is attributed to a diffusional flux mechanism and is called *spinodal decomposition*. On the other hand, if the system enters from a single-phase region into the metastable region, phase separation occurs by a mechanism resembling crystallization: slow nucleation followed by growth of the phase-separated domains. In this mechanism, small fluctuations in composition form a nucleus and, once it is formed, it grows by a conventional

diffusion process [6]. This mechanism is called *nucleation and growth* (Fig. 27.3).

27.3 COMPATIBILITY IN POLYMER BLENDS

The main motivation for blending immiscible polymers is to create materials with combinations of properties superior to those of the individual components. However, immiscible polymer blends have the disadvantage that they are not thermodynamically stable. Therefore, postmixing processing, such as molding or annealing, can significantly affect blend morphology. Changes in morphology may reduce or eliminate the benefits achieved by blending. To address this challenge, the morphological stability of immiscible polymer blends is often improved by adding a compatibilizer agent, which preferentially locates at the polymer–polymer interface. The addition of such compatibilizers can lead to more stable, finer scale morphologies, by reducing the effective interfacial tension and slowing phase coarsening [7]. Figure 27.4 shows the effect of a block copolymer on the morphology of a PS/PE (polyethylene) blend in which a continuous reduction in the dispersed phase size is observed as the compatibilizer content is increased [8].

A compatibilized blend exhibits no gross symptoms of phase separation and has a desirable set of final properties. This implies at least some mixing of polymer segments on a microscopic scale and a certain thermodynamic

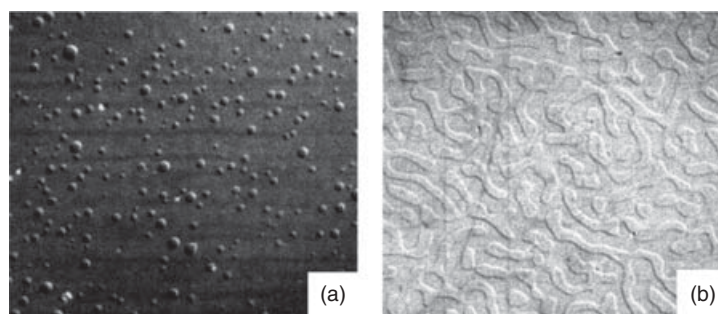


Figure 27.3 Blend images showing (a) nucleation and growth and (b) spinodal mechanisms.

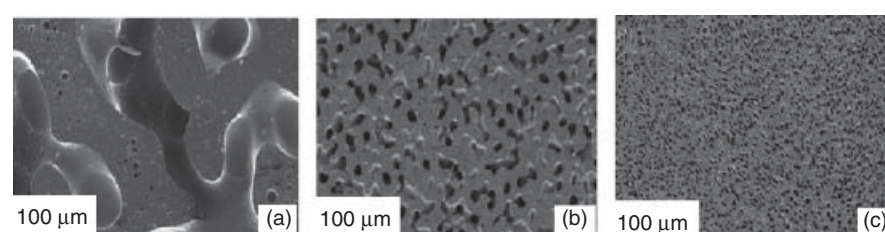


Figure 27.4 SEM micrographs of 50/50 PS/PE annealed polymer blends: (a) no block copolymer, (b) 0.3%, and (c) 1% of PS/PE block copolymer. *Source:* Reproduced with permission from Galloway JA, Jeon HK, Bell JR, Macosko CW. Polymer 2005;46(1):183–191 [8]. Copyright 2005 Elsevier.



compatibility that prevents demixing. It is important to realize that the highest degree of compatibility, in which complete miscibility has been reached ($\Delta G_m < 0$), does not always mean the best final properties. Most of the final mechanical properties require some amount of phase separation to produce the desired property [9].

The desired compatibilization can be obtained by different methods such as the addition of a third component (copolymer or functional polymer) or by inducing *in situ* chemical reactions (reactive blending) among blend components, leading to the modification of the polymer interfaces and tailoring the blend phase structure and the final properties. The final properties of a blend will be determined not only by the components properties but also by the phase morphology and the interface adhesion, both of which determine the stress transfer within the blend and its end-use applications.

The blend morphology is determined by the processing history to which the blend has been subjected. The processing history depends on several factors, such as type of mixer, rate of mixing, temperature, rheology of the blend components, and interfacial tension between phases.

Compatibilizers reduce the interfacial tension in the melt between blend components and retard the coalescence process via steric stabilization, leading to an extremely fine dispersion of one phase into the other one. Compatibilizers also improve stress transfer by increasing the adhesion between phases and stabilize the disperse phase against growth during further annealing.

One of the most studied approaches to compatibilize a blend is the addition of a third component, such as a block or graft copolymer. Copolymers that contain segments chemically identical to the blend components are frequently used because they enhance the miscibility between the copolymer segments and the corresponding blend component (Fig. 27.5).

To improve compatibilization, it is required that the copolymer preferentially locates at the blend interface.

The resistive force to diffusion increases with molecular weight; thus, copolymers with high molecular weight are preferred if long times are available during the mixing process and lower-molecular-weight copolymers must be used if available diffusion times are short. Although block copolymers are preferred over graft copolymers, they are often not commercially available and need to be tailor made for a particular blend [7, 9].

The addition of a functional or reactive polymer as a compatibilizer involves the use of a polymer chemically identical to one of the components of the blend, which has been functionalized with certain groups (e.g. polar groups) that have some affinity for the other blend component. This functional group may chemically react with the blend component or only interact with it by polar or ionic interactions.

The polymer may be modified with functional or reactive groups in a reactor or an extruder, via reactive extrusion. Polyolefin modified with maleic anhydride, acrylic acid, glycidyl methacrylate, acid groups neutralized with a metal cation (ionomer), itaconic acid, or anhydride or similar compounds have been widely reported as compatibilizers because these groups have the ability to form a chemical linkage or a polar or ionic interaction with polar polymers such as polyamides (PAs), polyesters, and others.

Another method for producing compatible blends is via reactive blending, which implies the *in situ* formation of copolymers during melt blending, with no need for addition of a separate compatibilizer. This method has found widely commercial application and can be carried out either in batch melt mixers or in continuous processing equipment using single- or twin-screw extruders. The use of twin-screw extruders in a continuous process allows better temperature control and can be designed to apply the shear stresses needed to improve blending and to remove the undesirable reaction byproducts by devolatilization.

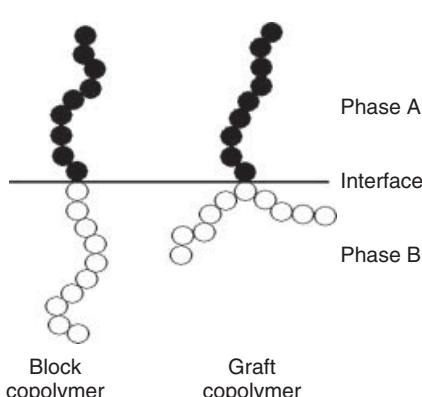


Figure 27.5 Schematic diagram showing interactions of block and graft copolymers through the interface.

27.4 TECHNIQUES FOR STUDYING BLEND MICROSTRUCTURE

Experimental study of blend miscibility or compatibility is more difficult for polymeric materials than for small molecules, because the heat of mixing (ΔH_m) is very small for polymers and is nearly impossible to measure directly. Because of the microscopic size of the dispersed phase, it is necessary to use special techniques to measure morphology on that very small scale. A brief sampling of the most important techniques used to study blend microstructure is offered below [6].

Measurement of the *glass transition temperature* of a blend is one of the most common ways to determine blend compatibility. Perhaps the most used criterion of polymer

compatibility is the detection of a single glass transition whose temperature is commonly intermediate between the glass transition temperatures corresponding to each one of the blend components. Thus, a general rule that has been applied is that if the blend displays two T_g s at or near the same temperatures of the blend components, then the blend is classified as incompatible. On the other hand, if the blend shows only a single transition temperature that is intermediate between those of the pure components, the blend is classified as compatible.

In addition, it is believed that a very broad, single glass transition in miscible polymer blends having little or very weak interactions is caused by the presence of concentration fluctuations that broaden the distribution of segmental relaxation times, which depend not only on blend composition but also on temperature. Further, it has been empirically observed that miscible polymer blends with large differences in T_g between the constituent components (ΔT_g) will give rise to failure of the time temperature superposition (TTS) principle. Glass transitions are determined with relative ease by thermal analysis using a differential scanning calorimeter (DSC), but this technique is limited to materials with significantly different T_g s and it cannot give information about the degree of compatibility.

Another technique commonly used is *light microscopy*, which is relatively simple and cheap, and requires non-complicated specimen preparation. The main disadvantage of this technique is the low resolution of light microscopes, which is limited by the wavelength of visible light. The visibility of blend phases can be enhanced by contrast techniques identifying the phases by staining or fluorescence. Samples made from two miscible or compatible polymers are optically clear, whereas those made from incompatible polymers are usually translucent or opaque. Some authors have reported that the critical domain size required for film transparency in a microheterogeneous blend is approximately 0.1 μm or 100 nm. The clarity observed in some blends is also affected by the refractive indices of the components or by the size of the dispersed phase, which could be smaller than the wavelength of visible light.

Scanning electron microscopy (SEM) can offer a good depth of field, good resolution, and easy specimen preparation. It can be used for immiscible polymer blends, where the phases are sufficiently large and can be easily debonded. Information on surface topography, size, and distribution of the dispersed phase and interfacial interaction between phases can be elucidated with this technique. Elemental analysis on the blend components can also be obtained if the SEM equipment includes an energy dispersion X-ray spectrometer (EDX).

Another microscopic technique is *transmission electron microscopy* (TEM), which offers higher resolution and

provides information on the fine structure of materials down to atomic or molecular levels and elemental analysis from small samples. A combination of the scanning and the transmission facilities can be obtained from a scanning transmission electron microscopy (STEM), which offers better image processing, much less beam damage of the analyzed samples, as well as accurate and high-quality diffraction patterns, which can be located on a specific area of the sample. It can be combined with other specific techniques such as back-scattered electrons or diffracted electrons to increase contrast.

This technique can be used to obtain structural information on very small scales approaching the molecular dimensions. It can be used to study surface morphology, internal structure, and crystallographic analysis. It can provide information about cocrystallization, very fine depression phases, or interfaces.

Spectroscopic techniques such as *FTIR*, *Raman*, or *NMR* can measure molecular interactions such as hydrogen bonds or specific chemical reactions. These techniques cannot give information about the phase inversion and are mostly nonquantitative.

Other techniques used with less frequency are *light*, *neutron* and *X-ray scattering*. In light scattering (Chapter 18), a laser beam is scattered on heterogeneities such as large molecules or molecular clusters. This technique can detect segregation of phases in solutions with temperature changes; thus, it can detect spinodal decompositions and can be used for the measurement of phase size and dispersion.

Neutron and X-ray scattering techniques use shorter wavelengths and require deuterated polymers for neutron and fluorinated polymers for X-ray scattering. The information obtained with these techniques is on the molecular scale and can reveal the arrangement of side groups, crystalline structure, and conformation of molecules.

27.5 PREPARATION OF POLYMER BLENDS

Preparation of polymer blends has been done by different types of machinery that includes internal mixers, such as single- or multishaft mixers, and extruders, such as single- or twin-screw extruders [9].

27.5.1 Mixers

Dry blends (powder blending) or blends of plasticized polymers are commonly prepared in a single-shaft mixer, such as ribbon blenders or paddle mixers.

Internal multishaft mixers that generate higher mechanical stress than single-shaft mixers whose shafts rotate at different speeds and whose charge is contained by a ram are used for melting and mixing of viscous masses. The

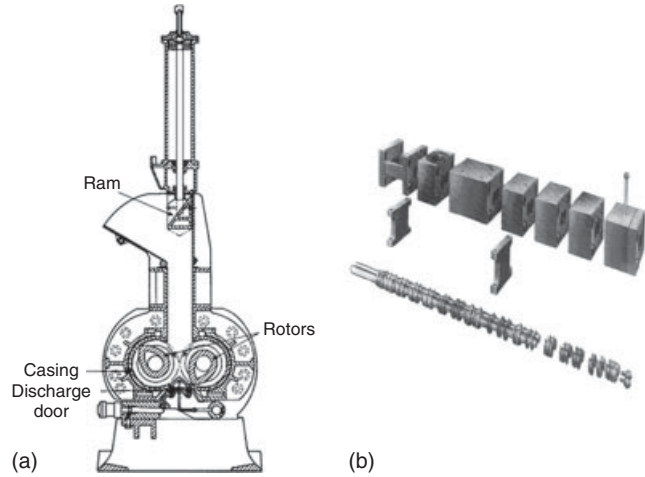


Figure 27.6 Devices used for polymer blend preparation: (a) internal multishaft batch mixer and (b) modular twin-screw extruder.

rotors are designed to cause flows to circulate through the mixer chamber. One of the most common internal mixers is the Banbury plasticizing batch mixer (Fig. 27.6a). This type of mixer is widely used for polymer blends such as rubbery polymer melts and blends of rubbers and plastics.

27.5.2 Extruders

Single-screw extruders have been widely used for blend preparation; however, they do not offer sufficiently high stress levels to improve mixing; thus, special designs of screws have been developed such as those with mixing heads or barrier zones that increase residence time and enhance blend mixing.

Twin-screw mixers (Fig. 27.6b) have demonstrated to be the most efficient devices to obtain higher mixing levels in polymer blends. An obvious advantage of these extruders over single-screw design is the additional distance along the periphery over which the melt is dragged in one revolution. These extruders are used for mixing, compounding, or reacting polymeric materials. They offer extreme versatility and allow their operation to be designed specifically for the blend formulation being processed. Twin-screw extruders (Chapter 23) are formed by two screws, side by side, placed within the extruder barrel; they could be either counter-rotating or corotating and intermeshing or nonintermeshing, depending on the way they rotate or the way they are matched together. The configurations of the screws may be varied using different types of mixing elements, such as forward conveying or reverse conveying, kneading blocks, vent stages, and other specific designs to achieve particular mixing characteristics. Corotating intermeshing units are

widely used for compounding materials where higher levels of mixing and high output rates are desirable.

The correct choice of compounder, operation conditions (rate, rpm, and temperature), feeding technique, and mixing elements of the compounder configuration has a significant effect on the quality of the resulting polymer blend. The capability of a compounder to generate shear stresses of sufficient magnitude to disrupt the stabilizing interfacial forces of the blend and the deformations field generated during plastication directly influences the dispersion mechanism.

27.6 FACTORS INFLUENCING THE MORPHOLOGY OF A POLYMER BLEND

Current commercial interest in blends is to a large degree focused on the dispersion and mixing characteristics of polymers in melt-compounding processing equipment, such as mixers and extruders. Controlling the factors that directly influence both control of interfacial modification and morphology, under melt processing conditions, have been widely studied over the years. The development and stability of morphology in multiphase polymer melts is a complex function of several factors, the most important being viscosity ratio, blend composition, applied shear stress, as well as elasticity and interfacial characteristics [9, 10].

A theory for the break up of individual droplets for Newtonian fluids has been developed and a relationship has been established between the capillary number (Ca), which is a ratio of shear to interfacial forces, and the viscosity ratio η_r ($\eta_r = \eta_d/\eta_m$ = dispersed phase viscosity/matrix phase viscosity), where G is shear rate, D is the diameter of the droplet, and γ is interfacial tension.

$$Ca = \frac{G\eta_m D}{2\gamma} \quad (27.5)$$

The predicted drop size for a simple field is proportional to interfacial tension and inversely proportional to shear rate and matrix phase viscosity. Although Newtonian systems are relatively well understood, there are many limitations to this theory for predicting the morphology of a multiphase polymer system. Other difficulties in comparison with such ideal systems may include the complex shear fields applied in processing and the relatively high concentrations of the dispersed phase in most commercial polymer blends.

27.6.1 Viscosity Ratio

Viscosity ratio is the ratio between viscosity of the dispersed phase and the viscosity of the matrix. This

ratio has been shown to be one of the most important factors for controlling blend morphology. If the minor component of the blend has lower viscosity than the major component, that component will be finely and homogeneously dispersed. On the other hand, the minor component will be coarsely dispersed if it has higher viscosity than the major component. Some authors have found a linear relationship between the average diameter of the dispersed phase (minor phase) particles and the viscosity ratio [9, 10]. They have also reported that fine dispersion can be achieved if the viscosity of the minor phase is low and the value of the viscosity ratio is near unity. It has been demonstrated that as the viscosity ratio moves away from unity in either direction, the dispersed particles become larger. A higher matrix viscosity will stabilize the dispersed phase against capillarity instabilities. Thus, increasing the matrix viscosity would result in a more evenly distributed dispersion, mainly because it delays the breakup time and inhibits premature relaxation of the dispersed phase.

27.6.2 Blend Composition

For a given A–B blend, the composition of each component will define a specific region: (i) a region for which phase A is dispersed in matrix B, (ii) an intermediate region of phase inversion for which both A and B are cocontinuous, and (iii) a region in which now phase B is dispersed in matrix A (Fig. 27.7).

A variety of morphological structures can be obtained by varying the components, composition. Increasing the fraction of the dispersed phase results in an increase in particle size mainly owing to coalescence. As the minor phase concentration is increased, particle–particle interactions may

significantly increase and promote coalescence. It is clear that the extent of coalescence will depend to a large degree on the interfacial tension of the immiscible polymer components.

27.6.3 Shear Stress

As discussed earlier, from Equation 27.5, the phase size is inversely proportional to the applied shear stress. It has been demonstrated that shearing at high shear stress results in much finer and dispersed morphologies. The reported results have indicated that large variations in shear stress are required for this to predominate over the viscosity ratio in controlling the dispersed particle size. Increasing shear stress results in higher deformation of the dispersed phase and a fiberlike dispersed phase could even be formed. High shear rates may have a negative effect on the transient breakup process by suppressing capillary instability during flow.

27.6.4 Elasticity

The effect of elasticity in determining the morphology in a polymer blend remains one of the least understood aspects in this field. Some studies have shown that the elastic contribution to interfacial tension can result in a tendency for the phase of higher elasticity to encapsulate the one with lower elasticity, indicating that it is generally difficult to deform a highly elastic material. It has been reported that polymer blend morphology is not highly sensitive to changes in shear stress and shear rate when mixing in an internal mixer, and this was attributed to the viscoelastic nature of the dispersed droplets [11]. Although internal mixers are predominantly shear mixing devices, they can also induce elongational flow to the dispersed particles. The efficiency of elongational flow in droplet breakup has been demonstrated; however, the elastic component of molten polymers allows them to better retain their shapes after deformation.

27.6.5 Interfacial Characteristics

As described earlier, compatibilizers can enhance compatibility in a polymer blend by promoting physical or chemical interactions with blend components. If the compatibilizer locates at the interface, it will bind the two components together interlacing their phases. The main effect of interfacial modification on the morphology of an immiscible blend is a reduction on the particle size and a narrowing of the particle size distribution. This reduction in particle size is related with a decrease in the interfacial tension and a reduction in the coalescence process. Interfacial modification seems to be the dominant factor for controlling the dispersed phase size, and the dependence of this phase size

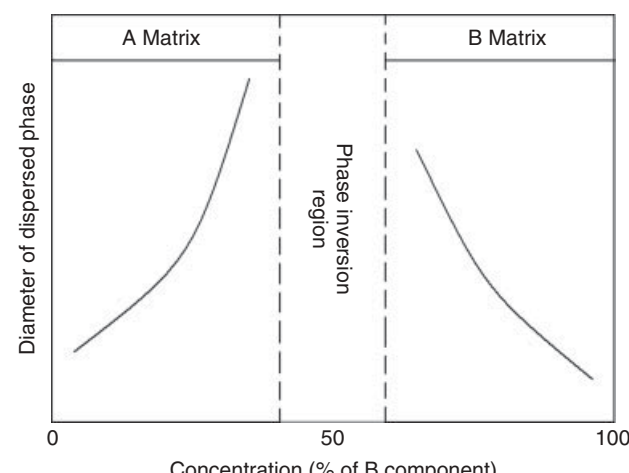


Figure 27.7 Variation of dispersed phase size in an A/B polymer blend as a function of component B concentration.

versus viscosity ratio is less pronounced for compatibilized systems in which an interfacial modification has occurred. The particle size on addition of an interfacial modifier is due to the reduction in interfacial tension as well as to reduced coalescence.

It has been demonstrated that when the rates of drop breakup and coalescence are in dynamic equilibrium, the particle size decreases as the applied stress increases and the interfacial tension between the phases decreases. For two particles to fuse in a bigger particle, they must first come into close proximity to each other by some flow process driven by a shear field, hydrodynamic interactions, gravity, or other forces. Once the two particles are in near contact, there is only a finite chance that coalescence of the particles will occur. Coalescence depends, among other variables, on the viscosity of the matrix phase that would allow sufficient time for drainage of the film between the dispersed phase domains. Several studies [12, 13] have shown that the dispersed phase particle size developed during processing can increase, decrease, or show a complex nonmonotonic behavior as the shear rate is increased, mainly because of the competing effects of increased particle–particle contacts versus decreased contact times. In addition, changes in polymer elasticity at high shear rates may also affect the dynamic equilibrium between coalescence and particle breakup.

27.7 PROPERTIES OF POLYMER BLENDS

27.7.1 Mechanical Properties

Mixing two or more polymers to produce blends or alloys is a well-established route to achieve a certain level of physical properties, without the need to synthesize specialized polymer systems. For example, an amorphous and brittle polymer, such as polystyrene, can increase its toughness when blending with polyethylene and a compatibilizer.

The goal of combining two or more polymers in a blend is to achieve a combination of favorable properties from each polymer. Figure 27.8 shows idealized expected property combinations from blending two polymers that are either miscible (center line), immiscible, and uncompatibilized (bottom line), or immiscible and compatibilized (top line). In the case of polymers that are miscible in all proportions, we can only obtain an average of their physical properties depending on the proportion of each polymer present. When two immiscible polymers are blended without compatibilization, one generally obtains physical properties worse than those of either individual polymer (antisynergic effect). Usually such a blend has poor structural integrity and poor heat stability because there is no mechanism for stabilizing a dispersion of one polymer in a

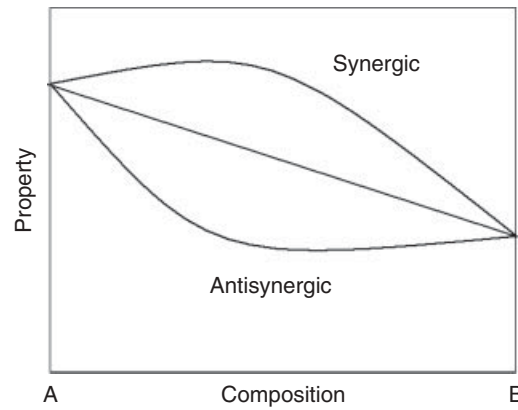


Figure 27.8 Schematic representation of blend property as a function of blend composition.

matrix of the other. On a macroscopic scale, the blend may appear heterogeneous and in the extreme case delaminated. When two immiscible polymers are blended with compatibilization, one may expect a synergistic combination of properties from each polymer [2, 14].

In most cases, melt mixing two polymers results in blends that are weak and brittle. The incorporation of a dispersed phase into a matrix mostly leads to the presence of stress concentrations and weak interfaces, arising from poor mechanical coupling between phases.

The mechanical properties and end-use performance of a blend have been improved by compatibilization. From a practical point of view, a blend is often considered to be compatible if a certain set of mechanical properties is achieved.

The well-known examples of blends are impact modified, toughened polymers, where polymers with different glass transition temperatures are blended, such as a rubber with a thermoplastic. Many other blends are known, such as barrier polymers for packaging, where specific polar or non-polar polymers improve the properties of polymer blends, combined to increase the resistance against transport of water and a certain gas (oxygen, carbon dioxide, etc.), such as PA (barrier to oxygen) with a polyolefin (barrier to water vapor).

The incorporation of rubber particles within the matrix of brittle plastics may enormously improve their impact resistance. When a force is applied to a blend, several deformation mechanisms of the major phase and of cracks that are formed in the blend are important. Their relative importance may depend on the polymer and on the nature of the loading. The best-known effect from compatibilization is the reduction of the interfacial tension in the melt. This causes an emulsifying effect and leads to an extremely fine dispersion of one phase into the other. A second effect is the increase of the adhesion at phase boundaries giving

improved stress transfer. For this effect, the interaction between the compatibilizing copolymer chain and the polymer chains of the dispersed phase and the matrix phase will be important. The third effect is the inhibition of coalescence of the dispersed phase by modifying the phase boundary interface.

The change induced in the stress-strain behavior by incorporation of elastomeric particles into a PS matrix has been reported [15]. On toughening, PS brittle behavior changes into ductile with flow. The rubber-modified polymer absorbs considerably more energy; thus, higher elongation to break can be achieved. By contrast, an addition of rigid resin to a ductile polymer enhances the modulus and the heat deflection temperature.

In general, two mechanisms are responsible for plastic deformation in rigid polymers: crazing and shear yielding. Crazing is an important source of toughness in rubber-modified thermoplastics. A craze can be described as a layer of polymer, a nanometer to few micrometers thick, which has undergone plastic deformation approximately in the direction normal to the craze plane as a response to tension applied in this direction. Shear yielding is a mechanism in which a thin layer of polymer deforms in shear at constant volume. It is characterized by regions of sheared polymer oriented to the tensile or compression stress. Unlike crazing, shear flow is essentially a process continuous in space. Shear yielding is much less sensitive to environmental effects. Both crazing and shear yielding involve the absorption of energy, and most methods of toughening polymers involve modifying the polymer such that more crazing and shear yielding take place. The rubber-modified polymer absorbs considerably more energy in a tensile test because of its higher elongation to break, which can be achieved only as a result of yielding in the matrix. The rubber particles accelerate yielding by acting as stress concentrators initiating deformation in the matrix; secondly, they respond to the hydrostatic component of the stress by cavitating and increasing in volume, thus allowing the strain in the matrix to increase; and thirdly, in their cavitated and extended state, they stabilize the yielded polymer by carrying a share of the applied stress. Various types of response of the rubber particles have been observed experimentally as the polymer yields, which includes debonding between rubber and matrix, cavitation within the particle, crazelike fibrillation of the rubber phase, and crazing within subinclusions.

The mechanisms of deformation under tension of polymer blends are strongly related to the behavior of the microdomains and their adhesion to the matrix. It has been demonstrated that the formation of microcavities under tension tests is responsible for the propagation of fractures. Most homopolymers have a limited range of stable fatigue-crack growth. However, the range of stable fatigue-crack growth can be increased by blending

rubber particles or some organic filler into the polymer matrix. Rubber particles provide a crack-tip mechanism that involves rubber-particle cavitations and matrix plasticity. The crack growth rate may be affected by several external parameters such as a change in mean stress, variation in stress amplitude, and the presence of a notch in the sample.

Theoretical understanding regarding toughening mechanisms has been advanced for both rubber and thermoplastic toughened blends. Some theories based on the early toughening mechanisms of toughened thermoplastics suggested that the energy absorbed in a fracture is the sum of the energy required to fracture the matrix and to break the rubber particles. Microcracks due to rubber particles cause tensile yielding and, thus, a large tensile deformation. Voids result when the microcracks open, and these voids permit large strains. Debonding or microcracking effectively lowers the modulus in the frontal process zone around the crack tip and, thus, effectively reduces the stress intensity there. This theory [16] cannot explain many phenomena, such as stress-whitening, the large amount of plastic deformations, higher fracture toughness at a higher temperature, and the fact that nonreactive rigid thermoplastic particles may also toughen some systems. Another theory [17] proposes a mechanism that involves dilatational deformation of the matrix and cavitation of the rubber particles in response to the triaxial stresses near the crack tip, combined with shear yielding between the holes formed by the cavitated rubber particles. The stress-whitening was attributed to light scattering by these holes, and the major energy absorption mechanism was suggested to be the plastic deformation of the matrix. Plastic deformation blunts the crack tip, which reduces the local stress concentration and allows the material to support higher loads before failure occurs. Other authors have proposed that additional crack-tip shielding in rubber-modified resins occurs due to the reduction in yield stress by the stress concentration of the compliant rubber particles that facilitate shear yielding. Even though there are various toughening mechanisms proposed by different researchers, it seems that a single theory cannot explain every experimental result and phenomenon of toughening. Figure 27.9 shows a scheme that describes the several toughening mechanisms involved in the fracture of rubber-toughened polymer blends.

27.7.2 Rheological Properties

The rheology of polymer blends has received a lot of attention because of its technological importance in polymer processing. Rheology studies can be classified into three groups: studies dealing with the rheology of polymer mixtures in, respectively, homogeneous, phase-separated, and transition regimes. Research on homogeneous blends is focused mainly on the concentration dependence of viscosity and linear dynamic properties [6, 18–20]. Rheological

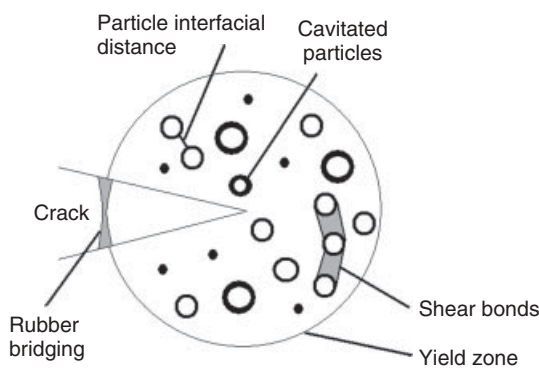


Figure 27.9 Scheme of the different mechanisms involved in the fracture of rubber-toughened polymer blends.

properties can be studied by taking into account the differences in molecular shape of the components. It is important to note that the TTS is applicable when polymer blends are in the homogeneous state far from the transition temperature and there is no obvious dynamic asymmetry of the components. In phase-separated polymer blends, the polymer blends show pronounced elastic properties, very long relaxation times, and a failure of the TTS. Complex changes in the linear viscoelastic properties were observed when polymer blends of a given composition were heated (for LCST systems) or cooled (for UCST systems) from the homogeneous regime to the phase separation regime.

When the size of dispersed particles is in the submicron range, fluid particles will remain spherical mainly because of the influence of interfacial tension. This system will have many common characteristics with dispersions of rigid particles.

When both phases are fluid, such as melt polymer blends, no general predictions of macrorheological behavior can be established. Generally, two distinct morphologies are observed, with the dispersed phase distributed either as ribbons or droplets. Droplets appear to be less deformable than an equivalent viscous Newtonian droplet. The resistance to breakdown in shear often makes most intensive shear mixers ineffective and leads to the need of employing other flow fields different from shear to achieve a good dispersion.

Morphology of a blend will depend on the detailed processing history. Morphologies such as ribbon type are stable in flow only if preserved by crystallization or quenching, and this type of morphology will break up rapidly when the flow ceases. This may affect the final properties of the final sample depending on if it was prepared by extrusion or injection molding. The great variety of morphologies observed in polymer blends has been attributed to the viscoelasticity of each polymer component.

Some authors report the next guide principles that may be applied for blend morphology after processing. (i) Drops with viscosity ratios higher than 3.5 cannot be dispersed in shear but can be in extension flow instead. (ii) The larger the interfacial tension coefficient, the less the droplets will deform. (iii) The time necessary to break up a droplet (T_b) and the critical capillary number (Ca_c) are two important parameters describing the breakup process. (iv) The effect of coalescence must be considered even for relatively low concentrations of the dispersed phase.

The addition of compatibilizers to polymer blends extensively affects their flow behavior. Chemical reactions occurring between the components of the blend upon compatibilization generally increase the viscosity of the system. Normally, the melt viscosity of polymer blends shows three types of behavior: (i) positive deviation behavior, where the blend viscosities show a synergist behavior, that is, blend viscosity is higher than the log additivity value; (ii) negative deviation behavior, where the blend viscosity shows a negative deviation from log additivity values; and (iii) a positive–negative deviation behavior. In the last case, the same blend exhibits both positive and negative deviation behavior depending on the composition, morphology, and processing conditions.

27.7.3 Optical Properties

Optical properties of blends have been studied to determine the factors leading to turbidity and hence to the design of blends with superior appearance. The analysis of the scattering of light and X-ray provides information about the morphology of the blends, allowing to measure the size and shape of the domain, as well as the differences in refractive index or electron density between components.

27.7.4 Barrier Properties

Polymer blending has been established as an effective means for building up new properties gradually altering transport properties of polymeric materials. Examples include blends of nylon and polyethylene that exhibit combined permeability to water vapor and oxygen, which in some cases is lower than the permeability to either component.

As the molecular size of most gases is much smaller than any scale of structure expected in polymer blend morphology, diffusion and permeability of gases can be employed to determine the phase behavior of a polymer blend. Therefore, the study of transport phenomena in blends would be motivated not only by the requirements of producing improved barrier materials but also by the continuous interest in the nature and characterization of polymer blend morphology.

27.8 APPLICATIONS OF POLYMER BLENDS

The worldwide commercialization of polymer blends has been directed at the replacement of traditional materials, such as metals and ceramics. Even though plastics can be more costly than other types of materials on a weight basis, they are often more economical in terms of production and manufacturing cost, mainly attributed to the less complex assembly of plastic parts that can be easily formed in complex-finished shapes [1, 21–26]. Blending is a convenient route to the time-efficient and cost-effective upgrading of commodity resins and to the tailoring of these resins to specific performance profiles for the desired application. The most common polymer blends and their applications are described below.

PPE/HIPS (*Polyphenyl-Ether/High Impact Polystyrene*). This type of blend features good dimensional stability, impact resistance, high resistance to moisture, low temperature impact strength, low creep, and improved processing. Applications include automotive instrument panels, interior trim, business equipment chassis, appliances, and electrical applications, including those requiring flame retardancy, building and construction, and medical applications.

PPE/PA. It features good chemical resistance, high continuous use temperature, high deflection temperature under load (DTUL), ease of processing, high modulus, and high impact. Applications include injection-molded automotive body panels, thermoformed truck body panels, trim components, mirror housings, wheel covers, under-the-hood electrical connectors, conductive grades for electrostatic painting, and fluid handling.

PET/PBT (*Polyethylene Terephthalate/Polybutylene Terephthalate*). Good colorability, excellent surface aesthetics, chemical resistance, gloss, good impact, and electrical properties. Applications include appliances, electrical applications, building, and construction.

PBT/Elastomers. It features chemical resistance, high notch Izod impact strength, and heat resistance.

PET/Elastomers. This blend features good stiffness, impact strength, and processability. Applications are in the automotive sector, such as in body parts, steering wheels, and under-the-hood components.

PET/PSF (*Polyethylene Terephthalate/Polysulfone*). It features warp resistance, stiffness, dimensional stability, high temperature performance, and chemical resistance. Applications include industrial process equipment, electrical connectors, and food-processing equipment.

PC/ABS (*Polycarbonate/Acrylonitrile-Butadiene-Styrene*). It has good heat resistance, toughness, tensile strength, creep resistance, color stability, flame resistance, moldability, and surface appearance. It is used in business

machine housings, exterior automotive trim, wheel covers, IPs, and interior parts. This blend replaces over-engineered straight PC in applications where a higher heat or impact resistance than straight ABS is required. Eliminating painting with a low gloss provides cost reduction, elimination of volatile organics, and better recyclability.

PC/PBT. It has low temperature impact, dimensional stability, and chemical resistance. It is applied in automotive bumpers.

PC/PET. This blend is transparent; it shows low temperature performance, chemical resistance, abrasion resistance, and impact resistance. Applications are in automotive parts, such as bumpers and exterior trim, in furniture, such as chair arm rests, support members, in appliances (housings), hand tools (housings), lawn and garden, such as motor housings, guards for electric hedge trimmers, and protective housings. Industrial applications include fluid handling equipment such as pump housings, valve bodies, and handles, as well as in electricals/electronics such as coil bobbins and connectors.

PC/TPU (*Thermoplastic Polyurethane Elastomer*). It is used in exterior motor vehicle for chemical resistance and strength.

PA/ABS. It has high temperature warp resistance, chemical resistance, good processability, and superior appearance. It can be applied in automotive parts such as body panels, under-the-hood connectors and components, fuel tanks, bearings, bushings, and cams.

PA/PE. It exhibits chemical resistance to gasoline and is used in fuel tanks.

PA/PTFE (*Polyamide/Polytetrafluoroethylene*). It shows low coefficient of friction and high temperature resistance. It is used in mechanical parts such as bearings, bushings, thrust washers, and construction hardware such as door latches.

TPU/ABS. It has low temperature toughness, chemical resistance, abrasion resistance, and superior toughness.

POM/Elastomer (*Polyacetal or Polyoxymethylene*). It has toughness, good notched Izod resistance, and chemical resistance. It is used in interior automotive, gears, cams, etc.

PPS/PTFE (*Polyphenylene Sulfide/Polytetrafluoroethylene*). It has high durability and wear resistance, tensile strength, hydraulic stability, and heat resistance. Applications include seals, valves, and bushings.

PE/PIB (*Polyethylene/Polyisobutylene*). It is used in sheet and film for barrier properties.

PE/Ionomer. It has impact resistance, stiffness, and heat resistance, and it is easy to process.

PP/EPDM, PE/EPDM (*Polypropylene/Ethylene-Propylene-Diene-Monomer*). It shows low temperature performance and toughness; rubberlike; used in wire and

cable insulation, hose and tubing, interior automotive trim, and mechanical components.

PVC/CPE or PVC/EVA (Poly(vinyl Chloride)/Chlorinated-Polyethylene) or (Poly(vinyl Chloride)/Ethylene-Vinyl Acetate Copolymer). They have impact resistance and UV stability and are used in the construction industry as siding, pipes, conduit, foamed material, and rigid sheets.

PVC/NBR (Nitrile Rubber). It exhibits oil and other organic fluid resistance and is used in hoses, belts, wire and cable insulation, and appliance parts.

PVC/TPU. It shows thermal stability, chemical resistance, and low temperature flexibility for footwear.

PVC/PMMA (Poly(Methyl Methacrylate)). This blend sometimes includes a small amount of MMA copolymer to improve the melt strength and as a processing aid. It is used in business machine housings, furniture, mass transit seating, and food service trays. MBS or MABS (methacrylate acrylonitrile butadiene styrene) can be added to improve low temperature toughness. Improved grades are used in siding, pipe, and fittings.

SAN/EPDM (Styrene acrylonitrile). It has good weatherability, impact strength, chemical resistance, and good processing. It is used in construction products and sporting goods.

REFERENCES

1. Utracki LA. *Polymer Blends Handbook*. Dordrecht, The Netherlands: Kluwer Academic Publishers; 2002.
2. Robeson LM. *Polymer Blends: A Comprehensive Review*. Munich, Germany: Hanser Publishers; 2007.
3. Huyskens PL, Luck WA, Huyskens T. *Intermolecular Forces*. New York: Springer-Verlag; 1991.
4. Koenhen DM, Smolders CA. *J Appl Polym Sci* 1975;19:1163.
5. Paul DR, Bucknall CB. *Polymer Blends*. Volume 1 and 2. NY, USA: Wiley; 2000.
6. Folkes MJ, Hope PS. *Polymer Blends and Alloys*. London, Great Britain: Blackie Academic and Professional; 1993.
7. Datta S, Lohse DJ. *Polymeric Compatibilizers*. NY, USA: Hanser Publishers; 1996.
8. Galloway JA, Jeon HK, Bell JR, Macosko CW. *Polymer* 2005;46:183.
9. Paul DR, Newman S. *Polymer Blends*. New York: Academic Press, Inc.; 1978.
10. Favis BD. *Macromol Symp* 1992;56:143.
11. Harrats C, Groeninckx G, Ciardelli, F. and Penczek, S. (Eds), *Modification and Blending of Synthetic and Natural Macromolecules*. Nato Science Series. Dordrecht, The Netherlands: Kluwer Academic Publishers; Volume 175. USA: 2004. p 155.
12. Angola JC, Fujita Y, Sakai T, Inoue T. *J Polym Sci Polym Phys* 1989;26:807.
13. Choudhary V, Varma HS, Varma K. *Polymer* 1991;32:2541.
14. Kulshreshtha AK, Vasile C. *Handbook of Polymer Blends and Composites*. Volume 3. Shawbury, UK: Rapra Technology Limited; 2003.
15. Bucknall CB, Clayton D, Keast WE. *J Mat Sci* 1972;7:1443.
16. Bucknall CB, Smith RR. *Polymer* 1965;6:437.
17. Donald AM, Kramer EJ. *J Mat Sci* 1982;17:1739.
18. Mikitaev AK, Ligidov MK, Zaikov GE. *Polymers, Polymer Blends, Polymer Composites and Filled Polymers: Synthesis, Properties, Applications*. Moscow, Russia: Nova Science Publishers, Inc.; 2006.
19. Utracki LA. *Polymer Blends*. Shawbury, UK: Rapra Technology Limited; 2000;11(3).
20. Mai YW, Yu ZZ. *Polymer Nanocomposites*. Cambridge, UK: Woodhead Publishing Ltd; 2006.
21. Thomas S, Zaikov GE. *Polymer Nanocomposites Research Advances*. NY, USA: Nova Science Publishers; 2008.
22. Yu L. *Biodegradable Polymer Blends and Composites from Renewable Resources*. New Jersey: Wiley; 2009.
23. Nwabunma D, Kyu T. *Polyolefin Blends*. New Jersey: Wiley; 2008.
24. Isayev AI. *Encyclopedia of Polymer Blends*. Fundamentals. Volume 1. Weinheim, Germany: Wiley; 2010.
25. Boudenne A. *Handbook of Multiphase Polymer Systems*. West Sussex, UK: Wiley; 2011.
26. Olabisi O, Robeson LM, Shaw MT. *Polymer-Polymer Miscibility*. Academic Press: New York; 1979.



28

THERMOSETTING POLYMERS

JEAN-PIERRE PASCAULT AND ROBERTO J.J. WILLIAMS

28.1 INTRODUCTION

Thermosetting polymers (also called *thermosets*) are a family of plastics characterized by the fact that they are formed starting from a liquid solution that irreversibly leads to a solid material during a heating step. In this sense, they exhibit an opposite behavior than the one of thermoplastic polymers that, with some exceptions, show a reversible solid-to-liquid transition when heated to a convenient temperature. Although the irreversible liquid-to-solid transition can be also produced by other means such as UV or electron beam irradiation, the resulting products are also called *thermosetting polymers*. The process by which the initial liquid solution is transformed into a solid is usually known as the *cure of the material*.

The initial liquid solution is usually composed of several ingredients, the most important ones being a mixture of comonomers that can react among themselves by an external action such as heating, UV-irradiation, etc. The self-reaction of a single monomer can be also employed. The rest of the ingredients can be initiators, catalysts, rubbers, fillers, fibers, pigments, etc. The necessary condition to generate a thermosetting polymer is that the single monomer or one or more of the comonomers has three or more reactive groups per molecule. This produces a tridimensional crosslinked structure that occupies all the reaction volume. The chemical reaction is, in most cases, irreversible so that turning the resulting material into a liquid state would require the breaking of the generated covalent chemical bonds, a process that leads to degradation of the material instead of the recuperation of the initial comonomers. This imposes a severe restriction on the process leading to a thermosetting polymer. Once the chemical reaction has been completed, it is not possible to reshape the final material.

The only possible action is to mill the solid material and use it as a filler. Knowledge of the chemical reactions taking place and the reaction heat is essential to design a cure process. Thermoplastic polymers are easier to process in the sense that their transformation from a solid to a liquid (heating) and back to a solid (cooling) is reversible. If there is a mistake, the final material (e.g., without the required thickness, size, or shape) can be recycled to the process.

A large variety of families of thermosetting polymers is used in industry. Phenolics were the first synthetic plastic produced in an industrial scale since the beginning of the twentieth century. They are thermosetting polymers formed by the reaction of phenol (a monomer with three reactive sites located in *o*, *o'*, and *p* positions) with formaldehyde (a comonomer with two reactive sites), and eventually another multifunctional comonomer, such as hexamethylenetetramine, added in a second step (for two-step processes). Of interest is the fact that they were produced by industry almost 15 years before the macromolecular structure of a polymer was formulated by Herman Staudinger, proving that on many occasions industrial innovations precede the formulation of the scientific background on which they are based. A second fact of interest is that phenolics still keep a niche in the market due to their outstanding dimensional stability, electrical properties, and resistance to creep at elevated temperatures. For example, formulations based on phenolics are used as the dielectric insulator in connectors for the space shuttle.

Many other families of thermosetting polymers have also found their niches in the global market. Some common examples are urea-formaldehyde and melamine-formaldehyde polymers, epoxies, unsaturated polyesters (UPs), and polyurethanes (PUs). Some typical

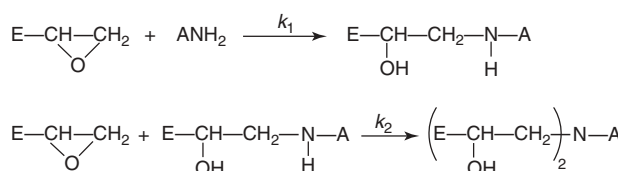
applications of these polymers are in wood agglomerates for furnishing (urea-formaldehyde polymers), laminates (melamine-formaldehyde polymers), coatings, adhesives, composite materials, electronic applications (epoxies), glass-fiber-reinforced plastics (UP), and insulating foams (PU). Formulations based on these polymers with a set of improved properties are continuously being developed by introducing new modifiers such as carbon nanotubes (CNTs), clays, or polyhedral oligomeric silsesquioxanes (POSS), or producing nanostructures using block copolymers (BCPs) or amphiphilic monomers [1]. These formulations are focused on high tech applications (optoelectronics and multimedia, telecommunications, energy storage and production, medical applications, etc.). New processing techniques with their corresponding equipment are continuously offered by several companies, proving the dynamic character of this field.

Although epoxies are mainly classified as thermosets, it is also possible to produce linear epoxy polymers using comonomers with two reactive sites per molecule. These linear polymers behave as thermoplastics and can be amorphous or semicrystalline. They exhibit some outstanding optical and barrier properties. Similarly, PUs can be either thermoplastics or thermosets depending on the number of reactive sites per molecule of monomers and comonomers.

Other thermosetting polymers are cyanate esters (CEs), benzoxazines, PU acrylates, bismaleimides (BMIs), dicyclopentadienes (DCPDs), diallyl phthalates (DAPs), etc. Formulations based on these polymers are used for specific applications where their particular properties are required. For example, DAP has long been the material of choice for electrical components where long-term reliability is required.

28.2 CHEMISTRIES OF NETWORK FORMATION

The description of the variety of chemistries that are used to produce thermosetting polymers can be the subject of a whole book and is beyond the scope of this chapter. A description of chemistries involved in the synthesis of several families of thermosets can be found elsewhere [2]. In this section, we focus on some aspects of the chemistry of epoxy polymers because it provides examples of both step-growth and chain-growth polymerizations employed in the synthesis of polymer networks.



Scheme 28.1 Reaction of epoxy groups with amines.

The epoxy group (oxirane ring) can react with both nucleophilic and electrophilic reagents. The most typical example of a step-growth polymerization of epoxy monomers is the reaction with amines, which are the most commonly curing agents/hardeners used to build up epoxy networks. The reactions shown in Scheme 28.1 take place in this case.

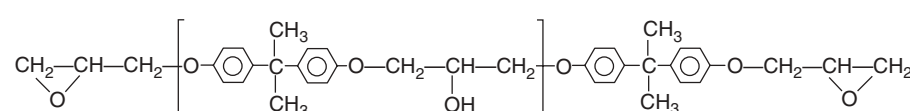
The multifunctional monomer with more than two reactive sites per molecule may be either the epoxy monomer or the amine comonomer. Diglycidylether of bisphenol A (DGEBA), with two epoxy groups per molecule, is a typical epoxy monomer (Scheme 28.2).

The step-growth polymerization between the 2-functional DGEBA and a 4-functional diamine (containing four active amine hydrogens in the structure) leads to a polymer network. The reactivity of the amine increases with its nucleophilic character: aliphatic > cycloaliphatic > aromatic. While for aliphatic and cycloaliphatic amines, primary and secondary amine hydrogens exhibit similar reactivities, for aromatic amines the reactivity of the secondary amine is 2–5 times less than the reactivity of the primary amine hydrogen. This means that once the primary amine reacts, the generated secondary amine exhibits a lower reactivity, a fact that is called a *substitution effect*. Aliphatic amines are used in low temperature curing formulations such as adhesives and coatings, while aromatic amines are used for high temperature cure cycles as those used for the manufacture of composite materials.

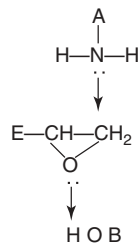
Hydroxyl groups catalyze the reaction through the formation of a trimolecular complex that favors the nucleophilic attack of the amino group, as shown in Scheme 28.3.

Apart from species containing OH groups that may be added as catalysts, the epoxy–amine reaction generates OH groups. Therefore, the reaction is self-catalyzed by reaction products, a fact that leads to sigmoidal conversion versus time curves when the polymerization is performed at a constant temperature.

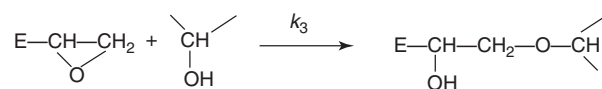
In most cases, when stoichiometric amounts of epoxy and amine comonomers are used, no side reaction takes



Scheme 28.2 Structure of diglycidyl ether of bisphenol A (DGEBA).



Scheme 28.3 Trimolecular complex that catalyzes the epoxy-amine reaction.



Scheme 28.4 Reaction of epoxy groups with secondary alcohols.

place. When there is an excess of epoxy groups, the reaction shown in Scheme 28.4 can take place after most of the amine hydrogens have reacted.

Epoxy monomers undergo a chain homopolymerization in the presence of both the Lewis acids as boron trifluoride complexes (cationic homopolymerization) or bases such as tertiary amines, imidazoles, and ammonium salts (anionic homopolymerization). These acids and bases are called *initiators* of the chain polymerization. In this reaction, each epoxy group acts as a bifunctional reagent in the propagation step, and therefore, a diepoxy monomer such as DGEBA becomes a 4-functional monomer leading to a polymer network. Figure 28.1 shows initiation and propagation steps of the anionic homopolymerization of epoxy groups. The scheme is completed by transfer reactions involving the transfer of an H from an OH group to the propagating chain, and complex termination reactions that depend on the particular formulation.

Initiation and propagation steps taking place in the cationic polymerization of epoxy monomers initiated by BF_3 complexes are shown in Figure 28.2.

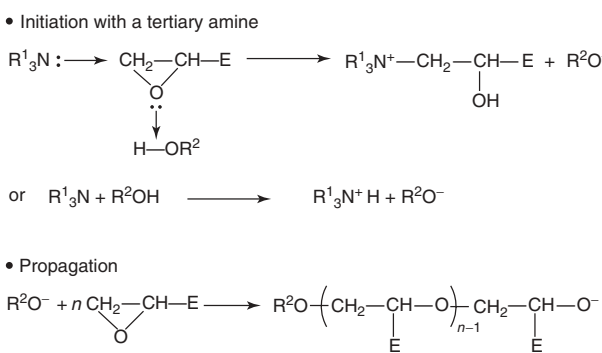
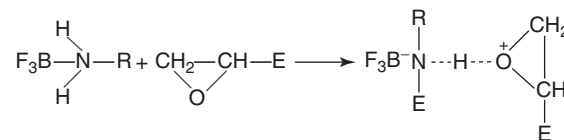


Figure 28.1 Initiation and propagation steps of the anionic homopolymerization of epoxy groups.

• Initiation with BF_3 complexes



• Propagation

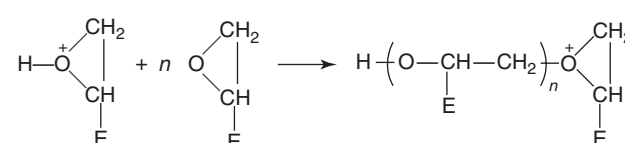


Figure 28.2 Initiation and propagation steps taking place in the cationic polymerization of epoxy monomers initiated by BF_3 complexes.

An usual way to generate a strong acid as an initiator of cationic polymerizations is by the UV decomposition of a complex aromatic salt of a Lewis acid. Cycloaliphatic epoxy monomers are used in this reaction because they exhibit higher reactivities than those of glycidylether epoxies such as DGEBA. These formulations are used in photopolymerization processes whose main advantage apart from the fast reaction rate is the insensitivity to oxygen (contrary to free-radical polymerizations).

Another usual family of hardeners employed to cure epoxy monomers are cyclic anhydrides, with the reaction initiated by tertiary amines or ammonium salts. The reaction proceeds through an alternating chainwise copolymerization, as shown in Figure 28.3.

The reaction of an alkoxide group with a cyclic anhydride is much faster than the reaction of a carboxylate group with an epoxy ring.

Several epoxy formulations are cured by both step-growth and chain-growth polymerizations occurring sequentially or in parallel. For example, BF_3 complexes or tertiary amines may be added as catalysts of an amine–epoxy reaction, leading to different reaction mechanisms taking place whose relative significance depends on the cure temperature (or thermal cycle) and the initial stoichiometry. The structure and properties of the resulting polymer networks depend on the relative contribution of both mechanisms.

28.3 STRUCTURAL TRANSFORMATIONS DURING NETWORK FORMATION

28.3.1 Gelation

Gelation occurs at a conversion where percolation of a giant molecule takes place throughout the system. At this critical

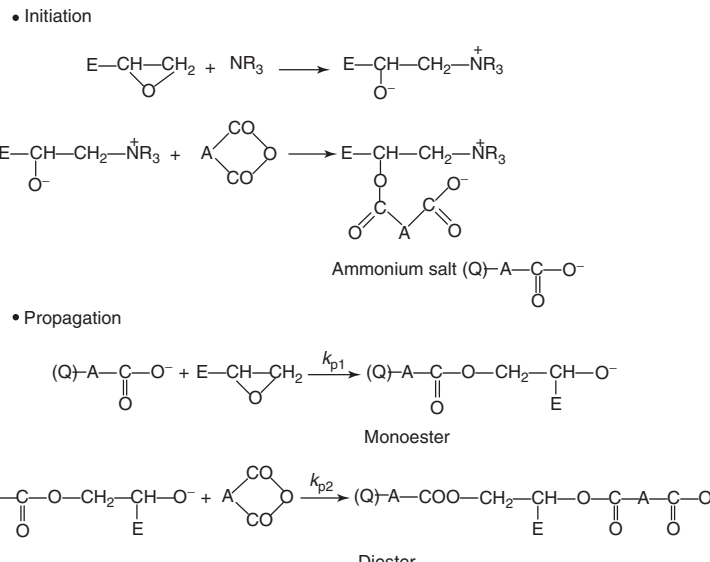


Figure 28.3 Chainwise copolymerization of epoxy monomers with cyclic anhydrides.

conversion, the system consists of a large number of finite molecules (the sol fraction) and one giant molecule (the gel fraction). From the macroscopic point of view, this implies the irreversible transition from a liquidlike to a solidlike behavior, which enables its characterization by monitoring the viscoelasticity of the sample during reaction. Gelation can be estimated as the time (conversion) where the elastic modulus becomes higher than the loss modulus. A more precise definition of gelation arises from the time (conversion) at which the ratio of both moduli ($\tan \delta$) becomes independent of the frequency of the experimental run [2]. The gel conversion depends on the functionality (number of reactive sites) of comonomers. The higher the functionality, the lower the gel conversion.

28.3.1.1 Stepwise Polymerizations For stepwise polymerizations of stoichiometric formulations of comonomers with f and g active sites per molecule exhibiting an ideal behavior (equal reactivity of functional groups, absence of both substitution effects and intramolecular cycles), the gel conversion (x_{gel}) is given by:

$$x_{\text{gel}} = \frac{1}{[(f-1)(g-1)]^{1/2}} \quad (28.1)$$

For the ideal step-growth polymerization of a diepoxy monomer such as DGEBA ($f = 2$) with a diamine ($g = 4$), the gel conversion is $x_{\text{gel}} = 0.577$. Experimental values close to 0.60 have been reported for many DGEBA-diamine formulations in close agreement with the theoretical prediction. The slight departure from the ideal value is often ascribed to the presence of substitution effects.

28.3.1.2 Chainwise Polymerizations A typical example of a thermoset produced by a chainwise polymerization is the case of the cure of unsaturated polyesters with styrene by a free-radical mechanism. Styrene is a bifunctional monomer, A_2 , characterized by the presence of one $\text{C}=\text{C}$ group that is transformed into a $-\text{C}-\text{C}-$ bond in the polymerization reaction. The unsaturated polyester is a multifunctional monomer, A_f , characterized by the presence of $(f/2)$ $\text{C}=\text{C}$ groups in its chemical structure. The molar fraction of $\text{C}=\text{C}$ groups belonging to the multifunctional monomer is given by:

$$a_f = \frac{f A_f}{2 A_2 + f A_f} \quad (28.2)$$

The gel conversion for the ideal chainwise polymerizations of an $A_2 + A_f$ system is given by the following equation [3]:

$$x_{\text{gel}} = \frac{2}{[a_f(f-2)(DP_w - 1)]} \quad (28.3)$$

where DP_w is the mass-average degree of polymerization of primary chains produced by single activation and termination steps. Its value is given by:

$$DP_w = \frac{1+q+\zeta}{1-q} \quad (28.4)$$

where

$$q = \frac{R_p}{R_p + R_t + R_d + R_c} \quad (28.5)$$

$$\zeta = \frac{R_c}{R_t + R_d + R_c} \quad (28.6)$$

Once initiated, a chain propagates at a rate R_p until termination takes place by one of the following events: chain transfer (rate R_t), chain disproportionation (rate R_d), or chain combination (rate R_c). For free-radical polymerizations, the probability of chain propagation is very much larger than the probability of termination by any one of the possible mechanisms. This means that $q \rightarrow 1$ and $x_{\text{gel}} \rightarrow 0$. In practice, the polymerization is far from being ideal. A large fraction of intramolecular cycles is produced leading to high crosslinked domains (microgels) embedded in a solution of unreacted monomers. Eventually, these microgels form an interconnected structure and macrogelation is produced, typically at conversions in the range of 5–15%.

28.3.2 Vitrification

The other independent transformation that can take place during network formation is vitrification. This transition occurs at the particular conversion where the increasing glass-transition temperature (T_g) of the reacting system equals the instantaneous value of the cure temperature. At this time, the macroscopic behavior of the system changes from a liquid or rubber to a glass. This means an increase of several decades in the value of the storage modulus.

Several equations have been proposed to describe the increase of T_g with conversion (x). A particular expression that was used to fit experimental data of a large variety of thermosetting polymers is the following one [4]:

$$\frac{T_g - T_{g0}}{T_{g\infty} - T_{g0}} = \frac{\lambda x}{1 - (1 - \lambda)x} \quad (28.7)$$

where T_g is the value of the glass-transition temperature at the particular conversion x , T_{g0} and $T_{g\infty}$ are, respectively, the initial ($x = 0$) and final ($x = 1$) values of the glass transition temperature, and $\lambda = \Delta C_{p\infty}/\Delta C_{p0}$ is the ratio of specific heats between liquid or rubber and glass, for the final material ($\Delta C_{p\infty}$) and the initial material (ΔC_{p0}). The evolution of T_g with conversion may be predicted by characterizing the initial and final materials using differential scanning calorimetry (DSC). For some polymer networks, full conversion cannot be attained due to limitations imposed by topology or by degradation when the temperature is increased to avoid vitrification. A specific system where full conversion cannot be attained is the reaction between epoxidized novolacs with aromatic diamines [5]. For these thermosetting polymers, Equation 28.7 can still be applied by replacing $T_{g\infty}$ by $T_{g\max}$, x by x/x_{\max} , and λ by $\lambda' = \Delta C_{p\max}/\Delta C_{p0}$, where $T_{g\max}$ and $\Delta C_{p\max}$ are the values obtained at the maximum attained conversion, x_{\max} [5, 6].

28.3.3 Conversion-Temperature Transformation (CTT) Diagram

Gelation, vitrification, and degradation curves can be plotted in the conversion-temperature transformation (CTT) diagram shown in Figure 28.4 [2, 6, 7]. The degradation curve is the boundary of a high temperature region where chemical degradation of the polymer network takes place. It is assumed that the stability toward thermal degradation of the reacting polymer increases with conversion.

Below the degradation curve, the diagram shows four different regions separated by the gelation and vitrification curves. Below the vitrification curve, the partially reacted thermosetting polymer is in the glassy state, either as an ungelled or as a gelled glass. Above the vitrification curve, the reactive polymer is present as a liquid or as a rubber, depending on the location of its actual conversion with respect to the gel conversion.

How do gelation and vitrification affect the kinetics of network formation? Let us first consider gelation. This transition is related to the formation of a percolating structure in the reaction medium, a fact that does not alter the reaction probability of chemical groups (they do not sense the occurrence of percolation). This means that kinetic equations are not influenced by gelation. For stepwise polymerizations, reactions paths that describe the kinetics of network formation depend only on concentration of reactants and temperature. The same equations describe the kinetics before and after gelation. For chainwise polymerization, some of the elementary steps must be expressed as a continuous function of conversion (e.g., Ref. 8). An acceleration in the overall reaction rate is usually observed due to the decrease in the rate of termination steps requiring the mobility of long chains (the so-called Tromsdorff's effect). However, there is no special change in the kinetic

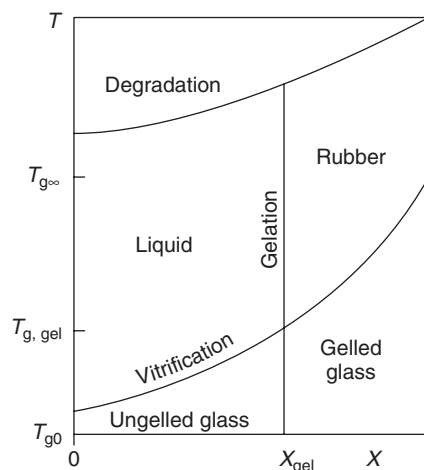


Figure 28.4 Conversion-temperature transformation (CTT) diagram.

equations due to gelation. On the other hand, vitrification produces a large decrease in the polymerization kinetics because it is directly related to the mobility of polymer segments. Kinetic equations must include a diffusional resistance that increases in importance as the system evolves beyond the vitrification curve. At some point, inside the glassy region chemical reactions become practically arrested and the polymer needs to be heated to the other side of the vitrification curve to continue the polymerization.

At room temperature, most thermosetting polymers are present as gelled glasses. Therefore, the most important properties of thermosetting polymers for practical purposes are those in the glassy state.

The CTT diagram may be employed to visualize the transformations occurring during specific thermal cycles selected for the polymerization. Isothermal trajectories at temperatures comprised between T_{g0} and $T_{g,gel}$ (temperature at which vitrification and gelation curves intersect) lead to a material that vitrifies before gelation. Vitrification is not a sharp transition, but it extends over a conversion range with its amplitude depending on the structure of the specific thermosetting polymer. For usual ways of defining the glass transition, the reacting polymer increases its conversion beyond the vitrification curve up to a point where the difference ($T_g - T$) is in the order of 20–30 °C. If this point is located in the region of an ungelled glass, the partially reacted polymer may be reactivated and processed by heating to a temperature located in the liquid region of the CCT diagram.

A partially reacted thermosetting polymer located in the ungelled glass region is denominated (in some old literature) as the B-stage of the polymer. This simply means that the polymer can be reconverted to a liquid by heating and then processed with conventional techniques. However, keeping isothermal trajectories is not easy in industrial practice due to the high exothermic reaction heat of most thermosetting polymers. These thermal excursions can lead to degradation of the polymer, making it necessary to model the expected evolution of temperature profiles in the material through mass and energy balances [2]. These models enable to select cure cycles that conduct the reacting polymer through the liquid and rubbery regions, ending at a temperature higher than $T_{g\infty}$ at full conversion.

28.4 PROCESSING

28.4.1 Formulations

The monomers, comonomers (hardeners), catalysts, and initiators are the components of the formulation that define the thermosetting polymer. Depending on the desired properties of the final material, a variety of other components may be part of the initial formulation. Fillers

(e.g., calcium carbonate, sawdust, recycled powdered thermosets, etc.) are used to improve mechanical properties and/or to reduce costs. Short fibers (glass, carbon, cellulose, etc.) are used to improve mechanical properties. Continuous fibers (glass, carbon, aromatic amides, etc.) are used in the manufacture of composite materials where the thermosetting polymer acts as the matrix that fixes the structure made of continuous fibers. Main mechanical properties are determined by the structure of fibers. Other usual additives are pigments and processing aids (e.g., additives that facilitate demolding of a cured part).

The intrinsic brittleness of most thermosetting polymers is a problem for their use as adhesives and coatings. Toughening can be achieved by producing a dispersion of rubbery particles or thermoplastic polymers inside the thermosetting polymer [9]. Core-shell particles with a rubbery core and a thin shell compatible with the thermosetting polymer can be used for these purposes. These particles can be produced by a two-stage latex emulsion polymerization technique. The core is a graftable crosslinked elastomer ranging in size from about 30 nm to 2 μm. The shell is grafted to the core and its chemical composition is selected to be as compatible as possible with the thermosetting polymer. This enables to achieve the formation of stable dispersions that can eventually generate partial aggregates during the cure. Another way to produce a dispersion of rubbery or thermoplastic particles is to start with a solution of a rubber or a thermoplastic in the precursors of the thermosetting polymer. Solubility is achieved by using low molar masses and compatible chemical structures. During polymerization a reaction-induced phase separation (RIPS) takes place mainly due to the decrease of the entropic contribution to the free energy of mixing [10]. This produces a dispersion of particles of the linear polymer in the thermoset. In general, rubbers exhibit an expected better toughening behavior than thermoplastic particles but produce a decrease in the elastic modulus and the glass transition temperature. Some thermoplastics give a reasonable toughening without deleterious effects on thermal and mechanical properties.

28.4.2 Rules for Processing Thermosetting Polymers

The main characteristic of thermosetting polymers is that polymerization and final shaping are performed in the same process. For a clear understanding, the evolutions of viscosity and modulus during curing at constant temperature are schematically plotted as a function of reaction time as shown in Figure 28.5.

Before gelation the material is a liquid with a finite value of viscosity. As the reaction proceeds, the viscosity increases and it tends to infinite at the sol–gel critical transition when a giant macromolecule percolates through the sample. After gelation, the mass fraction of the insoluble

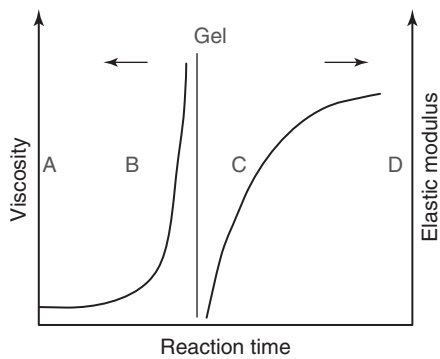


Figure 28.5 Evolution of viscosity and elastic modulus during the cure of a thermosetting polymer.

giant structure increases continuously and so does the elastic modulus of the sample. Shaping of the part has to be performed before the gel point where the material is still in the liquid state.

Most of the processing techniques have to take into account four different steps that depend on temperature, pressure, reaction rate, and the evolution of viscoelastic properties:

1. the pot life of the reactive system at the storage temperature (important before the beginning of the process);
2. flow inside the processing machine and into the mold (processing window);
3. reactions in the mold or on a substrate (for coatings and adhesives);
4. demolding and eventual postreaction.

The reactive system can be a one- or a two-pack system. Normally end users prefer a one-component system with a long pot life at room temperature and a high reactivity in the mold at a temperature as lower as possible. These two conditions are in contradiction with the Arrhenius law that can, however, be bypassed by the use of blocked reactants or by reactions activated by radiations.

The rheological evolution of the reactive system depends both on temperature and conversion. The chemoviscosity of thermosetting polymers is an important issue in relation to processing [11].

Processing techniques for thermosetting polymers are described in what follows in relation to the most extended applications.

28.4.3 Thermosetting Polymers for Adhesives, Coatings, and Paintings

28.4.3.1 Chemistries A large majority of adhesive and coating films in the end-use state exist in the form of a polymer network. Chemistries for adhesives and

coatings are either classical step-growth (epoxy/amine, epoxy/acid, isocyanate reactions, phenolics, trans-reactions of melamine, etc.) or chain-growth polymerizations (radical polymerization of acrylic or unsaturated polyesters, cationic polymerization of epoxies, etc.). Network formation is a very important process in film formation and the structure of the thermosetting polymer determines the application properties of the film [12]. Formulations are rather complex and additional components such as solvents, pigments, fillers are usually introduced to control the final properties.

Because of their excellent photooxidative durability, acrylic monomers are most often used in coatings. Hardness and softness, refractive index, chemical and humidity resistance, degree of durability, and degree of crosslinking are easily designed with an acrylic copolymer. Inherently, however, acrylic copolymers are not very flexible. To solve this problem, low T_g oligomers with acrylic functional groups are introduced in the formulation.

Formulations containing aromatic molecules such as aromatic isocyanates or epoxies not only suffer from poorer durability than formulations based on aliphatic monomers but they yellow severely on exposure to sunlight.

28.4.3.2 Solvent-Borne Coatings The majority of conventional coatings are solvent borne, traditionally containing about 25% solids. Organic solvents are added to coatings to disperse the different constituents of the formulation and to provide the low viscosity needed for conventional application methods (spray, roller coating, etc.). Once solvents are eliminated, the thermosetting polymer provides the physical properties of the coating.

Solvent-based coating films are formed by simultaneous crosslinking of polymer network precursors and solvent evaporation. This is a complex process in which the crosslinking rate and the development of the network depend on the content and nature of the solvent. Solvent evaporation depends not only on solvent volatility but also on the structure of the crosslinking system (thermodynamic interactions and chemical potential). The progress of chemical reaction and the rate of solvent evaporation determine the increase in T_g . When T_g approaches or exceeds the reaction temperature, the curing reaction becomes diffusion controlled and greatly retarded. The solvent evaporation slows down as well. The retention of residual solvent in the coating film even after long drying times (especially in the case of ambient temperature drying) is a very serious problem affecting the quality and durability of coating films [13].

As coating and paint producers as well as end users wish to reduce the volatile organic compound (VOC) emissions, progresses are made to increase the solids contents of solvent-based liquid coatings (high solid formulations). The challenges are finding more effective rheology-control agents, polymer architectures giving better control of the

placement of functional groups, and adequate catalysis to control the rate of curing.

28.4.3.3 Waterborne Coatings Water-borne coatings are based on formulations in which water is the primary “solvent.” Water-borne coatings constitute a strongly growing segment of the coatings’ market. Not only do water-borne formulations result in lower odor, easier clean-up, and decreased fire hazards than their solvent-borne counterparts, but they are also one of the key choices for reducing VOC emissions.

The polymers used in waterborne coatings can be either soluble or dispersed in water (or a combination of water and a cosolvent). The problem of formulations containing soluble polymers is that the presence of polar/hydrophilic groups in the polymer makes the final films more sensitive to humidity. For this reason, a better solution is to formulate hydrophobic polymers that are stabilized in water by internal or external surfactants forming emulsions. Emulsified polymers have high molar masses but because they are dispersed in a particulate form, the viscosity of the media is not sensitive to their molar masses. Therefore, the physical properties are expected to be less dependent on the cure reactions.

An important class of waterborne coatings is the family of polyurethane dispersions (PUDs). Ionizable groups (usually carboxyl) incorporated to the PU backbone allow the polymer to be dispersed in water after neutralization with amines. The properties can be varied substantially depending on the structure of the polyol and diisocyanate used to prepare them. Aliphatic and cycloaliphatic isocyanates are preferred because of their low reactivity with water and

to prevent yellowing of the film. However, the key problem is to control the coalescence of the initially stabilized polymer particles. Coalescence of these particles is often incomplete in the final film and may take a long time to reach equilibrium. In some cases, the film is postcured by a polyisocyanate leading to isocyanurate (or uretdione) structures (Fig. 28.6), to increase its thermal stability. This is accomplished by the use of a two-component system.

28.4.3.4 Radiation-Cured Coatings Radiation (ultraviolet light and electron beam) is a means of curing coatings that can be effectively used for heat-sensitive substrates because the curing can be carried out at ambient temperature. In addition, UV curing can bring many benefits to the coatings manufacturer in terms of increased productivity and lower labor costs as well as providing the possibility to reach the ever-increasing demands of legislation in terms of environmental compatibility. Within UV-cured coatings, the key and most critical part of the formulation is the photoinitiator. The two commonly used functional groups are (meth)acrylates (requiring free-radical initiators) and epoxies (that need cationic initiators). The other problem to solve is to find a compromise between the viscosity of the initial formulation, the final crosslink density, and the film hardness and toughness. This can be achieved by adjusting the ratio between different monomers and reactive oligomers of different molar masses [2]. However, as the morphology of photo-cured acrylate films is rather complex [14], properties of films such as elongation at break are limited compared to those of PU coatings.

28.4.3.5 Powder Coatings Powder coatings are produced by an extrusion process. The two-component powder

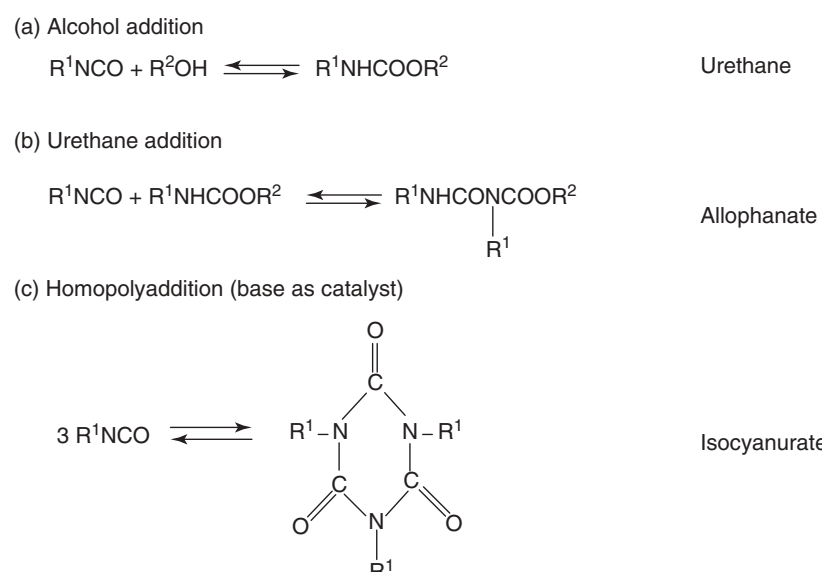


Figure 28.6 Different reactions of isocyanate groups.

(plus additives) is applied onto the substrate by electro-spray; then, the substrate is heated above T_g (or the melting temperature, T_m) to produce film flow and crosslinking. The requirements for a powder coating formulation are as follows:

1. T_g (or T_m) must be at least 20–30 °C above ambient conditions to store and handle powders.
2. Low molar mass to allow enough flow above T_g (or T_m), to obtain smooth films before the beginning of cure (processing window).
3. The cure temperature must be placed at 40–50 °C above T_g (or T_m) to achieve a convenient flow leading to film homogeneity. If the flow is controlled by T_m instead of T_g , the situation is slightly eased because the melting point is a much sharper transition than the glass transition.

Various systems are available depending on the end use. Typical systems are based on saturated polyesters, α,ω -acid-terminated cured with an epoxy (triglycidyl isocyanurate TGIC), or α,ω -OH-terminated cured with an isocyanate (or a blocked isocyanate). Recently, bio-based formulations with aliphatic nonyellowing monomers have been proposed [15].

The generation of a convenient processing window is difficult for most known crosslinking chemistries. This has limited the use of powder coatings at temperatures lower than about 130 °C, a fact that precludes their use on many plastic substrates. Efforts to develop radiation-curable powder coatings are ongoing.

28.4.4 Reaction Injection Molding

Reaction injection molding (RIM) is similar to thermoplastic injection molding except that thermosetting polymers are used, making it necessary a curing reaction to occur within the mold. The process involves the high speed mixing of two or more reactive chemicals, just as they are injected into the mold. The low viscous mixture fills the mold at relatively low temperatures and pressures. The reactions must be synchronized with the process so that gelation does not occur during the filling time [16].

The high pressure metering unit is one key element of the process. It must deliver the highly reactive starting ingredients to the mixhead with precise synchronization of two liquid streams, and within a few seconds inject them into the mold under high pressure using an impinging mixer. The other key element is the mixhead, which must deliver each stream at high velocity into the mixing chamber, accomplish this under precisely synchronized conditions, develop turbulence in the mix chamber so that the two streams are fully and rapidly mixed, and clean the chamber so that there is no build-up. The mixture is allowed

to stay in the mold up to the time necessary to advance the cure to the point where mechanical properties of the part allow demolding. For some formulations, reaction is accompanied by foaming. Heat generated by the chemical reaction helps to cure the material, but the mold must be heated so that the edges do not cool more rapidly than the core. The entire process, from mixing to demolding, typically takes less than 1 min.

From the perspective of a life cycle analysis (LCA), the RIM process presents two winning cards with respect to thermoplastic injection molding: the use of liquids instead of thermoplastic granules and the necessity to use much less clamping force during the molding process.

Because isocyanate/alcohol and isocyanate/amine reactions are very fast, give no by-products, and attain high degree of conversion, they are well suited for RIM. For PU-RIM, part A in Figure 28.4 is filled with the diols plus a catalyst and usual additives such as antioxidants, pigments, etc., and part B with the isocyanate. Several nonisocyanate chemical systems such as the metathesis polymerization of a diolefin monomer, DCPD, epoxy, and free-radical chemistries have also been developed for RIM. The required temperatures to generate convenient processing windows vary for each of these systems. For a DCPD-RIM formulation, part A contains DCPD monomer, initiator, activator, and other additives; part B also contains DCPD monomer, the coinitiator, and additives. Ring opening polymerization of caprolactam adapted to RIM leads to a linear polymer, polyamide 6.

Common items made via RIM include rigid structural foams (for business equipment, housings, furniture, and building materials), low modulus elastomers (for automobile fascias, bumper, air spoilers, and fenders), high modulus elastomers (for large industrial and consumer parts requiring toughness and rigidity), and also some specialties such as ophthalmic lenses [17].

When reinforcing agents such as short glass fibers are added to the mixture, the process is known as *reinforced reaction injection molding (RRIM)*. This process is used to produce rigid foam automotive panels. A subset of RRIM is structural reaction injection molding (SRIM), which uses fiber meshes previously placed in the mold as reinforcing agent.

Another similar process is in mold coating (IMC). The IMC is similar to the RIM process: a thermosetting formulation is first introduced into a closed mold and then cured by the high temperature of an injected thermoplastic [18]. This produces a coating (surface finish) of the thermoplastic part reducing time, space, material, and machinery requirements compared to a conventional two-step process. The process allows painted parts to be produced in similar cycle times as those used to produce the uncoated parts.

28.4.5 Thermosetting Polymers for Composite Materials

28.4.5.1 Introduction Composites are materials consisting of a combination at a macroscopic scale of high strength stiff fibers embedded in a matrix. In this section, the discussion is restricted to composites where the matrix is a thermosetting polymer. The matrix holds the reinforcement in the desired shape while the reinforcement improves the overall mechanical properties of the matrix. When designed properly, the new combined material exhibits better strength than the one of each individual material. This is the basic difference between reinforced and filled systems in which fillers are used to reduce cost but often degrade the mechanical properties.

Fiber-reinforced composite materials can be divided into two main categories normally referred to as *short fiber-reinforced materials* ($L/D < 100$) and *continuous fiber-reinforced materials* ($L/D > 100$). They can be also categorized by their fiber characteristics such as (i) type (glass, carbon, aramide, etc.), properties (strength, stiffness, tensile elongation), and content; (ii) form (discontinuous or continuous); (iii) fiber alignment (random or unidirectional); and (iv) composite's layout (e.g., laminar with a given stacking sequence of plies). All these parameters affect the strength and stiffness of the final material. With these data, the material can be classified as high fiber volume or high performance composite. As an example, materials made by a build-up of plies in which the continuous fibers are oriented unidirectionally are often referred to as *advanced or high performance composites*.

The matrix allows the necessary positioning of the fibers, transfers the load to the fibers and distributes the stress among them, and is also responsible for protecting the reinforcement from the environment. However, the matrix is often the weakest component of a composite. One important parameter for the material properties is the fiber–matrix interface (or interphase), which guarantees the stress transfer from fiber to fiber via the matrix. The interface/interphase is a finite thin layer with its own (very often unknown) physical and chemical properties that depend on the fiber–matrix combination. Because of the low viscosity of the thermoset precursors, they wet the reinforcement better than a thermoplastic polymer.

The matrix is the weakest component of the composite determining the allowed maximum stress and the maximum service temperature. Great efforts have been undertaken to develop thermosetting polymers with increased temperature resistance. Cyanate-esters (CEs), BMI, and polyimides are the actual thermosetting matrices with higher thermal resistance.

Unique to the composites industry is the ability to create a product using many different manufacturing processes. The matrix and reinforcement (short or long fibers) can

be combined in different ways to produce a wide variety of preforms and prefabricates, including granules, pellets, prepgs, and textile fabrics. Their form and appearance determine the processing alternatives for converting them to structural parts. The thermoset precursors can be put in contact with the fibers before or after placing the reinforcement material into the mold cavity or onto the mold surface. Once they are combined, they are compacted and cured.

Manufacturing processes can be split into two categories depending on the use of an open or a closed mold. A universal disadvantage of open-mold processes is that the material is only in contact with one side of the mold. Processes included in the open-mold category are wet lay-up techniques and bag molding. Processes pertaining to the closed-mold category are transfer molding, compression molding, and injection molding.

The physical changes that take place during composite manufacture include heating and cooling, pressure changes, fluid flow, and solidification (Fig. 28.5). Many interrelated issues are common to all composite processing techniques based on thermosetting polymers: (i) kinetic, statistical, and rheological aspects of network formation (viscosity vs extent of reaction, gelation time); (ii) matrix–fiber interfacial interactions; (iii) macroscopic and microscopic flow of the reacting thermosetting polymer in a confined geometry, preform deformation; (iv) heat transfer and heat production by chemical reaction; (v) temperature and conversion profiles; and (vi) dimensional stability (control of the shrinkage due to reaction and temperature variation).

Each one of the previous issues can influence the performance of the processing technique and the resulting composite in a variety of ways. Insufficient cure may result in a low T_g and a consequent creep under stress. Inadequate flow may result in high levels of porosity or large voids. Online sensor systems permit process control [19] and are a useful tool toward improved quality in composites manufacture. Dielectric techniques have achieved the greatest success as commercial *in-process* monitoring systems. Optical-fiber methods show promise for further development, most notably where distinct features in chemical spectra can be obtained.

For the choice of a process, an important factor is the amount of material to be produced. Large quantities can be used to justify high capital expenditures for rapid and automated manufacturing technology. Small production quantities are accommodated with lower capital expenditures but higher work and tooling costs at a correspondingly slower rate.

The finishing of the composite parts is also critical in the final design. Many of these finishes will include exterior erosion coatings, which can be deposited *in situ* (IMC) or during a separate operation.

28.4.5.2 Processes for Small Series

Wet Lay-Up Process. Formulations are impregnated by hand or sprayed into fibers that are in the form of woven, knitted, stitched, or bonded fabrics. This is usually accomplished by rollers or brushes. Spray-up is a partly mechanized version of the hand lay-up process. The thermoset precursor is applied by means of a spray gun to the mold surface simultaneously with the chopped glass-fiber roving. Laminates are left to cure under standard atmospheric conditions.

Both spray-up and hand lay-up cannot achieve a high volume fraction of fibers. Therefore, these techniques are not suitable for high performance applications. They are most suited to large sheetlike components such as boat hulls and furniture. There is virtually no limit to the size of the part that can be made. The molds can be made of wood, metal, neat polymers, or polymer composites with glass fibers. Unlike other processes, they require little or no pressure.

Bag Molding Bag molding is essentially an extension of the lay-up process. The lay-up structure is covered by a flexible airtight bag and either an external pressure is applied or vacuum is created inside the bag-mold enclosure. This improves the properties of the resultant composite by driving out volatile substances and increasing the volume fraction of reinforcement.

28.4.5.3 Processes for Medium Series

Prepregs Prepregs are thin sheets of fibers impregnated with formulated thermoset precursors. The thermoset precursor formulation in the prepreg is in the so-called B-stage that characterizes an ungelled liquid of very high viscosity, but with the necessary tack, flexibility, and shelf life to facilitate part production.

There are different ways to impregnate the fabric and reach the B-stage. In a chemical B-stage, the viscosity of the formulated thermoset precursor is reduced by heating. In a physical B-stage, the so-called hot melt process is carried out by impregnating reinforcements at high temperature to reduce viscosity, followed by cooling to reach the initial viscosity at room temperature. A solvent can be also used, followed by its removal by heating. In both cases, chemistry and heating have to be managed to control the beginning of the reaction and to advance the conversion to a point well below gelation.

After its manufacture, the prepreg is backed with release film for storage in a cool dry place or in a refrigerator until its use. Typically prepregs have a guaranteed shelf life of 12 months at -18°C . Tack life at 23°C depends on the thermosetting polymer.

Vacuum bag and autoclave processing are the two main methods for the manufacture of final parts from prepregs. Consolidation involves the cutting and stacking of prepreg

layers in a predetermined sequence of fiber orientations within a mold containing release agent and absorption layers. An upper plate is laid on top and this assembly is sealed in a vacuum bag. The thermosetting matrix is cured by exposure to a defined combination of temperature and pressure. When the lay-up is heated, the constraint offered by the thermosetting matrix decreases as its viscosity falls. Application of pressure forces the fibers together. Therefore, the temperature and pressure cycle affect not only the fiber volume fraction and void content but also the fiber distribution and alignment.

The constant fiber content allows the production of constant high quality composites. Main applications are in the aerospace sector (mostly using multifunctional epoxy monomers), sporting goods (rackets, skis, bike frames, golf items, baseball bats, etc.), and in the electronic industry (printed circuit boards). Autoclaves usually required for the reaction are expensive, slow to operate, and limited in size.

One application is honeycomb sandwich construction that consists of thin high strength prepreg skins bonded to a thicker honeycomb, foam, or balsa core. The advantages are very low weight, high stiffness, durable, design freedom, and reduced production costs.

Infusion Process In these transfer molding processes, dry fabrics, core materials, and various inserts are placed manually or robotically in a mold that can be internally heated. The thermosetting matrix is infused under vacuum, either as a semisolid film previously interleaved with the dry fabrics that are wetted when it flows or as a liquid that flows into the fibers with the assistance of vacuum. Just one “lower mold” is necessary; the “upper mold” is a sealed semipermeable vacuum foil (for vacuum-assisted resin transfer molding, VARTM) or an impermeable vacuum bag (for SCRIMP, Seemann composite resin infusion molding). Therefore, no clamping force is required. The assembly is placed into an autoclave. This process is generally performed at both elevated pressure and elevated temperature. The use of elevated pressure facilitates a high fiber volume fraction (typically 50–65% by volume or 60–75% by weight) and low void content for maximum structural efficiency.

These processes are well suited to the production of very large parts ranging from turbine blades and boats to rail cars and bridge decks with relatively low equipment investment. Compared to the conventional composite fabrication methods used in the aeronautical field, these infusion processes are an ideal technique using low cost materials without prepregs and autoclaves.

Resin Transfer Molding Resin transfer molding (RTM) is a closed mold infusion process in which reinforcement material is placed between two matching mold surfaces (Fig. 28.7). The matching mold set is then closed and

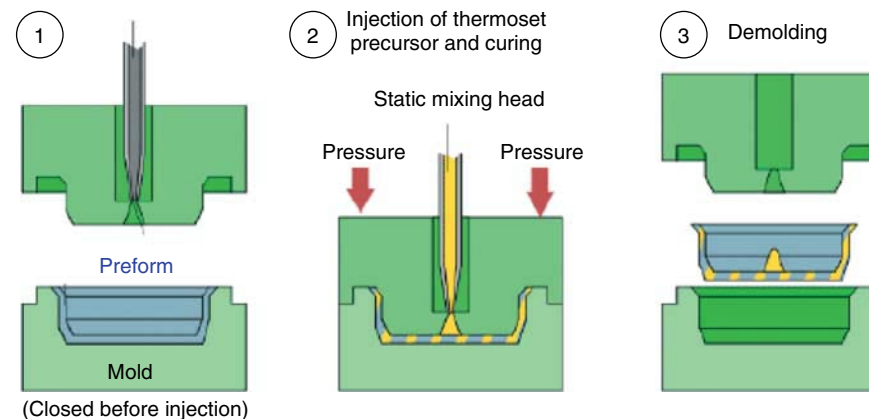


Figure 28.7 Scheme of the RTM process.

clamped and a low viscosity thermoset precursor is injected under moderate pressures (typically, 0.1–0.4 MPa) into the mold cavity through a port (or series of ports). The thermoset precursor fills voids within the mold set and wets the reinforcing materials. Vacuum is sometimes used to enhance flow and reduce void formation. The part is typically cured with heat. In some applications, the exothermic reaction of the thermosetting matrix may be sufficient for proper cure.

RTM is compatible with a variety of thermosetting polymers including polyester, vinyl ester, epoxy, phenolic, modified acrylic, and hybrid polyester–urethane. A convenient typical viscosity of thermoset precursors is in the range of 0.2–0.6 Pa s. The RTM process has the following advantages: (i) emissions are lower than in open-mold processes such as spray-up or hand lay-up; (ii) it can produce parts faster, as much as 5–20 times faster than open-mold techniques; (iii) the mold surface can produce a high quality finish; (iv) complex mold shapes can be achieved; and (v) cabling and other fittings can be incorporated into the design of the mold. However, it has one disadvantage: the contents of reinforcement are limited to allow the flow of thermoset precursors and saturation of the fibers.

28.4.5.4 Processes for Large Series

Compression Molding Compression molding is the most common method for molding thermosetting materials using processes such as sheet molding compound (SMC) or bulk molding compound (BMC). In these techniques, a compression press is used to apply heat and pressure to a sheet or bulk molding compound. The heated molding compound fills the mold and cures to produce the desired shape. Today, this is the only way to produce thermosetting composite parts in large series (higher than 10,000 parts/year).

SMC is a flat sheetlike compound, produced on a continuous moving belt process. The thermoset precursor is an UP-resin composed of an unsaturated polyester

TABLE 28.1 Typical Formulations for SMC and BMC

Raw Material	SMC Parts by Weight	BMC Parts by Weight
UP-resin	60	60
LPA	20–40	0–40
Initiator	1.5	1.5
Fillers	150	200
Release agent	4	4
Magnesium oxide	~1	~1
Glass fibers	25% on total formulation	15% on total formulation

Abbreviation: LPA, low profile additive.

prepolymer dissolved in a monomer, usually styrene [2]. The UP-resin is premixed with all the components of the formulation to form a paste. A typical formulation is shown in Table 28.1. Calcium carbonate (chalk) is the most commonly used filler. The role of the low profile additive, LPA is to compensate the shrinkage mainly due to the polymerization of styrene.

A scheme of the SMC process is shown in Figure 28.8. The paste is dosed on a polyamide or polyethylene film and glass rovings are cut to lengths of 25–50 mm and sprinkled on the top of the resin paste layer. A second film, on which a resin paste is also applied, is then put on the top of the glass-fiber layer. The thickening agent (MgO) reacts with the free acid groups of the UP prepolymer, producing an enormous increase in the viscosity of the SMC formulation after several days. A leatherlike sheet is formed, which is almost nonsticky and is easy to handle. In this stage, the UP-resin is still not polymerized.

For the production of complex parts, BMC may be used instead of SMC. The starting formulation for BMC has the aspect of a doughlike material made by mixing all ingredients together. A typical formulation is shown in Table 28.1. Depending on the requirements for the finished

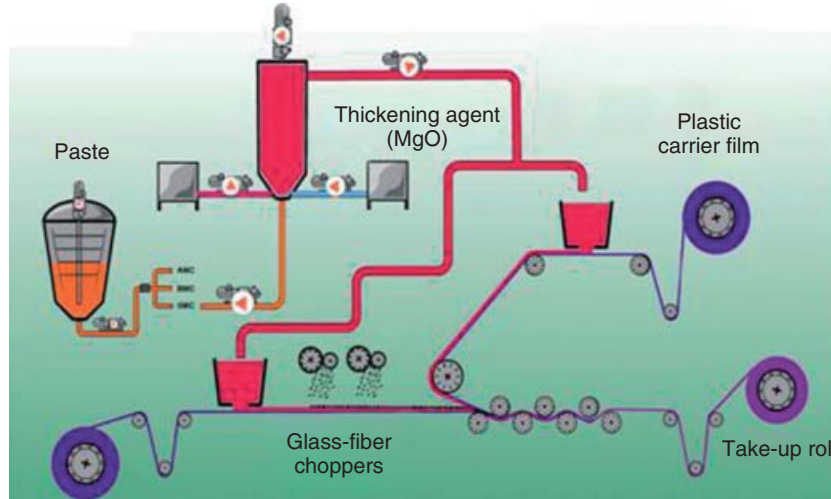


Figure 28.8 Scheme of the SMC process.

product, a wide variety of formulations is nowadays available. Products are made that possess high corrosion resistance, excellent surface finish, and high mechanical properties.

Injection Molding The processing and equipment for injection molding of thermosetting polymers differs slightly from the conventional injection machines used for thermoplastics. Reasons are (i) the thermosetting formulation must have a short residence time in the barrel or nozzle and (ii) the injection pressure is reduced after the mold is filled.

Free flowing molding powders are used in the production of electrical and electronic parts, such as connectors and switches. The powders consist of mixtures of thermoset precursors (phenolic, epoxy, silicone, or diallyl phthalate), fillers, short glass fibers, pigments, initiators or catalysts, etc. They are produced in high shear mixing and extruding equipment. Powders are fed into the mold and cured under high pressure at temperatures up to 180 °C.

BMC formulations can also be processed by injection molding. A typical product made of a BMC formulation is a headlamp reflector produced by a fully automatic injection molding process in very short cycle times. Modern installations produce several thousands of these products per day.

RRIM and SRIM are also injection molding processes, described in Section 28.4.4.

28.4.5.5 Processes for Unfilled Parts

Filament Winding The filament winding process is used in the fabrication of tubular composite parts. Typical examples are composite pipe, electrical conduit, containers, and composite tanks. Fiber-glass roving strands are impregnated by passing through a bath containing the liquid thermoset precursors. Then, they are wound onto a mandrel in a variety

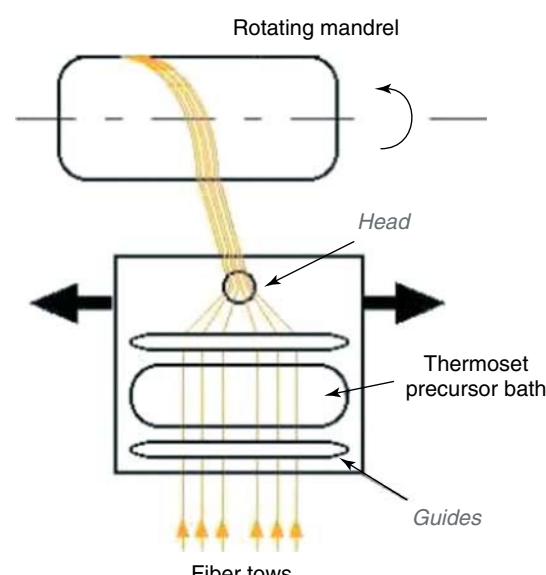


Figure 28.9 Scheme of the filament winding process. Source: Adapted from <http://www.polymerprocessing.com/operations/filwind/index.html>, with permission.

of orientations that are controlled by the fiber feeding mechanism and the rate of rotation of the mandrel (Fig. 28.9). Usually epoxy (mainly epoxy-anhydride systems), unsaturated polyester, or vinyl ester systems are used because of their long pot-life at ambient atmosphere during the impregnation step. When the winding operation is completed, the thermosetting matrix is polymerized and the composite part is removed from the mandrel.

Capital investment is relatively high compared to open-mold processes mainly due to the cost of the winding mandrel for a specific application.

Rotomolding Rotomolding or centrifugal casting is an industrial process for the production of pipes, masts, rollers, and containers. The casting equipment consists of a cylinder (often made of steel), which lies on the top of a series of roller bearings. It can be rotated at variable speed. A mixture of glass fibers and thermoset precursors is dosed simultaneously into the rotating cylinder. As a result of the centrifugal forces, the glass fibers are impregnated and deaerated. The resulting product is a tube with a good inner surface quality and mechanical properties determined by the amount of reinforcing fibers and the turning speed of the cylinder.

28.4.5.6 Continuous Processes Pultrusion is a continuous and highly automated molding process used in the fabrication of composite parts that have a constant cross-sectional profile. Dry glass-fiber rovings are pulled through a thermoset precursor bath in which they are impregnated with epoxy, unsaturated polyester, or vinyl ester systems. The impregnated fibers are pulled through a heated metal die in which the thermosetting precursors polymerize at temperatures of 110–160 °C. The flow through the die completes the impregnation of the fibers and controls the fiber content. Polymerization produces the material into its final shape. The cured profiles with a constant cross-section and very straight fibers are cooled down and cut to the desired length. The process is fast and the fiber content can be very high and accurately controlled.

The high glass fibers content gives very high mechanical properties to the profiles obtained. This is a particular advantage for civil engineering applications such as bridges and large structures. Compared to steel profiles, pultruded profiles based on glass-reinforced thermosets show a much better corrosion resistance and electrical insulating properties.

28.5 CONCLUSIONS

The large number of manufacturing processes reflects the variety of applications of thermosetting polymers in structural and functional materials. They can be deposited on substrates for adhesives, paintings, and coating, and they can be used as foams or as matrices for composites. In all these applications, chemistry and processing are strongly interrelated.

The thermosetting polymer field is continuously changing. Different precursors, combinations of materials, and modifications of existing manufacturing methods are introduced for new applications. The sustainable development is the major trend for the future. LCA is a new tool for the choice of a reactive system coupled with a processing technique. Efforts are made to decrease the energy consumption by the use of solvent-free and nontoxic chemistries enabling

to produce the cure at low temperatures and reduce the number of steps to obtain the final material.

Concerning advanced composite materials, optimal ways to impregnate the reinforcement material with the thermoset formulation and shape and cure the part as fast as possible and with low energy consumption are continuously searched. The density-related performance of these advanced composites is the key to their penetration as lightweight structural components. As reinforcement materials, carbon fibers are extending their use from high tech to more traditional applications.

Functional materials with applications in electronic, optical and magnetic devices, sensors, and catalysts can be produced by dispersing liquid crystals, organic crystals, metallic or inorganic oxide nanoparticles (NPs) in thermosetting polymers. BCPs with a variety of morphologies can be stabilized in thermosetting polymers [20–22]. To keep the dispersion of micelles in the final material, it is necessary that one of the blocks remains miscible with the reactive thermosetting polymer at least up to the gel point. The remaining blocks may be initial immiscible with the thermoset precursors or become phase separated at low conversions. Nanocomposites produced by a dispersion of micelles of BCP in a thermosetting polymer exhibit a significant increase in toughness, much higher than the one obtained by dispersing conventional rubbers or thermoplastics [23, 24]. Detailed mechanistic investigations revealed that the dominant toughening mechanism is BCP micelle cavitation-induced matrix shear banding [25, 26]. Also important is the fact that the glass transition temperature and the Young modulus of the thermosetting polymer are not affected by this modification.

The thermosetting polymer may also be the host of a variety of NPs such as POSS, CNTs, and nanoclays [21]. Self-healing thermosetting polymers with potential applications in paints and coatings have been developed [27, 28]. Thermosetting polymers also have a great potential as shape-memory actuators [29, 30].

REFERENCES

- Pascault JP, Williams RJ, editors. *Epoxy Polymers: New Materials and Innovations*. Weinheim: Wiley-VCH; 2010.
- Pascault JP, Sautereau H, Verdu J, Williams RJ. *Thermosetting Polymers*. New York: Marcel Dekker; 2002.
- Stockmayer WH. *J Chem Phys* 1944;12:125.
- Pascault JP, Williams RJ. *J Polym Sci B: Polym Phys* 1990; 28:85.
- Oyanguren PA, Williams RJ. *J Appl Polym Sci* 1993;47: 1361.
- Williams RJ. Transitions during network formation. In: Stepto RFT, editor. *Polymer Networks: Principles of Their Formation, Structure and Properties*. London: Blackie Academic & Professional; 1998. p 93–124.

7. Adabbo HE, Williams RJJ. *J Appl Polym Sci* 1982;27:1327.
8. Soulé ER, Borrajo J, Williams RJJ. *Polym Eng Sci* 2006;46:1641.
9. Riew CK, Kinloch AJ, editors. *Toughened Plastics I, Science and Engineering. Adv Chem Ser* 233. Washington, DC: American Chemical Society; 1993.
10. Williams RJJ, Rozenberg BA, Pascault JP. *Adv Polym Sci* 1997;128:95.
11. Halley PJ, MacKay ME. *Polym Eng Sci* 1996;36:593.
12. Dušek K, Dušková-Smrčková M. *Prog Polym Sci* 2000;25:1215.
13. Dušková-Smrčková M, Dušek K, Vlasák M. *Macromol Symp* 2003;198:259.
14. Barbeau P, Gerard JF, Magny B, Pascault JP, Vigier G. *J Polym Sci B: Polym Phys* 1999;37:919.
15. Noordover BAJ, van Staalduin VG, Duchateau R, Koning CE, van Benthem RATM, Mak M, Heise A, Frissen AE, van Haveren J. *Biomacromolecules* 2006;7:3406.
16. Macosko CW. *RIM, Fundamentals of Reaction Injection Molding*. New York: Hanser Publishers; 1989.
17. Lesartre N, Méchin F, Pascault JP, inventors; Institut National Des Sciences Appliquées, assignee. US Patent 2008/090989 A1. 2008.
18. Goodship V, Cook N, Dargue I, Lobjot C, Makenji K, Smith GF. *Plast Rubber Compos* 2007;36:34.
19. Summerscales J. In-process monitoring for control of closed-mold techniques for the manufacture of thermosetting matrix composites. In: Shonaike GO, Advani SG, editors. *Advanced Polymeric Materials: Structure–Property Relationships*. Boca Raton, FL: CRC Press; 2003. p 57 ff.
20. Ritzenthaler S, Court F, David L, Girard-Reydet E, Leibler L, Pascault JP. *Macromolecules* 2002;35:6245.
21. Pascault JP, Williams RJJ. Phase morphology of nanostructured thermosetting multiphase blends. In: Harrats C, Thomas S, Groeninckx G, editors. *Micro- and Nanostructured Multiphase Polymer Blend Systems: Phase Morphology and Interfaces*. Boca Raton, FL: CRC-Taylor and Francis; 2006. p 359 ff.
22. Zheng S. Nanostructured epoxies by use of block copolymers. In: Pascault JP, Williams RJJ, editors. *Epoxy Polymers: New Materials and Innovations*. Weinheim: Wiley-VCH; 2010. p 79 ff.
23. Gerard P, Boupat NP, Fine T, Gervat L, Pascault JP. *Macromol Symp* 2007;256:55.
24. Ruiz-Pérez L, Royston GJ, Fairclough PA, Ryan AJ. *Polymer* 2008;49:4475.
25. Liu JD, Sue HJ, Thompson ZJ, Bates FS, Dettloff M, Jacob G, Verghese N, Pham H. *Macromolecules* 2008;41:7616.
26. Liu JD, Sue HJ, Thompson ZJ, Bates FS, Dettloff M, Jacob G, Verghese N, Pham H. *Polymer* 2009;50:4683.
27. Xiao DS, Yuan YC, Rong MZ, Zhang MQ. *Polymer* 2009;50:2967.
28. Keller MW. Self-healing epoxy composites. In: Pascault JP, Williams RJJ, editors. *Epoxy Polymers: New Materials and Innovations*. Weinheim: Wiley-VCH; 2010. p 325 ff.
29. Xie T, Rousseau IA. *Polymer* 1852;2009:50.
30. Voit W, Ware T, Dasari RR, Smith P, Danz L, Simon D, Barlow S, Marder SR, Gall K. *Adv Funct Mater* 2010;20:162.

PART VI

POLYMERS FOR ADVANCED TECHNOLOGIES

29

CONDUCTING POLYMERS

MARÍA JUDITH PERCINO AND VÍCTOR MANUEL CHAPELA

29.1 INTRODUCTION

A polymer (material containing a long chain of similar molecular structures) is the first and foremost electrical and heat insulator. The idea that polymers or plastics could conduct electricity had been considered absurd. Their wide application as an insulating material is the reason they are studied and developed in the first place. In fact, these materials are commonly used for surrounding copper wires and manufacturing the outer structures of electrical appliances that prevent humans from coming in direct contact with electricity.

In 1958, polyacetylene was first synthesized by Natta et al. [1] as a black powder. The polyacetylene was found to be a semiconductor with conductivity between 7×10^{-11} to 7×10^{-3} S/m, depending upon how the polymer was processed and manipulated. The conventional method of polymerization in the laboratory requires a catalyst solution to be stirred thoroughly to carry out the reaction under homogeneous conditions. Acetylene polymerization was no exception. It had become customary for polymer chemists who synthesized polyacetylene to bubble acetylene gas into a catalyst solution with stirring. As a matter of fact, the product was obtained as an intractable black powder, from which it was very difficult to make specimens in a shape suitable for measurement of various spectra and properties because of its insolubility and infusibility. Soon after Shirakawa H. joined Ikeda's group [2], he succeeded in synthesizing polyacetylene directly in a form of thin film [3] by a fortuitous error in 1967. After a series of experiments to reproduce the error, they noted that a concentration of the Ziegler–Natta catalyst nearly a thousand times (10^3) as large as usual had been used. It is worth noting that the

insolubility of polyacetylene contributes to the formation of film. One important factor that should be added is that the catalyst used at that time, $Ti(O-n-C_4H_9)_4 - (C_2H_5)_3Al$, is a quite unique one from the viewpoint of its good solubility in organic solvents such as hexane or toluene to give a homogeneous solution and its high activity to give exclusively high molecular weight and crystalline polymers. By contrast, most Ziegler–Natta catalysts form precipitates that give an inhomogeneous solution when a titanium compound is mixed with alkyl aluminum.

The polymer is called a *conjugated polymer* because of the alternating single and double bonds in the polymer chain. Because of the special conjugation in their chains, it enables the electrons to delocalize throughout the whole system and thus many atoms may share them. The delocalized electrons may move around the whole system and become the charge carriers to make them conductive. It has been recognized for many years that a very long linear conjugated polyene might have various interesting properties, especially optical, electrical, and magnetic properties. A polyene is an even number of methyne ($=CH-$) groups, covalently bonded to form a linear carbon chain bearing one *p* electron on each carbon atom. Therefore, the chemical structure of the polyene is best represented by the formula $H(CH=CH)_nH$, where *n* denotes the number of repeating units. Recently, the word *polyacetylene* has become more popular than polyene because polyacetylene has been a great object of study.

The polyene can be transformed into a conducting form when electrons are removed from the backbone resulting in cations or added to the backbone resulting in anions. Anions and cations act as charge carriers, hopping from one site to another under the influence of an electrical

field, thus increasing conductivity. However, the conjugated polymers are not conductive, since they are covalently bonded and do not contain valence band as pure metal does. It is universally agreed that the doping process is an effective method to produce conducting polymers. Doping allows electrons to flow due to the formation of conduction bands. As doping occurs, the electrons in the conjugated system, which are loosely bound, are able to jump around the polymer chain. Electric current will be produced when the electrons are moving along the polymer chains. Some examples [4] of conjugated conducting polymers are polyacetylene, polypyrrole, polyaniline, and polythiopene (Fig. 29.1). In future, conductive polymers or organic metals may replace inorganic metal in several critical areas. Certain aspects of the inorganic metals, such as not being environmentally friendly and having a high toxicity, are the reason why these organic metals have potential benefits as substitutes. The potential applications of these organic metals include corrosion protection, radars, batteries, sensors, as well as electrochromic cells. Much research will be needed before the applications may become a reality, since conjugated conducting polymers still have some drawbacks such as not being water soluble, having poor mechanical strength, and not being biodegradable [6, 7].

29.2 HISTORICAL BACKGROUND

Conducting-polymer research dates back to the 1960s, when Pohl, Katon, and their coworkers, first synthesized and characterized semiconducting polymers [8, 9]. The discovery of the high conductivity of polysulfurnitride (SN_x), a polymeric material containing interesting electrical properties, was a step forward for research in conducting polymers. The beginning of conducting-polymer research began nearly a quarter of a century ago, when films of polyacetylene were found to exhibit profound increases in electrical conductivity when exposed to halogen vapor [10–13]. Heeger, Shirakawa, and MacDiarmid produced conjugated conducting polyacetylene when monomer of acetylene was doped with bromine or iodine vapor; the resulting electrical conductivity was 10 times higher than that obtained with the undoped monomers. Further investigations, initially aimed to produce thin films of graphite, showed that exposure of this form of polyacetylene to halogens increased its conductivity a billion fold. When undoped, the polymer was silvery, insoluble, and intractable, with a conductivity similar to that of semiconductors. When it was weakly oxidized by compounds such as iodine, it turned a golden color and its conductivity increased to about 10^4 S/m . In the 1980s, polyheterocycles were first developed. Polyheterocycles were

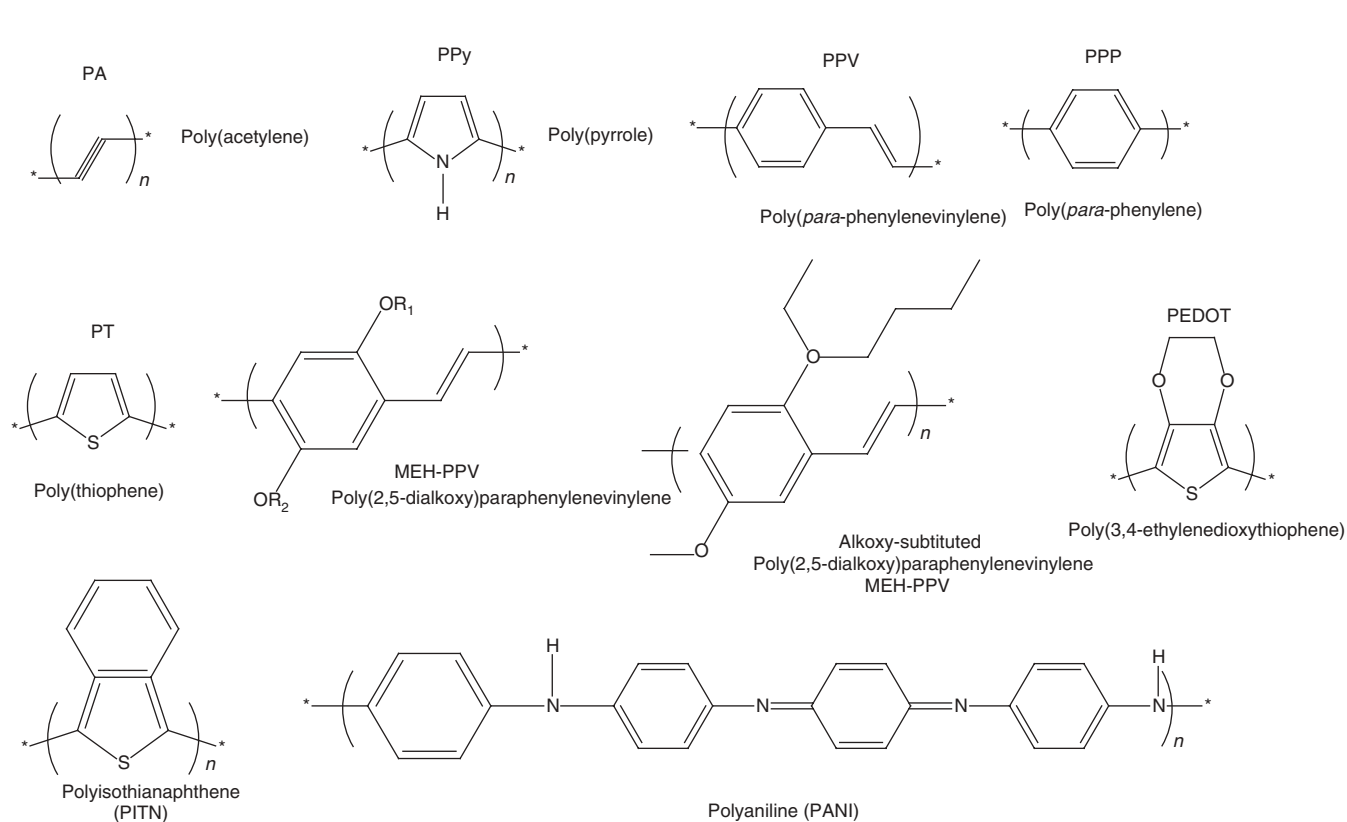


Figure 29.1 Examples of conjugated polymers [5].

found to be much more air stable than polyacetylene, although their conductivities were not so high, typically about 10^3 S/m. By adding various side groups to the polymer backbone, derivatives that were soluble in various solvents were prepared. Other side groups affected properties such as their color and their reactivity to oxidizing and reducing agents. A logarithmic conductivity ladder of some of these polymers is shown below. Since then it has been found that about a dozen different polymers and polymer derivatives undergo this transition when doped with a weak oxidation agent or reducing agent. They are all conjugated polymers. This early work has led to an understanding of the mechanisms of charge storage and charge transfer in these systems. All have a highly conjugated electronic state. This also causes the main problems with the use of these systems, those of processability and stability. The most recent research in this has been the development of highly conducting polymers with good stability and acceptable processing attributes. After their discovery, research papers dealing with polyconjugated systems were very extensive and systematic. The trend was to understand the chemical and physical aspects, either in neutral (undoped) state or charged (doped) states. According to SCIFINDER, more than 40,000 scientific papers have been published in this field of research since 1977 [14]. This previously underestimated family of macromolecular compounds turned out to be extremely interesting, from both the basic research and application points of view. In 2000, these three brilliant scientists, founders of the conjugated conducting-polymer science, were granted the Nobel Prize in chemistry.

29.3 THE STRUCTURES OF CONDUCTING POLYMERS

All materials can be divided into three main groups: conductors or metals, insulators, and semiconductors; they are differentiated by their ability to conduct or the ability to allow the flow of current. Generally, conducting polymers

are classified as semiconductors, although some highly conducting polymers, such as polyacetylene, fall into the metal category. Table 29.1 [6] compares some of the physical properties of insulators, semiconductors, and conductors.

Conjugated organic polymers that can have their conductivity increased by several orders of magnitude from the semiconductor regime are generally referred to as *electronic polymers* and have become of very great scientific and technological importance since 1990 because of their use in light-emitting diodes (LEDs) [7, 15]. The emeraldine base form of polyaniline and *trans*-(CH)_x are shown in Table 29.2 to illustrate the increases in electrical conductivity of many orders of magnitude that can be obtained by doping. The conductivity attainable by an electronic polymer has very recently been increased an infinite number of times by the discovery of superconductivity in regioregular poly(3-hexylthiophene) [16]. Although this phenomenon was present only in a very thin layer of the polymer in a field effect (FET) configuration at a very low temperature (circa 2 K), it represents a historical quantum-leap superconductivity in an organic polymer.

29.4 CHARGE STORAGE

One early explanation of conducting polymers used band theory as a method of conduction. This proposed that a half-filled valence band would be formed from a continuous delocalized π -system. This would be an ideal condition for conduction of electricity. However, it turns out that the polymer can more efficiently lower its energy by bond alteration (alternating short and long bonds), which introduces a band width of 1.5 eV, making it a high energy gap semiconductor. The polymer is transformed into a conductor by doping it with either an electron donator or an electron acceptor. This is reminiscent of doping of silicon-based semiconductors where silicon is doped with either arsenic or boron. However, while the doping of silicon

TABLE 29.1 Comparison of Physical Properties of Metals, Insulators, and Conducting Polymers*

Property	Conducting Polymers	Metals	Insulators
Electrical conductivity (S/cm)	$10^{-11} - 10^3$	$10^{-4} - 10^6$	$10^{-20} - 10^{-12}$
Carriers	Electrons of conjugated double bonds	Valence electrons of half-filled band	—
Concentrations of carriers per cm ³	$10^{12} - 10^{19}$	$10^{22} - 10^{23}$	—
Effect of impurity	Impurities of 0.1–1% change conductivity by two to three orders of magnitude	Effect comparatively slight	Strong effect
Magnetic properties	Paramagnetic	Ferro and diamagnets	Diamagnets

*Ref. 6.

TABLE 29.2 Conductivity between Conductive Polymers and Other Materials*

	Conductivity, S/cm		
Doped <i>trans</i> -(CH) _x -10 ⁵ S/cm	10 ⁶	Ag, Cu	<i>Metals</i>
Doped polyaniline 10 ³ S/cm	10 ⁵	Fe	
	10 ⁴	Mg	
	10 ³	In, Sn	<i>Semimetals</i>
	10 ²	Ge	
	10 ¹		
	10 ⁻²		
Undoped-(CH) _x -10 ⁻⁵ S/cm	10 ⁻⁴		
Undoped polyaniline 10 ⁻¹⁰ S/cm	10 ⁻⁶		
	10 ⁻⁸	Si	<i>Insulators</i>
	10 ⁻¹⁰	AgBr	
	10 ⁻¹²	Glass	
	10 ⁻¹⁴	Diamond	
	10 ⁻¹⁶	Nylon	
	10 ⁻¹⁸	Quartz	
	10 ⁻²⁰		

*Ref. 5.

produces a donor energy level close to the conduction band or an acceptor level close to the valence band, this is not the case with conducting polymers. The evidence for this is that the resulting polymers do not have a high enough concentration of free spins, as determined by electron spin spectroscopy. Initially the free spin concentration increases with the concentration of dopant. At larger concentrations, however, the concentration of free spins levels off at a maximum. To understand this, it is necessary to examine the way in which charge is stored along the polymer chain and its effect.

The polymer may store charge in two ways. In an oxidation process, it could either lose an electron from one of the bands or it could localize the charge over a small section of the chain. Localizing the charge causes a local distortion due to a change in geometry, which costs the polymer some energy. However, the generation of this local geometry decreases the ionization energy of the polymer chain and increases its electron affinity, making it able to accommodate the newly formed charges. This method increases the energy of the polymer less than it would if the charge was delocalized and, hence, takes place in preference of charge delocalization. This is consistent with an increase in disorder detected by Raman spectroscopy after doping. A similar scenario occurs for a reductive process. Typical oxidizing dopants used include iodine, arsenic pentachloride, iron(III) chloride, and (NO₂)₂PF₆ nitrosium hexafluorophosphate. A typical reductive dopant is sodium naphthalide. The main criterion is its ability to oxidize or reduce the polymer without lowering its stability or whether they are capable of initiating side reactions that inhibit the polymers ability to conduct electricity.

An example of the latter is the doping of a conjugated polymer with bromine. Bromine is too powerful an oxidant and adds across the double bonds to form sp³ carbons. The same problem may also occur with NO₂PF₆ if left too long. The oxidative doping of polypyrrole proceeds in the following way. An electron is removed from the p-system of the backbone producing a free radical and a spinless positive charge. The radical and cation are coupled to each other via local resonance of the charge and the radical. In this case, a sequence of quinoid-like rings is used. The distortion produced by this is of higher energy than the remaining portion of the chain. The creation and separation of these defects costs a considerable amount of energy. This limits the number of quinoid-like rings that can link these two bound species together. In the case of polypyrrole, it is believed that the lattice distortion extends over four pyrrole rings. This combination of a charge site and a radical is called a *polaron*. This could be either a radical cation or radical anion. This creates a new localized electronic state in the gap, with the lower energy states being occupied by single unpaired electrons. The polaron states of polypyrrole are symmetrically located about 0.5 eV from the band edges.

Upon further oxidation, the free radical of the polaron is removed, creating a new spinless defect called a *bipolaron*. This mechanism is of lower energy than the creation of two distinct polarons. At higher doping levels, it becomes possible that two polarons combine to form a bipolaron. Thus, at higher doping levels, the polarons are replaced with bipolarons. The bipolarons are located symmetrically with a band gap of 0.75 eV for polypyrrole. This, eventually, with continued doping, forms into a continuous bipolaron bands. Their band gap also increases as newly formed bipolarons are made at the expense of the band edges. For a very

heavily doped polymer, it is conceivable that the upper and the lower bipolaron bands will merge with the conduction and the valence bands, respectively, to produce partially filled bands and metallic conductivity. This is shown in Figure 29.2.

Conjugated polymers with a degenerate ground state have a slightly different mechanism. As with polypyrrole, polarons and bipolarons are produced on oxidation. However, because the ground-state structure of such polymers are twofold degenerate, the charged cations are not bound to each other by a higher energy bonding configuration and can freely separate along the chain. The effect of this is that the charged defects are independent of one another and can form domain walls that separate two phases of opposite orientation and identical energy. These are called *solitons* and can sometimes be neutral. Solitons produced in polyacetylene are believed to be delocalized over about 15 CH units with the maximum charge density next to the dopant counterion. The bonds closer to the defect show less amount of bond alternation than the bonds away from the center. Soliton formation results in the creation of new localized electronic states that appear in the middle of the energy gap. At high doping levels, the charged solitons interact with each other to form a soliton band that can eventually merge with the band edges to create true metallic conductivity. This is shown in Figure 29.3.

29.5 DOPING

The concept of doping is the unique, central, underlying, and unifying theme, which distinguishes conducting polymers from all other types of polymers [17, 18]. During the doping process, an organic polymer, either an insulator or a semiconductor having a small conductivity, typically in the range 10^{-10} – 10^{-5} S/cm, is converted into a polymer, which is in the “metallic” conducting regime (circa 1– 10^4 S/cm). The controlled addition of known, usually small ($\leq 10\%$), nonstoichiometric quantities of chemical species results in significant changes in the electronic, electrical, magnetic, optical, and structural properties of the polymer. Doping is reversible to produce the original polymer with little or no degradation of the polymer backbone. Both doping and undoping processes, involving dopant counterions that stabilize the doped state, may be carried out chemically or electrochemically [19].

29.5.1 Redox Doping

All conducting polymers (and most of their derivatives), for example, poly(paraphenylene), poly(phenylene vinylene), polypyrrole, polythiophene (PT), polyfuran, poly(heteroaromatic vinylenes), and polyaniline (Fig. 29.1), undergo p- and/or n-redox doping.

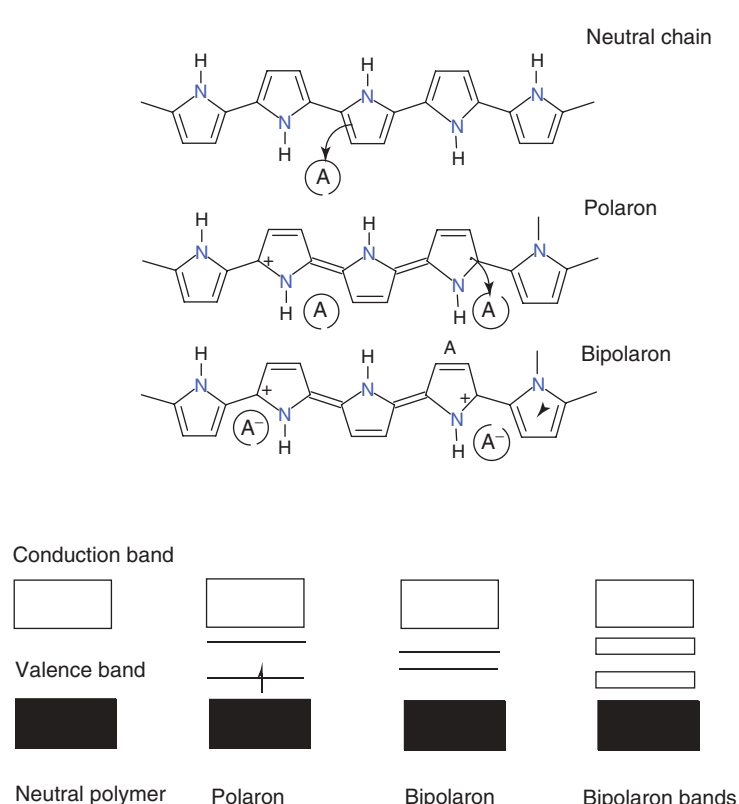
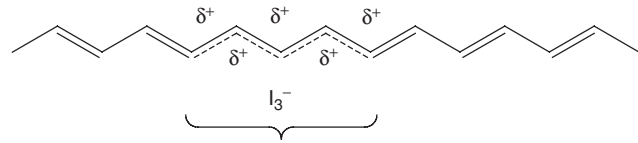


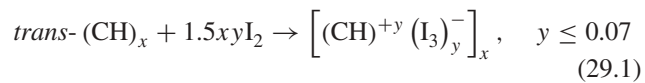
Figure 29.2 Mechanism of conduction on polymer doping.



Scheme 29.1 Charge delocalization in a soliton.

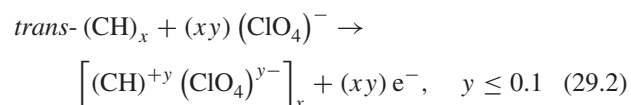
29.5.2 Chemical and Electrochemical p-Doping

p-Doping, that is, partial oxidation of the *p* backbone of an organic polymer, was first discovered by treating *trans*-(CH)_x with an oxidizing agent such as iodine [17, 18]:



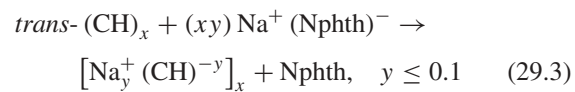
This process was accompanied by an increase in conductivity from circa 10⁻⁵ to circa 10³ S/cm. If the polymer is stretch-oriented five- to sixfold before doping, conductivities parallel to the direction of stretching up to about 10⁵ S/cm can be obtained [15, 19]. Approximately 85% of the positive charge is delocalized over 15 CH units (depicted in Scheme 29.1 for simplicity over only five units) to give a positive soliton.

p-Doping can also be accomplished by electrochemical anodic oxidation by immersing a *trans*-(CH)_x film in, for example, a solution of LiClO₄ dissolved in propylene carbonate and attaching it to the positive terminal of a DC (direct current) power source, the negative terminal being attached to an electrode also immersed in the solution [20]:



29.5.3 Chemical and Electrochemical n-Doping

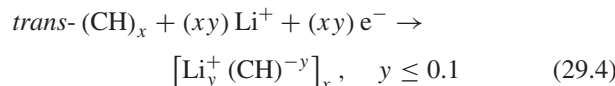
n-Doping, that is, partial reduction of the backbone *p*-system of an organic polymer, was also discovered using *trans*-(CH)_x by treating it with a reducing agent such as liquid sodium amalgam or preferably sodium naphthalene [17, 18], (Nphth,):



The antibonding π -system is partially populated by this process, which is accompanied by an increase in conductivity of about 10³ S/cm.

n-Doping can also be carried out by electrochemical cathodic [21], by immersing a *trans*-(CH)_x film in, for example, a solution of LiClO, dissolved in tetrahydrofuran and attaching it to the negative terminal of a DC power

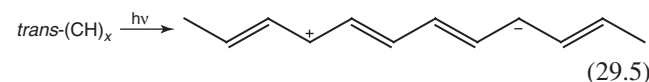
source, the positive terminal being attached to an electrode also immersed in the solution:



In all chemical and electrochemical p- and n-doping processes discovered for (CH)_x and for the analogous processes in other conducting polymers, counter “dopant” ions are introduced, which stabilize the charge on the polymer backbone. However, other types of doping that can provide information not obtainable by chemical or electrochemical doping are the redox doping, which can be termed *photodoping* and the *charge-injection doping*.

29.5.4 Doping Involving No Dopant Ions

29.5.4.1 Photodoping When *trans*-(CH)_x, for example, is exposed to radiation of energy greater than its band gap, electrons are promoted across the gap and the polymer undergoes “photodoping.” Under appropriate experimental conditions, spectroscopic signatures characteristic of, for example, solitons can be observed [22].



The positive and negative solitons are here illustrated diagrammatically for simplicity as residing only on one CH unit; they are actually delocalized over circa 15 CH units. They disappear rapidly because of the recombination of electrons and holes when irradiation is discontinued. If a potential is applied during irradiation, then the electrons and holes separate and photoconductivity is observed.

29.5.4.2 Charge-Injection Doping Charge-injection doping is most conveniently carried out using a metal/insulator/semiconductor (MIS) configuration involving a metal and a conducting polymer separated by a thin layer of a high dielectric strength insulator. It was this approach that resulted in the observance of superconductivity in a PT derivative, as described previously. Application of an appropriate potential across the structure can give rise, for example, to a surface charge layer, the “accumulation” layer that has been extensively investigated for conducting polymers [23–25]. The resulting charges in the polymer, for example, (CH)_x or poly(3-hexylthiophene), are present without any associated dopant ion. The spectroscopic properties of the charged species so formed can, therefore, be examined in the absence of dopant ion. Using this approach, spectroscopic studies of (CH)_x show the signatures characteristic of solitons and the mid-gap absorption band observed in the chemically and electrochemically doped polymer. However, Coulombic interaction between charge

on the chain and dopant ion is a very strong interaction and one that can totally alter the energetics of the system.

29.5.5 Nonredox Doping

This type of doping differs from redox doping described above in that the number of electrons associated with the polymer backbone does not change during the doping process. The energy levels are rearranged during doping. The emeraldine base form of polyaniline was the first example of the doping of an organic polymer to a highly conducting regime by a process of this type to produce an environmentally stable polysemiquinone radical cation. This was accomplished by treating emeraldine base with aqueous protonic acids (Scheme 29.2) and is accompanied by a nine to ten orders of magnitude increase in conductivity (up to around 3 S/cm) to produce the protonated emeraldine base [26–29]. Protonic acid doping has subsequently been extended to systems such as poly(heteroaromatic vinylenes) [30].

29.6 POLYANILINES

Polyanilines refer to an important class of electronic/conducting polymers. They can be considered as being derived from a polymer, the base form of which has the generalized composition given in Scheme 29.3a, which consists of alternating reduced and oxidized repeating units (Scheme 29.3a) [24–26]. The average oxidation state can be varied continuously from $y = 1$ to give the completely reduced polymer, to $y = 0.5$ to give the “half-oxidized” polymer, to $y = 0$ to give the completely oxidized polymer (Scheme 29.3b–d). The terms *leucoemeraldine*, *emeraldine*, and *pernigraniline* refer to the different oxidation states of the polymer, where y is 1, 0.5, and 0, respectively, either in the base form, for example, emeraldine base, or in the protonated salt form, for example, emeraldine hydrochloride [26–28]. In principle, the imine nitrogen atoms can be protonated in whole or in part to give the corresponding salts, the degree of protonation of the polymeric base depending

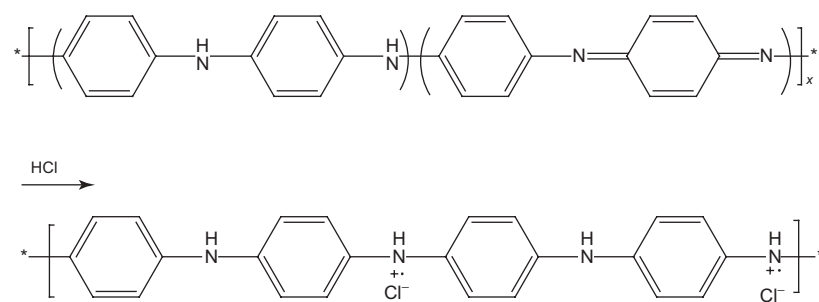
on its oxidation state and on the pH of the aqueous acid. Complete protonation of the imine nitrogen atoms in emeraldine base by aqueous HCl, for example, results in the formation of a delocalized polysemiquinone radical cation [26, 27] and is accompanied by an increase in conductivity of about 10^{10} . The partly protonated emeraldine hydrochloride salt can be easily synthesized, either by the chemical or electrochemical oxidative polymerization of aniline [26–28]. It can be deprotonated by aqueous ammonium hydroxide to give emeraldine base powder (a semiconductor).

29.6.1 Allowed Oxidation States

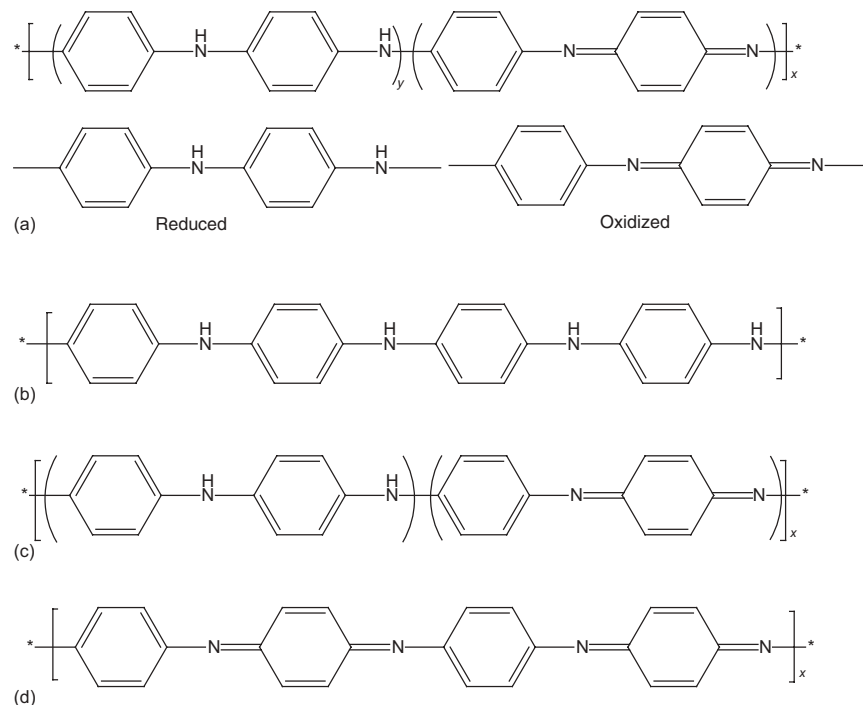
As can be seen from the generalized formula of polyaniline base (Scheme 29.4a), the polymer could, in principle, exist in a continuum of oxidation states ranging from the completely reduced material in the leucoemeraldine oxidation state, $y = 1$, to the completely oxidized material in the pernigraniline oxidation state, $y = 0$. However, we have shown [28, 29] that at least in *N*-methyl-2-pyrrolidinone (NMP) solution in the range $y = 1$ to $y = 0.5$ (emeraldine oxidation state), only two chromophores are present, characteristic of $y = 1$, and $y = 0.5$ species, and that all intermediate oxidation states consist, at the molecular level, only of mixtures of the chromophores characteristic of these two states. Since most of the properties of polyaniline of interest are concerned with the solid state, the authors have carried out a series of studies in the solid state that show that the same phenomenon is true in the oxidation-state ranges of $y = 1$ to 0.5 and $y = 0.5$ to 0. Within each of these ranges, all intermediate oxidation states consist, at the molecular level, only of mixtures of the chromophores characteristic of the two states defining the beginning and end of each range [30–32].

29.6.2 Doping

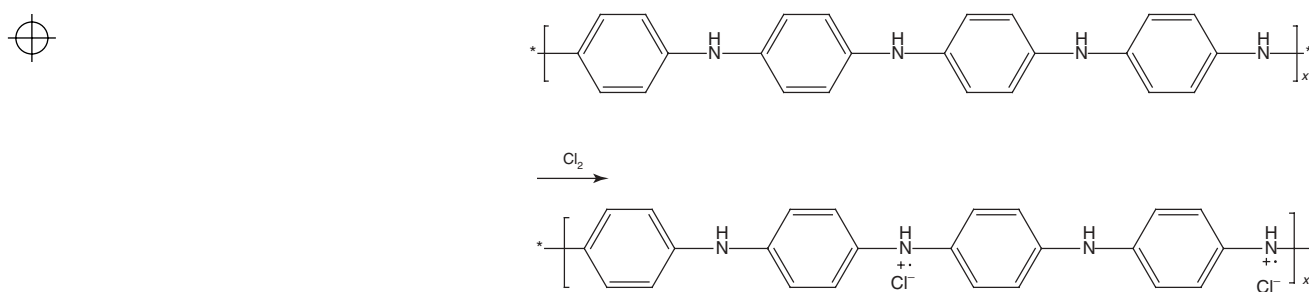
Polyaniline holds a special position among conducting polymers in that its most highly doped form can be reached by two completely different processes: protonic acid doping and oxidative doping. Protonic acid doping of emeraldine



Scheme 29.2 Treatment of emeraldine base with acid.



Scheme 29.3 Generalized composition of polyanilines indicating the (a) reduced and oxidized units, (b) completely reduced polymers, (c) half-oxidized polymer, and (d) fully oxidized polymer.



Scheme 29.4 Oxidative doping of polyaniline.

base units with, for example, 1 M aqueous HCl, results in complete protonation of the imine nitrogen atoms to give the fully protonated hydrochloride salt [26, 27]. The same doped polymer can be obtained by chemical oxidation (p-doping) of leucoemeraldine base [28]. This actually involves the oxidation of the α/π -system rather than just the p-system of the polymer as is usually the case in p-type doping. Its reaction with a solution of chlorine in carbon tetrachloride proceeds to give emeraldine hydrochloride (Scheme 29.4).

29.7 CHARGE TRANSPORT

Although solitons and bipolarons are known to be the main source of charge carriers, the precise mechanism is not

yet fully understood. The problem lies in attempting to trace the path of the charge carriers through the polymer. All of these polymers are highly disordered, containing a mixture of crystalline and amorphous regions. It is necessary to consider the transport along and between the polymer chains and also the complex boundaries established by the multiple numbers of phases. This has been studied by examining the effect of doping, temperature, magnetism, and the frequency of the current used. These tests show that a variety of conduction mechanisms are used. The main mechanism used is by movement of charge carriers between localized sites or among the soliton, polaron, or bipolaron states. Alternatively, where inhomogeneous doping produces metallic islands dispersed in an insulating matrix, conduction is by movement of

charge carriers between highly conducting domains. Charge transfer between these conducting domains also occurs by thermally activated hopping or tunneling. This is consistent with conductivity being proportional to temperature.

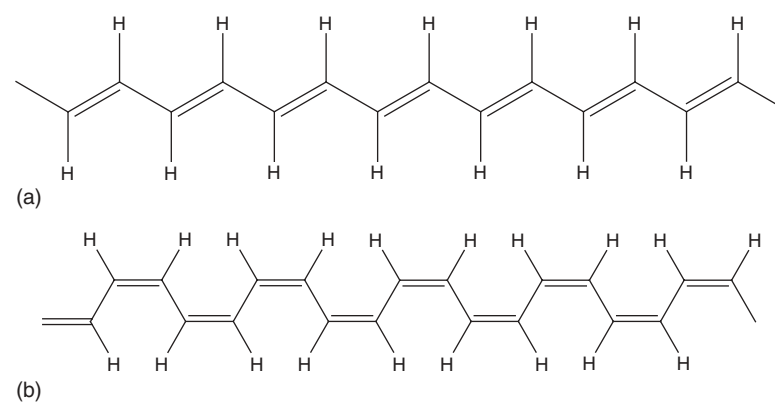
29.8 SYNTHESES

Synthesized conjugated conducting polymers can be classified into two major categories: chemically polymerized and electrochemically polymerized materials. Via chemical polymerization, conjugated monomers react with an excess amount of an oxidant in a suitable solvent, such as acid. The polymerization takes place spontaneously and requires constant stirring. The second method is via electrochemical polymerization, which involves placing both counter and reference electrodes (such as platinum), into the solution containing diluted monomer and electrolyte (the dopant) in a solvent. After applying a suitable voltage, the polymer film immediately starts to form on the working electrolyte. A major advantage of chemical polymerization concerns the possibility of mass-production at a reasonable cost [33, 34]. This is often difficult with electrochemical methods. On the other hand, an important feature of the electropolymerization technique is the direct formation of conducting-polymer films that are highly conductive, simple, and suitable for use especially in electronic devices.

upon the species of Ziegler–Natta catalyst employed. They also observed the formation of alkylbenzenes as a minor by-product of acetylene polymerization, with a catalyst system composed of titanium tetrachloride and trialkylaluminum. In a series of experiments using carbon-14 and deuterium, they noted that the ethyl group is introduced in the ethylbenzene when triethylaluminum labeled with carbon-14 or deuterium is used as the cocatalyst [35]. In other experiments, in which polyacetylene was oxidized by alkaline potassium permanganate, they observed the formation of propionic and acetic acids that are derived from the alkyl groups in trialkylaluminum used as the cocatalyst [35]. From these results, they concluded that polyacetylene and benzene could be formed from the same active site of the catalyst system. Thus, the reaction proceeds by *cis* opening of the triple bond in acetylene, followed by a *cis* insertion into the titaniumalkyl bond of the catalyst. This mechanism fits the orbital interaction model for the role of the catalyst by Fukui and Inagaki [36], according to which the initially formed configuration of the double bond is *cis* as a result of favored orbital interaction between the inserting acetylene and the active site of the catalyst. Whether cyclic trimerization occurs to give benzene or polymerization and proceeds to give polyacetylene is determined by the conformation of the growing chain, which takes either *cisoid* or *transoid* structure at the vicinity of the active site of the catalyst [36, 37]. As no *cis* form had been known until then, an important question remained, namely, why the mechanism is capable of yielding only *trans* configuration of the double bonds in polyacetylene [1, 38]. Scheme 29.5 shows the all-*cis* and all-*trans* forms of polyacetylene.

The configuration of the double bonds strongly depends on the temperature of polymerization. The *trans* content of polyacetylene prepared by the Ziegler–Natta catalysts decreases with decreasing polymerization temperature, as listed in Table 29.3, determined by infrared spectroscopy.

A thermal study by Ito et al. [39] indicated that irreversible isomerization of the *cis* form occurs at



Scheme 29.5 All-*trans* (a) and all-*cis* (b) polyacetylene.

TABLE 29.3 The Trans Contents of Polyacetylene Prepared at Different Temperatures*

Temperature, °C	Trans Content, %
150	100.0
100	92.5
50	67.6
18	40.7
0	21.4
-18	4.6
-78	1.9

Catalyst: $\text{Ti}(\text{O}-n\text{-C}_4\text{H}_9)_4 - (\text{C}_2\text{H}_5)_3\text{Al}$, $\text{Ti}/\text{Al} = 4$, $[\text{Ti}] = 10 \text{ mmol/l}$.

*Ref. 39.

temperatures higher than 145°C to give a *trans* form (Fig. 29.4). Thus, the *cis* form is thermodynamically less stable than the *trans* one. The observed *cis*-rich polyacetylene synthesized at lower temperatures suggested the *cis* opening of the triple bond of an acetylene monomer. When the polymerization was carried out at higher temperatures, spontaneous isomerization of the growing *cis* double bonds occurred to give *trans* ones, consistent with the *cis* opening mechanism proposed by Ikeda [37].

The electrical resistivity of films obtained with various *cis/trans* contents by the above preparation was measured by the conventional two-probe method under vacuum in a temperature range of -120 to 20°C [40]. The resistivity and energy gap of *trans*-rich polyacetylene were $1.03 \times 10^4 \Omega \text{ cm}$ and 0.56 eV , respectively, whereas the values of a *cis*-rich (80%) one were $2.43 \times 10^8 \Omega \text{ cm}$ and 0.93 eV , respectively. Hatano et al. [41] reported that the resistivity and energy gap measured on compressed pellets of powder

polyacetylene synthesized by the same catalyst system were in the range of 1.4×10^4 and $4.2 \times 10^5 \Omega \text{ cm}$ and 0.46 eV , respectively, in good agreement with those for *trans*-rich polyacetylene film. In conclusion, it became apparent that the intrinsic electrical properties do not change much between powder and film.

29.9.2 Polyaniline

Among the family of conjugated polymers, polyaniline is one of the most useful since it is air- and moisture-stable in both its doped, conducting form, and in its dedoped, insulating form [42–44]. Polyaniline is also unique among conducting polymers in that it has a very simple acid/base doping/dedoping chemistry (Fig. 29.4).

It has a great variety of potential applications, including anticorrosion coatings, batteries, sensors, separation membranes, and antistatic coatings [5, 46]. Conventional polyaniline synthesis (Fig. 29.5) is known to produce particulate products with irregular shapes. Therefore, many methods have been developed to make nanostructures of polyaniline (with diameters smaller than 100 nm) by introducing “structural directing agents” during the chemical polymerizing reaction. A great variety of such agents have been reported in the literature, and these include surfactants [47–50], liquid crystals [51], polyelectrolytes [52], nanowire seeds [53], aniline oligomers [54], and, relatively complex, bulky organic dopants [55–59]. It is believed that such functional molecules can either directly act as templates (e.g., polyelectrolytes) or promote the self-assembly of ordered “soft templates” (e.g., micelles, emulsions) that guide the formation of polyaniline nanostructures.

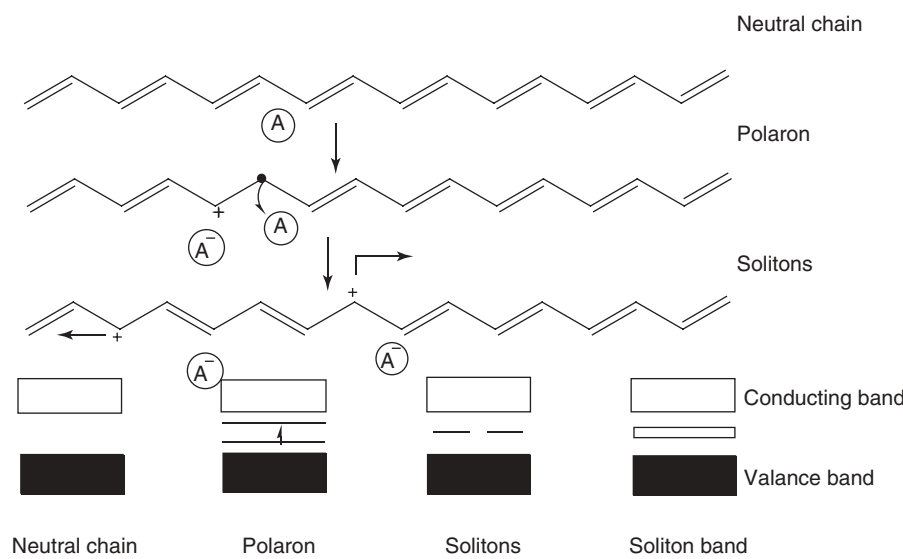


Figure 29.3 Mechanism of conduction upon polymer doping for conjugated polymers with a degenerate ground state.

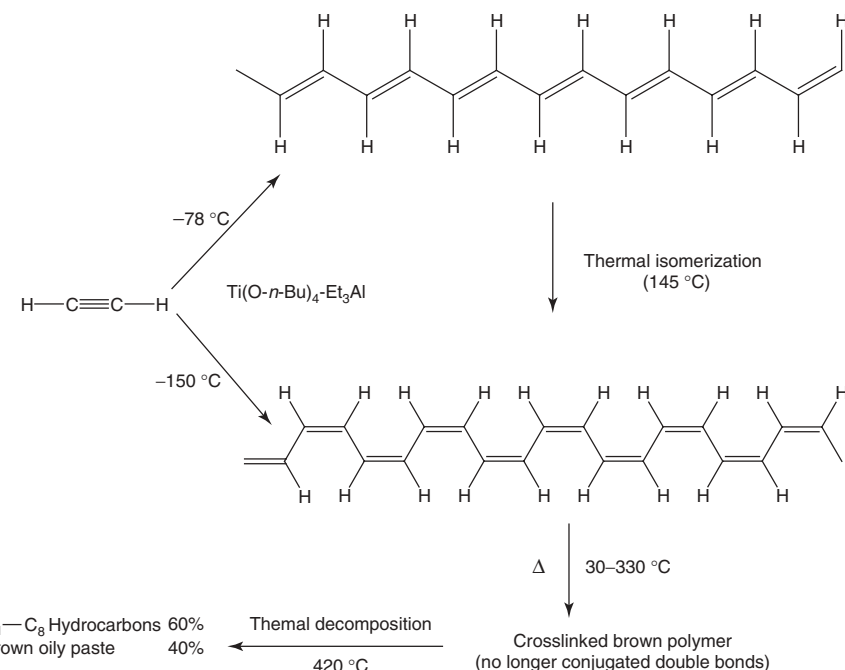


Figure 29.4 Thermal characterization of polyacetylene [39].

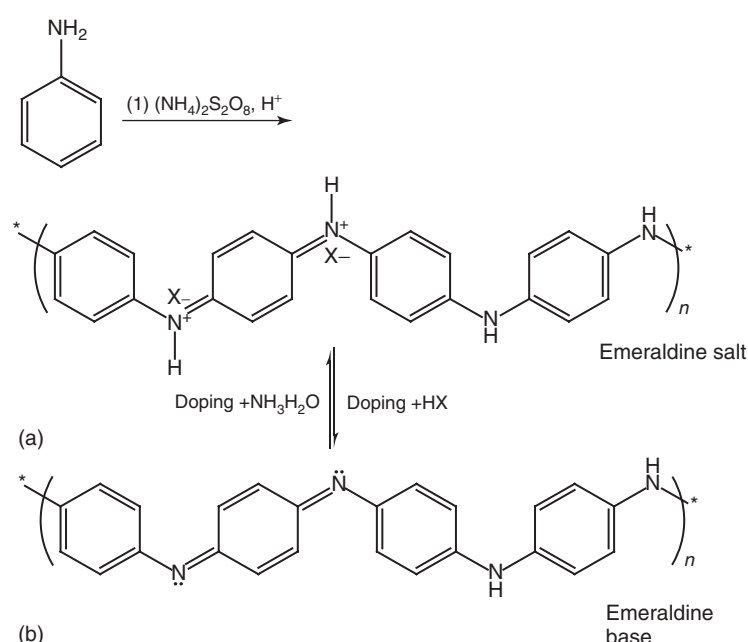


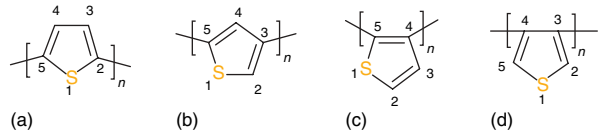
Figure 29.5 The conventional synthesis of polyaniline and its morphology. (a, b) The oxidative polymerization reaction of aniline is typically carried out in an acidic solution (e.g., 1 M HCl) [45].

29.9.3 Polythiophene

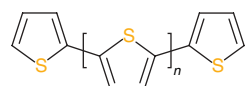
Another interesting family of conjugated polymers is the sulfur-containing polymers; above all, PT, its derivatives, and analogs attract the attention of researchers owing to a wide spectrum of valuable properties. PTs represent a special class of π processability and mechanical strength

[60]. Scheme 29.6 shows the possible arrangements of the repeating unit in PT.

The first PT synthesis was described in 1883. Washing of benzene with sulfuric acid afforded after further treatment with sulfuric acid a black insoluble material [61]. Oligomerization of thiophene induced by phosphoric



Scheme 29.6 Possible arrangements of the repeating unit of polythiophene.

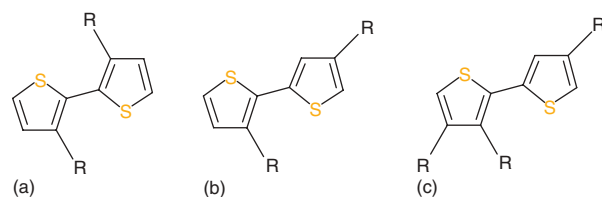


Scheme 29.7 Polythiophene.

acid leads to the formation of the trimer [62]. It was not until the early 1980s, however, that any well-defined polymeric material was obtained. After the first syntheses by Yamamoto et al. [63] and using the Grignard-type coupling [64] of 2,5-dibromothiophene, a vast number of articles concerning the synthesis and properties of PTs have been published. PTs (Scheme 29.7) exhibit favorable properties such as stability in both the neutral and the oxidized state under ambient conditions, but the numerous studies are also a result of the synthetic know-how for the preparation of (poly)thiophene and its derivatives [65].

The early problems concerning structural defects and solubility have attained much attention in the course of PT research, and some elegant solutions have been found. Extended π -conjugation in PTs is only possible in polymers with perfect 2,5-linked repeating units. Unfortunately, 2,4- and 2,3-couplings can be found as well. These undesired couplings are found when the polymers are prepared by (electro)oxidative polymerization methods. This is due to the fact that, during the polymerization, both the absolute oxidation potential of the α -position and the oxidation potential difference between the α - and β -positions decrease as the number of rings increases. The occurrence of α , β -linked thiophene rings interrupts the conjugation and as a result will give rise to inferior materials. PTs are, as other polycyclic aromatic compounds, insoluble in organic solvents due to their rigid backbone. This insolubility and related problems, such as characterization and processability, have been overcome by the introduction of flexible side chains at one of the P -positions. Appropriate solubility is achieved by using thiophenes with one alkyl side chain consisting of more than three carbon units at every repeating unit [66]. However, in 3-substituted PTs, there are several coupling patterns possible (Scheme 29.8): the head-to-head, head-to-tail, and tail-to-tail isomers [67, 68].

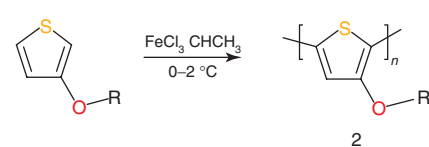
The head-to-head coupling is sterically unfavorable for coplanarity and causes considerable loss of conjugation, whereas the head-to-tail coupling displays only a limited effect on the conjugation. These significant differences



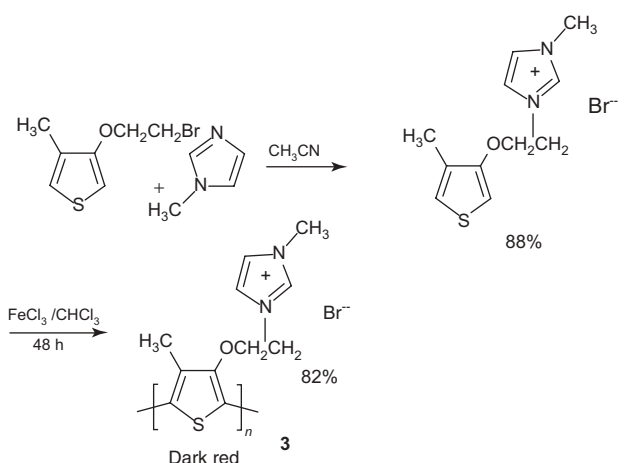
Scheme 29.8 (a) Head-to-head, (b) head-to-tail, and (c) tail-to-tail coupling patterns in substituted polythiophenes.

in coplanarity between head-to-head and head-to-tail couplings show the subtleties in the trade-off between resonance energy and steric hindrance in polyheterocycles. Studies of regioregular PTs, recently made accessible via a number of elegant synthetic routes, have shown that the crystallinity is increased with regioregularity and that the possibility of side-chain crystallinity is essential for optimal properties. For the case of regio-random polymers, the optimal chain length of the alkyl side chains for properties such as conductivity and optical nonlinearities has been determined to be in the range of seven to nine carbon atoms [69]; the conductivity of doped regioregular PT with an *n*-dodecyl side chain surpasses that of the *n*-octyl-substituted polymer [70].

PTs are usually synthesized by the oxidative dehydrogenation of thiophene and its derivatives that uses iron(III) chloride as an oxidizer and methylene chloride, chloroform, or nitromethane as solvents [71]. The principal direction of research in this area is the search for possible ways to improve engineering and service behavior of PTs through variation of the structure of parent monomers and resulting polymers. Thus, for example, the insertion of movable alkoxy groups into position 3 of the thiophene ring increases the solubility and processability of PTs and modifies their electric properties [72]. This phenomenon may be attributed to the electron-donor effect of alkoxy groups or to a more coplanar conformation of the corresponding PT as compared to products arising from the polymerization of common alkyl thiophenes [73]. The oxidative polycondensation of 3-alkoxythiophene at low temperatures and controlled addition of the monomer yields polymers with $M = 2340–3140$ and small structural defects (Scheme 29.9) [74].



Scheme 29.9 Oxidative polycondensation of 3-alkoxythiophene at low temperature.



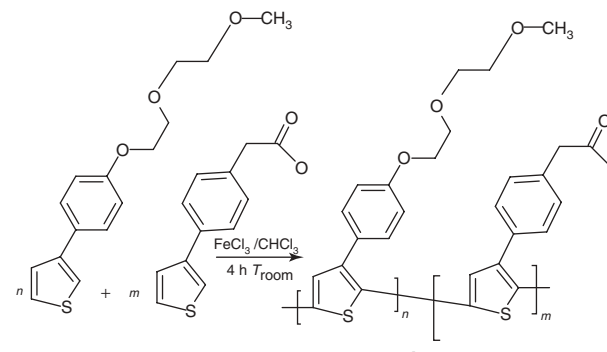
Scheme 29.10 Preparation of an imidazolinium-substituted PT-3.

Their thermal stability is slightly lower than that of the unsubstituted PT, and the value of T_g depends on the character of the alkoxy group ($R = \text{Me, Bu, Hex, Octyl}$). The same strategy was employed for the synthesis of ionochromic PTs containing crown ether side groups [75]; these polymers show good solubility in chloroform, THF, acetone, and ethyl acetate. The incorporation of hydrocarbon substituents into side chains improves the solubility of PTs in polar solvents even more greatly and ensures their compatibility. PT derivatives have also found application in biochemistry. Thus, an imidazolinium-substituted PT-3 (Scheme 29.10) that was prepared by the dehydropolycondensation of the corresponding monomer is used for the optical (colorimetric and fluorescent) determination of nucleic acids [76, 77].

This selective and universal method is based on conformational modifications of a cationic PT-5 [78] that occur via interaction with oligonucleotides or nucleic acids. As a result, the coloration of PT changes from dark red to blue or green. The synthesis of a soluble copolymer PT-4 ($M = 2.4 \times 10^4$) containing carboxyl and ether bonds is depicted in Scheme 29.11 [79].

29.9.4 Polypyrrole

The first synthesis of polypyrrole, appreciating its conducting properties, was described in 1968 [80]. Electrochemical oxidation of a pyrrole solution in 0.1 N sulfuric acid afforded a black conducting film. Improvements through the use of organic solvents and different electrolytes have been made [81, 82] and the electrochemical method has been the most employed polymerization technique ever since. Oxidized polypyrrole is stable under ambient conditions and up to temperatures exceeding 300 °C [82]. The neutral form of polypyrrole, on the other hand, has not been isolated



Scheme 29.11 Synthesis of a soluble copolymer PT-4.

and characterized, due to its extreme susceptibility to oxidation. The electrochemical route to polypyrrole provides good quality films. Counterions have a considerable influence on the conductivity and mechanical properties [83]. Changing the counterion from oxalate to perchlorate increases the conductivity by a factor in the order of hundred thousand. Commercially available (BASF) polypyrrole with tosylate as counterion exhibits a conductivity of 15 Scm⁻¹ and the stability of the material at ambient conditions is extremely good; a decrease of less than 15% per year is reported. Alkylsulfonates and phosphates have been used as electrolyte as well [84] and processable polymer blends are formed by using sulfonated polystyrene as counterions in the polymer.

The oxidation of a neutral polypyrrole film with chemical oxidizing agents increases the conductivity relative to that of the electrochemical oxidized materials [85]. 2,2'-Bipyrrole has been used as monomer, but the properties of the polymer obtained are similar to those of the parent polymer obtained from pyrrole itself [86].

Pyrrole has been chemically polymerized with oxidants including sulfuric acid [87], bromine and iodine [88], copper(II) perchlorate [89], and iron(III) chloride [90]. Soluble polypyrrole can be prepared by the introduction of flexible side chains [91–93]. In contrast with the progress made in the synthesis of regioregular PTs, all 3-substituted polypyrrroles reported so far have a regio-random structure.

Substitution on the nitrogen affords a regular soluble polymer; however, the conductivity is reduced drastically due to the strong steric interactions of the nitrogen substituent and the hydrogen atoms at the 3- and 4-positions of the adjacent pyrrole ring. Both rings are forced to go out of plane resulting in a loss of conjugation and hence a reduced conductivity [94]. Although the differences between a 3-substituted polypyrrole and an N-substituted polypyrrole at first glance are small with regard to steric hindrance, their conductivities differ significantly, again showing the subtleties in the structure–property relationship. The chemical oxidative method has also

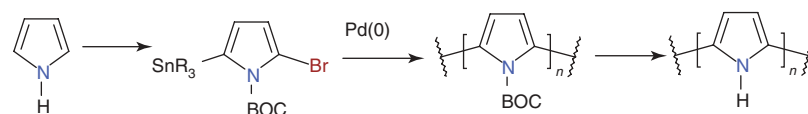
been applied to 3-alkyl pyrroles and to 3,4-dimethoxy pyrrole [95].

The introduction of sulfonic acid groups in the alkyl side chains affords water-soluble self-doped polypyrrole. Using the sodium salt of the 3-alkylsulfonic acid pyrrole, the monomer acts as electrolyte for the electrochemical synthesis as well. A second long alkyl chain on the opposite side of the pyrrole ring affords a highly ordered lamellar polymer also soluble in chloroform [96].

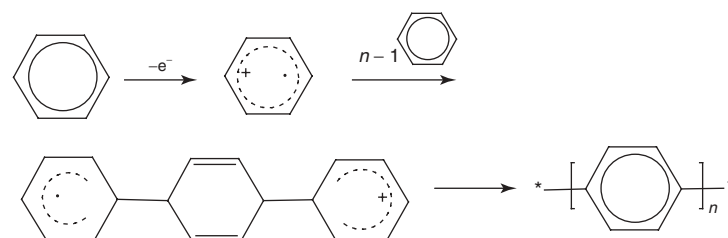
Structural defects such as α,β -couplings are inherent in oxidative polymerizations and to a minor extent can be present in the materials synthesized as described above. This failure to produce perfect 2,5-linked polypyrroles has been overcome by organometallic polymerization techniques. Thus, pyrroles with a Boc protecting group at nitrogen have been polymerized via the Stille coupling, affording a soluble nonplanar precursor polymer that has been deprotected by thermal treatment (Scheme 29.12). This polypyrrole, although of relatively low molecular weight (~ 3400), exhibits a perfect structure and is fully characterized. N-Boc-protected pyrrole has also been polymerized by the Ullmann coupling of the dibromo species, affording the same polymers as obtained by the Stille chemistry. A self-doped analog of polypyrrole has been obtained by means of the Ullmann coupling of *N*-butyl-2,5-dibromo-3,4-pyrrolidone [97].

29.9.5 Poly(paraphenylene)

Poly(paraphenylene) can be reduced or oxidized to produce conducting materials with conductivities up to 500 cm^{-1} . Both conducting species are highly sensitive toward water and oxygen, whereas neutral poly(paraphenylene) is stable, both thermodynamically and chemically. For the synthesis of poly(paraphenylene), a number of different routes have been employed, namely, oxidative coupling, organometallic coupling, and dehydrogenation of polycyclohexylenes.



Scheme 29.12 Polymerization and deprotection of N-Boc-protected pyrrole.



Scheme 29.13 Mechanism of the synthesis of poly(paraphenylene).

The first method reported for the synthesis of poly(paraphenylene) is the coupling of benzene by Lewis acid catalysis in the presence of an oxidant. In 1963, poly(paraphenylene) was synthesized by stirring benzene, aluminum chloride, and copper(II) chloride yielding an insoluble light brown powder [98]. The most favored mechanism is shown in Scheme 29.13. Benzene is oxidized to its radical cation that then propagates cationically. A second oxidation step produces the bis-cation, which loses two protons rearomatizing the terminal rings. Further oxidation of the dihydro structures finally affords the polymer [99].

Other Lewis acid/oxidant systems have been employed including $\text{ASF}_3/\text{AsF}_5$ [100] and liquid SO_2 or sulfuric acid and aluminum chloride [101]. Poly(paraphenylene) has been synthesized by the electrochemical oxidation of benzene in solvents such as liquid SO_2 [102] and concentrated sulfuric acid [103], or with the addition of Lewis acids including aluminum chloride [104], $\text{CuCl}_2/\text{LiAsF}_6$ [105], and BF_3OEt_2 [106], affording polymeric films. To improve the solubility, poly(paraphenylene) has been sulfonated [107] and alkylated [108] with propyl halides to give materials with enhanced solubility.

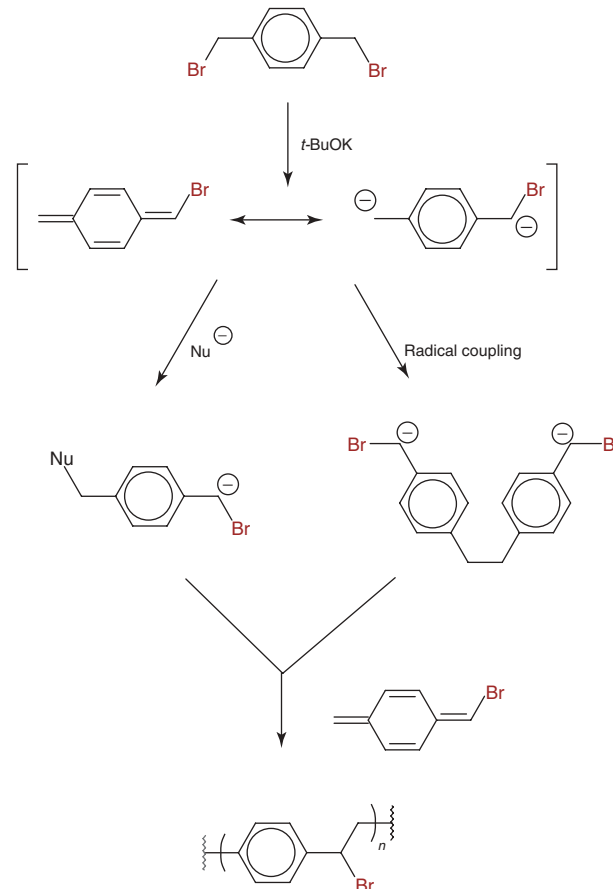
A number of different organometallic coupling methods have been used for the synthesis of poly(paraphenylene) including the Grignard cross-coupling of dihalobenzenes with a nickel catalyst [109, 110], the cross-coupling of dihalobenzenes with zero-valent nickel complexes, and the electrochemical reduction of dihalobenzenes activated by zero-valent nickel complexes [111]. Soluble poly(paraphenylene)s have been synthesized by the introduction of flexible alkyl side chains using the nickel catalyzed cross-coupling reactions with magnesium or borium, although the improved solubility does not have a stimulating effect on the average degree of polymerization, which is of the order of 13. Higher molecular

weight polymers, with an average degree of polymerization of approximately 100, have been obtained by the nickel (0)-induced polymerization of methyl 2,5-dichlorobenzoate, which on saponification and decarboxylation was transformed into poly(paraphenylenes) [112]. A polymerization without a transition metal catalyst has been achieved by the hexamethylphosphoramide-induced polymerization of 1-bromo-4-lithiobenzene to provide soluble poly(paraphenylenes) with molecular weights up to 2000. These materials, however, consist of a considerable percentage (20–30%) meta linkages, which probably accounts for the remarkably high solubility [113].

29.9.6 Poly(*p*-phenylene Vinylene)

Poly(*p*-phenylene vinylene) (PPV) is a conjugated polymer, which becomes conductive by the addition of electron donors or acceptors [114, 115]. Several methods have been reported for the synthesis of PPV [3, 4, 6]. Direct chemical polymerization, which was used in the first attempt of synthesizing PPV, gave a product in the form of an insoluble powder that limited the use of the polymer in many applications [116]. The most popular method for the preparation of PPV is base-induced polymerization of sulfonium salt monomer in aqueous solution [114–118]. In this method, PPV films are obtained from the precursor polymer after thermal elimination of the sulfonium groups. PPV has also been prepared electrochemically by reducing *p*-xylene-bis-(triphenylphosphonium). Two approaches are generally used for the synthesis of PPVs: the Wessling [119] route and the Gilch [120] route. The Wessling route involves treatment of *p*-xylylene sulfonium salts with an equal molar amount of base to form a soluble precursor polymer. The precursor polymer is then thermally treated to give the conjugated PPV. The Gilch route employs the treatment of α,α' -dihalo-*p*-xylenes with potassium *tert*-butoxide in organic solvents. Alkyl or alkoxy substituents on the aromatic ring are often used to impart solubility to the PPV. One of the most widely studied PPVs is poly(1-methoxy-4-(2-ethylhexyloxy)-*p*-phenylenevinylene) (MEHPPV) due to the enhanced solubility of this polymer [121]. The mechanism of this polymerization is not fully understood, and several processes have been suggested [8]. The polymerization is believed to proceed through a reactive quinodimethane intermediate that has been observed from UV spectra [122, 123]. However, the nature of the propagating species, radical or anionic, is not firmly established (Scheme 29.14).

Although many techniques to synthesize high molecular weight PPVs exist, they are largely limited to the synthesis of predominantly *trans*-PPVs [125]. Recent work by Katayama and Ozawa [126, 127] has, for the first time, provided access to all *cis*-PPVs by way of a stereospecific



Scheme 29.14 Polymerization mechanism of α,α' -dibromoethylene by anionic and radical polymerization [124].

Suzuki–Miyaura cross-coupling polymerization of 1,4-bis((*Z*)-2-bromovinyl)benzenes with aryl-bis-boronic acids. The interest has been in an alternative approach, where rather than building a PPV with a pre-ordained stereochemistry, a postpolymerization *syn*-selective reduction on a poly(phenylene ethynylene) (PPE) is used [125]. This scheme has the advantage that high molecular weight PPEs can be synthesized using either Pd-catalysis or alkyne metathesis. This route could also potentially allow for the access to an additional array of PPVs that are uniquely accessible from PPEs. The transformation of the triple bonds in PPEs and other acetylene building blocks to alkenes has considerable potential.

29.10 CHARACTERIZATION TECHNIQUES

As most other polymers, conducting polymers can be characterized through a variety of analytical techniques. Many examples exist in the literature, some of which include the following:

1. cyclic voltammetry, for understanding redox processes in conducting polymers and evaluating potential battery and electrochromic window material candidates;
2. optical characterization of conducting polymers, for electrochromic window and nonlinear optical materials;
3. nuclear magnetic resonance, for structure confirmation, chain orientation, and molecular motion;
4. gel permeation chromatography, for molecular weight;
5. Raman analysis, for vibrational assignments;
6. differential scanning calorimetric and thermogravimetric analysis, for evidence of glass and melting transitions and decomposition temperatures;
7. dependence of conductivity on temperature, electric field, and magnetic susceptibility, to understand the conductivity mechanism;
8. electroluminescence to screen for potential use in LEDs;
9. X-ray analysis, including Rutherford backscattering, to understand the crystal structure and to obtain elemental depth profiles, to gain insight into the conductivity mechanism.

29.11 PRESENT AND FUTURE POTENTIAL

29.11.1 Applications

Potential applications for conducting polymers are numerous; some potential applications for conducting polymers are discussed below.

29.11.1.1 Corrosion Protection The recent methods of corrosion protection are not very lasting and are coming under increased scrutiny by the Environmental Protection Agency (EPA). As an example, the use of chromium and cadmium for anticorrosion will soon be banned. A mechanism for corrosion protection involves the use of a sacrificial electrode, such as zinc coating, which will corrode (oxidize) in safekeeping the substrate. Unfortunately, the coatings do not last very long. The oxidized zinc metal is dissolved by water or moisture. For this reason, there are extreme environmental concerns, since toxic metals are being released into the ecosystem. Barrier coatings, such as epoxy, are employed extensively but are not very durable once a pit or hole in the coating has been formed. The corrosive species then attacks the underlying metal and thereby increases the exposed surface, accelerating the corrosion process. MacDiarmid first suggested the corrosion inhibiting property of conducting polymers in 1985 [128]. Initial studies on the protection of metal surfaces against corrosion

by conducting polymers were reported in the literature that same year. A major type of corrosion occurs by oxidation of a metallic surface by a water medium to produce oxides and hydroxides. As these are formed, soluble species are produced, the surface pits increase their surface area, and the rate of decomposition accelerates. One way to provide corrosion protection is to coat the metal with a barrier to prevent the reactive species from reaching the surface. Galvanization with zinc (or other metals with low oxidation potential) prevents corrosion via the creation of an interfacial potential at the metal–zinc interface. The zinc will corrode preferentially. While the reactive species may encounter the metal, the increased oxidation causes the metal to be insensitive. Corrosion is therefore inhibited.

29.11.1.2 Sensors and Electromechanical Devices

Since conducting polymers change properties by incorporation of ions and solvents (the property change easiest to measure is conductivity), it is possible to develop and market ion-specific sensors based on conducting polymers. Conducting polymers could permit the incorporation of sensors into clothing. There are some challenges involved, such as background noise due to water absorption, lifetime, selectivity, and sensitivity. Conducting polymers also change volume depending on their oxidation state. It is, therefore, possible for conducting polymers to convert electrical energy into mechanical work. Conducting polymers actuators were proposed by Baughmann et al. [13]. An oxidation-induced strain of polyaniline and polypyrrole-based actuators has been reported, and the first “self-contained” actuators were reported by MacDiarmid [128]. There are many interesting possibilities for conducting-polymer actuators, but a great deal of work needs to be done.

The conducting polymers have useful applications in the development of chemical sensors. During the past two decades, conducting polymers have emerged as one of the most interesting materials for the fabrication of electrochemical sensors [129]. The great advantage of conducting polymer-based sensors over other available techniques is that the conducting polymers have the potential to exhibit improved response properties and are sensitive to small perturbations. Earlier inert polymers were being used only to provide mechanical strength to the membranes, but conductive polymers improve the sensitivity of the sensors due to their electrical conductivity or charge transport properties. Conducting polymers are also known for their ability to be compatible with biological molecules in neutral aqueous solutions [130]. Moreover, the polymer itself can be modified to bind biomolecules to a biosensor [131]. Another advantage of conducting polymers is that the electrochemical synthesis allows direct deposition of a polymer film on the electrode substrate, followed by biomolecule immobilization [132]. It is thus possible to control the spatial distribution of

the immobilized enzymes, film thickness, and modulation of enzyme activity. Conducting polymers can act as an electron promoter. Moreover, conducting polymers can be deposited over defined areas of electrodes. The unique properties of conducting polymers have been exploited for the fabrication of electrochemical sensors and biosensors [130–134]. Among many analytical techniques available, the development of chemical sensors has made significant strides in the last two decades. The rapidly growing applications of chemical sensors reflect the extent to which analytical chemists require these devices for cheap, accurate, convenient, and quick analysis of various samples. Chemical sensors are miniaturized analytical devices, which can deliver real-time and online information about the presence of specific compounds or ions in complex samples. Usually, an analyte recognition process takes place, followed by the conversion of chemical information into an electrical or optical signal.

29.11.1.3 Batteries This field is the first area where conducting polymers promise to have a big commercial impact. Batteries have several key components: the electrodes allow for collection of current and transmission of power; the cathode material becomes reduced when the anode material is oxidized and vice versa; and the electrolyte provides a physical separation between the cathode and the anode, and provides a source of cations and anions to balance the redox reactions. Aside from picking the best conducting polymer available, there are many other issues, not related to conducting polymers, that affect battery performance, such as electrolyte stability and stability of the counter half-cell reaction (which is at least as important as the conducting-polymer electrode), and compatibility between the electrolyte and the materials.

There was a great deal of initial excitement about conducting polymers as active materials in batteries. Owing to their low density, it was thought that battery with power densities much higher than those of the ordinary lead/acid battery could be readily obtained. Since the charge on a polymer backbone is distributed over three or four repeat units, the charge capacity per unit of mass for conducting polymers is marginally better than that of metals. Conducting-polymer batteries were investigated by BASF/VARTA and Allied Signal. Bridgestone has marketed a button-sized battery using polyaniline and lithium. Conducting polymer still has a potential use in lithium-based high power density batteries, which use the high potential difference between lithium and the polymer to achieve high power densities, although stability and shelf life are still issues. As more and more individuals use cellular phones, laptop computers, and cordless drills, the importance of batteries that will handle many deep cycles (at least 60% depth of discharge)

becomes increasingly apparent. Conducting polymer-based batteries shows promise, but much work needs to be done.

29.11.1.4 Electrochromic Cell These cells are used to go from opaque to transmissive states at selected regions of the electromagnetic spectrum. Batteries and electrochromic cells have many common critical issues for commercial viability. They require cathodic and anodic reactions to be almost perfectly balanced (cyclic voltammetry is a good comparison tool for materials). The electrochromic window is similar to that of a battery with some additional requirements: at least one of the electrodes must be transparent to the given electromagnetic spectrum; the cathode material (which colors upon being oxidized) must be electrochemically reversible; and the ion-conducting electrolyte must not only provide physical separation between the cathode and anode, a source of cations and anions to balance redox reactions, but must also be transparent to the given region of the spectrum; and the anode material (which colors upon being reduced) must also be electrochemically reversible.

The ion-conducting electrolyte in electrochromic cells is usually an inorganic salt dissolved in a solvent such as propylene carbonate with a polymer such as poly(methyl methacrylate) added as a stiffener. The ion-conducting electrolyte acts as a source and sink for the ions as the various redox processes take place and maintains ionic contact between the materials. Conducting polymers also have an application in electrochromic cells, attenuating various regions of the electromagnetic spectrum. Aside from the batteries issues mentioned in the previous section, electrochromic cells have some additional requirements. Although thinner layers (for optical window) are usually sufficient, retention of extinction coefficient and contract ratios are critical. Many electrochromic cells need to last for more than 10,000 cycles and have switching times of a few minutes. In this case, spectroelectrochemistry is a good evaluation tool for conducting-polymer materials. Spectroelectrochemistry measures both the electrical and the optical response of the material in question. Again, it must be emphasized that this method is not suitable for devices; spectroelectrochemistry is usually performed in a great excess of electrolyte and, therefore, the counter half-cell reactions are often ill defined. There is a great deal of data that indicate that conducting polymers are good candidates for materials in electrochromic cells. In particular, polythiopene, polypyrrole, and polyaniline have been cycled more than 10,000 times. These data, although good for evaluating differences between polymers, may not accurately reflect the performance of conducting polymers in a sealed, self-contained device. This is because the counter half-cell reaction and those devices often require “deep cycle,” that is, near complete oxidation/reduction. The device usually starts to degrade at 10–100 times

fewer cycles than conducting polymers studied by cyclic voltammetry. This does not necessarily mean that polymer is degrading, as either the counter half-cell reaction or the limited amount of electrolyte may control the lifetime of the device. Furthermore, cyclic voltammetry measures the retention of charge capacity in a polymer film and not the electrochromic contrast ratio. Although a 20% drop in charge capacity might be acceptable in a battery, a 20% decrease in a contrast ratio for electrochromic cells may be unacceptable. In devices that are based on retention of surface conductivity, it appears that conductivity is lost long before a significant amount of charge capacity decreases. The evaluation of conducting polymer for battery and electrochromic application should be similar to the actual condition (depth of discharge, cycle time, and transmission of extinction ratio).

29.11.1.5 Controlled-Released Applications Another application for conducting polymers is controlled-released devices. Ions can be selectively released, as well as biologically active ions such as adenosine 5'-triphosphate (ATP) and heparin. A conducting polymer with a given oxidation potential is electrodeposited onto a substrate with a mobile counter ion. Another polymer layer (polymer B with a higher oxidation potential than polymer A) is electrodeposited (directly on top of polymer A) using an immobile counter ion (polyanion). During complete reduction (step 1), it is almost impossible for the polymeric anion (Y^-) to move into the electrolyte solution and, therefore, cations (M^+) from the solution must move into the outer polymer layer, but the mobile anions (X^-) from the inner layer move into the electrolyte. During selective oxidation of polymer A (2), the mobile anions (X^-) move from the solution to the inner layer. During oxidation of polymer B (3), the cations (M^+) move back into solution. This potential-dependent ion transport is an interesting way to deliver ionic drugs to certain biological systems. Anions can be exclusively delivered by cycling back and forth through step (2), cations can be exclusively delivered by cycling back and forth through step (3), or anions can be delivered and cations can be received by cycling through step (1). It is very important for the inner polymer layer to have a lower oxidation potential than the outer layer. If this is not the case, the inner layer, which is the one connected to the electrode, will act as an electrical insulator and will prevent the oxidation of the outer layer. Once the oxidation potential of the inner layer is reached, a pulse charge will occur, making selective ion transport difficult (rectification). Furthermore, a biologically compatible counter-half cell is necessary for a practical device. This might not present too much of a problem if the drug delivery system is used only once. If repeated uses of the same device are necessary, then issues such as reversibility

(as those of batteries and electrochromics) will need to be resolved.

29.11.1.6 Radar Application Radio direction and ranging (RADAR) uses electromagnetic waves that bounce off a particular target and are collected by a receiver, which analyzes the signal and determines the range, direction, and speed of the object in question. Reflections occur whenever there is a sharp impedance difference between the medium (usually air) and the object. Impedance differences are most notable between metals and air. Metals tend to reradiate (reflect) the incoming signal. Conducting-polymer camouflage works a little differently, in that it reflects back in a way that it has more continuously variable impedance. A conducting-polymer textile used for camouflage has no sharp edges or wings and tends to appear indistinguishable from the surrounding hills and trees and absorbs more than 50% of incident microwave radiation. Microwave (100 MHz–12 GHz) properties of conducting polymers have been studied, as have the millimeter wave (24–40 GHz) properties of polypyrrole-coated fibers. Conducting polymers as radar absorbers in antennas, Salisbury screens, camouflage, and other types of shielding are of interest to the military.

29.11.1.7 LEDs A significant event occurred when Friend et al. [134, 135] published an electroluminescence study on the neutral (nonconducting) form of para-phenylene vinylene. This work has opened up a new avenue of research and, more importantly, a potential market for the material. The electroinjecting electrode is usually a low work function (easily oxidized) metal and the hole-injection electrode is a high work function metal, or indium tin oxide, or a conducting polymer with an oxidation potential higher than that of the active layer. Some general trends have been observed: as a lower work function metal (less stable because it is easily oxidized) is used, the efficiency increases but the lifetime decreases. Studies have been reported in which a layer of neutral conjugated polymer, with a reduction potential closer to zero than that of the active conducting-polymer layer, increases efficiency. A simplistic overview of the function of an LED is as follows: an electron is injected into the polymer from the cathode while a hole is injected from the anode; there is an oxidized polymer on one side of the polymer film and a reduced polymer on the other side. The hole and the electron then migrate toward the center of the film and, when they meet each other, they recombine and give off light. The frequency of the light emitted is roughly equal to the difference between the oxidation and the reduction potential of the polymer (the electrochemical band gap) and, therefore, is related to the electronic band gap. Polymers with a different band gap have distinct values for the difference between oxidation and reduction

potential, and emit different wavelength of light. Several articles on conducting polymer LEDs and the effect of various additives, electrode modifications, tuning emission, the effect of impurities, and discussions of hole tunneling, photoexcitation, and unusual symmetric bias, have been published. The efficiency of LEDs is constantly being improved along with novel developments such as flexible LEDs, polarized LEDs, and light-emitting electrochemical cells. The emission of red, green, blue, and white light have all been demonstrated, and so has brightness in the order of 400 cd/m, which is similar in brightness to fluorescent lights or computer displays.

A challenge in the operation of LEDs is the fact that it appears that the mobility of the hole is higher than the mobility of the electron. The barrier height (as a resistance) between the polymer and each of the electrodes must be low and roughly equal, so that the hole and the electron recombine near the center of the conducting-polymer layer, to ensure good operation. Another limiting factor is the competition between radiative and nonradiative decay that, for PPV-type systems, is about 25%, which does not limit device performance at this juncture. Yet another challenge is the fact that the polymers that initially perform well in LEDs contain electron-rich double bonds. These double bonds are fairly easy to oxidize and are most likely one of the major causes for device degradation. Thermal and photo-oxidation of the double bonds in LED polymers have been discussed in detail. The efficiency, lifetime, and brightness depend on a variety of factors. One major challenge is balancing the electron mobility to that of the hole mobility. This is done by adding electron transport layers and hole transport layers such as trisubstituted amines. These layers reduce the barrier height and encourage the holes and electrons to combine near the center of the film. Electron and hole transport layers could permit the use of more stable metals without compromising efficiency. Conducting polymers enable a wide variety of structures to be synthesized and therefore many different wavelengths of light are possible. Although conducting polymers will not replace fluorescent light bulbs (which have efficiencies of around 70%), because conducting-polymer LEDs are easily patterned, operate at low DC voltages, and have uniform areas of light, there is a potential market for low level backlighting and alphanumeric displays.

REFERENCES

1. Natta G, Mazzanti G, Corradini P. Atti Accad Naz Lincei Cl Sci Fis Mat Rend 1958;25(8):3. Natta G, Mazzanti G, Corradini P. Atti Accad Naz Lincei Cl Sci Fis Mat Nat Rend 1958;25:2.
2. Shirakawa H. Rev Mod Phys 2001;73:713.
3. Ito T, Shirakawa H, Ikeda S. J Polym Sci Polym Chem Ed 1974;12:11.
4. Heeger AJ. Rev Mod Phys 2001;73:681.
5. MacDiarmid AG. Angew Chem Int Ed 2001;40:2581.
6. Harun MH, Saion E, Kassim A, Yahya N, Mahmud E. J Acoust Soc Am 2007;2:63.
7. Skotheim TA, Elsenbaumer RL, Reynolds JR, editors. Handbook of Conducting Polymers. 2nd ed. New York: Marcel Dekker; 1998.
8. Pohl HA, Bommann JA, Itoh W. Am Chem Soc Div Polym Chem Preprints 1961;2(1):211.
9. Katon JE, Wild BS. J Chem Phys 1964;40(10):2977.
10. Bredas JL, Chance RR, Silbey R. Phys Rev B 1982;26:5843.
11. Clarke TC, Geiss RH, Kwak JF, Street GB. J Chem Soc Chem Commun 1978;(12):489.
12. Pron A, Rannou P. Prog Polym Sci 2002;27:135.
13. Shirakawa H, Louis EJ, MacDiarmid AG, Chiang CK, Heeger AJ. J Chem Soc Chem Commun 1977;(16):578.
14. Stenger-Smith JD. Prog Polym Sci 1998;23:57.
15. Nalwa HS. In: Nalwa HS, editor. *Handbook of Organic Conductive Molecules and Polymers*. New York: Wiley; 1997.
16. Schon JH, Dodabalapur A, Bao Z, Kloc C, Schenker O, Batlogg B. Nature 2001;410:189.
17. Chiang CK, Jr Fincher CR, Park YW, Heeger AJ, Shirakawa H, Louis EJ, MacDiarmid AG. Phys Rev Lett 1977;39:109.
18. Chiang CK, Druy MA, Gau SC, Heeger AJ, Louis EJ, MacDiarmid AG. J Am Chem Soc 1978;100:1013.
19. Kanatzidis MG. Chem Eng News 1990;68(49):36.
20. Nigrey PJ, MacDiarmid AG, Heeger AJ. J Chem Soc Chem Commun 1979;(14):594.
21. Jr MacInnes D, Druy MA, Nigrey PJ, Nairns DP, MacDiarmid AG, Heeger AJ. J Chem Soc Chem Commun 1981;7:317.
22. Heeger AJ, Kivelson S, Schrieffer JR, Su W-P. Rev Mod Phys 1988;60:781.
23. Ziemelis KE, Hussain AT, Bradley DDC, Friend RH, Rilhe J, Wegner G. Phys Rev Lett 1991;66:2231.
24. Burroughes JH, Jones CA, Friend RH. Nature 1988;335:137.
25. Burroughes JH, Bradley DDC, Brown AR, Marks RN, Mackay K, Friend RH, Burns PL, Holmes AB. Nature 1990;347:539.
26. Chiang J-C, MacDiarmid AG. Synth Met 1986;13:193.
27. MacDiarmid AG, Chiang J-C, Richter AF, Epstein AJ. Synth Met 1987;18:285.
28. MacDiarmid AG, Epstein AJ. Faraday Discuss Chem Soc 1989;(88):317.
29. MacDiarmid AG, Epstein AJ. In: Salaneck WR, Clark DT, Samuels EJ, editors. *Science and Applications of Conducting Polymers*. Bristol: Adam Hilger; 1990. p 117.
30. Han CC, Elsenbaumer RL. Synth Met 1989;30:123.
31. Lu FL, Wudl F, Nowak M, Heeger AJ. J Am Chem Soc 1986;108:8311.

556 CONDUCTING POLYMERS

32. Sun Y, MacDiarmid AG, Epstein AJ. *J Chem Soc Chem Commun* 1990;(7):529.
33. Toshima N, Hara S. *Prog Polym Sci* 1995;20:155.
34. Chao TH, March J. *J Polym Sci A Polym Chem* 1988;26:743.
35. Ikeda S, Tamaki A. *J Polym Sci Polym Phys Ed* 1966;4:605.
36. Fukui K, Inagaki S. *J Am Chem Soc* 1975;96:4445.
37. Ikeda S. *Kogyo Kagaku Zasshi* 1880;1967:70.
38. Berets DJ, Smith DS. *Trans Faraday Soc* 1968;64:823.
39. Ito T, Shirakawa H, Ikeda S. *J Polym Sci Polym Chem Ed* 1975;13:1943.
40. Shirakawa H, Ito T, Ikeda S. *Makromol Chem* 1978;179: 1565.
41. Hatano M, Kambara S, Okamoto S. *J Polym Sci* 1961;51: S26.
42. Huang WS, Humphrey BD, MacDiarmid AG. *J Chem Soc Faraday Trans* 1986;82:2385.
43. MacDiarmid AG. *Synth Met* 1997;84:27.
44. MacDiarmid AG, Chiang JC, Halpern M, Huang WS, Mu SL, Somasiri NLD, Wu WQ, Yaniger SI. *Mol Cryst Liq Cryst* 1985;121:173.
45. Huang J. *Pure Appl Chem* 2006;78(1):15.
46. Chandrasekhar P. *Conducting Polymers, Fundamentals and Applications: A Practical Approach*. Boston: Kluwer Academic; 1999. p 760.
47. Zhang X, Manohar SK. *Chem Commun* 2004;20:2360.
48. Yu L, Lee JI, Shin KW, Park CE, Holze R. *J Appl Polym Sci* 2003;88:1550.
49. Michaelson JC, McEvoy AJ. *Chem Commun* 1994;79:18.
50. Li GC, Zhang ZK. *Macromolecules* 2004;37:2683.
51. Huang LM, Wang ZB, Wang HT, Cheng XL, Mitra A, Yan YX. *J Mater Chem* 2002;12:388.
52. Liu JM, Yang SC. *J Chem Soc Chem Commun* 1991;(21): 1529.
53. Zhang X, Goux WJ, Manohar SK. *J Am Chem Soc* 2004;126:4502.
54. Li WG, Wang HL. *J Am Chem Soc* 2004;126:2278.
55. Qiu HJ, Wan MX, Matthews B, Dai LM. *Macromolecules* 2001;34:675.
56. Wei ZX, Wan MX. *J Appl Polym Sci* 2003;87:1297.
57. Wei ZX, Zhang ZM, Wan MX. *Langmuir* 2002;18:917.
58. Wan MX. Conducting Polymer Nanotubes In: Nalwa HS, editor. *Encyclopedia of Nanoscience and Nanotechnology*. Vol. 2. Los Angeles: American Scientific Publishers; 2004. p 153.
59. Qiu HJ, Wan MX. *J Polym Sci A Polym Chem* 2001;39: 3485.
60. Chen S-A, Tsai C-C. *Macromolecules* 1993;26:2234.
61. Meyer V. *Chem Ber* 1883;16:1465.
62. Meisel SL, Johnson GC, Hartough HD. *J Am Chem Soc* 1950;72:1910.
63. Yamamoto T, Sanechika K, Yamamoto A. *J Polym Sci Polym Lett* 1980;18:9.
64. Lin Lin JW-P, Dudek LP. *J Polym Sci A Polym Chem* 1980;18:2869.
65. Gronowitz S, editor. *Thiophene and Its Derivatives, Part I*. The chemistry of heterocyclic compound. Vol. 44. New York: John Wiley & Sons; 1985.
66. Jen K-W, Miller GG, Elsenbaumer RL. *J Chem Soc Chem Commun* 1986;(17):1346.
67. Sato M, Morii H. *Macromolecules* 1991;24:1196.
68. Leclerc M, Diaz FM, Wegner G. *Makromol Chem* 1989;190:3105.
69. Roncali J, Garreau R, Yasser A, Marque P, Gamier F, Lemaire M. *J Phys Chem* 1987;91:6706.
70. McCullough RD, Tristram-Nagle S, Williams SP, Lowe RD, Jayaraman M. *J Am Chem Soc* 1993;115:4910.
71. [a]Fichou D, editor. *Handbook of Oligo- and Polythiophenes*. Vol. 3. Weinheim: Wiley-VCH; 1999.[b]McCullough RD. *Adv Mater* 1998;10:93.
72. Roncali J. *Chem Rev* 1997;97:173.
73. Leclerc M, Daoust G. *Synth Met* 1991;41:529.
74. Hu X, Xu L. *Polymer* 2000;41:9147.
75. Boldea A, Levesque L, Leclerc M. *J Mater Chem* 1999;9: 2133.
76. Tyagi S, Kramer FR. *Nat Biotechnol* 1996;14:303.
77. Taton TA, Mirkin CA, Letsinger RL. *Science* 2000;289: 1757.
78. Ho H-A, Boissinot M, Bergeron MG. *Polym Prepr (Am Chem Soc Div Polym Chem)* 2002;43:133.
79. Jonforsen M, Ahmad I, Johansson T. *Synth Met* 2001;119: 529.
80. Dall'Olio A, Dascola G, Varacca V, Bocchi VC. *R Acad Sei 1968;C 267:433.*
81. Diaz AF, Kanazawa KK, Gardini GP. *J Chem Soc Chem Commun* 1979;(14):635.
82. Kanazawa KK, Diaz AF, Gill WD, Grant PM, Street GB, Gardini GP, Kwak JF. *Synth Met* 1979;180(1):329.
83. Qian R, Qiu J, Shen D. *Synth Met* 1987;18:13.
84. Wernet W, Monkenbusch M, Wegner G. *Mol Cryst Liq Cryst* 1985;118:193.
85. Street GB, Clarke TC, Krounbi M, Kanazawa K, Lee V, Pfluger P, Scott JC, Weiser G. *Mol Cryst Liq Cryst* 1982;83:253.
86. Lindenberger H, SchXfer-Siebert D, Roth S, Hanack M. *Synth Met* 1987;18:37.
87. Salmon M, Kanazawa KK, Diaz AF, Krounbi M. *J Polym Sci Polym Lett* 1982;20:187.
88. Chan HS, Munro HS, Davies C, Kang ET. *Synth Met* 1988;22:365.
89. Castillo-Ortega NM, Inoue MB, Inoue M. *Synth Met* 1989;28:C65.
90. Lei J, Cai Z, Martin CR. *Synth Met* 1992;46:53.
91. Rllhe J, Ezquerra TA, Wegner G. *Synth Met* 1989;28:C177.
92. Masuda H, Tanaka S, Keariyama K. *J Chem Soc Chem Commun* 1989;(11):725.

93. Zotti G, Schiavon G, Berlin A, Pagani G. *Synth Met* 1989;28:C183.
94. Kanazawa KK, Diaz AF, Geiss RH, Gill WD, Kwak JF, Logan JA, Rabolt JF, Street GB. *J Chem Soc Chem Commun* 1979;19:854.
95. Merz A, Schwarz R, Schropp R. *Adv Mater* 1992; 4:409.
96. Collard DM, Fox MA. *J Am Chem Soc* 1991;113:9414.
97. Brockmann TW, Tour JM. *J Am Chem Soc* 1994;116: 7435.
98. Kovacic P, Kyriakis A. *J Am Chem Soc* 1963;85:454.
99. Milosevich S, Saichek K, Hinche L, England WB, Kovacic P. *J Am Chem Soc* 1983;105:1088.
100. Aldissi M, Lepins R. *J Chem Soc Chem Commun* 1984;4:255.
101. Aeiyach S, Soubiran S, Lacaze PC, Froyer J, Pelous Y. *Synth Met* 1989;32:103.
102. Delamare M, Lacaze P-C, Dumousseau J-Y, Dubois J-E. *Electrochim Acta* 1982;27:61.
103. Levi MD, Pisarevskaya EY, Molodkina EB, Danilov AI. *J Chem Soc Chem Commun* 1992;1:14.
104. Kacriyama K, Sato M, Somoto K, Tanaka S. *J Chem Soc Chem Commun* 1984;18:1199.
105. Sato M, Tanaka M, Kaneto K, Yoshino K. *Polym Commun* 1985;26:356.
106. Oshawa T, Inoue T, Takeda S, Kaneto K, Yoshino K. *Polym Commun* 1986;27:61.
107. Kovacic P, Marchionna VJ, Koch FW, Oziomek J. *J Org Chem* 1966;31:2467.
108. Jones MB, Kovacic P, Lanska D. *J Polym Sci A Polym Chem* 1981;19:89.
109. Taylor SK, Bennett SG, Khouri I, Kovacic P. *J Polym Sci Polym Lett* 1981;19:85.
110. Toshima N, Asakura T. *Bull Chem Soc Jpn* 1993;66: 948.
111. Aboulkassim A, Chevrot C. *Polymer* 1993;34:401.
112. Chaturvedi V, Tanaka S, Kaeriyama K. *Macromolecules* 1993;26:2607.
113. Tour JM, Stephens EB. *J Am Chem Soc* 1991;113:2309.
114. Murase I, Ohnishi T, Naguchi T, Hirooka T. *Polym Commun* 1984;25:1327.
115. Gagnon DR, Capistran JD, Karasz FE, Lenz RW, Antoun S. *Polymer* 1987;28:567.
116. Gourley KD, Lillya CD, Reynolds JR, Chien JCW. *Macromolecules* 1984;17:1025.
117. Wessling RA. *J Polym Sci Polym Symp* 1986;72:55.
118. Lenz RW, Han CC, Karasz FE. *J Polym Sci A Polym Chem* 1988;26:3241.
119. Wessling RA, Zimmerman RG, inventors. US patent 3,401,152. 1968; Wessling RA, Zimmerman RG, inventors. US patent 3,532,643. 1970.
120. Gilch HG, Wheelwright WL. *J Polym Sci A Polym Chem* 1966;4:1337.
121. Pohl HA. *Chem Eng* 1961;68(22):105.
122. Lahti PM, Modarelli DA, Denton FR, Lenz RW, Karasz FE. *J Am Chem Soc* 1988;110:7258.
123. Denton FR, Sarker A, Lahti PM, Garay RO, Karasz FE. *J Polym Sci A Polym Chem* 1992;30:2233.
124. Neef CJ, Ferraris JP. *Macromolecules* 2000;33:2311.
125. Moslin RM, Espino CG, Swager TM. *Macromolecules* 2008;42(1):452.
126. Katayama H, Nagao M, Nishimura T, Matsui Y, Umeda K, Akamatsu K, Tsuruoka T, Nawafune H, Ozawa F. *J Am Chem Soc* 2005;127:4350.
127. Katayama H, Nagao M, Nishimura T, Matsui Y, Fukuse Y, Wakioka M, Ozawa F. *Macromolecules* 2003;2006:39.
128. MacDiarmid AG. *Short Course on Conducting Polymers*. New York: New Platz; 1985.
129. Guiseppi-Elie A, Wallace GG, Matsue T. *Chemical and Biological Sensors Based on Electrically Conducting Polymers* In: Skotheim TA, Elsenbaumer R, Reynolds JR, editors. *Handbook of Conducting Polymers*. 2nd ed. New York: Marcel Dekker; 1998. p 963.
130. Chaubey A, Malhotra BD. *Biosens Bioelectron* 2002;17:441.
131. Mulchandani AK, Wang CL. *Electroanalysis* 1996;8: 414–419.
132. Bartlett PN, Whitaker RG. *Biosensors* 1988;3:359–379.
133. Arbizzani C, Mastragostino M, Scrosati B. *Conducting polymers for batteries, supercapacitors and optical devices* In: Nalwa HS, editor. *Handbook of Organic Conductive Molecules Sensors and Polymers*. Vol. 4. Chichester: Wiley; 1997. p 595–619 Chapter 11.
134. Friend RH, Gymer RW, Holmes AB, Burroughes JH, Marks RN, Taliani C, Bradley DDC, Dos Santos DA, Brédas JL, Lögdlund M, Salaneck WR. *Nature* 1999;397(14):121.
135. Friend RH. *Pure Appl Chem* 2001;73(3):425.

30

DENDRITIC POLYMERS

JASON DOCKENDORFF AND MARIO GAUTHIER

30.1 INTRODUCTION

Dendritic species represent the most recently discovered class of branched macromolecular architecture. Major developments in linear, crosslinked, and branched architectures date back roughly to the 1930s, 1940s, and 1960s, respectively. The first synthetic dendritic species were reported in 1978 [1]; however, much of the work in this area began to build momentum only in the mid-1980s. A chronology of the key developments in dendritic polymers is provided in Table 30.1.

Dendritic patterns can be found all around us in nature and within us. The drainage pattern of rivers and their tributaries, plant roots and foliage, and neurons within our body are but a few examples of unique branched systems ranging in size from kilometers down to micrometers. Molecular dendritic species recreate fractal-like patterns on the nanometric scale. Dendritic macromolecules can be divided into three subclasses on the basis of their structural characteristics: dendrimers, hyperbranched polymers, and dendrigraft polymers (including arborescent polymers). Dendrimers should ideally have a perfect branched structure, hyperbranched polymers rely on statistical branching giving a highly imperfect structure, while the architecture of dendrigraft polymers is best described as semi-controlled. A second subclass of controlled structures is the dendrons, which are dendritic fragments formed by a monofunctional initiator or core.

A graphical comparison of the structure of dendrons, dendrimers, hyperbranched polymers, and dendrigraft polymers is shown in Figure 30.1. The stepwise synthesis of dendrimers involves multiple cycles of protection, condensation, and deprotection reactions to produce strictly

controlled branched structures and extremely narrow molecular weight distributions (MWD): the molecular weight dispersity ($\mathcal{D} = M_w/M_n$) attained for such molecules can be less than 1.01. The preparation of dendrigraft polymers also relies on stepwise, generation-based synthetic procedures but uses polymeric building blocks rather than small molecules and branching points randomly distributed on the coupling substrate. Under appropriate reaction conditions, usually involving ionic polymerization and grafting, low molecular weight dispersities can also be achieved for these systems ($\mathcal{D} \approx 1.05\text{--}1.10$). The completely random branching process used in the synthesis of hyperbranched polymers, typically resulting from the condensation of nonprotected polyfunctional monomers, provides the least defined structures, a $\mathcal{D} > 2$ being obtained in most cases.

Each color in Figure 30.1 represents the branching levels derived from building blocks introduced in successive generations, these being small molecules for dendrons, dendrimers, and hyperbranched polymers (Fig. 30.1a–c), and polymeric segments for the dendrigraft polymers (Fig. 30.1d). Dendrons are closely related to the dendrimers of Figure 30.1b, the main distinction being the number of functional groups available on the substrate serving as core in the first reaction step. It should also be noted that hyperbranched polymers can be obtained from polymeric segments (e.g., macromonomers) as well as small molecules.

Dendritic macromolecules constructed from small-molecule monomers incorporate three major components: a core, repeating branch cell units, and a corona or outer shell. The branch cells (BC), also known as *repeating units* (RU), are defined in terms of a branching angle,

TABLE 30.1 Dendritic Molecule Discoveries in the Literature

Year	Authors
<i>Cascade Growth and Dendrimers</i>	
1978	Vögtle [1]
1982	Maciejewski [3]
1983	de Gennes [4]
1985	Tomalia [5], Newkome [6]
1990	Hawker and Fréchet [7], Miller and Neenan [8]
<i>Random Hyperbranched Polymers</i>	
1988	Gunatillake et al. [9]
1990	Kim and Webster [10]
1991	Hawker et al. [11]
<i>Dendrigraft Polymers</i>	
1991	Gauthier and Möller [12], Tomalia et al. [13]

Source: Adapted with permission from Tomalia DA, Fréchet JMJ. *J Polym Sci A Polym Chem* 2002;40:2719 [2]. Copyright John Wiley and Sons.

rotation angles, RU lengths, and terminal groups. The covalent assembly of these BC can take place in a symmetrical manner, as in dendrimers, or into random irregular patterns for hyperbranched polymers. The size,

shape, and functionality of the dendritic species depend on the synthetic strategy employed and can be different for each generation and/or each subclass of dendritic species.

The unique architecture of dendritic polymers affords distinct physical properties to these molecules as compared to their linear polymer analogues. For example, as shown in Figure 30.2, branched molecules have a much lower intrinsic viscosity than their linear analogues. Their compact and dense molecular configuration also leads to enhanced solubility at high molecular weights.

Some of the procedures used to synthesize dendritic molecules can be quite involved, and many different methods have been reported. The following three sections provide an overview of some of the pioneering work yielding each of the three main subclasses of dendritic polymers, namely, dendrimers, hyperbranched polymers, and dendrigraft polymers. The general characteristics and properties of these materials are also considered, as well as some of the more recent work including potential applications for these extremely versatile materials.

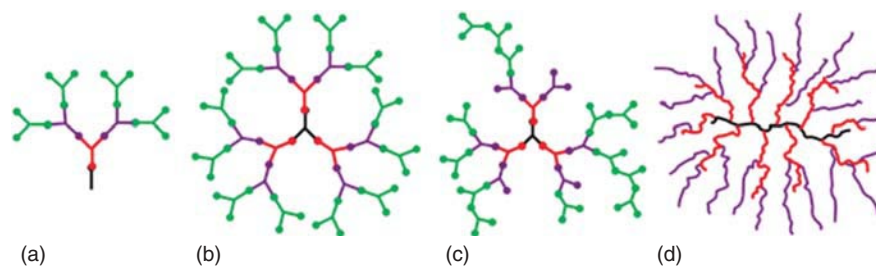


Figure 30.1 Structure of four types of dendritic polymers: (a) dendron, (b) dendrimer, (c) hyperbranched polymer, and (d) dendrigraft polymer. (See insert for the color representation of the figure.)

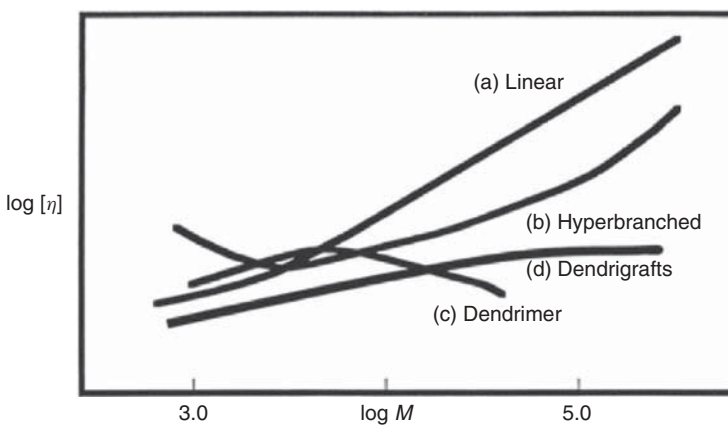


Figure 30.2 Molecular weight dependence of intrinsic viscosity $[\eta]$ for polymers with (a) linear, (b) hyperbranched, (c) dendrimer, and (d) dendrigraft architectures. Source: Reproduced with permission from Tomalia DA, Fréchet JMJ. Introduction to the dendritic state. In: Tomalia DA, Fréchet JMJ, editors. *Dendrimers and Other Dendritic Polymers*. West Sussex: Wiley; 2001. p 3 [14]. Copyright 2001 John Wiley and Sons.

30.2 DENDRIMERS

The word *dendrimer* is derived from the Greek words for tree- or branchlike (*dendron*) and part (*meros*). The strictly controlled structure of ideal dendrimers results from the layered assembly of BC surrounding the core, which is attained through sequential reaction cycles. This can be achieved in two different ways, namely, by divergent (core-first) or convergent (arm-first/core-last) methods.

30.2.1 Synthetic Strategies and Properties

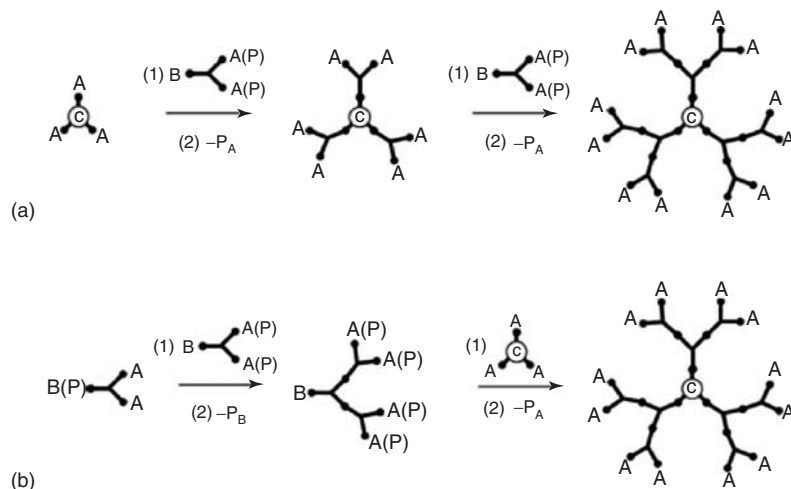
The divergent approach begins with a multifunctional core onto which polyfunctional monomers of the AB_n -type are added. Dendrimers result when the branching multiplicity (subscript n) of the monomer unit is at least 2. Following the addition of these small-molecule building blocks, the subsequent layer can be added after deprotection of the end groups and another monomer condensation reaction. The structure resulting after the first addition cycle is known as a *generation 1 (G1) dendrimer*. Further reaction cycles are employed to prepare dendrimers of the desired generation, size, or molecular weight.

The convergent approach uses monomers similar to the divergent strategy and provides branched molecules with the same characteristics and predictability; however, wedgelike dendrons are first synthesized and subsequently anchored on a core to complete the dendritic structure. The number of dendrons that can be coupled with a core is governed by the core functionality. Convergent growth of the dendron occurs through selective protection of one of the functional groups, followed by a condensation reaction, resulting in directional growth. The dendron unit is interesting in itself, and it has been investigated as its own entity, but deprotection and coupling with a multifunctional “anchor” core is required to complete the dendrimer structure.

A comparison of the divergent and convergent strategies for the synthesis of a generation 2 (G2) dendrimer is provided in Scheme 30.1, where functionality A selectively reacts with functionality B, and P represents a protecting group for the associated functional group.

The divergent synthesis (Scheme 30.1a) begins with an unprotected trifunctional initiating core ($N_c = 3$). The G0 core can be coupled with a partially protected monomer, $BA_2(P)_2$, having a branching multiplicity (N_b) of 2. The G1 dendrimer results after removal of the protecting group on the A functionality (- P_A). Coupling of this substrate with the protected monomer yields what is referred to as a *half-generation dendrimer* (G1.5), and the G2 dendrimer is obtained on deprotection. The convergent synthesis starts by coupling a partially protected monomer, $B(P)A_2$, with a complementary protected monomer, $BA_2(P)_2$, to yield a dendron. Deprotection of the B group (- P_B) at the focal point of the dendron allows selective coupling with the G0 core (A_3) to obtain the G1.5 dendrimer. Deprotection of the terminal A functionalities provides the G2 dendrimer. Specific details on the chemistry for the functionalization, condensation, and protection processes are discussed subsequently.

The radial core-to-surface direction of the synthesis for the divergent strategy and surface-to-core direction for the convergent method should yield identical architectures, albeit some differences in properties have been observed for molecules obtained by both methods and deemed to have identical compositions. This can be explained in terms of the degree of structural perfection attained in each case. The divergent strategy requires the reaction of an exponentially increasing number of functional groups over successive generations. Considering the large number of reactions required for the complete conversion of all terminal groups, the probability of attaining a perfect structure is reduced.



Scheme 30.1 Synthesis of a G2 dendrimer by (a) divergent and (b) convergent strategies.

This contrasts with the small number of coupling reactions involved in each cycle of a convergent synthesis. A lower degree of surface congestion also exists for the synthesis of individual dendrons, which favors complete reactions.

While the convergent strategy facilitates monomer coupling for upper generations independently of surface packing, the coupling of large dendrons to the anchor core is also more difficult due to steric hindrance making the focal point less accessible. Reduced coupling efficiency of the dendrons with the core has a more profound effect on the homogeneity of the dendritic species generated as compared to a reduced coupling efficiency for small-molecule monomers on the periphery of dendrimer in a divergent approach. The extent of surface congestion by terminal dendrimer groups can be estimated from the ratio of the dendrimer surface area (A_D) to the number of surface groups (Z) according to Equation 30.1, corresponding the surface area occupied per end group (A_z):

$$A_z = \frac{A_D}{Z} = \frac{4\pi r^2}{N_c N_b^G} \quad (30.1)$$

The generation at which the area available per end group approaches the actual dimensions of the end group is the point where incomplete reactions should become significant, resulting in an imperfect structure. This dense or critical packing state was predicted by de Gennes for polyamidoamine (PAMAM) dendrimers [4]. It was thus predicted that the onset of deviation in molecular weight from the ideal structure would occur around generation 9 or 10 for dendrimers, while molecular weight deviations were experimentally observed for generations as low as 4, but these nonetheless became more predominant from generations 9 or 10 as expected. Surface crowding effects and surface functionalization can play important roles in the application of dendrimers as scaffolds or containers: for example, a densely packed surface may inhibit loading of the dendrimer and rather favor surface coordination. Conversely, the flexible and more open structure of lower generation dendrimers should enhance their ability to house materials within their interior.

30.2.2 General Characteristics

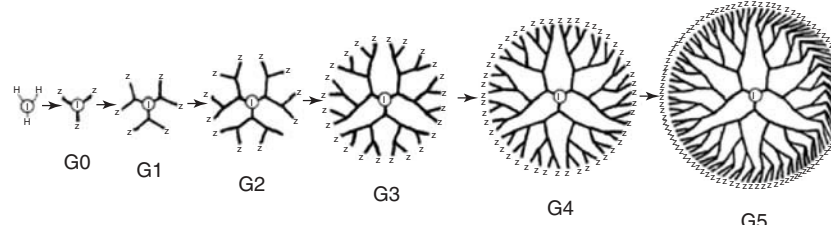
The size, shape, and molecular weight of a dendrimer depend on the molecular weight and the branching multiplicity of the monomer, as well as its generation number. Molecular weights can range from the hundreds or thousands for low generations, to over 10^5 for generations 10 and above. The corresponding diameter of these structures ranges from circa 1 to above 10 nm. Different generations of dendrimers derived from a trifunctional core are compared in Scheme 30.2.

The three-dimensional topology of dendrimers displays a transition from ellipsoidal to spherical for increasing generations [16]. The onset of the morphogenesis is reliant on the core multiplicity and the synthetic strategy (divergent or convergent) used. Increased core multiplicity ($N_c = 3$ or 4 vs $N_c = 2$) forces a shape change at least one generation earlier. The convergent method has a similar effect due to the more perfect structure (increased crowding) attained for a particular generation. The most significant transformations occur between generations 3 and 5, after which the dendritic species adopt either spheroidal or slightly ellipsoidal geometries. An increase in generation number also brings enhanced surface group congestion, until a maximum known as the *dense packing state* is reached. Beyond this point, only a fraction of the end groups can participate in the next cycle of monomer addition.

Targeting a specific molecular weight and number of functional groups in dendrimer synthesis is relatively easy due to the uniform structure of the molecules, in as much as complete reactions are possible. The molecular weight (MW) and the number of terminal functional groups (Z) of dendrimers are well-defined functions of the core multiplicity (branching functionality N_c), the branch cell multiplicity (N_b), and the generation number (G) of the molecules. The number of functional groups can be calculated according to the following equation:

$$Z = N_c N_b^G \quad (30.2)$$

The number of end groups is directly related to the number of covalent bonds formed in each reaction cycle,



Scheme 30.2 Dendrimer generations derived from a trifunctional core and a monomer with a branching multiplicity of 2. *Source:* Reproduced with permission from Tomalia DA, Berry V, Hall M, Hedstrand DM. *Macromolecules* 1987;20:1164 [15]. Copyright 1987 American Chemical Society.

which increases according to the power law. The total number of BC in the structure can be calculated from Equation 30.3. The total number of BC is analogous to the degree of polymerization (DP) commonly cited for linear polymers and is also equivalent to the number of covalent bonds formed in the dendrimer:

$$BC = N_c \left[\frac{N_b^G - 1}{N_b - 1} \right] \quad (30.3)$$

The overall molecular weight of the dendrimer can be calculated by factoring in the molar mass of the various components including the core (M_c), repeat units (M_{RU}), and terminal groups (M_Z), as expressed in the following equation:

$$MW = M_c + N_c \left[M_{RU} \left(\frac{N_b^G - 1}{N_b - 1} \right) + M_Z N_b^G \right] \quad (30.4)$$

30.2.3 Common Structures

30.2.3.1 Dendrimers Synthesized by a Divergent Strategy The concept of branched macromolecules derived from repetitive reaction cycles of multifunctional small molecules was first introduced in 1978 [1]. Vögtle thus reported a cascade-type divergent synthesis for low molecular weight polypropylenimine by the cyanoethylation of various amines cited in Reference 1, using acrylonitrile in glacial acetic acid at reflux for 24 h. Subsequent reduction of the cyano functionalities with cobalt(II) chloride hexahydrate and NaBH_4 in methanol converted the terminal cyanoethyl groups to primary propylamine functionalities, which were subjected to further cyanoethylation and reduction reactions to obtain the upper generation cascade polymers.

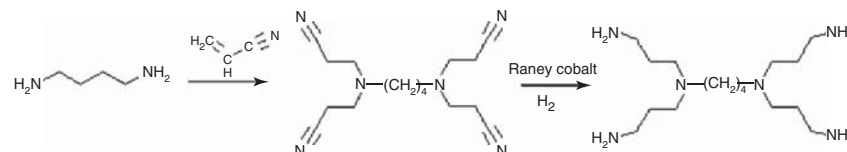
The yield of the cyanoethylation and reduction reactions in Vögtle's work was less than ideal, varying from 76% for the zeroth generation to 35% for the G1 product. These low yields resulted in ill-defined structures and prevented the synthesis of the upper generation structures. This procedure was nevertheless improved upon in the early 1990s after optimizing the cyanoethylation and hydrogenation reactions, by working in aqueous solutions at 80 °C and through hydrogenation with Raney cobalt, respectively [17, 18]. In this case, diaminobutane (DAB) served as multifunctional core to generate DAB-*dendr*-(CN)_x and

DAB-*dendr*-(NH₂)_x dendrimers after the cyanoethylation and hydrogenation reactions, respectively. The reaction sequence for the divergent synthesis of polypropylenimine dendrimers is shown in Scheme 30.3.

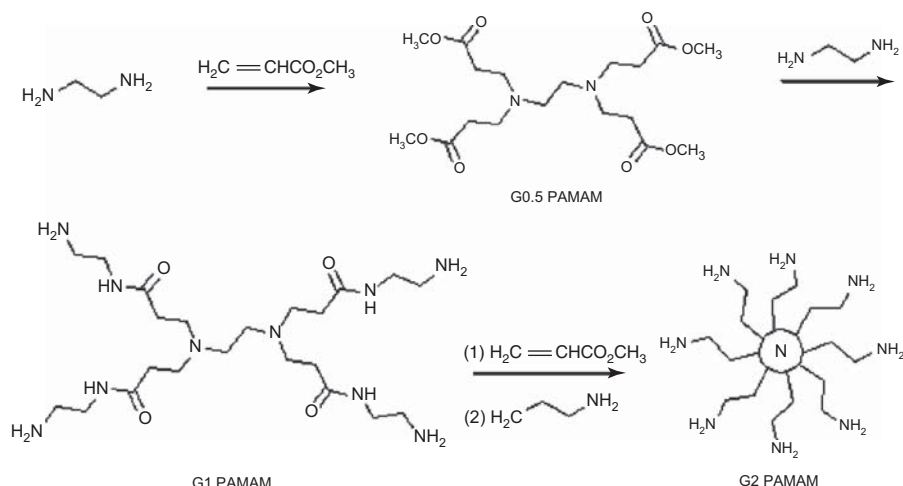
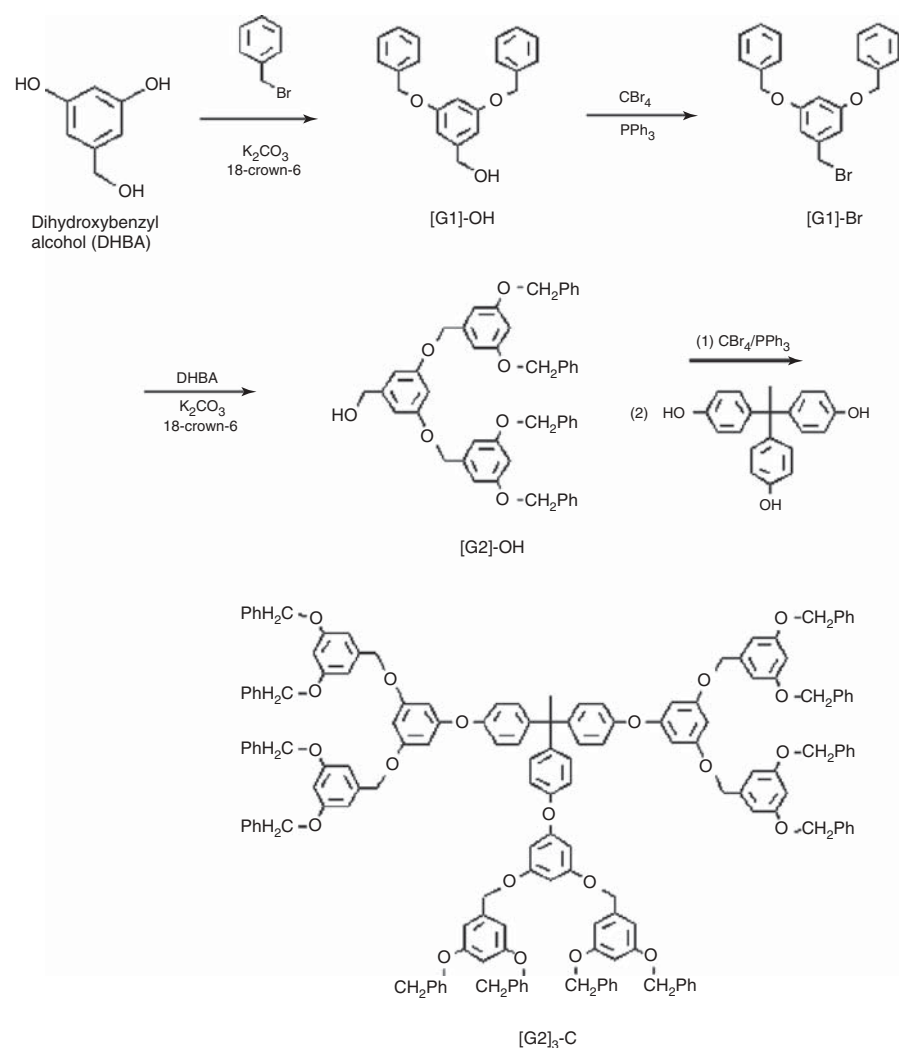
PAMAM dendrimers, synthesized subsequently, are likely the most widely investigated and used dendritic polymers to date. The first dendrimers commercialized in that family were the Starburst® systems. These species were developed in the mid-1980s by Tomalia [5], at about the same time when Newkome developed similar dendritic architectures named *Arborols* [6]. A major incentive for the development of these molecules was the creation of covalently bonded (unimolecular) micelles comparable to the well-known multi- or intermolecular micellar systems.

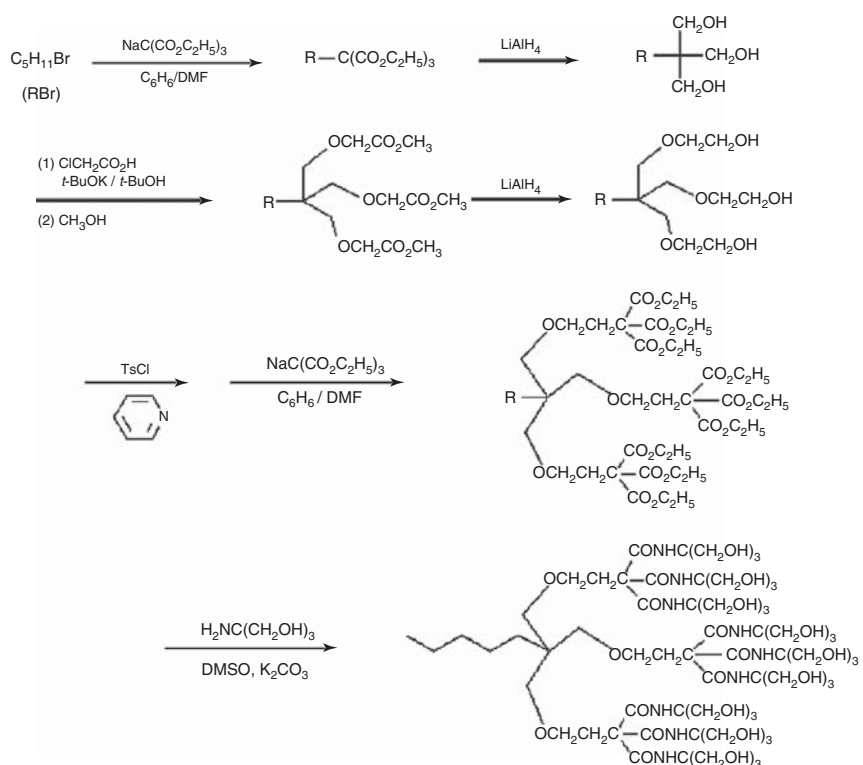
PAMAM dendrimers are versatile in that their terminal groups can be easily modified for targeted functionality or reactivity. These compounds are synthesized by the condensation of amines and acrylates. An initiating core containing one or more amine functionalities is first reacted with an excess of methyl acrylate, resulting in an alkyl ester branch addition at each amino hydrogen (Scheme 30.4). This ester-terminated product is referred to as the *G0.5 dendrimer*. Amidation of the ester with ethylenediamine (EDA) causes branch extension with terminal amino groups. This amine-terminated dendrimer is referred to as a *G1 PAMAM dendrimer*. Repetitive cycles of Michael addition of the acrylate ester and amidation with EDA leads to successive generations of dendrimers. Functional group modification chemistry can also be performed on the terminal ester or amine groups. Thus, the treatment of the half-generation (ester-terminated) PAMAM dendrimers with alkali metal hydroxides yields carboxylate functionalities.

30.2.3.2 Dendrimers Synthesized by a Convergent Strategy Hawker and Fréchet [7] made a major contribution to the dendritic polymer chemistry field by developing a convergent approach to dendrimer synthesis in 1990. Dendritic fragments (dendrons) of benzyl ether were thus created by coupling phenols with benzylic halides. This approach represents a surface-to-core method, where the monomers are assembled from the peripheral units toward the core. Benzyl bromide was first coupled with dihydroxybenzyl alcohol (DHBA) in the presence of potassium carbonate and 18-crown-6 as a phase transfer catalyst in acetone as shown in Scheme 30.5. Following isolation and purification of the product, the



Scheme 30.3 Preparation of polypropylenimine dendrimers.

**Scheme 30.4** Divergent PAMAM dendrimer synthesis starting from a diamine (EDA) core.**Scheme 30.5** Synthesis of a Fréchet-type benzyl ether dendrimer by a convergent approach.



Scheme 30.6 Arborol synthesis according to Newkome.

G1 dendritic benzyl alcohol was converted to a benzylic bromide by treatment with carbon tetrabromide and triphenylphosphine. Further cycles of DHBA monomer coupling were performed to obtain subsequent dendron generations. To obtain a symmetrical dendrimer, the dendritic wedges carrying a bromide functionality at their focal point can be coupled with a polyfunctional core such as 1,1,1-tris(4'-hydroxyphenyl)ethane.

A convergent strategy such as this, with only one final coupling step for the dendron wedges, facilitates high yield reactions leading to well-defined structures. The symmetry of the molecules can be controlled through the functionality of the anchoring core.

In fact Newkome was really the first one to report a convergent dendron synthesis for the preparation of arborols, but the generation number and the molecular weight attained were limited [6]. The synthesis of arborols started from a trifunctional branch cell formed by treating an alkyl halide with triethyl sodium methanetricarboxylate. Subsequent reduction of the ester with LiAlH₄ yielded a triol. The formation of the second tier through another cycle of esterification was attempted by tosylation with tosyl chloride in pyridine and treatment with the methylsodium triester, but the yield was very low due to inefficient nucleophilic attack at the three terminal sites as a result of steric crowding. To solve this issue, extension of the ester was performed before tosylation and coupling with the methylsodium triester

to afford the nonaester. The third generation of this cascade molecule, obtained through amide functionalization with tris(hydroxymethyl)aminomethane, was completely water soluble. The reaction scheme for Newkome's synthesis of a 27-arm arborol is shown in Scheme 30.6.

30.2.4 Applications and Recent Trends

Considering the extensive control achieved over the size, shape, and surface functionality of dendrimers, it is not surprising that these molecules have a wide range of potential applications. On examination of the structural features of a dendrimer, one can visualize sector-specific uses as shown in Figure 30.3.

The first application examined, and one of the primary motivations for dendrimer syntheses, was as unimolecular micelles. In contrast to common micellar structures formed through intermolecular association or aggregation, dendrimers are covalently bonded structures unaffected by their surrounding environment. Consequently, the ability of amphiphilic dendrimers to encapsulate guest compounds should be independent of changes in concentration, solvent, and pH, among others. A strong incentive for dendrimer micelles is in catalysis. Considering the structure and functionality control attained, catalytic sites can be introduced specifically within the core, on the periphery of dendrimers, or both, as illustrated in Figure 30.4.

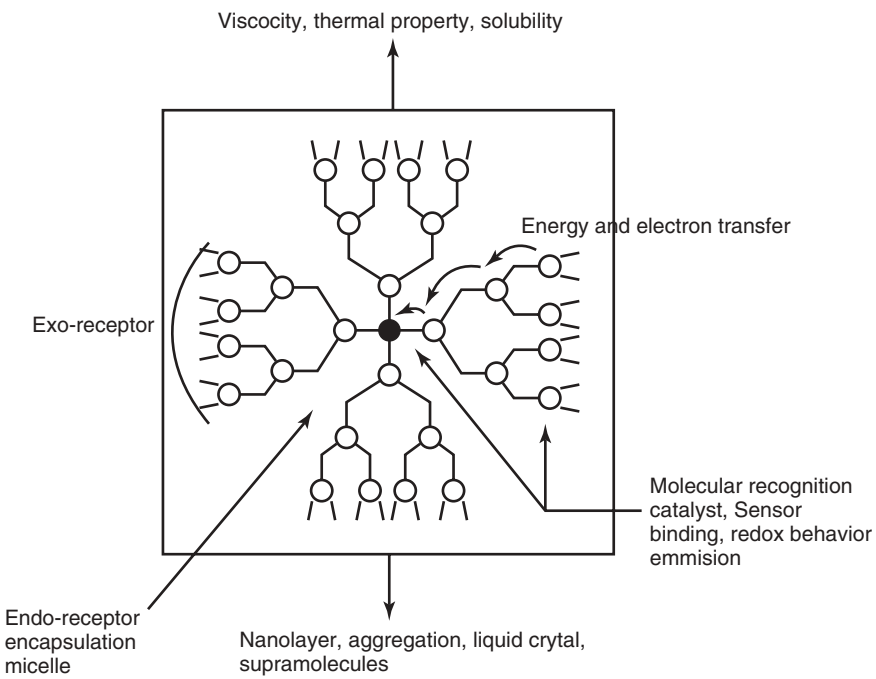


Figure 30.3 Structural features and potential uses of dendrimers. *Source:* Reproduced with permission from Inoue K. *Prog Polym Sci* 2000;25:453 [19]. Copyright 2000 Elsevier.

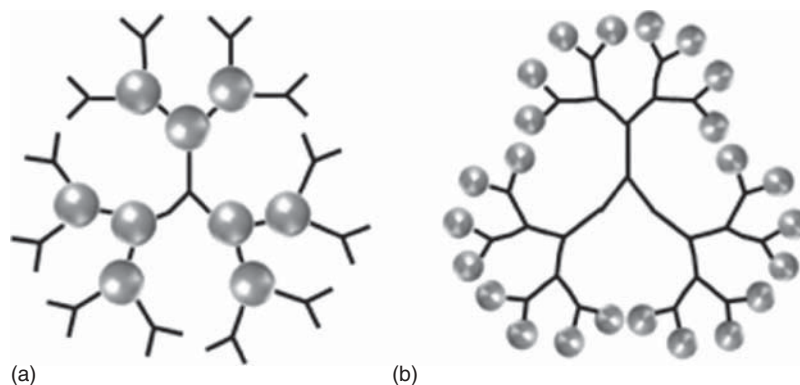


Figure 30.4 (a) Internal and (b) peripheral dendrimer functionalization.

The preparation of metalodendrimers, incorporating metallic species within their structure, is a relatively facile process given the ease and versatility of dendrimer functionalization which can be tailored for metal coordination. For example, the PAMAM dendrimers discussed earlier can coordinate different transition metals through their nitrogen atoms. Metals able to coordinate with the PAMAM structure include among others Cu [20, 21], Au [22], Pd [23], Pt [24], Ag [25], Co [26], as well as bimetallic systems such as Pd–Au [27] and Pt–Ru [28]. Dendritic catalyst selectivity, activity, and stability can vary on the basis of steric effects, the location of the catalyst, and the architecture of the dendritic support [29, 30].

Coronal functionalization of the dendrimers with metals is typically performed by a divergent approach, that is, with the metal binding process occurring in the final step. Catalysis on the periphery of dendrimers provides easily accessible sites; however, steric crowding of the reactants can influence the activity level observed. In theory, such a system should have a performance comparable to homogeneous (nonsupported) systems [31]. A higher loading level (catalyst/dendrimer) is possible with peripheral loading, as there is a larger number of terminal groups as compared to junctions within the dendrimer skeleton; however, core-functionalized metalodendrimers offer isolated catalytic sites that can be attractive for

certain applications. In many cases, the reduction of the noble metal salts is necessary after loading into the dendrimer. Alternately, the reduction of surface-bound metals could result in encasement of the dendritic structure, and potentially eliminate some of the inherent benefits that the core may have, or create a barrier to core loading. Careful selection of the surface functionality and the degree of functionality are critical. In both core- and periphery-functionalized metallocendrimers, isolation of the catalyst from the crude product is conveniently achieved by nanofiltration. Several reviews have been published on this topic [31, 32].

Examples of peripherally functionalized catalysts include carbosilane dendrimers with Ni at their peripheral functional sites serving in the Kharasch addition of polyhalogenoalkanes to terminal carbon–carbon double bonds, which displayed regioselectivity [33]. Polypropylenimine dendrimers have likewise been end-functionalized with palladium, rhodium, iridium, and Pd–Ni bimetallic catalysts for use in the Heck reaction and hydroformylation [34]. PAMAM dendrimers supported on silica were complexed with rhodium for heterogeneous catalysis in the hydroformylation of styrene and various other olefins. The highly active catalyst yielded branched chain aldehydes with high selectivity from aryl olefins and vinyl esters. The catalyst was easily recovered, and no significant loss in selectivity or activity was observed on reuse [35].

Core-functionalized metallocendrimer catalysts are sometimes referred to as *dendrymes* by analogy to biological systems and due to the observed influence of the generation number on selectivity. Ferrocenylphosphine core-functionalized carbosilane dendrimers have thus been prepared as Pd ligands for the homogeneous catalysis of allylic alkylation reactions, and displayed variations in product selectivity for the largest dendrimers investigated [36]. Fréchet-type polyether dendrons were complexed with Pt for use as SO₂ sensor and with Ni for the Kharasch addition of CCl₄ to methyl methacrylate [37]. The dendron wedges, when functionalized at their focal point, displayed adequate catalytic activity with easy recovery and good stability.

Mimicking biological species is a major investigation area for dendrimers, particularly for PAMAM-based structures due to their similarities in size, shape, and chemical make-up with globular proteins. Thus, the immunodiagnostic capabilities of dendrimers have been investigated [38], as well as *in vitro* and *in vivo* gene delivery [39] and gene expression [40]. These species possess an exterior barrier controlled through end-group functionalization, as well as void spaces within their interior, much like liposomes. The tailored unimolecular micelle characteristics of dendrimers, with an open interior (in contrast to typical micelles), allows them to entrap guest molecules of various sizes and to selectively release them under certain conditions [41]. These

characteristics have led to the development of macromolecular drug delivery systems from dendrimers. In analogy to other complexation processes, drug molecules can be loaded inside or attached at the periphery of the molecules, to form dendrimer–drug conjugates. In the latter category, it has been demonstrated that PAMAM dendrimer–platinate conjugates have antitumor activity [42]. More recently, it was shown that the encapsulation or complexation of camptothecin (a plant alkaloid known for its anticancer potency) with PAMAM dendrimers increased its solubility, which represents a step toward the effective delivery of this drug to cancerous cells [43]. PAMAM dendrimer–glucosamine conjugates have even been shown to prevent scar tissue formation [44]. Lastly, dendrimers have been investigated for light-harvesting applications [45]. Their branched architecture provides an interesting framework in which energy transfer can occur from peripheral chromophores to an energy sink located at the core of the molecules. This property can be exploited in light-emitting diodes, frequency converters, fluorescent sensors, or as a mimic for the natural photosynthesis process.

30.3 HYPERBRANCHED POLYMERS

Hyperbranched polymers also possess a dendritic architecture, but with imperfect branching. The basic structural features present in these molecules are the same as in dendrimers, namely, a core surrounded by layers of BC capped with terminal units. The one-pot syntheses used to create these treelike structures also rely upon AB_n-type monomers (Scheme 30.1), but without protecting groups preventing simultaneous condensation reactions. The resulting polymers typically have broad MWD ($D > 2$), with multiple isomers and geometries. Because they are created in a single reaction step, hyperbranched polymers are more economical to produce than dendrimers as their synthesis is less time and resource intensive. This trait represents a major draw for industry and the development of commercial applications for dendritic polymers

30.3.1 General Features

Many methods have been reported to synthesize hyperbranched polymers. These materials were first reported in the late 1980s and early 1990s by Odian and Tomalia [9], Kim and Webster [10], and Hawker and Fréchet [11]. As early as 1952, Flory actually developed a model for the polymerization of AB_n-type monomers and the branched structures that would result, identified as random AB_n polycondensates [46]. Condensation step-growth polymerization is likely the most commonly used approach; however, it is not the only method reported for the synthesis of statistically branched dendritic polymers: chain growth and ring-opening polymerization methods have also been applied,

among others. In a one-pot (or concurrent) method, the monomers simply add in alternate manners into patterns that can be modeled statistically. Structures can be grown in the presence or the absence of a central core, as illustrated in Scheme 30.7 for a simplified system.

Ideally no intermolecular reactions should occur between the branched structures, but this is difficult to avoid in many cases and is a drawback to this method. For such an ideal (and simplified) case with an AB_2 -type monomer, the branching coefficient (α), representing the probability that a branch unit has reacted, and is thus connected to another branch unit, is equal to the fraction of B groups reacted (p_B), if it is assumed that the two B moieties are equally reactive. The probability or fraction of A groups having reacted (p_A) can then be considered to represent the extent of reaction, which leads to the relation between the extent of reaction (p), the branching coefficient (α), and the functionality of the AB_x monomer (f) given by the following equation [46]:

$$\alpha = p_B \text{ and } p_A = p_b (f - 1); \text{ therefore,}$$

$$\alpha = \frac{p_A}{f - 1} = \frac{p}{f - 1} \quad (30.5)$$

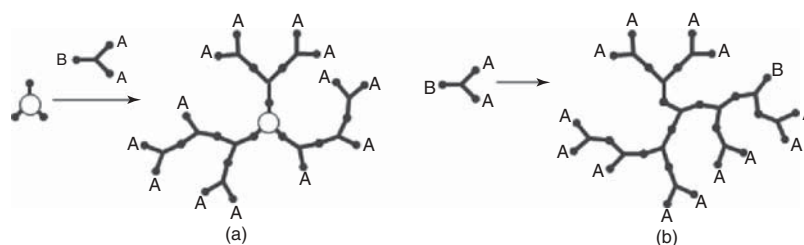
Fréchet proposed to use the ratio of the number of fully branched monomer units to the total number of monomer units contained within the polymer (N_0) to describe the degree of structural perfection of hyperbranched polymers

derived from AB_2 -type monomers [11]. In a dendrimer with a perfect structure, two types of monomer units are present in equal proportions, the terminal (T) and the dendritic (D) units, and thus the degree of branching is equal to 1. In a hyperbranched structure, some of the dendritic units are unreacted, leading to the formation of a third monomer unit described as a linear (L) segment. The degree of branching (α_{Fr}) attained under these conditions can be expressed by Equation 30.6, where D , T , and L represent the total number of each type of unit:

$$\alpha_{\text{Fr}} = \frac{D + T}{D + T + L} = \frac{D + T}{N_0} \quad (30.6)$$

The different types of dendritic monomer units are shown in Figure 30.5, where the dendrimer (Fig. 30.5a) contains three dendritic and six terminal groups, while the hyperbranched structure (Fig. 30.5b) has two dendritic, three linear, and five terminal units, yielding branching functionalities (as defined by Fréchet [11]) of 1 and 0.7, respectively.

The relative amounts of each of the three types of monomer units can, in some cases, be determined by NMR analysis or by other spectroscopic methods. In situations where the units cannot be differentiated by these methods, selective labeling and/or degradation can be performed, followed by spectroscopic analysis. It should be noted that Equation 30.6 does not tend toward zero for linear polymers as it should. This discrepancy prompted the development



Scheme 30.7 (a) Core and (b) noncore methods for the synthesis of hyperbranched polymers.

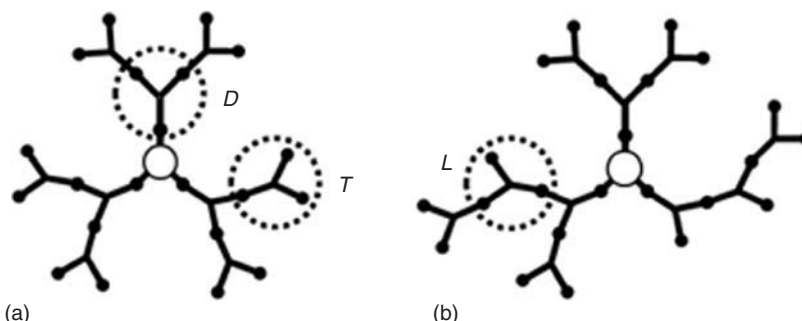


Figure 30.5 Structural units in a dendrimer (a, $\alpha_{\text{Fr}} = 1$) and a hyperbranched polymer (b, $\alpha_{\text{Fr}} = 0.7$): dendritic (D), linear (L), and terminal (T).

of a corrected expression for branching functionality (α' , Eq. 30.7) by two different groups in 1997 [47, 48]. Expressions for the universal degree of branching were also derived for higher order functionalities and can be found in the respective references:

$$\alpha' = \frac{2D}{2D + L} \quad (30.7)$$

In his original 1952 article [46], Flory also predicted the influence of branching on the DP and molecular weight dispersity, as shown in the following equation, which is derived from Equation 30.5:

$$D = \frac{X_w}{X_n} = \frac{1 - \alpha^2(f - 1)}{1 - \alpha(f - 1)} \quad (30.8)$$

It is apparent that the breadth of the MWD is highly dependent on the extent of reaction (conversion) attained in these reactions, as D increases with the conversion. At low conversions, the MWD for an AB_n system corresponds to a Flory distribution ($D \approx 2$); however, D trends toward infinity as full conversion is approached. For trifunctional monomers, including equally reactive A_3 monomers and ABC monomers with reactivity differentials, the MWD also depends on the DP but in a different way: D is proportional to DP in an A_3 system, while for an ABC system it is proportional to $(DP)^{1/2}$ [49, 50].

Unfortunately, the one-pot reaction scheme for the preparation of hyperbranched polymers offers no option for molecular weight control, which ultimately leads to gelation. Intramolecular side reactions such as cyclization resulting from “backbiting” processes are also common in these reactions. One technique developed to avoid or reduce side reactions uses a slow monomer addition protocol, by adding monomer throughout the reaction. This method has been termed *concurrent slow addition* [51–53]. The copolymerization of AB monomers with AB_2 monomers has also been employed to control the molecular weight and reduce D in these reactions [51, 54]. Multifunctional initiators (B_y monomers), when used in batchwise or concurrent slow addition protocols, have also shown promise in controlling the breadth of the MWD [55, 56].

30.3.2 Synthetic Strategies and Common Structures

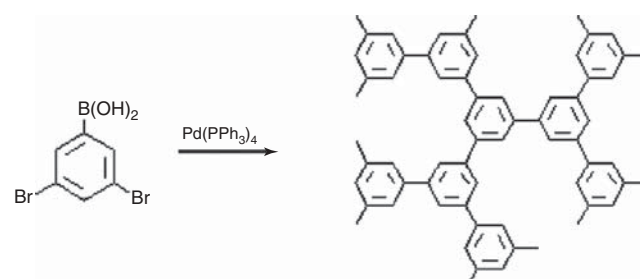
Hyperbranched polymers can be synthesized by either single- or double-monomer methods. Falling in the single-monomer methodology (SMM) are common polymerization techniques including the polycondensation of AB_n monomers, self-condensing vinyl polymerization (SCVP), self-condensing ring-opening polymerization (SCROP),

and proton-transfer polymerization (PTP). The double-monomer methodology (DMM), as the name suggests, relies on monomer pairs that can be subdivided into two strategies: $A_2 + B_3$ reactions, and the couple-monomer methodology (CMM). Many combinations of compatible monomers have been successfully applied to these strategies. Considering the broad scope of this topic, only a few examples of the pioneering work and some of the simpler methods are provided for the different strategies. A more detailed review on synthetic strategies for the preparation of hyperbranched polymers was provided by Gao and Yan [57].

30.3.2.1 Single-Monomer Methodology Kim and Webster reported the first example of a single-monomer polycondensation technique using 3,5-dibromophenylboronic acid and aqueous sodium carbonate in the presence of a Pd catalyst [10]. A general scheme corresponding to this reaction and the resulting hyperbranched structure obtained are shown in Scheme 30.8.

The single-monomer polycondensation scheme has also been used to synthesize hyperbranched polyethers [58], polyesters [59], polyurethanes [60], polysiloxanes [61], as well as polycarbonates [62]. Higher order monomers including AB_3 , AB_4 , AB_5 , and AB_6 have also been applied in single-monomer polycondensation syntheses of hyperbranched polymers [63, 64].

SCVP requires a monomer not only with a vinyl group but also with a pendant moiety that can act as an initiating site for other vinyl pendants. This type of monomer is referred to as an *inimer* (initiator + monomer). Fréchet developed both free radical [65] and cationic [66] SCVP methods for the synthesis of hyperbranched molecules using inimers. These techniques all depend upon the same principle: new initiating species are formed from a specific functionality within the inimer molecules. Once activated, this site can propagate through vinyl groups on other monomers or inimers. As propagation continues, macromonomers formed from inimers in the reaction eventually react with the propagating center, resulting in branching.



Scheme 30.8 Hyperbranched polyphenylene synthesis by the single-monomer polycondensation method.

In Fréchet's cationic method, 3-(1-chloroethyl)-ethenylbenzene is activated with SnCl_4 to yield a cationic initiating site from the chloroethyl functionality. This site can propagate through vinyl-containing species, producing chains with pendant initiating sites that form branches once they become active and participate in chain propagation. Similar reaction sequences are involved in the radical systems, for example, with a styrenic inimer containing a benzylic nitroxide functionality [65]. In this case, the hyperbranching process begins with the thermolysis of the benzylic nitroxide, producing radical species that propagate through the pendant vinyl group of the styrene moieties. Residual nitroxides can also cleave along the polymer backbone to form radical sites and propagate branch growth. The cationic and radical hyperbranching processes are illustrated in Scheme 30.9a and b, respectively.

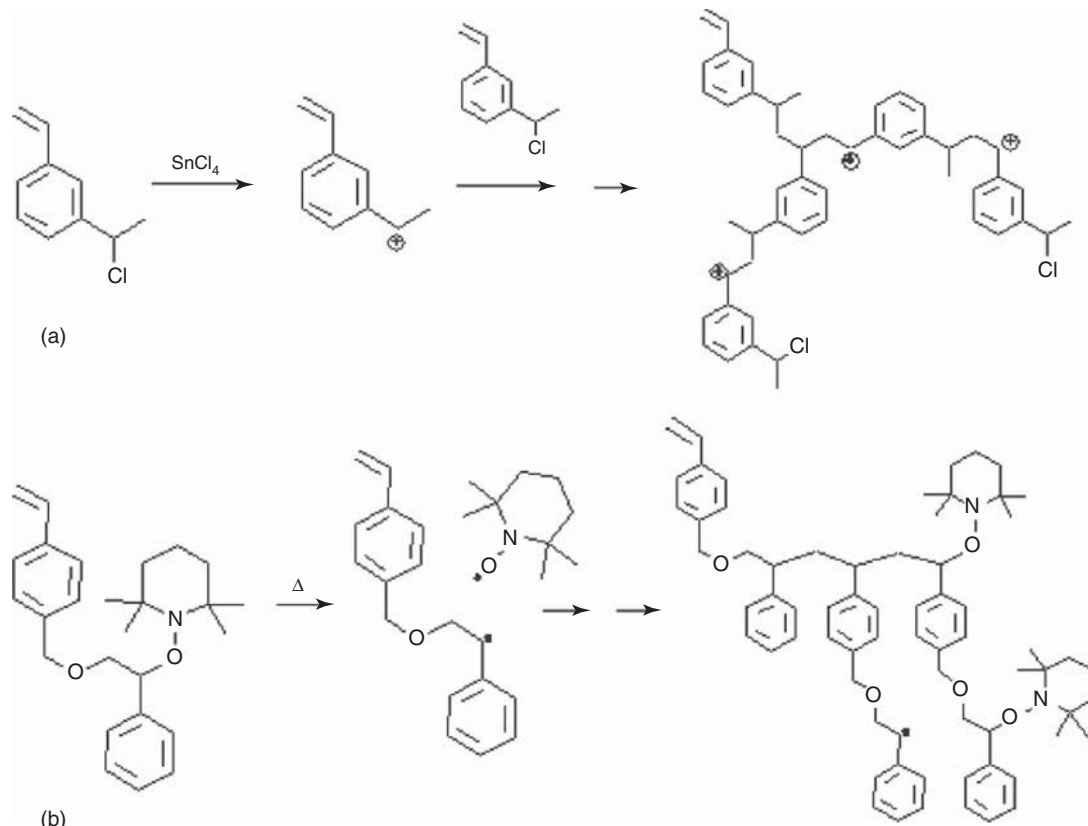
The degree of branching attained in SCVP reactions is governed by the reactivity difference between chain growth through the vinyl groups and step growth addition at the initiating site. In some cases, the degree of branching attained can be controlled by adjusting the reaction conditions used. The radical SCVP procedure requires additional considerations, however, since side reactions leading to gelation are more probable at longer reaction times.

Polymerization by the inimer technology has received much attention from Kennedy and Puskas, specifically for the synthesis of hyperbranched polyisobutylenes (PIB)s and copolymers thereof in a one-pot method [67]. While this convergent approach complicates the structural analysis of the branched polymers, fragmentation of the resulting polymer is possible in some cases to allow such analysis [68]. Branching ratios (BR) can be calculated directly from the molecular weight of the branched polymer as per Equation 30.9, to give an indication of the number of branches contained within the molecules, as the ratio of the measured M_n for the polymer obtained to the theoretical M_n (M_n^{theo}).

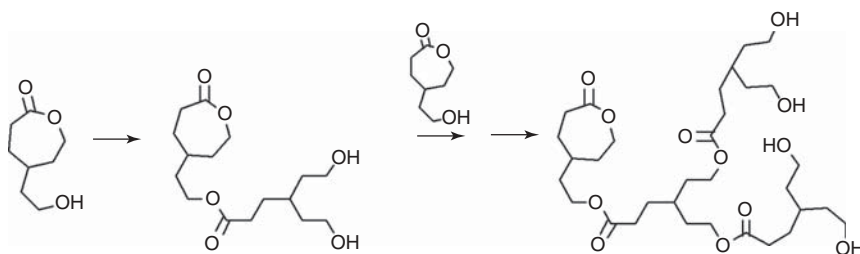
$$\text{BR} = \frac{M_n}{M_n^{\text{theo}}} - 1 \quad (30.9)$$

The theoretical M_n is calculated by assuming that all the inimer molecules in the reaction act solely as monofunctional initiator and not as a branching agent. This quantity is calculated from the mass of monomer (m_m) and the moles of inimer (n_i) in the reaction as described by the following equation:

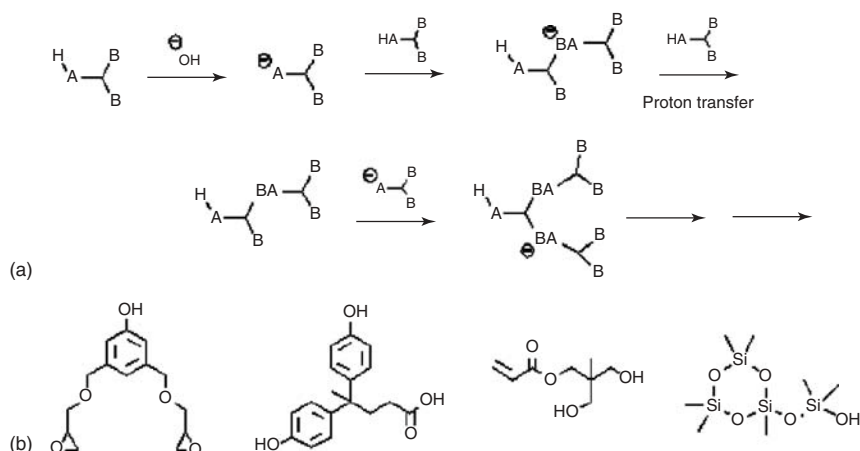
$$M_n^{\text{theo}} = \frac{m_m}{n_i} \quad (30.10)$$



Scheme 30.9 Formation of hyperbranched polymers by (a) cationic and (b) radical SCVP.



Scheme 30.10 SCROP of hydroxyl-functionalized caprolactone.



Scheme 30.11 (a) Generalized PTP synthetic scheme and (b) examples of monomers used in PTP syntheses.

SCROP and ring-opening multibranching polymerization (ROMBP) are similar to SCVP; however, in these cases, the inimer is a cyclic monomer carrying an initiating functionality. A good example of this approach is shown in Scheme 30.10, where hyperbranched polyesters are formed from inimers containing an alcohol functionality and a caprolactone group [69].

The dominant contribution of simultaneous chain growth from all the chain ends, controlled by the deprotonation level of the initiator, leads to relatively narrow MWD ($D \approx 1.1\text{--}1.4$) while maintaining branching levels typical of random polycondensation reactions (degree of branching $\alpha' \approx 0.5$, Eq. 30.7) [70]. The SCROP technique has also been used to synthesize hyperbranched polyglycerols [70], polyethers [71], and polyamines [72].

PTP, which began to gain momentum in the late 1990s, relies on a reaction sequence of the type shown in Scheme 30.11a, where a catalytic amount of initiator is added to the monomer for proton abstraction. Following coupling with another neutral monomer unit, a thermodynamically favorable proton-transfer reaction occurs from another free monomer unit to the dimer. The activated monomer can then couple with another monomer unit or with an existing branched species. The proton-transfer step

does not propagate to a significant extent as it is a kinetically slower process. Specific monomers that have been investigated for the PTP method are shown in Scheme 30.11b.

30.3.2.2 Double-Monomer Methodology The most versatile approach to hyperbranched polymer synthesis is likely the double-monomer methodology (DMM), due to the wide range of monomers and chemical functionalities to which it can be applied. The two categories of DMM reactions only differ in terms of the reactivity of the functional groups involved: in $A_2 + B_3$ reactions, all the moieties within each monomer have the same reactivity, while varying degrees of reactivity describe the couple-monomer methodology (CMM).

The chemistry behind the $A_2 + B_3$ method is analogous to the previously described AB_n reactions, but the compatible reactive sites are separated on two different monomers. A significant obstacle in this approach is the occurrence of gelation, commonly observed for the direct polycondensation of A_2 and B_3 monomers. This problem can be minimized through slow monomer addition, capping agents, reaction quenching by precipitation, or the addition of catalysts or condensation agents before reaching the critical conversion point. A few of the less exotic monomer combinations that have been used in $A_2 + B_3$ reactions are depicted in Figure 30.6. These examples include monomers

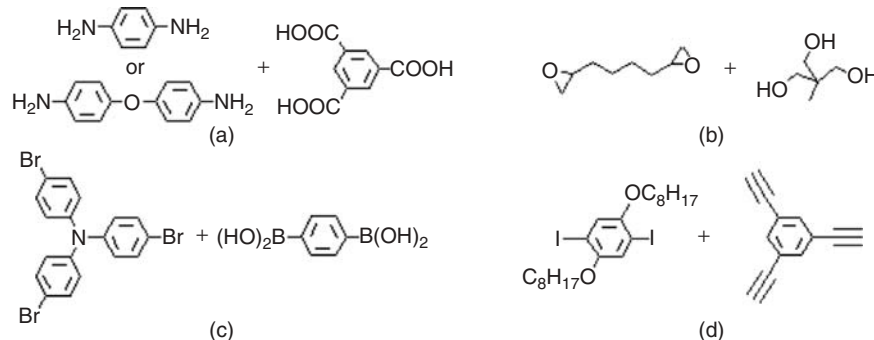


Figure 30.6 Examples of monomer combinations for the $A_2 + B_3$ double-monomer synthesis of hyperbranched polymers.

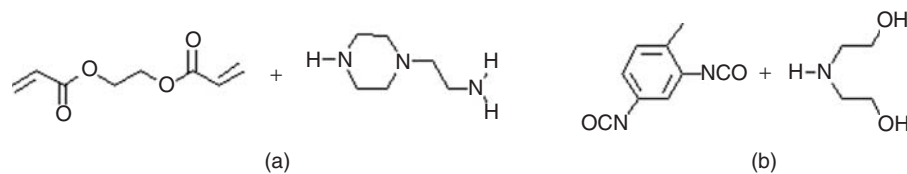


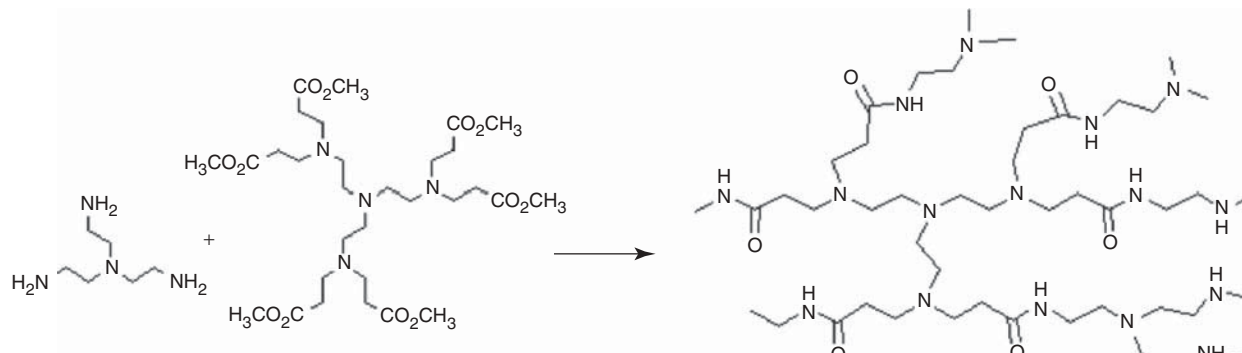
Figure 30.7 CMM monomers for (a) $A_2 + B' B_2$ and (b) $A_2 + CB_n$ reactions.

with the following chemical functionality combinations: aromatic diamine and triacid (Fig. 30.6a) [73], diepoxy and trihydroxy (Fig. 30.6b) [74], trisbromophenyl and diboronic acid, (Fig. 30.6c) [75], and diiodophenyl and triethynylphenyl (Fig. 30.6d) [76].

The CMM provides improved control over the branching process through reactivity tailoring, resulting in soluble (nongelled) hyperbranched polymers in most cases. Gelation can be avoided through careful monomer selection whereby the reactivity of the functional groups differs. Many different monomer combinations have been reported fulfilling this requirement, two of which are $A_2 + B' B_2$ and $A_2 + CB_n$ systems. In the first case, both A groups have the same chemistry and reactivity, and likewise for the B groups, however, B' has the same chemical make-up as B but differs in reactivity. In the $A_2 + CB_n$ system, the A groups and B groups have equivalent reactivity, but

C differs in chemical structure and reactivity. Examples of monomers corresponding to each of these CMM classes are provided in Figure 30.7.

The first example, Figure 30.7a, is an $A_2 + B' B_2$ system with two equally reactive vinyl groups (A_2) and three amine functionalities, where the tertiary amine is unreactive under the conditions used. The primary and secondary amines differ in terms of reactivity and are bi- and monofunctional, respectively ($B_2 B'$). In the $A_2 + CB_n$ case, Figure 30.7b, the isocyanate groups are considered to be equally reactive based on the CMM naming conventions (A_2), as are the hydroxyl groups (B_2), the third functional group being a secondary amine (C). Higher order functionalities have also been investigated. A hyperbranched analog of the commercially available PAMAM dendrimers (HYPAM) has thus been synthesized by a one-pot method shown in Scheme 30.12 [77]. This approach can be described as an



Scheme 30.12 Synthesis of hyperbranched PAMAM (HYPAM).

$A_6 + B_6$ reaction of tris(2-aminoethyl)amine with tris(2-di(methyl acrylate)aminoethyl)amine.

30.3.3 Applications and Recent Trends

The comparable architecture and chemical functionality of dendrimers and hyperbranched polymers lead to similar applications for these two families of dendritic polymers. The main benefit in using hyperbranched polymers to replace dendrimers lies in their simpler synthesis, provided that the perfect structure of dendrimers can be sacrificed for their broadly distributed hyperbranched analogs. The one-pot syntheses require less time and resources, resulting in less expensive processes that make hyperbranched polymers excellent candidates for commercial applications. Pertinent to the hyperbranched architecture are applications as electronic, magnetic, and catalytic materials, as well as numerous uses in the biomedical field; some of these are considered herein.

The incorporation of transition metals in hyperbranched polymers has received considerable attention. Like dendrimers, hyperbranched materials can be loaded with metals within their interior, on their exterior, or throughout the whole molecule, the exact location of the coordination sites depending on the functionality of the polymer, as shown previously in Figure 30.4. Salazar thus modified hyperbranched polyglycerol with hydroxyl end groups to a structure containing tertiary amines on its periphery [78]. The hyperbranched polyamines were coordinated with copper chloride and were successfully used as catalysts in the oxidative coupling reaction of phenylacetylene. Similarly, NCN-pincer platinum(II) carboxylates were complexed with hyperbranched polyglycerols to form endo-receptors to catalyze the coupling reaction of methyl vinyl ketone and ethyl α -isocyanopropionate by Michael addition [79, 80]. These systems displayed improved performance due to the enhanced accessibility of the catalytic sites and the high local reagent concentration; the catalysts could be isolated from the reaction product in high yield (>97%) by dialysis. Other mainstream hyperbranched polymers such as polyethylenimines [81] and PAMAMs [77] have also been used to stabilize various transition metals for catalytic applications. These molecules contain multiple metal-coordinating sites, both internal and peripheral, due to their high nitrogen content. The terminal primary amine groups of these polymers can also serve as functionalization sites to enhance the stability of the metal–polymer complexes under different solvency conditions. Thus, in the case of hyperbranched polyethylenimines, the aqueous solubility of the polymers loaded with transition metals (Cu, Ag, Au, and Pt) was ensured by encapsulating the structure with a carbohydrate shell [81].

The postpolymerization functionalization method to incorporate transition metals into hyperbranched polymer

structures can target the interior cavities and the functional groups of the molecules alike. One of the more exotic applications proposed for a metal-loaded hyperbranched polymer is a combination of a semiconductor polymer of conjugated poly(*p*-phenylenevinylene) (PPV) and colloidal semiconducting CdS nanocrystals at various locations within the structure [82]. This was accomplished by incorporating alkoxy substituents within the monomer before the hyperbranched polymer synthesis, to provide coordinating sites for cadmium. The deposition of cadmium within the branched structure increased the dispersion of the nanoparticles and reduced their aggregation within the PPV-CdS hybrid, in addition to providing efficient energy transfer. The unique photochemical activity displayed by these nanostructured CdS materials make them excellent candidates for power conversion in hybrid photovoltaic systems [83]. Using a similar approach, a scaffold containing triple bonds acting as ligand sites was used to template the deposition of cobalt carbonyl, $Co_2(CO)_8$. The cobalt-containing hyperbranched polyynes were synthesized by Häußler et al. for the preparation of nanostructured magnetoceramics [84]. The cobalt was incorporated in the core of the hyperbranched polyynes through cobalt-triple bond coordination within the hyperbranched backbone. The structural units of the polymers used to template CdS and cobalt deposition are compared in Figure 30.8.

The incorporation of metals within dendritic structures during the synthesis of the molecules has been achieved using metal-containing AB_2 monomers. Onitsuka used this approach in the synthesis of hyperbranched polyyne from Pt-functionalized monomers [85]. These displayed liquid crystalline properties under the influence of a magnetic field, similar to the analogous one-dimensional linear structures [86]. The predetermined location of the metal within the monomer ensures its even and regular distribution throughout the entire polymer structure. An analogous Pt-containing dendrimer structure has also been reported [87]. The formation of a hyperbranched structure from the platinum–acetylide monomer proceeds as shown in Scheme 30.13.

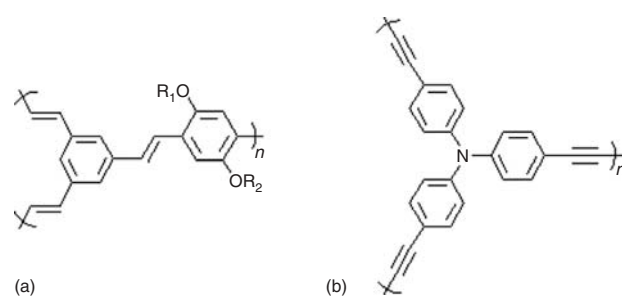
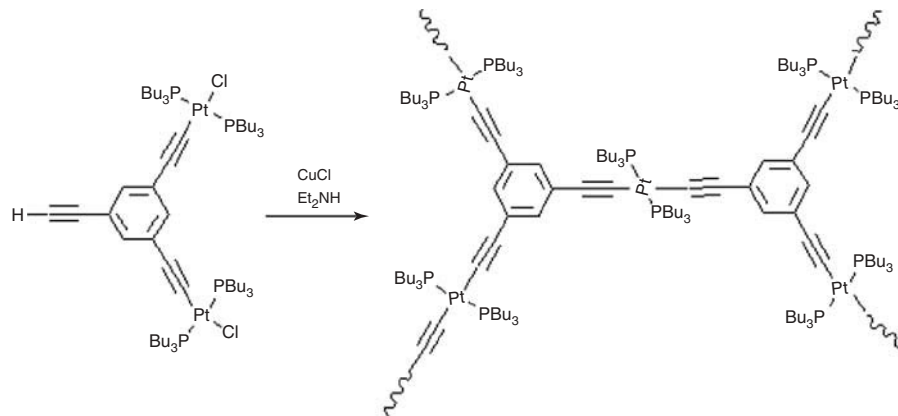


Figure 30.8 Conjugated hyperbranched polymers used to template (a) CdS and (b) cobalt deposition.



Scheme 30.13 Synthesis of a hyperbranched polymer from a platinum-containing acetylide monomer.

Hyperbranched polymers are also gaining interest as biomaterials, specifically as hosts for bioactive molecules such as drugs, labels, or probes. Hyperbranched polyglycerols are one of the candidates considered for this application as their synthesis is well-established and controlled, but more importantly they are biocompatible and biodegradable. End-group functionalization is also a versatile method that can be easily adapted for enhanced biocompatibility, for site targeting, or to serve as binding sites for guest molecules [88]. Similar polymers have been applied to protein immobilization [89, 90] or to support cell growth [91]. Hyperbranched PIB-based copolymers have likewise received significant attention as biomaterials, with specific interest as coatings in arterial stents [92, 93]. This is due to the fact that a linear triblock copolymer analog, poly(styrene-*b*-isobutylene-*b*-styrene) (SIBS), has received approval from the United States Food and Drug Administration (FDA) for use as medical device coating. More specifically, copolymers of PIB and styrenic monomers were shown to display thermoplastic elastomeric (TPE) properties and are being assessed for their degree of biocompatibility [94, 95]. The TPE properties of these materials arise from microphase separation of the polystyrene (PS) chain segments within the polymer matrix providing physical cross-links, in analogy to the common block copolymer TPE. Consequently, these materials behave like covalently crosslinked (vulcanized) rubbers at room temperature, but they can be processed like thermoplastics at temperatures above the glass transition temperature of the PS segments.

30.4 DENDRIGRAFT POLYMERS

30.4.1 General Characteristics

These macromolecules have a dendritic architecture reminiscent of dendrimers and hyperbranched polymers, but

are derived from polymeric building blocks rather than small-molecule monomers. While the molecular weights attained for dendrigraft polymers can be much higher than for the other dendritic polymer families, their MWD typically remains relatively narrow ($P < 1.1$), and thus they are referred to as *semicontrolled dendritic structures* [96]. Synthetic schemes have been developed for the preparation of dendritic graft polymers by different methods including anionic, cationic, radical, and ring-opening polymerization. Three distinct methodologies can be distinguished in the literature, namely, divergent *grafting-onto*, divergent *grafting-from*, and convergent *grafting-through* techniques.

The divergent approach relies on successive grafting reactions starting from a linear substrate (equivalent to the core in dendrimer syntheses). In the divergent grafting-onto method, polymeric side chains are coupled with the substrate, while in the divergent grafting-from method, the side chains are grown from initiating sites on the substrate. Successive grafting reactions lead to consecutive generations of branched polymers in both cases. The convergent grafting-through methodology is a one-pot technique, whereby building blocks are produced and coupled *in situ* to yield branched structures in a single reaction step. This represents the main advantage of the grafting-through methods, in analogy to the hyperbranched polymer syntheses, as it requires less time, effort, and resources to obtain high molecular weight dendritic structures. The grafting-onto and grafting-from methods, in contrast, involve distinct steps of substrate functionalization, grafting, and product isolation for each generation.

30.4.2 Synthetic Strategies, Common Structures, and Properties

30.4.2.1 Divergent Grafting-Onto Strategy The first dendrigraft polymer syntheses were reported independently by two research groups in 1991. Gauthier and Möller [12]

developed a divergent anionic grafting-onto method for the preparation of branched PSs denominated arborescent polymers. The term *arborescent* referred to the treelike architecture of the molecules, with symmetric long branches. Tomalia et al. [13], on the other hand, employed cationic polymerization in a similar divergent grafting-onto scheme to synthesize branched polyethylenimines, initially called *Comb-burst® polymers*. The term *dendrigrad polymers* has meanwhile become widely accepted to designate arborescent, Comb-burst, and other related dendritic graft polymer architectures collectively. The divergent grafting-onto strategy is represented schematically in Figure 30.9. Specific details of the anionic and the cationic grafting methods developed by Gauthier and Möller and by Tomalia et al., respectively, are discussed in the subsequent sections.

Arborescent Polymers The first grafting technique developed for the synthesis of arborescent polymers used chloromethyl coupling sites located on the phenyl pendants of PS substrates. Coupling “living” polystyryl anions

with the chloromethyl sites on the substrate thus resulted in a comb-branched, or generation 0 (G0) arborescent PS structure. Repetition of the functionalization and grafting reactions led to arborescent polymers of generations G1, G2, G3, etc. Efficient coupling with the substrate required “capping” of the living chains with a single 1,1-diphenylethylene unit to suppress metal-halogen exchange side reactions. One of the major problems encountered in this approach was associated with the use of hazardous chloromethyl methyl ether for the introduction of the chloromethyl coupling sites on the substrate. This issue was solved in 2001, when Li and Gauthier [97] developed an alternate grafting method based on acetyl coupling sites (derived from acetyl chloride). In this case, the living PS chains were capped with a few 2-vinylpyridine units before coupling with the acetylated substrate, and LiCl was added to suppress proton abstraction from the acetyl groups leading to chain termination. The synthetic paths for the preparation of G0 arborescent PS using both chloromethyl and acetyl coupling sites are compared in Scheme 30.14.

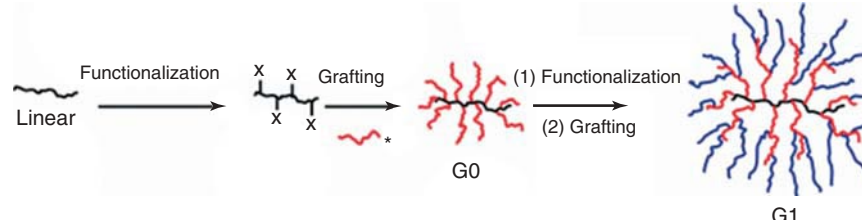
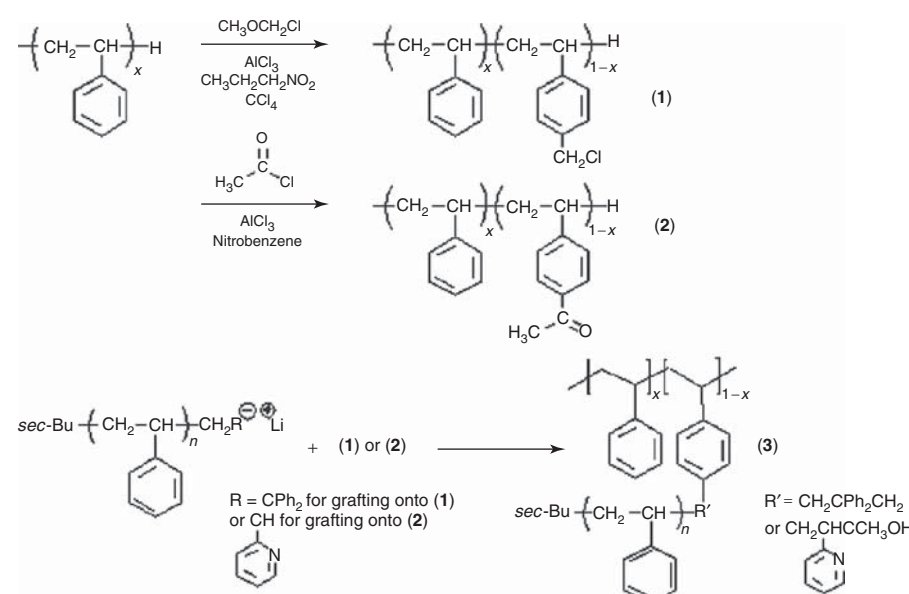


Figure 30.9 Schematic representation of the generation-based synthesis of dendrigrad polymers by a divergent grafting-onto method. (See insert for the color representation of the figure.)



Scheme 30.14 Arborescent polystyrene synthesis: linear substrate functionalization by chloromethylation (1) or acetylation (2), and coupling with living polystyrene to yield a G0 molecule (3).

The scope of the grafting methods initially developed for PS was expanded over the years to the synthesis of arborescent copolymers, mainly by grafting a polymer with a different composition in the final reaction cycle. Copolymers with core–shell morphologies were thus synthesized by grafting living poly(2-vinylpyridine) (P2VP) chains onto chloromethylated or acetylated PS substrates [98, 99]. Polystyrene-*g*-polyisoprene [100] and polystyrene-*g*-poly(*tert*-butyl methacrylate) [101] copolymers were also synthesized by a similar approach. Alternatively, molecules with an inner P2VP shell embedded between a core and a corona of PS were obtained by grafting a PS-*b*-P2VP block copolymer onto arborescent PS substrates [102].

Depending on the molecular weight of the side chains and the functionalization level of the substrate used in the reaction, very high overall molecular weights can be achieved in only a few grafting cycles. If the number of coupling sites (f) available per side chain on the substrate and the molecular weight of the side chains (M_{br}) remain constant for each cycle, the molecular weight (M) of an arborescent polymer can be calculated according to the following equation:

$$\begin{aligned} M &= M_{\text{br}} + M_{\text{br}}f + M_{\text{br}}f^2 + M_{\text{br}}f^3 + \dots \\ &= \sum_{x=0}^{G+1} M_{\text{br}}f^x \end{aligned} \quad (30.11)$$

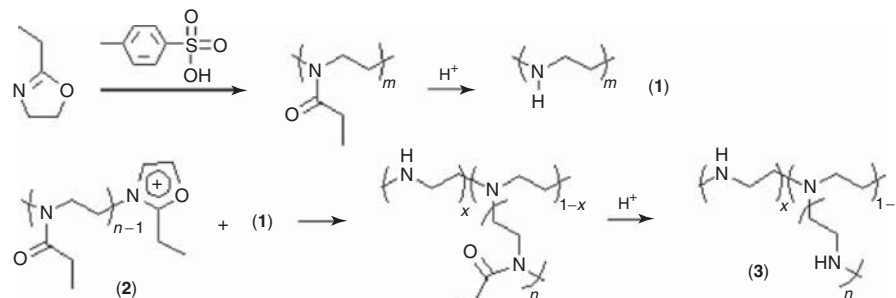
Three key parameters characterize the success of a grafting reaction: the grafting yield (G_y), defined as the fraction of side chains generated in the reaction becoming attached on the substrate; the branching functionality (f_w), corresponding to the number of chains added in a grafting reaction; and the coupling efficiency (C_e), which is the fraction of coupling sites grafted with side chains. Arborescent polymers are typically synthesized from linear polymer building blocks having a molecular weight of about 5000 g/mol and substrates with target functionalization levels of circa 25–30 mol%. This provides a large number of coupling sites on the substrate (10–15 per side chain), while minimizing steric hindrance effects that would become more important at higher grafting densities. The grafting of coronal side chains has been investigated for both long (30,000 g/mol) and short (5000 g/mol) chain segments, resulting in either starlike or crew-cut [103] architectures, respectively. For increased side-chain lengths, the grafting yield and the coupling efficiency decrease due to enhanced steric crowding by the longer chains. The same effect also comes into play when grafting onto substrates of the upper generations. The small molecules used in the substrate functionalization process can easily diffuse on the periphery and the interior of the branched structures. The ability of polymeric chains to diffuse to the coupling

sites located within the interior of the branched substrates decreases as their size increases, however, which reduces the grafting yield and the coupling efficiency. Typical values of grafting yield and coupling efficiency thus range from upward of 90% in G0 polymer syntheses, down to circa 20% for G4 polymers. Narrow MWD are maintained over successive grafting reactions, and D sometimes even decreases marginally as a result of averaging of the side-chain length distribution. The molecular weight of these polymers can range from circa 5×10^4 g/mol for G0 to over 10^7 g/mol for G4 polymers, depending on the length of the side chains and the grafting density used in the synthesis.

The spherical topology of arborescent polymers is a consequence of the molecular weight of the polymer chains used in their synthesis: a prolate spheroid having at most a 3 : 2 axis ratio is expected for a G0 molecule (if it were to adopt a fully extended chain conformation) when grafting side chains having the same molecular weight as the linear substrate (e.g., 5000 g/mol for both components). This changes to an increasingly spherical topology over successive grafting cycles (5 : 3 axis ratio for a G1 polymer, 7 : 5 for G2, and so on). This topology is reflected in the dilute-solution properties of arborescent polymers in terms of their scaling behavior (molecular weight dependence) for the second virial coefficient (A_2), the z -average translational diffusion coefficient (D_z), and the radius of gyration (r_g), which are all comparable to rigid spheres [104]. More recently, it was shown through small-angle neutron scattering measurements that the chain segment density of arborescent polymer molecules becomes relatively constant at their center after a few grafting cycles, but decreases according to a power law within their corona [105].

Comb-burst Polymers The divergent grafting-onto method suggested by Tomalia et al. [13] for the synthesis of Comb-burst polymers yields a molecular architecture similar to the arborescent systems, but these polymers are produced through cationic polymerization of 2-ethyl-2-oxazoline. The side chains inherently contain protected coupling sites that are activated by deacylation under acidic conditions. The secondary amine sites generated along the substrate polymer can be coupled with living poly(2-ethyl-2-oxazoline) in a predetermined molar ratio to control the branching density. Another possibility is through partial deacylation of a fraction of the secondary amine sites. Depicted in Scheme 30.15 is the cationic synthesis of Comb-burst poly(2-ethyl-2-oxazoline), by initiation of the polymerization with methyl tosylate, as well as substrate activation and grafting to yield a G0 polyethylenimine (3).

The number of RU (N_{RU}) and the molecular weight (M) of Comb-burst polymers can be predicted from the number



Scheme 30.15 Grafting of living poly(2-ethyl-2-oxazoline) (**2**) onto a linear polyethylenimine (**1**) to yield a G0 Comb-burst polyethylenimine (**3**).

of coupling sites on the branches (N_b) and the core (N_c), the molecular weight of the core (M_c), the molecular weight of the RU (M_{RU}), and the molecular weight of the end groups (M_z), according to the following expressions:

$$N_{RU} = N_c \left(\frac{N_b^{G+1} - 1}{N_b - 1} \right)$$

$$M = M_c + N_c \left[M_{RU} \left(\frac{N_b^{G+1} - 1}{N_b - 1} \right) + M_z N_b^{G+1} \right] \quad (30.12)$$

A series of Comb-burst polyethylenimine was thus synthesized with a side-chain DP increasing from 10 to 20 for the first two generations, and then maintained constant at 100 for the subsequent generations [106]. A geometric increase in molecular weight was observed as predicted by Equation 30.12, with grafting yield variations similar to those observed for arborescent systems.

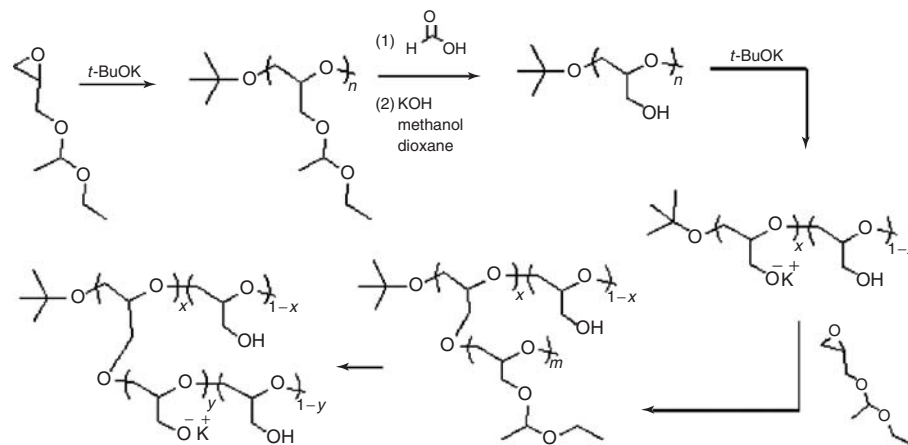
30.4.2.2 Divergent Grafting-From Strategy In a divergent grafting-from method, polymer chains are grown from a substrate acting as a polyfunctional initiator. This approach is particularly advantageous for the preparation of copolymers with core-shell morphologies, as these can be obtained simply through the addition of different monomers in the side-chain growth process. As with the grafting-onto method, variations in the dimensions of the initiating core relatively to the side chains, as well as the location of the initiating sites, can produce different topologies. Spherical molecules result when the core has dimensions comparable to the side chains and the latter are evenly distributed around the core. If the DP of the side chains in the first grafting cycle (G0 polymer synthesis) is significantly lower than that of the core, cylindrical structures will result. A G0 (comb-branched) molecule exhibiting this topology is commonly referred to as a *polymeric brush*.

The divergent grafting-from method suffers from a significant drawback in terms of structural characterization. In the grafting-onto techniques, a sample of the side chains can be removed for analysis before the grafting

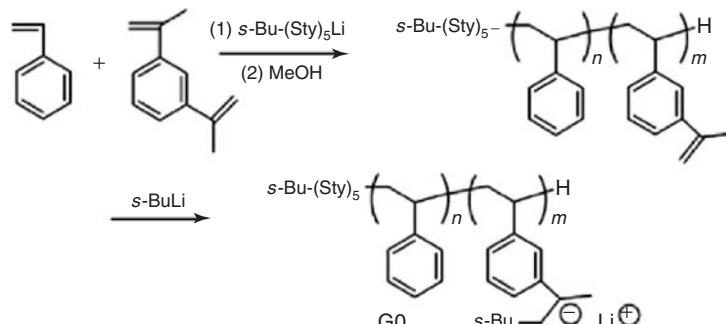
reaction. Unfortunately, this cannot be done in the grafting-from approaches, in analogy to hyperbranched polymer syntheses. Characterization of the side chains is only possible if they can be cleaved from the substrate after the reaction. Another drawback of this method is that it often yields broadly dispersed products, due to the increased probability of side reactions and the influence of steric hindrance resulting in the retardation of propagation for some of the chains.

This approach was first developed by Six and Gnanou for the synthesis of starlike dendritic poly(ethylene oxide) [107]. Analogous results have also been obtained using dendrimerlike multifunctional initiators [108, 109]; however, we focus on methods starting from linear macroinitiator substrates in this section. One such method was reported for the synthesis of arborescent polyglycidols, starting from a linear polyglycidol macroinitiator with anionic ring-opening polymerization [110]. The linear substrate was obtained by initiating the polymerization of glycidol acetal with potassium *tert*-butoxide, and treatments with formic acid and KOH/methanol/dioxane to deprotect the hydroxyl functionalities. The initiating sites were activated by treatment with potassium *tert*-butoxide, and glycidol acetal monomer was added to grow branches from the substrate and produce a G0 structure. Further reaction cycles led to arborescent polyglycidols of generations up to G2. The synthesis of a G0 arborescent polyglycidol starting from the polymerization of the acetal monomer is illustrated in Scheme 30.16 as an example.

Relatively low D values were obtained in this synthesis ($D \approx 1.2\text{--}1.4$), albeit with MWD broadening over successive generations. Substrate activation with *tert*-butoxide targeted a 10% neutralization level, to provide adequate spacing for the side chains, but much higher branching densities (reaching 90%) were observed in practice. This is due to hopping of the potassium counterions among the hydroxyl groups on the macroinitiator substrate, leading to chain growth from most of the deprotected functional groups. Monomer conversion reached 99% during the first



Scheme 30.16 Synthesis of a G0 arborescent polyglycidol molecule.



Scheme 30.17 One-pot synthesis of arborescent polystyrene by a semibatch process with mixed monomer additions. Source: Reproduced with permission from Yuan Z, Gauthier M. Macromolecules 2003;2006:39 [114]. Copyright 2006 American Chemical Society.

two grafting cycles, but decreased to 27% for the G2 polyglycidol due to poor solubility of the graft polymer.

An approach similar to the previous divergent grafting-from method also served to synthesize dendrigraft poly(L-lysine) by ring-opening polymerization [111], styrene homopolymers and styrene-methacrylate copolymers by a combination of stable free-radical polymerization and atom transfer radical polymerization (ATRP) [112], and copolymers of 2-hydroxyethyl methacrylate with styrene or *tert*-butyl methacrylate by ATRP [113].

Another embodiment of this technique was used for the synthesis of high molecular weight, low \mathcal{D} arborescent polymers by Yuan and Gauthier in a one-pot synthesis of arborescent PSs [114]. In this case, the anionic copolymerization of styrene (Sty) and 1,3-diisopropenylbenzene (DIB) initiated by *sec*-butyllithium was carried out in a semibatch process. Following complete monomer conversion, the chains were terminated and the isopropenyl moieties of the DIB units were activated with *sec*-butyllithium to produce a polyfunctional anionic macroinitiator without additional workup. Further styrene-DIB monomer mixture additions yielded a comb-branched (G0) copolymer, and

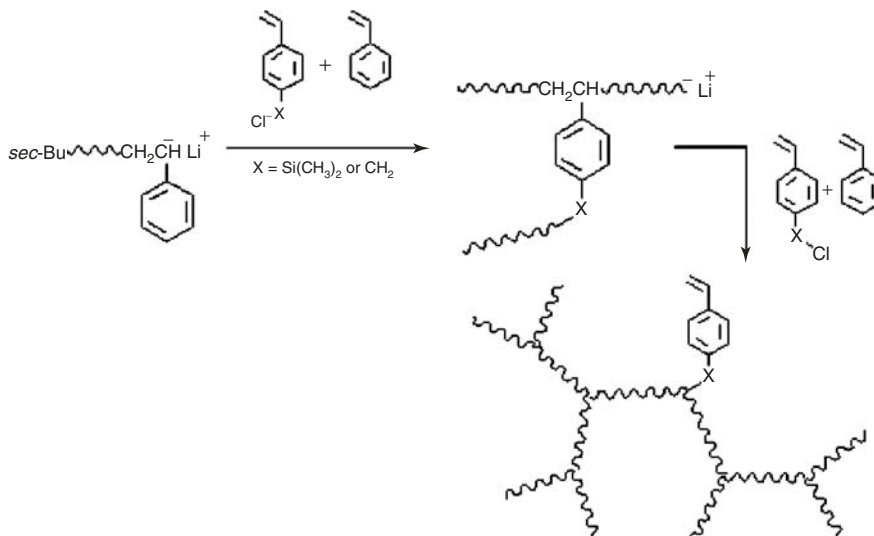
subsequently G1 arborescent PS molecules after activation and styrene addition. An illustration of this synthetic technique is provided in Scheme 30.17.

Control over the side-chain molecular weight was achieved through the amount of monomer added to the activated substrates. The \mathcal{D} values obtained ranged from 1.1 to 1.3 for molecular weights (M_w) reaching 7×10^6 g/mol. The same technique was also used to synthesize arborescent copolymers, by adding other monomers in the last side-chain growth cycle, namely, arborescent polystyrene-*g*-poly(*tert*-butyl methacrylate) and polystyrene-*g*-[polystyrene-*b*-poly(2-vinylpyridine)] copolymers [115].

Hybrid techniques combining grafting-onto and grafting-from methodologies have also been investigated for arborescent polymer molecules, by introducing functional groups at the chain ends of an arborescent polymer and activating them to grow a corona of polymer segments with a different chemical composition [116].

30.4.2.3 Convergent Grafting-Through Strategy

The convergent grafting-through method is the least time- and



Scheme 30.18 One-pot *grafting-through* method to for the convergent synthesis of dendrigrift polystyrene.

resource-intensive approach for the synthesis of dendrigrift polymers. This self-branching system, carried in a one-pot reaction, makes use of bifunctional monomers carrying a vinyl group and a second functional group capable of coupling *in situ* with the living chains. The bifunctional monomer can be added slowly at different stages of the reaction to induce the formation of branching points, while maintaining relatively low D typical for dendrigrift polymers.

This technique was first developed by Knauss et al. for the convergent anionic synthesis of PS. On addition of a bifunctional monomer such as 4-(chlorodimethylsilyl)styrene [117] or vinylbenzyl chloride [118] to living polystyryllithium, a portion of the living chains undergo nucleophilic substitution at their chloromethyl or chlorosilyl site, while propagation may take place via the vinyl group. The branched macromonomers generated in the coupling reaction quickly become sterically crowded, which limits the attainable molecular weight, but this growth mechanism is also believed to be at the origin of the relatively narrow MWD observed in some cases ($D \approx 1.1\text{--}1.8$). To facilitate the attainment of higher molecular weights and branching functionalities, styrene monomer can be added along with the bifunctional monomer to introduce PS segment spacers between the branching points, thus reducing the influence of steric crowding on the branching process. In the absence of PS spacers, the branched structures obtained are closer to star-branched polymers than to dendrigrift polymers. A polymerization process with styrene addition to produce spacers between the branching points is depicted in Scheme 30.18.

The branched structure of dendrigrift polymers obtained by the convergent grafting-through method can be described

in terms of an average generation number (G) determined from Equation 30.13, where M_G and M_0 correspond to the M_n for the graft polymer and the primary chains (before addition of the coupling agent), respectively, and M_B is the molecular weight of the structural unit derived from the coupling agent:

$$G = \log(M_G) - \log(M_0 + M_B) \quad (30.13)$$

The bifunctional monomer approach, with continuous addition of the monomer and the branching agent, is analogous to hyperbranched polymer syntheses using the inimer technology, but the MWD obtained are significantly narrower: the D values reported vary from 1.2 to 2.0, albeit the molecular weight is also limited to circa 10^5 g/mol [117, 118].

A similar approach was used to construct a unique tri-block copolymer having dendritic termini connected by linear segment. The synthesis of the dendritic-block-linear-block-dendritic PS, referred to as the *pom-pom* structure due to its dumbbell-like shape, results from a convergent anionic polymerization procedure using dichlorodimethylsilane as a coupling agent [119].

30.4.3 Applications and Recent Trends

Considering the versatility of dendrigrift polymer syntheses, it is relatively easy to introduce features in the molecules of interest for specific applications. Since the chain segments of dendrigrift polymers are covalently bonded, copolymers with amphiphilic character behave like unimolecular micelles that provide an interesting basis for comparison with regular micelles. The self-assembly of

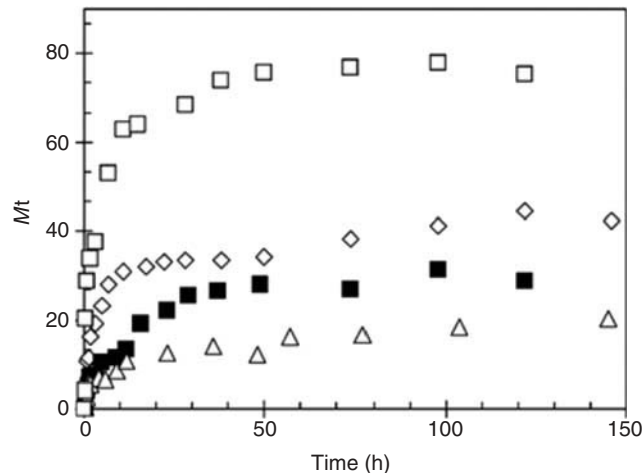


Figure 30.10 Percent mass fraction of lidocaine released from an arborescent PS-*g*-P2VP G1 (□) copolymer, and of indomethacin released from G1 (◊), G2 (■), and G3 (△) copolymers. *Source:* Reproduced with permission from Njikang GN, Gauthier M, Li J. Polymer 2008;49:5474 [120]. Copyright 2008 Elsevier.

block copolymers into micelles under selective solvency conditions is indeed concentration dependent, requiring a minimum concentration (the critical micelle concentration (CMC)), which is nonexistent for unimolecular micelles. Thus, depending on the specific application targeted, the dynamic character of block copolymer assemblies and their sensitivity to solvency conditions may be problematic, for example, when trying to load host molecules within their core.

The core–shell morphology of amphiphilic dendrigraft polymers, and the ability to control their characteristics (hydrophobic core size, hydrophilic corona thickness) independently, provides a wider range of structures than can be achieved for block copolymer micelles. A good example of this is arborescent amphiphiles incorporating a hydrophobic arborescent PS core and a corona of polar P2VP segments [98, 99]. These copolymers are interesting in terms of their solubilization properties [99] and their ability to host and slowly release hydrophobic compounds [120]. *In vitro* loading and release studies of indomethacin and lidocaine from PS-*g*-P2VP arborescent copolymers of different generations showed that the release profiles for

the model drugs displayed an initial burst release, followed by more gradual release over extended time periods. The release profiles obtained for indomethacin and lidocaine from different host PS-*g*-P2VP copolymers are compared in Figure 30.10 as an example.

It is clear from Figure 30.10 that the release from upper generation copolymers is more gradual, which can be attributed to the increased branching functionality of the molecules. It should also be noted that ionic interactions are present between the carboxylic acid group of the drug and the nitrogen atom of the pyridine pendants, which explains the much slower overall release rate for indomethacin as compared to lidocaine.

The usefulness of analogous arborescent copolymers characterized by a layered architecture, with an inner shell of P2VP segments, has been recently demonstrated as unimolecular templates for the preparation of metallic nanoparticles in nonpolar solvents [102]. Metallic nanoparticles are being intensively investigated for applications including imaging agents, microelectronics, separation science, catalysis, and biological uses such as targeted labeling and delivery systems or cell therapy. Arborescent copolymers with reverse micelle characteristics are obtained by grafting living PS-*b*-P2VP block copolymers onto arborescent PS substrates according to the methods described previously [12, 97]. A schematic representation of the synthesis of a template molecule, its loading with a metallic salt, and the reduction of the salt to metallic nanoparticles is shown in Figure 30.11. Since the living end of the block copolymer serving as side-chains is located at the end of the P2VP segment, a core–shell–corona copolymer architecture is obtained, with a corona of PS chains providing compatibility with nonpolar organic solvents, an inner shell of P2VP, and a PS core. The P2VP shell enables the loading of polar compounds, for example, through coordination with transition metals or, for charged species, through ionic interactions. This templating approach to the preparation of metallic nanoparticles has so far been explored using HAuCl₄.

The metals loaded in the arborescent templates may be easily viewed by transmission electron microscopy (TEM) as shown in Figure 30.12 [102]. The generation number of the PS-*g*-(P2VP-*b*-PS) templates governs the distribution of the metallic species within the molecules: the G0 templates (Fig. 30.12a), having an ill-defined core comprised of a

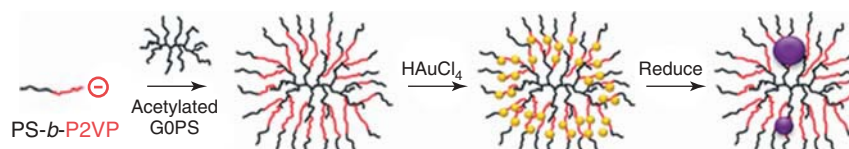


Figure 30.11 Synthesis of an arborescent copolymer, G0PS-*g*-(P2VP-*b*-PS), its application to templating HAuCl₄ deposition, and reduction to gold nanoparticles. (See insert for the color representation of the figure.)

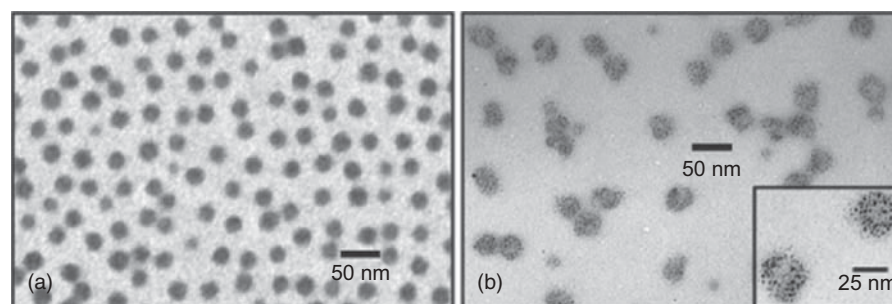
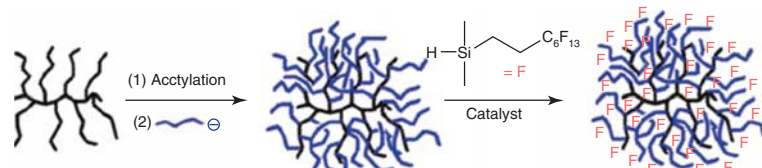


Figure 30.12 TEM micrographs for (a) PS-*g*-(P2VP-*b*-PS) and (b) G1PS-*g*-(P2VP-*b*-PS) loaded with HAuCl₄; the high magnification inset depicts the ring-like arrangement of Au. *Source:* Reproduced with permission from Dockendorff J, Gauthier M, Mourran A, Möller M. *Macromolecules* 2008;41:6621 [102]. Copyright 2008 American Chemical Society.



Scheme 30.19 Synthesis of G0PS-*g*-PIP copolymer followed by hydrosilation with a fluorohydrosilane for use as a processing aid. *Source:* Reproduced with permission from Gauthier M, Lin W-Y, Teertstra SJ, Tzoganakis C. *Polymer* 2010;51:3123 [121]. Copyright 2010 Elsevier. (See insert for the color representation of the figure.)

single linear PS chain, provide a uniform distribution of gold, while the G2 species (Fig. 30.12b), incorporating a larger noncoordinating G1PS core, display a metal-depleted region at the center of the nanoparticles.

The high molecular weight, compact structure, and spherical topology of arborescent polymers confer them a low viscosity as compared to their linear counterparts. These characteristics are also attractive for their potential application as polymer processing additives. It has indeed been demonstrated that branched polymers with a high degree of symmetry have a greater tendency to diffuse to the surface of polymer blends [121], and so they can interact more efficiently with the die wall surface and modify the processing characteristics of the host polymer. Linear fluoroelastomers have been instated as polymer processing additives for many years due to their ability to induce slippage at the walls of processing equipment, which leads to reduced melt defects and energy consumption. For that reason, fluorine-containing arborescent polystyrene-*g*-polyisoprene copolymers, combining the inherent properties of branched polymers with the surface energy reduction of fluorinated polymers, have been investigated as processing aids [121]. Arborescent copolymers with a PS core and polyisoprene (PIP) side chains were synthesized by a divergent grafting-onto method [97] and hydrosilylated with a fluorohydrosilane as depicted in Scheme 30.19.

Capillary rheometer extrusion tests were performed by monitoring the applied pressure and the extrudate appearance as a function of the deformation (shear) rate, for blends of the arborescent copolymers at 0.5% w/w with a commercial linear low density polyethylene (LLDPE) resin. In all cases, the backpressure was reduced for the blends as compared to virgin LLDPE; however, the performance of the arborescent additives was inferior to a commercial additive used for comparison.

30.5 CONCLUDING REMARKS

The dendritic polymer literature reviewed herein provides compelling evidence that these materials are a unique and versatile class of branched polymers. The synthesis of dendritic macromolecules can be accomplished by numerous methods allowing for specific tailoring of the characteristics of the polymer, to yield desired properties or functionality. While some of the procedures reported are quite intricate, requiring multiple cycles of synthetic steps and work-up, one-pot syntheses have also been developed for hyperbranched and dendrigraft polymers, making these materials more viable for (large-scale) commercial production and industrial applications.

The low viscosity [122] of dendritic polymers is interesting in terms of their potential applications as rheological (or

viscosity) modifiers and/or as polymer processing aids. Furthermore, the multiple chemical functionalities available for these materials offers a wide range of applications in different areas including stabilized catalysts, biological markers, sensors, and micelle mimics.

Dendritic polymers have been the focus of a great deal of application-oriented research in recent years. The number of U.S. patents related to dendritic polymers issued between 1990 and 1999 totaled 62, and only three patents were issued before 1990. From 2000 until July 2010, approximately 240 additional dendrimer-related patents were issued, that is almost four times the number issued in the previous decade.¹ The number of patent applications relating to dendritic species over the same period totaled approximately 430, demonstrating that this field is receiving even more attention than the number of already issued patents suggests. Recent emphasis on more exotic applications within the fields of nanotechnology, pharmaceuticals, and biotechnology has resulted in rapid growth in the number of filings. Further investigation into these fields as well as the new synthetic approaches and hybrid methodologies being developed will certainly broaden the scope of dendritic polymer applications in the future.

REFERENCES

- Buhleier E, Wehner W, Vögtle F. *Synthesis* 1978;2:155.
- Tomalia DA, Fréchet JMJ. *J Polym Sci A Polym Chem* 2002;40:2719.
- Maciejewski M. *J Macromol Sci Pure Appl Chem* 1982;17:689.
- de Gennes PG, Hervet H. *J Physique Lett* 1983;44:L-351.
- Tomalia DA, Baker H, Dewald J, Hall M, Kallos G, Martin S, Roeck J, Ryder J, Smith P. *Polym J* 1985;17:117.
- Newkome GR, Yao Z-q, Baker GR, Gupta VK. *J Org Chem* 1985;50:2003.
- Hawker CJ, Fréchet JMJ. *J Am Chem Soc* 1990;112:7638.
- Miller TM, Neenan TX. *Chem Mater* 1990;2:346.
- Gunatillake PA, Odian G, Tomalia DA. *Macromolecules* 1988;21:1556.
- Kim YH, Webster OW. *J Am Chem Soc* 1990;112:4592.
- Hawker CJ, Lee R, Fréchet JMJ. *J Am Chem Soc* 1991;113:4583.
- Gauthier M, Möller M. *Macromolecules* 1991;24:4548.
- Tomalia DA, Hedstrand DM, Ferritto MS. *Macromolecules* 1991;24:1435.
- Tomalia DA, Fréchet JMJ. Introduction to the dendritic state. In: Tomalia DA, Fréchet JMJ, editors. *Dendrimers and Other Dendritic Polymers*. West Sussex: Wiley; 2001. p 3.
- Tomalia DA, Berry V, Hall M, Hedstrand DM. *Macromolecules* 1987;20:1164.
- Naylor AM, Goddard WA III, Kiefer GE, Tomalia DA. *J Am Chem Soc* 1989;111:2339.
- Wörner C, Mülhaupt R. *Angew Chem Int Ed Engl* 1993;32:1306.
- de Brabander-van den Berg EMM, Meijer EW. *Angew Chem Int Ed Engl* 1993;32:1308.
- Inoue K. *Prog Polym Sci* 2000;25:453.
- Zhao M, Sun L, Crooks RM. *J Am Chem Soc* 1998;120:4877.
- Balogh L, Tomalia DA. *J Am Chem Soc* 1998;120:7355.
- Gröhn F, Bauer BJ, Akpalu YA, Jackson CL, Amis EJ. *Macromolecules* 2000;33:6042.
- Scott RWJ, Ye H, Henriquez RR, Crooks RM. *Chem Mater* 2003;15:3873.
- Gu Y, Xie H, Gao J, Liu D, Williams CT, Murphy CJ, Ploehn HJ. *Langmuir* 2005;21:3122.
- Peng Z, Zhang J, Sun X, Yang J, Diao J. *Colloid Polym Sci* 2009;287:609.
- Atwater JE, Akse JR, Holtsnider JT. *Mater Lett* 2008;62:3131.
- Scott RWJ, Wilson OM, Oh S-K, Kenik EA, Crooks RM. *J Am Chem Soc* 2004;126:15583.
- Gu Y, Wu G, Hu XF, Chen DA, Hansen T, zur Loye H-C, Ploehn HJ. *J Power Sources* 2010;195:425.
- Newkome GR, He E, Moorefield CN. *Chem Rev* 1999;99:1689.
- Cuadrado I, Morán M, Casado CM, Alonso B, Losada J. *Coord Chem Rev* 1999;193–195:395.
- Berger A, Gebbink RJMK, van Koten G. *Top Organomet Chem* 2006;20:1.
- [a] Ribaudo F, van Leeuwen PWNM, Reek JNH. *Top Organomet Chem* 2006;20:39. [b] King ASH, Twyman LJ. *J Chem Soc Perkin Trans 1* 2002;2209. [c] van Heerbeek R, Kamer PCJ, van Leeuwen PWNM, Reek JNH. *Chem Rev* 2002;102:3717.
- Knapen JWJ, van der Made AW, de Wilde JC, van Leeuwen PWNM, Wijkens P, Grove DM, van Koten G. *Nature* 1994;372:659.
- Reetz MT, Lohmer G, Schwickardi R. *Angew Chem Int Ed Engl* 1997;36:1526.
- Bourque SC, Maltais F, Xiao W-J, Tardif O, Alper H, Arya P, Manzer LE. *J Am Chem Soc* 1999;121:3035.
- Oosterom GE, van Haaren RJ, Reek JNH, Kamer PCJ, van Leeuwen PWNM. *Chem Commun* 1999;1119.
- Albrecht M, Hovestad NJ, Boersma J, van Koten G. *Chem Eur J* 2001;7:1289.
- Fischer M, Vögtle F. *Angew Chem Int Ed* 1999;38:884.
- Navarro G, de ILarduya CT. *Nanomedicine* 2009;5:287.

¹Note: Patent search results from an “advanced search” performed at <http://patft.uspto.gov/> on July 13, 2010. Query included appropriate Issue Date and keyword search of “dendrimer or arborescent or dendrigraft or hyperbranched” within the abstract. An example of a query string was as follows: ISD/1/2000->7/13/2010 and ABST/(dendrimer or arborescent or dendrigraft or hyperbranched).

40. Bielinska A, Kukowska-Latallo JF, Johnson J, Tomalia DA, Baker JR Jr. *Nucleic Acids Res* 1996;24:2176.
41. Jansen JFGA, Meijer EW, de Brabander-van den Berg EMM. *J Am Chem Soc* 1995;117:4417.
42. [a] Malik N, Evagorou EG, Duncan R. *Anticancer Drugs* 1999;10:767. [b] Howell BA, Fan D. *Proc Math Phys Eng Sci* 2010;466:1515.
43. Cheng Y, Li M, Xu T. *Eur J Med Chem* 2008;43:1791.
44. Shaunak S, Thomas S, Gianasi E, Godwin A, Jones E, Teo I, Mireskandari K, Luthert P, Duncan R, Patterson S, Khaw P, Brocchini S. *Nat Nanobiotechnol* 2004;22:977.
45. [a] Nantalaksakul A, Reddy DR, Bardeen CJ, Thayumanavan S. *Photosynth Res* 2006;87:133. [b] Adronov A, Fréchet JMJ. *Chem Commun* 2000;1701. [c] Devadoss C, Bharathi P, Moore JS. *J Am Chem Soc* 1996;118:9635. [d] Lo S-C, Burn PL. *Chem Rev* 2007;107:1097.
46. Flory PJ. *J Am Chem Soc* 1952;74:2718.
47. Yan D, Müller AHE, Matyjaszewski K. *Macromolecules* 1997;30:7024.
48. Höller D, Burgath A, Frey H. *Acta Polym* 1997;48:30.
49. Erlander S, French D. *J Polym Sci* 1956;20:7.
50. Burchard W. *Macromolecules* 1972;5:604.
51. Hanselmann R, Höller D, Frey H. *Macromolecules* 1998;31:3790.
52. Bharathi P, Moore JS. *Macromolecules* 2000;33:3212.
53. Gong C, Miravet J, Fréchet JMJ. *J Polym Sci A Polym Chem* 1999;37:3193.
54. Schallausky F, Erber M, Komber H, Lederer A. *Macromol Chem Phys* 2008;209:2331.
55. Radke W, Litvinenko G, Müller AHE. *Macromolecules* 1998;31:239.
56. Yan D, Zhou Z, Müller AHE. *Macromolecules* 1999;32:245.
57. Gao C, Yan D. *Prog Polym Sci* 2004;29:183.
58. Miller TM, Neenan TX, Kwock EW, Stein SM. *J Am Chem Soc* 1993;115:356.
59. Wooley KL, Hawker CJ, Lee R, Fréchet JMJ. *Polym J* 1994;26:187.
60. Spindler R, Fréchet JMJ. *Macromolecules* 1993;26:4809.
61. Mathias LJ, Carothers TW. *J Am Chem Soc* 1991;113:4043.
62. Bolton DH, Wooley KL. *Macromolecules* 1890;1997:30.
63. Yoon K, Son DY. *Macromolecules* 1999;32:5210.
64. Miravet JF, Fréchet JMJ. *Macromolecules* 1998;31:3461.
65. Hawker CJ, Fréchet JMJ, Grubbs RB, Dao J. *J Am Chem Soc* 1995;117:10763.
66. Fréchet JMJ, Henmi M, Gitsov I, Aoshima S, Leduc MR, Grubbs RB. *Science* 1995;269:1080.
67. [a] Paulo C, Puskas JE. *Macromolecules* 2001;34:734. [b] Puskas JE, Dos Santos LM, Kaszas G, Kulbaba K. *J Polym Sci A Polym Chem* 2009;47:1148.
68. Foreman EA, Puskas JE, Kaszas G. *J Polym Sci A Polym Chem* 2007;45:5847.
69. Liu M, Vladimirov N, Fréchet JMJ. *Macromolecules* 1999;32:6881.
70. Sunder A, Hanselmann R, Frey H, Mühlaupt R. *Macromolecules* 1999;32:4240.
71. Magnusson H, Malmström E, Hult A. *Macromol Rapid Commun* 1999;20:453.
72. Suzuki M, Ii A, Saegusa T. *Macromolecules* 1992;25:7071.
73. Jiikei M, Chon S-H, Kakimoto M-a, Kawauchi S, Imase T, Watanebe J. *Macromolecules* 1999;32:2061.
74. Emrick T, Chang H-T, Fréchet JMJ. *Macromolecules* 1999;32:6380.
75. Tanaka S, Takeuchi K, Asai M, Iso T, Ueda M. *Synth Met* 2001;119:139.
76. Mendez JD, Schroeter M, Weder C. *Macromol Chem Phys* 2007;208:1625.
77. Pérignon N, Mingotaud A-F, Marty J-D, Rico-Lattes I, Mingotaud C. *Chem Mater* 2004;16:4856.
78. Salazar R, Fomina L, Fomine S. *Polym Bull* 2001;47:151.
79. Slagt MQ, Stiriba S-E, Klein Gebbink RMJ, Kautz H, Frey H, van Koten G. *Macromolecules* 2002;35:5734.
80. Slagt MQ, Stiriba S-E, Kautz H, Klein Gebbink RJM, Frey H, van Koten G. *Organometallics* 2004;23:1525.
81. Krämer M, Pérignon N, Haag R, Marty J-D, Thomann R, Lauth-de Viguerie N, Mingotaud C. *Macromolecules* 2005;38:8308.
82. Yang J, Lin H, He Q, Ling L, Zhu C, Bai F. *Langmuir* 2001;17:5978.
83. Lee J-C, Lee W, Han S-H, Kim TG, Sung Y-M. *Electrochem Commun* 2009;11:231.
84. Häußler M, Lam JWY, Zheng R, Dong H, Tong H, Tang BZ. *J Inorg Organomet Polym Mater* 2005;15:519.
85. Onitsuka K, Ohshiro N, Fujimoto M, Takei F, Takahashi S. *Mol Cryst Liq Cryst* 2000;342:159.
86. Hagihara N, Sonogashira K, Takahashi S. *Adv Polym Sci* 1981;41:149.
87. Takahashi S, Onitsuka K, Takei F. *Macromol Symp* 2000;156:69.
88. Frey H, Haag R. *Rev Mol Biotechnol* 2002;90:257.
89. Cosulich ME, Russo S, Pasquale S, Mariani A. *Polymer* 2000;41:4951.
90. Boulares-Pender A, Prager-Duschke A, Elsner C, Buchmeiser MR. *J Appl Polym Sci* 2009;112:2701.
91. Muthukrishnan S, Nitschke M, Gramm S, Özyürek Z, Voit B, Werner C, Müller AHE. *Macromol Biosci* 2006;6:658.
92. Puskas JE, Dos Santos LM, Fischer F, Götz C, El Fray M, Altstädt V, Tomkins M. *Polymer* 2009;50:591.
93. Puskas JE, Chen Y, Dahman Y, Padavan D. *J Polym Sci A Polym Chem* 2004;42:3091.
94. [a] Puskas JE, Chen Y, Antony P, Kwon Y, Kovar M, Harbottle RR, De Jong K, Norton PR, Cadieux P, Burton J, Reid G, Beiko D, Watterson JD, Denstedt J. *Polym Adv Technol* 2003;14:763. [b] Foreman E, Puskas JE, El Fray M, Prowans P, Piątek M. *Polym Prepr* 2008;49(1):822.
95. Cadieux P, Watterson JD, Denstedt J, Harbottle RR, Puskas J, Howard J, Gan BS, Reid G. *Colloids Surf B Biointerfaces* 2003;28:95.

96. Kee RA, Gauthier M, Tomalia DA. Semi-controlled dendritic structure synthesis. In: Tomalia DA, Fréchet JMJ, editors. *Dendrimers and Other Dendritic Polymers*. West Sussex: Wiley; 2001. p 209.
97. Li J, Gauthier M. *Macromolecules* 2001;34:8918.
98. Kee RA, Gauthier M. *Macromolecules* 2002;35:6526.
99. Gauthier M, Li J, Dockendorff J. *Macromolecules* 2003;36:2642.
100. Kee RA, Gauthier M. *Macromolecules* 1999;32:6478.
101. Kee RA, Gauthier M. *J Polym Sci A Polym Chem* 2008;46:2335.
102. Dockendorff J, Gauthier M, Mourran A, Möller M. *Macromolecules* 2008;41:6621.
103. Zhang L, Eisenberg A. *J Am Chem Soc* 1996;118:3168.
104. Gauthier M, Möller M, Burchard W. *Macromol Symp* 1994;77:43.
105. Il Yun S, Lai K-C, Briber RM, Teertstra SJ, Gauthier M, Bauer BJ. *Macromolecules* 2008;41:175.
106. Yin R, Swanson DR, Tomalia DA. *Polym Mater Sci Eng* 1995;73:277.
107. Six J-L, Gnanou Y. *Macromol Symp* 1995;95:137.
108. Hirao A, Sugiyama K, Tsunoda Y, Matsuo A, Watanabe T. *J Polym Sci A Polym Chem* 2006;44:6659.
109. Trollsås M, Hedrick JL. *J Am Chem Soc* 1998;120:4644.
110. Walach W, Kowalcuk A, Trzebicka B, Dworak A. *Macromol Rapid Commun* 2001;22:1272.
111. Klok H-A, Rodríguez-Hernández J. *Macromolecules* 2002;35:8718.
112. Grubbs RB, Hawker CJ, Dao J, Fréchet JMJ. *Angew Chem Int Ed Engl* 1997;36:270.
113. Cheng G, Böker A, Zhang M, Krausch G, Müller AHE. *Macromolecules* 2001;34:6883.
114. Yuan Z, Gauthier M. *Macromolecules* 2003;2006:39.
115. Yuan Z, Gauthier M. *Macromol Chem Phys* 2007;208:1615.
116. Gauthier M, Tichagwa L, Downey JS, Gao S. *Macromolecules* 1996;29:519.
117. Knauss DM, Al-Muallem HA, Huang T, Wu DT. *Macromolecules* 2000;33:3557.
118. Knauss DM, Al-Muallem HA. *J Polym Sci A Polym Chem* 2000;38:4289.
119. Knauss DM, Huang T. *Macromolecules* 2005;2002:35.
120. Njikang GN, Gauthier M, Li J. *Polymer* 2008;49:5474.
121. Gauthier M, Lin W-Y, Teertstra SJ, Tzoganakis C. *Polymer* 2010;51:3123.
122. Puskas JE, Kaszas G. *Prog Polym Sci* 2000;25:403.

31

POLYMER NANOCOMPOSITES

OCTAVIO MANERO AND ANTONIO SANCHEZ-SOLIS

31.1 INTRODUCTION

Polymeric nanocomposites are a class of relatively new materials with ample potential applications. Products with commercial applications appeared during the last decade [1], and much industrial and academic interest has been created. Reports on the manufacture of nanocomposites include those made with polyamides [2–5], polyolefins [6–9], polystyrene (PS) and PS copolymers [10, 11], ethylene vinyl alcohol [12–15], acrylics [16–18], polyesters [19, 20], polycarbonate [21, 22], liquid crystalline polymers [8, 23–25], fluoropolymers [26–28], thermoset resins [29–31], polyurethanes [32–37], ethylene-propylene oxide [38], vinyl carbazole [39, 40], polydiacetylene [41], and polyimides (PIs) [42], among others.

Generally, polymer nanocomposites can be obtained through two routes: the first one is the polymerization of monomers in contact with the exfoliated clay and the second one uses existing transformation processes to produce nanocomposites, for example, by a reactive extrusion. There are, however, problems present due to the lack of affinity of the clay–polymer system because of the hydrophilic character of the particles. It is then necessary to treat the clay chemically to increase its affinity with the polymer matrix. This constitutes another whole area of research in the nanocomposites production.

The mixing of the nanoparticle with the polymer requires an intercalation process of the macromolecule into the clay galleries gap. This is a diffusion-controlled process that requires long contact times between the polymer and the clay under the pressure produced inside the extruder. The intercalation process leads to the exfoliation of the clay. However, low screw speeds and long residence times in

the extruder may cause polymer degradation. To avoid such problem that would enable complete clay exfoliation, it would be necessary to change the screw configuration or to consider the chemical modification of the clay. Moreover, clay exfoliation is not a sufficient condition to obtain optimum system performance. The problem of compatibility of the clay–polymer matrix is an outstanding one, and the thermodynamic processes involved in the synthesis of these materials [43, 44] constitute areas that are currently under investigation.

The macroscopic effects of the integration of nanoparticles into the polymer matrix are quite remarkable. For example, the barrier properties of the new systems are enhanced since the diffusion of gas molecules through the material is largely retarded. A lower permeability of O₂ is obtained without substantially modifying the production method of films, containers, bottles, etc. Oxygen permeability decreases drastically with nanoparticle concentration.

This chapter covers fundamental and applied research on polyester/clay nanocomposites (Section 31.2), which includes polyethylene terephthalate (PET), blends of PET and poly(ethylene 2,6-naphthalene dicarboxylate) (PEN), and unsaturated polyester resins. Section 31.3 deals with polyethylene (PE) and polypropylene (PP)–montmorillonite (MMT) nanocomposites, including blends of low density polyethylene (LDPE), linear low density polyethylene (LLDPE), and high density polyethylene (HDPE). Section 31.4 analyzes the fire-retardant properties of nanocomposites made of high impact polystyrene (HIPS), layered clays, and nonhalogenated additives. Section 31.5 discusses the conductive properties of blends of PET/PMMA (poly (methyl methacrylate)) and PET/HDPE combined with several types of carbon

black (CB). The synthesis and potential applications of barium sulfate particles with various morphologies (fibers, spherical) are discussed in Section 31.6, and finally, in Section 31.7 the new nanocomposites of graphene are briefly exposed.

31.2 POLYESTER/CLAY NANOCOMPOSITES

31.2.1 PET–Clay Nanocomposites

The processing of polymeric nanocomposites based on PET and a clay, MMT, was analyzed elsewhere [45]. The clay was chemically modified with a quaternary ammonium salt, and this was subsequently incorporated into the polymer using maleic anhydride (MAH) and pentaerythritol (PENTA) as compatibilizing agents.

An interesting observation is the reported decrease in melt viscosity of organo-clay composites, with respect to the matrix viscosity [46, 47]. Results reveal that PET nanocomposites behave quite differently in shear as opposed to elongation.

Nanocomposites of MMT polymer can be obtained by direct polymer melt intercalation where the polymer chains diffuse into the space between the clay galleries. This process can be carried out through a conventional melt-compounding process [6, 4].

Exfoliated and homogeneous dispersions of the silicate layers can be obtained in a straightforward manner when the polymer contains functional groups, for example, amide or imide groups [48, 49]. This is due to the fact that the silicate layers of the clay have polar hydroxyl groups, which are compatible with polymers containing polar functional groups [50]. Compatibilizers are usually small molecules (such as oligomers) containing polar groups that facilitate the intercalation of polymers between the silicate layers. As intercalation proceeds, the interlayer spacing of the clay increases, and the interaction of layers weakens. The intercalated clays containing the oligomers contact the polymer under a strong shear field. If the miscibility of the oligomer with the polymer is good enough to disperse at the molecular level, the exfoliation of the intercalated clay should occur. If miscibility is not good, phase separation occurs with no exfoliation.

Rheological studies of PET nanocomposites are not ample, but show very interesting features. In the low frequency range, the nanocomposites display a more elastic behavior than that of PET. It appears that there are some physical network structures formed due to filler interactions, collapsed by shear force, and after all the interactions have collapsed, the melt state becomes isotropic and homogeneous. Linear viscoelastic properties of polycaprolactone and Nylon-6 [51] with MMT display a pseudo-solidlike behavior in the low frequency range of

the spectrum, consisting of power-law dependence of the moduli with frequency. If shear flow is applied before, the magnitude of the moduli decreases in the aligned sample, implying that the weak interactions are destroyed by the flow. Nonterminal low frequency rheological behavior has also been observed in ordered block copolymers and smectic liquid crystalline small molecules [52, 53].

In highly interactive polymer–particle systems, solidlike yield behavior can be observed even at temperatures above the glass transition temperature of the polymer [54]. Polymer molecules can adopt stretched configurations that allow them to adsorb to the surfaces of many particles. Relative motion between polymer chains is retarded by immobilization due to polymer confinement between nanoparticle surfaces. The equilibrium thickness of the immobilized polymer layer is of the order of the radius of gyration of the molecule. Filler particles can be regarded as hard cores surrounded by immobilized polymer shells of comparable size.

According to small-angle neutron scattering (SANS) and birefringence experiments by Schmidt et al. [55–57], the influence of shear on viscoelastic-polymer–clay solutions gives rise to an alignment of the platelets along the flow direction and with increasing shear the polymer chains start to stretch. Polymer chains are in dynamic adsorption–desorption equilibrium with the clay particles to form a network. This network is highly elastic, since cessation of shear flow leads to fast recovery.

Another example of network formation is found in PEO (poly(ethylene oxide))–silica systems [58, 59]. At relatively small-particle concentrations, the elastic modulus increases at low frequencies, suggesting that stress relaxation of these hybrids is effectively arrested by the presence of silica nanoparticles. This is indicative of a transition from liquidlike to solidlike behavior. At high frequencies, the effect of particles is weak, indicating that the influence of particles on stress relaxation dynamics is much stronger than their influence on the plateau modulus.

A noteworthy finding has been that all the materials show two distinct relaxation dynamics, a fast and a slow relaxation [60]. The fast mode corresponds to relaxation of bulky polymer molecules, while the slow mode is related to relaxation of the filler structure with much longer time scales. As silica particles are physically connected with adsorbed polymer molecules, the formed polymer–particle network is a temporary physical network. On a long time scale, relaxation of this network occurs when immobilized polymer molecules connecting silica particles become free, via dissociation from silica particles or disentanglement from other immobilized polymer molecules.

Another interesting observation [61] is that remarkable increases in the elastic modulus at low frequency with low values of the molecular weight reflect the fact that an elastic network is formed due to the presence of the clays.

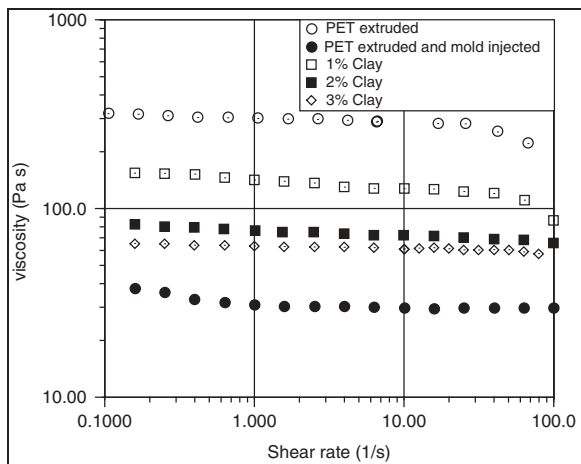


Figure 31.1 The processing of PET leads to loss of viscosity, while the addition of clays increases the viscosity at low contents. Extrusion screw speed is 50 rpm. Mold injection temperature is 7°C. The tests were made in a rheometer with parallel plates of 25 mm diameter. *Source:* Reproduced with permission from Sánchez-Solís A, Romero I, Estrada MR, Calderas F, Manero O. Polym Eng Sci 2004;44:1094 [61]. Copyright 2004 John Wiley and Sons, Inc.

On the other hand, another remarkable result is that the largest increases in the mechanical properties are observed in samples where the viscoelastic properties are of small magnitudes and have some of the lowest molecular weights. It seems that nanocomposites behave drastically different under tension as opposed to shear. This is advantageous with regard to molding operations, where the viscosity is low and the mold fills conveniently (Figs 31.1 and 31.2).

For example, the observed decrease in the shear viscosity with the addition of MAH and PENTA leads to lower pressure in the filling of the mold in the mold-injection operation. In fact, the injection pressure diminishes from 40,680 kPa for PET to 24,822 kPa in the system PET-clay-MAH (1 wt%) and to 13,790 kPa in the system PET-clay-PENTA under the same processing conditions. This corresponds to a threefold decrease in the viscosity. However, it is necessary to point out that the viscosity curves reported are built from simple shear rheometric flows. In the actual process operation, the fluid that fills the mold is subjected to a nonhomogeneous stress field, which is likely to develop slip at the walls and another complicated flow behavior [62]. In these circumstances, the *in situ* viscosity is probably lower than that measured in the rotational rheometer. Measurements of pressure drop versus flow rate made on the fluid that enters the mold would surely provide a more reliable value of the “process viscosity,” and hence a better evaluation of the effect of the nanoparticles on the flow behavior of PET.

31.2.2 PET-PEN/Clay Nanocomposites

PET and PEN form immiscible mixtures. Improved miscibility can be obtained by performing a transesterification reaction between both ingredients to produce copolyesters, which act as compatibilizers in the interface of the blend. This reaction, when carried out in a melt extruder, depends strongly on temperature and residence time, in particular, within 50–80 wt% PEN content [63]. Physical and mechanical properties of the resulting blend depend on the degree of transesterification and also on the resulting copolymer

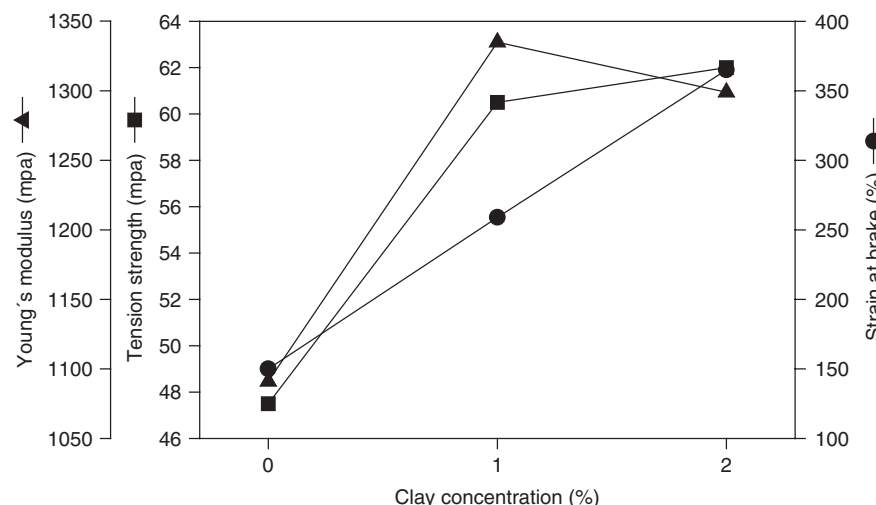


Figure 31.2 Mechanical properties of two modified clays, Clay-MAH and Clay-PENTA, in a 3–1 proportion are shown. Tension strength, Young's modulus, and strain at brake of PET matrix were improved by 18%, 30%, and 140% with 1% clay content, respectively. *Source:* Reproduced with permission from Sánchez-Solís A, Romero I, Estrada MR, Calderas F, Manero O. Polym Eng Sci 2004;44:1094 [61]. Copyright 2004 John Wiley and Sons, Inc.

microstructure, that is, whether it contains block or random substructures.

A great deal of attention on PET/PEN blends has been paid to elucidate the type of kinetics of the transesterification reaction, and, in particular, reversible second-order kinetics has been found in solution [64]. On the other hand, the reaction kinetics is strongly affected by terminal hydroxyl groups when the reaction is carried out in a mixing chamber [65]. In the same device, studies on the thermal, rheological, and mechanical properties for blends with 25, 50, and 75 wt% of PEN content have also been reported [66]. By using a twin-screw extruder, a block copolymer may be obtained via melt extrusion when the PEN content is 20 wt% [67].

From the industrial point of view, PET–PEN blends are attractive in the production of bottles for carbonated liquids filled at high temperatures. PEN imparts the blend a higher resistance to gas diffusion, better mechanical properties, and increased glass transition temperature (T_g). However, these benefits are partly offset by the cost of PEN, and for this reason, PEN contents in the blend higher than 20 wt% are not suitable. Besides, there are some problems in the production of this blend, since transesterification is promoted in systems with similar viscosity [68], but this requirement is difficult to meet since melt viscosity of the ingredients can be widely different. Another problem is that agents that promote miscibility can only be processed at small concentrations, of the order of 2 wt%; otherwise, mechanical properties are negatively affected [69]. Furthermore, for certain concentrations of the ingredients in the blend and the preparation method of the sample, for instance, film under pressure and quenching, some properties increase (such as tensile strength), but others decrease (such as Young's modulus) [70]. On the other hand, when the sample film is bioriented, both tensile strength and modulus improve [71]. It seems that the full relationship between transesterification and mechanical properties is not well understood yet because of the numerous factors and variables that affect this relationship.

Finally, shear viscosity is strongly affected by the clay in the blends, especially at high PEN contents. A lubricating effect rather than a filler effect reveals the possibility that the clay is not well dispersed in the polymer blend, and migration of particles in the flow to the wall region can explain the observed reduction in shear viscosity. When MMT clay is mixed with crystallizable polymers such as polyesters, some processing problems arise because the crystallization process is modified by nucleation effects induced by the nanoparticles. Moreover, these particles also influence the kinetics of transesterification between PET and PEN, besides other factors such as the reaction time and extruder processing temperature. In Reference 72, a quaternary alkyl ammonium compound (C18) and MAH were used to modify the surface properties of the clay

particles. Thereafter, the particles were mixed with PET and PEN to produce blends whose properties were examined. The PET–PEN/clay–C18 blend possesses a higher proportion of amorphous phase, because of the restriction to the normal crystallization process due to the particles, as evidenced in the low value of the crystallization enthalpy.

In the transesterification reaction, clay–C18 induces the largest proportion of NET (naphthalate-ethylene-terephthalate) groups as opposed to clay–Na⁺, which produces 22 times less NET groups. In spite of the fact that clay–Na⁺ is hydrophilic, the surfaces of all samples possess a hydrophobic character. This clay is highly incorporated into the polymer and presumably has a low concentration at the surface, as evidenced in the receding contact angle results that show a predominantly hydrophobic character of the surface. This blend also presents a solidlike behavior, as disclosed by the values of the storage modulus in the low frequency range of the spectrum, which provides evidence for the presence of a high entanglement density and large polymer–particle interactions (Fig. 31.3).

The rheological behavior of these materials is still far from being fully understood but relationships between their rheology and the degree of exfoliation of the nanoparticles have been reported [73]. An increase in the steady shear flow viscosity with the clay content has been reported for most systems [62, 74], while in some cases, viscosity decreases with low clay loading [46, 75]. Another important characteristic of exfoliated nanocomposites is the loss of the complex viscosity Newtonian plateau in oscillatory shear flow [76–80]. Transient experiments have also been used to study the rheological response of polymer nanocomposites. The degree of exfoliation is associated with the amplitude of stress overshoots in start-up experiment [81]. Two main modes of relaxation have been observed in the stress relaxation (step shear) test, namely, a fast mode associated with the polymer matrix and a slow mode associated with the polymer–clay network [60]. The presence of a clay–polymer network has also been evidenced by Cole–Cole plots [82].

The nanocomposite PET–PEN/MMT clay was studied under steady shear, instantaneous stress relaxation, and relaxation after cessation of steady flow [83]. Relaxation times of the slow mode in instantaneous stress relaxation were longer for the systems that have presumably permanent crosslinking networks (PET–PEN) or dynamic networks (PET–PEN–MMT). These results are consistent with those found in relaxation after cessation of flow (Fig. 31.4). Nanoclay addition somehow restricts the slow relaxation (due to polymer–particle interactions). The nanocomposite exhibits lower steady-state viscosity as compared to the polymer–matrix system. This is thought to be caused by polymer–polymer slipping, as revealed by the SEM observations (Fig. 31.5a and b).

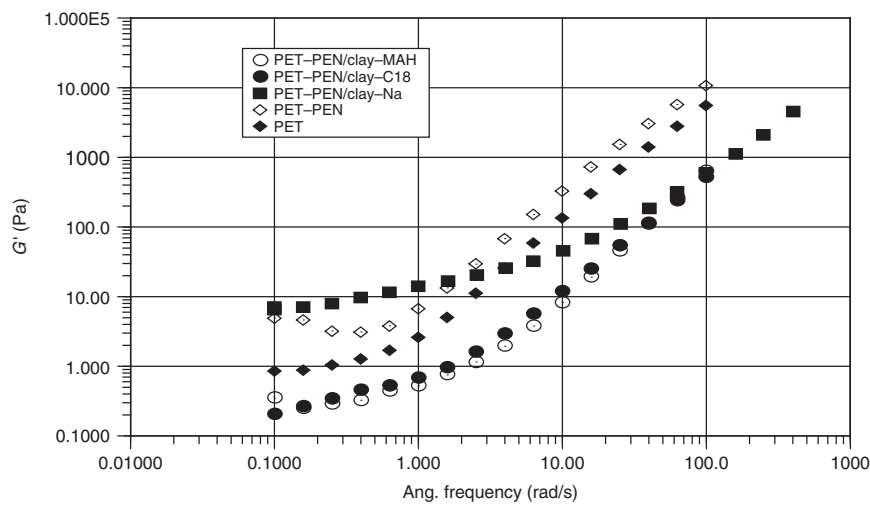


Figure 31.3 Variation of the storage modulus with frequency for PET/PEN–clay systems. *Source:* Reproduced with permission from Sánchez-Solís A, García-Rejón A, Estrada M, Martínez-Richa A, Sánchez G, Manero O. Polym Int 2005;54:1669 [72]. Copyright 2005 John Wiley and Sons, Inc.

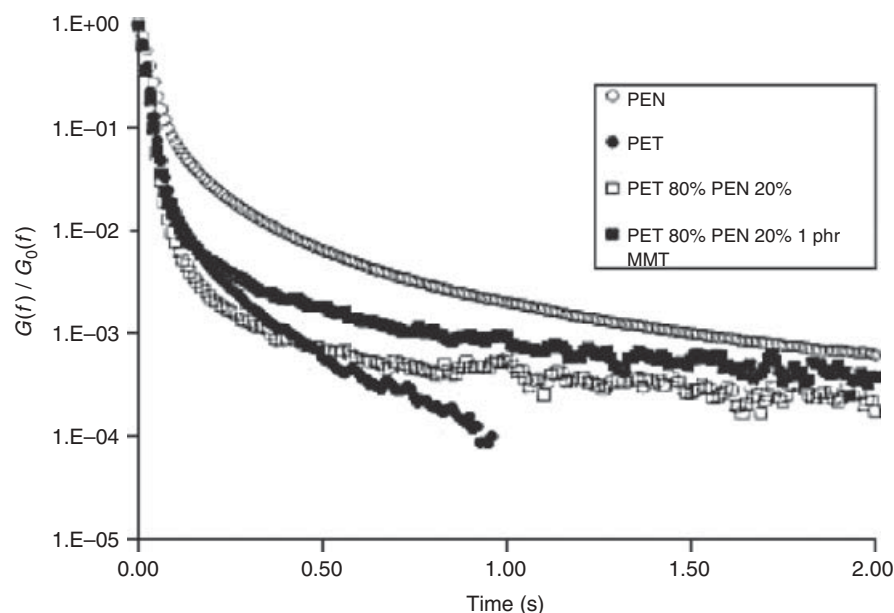


Figure 31.4 Stress relaxation curves after cessation of steady shear flow for the PET/PEN–clay systems (shear rate is 10 s^{-1}). *Source:* Reproduced with permission from Calderas F, Sánchez-Solís A, Maciel A, Manero O. Macromol Symp 2009;283:354 [83]. Copyright 2009 Wiley-VCH Verlag GmbH & Co. KGaA.

31.2.3 Polyester Resin/Clay Nanocomposites

Unsaturated polyester resins are produced by a crosslinking reaction in solution of a prepolymer dissolved in styrene initiated with peroxides. This curing reaction renders an insoluble and infusible crosslinked matrix with high rigidity, but fragile. This matrix is usually reinforced with glass fibers or fillers of micrometric size. Since the mechanical properties of such materials depend strongly on

the interaction among phases, attention has been given to the analysis of matrix–filler interactions.

The effect of high shear mechanical mixing and sonication methods on the physical properties of the nanocomposites has been analyzed [84] using modified clays with a quaternary ammonium salt and calcium carbonate [85] and silane-treated clays [31]. Although the nanoclay is usually chemically modified to make it organophilic and compatible with the polymer matrix, untreated MMT was

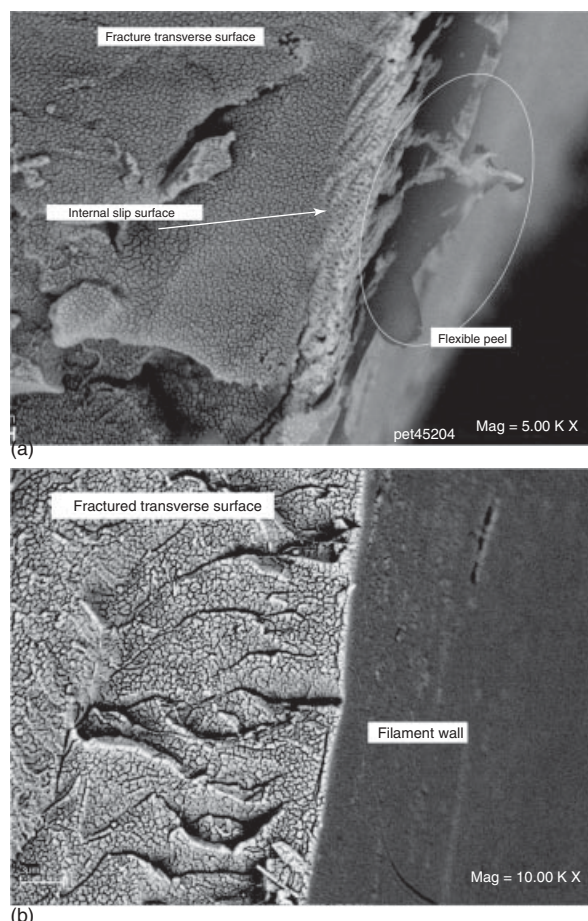


Figure 31.5 SEM micrograph of the edge region of a capillary filament: (a) blend with clay and (b) blend without clay. *Source:* Reproduced with permission from Calderas F, Sánchez-Solís A, Maciel A, Manero O. *Macromol Symp* 2009;283:354 [83]. Copyright 2009 Wiley-VCH Verlag GmbH & Co. KGaA.

also used, taking advantage of its high swelling capacity in polar liquids such as water or alcohol, allowing the expansion of the interlaminar spacing and the subsequent intercalation or exfoliation of the clay after polymerization.

Exfoliation of MMT in the polymer matrix has been shown to occur through a process called *slurry compounding*, in which the MMT swells in water and then is mixed with Nylon-6 under extrusion [86]. Other techniques include the addition of MMT to water and the subsequent replacement of water by alcohol or acetone with further addition of a silane agent to modify the clay and make it compatible with the polymer matrix [87–89]. Intercalated nanocomposites were also obtained by slurry compounding introducing an epoxy monomer in the hydrated MMT galleries [90].

Preparation of nanocomposites using the slurry compounding process has been carried out with Nylon and epoxy resins. In Reference 91, this method is implemented

to obtain polyester resin–clay nanocomposites. The influence of MMT slurry on the crosslinking reaction with the unsaturated polyester resin, and the effect of the clay hydration on the thermal and mechanical properties of the resulting nanocomposites have been analyzed. In addition, changes with respect to the pristine polyester resin on the gelation temperature and morphology of the nanocomposites prepared with this novel method were also analyzed in detail.

The procedure to obtain nanocomposites based on unsaturated polyester resins leads to improvements in the order of 120% in the flexural modulus, 14% in flexural strength and 57% increase in tensile modulus with 4.7% of clay slurry content. Thermal stability augments and the gelation temperature increases to 45 °C, as compared to that of the resin (Fig. 31.6). It seems that adding water to the MMT allows better intercalation of polymer chains into the interlamellar space. Because clay is first suspended in water, this improves dispersion and distribution of the particles in the resin matrix. Longer gelation times lead to more uniform and mechanically stronger structures and to yield stresses (Fig. 31.7). Enhanced polymer–clay interactions are revealed by XPS in this case (Fig. 31.8).

31.3 POLYOLEFIN/CLAY NANOCOMPOSITES

31.3.1 Polyethylene/Clay Nanocomposites

As pointed out before, the polymer may be functionalized with polar groups to enhance compatibility with the modified clay. Bellucci et al. [92] have reported that the formation of polymer–clay nanocomposites depends mostly on the polymer properties, clay characteristics, and type of organic modifier.

In the case of LDPE–clay nanocomposites, the mechanical behavior does not depend only on the degree of exfoliation or the clay content but also on the presence of substantial amounts of compatibilizer [93, 94]. Besides the chemical modification of the clay, it is then necessary to turn the polymer matrix more polar with the grafting of polar groups. Traditionally, MAH has been used as the polar group to induce compatibility due to the high reactivity of the anhydride group.

The use of organically modified clays and PE grafted with MAH allows for the production of polymer nanocomposites with improved mechanical properties [95, 96]. Liang et al. [97] reported improvements in the mechanical properties when the HDPE concentration is larger than 6 wt%. Wang et al. [98] reported that the most important factors for improved PE–clay nanocomposites are the chain length of the intercalant (chains with more than 16 carbon atoms) and low amount of grafting (0.1 wt%). Chrissopoulos et al. [99] observed that exfoliated structures are obtained when the proportion of MAH-g-PE/clay is

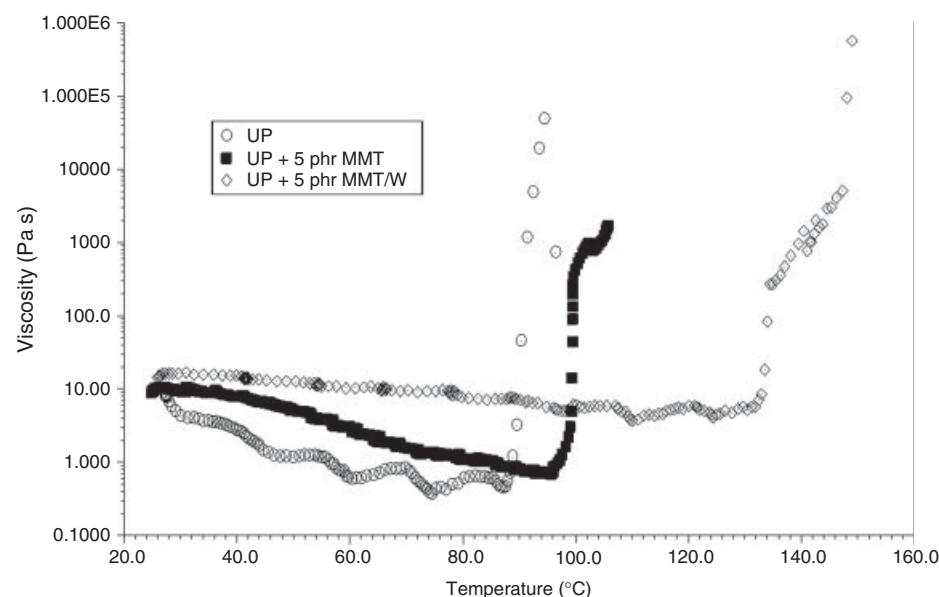


Figure 31.6 Shear viscosity versus temperature for an unsaturated polyester resin (UP)–clay slurry indicating the temperature for the onset of the gelation reaction. *Source:* Reproduced with permission from Rivera-Gonzaga JA, Sanchez-Solis A, Manero O. *J Polym Eng* 2012;32,1 [91]. Copyright 2012 De Gruyter.

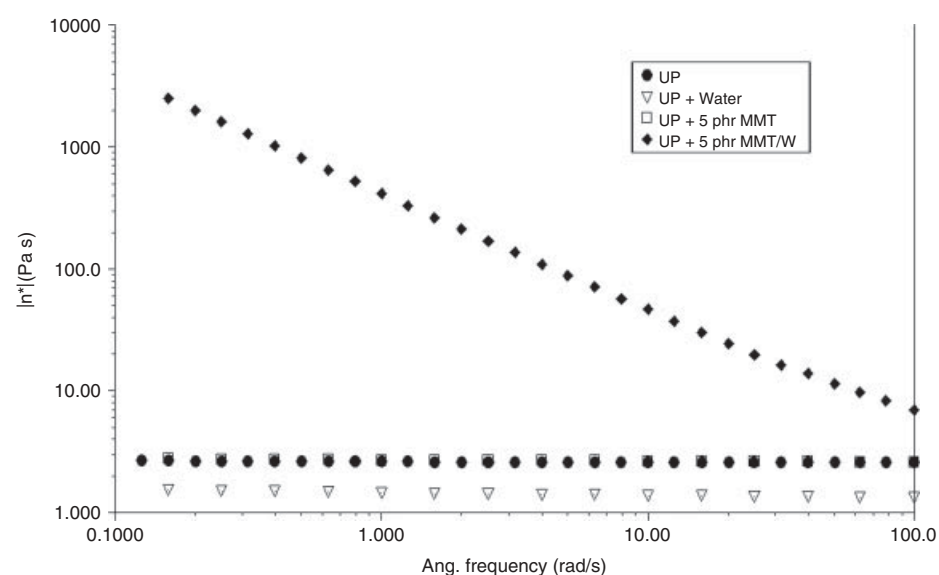


Figure 31.7 Complex viscosity as a function of oscillation frequency for an unsaturated polyester resin–clay slurry system. *Source:* Reproduced with permission from Rivera-Gonzaga JA, Sanchez-Solis A, Manero O. *J Polym Eng* 2012;32,1 [91]. Copyright 2012 De Gruyter.

larger than 4.5/1. Arrunvisut et al. [100] further agreed in that hydrogen bridging between the MAH-grafted groups and hydroxyl groups from the clay edges favor phase compatibility.

Nanocomposites exhibiting improved mechanical properties reveal strong polymer–clay interfacial adhesion, increasing with the exfoliation degree of the clay [96, 101].

However, in addition to this, there is evidence of improvements found with partial exfoliation [102, 103] of tactoids formed by 10–20 lamellas, due to required flexibility of the dispersed particles. Interfacial interactions are of fundamental importance in the structure and properties of nanocomposites. Lee et al. [104] proposed that the interactions of the polar maleic groups grafted to PP with hydroxyl groups of

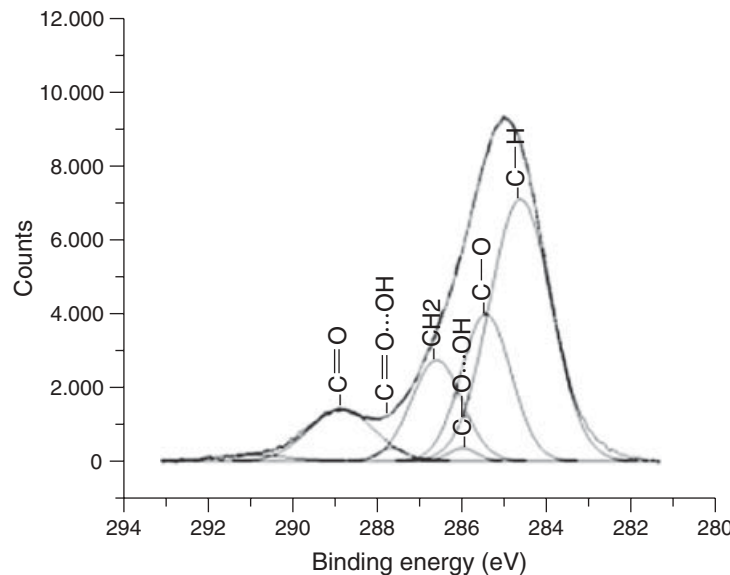


Figure 31.8 XPS of the UP-MMT/W system revealing interactions between $\text{C}=\text{O}\cdots\text{HO}$ and $\text{C}-\text{O}\cdots\text{HO}$ groups. *Source:* Reproduced with permission from Rivera-Gonzaga JA, Sanchez-Solis A, Manero O. *J Polym Eng* 2012;32,1 [91]. Copyright 2012 De Gruyter.

the clay are of the van der Waals type and no chemical reactions are likely. Xie et al. [105] suggested, alternatively, a possible formation of links between the maleic groups of PP and the ammonium groups in the clay galleries. In addition, Walter et al. [106] mentioned the possibility of a reaction between the MAH and octadecyl amine, used to modify the clay.

The ternary blends mentioned, nonetheless, are used in stretch and thermoshrinkable films in the packing industry and in the agricultural uses to protect crops. In this regard, an improved understanding of the particle–polymer interactions may motivate the formulation of new materials with specific properties.

In Reference 107, the effect of grafting of a polar group (MAH) onto LDPE chains and the chemical modification of clay particles with 2,6-diaminocaproic acid (*L*-lysine monohydrochloride) to produce nanocomposites with a matrix composed of a ternary blend of PEs (LDPE, LLDPE, and HDPE) was studied in detail. X-ray diffraction was used to determine the exfoliation degree of the clay. Morphological features were revealed by scanning electron microscopy and thermal analysis disclosed the thermal stability of the samples. Comparative analyses of the mechanical (under tension) and rheological properties of the nanocomposites were carried out as well.

It was shown that the PE ternary blend composed of 25%, 42%, and 33% HDPE, LLDPE, and LDPE, respectively, possessed the required mechanical properties to resist tear forces in films for packing and agricultural uses. MAH grafting on LDPE (0.36%) in addition to *L*-lysine-modified clay induced a large clay-grafted polymer

interaction. With respect to the reference ternary blend, the resulting system presented increases of 13% in tensile strength, 140% strain at break, 111% strength at break, and 11% tear strength with no substantial changes in the modulus. Rheological data revealed a shear-thinning behavior in viscosity consistent with high orientation at high shear rates, assisted by the clay particles. The decrease in the slope of the storage modulus in the low frequency range under oscillatory shear manifested high clay particle-grafted LDPE interaction. The entanglement density and the relaxation time were strongly affected by the presence of the modified clay particles if no MAH-grafted chains were present to promote polymer–clay-enhanced interactions.

The improvement in the mechanical properties of the nanocomposite LDPE-*g*-MAH/bentonite-*L*-lysine as compared to those of the blend HDPE–LLDPE–LDPE were explained in terms of a good exfoliation degree and uniform dispersion of the platelets in the polymer matrix. To prove this relationship, diffraction X-ray spectra, TEM, and rheological tests revealed changes in the morphology and linear viscoelastic properties identified with the compatibilizer action through the polar groups. The nanocomposite synthesis was possible even at very low grafting (0.45 wt%) and with small amounts of organo-clay (0.49%).

31.3.2 Polypropylene/Clay Nanocomposites

PP is a commodity polymer used in mostly automobile applications (bumpers and interiors) and in packaging and food containers. Mica and talc are used as fillers (from 20% to 40%) to improve dimensional stability and mechanical

properties. Clays of several kinds can enhance stiffness and resistance at much lower loadings. They can also yield improved barrier resistance and flame retardance. In the case of PP, from 5 to 10 wt% clay content, improvements in the polymer properties are found. Melt compounding has been used by Okada et al. [6, 7, 108] for PP-layered silicate nanocomposites.

The interactions between the oxygen atoms of the clay surface and the polymeric compatibilizer must be stronger than the interactions between the clay surface and the surfactant to obtain delamination of the silicates [109]. The length of the surfactant chain is an important variable that influences the level of exfoliation. In the case of alkyl amides, the chain must contain more than eight carbon atoms for the clay to be exfoliated in PP. Some authors [110] have found that with 1 wt% MA content in PP-g-MAH, a 2 : 1 ratio is adequate to obtain exfoliation of the clay. A major limitation to the grafting reaction is polymer degradation. As the grafting content increases, the molecular weight of PP is reduced and, hence, the mechanical properties.

Procedures for melt compounding usually mix the clay with the functionalized grafted polymer (PP-g-MAH) in a 1 : 3 proportion and this concentrate may be thereafter mixed with PP to get a final 80/15/5 PP/PP-g-MAH/clay proportion. Other procedures suggest first mixing the grafted polymer with the clay for exfoliation and thereafter these ingredients are mixed with PP with peroxides. A third method suggests the incorporation of clay to a mixture of PP, PP-g-MAH, and surfactant using a ratio of 6 : 1 of PP-g-MAH to clay [111]. An example of the improved adhesion of fibers to the PP matrix due to the compatibilization action by the polar groups is shown in Figures 31.9 and 31.10.

The rheological properties of the nanocomposites show an increase of the elastic modulus with MAH content of the grafted polymer and also an increase of the modulus with clay content. Under small amplitude oscillatory flow, plots of the dynamic viscosity with complex modulus show that in composites, the dynamic viscosity increases sharply with decreasing stress, in fact revealing the presence of a yield stress in clay systems as compared to silicate-free melts [112]. Under extensional flow, the nanocomposites display strain hardening, which is absent in the PP matrix or in the grafted PP. Orientation of the platelets normal to the flow in uniaxial extension contrasts to that under biaxial extension, where the platelets are now positioned along the flow direction [113]. When the nanocomposites were extruded through a converging die section, with strong uniaxial extensional flow, the platelets are in this case oriented along the flow direction. Research on mechanical properties and fire-retardant properties may be found elsewhere [114, 115].

31.4 POLYSTYRENE/CLAY NANOCOMPOSITES

31.4.1 HIPS/Clay Nanocomposites

Improvements in the reduction of flammability of polymers with low clay contents and better processability have been reported, in addition to reductions in the concentration of toxic vapors produced in the combustion stage [116–120]. In connection to their flame-retardant properties, exfoliated nanocomposites based on PP [121, 122, 115, 123], PS [115, 123, 124], poly(ethylene-vinyl acetate) [125, 126], styrene-butadiene rubber [127], PMMA [128], polyesters [129], acrylonitrile butadiene styrene [130], and polymeric foams [131] have been the subject of increasing attention.

The flame-retardant mechanism involves the formation of a carbonaceous char layer on the surface of the burning material due to the presence of clay particles that act as an insulating barrier. The extent of this layer depends, among various factors, on the concentration, distribution, dispersion, and compatibility of the particles with the polymer. Phosphorous compounds are among the most popular nonhalogenated flame-retardant agents used with thermoplastic polymers, thermosets, textiles, and coatings. In these systems, the mechanism of flame-retarding depends mainly on the type of phosphorous compound and on the polymer microstructure [132].

In some cases, such as in the PET system, it is possible to exfoliate the clay by extrusion without previous clay treatment [61]. In Reference 133, a comparative study is carried out on the use of pristine-layered MMT-Na⁺ and MMT-Na⁺ intercalated with triphenyl phosphate (TPP), as flame-retardant agents when mixed with HIPS. Results of the burning rate, mechanical, impact, and rheological properties of the HIPS nanocomposite were presented. The HIPS-MMT clay (MMT-Na⁺) blends present increasing burning rate with clay content as compared to that of HIPS alone, even at high clay concentrations. TPP acts as a flame-retardant agent when it is intercalated in the clay galleries. These results have been explained on the basis of the combined effect of decreasing viscosity of the flowing blend and temperature.

In the blends with TPP (4.7%), the mechanical properties of HIPS are retained. For TPP concentrations larger than 5.6%, the material self-extinguishes as dripping of the burning material occurs. In the MMT-i-TPP blends, the degradation temperature of the nanocomposite compared with that of HIPS is not affected. MMT-i-TPP blends work as a fire-retardant agent, although in the extrusion process the clay with TPP is not exfoliated.

31.4.2 HIPS-PET/Clay Nanocomposites

HIPS is widely used in the audio, video, automotive, aircraft industries, and in electric appliances, among others.



Figure 31.9 Mix of PP-PP-g-MAH with glass fibers. Adhesion between the fibers and matrix is poor.



Figure 31.10 Mix of PP/PP-g-MAH/clay-L-lysine. Adhesion of the fibers to the matrix is apparent, brought about by the change in surface tension with the modified clay.

Small rubber particles embedded in the PS matrix provide high impact resistance [134, 135]. However, this polymer is highly flammable as it is exposed to fire, due to its chemical structure, where aliphatic groups bound to aromatic moieties provide hydrogen to the combustion reaction without forming any char layer that may prevent fire propagation [132, 136].

To improve flame retardation in HIPS, agents formulated from halogenated compounds have been traditionally used [137, 138]. These compounds form, nevertheless, highly toxic vapors during the combustion process. Recently, alternative flame-retardant compounds have been developed, ensuring that no toxic vapors are expelled, presenting an augmented thermal stability. Furthermore,

reports have highlighted that a carbonaceous layer is easily formed during combustion, acting as a barrier to energy transfer and mass loss [118–120]. Attention in the recent literature has been given to the flame retardation properties of polymer nanocomposites [139–141].

In Reference 142, PET was used in blends with HIPS and modified MMT clay. The use of PET was justified since this polymer self-extinguishes under fire. In addition to study the flame-retardant properties of the HIPS–clay and HIPS–PET–clay systems, mechanical and rheological properties were measured to provide explanations on the

mechanism by which the polymer nanocomposites inhibit flame propagation. The mechanism proposed considered that clay particles stay at the interface between both polymers, since the interfacial tension of the particles with HIPS is larger than that with PET. The clay particles in the PET microspheres then promote the formation of the carbonaceous layer that leads to diminishing burning rate (Figs 31.11 and 31.12).

In Reference 143, the analysis of the processes aimed at reducing the flammability properties of HIPS with the use of clays and a nonhalogenated flame-retardant

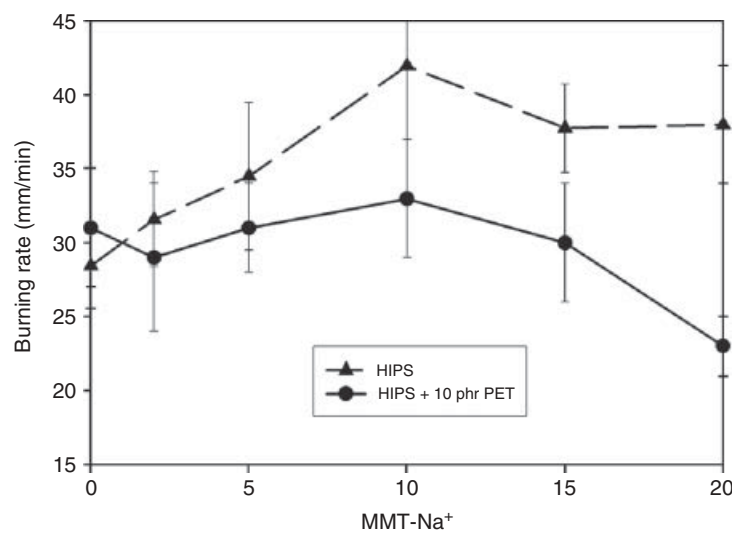


Figure 31.11 HIPS–clay and HIPS–PET–clay systems. Burning rate as a function of clay content. *Source:* Reproduced with permission from Rivera-Gonzaga JA, Sanchez-Solis A, Manero O. J Polym Eng 2012;32,1 [91]. Copyright 2012 De Gruyter.

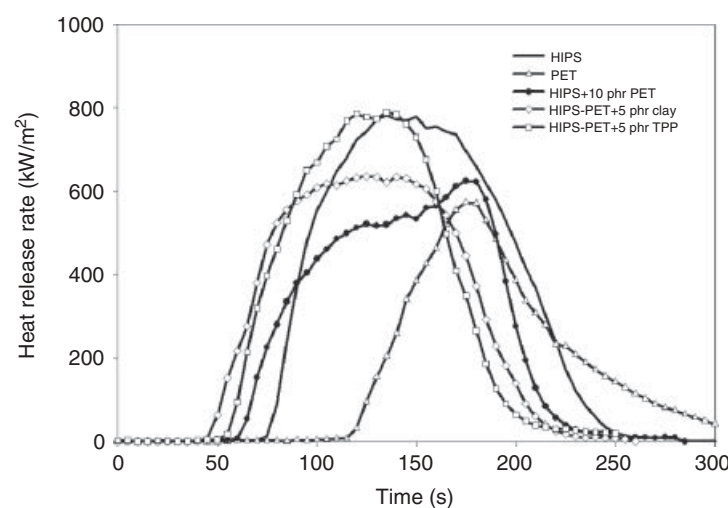


Figure 31.12 Heat release rate plotted with time for HIPS, PET, HIPS–PET (10 phr), HIPS–PET(10 phr) + 5 phr clay; and HIPS–PET(10 phr) + 5 phr TPP. *Source:* Reproduced with permission from Sanchez-Olivares G, Sanchez-Solis A, Manero O. Int J Polym Mater 2008;57:417 [142]. Copyright 2008 Taylor & Francis.

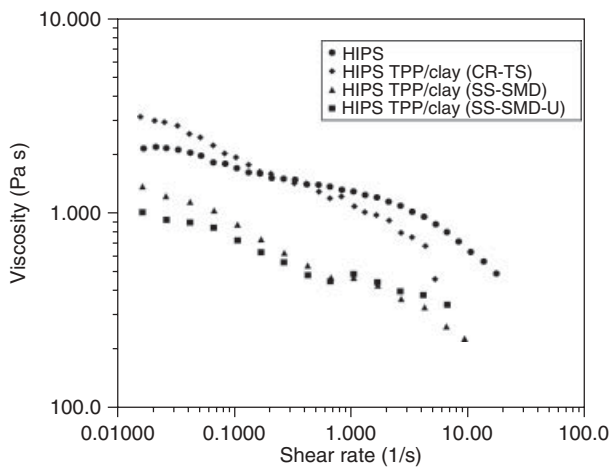


Figure 31.13 Shear viscosity as a function of the shear rate for the HIPS–TPP/clay blends. CR-TS, twin-screw counter-rotating extruder; SS-SMD, single-screw extruder with the static mixing die; SS-SMD-U, single-screw extruder with the static mixing die and sonication. *Source:* Reproduced with permission from Sanchez-Olivares G, Sanchez-Solis A, Camino G, Manero O. Express Polym Lett 2008;2:569 [143]. Copyright 2008 BME-PT.

additive, maintaining the original mechanical properties of HIPS, mainly the impact resistance, was carried out. The use of different extrusion processes was intended to improve clay and flame-retardant agent dispersion to reduce HIPS flammability. The extrusion processes considered include intermeshing counter-rotating twin-screw, single-screw with a static-mixing die, and the latter with sonication transducers placed on the die itself (Fig. 31.13).

This study demonstrated that the HIPS–TPP/clay blend properties (flammability, combustion, thermal, rheological, and mechanical) depend on the dispersion and distribution of the particles into the polymer matrix. Three extrusion processes were considered to produce different degrees of

particle dispersion. When this was good (single-screw with the static mixing die process), the peak in the heat release rate diminished in cone-calorimetric tests. The contrary occurred (twin-screw process) when particle dispersion was not uniform (Figs 31.13 and 31.14).

31.5 POLYMER/CARBON BLACK NANOCOMPOSITES

31.5.1 PET – PMMA/Carbon Black Nanocomposites

The electrical properties of insulating polymers may be modified when they are mixed with conductive particles such as metal powder, CB, graphite, or an intrinsically conducting polymer. Among the available fillers, the most popular is carbon CB. The selective localization of CB particles in multiphase polymeric materials is a favorable condition for obtaining heterogeneous microdispersion of CB [144–152]. It was found that CB distributes unevenly in each component of the immiscible polymer blend. Two types of distribution were observed: in the first, CB was distributed predominantly in one phase of the blend homogeneously. In the second, the conductive particles concentrated at the interface of the two phases. The conductivity of these composites was determined by two factors: the preferential concentration of CB in one phase and the structural continuity of this phase. This double percolation, that is, percolation of the polymer phases and percolation of the CB particles, or cocontinuous phase morphology, depicts especially low resistivity values. Interfacial free energies, mixing kinetics and viscosities, and polymer polarity and crystallinity are important factors governing the selective localization of CB. The production of low conductive materials with permanent antistatic properties using polymeric alloys has been given attention by Lee [153].

In Reference 154, PMMA was selected as it is immiscible with PET. The description of the electroconductive properties of this immiscible polymer blend filled with CB was carried out. To properly analyze the results obtained, models that predicted the selective location of CB in the blend were considered. The presence of CB extensively modified the rheological and conductive properties of the blend. Resistivity decreased similarly in both PET and PMMA with CB concentration. However, the immiscible polymer blend extensively modified this behavior because resistivity became a function of morphology and location of CB in the polymers. Viscosity was observed to be a strong function of PET content at high CB concentrations. Indeed, resistivity decreases continuously (a drop of seven decades) for 20% CB (PET basis) from 0% to 60% PET content. The same behavior (similar slope) was observed for 5% CB, but the conductivity curve was shifted to higher PET contents. It was shown that the preferential CB location in

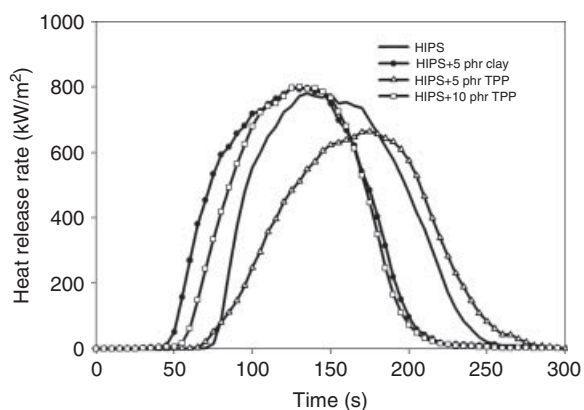


Figure 31.14 Heat release rate plotted with time for HIPS and blends with clay and TPP. *Source:* Reproduced with permission from Sanchez-Olivares G, Sanchez-Solis A, Camino G, Manero O. Express Polym Lett 2008;2:569 [143]. Copyright 2008 BME-PT.

the PET phase is explained on the basis of surface tension values. The polar groups of PET interacted more strongly with the conductive CB particles, resulting in a relatively higher concentration of CB in PET.

31.5.2 PET-HDPE/Carbon Black Nanocomposites

In these systems, it is possible to obtain low percolation thresholds if a double percolation is present, that is, particle and phase percolation. This effect may be observed when the conductive particles, localized preferentially in one polymer phase, have a concentration equal or larger than the electric percolation threshold, and when the host polymer phase is the matrix or continuous phase of the polymer blend [155]. There are several models that describe the electroconductivity of these systems: the effective medium theory, the onset for percolation theory, and thermodynamic models. Sumita's model considers the formation of chainlike conductive structures [151, 156].

The study of electroconductive polymer systems, based on conductive particles and polymer blends, has been quite intensive during the recent past. Gubbels et al. [149] studied the selective localization of CB particles in multiphase polymeric materials (PS and PE). According to these results, the percolation threshold may be reduced by the selective localization of CB. The minimum resistivity was obtained when double percolation (phase and particle percolation) exists in the PS-PE blend. In addition, it was found that the percolation threshold may be obtained at very low particle concentrations, provided that CB is selectively localized at the interface of the blend components. Soares et al. [150] found that the type of CB (i.e., different surface areas) does not affect the conductivity of the blend with 45/55 PS/PIP (polyisoprene) composition.

Blends of PET/HDPE have been treated previously in the literature [157, 158]. These are immiscible, but the addition of compatibilizers improves the mechanical properties of the blend, such as styrene-ethylene/butylene-styrene (SEBS) and ethylene propylene diene monomer (EPDM) [157], MAH [158], Poly(ethylene-stat-glycidyl methacrylate)-graft-poly(acrylonitrile-stat-styrene) (EGMA), poly(ethylene acrylic acid), and maleated copolymers of SEBS, HDPE, ethylene-propylene copolymer (EP). The addition of compatibilizers modifies the rheological properties of blends of PET with HDPE, in such a way that increases in viscosity are observed as the component interactions augment. Changes in crystallization of PET were evaluated in blends with Polyphenylene sulfide (PPS), PMMA, HDPE aromatic polyamides, and copolyesters [159].

CB easily mixes with elastomers and thermoplastics. It is made of colloidal-size particles that provide a good dispersion in the matrix and also good mechanical properties [160, 161]. The manufacturing process of CB involves the thermal decomposition of petroleum or natural gas [162].

The product leaves the oven at high temperature in the form of particle agglomerates with high surface area and with a quasigraphite conformation. The most important properties of CB are structure and surface area. The structure of CB is characterized by the arrangement, distribution and ordering of the particles, which is itself a function of the surface area, and number of particles in each aggregate. The structure is characterized by the value of the absorption of dibutylphthalate (DBP) or by the Brunauer-Emmet-Teller method. In Reference 163, attention was given to the rheological and electroconductive properties of PET/HDPE blends filled with CB. Particular emphasis was given to the effect of different types of CB, comprising different surface areas, structure, and porosity, upon the resulting rheological and electroconductive properties of the blend.

The rheological properties of the blends affect the structural arrangement of particles in the matrix formed by the blend of two immiscible polymers. Particle structure, chemical properties of the surface, morphology of the surface, size, content, and orientation are important factors, besides the properties of the matrix, to obtain conducting blends. Higher viscosities are recorded in the systems with more structured CB samples. CB is preferentially located in the more viscous phase (HDPE) due to the lower interfacial tension between CB and HDPE. In more structured CBs, the percolation threshold is observed to occur at low concentrations of CB particles, in the region of high HDPE content. The system exhibits high conductivity when HDPE is the dispersed phase. In this case it is likely that CB forms conductive pathways either in the dispersed HDPE phase or at the interface between the two polymers.

31.6 NANOPARTICLES OF BARIUM SULFATE

Barium sulfate (BaSO_4) has an industrial relevance due to its whiteness, inertness, high specific gravity, and optical properties, such as opacity to UV rays and X-rays [164–167]. It is mainly used as a radio-contrast agent, filler in plastics, extender in paints, coatings and additive in pharmaceutical products, and in printing ink. Nowadays, interest on this material has been renewed with the development of methods to produce nanosized particles, supraparticles of a well-controlled number of nanoparticles and mesocrystals that mimic biomimetic processes.

Among the methods for nanoparticle synthesis, controlled precipitation has the advantage of good reproducibility, low cost, and the use of mild reaction conditions within a relatively simple process. This method can improve the quality of the product in terms of controlling the particle size and the particle size distribution. Concentration, pH, temperature, reaction media, and the introduction of stabilizing agents (chelating agents, polymeric inhibitors, surfactants, and other organic additives) are the most important parameters to promote nucleation and controlled growth.

The control of shapes of BaSO_4 has been the object of numerous studies. Li et al. prepared ellipsoidal nanocrystals by using ethylene diamine tetraacetic acid (EDTA) [168], while Yu et al. obtained fibers in presence of sodium polyacrylate [169]. Likewise, using the same agent, Wang et al. have reported a well-established method to obtain cones, fiber bundles as well as elucidating their crystallization and its associated kinetic mechanisms [170, 171]. The kinetics of the crystallization process involves the nucleation and growth rates of the crystal, which are directly dependent on the saturation ratio. This ratio is the driving force for nucleation and growth and determines the induction period along which a stationary cluster distribution is reached and critical nuclei are formed [172]. Judat and Kind proposed a mechanism for BaSO_4 formation that involves molecular and aggregative growth [173]. Qi et al. synthesized a variety of well-defined morphologies using double-hydrophilic block copolymers as crystal growth modifiers to direct the controlled precipitation as a function of pH [174, 175]. A possible mechanism for the development of (defect-free growth) bundles of BaSO_4 nanofilaments from the amorphous precursor particles by attractive van der Waals forces and crystal multipole forces was proposed (vectorially directing).

In Reference 176, the morphology of BaSO_4 nanostructures, synthesized by controlled precipitation, was studied in detail. The influence of the capping agent, pH, reaction media, and aging, on the agglomerate shape, primary, and secondary particle size, was further analyzed. The synthesis of nanometric BaSO_4 in dimethyl sulfoxide (DMSO) allows the production of long fibers (Fig. 31.15). HRTEM observations allowed a direct assessment of self-assembled primary barium sulfate nanoparticles, which suggest a brick-by-brick assembling mechanism via hierarchical organization during aging processes. Direct observation of self-assembled primary particles by HRTEM reveals that fibers are formed via hierarchical organization of barium sulfate nanoparticles during aging processes (Fig. 31.16).

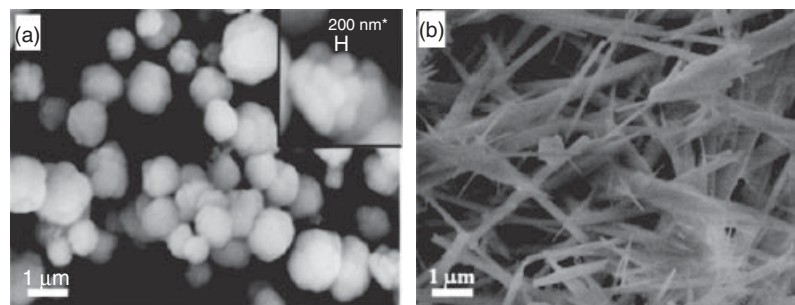


Figure 31.15 BaSO_4 aggregates at room temperature: (a) after the reaction and (b) past eight days of aging. *Source:* Reproduced with permission from Romero-Ibarra IC, Rodriguez Gattorno G, Garcia Sanchez MF, Sánchez Solís A, Manero O. Langmuir 2010;26: 6954 [176]. Copyright 2010 American Chemical Society.

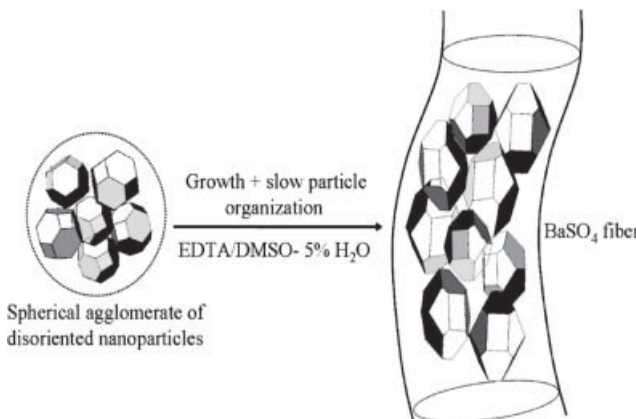


Figure 31.16 Schematic representation of the BaSO_4 fiber formation mechanism by electrostatic multipolar interactions. *Source:* Reproduced with permission from Romero-Ibarra IC, Rodriguez Gattorno G, Garcia Sanchez MF, Sánchez Solís A, Manero O. Langmuir 2010;26:6954 [176]. Copyright 2010 American Chemical Society.

31.7 POLYMER/GRAFENE NANOCOMPOSITES

Graphene–polymer nanocomposites share with other nanocomposites the characteristic of remarkable improvements in properties and percolation thresholds at very low filler contents. Although the majority of research has focused on polymer nanocomposites based on layered materials of natural origin, such as an MMT type of layered silicate compounds or synthetic clay (layered double hydroxide), the electrical and thermal conductivity of clay minerals are quite poor [177]. To overcome these shortcomings, carbon-based nanofillers, such as CB, carbon nanotubes, carbon nanofibers, and graphite have been introduced to the preparation of polymer nanocomposites. Among these, carbon nanotubes have proven to be very effective as conductive fillers. An important drawback of them as nanofillers is their high production costs, which

impede their mass production of composite materials. In this regard, graphene can provide new means in the field of nanocomposite production.

Graphene is considered bidimensional carbon nanofiller with a one-atom-thick planar sheet of sp^2 -bonded carbon atoms that are densely packed in a honeycomb crystal lattice. It is regarded as one of the thinnest materials with tremendous application potential. Graphene and polymer/graphene nanocomposites have remarkable properties, among these:

1. *Mechanical Properties.* The tensile strength of graphene is similar or slightly higher than carbon nanotubes, but much higher than steel, Kevlar, HDPE, and natural rubber [178]. Graphene-based polymer nanocomposites exhibit superior mechanical properties compared to the neat polymer or conventional graphite based composites. This is attributed to the very high aspect ratio of the graphene filler.
2. *Thermal Stability and Conductivity.* Thermal degradation temperature of PMMA, PS, and PVA (poly(vinyl alcohol)) nanocomposites shifts up by 10–100 °C. During combustion [179], nanoparticles form a network of char layers that retards the transport of decomposition products. The thermal conductivity of epoxy composites is four times higher than that of the neat epoxy resin with 5 wt% loads.
3. *Dimensional Stability.* Since graphite has a negative thermal expansion coefficient [180], graphene can

prevent dimensional changes in polymers when incorporated and oriented appropriately.

4. *Gas Permeation.* Nanocomposites with homogeneously dispersed graphene in the polymer matrix also exhibited good barrier properties [181]. N_2 and He permeation rates were suppressed several-fold by the addition of functionalized graphene.
5. *Electrical Conductivity.* Graphene-based polymer nanocomposites exhibit a several-fold increase in electrical conductivity [182]. These improvements are due to the formation of a conducting network by graphene sheets in the polymer matrix. The maximum or very high electrical conductivity was obtained using a very low graphene loading in different polymer matrices compared to other carbon fillers. Conducting polymer/graphene composites can also be used as electrode materials in a range of electrochromic devices. The polymer/graphene flexible electrode has some commercial applications in LEDs, transparent conducting coatings for solar cells and displays.

31.7.1 Synthesis and Structural Features of Graphene

Graphene can be prepared using four different methods [183]. The first is chemical vapor deposition (CVD) and epitaxial growth, such as the decomposition of ethylene on nickel surfaces. The second is the micromechanical exfoliation of graphite. The third method is epitaxial growth on electrically insulating surfaces, such as SiC, and the fourth is the solution-based reduction of graphene oxide (Fig. 31.17).

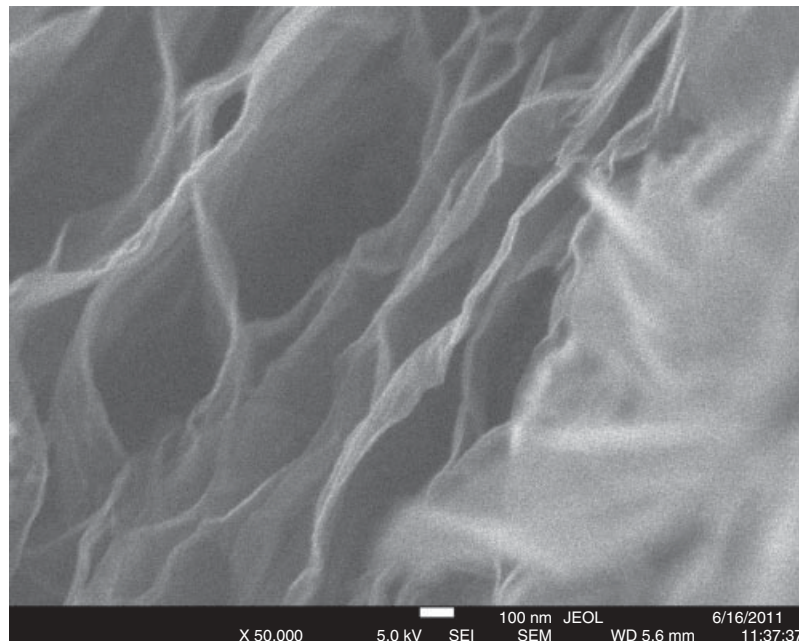


Figure 31.17 HRSEM micrograph of graphene laminates obtained from graphite oxide through the Hummers and Offeman procedure [184].

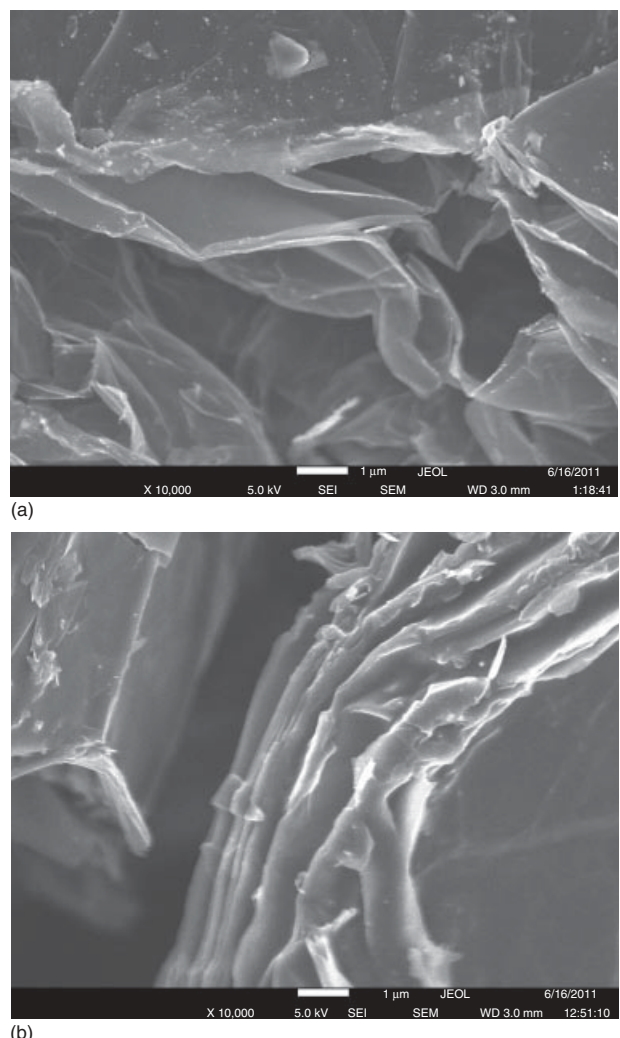


Figure 31.18 (a) HRSEM micrographs of graphene laminates modified with urea and (b) with L-lysine amino acid.

31.7.2 Surface Modification of Graphene

Pristine graphene materials are unsuitable for intercalation by large species, such as polymer chains, because graphene as a bulk material has a pronounced tendency to agglomerate in a polymer matrix [185]. Considerable work has been carried out on the amination, esterification, isocyanate modification, and polymer wrapping as routes for the functionalization of graphene (Fig. 31.18a and b). The electrochemical modification of graphene using ionic liquids has also been reported.

31.7.3 Polymer/Graphene Nanocomposites

The most important aspect of these nanocomposites is that all these improvements are obtained at very low filler loadings in the polymer matrix. Different types of

nanographite forms, such as expanded graphite and exfoliated graphite, have also been used to produce conducting nanocomposites with improved physicochemical properties. Polymer-graphene nanocomposites include those of epoxy [186], PS [187], polyaniline [188], PVA [189], Polyurethane (PU) [190], Polyvinilidene fluoride (PVDF) [191], PET [192], and PC [193] nanocomposites.

31.7.4 Preparation Methods of Polymer/Graphene Nanocomposites

31.7.4.1 In Situ Intercalative Polymerization A variety of polymer nanocomposites have been prepared using this method, that is, PS/graphene, PMMA/expanded graphite, poly(styrene sulfonate) (PSS)/layered double hydroxyl (LDH), PI/LDH, and PET/LDH.

31.7.4.2 Solution Intercalation Graphene or modified graphene can be dispersed easily in a suitable solvent, such as water, acetone, chloroform, tetrahydrofuran (THF), dimethyl formamide (DMF), or toluene, owing to the weak forces that stack the layers together. Polymer nanocomposites based on PE-g-MAH/graphite, epoxy/LDH, PS, PP, PVA/graphene, poly(vinyl chloride) (PVC)/carbon nanotubes, ethylene vinyl acetate (EVA)/LDH have been prepared using this method.

31.7.4.3 Melt Intercalation A thermoplastic polymer is mixed mechanically with graphite or graphene or modified graphene at elevated temperatures using conventional methods, such as extrusion and injection molding. A wide range of polymer nanocomposites, such as expanded graphite with HDPE, PPS, and PA6, have been prepared using this method.

31.7.4.4 Dispersion of Graphene into Polymers The improvement in the physicochemical properties of the nanocomposites depends on the distribution of graphene layers in the polymer matrix as well as interfacial bonding between the graphene layers and polymer matrix. Interfacial bonding between graphene and the host polymer dictates the final properties of the graphene-reinforced polymer nanocomposite.

TEM can provide direct images of dispersion and has been widely used to visualize layered silicates in polymers. In addition, rheology can be an effective tool for quantifying nanocomposite dispersion. It averages over many particles and is also useful in its own right for predicting processability. The onset of network formation can be inferred from small strain oscillatory shear versus frequency plots of the storage modulus for a series of concentrations of graphene. The storage modulus becomes independent of frequency at low frequency, a signature of solidlike network formation. The modulus data may

indicate that polymer chains can bridge between particles causing network percolation at a lower concentrations than conductivity percolation.

31.8 CONCLUSIONS

In this chapter, we have reviewed important issues regarding the fundamental and applied research on polymer/clay nanocomposites, including the contributions of our group to the understanding of the properties and behavior of these complex materials. It was not the intention to cover most of the polymer nanocomposite field, rather to expose some of the most important issues and challenges in this area. The last section of this chapter (polymer/graphene systems) shows that this field is fast developing, ensuring a wide research activity and the production of new materials for the future.

ACKNOWLEDGMENTS

We acknowledge the support from UNAM through project PAPIIT IN 116510 and we thank Omar Novelo for the SEM micrographs.

REFERENCES

1. Kojima Y, Usuki A, Kawasumi M, Okada A, Fukushima Y, Kurauchi T, Kamigaito O. *J Mater Res* 1993;8:1185.
2. Okada A, Usuki A. *Mater Sci Eng* 1995;C3:109.
3. Akkapeddi MK. *Polym Comp* 2000;21(4):576.
4. Liu L, Qi Z, Zhu X. *J Appl Polym Sci* 1999;71(7):1133.
5. Cheng LP, Lin DJ, Yang KC. *J Memb Sci* 2000;172:157.
6. Kawasumi M, Hasegawa N, Kato M, Usuki A, Okada A. *Macromolecules* 1997;30:6333.
7. Kato M, Usuki A, Okada A. *J Appl Polym Sci* 1997;66(9):1781.
8. Heinemann J, Reichert P, Thomann R, Mulhaupt R. *Macromol Rapid Commun* 1999;20(8):423.
9. Jeong HG, Jung HT, Lee SW, Hudson SD. *Polym Bull* 1998;41(1):107.
10. Noh MH, Lee DC. *J Appl Polym Sci* 1999;74(12):2811.
11. Fu X, Qutubuddin S. *Polymer* 2001;42(2):807.
12. Messersmith PB, Giannelis EP. *Chem Mater* 1993;5(8):1064.
13. Vaia RA, Vasudevan S, Krawiec W, Scanlon LG, Giannelis EP. *Adv Mater (Weinheim)* 1995;7(2):154.
14. Levy R, Francis CW. *J Colloid Interface Sci* 1975;50(3):442.
15. Greenland DJ. *J Colloid Sci* 1963;18:647.
16. Muzny CD, Butler BD, Hanley HJM, Tsvetkov F, Peiffer DG. *Mater Lett* 1996;28(4):379.
17. Okamoto M, Morita S, Taguchi H, Kim YH, Kotaka T, Tateyama H. *Polymer* 2000;41(10):3887.
18. Dietsche F, Mulhaupt R. *Polym Bull* 1999;43(4–5):395.
19. Ke Y, Long C, Qi Z. *J Appl Polym Sci* 1999;71(7):1139.
20. Matayabas JC, Turner SR, Sublett BJ, Connell GW, Gilmer JW, Barbee RB, inventors. High I.V. polyester compositions platelet particles. US patent 6084019. 2000.
21. Rosenquist NR, Miller KF, inventors. Composite comprising polymerizes cyclic carbonate oligomer. US patent 4,786,710. 1988.
22. Huang X, Lewis S, Brittain WJ, Vaia RA. *Macromolecules* 2000;33(6):2000.
23. Giannelis EP. *Adv Mater* 1996;8(1):29.
24. Aranda P, Ruiz-Hitzky E. *Appl Clay Sci* 1999;15:119.
25. Usuki A, Koiwai A, Kojima Y, Kawasumi M, Okada A, Kurauchi T, Kamigaito O. *J Appl Polym Sci* 1995;15:119.
26. Michalczyk MJ, Sharp KG, Stewart CW, inventors. US patent 5,726,247. 1998.
27. Badesha S, Henry A, Maliborski J, Clifford E, inventors. US patent 5,840,796. 1998.
28. Ellsworth MW, inventor. US patent 5,962,553. 1999.
29. Wang M, Pinnavaia TJ. *Chem Mater* 1994;6(4):468.
30. Zilg C, Mulhaupt R, Finter J. *Macromol Chem Phys* 1999;200(3):661.
31. Kornmann X, Berglund LA, Sterte J, Giannelis EP. *Polym Eng Sci* 1998;38(8):1351.
32. Chen L, Liu K, Yang CZ. *Polym Bull* 1996;37(3):377.
33. Hirai T, Miyamoto M, Komasawa I. *J Mater Chem* 1999;9(6):1217.
34. Wang Z, Pinnavaia TJ. *Chem Mater* 1998;10(12):3769.
35. Zilg C, Thomann R, Mulhaupt R, Finter J. *Adv Mater* 1999;11(1):49.
36. Chen TK, Tien YI, Wei KH. *J Appl Polym Sci Polym Chem* 1999;37(13):2225.
37. Chen TK, Tien YI, Wei KH. *Polymer* 2000;41(4):1345.
38. Spenleuhauer G, Bazile D, Veillard M, Prud'Homme C, Michalon JP, inventors. US patent 5,766,635. 1998.
39. Biswas M, Sinha Ray S. *Polymer* 1998;39(25):6423.
40. Sinha Ray S, Biswas M. *J Appl Polym Sci* 1999;73(14):2971.
41. Srikririn T, Moet A, Lando JB. *Polym Adv Technol* 1998;9(8):491.
42. Tyan H, Liu Y, Wei K. *Chem Mater* 1999;11(7):1942.
43. Vaia RA, Giannelis EP. *Macromolecules* 1997;30:7990.
44. Vaia RA, Giannelis EP. *Macromolecules* 1997;30:8000.
45. Sánchez-Solís A, García-Rejón A, Manero O. *Macromol Symp* 2003;192:281.
46. Cho JW, Paul DR. *Polymer* 2001;42:1083.
47. Chung S-C, Hahm W-G, Im S-S, Oh S-G. *Macromol Res* 2002;10:221.
48. Usuki A, Kawasumi Y, Kojima M, Fukushima Y, Okada A, Kurauchi T, Kamigaito O. *J Mater Res* 1993;8:1179.
49. Yano K, Usuki A, Okada A, Kurauchi T, Kamigaito O. *J Polym Sci A: Polym Chem* 1993;31:2493.

50. Yangchuan K, Chenfen L, Zongneng Q. *J Appl Polym Sci* 1999;71:1139.
51. Krishnamoorti R, Giannelis E. *Macromolecules* 1997;30: 4097.
52. Rosedale JH, Bates FS. *Macromolecules* 1990;23:2329.
53. Larson RG, Winey KI, Patel SS, Watanabe H, Bruisma R. *Rheol Acta* 1993;32:245.
54. Gelfer M, Song HH, Liu L, Avila C, Yang L, Si M, Hsiao BS, Chu B, Rafailovich M, Tsou AH. *Polym Eng Sci* 1984;20:2002:42.
55. Schmidt G, Nakatani AI, Butler PD, Han CC. *Macromolecules* 2002;35:725.
56. Schmidt G, Nakatani AI, Butler PD, Karim A, Han CC. *Macromol Commun* 2000;33:20.
57. Schmidt G, Nakatani AI, Han CC. *Rheol Acta* 2002;41:45.
58. Hacket E, Manias E, Giannelis EP. *Chem Mater* 2000;12: 2161.
59. Krishnamoorti R, Vaia RA, Giannelis EP. *Chem Mater* 1996;8:1728.
60. Zhang Q, Archer LA. *Langmuir* 2002;18:10435.
61. Sánchez-Solís A, Romero I, Estrada MR, Calderas F, Manero O. *Polym Eng Sci* 2004;44:1094.
62. Utracki LA, Lyngaae-Jorgensen J. *Rheol Acta* 2002;41:394.
63. Stewart ME, Cox AJ, Naylor DM. *Polymer* 1993;34:4060.
64. Alexandrova L, Cabrera A, Hernández MA, Cruz MJ, Abadie MJM, Manero O, Likatchev D. *Polymer* 2002;43: 5397.
65. Kenwright AM, Peace SK, Richards RW, Bunn A, MacDonald WA. *Polymer* 1999;40:5851.
66. Kyotani M, Pudjastuti W, Saeed A. *J Macromol Sci Phys* 1999;38:197.
67. Chen P, Music K, McNeely G, inventors. WO patent 96/35571P. 1996.
68. Tharmapuram SR, Jabarin SA. *Adv Polym Technol* 2003;22: 137.
69. Sánchez-Solís A, Estrada MR, Cruz J, Manero O. *Polym Eng Sci* 2000;40:1216.
70. Ito M, Takahashi M, Kanamoto T. *Polymer* 2002;43:3675.
71. Sánchez-Solís A, García-Rejón A, Martínez-Richa A, Calderas F, Manero O. *J Polym Eng* 2005;25:553.
72. Sánchez-Solís A, García-Rejón A, Estrada M, Martínez-Richa A, Sánchez G, Manero O. *Polym Int* 2005;54:1669.
73. Wagener R, Reisinger T. *Polymer* 2003;44:7513.
74. Krishnamoorti R, Vaia RA, Giannelis EP. *Chem Mater* 1996;8:1728.
75. Fornes TD, Yoon PJ, Keskkula H, Paul DR. *Polymer* 2001; 42:9929.
76. Hyun Y, Lim S, Choi S, H, Jhon M. *Macromolecules* 2001; 34:8084.
77. McAlpine M, Hudson N, Liggat J, Pethrick J, Pugh D, Rhoney I. *J Appl Polym Sci* 2006;99:2614.
78. Wang Z, Xie G, Wang X, Zhang Z. *J Appl Polym Sci* 2006;1000:4434.
79. Lertwimolnun W, Vergnes B. *Polymer* 2005;46:3462.
80. Lertwimolnun W, Vergnes B. *Polym Eng Sci* 2006;46:314.
81. Letwimolnun W, Vergnes B, Ausias G, Carreau PJ. *J NonNewton Fluid Mech* 2007;141:167.
82. Abrányi A, Százdi L, Pukánszky B, Vancsó GJ. *Macromol Rapid Commun* 2006;27:132.
83. Calderas F, Sánchez-Solís A, Maciel A, Manero O. *Macromol Symp* 2009;283:354.
84. Mironi-Harpaz I, Narkis M. *Polym Eng Sci* 2005;45: 174–185.
85. Xu L, Lee J. *Polym Eng Sci* 2005;45:496.
86. Hasegawa N, Okamoto H, Kato M, Usuki A, Sato N. *Polymer* 2003;44:2933.
87. Wang K, Wang L, Wu J, Chen L, He C. *Langmuir* 2005;21: 3613.
88. Wang K, Wu J, Chen L, Toh ML, He C, Yee AF. *Macromolecules* 2005;38:788.
89. Wang K, Chen L, Kotaki M, Ch H. *Compos Appl Sci Manuf* 2007;38:192.
90. Bongiovanni R, Mazza D, Ronchetti S, Turcato EA. *J Colloid Interface Sci* 2006;296:515.
91. Rivera-Gonzaga JA, Sanchez-Solis A, Manero O. *J Polym Eng* 2012;32,1.
92. Bellucci F, Terenzi A, Leuteritz A, Pospiech D, Frache A, Traversa G, Camino G. *Polym Adv Technol* 2008;19:547.
93. Morawiek J, Pawlak A, Slouf M, Galeski A, Piorkowska E, Krasnikowa N. *Eur Polym J* 2005;41:1115.
94. Osman M, Rupp J. *Macromol Rapid Commun* 2005;26:880.
95. Zhou Z, Zhai H, Xu W, Guo H, Liu C, Pan P. *J Appl Polym Sci* 2006;101:805.
96. Wang K, Choi M, Koo C, Xu M, Chung I, Jang M, Choi S, Song H. *J Polym Sci Polym Phys* 2002;40:1454.
97. Liang G, Xu J, Bao S, Xu W. *J Appl Polym Sci* 2004;91: 3974.
98. Wang K, Choi M, Koo C, Choi Y, Chung I. *Polymer* 2001; 42:9819.
99. Chrissopoulou K, Altintzi I, Anastasiadis S, Giannelis E, Pitsikalis M, Hadjichristidis N, Theophilou N. *Polymer* 2005;46:12440.
100. Arunvisut S, Phummanee S, Somwangthanaroj A. *J Appl Polym Sci* 2007;106:2210.
101. Gopakumar T, Kontopoulou M, Parent J. *Polymer* 2002;43: 5483.
102. Stoeffler K, Lafleur P, Denault J. *Polym Eng Sci* 2008;48: 2459.
103. Bousmina M. *Macromolecules* 2006;39:4259.
104. Lee W, Eung S, Hun S, Jin-San Y. *J Appl Polym Sci* 2005;98:1229.
105. Xie Y, Yu D, Kong J, Fan X, Qiao W. *J Appl Polym Sci* 2006;100:4004.
106. Walter P, Mader D, Reichert P, Mulhaupt R. *J Macromol Sci* 1999;A36:1613.
107. Bonilla E, Sanchez-Solís A, Manero O. *J Polym Eng* 2008;28:553.

108. Hasegawa N, Kawasumi M, Kato M, Usuki A, Okada A. *J Appl Polym Sci* 1998;67:87.
109. Manias E, Touny A, Wu L, Strawhecker K, Lu B, Chung TC. *Chem Mater* 2001;13:3516.
110. Ton-That MT, Perrin F, Cole KC, Bureau MN, Denault J. *Polym Eng Sci* 2004;44, 1212.
111. Kato M, Matsushita M, Fukumori K. *Polym Eng Sci* 2004;44:1205.
112. Marchant D, Jarayaman K. *Ind Eng Chem Res* 2002;41: 6402.
113. Okamoto M, Nam PH, Maiti P, Kotaka T, Hasegawa N, Usuki A. *Nano Lett* 2001;1:295.
114. Svoboda P, Zeng C, Wang H, Lee L, Tomasko D. *J Appl Polym Sci* 2002;85:1562.
115. Gilman J, Jackson C, Morgan A, Harris R, Manias E, Giannelis E, Wuhenow M, Hilton D, Phillips S. *Chem Mater* 2000;12:1866.
116. Nalwa H. *Encyclopedia of Nanoscience and Nanotechnology, Polymer-Clay Nanocomposites*. Vol. 8. American Scientific Publishers; 2004. p 823–824.
117. Pinnavaia T, Beall G. *Polymer-Clay Nanocomposites*. London: Wiley; 2000. p 193.
118. Gilman J. *Appl Clay Sci* 1999;15:31.
119. Zhu J, Wilkie C. *Polym Int* 2000;49:1158.
120. Porter D, Metcalfe E, Thomas M. *Fire Mater* 2000;24:45.
121. Gianelli W, Ferrara G, Camino G, Pellegatti G, Rosenthal J, Trombini R. *Polymer* 2005;46:7037.
122. Ramos L, Melo T, Rabello M, Silva S. *Polym Degrad Stab* 2005;89,383.
123. Marosi G, Anna P, Marton A, Bertalan G, Bota A, Toth A, Mohai M, Racz I. *Polym Adv Technol* 2002;13:1103.
124. Morgan A, Harris J, Kashiwagi R, Chyall L, Gilman J. *Fire Mater* 2002;26:247.
125. Zanetti M, Camino G, Toman R, Mulhaupt R. *Polymer* 2001;42:4501.
126. Alexandre M, Beyer G, Henrist C, Cloots R, Rulmont A, Jerome R. *Macromol Rapid Commun* 2001;22:643.
127. Zhang H, Wang Y, Wu Y, Zhang L, Yang J. *J Appl Polym Sci* 2005;98:844.
128. Costache M, Wang D, Heidecker J, Manias E, Wilkie C. *Polym Adv Technol* 2006;17:272.
129. Gianelli W, Camino G, Tabuani D, Bortolon V, Savadori T, Monticelli O. *Fire Mater* 2006;30:333.
130. Wang S, Hu Y, Lin Z, Gui Z, Wang Z, Chen Z, Fan W. *Polym Int* 2003;52:1045.
131. Wang J, Chow W. *J Appl Polym Sci* 2005;97:366.
132. Grand A, Wilkie C. *Fire Retardancy of Polymeric Materials*. M. Dekker: New York (NY), USA. 2000. p 147.
133. Sanchez-Olivares G, Sanchez-Solis A, Manero O. *Int J Polym Mater* 2008;57:245.
134. Paul DR, Rios-Guerrero L. *Polymer* 2000;41:542.
135. Donald AM, Kramer EJ. *J Appl Polym Sci* 1982;27:3729.
136. van Krevelen DW. *Properties of Polymers*. 3rd ed. Elsevier; Amsterdam, The Netherlands. 1990. p 641.
137. Utevski L, Scheinker M, Georlette P, Shoshana L. *J Fire Sci* 1997;15:375.
138. Song JH. *J Vinyl Addit Technol* 1995;1:1.
139. Zanetti M, Camino G, Canavese D, Morgan A, Lamelas F, Wilkie C. *Chem Mater* 2002;14:189.
140. Hu Y, Wang S, Ling Z, Zhuang Y, Chen Z, Fan W. *Macromol Mater Eng* 2003;288:272.
141. Morgan A. *Polym Adv Technol* 2006;17:206.
142. Sanchez-Olivares G, Sanchez-Solis A, Manero O. *Int J Polym Mater* 2008;57:417.
143. Sanchez-Olivares G, Sanchez-Solis A, Camino G, Manero O. *Express Polym Lett* 2008;2:569.
144. Asai S, Sakata K, Sumita M, Miyasaka K. *Polym J* 1992;24: 415.
145. Sumita M, Sakata K, Hayakawa Y, Asai S, Miyasaka K, Tanemura M. *Colloid Polym Sci* 1992;270:134.
146. Gamboa KMN, Ferreira AJB, Camargo SS, Soares BG. *Polym Bull* 1997;38:95.
147. Tchoudakov R, Breuer O, Narkis M. *Polym Eng Sci* 1996;36: 1336.
148. Tchoudakov R, Breuer O, Narkis M, Siegmann A. *Polym Eng Sci* 1928;1997:37.
149. Gubbels F, Blacher S, Vanlathem E, Jerome R, Deltour R, Brouers F, Teyssie P. *Macromolecules* 1994;28:1559.
150. Soares BG, Gubbels F, Jerome R, Teyssie P, Vanlathem E, Deltour R. *Polym Bull* 1995;35:223.
151. Sumita M, Alai S, Miyadera N, Jojima E, Miyasaka K. *Colloid Polym Sci* 1986;264:212.
152. Brewer O, Tchoudakov R, Narkis M, Siegmann A. *J Appl Polym Sci* 1997;64:1097.
153. Lee B. *Polym Eng Sci* 1992;32:36.
154. Mallette JG, Marquez A, Manero O. *Polym Eng Sci* 2000; 40:2272.
155. Foulger SH. *J Appl Polym Sci* 1899;1999:37.
156. Miyasaka K, Watanabe K, Jojima E, Aida H, Sumita M, Ishkiwa K. *J Mater Sci* 1982;17:1610.
157. Traugott D, Barlow JW, Paul DR. *J Appl Polym Sci* 1983; 28:2947.
158. Sambaru P, Jabarin SA. *Polym Eng Sci* 1993;33:827.
159. Nadkarni VM, Shingankuli VL, Jog JP. *J Appl Polym Sci* 1992;46:339.
160. Blaszkiewicz M, McLachlan DS, Newnham RE. *Polym Eng Sci* 1992;32:421.
161. Mather PJ, Thomas KM. *J Mater Sci* 1997;32:401.
162. Sichel EK. *Carbon Black-Polymer Composites: The Physics of Electrically Conducting Composites*. Marcel Dekker: New York (NY), USA. 1982.
163. Mallette JG, Quej LM, Marquez A, Manero O. *J Appl Polym Sci* 2001;81:562.
164. Bala H, Fu W, Guo Y, Zhao J, Jiang Y, Ding X, Yu K, Li M, Wang Z. *Colloids Surf* 2006;274:71.
165. Fenter P, McBride MT, Srajer G, Sturchio NC, Bosbach D. *J Phys Chem B* 2001;105:8112.

166. Nagaraja BM, Abimanyu H, Jung KD, Yoo KS. *J Colloid Interface Sci* 2007;316:645.
167. Nuutinen JP, Clerc C, Törmälä PJ. *J Biomater Sci Polym Ed* 2003;14:665.
168. Li J, Xu Y, Wu D, Sun Y. *Chin Particulol* 2003;1:134.
169. Yu S-H, Antonietti M, Cölfen H, Hartmann J. *Nano Lett* 2003;3:379.
170. Wang T, Cölfen H. *Langmuir* 2006;22:8975.
171. Wang T, Reinecke A, Cölfen H. *Langmuir* 2006;22:8986.
172. Öncü AA, Sundmacher K, Seidel-Morgenstern A, Thévenin D. *Chem Eng Sci* 2006;61:652.
173. Judat B, Kind MJ. *J Colloid Interf Sci* 2004;269:341.
174. Qi L, Cölfen H, Antonietti M. *Angew Chem Int Ed* 2000;39:604.
175. Qi L, Cölfen H, Antonietti M. *Chem Mater* 2000;12:2392.
176. Romero-Ibarra IC, Rodriguez Gattorno G, Garcia Sanchez MF, Sánchez Solís A, Manero O. *Langmuir* 2010;26:6954.
177. Garcia NJ, Bazan JC. *Clay Miner* 2009;44:81.
178. Lee C, Wei X, Kysar JW, Hone J. *Science* 2008;321:385.
179. Liu N, Luo F, Wu H, Liu Y, Zhang C, Chen J. *J Adv Funct Mater* 2008;18:1518.
180. Kelly BT. *Carbon* 1972;10:429.
181. Bunch JS, Verbridge SS, Alden JS, van der Zande AM, Parpia JM, Craighead HG, McEuen PL. *Nano Lett* 2008;8:2458.
182. Steurer P, Wissert R, Thomann R, Muelhaupt R. *Macromol Rapid Commun* 2009;30:316.
183. Li D, Muller MB, Gilje S, Kaner RB, Wallace GG. *Nat Nanotech* 2007;3:101.
184. Hummers WS, Offeman RE. *J Am Chem Soc* 1958;80(6):1339.
185. Worsley KA, Ramesh P, Mandal SK, Niyogi S, Itkis ME, Haddon RC. *Chem Phys Lett* 2007;445:51.
186. Wang S, Tamraparni M, Qiu J, Tipton J, Dean D. *Macromolecules* 2009;42:5251.
187. Stankovich S, Dikin DA, Dommett GH, Kohlhaas KM, Zimney EJ, Stach EA, Piner RD, Nguyen ST, Ruoff RS. *Nature* 2006;442:282.
188. Wang DW, Li F, Zhao J, Ren W, Chen ZG, Tan J, Wu ZS, Gentle I, Lu GQ, Cheng HM. *ACS Nano* 2009;7:1745.
189. Liang J, Huang Y, Zhang L, Wang Y, Ma Y, Guo T, Chen Y. *Adv Funct Mater* 2009;19:2297.
190. Lee YR, Raghu AV, Jeong HM, Kim BK. *Macromol Chem Phys* 2009;210:1247.
191. Ansari S, Giannelis EP. *J Polym Sci Polym Phys* 2009;47:888.
192. Zhang HB, Zheng WG, Yan Q, Yang Y, Wang J, Lu ZH, Ji GY, Yu ZZ. *Polymer* 2010;51:1191.
193. Kim H, Macosko CW. *Polymer* 2009;50:3797.

INDEX

ABS, *see* Acrylonitrile-butadiene-styrene terpolymer
Abstraction of hydrogen atoms, 206, 208, 214
Acrylates, (meth)acrylates, 520, 526
Acrylics, 279, 525, 530
Acrylonitrile-butadiene rubber copolymer, 13, 106, 517
Acrylonitrile-butadiene-styrene terpolymer
general, 13, 106, 209–212, 227, 236, 278–9, 306, 361
in blends, 516
processing, 460
Acrylonitrile-styrene-acrylate polymers, 210
Addition polymers, 8–10, 43, 427
Adhesives, 520, 524–5, 532
Aggregation
definition, 296
in dispersion polymerization, 305
Alkyd resins, 56, 59
Alpha-relaxation, 20
Amorphous phase, 17, 19, 24, 391–3, 397, 588
Amphiphilic, 520, 565, 579

Anionic polymerization
block copolymer synthesis, 150–152
chain-end functionalized polymer synthesis
carbonation, 156
hydroxylation, 156
reactions with silyl halides, 156
silyl hydride functionalization and hydrosilation 156–7
termination with electrophilic reagents, 155
copolymerization of styrenes and dienes, 148–150
SBR (styrene-butadiene)
random copolymer, 149–150
tapered block copolymers, 148–9
diene monomers
kinetics and mechanism, 134–9
stereochemistry, 144–6
initiation by electron transfer
alkali metals, 130
radical anions, 131
initiation by nucleophilic addition
1,1-diphenylmethyl carbanions, 134

alkyllithium compounds, 131
ate complexes, 133
difunctional initiators, 133–4
functionalized initiators, 134
organoalkali initiators, 133
organoalkaline earth initiators, 133
polar monomers
cyclic carbonates, 143
ethylene oxide, 140–141
methyl methacrylate, 140, 146–7
propylene oxide, 141–2
propylene sulfide, 142
siloxanes, 143–4
vinylpyridines, 148
 β -propiolactone, 142
 ε -caprolactone, 143
solvents, 130
star-branch polymer synthesis, 153–5
styrene
kinetics and mechanism, 134–9
stereochemistry, 147–8
Apparent rate constants, *see*
Pseudokinetic rate constant method
Arborescent polymers, 559, 574
amphiphilic, 579–580

- Arborescent polymers (*Continued*)
 architecture, 575–6, 580
 copolymers, 576–580
 poly(2-vinylpyridine), 576, 578,
 580
 poly(ethylene oxide), 577
 poly(tert-butyl methacrylate), 576,
 578
 polyisoprene, 576, 581
 polystyrene, 575–9, 581
- Arborols, 563, 565
- Architecture, *see also* Topologies, 559–61, 563, 566–7, 573–6, 580
- Arrhenius-type relaxation
 activation energy, 29
 beta-relaxation, 27–8
 high-frequency relaxation, 34–5
 sigma-relaxation, 16, 20, 30, 32–4
- ASA *see*
 Acrylonitrile-styrene-acrylate polymers
- Atom transfer radical polymerization
 AGET, ARGET, ICAR, 80
 characterization of polymers synthesized by, 352–3
 copolymers, 107
 crosslinking, 199
 dendrimers, 578
 general considerations, 78
 grafting, 206–8, 211, 213, 218
 in aqueous dispersions, 308–9
 in ionic liquids, 325
 in microreactors, 330
 metalloradical, 80
 polymerization rate, 80
- ATRP *see* Atom transfer radical polymerization
- Autoacceleration *see* Trommsdorff effect
- Autoclave processing, 529
- Average molecular weight between crosslinks, M_c , 191, 194–5
- Axial diffusion, 252
- Azeotropy, 260
- Bag molding, 528–9
- Banbury mixer, 451–2
- Barrier properties, 511, 513, 515–6
- Bead polymerization, *see* suspension polymerization
- Benzoxazines, 520
- Beta-relaxation, 20
- Binomial theorem, 254–5
- Bio-based formulations, 527
- Biodegradable polymer, 12, 242, 538, 574
- Bismaleimides (BMI), 520, 528
- Bivariate distribution, 254–5, 265
- Blow molding, 243, 282, 437, 445
- Blown films
 blow-up ratio, *see also* BUR, 464
 BUR, 464–6
 DR, 464, 466–472
 draw ratio, *see also* DR, 464, 469, 471
 freeze line, 464, 467, 469
 modeling, 465–6
 stretching force, 463–470
 thickness ratio, 464
- Bond energy, 507
- Bottle blowing, 455–6,
- Brabender mixer, 451–2
- Bragg's law, 395
- Branching
 branched polymer, 254, 256, 258–263
 branching point, *see also* crosslink point, 10, 178, 191, 559, 579
 density, 576
 distribution of, 265
 effect on mechanical and rheological behavior, 437, 439, 441
 functionality, 562, 569, 576, 580
 long-chain branching, LCB, 256, 262
 number average of branches, 255
 ratio, 570
 short-chain branching, SCB, 263
 statistical, 559, 567–8
- b-scission (β -scission), 262
- Bulk molding compound (BMC), 530–31
- Bulk polymerization, 258–9, 261, 263
- Cannon-Fenske viscometer, 362–3
- Capillary number, 511, 515
- Carbenium ion, 163–5, 168–9, 171
- Catalyst, 520–21, 524, 527, 531–2, 566–7, 573, 581
- Cationic polymerization
 isobutene, 165–8
 mechanism, 163–4
 prospects, 181
 styrene and derivatives, 171–2
 vinyl ethers, 168–71
- Cationic ring-opening polymerization
 azetidines, 178
 aziridines, 176–8
 cyclic imino-ethers, 178–81
 poly(ethylene oxide), 172–3
 poly(oxetane), 173
 poly(tetrahydrofuran), 173–5
- Chain composition
 average composition, 256
 calculation of, 260
 chain composition distribution, 256, 261
 composition drift, 260–61
 control of, 258, 260
 cumulative composition distribution, CCD, 261
 effect of transfer reactions on, 258
 effects on termination rate constant, 262
 instantaneous copolymer composition, ICC, 260–61
- Chain length distribution, CLD, 7, 76, 93, 95–7, 100, 199–200, 202, 253–4, 258, 576
- Chain microstructure, 258
- Chain orientation, 470
- Chain polymerization, 9–10, 43
- Chain stereoregularity, 258
- Chain topology, 258
- Chain transfer agents (CTAs), 258, 261, 263–4, 298
 and average number of radicals per particle, 301
 and desorption of radicals, 300–301
 and molecular weight in emulsion polymerization, 302
 in suspension polymerization, 307
- Charlesby-Pinner's equation, 201
- Chemoviscosity, 525
- Chlorinated-Polyethylene, 517
- Clays, nanoclays, 520, 532
- Coagulation
 catastrophic, 306
 definition, 296
 limited, 299
- Coalescence, 306, 471, 505, 509, 512–5
- Coatings, 520, 524–8, 532
- Colloidal stability, 296
- Comb-branched, 575, 577–8
- Comb-burst®, 575–7

- Commercial polymer grafting, *see*
Graft copolymers
- Compatibilizer, 505, 508–9, 512–3,
515
- Composites, composite materials,
520, 524, 528–32
- Compounding
generalities, 451–2, 454,
in fiber composites, 496
in polymer blends, 505, 511
in polymer composites, 585, 590,
592–3
- Compression molding, 459, 460, 528,
530
- Computational fluid dynamics (CFD)
simulations, 444–8
- Condensation polymers, 8, 10–12,
43, 48, 51, 53, 55, 57, 59, 241,
561, 563, 567, 569, 571
- Conducting polymers
applications, 552–5
characterization, 551–2
charge storage, 541
charge transport, 544–5
chemical and electrochemical
n-doping, 542
chemical and electrochemical
p-doping, 542
doping involving no dopant ions
charge-injection doping, 542–3
photo-doping, 542
electrospinning, 488
non-redox doping, 543
poly(paraphenylene), 550–51
poly(p-phenylenevinylene), 551,
573
polyacetylene, 545–6
polyaniline, 218, 241, 543–4,
546–7
polypyrrole, 218, 241, 338,
549–550
polythiophene, 241, 547–9
potential, 552–5
redox doping, 541
structure, 539, 541, 546, 552
synthesis, 545
- Conductivity, 16, 18–19, 21–2, 24,
27–37, 193, 206–7, 218, 243,
324, 451, 488, 537–43, 545,
548–9, 552, 554, 596–9, 601
- Conformation of polymer chains
bond rotation, 475
distribution function, 475
- excluded volume, 364, 375, 384,
476
- Gaussian coil (ideal chain),
475
- radius of gyration, 475, 481
- root-mean-square end-to-end
distance, 475
- Controlled radical polymerization,
CRP
ATRP in aqueous dispersions,
308–9
bulk and solution, 78–81, 262,
265–6
challenges in aqueous dispersion
systems, 308
in ionic liquids, microwave
activated or microreactors
ATRP, 325, 330
NMRP, 330
RAFT, 328, 330–31
miniemulsion systems, 308–9
NMRP in aqueous dispersions,
308
RAFT in aqueous dispersions,
309
- Controlled-living radical
polymerization, CLRP, *see also*
Controlled Radical
Polymerization, 78, 107, 199,
217
- Conversion-temperature
transformation diagram, CTT,
523–4
- Coordination polymerization, 85
Cossee-Arlman, 93
early transition metal-based
catalysts, 91
McConville, 91
phenoxyamine, 86, 91–2
Schrock, 91
Stephan, 91
elastomers, 85, 87, 89–92
cis-1,4-polybutadiene, 87, 89
ethylene-propylene diene
copolymers, (EPDM), 85
ethylene-propylene rubber
(EPR), 87
random ethylene- α -olefin
copolymers, 87
trans-1,4-polybutadiene, 89
- late transition metal catalysts, 86,
96–8
Brookhart, 86, 92
Gibson, 86, 92
- Grubbs, 86, 92
Versipol, 92
- mathematical modeling, 93
method of moments, 95, 97–8
Monte Carlo technique, 97
multigrain model, 97
polymer microstructural
models, 93
Stockmayer distribution, 95–6
- mechanism, 1, 87, 94–5
- monomer types, 87
alfa-olefins, 88
conjugated dienes, 88
dienes, 88
non-conjugated dienes, 88
propylene, 85–7
styrene, 86–7, 91
- Phillips catalysts, 85–7, 95, 98
- plastomers, 87
- polymerization kinetics, 93, 97–9,
101
basic mechanism, 94
chemical equations, 94
- single-site catalysts, 86, 89, 91–3,
95, 98
constrained geometry, 86, 89,
91
- Ishihara's catalyst, 91
- metallocene, 86, 89–95, 98
- monocyclopentadienyl, 86,
90–91
- non-metallocene catalysts, 91
- supported single site catalysts,
92
- thermoplastics, 87
cycloolefins, 87
ethylene-propylene copolymers,
87
- high density polyethylene
(HDPE), 87
- isotactic polypropylene, 87
- linear low density polyethylene
(LLDPE), 87, 92
- styrene-ethylene copolymers,
87, 91
- syndiotactic polypropylene
(sPP), 87, 89, 90, 92
- syndiotactic polystyrene (sPs),
86, 87, 90, 92
- trans-1,4-polyisoprene, 87
- Ziegler-Natta catalysts, 85–90, 94,
98
- Ziegler-Natta polymerization, 262
- Copolymer, 505, 508–9, 514, 517

- Copolymer composition
 azeotropic, 111, 120, 260, 277
 composition behaviors, 110
 cumulative, 109
 equation, *see* Mayo Lewis
 equation
 instantaneous, 109
 instantaneous multicomponent, 117
 measurement methods, 116
 microstructures, 107
 policies to minimize composition
 drift, 120
- Copolymerization
 alternating
 2-D NMR analysis, 348
 chainwise, 522
 copolymer composition,
 110–111
 definition, 106
 direct copolymerization, 205
- block
 anionic synthesis, 150
 compatibility in polymer
 blends, 509
 definition, 107
 polycondensation, 50, 520, 532
 tapered, 148
- copolymerization equation, *see*
 Mayo Lewis equation
- copolymerization rate, 118
 definition, 105
 effect of pressure, 120
 effect of temperature, 118
 gradient, 107
 ideal, 110
 models
 complex dissociation model,
 113
 complex participation model,
 113
 depropagation model, 113
 model discrimination, 114
 penultimate model, 96, 112, 256
 terminal model, 94, 96, 107–8,
 117, 255–6, 258–265
 multicomponent, 105, 116, 256,
 258, 260
 nomenclature, 107
 random, *see* statistical
 copolymerization
 reaction media, 119
 sequence length distribution, 115,
 258
 statistical, 106, 115, 180
- step-growth, 106
 types, 106
- Core-shell particles, 524
- Coupling efficiency, 562, 576
- Crazing, 514
- Critical micelle concentration (CMC),
 296–7, 299–303
- Crosslink density, 187–8, 190–91,
 193–4, 201, 526
- Crosslink point, 187–9, 192,
 200–201
- Crosslinking, 55, 57, 116, 121, 173,
 187–204, 216, 225–6, 241–2,
 259, 262–5, 269, 278–9, 298,
 321–2, 327, 329, 387, 427,
 429, 437, 525, 527, 588–590
- Crystalline phase, 392–3, 427
- Cumulative properties
 cumulative copolymer
 composition, *see also* Chain
 composition, 260–61
 cumulative number-average
 molecular weight, 264
 cumulative weight-average
 molecular weight, 259–61
 definition, 261
- Curing, 56, 191–2, 242, 328–9, 341,
 415, 455, 459, 460, 483,
 519–521, 523–530, 532, 589
- Curing agent, 520
- Cyanate esters (CE), 520, 528
- Cyclization, 175, 188, 190, 192, 195,
 199, 281
 definition, 190
 effect of dilution on, 194
 primary cycles or intramolecular
 cyclization, 143–4, 190,
 527–8, 569
 secondary cycles, 190, 264
- Dangling chain, 188, 192, 194,
- DC conductivity, 21
- Dead polymer, 253–9, 262, 264–5
- Degradation, 523–4
- Dendrigraft polymers, *see also*
 Arborescent polymers,
 559–560, 574
- Dendrimer, 559–61
- Dendrzyme, 567
- Dendron, 559–63, 565, 567
- Depropagation, 259
- Diallyl phthalate (DAP), 520, 531
- Dicyclopentadienes (DCPD), 520,
 527
- Dielectric analysis, DEA, 193
- Dielectric fundamentals, 18
- Dielectric relaxation in solid
 polymers, 19, 27
- Dielectric spectra: general features,
 24
- Differential scanning calorimetry,
 DSC, 16–18, 23, 25, 32, 34, 36,
 193, 230, 259, 288, 510, 523
- Diffusional effects, 258–62
- Diglycidyl ether of bisphenol A
 (DGEBA), 523
- Dimensional stability, 520–22
- Dispersed phase, 469–71
- Dispersion polymerization, 305
- Divinyl monomer, 262, 265, 267–9
- DLVO theory, 296
- Double-monomer methodology, 569,
 571
- Droplets
 as dispersed phase, 295
 as nucleation site, 299–300,
 304–5, 308–9
 formation of monomer droplets
 in macroemulsions, 297, 299
 in miniemulsions, 308
 in suspension polymerization,
 305–6
 role in emulsion polymerization,
 300–301
- size distribution (DSD)
 in macroemulsions, 297
 in miniemulsions, 304
- Dynamic light scattering, DLS
 apparent diffusion coefficient, 381
 average diffusion coefficient, 381
 by flexible polymers
 concentrated solutions, 385–7
 fast mode, 385–6
 intermediate q region, 385
 Rouse model, 384
 Rouse relaxation times, 384
 scattering correlation function
 for a Rouse chain, 384
 semi dilute regime, 385–7
 slow mode, 385–6
 Zimm relaxation times, 384
- exponential sampling method, 381
- heterodyning, 378
- homodyne, 378
- intensity-intensity time correlation
 function, 378
- measurement of diffusion
 coefficient by DLS, 379

- method of cumulants, 381
 of thin rods
 coupling of translational and rotational motions, 382
 of thin rods
 depolarized dynamic light scattering, 382–3
 first cumulant for thin rods, 382
 scattered intensity of thin rod, 382
 tobacco mosaic virus (TMV), 382–3
 other inversion methods, 381
 particle sizing, 377, 379
 photon correlation spectroscopy, 378
 polydispersity index, 381
 Provencher's CONTIN, 381
 Siegert relationship, 378
 size distribution by DLS, 380
 Stokes-Einstein relation, 379
 time dependent scattering intensity, 378–82
 Dynamic mechanical analysis, DMA, 16–17, 33–4, 36, 193–4, 428
 Dynamics of block copolymers close to the order-disorder transition
 C-mode, 386–7
 cooperative diffusion, 386–7
 H-mode, 386–7
 internal mode, 386–7
 EAA, *see* Ethylene-acrylic acid copolymer
 Effective chains, Ne, 194
 Elasticity, 511–13
 Elastomer, 4–5, 8, 52, 85, 87, 89–92, 165, 168, 172, 175, 181, 190–92, 207–8, 210–11, 213, 233, 241, 286, 428, 432, 437–8, 516, 522, 524–5, 527, 532, 574, 581, 597
 Electrode and Interfacial Polarization Effects, 26
 Electron beam curing, 527
 Electrospray, 526
 Elemental analysis
 copolymer composition, 338, 343
 general, 337–8
 molecular weight determination, 338
 monomer composition, 338
 Elementary reactions, 252–3, 267
 Emulsion polymerization
 ab initio
 conventional, 300, 303
 CRP, 308–9
 compartmentalization, 301
 composition control in
 copolymerizations, 302
 formulation components, 298–9
 free-radical capture, 299–302
 Harkins theory, 295
 heat transfer aspects, 303
 historical developments, 295
 intervals, 300
 kinetics, 297, 300–301
 molecular weight issues, 302
 monomer partitioning and swelling
 in polymer latexes, 297
 monomer-flooded conditions, 302
 monomer-starved conditions, 302
 morphology of polymer latex particles, 303
 characterization, 303
 in suspension polymerization, 306
 Morton, Kaizerman and Altier (MKA) equation, 297–8
 nucleation mechanisms
 homogeneous, 299–300
 micellar, 299–300
 number of particles (N), 298, 300–302
 Ostwald ripening effect, 304, 308
 overall description, 252, 259, 262, 299
 seeded, 300, 303, 308
 semibatch and continuous processes, 302–3
 Smith and Ewart (S-E) theory, 295, 300–301
 superswelling, 308–9
 toughening, 524
 typical monomers, 298
 Windsor I system, 297
 zero-one system, 301
 Emulsions, 297
 End-linking, 191–2, 201
 Energy balance, 263, 288–9
 EPDM, *see*
 Ethylene-propylene-diene-monomer copolymer
 Epoxidized novolac, 527
 Epoxy resins, 8, 55, 191, 415, 431, 523, 590, 599
 EPS *see* Expandable polystyrene
 Ergodic hypothesis, 257
 Error-in-variables model, EVM, 260
 Ethylene-acrylic acid copolymer, 105
 Ethylene-propylene-diene-monomer copolymer
 abbreviation, 13
 antioxidants, 227
 blend with styrene acrylonitrile, 517
 blend with polypropylene and polyethylene, 516
 characteristics, 106
 coordination polymerization, 85, 87, 91
 grafting, 208, 210–14
 Ethylene-vinyl acetate copolymer
 abbreviation, 13
 blend with poly(vinyl chloride), 517
 characteristics, 105
 GPC characterization, 361
 reactivity ratios, 109
 solution intercalation, 600
 EVA, *see* Ethylene-vinyl acetate copolymer
 Evaporators, 276–7
 extruder, 292
 falling strand, 276, 292
 filmextruder, 276
 flash Devol, 291
 wiped film, 276, 292
 Expandable polystyrene, 13, 306
 Extruder
 CFD simulation, 446–8
 die, 452–6
 for blow and ribbon extrusion, 463
 for nanocomposites, 585, 587–8, 596
 for polymer blends, 509–511
 for solvent removal, 285, 292
 in natural fiber composites, 496
 single-screw, 453, 511, 596
 twin-screw, 292, 447–8, 452–4, 463, 509–511, 588, 596
 Extrusion
 constitutive equations in, 444–5
 film and ribbon, 463–7, 469–470
 generalities, 451–6, 460,
 in nanocomposites, 585, 588, 590, 593, 595–6, 600
 in polymer blends, 509, 515
 multiple extrusion, 229–230, 232
 of natural fiber composites, 495–7
 polymer rheology in, 437, 439
 powder coating, 526

- Extrusion (*Continued*)
 reactive, 444
 ribbon
 cooling length, 464, 467–8, 471
 modeling, 466
 ribbon thickness, 464
 ribbon width, 464, 468
 stretching force, 463–470
 sulfur extrusion, 142
- Fatigue, 514
- Feed policies, 261
- Fiber forming processing
 dry spinning, 488
 electrospinning, 488
 gel spinning, 488
 wet spinning, 487
- Fiber-matrix interface, 519–22, 525–7, 529–530, 531–2
- Fiber-reinforced composite materials, 528
- Fibers, 470–72, 528
- Filament winding, 524, 527–8, 529–32
- Fillers, 531
- Film blowing, 454, 463–7, 469–470
- Film extrusion, 454–5, 460
- Film forming processing
 coating
 pre-metered coating, 483
 self-metered coating, 483
 epitaxy, 487
 Langmuir-Blodgett deposition, 487
 layer-by-layer deposition, 487
 solvent casting
 belt casting process, 482
 wheel casting process, 482
 spin coating
 basic stages, 484
 Bornside et al. approach, 486
 Cregan and O'Brien approach, 486
 Emslie Bonner and Peck model, 485
 film thinning, 484
 Meyerhofer approach, 485
 surface-oriented phase separation, 486
 thin films, 484
- Film properties
 composition, 463
 elastic modulus, 465, 470–71
 elongation at break, 470–71
 final dimensions, 463, 465, 467
 mean failure energy (MFE), 471–2
 morphology, 463, 467, 469–71
 tensile modulus, 470
 tensile strength, 470–71
- Films, 524–5, 528, 530–31
- Flory interaction parameter, 191, 297–8, 476, 478, 507
- Flory-Huggins equation, 191, 290–91, 297–8, 476–7, 506–7
- Flory-Huggins lattice theory
 change in enthalpy of mixing, 473–4, 478
 change in entropy of mixing, 473–4, 478
 change in Gibbs free energy of mixing, 474, 476, 478
 chemical potential, 476, 479–80
 ideal solution, 476, 481
 osmotic pressure, 476, 479–81
 regular solution, 476
- Flory-Rehner equation
 affine deformation model, 191, 194
 phantom model, 194
- Flory-Schulz distribution, 261
- Fluoroelastomer, 581
- Foams, 525–7, 529
- Folded chain, 392
- Fréchet, 560, 563–4, 567–570
- Free radical copolymerization, 187, 191–3, 195, 197–202, 321–2
- Free radical initiators
 azo-compounds, 65, 68–9, 73
 half-life time, 66
 initiator efficiency, 66, 73–4, 81
 peroxides, 65, 69, 73
- Free radical polymerization
 backbiting reactions, 71
 ceiling temperature, 77
 chain transfer agents, 69
 chain transfer to impurities, 70
 chain transfer to initiator, 69
 chain transfer to monomer, 69
 chain transfer to polymer, 70
 chain transfer to small species, 68–9, 71
 chain transfer to solvent, 69–70
 floor temperature, 77
 free radicals, 65–6, 68, 71, 73, 75, 78–9
 general considerations, 65
 heat of polymerization, 77
 inhibition, 71
 initiation, 65–6, 71–5
- kinetic modeling, 252–4, 258, 261, 264
 kinetics, 71–4
 mechanism, 66–7
 molecular weight distribution
 Flory-Schulz distribution, 75
 full distribution, 74–6, 81
 M_n , 74–6, 80
 polydispersity index or dispersity, 76, 78, 81
 monomer addition, 66–8, 71
 propagation, 65–9, 71–5, 77
 quasi-steady state, 73
 rate constants
 chain transfer to impurities, 70
 chain transfer to initiator, 69
 chain transfer to monomer, 69
 chain transfer to polymer, 70
 chain transfer to solvent, 69–70
 propagation rate (k_p) constants, 66–8, 71–80
 pulsed laser polymerization, 76
 termination, 65–6, 68–9, 71–6
 thermodynamic aspects, 77
- Free volume, 443
- Fringe micelles, 189
- Functionalization
 acetylation, 575
 chloromethylation, 575
 dendrimer, 566
 direct copolymerization, 205
 end-functionalization, 205
 functionalization-grafting, 205
- Galerkin finite-elements method, GF, 199, 323
- Gel conversion, 520, 527, 529, 532
- Gel effect, *see* Trommsdorff effect
- Gel permeation chromatography, GPC,
see size exclusion chromatography
- Gelation, 187–204, 238, 256, 263, 521–4, 527–9, 569, 570–72, 590–91
 classical theory, *see* statistical theories
 critical conversion, 196–8
 effect of cyclization on gelation, 190
 gel, 256, 262–4
 gel fraction, 191, 521–4, 527, 528–9

- gelation point, 191, 193, 263–4, 322, 521–3
 post-gelation, 197, 199, 201, 256
 pre-gelation, 193, 199, 201, 256
 prevention of, 187
 sol fraction, 191, 194, 529–530
- Generation, 559–63, 565, 567, 574–7, 579–580
- Glass transition temperature, T_g
 alpha-relaxation
 chitin, 22–4, 28
 chitosan, 30, 31
 generalities, 16–18
 PVA, 34
 water content effect, 32–3
 generalities, 15–16, 259, 281, 283, 446, 505, 509, 510, 513, 525, 532
- Glass-fiber reinforced plastics, 520, 527–32
- Graft copolymers
 general, 10, 107
 in polymer blends, 509
 polyol polyethers, 210
- Graft polyolefins
 anionic copolymerization, 211
 borane compounds, 210
 cationic copolymerization, 211
 controlled radical polymerization techniques, 212–4
 metallocenes, 211
 Ziegler-Natta, 211
- Grafting density, 576
- Grafting from inorganic surfaces
 anchoring groups, 207
 controlled radical polymerization techniques
 general, 211–18
 ATRP, 215–18
 NMRP, 214–18
 RAFT, 215–17
 free radical polymerization techniques, 214, 216–17
 grafting density, 207, 215–16
- Grafting from polymer surfaces
 controlled radical polymerization techniques
 general, 211–14
 ATRP, 213
 NMRP, 211–13
 RAFT, 214
 free radical polymerization techniques, 207–211
- Grafting yield, 576–7
Grafting, see Synthetic strategies
- Haake mixer, 451–2
- Hand lay-up process, 523–5, 527–8, 532
- Hardener, 529–530
- HDPE *see* High density polyethylene
- Heat effects, 263
- Heat of polymerization, 274, 287
- Heterogeneous coordination catalyst, 258
- Heterogeneous system, 252, 262, 264
- High density polyethylene, HDPE
 additives, 230, 236
 composites, 432
 coordination polymerization, 85, 87
 general, 8, 10, 12–13
 in blown films and ribbon extrusion, 467, 469–71
 in natural fiber composites, 495, 497–8, 500–501
 modified or grafted, 213
 nanocomposites, 585, 590, 592, 597, 599–600
 processing, 452, 457, 459
 solution process, 287
- High-frequency relaxations, 34
- High-temperature relaxations, 33
- History, 273
- Hollow articles in polymer processing, 455, 458
- Homogeneous system, 252, 261, 264
- Homopolymerization
 capability of, 260
 effect of impurities in, 258
 mathematical model for, 264, 255–7
 similarities of copolymerization with, 262
 stereoregularity in, 258
- Hot melt process, 520–21, 524
- Hybrid materials physisorption, 207
- Hybrid materials synthesis
 carbon black-g-polymer
 FRP, 216
 NMRP, 216
 carbon nanotubes
 ATRP, 217–18
 FRP, 216–17
 NMRP, 217–18
 RAFT, 217
 CdSe-g-polymer
- NMRP, 215
 RAFT, 215
- covalent bonding, 207
- electrostatic absorption, 207
- fullerenes-g-polymer
 FRP, 216
 NMRP, 216
- in thermosets, 573, 578, 582
- nanomagnetite-g-polymer
 ATRP, 215
 NMRP, 214–15
 nano-onions, 216
 ATRP, 216
- NPSiO₂-g-polymer
 ATRP, 215
 FRP, 214
 NMRP, 214–15
 RAFT, 215
- Hydrogen bonding, 506, 507
- HYPAM, 572
- Hyperbranched polymers, 559–560, 567
- Impurities, 258
- Infrared spectroscopy
 attenuated total reflectance (ATR), 341
 FT-IR microscopy, 341
 generalities, 339, 341
 instrumentation
 Fourier transform spectrometers, 339
 interferometer, 339
 polyethylene, 342, 352
 poly(hydroxyalkanoate), 343
 qualitative analysis
 fingerprint, 339–340
 generalities, 339
 functional group, 339–340
 generalities, 340–41
 Lambert-Beer law, 340–41
 real time IR spectroscopy
 crosslinked polymers and copolymers, 342
 generalities, 341
 interpenetrating polymer networks, 342
 photopolymerization, 341
 UV curing, 341
 sampling methods, 341
 symmetric and assymmetric stretchings, 339, 341–2
- Infusion process, 529
- Inimer, 570–71, 579

Initiation
 initiation reaction, 256–7, 259–62, 264–5
 initiator, 258, 261–2, 264, 268, initiator decomposition, 254, 258, 264, 267
 initiator efficiency, 262
 thermal initiation, 267, 269
 Initiator, 529
 Injection molding, 521, 524, 526–7, 530–31
 compression molding, 459–460
 defects, 457–8
 for thermosets, 521, 524, 526–7, 530–31
 generalities, 8, 48, 455–6
 limitations, 457
 rotational molding, 458–9
 Injection processing,
 applications, 282
 for nanocomposites, 587, 600
 for polymer blends, 515–6
 for thermosetting polymers, 528, 531
 in natural fiber composites, 493, 496–8
 In-mold coating, IMC, 528, 531
 Inorganic condensation polymers, 53, 54
 Inorganic polymer, 11–12, 54, 415
 Instantaneous property
 instantaneous copolymer
 composition, ICC, *see also*
 Chain composition, 260
 instantaneous MWD, 261
 instantaneous radical-type
 distribution, 257
 instantaneous value of mass, 252
 instantaneous vs cumulative
 property, 261
 Interfacial adhesion, 470
 Interfacial properties or
 characteristics, 506, 508–13, 515
 Interfacial tension
 role in particle morphology, 303
 role in particle swelling, 297–8
 role in suspension polymerization, 306
 Intermediate species, 252
 Intermolecular crosslinking, 190, 192, 199
 Intermolecular forces, 507

Internal double bond polymerization, IDB, 262–4
 Intramolecular crosslinking, *see also*
 cyclization, 190, 192, 195, 199–200
 Intramolecular cycles, 527–8
 Intrinsic viscosity, 7, 190, 282, 356, 361–5, 560
 Ionic liquids, 317, 324–9
 cellulose, 326, 328
 microwave energy, 328–9
 recycling, 325, 327–9
 solvents for polymerizations, 324–9
 surfactants in polymerizations, 329
 Ionic polymerization, 252, 258, 261
 Ionomer, 509, 516
 Junction points, *see also* crosslink point, 188, 189, 194
 Junction zones, 189
 Kinetic rate coefficient, 253
 Kinetic theories, 198
 Kraemer-Hügins plot, 363
 Kuhn segment, 195
 Lamellar structure, 391–3, 404
 Lamellar stacking model, 404–5
 Lamellar thickness, 393, 401
 Laminates, 522–3
 LCST *see* Lower critical solution temperature
 LDPE *see* Low density polyethylene
 Lewis acids, 520, 529
 Life cycle analysis, LCA, 521
 Light scattering, LS
 concentration fluctuations, 367, 370
 correlation length, 369, 370
 density fluctuations, 367, 370
 dielectric constant fluctuations, 367, 370
 dielectric correlation function, 368–370
 Mie, 368
 molecular weight dispersity, 375–6
 Rayleigh-Debye-Gans
 approximation, 368
 Rayleigh ratio, 369–370
 SANS, 367, 369–370, 376, 378
 SAXS, 367, 369, 376
 scattered intensity, 368

thermodynamic limit, 369–370
 T-Matrix, 368
 use of the technique, 259
 Limiting conversion, 259
 Linear polymerization, 256, 259, 262–5
 Live polymer, 253–7, 263
 Long chain hypothesis (LCH), 108, 256
 Long-chain approximation, LCA, 260
 Low density polyethylene, LDPE
 additives, 230, 236
 bulk process, 273
 composites, 432–3
 general, 8, 10, 12–13, 92
 in blown films and ribbon extrusion, 467, 469–71
 in natural fiber composites, 496–7
 Mark-Houwink parameters, 364
 modified, 213
 nanocomposites, 585, 590, 592
 processing, 452, 457, 459
 Low profile additive, LPA, 522
 Low-frequency relaxations, 28
 Low-temperature relaxations, 30

MABS *see* Methyl methacrylate-acrylonitrile-butadiene-styrene polymers
 Macroemulsion, 262
 Macromonomers
 in anionic polymerization, 130, 134
 in coordination polymerization, 94, 96
 in dendritic polymers, 559, 569, 579
 in functional polymers, 206
 in grafting, 211, 213
 in green solvent polymerization, 232
 in polycondensation, 51, 61
 Mark-Houwink-Sakurada equation, 7, 21, 359, 364–5
 Mass action law, 253–4
 Mass balance equation, 252, 265
 Mass spectroscopy
 detection limit, 351
 electron ionization, 351
 generalities, 348, 351–2
 matrix assisted laser desorption / ionization (MALDI)

- in addition-fragmentation transfer polymerization (RAFT), 352
- in atom transfer radical polymerization (ATRP), 353
- generalities, 352–3
- nonpolar polymers, 354
- tandem mass spectrometry, 355
- sample introduction, 351
- sensitivity, 342, 344, 351
- signal to noise ratio, 343, 351
- Matrix, 469, 471
- Mayo-Lewis, 260
- Mayo-Lewis equation, 95, 108–9, 119, 148, 260
- MBS *see* Methyl methacrylate-butadiene-styrene polymers
- Mechanical properties, 425
- compliance, 430
- composites, 431
- generalities, 14–15, 18–19, 32, 51, 86, 191, 207, 227, 230, 234–6, 243, 282, 410–11, 414, 425–431, 433–4, 463, 469–471, 475, 549
- modulus
- bulk, 427
 - compression, 428
 - dynamic, 431
 - elastic, 427, 432–4, 519, 528
 - loss, 193–4, 431, 522, 527, 532
 - shear, 427–8
 - storage, 431, 519, 520, 522, 528
- molecular structure, 428
- of nanocomposites, 587–593, 595, 597–8
- of polymer blends, 509, 513
- of thermosetting polymers, 524, 527–8, 531–2
- of wood composites, 493–5, 497–8
- polymer, 426
- strain, 426
- constant, 430
 - deformation, 427
 - simple, 428
 - sinusoidal, 430
 - stress test, 427
- strength
- impact, 427
 - tensile, 425, 431–4
 - ultimate, 428
- stress, 425
- concentration, 433
- decay, 430
- relaxation, 430
- sinusoidal, 431
- strain curve, 427
- transfer, 432
- Melamine-formaldehyde polymer, 46–7, 519–520, 530
- Melt
- in film and ribbon extrusion, 463–4, 467–8
 - processing pressure, 451–9, 461
 - processing temperature, 451–2, 456–461
- Melting point, 281, 519–520
- Metallocendrimer, 566–7
- Method of moments, 253, 255, 268
- Methyl methacrylate (MMA)
- polymerization
 - in sc-CO₂, 264
 - limiting conversion, 259
 - terminal double bonds formation, 262
- Methyl methacrylate-acrylonitrile-butadiene-styrene polymers, 209, 517
- Methyl
- methacrylate-butadiene-styrene polymers, 13, 210, 517
- Meyer-Lowry equation, 261
- Micelles
- and micellar nucleation, 299
 - conditions to form micelles, 296–7
 - definition, 296
 - in emulsion polymerization, 299
 - in microemulsion polymerization, 304
 - in miniemulsion polymerization, 304
 - solubilization of hydrophobic liquids in, 297
- Michael addition, 563, 573
- Microchannels, 329–330
- Microemulsion polymerization, 304
- Microgels, 154, 190, 192, 199, 200, 523, 527
- Microreactors, 329–331
- chip-based reactor, 329–331
 - column reactor, 330
 - tubular reactor, 329–331
- Microscopy
- 2D image analysis, *see also* 2D image, 416–9
 - 3D image analysis, 416–421
 - composition, 409–410, 412, 414–5, 417
 - confocal microscopy, 416
 - electron diffraction energy-loss spectroscopy, EELS, 409, 412, 414–5
 - electron holography, 409–410
 - energy dispersive X-ray analysis, EDX, 409, 412, 414
 - energy-filtered transmission electron microscopy, EFTEM, 409, 414–5
 - environmental scanning electron microscopy, ESEM, 410, 413
 - high resolution transmission electron microscopy, HRTEM, 409, 413, 415
 - laser scanning confocal microscopy, 416
 - light microscopy, 510
 - materials evaluated
 - blend, 414–7, 420
 - block copolymer, 411–2, 416–420
 - copolymer, 411–3, 415–420
 - nanocomposites, 412–3, 415, 418
 - nanoparticles, 412, 415 - morphology, 412–5, 419
 - phase contrast, 410, 413, 417
 - resolution, 409–411, 414–5, 417–8
 - scanning electron microscopy, SEM, 409–412, 416–7, 510
 - scanning transmission electron microscopy, STEM, 409, 411–5
 - staining, 412
 - structure (micro, nano) analysis, 409–420
 - topology, 409, 416, 419–420
 - transmission electron microscopy, TEM, 409–413, 415, 418–9
 - annular dark field, 412–3
 - conventional TEM, CTEM, 409, 412–3, 418, 510
 - cryogenic HRTEM or cryo-HRTEM, 413
 - cryogenic TEM or cryo-TEM, 409, 413
 - high angle annular dark field, 409, 413

- Microscopy (*Continued*)**
- high voltage transmission electron microscopy, HV-TEM, 414
 - in situ* TEM, 409–412
 - low voltage transmission electron microscopy, LV-TEM, 414
 - transmission electron microtomography, TEMT, 416–420
 - Z-contrast, 409, 413–4
 - ultramicrotomy 413
 - X-ray microtomography, X-ray m-CT, 416–8, 420
- Microstructure, 505, 509**
- Microwave energy, 327–9**
- cellulose, 328
 - ionic liquids, 327–329
 - polymer processing, 328
 - polymerization reactions, 328–9
- Miniemulsion polymerization, 303–4**
- Mixer, 509–512, 515**
- Mixing, 291**
- Modeling**
- chemical reactor modeling, 252, 262
 - monofunctional polymer molecule assumption, 264
 - multifunctional polymer molecule assumption, 265
 - of bivariate distribution, 254
 - of molecular weight distribution, 256
 - tips for, 257
- Modification of polymers by grafting**
- grafting-from, 205–7, 211, 215–8
 - grafting-onto, 206, 214, 216
 - grafting-through, 206, 211
- Moisture content effects on molecular relaxations, 17**
- Molding powders, 523**
- Molecular dynamic simulations, 445–6**
- Molecular weight**
- molecular weight dispersity
 - anionic polymerization, 129, 142
 - cationic polymerization, 166, 170
 - control, 258, 261
 - coordination polymerization, 95
 - definition, 7
 - suspension polymerization, 306
 - tips related to MWD issues, 256–264
- number average**
- control in anionic polymerization, 128
 - control in condensation polymerization, 57
- hyperbranched polymers, 559, 569**
- in crosslinked polymers, 192, 202**
- in graft polymers, 211, 213**
- measurement, 356–9**
- microreactors, 331**
- microwave polymerization, 328**
- polymer processing, 425**
- radical polymerization, 76, 78, 80–81**
- molecular weight distribution (MWD)**
- anionic polymerization, 129–134, 139–143, 152–4, 172
 - bulk polymerization, 276–7, 280–283, 285, 287, 291
 - copolymers, 256, 265
 - definition, 6–7
 - effect on miscibility, 505–7, 509
 - graft copolymers, 211
 - hyperbranched polymers, 559, 567
 - influence on polymer properties, 425–6
 - influence on rheological properties, 439, 443
 - measurement, 352–355
 - method of moments, 253–6, 264, 268, 323
 - microreactors, 331
 - moments, 6–7, 76, 253
 - moments in catalysis
 - coordination polymerization, 95, 97–8
 - moments in polymer network modeling, 195, 198, 266–7
 - polymer solution, 479
 - radical polymerization, 74–5
 - step-growth polymerization, 44–5, 53
- Monte Carlo simulation, 97–98, 195, 197–9, 301, 413, 476**
- Morphology, 505, 508–512, 515**
- Most probable distribution, see Flory-Schulz distribution**
- Multifunctional assumption, 198, 265, 266**
- Nanofibers, 432**
- composites, 433
- Nanofiller, 446**
- Nanoparticle, 532, 573, 580–581**
- Nanotubes, 432**
- carbon (CNT), 520, 532
 - composites, 434
- Natural fiber composites**

- decay factors
 interface, 500–501
 moisture, 500
 particle size, 500
 wood/polymer ratio, 500
- durability, 493, 495, 498, 500–501
- manufacturing process, 493, 495, 497
- mechanical properties, 498–9
- properties, 493–5, 497
- raw materials
 additives, 495
 interface, 494–7
 moisture content, 496
 natural fibers, 494
 particle size, 496
 polymers, 495
 uses, 493, 501
- water absorption, 497–8
- wood/polymer ratio, 496
- Natural fibers, 432
- Natural fillers, 446
- Natural polymer, 3, 11, 16, 356, 391
- NBR, *see* Acrylonitrile-butadiene rubber copolymer
- Neutralized and nonneutralized chitin films, 21
- Newkome, 560, 563, 565
- Nitrile rubber, 517
- Nitroxide-mediated radical polymerization
 alkoxyamine, 79
 characterization of polymers
 synthesized by, 352
- copolymers, 107
- crosslinking, 199
- degree of polymerization, 79
- fundamentals, 78–80
- grafting, 207–8, 211–8
- in aqueous dispersions, 308–9
- in microreactors, 330
- kinetics, 79
- mathematical modeling, 266–9
- mechanism, 78
- microwave process, 328
- nitroxide radicals, 79
- NMP *see* Nitroxide-mediated radical polymerization
- NMRP *see* Nitroxide-mediated radical polymerization
- Nonlinear polymerization, 256, 264–5
- Non-mean field theory, 197
- Non-Newtonian behavior or flow, 438, 441, 448, 463
- Non-Newtonian fluid, 4, 438, 451, 485
- Non-steady-state, 252
- Nuclear magnetic resonance (NMR)
 chemical shift, 343–5, 348–9, 351–2
 generalities, 338, 343–352
 instrumentation
 continuous wave, 345
 Fourier transform, 345
 qualitative analysis
 general, 346
 poly(dimethylsiloxane), 347
 polystyrene, 346, 350
 quantitative and compositional analysis
 end groups, 350, 352
 functional groups, 349, 352
 general, 349–351
 stereochemistry (tacticity), 350
- sample preparation, 345
- spin-spin coupling, 345, 348
- two dimensional NMR analysis
 general, 348, 351
- use for characterization of several polymers, 114, 116, 133, 135, 150, 156, 194, 211, 357, 479, 510, 552, 568
- 2D-INADEQUATE, 348
- heteronuclear correlation spectroscopy (HETCOR), 348
- homonuclear correlation spectroscopy (COSY), 348
- Overhauser effect (NOE), 348
- Number-average molecular weight, 258–261, 264, 269
- Numerical fractionation technique, NFT, 195
- Nylon, 5, 8, 13, 48, 106, 208, 283, 338, 360, 364–5, 427, 507, 515, 540, 586, 590
- Optical properties, 515
- Origin of dielectric response, 19
- Osmometry, 338, 357, 371
 membrane osmometry, 480
 vapor pressure osmometry, 480–481
- Paintings, 520–521, 523, 525, 528
- PAMAM, 562–4, 566–7, 572–3
- Particle deformation, 469
- Particle size distribution (PSD)
 characterization, 303
 in emulsion polymerization, 303
 in suspension polymerization, 306–8
 modeling, 307
 simulation by CFD, 308
- PE *see* Polyethylene
- Pearl polymerization, *see* suspension polymerization
- Pendant double bond, 154, 192–3, 199, 262, 264–5
- Percolation theory, 193, 195, 197–8, 521, 523, 596–8, 601
- Phase diagram, 478
 molecular weight dispersity 320
- Phase equilibria
 binodal and spinodal curves, 478
 critical concentration, 478
 critical temperature, 478
 lower critical solution temperature, 318–9, 478–9, 507
 phase separation, 478
 upper critical solution temperature, 318–320, 478–9, 507
- Phenol polymers, 46
- Phenolic resins, 55–6, 60, 525, 532
- Pigments, 519, 525, 530–531
- Pi-pi interactions, 189
- Poly(butylene terephthalate), PBT, 13, 227, 230, 236, 242, 281–3, 361, 415, 461, 516
- Poly(ethylene glycol), PEG, 172, 352, 358–9, 412
- Poly(ethylene oxide), PEO, 12–13, 172, 179, 211, 216, 218, 359, 376, 378, 385–6, 577, 586
- Poly(ethylene terephthalate), PET, 12–14, 47, 206–7, 227, 230, 236, 239, 242–3, 273, 281–3, 361–3, 365, 391, 399, 427, 455, 461, 463, 507, 583, 586–9, 593, 595–7
- Poly(lactic acid), PLA, 12–13, 414
- Poly(methyl methacrylate), PMMA, 5, 10, 12–13, 133, 147, 152, 211, 213–8, 227, 233, 236, 273, 279, 306, 321, 338, 350, 353, 359, 361, 364, 411–2, 415, 452, 457, 460, 486, 507, 517, 553, 585, 593, 596–7, 599–600
- Poly(phenylene sulfide), 516

Poly(phenyl–ether), 516
 Poly(tetrafluoroethylene), PTFE, 13, 237, 273, 516
 Poly(vinyl acetate), 306
 Poly(vinyl alcohol), PVA
 dielectric relaxations, 34–8
 generalities, 13, 15–18, 20–21, 201, 358–9, 410, 599
 Poly(vinyl butyral), PVB, 463
 Poly(vinyl chloride), PVC
 for film and ribbon extrusion, 463
 generalities, 8, 10, 12–13, 210, 213, 225–7, 236, 238–240, 243, 245, 261, 263, 361, 364, 415, 429, 458–460, 463, 495, 498, 600
 heat stabilizers
 costabilizers, 232
 examples, 232–3
 metal-free heat stabilizers, 232
 mixed metal salts, 231
 organotin heat stabilizers, 231
 testing, 232
 in polymer blends, 507, 517
 synthesis in dispersed phase, 306
 synthesized in bulk and solution, 273
 Polyacrylonitrile, 507
 Polyamide, PA, 5, 8–9, 11, 13, 46–50, 178, 227, 229, 230, 233, 236, 238, 240, 241, 273, 283–4, 328, 331, 361, 391, 413, 428, 459, 488, 509, 516, 527, 530, 585, 597
 Polyamidoamine, *see* PAMAM
 Polyaniline, 218, 241, 538–541, 543–4, 546–7, 552–3, 600
 Polycarbonate, PC, 13, 46, 143, 227, 283–5, 321, 361, 414–5, 460, 516, 569, 581
 Polydispersity, *see* Molecular weight dispersity
 Polyester dendrimer, 569
 Polyesters, 8–9, 11, 45–52, 55–7, 191, 233, 241, 273, 281, 323–4, 360, 488, 431, 509, 519, 522, 525, 527, 530–532, 569, 571, 585–7, 591, 593, 597
 Polyethers, 50, 51, 210, 216, 323, 360, 567, 569, 571
 Polyethylene
 additives, 230–231, 233, 240–243
 anionic polymerization, 129
 blends, 507–8, 513, 515–7

characterization, 340, 342, 356, 358–361
 coordination polymerization, 85, 87, 91–2
 gel spinning, 488
 general, 4–5, 8, 12–13, 70, 451
 in natural fiber composites, 495–8, 500
 injection, 457
 microscopy, 409, 411, 413–4
 modified or grafted, 205, 211–3, 217
 nanocomposites, 585, 590, 592, 597, 600
 semicrystalline nature, 391–2
 solution/bulk process, 273, 281–2, 287
 T_g , 428
 thermoforming, 460
 x-ray scattering, 400
 Polyethylenimine, 573, 575–7
 Polyglycidol, 578
 Polyhedral oligomeric silsesquioxanes (POSS), 524–5, 527, 531
 Polyimides, 46, 50–51, 227, 520, 528, 532, 585
 Polyisobutylene, 516
 Polymer
 abbreviations, 12–13, 361
 classification, 7–9, 11, 43
 common names, 12–13
 conventional nomenclature, 12
 definition, 3
 history, 3–4
 IUPAC nomenclature, 13, 43, 189–190
 nomenclature, 12–13
 production volume, 12, 290
 uses, 7
 Polymer additives
 active protection additives
 content protection, 243–4
 heat control, 244
 productivity enhancer, 244
 additives to enhance processing, 240
 additives to influence morphology
 and crystallinity, 242–3
 additives to modify plastic surface properties, 240–241
 animal repellents, 244
 antifogging agents, 206, 225, 240–241
 antimicrobials, 243

antioxidants
 examples, 230–231
 general, 225–8, 244–5, 278, 286, 527
 other antioxidative stabilizers, 229
 primary antioxidants, 228–9
 secondary antioxidants, 229
 testing, 229–230
 antistatic agents, 225, 241, 463, 482, 546, 596
 blowing agents, 244
 coupling agents / compatibilizers, 243
 flame retardants
 examples, 238
 general, 225, 227, 235–8, 245, 324, 593–5
 halogenated flame retardants, 235
 inorganic flame retardants, 235–6
 phosphorus and nitrogen containing flame retardants, 236–7
 testing of flame retardancy, 237–8
 light stabilizers
 examples, 235
 general, 225–6, 233–5, 245, 495
 hindered amine light stabilizers, 233–5
 testing, 235
 UV absorbers, 233
 markers, 244
 nucleating agents / clarifiers, 242–3
 odor masking, 244
 plasticizers, 18, 225, 231–2, 238–9, 279, 324, 482
 polymer chain modifiers
 chain extenders, 241
 controlled degradation, 241–2
 prodegradants, 242
 scavenging agents
 acid scavengers, 239
 aldehyde scavenger, 239–240
 odor reduction, 240
 slip and antiblocking agents, 240
 smart additives, *see* active protection additives

- thermal conductivity enhancers, 243
trends, 245
- Polymer architecture classes, 559–560
- Polymer blends
in film and ribbon extrusion, 463, 469, 470, 471
blend composition, 505–6, 510–513
compatibilized, 505, 508, 513
compatible, 505, 509–510, 513
immiscible, 505–8, 510, 512, 513
miscible, 505–7, 510, 512–3
- Polymer characterization
composition analysis, 337–8, 342–3, 348–9
differential scanning calorimetry (DSC), 510, 528
generalities, 337, 352
polymer structure, 337, 347–8
- Polymeric melts
electrical conductivity, 446
infrared spectroscopy, 443
light birefringence, 443
polarized light microscopy (POM), 443
small angle light scattering, 443
thermal conductivity, 446
- Polymer gel, *see also* gelation, 190, 191
- Polymer latex
applications, 304
characterization, 303
definition, 295
monomer partitioning and swelling, 297
superswelling, 308–9
- Polymer nanocomposites
generalities, 531, 585
HIPS/clay, 593
HIPS-PET/clay, 593
nanoparticles of barium sulfate, 597
PET/clay, 586
PET-HDPE/carbon black, 597
PET-PEN/clay, 587
PET-PMMA/carbon black, 596
polyolefin/clay nanocomposites, 590
polyester resin/clay, 589
polyester/clay, 586
polymer carbon black
nanocomposites, 596
- polymer/graphene nanocomposites, 598
- polypropylene/clay, 592
- polystyrene/clay nanocomposites, 593
- polyethylene/clay, 590
- preparation methods
polymer/graphene
adsorption-desorption equilibrium, 586
amorphous phase, 588
aspect ratio, 599
barium sulfate, 586, 597–8
birefringence, 586
burning rate, 593, 595
carbon black, 596–7
carbon nanotubes, 598, 600
carbonaceous char, 593
CB, 586, 596–8
char layer, 593, 599
clay, 585–596, 598
Cole-Cole, 588
combustion, 593–4, 596, 599
compatibility, 585, 590, 593
compatibilizers, 586–7, 597
complex viscosity, 588, 591
conductive fillers, 598
crosslinking, 589
crystallization, 588, 597–8
dispersion, 586, 590, 592–3, 595–7, 600
distribution, 590, 593, 596–8, 600
elastic modulus, 586, 593
exfoliation, 585–6, 588–593, 599
extensional flow, 593
fire retardant, 593
flame retardant, 593–5
gas diffusion, 588
gelation temperature, 590
glass transition temperature, 586, 588
grafting, 590, 592–3
grapheme, 586, 598–9, 600
HDPE, 585, 592, 597, 600
HIPS, 585, 594–6
hydrophilic, 585, 588, 598
hydrophobic, 588
immiscible, 587, 596–7
intercalation, 585–6, 589–590, 599–600
interfacial interactions, 591
- LDPE, 585, 590, 592
- L-lysine, 592, 594, 600
- MAH, 586–594, 597, 600
- mechanical properties, 587–593, 595, 597–9
- melt compounding, 592–3
- melt viscosity, 586, 588
- miscibility, 586–8
- mixing, 585, 588–9, 593, 596
- nonhalogenated flame-retardant, 593, 595
- nucleation, 588, 597–8
- oscillatory shear, 588, 592, 600
- PEN, 585, 587–9
- PENTA, 586–7
- percolation, 596–8, 600
- permeability, 585
- PET, 585–590, 593, 595–7, 600
- phosphorous compound, 593
- PP, 585, 591–4
- processing, 586–8
- relaxation, 586, 588, 592
- resistivity, 596–7
- rheological properties, 592–3, 595, 597
- slurry, 590–591
- sonication, 589, 596
- tear, 592
- transesterification reaction, 587–8
- triphenyl phosphate, 593
- unsaturated polyester resin, 585, 589–591
- viscoelastic properties, 586–7, 592
- surface modification of graphene, 599
- synthesis and structural features of graphene, 599
- Polymer network
by cationic ring opening polymerization (CROP), 51, 174, 178
by free-radical copolymerization (FRC), 263
by step-growth polymerization, 520–521, 523, 525, 532
characterization techniques, 193, 342
chemical networks, 189, 191
defects, 188, 192
definition, 187

Polymer network (*Continued*)
 from radiation-induced
 polymerization, 329
 Gaussian network, 194
 homogeneous, 188–190, 199
 ideal, 188–9, 199
 imperfect, 188
 interpenetrating, 189
 model, 188–9, 192
 perfect, 188–9
 physical networks, 189
 semi-interpenetrating, 189
 structure, 187
 Polymer post-modification
 copper-catalyzed, 207
 coupling reactions, 207
 Diels-Alder, 207
 metal-free, 207
 polydienes by NMRP, 211–2
 polyolefins by CRP, 212–4
 Polymer processing, 437, 438, 444,
 445, 446
 additives, 532, 581
 blow molding, 437, 445
 extrusion, 437, 439, 444–5
 film blowing, 437
 injection molding, 437
 production of thermosets, 524–7
 Polymer reaction engineering, 251,
 257
 Polymer rheology
 Bagley correction, 441–2
 capillary rheometer, 441–2
 constitutive equations, 437, 443,
 445
 Criminale-Ericsen-Filbey
 (CEF), 445
 Goddard–Miller (G-M)
 equation, 445
 Kaye-Bernstein-Kearsly-Zapas
 (K-BKZ), 445
 Maxwell model, 444
 power law model, 441–2, 444
 Yasuda-Carreau equation, 444
 creep, *see also* retardation process,
 440, 444, 519, 528
 dilatant, 438
 dynamic moduli, 442
 dynamic rheometers, 442
 extensional viscosity, 443
 extrudate swelling, 438–9, 445
 generalized Newtonian fluid
 (GNF), 444–5
 Hookean solid, 437–8, 440

linear strain, 439
 linear viscoelasticity, 440–441,
 445
 master curve, 443
 melt flow index (MFI), 442–3
 Newtonian liquids, 437–8
 Newtonian viscosity, 273, 276,
 281, 290–291, 444
 non-Newtonian viscosity, 448
 normal stress differences, 442, 445
 normal stresses, 438
 pressure effect on viscosity, 443
 pseudoplastic, 438
 Rabinowitch correction, 441–2
 relaxation modulus, 440, 445
 relaxation spectrum, 443
 relaxation time, 445
 retardation process, 440
 rheological properties, 514
 rotational rheometers, *see also*
 dynamic rheometers, 442
 cone-and-plate, 442
 parallel plate, 442
 shear strain, 439, 440
 shear stress, 509, 511–2
 shear thickening, *see also* dilatant,
 438
 shear thinning, *see also*
 pseudoplastic, 438, 441, 444,
 446
 temperature effects on viscosity,
 443–4
 viscoelasticity, 521, 525
 viscosity, 520–523, 525
 viscosity ratio, 511–3
 viscous dissipation, 444–5
 Voigt model, 444
 Weissenber effect, 438
 WLF equation, 443
 zero-shear-rate viscosity, 441–4,
 446
 Polymer solution thermodynamics,
 505–6, 508
 energy of mixing, 505–7
 enthalpy, 506–7,
 entropy, 505–7
 heat of mixing, 506–7, 509
 lower critical solution temperature,
 507–8
 phase diagrams
 binodal curve, 507–8
 spinodal curve, 507–8, 510
 solubility parameters, 507
 spinodal decomposition, 508
 upper critical solution temperature,
 508
 Van der Waals, 507
 Polymeric liquids, 438, 440–442
 polymer melts, 438–446
 polymer solutions
 concentrated, 473
 dilute, 473, 476, 480
 rheological issues, 438, 441
 semidilute, 473, 481
 solubility, 474, 477
 polymer suspensions, 438, 441
 Polymerization
 anionic, 527, 574–5, 577–9
 atom transfer radical
 polymerization, 578
 catalysts, 281, 285, 287
 cationic, 521, 526, 569, 570,
 574–6
 chain transfer agents, 278
 chain-growth, 521–3, 525, 527
 crosslinking, 278
 depropagation, 280
 free radical, 275, 519–520, 526–7,
 530, 576–7
 high temperature, 277, 280
 initiators, 276, 279–280, 285
 ionic, 285
 metathesis, 520–523, 525
 photo, 520–521, 523, 525
 proton-transfer polymerization,
 569, 571
 rate
 in bulk or solution, 258–263
 in dispersion, 305
 in emulsion, 297, 301
 in microemulsion, 304
 in miniemulsion, 304
 ring-opening, 525, 531, 569, 571,
 574, 577–8
 ring-opening multibranching
 polymerization, 571
 self-condensing ring-opening
 polymerization, 569, 571
 self-condensing vinyl
 polymerization, 569–571
 solid state, 281, 283
 step growth, 280, 281, 526–7,
 559, 561, 563, 567, 569,
 571
 transesterification, 281, 283
 Polyoxyethylene, 516
 Polyphenylene, 569
 Polyphosphazenes, 54

- Polypropylene
 additives, 225–7, 230–231, 233, 235–8, 241–3
 blends, 507, 516
 characterization, 358, 360–361
 composites, 432–3
 coordination polymerization, 88, 90, 92–3, 411
 general, 5, 8, 12–13, 85–6, 426
 in natural fiber composites, 495–6, 498–500
 injection, 457
 isotactic, 87, 391
 kinetics mathematical modeling, 96
 microscopy of blends, 414
 modified or grafted, 205, 211–4
 nanocomposites, 585, 591–4
 syndiotactic, 87, 89–90
 T_g , 429
 Thermoforming, 460
 Polypropylenimine, 563
 Polysilanes, 53
 Polysiloxanes, 46, 53, 243, 321, 410
 Polystyrene, PS
 anionic polymerization, 132, 147, 149–152, 155–6
 blends, 414, 417, 507, 513, 516
 branched, 411
 cationic polymerization, 168, 172
 controlled radical polymerization, 308
 dendrigraft polymer, 410, 575–6, 578, 581
 emulsion polymerization, 298
 expandable (EPS), 306
 for film and ribbon extrusion, 467, 470–471
 for ion exchange resins, 306
 form factor (light scattering), 374
 fungal attack, 498
 general, 5, 8, 9, 12–13, 68, 207–8, 241, 243, 262, 273, 276–7, 285, 356
 high-impact polystyrene (HIPS), 207–9, 212, 278, 306, 516
 microreactors, 330
 MWD measurement, 361
 nanocomposites, 585
 SEC columns, 355
 SEC standards, 359–360
 segments in thermoplastic elastomers, 574
 SIS copolymer, 418
 spin coating, 486
 sulfonated, 549
 suspension polymerization, 306
 syndiotactic polystyrene, 86–7, 90, 92
 synthesized in supercritical fluids, 321, 323
 Polysulfones, 285, 516
 Polyurethanes, PU, 8–9, 11, 13, 46–7, 50, 52–3, 165, 191, 210, 216, 273, 328, 417–8, 495, 516, 519, 526, 528, 569, 585, 600
 Pom-pom, 579
 Pot life, *see* Shelf life, 528–9
 Powder coatings, 524–5, 528, 531–2
 PP *see* Polypropylene
 Preform in polymer processing, 455, 528
 Preforms, 524
 Prepregs, 525
 Pressure (reactor), 276, 290
 Primary chains, 190, 192, 200–202
 Productivity, 258, 263
 Propagation reaction step, 254–6, 258–262, 264–5, 267, 269
 Pseudo-homopolymer approach, *see* Pseudokinetic Rate Constant method
 Pseudo-kinetic rate constant method, PKRCM, 255–6, 264–5
 Pultrusion, 527
 Quasi-steady-state approximation (QSSA)
 definition, 73
 in Mayo-Lewis equation, 108, 110
 in polymer reaction engineering, 256, 259
 Radiation-cured coatings, 527, 531
 Radical lifetime, 258
 RAFT *see* Reversible addition–fragmentation chain transfer polymerization
 Rate constant, *see* kinetic rate coefficient
 Reaction injection molding, RIM, 8, 527–530
 Reaction mechanism
 definition, 252
 for free radical polymerization, 254
 for LCB, 260
 for multicomponent copolymerization, 256
 for transfer to polymer, 255
 Reaction rate expression, 252–3
 Reaction-diffusion, 263
 Reaction-induced phase separation, RIPS, 525, 528
 Reactive blending, 509
 Reactive sites
 active center, 266
 active sites, 258
 dormant center, 266
 poisoning, 266
 Reactivity ratios
 anionic copolymerization, 148–150
 Arrhenius-type equation, 119
 definition, 108
 estimation, 114, 260
 pseudoreactivity ratios, 112, 255, 256
 values, 109, 148
 Reactor, 252
 autoclave, 275, 287
 batch reactor, 252–4, 259, 260–261, 263, 274, 277
 continuous stirred tank reactor, CSTR, 252, 261, 263, 274, 276–8, 281, 283, 287–8
 loop, 275, 287
 molds, *see also* casts, 275–6, 279
 polymerization reactor, 252
 semibatch reactor, 256, 260, 261, 274, 279
 series of reactors, 274, 281, 289
 size, 276
 tubular reactor, 252, 256, 263, 275–7, 281, 289
 Reinforced reaction injection molding, RRIM, 532
 Relaxation time, 16–20, 28–31, 33, 35–7
 Residence time, 276
 Resin transfer molding, RTM, 527
 Resins, 46, 47, 55–7, 59–60
 Retardation effect, 258
 Reversible addition–fragmentation chain transfer polymerization
 characterization of polymers
 synthesized by, 352
 copolymers, 107
 crosslinking, 199
 degree of polymerization, 81
 grafting, 207–8, 211, 214–5, 217

- Reversible addition–fragmentation chain transfer polymerization (*Continued*)
 in aqueous dispersions, 309
 in microreactors, 330
 microwave process, 328
 molecular weight distribution, 81
- Rheological properties of nanocomposites, 592–3, 595, 597
- Rheological properties of polymer blends, 514
- Rheological properties of polymers, 4, 10, 71, 419, 437, 468, 482
- Rotational molding (rotomolding), 451, 458, 459, 529
- Rubber, 505, 511, 513–5, 517
- Runaway, 263
- SAN, *see* Styrene-acrylonitrile copolymer
- Saturated polyesters, 532
- SBR, *see* Styrene-butadiene rubber copolymer
- SBS, *see* Styrene-butadiene-styrene block copolymers
- Scattering, 510, 514, 515
- Scission, 201, 262, 277, 280
- Second virial coefficient, 373, 477, 480, 576
- Seemann composite resin infusion molding, SCRIMP, 532
- Self-branching, 579
- Self-healing, 530, 531
- Semicontrolled structure, 559, 574
- Semidilute polymer solutions
 Blob model, 481
 scaling theory, 482
- SFRP *see* Nitroxide-mediated radical polymerization
- Shape-memory, 529
- Sheet molding compound, SMC, 528, 530
- Shelf life, *see* Pot life, 531
- Shrinkage, 522
- Silicone, 525
- Single-monomer methodology, 569
- SIS *see* Styrene-isoprene-styrene block copolymers
- Size exclusion chromatography, 259–260, 338, 355–362, 365, 443, 479–480, 552
 branching measurement, 361
 calibration, 359
- detectors, 358–9
 equipment, 358–9
 high-temperature, 360–361
 principles, 356–7
 sample preparation, 361
 universal calibration, 359
- Sol, *see also* gelation, 263
- Solid-phase synthesis, 59, 61
- Solubility parameter
 general, 365, 425, 426, 477–8, 507
 Hansen solubility parameters, 478
 Hildebrand solubility parameter, 477
- Solution polymerization, 258, 260–261, 263
- Solvent, 258, 260–261, 263, 267–8, 269, 273, 277
- Solvent-borne coatings, 519
- Spin-lattice relaxation time, T1, 194
- Spin-spin relaxation time, T2, 194
- Spray-up process, 523
- Stable free radical polymerization,
see Nitroxide-mediated radical polymerization
- Star-branched, 579
- Star-burst®, 563
- Starlike, 576–7
- Static light scattering in dilute polymer solutions
 apparent molecular weight in copolymers, 371–2
 branched polymers form factor, 375–6
 Einstein–Smoluchowski fluctuation theory, 370
 form factor, 373, 375–6, 379, 381
 Kirkwood and Goldberg theory, 370
 molecular weight determination, 370–372
 osmotic pressure, 370–371
 preferential sorption effects, 372
 radius of gyration, 374
 spherical thin shells form factor, 376
 virial coefficients, 371
 worm-like micelles, 376, 378
- Zimm plot, 374
- Stationary state hypothesis, *see* Quasi-steady-state assumption
- Statistical theories
 Flory's theory, 195–6, 199
 mean-field theory, 195, 197–9
- Staudinger, 527, 531
- Steady-state operation, 252, 274
- Steady-state viscosity, 193
- Step-growth polymerization, 9–10, 43–63, 106, 187, 191, 195, 201
- Storage modulus, 193–4, 431, 523, 588–9, 592, 600
- Structural reaction injection molding (SRIM), 525–7, 532
- Structural units, 568
- Structure, 425
 chemical, 426
 macromolecular, 425
 molecular, 428
- Styrene maleic anhydride copolymer, SMA, 13, 113
- Styrene polymerization
 heat effects in, 263
 termination, 262
 transfer to monomer, 262
- Styrene-acrylonitrile copolymer
 3D microscopy, 419, 420
 abbreviation, 13
 blend with ethylene-propylene-diene-monomer, 517
 blends, 517
 characteristics, 106
 energy-filtered transmission electron microscopy, 415
 grafting, 209, 210
 light stabilizers, 233
- Mark-Houwink-Sakurada constants, 364
 production process, 277, 306
 reactivity ratios, 109
- Styrene-butadiene rubber copolymer
 abbreviation, 13
 anionic polymerization, 128, 146, 149
 characteristics, 105
 effects of light stabilizers in, 236
 GPC characterization, 361
 grafting, 208, 211, 212
- Mark-Houwink-Sakurada constants, 364
 reactivity ratios, 109
 solution process, 285–6
- Styrene-butadiene-styrene block copolymers, 13, 211–2, 227, 286, 361
- Styrene-isoprene-styrene block copolymers, 13, 211–2, 286, 418–9
- Substitution effect, 529

- Substrate, 519–520, 524, 527–8, 532, 559, 561, 574–8, 580
- Summation operator, 255
- Supercritical carbon dioxide copolymerization, 321–2
crosslinking, 322
homopolymerization, 321
mathematical modeling, 321–2
comparison, 321
MMA, 321, 323
TFE/Vac, 321
vinyl/divinyl monomers, 322
- polymerization, 206, 212, 321
properties, 320–321
- Supercritical fluids
LCEP, 318
LCST, 318–320
phase equilibria, 317
UCEP, 318
UCST, 318–320
- Surface modification
corona discharge, 206
electron beam, 206
gamma-rays, 206
ozone, 206
UV-irradiation, 206
- Surfactant, 296
adsorption, 296
hydrophilic-lyophilic balance (HLB), 298
in emulsion polymerization, 298
Kraft point, 297
specific area (as), 296, 300
types, 296
- Suspending agents, 306
- Suspension polymerization, 305–8
advantages and disadvantages, 306
commercial resins manufactured by, 306
generalities, 252, 261–3, 305–6
scaling up, 307
summary of studied CRP systems, 309
- Swelling index, 188, 190–191, 194, 278
- Synthesis, *see* Polymerization or Synthetic strategies
- Synthetic strategies
arm-first, 561
cascade, 560, 563, 565
convergent, 561–5, 570, 574, 578–9
core, 568
core-last, 561
- divergent, 561–4, 566, 574–8, 581
grafting from, 574, 577
grafting onto, 574–6
grafting through, 578–9
noncore, 568
one-pot, 567–570, 573–4, 578–9, 581
semibatch, 578
stepwise, *see also* Polymerization, 559
- Tack life, 519, 520, 522, 524, 528–532
- Temperature
effects on disproportion termination, 262
effects on limiting conversion, 259
effects on molecular weight, 261
effects on productivity, 258
effects on reactivity ratios, 260
effects on stereoregularity, 258
effects on transfer to monomer, 262
effects on transfer to polymer, 258
gradients of, 263
- Temperature (reactor), 274, 276–9, 281–3, 286
- Temperature control
adiabatic temperature rise, 287
condensers, 276
cooling, 274, 276
heat exchanger, 276
isothermal, 276
self-accelerating temperature (SAT), 288
- Template, 573, 580
- TEMPO,
crosslinking, 199
grafting, 212–216
in controlled radical polymerization, 71, 72, 79
in suspension polymerization, 309
- Terminal double bond, TDB
polymerization, 258, 259
- Terminal model, 255–6
- Termination reaction,
chemically controlled termination, 262, 255
diffusion-controlled termination, 259–261
- Terpolymer, 105
- Thermoforming, 451, 460, 461, 497
- Thermoplastic polyurethane elastomer, TPU, 516
- Thermoplastics, 437, 441, 442, 446, 519, 520, 523–5, 527–532
- Thermoset, 530
- Thermosetting polymers, 55, 524, 532
- Theta conditions, 364–365
- Theta temperature, 477, 480
- Thickening agent, 523
- Tomalia, 560, 563, 567, 575–6
- Topologies,
brush, 577
core-shell, 576, 577, 580
core-shell-corona, 580
cylindrical, 577
dumbbell, 579
spherical, 562, 576, 577, 581
- Total transverse relaxation function, M(t), 194
- Toughening, 519, 520, 522, 525, 530–32
- Transfer reaction step
chain transfer agent, CTA, 258, 263
effects of, 258
transfer to dimer, 269
transfer to initiator, 267, 269
transfer to monomer, 258, 259, 261, 262, 269
transfer to polymer, 254, 255, 258–265, 269
transfer to small molecule, T, 264
transfer to solvent, 269
- Trommsdorff effect, 73–4, 259, 301–2
- Ubbelohde viscometer, 362
- UCST *see* Upper critical solution temperature
- Ultraviolet radiation, 329
polymerization reactions, 329
- Unimolecular micelle, 579–80
- Unit cell, 15, 23, 391–2
- Unsaturated polyesters, UP, 519, 521, 526
- Urea polymers, 31, 46–7, 190, 191, 216, 239–240, 519, 520
- Urea-formaldehyde polymers, 529
- UV-curing, 529
- Vacuum bag, 530–532
- Vacuum-assisted resin transfer molding, VARTM, 522, 525

VDC/VCM, *see* Vinylidene chloride–vinyl chloride copolymer
Vinyl ester, 524–530
Vinylidene chloride–vinyl chloride copolymer, 106
Viscoelastic behavior, 425, 429–431
melt, 425
rubber, 425
Viscometry, 441, 443
Vitrification, 523, 524
Vögtle, 560, 563
Volatile organic compound emissions, VOC, 525–6
Volatile organic compounds, 317, 326–329
Vulcanization, 191–2, 200

Water soluble polymers, 280
Waterborne coatings, 526
Weight-average chain length, 6, 196–7, 200–202, 327
Weight-average molecular weight, 253, 255, 258–9, 261–2
Wet lay-up process, 528–9
Wire coating, 454–5
X-ray diffraction, 23, 25, 592
X-ray scattering, correlation function, 399–400, 402–3
Debye's equation, 404
diffraction intensity, 395
electron density distribution, 400

fluctuations, 399–400
function, 393–4, 402
general, 391, 393, 398
Fourier transform, 394, 397–8, 400, 402, 405
interface distribution function, 402–3, 405–6
long period, *see* periodicity
Lorentz factor, 395–6
multiplicity factor, 395
periodicity, 395–7, 400–401, 405
polarization factor, 395
random orientation, 396
reciprocal space, 391, 393–7, 402, 405
scattering vector, 393, 394–5, 404